

Quarterly Publication

ISSN 2383 - 3572

---



# Global Journal of Environmental Science and Management

Volume 10, Number 1, Winter 2024



## Publisher and Editor in Chief

Professor J. Nouri  
Tehran University of Medical Sciences,  
Tehran, Iran  
Email: [editor@gjesm.net](mailto:editor@gjesm.net)  
[nourijafar@gmail.com](mailto:nourijafar@gmail.com)

## Managing Editor

Professor D. Sivakumar  
Kalasalingam Academy of Research and  
Education, Tamil Nadu, India  
Email: [sivakumar.gjesm@gmail.com](mailto:sivakumar.gjesm@gmail.com)

## Assistant Editor

Dr. S.M. Tehrani  
International Journal of Human  
Capital in Urban Management  
Email: [tehranishohre@gmail.com](mailto:tehranishohre@gmail.com)

## Page Designer

A. Rezaye Soltanabadi  
Imajgaran Danesh

## Website Manager

M. Dorani  
Sinaweb Management System

## Editorial Contact Information

Z, Kouhestan Deadend,  
Janpour Street, Darabad Square,  
Tehran, Iran  
Phone: +9821-26105110  
Email: [gjesm.publication@gmail.com](mailto:gjesm.publication@gmail.com)  
[editor@gjesm.net](mailto:editor@gjesm.net)

Website: <https://www.gjesm.net/>

## Publication Center

GJESM Publisher  
[publisher@gjesm.net](mailto:publisher@gjesm.net)

(QUARTERLY PUBLICATION)



## Editorial Board

*Professor V.K. Gupta; University of Johannesburg, South Africa*

*Professor A. Fauzi Ismail; Universiti Teknologi Malaysia, Malaysia*

*Professor A.T. Peterson; University of Kansas, USA*

*Professor M. Sillanpää; Lappeenranta University of Technology, Finland*

*Professor A. Cerda; University of Valencia, Spain*

*Professor J.-D. Gu; University of Hong Kong, P.R. China*

*Professor S.I. Allakhverdiev; Russian Academy of Sciences, Russia*

*Professor D. Wen; University of Leeds, UK*

*Professor T. Yigitcanlar; Queensland University of Technology, Australia*

*Professor A. Z. Aris, Universiti Putra Malaysia, Malaysia*

*Professor K. Yetilmezsoy, Yildiz Technical University, Turkey*

*Professor K.E. Noll; Illinois Institute of Technology, USA*

*Professor J. Nouri; Tehran University of Medical Sciences, Iran*

*Professor D. Sivakumar; Kalasalingam Academy of Research and Education, India*

*Professor M.H. Sayadi; University of Birjand, Birjand, Iran*

GJESM is licensed under a "Creative Commons Attribution 4.0 International (CC-BY 4.0)"

Publication authorization is certified by the Ministry of Culture and Islamic Guidance; No. 93/3629; 14 May 2014

Scientific-Research grade is accredited by the Ministry of Science, Research and Technology; No. 3/18/59975; 20 June 2015

**Circulation: 500**

**pISSN 2383 - 3572**

**eISSN 2383 - 3866**

**Aims and Scope**

Global Journal of Environmental Science and Management (GJESM) is an international scholarly refereed research journal which aims to promote the theory and practice of environmental science and management. A broad outline of the journal's scope includes; peer reviewed original research articles, case and technical reports, reviews and analyses papers, short communications and notes to the editor, in interdisciplinary information on the practice and status of research in environmental science and management, both natural and man-made. The main aspects of research areas include, but are not exclusive to; environmental chemistry and biology, environments pollution control and monitoring, transport and fate of pollutants in the environment, concentrations and dispersion and trace of wastes in air, water, and soil, point and non-point sources pollution, heavy metals and organic compounds in the environment, atmospheric pollutants and trace gases, solid and hazardous waste management; soil biodegradation and bioremediation of contaminated sites; environmental impact assessment, industrial ecology, ecological and human risk assessment; improved energy management and auditing efficiency and environmental standards and criteria.

**Vision and Mission**

Global Journal of Environmental Science and Management (GJESM) publishes original. Peer-reviewed and technical environmental articles serve those environmental science and management through the on time quarterly publication with reliable information. GJESM is an integral partner with the scientific and technical communities, delivering superior information products and services that foster communication, build insights and enables individual and collective advancement in environmental research. Providing environmental science and management information to the general public with descriptions of contemporary advances in environmental issues to be used in improving environmental protection and management.

**Abstracting and Indexing**

Web of Science (ESCI); Scopus; Scimago Journal Rank (SJR); ProQuest (Agricultural and Environmental Science + Natural Science Collection + Ulrichsweb); Chemical Abstract (CAS); CABI Abstract; Global Health Abstract; Agricola; Committee on Publication Ethics (COPE); PubMed-NCBI; DOAJ; Open J-Gate; Google Scholar; Academia.edu; Geomar; WorldCat; Academic Resource Index; Environmental XPRT; Information Matrix for the Analysis of Journals (MIAR); Bibliothek Humburg; ScienceMedia; JournalTOCs; MSRT; ISC; RICEST; SID; Civilica; Magiran.

# Global Journal of Environmental Science and Management (GJESM)

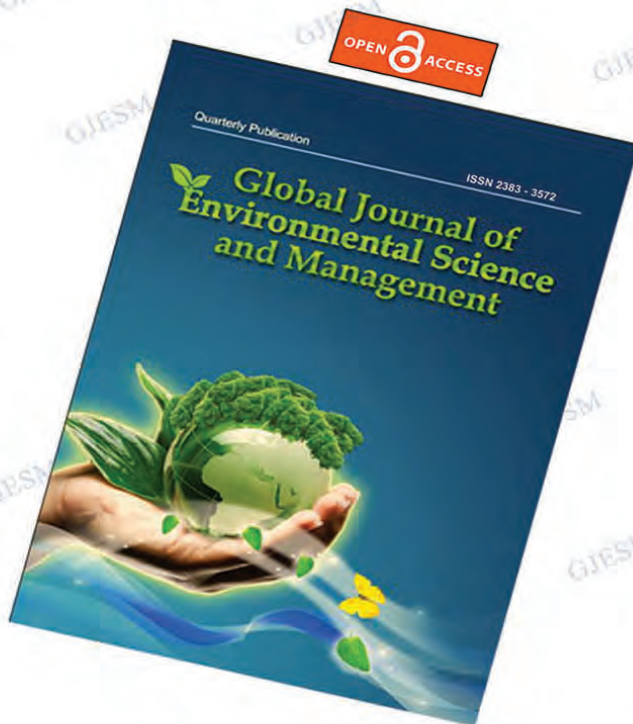
*Editor-in-Chief*  
*Professor J. Nouri*

pISSN 2383 - 3572

eISSN 2383 - 3866

**QUARTERLY FULL OPEN ACCESS PEER REVIEWED PUBLICATION**

**Journal Abbreviation: Global J. Environ. Sci. Manage.**



## CALL FOR PAPERS

Publication benefits in  
Global Journal of Environmental  
Science and Management

- *Quarterly Publication journal*
- *Online submission and reviewing*
- *Online status inquiry*
- *Double blind peer reviewing*
- *Rapid evaluation and publication*
- *Immediate publication on the net*
- *Open access to all PDF full text of published articles*
- *No pay charge for publication*
- *Indexed and cited in well-known databases;  
particularly Web of Science and Scopus*

[www.gjesm.net](http://www.gjesm.net)  
[www.gjesm.org](http://www.gjesm.org)

[editor@gjesm.net](mailto:editor@gjesm.net)  
[global.jesm@gmail.com](mailto:global.jesm@gmail.com)  
[gjesm.publication@gmail.com](mailto:gjesm.publication@gmail.com)

Tel.: +9821 2610 5110

Fax: +9821 2610 5111



# CONTENTS

Volume 10, Number 1, Winter 2024

1	Economics and cost effectiveness of a rain garden for flood-resistant urban design	1
	<b>D. Rinchumphu; N. Suriyanon; N. Phichetkunbodee; S. Munlikawong; C. Wanitchayapaisit; S. Sitthikankun (THAILAND/ TAIWAN)</b>	
2	Green synthesis of titanium dioxide photocatalyst using <i>Lactobacillus bulgaricus</i> for processing palm oil mill effluent	13
	<b>L. Agustina; M. Romli; P. Suryadarma; S. Suprihatin (INDONESIA)</b>	
3	Efficient biosorption of cadmium by <i>Eucalyptus globulus</i> fruit biomass using process parameters optimization	27
	<b>M. Samimi (IRAN)</b>	
4	Silver-based plasmonic nanoparticles for biosensor organophosphate pesticides using a single film containing acetylcholinesterase/choline oxidase	39
	<b>D. Hermanto; N. Ismillayli; H. Muliasari; R. Wirawan; S.R. Kamali (INDONESIA/ CHINA)</b>	
5	Analyzing cellulolytic bacteria diversity in mangrove ecosystem soil using 16 svedberg ribosomal ribonucleic acid gene	51
	<b>I. Dewiyanti; D. Darmawi; Z.A. Muchlisin; T.Z. Helmi (INDONESIA)</b>	
6	Evaluation of municipal waste collection performance using operational data	69
	<b>G.M. Hoang; H.T.T. Ung; N.T.L. Le; T.D. Nguyen (VIETNAM)</b>	
7	Wetland degradation monitoring using multi-temporal remote sensing data and watershed land degradation index	83
	<b>I. Ridwan; S. Kadir; N. Nurlina (INDONESIA)</b>	
8	Exploring the upper ocean characteristics of a bay using coastal and regional ocean community model	97
	<b>D. Jaishree; P.T. Ravichandran (INDIA)</b>	
9	Application of fuzzy logic in decision-making process for relocation of floating net cages in river fish farming	117
	<b>R. Pramana; B.Y. Suprpto; Z. Nawawi (INDONESIA)</b>	
10	Factors affecting cadmium toxicity to rice germinated in soils collected from downstream areas of abandoned zinc mines	133
	<b>P. Chanpiwat; A. Numprasanthai (THAILAND)</b>	
11	Impact of environmental and geographical position on the chemometric classification of ethanol extracts from <i>Isotoma longiflora</i> leaves	155
	<b>E. Imelda; K. Khairan; R.R. Lubis; T. Karma; R. Idroes (INDONESIA)</b>	
12	Torrefaction of bamboo pellets using a fixed counterflow multibaffle reactor for renewable energy applications	169
	<b>W. Hidayat; B.A. Wijaya; B. Saputra; I.T. Rani; S. Kim; S. Lee; J. Yoo; B.B. Park; L. Suryanegara; M.A.R. Lubis (INDONESIA/ KOREA)</b>	
13	Evaluation of mineral and near-infrared forecasting of wheat yield varieties using spectrophotometric techniques	189
	<b>H.A. Pardhe; N. Krishnaveni; B.K. Chekraverthy; S. Patel; S. Naveen; V. Rashmi; P.C. Govinden (INDIA/ MAURITIUS)</b>	
14	Presence of microplastics contamination in table salt and estimated exposure in humans	205
	<b>D.A. Syamsu; D. Deswati; S. Syafrizayanti; A. Putra; Y. Suteja (INDONESIA)</b>	

15	Generalization of artificial neural network for predicting methane production in laboratory-scale anaerobic bioreactor landfills	225
	<b>M.J. Zoqi (IRAN)</b>	
16	Modeling regional aboveground carbon stock dynamics affected by land use and land cover changes	245
	<b>A.D. Malik; M.C.W. Arief; S. Withaningsih; P. Parikesit (INDONESIA)</b>	
17	Root growth and arbuscular mycorrhizal fungi on woody plants for vegetative stabilization of tropical slopes	267
	<b>I.G. Tejakusuma; E.H. Sittadewi; T. Handayani; T. Hernaningsih; W. Wisyanto; A. Rifai (INDONESIA)</b>	
18	Role of <i>Cylindrospermopsis sp.</i> in vertical nitrogen changes observed in tropical oxidation wastewater treatment ponds	287
	<b>M. Srichomphu; O. Phewnil; T. Pattamapitoon; Ratcha Chaichana; K. Chunkao; W. Wararam; N. Dampin; P. Maskulrath (THAILAND)</b>	
19	Flood susceptibility mapping based on watershed geomorphometric characteristics and land use/land cover on a small island	301
	<b>B.H. Narendra; O. Setiawan; R.A. Hasan; C.A. Siregar; , Pratiwi; N. Sari; A. Sukmana; I.W.S. Dharmawan; R. Nandini (INDONESIA)</b>	
20	Machine learning using random forest to model heavy metals removal efficiency using a zeolite-embedded sheet in water	321
	<b>N.D. Takarina; N. Matsue; E. Johan; A. Adiwibowo; M.F.N.K. Rahmawati; S.A. Pramudyawardhani; T. Wukirsari (INDONESIA/ JAPAN)</b>	
21	Cocoa farmers' characteristics on climate variability and its effects on climate change adaptation strategy	337
	<b>I. Idawati; N.A. Sasongko; A.D. Santoso; M. Septiani; T. Handayani; A.Y.N. Sakti; B.D. Purnamasari (INDONESIA)</b>	
22	An analysis on the economic development and deforestation	355
	<b>E.S. Siregar; S.U. Sentosa; A. Satrianto (INDONESIA)</b>	
23	Ecotoxicological insight of phytochemicals, toxicological informatics, and heavy metal concentration in <i>Tridax procumbens</i> L. in geothermal areas	369
	<b>N.B. Maulydia; R. Idroes; K. Khairan; T.E. Tallei; F. Mohd Fauzi (INDONESIA/ MALAYSIA)</b>	
24	A state of the art review on geotechnical reinforcement with end life tires	385
	<b>M. Shariati; M. Afrazi; H. Kamyab; S. Rouhanifar; E. Toghrol; M. Safa; Sh. Chelliapan; H. Afrazi (ECUADOR/ USA/ MALAYSIA/ IRAN/ AUSTRALIA/ VIETNAM)</b>	
25	Abnormality in optimal forest management by indigenous people in deforestation	405
	<b>A. Mutolib; Y. Yonariza; A. Rahmat (INDONESIA)</b>	



ORIGINAL RESEARCH PAPER

## Economics and cost effectiveness of a rain garden for flood-resistant urban design

D. Rinchumphu<sup>1</sup>, N. Suriyanon<sup>1</sup>, N. Phichetkunbodee<sup>2</sup>, S. Munlikawong<sup>1</sup>, C. Wanitchayapaisit<sup>3</sup>, S. Sitthikankun<sup>1</sup>

<sup>1</sup> Department of Civil Engineering, Faculty of Engineering, Chiang Mai University, Thailand

<sup>2</sup> Department of Civil Engineering, Faculty of Engineering, National Taiwan University, Taiwan

<sup>3</sup> Department of Plant and Soil Sciences, Faculty of Agriculture, Chiang Mai University, Thailand

### ARTICLE INFO

#### Article History:

Received 08 January 2023

Revised 18 March 2023

Accepted 18 April 2023

#### Keywords:

Cost efficiency

Green infrastructure

Infiltration

Rain garden

Stormwater management

### ABSTRACT

**BACKGROUND AND OBJECTIVES:** Rapid urbanization negatively affects the hydrologic cycle and makes cities vulnerable to disastrous flash floods. It can additionally cause erosion and water pollution in natural ecosystems. Global climate changes have exacerbated such issues, further upsetting hydrologic patterns. Therefore, many regions have considered the rain garden as green infrastructure, which can help mitigate urban runoff. However, design guidelines and the means of assessing rain garden cost effectiveness in the Global South are limited. Furthermore, as many countries in the Global South experience a tropical climate, design guidelines developed in the temperate Global North may not be directly transferable. The need for more information on design and cost effectiveness can make designers and decision makers hesitate to implement such a new strategy. The main objective of the present study is to create a design approach and simultaneously specify the cost of the infiltration rate of the rain garden in urban areas.

**METHODS:** This study focuses on the ability of rain garden design to determine accurately the cost of materials used for construction. Sand and gravel are used in different sand ratios in the filter media layer, namely 1:1, 1:2, 1:3, and 1:4. The storage layer uses gravel only and has only one design. The aim is to determine the change in infiltration rate with an increase in the amount of sand. Knowing the amount of sand can determine the cost per infiltration rate.

**FINDINGS:** The results showed that the most efficient design was a rain garden with a soil:sand ratio of 1:4, which increased the infiltration rate per cost by 2.00 millimeters per hour per United States Dollar per square meter. The lowest efficiency option was a soil:sand ratio of 1:1, which increased the infiltration rate per cost by 1.33 millimeters per hour per United States Dollar per square meter.

**CONCLUSION:** This study will serve as a guide for designers to design a rain garden area according to the needs of the area, having determined the construction cost per infiltration rate. However, spatial requirements, construction costs, and social factors may influence future decisions on rain garden design and must be studied further.

DOI: [10.22035/gjesm.2024.01.01](https://doi.org/10.22035/gjesm.2024.01.01)

This is an open access article under the CC BY license (<http://creativecommons.org/licenses/by/4.0/>).



NUMBER OF REFERENCES

35



NUMBER OF FIGURES

7



NUMBER OF TABLES

2

\*Corresponding Author:

Email: [sitthikorn\\_sit@cmu.ac.th](mailto:sitthikorn_sit@cmu.ac.th)

Phone: +669 5146 6767

ORCID: [0000-0001-6107-8010](https://orcid.org/0000-0001-6107-8010)

Note: Discussion period for this manuscript open until January 1, 2024 on GJESM website at the "Show Article".

## INTRODUCTION

Rapid growth in urban areas has increased stormwater runoff. The water permeability of the soil surface decreases continuously owing to the vast and rising expansion of constructed works which have been reducing the natural land surface in urban areas. Structures such as buildings and roads are necessary living facilities, which are increasingly required as the population grows (Mardianti and Purba, 2023). In addition, climate change, unpredictable increases in rainfall, insufficient existing drainage systems for stormwater runoff catchment, and low sewerage treatment capacity result in prolonged waterlogging and affect life and traffic in urban areas. Therefore, methods to create a better infiltration rate on existing land surface areas are an exciting prospect for alleviating such problems. Water sensitive urban design (WSUD) in Australia or low impact development (LID) in the United States are examples of common approaches to improving soil surfaces for higher infiltration rates (Huang et al., 2015; Li et al., 2019). Rain gardens or bioretention systems are especially well known and could be implemented in urban areas, as they are well permeable to the original soil (Morash et al., 2019; Sharma and Malaviya, 2021; Suharyanto et al., 2023). A rain garden is a system of soil layers to increase the permeability of the soil surface. It consists of three main layers: 1) filter media, 2) transition layer, and 3) storage layer (Parker and Zingoni de Baro, 2019; SSQTA, 2020). The efficiency indicator is the increased infiltration rate of the entire system, which must increase the permeability of the original soil (Qin et al., 2021; Shi, Zhao et al., 2022). Mixing sand into the soil is the typical method of increasing porosity and hence the water infiltration rate of the soil (Sittisom et al., 2022). However, the key factor in design and construction is cost (Van der Meulen, 2019; Zeng et al., 2021). How much the soil must be changed to achieve improved infiltration rates is not yet known, but adding a proportion of sand to increase the infiltration rate raises the cost (Zeng et al., 2021). The study aims to design a rain garden to determine the construction cost and infiltration rate efficiency to inform further application guidelines. This study has been carried out in Thailand in 2023.

### *Hydrology principle and stormwater runoff*

The hydrologic cycle, commonly called the water cycle, lacks a definitive starting point. Nevertheless, it

is crucial to assign precipitation, which encompasses rainfall, hail, and snow, as the first step in the cycle. This water condenses in the atmosphere and returns to the Earth's surface. Before reaching the ground, a portion of the precipitation is intercepted by natural features, such as leaves and plant branches, and human-made structures, such as rooftops, in a process referred to as interception. In cases where the amount of precipitation surpasses the soil's capacity to absorb it, the excess water flows over the land surface as overland flow (Monger et al., 2022). When water naturally flows from high areas to low ones and then to a river, it is called surface runoff. After that, some water that infiltrates the soil (infiltration) will flow to lower areas, a phenomenon called interflow. Water that infiltrates deeper and accumulates in aquifers is called groundwater, which can flow into lower areas, rivers, and the sea. As the water flows, it receives thermal energy from the sun. This water then disperses into the atmosphere through evaporation, which is the process by which a liquid changes into a gas. Transpiration is the process by which plants release water vapor into the atmosphere through tiny pores in their leaves. Evaporation can occur from any wet surface, while transpiration is specific to plants. When more vapor condenses in the atmosphere, it becomes precipitation again (Sittisom et al., 2022). The hydrologic cycle can be written as a hydrologic balance equation to describe the relationship using Eq. 1 (Sittisom et al., 2022).

$$P = Q + G + E + T + I + S \quad (1)$$

where P is rainfall, Q is surface runoff, G is underground water volume, E is surface water evaporation, T is plant transpiration, and S is water changes on the soil surface. However, the critical consideration is alleviating the severity of prolonged waterlogging caused by stormwater runoff. Therefore, the equation is applied in designing a rain garden.

### *Rain garden design*

The rain garden is an area intended to efficiently catch stormwater runoff in urban areas (water sensitive design). Rain gardens and bioretention are very similar. The design of rain gardens appears in many standards used in water catchment areas, for example in Singapore's Waters Design Guidelines: Active, Beautiful, Clean (PUB, 2014) and Low

Impact Development: Technical Guidance Manual (Puget Sound Action Team, 2012), which has been implemented in many states in the United States of America (Batalini de Macedo *et al.*, 2022). The rain garden is often located in low areas to slow down the water and reduce the stormwater runoff flow rate. It also temporarily collects water in instances where the rain garden is designed as a basin. It often looks like a garden. Hence, a rain garden can be created in many kinds of public areas, such as traffic islands, gardens in residential projects, and city parks. Apart from the stormwater runoff reduction, it also enhances aesthetics and increases green areas (Bağ and Barjenbruch, 2022; Wilbers *et al.*, 2022). The critical function of a rain garden is the ability to enhance the underground infiltration rate. Therefore, the design of each layer and the material properties of each is essential. Various designs are described in the literature; for example, the Australian guidelines (Melbourne Water, 2013) recommend the layer design as follows: ponding depth layer 20–30 cm, filter media layer 30 cm, transition layer 10 cm, storage layer 30–40 cm. The materials are sand and sandy loam for the filter media layer, small gravel for the transition layer, and large gravel for the storage layer. An example of landscape architecture design is presented in Fig. 1.

In addition, Wanitchayapaisit *et al.* (2022) designed two variations of a rain garden for rainwater management in Chiang Mai, Thailand: 1) ponding depth layer 60 cm, planting soil layer 30 cm, storage layer 40 cm; and 2) ponding depth layer 40 cm, planting soil layer or filter media layer 70 cm, storage

layer 20 cm. The materials for the two designs are soil mixed with sandy loam (filter media layer) and gravel (storage layer). The results showed that the efficiency of rainwater harvesting of variant 1) was higher than that of variant 2). However, variant 2) was more efficient than the unchanged original soil and many other designs (Yuan *et al.*, 2017; Zhou and Guo, 2022). Moreover, the rain garden reduces runoff pollution (Chen *et al.*, 2023; Makbul *et al.*, 2021). An area with a higher infiltration rate serves to reduce the duration and severity of stormwater runoff; the retention of increased volumes of water in the drainage systems of urban areas is prevented. Common critical gaps in creating rain gardens are as follows. 1) In the Thai context, although the design guidelines of a rain garden have yet to be standardized, the variety of designs results in difficulty in implementation. Furthermore, the design is implemented in specific areas and depends on the knowledge and experience of each designer, which may need clarification. Because of that, the technique proposed by Wanitchayapaisit *et al.* (2022) is an appropriate approach for estimating the construction cost for infiltration rates because the design takes into account the characteristics of weather, soil, and rainfall in the areas under consideration. 2) The cost per infiltration rate still needs to be standardized, and it is difficult to design appropriately to serve an area's needs and the break-even points. The permeability rate obtained by mixing sand with soil in various ratios (Sittisom *et al.*, 2022) was used as a guideline for this study. 3) The literature review revealed a problem in determining rain gardens' cost per infiltration rate.

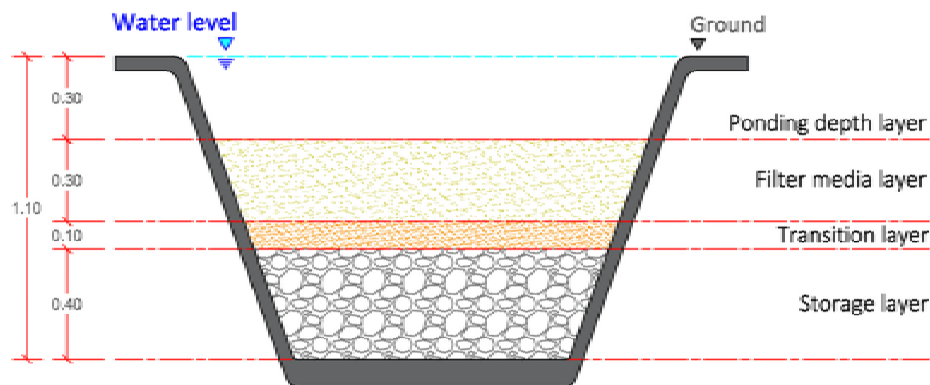


Fig. 1: Example of soil layer design for a rain garden (Melbourne Water, 2013)

The cost efficiency of a rain garden

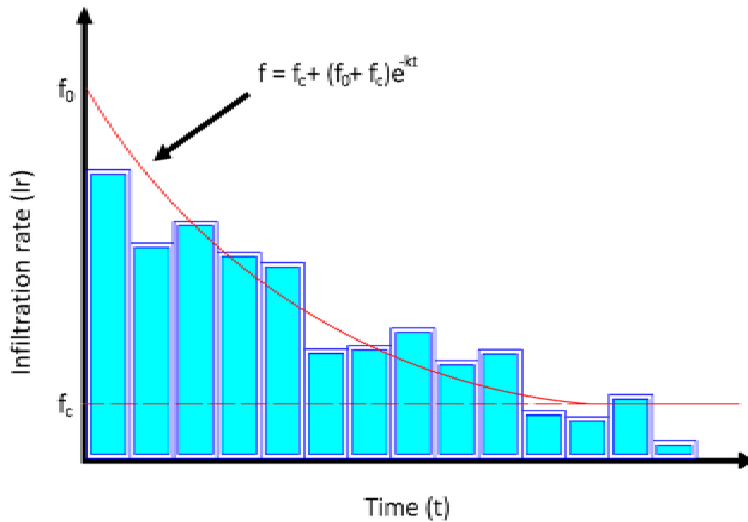


Fig. 2: Characteristics of the occurrence of the infiltration rate per time of change (Sittisom *et al.*, 2022)

The primary objective is to create a design approach considering both infiltration rate and cost for rain gardens in urban areas. Assess the efficiency of a rain garden, and it is essential to understand the principles and techniques used to measure infiltration rates.

*Principle of the infiltration rate*

As the water moves from high to low areas, it infiltrates into the soil; some of it becomes simply as soil moisture, whereas some parts penetrate deeper and become groundwater. The infiltration rate of soil relies on many factors, such as rainfall intensity, temperature, soil physical characteristics (Mongil-Manso *et al.*, 2022), types of cover crops, land use characteristics, and initial soil moisture content (Abdelmoneim *et al.*, 2021; Sittisom *et al.*, 2022). Horton’s theory is applied to calculate the quantity of permeable water in the soil.

The design and measurement of the infiltration rate of the rain garden can be written using Eq. 2 (Sittisom *et al.*, 2022).

$$f_t = f_c + (f_0 - f_c) e^{-kt} \quad (2)$$

where  $f_t$  is the infiltration rate measured in millimeters per hour (mm/h),  $f_c$  is a constant infiltration rate (mm/h),  $f_0$  is the initial infiltration rate (mm/h), and  $k$  is a constant value showing a decrease

in the soil infiltration rate.

To measure the infiltration rate for soil design following Horton’s theory, an instrument called a double-ring infiltrometer is used (Raju and Hussain, 2019; Atta-Darkwa *et al.*, 2022).

*Double-ring infiltrometer technique*

The permeability determination approach is applied to discover the potential based on urban catchment management principles. One method used to determine soil permeability is the double-ring infiltrometer technique, according to ASTM D 3385-03, as illustrated in Fig. 3.

The double-ring infiltration technique (Fig. 3) is applied following the prediction equation in Horton’s theory of permeability, which was first proposed in the 1940s (Abdelmoneim *et al.*, 2021; Geberemariam, 2019). The literature review showed that the single-ring infiltrometer technique is another practical technique for examining the infiltration rate. It is important to know the infiltration rate of the soil composite because infiltration measurement techniques are only applied to determine the soil permeability. To increase the soil infiltration rate, a basic technique to increase the soil porosity is to mix sand into the soil. The use of sand as filter media (Melbourne Water, 2013; Sittisom *et al.*, 2022) is a standard method to increase soil infiltration efficiency.

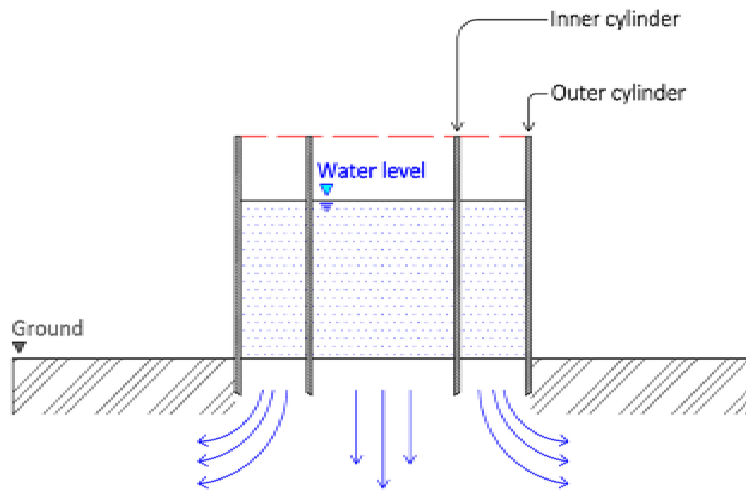


Fig. 3: Double-ring infiltration technique (Sittisom *et al.*, 2022)

#### The construction cost of a rain garden

The cost estimate is a process of estimating the quantity of materials and reasonable prices for actual projects. There are two types of cost estimate: approximate and detailed.

#### Approximate estimation

An approximate estimation is a method for price estimation that does not rely on detailed plans or precise quantities. This method can be conducted instantly and involves estimating areas, height, length, or quantities, relying on the experience of the estimator. The approximate price estimation may consist of price per unit of use, price per unit area or per unit volume, or assembly price per unit.

#### Detailed estimation

A detailed estimation takes into account all relevant components, such as the quantity of materials, material prices, labor costs, machine costs, operating costs, profits, taxes, interest, and other price-related details. This estimate requires a detailed plan that is complete and clear. It is accurate but takes more time than the approximate estimate (Sittikankun *et al.*, 2021). The present study aims to determine the construction cost and infiltration rate efficiency of a garden design in order to construct further application guidelines for Thailand. The study was conducted using the rain garden design model of

Wanitchayapaisit *et al.* (2022), which selected Chiang Mai University as the study site, located in the same area as this study. The material cost for rain garden construction was obtained from a survey in Chiang Mai in 2022.

#### MATERIALS AND METHODS

1) Rain garden design. In order to determine the construction cost, the size of the rain garden is first described. It consists of a ponding depth layer of 60 cm, a filter media layer of 30 cm, and a storage layer of 40 cm, as shown in Fig. 4.

2) Determination of infiltration rate. The sand-to-infiltration rate ratio can be calculated using Eq. 3 (Sittisom *et al.*, 2022):

$$I_r = 6.025e^{1.994(S_r)} \quad (3)$$

where  $I_r$  is the infiltration rate, and  $S_r$  is the sand ratio. Once the infiltration rate is determined, the next step is to determine the cost of the design.

3) Determination of cost. The material cost for rain garden construction was obtained from a survey in the Muang Chiang Mai District, Chiang Mai, in January 2023. The price for general coarse sand was 14.29 United States Dollar per cubic meter (USD/m<sup>3</sup>), and for 3/8 inch gravel was 20 USD/m<sup>3</sup>. The original soil in the test area was used, so there was

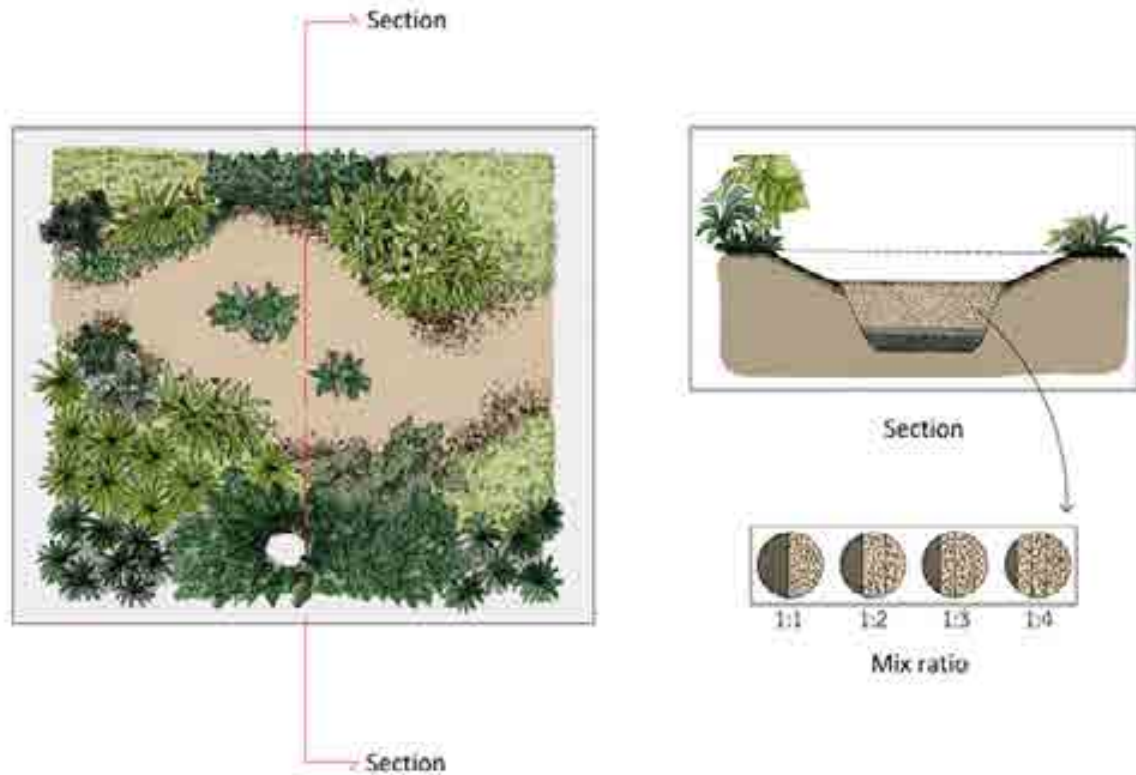


Fig. 4: Example of rain garden design.

no cost. Hence, the price takes into account only the cost of materials. Labor costs, transportation costs, and other costs are not considered. The price is the average price from the stores that have been found to stock the materials, as shown in Table 1.

#### Cost-efficiency calculation

Cost is inevitably an important factor in rain garden construction. After deciding on the garden design, estimating the construction material cost and determining the sand-to-infiltration rate ratio retrieved from Eq. 3, the permeability rate to cost can be calculated, as shown in Eq. 4 (Combes et al., 2018; Hoang et al., 2021).

$$\text{Cost efficiency } (C_e) = \frac{\text{Infiltration rate } (I_r)}{\text{Cost } (C)} \quad (4)$$

where the infiltration rate ( $I_r$ ) and the cost ( $C$ ) is for the coarse sand and 3/8 inch gravel.

## RESULTS AND DISCUSSION

Increasing the filter media layer's porosity by mixing more sand into the soil was found to raise the infiltration rate, but the cost also went up simultaneously. However, the application depended on the stormwater runoff characteristics in the design area. What was important was the cost of the infiltration rate that the designer considered reasonable, Sittisom et al. (2022) tested the filter media layer of bioretention using different mixing ratios. The sand-to-aggregate ratio and infiltration rate are summarized in Fig. 5.

In Fig. 5,  $I_r$  is the infiltration rate (mm/h), and  $S_r$  is the sand-to-aggregate ratio. Design the infiltration rate by using Eq. 4 and calculate by using the best design layer of rain garden from (Wanitchayapaisit et al., 2022) is the ponding depth layer 60 cm, the filter media layer 30 cm, the storage layer 40 cm, which is estimated to be an area of 1 square meter ( $m^2$ ). Price per unit volume will be the cost estimation

Table 1: Price survey of general coarse sand around Chiang Mai Province

Store name	Price (USD/m <sup>3</sup> )	
	Sand	Gravel
Chuchai	12.86	17.14
Thanasap	14.29	21.43
CMR Sum dang det	15.71	20.00
P.Lansai	17.14	21.43
Huay Sai Lan Sai	11.43	20.00
Lan Sai Khun Yo	11.43	17.14
Lan Sai Ruamchok	17.14	20.00
New Chok Amnuai Sai	14.29	22.86
Average	14.29	20.00

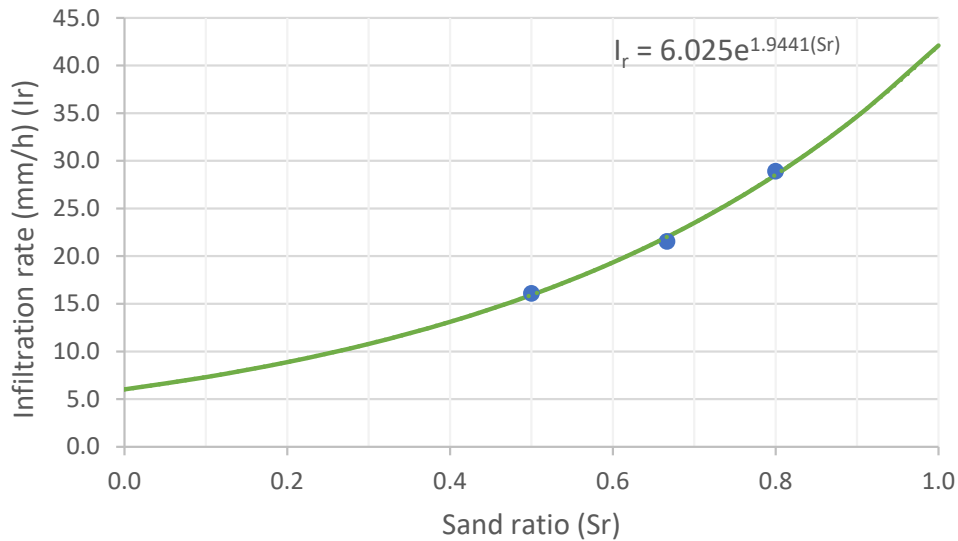


Fig. 5: The ratio of sand to aggregate with the infiltration rate (Sittisom et al., 2022)

method used in this study because there is no plan, and the width and length of the rain garden need to be specified. As shown in Fig. 6, the price per unit volume method has a mistake in price of 10–25%.

Although there is a risk of a price mistake from the price per unit volume method, it has the advantage of arriving at an estimate more quickly than other estimation methods (Sitthikankun et al., 2021). Therefore, this method was chosen in order to be able to use the price per volume to calculate the cost efficiency, as shown in Table 2.

The mixture rate to infiltration rate considered in 4 alternative could be used to determine the cost, as seen in Table 3.

The construction cost is an essential factor in building

a rain garden. To be able to forecast the increased cost-to-infiltration rate, four alternatives are presented. The results of the relationship between the cost-to-infiltration rate and sand mixing ratio (Fig. 7) are beneficial for further costing of the rain garden design. Moreover, the information can be used to create the following equation:  $C_e = 19.229e^{1.3584(Sr)}$  where  $C_e$  is Cost efficiency (mm/h/USD), and  $Sr$  is a sand-to-aggregate ratio. The equation test value is 0.9998, which is a reliable value (Rinchumphu et al., 2013).

Fig. 7 shows that, when the filter media layer becomes more porous owing to the addition of sand, the infiltration rate also increases (Sittisom et al., 2022), but the cost of sand and gravel rises as well. This can be used as a guideline for determining the

The cost efficiency of a rain garden

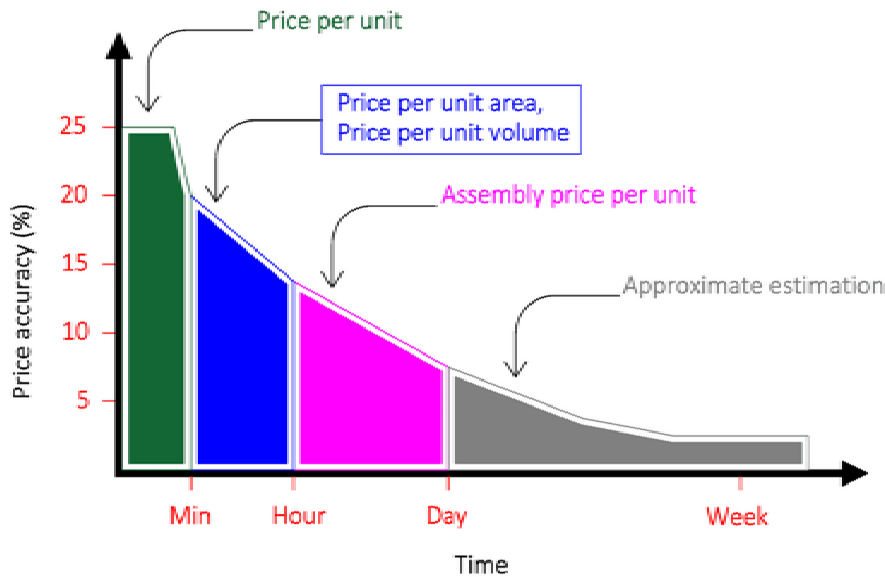


Fig. 6: The accuracy of cost estimation for each method (Sithikankun *et al.*, 2021).

Table 2: The mixing ratio of the filter media layer in each type

Alternative ratio, soil, and sand	Soil volume (m <sup>3</sup> )	Sand volume (m <sup>3</sup> )	Gravel volume (m <sup>3</sup> )	Infiltration rate (mm/h)	Cost (USD)	Cost efficiency (mm/h/USD)
1) 1:1	0.30	0.30	0.40	16.33	12.29	1.33
2) 1:2	0.20	0.40	0.40	22.77	13.72	1.66
3) 1:3	0.15	0.45	0.40	26.88	14.43	1.86
4) 1:4	0.12	0.48	0.40	29.70	14.86	2.00

Table 3: The cost to infiltration rate

1	Alternative 1: The cost of sand was USD 4.29. The cost of gravel was USD 8. The total cost was 12.29 United States Dollar per square meter (USD/m <sup>2</sup> ), with cost efficiency = 1.33 millimeters per hour per United States Dollar per square meter (mm/h/USD/m <sup>2</sup> )
2	Alternative 2: The cost of sand was 5.71 USD. The cost of gravel was 8 USD. The total cost was 13.72 USD/m <sup>2</sup> , with cost efficiency = 1.66 mm/h/USD/m <sup>2</sup>
3	Alternative 3: The cost of sand was 6.43 USD. The cost of gravel was 8 USD. The total cost was 14.43 USD/m <sup>2</sup> , with cost efficiency = 1.86 mm/h/USD/m <sup>2</sup>
4	Alternative 4: The cost of sand was 6.86 USD. The cost of gravel was 8 USD. The total cost was 14.86 USD/m <sup>2</sup> , with cost efficiency = 2.00 mm/h/USD/m <sup>2</sup>

permeation rate to cost in the construction of a rain garden. Nevertheless, the limitation of this study was that the cost survey was conducted only in Chiang Mai and only during January 2023. For more appropriate and practical approaches to further rain garden developments, it is necessary to consider the

differences in area and duration that affect the cost according to the theoretical principles of construction cost estimates. When designers can estimate the increasing cost accurately and quickly, more effective decisions can be made on the type and size of the rain garden.

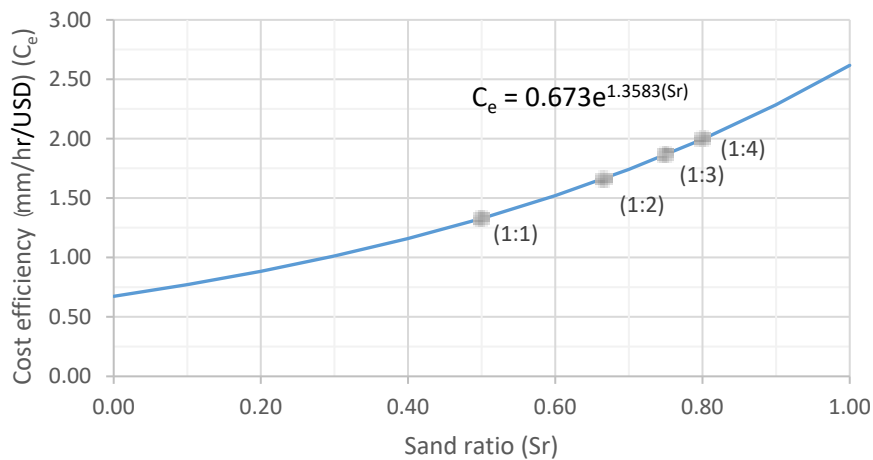


Fig. 7: Ratio of sand to cost.

## CONCLUSION

This study shows that rain gardens can help reduce stormwater runoff in urban areas by delaying the runoff from inside the rain garden; they act like retention ponds and allow water to infiltrate the soil instead of flowing onto the surface. Increasing the permeation rate of the filter media layer by using sand as the base layer is a method that is feasible with easily obtainable materials. Water can penetrate through sand very well. The results set out the cost of rain garden construction, which could be helpful for those involved in making decisions about the design. In order to advance the use of rain gardens, the determination of construction costs and standardized designs are, therefore, important factors. The study examined the relationship between infiltration rate and the cost of building a rain garden across four different cost alternatives. Based on the study's results, an equation was developed to determine the infiltration rate per cost accurately. The equation was tested and found to have a highly reliable test value of 0.9998. This study yielded two main results. 1) The rain garden design consists of a ponding depth layer of 60 cm as the top layer, a filter media layer of 30 cm as the next layer, and a storage layer of 40 cm as the bottom layer. 2) It is possible to set the permeation rate per cost to design the rain garden to meet local needs. This flexibility allows

urban planners and policymakers to tailor their rain garden design to meet the required permeation rate and budgetary limitations. This study had a limitation in the cost analysis, as the prices used to determine the costs were based on local prices in Chiang Mai, Thailand. For another location, it will be essential to consider the cost of local materials in that area. In order to create a more comprehensive dataset that includes different rain gardens suitable for use in Thailand, it is recommended that future studies investigate other aspects of rain gardening, such as cost-effectiveness, maintenance costs, and incentives available for creating rain gardens. Such studies would provide valuable information for urban planners and policymakers seeking to adopt rain gardens as part of their flood-resistant urban design strategy in Thailand.

## AUTHOR CONTRIBUTIONS

D. Rinchumphu supervised the fourth author in analyzing and summarizing the test results, including giving advice on techniques and methods. S. Munlikawong researched and collected local material prices. C. Wanitchayapaisit participated in advising on the performance analysis of rain gardens and preparing illustrations. S. Sitthikankun, the corresponding author, collected all data, analyzed the results, and drew conclusions. N. Phichetkunbodee and N. Suriyanon contributed to the data analysis.

## ACKNOWLEDGEMENT

The authors wish to thank support staff from the City Research and Development Center (City R&D), Faculty of Engineering, Chiang Mai University, and the Center of Excellence in Natural Disaster Management (CENDiM), Chiang Mai University, Thailand. This research has received funding support from the NSRF via the Program Management Unit for Human Resources and Institutional Development, Research and Innovation [Grant number B16F640172]. This research was partially supported by Chiang Mai University.

## CONFLICT OF INTEREST

The author declares that there is no conflict of interests regarding the publication of this manuscript. In addition, the ethical issues, including plagiarism, informed consent, misconduct, data fabrication and/or falsification, double publication and/or submission, and redundancy have been completely observed by the authors.

## OPEN ACCESS

©2023 The author(s). This article is licensed under a Creative Commons Attribution 4.0 International License, which permits use, sharing, adaptation, distribution, and reproduction in any medium or format, as long as appropriate credit is given to the original author(s) and the source, a link to the Creative Commons license is provided, and any changes made indicated. The images or other third-party material in this article are included in the article's Creative Commons license, unless indicated otherwise in a credit line to the material. If material is not included in the article's Creative Commons license and your intended use is not permitted by statutory regulation or exceeds the permitted use, you will need to obtain permission directly from the copyright holder. To view a copy of this license, visit: <http://creativecommons.org/licenses/by/4.0/>

## PUBLISHER'S NOTE

GJESM Publisher remains neutral with regard to jurisdictional claims with regard to published maps and institutional affiliations.

## ABBREVIATIONS

%	Percent
cm	Centimeter
C	Cost
$C_e$	Cost efficiency
E	Surface water evaporation
Eq.	Equation
Fig.	Figure
$f_0$	Initial infiltration rate
$f_c$	Constant infiltration rate
$f_t$	Infiltration rate at time (t)
G	Underground water volume
Ir	Infiltration rate
in	Inch
k	Constant value showing a decrease in the soil infiltration rate
LID	Low impact development
mm/h	Millimeters per hour
mm/h/USD/m <sup>2</sup>	Millimeters per hour per United States Dolla per square meter
m <sup>2</sup>	Square meter
m <sup>3</sup>	Cubic meter
p	Rainfall
Q	Surface runoff
S	Water changes on the soil surface
Sr	Sand ratio
t	Time
T	Plant transpiration
USD	United States Dolla
USD/m <sup>2</sup>	United States Dolla per square meter
USD/m <sup>3</sup>	United States Dolla per cubic meter
WSUD	Water sensitive urban design

## REFERENCES

- Abdelmoneim, A.A.; Daccache, A.; Khadra, R.; Bhanot, M.; Dragonetti, G., (2021). Internet of Things (IoT) for double ring infiltrometer automation. *Comput. Electron. Agric.*, 188: 106324 **(10 pages)**.
- Atta-Darkwa, T.; Asare, A.; Amponsah, W.; Oppong, E.D.; Agbeshie, A.A.; Budu, M.; Larbi, I.; Akolgo, G.A.; Quaye, D.N.D., (2022). Performance evaluation of infiltration models under different tillage operations in a tropical climate. *Sci. Afr.*, 17: e01318 **(13 pages)**.
- Bak, J.; Barjenbruch, M., (2022). Benefits, Inconveniences, and Facilities of the Application of Rain Gardens in Urban Spaces from the Perspective of Climate Change and mdash;A Review. *Water*, 14(7): 1153 **(19 pages)**.
- Batalini de Macedo, M.; Nóbrega Gomes Júnior, M.; Pereira de Oliveira, T.R.; H. Giacomoni, M.; Imani, M.; Zhang, K.; Ambrogi Ferreira do Lago, C.; Mendiondo, E.M., (2022). Low Impact Development practices in the context of United Nations Sustainable Development Goals: A new concept, lessons learned and challenges. *Crit. Rev. Environ. Sci. Technol.*, 52(14): 2538-2581 **(44 pages)**.
- Bodhinayake, W.; Si, B.C.; Noborio, K., (2004). Determination of hydraulic properties in sloping landscapes from tension and double-ring infiltrometers. *Vadose Zone J.*, 3(3): 964-970 **(7 pages)**.
- Chen, C.; Li, Y.; Le, W.; You, C.; Liu, Z.; Liu, W.; Zhang, R., (2023). Field performance of rain garden in red soil area in southern China. *Water*, 15(2): 267 **(14 pages)**.
- Combes, P-P; Duranton, G.; and Gobillon, L., (2018). The costs of agglomeration: house and land prices in french cities. *The Rev. Econ. Stud.*, 86(4): 1556-1589 **(48 pages)**.
- Geberemariam, T.K., (2019). Finite difference method to design sustainable infiltration based stormwater management system. *Preprints 2019* **(17 pages)**.
- Hoang, N.H.; Ishigaki, T.; Kubota, R.; Tong, T.K.; Nguyen, T.T.; Nguyen, H. G.; Yamada M.; Kawamoto, K., (2021). Financial and economic evaluation of construction and demolition waste recycling in Hanoi, Vietnam. *Waste Manage.*, 131: 294-304.
- Huang, C.-L.; Hsu, N.-S.; Wei, C.-C.; Luo, W.-J., (2015). Optimal spatial design of capacity and quantity of rainwater harvesting systems for urban flood mitigation. *Water*. 7(9): 5173-5202 **(30 pages)**.
- Li, C.; Peng, C.; Chiang, P.-C.; Cai, Y.; Wang, X.; Yang, Z., (2019). Mechanisms and applications of green infrastructure practices for stormwater control: A review. *J. Hydrol.*, 568: 626-637 **(12 pages)**.
- Makbul, R.; Desi, N.; Sudirman., (2021). Reduction of gray water and run-off in a residential environment with eain garden model. Case study: Settlements in Makassar City. *IOP Conference Series: Earth Environ. Sci.*, 21(1): 012021 **(7 pages)**.
- Mardianti, F.; Purba, D.E., (2023). Effects of citizen participation on urban water management based on socioeconomic factors. *Global J. Environ. Sci. Manage.*, 9(4): 915-932 **(18 pages)**.
- Melbourne Water, (2013). Building an infiltration raingarden.
- Monger, F.; Bond, S.; Spracklen, D.V.; and Kirkby, M.J., (2022). Overland flow velocity and soil properties in established semi-natural woodland and wood pasture in an upland catchment. *Hydrol. Processes*, 36(4): e14567.
- Mongil-Manso, J.; Navarro-Hevia, J.; and San Martín, R., (2022). Impact of Land Use Change and Afforestation on Soil Properties in a Mediterranean Mountain Area of Central Spain. *Land*, 11(7): 1043 **(23 pages)**.
- Morash, J.; Wright, A.; LeBleu, C.; Meder, A.; Kessler, R.; Brantley, E.; Howe, J., (2019). Increasing sustainability of residential areas using rain gardens to improve pollutant capture, biodiversity and ecosystem resilience. *Sustainability*. 11(12): 3269 **(18 pages)**.
- Parker, J.; Zingoni de Baro, M.E., (2019). Green infrastructure in the urban environment: a systematic quantitative review. *Sustainability*, 11(11) **(20 pages)**.
- PUB, (2014). Active, beautiful, clean (ABC) waters design guidelines: Singapore's National Water Agency. Public Utilities Board **(112 pages)**.
- Puget Sound Action Team. (2012). Low Impact Development: Technical Guidance Manual. Washington: Pierce County Extension **(365 pages)**.
- Qin, Y.; Chen, M.; Li, X.; Qiu, J., (2021). Factors affecting the hydrological response of substrate material for green roofs and bioretention. *IOP Conferenc Series: Earth Environ. Sci.*, 821(1): 012009 **(10 pages)**.
- Raju, Y.K.; Hussain, M., (2019). Fitting infiltration equations using double ring infiltrometer to design and evaluate irrigation methods. *Int. J. Recent Technol. Eng.*, 8 **(4 pages)**.
- Rinchumphu, D.; Eves, C.; Susilawati, C., (2013). Brand value of property in Bangkok Metropolitan Region (BMR), Thailand. *Int. Real estate Rev.* 16(3): 296-322 **(28 pages)**.
- Sharma, R.; Malaviya, P., (2021). Management of stormwater pollution using green infrastructure: the role of rain gardens. *WIREs Water*, 8(2): e1507 **(21 pages)**.
- Shi, S.; Zhao, F.; Ren, X.; Meng, Z.; Dang, X.; and Wu, X., (2022). Soil Infiltration Properties Are Affected by Typical Plant Communities in a Semi-Arid Desert Grassland in China. *Water*, 14(20): 3301 **(14 pages)**.
- Sitthikankun, S.; Rinchumphu, D.; Buachart, C.; Pacharawongsakda, E., (2021). Construction cost estimation for government building using Artificial Neural Network. *Int. Trans. J. Eng. Manag. Appl. Sci. Technol*, 12: 1-12 **(12 pages)**.
- Sittisom, P.; Tangsongsuwan, R.; Munlikawong, S.; Wongsapai, W.; Sitthikankun, S.; Rinchumphu, D., (2022). The determination of doil infiltration rate of urban bioretention design process in Chiang Mai, Thailand. *Nakhara: J. Environ. Des. Plann.*, 21(3): Article 228 **(11 pages)**.
- SSQTA, (2020). Biofiltration systems in development services schemes. Senior Stormwater Quality Technical Advisor **(65 pages)**.
- Suharyanto, A.; Maulana, A.; Suprayogo, D.; Devia, Y.P.; Kurniawan, S., (2023). Land surface temperature changes caused by land cover/ land use properties and their impact on rainfall characteristics. *Global J. Environ., Sci. Manage.*, 9(3): 353-372 **(20 pages)**.
- Van der Meulen, S.H., (2019). Costs and benefits of green roof types for cities and building owners. *Journal of sustainable development of energy. Water Environ. Syst.*, 7(1): 57-71 **(15 pages)**.
- Wanitchayapaisit, C.; Suppakittpaisarn, P.; Charoenlerthanakit, N.; Surinseng, V.; Yaipimol, E.; Rinchumphu, D., (2022). Rain garden design for stormwater management in Chiang Mai, Thailand: a research-through-design study. *Nakhara: J. Environ. Des. Plann.*, 21(3): Article 222 **(23 pages)**.

- Wilbers, G.J.; de Bruin, K.; Seifert-Dähnn, I.; Lekkerkerk, W.; Li, H.; and Budding-Polo Ballinas, M., (2022). Investing in Urban Blue and ndash;Green Infrastructure and mdash;Assessing the Costs and Benefits of Stormwater Management in a Peri-Urban Catchment in Oslo, Norway. *Sustainability*, 14(3): 1934 (17 pages).
- Yuan, J.; Dunnett, N.; Stovin, V., (2017). The influence of vegetation on rain garden hydrological performance. *Urban Water J.*, 14(10): 1083-1089 (7 pages).
- Zeng, J.; Lin, G.; Huang, G., (2021). Evaluation of the cost-effectiveness of green infrastructure in climate change scenarios using TOPSIS. *Urban For. Urban Greening*. 64: 127287 (9 pages).
- Zhou, Z.; Guo, Q., (2022). Drainage alternatives for rain gardens on subsoil of low permeability: balance among ponding time, soil moisture, and runoff reduction. *J. Sustainable Water Built Environ.*, 8(3): 05022002 (12 pages).

#### AUTHOR (S) BIOSKETCHES

**Rinchumphu, D.**, Ph.D., Assistant Professor, Department of Civil Engineering, Chiang Mai University, Thailand.

- Email: [damrongsak.r@cmu.ac.th](mailto:damrongsak.r@cmu.ac.th)
- ORCID: 0000-0002-6037-4974
- Web of Science ResearcherID: NA
- Scopus Author ID: 57219602276
- Homepage: <https://civil.eng.cmu.ac.th/people/damrongsak-rinchumphu>

**Suriyanon, N.**, Ph.D., Lecturer, Department of Civil Engineering, Chiang Mai University, Thailand.

- Email: [natee.suriyanon@cmu.ac.th](mailto:natee.suriyanon@cmu.ac.th)
- ORCID: 0009-0003-0669-4138
- Web of Science ResearcherID: NA
- Scopus Author ID: 54788469300
- Homepage: <https://civil.eng.cmu.ac.th/people/natee-suriyanon>

**Phichetkunbodee, N.**, Ph.D. Candidate, Department of Civil Engineering, National Taiwan University, Taiwan.

- Email: [d11521023@ntu.edu.tw](mailto:d11521023@ntu.edu.tw)
- ORCID: 0000-0003-4569-669X
- Web of Science ResearcherID: NA
- Scopus Author ID: 57222813126
- Homepage: <https://www.ce.ntu.edu.tw/en/home>

**Munlikawong, S.**, M.Eng. Student, Department of Civil Engineering, Chiang Mai University, Thailand.

- Email: [sikarint\\_m@cmu.ac.th](mailto:sikarint_m@cmu.ac.th)
- ORCID: 0009-0007-0714-5180
- Web of Science ResearcherID: NA
- Scopus Author ID: NA
- Homepage: <https://civil.eng.cmu.ac.th/>

**Wanitchayapaisit, C.**, Lecturer, Faculty of Agriculture, Chiang Mai University, Thailand

- Email: [chulalux.w@cmu.ac.th](mailto:chulalux.w@cmu.ac.th)
- ORCID: 0000-0002-9428-9567
- Web of Science ResearcherID: NA
- Scopus Author ID: 57216993964
- Homepage: [https://mis.agri.cmu.ac.th/mis/Main/member\\_detail/QUdSSU1JUzlwMjExMDEz](https://mis.agri.cmu.ac.th/mis/Main/member_detail/QUdSSU1JUzlwMjExMDEz)

**Sitthikankun, S.**, Ph.D. Candidate, Department of Civil Engineering, Chiang Mai University, Thailand.

- Email: [sitthikorn\\_sit@cmu.ac.th](mailto:sitthikorn_sit@cmu.ac.th)
- ORCID: 0000-0001-6107-8010
- Web of Science ResearcherID: NA
- Scopus Author ID: 57437092300
- Homepage: <https://civil.eng.cmu.ac.th/>

#### HOW TO CITE THIS ARTICLE

Rinchumphu, D.; Suriyanon, N.; Phichetkunbodee, N.; Munlikawong, S.; Wanitchayapaisit, C.; Sitthikankun, S., (2024). Economics and cost-effectiveness of rain garden for flood-resistant urban design. *Global J. Environ. Sci. Manage.*, 9(4): 1-12.

DOI: 10.22035/gjesm.2024.01.01

URL: [https://www.gjesm.net/article\\_704363.html](https://www.gjesm.net/article_704363.html)





## ORIGINAL RESEARCH PAPER

Green synthesis of titanium dioxide photocatalyst using *Lactobacillus bulgaricus* for processing palm oil mill effluentL. Agustina<sup>1</sup>, M. Romli<sup>2</sup>, P. Suryadarma<sup>2</sup>, S. Suprihatin<sup>2\*</sup><sup>1</sup> Agroindustrial Engineering Study Program of Graduate School, IPB University, PO Box 220, Bogor, West Java, Indonesia<sup>2</sup> Department of Agroindustrial Technology, Faculty of Agricultural Engineering and Technology, IPB University, PO Box 220, Bogor, West Java, Indonesia

## ARTICLE INFO

**Article History:**

Received 16 January 2023

Revised 02 June 2023

Accepted 11 July 2023

**Keywords:**

Advanced wastewater treatment

Green synthesis

Palm oil mill effluent

Nano titanium dioxide

Photocatalytic process

## ABSTRACT

**BACKGROUND AND OBJECTIVES:** To improve photocatalytic degradation performance, photocatalyst particles with a larger surface area preferred. The effectiveness of titanium dioxide as a photocatalyst depends on the synthesis method used. The method affect the particle size, crystallinity and phase composition of the produced catalyst. This study aims to develop a green synthesis process of nano- titanium dioxide photocatalysts for the advanced treatment of palm oil mill effluent.

**METHODS:** The green synthesis of titanium dioxide nanoparticles used de Man-Rogosa-Sharpe broth media containing *Lactobacillus bulgaricus* culture and titanium oxyhydroxide metal oxide. The factors investigated were the molarity of titanium oxyhydroxide (0.025 molar; 0.035 molar and 0.045 molar) and temperature (40; 50 and 60 degrees Celsius). The synthesized photocatalyst was characterized using a particle size analyzer to determine the particle size. The produced photocatalyst with a nanoparticle size range of 1-100 nanometer was further characterized using scanning electron microscopy-energy dispersive X-ray and X-ray diffraction. The photocatalyst was tested for advanced treatment of palm oil mill secondary effluent. The factors investigated in this test included the irradiation time and titanium dioxide photocatalyst dosage. The treatment performance was evaluated in terms of effluent quality and pollutant elimination efficiency.

**FINDINGS:** Nano titanium dioxide photocatalysts have been synthesized through titanium oxyhydroxide metal oxide biologically using *Lactobacillus bulgaricus*. The synthesis process at a temperature of 60 degrees Celsius and a 0.025 molar metal oxide solution produced a titanium dioxide photocatalyst with a size of 33.28 nanometer. The content of titanium and oxygen constituents in the photocatalyst was confirmed to be 39.06 percent and 47.95 percent respectively, with 67.6 percent titanium dioxide crystallinity in a theta degree of 25.4. This indicates that the green synthesis has produced an anatase diffraction nano titanium dioxide photocatalyst. Testing the titanium dioxide photocatalyst to treat palm oil mill secondary effluent yielded in elimination efficiency of 16.16-27.27 percent for chemical oxygen demand and 11.05-21.95 percent for biological oxygen demand. Phenol, which is toxic and difficult to degrade biologically, could eliminated significantly (up to 81.12 percent) using a photocatalyst dose of 1 gram per liter at a time irradiation of 2.5 hour.

**CONCLUSION:** The biological synthesis of nano titanium dioxide photocatalysts is affected by temperatures and metal oxide concentrations. The photocatalytic process for advanced treatment of palm oil mill secondary effluent shows that this synthesis process effectively eliminates phenols. Some compounds such as lignin, amino acids, and pectin are not significantly mineralized using this process.

DOI: [10.22034/gjesm.2024.01.02](https://doi.org/10.22034/gjesm.2024.01.02)This is an open access article under the CC BY license (<http://creativecommons.org/licenses/by/4.0/>).

NUMBER OF REFERENCES

42



NUMBER OF FIGURES

6



NUMBER OF TABLES

3

\*Corresponding Author:

Email: [suprihatin@apps.ipb.ac.id](mailto:suprihatin@apps.ipb.ac.id)

Phone: +62813 1089 5109

ORCID: [0000-0001-9641-8820](https://orcid.org/0000-0001-9641-8820)

Note: Discussion period for this manuscript open until April 1, 2024 on GJESM website at the "Show Article".

## INTRODUCTION

The increase in crude palm oil (CPO) production increases in the amount of liquid waste (Palm Oil Mill Effluent/POME) produced (Agustina et al., 2021). Biological treatment (anaerobic and aerobic) has been widely applied to treat POME because the processing costs are low. However, the resulting effluent still contains contaminants in the form of suspended and dissolved materials difficult to degrade biologically (recalcitrant), such as pectin, lignin, tannins, and other phenolic compounds (Zainuri et al., 2018; Samimi and Shahriari-Moghadam, 2020). These materials can cause the effluent to be colored, causing water pollution problems and ecosystem disturbances. The remaining pollutants in the effluent need to be removed using appropriate methods to produce clean water to support palm oil mill activities, where the need for clean water at factory sites is now becoming a problem. Therefore, the development of a wastewater recycling process in palm oil mills can be a win-win solution for environmental and economic interests. Considering that pollutants in the effluent of biological processes are generally difficult to degrade biologically (recalcitrant), non-biological process is suitable for eliminating these pollutants. To achieve this goal, the research plan is intended to develop a photocatalytic degradation process for eliminating dissolved organic pollutants difficult to degrade biologically. A review of the results of previous research shows that this method has various advantages for advanced wastewater treatment (Wang et al., 2022), such as being effective for recalcitrant pollutants, and the process is fast, does not depend on microbial activity, and can utilize local resources (Li Puma, 2003; Fathinia and Khataee, 2013; Ng and Cheng, 2015; Ng et al., 2019). The performance of the photocatalytic process is mainly determined by the photocatalyst used (Nguyen et al., 2021; Hidayah et al., 2022). One of the prospective metal oxides is titanium dioxide ( $\text{TiO}_2$ ) because it is inert, harmless, cheap, chemical corrosion resistant, and has good optical characteristics (Khan et al., 2015; Fares et al., 2022). The requirement for a good catalyst is to have a large surface area (Supriyanto et al., 2014) to increase the adsorption capacity so that a larger photocurrent is produced (Sucahya et al., 2016). Therefore, the particle size of a good catalyst needs to be reduced/reduced to nano size. Several studies in this field have used  $\text{TiO}_2$  photocatalysts doped with other metal oxides in a photocatalytic system (Fadzil et al., 2013), where the

$\text{TiO}_2$  photocatalyst is combined with feroxalate and exposed to a stream of ozone, yielding a 54 percent (%) decrease in organic compound content (as measured by the decrease in chemical oxygen demand (COD) value). A decolorization effect of 90% on congo red with the use of  $\text{TiO}_2$  combined with gadolinium has also been achieved in previous research (Khademalrasool et al., 2016). This research used a  $\text{TiO}_2$  nanoparticle as the photocatalyst to provide an improved effect on degradation of palm oil mill wastewater. Efforts were made in this research to improve the characteristics of  $\text{TiO}_2$  through green synthesis. Method for creating nanoparticles, include physical, chemical, and biological processes. However the biological method is the simplest and uses no chemicals (Agustina et al., 2020). This method can improve the properties of  $\text{TiO}_2$  photocatalysts thus, the biological approach is thought to be more ecologically friendly (Mukherjee and Nethi, 2019) and efficient.  $\text{TiO}_2$  nanoparticles with a size of 30 nanometer (nm) with a tetragonal structure and anatase phase (which has the best ability to degrade organic compounds because it has the highest bandgap) have been proven in research (Jha et al., 2009) using *Lactobacillus* on nutrient-broth media. To increase the adsorption ability of a  $\text{TiO}_2$  photocatalyst (Azhar et al., 2011) performed synthesis with the help of *Lactobacillus* on de Man-Rogosa-Sharp (MRS) broth media, however the size of the  $\text{TiO}_2$  photocatalyst produced was still large (150 nm). Based on the results obtained from their research, green synthesis of  $\text{TiO}_2$  was performed in this research to improve its physical and chemical characteristics so that it can be used as a photocatalyst in the processing of palm oil liquid waste using the photocatalytic method. The green synthesis method is expected to provide advantages that are not obtained in physical and chemical synthesis (Bandeira et al., 2020). Polysaccharides from MRS broth media, which promote the stability of synthesis, are the medium to be used in green synthesis (Makarov et al., 2014). According to Jha et al. (2009), *Lactobacillus* is a non-pathogenic, partially oxygen-tolerant, gram-positive, prokaryotic, anaerobic-mesophilic bacterium with adaptability and high metabolism. It can be used to enhance the synthesis condition by assisting in the formation of nanoparticles from  $\text{TiO}_2$ . The green synthesized  $\text{TiO}_2$  photocatalyst also has other potential applications besides POME treatment. For example, it can be used for air purification (removal of air pollutants, including volatile organic compounds,

nitrogen oxides, and sulfur oxides (Prasetya *et al.* 2021); coating self-cleaning surfaces such as glass, ceramics, and metals; solar energy conversion; environmental remediation, which is related to this study (degradation of organic recalcitrant in case of a water purification process). Table 1 shows some important research conducted related to the synthesis of nanoparticles for photocatalysts.

To date, no specific information about the successful implementation of green synthesis using *Lactobacillus bulgaricus* (*L. bulgaricus*) for palm oil mill secondary effluent (POMSE) treatment on an industrial scale has been found. This study was conducted to solve the following problems; 1) How to determine the best conditions for performing green synthesis of TiO<sub>2</sub> photocatalysts with superior characteristics to degrade recalcitrant pollutants in advanced processing of palm oil mill wastewater; 2) How to determine the performance of the photocatalytic process using green synthesized TiO<sub>2</sub> photocatalysts for advanced treatment of POMSE. The main objective of this study is to develop a photocatalytic process with a focus on green synthesis of TiO<sub>2</sub> photocatalysts so that the produced photocatalyst can be used for advanced processing of liquid waste, as an effort to apply the concept of recycled wastewater in palm oil mills.

Furthermore, the specific aims of this research are as follows: 1) To produce TiO<sub>2</sub> photocatalysts through a green synthesis process using *L. bulgaricus* as a bio-reductor; 2) To obtain the performance value of the photocatalytic process (using the main parameter: COD, biological oxygen demand (BOD<sub>5</sub>) and phenol degradation). This study was conducted from 2021 to 2022, using samples of palm oil liquid waste from a factory located in South Kalimantan, Indonesia.

## MATERIALS AND METHODS

### Material

The materials used were metal oxide titanium oxyhydroxide: TiO(OH)<sub>2</sub>, MRS broth, MRS agar, *L. bulgaricus* culture, POME, POMSE, TiO<sub>2</sub> photocatalyst from green synthesis, polyaluminium chloride (PAC), filter paper, distilled water and other materials for analysis. The tools used are photoreactors, hot plates (with stirrers), water bath, incubators and glassware for synthesis and analysis.

### Green synthesis of TiO<sub>2</sub> photocatalyst

Synthesis using specific media (MRS broth containing *L. bulgaricus* and metal oxide TiO(OH)<sub>2</sub>) was performed in the following steps (work procedures adjusted from the study of (Jha *et al.*, 2009):

Table 1: Research on photocatalyst synthesis

No.	Results	Sources
1.	Nano TiO <sub>2</sub> films have significantly better climatic resistance than blank polyethylene films. TiO <sub>2</sub> nanoparticles were added, which increased in water vapor transmission from 18.1 to 24.6 g/m <sup>2</sup> in 24 h. Results showed that TiO <sub>2</sub> nanoparticles incorporated into polyethylen-based films have a good potential application as an active food packaging solution.	Xing <i>et al.</i> (2012)
2.	TiO <sub>2</sub> nanoparticles made from <i>Planomicrobium sp.</i> , a microbial species isolated from melting ice, were resistant to the growth of <i>Bacillus subtilis</i> , <i>Klebsiella planticola</i> , and <i>Aspergillus niger</i> bacteria. This nanoparticle synthesis used an eco-friendly, cost-effective process.	Chelladurai <i>et al.</i> (2013)
3.	Nanobiotechnology procedures involving biological synthesis have a tremendous potential to increase the production of nanoparticles without the use of harsh, expensive, and toxic chemicals typically used in conventional physical and chemical processes.	Shah <i>et al.</i> (2015)
4.	Catalytic activity during the photodegradation of dyes significantly diminished when TiO <sub>2</sub> was substituted with zinc oxide (ZnO) because ZnO is unstable and results in inconsistent dissolution processes to form zinc hydroxide (Zn(OH) <sub>2</sub> ) on the ZnO particle surfaces, leading to catalyst deactivation.	Amini and Ashrafi (2016)
5.	Analyses of the experimental conditions, nanoparticle properties, and possible uses of nanoparticles in pharmaceuticals and biomedical applications were presented for the production of high-value nanoparticles from food waste (in aquaculture and horticulture).	Ghosh <i>et al.</i> (2017)
6.	The reduction of aromatic aldehydes was facilitated using produced metal oxide nanoparticles. Ammonium formate was used as a green hydrogen donor during the reduction, and the corresponding alcohols were produced in excellent yields in 2–24 h.	Muthuvinothini and Stella (2019)
7.	Current analysis of various biological substrate sources, green synthesis processes, and effects on the characteristics of zinc oxide nanoparticles.	Bandeira <i>et al.</i> (2020)

the main culture with various dilutions was added to MRS broth (culture: MRS broth; 25 millilitre (mL): 75 mL) and incubated for 24 h at 27 degrees Celsius (°C). Then a 20 mL TiO(OH)<sub>2</sub> solution was added with the molarity according to the factor applied to the treatment combination. Heat the solution in a water bath (temperature adjusted according to the treatment combination) for 20-25 min until a white precipitate forms at the bottom of the Erlenmeyer flask. The solution was then incubated at room temperature (25°C) for 48 h until a stable white precipitate formed on the Erlenmeyer flask bottom. The goal of the synthesis is to obtain the appropriate size (1-100 nm) in the size range of nanoparticles (Carvalho *et al.*, 2018); thus the initial design applied was a-completely randomized (two replications) at different temperatures of 40°C, 50°C, and 60°C and molarity levels of 0.025, 0.035, and 0.045 M. The Determination of the levels was based on the research results of Jha *et al.* (2009). The molarity level and temperature chosen to synthesize *Lactobacillus sp.* in this study were 0.025 M TiO(OH)<sub>2</sub> and 50°C, respectively. The mesophilic *Lactobacillus* bacterium can thrive between 35°C and 45°C. The ideal growth temperature for *L. bulgaricus* is between 45°C and 47°C. According to previous research findings, green synthesis of TiO<sub>2</sub> nanoparticles was conducted over a temperature range of 37°C–60°C; thus, the temperature was set at 40°C, 50°C, and 60°C. Determination of the molarity levels of 0.025, 0.035, and 0.045 M considered the research results of

Jha *et al.* (2009) that used a minimum molarity level of 0.025 M. It was then expected that the higher concentrations would help the synthesis process to produce the desired nanocatalyst characteristics. The synthesized photocatalyst was tested for size using a particle size analyzer (PSA) in Laboratory of Materials Physics, Institut Teknologi Sepuluh Nopember, Surabaya, Indonesia, if the size of the produced photocatalyst is within the nanoparticle size range, proceed with another characterization using scanning electron microscopy-energy dispersive X-ray (SEM EDX) spectroscopy at Integrated Laboratory and Technology Innovation Center, University of Lampung and X-ray diffraction (XRD) Institut Teknologi Bandung Nanoscience and Nanotechnology Research Center.

#### Photocatalytic process

The performance of the photocatalyst obtained through the green synthesis process was tested by applying the photocatalytic process to POMSE in a suspended photoreactor, as shown in Fig. 1. In this study stage, the POMSE sample was first coagulated and filtered using filter paper to homogenize the solution, and then, it was tested for the COD, BOD<sub>5</sub> and phenol. The analysis was performed in South Kalimantan Province Health Laboratory. The factors studied were catalyst dose and irradiation time for the photocatalytic process using a completely randomized trial design with two replications. The photocatalytic process was performed under the following conditions: (a) the photocatalyst used

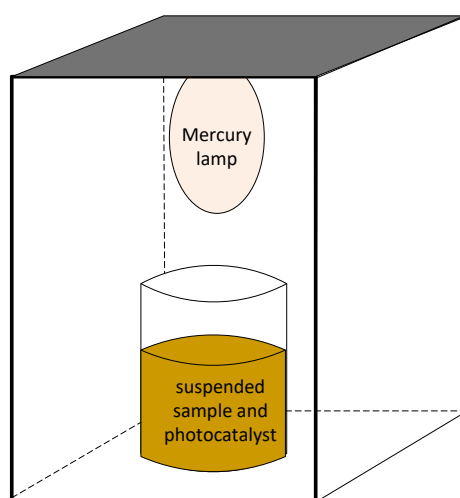


Fig. 1: Scheme of photoreactor

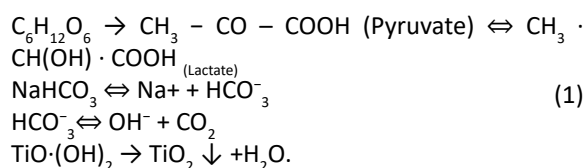
was TiO<sub>2</sub> resulting from green synthesis; (b) the photocatalyst dosages used were 1 gram (g), 1.5 g, and 2 g (Thota *et al.*, 2014; Lestari, 2017);

(c) irradiation times (contact time) in the photocatalytic process were 1.5, 2, and 2.5 h; (d) the light source used was a 350-W Philips mercury lamp.

## RESULTS AND DISCUSSION

### Green synthesis of TiO<sub>2</sub> photocatalyst

The research phase begins with the preparation of the microorganism culture (*L. bulgaricus*) used for experiments. Furthermore, the main culture of *L. bulgaricus* was made on MRS broth media with four times dilution. In this synthesis, atoms and molecules mix to create precursor blocks, which are later self-assembled into nanoparticles (Ealia and Saravanakumar, 2017). This method is known as a bottom-up technique. The primary biological factor affecting the synthesis of a substance is the cell membrane, which is composed of lipids and membranes. In the cell membrane, synthetic biochemical conversion occurs following the oxidation and reduction mechanisms. Because the composition of the membrane is dynamic and flexible, the effect of the composition is not always constant and facilitates the synthesis (Capeness *et al.*, 2019). It is anticipated that green synthesis of TiO<sub>2</sub> nanoparticles will be able to use extracellular and intracellular microorganisms under suitable environmental conditions. Electrostatic interaction between the membranes of microorganisms containing negatively charged phospholipids and the combination of metal oxides used can also result in the extracellular creation of nanoparticles (Anandgaonker *et al.*, 2019). Eq. 1 is the chemical reaction that probably occurs (Makarov *et al.*, 2014).



According to Malik *et al.* (2014), additional research into other metal oxides and culture variables is necessary to produce certain nanoparticles. However, the types of nanoparticles produced also depend on the temperature used during the synthesis. The color change of the media to a lighter

shade is one of the early signs of the production of high-quality nanoparticles (Ridhawati and Fajar, 2017). Based on the self-defense mechanisms of microbes, microorganisms are used in the fabrication of nanoparticles (Ghosh *et al.*, 2017). The biological mechanism converts reactive ions into stable atoms because high ion concentrations are typically lethal to bacterial cells. In this investigation, *L. bulgaricus* cells were cultivated for 36 h in sterile distilled water containing carbon and nitrogen sources. A white precipitate appeared at the bottom of the Erlenmeyer flask after 20 mL of TiO(OH)<sub>2</sub> was heated in a water bath at 50°C for 20–25 min to create the metal oxide. This precipitate appearance is proof that TiO<sub>2</sub> nanoparticles have formed. The solution was then incubated at room temperature (25°C) for 48 h until a stable white precipitate formed on the Erlenmeyer flask base. Fig. 2 depicts the green synthesis process of TiO<sub>2</sub>.

### Measurement using PSA

The results of particle size analysis using the PSA showed a different pattern. From Fig. 3a, at a constant treatment temperature of 40°C but increasing concentrations (0.025, 0.035, and 0.045 M), the size of the particles formed increases. From Fig. 3b, using the same concentration of 0.025 M but at different temperatures of 40°C, 50°C, and 60°C produced better synthesis results, with the particle size decreasing. At 60°C and 0.025 M the results were significant, with the obtained particle size within the size range of nanoparticles (33.28 nm). TiO<sub>2</sub> nanoparticles have high protein affinity for binding metals, which prevents particle aggregation. Proteins and polysaccharides are produced when *L. bulgaricus* is used as a bio-reductor during the synthesis of TiO<sub>2</sub> nanoparticles, which is not the case when the synthesis is performed using physical or chemical methods. This aids in the process of synthesizing metal oxide bonds so that they do not cause protein agglomeration. (Makarov *et al.*, 2014). Regulation of the synthesis media is necessary to create an optimal synthesis environment.

Factors affecting the synthesis include pH, metal oxide concentration, and temperature. Generally, glucose-containing media support the growth of microorganisms, particularly *Lactobacillus* grown on MRS media. As glucose is a reducing agent, it tends to reduce the value of the oxidation reduction

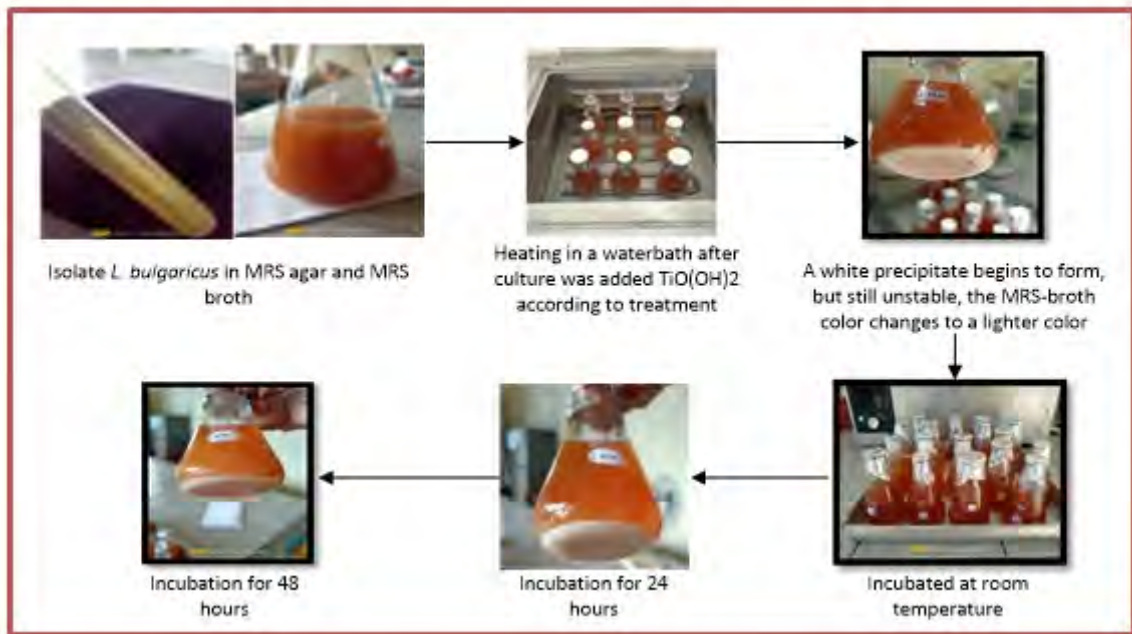
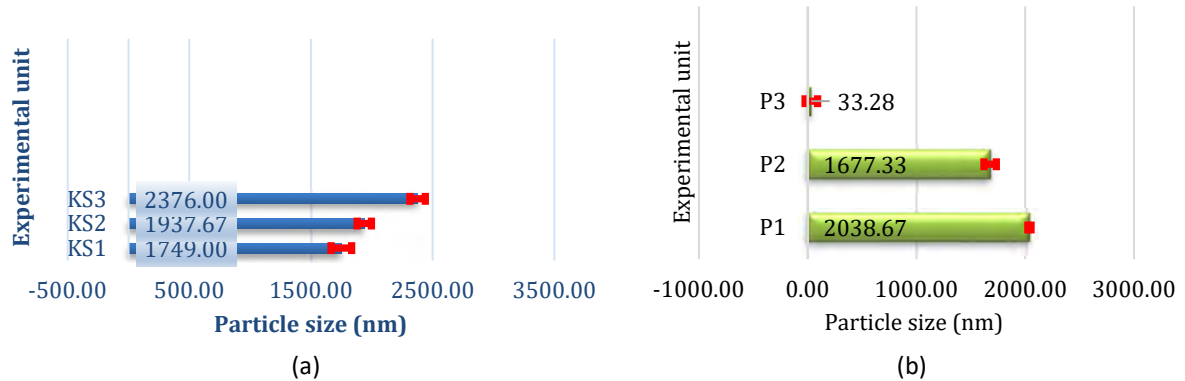


Fig. 2: Green synthesis of  $\text{TiO}_2$  photocatalyst using *L. bulgaricus*



Experimental unit:

KS1 : 40° C; 0.025 M;

KS2 : 40° C; 0.035 M;

KS3 : 40° C; 0.045 M;

P1 = 40° C; 0.025 M;

P2 = 50° C; 0.025 M;

P3 = 60° C; 0.025 M;

Fig. 3: Graph of particle measurement results a) fixed temperature with increasing concentration, b) increasing temperature with fixed concentration

potential. The degree of aerobiosis is quantified by the oxidation-reduction potential, which is written as the oxidation reduction potential ( $r\text{-H}_2$ ); the negative logarithm of the partial pressure of hydrogen gas. The

pH of the medium and the overall  $r\text{-H}_2$ , both of which are partially controlled by bicarbonate, have an impact on the synthesis conditions of  $\text{TiO}_2$  nanoparticles in addition to the use of glucose, an energy-

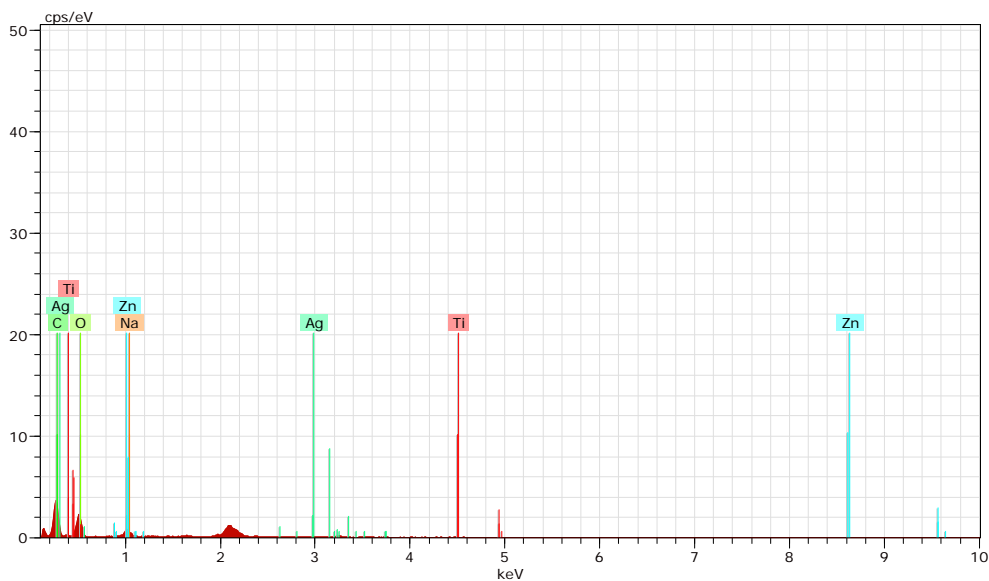


Fig. 4: Spectrum of  $\text{TiO}_2$  based on SEM EDX analysis

generating substance (in the synthesis medium). The membrane-bound oxidoreductase is activated by the anticipated slightly acidic pH and decreased  $r\text{-H}_2$ . The temperature also plays a significant role in the synthesis process. The mesophilic *Lactobacillus bulgaricus* bacterium can thrive between  $35^\circ\text{C}$  and  $45^\circ\text{C}$ . The ideal growth temperature for *L. bulgaricus* is  $45^\circ\text{C}$  and  $47^\circ\text{C}$ . According to earlier research findings, green synthesis of  $\text{TiO}_2$  nanoparticles was conducted over a temperature range of  $37^\circ\text{C}$ – $60^\circ\text{C}$  (Jha *et al.*, 2009). However, the present study's findings indicate that the best green synthesis conditions occurred at  $60^\circ\text{C}$ . This suggests that for nanoparticle synthesis to occur, the temperature must be raised above the range for growth. The concentration of metal oxides used during catalyst synthesis may have effects on the process. Higher concentrations may lead to agglomeration of metal oxide particles, resulting in decreased surface areas and reduced accessibility of active sites. Conversely, lower concentrations can promote better dispersion and higher surface areas, which can enhance catalytic activity. In this study the main factors studied were the process temperature and concentration of the metal oxide used.

#### Nanoparticle characterization (using SEM EDX and XRD)

Based on the results of particle measurements resulting from the green synthesis, the treatment

product was determined at  $60^\circ\text{C}$  with a molarity level of 0.025 M which was further characterized using SEM EDX. The characterization results were also used to determine whether the product can be synthesized in larger quantities so that it can be used as a photocatalyst in processing palm oil mill wastewater using the photocatalytic technique. Confirmation of the content of the synthesized  $\text{TiO}_2$  elements was performed using SEM EDX. As shown in the spectrum in Fig. 4, the amounts of the titanium (Ti) and oxygen (O) elements are 39.06% and 47.95%, respectively.

Table 2 shows the overall results of the constituent elements in the  $\text{TiO}_2$  nanocatalyst synthesis process (in atomic and weight percentages). Through SEM EDX it is possible to identify the constituent elements in the synthesis in detail. In addition, to Ti and O, the other elements were carbon (C), zinc (Zn), silver (Ag) and sodium (Na).

The peak area formed (Fig. 5) shows that the crystallinity of  $\text{TiO}_2$  is 67.6%, which also indicates the amount of  $\text{TiO}_2$  in the mixture is 67.6%, with the remaining 32.4% being an amorphous component. The highest peak is in the range of 25.4 degrees theta, indicating anatase diffraction formed by  $\text{TiO}_2$ .

#### Photocatalyst performance

Through photocatalysis, the  $\text{TiO}_2$  photocatalyst is crucial in the treatment of POMSE, which is a waste

Table 2: Elements in TiO<sub>2</sub> nanocatalyst synthesis process

Formula	Mass (%)	Atom (%)
C	0.41	0.13
O	47.95	59.98
Zn	8.62	1.98
Ag	2.63	0.37
Na	1.33	0.87
Ti	39.06	36.68
Total	100	100

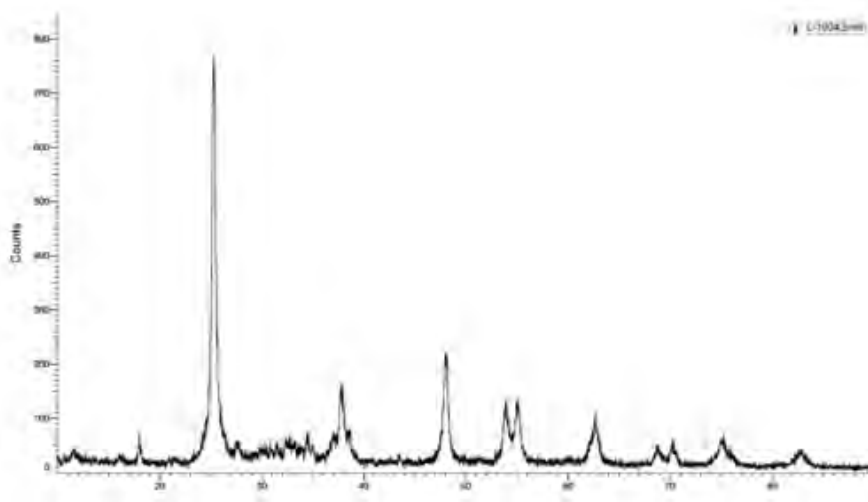
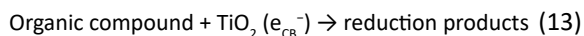
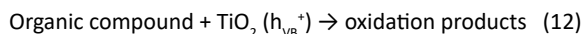
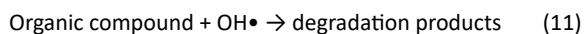
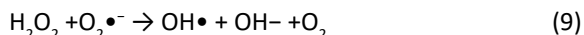
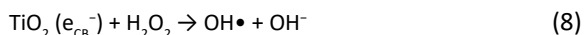
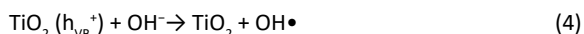
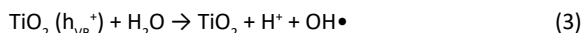
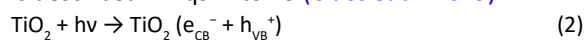


Fig. 5: Peak area of TiO<sub>2</sub> based on XRD analysis

product of the extraction of palm oil that contains significant concentrations of organic contaminants, suspended particles, and nutrients making it hazardous to the environment if released into the environment untreated. When exposed to light energy, especially in the ultraviolet spectrum, the TiO<sub>2</sub> photocatalyst can start and accelerate chemical reactions through the photocatalytic process. When TiO<sub>2</sub> is exposed to ultraviolet light, electron hole pairs are produced, where electrons and holes develop into highly reactive species. The TiO<sub>2</sub> photocatalyst can assist with the overall remediation process in the context of treating POMSE in organic pollutant degradation. The reactive species generated by TiO<sub>2</sub>, such as hydroxyl radicals (•OH), can oxidize and break down complex organic compounds in POMSE. These radicals react with organic pollutants, converting them into simpler and less harmful substances, such as carbon dioxide and water. The general mechanism is described in Eqs. 2 to 13 (Claes *et al.* 2019).



Increasing the amount of O<sub>2</sub> in the liquid waste affects the BOD<sub>5</sub> and COD values, because the availability of sufficient O<sub>2</sub> in the liquid waste helps the degradation process of organic components, thereby reducing the BOD<sub>5</sub> and COD values in the liquid waste. The reduction and percentage of the elimination parameters COD, BOD<sub>5</sub> and phenol are presented in Table 3. According to Table 3, the measurement results of the waste quality parameters after the photocatalytic process was applied did not meet the specified quality standards.

The percentage reductions of COD (Table 3 and Fig. 6) ranged from 16.16% to 27.27%. This shows that the ability of the TiO<sub>2</sub> catalyst to degrade organic pollutants ranges from 16.16% to 27.27% for 2.3 h. The assumption that can be given from these results is that in 150 min, organic pollutants which account for approximately 16-27% of the total organic pollutants have been mineralized. Meanwhile, the rest, which are complex compounds (lignin, amino acids, pectin) and some phenols remain in the depolymerization stage to form molecules with smaller molecular weights (micro-molecules) as intermediate compounds, which require a longer total mineralization time. This is based on visual observations of the color of POMSE (presumably from lignin) before and after 150 min of photocatalysis, which did not exhibit a significant color change. The presence of sufficient dissolved oxygen in the reactor, which enables microorganisms to break down polluting substances, is one environmental aspect that contributes to the high COD value (Elystia *et al.*, 2022). Palm liquid waste contains high protein (in the form of amino acids); thus, it also contains high organic matter and causes pollutant concentrations to remain high (Alhaji *et al.*, 2016). This statement is reinforced

by research conducted by (Chang and Wu, 2010) who reported that under the same pH conditions (7-8), it takes 960 min of degradation time, to degrade lignin up to 88% with a TiO<sub>2</sub> photocatalyst concentration of 10 gram per liter (g/L) without the addition of air. Concerning the degradation of amino acids, some researchers have stated that the degradation of amino acids is affected by the molecular structure of its constituents (especially the side chains) and the interactions between the amino acid side chains and the catalyst surface which vary with pH (Tran *et al.*, 2006). Thus, not all amino acids can be degraded at similar pH values.

Research related to the application of the photocatalytic process to POMSE has been conducted, but the TiO<sub>2</sub> photocatalyst used is a result of chemical synthesis. The TiO<sub>2</sub> photocatalyst can degrade organic compounds (COD) and effectively eliminate phenolic pollutants in POMSE (31.36% COD degradation performance and up to 96.66% phenol elimination by TiO<sub>2</sub> loading of 1.5 g/L; air flow rate of 10 cc/min) at 120 min (Lestari *et al.* 2017). Another research by Nawaz *et al.* (2023) investigated the effectiveness of photocatalytic remediation of treated POME-containing phenolic compounds using TiO<sub>2</sub> nanomaterials. Chemical precipitation was used to prepare the TiO<sub>2</sub> nanomaterial. Under visible light illumination, 78.32% of 224.85 milligram per liter (mg/L) phenolic compounds were broken down in 180 min at the optimal TiO<sub>2</sub> dosage (0.9 g/L). The reaction of hydroxyl free radicals is non-selective, thus, some free radicals attack phenols, whereas others attack other organic pollutants; when almost all phenols are mineralized, the hydroxyl radicals formed oxidize other organic pollutants in POMSE. Based on this, the

Table 3: Measurement results and percentage of elimination parameters COD, BOD<sub>5</sub> and phenol

Variables	Measurement results (mg/L)			Elimination percentage (%)		
	BOD <sub>5</sub>	COD	phenol	BOD <sub>5</sub>	COD	phenol
Quality standard	50	100	0.5	-	-	-
POMSE	2061.50	4852.50	4.28	-	-	-
F1 (1 g/L TiO <sub>2</sub> ; 1.5 h of irradiation)	1790.5	3940.4	3.37	13.21	18.86	21.25
F2 (1,5 g/L TiO <sub>2</sub> ; 1.5 h of irradiation)	1740	3700.6	3.45	15.66	23.79	19.48
F3 (2 g/L TiO <sub>2</sub> ; 1.5 h of irradiation)	1609	3529.1	1.86	22.01	27.32	56.57
F4 (1 g/L TiO <sub>2</sub> ; 2 h of irradiation)	1801	3949.3	1.93	12.70	18.67	54.85
F5 (1,5 g/L TiO <sub>2</sub> ; 2 h of irradiation)	1786.5	3918.1	1.83	13.40	19.31	57.20
F6 (2 g/L TiO <sub>2</sub> ; 2 h of irradiation)	1833.75	3856.9	1.09	11.11	20.57	74.62
F7 (1 g/L TiO <sub>2</sub> ; 2.5 h of irradiation)	1746.1	3828.65	0.81	15.36	21.16	81.12
F8 (1,5 g/L TiO <sub>2</sub> ; 2.5 h of irradiation)	1814.95	3930.3	1.55	12.02	19.06	63.73
F9 (2 g/L TiO <sub>2</sub> ; 2.5 h of irradiation)	1813.5	4067.8	1.65	12.09	16.23	61.54

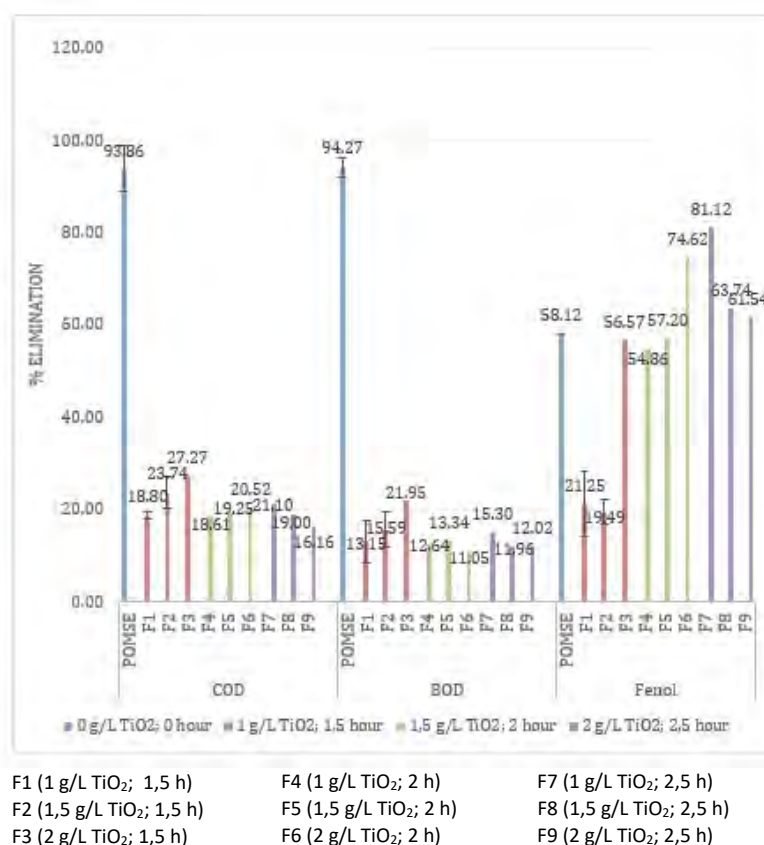


Fig. 6: Effect of irradiation time and  $\text{TiO}_2$  photocatalyst dosage on elimination percentage of COD,  $\text{BOD}_5$  and Phenol

assumption that can be given is that approximately 70% of the pollutants not been mineralized are intermediate compounds resulting from the degradation of lignin, amino acids, phenols, pectin, oils and greases, as well as macromolecules, which are constituent of organic pollutants in POMSE. However, COD could only be reduced by 16.16%-27.27%. Phenol, which is a hazardous substance, toxic, and difficult to degrade by decomposer organisms, can be reduced significantly to close to environmental quality standards (0.5 part per million). The experimental unit F7 (dose of 1 g/L; irradiation of 2.5 h) resulted in phenol elimination of up to 81.12%, producing an effluent phenol concentration of 0.81 mg/L.

#### *Benefits of using a green synthesis approach for $\text{TiO}_2$ photocatalyst production*

Utilizing a green synthesis approach for  $\text{TiO}_2$  photocatalyst production can offer several

environmental benefits compared with conventional methods. Here are some key advantages,

- **Reduced energy consumption:** green synthesis methods typically employ milder reaction conditions, such as lower temperatures and pressures, resulting in reduced energy requirements. This decrease in energy consumption contributes to lower greenhouse gas emissions and overall environmental impact.
- **Decreased chemical waste:** green synthesis approaches typically emphasize the use of environmentally friendly solvents and reagents, minimizing the generation of hazardous byproducts and chemical waste. This aspect reduces the risk of water and soil contamination and helps preserve ecosystem health.
- **Lower toxicity and pollution potential:** conventional synthesis methods may involve the use of toxic chemicals and hazardous reagents, which can pose risks to human health and the environment. Green

synthesis techniques prioritize the use of nontoxic or low-toxicity substances, thereby minimizing the potential for pollution and associated adverse effects.

- Renewable feedstock: green synthesis approaches typically utilize renewable feedstock or bio-based materials as starting materials, reducing reliance on non-renewable resources. By utilizing sustainable sources, such as biomass or agricultural waste, the environmental impact of the synthesis process is reduced, and the overall sustainability is improved.

- Water and energy conservation: certain green synthesis methods emphasize water-based reactions or solvent-free approaches, reducing water consumption and minimizing the need for organic solvents. Furthermore, by optimizing the synthesis process, green approaches can reduce the overall reaction time, thereby saving energy.

- Enhanced product performance: green synthesis methods can prepare  $\text{TiO}_2$  photocatalysts with improved performance characteristics, such as higher surface areas, better crystallinity, or narrower particle size distributions. Enhanced product performance can lead to more efficient photocatalytic reactions, reducing the amount of catalyst required and thus minimizing the overall environmental impact.

## CONCLUSION

Green synthesis of  $\text{TiO}_2$  photocatalysts was performed using  $\text{TiO}(\text{OH})_2$  metal oxide, yielding a  $\text{TiO}_2$  photocatalyst with a particle size of 33.28 nm at 60°C and a 0.025 M metal oxide solution. The content of Ti and O constituents in the  $\text{TiO}_2$  photocatalyst was confirmed to be 39.06% and 47.95%, respectively, with  $\text{TiO}_2$  crystallinity of 67.6% in the range of 25.4 degrees theta, indicating that the results of the green synthesis have formed anatase diffraction. The process temperature and metal oxide concentration are the factors influencing the formation of nanoparticles. By applying a photocatalytic to POMSE using synthesized  $\text{TiO}_2$  photocatalyst, the following results were obtained; COD can be reduced by 16.16%-27.27%,  $\text{BOD}_5$  by 11.05%-21.95%, and phenol by 19.49% up to 81.12%. The concentration of dissolved carbon dioxide ( $\text{CO}_2$ ) in water influences the increase in the amount of oxygen ( $\text{O}_2$ ). Generally, this is because  $\text{CO}_2$  triggers an increase in the concentration of hydrogen (H) ions which decreases the pH of water to neutral, from 8.39 to a neutral pH value of 6.83-6.91. In the mechanism of the photocatalytic process, the photocatalyst used

(in this case  $\text{TiO}_2$ ) functions to absorb photon energy and produce holes ( $\text{h}^+$ ).  $\text{h}^+$  oxidizes organic molecules and reacts with hydroxide ( $\text{OH}^-$ ) or hydrogen dioxide ( $\text{H}_2\text{O}$ ). Increasing the amount of oxygen ( $\text{O}_2$ ) in the liquid waste affects the  $\text{BOD}_5$  and COD values, because the availability of sufficient  $\text{O}_2$  in the liquid waste helps the degradation process of organic components, thereby reducing the  $\text{BOD}_5$  and COD values in the liquid waste. The synthesized  $\text{TiO}_2$  photocatalyst seems to specifically degrade phenol. Phenol experienced a significant reduction of up to 81.12% at a photocatalyst dose of 1 g/L and time irradiation of 2.5 h. Overall, adopting a green synthesis approach for  $\text{TiO}_2$  photocatalyst production offers significant environmental benefits, including reduced energy consumption, decreased chemical waste, lower toxicity and pollution potential, renewable feedstock utilization, water and energy conservation, and improved product performance. These advantages contribute to a more sustainable and environmentally friendly production process for  $\text{TiO}_2$  photocatalysts. Notably, while there are challenges associated with the green synthesis of  $\text{TiO}_2$  photocatalysts using *L. bulgaricus*, these limitations can be addressed through further research in terms of process optimization and technological advancements. Green synthesis methods hold great potential for sustainable and eco-friendly production of  $\text{TiO}_2$  nanoparticles, and ongoing efforts aim to overcome these challenges to make them viable alternatives to conventional synthesis methods.

## AUTHOR CONTRIBUTIONS

L. Agustina contributed to the process of sampling and experimental research on laboratory (green synthesis and photocatalytic process), manuscript preparation and revision. M. Romli sharpened the background, supervised the experimental research on laboratory related to photocatalytic process, extended the discussion, and improvement recommendations. P. Suryadarma sharpened the implemented methodology, supervised the experimental research on laboratory related to green synthesis, extended the discussion, and improvement recommendations. S. Suprihatin, the corresponding author, supervised the experimental research on laboratory, organized the discussion, and proofread the manuscript.

## ACKNOWLEDGEMENT

This study was financially supported by the Ministry of Research, Technology and Higher Education of the

Republic of Indonesia through a BPPDN (Beasiswa Pendidikan Pascasarjana Dalam Negeri, [Grant Number: 190031088303]).

### CONFLICT OF INTEREST

The authors declare that there is no conflict of interests regarding the publication of this manuscript. In addition, the ethical issues, including plagiarism, informed consent, misconduct, data fabrication and/or falsification, double publication and/or submission, and redundancy, have been completely observed by the authors.

### OPEN ACCESS

©2024 The author(s). This article is licensed under a Creative Commons Attribution 4.0 International License, which permits use, sharing, adaptation, distribution and reproduction in any medium or format, as long as you give appropriate credit to the original author(s) and the source, provide a link to the Creative Commons license, and indicate if changes were made. The images or other third-party material in this article are included in the article's Creative Commons license, unless indicated otherwise in a credit line to the material. If material is not included in the article's Creative Commons license and your intended use is not permitted by statutory regulation or exceeds the permitted use, you will need to obtain permission directly from the copyright holder. To view a copy of this license, visit: <http://creativecommons.org/licenses/by/4.0/>.

### PUBLISHER'S NOTE

GJESM Publisher remains neutral with regard to jurisdictional claims in published maps and institutional affiliations.

### ABBREVIATIONS

%	Per cent
Ag	Argentum
BOD <sub>5</sub>	Biochemical oxygen demand
C	Carbon
CO <sub>2</sub>	Carbon dioxide
COD	Chemical oxygen demand
CPO	Crude palm oil
Eq.	Equation
F1	1 g/L dosage of TiO <sub>2</sub> ; 1.5 hour irradiation time

F2	1.5 g/L dosage of TiO <sub>2</sub> ; 1.5 hour irradiation time
F3	2 g/L dosage of TiO <sub>2</sub> ; 1.5 hour irradiation time
F4	1 g/L dosage of TiO <sub>2</sub> ; 2 hour irradiation time
F5	1.5 g/L dosage of TiO <sub>2</sub> ; 2 hour irradiation time
F6	2 g/L dosage of TiO <sub>2</sub> ; 2 hour irradiation time
F7	1 g/L dosage of TiO <sub>2</sub> ; 2.5 hour irradiation time
F8	1.5 g/L dosage of TiO <sub>2</sub> ; 2.5 hour irradiation time
F9	2 g/L dosage of TiO <sub>2</sub> ; 2.5 hour irradiation time
g	Gram
g/L	Gram per liter
H	Hydrogen
h+	Holes
H <sub>2</sub> O	Hydrogen dioxide
ITB	Institut Teknologi Bandung
KS1	40° C; 0.025 M
KS2	40° C; 0.035 M
KS3	40° C; 0.045 M
L	Liter
L.	
<i>L. bulgaricus</i>	Lactobacillus bulgaricus
M	Molarity
mg	Milligram
mL	Milliliter
MRS	de Man Rogosa and Sharpe
Na	Natrium
nm	Nanometer
O	Oxygen
O <sub>2</sub>	Oxygen
OH <sup>-</sup>	Hydroxide
°C	Celcius degrees
P1	40° C; 0.025 M
P2	50° C; 0.025 M
P3	60° C; 0.025 M
PAC	Poly aluminium chloride
pH	Potential hydrogen
POME	Palm oil mill effluent
POMSE	Palm oil mill secondary effluent

ppm	Part per million
$r-H_2$	oxidation-reduction potential
SEM-EDX	Scanning Electron Microscope-Energy Dispersive X-ray
Ti	Titanium
$TiO(OH)_2$	Titanium oxyhydroxide
$TiO_2$	Titanium dioxide
TSS	Total Suspended Solid
W	Watt
XRD	X-ray Diffraction
Zn	Zinc

## REFERENCES

- Agustina, L.; Suprihatin, S.; Romli, M.; Suryadarma, P., (2020). Current development, potentials, and challenges of biological synthesis of nanoparticle (as a photocatalyst): a review. IOP Conf. Ser. Mater. Sci. Eng., 980 (11 pages).
- Agustina, L.; Suprihatin, S.; Romli, M.; Suryadarma, P., (2021). Processing of palm mill oil effluent using photocatalytic: a literature review. J. Ecol. Eng., 22(11): 43-52 (10 pages).
- Alhaji, M.H.; Sanaullah, K.; Lim, S.; Khan, A.; Hipolito, C.N.; Abdullah, M.O.; Bhawani, S.A.; Jamil, T., (2016). Photocatalytic treatment technology for palm oil mill effluent (POME) – A review. Process Saf. Environ. Protect., 102: 673-686 (14 pages).
- Anandgaonker, P.; Kulkarni, G.; Gaikwad, S.; Rajbhoj, A., (2019). Synthesis of  $TiO_2$  nanoparticles by electrochemical method and their antibacterial application. Arab. J. Chem., 12(8): 1815-1822 (8 pages).
- Azhar, A.M.; Ladan, S.A.B.; Ebrahimi, M.T.; Heydari, M., (2011). Lactobacillus-mediated biosynthesis of titanium nanoparticles in mrs-broth medium. NANOCON 2011 - Conference Proceedings, 3rd International Conference (5 pages).
- Amini, M.; Ashrafi, M., (2016). Photocatalytic degradation of some organic dyes under solar light irradiation using  $TiO_2$  and ZnO nanoparticles. Nano. Chem. Res., 1(1): 79-86 (8 pages).
- Bandeira, M.; Giovanela, M.; Roesch-Ely, M.; Devine, D.M.; Crespo, J.S., (2020). Green synthesis of zinc oxide nanoparticles: a review of the synthesis methodology and mechanism of formation. Sustainable Chem. Pharm., 15: 100223 (10 pages).
- Capeness, M.J.; Bravo, V.E.; Horsfall, L.E., (2019). Production of biogenic nanoparticles for the reduction of 4-nitrophenol and oxidative laccase-like reactions. Front. Microbiol., 10: 997 (9 pages).
- Carvalho, P.M.; Felício, M.R.; Santos, N.C.; Gonçalves, S.; Domingues, M.M., (2018). Application of light scattering techniques to nanoparticle characterization and development. Front. Chem., 6: 237 (17 pages).
- Chelladurai, M.; Chitra, K.; Shanmugam, R.; Gnanajobitha, G.; Paulkumar, K.; Vanaja, M.; Gurusamy, A., (2013). Novel eco-friendly synthesis of titanium oxide nanoparticles by using Planomicrobium sp. and its antimicrobial evaluation. Der Pharmacia. Sinica. 4(3): 59-66 (8 pages).
- Chang, C.Y.; Wu, N.L., (2010). Process analysis on photocatalyzed dye decomposition for water treatment with  $TiO_2$ -coated rotating disk reactor. Ind. Eng. Chem. Res., 49(23): 12173–12179 (7 pages).
- Claes, T.; Dilissen, A.; Leblebici, M.E.; Gerven, T.V., (2019). Translucent packed bed structures for high throughput photocatalytic reactors. Chem. Eng. J., 361: 725-735 (10 pages).
- Ealia, S.A.M.; Saravanakumar, M.P., (2017). A review on the classification, characterisation, synthesis of nanoparticles and their application. IOP Conference Series. Mater. Sci. Eng., 263 (16 pages).
- Elystia, S.; Hasti, F.A.; Muria, S.R., (2022). Penyisihan COD dan nitrogen total pada limbah cair sawit menggunakan Chlorella sp. yang diimobilisasi dalam flat-fotobioreaktor. J. Sains dan Teknologi., 11(1): 67-76 (10 pages).
- Fadzil, N.A.M.; Zainal, Z.; Abdullah, A.Z., (2013). COD removal for palm oil mill secondary effluent by using UV/ferrioxalate/ $TiO_2/O_3$  system. Int. J. Emerg. Technol. Adv. Eng., 3(7): 237–243 (6 pages).
- Fares, E.; Aïssa, B.; Isaïfan, R.J. (2022). Inkjet printing of metal oxide coatings for enhanced photovoltaic soiling environmental applications. Global J. Environ. Sci. Manage., 8(4): 485-502 (18 page).
- Fathinia, M.; Khataee, A.R., (2013). Residence time distribution analysis and optimization of photocatalysis of phenazopyridine using immobilized  $TiO_2$  nanoparticles in a rectangular photoreactor. J. Ind. Eng. Chem., 19(5): 1525–1534 (9 pages).
- Ghosh, P.R.; Fawcett, D.; Sharma, S.B.; Poinern, G.E.J., (2017). Production of high-value nanoparticles via biogenic processes using aquacultural and horticultural food waste. Materials (Basel). 10(8): 852 (19 pages).
- Hidayah, E.N.; Pachwarya, R.B.; Cahyugroho, O.H., (2022). Immobilization of resin photocatalyst in removal of soluble effluent organic matter and potential for disinfection by-products. Global J. Environ. Sci. Manage., 8(3): 437-448 (12 pages).
- Jha, A.K.; Prasad, K.; Kulkarni, A.R., (2009). Synthesis of  $TiO_2$  nanoparticles using microorganisms. Colloids Surfaces B: Biointerfaces. 71(2): 226–229 (4 pages).
- Khademalrasool, M.; Farbod, M.; Talebzadeh, M.D., (2016). The improvement of photocatalytic processes: design of a photoreactor using high-power LEDs. J. Sci. Adv. Mater. Devices. 1(3): 382–387 (6 pages).
- Khan, M.M.; Adil, S.F.; Al-Mayouf, A., (2015). Metal oxides as photocatalysts. J. Saudi Chem. Soc., 19(5): 462-464 (3 pages).
- Lestari, I., (2017). Degradasi senyawa organik pada palm oil mill secondary effluent menggunakan fotokatalis  $TiO_2$ . Citra Widya Edukasi., IX(2): 143–152 (10 pages).
- Li Puma, G., (2003). Modeling of thin-film slurry photocatalytic reactors affected by radiation scattering. Environ. Sci. Technol., 37(24): 5783–5791 (9 pages).
- Makarov, V.V.; Love, A.J.; Sinityna, O.V.; Makarova, S.S.; Yaminsky I.V.; Taliansky, M.E.; Kalinina, N.O., (2014). "Green" nanotechnologies: synthesis of metal nanoparticles using plants. Handbook of Families and Health. 6: 35–44 (10 pages).
- Malik, P.; Shankar, R.; Malik, V.; Sharma, N.; Mukherjee, T.K., (2014). Green chemistry based benign routes for nanoparticle synthesis. J. Nanopart., 1–14 (14 pages).
- Mukherjee, S.; Nethi, S.K., (2019). Biological synthesis of nanoparticles using bacteria, in: Panpatte, D., Jhala, Y., (Eds), Nanotechnol. Agric. Springer.
- Muthuvinothini, A.; Stella, S., (2019). Green synthesis of metal oxide nanoparticles and their catalytic activity for the reduction of aldehydes. Process Biochem., 77 (9 pages).
- Nawaz, R.; Kait, C.F.; Chia, H.Y.; Isa, M.H.; Huei, L.W., (2020). Photocatalytic remediation of treated palm oil mill effluent contaminated with phenolic compounds using  $TiO_2$  nanomaterial. Desalin. Water. Treat., 183 (11 pages).
- Ng, K.H.; Cheng, C.K., (2015). A novel photomineralization of POME over UV-responsive  $TiO_2$  photocatalyst: kinetics of POME

- degradation and gaseous product formations. RSC Adv., 5(65): 53100–53110 (11 pages).
- Ng, K.H.; Yuan, L.S.; Cheng, C.K.; Chen, K.; Fang, C., (2019). TiO<sub>2</sub> and ZnO photocatalytic treatment of palm oil mill effluent (POME) and feasibility of renewable energy generation. J. Clean Prod., 233:209–225 (17 pages).
- Nguyen, C.C.; Nguyen, D.L.T.; Nguyen, D.M.T.; Van-Huy Nguyen, V.; Nanda, S.; Vo, D.N.; Shokouhimehr, M.; Do, H.H.; Kim, S.Y.; Le, Q.V., (2021). Nanostructured photocatalysts: introduction to photocatalytic mechanism and nanomaterials for energy and environmental applications, in: Nguyen, V., Vo, D.N., Nanda, S., (Eds), Nanostructured Photocatalysts. Elsevier B.V.
- Prasetya, H.; Agustina, L.; Rinovian, A.; Muttaqin, F.D., (2022). Assessment of ceramic based photocatalytic as indoor air purifier during covid-19 pandemic. IOP Conf. Ser.: Earth Environ Sci., 986 (10 pages).
- Ridhawati.; Fajar, H.R., (2017). Sintesis dan karakterisasi nanopartikel titanium dioksida dengan bioreduktor ekstrak kayu manis (*Cinnamomum* sp.). Prosiding Seminar Hasil Penelitian. SNP2M., 2: 101-104 (4 pages).
- Samimi, M.; Shahriari Moghadam, M., (2020). Phenol biodegradation by bacterial strain O-CH1 isolated from seashore. Global J. Environ. Sci. Manage., 6(1): 109-118 (10 pages).
- Shah, M.; Fawcett, D.; Sharma, S.; Tripathy, S.K.; Poinern, G.E.J., (2015). Green synthesis of metallic nanoparticles via biological entities. Materials (Basel). 8(11): 7278-7308 (30 pages).
- Sucahya, T.N.; Permatasari, N.; Nandiyanto, A.B.D., (2016). Review: fotokatalis untuk pengolahan limbah cair. J. Integrasi Proses., 6(1): 1-15 (15 pages).
- Supriyanto, E.; Holikin, A.; Suwardiyanto., (2014). The thermal annealing effect on crystal structure and morphology of titanium dioxide (TiO<sub>2</sub>) powder. J. Ilmiah Dasar., 15(1): 37-41 (6 pages).
- Thota, S.; Tirukkovalluri, S.R.; Bojja, S., (2014). Visible light induced photocatalytic degradation of methyl red with codoped titania. J. Catal., 2014: 1-7 (7 pages).
- Wang, H.; Li, X.; Zhao, X.; Li, C.; Song, X.; Zhang, P.; Huo, P.; Li, X., (2022). A review on heterogeneous photocatalysis for environmental remediation: from semiconductors to modification strategies. Chin. J. Catal., 43(2): 178-214 (36 pages).
- Xing, Y.; Li, X.; Zhang, L.; Xu, Q.; Che, Z.; Li, W.; Bai, Y.; Li, K., Effect of TiO<sub>2</sub> nanoparticles on the antibacterial and physical properties of polyethylene-based film. Prog. Org. Coat., 73(2-3): 219-224 (6 pages).
- Zainuri, N.Z.; Hairom, N.H.H.; Sidik, D.A.B.; Desa, A.L.; Misdan, N.; Yusof, N.; Mohammad, A.W., (2018). Palm oil mill secondary effluent (POMSE) treatment via photocatalysis process in presence of ZnO-PEG nanoparticles. J. Water Process Eng., 26: 10-16 (7 pages).

#### AUTHOR (S) BIOSKETCHES

**Agustina, L.**, Ph.D. Candidate, Agroindustrial Engineering Study Program of Graduate School, IPB University, PO Box 220, Bogor, West Java, Indonesia.

- Email: [lya.agustina@ulm.ac.id](mailto:lya.agustina@ulm.ac.id)
- ORCID: 0000-0001-6780-0158
- Web of Science Researcher ID: GOG-9829-2022
- Scopus Author ID: 57210411885
- Homepage: <http://tip.ulm.ac.id/id/dosen/>

**Romli, M.**, Ph.D., Professor, Department of Agroindustrial Technology, Faculty of Agricultural Engineering and Technology, IPB University, PO Box 220, Bogor, West Java, Indonesia.

- Email: [mromli@apps.ipb.ac.id](mailto:mromli@apps.ipb.ac.id)
- ORCID: 0000-0002-1533-325X
- Web of Science Researcher ID: GPW-9612-2022
- Scopus Author ID: 55574122275
- Homepage: <https://tin.ipb.ac.id/>

**Suryadarma, P.**, Ph.D., Associate Professor, Department of Agroindustrial Technology, Faculty of Agricultural Engineering and Technology, IPB University, PO Box 220, Bogor, West Java, Indonesia.

- Email: [prayoga@apps.ipb.ac.id](mailto:prayoga@apps.ipb.ac.id)
- ORCID: 0000-0002-1655-3035
- Web of Science Researcher ID: AAW-3282-2021
- Scopus Author ID: 54879446100
- Homepage: <https://tin.ipb.ac.id/>

**Suprihatin, S.**, Ph.D., Professor, Department of Agroindustrial Technology, Faculty of Agricultural Engineering and Technology, IPB University, PO Box 220, Bogor, West Java, Indonesia.

- Email: [suprihatin@apps.ipb.ac.id](mailto:suprihatin@apps.ipb.ac.id)
- ORCID: 0000-0001-9641-8820
- Web of Science Researcher ID: GNH-5658-2022
- Scopus Author ID: 56085767200
- Homepage: <https://tin.ipb.ac.id/>

#### HOW TO CITE THIS ARTICLE

Agustina, L.; Romli, M.; Suryadarma, P.; Suprihatin, S., (2024). Green synthesis of titanium dioxide photocatalyst using *Lactobacillus bulgaricus* for processing palm oil mill effluent. *Global J. Environ. Sci. Manage.*, 10(1): 13-26.

DOI: [10.22034/gjesm.2024.01.02](https://doi.org/10.22034/gjesm.2024.01.02)

URL: [https://www.gjesm.net/article\\_706081.html](https://www.gjesm.net/article_706081.html)





## ORIGINAL RESEARCH PAPER

Efficient biosorption of cadmium by *Eucalyptus globulus* fruit biomass using process parameters optimization

M. Samimi

Department of Chemical Engineering, Faculty of Engineering, Kermanshah University of Technology, Kermanshah, Iran

## ARTICLE INFO

**Article History:**

Received 04 March 2023

Revised 17 June 2023

Accepted 20 July 2023

**Keywords:**

Biomass

Biosorption kinetics

Box-Behnken design

E. globulus fruit

## ABSTRACT

**BACKGROUND AND OBJECTIVES:** Industrial wastewater usually contains metal ions which are hazardous to human and aquatic organisms. Nowadays, the application of inexpensive biomaterials in adsorptive removal of metal ions, such as plant biomass, has been widely considered. In this study, the efficiency of *Eucalyptus globulus* fruit biomass for biological adsorption of cadmium ions from aquatic environments has been evaluated.

**METHODS:** After drying, the collected biosorbent was ground and powdered. The dried biomass, after screening with particle size of less than 45 micrometers, was used in all experiments. The effects of operating factors, such as biosorbent to cadmium ratio, pH value of the solution and residence time of biomass and metal, on the amount of analyte adsorption were evaluated by response surface methodology. The optimum conditions for maximum metal uptake by *Eucalyptus globulus* fruit biomass were also evaluated using the *Box-Behnken* Design model. Kinetic studies were statistically described to investigate the metal adsorption process.

**FINDINGS:** Validation experiments showed the accuracy of the model proposed for determining the optimum conditions for the cadmium biosorption process. Based on the experimental data, the values of coefficient of determination, adjusted coefficient and predicted coefficient used in the model were determined as 0.9948, 0.9855 and 0.9245, respectively. Using the model, the maximum cadmium ion adsorption by biomass was obtained at 93.65 percent, biosorbent-to-metal ratio of 9:1, pH value of 6, and contact time of 80 minutes.

**CONCLUSION:** In the present study, the *Eucalyptus globulus* fruit biomass, under optimal operating conditions, proved to be an efficient sorbent for cadmium uptake from aqueous environments. The results from the experimental data of the adsorption studies were consistent with pseudo-second-order kinetics (maximum capacity of 128.2 milligram per gram), indicating that the chemical adsorption of cadmium on the used biomass occurring in monolayers.

DOI: [10.22034/gjesm.2024.01.03](https://doi.org/10.22034/gjesm.2024.01.03)This is an open access article under the CC BY license (<http://creativecommons.org/licenses/by/4.0/>).

NUMBER OF REFERENCES

42



NUMBER OF FIGURES

6



NUMBER OF TABLES

5

\*Corresponding Author:

Email: [m.samimi@kut.ac.ir](mailto:m.samimi@kut.ac.ir)

Phone: +98918 836 5523

ORCID: [0000-0003-3098-7283](https://orcid.org/0000-0003-3098-7283)

Note: Discussion period for this manuscript open until April 1, 2024 on GJESM website at the "Show Article".

## INTRODUCTION

Heavy metals enter the environment and water resources through various processes such as battery manufacturing, metal plating, dyeing, etc. (Vilar *et al.*, 2007; Ehzari *et al.*, 2022a; Justus Reymond and Sudalaimuthu, 2023; Sulistyowati *et al.*, 2023; Sabilillah *et al.*, 2023; Sulistyowati *et al.*, 2023). Recent studies have shown that around 1.6 billion people cannot access clean water (Biswas, 2022). This trend is dramatically increasing with the growth of population, showing the necessity of using efficient methods to remove pollutants (Tauqeer *et al.*, 2021). So far, various methods, such as oxidative degradation, reverse osmosis, coagulation, photocatalysis, membrane separation and ultrafiltration, have been used to purify water and remove pollutants from aquatic environments (Azimi *et al.*, 2019; Samimi and Shahriari-Moghadam, 2020; Janani *et al.*, 2022; Ehzari *et al.*, 2022b). These methods are costly, complex and time-consuming and require high energy consumption and skilled labor. In recent decades, the use of biosorbent has become more common due its high efficiency, simplicity, low cost, and environmental friendliness, compared to the mentioned methods (Abdelfattah *et al.*, 2016; Rafiq *et al.*, 2016; Wang *et al.*, 2021). Low concentrations of heavy metals lead to the production of free oxygen radicals causing cytotoxicity. Therefore, the removal of these contaminants, rather than other water pollutants, has been considered extensively (Islam *et al.*, 2021). Cadmium, as one of the heavy metals, is widely used in various industries. Cadmium ions are very toxic even at low concentrations, causing liver and kidney damage, high blood pressure, increased bone fragility, and decreased red blood cell count (Briffa *et al.*, 2020; Zhang *et al.*, 2020; Pipoyan *et al.*, 2023). Due to toxic properties and bioaccumulation of cadmium, it has been identified as one of the most dangerous metal pollutants by the United States Environmental Protection Agency (Parker *et al.*, 2022). The natural properties of the adsorbent are important in the adsorption processes aided by biological adsorbents. Various adsorbents have been studied and introduced for removing different compounds from aquatic environments (Safari *et al.*, 2019; Samimi and Moeini, 2020; Shourije *et al.*, 2023). Several studies have also been conducted on different parts of eucalyptus tree as an adsorbent. For instance, the activated charcoal produced from *Eucalyptus urograndis* wood

was used as an adsorbent for copper, cadmium, and nickel ions (de Souza *et al.*, 2023); *E. globulus* leaves were used as an efficient biosorbent for methyl blue dye (Ouldmoumna *et al.*, 2013); *E. camaldulensis* leaves were utilized for the removal of lead ions from aquatic environments (Sabri *et al.*, 2018); *E. globulus* wood was applied for the removal of lead ions (Tejada-Tovar *et al.*, 2021); and *Eucalyptus* leaf ash was used for the removal of cadmium, cobalt, and nickel ions from aqueous systems (Zavarmousavi and Khalegh, 2013). Eucalyptus tree belongs to the Myrtaceae family and includes about nine hundred species and subspecies. This evergreen plant, ranging from shrubs to tall trees, is native to Australia and Tasmania. Among various species of this genus grown in different regions of the world, *E. globulus* is the highly distributed one (Chandorkar *et al.*, 2021). Although numerous studies have been conducted on heavy metals removal by plant adsorbents, no study has investigated the efficiency of *Eucalyptus globulus* fruit for the removal of metal pollutants. The aim of this study was to evaluate the efficiency of *E. globulus* fruit biomass (EFB) for the biological removal of divalent cadmium (Cd(II)) from aqueous environments. In addition, biomass characteristics, optimization of operational factors by Response Surface Methodology (RSM) and Box-Behnken design (BBD), biosorption mechanism, and adsorption kinetics of the biosorbent in the biological adsorption of the analyte were investigated. This study has been carried out in Kermanshah, Iran in 2023.

## MATERIALS AND METHODS

### *Preparation of biomass and the equipment*

The *E. globulus* fruit was collected from Zabol city in Sistan and Baluchistan - Iran. The biomass preparation process was carried out according to the study conducted by Samimi and Shahriari-Moghadam (2023). The fruits were washed with deionized water to remove impurities from the surface of the biosorbent and then dried at 35 degrees Celsius (°C) in an oven for 48 hours. The dried adsorbent was ground, powdered, and sieved. Finally, the prepared EFB, with a particle size <45 micrometer (µm), was applied in further studies. Metals measurements were performed using a flame atomic absorption spectrometer (Savant AA model, Australia) and Fourier-transform infrared spectroscopy (FTIR) by a spectrometer (Bruker Ltd., Germany).

### Batch adsorption

A certain amount of cadmium sulfate ( $\text{CdSO}_4 \cdot 2\text{H}_2\text{O}$ ) salt was dissolved in double distilled water and stirred at 100 revolutions per minute (rpm) for 15 min to achieve 1000 milligram per liter (mg/L) of Cd(II) solution. The solutions, with different conditions, required for the experiments were prepared by diluting the stock solution. To evaluate the ability of EFB in Cd(II) adsorption, 100 mg of biosorbent was added to 100 milliliter (mL) of the analyte solution (at 120 rpm) with different concentrations of metal ions. The analyte solution was vortexed and stirred at different times of the experimental design. The EFB-Cd solution was centrifuged (using centrifuge model Z205-A - USA) at 5500 rpm for 15 min to separate any solids from it. The amount of cadmium ions adsorption was indirectly analyzed by determining the residual metal in the supernatant. The kinetics of Cd(II) biosorption by EFB was studied in batch systems at room temperature. Cadmium uptake per gram of EFB and its removal efficiency were calculated using Eqs. 1, 2 and 3 (Samimi and Safari, 2022). Adsorbate removal efficiency (%):

$$\frac{(C_0 - C_e)}{C_0} \times 100 \quad (1)$$

$$q_e = \frac{(C_0 - C_e)}{M} \times V \quad (2)$$

$$q_t = (C_0 - C_t) \times \frac{V}{M} \quad (3)$$

Where,  $q_e$  and  $q_t$  are the EFB uptake capacity expressed in milligram per gram (mg/g) at equilibrium and time  $t$  (min), respectively;  $C_0$  and  $C_e$  are the initial and final cadmium concentrations (mg/g), respectively;  $M$  is the EFB dosage (g); and  $V$  is the cadmium solution volume (L).

### Design of experiments (DOE) and removal optimization

According to the number of operating variables,

the Box-Behnken Design (BBD) model was used to determine the conditions of the experimental parameters. Minitab-18 software was used to implement the model. The RSM was used to achieve optimal conditions for the adsorbate removal process. The influence of the *E. globulus fruit* biomass (EFB)-to-cadmium ratio (EC), the potential of hydrogen (pH) of an aqueous solution containing cadmium ions, and the contact time ( $t$ ) were evaluated as the most important experimental variables for the adsorptive removal of Cd(II). The operating parameters and their variety of levels (coded from -1 to +1) are summarized in Table 1.

The experimental variables were examined at EFB-to-cadmium ratios of 3:1, 6:1 and 9:1, pH values of 2, 4 and 6 and contact times of 10, 45 and 80 min. For this purpose, 15 tests were carried out based on the BBD model (13 tests and 2 duplicate tests to determine the errors). The DOE for operating variables and their results are reported in Table 2. For further statistical analysis of the mathematical model, an analysis of variance (ANOVA) was also performed with a significance level of 5 percent (%).

The full quadratic model for the correlation between the Cd(II) removal percent (CR%) and the response variables are expressed using Eq. 4 (Oliver Paul Nayagam and Prasanna, 2023).

$$CR\% = \alpha_0 + \sum_{i=1}^3 \alpha_i X_i + \sum_{i=1}^3 \alpha_{ii} X_i^2 + \sum_{i=1}^2 \sum_{j=i+1}^3 \alpha_{ij} X_{ij} \quad (4)$$

Where, CR% is the response;  $X_i$  and  $X_{ij}$  are independent variables; and  $\alpha_0$ ,  $\alpha_i$ ,  $\alpha_{ii}$  and  $\alpha_{ij}$  are intercept (offset term), linear, quadratic and interaction terms (regression coefficients), respectively. The F-value used for analyzing the statistical significance of the second-order models was calculated by dividing the mean-square regression value by the mean-square residual, as presented in previous studies (Moghadam and Samimi, 2022).

Table 1: The operational factors and variety of levels

Variables		Rang of levels		
Main factors	Symbol	-1	0	+1
EFB-to-cadmium ratio	EC	3:1	6:1	9:1
The pH value of analyte solution	pH	2	4	6
Contact time (min)	t	10	45	80

## RESULTS AND DISCUSSION

### Analysis of response variance and process optimization

Based on the BBD model, a least squares quadratic model (regression equation in uncoded units) was derived for the cadmium uptake as explained by Eq. 5 (Samimi and Shahriari-Moghadam, 2018).

$$CR \% = 51.63 + 11.265X_{EC} + 8.224X_{pH} + 18.426X_t - 1.74X_{EC}^2 - 2.20X_{pH}^2 - 12.73X_t^2 + 7.24X_{EC} \cdot X_{pH} + 7.02X_{EC} \cdot X_t + 6.52X_{pH} \cdot X_t \quad (5)$$

The model, selected based on the comparison between the measured and predicted amounts of CR%, had coefficient of determination ( $R^2$ ), adjusted coefficient ( $R_{adj}^2$ ), and predicted coefficient ( $R_{pred}^2$ ) values of 0.9948, 0.9855, and 0.9245, respectively. The ANOVA of the quadratic model for cadmium adsorption is presented in Table 3. Based on the results, the total degrees of freedom (DF), the DF for regression, and the DF for residual error were 14, 9, and 5, respectively. The higher the F-value with the p-values less than 0.05, the greater the significance

Table 2: DOE and responses for three independent factors

Run. No.	Manipulated variables			Response
	$X_{EC}$	$X_{pH}$	$X_t$	CR%
1	0	0	0	51.68
2	-1	-1	0	33.21
3	0	0	0	52.84
4	1	-1	0	44.67
5	-1	1	0	36.24
6	-1	0	1	39.11
7	1	0	1	72.28
8	0	0	0	50.37
9	1	0	-1	21.17
10	-1	0	-1	16.08
11	0	1	-1	19.55
12	0	-1	-1	17.20
13	1	1	0	76.64
14	0	-1	1	40.79
15	0	1	1	69.23

Table 3: The ANOVA of the quadratic model for cadmium adsorption

Source	DF	Sum of squares	Mean squares	F-Value	P-Value	Degree of significance
Regression	9	5455.07	606.12	106.40	< 0.001	Significant
Linear	3	4272.46	1424.15	249.99	< 0.001	Significant
$X_{EC}$	1	1015.20	1015.20	178.20	< 0.001	Significant
$X_{pH}$	1	541.04	541.04	94.97	< 0.001	Significant
$X_t$	1	2716.21	2716.21	476.79	< 0.001	Significant
Square	3	605.94	201.98	35.45	0.001	Significant
$X_{EC}^2$	1	11.13	11.13	1.95	0.221	Not significant
$X_{pH}^2$	1	17.93	17.93	3.15	0.136	Not significant
$X_t^2$	1	598.70	598.70	105.09	< 0.001	Significant
2-Way Interaction	3	576.67	192.22	33.74	0.001	Significant
$X_{EC} \cdot X_{pH}$	1	209.38	209.38	36.75	0.002	Significant
$X_{EC} \cdot X_t$	1	197.12	197.12	34.60	0.002	Significant
$X_{pH} \cdot X_t$	1	170.17	170.17	29.87	0.003	Significant
Residual error	5	28.48	5.70	-	-	-
Lack-of-Fit	3	25.43	8.48	5.55	0.156	Not significant
Pure Error	2	3.05	1.53	-	-	-
Total	14	5483.56	-	-	-	-

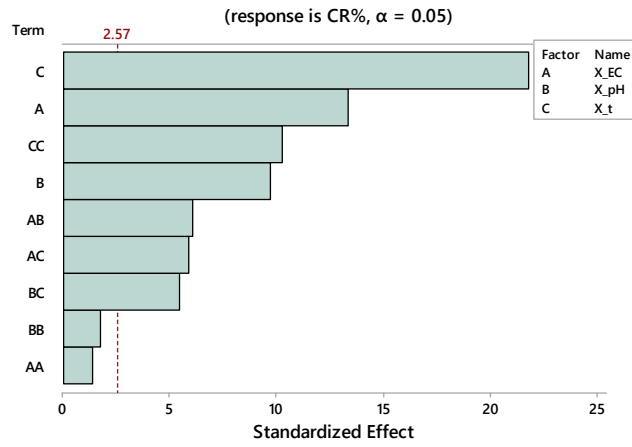


Fig. 1: Pareto graphical evaluation of the impact of standardized factors on CR%

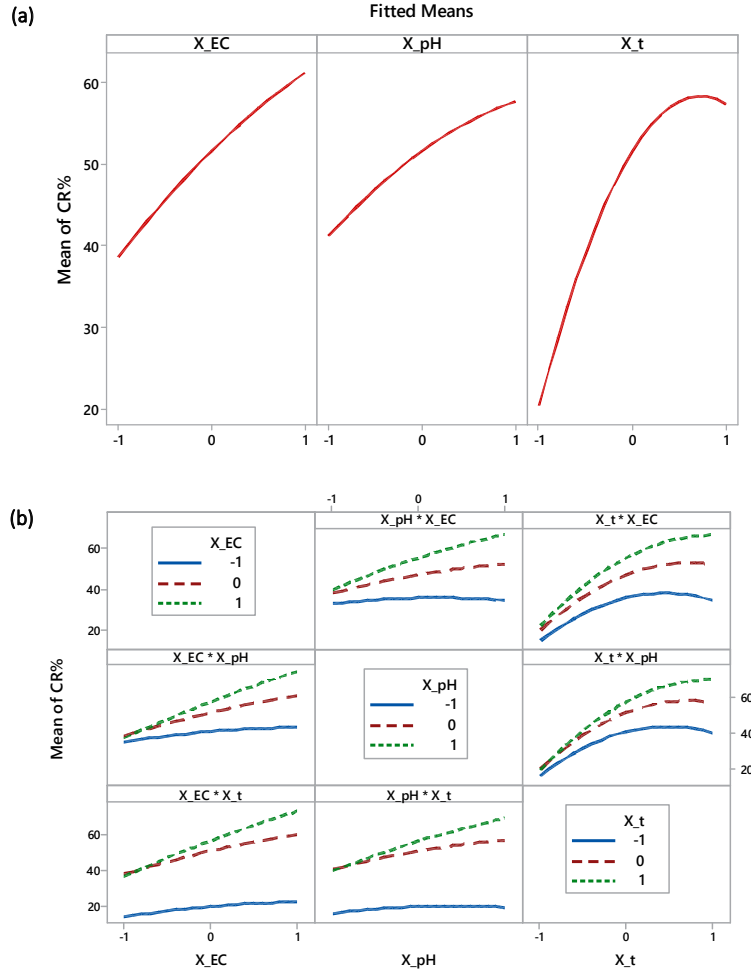


Fig. 2: The mean effects (a) and 2-way interaction diagrams (b) of coded operational parameters on CR%

level of the factors, the coded terms of  $X_{EC}$ ,  $X_{pH}$ ,  $X_t$ ,  $X_t^2$  and the 2-way interaction terms (namely  $X_{EC} \cdot X_{pH}$ ,  $X_{EC} \cdot X_t$ , and  $X_{pH} \cdot X_t$ ). However, the parameters with p-values greater than 0.05, such as  $X_{EC}^2$  and  $X_{pH}^2$ , were not significant.

As shown in the graphical Pareto analysis (Fig. 1), all terms except BB and AA (namely  $X_{EC}^2$  and  $X_{pH}^2$ ) crossed the hypothetical point boundary, confirming their importance as they were further from the vertical line (Samimi et al., 2023a). The analysis result confirmed the data calculated from the regression equation.

The plot of the main effects and the mutual interactions of the encoded operating parameters on the average cadmium removal percentage based on the BBD model are shown in Fig. 2. Obviously, the cadmium uptake was higher at high levels of all operating parameters, and the increasing slope of  $X_t$

factor on the removal percentage was more evident. The interaction effects of the parameters also confirmed this trend. Fig. 3 shows the experimental model of CR% in contour plots created by Minitab software tool in different modes. In Fig. 3a, the contour diagram of cadmium sorption was plotted based on  $X_t$  and  $X_{pH}$  (with the encoded EFB-to-cadmium ratio at the average level:  $X_{EC} = 0$ ). In Fig. 3b, the contour plot of CR% was drawn based on  $X_t$  and  $X_{EC}$  (with the encoded pH at the average level:  $X_{pH} = 0$ ) and in Fig. 3c it was sketched based on  $X_{pH}$  and  $X_{EC}$  (with the encoded time at the  $X_t = 0$ ). As shown in Fig. 3a, at the biosorbent-to-metal ratio of 6:1, the CR% increases with the simultaneous increase in contact time and pH value. The results of Fig. 3b at the medium pH level (i.e. pH=4) illustrated that the highest CR% was proportional to the simultaneous increase of the contact time and the

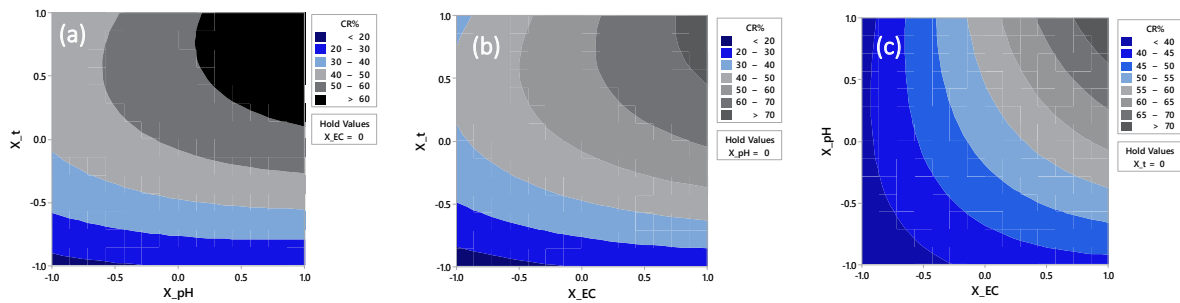


Fig. 3: The contour diagrams of the effect of operational variables on CR% for a) versus XpH; b) versus ; and c) versus .

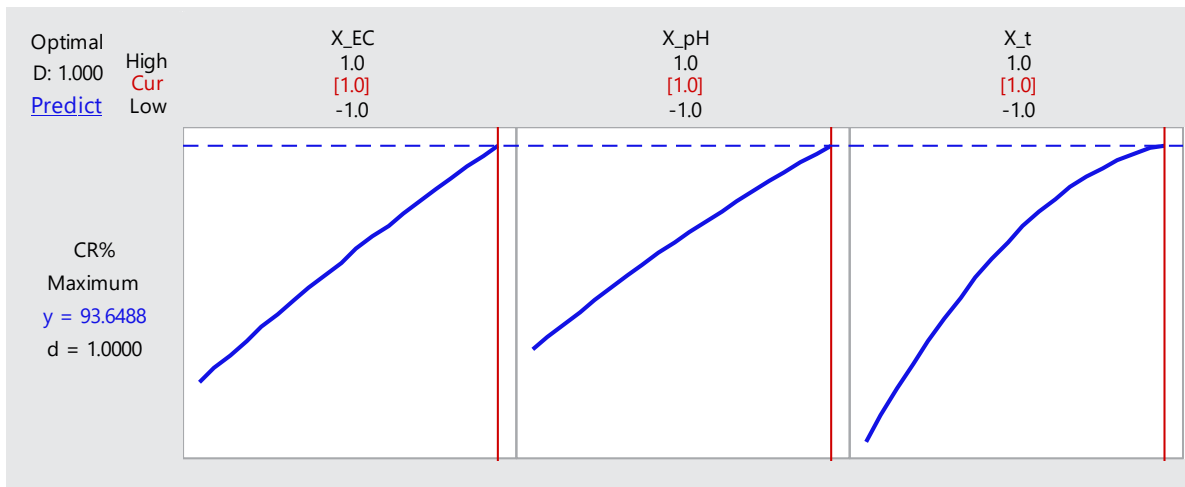


Fig. 4: Optimization diagram of the operating conditions in cadmium biosorption process by EFB

*Eucalyptus globulus* fruit biomass for adsorptive cadmium removal

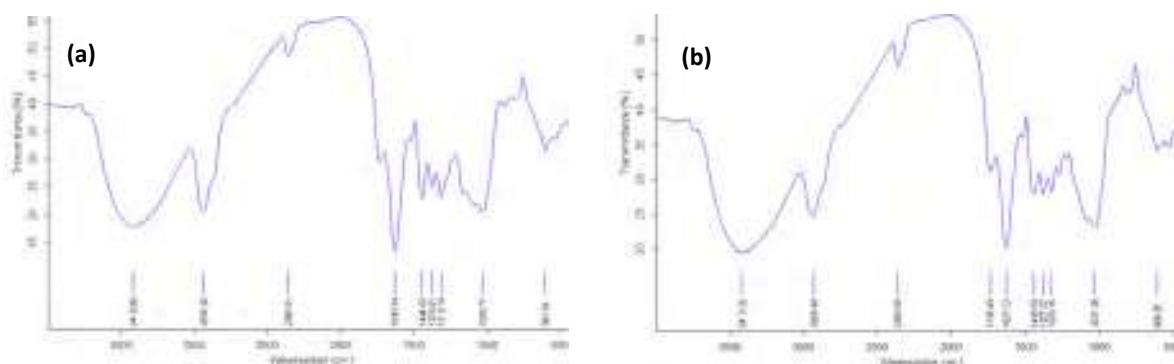


Fig. 5: The FTIR analysis for a) EFB and b) EFB-Cd(II)

Table 4. Constants of PFO, PSO and IDM in the Model

Models	PFO			PSO			IDM		
	$q_e$	$k_1$	$R^2$	$q_e$	$k_2$	$R^2$	$k_p$	$C$	$R^2$
	132.26	0.0514	0.946	128.205	$1.85 \times 10^{-4}$	0.979	10.15	-3.782	0.969

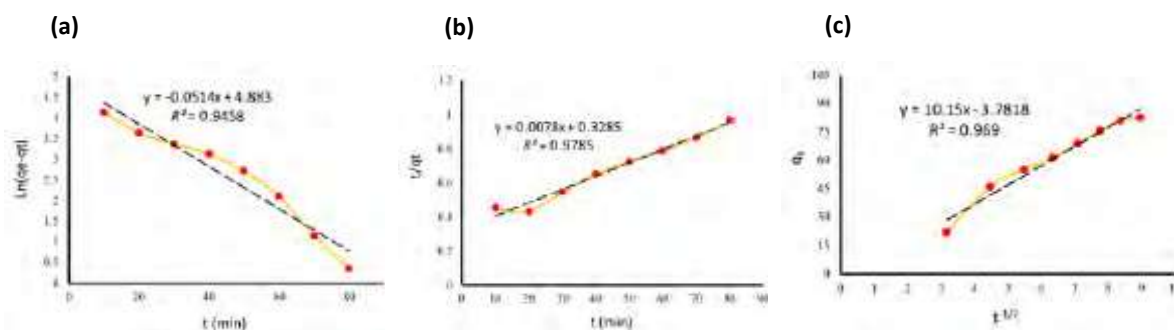


Fig. 6: Kinetics diagram of a) PFO, b) PSO, and c) IDM for Cd(II) biosorption by EFB

Table 5: Adsorption capacities of different biosorbents for the removal of heavy metals

Biosorbent	Analyte	Removal%	$q_{max}$ (mg/g)	Optimal pH	Sources
Banana leaves activated carbon	Copper	83	66.2	5	Darweesh <i>et al.</i> , 2022
<i>Corchorus olitorius</i> leaf	Zinc	-	11.63	6	Ali and Bhakta, 2020
Activated <i>Eupatorium adenophorum</i>	Cadmium	88.9	45.45	7	Joshi <i>et al.</i> , 2022
Activated <i>Acer oblongum</i>	Cadmium	96	44.64	7	Joshi <i>et al.</i> , 2022
Strain-MS3	Lead	58.69	138.88	6.6	Samimi and Shahriari-Moghadam, 2021
EFB biosorbent	Cadmium	89.57	128.205	6	The current study

EFB-to-cadmium ratio. However, the pH increase in Fig. 3a or the sorbent-to-analyte ratio increase in Fig. 3b at low-time contact did not not considerably affect CR%. According to the direction of the lines and curves, the contour diagram of Fig. 3c at resident

time of 45 min also revealed that the CR% increased with a simultaneous increase in pH value and EFB-to-cadmium ratio. However, at low sorbent-to-metal ratio levels, the pH changes did not significantly affect CR%.

Numerical optimization of the BBD was performed to predict the optimal conditions of EFB for achieving the maximum metal sorption. According to the optimization results presented in Fig. 4, the maximum CR% in aqueous environment, obtained at EC of 9:1, pH of 6 and contact time of 80 min, was 93.65%.

As shown in the BBD results (Table 3), the p-value of the *lack-of-fit* term was not significant (0.156), confirming the model's validity (Samimi et al., 2023a). However, based on the experimental validation test under optimal conditions, the removal of cadmium from aqueous environments by EFB was found to be 89.57%. The small difference (<5%) between the value predicted by the model (93.65%) and the actual value (89.57%) demonstrated the high accuracy and validity of the proposed model.

#### FTIR analysis for biosorbent/metal

The prepared biosorbent was analyzed by FTIR spectroscopy to identify the functional groups of EFB. The FTIR spectrum of the biosorbent is shown in Fig. 5. According to Fig. 5a, the absorption peak at 3419/cm corresponded to the -OH group in EFB. The absorption band at 2936/cm was associated with the stretching vibration of the methyl group (C-H bonds). Other stretching vibration peaks were attributed to the C=O, C-C, and C-O bonds. The above active sites on the EFB surface could affect the adsorption of Cd(II). The shifted peaks after metal biosorption showed that Cd(II) was adsorbed on the surface of EFB (Fig. 5b).

#### Kinetics of metal biosorption

Cadmium uptake rate by EFB versus contact time were generally evaluated using adsorption kinetics by pseudo-first-order (PFO) and pseudo-second-order (PSO) kinetic models and intraparticle diffusion mechanism (IDM). The linear forms of the mentioned models are expressed by Eqs. 6, 7 and 8, respectively (Samimi et al., 2023b).

$$\ln(q_e - q_t) = \ln q_e - k_1 t \quad (6)$$

$$\frac{t}{q_t} = \frac{1}{k_2 q_e^2} + \frac{t}{q_e} \quad (7)$$

$$q_t = k_p t^{\frac{1}{2}} + C \quad (8)$$

Where,  $k_2$  (g/mg/min) and  $k_1$  (1/min) are adsorption rate constants for PSO and PFO kinetics, respectively; and  $k_p$  (mg/g/min<sup>1/2</sup>) parameter is IDM constant. All the kinetics experiments were done at pH value of 6. The kinetics diagrams of PFO, PSO and IDM for cadmium adsorption are shown in Fig. 6a to c. As described in Table 4, the higher value of  $R^2$  for PSO kinetics rather than PFO and IDM indicated that the rate-controlling stage in cadmium uptake was the chemical interaction between the EFB functional groups and Cd(II). Comparison of the cadmium uptake capacity obtained in this study and the adsorption capacities of different biosorbents reported in other studies has been presented in Table 5.

#### CONCLUSION

Cadmium ions, as one of the heavy metals, find their way into the aquatic environments through industrial applications. In the present study, a novel biomass derived from *E. globulus* fruit was evaluated for cadmium uptake from aquatic environments. The results of the regression equation, *Pareto* graphical analysis and contour plots revealed that all the selected experimental parameters, such as biomass-to-metal ratio, pH value of the solution, and contact time, significantly affected the cadmium biosorption by EFB biosorbent. Investigation of the parameters and numerical optimization of the quadratic model were performed to predict the optimum conditions for achieving the maximum cadmium uptake by EFB. The maximum metal uptake (at biosorbent-to-metal ratio of 9:1, pH value of 6 and residence time of 80 min) was determined as 93.65%. The statistical analysis and validation tests revealed the high accuracy of the BBD model in predicting the optimum conditions for cadmium adsorption by EFB. Based on the comparison between the measured and predicted amounts of CR%, coefficients of  $R^2$ ,  $R_{adj}^2$ , and  $R_{pred}^2$  in the BBD model were 0.9948, 0.9855, and 0.9245, respectively. According to the results, the cadmium adsorption followed a PSO kinetic model, indicating that the rate-controlling stage in cadmium sorption was the chemical interaction between functional groups in EFB and Cd(II) ions. However, the  $q_e$  values calculated by PFO and PSO models (132.36 and 128.2 mg/g, respectively) were obtained from the experiments in optimal conditions based on the BBD model. The results of FTIR analysis, proved the

active role of functional groups (e.g. methyl group and hydroxy group) on the EFB surface. The EFB, as a biomass prepared from worthless and unusable fruit for humans, showed a significant potential for the removal of heavy metals from wastewater. The present study illustrated that cadmium could be simply removed from aqueous environments using this naturally occurring adsorbent.

#### AUTHOR CONTRIBUTIONS

The corresponding author, M. Samimi, managed the project, supervised various stages of the study, wrote the original draft, performed the analysis and validation tests, and reviewed and edited the manuscript.

#### ACKNOWLEDGEMENT

The author would like to acknowledge the financial support of Kermanshah University of Technology for the current study under [Grant number S/P/T 1452]. The author also thank the University of Zabol for providing FTIR analysis.

#### CONFLICT OF INTEREST

The author declares that there is no conflict of interests regarding the publication of this manuscript. In addition, the ethical issues, including plagiarism, informed consent, misconduct, data fabrication and/or falsification, double publication and/or submission, and redundancy have been completely observed by the authors.

#### OPEN ACCESS

©2024 The author. This article is licensed under a Creative Commons Attribution 4.0 International License, which permits use, sharing, adaptation, distribution and reproduction in any medium or format, as long as you give appropriate credit to the original author(s) and the source, provide a link to the Creative Commons license, and indicate if changes were made. The images or other third-party material in this article are included in the article's Creative Commons license, unless indicated otherwise in a credit line to the material. If material is not included in the article's Creative Commons license and your intended use is not permitted by statutory regulation or exceeds the permitted use, you will need to obtain permission directly from the copyright holder. To view a copy of this license, visit:

<http://creativecommons.org/licenses/by/4.0/>

#### PUBLISHER'S NOTE

GJESM Publisher remains neutral with regard to jurisdictional claims with regard to published maps and institutional affiliations.

#### ABBREVIATIONS

%	Percent
°C	Degree Celsius
$\mu\text{m}$	Micrometre
ANOVA	Analysis of variance
BBD	Box-Behnken Design
$C_0$	Initial cadmium concentrations
Cd(II)	Divalent cadmium
$\text{CdSO}_4 \cdot 2\text{H}_2\text{O}$	Cadmium sulfate
$C_e$	Final cadmium concentrations
CR	Cadmium removal
$C_t$	Cadmium concentrations at time t
DOE	Design of experiments
EC	EFB-to-Cadmium ratio
EFB	<i>E. globulus</i> fruit biomass
Eq.	Equation
Fig.	Figure
FTIR	Fourier-transform infrared spectroscopy
g	Gram
IDM	Intraparticle diffusion mechanism
L	Liter
mg	Milligram
mg/g	Milligram per gram
mg/L	Milligram per liter
mL	Milliliter
min	Minute
No.	Number
OD	Optical Density
PFO	pseudo-first-order
pH	Potential of hydrogen
PSO	pseudo-second-order
$q_e$	Uptake capacity (at equilibrium)
$q_t$	Uptake capacity (at time t)
$R^2$	Coefficient of determination
$R^2_{\text{adj}}$	Adjusted $R^2$
$R^2_{\text{pred}}$	Predicted $R^2$
rpm	Revolutions per minute

RSM	Response surface methodology
V	Volume
$X_{EC}$	EFB to cadmium ratio - Coded factor
$X_{pH}$	pH value - Coded factor
$X_t$	Contact time - Coded factor
$\alpha_0$	Offset term
$\alpha_i$	Linear term
$\alpha_{ii}$	Quadratic term
$\alpha_{ij}$	Interaction term

## REFERENCES

- Abdelfattah, I.; Ismail, A.A.; Al Sayed, F.; Almedolab, A.; Aboelghait, K., (2016). Biosorption of heavy metals ions in real industrial wastewater using peanut husk as efficient and cost effective adsorbent. *Environ. Nanotechnol. Monit. Manag.*, 6: 176-183 (8 pages).
- Ali, M.M.; Bhakta, J.N., (2020). Biosorption of zinc from aqueous solution using leaves of *Corchorus olitorius* as a low-cost biosorbent. *Water Environ. Res.*, 92(6), 821-828 (8 pages).
- Azimi, N.; Azimi, P.; Samimi, M.; Mansouri Jalilian, T., (2019). Ultrasonic-assisted adsorption of Ni (II) ions from aqueous solution onto Fe<sub>3</sub>O<sub>4</sub> nanoparticles. *Adv. Nanochem.*, 1(2): 66-72 (7 pages).
- Biswas, A.K., (2022). Urban water security for developing countries. *River*. 1(1): 15-24 (10 pages).
- Briffa, J.; Sinagra, E.; Blundell, R., (2020). Heavy metal pollution in the environment and their toxicological effects on humans. *Heliyon*. 6(9): e04691 (26 pages).
- Darweesh, M.A.; Elgendy, M.Y.; Ayad, M.I.; Ahmed, A.M.; Elsayed, N.K.; Hammad, W.A., (2022). Adsorption isotherm, kinetic, and optimization studies for copper (II) removal from aqueous solutions by banana leaves and derived activated carbon. *S. Afr. J. Chem. Eng.*, 40, 10-20 (11 pages).
- Chandorkar, N.; Tambe, S.; Amin, P.; Madankar, C., (2021). A systematic and comprehensive review on current understanding of the pharmacological actions, molecular mechanisms, and clinical implications of the genus *Eucalyptus*. *Phytomedicine Plus*, 1(4): 100089 (20 pages).
- Daifullah, A.; Yakout, S.; Elreefy, S., (2007). Adsorption of fluoride in aqueous solutions using KMnO<sub>4</sub>-modified activated carbon derived from steam pyrolysis of rice straw. *J. Hazard. Mater.*, 147(1-2): 633-643 (11 pages).
- de Souza, E.C.; Pimenta, A.S.; da Silva, A.J.F.; do Nascimento, P.F.P.; Ighalo, J.O., (2023). Oxidized eucalyptus charcoal: a renewable biosorbent for removing heavy metals from aqueous solutions. *Biomass Convers. Biorefin.*, 13: 4105-4119 (15 pages).
- Ehzari, H.; Amiri, M.; Safari, M.; Samimi, M., (2022a). Zn-based metal-organic frameworks and p-aminobenzoic acid for electrochemical sensing of copper ions in milk and milk powder samples. *Int. J. Environ. Anal. Chem.*, 102(16): 4364-4377 (14 pages).
- Ehzari, H.; Safari, M.; Samimi, M.; Shamsipur, M.; Gholivand, M.B., (2022b). A highly sensitive electrochemical biosensor for chlorpyrifos pesticide detection using the adsorbent nanomatrix contain the human serum albumin and the Pd: CdTe quantum dots. *Microchem. J.*, 179: 107424 (10 pages).
- Guarin, J.R.; Moreno-Pirajan, J.C.; Giraldo, L., (2018). Kinetic Study of the Bioadsorption of Methylene Blue on the Surface of the Biomass Obtained from the Algae *D. antarctica*. *J. Chem.*, 2018: 2124845 (12 pages).
- Ho, Y.S.; McKay, G., (1999). Pseudo-second order model for sorption processes. *Process Biochem.*, 34(5): 451-465 (15 pages).
- Islam, A.; Teo, S.H.; Taufiq-Yap, Y.H.; Ng, C.H.; Vo, D.V.N.; Ibrahim, M.L.; Hasan, M.M.; Khan, M.A.R.; Nur, A.S.; Awual, M.R., (2021). Step towards the sustainable toxic dyes removal and recycling from aqueous solution-A comprehensive review. *Resour. Conserv. Recycl.*, 175: 105849 (24 pages).
- Janani, R.; Gurunathan, B.; Sivakumar, K.; Varjani, S.; Ngo, H.H.; Gnansounou, E., (2022). Advancements in heavy metals removal from effluents employing nano-adsorbents: way towards cleaner production. *Environ. Res.*, 203: 111815 (14 pages).
- Joshi, H.K.; Vishwakarma, M.C.; Kumar, R.; Sharma, H.; Joshi, S. K.; Bhandari, N.S., (2022). Adsorption of Cd<sup>2+</sup> from synthetic wastewater by modified leaves of *Eupatorium adenophorum* and *Acer oblongum*: thermodynamics, kinetics and equilibrium studies. *Discover Water*: 2(1), 9 (16 pages).
- Justus Reymond, D.; Sudalaimuthu, K., (2023). Geospatial visualization and seasonal variation of heavy metals in river sediments. *Global J. Environ. Sci. Manage.*, 9(2): 309-322 (14 pages).
- Moghadam, H.; Samimi, M., (2022). Effect of condenser geometrical feature on evacuated tube collector basin solar still performance: Productivity optimization using a Box-Behnken design model. *Desalination*, 542: 116092 (8 pages).
- Oliver Paul Nayagam, J.; Prasanna, K., (2023). Response surface methodology and adaptive neuro-fuzzy inference system for adsorption of reactive orange 16 by hydrochar. *Global J. Environ. Sci. Manage.*, 9(3): 373-388 (16 pages).
- Ouldoumna, A.; Reinert, L.; Benderdouche, N.; Bestani, B.; Duclaux, L., (2013). Characterization and application of three novel biosorbents "*Eucalyptus globulus*, *Cynara cardunculus*, and *Prunus cerasifera*" to dye removal. *Desalin. Water Treat.*, 51(16-18): 3527-3538 (12 pages).
- Parker, G.H.; Gillie, C.E.; Miller, J.V.; Badger, D.E.; Kreider, M.L., (2022). Human health risk assessment of arsenic, cadmium,

- lead, and mercury ingestion from baby foods. *Toxicol. Rep.*, 9: 238-249 (12 pages).
- Pipoyan, D.; Stepanyan, S.; Beglaryan, M.; Stepanyan, S.; Mendelsohn, R.; Deziel, N.C., (2023). Health risks of heavy metals in food and their economic burden in Armenia. *Environ. Int.*, 172, 107794 (8 pages).
- Rafiq, M.; Farooq, U.; Athar, M.; Salman, M.; Aslam, M.; Raza, H.H., (2016). *Gardenia jasminoides*: an ornamental plant for the biosorption of lead and cadmium ions. *Desalin. Water Treat.*, 57(22), 10432-10442 (11 pages).
- Sabilillah, A.M.; Palupi, F.R.; Adji, B.K.; Nugroho, A.P., (2023). Health risk assessment and microplastic pollution in streams through accumulation and interaction of heavy metals. *Global J. Environ. Sci. Manage.*, 9(4): 719-740 (22 pages).
- Sabri, M.A.; Ibrahim, T.H.; Khamis, M.I.; Al-Asheh, S.; Hassan, M.F., (2018). Use of *Eucalyptus camaldulensis* as biosorbent for lead removal from aqueous solution. *Int. J. Environ. Res.*, 12(4), 513-529 (17 pages).
- Safari, M.; Moghadam, M.S.; Samimi, M.; Azizi, Z., (2019). Study of the Optimal Conditions for Zn<sup>+2</sup> Removal Using the Biomass of Isolated Bacteria from Ravang Mine. *Iran. J. Soil Water Res.*, 50(1): 149-160 (12 pages).
- Samimi, M.; Moieni, S., (2020). Optimization of the Ba<sup>+</sup> 2 uptake in the formation process of hydrogels using central composite design: Kinetics and thermodynamic studies of malachite green removal by Ba-alginate particles. *J Part. Sci. Technol.*, 6(2): 95-102 (8 pages).
- Samimi, M.; Safari, M., (2022). TMU-24 (Zn-based MOF) as an advance and recyclable adsorbent for the efficient removal of eosin B: Characterization, equilibrium, and thermodynamic studies. *Environ. Prog. Sustainable Energy*, 41(5): e13859 (9 pages).
- Samimi, M.; Mohammadzadeh, E.; Mohammadzadeh, A., (2023a). Rate enhancement of plant growth using Ormus solution: optimization of operating factors by response surface methodology. *Int. J. Phytoremediation*, 1-7 (7 pages).
- Samimi, M.; Shahriari-Moghadam, M., (2021). Isolation and identification of *Delftia lacustris* Strain-MS3 as a novel and efficient adsorbent for lead biosorption: Kinetics and thermodynamic studies, optimization of operating variables. *Biochem. Eng. J.*, 173: 108091 (9 pages).
- Samimi, M.; Shahriari Moghadam, M., (2018). Optimal conditions for the biological removal of ammonia from wastewater of a petrochemical plant using the response surface methodology. *Global J. Environ. Sci. Manag.*, 4(3): 315-324 (10 pages).
- Samimi, M.; Shahriari Moghadam, M., (2020). Phenol biodegradation by bacterial strain O-CH1 isolated from seashore. *Global J. Environ. Sci. Manag.*, 6(1): 109-118 (10 pages).
- Samimi, M.; Shahriari-Moghadam, M., (2023). The Lantana camara L. stem biomass as an inexpensive and efficient biosorbent for the adsorptive removal of malachite green from aquatic environments: kinetics, equilibrium and thermodynamic studies. *Int. J. Phytoremediation*, 25(10): 1-9 (9 pages).
- Samimi, M.; Zakeri, M.; Alobaid, F.; Aghel, B., (2023b). A Brief Review of Recent Results in Arsenic Adsorption Process from Aquatic Environments by Metal-Organic Frameworks: Classification Based on Kinetics, Isotherms and Thermodynamics Behaviors. *Nanomater.*, 13(1): 60 (12 pages).
- Shourije, S.M.J.S.; Dehghan, P.; Bahrololoom, M.E.; Cobley, A.J.; Vitry, V.; Azar, G.T.P., Kamyab, H; Mesbah, M., (2023). Using fish scales as a new biosorbent for adsorption of nickel and copper ions from wastewater and investigating the effects of electric and magnetic fields on the adsorption process. *Chemosphere*. 317: 137829 (12 pages).
- Sulistyowati, L.; Nurhasanah; Riani, E.; Cordova, M.R., (2022). Heavy metals concentration in the sediment of the aquatic environment caused by the leachate discharge from a landfill. *Global J. Environ. Sci. Manage.*, 9(2): 323-336 (14 pages).
- Sulistyowati, L.; Yolanda, Y.; Andareswari, N., (2023). Harbor water pollution by heavy metal concentrations in sediments. *Global J. Environ. Sci. Manage.*, 9(4): 885-898 (14 pages).
- Tauqeer, M.; Khan, M.E.; Ji, R.S.; Bansal, P.; Mohammad, A., (2021). Metal and Metal Oxide Nanomaterials for Wastewater Decontamination. In *Metal, Metal-Oxides and Metal-Organic Frameworks for Environmental Remediation*. Springer Cham, 64: 63-95 (33 pages).
- Tejada-Tovar, C.; Villabona-Ortiz, A.; Ortega-Toro, R.; Mancilla-Bonilla, H.; Espinoza-León, F., (2021). Potential use of residual sawdust of *Eucalyptus globulus* Labill in Pb (II) adsorption: Modelling of the kinetics and equilibrium. *Appl. Sci.*, 11(7): 3125 (12 pages).
- Vilar, V.J.; Botelho, C.M.; Boaventura, R.A., (2007). Chromium and zinc uptake by algae *Gelidium* and agar extraction algal waste: Kinetics and equilibrium. *J. Hazard. Mater.*, 149(3): 643-649 (7 pages).
- Wang, C.; Xiong, C.; He, Y.; Yang, C.; Li, X.; Zheng, J.; Wang, S., (2021). Facile preparation of magnetic Zr-MOF for adsorption of Pb (II) and Cr (VI) from water: Adsorption characteristics and mechanisms. *Chem. Eng. J.*, 415: 128923 (11 pages).
- Zhang, S.; Sun, L.; Zhang, J.; Liu, S.; Han, J.; Liu, Y., (2020). Adverse impact of heavy metals on bone cells and bone metabolism dependently and independently through anemia. *Adv. Sci.*, 7(19): 2000383 (15 pages).

**AUTHOR (S) BIOSKETCHES**

**Samimi, M.**, Ph.D., Assistant Professor, Department of Chemical Engineering, Faculty of Engineering, Kermanshah University of Technology, Kermanshah, Iran.

- Email: [m.samimi@kut.ac.ir](mailto:m.samimi@kut.ac.ir)
- ORCID: [0000-0003-3098-7283](https://orcid.org/0000-0003-3098-7283)
- Web of Science Researcher ID: AAT-2290-2021
- Scopus Author ID: 24478806000
- Homepage: <http://research.kut.ac.ir/~msamimi/en/>

**HOW TO CITE THIS ARTICLE**

Samimi, M., (2024). Efficient biosorption of cadmium by *Eucalyptus globulus* fruit biomass using process parameters optimization. *Global J. Environ. Sci. Manage.*, 10(1) 27-38.

DOI: [10.22034/gjesm.2024.01.03](https://doi.org/10.22034/gjesm.2024.01.03)

URL: [https://www.gjesm.net/article\\_706328.html](https://www.gjesm.net/article_706328.html)





## ORIGINAL RESEARCH ARTICLE

## Silver-based plasmonic nanoparticles for biosensor organophosphate pesticides using a single film containing acetylcholinesterase/choline oxidase

D. Hermanto<sup>1,\*</sup>, N. Ismillayli<sup>1</sup>, H. Muliarsi<sup>2</sup>, R. Wirawan<sup>3</sup>, S.R. Kamali<sup>4</sup><sup>1</sup> Department of Chemistry, University of Mataram, Jl. Majapahit 62 Mataram, NTB 83125, Indonesia<sup>2</sup> Department of Pharmacy, University of Mataram, Jl. Majapahit 62 Mataram, NTB 83125, Indonesia<sup>3</sup> Department of Physics, University of Mataram, Jl. Majapahit 62 Mataram, NTB 83125, Indonesia<sup>4</sup> Department of Applied Chemistry, Chaoyang University of Technology, Wufeng, 41349, Republic of China

## ARTICLE INFO

**Article History:**

Received 26 January 2023

Revised 09 March 2023

Accepted 24 May 2023

**Keywords:**

Biosensor

Colorimetric indicator

Organophosphate pesticides

Silver nanoparticle

Single film

## ABSTRACT

**BACKGROUND AND OBJECTIVES:** To address the potential harm caused by the intensive use of pesticides in pest control in agriculture, there is a need for accurate and efficient methods to detect and monitor pesticide residues. Therefore, this study aimed to develop a biosensor that can detect organophosphate pesticides highly toxic to humans and the environment.**METHODS:** Biosensor organophosphate pesticides using a single film containing acetylcholinesterase/choline oxidase have been designed using silver-based plasmonic nanoparticles as a colorimetric indicator. In the presence of acetylcholinesterase, acetylcholine is hydrolyzed to choline and acetic acid, then choline oxidase catalyzes the oxidation of choline to hydrogen peroxide and betaine. Hydrogen peroxide reacts with the silver nanoparticles, and the discoloration of the brown solution occurs due to the oxidation of silver+.**FINDINGS:** As a biosensor indicator, silver nanoparticles were extremely accurate, sensitive, and stable over a long period of storage. Transmission Electron Microscope images confirmed the reduction in size of nanoparticles from  $16.82 \pm 4.36$  to  $9.63 \pm 2.29$  nanometers. The analyte profenofos, one of the organophosphate pesticides, inhibits the activity of acetylcholinesterase, thereby reducing the concentration decrease of silver nanoparticles by releasing less hydrogen peroxide. Optimum conditions for biosensors were achieved with a potential of Hydrogen of 7, buffer, and acetylcholinesterase concentrations of 7 and 70 millimolar, respectively, with an incubation time of 5 minutes. Biosensor response showed a linear range at profenofos concentrations of 0.05-2.00 milligrams per liter, with limits of detection and quantization of 0.04 and 0.13 milligrams/liter, respectively. Biosensor also has excellent sensitivity, reproducibility, and stability, with a Relative Standard Deviation of 2.5 percent and a stable response of up to 4 months. Subsequently, using a biosensor in the chilli as a sample resulted in a profenofos level of 0.04 milligrams per liter, making it safe for consumption.**CONCLUSION:** Biosensor measurement outcome aligned with the gas chromatography-mass spectrometry result, which is the accepted standard method for detecting profenofos. Additionally, the proposed biosensor offers several advantages such as ease of use, fast, low-cost, and on-site analysis. Hence, this method is suitable for monitoring and controlling pesticide residues, particularly organophosphate, in agricultural products and the environment.DOI: [10.22034/gjesm.2024.01.04](https://doi.org/10.22034/gjesm.2024.01.04)This is an open access article under the CC BY license (<http://creativecommons.org/licenses/by/4.0/>).

NUMBER OF REFERENCES

31



NUMBER OF FIGURES

6



NUMBER OF TABLES

1

\*Corresponding Author:

Email: [dhony.hermanto@unram.ac.id](mailto:dhony.hermanto@unram.ac.id)

Phone: +62370 646 506

ORCID: [0000-0001-6907-0021](https://orcid.org/0000-0001-6907-0021)

Note: Discussion period for this manuscript open until April 1, 2024 on GJESM website at the "Show Article".

## INTRODUCTION

Pesticide is the most effective solution in controlling pests such as insects, fungi, and weeds due to its effectiveness in killing nuisance organisms (Tudi et al., 2021). The advantages of using pesticides include their ease of use, high success rate, easy to obtain, readily available, and relatively low cost. Their significant role in reducing disease and increasing crop yield has resulted in their widespread use, which, in turn, has led to excessive use of pesticides, including increased dosage, usage frequency, and the use of different types and compositions. Although some pesticides have a low persistence in the environment, they are harmful to humans and the ecosystem due to their high active toxicity (Damalas and Koutroubas, 2016; Mesnage et al., 2014). Consumers are exposed to pesticide residues present in crops, including residues from the soil that are absorbed by the roots and tubers of harvested plants. To ensure food safety, the Indonesian National Standard Agency regulated the maximum allowable limit for pesticide residues in plants, with the concentration of organophosphate residues in vegetables not exceeding 0.05 milligrams per kilogram (mg/kg) (SNI, 2008). Ensuring the safety of agricultural products necessitates the detection of pesticides. Although several analytical methods have been reported in the literature for determining organophosphate pesticides, ultraviolet-visible (UV-Vis) and Fourier Transform infrared (FTIR) spectrophotometry remain the standard analysis methods due to their simplicity (Li et al., 2018; Sahu et al., 2020). However, this method uses reagents that are toxic and not environmentally friendly; this will cause new problems when the measured waste is disposed of into the environment. Other methods such as gas chromatography (GC) (Gaber, 2014), gas chromatography-mass spectrometry (GC-MS) (Yang et al., 2018), high-performance liquid chromatography (HPLC) (Rajput et al., 2018), high-performance thin layer chromatography (HPTLC) (Hussain et al., 2020), and liquid chromatography-mass spectrometry (LC-MS) (Stachniuk et al., 2017) have also been commonly used in determining organophosphate because of their efficiency. However, these methods require relatively long preparation, skilled labor, and sophisticated and expensive equipment. To overcome this problem, enzyme-based biosensors have been developed as an alternative method. For example, various types of cholinesterase biosensing agents were used to measure

the inhibition of enzyme activity due to the addition of pesticide analytes in enzymatic reactions (Kuswandi et al., 2008). Acetylcholinesterase (AChE) biosensor has been proposed for detecting organophosphate pesticides using potentiometric (Mashuni et al., 2022), amperometric (Zhang et al., 2019), and optical transducers (spectrometry or fluorometric) (Yan et al., 2019; Shah et al., 2021). The optical sensor, especially colorimetric sensors employ an indicator for detecting the pesticide, such as a zwitterionic polymer (Zhu et al., 2008) and bromothymol blue (Kuswandi et al., 2008) but these indicators are toxic and have a limited range of action due to their dependence on the potential of hydrogen (pH). The weakness can be overcome by using silver nanoparticles (AgNPs) as a colorimetric detector. AgNP has unique properties, such as a high-sensitivity SPR spectral effect, making it a colored solution. (Loisea et al., 2019). The optical biosensor for detecting pesticides is proposed to utilize the SPR of AgNPs. The sensor mechanism is based on AChE inhibition due to the presence of analytes (Kaur and Singh, 2020). AChE enzyme hydrolyzes acetylcholine (ACh) to produce choline (Ch) and acetic acid in the presence of oxygen and water is oxidized to betaine and hydrogen peroxide ( $H_2O_2$ ) through the catalytic activity of choline oxidase (ChO) (Bodur et al., 2021). Hydrogen peroxide spontaneously undergoes a redox reaction in the presence of colloidal AgNPs in an aqueous system (Sequeira, 2021; Tagad et al., 2013), where the AgNPs serve as an indicator. By combining these two enzymes with a colloidal AgNPs coupled biosensor system, biosensors are being developed. As the mechanism of action of the biosensor developed is based on the activity of the AChE enzyme, pesticides with a mechanism of action to inhibit AChE can be detected using this biosensor, such as organophosphate and carbamate pesticide. In this study, prefonofos (an organophosphate) is used as an analyte that inhibits AChE activity, while the enzymes AChE and ChO were trapped in one film by a simple procedure without further chemical modifications. Subsequently, enzyme immobilization on a suitable matrix can maintain its activity and increase its resistance to changes in reaction condition such as pH and temperature (Hermanto et al., 2020). The film was placed into colloidal AgNPs with added substrate and analytes, and measurements were carried out in a batch system. The validation of biosensor results compared to GC method was described. The application of biosensor

in determining profenofos in the real sample also was conducted. Therefore, this study aimed to develop a biosensor for organophosphate determination and was carried out in Mataram, West Nusa Tenggara, Indonesia in 2023.

## MATERIALS AND METHODS

### Chemicals

AChE from *Electrophorus electricus* (EC 3.1.1.7, type Type VI-S, 200 units/milliliter, units/mL), ChO from *Alcaligenes sp.* (EC 1.1.3.17, the activity of  $\geq 10$  units/mL), ACh chloride ( $\geq 99$  percent: %, TLC), sodium alginate from brown alga (300-400 centipoise, cP), chitosan from crab shell (95% deacetylated), and profenofos (Sigma Pestanal®) were obtained from Sigma Aldrich (St. Louis, Missouri, USA). The 2-pyrimidine aldoxime methiodide (2-PAM) was purchased from Merck. All chemicals were of analytical grade and used as received without further purification, and double distilled water was used to prepare the solutions.

### Preparation of film and immobilization procedure

Based on the previous study, a solid support film for the immobilization of AChE and ChO was prepared by mixing both chitosan and alginate hydrosols (Hermanto *et al.*, 2020). The alginate-chitosan hydrosol 3 microliter ( $\mu\text{L}$ ) was added to 1  $\mu\text{L}$  Tris hydrochloric acid (HCl) buffer (pH 6.5). The buffer mixture was added to 10  $\mu\text{L}$  of the bi-enzyme mixture. The prepared bi-enzyme mixture consisted of AChE (10 microliters:  $\mu\text{L}$ , 200.0 units/mL) and ChO (200  $\mu\text{L}$ , 10.0 units/mL) at a 1:1 enzyme ratio in 40  $\mu\text{L}$  of Tris-HCl buffer solution (pH 7.0). Furthermore, the enzyme

activity was maintained using a Tris-HCl buffer in a modified hydrosol process. The mixture was flattened immediately using a magnetic stirrer (300 rotations per minute (rpm) for 10 seconds, then stored for the aging process for 72 hours (h) and 4 degree Celsius ( $^{\circ}\text{C}$ ). The produced film was stored in a closed container at  $4^{\circ}\text{C}$  until used (Hermanto *et al.*, 2022).

### Preparation colloidal AgNPs

The proposed method for preparing colloidal AgNPs is a conventional synthesis method using green electrolysis, as described by Hermanto, *et al.* (2023). The synthesized colloidal AgNPs were further separated and purified by centrifugation (Tomy Centrifuge MDX 310, Japan) at 12,000 rpm, followed by freeze drying (Freeze dryer Alpha 1-2LDplus with RZ 2.5 vacuum pump, Germany) before being used as an indicator biosensor.

### Fabrication optical biosensor

A single alginate-chitosan-immobilized AChE/ChO film was cut into a cuvette size (10  $\times$  45 millimeters (mm) and carefully placed into the cuvette (Fig. 1). Furthermore, 2 mL of colloidal AgNP was added to the cuvette (10 mg of separated AgNP was taken and redispersed using 1 L double distilled water). The measurements were carried out using atomic absorption spectrophotometer (AAS) Thermo scientific iCE3000 USA, obtaining an Ag concentration of 10.38 milligram/liter (mg/L). Next, 1 mL of ACh chloride (substrate) was added to the cuvette. Finally, at the same time, 1 mL of organophosphate pesticide (profenofos pesticide) was also added to the cuvette

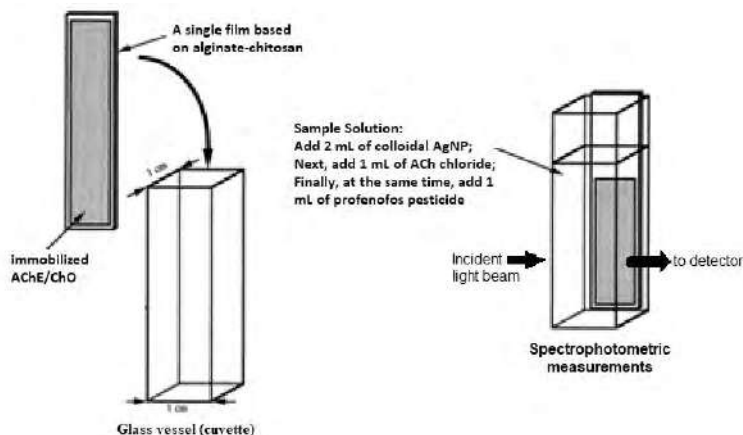


Fig. 1: Biosensor design

with various concentrations to make a standard curve. Incubation for 30 minutes (min) was required to complete the inhibition reaction. A blank solution was prepared using the above procedure without pesticide profenofos.

#### Measurement procedure

The absorbance of colloidal AgNPs as indicator of biosensor was then measured using UV-Vis Spectrophotometer (Spectrophotometer 7809, Labo-hub, China). The increase in the concentration of profenofos pesticide is proportional to the increase in inhibition. It affected the intensity of the SPR absorbance of the AgNPs colloid due to the redox reaction between hydrogen peroxide (product of the enzyme-substrate reaction) and AgNPs. The response of the optical biosensor is shown as a calibration curve, in which there is a linear correlation between the concentration of profenofos and the SPR intensity of colloidal AgNPs.

#### Determination with GC-MS methods

For comparison, GC-MS detection method (GC-MS QP210 Ultra, Shimadzu) equipped with an RTX®-5MS fused-silica capillary column (methyl polysiloxane type containing 5% Diphenyl and 95% Dimethyl Polysiloxane, length 30 meters (m) × 0.25 mm id. × 0.25 micrometer (µm) film thickness in static phase) was also used as a reference method for determining profenofos pesticide in actual samples. High-purity helium carrier gas was used as the mobile phase (1.5 mL/min). The automatic injection process (Auto sampler carousel, AOC, Ahimadzu type) in GC-MS device was performed by injecting 1 µL at an injection temperature of 250 °C. In contrast, the interface

temperature and the ion source were set at 300 °C (Alen *et al.*, 2016). Identifying profenofos pesticide based on peak chromatograms was performed, then its concentrations were determined using a calibration curve of peak area versus profenofos concentration.

#### Determination of profenofos in real sample

A real sample of Chilli (*Capsicum frutescens* L.) was obtained from the local market (Pagesangan, Mataram-Indonesia). A total of 100 g of crushed chilli was mixed with 50 mL of pH 7 Tris-HCl buffer under stirring conditions. The mixture was filtered and centrifuged at 8000 rpm for 5 min. The supernatant was separated and analyzed for the profenofos content.

## RESULTS AND DISCUSSION

#### Biosensor scheme

In this study, an optical biosensor was developed for detecting organophosphate pesticides based on a single film of alginate-chitosan modified with silver-based plasmonic nanoparticles. For this purpose, a simple alginate-chitosan film was prepared by immobilizing the double enzymes (AChE and ChO). The scheme of the enzymatic reaction of AChE and ChO enzymes immobilized on film with ACh is shown in Fig. 2. First, the hydrolysis reaction (reaction with water, H<sub>2</sub>O) of ACh to Ch and acetic acid occurs with AChE as a biocatalyst (Kuswandi *et al.*, 2008; 2021). Under the role of ChO, Ch released is oxidized to betaine. The ChO prosthetic group, namely Flavin Adenine Dinucleotide (FAD), is reduced to 1,5-dihydro-FAD (FADH<sub>2</sub>) by accepting electrons. This reaction is reversible. In the presence of oxygen (O<sub>2</sub>) as the electron acceptor, FADH<sub>2</sub> is oxidized to FAD. Therefore, the enzyme returns to its original form, while the oxygen as the electron

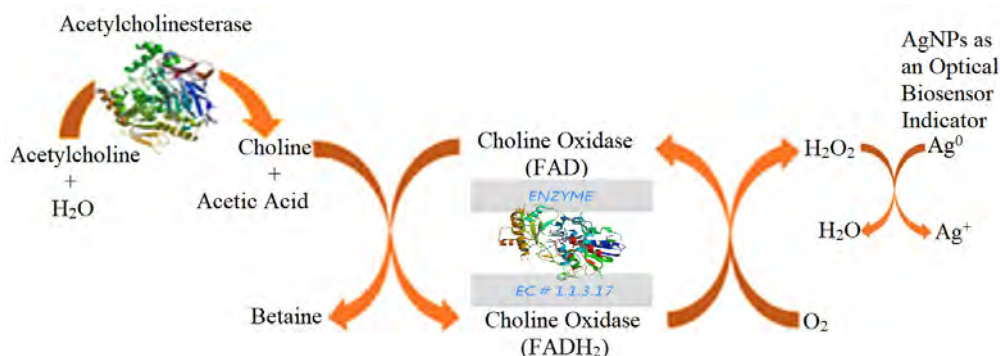


Fig. 2: Scheme of enzymatic reaction (AChE/ChO)

acceptor is reduced to hydrogen peroxide ( $H_2O_2$ ) (Bodur *et al.*, 2021). The hydrogen peroxide produced by this reaction enters the aqueous system with colloidal AgNPs. Hydrogen peroxide is oxidized into water molecules, while AgNPs as a biosensor indicator will decrease in concentration because silver ( $Ag^0$ ) is reduced to ionic silver ( $Ag^+$  ion) (Sequeira, 2021; Tagad *et al.*, 2013). The determination of ACh can be carried out by measuring changes in the intensity of the SPR absorbance of the AgNPs. The presence of profenofos (an organophosphate pesticide) as an inhibitor of ACh hydrolysis of the enzymatic reaction in Fig. 2 caused a reduction in the amount of  $H_2O_2$  released, and hence the discolouration of AgNP was reduced compared to the absence of profenofos.

In this study, a color change from brown to pale yellow causes a decrease in the intensity of the SPR AgNPs signal. This aspect is important because the operating range of AgNPs as an optical biosensor indicator closely matches the changes in hydrogen peroxide released in enzymatic reactions. On the other hand, the colloidal AgNPs are evenly distributed in the aqueous system to allow easy access to the enzymatic reaction products, resulting in the high sensitivity of the optical biosensor indicator, which is also responsible for reaction inhibition (the presence of organophosphate pesticide analytes). Besides reducing the SPR-AgNP signal intensity, the presence of hydrogen peroxide associated with the enzyme-substrate reaction leads to the erosion of the AgNP. This erosion results from the redox reaction, and hydrogen peroxide is reduced to a water molecule while AgNP is oxidized to  $Ag^+$ . It is demonstrated in Transmission Electron Microscope

(TEM) images of AgNPs before and after reacting with hydrogen peroxide associated with the enzyme-substrate reaction (Fig. 3).

In this study, Fig. 3a shows the TEM images of the AgNPs prepared. As shown above, nanoparticles are spherical with a quasi-uniform size, and the estimated mean diameter is  $16.82 \pm 4.36$  nanometer (nm) (Hermanto *et al.*, 2023). Fig. 3b shows a TEM image of an AgNP undergoing oxidation due to interaction with hydrogen peroxide. Nanoparticles have a quasi-uniform sphere size but decreasing size; In the mean distribution histogram, its diameter is  $9.63 \pm 2.29$  nm. Subsequently, TEM images confirm that the AgNPs before and after the reaction with hydrogen peroxide are spherical. This spherical AgNP allows all sides to interact well and spontaneously in the presence of hydrogen peroxide, and it can be used as a biosensing agent.

#### Optimization of experimental parameters

Before the analytical properties of biosensors can be determined, various parameters must be optimized through a series of preliminary investigations. Table 1 shows some of the experimental parameter ranges investigated and their optimum values.

The investigated experimental parameters influenced the enzymatic reaction, namely pH, buffer and substrate concentration (ACh), and incubation time. Tris-HCl buffer was utilized for this system, while phosphate buffer was avoided because of its interaction with AChE because it has the potential to compete with profenofos pesticide, which has a phosphate group. It was found that the buffer

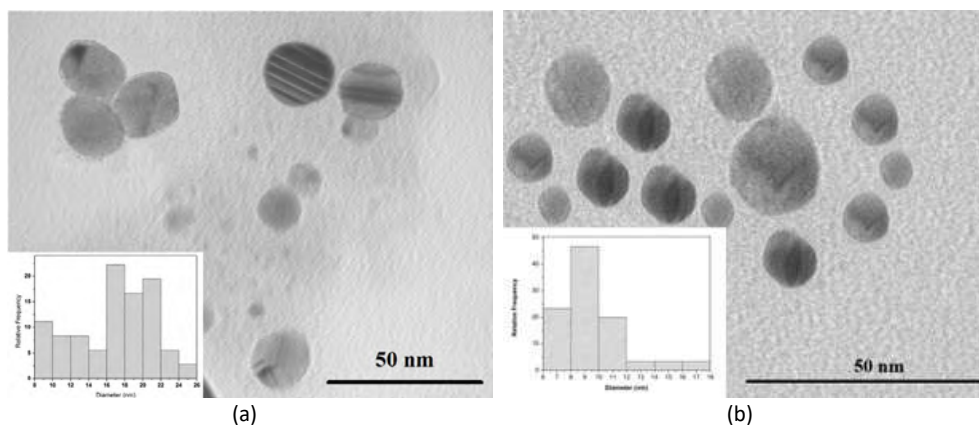


Fig. 3: TEM images of AgNPs (a) before (b) after reacting with hydrogen peroxide released in enzymatic reactions (Hermanto *et al.*, 2023)

concentration was 7 millimolar (mM), and pH 7 was the optimum buffer solution; this was used for further measurement. The enzymatic reaction proceeds efficiently when the concentration of ACh as a substrate is proportional to the activity of AChE enzyme. In order to achieve good reproducibility, the substrate concentration was optimized in the range of 10 to 100 mM ACh. The concentration of 70 mM is the optimum ACh concentration and is used for further measurements. The chemical environment around the enzyme influences biosensor response. In this case, the alginate-chitosan film act as the enzyme immobilization matrix. The substrate must diffuse and penetrate the film to interact with the enzyme, and a measurable response change was obtained. Incubation time to ensure the optimal enzymatic reaction was achieved and induced AgNPs color change. In this study, the reaction incubation time was 5 min.

#### The response of optical biosensor

The dynamic response of the profenofos biosensor was determined by changes in the SPR absorbance signal before and after inhibition at 425 nm under optimal conditions (Fig. 4a). The response of plasmonic-based biosensor to AChE and ChO activity

due to the presence of the profenofos pesticide is plotted as a calibration curve. The biosensor system detected a series of profenofos pesticide solutions at concentration intervals of 0.05–2.00 mg/L with three replicates (Fig. 4b). Samples containing profenofos interacted with AChE resulted in an inhibitory response to ACh production. Regeneration of inhibited enzyme activity was carried out by adding the 2-PAM solution to restore immobilized enzyme activity (Kuswandi and Suwandari, 2007). However, inhibited AChE regeneration cannot restore 100% of its activity due to the strong interaction between AChE and profenofos pesticide (as a competitive inhibitor). Therefore, it is considered an irreversible reaction, and regeneration can only be carried out on film. On the other hand, it is difficult to regenerate AgNPs as an indicator of optical biosensors due to the impossibility of obtaining their original shape and size. From Fig. 4a, it is known that the increase in the concentration of profenofos pesticide is proportional to the increase in SPR absorbance. Fig. 4b shows the relationship between the concentration of profenofos pesticide and SPR absorbance in a standard curve (linear plot).

A calibration curve was constructed by evaluating the level of inhibition against the profenofos pesticide

Table 1: Optimization of experimental parameters

Experimental parameters	Value range	Optimal value
The concentration of buffer (mM)	1 – 10	7
pH	6 – 8	7
ACh concentration (mM)	10 – 100	70
Incubation time (min)	1 – 10	5

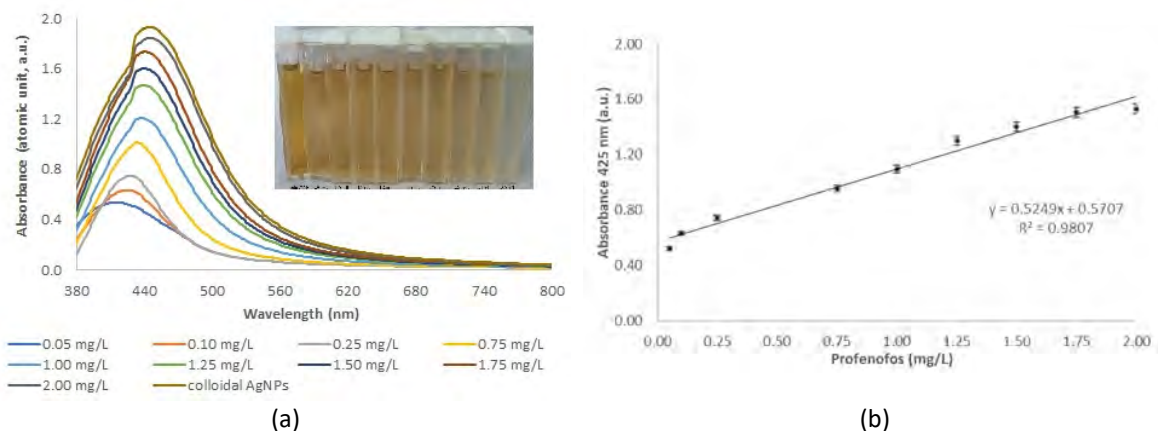


Fig. 4: SPR spectra of AgNPs as a biosensor detection system for profenofos at various concentrations (a); calibration curve (b)

concentration. A linear correlation ( $r$ ) of 0.99 was obtained for the working range of profenofos pesticide concentrations from 0.05 to 2.00 mg/L, as shown in Fig. 4b. A flat biosensor response was obtained for higher concentrations of pesticide profenofos, indicating that the response is approaching the optimal maximum SPR uptake of AgNP. Since the maximum concentration of analyte in the sample that falls within the linear range is 2.00 mg/L profenofos, for samples that provide absorbance above the linear range, dilution is required until the concentration is within the linear range. The limits of detection (LOD,  $3\sigma$ ) and limits of quantization (LOQ,  $10\sigma$ ) of the calculated results were 0.04 mg/L and 0.13 mg/L of profenofos pesticide, respectively. Determination of the pesticide chlorpyrifos by a previous study (Kuswandi *et al.*, 2008) through a fiber-optic biosensor based on AChE and bromothymol blue on a single sol-gel film was able to detect 0.04 mg/L of chlorpyrifos with a concentration range of 0.05-2.00 mg/L. This value represents the same LOD and linear range as this proposed biosensor. Another visible sensor that uses poly(sulfobetaine methacrylate)-coated paper for detecting profenofos has a higher detection limit of 4.891 mg/L (Zhu *et al.*, 2023). The proposed biosensor is better and allows the detection of profenofos at the maximum residue level (0.05 mg/kg) approved by the Indonesian government by Menkes and Mentan (1996) and SNI (2008). As a comparison for determining profenofos using HPLC in previous studies (Mahajan and Chatterjee, 2018), it showed a detection limit of 0.104 mg/L. The developed biosensor provides better analytical features with a lower measurement limit of 0.04 mg/L. AgNP as an indicator offered better sensitivity than the previous indicator, which used poly(sulfobetaine methacrylate) (Zhu *et al.*, 2023) and bromothymol blue (Kuswandi *et al.*, 2008) in visual/optical sensors for pesticide determination. It is indicated by the higher slope value of the change in pesticide absorbance per unit concentration, and the higher the slope value, the more sensitive the sensor. In this study, the slope was 0.5249 a.u L/mg, while the slope in the previous study was 0.0085 and 0.0331 a.u L/mg, respectively. In addition, AgNPs are highly accurate and stable over a long storage period (Hermanto *et al.*, 2023). In fabricating enzyme-based optical biosensors, recovery of inhibited enzymes is an advantage, and it is one of the purposes of immobilizing enzymes, repeatedly used, enabling biosensors to be more economical,

effective, and practical in handling. The phosphate group of profenofos has a strong interaction with AChE, and AChE exposed to profenofos has an ester bond between the phosphate and serine groups on AChE, making it difficult to restore its activity (competitive inhibitor) and repeated reactivation using Tris-HCl buffer solution and ACh was not achieved. However, reactivation using 1 mM 2-PAM can restore AChE activity effectively due to its strong nucleophilic character towards the electrophilic phosphorus atom of phosphorylated AChE, and phosphorus attached to AChE is released, producing a free and active form of AChE (Kuswandi and Suwandari, 2007). Then, washing with Tris-HCl buffer solution spontaneously restored ChO activity effectively. Biosensor reproducibility is another important analytical performance. The reproducibility of silver-based plasmonic nanoparticles proposed for biosensors is expressed as Relative Standard Deviation (RSD) or the Coefficient of Variation (CV) of determining the response of biosensor at a concentration of 0.05 to 2.00 mg/L with 3 repetitions on a same single film containing AChE/ChO. The reproducibility of biosensors (RSD) was an average of 2.5% (Fig. 4b), meaning the reproducibility was good. The repeated use of film from this biosensor produces a good response after being reactivated, which is expressed as the stability of the biosensor. The stability of this biosensor is good, and even after being used repeatedly for a week for the detection of profenofos pesticide, this biosensor can still provide a sensor response of about 90% of the initial response, as long as a film containing AChE/ChO is stored at 4 °C. Fig. 5 shows that sensor response can last up to 4 months, after which it gradually decreases, and the acceptable biosensor response  $\geq 60\%$  of the initial response. At four months of the storage period, namely the seventh measurement, biosensor response was reduced to 60%, probably due to the leaching of AChE/ChO from the film during film washing, which was carried out during the enzyme reactivation process in the film using a solution of 2-PAM, in this case, reactivation was carried out six times. In these conditions, film on biosensors can no longer be used to determine profenofos, and this result is better than the previous study (Kuswandi *et al.*, 2008). Considering the use of low-cost material for synthesizing film and AgNP, the production cost per biosensor unit is 5 USD. A technique of immobilizing the enzyme on film facilitates the reuse of the enzyme, offering a biosensor production

Biosensor for organophosphate determination

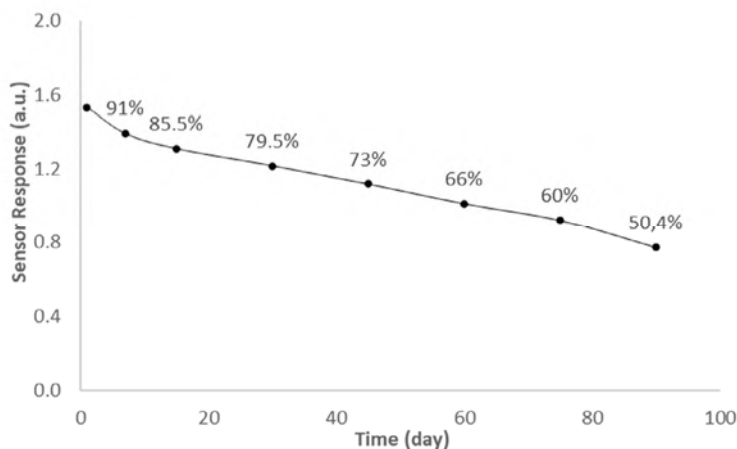


Fig. 5: Decrease in sensor response as a function of time, measurement using 2 mg/L profenofos

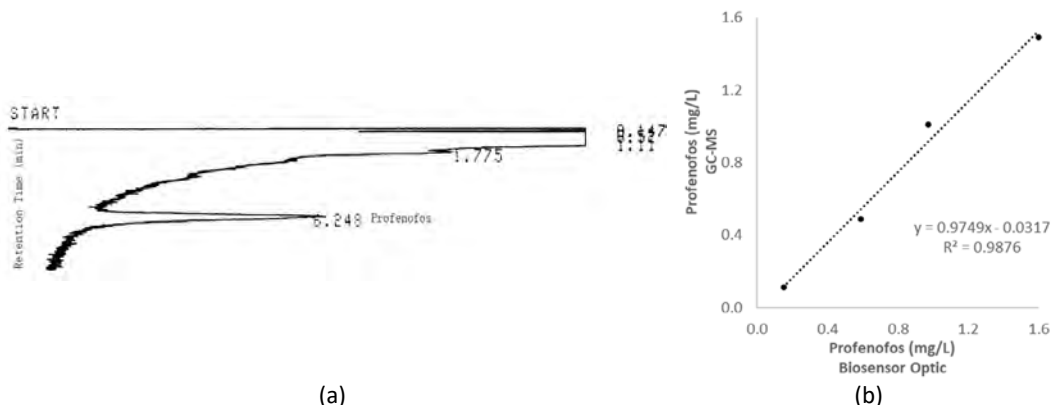


Fig. 6: Chromatogram of profenofos (a); and the linearity relationship of profenofos pesticide concentrations were measured using an optical biosensor and GC-MS as a reference method (b).

cost reduction of about 80%, and per unit film can be measured up to 7 times (6 times enzyme reactivation).

Validation of analytical methods is the evaluation of specific parameters using laboratory experiments to demonstrate that they meet the requirements for their use. Optical biosensor validation uses GC-MS as a standard method to determine profenofos pesticide in real samples. Subsequently, the samples were analyzed using both methods, in which samples spiked with profenofos were made in four different concentrations, 0.1, 0.5, 1.0, and 1.5 mg/L, with three times repetition. Fig. 6 shows the linear relationship between the measurements of profenofos pesticide using both methods.

Fig. 6a is the chromatogram of the profenofos

pesticide with a retention time as a qualitative parameter of about 6.248 min. Meanwhile, the peak area parameter of the chromatogram was used quantitatively by plotting it in the linear regression equation of the profenofos calibration curve to obtain the profenofos residue level in the sample. Based on Fig. 6b, the linear regression analysis shows a linear relationship ( $y=1.1637x-0.1795$ ), with a good agreement between the two methods ( $R^2 = 0.9876$ ). The regression coefficient is  $\approx 1$ , meaning there is no significant difference when comparing the optical biosensor method and GC-MS in determining profenofos pesticide. It is supported by the analysis of the slope of the linear regression curve of 0.9749 (close to the ideal value of 1.0). The measurement

results of the proposed optical biosensor, therefore, agree with the reference method (GC-MS), and the determination of the profenofos content in chilli as a real sample was determined using the proposed biosensor. The profenofos level in chilli was 0.04 mg/L; this value is below the maximum residue threshold permitted by the Government of Indonesia, making chilli safe for consumption. Compared to conventional method such as GC-MS and HPLC, the proposed biosensor is cheaper for fabricating and maintaining the apparatus and sample preparation, more accessible, faster, and allows on-site analysis. The reusability of biosensors can be achieved by using film as an immobilizing matrix for AChE/ChO enzyme and reactivation process. In addition, this method minimizes expensive solvents such as those used in HPLC analysis. Therefore, the developed biosensor is suitable for monitoring and controlling pesticide levels in agricultural products and the environment to ensure the safety of its consumption and minimize the negative impact of pesticides on non-target living things and the environment.

## **CONCLUSION**

A successful optical biosensor has been developed for detecting organophosphate pesticides based on an alginate-chitosan film containing AChE and ChO. In this system, the alginate-chitosan single film was used as a matrix of double enzymes (AChE and ChO), and silver-based plasmonic nanoparticles serve as a colorimetric indicator. As an indicator, the excellences of AgNP are highly accurate, sensitive, and stable over a long storage period. Silver nanoparticles are oxidized to silver ions in the presence of hydrogen peroxide produced by enzyme activity. A decrease in the concentration of nanoparticles is indicated by the fading of the solution color from brown to pale yellow in the system. Profenofos inhibits the ACh hydrolysis, reducing the amount of  $H_2O_2$  released. Therefore, the discoloration of AgNP was reduced compared to the absence of profenofos, and the increase in the concentration of profenofos pesticide was proportional to the increase in SPR absorbance of AgNP. The size reduction of AgNPs was confirmed by TEM images from  $16.82 \pm 4.36$  to  $9.63 \pm 2.29$  nm due to its reaction with  $H_2O_2$ . The optimum biosensor performance was at 7 mM buffer concentration, pH 7, 70 mM ACh concentration, and 5 min incubation time. Biosensor response due to

inhibition of profenofos showed a linear relationship with the concentration of profenofos in the range of 0.05 to 2.00 mg/L, with LOD 0.04 mg/L and LOQ 0.13 mg/L. The proposed organophosphate biosensor also has excellent sensitivity, reproducibility, and stability, with RSD of 2.5% and a stable response of about 4 months. The method validation through GC-MS analysis as a standard method in profenofos concentration of 0.1 to 1.5 mg/L shows good agreement between the results of the two methods. Applying biosensor in chilli as a sample gives profenofos level of 0.04 mg/L, and therefore it is safe for consumption. The advantages of biosensor include its simplicity, ease, cheapness, short time, and on-site analysis, making it suitable for routine analysis to ensure the safety of consumption of agricultural products and reduce the negative impact of pesticides on the environment. The film containing AChE/ChO enzymes must be stored at 4 °C when not in use to ensure the performance of the biosensor remains good for on-site detection of organophosphate pesticide.

## **AUTHOR CONTRIBUTION**

D. Hermanto performed the study conceptualization, methodology and writing-original draft. N. Ismillayli, performed the validation, data curation and the study supervision. R. Wirawan worked on the study software, resources and methodology. S.R. Kamali has done the study investigation, methodology and visualization. H. Muliastari investigated the formal analysis and project administration. All authors contributed to the study writing, review and editing.

## **ACKNOWLEDGEMENT**

The authors thank the Kementerian Pendidikan, Kebudayaan, Riset dan Teknologi Republik Indonesia (Kemendikbudristek RI) for the National Competitive Basic Research Program [decree number: 2349/UN18.L1/PP/2023].

## **CONFLICT OF INTEREST**

The author declares that there is no conflict of interests regarding the publication of this manuscript. In addition, the ethical issues, including plagiarism, informed consent, misconduct, data fabrication and/or falsification, double publication and/or submission, and redundancy have been completely observed by the authors.

**OPEN ACCESS**

©2024 The author(s). This article is licensed under a Creative Commons Attribution 4.0 International License, which permits use, sharing, adaptation, distribution and reproduction in any medium or format, as long as you give appropriate credit to the original author(s) and the source, provide a link to the Creative Commons license, and indicate if changes were made. The images or other third-party material in this article are included in the article's Creative Commons license, unless indicated otherwise in a credit line to the material. If material is not included in the article's Creative Commons license and your intended use is not permitted by statutory regulation or exceeds the permitted use, you will need to obtain permission directly from the copyright holder. To view a copy of this license, visit: <http://creativecommons.org/licenses/by/4.0/>

**PUBLISHER'S NOTE**

GJESM Publisher remains neutral with regard to jurisdictional claims in published maps and institutional affiliations.

**ABBREVIATIONS**

%	Percent	FAD	Flavin adenine dinucleotide
°C	Degree Celsius	FADH <sub>2</sub>	1,5-dihydro-FAD
μ	Micro	FTIR	Fourier transform infrared
μg	Microgram	GC	Gas chromatography
μL	Microliter	GC-MS	Gas chromatography combined with mass spectrometry
AAS	Atomic Absorption Spectrophotometer	h	Hour
ACh	Acetylcholine	H <sub>2</sub> O	Dihydrogen monoxide or water
AChE	Acetylcholinesterase	H <sub>2</sub> O <sub>2</sub>	Dihydrogen dioxide or hydrogen peroxide
Ag <sup>+</sup>	Ionic silver	HCl	hydrochloric acid
Ag <sup>0</sup>	Silver	HPLC	High-performance liquid chromatography
AgNP	Silver nanoparticle	HPTLC	High-performance thin layer chromatography
AOC	Auto sampler carousel	kg	Kilogram
a.u.	Atomic unit	L	Liter
C	Celsius	LC-MS	Liquid chromatography combined with mass spectrometry
Ch	Choline	LOD	Limits of detection
ChO	Choline oxidase	LOQ	Limits of quantization
cP	Centipoise	MDX	Magnetically-driven sealless circulator
CV	Coefficient of variation	m	Meter
EC	The Enzyme Commission number	mm	Millimeter
		mg	Milligram
		mg/kg	milligram per kilogram
		mL	Milliliter
		mg/L	Milligram per liter
		min	Minute
		mM	Millimolar
		Menkes	Menteri Kesehatan
		Mentan	Menteri Pertanian
		nm	Nanometer
		O <sub>2</sub>	Oxygen
		PAM	2-pyrimidine aldoxime methiodide
		pH	Potential of hydrogen
		QP	Quadrupole
		R	Linier Regression
		RSD	Relative standard deviation
		RTX	Column GC, Fused silica nonpolar phase
		RZ	Rotary vane pump

<i>Rpm</i>	Rotations per minute
<i>SNI</i>	Standar Nasional Indonesia
<i>SPR</i>	Surface plasmon resonance
<i>TEM</i>	Transmission electron microscopes
<i>TLC</i>	Thin layer chromatography
<i>USA</i>	United States of America
<i>UV</i>	Ultraviolet
<i>Vis.</i>	Visible

## REFERENCES

- Alen, Y.; Adriyani, F.; Suharti, N.; Nakajima, S.; Djamaan, A., (2016). Determination of profenofos pesticide residue in tomato (*Solanum lycopersicum* L.) using gas chromatography technique. *Der Pharmacia Let.*, 8(8): 137–141 (5 pages).
- Bodur, O.; Dinc, S.; Özmen, M.; Arslan, F., (2021). A sensitive amperometric detection of neurotransmitter acetylcholine using carbon dot-modified carbon paste electrode. *Biotechnol. Appl. Biochem.*, 68(1): 20–29 (10 pages).
- Damalas, C.A.; Koutroubas, S.D., (2016). Farmers' exposure to pesticides: Toxicity types and ways of prevention. *Toxics*. 4(1): 1–10 (10 pages).
- Gaber, S., (2014). Developing a gas chromatography-flame ionization detector analytical method for the analysis of organochlorine pesticides residues. *World Appl. Sci. J.*, 31(1): 1911–1916 (6 pages).
- Hermanto, D.; Ismillayli, N.; Irmawanti, I.; Fathulloh, I.; Cahyani, D.N.; Zuryati, U.K.; Muliastari, H.; Wirawan, R., (2023). Electrochemically synthesized biogenic silver nanoparticles using green tea extract as a promising antioxidant. *Karbala Int. J. Mod. Sci.*, 9(1): 80–88 (9 pages).
- Hermanto, D.; Mudasir, M.; Siswanta, D.; Kuswandi, B.; Ismillayli, N., (2019). Polyelectrolyte complex (PEC) of the alginate-chitosan membrane for immobilizing urease. *J. Math. Fund. Sci.*, 51(3): 309–319 (11 pages).
- Hermanto, D.; Mudasir, M.; Siswanta, D.; Kuswandi, B.; Ismillayli, N., (2020). The preparation and characterization of alginate-chitosan membranes as solid support for btb and urease entrapment. *J. Molekul*, 15(1): 40–47 (8 pages).
- Hermanto, D.; Mudasir, M.; Siswanta, D.; Kuswandi, B.; Ismillayli, N., (2022). Optical fiber mercury biosensor based on immobilized urease and bromothymol blue onto the alginate-chitosan membrane in the flow-system. *Kuwait J. Sci.*, 49(1): 1–13 (13 pages).
- Hussain, M.; Aftab, K.; Iqbal, M.; Ali, S.; Rizwan, M.; Alkahtani, S.; Abdel-Daim, M., (2020). Determination of pesticide residue in Brinjal sample using HPTLC and developing a cost-effective method alternative to HPLC. *J. Chem.*, 2020: 1–12 (12 pages).
- Kaur, J.; Singh, P., (2020). Enzyme-based optical biosensors for organophosphate class of pesticide detection. *Phys. Chem.*, 22(27): 15105–15119 (15 pages).
- Kuswandi, B.; Suwandari, N.W., (2007). A Simple and sensitive flow injection optical fibre biosensor based on immobilised enzyme for monitoring of pesticides. *Sens. Transducers*, 76(2): 978–990 (13 pages).
- Kuswandi, B.; Fikriyah, C.; Gani, A., (2008). An optical fiber biosensor for chlorpyrifos using a single sol-gel film containing acetylcholinesterase and bromothymol blue. *Talanta*, 74(4): 613–618 (6 pages).
- Kuswandi, B.; Taufikurrohman, M.; Nugraha, A., (2021). Communication—An optical fiber biosensor based on a lab-on-a-tip approach for user-friendly carbosulfan detection in vegetable samples. *J. Electrochem Soc.*, 168(7)(077502): 1–5 (5 pages).
- Li, Y.; Luo, Q.; Hu, R.; Chen, Z.; Qiu, P., (2018). A sensitive and rapid uv–vis spectrophotometry for organophosphorus pesticides detection based on Ytterbium (Yb<sup>3+</sup>) functionalized gold nanoparticle. *Chinese Chem. Lett.*, 29(12): 1845–1848 (4 pages).
- Loiseau, A.; Asila, V.; Boitel-Aullen, G.; Lam, M.; Salmain, M.; Boujday, S., (2019). Silver-based plasmonic nanoparticles for and their use in biosensing. *Biosens.*, 9(2)(78): 1–39 (39 pages).
- Mahajan, R.; Chatterjee, S., (2018). A simple HPLC–DAD method for simultaneous detection of two organophosphates, profenofos and fenthion, and validation by soil microcosm experiment. *Environ. Monit. Assess.*, 190(327): 1–8 (8 pages).
- Mashuni, M.; Ritonga, H.; Jahiding, M.; Rubak, B.; Hamid, F.H., (2022). Highly sensitive detection of carbaryl pesticides using potentiometric biosensor with nanocomposite Ag/r-graphene oxide/chitosan immobilized acetylcholinesterase enzyme. *Chemosens*. 10(4)(138): 1–9 (9 pages).
- Menkes; Mentan, (1996). Surat keputusan bersama menteri kesehatan dan menteri pertanian republik Indonesia No. 881/Menkes/SKB VIII/1996, N.771/Kpts/Tp.270/8/1996 tentang batas maksimum residu pestisida pada hasil pertanian (maximum limit of pesticide residues available on the agricultural): 1–43 (43 pages).
- Mesnage, R.; Defarge, N.; Spiroux De Vendômois, J.; Séralini, G., (2014). Major pesticides are more toxic to human cells than their declared active principles. *BioMed. Res. Int.*, 2014(179691): 1–8 (8 pages).
- Rajput, S.; Kumari, A.; Arora, S.; Kaur, R., (2018). Multi-residue pesticides analysis in water samples using reverse phase high performance liquid chromatography (RP-HPLC). *MethodsX*, 5: 744–751 (7 pages).
- Sahu, D.K.; Rai, J.; Rai, M.K.; Banjare, M.K.; Nirmal, M.; Wani, K.; Sahu, R.; Pandey, S.G.; Mundeja, P., (2020). Detection of flonicamid insecticide in vegetable samples by UV–Visible spectrophotometer and FTIR. *Results Chem.*, 2: 100059–100070 (12 pages).
- Sequeira, C., (2021). Silver Nanoparticles for Hydrogen Peroxide Sensors. *Biomed. J. Sci. Tech. Res.*, 40(4): 32438–32443 (6 pages).
- Shah, M.M.; Ren, W.; Irudayaraj, J.; Sajini, A.A.; Ali, M.I.; Ahmad, B., (2021). Colorimetric detection of organophosphate pesticides based on acetylcholinesterase and cysteamine capped gold nanoparticles as nanozyme. *Sens.*, 21(23): 1–12 (12 pages).
- SNI, (2008). Batas maksimum residu pestisida pada hasil pertanian (maximum limit of pesticide residues available on the agricultural): 1–147 (147 pages).
- Stachniuk, A.; Szmagara, A.; Czaczo, R.; Fornal, E.S., (2017). LC-MS/MS determination of pesticide residues in fruits and vegetables. *J. Environ. Sci. Health., Part B*, 52(7): 446–457 (12 pages).
- Tagad, C.K.; Kim, H.U.; Aiyyer, R.C.; More, P.; Kim, T.; Moh, S.H.; Kulkarni, A.; Sabharwal, S.G., (2013). A sensitive hydrogen peroxide optical sensor based on polysaccharide stabilized silver nanoparticles. *RSC Adv*, 3(45): 22940–22943 (4 pages).

- Tudi, M.; Ruan, H.D.; Wang, L.; Lyu, J.; Sadler, R.; Connell, D.; Chu, C., (2021). Agriculture development, pesticide application and its impact on the environment: Review. *Environ. Res. Public Health*, 18(1112): 1–23 (23 pages).
- Yan, X.; Kong, D.; Jin, R.; Zhao, X.; Li, H.; Liu, F.; Lin, Y.; Lu, G., (2019). Fluorometric and colorimetric analysis of carbamate pesticide via enzyme-triggered decomposition of Gold nanoclusters-anchored MnO<sub>2</sub> nanocomposite. *Sens. Actuators, B*, 290: 640–647 (8 pages).
- Yang, X.; Imasaka, T.; Imasaka, T. (2018). Determination of pesticides by gas chromatography combined with mass spectrometry using femtosecond lasers emitting at 267, 400, and 800 nm as the ionization source. *Anal. Chem.*, 90(7): 4886–4893 (8 pages).
- Zhang, P.; Sun, T.; Rong, S.; Zeng, D.; Yu, H.; Zhang, Z.; Chang, D.; Pan, H., (2019). A sensitive amperometric AChE-biosensor for organophosphate pesticides detection based on conjugated polymer and Ag-rGO-NH<sub>2</sub> nanocomposite. *Bioelectrochem.*, 127(1): 163–170 (8 pages).
- Zhu, J.; Yin, X.; Zhang, W.; Chen, M.; Feng, D.; Zhao, Y.; Zhu, Y. (2023). Simultaneous and sensitive detection of three pesticides using a functional poly (sulfobetaine methacrylate)-coated paper based-colorimetric sensor. *Biosens.*, 13(309): 1-16 (16 pages).

#### AUTHOR (S) BIOSKETCHES

**Hermanto, D.**, Ph.D., Assistant Professor, Department of Chemistry, University of Mataram, Jl. Majapahit 62 Mataram, NTB 83125, Indonesia.

- Email: [dhony.hermanto@unram.ac.id](mailto:dhony.hermanto@unram.ac.id)
- ORCID: 0000-0001-6907-0021
- Web of Science ResearcherID: AAB-5058-2021
- Scopus Author ID: 57210263037
- Homepage: <http://mipa.unram.ac.id/>

**Ismillayli, N.**, M.Sc., Assistant Professor, Department of Chemistry, University of Mataram, Jl. Majapahit 62 Mataram, NTB 83125, Indonesia.

- Email: [nurul.ismillayli@unram.ac.id](mailto:nurul.ismillayli@unram.ac.id)
- ORCID: 0000-0002-9038-0825
- Web of Science ResearcherID: AAZ-4060-2020
- Scopus Author ID: 57213188179
- Homepage: <http://mipa.unram.ac.id/>

**Muliasari, H.**, M.Si., Assistant Professor, Department of Pharmacy, University of Mataram, Jl. Majapahit 62 Mataram, NTB 83125, Indonesia.

- Email: [handamuliasari@unram.ac.id](mailto:handamuliasari@unram.ac.id)
- ORCID: 0000-0000-0000-0000
- Web of Science ResearcherID:
- Scopus Author ID: 57213604049
- Homepage: <https://fk.unram.ac.id/program-studi-farmasi/>

**Wirawan, R.**, Ph.D., Associate Professor, Department of Physics, University of Mataram, Jl. Majapahit 62 Mataram, NTB 83125, Indonesia.

- Email: [rwirawan@unram.ac.id](mailto:rwirawan@unram.ac.id)
- ORCID: 0000-0003-4080-1390
- Web of Science ResearcherID:
- Scopus Author ID: 55871401900
- Homepage: <http://mipa.unram.ac.id/>

**Kamali, S.R.**, Ph.D. Candidate, Department of Applied Chemistry, Chaoyang University of Technology, Wufeng, 41349, Republic of China

- Email: [sitikamali@gmail.com](mailto:sitikamali@gmail.com)
- ORCID: 0000-0002-9635-9469
- Web of Science ResearcherID:
- Scopus Author ID: 57204546439
- Homepage: <http://mipa.unram.ac.id/>

#### HOW TO CITE THIS ARTICLE

Hermanto, D.; Ismillayli, N.; Muliasari, H.; Wirawan, R.; Kamali, S.R., (2024). Silver-based plasmonic nanoparticles for biosensor organophosphate pesticides using a single film containing acetylcholinesterase/choline oxidase. *Global J. Environ. Sci. Manage.*, 10(1): 39-50.

DOI: 10.22034/gjesm.2024.01.04

URL: [https://www.gjesm.net/article\\_704983.html](https://www.gjesm.net/article_704983.html)





## ORIGINAL RESEARCH ARTICLE

# Analyzing cellulolytic bacteria diversity in mangrove ecosystem soil using 16 svedberg ribosomal ribonucleic acid gene

I. Dewiyanti<sup>1</sup>, D. Darmawi<sup>2\*</sup>, Z.A. Muchlisin<sup>3</sup>, T.Z. Helmi<sup>4</sup><sup>1</sup> Graduate School of Mathematics and Applied Sciences, Universitas Syiah Kuala, Banda Aceh 23111, Indonesia<sup>2</sup> Laboratory of Microbiology, Faculty of Veterinary Medicine, Universitas Syiah Kuala, Banda Aceh Aceh 23111, Indonesia<sup>3</sup> Aquaculture Department, Faculty of Marine and Fisheries, Universitas Syiah Kuala, Banda Aceh 23111, Indonesia<sup>4</sup> Laboratory of Biochemistry, Faculty of Veterinary Medicine, Universitas Syiah Kuala, Banda Aceh 23111, Indonesia

## ARTICLE INFO

**Article History:**

Received 28 February 2023

Revised 05 May 2023

Accepted 14 June 2023

**Keywords:**

16 svedberg ribosomal ribonucleic acid (16S rRNA)

Bacteria

Cellulase

Mangrove

Molecular biology

## ABSTRACT

**BACKGROUND AND OBJECTIVES:** Soil is an essential abiotic component serving as a habitat for numerous organisms, including cellulolytic bacteria commonly found in mangrove ecosystems. This bacteria could produce active enzymes needed to improve environmental quality by accelerating the organic matter decomposition. The unique mangrove environment may contain new types of cellulolytic bacteria with new characteristics. Despite several mangrove areas being explored as sources of cellulolytic bacteria, there is currently unexplored data on its diversity in Aceh Province, Indonesia. Accordingly, it is necessary to analyze the molecular biological approach, namely the 16 svedberg ribosomal ribonucleic acid gene, to identify the diversity of cellulolytic bacteria and analyze the phylogenetic relationships between them.**METHODS:** Bacteria isolates were collected from mangrove soil at six research locations with three replications. A purposive sampling method was applied to determine the research location. Isolates from soil samples were streaked and purified in carboxymethyl cellulose as selective media for cellulolytic bacteria. Molecular identification adopted 16 svedberg ribosomal ribonucleic acid gene sequencing, and the sequencing data were matched with GenBank data. Phylogenetic analysis and genetic distance between species were evaluated using molecular evolutionary genetics analysis.**FINDINGS:** Thirteen isolates were sequenced, and nine species of cellulolytic bacteria dominated by the *Bacillus* genus were identified. These species exhibited an identity value of 97.77-100 percent when compared to data from GenBank, and *B. velezensis* was found to have a close relationship with *B. amyloliquefaciens* at a value of 0.002 percent. Interestingly, the non-rehabilitated mangrove areas had more bacterial species than the rehabilitated ones. Two *Bacillus* genus had different nucleotide bases, proving they were distinct species.**CONCLUSION:** Nine cellulolytic bacteria species were identified; the two closely interspecies genetic distance related were *B. velezensis* and *B. amyloliquefaciens*, whereas the farthest were *Bacillus* sp1. and *Bacillus* sp2. Small genetic distances of interspecies indicate a close relationship between species. In comparing the two sampling sites, the non-rehabilitated mangrove contains higher bacterial cellulolytic species than the rehabilitated and *Bacillus-dominated* site. The findings provide valuable insights into the diversity of cellulolytic bacteria in mangrove ecosystems. The abundance of bacterial species could serve as sources of cellulase enzymes with different characteristics, essential in an environmental aquatic management.DOI: [10.22034/gjesm.2024.01.05](https://doi.org/10.22034/gjesm.2024.01.05)This is an open access article under the CC BY license (<http://creativecommons.org/licenses/by/4.0/>).

NUMBER OF REFERENCES

76



NUMBER OF FIGURES

7



NUMBER OF TABLES

5

\*Corresponding Author:

Email: [darmawi@usk.ac.id](mailto:darmawi@usk.ac.id)

Phone: + 62821 1615 7741

ORCID: [0000-0003-3499-8000](https://orcid.org/0000-0003-3499-8000)

Note: Discussion period for this manuscript open until April 1, 2024 on GJESM website at the "Show Article".

## INTRODUCTION

The mangrove ecosystem is a unique marine environment characterized by distinctive features, such as high productivity and providing a habitat for diverse aquatic organisms (Thatoi et al., 2013; Hu et al., 2022). Bacteria are the most abundant and diverse microorganisms found in the mangrove ecosystem, and its soil plays a crucial role in providing essential nutrients, such as carbon, nitrogen, and phosphorus, which contributes to high productivity (Becker et al., 2020; Palit et al., 2022; Saneha et al., 2023). However, as a heterotrophic microorganism, bacteria serve as primary decomposers within the ecosystem and are instrumental in decomposing organic matter, mineralization, and nutrient cycling for plant growth (McGuire et al., 2012; Liu et al., 2019; Pringgenies et al., 2023). In mangrove ecosystem, fallen vegetation litter contributes to the abundance of cellulose on the soil surface. These are rich in polysaccharides, such as cellulose and hemicellulose, and are major components of plant cell walls and a primary carbon source in the carbon cycle (Furusawa, 2019). Cellulolytic bacteria can digest cellulose and are widespread microorganisms (Watanabe and Tokuda, 2010). Cellulolytic bacteria is one of the essential bacteria types commonly found in mangrove soil; they contribute carbon sources to improve soil fertility. The diversity of bacteria in the ecosystem serves as an indicator of water fertility, and each species has its unique function and role, such as cellulolytic bacteria, which produces cellulase enzyme that accelerates cellulose degradation (Biswa et al., 2020; Nimnoi and Pongsilp, 2022). Microbial enzymes involved in plant cell wall degradation convert these polysaccharides into digestible components (Ejaz et al., 2021). Bacteria participate directly in the nutrient cycle and provide insight into soil environmental quality through decomposition (Hafich et al., 2012). Studying highly active cellulolytic bacteria is essential to understanding microbial cellulose degradation (Talia et al., 2012). Interest in cellulase enzymes has grown in recent years due to its application in bioenergy and biofuel production, alongside other industries, such as beverage, paper, and textile (Srivastava et al., 2015; Ejaz et al., 2021). Safika et al. (2018) stated that cellulolytic bacteria has been proposed as a cost-effective method for reducing fibrous feed and increasing its digestibility, as opposed to using commercial cellulase enzymes.

In the fisheries sector, cellulose degradation in feed ingredients can enhance fish growth by improving digestibility (Kurniawan et al., 2019). The isolation of cellulolytic bacteria from mangrove organic materials, like sediments and leaf litter, has been reported in several studies (Behera et al., 2014; Yahya et al., 2014; Chantarasiri, 2015; Kurniawan et al., 2018; Ningsih et al., 2014). Cellulolytic bacterial diversity isolated from the mangrove ecosystem using the 16S rDNA gene has been carried out. Pramono et al. (2021) reported the species found in mangrove soil, namely *Fictibacillus nanhaiensis*; Kurniawan et al. (2019) recorded two species, namely *Vibrio parahaemolyticus* and *Bacillus amyloliquefaciens* from mangrove soil. There are three species of cellulolytic bacteria from mangrove soil in Malaysia, namely *Anoxybacillus* sp., *Bacillus subtilis*, and *Paenibacillus dendritiformis* (Naresh et al., 2019). Bacterial diversity can be assessed using two approaches: cultivation and non-cultivation, with metagenomic analysis being a useful tool to overcome the limitations of cultivation-based methods (Glogauer et al., 2011). In studying bacterial diversity in forest soil enriched with cellulolytic bacteria, the 16S rDNA gene sequencing analysis is commonly employed (Talia et al., 2012). This method is useful for analyzing the diversity of microorganisms (Izquierdo et al., 2010). Diverse studies of cellulolytic bacteria in Indonesia's mangrove ecosystems have been carried out for morphology approach and molecular biology. However, there is no information about the diversity of cellulolytic bacteria in the soil of rehabilitated and non-rehabilitated mangrove areas in Aceh Besar and Banda Aceh, Aceh Province, Indonesia. Those areas have different bacterial populations, productivity, and soil characteristics, including organic carbon (OC) content and soil texture, making those interesting subjects to study. Non-rehabilitated mangrove areas exhibited higher OC content and cellulolytic bacterial populations than rehabilitated ones. Specifically, the OC content and bacterial populations in non-rehabilitated and rehabilitated mangrove areas were 1.21 percent (%) and 0.90%, categorized low and very low OC content (Dewiyanti et al., 2021), and  $5.07 \times 10^7$  colony form unit/gram (CFU/g) and  $3.47 \times 10^7$  (CFU/g), respectively. High bacterial diversity can be associated with the stability and fertility of an ecosystem. The suitable environmental management should be applied in mangrove ecosystem to increase

productivity and fertility. One way is to analyze the presence of cellulolytic bacteria and their species richness. Furthermore, the distinct environmental characteristics of mangrove soil harboring cellulolytic bacteria have encouraged several studies to discover new bacterial strains capable of producing cellulase enzymes with unique properties. Therefore, the current study aims to analyze the molecular biological approach, namely the 16S rRNA gene, to identify the diversity of cellulolytic bacteria species and to analyze the phylogenetic relationships between them in the mangrove ecosystems, Banda Aceh and Aceh Besar. This study was carried out in the northern coast of Aceh Province, Indonesia, in 2021–2022.

## MATERIALS AND METHODS

### Study area

Cellulolytic bacteria isolates were collected from the soil samples in rehabilitated and non-rehabilitated mangrove areas in the northern coast of Banda Aceh and Aceh Besar, Aceh Province, Indonesia. The rehabilitated mangrove is the vegetation planted after the tsunami catastrophe in 2004, while the non-rehabilitated is the ecosystem that was not destroyed by the tsunami. The rehabilitated mangroves were dominated by *Rhizophora* sp., but the three common species in the non-rehabilitated ecosystem included *Rhizophora* sp., *Avicennia marina*, and *Sonneratia alba*. Identifying these isolates was performed through molecular biological techniques, specifically the phylogenetic analysis of the 16S rRNA gene at the Research Laboratory, Faculty of Veterinary Medicine, Universitas Syiah Kuala (USK).

### Sample handling

The study involved using bacterial isolates sourced from the soil samples. These isolates were purified and then tested for their ability to produce cellulase enzymes in the rehabilitated and non-rehabilitated mangrove ecosystems. Then, the isolates producing cellulase continued to the molecular biology step. The soil samples were collected from six locations, with three located in the non-rehabilitated area and the remaining in the rehabilitated mangrove region in Aceh Besar and Banda Aceh. Stations one, two, and three were identified in Lambadeuk, Dayah Teungoh, and Gampong Pande (rehabilitated); four, five, and six were in Ruyung, Lamreh, and Gampong Lampanah (non-rehabilitated). The study area's geographic

location and soil sampling location are depicted in Fig. 1. Table 1 explains the location and coordinates of the study area.

### Production of carboxymethyl cellulose (CMC) liquid media

The preparation of selective media for cellulolytic bacteria was carried out by weighing specific amounts of various ingredients, such as 1 gram (g) of CMC, 0.02 g of magnesium sulfate heptahydrate ( $MgSO_4 \cdot 7H_2O$ ), 0.05 g of potassium dihydrogen phosphate ( $KH_2PO_4$ ), 0.075 g of potassium nitrate ( $KNO_3$ ), 0.002 g of ferrous sulfate ( $FeSO_4$ ), 0.004 g of calcium chloride ( $CaCl_2$ ), 0.2 g of yeast extract, and 0.1 g of glucose, which were then added to 100 milliliter (mL) of distilled water and placed in an Erlenmeyer flask. Subsequently, one bacterial isolate was introduced into the flask and then centrifuged. The Erlenmeyer flask containing the liquid media was covered with aluminum foil and plastic wrap before transporting to the research laboratory at the Faculty of Veterinary Medicine, USK, for bacterial deoxyribonucleic acid (DNA) extraction.

### DNA extraction

This process involved using the commercially available gDNA Presto™ Bacteria Mini kit (Geneaid) to extract the DNA separately. The purified total DNA of 50 microliter ( $\mu L$ ), ~200 microgram per milliliter ( $\mu g/mL$ ) was eluted and then used as a template for Polymerase Chain Reaction (PCR) testing (Sari et al., 2017). To begin the extraction process, a pellet was resuspended by vortexing in 200 mL of extraction buffer. Subsequently, 20 mL of proteinase K was added to the mixture, which was then incubated at 37 degree Celsius ( $^{\circ}C$ ) for 30 minutes (min), with the sample being inverted every 10 min, during the incubation period. The present study outlines a DNA extraction and purification protocol using a column-based method. Initially, 200  $\mu g$  of Genomic bind (GB) buffer was added to the sample, and the mixture vortexed for 10 seconds (s) before being incubated at  $70^{\circ}C$  for 10 min. The elution buffer is preheated to  $70^{\circ}C$  for the subsequent step, where 200 mL of absolute ethanol is added to the mixture and lysed using a shaker. The resulting sample is then transferred to a column tube of 2 mL capacity and centrifuged at 14.000–16.000 revolution per min (rpm) for 2 min. The supernatant is then discarded, and the pellet is transferred to a new 2 mL tube. Next, 400 mL of wash1 buffer is added to the column and centrifuged at

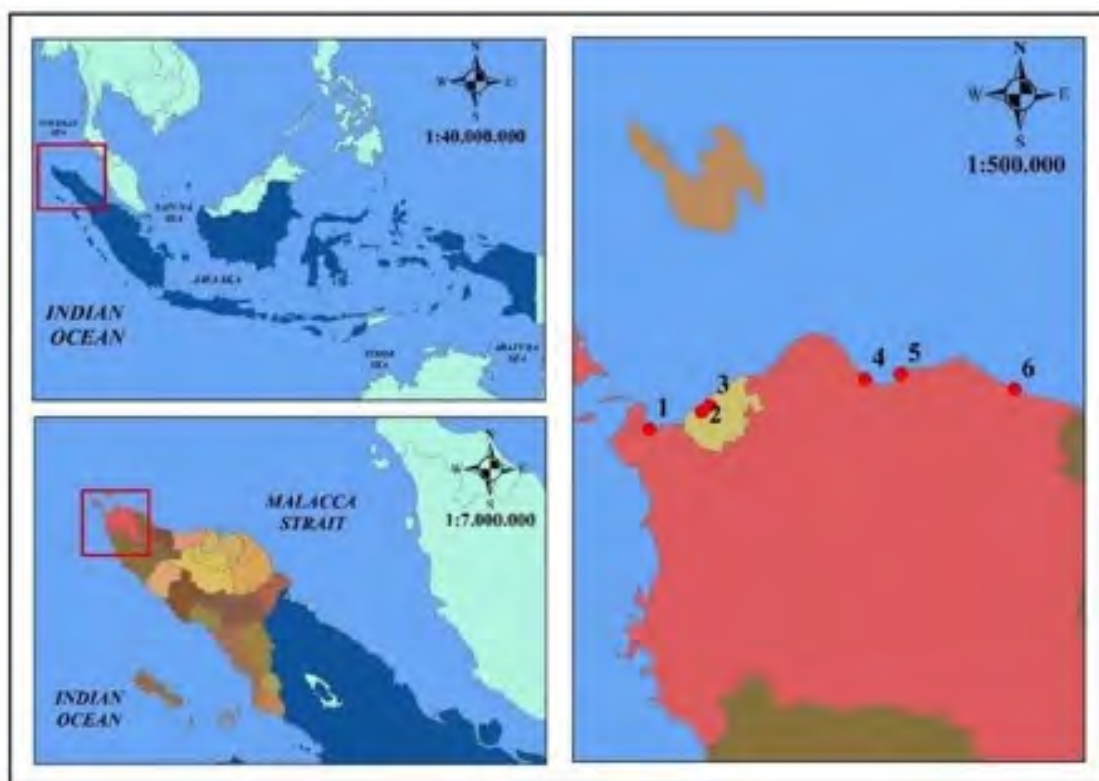


Fig. 1: Geographic location of the study area along with soil sampling locations with red dot in the mangrove ecosystem

Table 1: Location and coordinates of the study area

No.	Location	Coordinate
1	Gampong Lambadeuk	05°32'35.8"(North) N 95°14'30.9"E (East)
2	Gampong Dayan Teungoh	05°33'50.3"N 95°18'13.3"E
3	Gampong Pande	05°34'15.3"N 95°18'46.4"E
4	Gampong Ruyung	05°36'08.2"N 95°29'46.8"E
5	Gampong Lamreh	05°36'30.0"N 95°32'18.1"E
6	Gampong Lampanah	05°35'25.1"N 95°40'20.9"E

14.000–16.000 rpm for 30 s. The resulting supernatant is then discarded, and the process is repeated using 600 mL of wash buffer (containing ethanol). After the final centrifugation at 14.000–16.000 rpm for 30 s, the column is transferred to a 1.5 mL tube. Following this, preheated elution buffer (30–50 mL) is carefully added to the center of the column, and the DNA tube is allowed to incubate at room temperature for 3–5 min before being centrifuged at 14.000–16.000 rpm for 1 min. Finally, the purified DNA tube is stored at –20°C to prevent degradation until it is used in the PCR for DNA amplification.

#### DNA amplification

A study conducted by Sari *et al.* (2017) involved obtaining approximately 50 µL of pure DNA at a concentration of 200 µg/mL, which was then utilized as a template for PCR testing. The adopted primers were 63Forward (F) 5' (AGA GTT TGA TCM TGG CTC AG) 3' and 1387Reverse (R) 3' (TAC GGY TAC CTT GTT ACG ACT T) 5', thereby amplifying the 16S rRNA gene with a length of approximately 1500 base pair (bp). Meanwhile, 30 nanogram (ng) of DNA was combined with a total of 25 mL mixture containing 10 picomole (pmol) of each primer and 12.5 mL of the main mix

(Kapa Biosystems, Boston, Massachusetts, United States). The PCR amplification process involved 25 cycles and a pre-denaturation temperature of 95°C for 5 min. During each of the 25 cycles, denaturation was performed at 95°C for 1 min, followed by annealing at 50°C for 30 min, and extension at 72°C for 2 min. A final extension step was performed at 72°C for 10 min. In determining the purity and size of the amplification products, 1.2% weight/volume (w/v) agarose gel electrophoresis was used in 1× Tris-Acetate-ethylene diamine trisacetic acid (EDTA) buffer (TAE buffer), potential of hydrogen (pH) = 8.3 (containing 40 mM Tris-hydrochloric acid (HCl), 40 mM acetate, 1.0 mM EDTA), and the Gel Doc XR+ System (Bio-Rad) was used for analysis. TAE is commonly used as a buffer for nucleic acid electrophoresis.

#### *DNA electrophoresis and sequencing*

The Gel Doc XR+ System from Bio-Rad was used for analyzing the gel electrophoresis results. The resulting electrophoresis bands were visualized using an ultra-violet (UV) transilluminator, such as the UVITEC Fire-Reader V10-Plus machine. The presence of a single, clear band with a size of relatively 1500 bp indicates good PCR product visualization. PCR products showing satisfactory electrophoresis results were sent to First BASE Laboratories, in Malaysia for further analysis. Cycle sequencing was performed using the PCR Kapa 2G Fast ReadyMix kit with dye, and the reaction product was sequenced with Dye Terminator (3'-labeled dideoxy nucleotide triphosphate).

#### *Identification and Phylogenetic tree construction*

To identify the bacteria species, the 16S rRNA gene based on sequencing techniques commonly employed for detecting and classifying bacteria (Ntushelo, 2013). The 16S rRNA gene sequence is the most common genetic marker applied for almost all bacteria due its function has not changed over time, suitable for bacterial classification, and has sufficient variation to distinguish between taxa (Ntushelo, 2013; Manjul and Shirkot, 2018). The Clustal W program in the molecular evolutionary genetics analysis (MEGA X) version was used to align the obtained sequencing results alongside the sequencing data from GenBank (Tamura et al., 2013). The edited sequencing alignments were 1386 bp; it

is used to construct a phylogenetic tree with 1000× bootstrap support (Gusakov et al., 2011; Naresh et al., 2019; Sari et al., 2017). However, to confirm the species similarity with existing databases, the Basic Local Alignment Search Tool (BLAST) was used to analyze the obtained sequencing results and determine the similarity between DNA sequencing and that of bacteria. Meanwhile, the BLAST-nucleotide, programmed at the National Center for Biotechnology Information (NCBI), was adopted to analyze the homology of 16S rRNA gene sequencing using data in the GenBank database. Using the kimura-2-parameter (K2P) model, genetic distances were estimated, and bacterial relationships were presented in a phylogenetic tree constructed using the Neighboring Joining (NJ) method with 1000× bootstrap and the K2P model. The MEGA X program was used to construct the phylogenetic tree based on the methods that Kumar et al. (2018) and Tamura et al. (2013) adopted.

## RESULTS AND DISCUSSION

### *Composition of cellulolytic bacteria species in soil on mangrove ecosystems*

The 16S rRNA gene was amplified from cellulolytic bacteria using the primer pair 63F and 1387R, yielding a fragment size of 1500 bp upon alignment of the DNA ladder (Fig. 2). After alignment, the 16S rRNA gene fragment size was determined to be 1386 bp. This primer pair is capable of amplifying genes of approximately 1300 bp, resulting in an average size of ±1350 bp for the 16S rRNA gene fragment (Faturrahman, 2005; Kusumaningrum et al., 2016). The 16S rRNA is commonly used and selected as a method of bacterial identification because of its distribution in all bacteria species, its function that never changes, and this gene is large enough to reach 1500 bp in size (Safika et al., 2018).

The sequencing results were compared to the GenBank database, revealing species similarities ranging from 97.77% to 100%. The specific similarity values for each species are presented in Table 2. This indicates that the values between 97.77% and 100% of the sequencing matched the database. For instance, the isolates BTM121, BTM622, BTM632, and BTM511 were identified as *B. altitudinis* with 100% homology, whereas isolate BTM113 was identified as *Bacillus* sp1. with 97.77% homology, and *Bacillus* sp2. with 99.86%. According to Petti

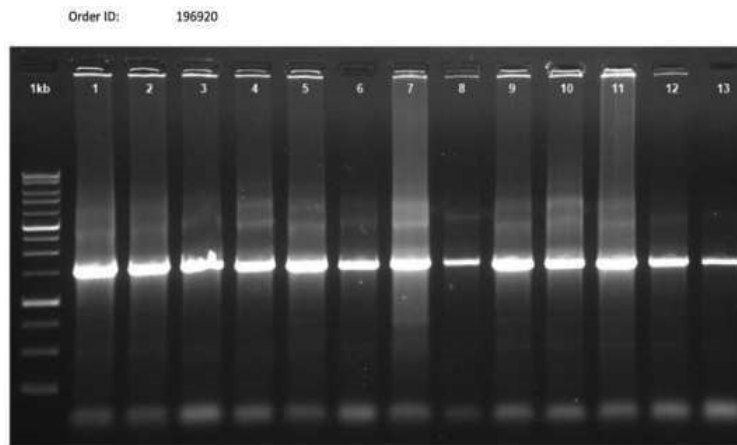


Fig. 2: Visualization of DNA from each cellulolytic bacterial isolate on geldoc Description: 1 kilobyte (kb) = 250 DNA Ladder (bp)

Table 2: Species of cellulolytic bacteria identified using 16S rRNA

No. of species	Sample code	Species	BLAST (%)	bp
1	BTM113	<i>Bacillus</i> sp1.	97.77	1386
2	BTM512	<i>Bacillus</i> sp2.	99.86	1386
3	BTM 121	<i>B. altitudinis</i>	100	1386
	BTM 622	<i>B. altitudinis</i>	100	1386
	BTM 632	<i>B. altitudinis</i>	100	1386
	BTM 511	<i>B. altitudinis</i>	100	1386
4	BTM211	<i>B. amyloliquefaciens</i>	99.78	1386
5	BTM533	<i>B. safensis</i>	100	1386
6	BTM123	<i>B. subtilis</i>	99.93	1386
	BTM621	<i>B. subtilis</i>	99.93	1386
7	BTM611	<i>B. velezensis</i>	99.93	1386
8	BTM431	<i>Brevibacillus</i> sp.	99.57	1386
9	BTM321	<i>P. aeruginosa</i>	98.85	1386

(2007), a genus is considered similar assuming the similarity score is 97%, and a species is deemed one supposing the similarity obtained is 99%. However, assuming *Bacillus* sp1. from isolate BTM113 does not reach the 99% to 100% homology threshold, it may suspect a new species, and there are nucleotide base differences compared to GenBank. The same sequencing result has not been recorded or registered in GenBank. Additionally, isolate Bakteri tanah mangrove (BTM)432 and BTM321 were identified as *Brevibacillus* sp., and *Pseudomonas aeruginosa*, with a 99.57% and 98.85% similarity to the data in GenBank. The highest individual composition is *B. altitudinis* followed by *B. subtilis*.

Briefly, nine species of cellulolytic bacteria were identified among the 13 sequenced isolates obtained from the mangrove ecosystem soil (Table 2). These

include *B. altitudinis*, *B. amyloliquefaciens*, *Bacillus* sp1., *Bacillus* sp2., *B. safensis*, *B. subtilis*, *B. velezensis*, *Brevibacillus* sp., and *P. aeruginosa*. However, among these species, *Bacillus* was the most commonly found genus, with four isolates identified as *B. altitudinis*, and two identified as *Bacillus* sp. and *B. subtilis*. This finding is consistent with previous studies, such as Shome et al. (1995) who identified 38 bacterial isolates, and reported that *Bacillus* sp. is the most dominant species (>50%) isolated from mangrove sediments in South Andaman. Yahya et al. (2014) reported that *Bacillus* sp. is the most abundant bacteria involved in the decomposition process of mangrove litter in the coast of Pasuruan Palace, thereby exhibiting the ability to degrade cellulose. Vásquez and Millones (2023) reported two species of bacteria that produce cellulase enzymes: *B. safensis*

and *B. subtilis*. *Bacillus* is a genus of Firmicutes group; Basak *et al.* (2016) found that Bacteroidetes, Acidobacteria, Firmicutes, Actinobacteria, Nitrospirae, Cyanobacteria, Planctomycetes, and Fusobacteri are groups of microorganisms mostly found in mangrove sediments in Dhulibhashani, India. *Brevibacillus* sp. is a type of cellulolytic bacteria that can produce cellulase enzymes. Liang *et al.* (2009) reported that strain JLX of *Brevibacillus* sp., can break down various unique polymers, including cellulose, and utilizes various carbohydrates, such as cellulose, cellobiose, glucose, and xylose. Several studies have reported that *P. aeruginosa* is another cellulase-producing bacteria found in soil (Gunavathy and Boominathan, 2015; Gunavathy and Boominathan, 2016) and sawdust (Agarwal *et al.*, 2014). Kurniawan *et al.* (2018a) identified *P. aeruginosa* as one of the cellulose-degrading bacteria found in mangrove forest soil in Bangka Island, Indonesia. The diversity of cellulolytic bacteria varies in each area of the mangrove ecosystem; various species can be found in different mangrove ecosystems due to differences in their environmental characteristics, such as soil and water. The higher the species diversity and abundance of bacteria, the faster process of organic matter degradation. The bacterial richness indicates ecosystem fertility because they uniquely functions as a decomposer, such as cellulolytic bacteria, which produces cellulase enzyme that accelerates cellulose degradation (Biswas *et al.*, 2020). Several studies have been conducted on mangrove soil's bacteria. For example, Kurniawan *et al.* (2019) found cellulolytic bacteria using molecular biology of the 16S rRNA gene, including TBL1 isolate with 85% similarity to *Vibrio parahaemolyticus*, and strains HY3 and TBL2 with 98% similarity to *B. amyloliquefaciens*. Pramono *et al.* (2021) identified isolate LG2 as the species *Fictibacillus nanhaiensis* strain JSM 082006, which produced the highest cellulase enzyme activity. Naresh *et al.* (2019) successfully identified three species using the 16S rRNA gene: *Anoxybacillus* sp., *B. subtilis*, and *Paenibacillus dendritiformis*, and Biswas *et al.* (2020) discovered strains T2-D2 as *Bacillus* sp. and E1-PT as *Pseudomonas* sp. The composition of cellulolytic bacteria found in mangrove sediments is high, reaching 87.87% (Pramono *et al.*, 2021). In the fisheries sector, several cellulase bacteria were found to have potential as probiotics. According to Yanbo and Zirong (2006) and Soltani *et al.* (2019),

*Bacillus* sp. is one of the bacteria believed to increase the digestibility of fish because these bacteria are classified as probiotics, so they are often applied to feed to increase feed digestibility. The species of *Bacillus* often applied as a probiotic is *B. subtilis* (El Dakar *et al.*, 2007; Olmos *et al.*, 2020; Truong *et al.*, 2021), and this bacterium was found at the study site. The use of *Bacillus* sp. as a probiotic bacterium in fish feed is believed to enhance their digestive capacity by converting unutilized feed into a digestible form (Putra *et al.*, 2021; Widanarni *et al.*, 2022). This approach can be an alternative to producing dual-function feed and indirectly improve feed quality.

#### Genetic distance of cellulolytic bacteria species

Table 3 shows the genetic distance within-species (intraspecies) values, and the values of interspecies distances. Four isolates detected as the *B. altitudinis* species exhibited a species distance of zero, meaning that these isolates are identical. Similarly, two isolates identified as the *B. subtilis* species exhibited a within-species distance of zero. *Bacillus* sp. has a interspecies distance value of 0.084%, indicating differences between the two species (*Bacillus* sp1. and *Bacillus* sp2.). The interspecies genetic distance is 0.069% between *Bacillus* sp2. and *B. amyloliquefaciens*, 0.067% between *Bacillus* sp2. and *B. altitudinis*, and 0.067% between *B. velezensis* and *Bacillus* sp2. The closest intraspecies distances were found to be between *B. velezensis* and *B. amyloliquefaciens* at 0.002%, followed by *B. safensis* and *B. altitudinis* at 0.004%, *B. velezensis* and *B. subtilis* at 0.004%, as well as *B. subtilis* and *B. amyloliquefaciens* at 0.006%. Maduppa *et al.* (2018) stated that a smaller genetic distance implies a closer a relationship between species and vice versa.

In a study by Fan *et al.* (2017), *B. velezensis*, *B. methylotrophicus*, and *B. amyloliquefaciens* were found to have a high degree of similarity in their nucleotide base sequence, depicting that they belong to the same clade. Furthermore, Hossain *et al.* (2015) reported that a recent phylogenomic study has shown that the genomes of *B. methylotrophicus*, *B. velezensis*, *B. oryzicola*, and *B. amyloliquefaciens* are highly similar. A specific strain isolate code of *B. amyloliquefaciens* (DSM 23117T), first identified as *B. amyloliquefaciens* in 2008 (Wang *et al.*, 2008), was later revised as *B. amyloliquefaciens* sub-sp. plantarum in 2011 (Borris *et al.*, 2011), and finally

Table 3: Within-species and interspecies distance values of cellulolytic bacteria

No.	Species	1	2	3	4	5	6	7	8	9	10	11	12	13
1	<i>B. altitudinis</i>	0												
2	<i>B. altitudinis</i>	0.000	0											
3	<i>B. altitudinis</i>	0.000	0.000	0										
4	<i>B. altitudinis</i>	0.000	0.000	0.000	0									
5	<i>B. amylo liquefaciens</i>	0.030	0.030	0.030	0.030	0								
6	<i>Bacillus</i> sp1.	0.045	0.045	0.045	0.045	0.019	0							
7	<i>Bacillus</i> sp2.	0.067	0.067	0.067	0.067	0.069	0.084	0						
8	<i>B. safensis</i>	0.004	0.004	0.004	0.004	0.032	0.048	0.067	0					
9	<i>B. subtilis</i>	0.029	0.029	0.029	0.029	0.006	0.021	0.066	0.031	0				
10	<i>B. subtilis</i>	0.029	0.029	0.029	0.029	0.006	0.021	0.066	0.031	0.000	0			
11	<i>B. velezensis</i>	0.028	0.028	0.028	0.028	0.002	0.019	0.067	0.030	0.004	0.004	0		
12	<i>Brevibacillus</i> sp.	0.969	0.969	0.969	0.969	0.960	1.006	0.914	0.963	0.957	0.957	0.960	0	
13	<i>P. aeruginosa</i>	5.428	5.428	5.428	5.428	N/A	N/A	0						

reclassified as *B. velezensis* in 2016 based on DNA hybridization, and phenotypic and phylogenetic analyses (Dunlap *et al.*, 2016). Although some recent publications and GenBank data sets still refer to this strain as *B. amylo liquefaciens*, it was later confirmed as *B. velezensis* strain using molecular methods (Fan *et al.*, 2017; Liu *et al.*, 2019; Santiago *et al.*, 2021). Despite having similar morphology, physiology, phenotypic properties, and 16S rRNA gene sequences, *B. velezensis* and *B. amylo liquefaciens* can be distinguished based on their fatty acid (FA) cellular composition, as noted by Huynh *et al.* (2022). Both *B. velezensis* and *B. amylo liquefaciens* belong to the *B. subtilis* group, which suggests a close taxonomic relationship (Fan *et al.*, 2017).

#### Phylogenetic tree of cellulolytic bacteria

Using the NJ method with 1000× bootstrap repetitions, the phylogenetic analysis consistently revealed that *B. velezensis* is closely related to *B. amylo liquefaciens* and *B. subtilis* and showed that *B. subtilis* is closely related to *B. safensis* (Fig. 3). Recently, Vásquez and Millones (2023) reported the close phylogenetic relationship of cellulolytic bacteria of *B. subtilis* and *B. safensis* isolated from solid waste of palm forests, Peru. Constructing the phylogenetic tree from 13 cellulolytic bacteria isolates divided into nine species, and two main clades (groups). Clade one consist of *B. altitudinis*, *B. safensis*, *B. amylo liquefaciens*, *B. subtilis*, *Bacillus* sp1. (BTM113), *Bacillus* sp2. (BTM512), *B. velezensis*, and *Brevibacillus* sp. Meanwhile, clade two consists of *P. aeruginosa* at 1000× bootstrap. One main clade was then divided

into two subclades, which separated *Brevibacillus* sp. Species of *A. hydrophila* (access code LR991675.1), an outgroup species in the phylogenetic tree (Fig. 3). The *Bacillus* and *Brevibacillus* genera gather in the same class and order, namely the Bacilli class and the order Bacillales, but in different families. *Bacillus* belongs to the Bacillaceae family while *Brevibacillus* belongs to the Paenibacillaceae family. Both families are the phylum Firmicutes. Sulistiyani *et al.* (2021) reported two families and three genera identified using the 16S rRNA gene, namely Bacillaceae (genus *Bacillus* and *Fictibacillus*), and Paenibacillaceae (genus *Brevibacillus*). These families can produce cellulase, xylanase, amylase, and lipase enzymes (Shanti and Roymon, 2018; Powthong and Suntornthicharoen, 2017).

Comparatively, there are five species of cellulolytic bacteria in the rehabilitated mangrove area: *B. amylo liquefaciens*, *Bacillus* sp1., *B. subtilis*, *B. altitudinis*, and *P. aeruginosa*. The non-rehabilitated area has six species of cellulolytic bacteria, including *Bacillus* sp2., *B. subtilis*, *B. altitudinis*, *B. velezensis*, *B. safensis*, and *Brevibacillus* sp. Based on the analysis, *Bacillus* sp1., *B. amylo liquefaciens*, and *P. aeruginosa* were not found in non-rehabilitated areas, while *Bacillus* sp2., *B. safensis*, *B. velezensis* and *Brevibacillus* sp. were also not found in the rehabilitated areas. The phylogenetic trees of the rehabilitated and non-rehabilitated mangrove areas, shown in Fig. 4a and Fig. 4b, respectively, consist of two main clades, with one serving as an outgroup. The species used as an outgroup in this phylogenetic tree is *A. hydrophila* (access code LR991675.1).

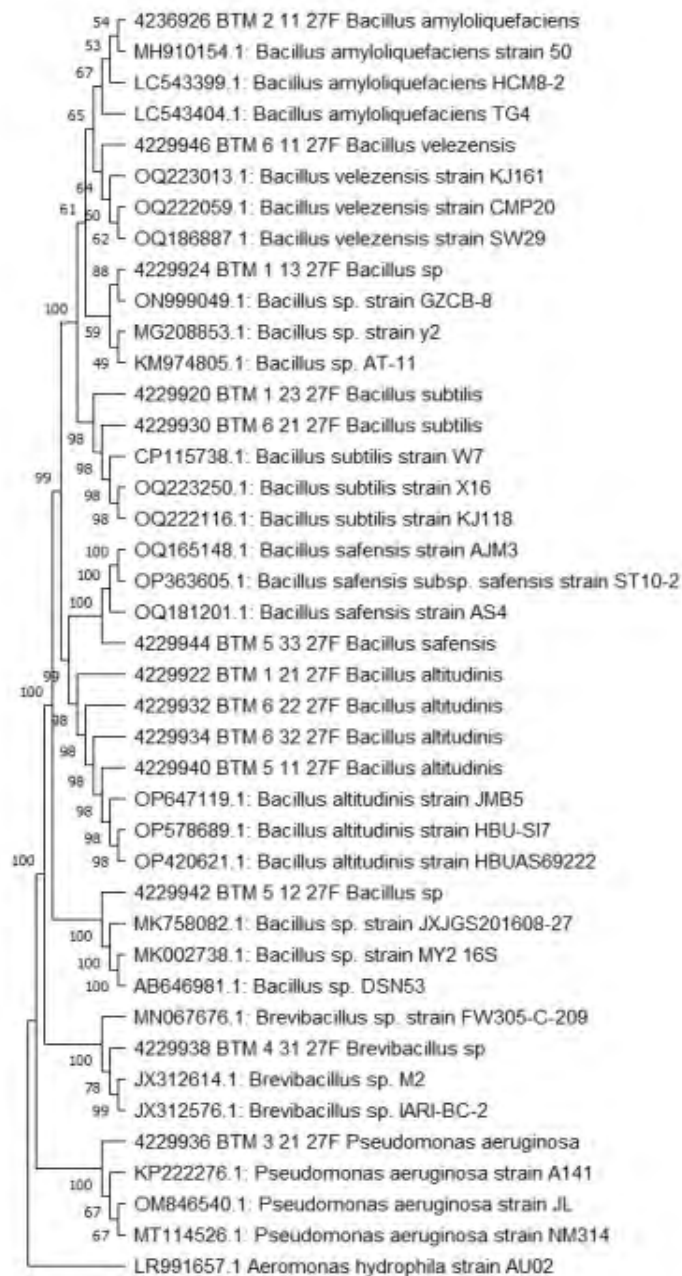


Fig. 3: Phylogenetic tree of 9 cellulolytic bacterial sequences isolated from mangrove soil using NJ method

The present study found that the number of cellulolytic bacteria species was higher in the non-rehabilitated mangrove area than in the rehabilitated one. Preliminary studies suggested that this difference in species richness was due to lower OC

in the rehabilitated mangrove soil. The OC in the non-rehabilitated and rehabilitated mangrove were 1.23% and 0.90% (Dewiyanti *et al.*, 2021), followed by a higher percentage of silt fraction (fine fraction) in non-rehabilitated mangrove (43%) than in

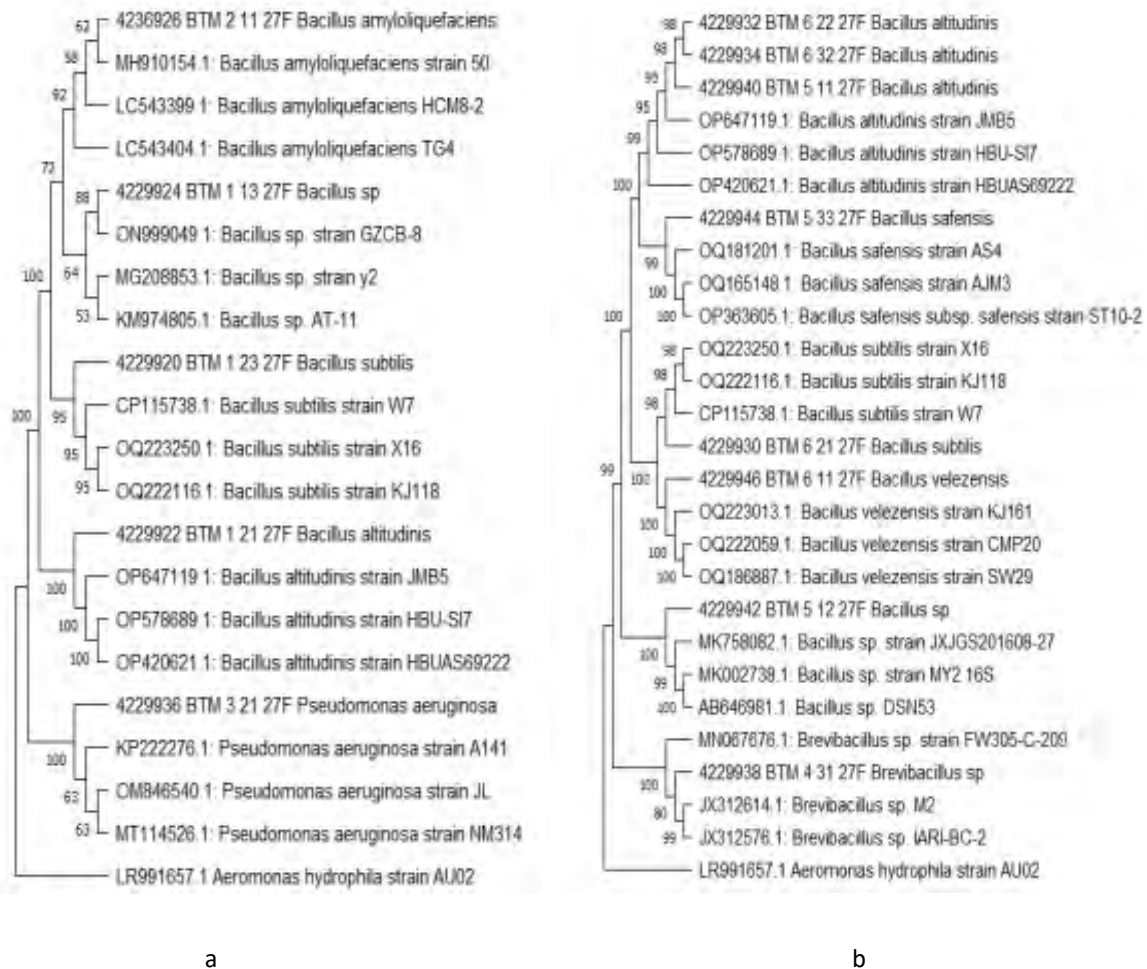


Fig. 4: Phylogenetic tree of cellulolytic bacteria in soil in mangrove ecosystems (a) rehabilitated mangrove (b) non-rehabilitated mangroves

rehabilitated (31%). Soil organic C content is higher in fine soil with small porosity (silt) than in coarse soil with big porosity (sand). Carney and Matson (2005) mentioned that fine-textured soils support more microbial biomass and species than their coarse-textured. Huang et al. (2019) supported this view, stating that bacterial diversity tends to increase with higher organic matter content in the soil. A higher number of mangrove vegetation in non-rehabilitated than in rehabilitated area was assumed to contribute more litter production that can increase OC content. There were 70 individuals/100 square meter (m<sup>2</sup>) in non-rehabilitated than 39 individuals/100 m<sup>2</sup> in rehabilitated. Litter production significantly

contributes OC into the soil, promoting the diversity of cellulolytic bacteria (Leff et al., 2012). Another factor that could explain the higher number of bacterial species in the non-rehabilitated areas is the more extensive root systems in these ecosystems. Batubara (2021) reported that the rhizosphere, the soil layer where roots grow, is enriched with nutrients from root exudates (materials released from living root cells, such as sugars, amino acids, organic acids, and FA) and other soil organisms. Bacteria tend to dominate in the rhizosphere due to organic matter abundance; many bacteria species form symbiotic relationships with plant roots, as these exudates serve as the primary food source for microorganisms

Table 4: Nucleotide base composition and accession number registered in GenBank of cellulolytic bacteria

No.	Bacterial isolate	Species	Accession number	T (%)	C (%)	A (%)	G (%)	GC (%)
1	BTM121	<i>B. altitudinis</i>	OQ152604	20.00	23.78	25.02	31.20	54.98
	BTM632	<i>B. altitudinis</i>	OQ152605	20.00	23.78	25.02	31.20	54.98
	BTM511	<i>B. altitudinis</i>	OQ152606	20.00	23.78	25.02	31.20	54.98
	BTM622	<i>B. altitudinis</i>	OP363153	20.00	23.78	25.02	31.20	54.98
2	BTM211	<i>B. amyloliquefaciens</i>	OQ152607	19.93	23.78	24.87	31.42	55.20
3	BTM113	<i>Bacillus</i> sp1.	OQ152608	20.65	22.98	24.95	31.42	54.40
4	BTM512	<i>Bacillus</i> sp2.	OQ152609	20.87	22.76	25.82	30.55	53.31
5	BTM123	<i>B. subtilis</i>	OQ152610	20.07	23.71	24.95	31.27	54.98
	BTM621	<i>B. subtilis</i>	OQ152611	20.00	23.64	25.02	31.35	54.98
6	BTM611	<i>B. velezensis</i>	OQ152612	20.00	23.64	25.02	31.35	54.98
7	BTM622	<i>B. safensis</i>	OP363154	19.93	23.71	24.87	31.49	55.20
8	BTM431	<i>Brevibacillus</i> sp.	OQ152613	20.51	23.64	24.80	31.05	54.69
9	BTM321	<i>P. aeruginosa</i>	OQ152614	20.36	22.62	25.38	31.64	54.25

Table 5: Average nucleotide composition

Nucleotide	Average	Minimum	Maximum
T %	20.18	19.93	20.87
C %	23.51	22.62	23.78
A %	25.06	24.80	25.82
G %	31.26	30.55	31.64
GC %	54.76	53.31	55.20

and their activities (Raaijmakers *et al.*, 2009; Sulistiyani *et al.*, 2020). A previous study investigating cellulolytic bacteria: *B. altitudinis* and *B. safensis* showed a higher cellulolytic index (CI) than other bacteria found in mangrove non-rehabilitated areas. Dewiyanti *et al.* (2022) reported that *B. safensis* had CI index of 4.82, followed by *B. altitudinis* with 2.09 CI index, categorized as a high CI index. A high CI index indicates high cellulase production (Naresh *et al.*, 2019). Enzyme produced by microorganism could be good indicators to ecosystem response's to environmental changes (Luo and Gu, 2015).

#### Composition of nucleotide bases in cellulolytic bacteria

The sequencing of 13 isolate samples resulted in nucleotides with a base length of 1386 bp, and Guanine (G) being the most abundant nucleotides, followed by Adenine (A), Cytosine (C), and Thymine (T). The nucleotide base composition for each cellulolytic bacterial species is presented in Table 4. The nucleotide composition had an average of

20.18% (T), 23.51% (C), 25.06% (A), and 31.26% (G). The GC content of the first, second, and third codon positions increased, with mean GC and AT contents of 27.39%, and 22.62%, respectively. The average nucleotide composition is shown in Table 5.

After conducting a nucleotide alignment, the two *Bacillus* sp. isolates were discovered to be distinct species, as revealed by Multalin (multiple sequence alignment) program (Fig. 5). The interspecies were identified in both isolates, with nucleotide base changes observed at several points, denoted by the following base sequence numbers 9, 11, 12, 16, 17, 28, 29, 74, 75, 118, 119, 120, 121, 122, etc. The nucleotide base of these two species had a variation of 106 base sequence points (7.7%) due to nucleotide base substitution. These nucleotide base variations are highlighted in blue and black (Fig. 5), and were primarily caused by nucleotide base changes, including transition and transversion substitutions. Transitions are changes between A and G bases (purines) or disparities between C and T bases (pyrimidines), while transversions are alterations



Fig. 5: Sequence alignment of *Bacillus* sp. (BTM113 and BTM512) using Multalin

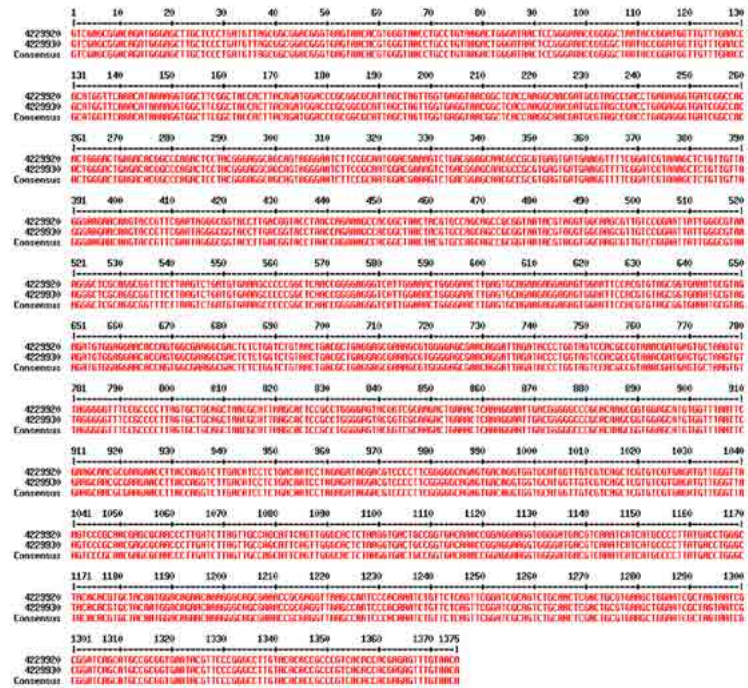


Fig. 6: Sequence alignment of *B. subtilis* (BTM123 and BTM621) using Multalin

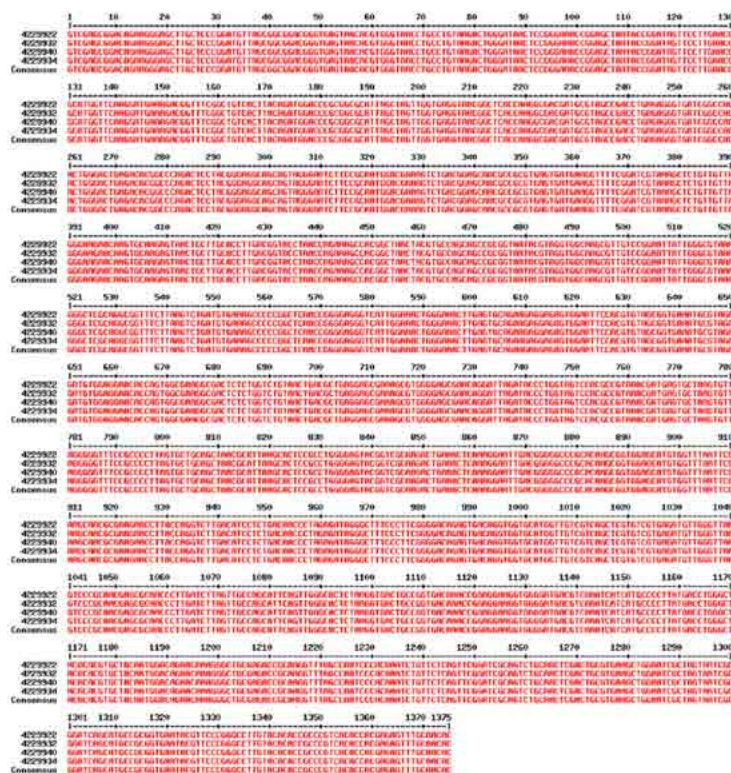


Fig. 7: Sequence alignment of *B. altitudinis* (BTM121, BTM622, BTM632 and BTM511) using Multalin

between a purine and pyrimidine base (Elyvra *et al.*, 2009; Nandy, 2009; Ubaidillah and Sutrisno, 2009). Specifically, the nucleotide chain polymorphism in *Bacillus* sp. includes 74 nucleotide transitions and 32 transversions. Among these substitutions, nucleotide transitions were more commonly found than transversions (Kochzius and Nuryanto, 2008). The nucleotide composition of *Bacillus* sp1 (BTM113) was 20.65% (T), 22.98% (C), 24.95% (A), and 31.42% (G), and the highest average was the G+C pair with a value of 27.2% while the lowest is the A+T pair (22.8%), the G+C nucleotide pair composition was also higher in *Bacillus* sp2. (BTM512). Assuming both species have a higher A+T nucleotide base value based on composition, the species will have many similarities due to independent parallel substitutions. Conversely, supposing both species have a higher G+C nucleotide base composition, the species will have fewer similarities (Lam and Morton, 2006). Transition mutations were found to occur more frequently and easily than transversion mutations, which explains

why transitions were more commonly found among substitutions (Graur and Li, 2000). Notably, the average content of the G+C nucleotide base was greater than that of the A+T nucleotide base in each identified species of cellulolytic bacteria, with values of 27.39% (GC) and 22.62% (AT), respectively. This formula also occurred in each identified species of cellulolytic bacteria. This finding is consistent with previous research suggesting that G+C nucleotide pairs are more prevalent in bacterial genomes.

Meanwhile, two isolates, identified as *B. subtilis*, and the four isolates, identified as *B. altitudinis*, were confirmed through alignment to be the same species. Figs. 6 and 7 show that the nucleotide base variations in these isolates were identical, indicating that they belonged to the same species.

**CONCLUSION**

The study results revealed cellulolytic bacteria in mangrove soil for rehabilitated and non-rehabilitated, Banda Aceh and Aceh Besar, Aceh Province, Indonesia.

Based on the alignment using MEGA X and comparing to the BLAST database in GeneBank, nine species were identified from the 13 isolates successfully sequenced using the 16S rRNA gene: *B. altitudinis*, *B. amyloliquefaciens*, *Bacillus* sp1., *Bacillus* sp2., *B. safensis*, *B. subtilis*, *B. velezensis*, *Brevibacillus* sp., and *P. aeruginosa*. The similarity of data sequencing and GenBank database ranged from 97.77% to 100%. The isolates BTM121, BTM622, BTM632, and BTM511 were identified as *B. altitudinis* with 100% homology, whereas isolate BTM113 was identified as *Bacillus* sp1. with 97.77% homology, and *Bacillus* sp2 with 99.86%. Species of *B. amyloliquefaciens*, *B. safensis*, *B. subtilis*, *B. velezensis*, and *P. aeruginosa* have 99.78%, 100%, 99.93%, 99.57%, and 98.85% homology, respectively. The species obtained are considered similar due to similarity achieving 97%, and categorized as same species with database if the similarity obtained 99%. Further analysis revealed that *B. velezensis* is closely related to *B. amyloliquefaciens*, with interspecific genetic distance of 0.002%. The farthest interspecies genetic distance was 0.084% related between *Bacillus* sp1. and *Bacillus* sp2. Small genetic distances of interspecies indicate a close relationship between species. Research studies were located at two kinds of mangrove habitats (rehabilitated and non-rehabilitated mangrove) with different characteristics, for example, substrate fraction, OC, and mangrove species. Previous research showed that non-rehabilitated mangrove contain higher OC, silt fraction, and mangrove vegetation species and abundance. This condition makes the non-rehabilitated mangrove soil acquire more bacterial cellulolytic species than the rehabilitated habitat. The characteristics of a suitable soil environment strongly support the life and diversity of cellulolytic bacteria, so an action is needed to increase the presence of cellulolytic bacteria in mangrove soils by applying cellulolytic species that produce high enzyme cellulase. The bacteria diversity is a critical aspect to the functioning of the ecosystem, managing the ecosystem while maintaining diversity may be one of the approaches to ensure the stability and productivity of the mangrove ecosystem in the study area. Notably, *Bacillus* is a genus commonly found in the study area, and two isolates from the *Bacillus* sp. were identified as different species, as proven by different nucleotide bases that have been aligned. *Bacillus* sp1. could be a novel species due to low

homology percentage and the absence of nucleotide bases identical to the aligned data on GenBank. *B. subtilis* found is a cellulolytic bacterium often applied in the industrial, animal husbandry, and fishery sectors.

#### AUTHOR CONTRIBUTIONS

D. Darmawi, as a corresponding author, developed the study idea and concepts and supervised the manuscript. I. Dewiyanti, as the first author, has contributed to study conceptualization, surveys, data collection and analysis, result interpretation, and manuscript preparation. Z.A. Muchlisin contributed to the research design, result interpretation, and manuscript review. T.Z. Helmi contributed to the result interpretation and manuscript review.

#### ACKNOWLEDGEMENT

The authors are grateful to the Directorate of Research and Community Service for providing research grants through the Doctoral Dissertation scheme, the contract research number was [154/SP2H/LT/DRPM/2021]. Furthermore, the authors are grateful to Dila, Iko, Nanda, Thariq, Fajar for their fieldwork and to the local people for support and cooperation during the study.

#### CONFLICT OF INTEREST

The authors declare that there is no conflict of interests regarding the publication of this manuscript. In addition, the ethical issues, including plagiarism, informed consent, misconduct, data fabrication and/or falsification, double publication and/or submission, and redundancy have been completely observed by the authors.

#### OPEN ACCESS

©2024 The author(s). This article is licensed under a Creative Commons Attribution 4.0 International License, which permits use, sharing, adaptation, distribution and reproduction in any medium or format, as long as you give appropriate credit to the original author(s) and the source, provide a link to the Creative Commons license, and indicate if changes were made. The images or other third-party material in this article are included in the article's Creative Commons license, unless indicated otherwise in a credit line to the material. If material is not included in the article's Creative Commons license and your

intended use is not permitted by statutory regulation or exceeds the permitted use, you will need to obtain permission directly from the copyright holder. To view a copy of this license, visit:

<http://creativecommons.org/licenses/by/4.0/>

#### PUBLISHER'S NOTE

GJESM Publisher remains neutral with regard to jurisdictional claims in published maps and institutional affiliations.

#### ABBREVIATIONS

<i>16S rRNA</i>	16 svedberg ribosomal ribonucleic acid	<i>HY3</i>	Isolate code of <i>B. amyloliquefaciens</i>
%	Percent	<i>JLX</i>	Genus in the <i>Brevibacillus</i>
$\mu\text{g}$	Microgram	<i>JSM</i>	Strain code
$\mu\text{L}$	Microliter	<i>K2P</i>	Kimura-2-parameter
$^{\circ}\text{C}$	Degree Celsius	$\text{KH}_2\text{PO}_4$	Potassium Dihydrogen Phosphate
A	Adenine	$\text{KNO}_3$	Potassium nitrate
<i>BTM</i>	Bakteri tanah mangrove (mangrove soil bacteria) as isolate code	<i>LG2</i>	Isolate code of <i>Fictibacillus nanhaiensis</i>
<i>BLAST</i>	Basic local alignment search tool	<i>LR991675.1</i>	Access code of <i>A. hydrophila</i>
<i>bp</i>	Basepair	$\text{m}^2$	Square meter
<i>C</i>	Cytosine	<i>MEGA</i>	Molecular evolutionary genetics analysis
$\text{CaCl}_2$	Calcium chloride	$\text{MgSO}_4 \cdot 7\text{H}_2\text{O}$	Magnesium sulfate heptahydrate
<i>CFU</i>	Colony form unit	<i>min</i>	Minute
<i>CI</i>	Cellulolytic index	<i>mL</i>	Mililiter
<i>CMC</i>	Carboxymethyl cellulose	<i>mM</i>	miliMolar
<i>DNA</i>	Deoxyribonucleic acid	Multalin	Multiple sequence alignment
DSM 23117T	Isolate code of <i>B. amyloliquefaciens</i>	<i>N</i>	North
<i>E1-PT</i>	Isolate code of <i>Pseudomonas</i> .	<i>NCBI</i>	National Center for Biotechnology Information
<i>E</i>	East	<i>ng</i>	Nanogram
<i>EDTA</i>	Ethylene diaminete traacetic acid	<i>NJ</i>	Neighboring joining
<i>etc</i>	et cetera	<i>No</i>	Number
<i>F</i>	Forward	<i>OC</i>	Organic carbon
$\text{FeSO}_4$	Ferrous sulphate monohydrate	<i>PCR</i>	Polymerase Chain Reaction
<i>FA</i>	Fatty acid	<i>pH</i>	Potential of hydrogen
<i>G</i>	Guanine	<i>pmol</i>	Picomole
<i>g</i>	Gram	<i>R</i>	Reverse
<i>GB</i>	Genomic bind	<i>rpm</i>	Revolution per minute
<i>HCL</i>	Hydrogen chloride	<i>s</i>	Second
		<i>T2-D2</i>	Isolate code of <i>Bacillus</i> sp.
		<i>T</i>	Thymine
		<i>TAE buffer</i>	Tris-acetate-EDTA buffer
		<i>TBL1</i>	Isolate code of <i>Vibrio parahaemolyticus</i>
		<i>TBL2</i>	Isolate code of <i>B. amyloliquefaciens</i>
		<i>USK</i>	Universitas Syiah Kuala
		<i>UV</i>	Ultra Violet
		<i>w/v</i>	Weight/volume

## REFERENCES

- Agarwal, T.; Saxena, M.K.; Chandrawat, M.P.S., (2014). Production and optimization of cellulase enzyme by *Pseudomonas aeruginosa* MTCC 4643 using sawdust as a substrate. *Int. J. Sci. Res.*, 4(1): 1-3 (3 pages).
- Becker, P.; Weber, L.; Suca, J.J.; Klopiz, J.K.; Mooney, T.A.; Apprill, A., (2020). Microbial and nutrient dynamics in mangrove, reef, and seagrass waters over tidal, and diurnal time scales. *Aquat. Microb. Ecol.*, 85: 101-119 (19 pages).
- Basak, P.; Pramanik, A.; Sengupta, S.; Nag, S.; Bhattacharyya, A.; Roy, D.; Pattanayak, R.; Ghosh, A.; Chattopadhyay, D.; Bhattacharyya, M., (2016). Bacterial diversity assessment of pristine mangrove microbial community from Dhulibhushani, Sundarbans using 16S rRNA gene tag sequencing. *Genom. Data.* 1(7): 76-78 (3 pages).
- Batubara, U.M.; Suparjo, S.; Maritsa, H.U.; Pujianto, E.; Herlini, M., (2022). Screening and determination of potential cellulolytic bacteria from mangrove ecosystem. *J. Perikanan dan Kelautan*, 27(2): 264-271 (8 pages).
- Behera, B.C.; Parida, S.; Dutta, S.K.; Thatoi, H.N., (2014). Isolation and identification of cellulose degrading bacteria from mangrove soil of Mahanadi River Delta and Their Cellulase. *Am. J. Microbiol. Res.*, 2(1): 41-46 (6 pages).
- Biswas, S.; Al Saber, Md.; Tripty, I.A.; Karim, A.Md.; Islam, A.Md.; Hasan, S.Md.; Rubayet Ul Alam, A.S.M.; Jahid, K.Md.I.; Hasan, N.Md., (2020). Molecular characterization of cellulolytic (endo- and exoglucanase) bacteria from the largest mangrove forest (Sundarbans), Bangladesh. *Anal. Microbiol.*, 7(70): 1-11 (11 pages).
- Borriess, R.; Chen, X.H.; Rückert, C.; Blom, J.; Becker, A.; Baumgarth, B.; Fan, B.; Pukall R.; Schumann, P.; Spröer, C., (2011). Relationship of *Bacillus amyloliquefaciens* clades associated with strains DSM 77 and FZB42T: A proposal for *Bacillus amyloliquefaciens* subsp. *amyloliquefaciens* subsp. nov. and *Bacillus amyloliquefaciens* subsp. *plantarum* subsp. nov. based on complete genome sequence comparisons. *Int. J. Syst. Evol. Microbiol.*, 61(8): 1786-1801 (16 pages).
- Carney, K.M.; Matson, P.A., (2005). Plant communities, soil microorganisms, and soil carbon cycling: does altering the world belowground matter to ecosystem functioning?. *Ecosystems.*, 8(8): 928-940 (13 pages).
- Chantarasiri, A., (2015). Aquatic *Bacillus cereus* JD0404 isolated from the muddy sediments of mangrove swamps in Thailand and characterization of its cellulolytic activity. *Egypt. J. Aquat. Res.*, 41(3): 257-64 (8 pages).
- Dewiyanti, I.; Darmawi, D.; Muchlisin, Z.A.; Helmi, T.Z.; Imelda, I.; Defira, C.N., (2021). Physical and chemical characteristics of soil in mangrove ecosystem based on differences habitat in Banda Aceh and Aceh Besar. IOP Conference Series. Earth. Environ. Sci., 674: 012092 (7 pages).
- Dewiyanti, I.; Darmawi, D.; Muchlisin, Z.A.; Helmi, T.Z.; Arisa, I.I.; Rahmiati, R.; Destri, E.; Fanisha, S., (2022). Characteristic and activity of cellulolytic bacteria isolated from mangrove soil in Northern Coast of Aceh Province, Indonesia. *Biodivers*
- Dunlap, C.A.; Jin Kim, S.; Wo Kwon, S.; Rooney, A.P., (2016). *Bacillus velezensis* is not a later heterotypic synonym of *Bacillus amyloliquefaciens*; *Bacillus methylophilicus*, *Bacillus amyloliquefaciens* subsp. *plantarum* and '*Bacillus oryzicola*' are later heterotypic synonyms of *Bacillus velezensis* based on phylogenomics. *Int. J. Syst. Evol. Microbiol.*, 66(3): 1212-1217 (6 pages).
- Ejaz, U.; Sohail, M.; Ghanemi, A., (2021). Cellulases: from bioactivity to a variety of industrial applications. *Biomimetics.*, 6(3): 44-54 (11 pages).
- El Dakar, A.Y.; Shalaby, S.M.; Saoud, I.P., (2007). Assessing the use of a dietary probiotic/prebiotics as an enhancer of spinefoot Rabbitfish *Siganus rivulatus* Survival and Growth. *Aquac. Nutr.*, 13(6): 407-412 (6 pages).
- Elyvra, R.; Solihin, D.D.; Affandi, R.; Junior, Z.; Yus, Y., (2009). Keanekaragaman genetika dan hubungan kekerabatan *Kryptopterus limpok* dan *Kryptopterus Apogon* dari Sungai Kampar dan Sungai Indragiri Riau berdasarkan Gen Sitokrom B1. *J. Ilmu-ilmu Perairan Indonesia.*, 16(1): 55-61 (7 pages).
- Fan, B.; Blom, J.; Klenk, H.P.; Borriess, R., (2017). *Bacillus amyloliquefaciens*, *Bacillus velezensis*, and *Bacillus siamensis* form an "Operational Group B. amyloliquefaciens" within the B. subtilis species complex. *Front. Microbiol.*, 8(22): 22-36 (15 pages).
- Faturrahman., (2005). Genetic diversity of *Clostridium bifementans* strains by amplified ribosomal DNA restriction analysis. *J. Biol. Tropi.*, 6(2): 57-64 (7 pages).
- Furusawa, G., (2019). Biodiversity of plant polysaccharide-degrading bacteria in mangrove ecosystem. *Trop. Life. Sci. Res.*, 30(3): 157-172 (17 pages).
- Glogauer, A.; Martini, V.P.; Faoro, H.; Couto, G.H.; Santos, M.M.; Monteiro, R.A.; Mitchell, D.A.; de Souza, E.M.; Pedrosa, F.O.; Krieger, N., (2011). Identification and characterization of a new true lipase isolated through metagenomic approach. *Microb. Cell. Fact.*, 10(54): 1-15 (15 pages).
- Graur, D.; Li, H.W. (2000). Fundamentals of molecular evolution. 2<sup>nd</sup> edition. Sinauer (439 pages).
- Gunavathy, P.; Boominathan, M., (2015). Isolation and molecular characterization of cellulase producing bacteria from soil of Sacred Grove, Puducherry, India. *Int. J. Curr. Microbiol. Appl. Sci.*, 4(12): 584-590 (7 pages).
- Gunavathy, P.; Boominathan., (2016). Optimization of cellulase production of *Pseudomonas aeruginosa* Sg21 isolated from sacred Groove, Puducherry, India. *Int. J. Sci. Res.*, 6(5): 603-607 (5 pages).
- Gusakov, A.V.; Kondratyeva, E.G.; Sinitsyn, A.P., (2011). Comparison of two methods for assaying reducing sugars in the determination of carbohydrase activities. *Int. J. Anal. Chem.*, 2011(283658): 1-4 (4 pages).
- Hafich, K.; Perkins, E.J.; Hauge, J.B.; Barry, D.; Eaton, W.D., (2012). Implications of land management on soil microbial communities and nutrient cycle dynamics in the lowland tropical forest of northern Costa Rica. *Trop. Ecol.*, 53(2): 215-224 (10 pages).
- Hossain, M.J.; Ran, C.; Liu, K.; Ryu, C.M.; Rasmussen-Ivey, C.R.; Williams, M.A., (2015). Deciphering the conserved genetic loci implicated in plant disease control through comparative genomics of *Bacillus amyloliquefaciens* subsp. *plantarum* strains. *Front. Plant. Sci.*, 17(6): 631-644 (14 pages).
- Hu, B.; Liao, J.; Zhang, Q.; Ding, S.; He, M.; Qiao, Y.; Zhang, Z.; Shang, C.; Chen, S., (2022). Diversity and vertical distribution of sedimentary bacterial communities and its association with metal bioavailability in three distinct mangrove reserves of South China. *Water.*, 14(6): 1-27 (27 pages).
- Huang, X.; Zhao, J.; Zhou, X.; Zhang, J.; Cai, Z., (2019). Differential responses of soil bacterial community and functional diversity to reductive soil disinfestation and chemical soil disinfestation. *Geoderma.*, 348(2019): 124-134 (11 pages).
- Huynh, T.; Vörös, M.; Kedves, O.; Turbat, A.; Sipos, G.; Leitgeb, B.; Kredics, L.; Vágvölgyi, C.; Szekeres, A., (2022). Discrimination between the two closely related species of the operational group B. *amyloliquefaciens* based on whole-cell fatty acid profiling. *Microorganisms.*, 10(2): 418-430 (13 pages).
- Izquierdo, J.A.; Sizova, M.; Lynd, L.R., (2010). Diversity of bacteria and glycosyl hydrolase family 48 genes in cellulolytic consortia enriched from thermophilic biocompost. *Appl. Environ. Microbiol.*, 76(11): 3545-53 (9 pages).
- Kochzius, M.; Nuryanto, A., (2008). Strong genetic population structure

- in the boring giant clam, *Tridacna crocea*, across the Indo-Malay Archipelago: implications related to evolutionary processes and connectivity. *Mol Ecol.*, 17(17): 3775-3787 (13 pages).
- Kumar, S.; Stecher, G.; Li, M.; Knyaz, C.; Tamura, K., (2018). MEGA X: molecular evolutionary genetics analysis across computing platforms. *Mol. Biol. Evol.*, 35(6): 1547-1549 (3 pages).
- Kurniawan, A.; Sari, S.P.; Asriani, E.; Kurniawan, A.; Sambah, A.B.; Prihanto, A.W., (2018). Cellulolytic bacteria mangrove leaf litter in Bangka Island. *Samakia.*, 9(2018): 06-11 (6 pages).
- Kurniawan, A.; Prihanto, A.A.; Sari, S.P.; Febriyanti, D.; Kurniawan, A.; Sambah, A.B.; Asriani, E., (2018a). Isolation and identification of cellulolytic bacteria from mangrove sediment in Bangka Island. *IOP Conference Series: Earth. Environ. Sci.*, 137: 012070 (7 pages).
- Kurniawan, A.; Suci, P.S.; Euis, A.; Andi, K.; Abu Bakar, S.; Asep, A.P., (2019). Molecular identification of cellulolytic bacteria from mangrove sediment at Tin Mining Region In West Bangka. *Int. J. Appl. Boil.*, 3(2019): 7-14 (14 pages).
- Kusumaningrum, H.D.; Handayani, L.; Novrianti, R., (2016). Partial sequencing of 16S rRNA gene of selected *Staphylococcus aureus* isolates and its antibiotic resistance. *Media Peternakan.*, 39(2016): 67-74 (8 pages).
- Lam, K.; Morton, B., (2006). Morphological and mitochondrial-DNA analysis of the Indo-West Pacific rock oysters (Ostreidae: Saccostrea species). *J. Molluscan. Stud.*, 72(2006): 235-245 (11 pages).
- Leff, J.W.; Nemerger, D.R.; Grandy, A.S.; O'Neil, S.P.; Wickings, K.; Townsend, A.R.; Cleveland, C.C., (2012). The effects of soil bacterial community structure on decomposition in a tropical rain forest. *Ecosystems.*, 15(2012): 284-298 (15 pages).
- Liang, Y.; Yesuf, J.; Schmitt, S.; Bender, K.; Bozzola, J., (2009). Study of cellulases from a newly isolated thermophilic and cellulolytic *Brevibacillus* sp. strain JXL. *J. Ind. Microbiol. Biotechnol.*, 36(2009): 961-970 (10 pages).
- Liu, M.; Huang, H.; Bao, S.; Tong, Y., (2019). Microbial community structure of soils in Bamenwan mangrove wetland. *Sci. Rep.*, 9(2019): 1-11 (11 pages).
- Luo, L.; Gu, J.D., (2015). Particle-size fractions-dependent extracellular enzyme activity in sediments and implications for resource allocation in a subtropical mangrove ecosystem. *Global J. Environ. Sci. Manage.*, 1(1): 15-26 (12 pages).
- Maduppa, H.H.; Timm, J.; Kochzius, M., (2018). Reduced genetic diversity in the clown anemonefish *Amphiprion ocellaris* in exploited reefs of Spermonde Archipelago, Indonesia. *Front. Mar. Sci.*, 5(80): 1-8 (8 pages).
- Manjul, A.S.; Shirkot, P., (2018). 16S rRNA gene sequencing for bacterial identification of pullulanase synthesizing thermophilic bacteria contributing to big data. *Intl. J. Chem. Stud.*, 6(2): 2769-277 (5 pages).
- McGuire, K.L.; Fierer, N.; Bateman, C.; Treseder, K.K.; Turner, B.L., (2012). Fungal community composition in neotropical rain forests: the influence of tree diversity and precipitation. *Microb. Ecol.*, 63(4): 804-812 (9 pages).
- Nandy, A., (2009). Empirical relationship between intra-purine and intrapyrimidine differences in conserved gene sequences. *PLoS ONE.*, 4(8): e6829 (12 pages).
- Nares, S.; Balakrishnan, K.; Ahmad, A.N.G.; Yi Peng., (2019). Isolation and partial characterisation of thermophilic cellulolytic bacteria from North Malaysian tropical mangrove soil. *Trop. Life Sci. Res.*, 30(1): 123-147 (25 pages).
- Nimnoi, P.; Pongsilp, N., (2022). Insights into bacterial communities and diversity of mangrove forest soils along the Upper Gulf of Thailand in response to environmental factors. *Biology.*, 11(2): 1-22 (22 pages).
- Ningsih, R.L.; Khotimah, S.; Lovadi, I., (2014). Cellulose degradation bacteria from *Avicennia alba* blume leaf litter in the safety mangrove forest in Pontianak Regency. *Protobiont.*, 3(1): 34-40 (7 pages).
- Ntushelo, K., (2013). Identifying bacteria and studying bacterial diversity using the 16S ribosomal RNA genebased sequencing techniques: a review. *Afr. J. Microbiol. Res.*, 7(49): 5533-5540 (8 pages).
- Olmos, J.; Acosta, M.; Mendoza, G.; Pitones, V., (2020). *Bacillus subtilis*, an ideal probiotic bacterium to shrimp and fish aquaculture that increase feed digestibility, prevent microbial diseases, and avoid water pollution. *Arch. Microbiol.*, 202(3): 427-435 (9 pages).
- Palit, K.; Rath, S.; Chatterjee, S.; Das, S., (2022). Microbial diversity and ecological interactions of microorganisms in the mangrove ecosystem: Threats, vulnerability, and adaptations. *Environ. Sci. Pollut. Res.*, 29(2022): 32467-32512 (45 pages).
- Petti, C.A., (2007). Detection and identification of microorganisms by gene amplification and sequencing. *Clin. Infect. Dis.*, 44(8): 1108-1114 (7 pages).
- Powthong, P.; Suntornthicharoen, P., (2017). Antimicrobial and enzyme activity produced by *Bacillus* spp. isolated from soil. *Int. J. Pharm.Sci.*, 9(3): 205 (6 pages).
- Pramono, H.; Mariana, A.; Ryandini, D.; Sudiana, E., (2021). Short communication: Diversity of cellulolytic bacteria isolated from coastal mangrove sediment in Logending Beach, Kebumen, Indonesia. *Biodiversitas.*, 22(4): 1869-1878 (10 pages).
- Pringgenies, D.; Setyati, W.A.; Feliatra, F.; Ariyanto, D., (2023). The antibacterial and antifungal potential of marine natural ingredients from the symbiotic bacteria of mangrove. *Global J. Environ. Sci. Manage.*, 9(4): 819-832 (14 pages).
- Putra, A.N.; Mustahal.; Syamsunarno, M.B.; Hermawan, D.; Fatimah, D.G.; Putri, P.B.; Sevia.; Isnaini, R.; Herjayanto, M., (2021). Dietary *Bacillus* NP5 supplement impacts on growth, nutrient digestibility, immune response, and resistance to *Aeromonas hydrophila* infection of African catfish, *Clarias gariepinus*. *Biodiversitas.*, 22(1): 253-261 (9 pages).
- Raaijmakers, J.M.; Paulitz, T.C.; Steinberg, C.; Alabouvette, C.; Moënne-Loccoz, Y., (2009). The rhizosphere: a playground and battlefield for soilborne pathogens and beneficial microorganisms. *Plant Soil.*, 321(2009): 341-361 (21 pages).
- Safika.; Sari, W.N.; Darmawi.; Fahrimal, Y.; Santosa, S.F., (2018). Isolation and identification of a cellulolytic *Bacillus* from rumen of Aceh's cattle. *Asian Jr. of Microbiol. Biotech. Env. Sc.*, 20(3): 798-804 (6 pages).
- Saneha, S.; Pattamapitoon, T.; Bualert, S.; Phewnil, O.; Wararam, W.; Semvimol, N.; Chunkao, K.; Tudsanaton, C.; Srichomphu, M.; Nachaiboon, U.; Wongsrikaew, O.; Wichittrakarn, P.; Chanthasoon, C., (2023). Relationship between bacteria and nitrogen dynamics in wastewater treatment oxidation ponds *Global J. Environ. Sci. Manage.*, 9(4): 707-718 (12 pages).
- Santiago, C.M.; De Vicenta, A.; Romero, D., (2021). Bacterial extracellular matrix as a natural source of biotechnologically multivalent materials. *Comput. Struct. Biotechnol. J.*, 19(2021): 2796-2805 (10 pages).
- Sari, W.N.; Safika, S.; Darmawi, D.; Fahrimal, Y., (2017). Isolation and identification of a cellulolytic Enterobacter from rumen of Aceh cattle. *Vet. World.*, 10(12): 1515-1520 (6 pages).
- Shanti, V.; Roymon, M.G., (2018). Isolation and screening of alkaline thermostable xylanase producing bacteria from soil in Bhilal durg region of Chhattisgarh, India. *Int. J. Curr. Microbiol. Appl. Sci.*, 3(8): 303-311 (9 pages).
- Shome, B.R.; Mandal, A.B.; Bandhopadhyay, A.K., (1995). Bacteri flora in mangrove of Andaman: part I: isolation, identification and antibiogram studies. *Ind. J. Mar. Sci.*, 24(1995): 97-98 (2 pages).
- Soltani, M.; Hosenifar, S.H.; Roy, S.; Kumar, V.; Lymbery, A.; Ringoe, E., (2019). Genus *Bacillus*, promising probiotics in aquaculture: aquatic animal origin, bio-active components, bioremediation and efficacy

- in fish and shellfish. *Rev. Fish.*, 27 (3): 331-379 (49 pages).
- Srivastava, N.; Srivastava, M.; Mishra, P. K.; Singh, P.; Ramteke, P. W., (2015). Application of cellulases in biofuels industries: An overview. *J. Biofuels. Bioenergy*, 1(1): 55-63 (9 pages).
- Sulistiyani, T.R.; Masrukhin; Purnaningsih; Napitupulu, T.P.; Budiyanoto, A.; Kanti, A.; Sudiana, I.M., (2020). Endophytic bacteria diversity from Zingiberaceae and anticandidal characterization produced by *Pseudomonas helmanticensis*. *J.Teknologi.*, 83(1): 7-17 (11 pages).
- Talia, P.; Sede, S.M.; Campos, E.; Rorig, M.; Principi, D.; Tosto, D.; Hopp, H.E.; Grasso, D.; Cataldi, A., (2012). Biodiversitas characterization of cellulolytic bacteria present on native Chaco soil by comparison of ribosomal RNA genes. *Res. Microbiol.*, 163(3): 221-232 (12 pages).
- Tamura, K.; Stecher, G.; Peterson, D.; Filipski, A.; Kumar, S., (2013). MEGA6: Molecular evolutionary genetics analysis version 4.0. *Mol. Biol. Evol.*, 30(12): 2725-2729 (4 pages).
- Thatoi, H.; Bikash, C.B.; Rashmi, R.M.; Sushil., (2013). Biodiversity and biotechnological potential of microorganisms from mangrove ecosystems: a review. *Ann. Microbiol.*, 63(2013): 1-19 (19 pages).
- Truong, Q.P.; Phan, T.C.T.; Vu, H.H.; Pham, T.T.N.; Huynh, T.G.; Vu, N.U., (2021). Isolation of potential probiotic *Bacillus subtilis* CM3.1 and its effects on water quality and growth performance of the white leg shrimp *Litopenaeus vannamei* in the Mekong Delta, Vietnam. *AACL. Bioflux.*, 14(6): 3347-3357 (11 pages).
- Ubaidillah, R.; Sutrisno, H., (2012). Pengantar biosistemika: teori dan praktek. Pusat Penelitian Biologi. Lembaga Ilmu Pengetahuan Indonesia. Bogor, Indonesia: LIPI Press. (198p).
- Vásquez, E.; Millones, C., (2023). Isolation and identification of bacteria of genus *Bacillus* from composting urban solid waste and palm forest in Northern Peru. *Microorganisms.*, 11(3): 1-16 (16 pages).
- Wang, L.T.; Lee, F.L.; Tai, C.J.; Kuo, H.P., (2008). *Bacillus velezensis* is a later heterotypic synonym of *Bacillus amyloliquefaciens*. *Int. J. Syst. Evol. Microbiol.*, 58(3): 671-675 (5 pages).
- Watanabe, H.; Tokuda, G., (2009). Cellulolytic systems in insects. *Annu. Rev. Entomol.*, 55(2009): 609-632 (23 pages).
- Widananarni.; Sukenda.; Anggraeni, A.A.; Maharani, R.B.A.; Mulyadin, A.; Yuhana, M., (2022). The effects of different dosage applications of *Bacillus* sp. NP5 para-probiotic on the growth performance and resistance of Nile tilapia against *Streptococcus agalactiae* infection. *J. Akuakultur Indonesia.*, 21(2): 186-197 (12 pages).
- Yahya.; Happy, N.; Yenny, R.; Soemarno., (2014). Characteristic of extracellular metabolic of coastal ecosystem bacteria producing histidine decarboxylase crude. *Int. Food Res. J.*, 21(4): 1337-1347 (11 pages).
- Yanbo, W.; Zirong, X., (2006). Effect of probiotics for common carp (*Cyprinus carpio*) based on growth performance and digestive enzyme activities. *Anim. Feed. Sci. Tec.*, 127(3-4): 283-292 (10 pages).

#### AUTHOR (S) BIOSKETCHES

**Dewiyanti, I.**, Ph.D. Candidate, Graduate School of Mathematics and Applied Science, Universitas Syiah Kuala, Banda Aceh 23111, Indonesia.

- Email: [irmadewiyanti@usk.ac.id](mailto:irmadewiyanti@usk.ac.id)
- ORCID: 0000-0002-1361-6280
- Web of Science ResearcherID: E-5877-2017
- Scopus Author ID: 56140589200
- Homepage: <https://fsd.usk.ac.id/irmadewiyanti/>

**Darmawi, D.**, Ph.D., Professor, Laboratory of Microbiology, Faculty of Veterinary Medicine, Universitas Syiah Kuala, Banda Aceh, Aceh 23111, Indonesia.

- Email: [darmawi@usk.ac.id](mailto:darmawi@usk.ac.id)
- ORCID: 000-0003-3499-8000
- Web of Science ResearcherID: NA
- Scopus Author ID: 57190664731
- Homepage: <https://fsd.usk.ac.id/darmawi/>

**Muchlisin, Z.A.**, Ph.D., Professor, Aquaculture Department, Faculty of Marine and Fisheries, Universitas Syiah Kuala, Banda Aceh 23111, Indonesia.

- Email: [muchlisinza@usk.ac.id](mailto:muchlisinza@usk.ac.id)
- ORCID: 0000-0002-0858-1853
- Web of Science ResearcherID: NA
- Scopus Author ID: 55937322900
- Homepage: <https://fsd.usk.ac.id/muchlisinza/>

**Helmi, T.Z.**, Ph.D., Assistant Professor, Laboratory of Biochemistry, Faculty of Veterinary Medicine, Universitas Syiah Kuala, Banda Aceh 23111, Indonesia.

- Email: [zahrial\\_fkh@usk.ac.id](mailto:zahrial_fkh@usk.ac.id)
- ORCID: 000-0001-8623-2854
- Web of Science ResearcherID: NA
- Scopus Author ID: 57192716683
- Homepage: <https://fsd.usk.ac.id/zahrial/>

#### HOW TO CITE THIS ARTICLE

Dewiyanti, I.; Darmawi, D.; Muchlisin, Z.A., Helmi, T.Z., (2024). Diversity of cellulolytic bacteria in mangrove ecosystems soil using the 16S rRNA Gene. *Global J. Environ. Sci. Manage.*, 10(1): 51-68.

DOI: [10.22034/gjesm.2024.01.05](https://doi.org/10.22034/gjesm.2024.01.05)

URL: [https://www.gjesm.net/article\\_705424.html](https://www.gjesm.net/article_705424.html)





## ORIGINAL RESEARCH PAPER

## Evaluation of municipal waste collection performance using operational data

H.M. Giang<sup>1,\*</sup>, U.T.T. Ha<sup>1</sup>, L.T.L. Ngan<sup>1</sup>, N.D. Toan<sup>2</sup><sup>1</sup> Faculty of Environmental Engineering, Hanoi University of Civil Engineering, 55 Giai Phong Road, Hai Ba Trung District, Hanoi, 113021, Vietnam<sup>2</sup> Institute of Natural Resources and Environment Training, Ministry of Natural Resources and Environment, No 83 Nguyen Chi Thanh, Dong Da, Hanoi, Vietnam

## ARTICLE INFO

**Article History:**

Received 16 February 2023

Revised 25 May 2023

Accepted 27 June 2023

**Keywords:**

Collection route

Deadheading rate

Transportation cost estimation

Waste collection efficiency

## ABSTRACT

**BACKGROUND AND OBJECTIVES:** Developing countries' governments face challenges in municipal solid waste collection, such as rapidly increased volume of waste, physical and social obstacles to collection routes, or funding shortages. The lack of practical evaluation of the waste collection performance is considered a gap in improving the waste collection system in these countries. This study aims to assess the efficiency of current municipal solid waste collection by analyzing operational data that can help enhance the collection.**METHODS:** The geographical information system and the geographical position system data of all active trucks were collected for 14 consecutive days using the digital map. Data on waste volume collected by trucks, waste volume at collection points, and operational time of trucks throughout a working day were collected by survey. The operational efficiency indicators, including the deadhead rate, waste collected per distance unit, stopping time rate, and costs, are estimated to evaluate the effectiveness of municipal solid waste collection services.**FINDINGS:** The results indicate that solid waste collection efficiency of 1.67 tons/kilometers is low for high-density population areas. The deadheading rate of approximately 20 percent shows that the collection route operated by drivers is meandering and inefficient. Although using small trucks (6–7 tons) for transporting waste to landfills over a long distance is inefficient, small vehicles are used more than large ones. Ineffective utilization of transfer stations could lead to high idle time, accounting for approximately 37.6 percent of a collection trip. The regulated estimating method for transportation costs is not comprehensively developed, which may cause mistakes in choosing collection vehicles for operation and transfer station usage.**CONCLUSION:** The research findings assess the performance and identify ineffective factors that require improvement of waste collection, aiming to enhance the solid waste management system. Waste collection routes of Hoan Kiem district must be designed using empirical data. The distance-based coefficients should be developed for all collection vehicles with different loading capacities to better estimate collection and transportation costs in Hanoi, helping decision-makers utilize the current transfer station more effectively and appropriately in choosing collection vehicles for operation.DOI: [10.22034/gjesm.2024.01.06](https://doi.org/10.22034/gjesm.2024.01.06)This is an open access article under the CC BY license (<http://creativecommons.org/licenses/by/4.0/>).

NUMBER OF REFERENCES

31



NUMBER OF FIGURES

8



NUMBER OF TABLES

2

\*Corresponding Author:

Email: [gianghm@huce.edu.vn](mailto:gianghm@huce.edu.vn)

Phone: +849 4943 8385

ORCID: [0000-0003-0006-4541](https://orcid.org/0000-0003-0006-4541)

Note: Discussion period for this manuscript open until April 1, 2024 on GJESM website at the "Show Article".

## INTRODUCTION

In developing countries, waste management systems often struggle to provide effective collection services to urban populations (Shekdar, 2009). Ineffective urban waste collection practices can spread disease and adverse environmental and socio-economic impacts due to fuel consumption and pollutant emissions (Zsigraiova et al., 2013). Collection accounted for a significant share of the waste management cost (Greco et al., 2015), averaging between 50 percent (%) and 70% of the total system (Hannan et al., 2020). Municipalities in developing countries have implemented numerous waste collection schemes. Urban areas cannot take advantage of these initiatives due to financial distress and limited resources (Soni, 2022). Guerrini et al. (2017) advocated that enhancing the efficiency of waste collection services must be prioritized for adequate financial support. Improving the performance of solid waste collection systems (WCS) is a major challenge for most developing countries. In developing cities, drivers were responsible for constructing the waste collection routes without considering the increasing demand. An efficient OCR is vital as cities expand due to urbanization (Hazra and Goel, 2009). Analyzing demand, performance analysis, and planning routes more effectively are necessary to meet this increasing demand. The performance analysis findings can help make decisions about corrective actions to improve performance to meet environmental needs, ensure public acceptance, encourage social participation, and inform investment decisions or other specific activities (Sulemana et al., 2018). Urban waste collection rate has increased gradually in cities and provinces in Vietnam. It rose from 81% in 2010 to 92% in 2019 (Monre, 2020). Major cities, such as Ha Noi, Ho Chi Minh, and Da Nang, had relatively high urban solid waste collection rates of 99% and 100%. The secondary waste collection efficiency is inadequate, causing adverse effects, such as traffic problems, unpleasant odors, and litter on the road, affecting the sewage system. The rapid increase in the generated waste and continuous change in waste composition due to socio-economic development leads to confusion in operational practices. According to the National Status of the Environment Report (Monre, 2020), the solid waste composition showed a significant change due to the lifestyle of urban residents. Biodegradable organic

matter in household waste dropped from a high rate of approximately 80–90% in the 2000s to 50–60% in 2015–2020. Recyclable materials, such as paper and plastic, including components challenging to handle, such as textile, leather, rubber, and low-valued plastic waste, tend to increase over the years (Hoang et al., 2017; Pham et al., 2021). Low-density waste in the composition leads to a relative increase in waste volume, affecting the WCS capacity and operational efficiencies. Current research on collection efficiency focused on evaluating the municipal solid waste (MSW) collection service performed by private companies and local governments. Salazar-Adams (2021) research reveals that private waste collection companies may outperform the government's efficiency. However, in terms of eco-efficiency in MSW collection service, Romano et al. (2020) demonstrated that publicly-owned waste operators tend to excel. In Vietnam, the number of publicly-owned waste collection operators surpasses that of private companies. Notably, the collection efficiency of both is subpar. Collection activities' performance analysis through operational data is more important than relying on operators' choices. Collection system optimization has gained significant attention as a research trend. Previous studies defined optimal collection routes by re-allocation of recycling stations (Le et al., 2022); developed optimal routes to reduce costs and greenhouse gas emissions (Hannan et al., 2020), minimizing the number of vehicles with transfer stations (Ghani et al., 2021), or maximizing waste volume collected (Son, 2014). A substantial amount of data input is needed to achieve accurate results using optimization models. This requirement necessitates data worthiness and timeliness, which lack in Vietnam. The problems in Vietnam are the lack of data and key performance indicators (KPIs) to assess the collection system. Literature assessed the KPIs of WCS, including the operational cost (Zsigraiova et al., 2013), vehicles' traveled distances (Tavares et al., 2009), and the number of trips (Kinobe et al., 2015). The operational scheduling and routing of collection vehicles are often considered as leading causes of poor performance of the collection system, but these factors are less considered in previous literature. This shortcoming occurs in many developing cities, including Ha Noi City (HNC). Regarding waste collection in densely populated urban areas, such as the city center of HNC, operational time is critical

in ensuring efficient and timely waste collection. The problem of traffic congestion during rush hour exacerbates the challenge of waste collection. Being efficient in the timely waste collection could help minimize traffic flow disruption. The operational time has been studied in previous literary works, yet these studies have been somewhat limited concerning its impact on enhancing the collection process. Operational time for each waste collection process, such as loading and unloading waste, moving, and off-route during operation, was not specified in the study of [Le et al. \(2021\)](#). The timely efficiency was evaluated in the study by [Nguyen \(2018\)](#) but did not consider factors affecting the running time, such as routes and distance from landfills and transfer stations. Weight collected per distance unit is a crucial measure for evaluating the efficacy of collection routes. It provides valuable insights into appropriate collection services based on area conditions, especially in high-density urban settlements ([Nguyen, 2018](#)). Other essential metrics for waste collection assessment are cost for collection and deadheading rate. The term 'deadheading' means the unnecessary distance traveled by collection trucks that do not collect trash. A high deadheading rate means more fuel, labor, and upkeep expenses with no income in return. Academic research tends to focus on the former ([Salazar-Adams, 2021](#); [Le et al., 2022](#); [Hannan et al., 2020](#)) and not consider the latter. An assessment of the rate of deadheading, accompanied by KPIs, such as weight collection per unit of routes and trucks, operational time, and cost analysis, can uncover potential strategies for improving the system. Previous studies have been found to overlook the issue of insufficient attention. A thorough analysis of these indicators and the factors that influence them is necessary to develop effective strategies for improvement. This study mainly aims to identify the primary factors that affect collection efficiency indicators and to devise strategies for enhancing WCS. This study was conducted in Hoan Kiem district (HKD), Ha Noi City, Vietnam in 2021.

## MATERIALS AND METHODS

Ha Noi is one of the most prominent cities in Vietnam with a population of 8.5 million people and plays a significant role in Vietnam's economy and culture. Like many rapidly growing cities, waste management in Ha Noi has become a critical issue in

recent years ([Monre, 2020](#)).

### Study area

HKD is one of the famous tourist destinations in Ha Noi ([Fig. 1](#)). Located in the city's heart, this district is famous for its peaceful beauty and cultural significance, offering visitors a glimpse into its rich heritage. The district is the smallest district of Ha Noi City, with a population of approximately 140 thousand.

The waste collection in the old quarter district often faces problems due to the complexity of the urban, high-density population, the significant number of tourists, and the inappropriate waste collection routes ([Phuong et al., 2021](#)). [Fig. 2](#) shows the waste flow and collection method applied in HKD.

Although vehicles and facilities are adequate, slow waste transportation due to inefficient route design causes various difficulties for collection activities. The daily waste generation in HKD is approximately 250–300 tons (t), primarily from household, tourist, commercial, and public activities, and this amount of waste is transported to Nam Son landfill (NSL), which is 50 kilometers (km) from the city.

### Survey and data collection

The global position system (GPS) loggers attached to Ha Noi urban environment company (URENCO) collection vehicles record the coordinate data by time. The database is stored and processed in URENCO digital map system for management. The GPS data of operational trucks operating in HKD is collected for 14 consecutive days (May 16–29, 2021) via Ha Noi URENCO digital map system ([Nordtest, 1995](#)). With 11 collection trucks (including six 6-ton loads, two 7-ton, two 10-ton, and one 11-ton vehicles) operating in the area, the team could collect operational data of approximately 197 collection rides (197 samples) for processing and analyzing the efficiency of the WCS. Quantum global information system (QGIS) ver. 3.30.1 software was used to map collection routes with collection points. The collection points' geographic coordinates are collected from Ha Noi URENCO. Due to no collection route being designed, the collection route in each area is defined by survey team members based on the location of collection points, and the road segment drivers travel most to collect waste in that area. The volume of waste in collection points and waiting time at collection points were observed

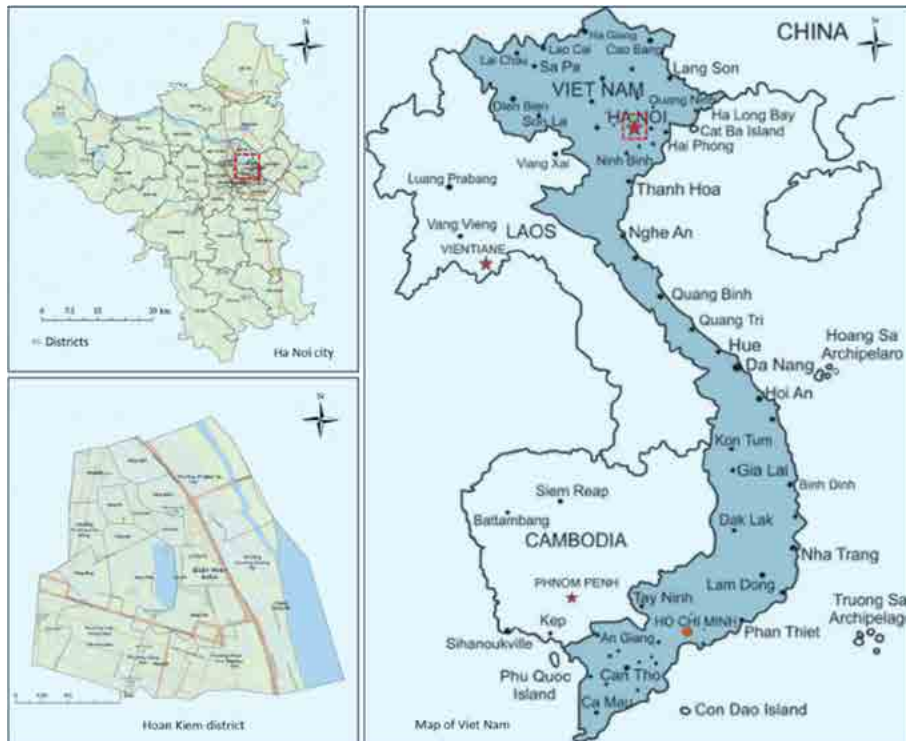


Fig. 1: Geographic location of the study area HKD, Ha Noi City, Vietnam



Fig. 2: Methods for collecting waste in HKD

by the field survey team in the collection points during the survey period. The collection cost for each trip was estimated and provided by URENCO as secondary data. The explanation of indicators, input data, and collection methods is presented in Table 1.

#### Data analysis

Several indicators evaluate the collection operation's effectiveness in this study. Firstly, the

effectiveness of the collection route and vehicle usage in the related tour is evaluated by the rate of waste collected amount per moving distance of collection trucks. This indicator is popular in comparing collection methods (Nguyen, 2018). In this study, indicator  $E_1$  (Eq. 1) assesses the route operated by collection drivers in each area while the indicator  $E_2$  (Eq. 2) evaluates the effectiveness of using collection vehicle types for the whole trip. The effectiveness of

Table 1: Factors and indicators for assessing the performance of the collection route

No.	Input data and indicators	Denotes	Units	Explanation and determination
1		$i,j,k$		Denote the collection truck, route, and vehicle type
2	Number of sample	$n^j$ $n_k$		The number of trucks collecting waste on route $j$ , and the number of collection trucks type $k$
3	Length of total collection trip	$Q_{i,j}$	Km	The total length of the trip (from garage to landfill and go back to garage) that the collection truck $i$ collecting waste on route $j$ . The data is collected from recorded data in the digital map of URENCO based on the registered plate of vehicles and time.
4	Operational time	$T_i$	minute (min)	The operational time of a collection truck $i$ for one trip. The data is collected from URENCO digital map.
5	Stopping time	$T_i^s$	min	The total stopping time of collection truck $i$ during the operation. Survey team members collect and calculate the data by tracking vehicle $i$ on each trip on URENCO digital map.
6	The length of the collection route	$D_j$	km	The length of route $j$ traveled by collection trucks from the first collection point to the last. $D_j$ is determined based on the digital map after survey team members create the collection route.
7	The length of the deadhead	$D_j^h$	km	The total segment length of that collection vehicle traveled more than once in route $j$ without waste collection. $D_j^h$ was defined by survey team members based on the movement of the collection truck in the collection route map.
8	Collected waste amount of a vehicle in one trip	$M_i$	t	The amount of waste that the collection truck $i$ collected in one route. Data of $M_i$ are collected from recorded data of weighbridge in NSL according to the registered plate of vehicles and the time the vehicle arrived
9	The efficiency of the collection route	$E_0^j$	t/km	The rate of the waste amount per distance of the collection route $j$ inside the city
10	The route efficiency of collection vehicles (truck types)	$E_1^k$	t/km	The rate of the waste amount that trucks type $k$ (small and large) transport over the distance of the collection routes
11	The trip efficiency of the collection vehicles (truck types)	$E_2^k$	t/km	The rate of the waste amount that trucks type $k$ (small and large) transport over the distance of the collection trips
12	The indicator for deadheading rate assessment	$E_3$	%	The percentage of the deadheading segment length and the length of the collection route (Mcbride, 1982)
13	The indicator for time usage effectiveness assessment	$E_4$	%	The percentage of stopping time over operational time

route  $j$  was calculated using Eq. 1 (Nguyen, 2018).

$$E_0^j = \frac{\sum_i \frac{M_{i,j}}{D_j}}{n_j} \quad (1)$$

The effectiveness of trucks type  $k$  was calculated using Eq. 2 (The current study result).

$$E_1^k = \frac{\sum_{i,j} \frac{M_{i,j,k}}{D_{j,k}}}{n_k} \quad (2)$$

The effectiveness of collection vehicles for the

whole tour was calculated using Eq. 3 (The current study result).

$$E_2^k = \frac{\sum_{i,j} \frac{M_{i,j,k}}{Q_{i,j,k}}}{n_k} \quad (3)$$

The deadhead indicator presents the proportion of ineffective road segments applied to evaluate the collection route drivers' superiority based on their experience with city traffic and area conditions. A higher deadhead rate indicates the current collection route is meandering and inefficient. The deadheading rate was calculated using Eq. 4 (Cortés et al., 2011).

$$E_3 = \frac{D_j^h}{D_j} \times 100 \quad (4)$$

The indicator of collection time usage evaluates the ratio of stopped time (including waste collection time) to the total operating time of the collection vehicle. A higher ratio indicates a longer idle time for the vehicle. A high ratio implies that the vehicle has to stop frequently during its operation, and the utilization of the collection vehicle's operation time along the route is inefficient. Stopping time can be affected by the local traffic condition or the road characteristics in downtown areas. The time usage effectiveness was calculated using Eq. 5 (The current study result).

$$E_4 = \frac{T_i^s}{T_i} \times 100 \quad (5)$$

## RESULTS AND DISCUSSION

Fig. 3 presents the maps of collection routes for waste collection in each area in HKD, as re-created by GPS data of collection vehicles during the survey. The red lines present the actual moving pathway of collection vehicles from the garage to collection areas, and the blue lines describe the route for collecting waste in assigned areas, defined by collection points in the areas and the highest moving frequency of collection vehicles.

The collection routes are not properly planned; the drivers choose the optimal route based on their experience and understanding of traffic conditions in the collection area. The collection routes in Hang Bai, Tran Hung Dao, and Cua Nam vary among collection trips. The drivers' unstable routes made the management and operation difficult, especially in assessing the effectiveness of waste collection activities. Analyzing and assessing collection activities' efficiency is impossible when drivers operate different routes time by time. Thus, the current collection face difficulties in improvement due to a lack of assessment data. Determination of route collection maps helps estimate the length, deadheading rates, and route efficiency.

### Efficiency of collection routes

Table 2 presents the daily data of collection routes, cost and efficiency, and the rate of truck types used for

each route defined in the maps. Based on the created maps, the average length of a waste collection route is 5.3 km, with an average frequency of approximately 1.5 trips per day. The means of route efficiency of trucks is approximately 1.67 tons per kilometer (t/km), higher than Da Nang city (0.6–1.65 t/km) (Nguyen, 2018). The distance between the city and the disposal site is a key factor in collection efficiency. The routes with the highest effectiveness are Trang Tien, Tran Hung Dao, and Phan Chau Trinh, while those with the lowest effectiveness are Hang Dao, Le Van Linh, and Ly Thai To. Although the latter routes generate high volumes of waste, their collection efficiency is only approximately 1 t/km. Long-distance routes and dense populations decrease collection efficiency in these areas. The effectiveness of a route is also affected by the utilization of vehicles, as shown in this case study. Using larger vehicles can increase the amount of waste collected per distance unit and potentially increase collection costs. The cost column indicates the fee for collecting and transporting one ton of MSW from the city to the landfill for disposal, thereby representing the unit cost of a truck for this purpose.

### The deadheading rates

The high proportion of deadheading segments is attributed to the characteristics of the assigned area's terrain, road, and traffic conditions. One of the main factors is the inefficient routing and scheduling of waste collection trucks. Poor route design can lead to long detours and backtracking, wasting time, fuel, and resources. The deadheading rate significantly impacts the effectiveness of waste collection routes, but it lacks attention in waste collection studies in Vietnam. Fig. 4 illustrates the deadheading rate of waste collection routes, indicating that the average deadheading rate is approximately 20%. The collection routes with the highest deadhead are Hang Bai (50%) and Le Van Linh (30%). Due to its low deadheading rate, the Trang Tien route is the most efficient moving distance. The box plot reveals several outliers for the Bach Dang, Cua Nam, Hang Dao, Hang Bai, and Ly Thai To routes, indicating that collection vehicles traveled differently on each trip due to drivers' choices, increasing deadheading rates. The deadheading rate in waste collection routes got little attention in previous literature, and other Vietnamese cities' information on the deadheading

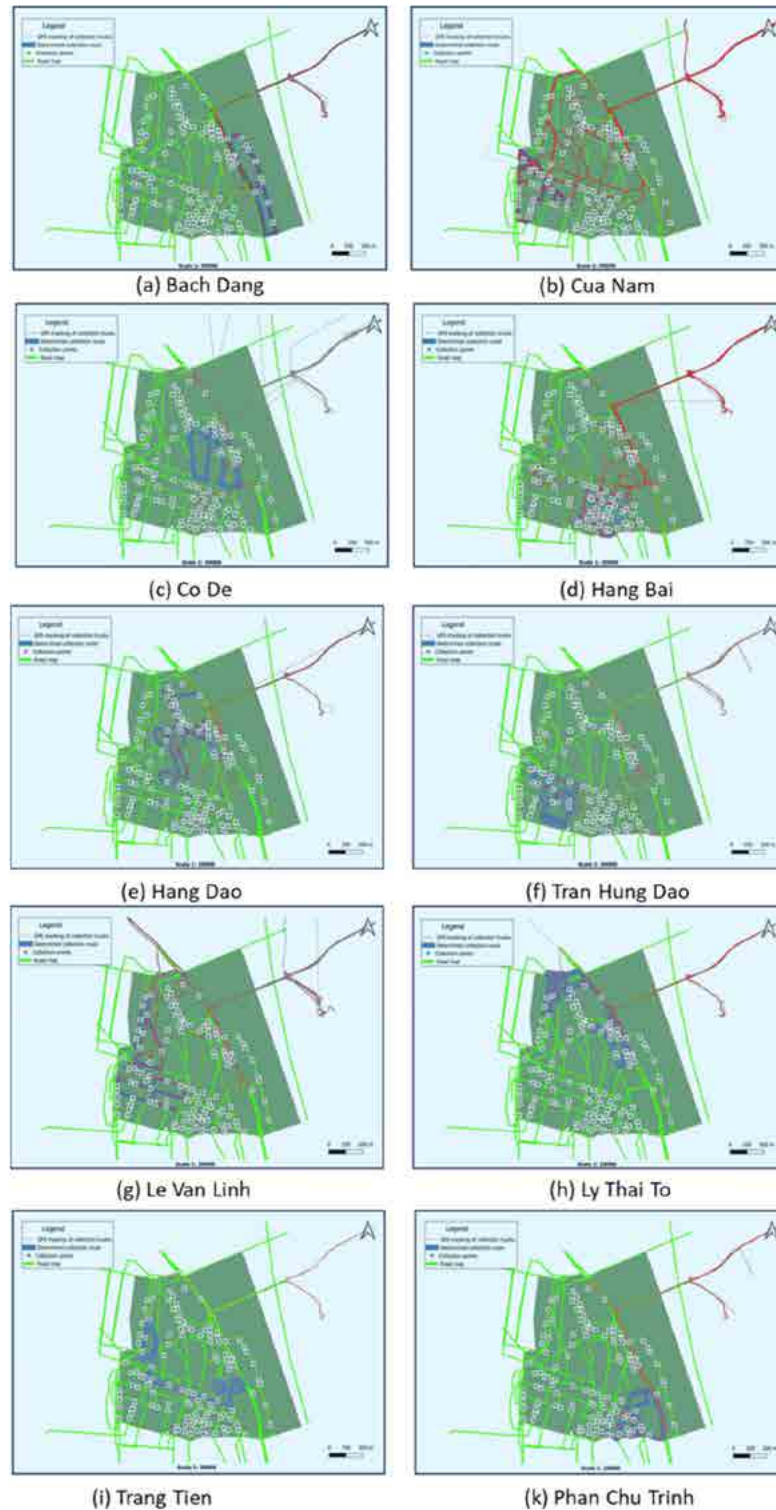


Fig. 3: Waste collection routes of HKD. The red and orange line shows the actual moving of collection vehicles, while the blue lines show the collection route in different areas. Handcart icons and their address present the collection points

### Waste collection efficiency assessment

Table 2: Data and parameters of collection routes in Hoan Kiem

Route	$D_j$ (km)	Efficiency $E_0^j$ (t/km)	Daily collected (t/day)	Cost (VND/t)	Frequency (trips/day)	Percentage of 6 and 7-ton trucks (%)
Trang Tien	4.4	2.53	3.2	271,850	0.3	0
Tran Hung Dao	4.2	2.82	12.7	268,681	1.1	0
Phan Chau Trinh	4.9	2.47	10.4	271,226	0.9	8
Ly Thai To	7.2	1.00	13.4	244,622	1.9	100
Le Van Linh	7.8	1.30	31.1	250,027	3.1	50
Hang Dao	7.9	0.98	13.2	247,020	1.7	100
Hang Bai	4.6	1.71	11.7	249,875	1.5	95
Cua Nam	3.8	1.98	12.5	262,147	1.6	100
Co De	4.3	1.79	4.4	257,808	0.6	100
Bach Dang	3.7	2.14	12.3	248,039	1.6	100
Average	5.3	1.67	12.5	257,130	1.4	65

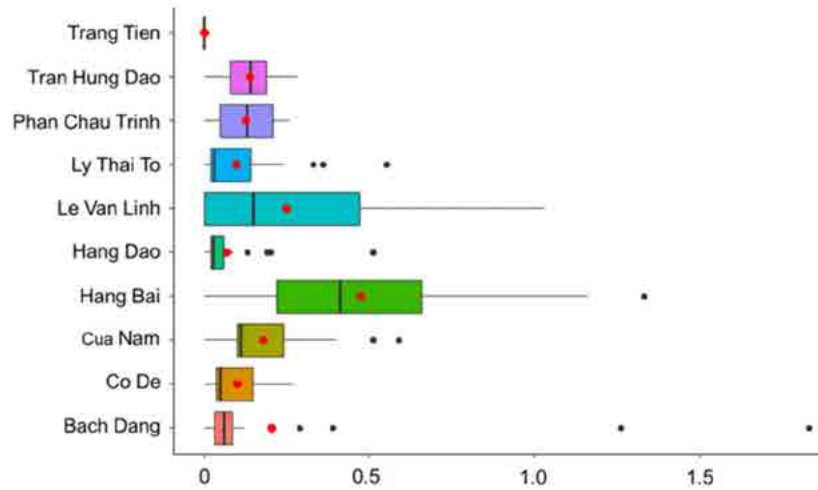


Fig. 4: The deadheading rate of collection routes

rate of waste collection routes is unavailable.

To reduce deadheading rates in waste collection routes, waste collection companies can invest in better route optimization and scheduling software to optimize routes based on real-time data on waste generation patterns (Ramos *et al.*, 2018). Various optimization methods are successfully applied to optimize collection systems, such as variable routing optimization (Hannan *et al.*, 2020); GIS approaches (Tavares *et al.*, 2009), mixed integer programming (Bhambulkar and Khedikar, 2011) or Integer Linear Programming (Ghani *et al.*, 2021). In addition to optimizing routes and schedules, URENCO can undertake alternative waste collection methods, such as on-demand or subscription-based collection

services, that can reduce deadheading rates by aligning collection schedules with waste generation amount more effectively. Such approaches can also provide more flexible and customized waste collection services to businesses and households with home businesses, leading to higher customer satisfaction and loyalty.

#### *The efficiency of collection vehicles*

Fig. 5 shows the result of effectiveness indicators  $E_1$  and  $E_2$  in assessing the effectiveness of truck usage for collection inside and outside the city center. The mean collection efficiency of vehicles over the trip is approximately 0.1 t/km, relatively lower than in Hoi An City (0.5 t/km) (Le *et al.*, 2021).

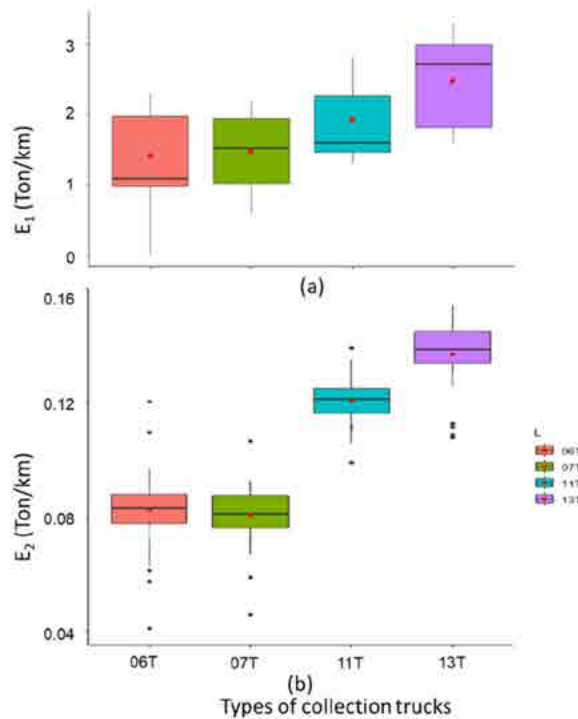


Fig. 5: The collection vehicles' effectiveness assessment

The variance in the efficiency of route collection across various vehicle types (from 1.5–2.1) (Fig. 5a) is considerably smaller than that of the efficiency of the trip (from 0.08–0.13) (Fig. 5b). These results indicate that small collection trucks (6-ton and 7-ton) are more effective for short trips, and big trucks (11-tons and 13-tons) are suitable for long trips. Using small trucks for transporting waste to landfills over a long distance is inefficient. To enhance the effectiveness of WCS, small trucks for the direct transportation of waste to NSL should be reduced, and a transfer station should rather be utilized (Worrell and Vesilind, 2010).

#### Collection time

Fig. 6 assessed the time usage efficiency of each vehicle used for transportation. On average, an entire collection trip took approximately 291 min (approximately 6 hours), and the stopping time is approximately 108 min (approximately 2 hours), accounting for approximately 37.6% of the traveled time. The operation and stopping times are significantly varied, while the total distance of

collection trips is constant, approximately 93 km. Le et al. (2021) recent study discovered that the average cumulative operational hours for each type of vehicle across four working shifts in Hoi An City is approximately 3 hours. Vehicles can operate on four shifts per day. Shorter transportation distances result in better efficient use of vehicles, while longer distances pose challenges in controlling operational time (Nguyen, 2018). Implementing a waste transfer station presents an optimal solution to the time inefficiencies the vehicles face.

Fig. 7 illustrates the correlation between waste volume collected by a vehicle ( $M_i$ ) and the stopping time of each vehicle. The correlation coefficient is 0.22, indicating that the stopping time of vehicles is not affected by the amount of loading waste. This result is consistent with a previous study by Nguyen (2018). The field observation results showed that the average loading time of small and large vehicles, considered part of stopping time in this study, is approximately 45 and 70 minutes (min). The unknown-reason stopping time is approximately 40–60 min, accounting for 13–20% of the overall collection time of vehicles, considered as

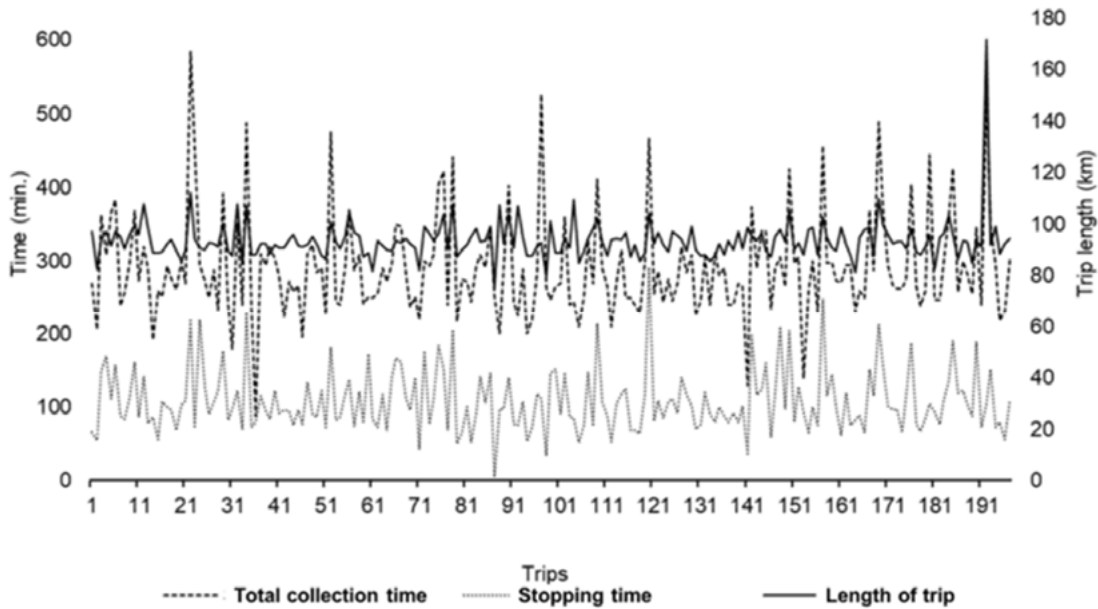


Fig. 6: Time usage of different collection trips

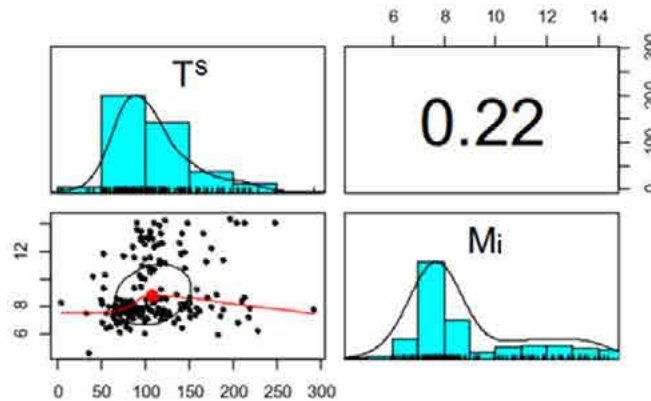


Fig. 7: Correlation of stopping time and loading waste of vehicle.

off-route factors. This result is consistent with the off-route factors defined in the study of Tchobanoglous et al. (1993), which varies from 10–40% of collection time, and a rate of 15% is the representative off-route factor for most operations. This study indicates that the drivers made efficient use of their time while gathering and carrying waste despite working a six-hours-extended shift.

Despite the Lam Du transfer station located approximately 5 km from the city center, it is not

being utilized to transform small collection trucks into large vehicles (Ghiani et al., 2021). Fig. 8 shows the cost for collection and the number of trips using small vehicles (7 t maximum loading capacity) and using large vehicles (13 t maximum loading capacity). The unit costs for transporting one t of waste using small compressor trucks are cheaper than that for large ones. URENCO Hanoi uses small trucks for transporting waste to landfills more frequently. It can be explained by the collection

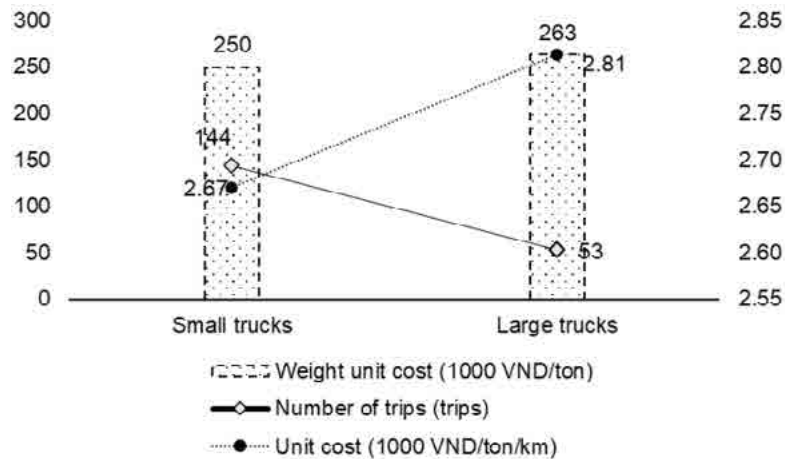


Fig. 8: Collection cost

cost estimates method regulated by the decision 30/2020/QĐ-UBND on Nov 26<sup>th</sup>, 2020, on issuing procedures, standards, and cost estimation for environmental sanitation maintenance in Ha Noi City (HPC, 2020). The method applied the same distance-based adjustment coefficients for labor and equipment costs for all vehicles. The unit cost of small trucks is always lower than that of big trucks. This study result contrasts prior studies of waste transfer stations (Ouan, 1983) and the theory for estimating transportation cost (Worrell and Vesilind, 2010), indicating that the slope of unit cost per weight of small trucks is greater than that of large trucks. The unit cost per t per km of small trucks should be greater than that of large ones (Ouan, 1983). Since the large vehicle unit cost is higher than the small vehicle unit cost, the transfer station is inappropriate in Ha Noi. It requires developing the distance-based adjustment coefficients appropriate for different truck capacities to improve the cost-estimating method of waste transportation.

## CONCLUSION

The study investigated HKD's secondary collection system through operational data and four KPIs. The analysis of these indicators has revealed the interdependence of these factors and their consequential impact on the overall operation of the collection system. Notably, this research pioneers analyzing and evaluating the deadheading rate indicator. The result indicates that the existing

collection routes, established by drivers based on their experience with local traffic, are meandering and ineffective. The mean deadheading rate is relatively high, at approximately 20%. Hang Bai route exhibits the highest deadheading of approximately 50%. The mean collection efficiency of vehicles throughout the trip, estimated to be approximately 0.1 t/km, is relatively low compared to other cities in Vietnam. The mean operational time of a collection trip is approximately 6 hours, and the driver must work a prolonged shift. The collection system requires more workers and trucks due to the long operational time. The study also shows that the transportation cost estimation method is inappropriate when applying the same distance coefficient for small and big trucks. It can also explain the ineffective utilization of transfer stations and the relatively high operational time and long transportation distance in HKD. After analyzing the collection efficiency indicators and the contributing factors, the primary strategies for enhancing efficiency have been identified. Following the initiative to promote scientific-based decision-making in Vietnam, it is recommended that a study be conducted to determine the distance factors for waste transportation trucks of varying types. The results should then be disseminated and discussed with relevant authorities. Precise calculations and collection cost projections can efficiently utilize collection vehicles and transfer stations. Next, vehicle routing should be re-designed to reduce the

deadheading rate and optimize waste collection. By illuminating these strategies, communities and URENCO could better manage and streamline their waste management processes, leading to more sustainable and environmentally friendly practices.

#### AUTHOR CONTRIBUTIONS

G.M. Hoang, the corresponding author, has contributed to planning the research, interpreting results and preparing the manuscript. T.D. Nguyen conducted secondary data collection and reviewed, commented, and edited the manuscript., H.T.T. Ung conducted survey and and N.T.L. Le carried out data analysis.

#### ACKNOWLEDGEMENT

The authors thank the Ministry of Education and Training, Vietnam, for supporting our research under the grant financial Number [B2019-XDA-01]. The authors sincerely thank Mr. Tran Nhat Hoai, our student, for his active assistance in preparing the maps of the article.

#### CONFLICT OF INTEREST

The author declares that there is no conflict of interest regarding the publication of this manuscript. In addition, the ethical issues, including plagiarism, informed consent, misconduct, data fabrication and/or falsification, double publication and/or submission, and redundancy, have been ultimately observed by the authors.

#### OPEN ACCESS

©2024 The author(s). This article is licensed under a Creative Commons Attribution 4.0 International License, which permits use, sharing, adaptation, distribution and reproduction in any medium or format, as long as you give appropriate credit to the original author(s) and the source, provide a link to the Creative Commons license, and indicate if changes were made. The images or other third-party material in this article are included in the article's Creative Commons license, unless indicated otherwise in a credit line to the material. If material is not included in the article's Creative Commons license and your intended use is not permitted by statutory regulation or exceeds the permitted use, you will need to obtain

permission directly from the copyright holder. To view a copy of this license, visit: <http://creativecommons.org/licenses/by/4.0/>

#### PUBLISHER'S NOTE

GJESM Publisher remains neutral with regard to jurisdictional claims in published maps and institutional affiliations.

#### ABBREVIATIONS

%	Percent
$D_j$	Distance of collection route
$D_j^h$	Distance of deadhead
$E_0$	Efficiency of collection route
$E_1$	Route efficiency of collection trucks
$E_2$	Trip efficiency of collection trucks
$E_3$	Percentage of deadheading length
$E_4$	Percentage of stopping time
GIS	Global information system
GPS	Global position system
HKD	Hoan Kiem district
km	kilometers
$M_i$	Amount of waste that a collection truck collected
min.	minutes
MSW	Municipal solid waste
min	minute
NSL	Nam Son landfill
OCR	operational collection route
$Q_{i,j}$	The total distance of the collection trip
QGIS	Quantum GIS
t	Ton
$T_i$	Operational time
$T_i^s$	Stopping time
URENCO	Urban environment company
WCS	waste collection systems

## REFERENCES

- Akhtar, M.; Hannan, M.A.; Begum, R.A., (2017). Backtracking search algorithm in CVRP models for efficient solid waste collection and route optimization. *Waste Manage.*, 61: 117–128 **(12 pages)**.
- Ashish, S.; Pankaj K.D.; Abdul, W.H.; Mohammad Y.; Hesam K.; Shreshivadasan C., (2022). Challenges and opportunities of utilizing municipal solid waste as alternative building materials for sustainable development goals: a review. *Sustainable Chem. Pharm.*, 27(2022): 100706 **(33 pages)**.
- Bhambulkar, A.V.; Khedikar I.P., (2011). Municipal solid waste collection route for Laxmi Nagar by geographical information system. *Int. J. Adv. Eng. Technol.*, 2(4): 48–53 **(6 pages)**.
- Cortés, C.E.; Jara-Díaz, S.; Tirachini, A., (2011). Integrating short turning and deadheading in the optimization of transit services. *Transp. Res. Part A Policy Pract.*, 45(5): 419-434 **(15 pages)**.
- Ghiani, G.; Manni, A.; Manni, E.; Moretto, V., (2021). Optimizing a waste collection system with solid waste transfer stations. *Comput. Ind. Eng.*, 161: 107618 **(7 pages)**.
- Greco, G.; Allegrini, M.; Lungo, C. D.; Savellini, P.G.; Gabellini, L., (2015). Drivers of solid waste collection costs. Empirical evidence from Italy. *J. Clean. Prod.*, 106: 364–371 **(8 pages)**.
- Guerrini, A.; Carvalho, P.; Romano, G.; Marques, R.C.; Leardini, C., (2017). Assessing efficiency drivers in municipal solid waste collection services through a non-parametric method. *J. Clean. Prod.*, 147: 431–441 **(11 pages)**.
- Hannan, M.A.; Begum, R.A.; Al-Shetwi, A.Q.; Ker, P.J.; Al Mamun, M.A.; Hussain, A.; Basri, H.; Mahlia, T.M.I., (2020). Waste collection route optimisation model for linking cost saving and emission reduction to achieve sustainable development goals. *Sustainable Cities Soc.*, 62: 102393 **(11 pages)**.
- Hazra, T.; Goel, S., (2009). Solid waste management in Kolkata, India: practices and challenges. *Waste Manage.*, 29(1): 470–478 **(9 pages)**.
- Hoang, M.G.; Fujiwara T.; Pham P.S.T., (2017). Municipal waste generation and composition in a tourist city - Hoi An, Vietnam. *J Japan Soc. Civ. Eng.*, 5: 123–132 **(10 pages)**.
- HPC, (2020). Decision 30/2020/QĐ-UBND, Procedures, standards, and cost estimation for environmental sanitation maintenance in Hanoi city.
- Kinobe, J.R.; Bosona, T.; Gebresenbet, G.; Niwagab, C.B.; Vinnerås, B., (2015). Optimization of waste collection and disposal in Kampala city. *Habitat Int.*, 49: 126–137 **(12 pages)**.
- Le, D.C.; Fujiwara, T.; Asari, M.; Pham, P.S.T., (2021). Solid waste collection system in tourism destination – The status, problems and challenges. *Chem. Eng. Trans.*, 83: 43–48 **(6 pages)**.
- Le, D.C.; Fujiwara, T.; Asari, M.; Pham, P.S.T., (2022). Optimization of solid waste collection system in a tourism destination. *Global J. Environ. Sci. Manage.*, 8 (3):419–436 **(18 pages)**.
- Mcbride, R., (1982). Controlling left and u-turns in the routing of refuse collection vehicles. *Comput. Oper. Res.*, 9(2): 145–152 **(8 pages)**.
- Monre, (2020). National report on the Environment status 2019: Domestic waste management. Dan Tri publisher.
- Nguyen, H.D., (2018). Assessment of waste collection systems and separate collection alternatives in Vietnam. PhD. Dissertation, Okayama University. Japan.
- Nguyen, T.T.T.; Wilson, B.G., (2010). Fuel consumption estimation for kerbside municipal solid waste collection activities. *Waste Manage. Res.*, 28: 289–297 **(9 pages)**.
- Nordtest, (1995). Solid waste, municipal: Sampling and characterisation **(12 pages)**.
- Ouano, E.A.R., (1983). Hauling distance and transfer station location. *J. Environ. Eng.*, 109(6): 1429–1433 **(5 pages)**.
- Pham, P.S.T.; Fujiwara, T.; Akasaki, N.; Le, D.C.; Hoang, M.G.; Pham, V.D., (2021). Analyzing the characterization of municipal solid waste in Da Nang City, Vietnam. *Chem. Eng. Trans.*, 83: 241–246 **(6 pages)**.
- Phuong, N.T.L.; Yabar, H.; Mizunoya, T., (2021). Characterization and analysis of household solid waste composition to identify the optimal waste management method: a case study in Hanoi city, Vietnam. *Earth*. 2(4): 1046–1058 **(13 pages)**.
- Ramos, T.R.P.; de Moraes, C.S.; Barbosa-Póvoa, A.P., (2018). The smart waste collection routing problem: Alternative operational management approaches. *Expert Syst. Appl.*, 103: 146–158 **(13 pages)**.
- Romano, G.; Molinos-Senante, M., (2020). Factors affecting eco-efficiency of municipal waste services in Tuscan municipalities: an empirical investigation of different management models. *Waste Manage.*, 105: 384–394 **(11 pages)**.
- Salazar-Adams, A., (2021). The efficiency of municipal solid waste collection in Mexico. *Waste Manage.*, 133(2021): 71–79 **(9 pages)**.
- Shekdar, A.V., (2009). Sustainable solid waste management: An integrated approach for Asian countries. *Waste Manage.*, 29(2009): 1438–1448 **(11 pages)**.
- Son, L.H., (2014) Optimizing municipal solid waste collection using chaotic particle swarm optimization in GIS based environments: a case study at Danang city, Vietnam. *Expert Syst. Appl.*, 41: 8062–8074 **(13 pages)**.
- Sulemana, A.; Donkor, E.A.; Forkuo, E.K.; Oduro-kwarteng, S., (2018). Optimal routing of solid waste collection trucks: a review of methods. *J. Eng.*, 2018: 4586376 **(12 pages)**.
- Tavares, G.; Zsigraiova, Z.; Semiao, V.; Carvalho, M.G., (2009). Optimisation of MSW collection routes for minimum fuel consumption using 3D GIS modelling. *Waste Manage.*, 29(3): 1176–1185 **(10 pages)**.
- Tchobanoglous, G.; Thelsen, H.; Vigil, S., (1993). Integrated solid waste management: engineering principles and management issues, McGraw-Hill, Inc.
- Worrell, W.A.; Vesilind, A.P., (2012). Solid waste engineering, Second E., Cengage Learning, Stamford.
- Zsigraiova, Z.; Semiao, V.; Beijoco, F., (2013). Operation costs and pollutant emissions reduction by definition of new collection scheduling and optimization of MSW collection routes using GIS. The case study of Barreiro, Portugal. *Waste Manage.*, 33(4): 793–806 **(14 pages)**.

#### AUTHOR (S) BIOSKETCHES

**Giang, H.M.**, Ph.D., Assistant Professor, Faculty of Environmental Engineering, Hanoi University of Civil Engineering, 55 Giai Phong Road, Hai Ba Trung District, Hanoi, 113021, Vietnam.

- Email: [gianghm@huce.edu.vn](mailto:gianghm@huce.edu.vn)
- ORCID: [0000-0003-0006-4541](https://orcid.org/0000-0003-0006-4541)
- Web of Science ResearcherID: O-5640-2017
- Scopus Author ID: 57201072500
- Homepage: <https://moitruong.huce.edu.vn/ts-hoang-minh-giang>

**Ha, U.T.T.**, Dr., Senior Lecturer, Faculty of Environmental Engineering, Hanoi University of Civil Engineering, 55 Giai Phong Road, Hai Ba Trung District, Hanoi, 113021, Vietnam.

- Email: [hautt@huce.edu.vn](mailto:hautt@huce.edu.vn)
- ORCID: [0000-0003-3401-1536](https://orcid.org/0000-0003-3401-1536)
- Web of Science ResearcherID: NA
- Scopus Author ID: NA
- Homepage: <https://moitruong.huce.edu.vn/ths-gvc-ung-thi-thuy-ha>

**Ngan, L.T.L.**, B.Sc., Master Student, Faculty of Environmental Engineering, Hanoi University of Civil Engineering, 55 Giai Phong Road, Hai Ba Trung District, Hanoi, 113021, Vietnam.

- Email: [nganngan.211196@gmail.com](mailto:nganngan.211196@gmail.com)
- ORCID: [0000-0002-7552-3311](https://orcid.org/0000-0002-7552-3311)
- Web of Science ResearcherID: NA
- Scopus Author ID: NA
- Homepage: <https://moitruong.huce.edu.vn/he-thac-sy>

**Toan, N.D.**, Ph.D., Director, Institute of Natural Resources and Environment Training, Ministry of Natural Resources and Environment, No 83 Nguyen Chi Thanh, Dong Da, Hanoi, Vietnam.

- Email: [toantnmt@gmail.com](mailto:toantnmt@gmail.com)
- ORCID: [0000-0002-2970-0938](https://orcid.org/0000-0002-2970-0938)
- Web of Science ResearcherID: NA
- Scopus Author ID: NA
- Homepage: <http://innet.gov.vn/>

#### HOW TO CITE THIS ARTICLE

Hoang, M.G.; Ung, T.T.H.; Le, T.L.N.; Nguyen, D.T., (2024). Evaluation of municipal waste collection performance using operational data. *Global J. Environ. Sci. Manage.*, 10(1): 69-82.

DOI: [10.22034/gjesm.2024.01.06](https://doi.org/10.22034/gjesm.2024.01.06)

URL: [https://www.gjesm.net/article\\_705675.html](https://www.gjesm.net/article_705675.html)





## ORIGINAL RESEARCH PAPER

## Wetland degradation monitoring using multi-temporal remote sensing data and watershed land degradation index

I. Ridwan<sup>1,\*</sup>, S. Kadir<sup>2</sup>, N. Nurlina<sup>1</sup><sup>1</sup> Geophysics, Lambung Mangkurat University, Jl. Ahmad Yani km 36, Banjarbaru, South Kalimantan, Indonesia<sup>2</sup> Forest Faculty, Lambung Mangkurat University, Jl. Ahmad Yani km 36, Banjarbaru, South Kalimantan, Indonesia

## ARTICLE INFO

**Article History:**

Received 17 March 2023

Revised 24 May 2023

Accepted 30 July 2023

**Keywords:**Land degradation index  
land use/land cover (LULC)  
Soil erosion  
Soil moisture content  
Vegetation coverage

## ABSTRACT

**BACKGROUND AND OBJECTIVES:** The condition of the watershed area, particularly the Tabunio Watershed, is one with priority treatment due to the condition of the land where it is located, which qualifies for the "very high recovery" category with a critical land area of 19,109.89 hectares. Moreover, the diminishing water absorption also results in flooding during the rainy season and drought in the dry season. Environmental damage in the Tabunio Watershed is exacerbated by the existence of traditional gold mining and has become a concern for many parties. With this in mind, the perceived increase in natural disasters, such as floods, landslides, and droughts from year to year requires an evaluation of land degradation in the Tabunio Watershed.**METHODS:** The objective of this study was to monitor and simulate the spatial and temporal aspects of land degradation in the Tabunio Watershed. It was suggested that a complete land degradation index be developed to capture the spatial and temporal aspects of land degradation between the years 2005 and 2020. This index integrates land use land cover, vegetation coverage, soil erosion, and soil moisture content.**FINDINGS:** The proposed comprehensive land degradation index in this study demonstrated that (a) the land degradation index, which successfully monitored the spatio-temporal aspect of land degradation (kappa coefficient > 0.73 and overall accuracy > 86 percent), is regarded as having high accuracy. (b) In comparison to the individual indices, the land degradation index is capable of revealing land degradation in a more comprehensive manner. (c) land degradation index is readily transferable and applicable to other study areas due to the fact that all of its land degradation indices can be quickly extracted from remotely sensed imagery. (d) land degradation index can be used in a wide variety of contexts, which also accounts for the provision of quantitative predictions with regard to the possibility of land degradation. (e) The rate of land degradation will generally increase from 2005 to 2020, with 2010 being the most extreme year.**CONCLUSION:** The proposed comprehensive land degradation index method is capable of describing the spatial and temporal aspect of land degradation from 2005 to 2020 in the watershed area. Moreover, the proposed approach shows that the level of land degradation from 2005 to 2020 normally increases, recording the extreme years as the 2010s. In addition, in most years, the amount of land degradation was moderate, only few of which had severe or extreme degradation. As a consequence of this, some land degradation management measures ought to be created in advance, guaranteeing the protection of this vital region, which is a source of freshwater. The study provides a substantial understanding of the effect of land degradation on sustainable environment management and development in the watershed.DOI: [10.22034/gjesm.2024.01.07](https://doi.org/10.22034/gjesm.2024.01.07)This is an open access article under the CC BY license (<http://creativecommons.org/licenses/by/4.0/>).

NUMBER OF REFERENCES

62



NUMBER OF FIGURES

3



NUMBER OF TABLES

3

\*Corresponding Author:

Email: [ichsanridwan@ulm.ac.id](mailto:ichsanridwan@ulm.ac.id)

Phone: +813 5103 7167

ORCID: [0000-0002-8739-5038](https://orcid.org/0000-0002-8739-5038)

Note: Discussion period for this manuscript open until April 1, 2024 on GJESM website at the "Show Article".

## INTRODUCTION

The resources provided by the land constitute an essential component of the material basis for human existence and advancement. In recent years, the irresponsible use of land resources, combined with the poor management of those resources, as well as the growth of the world's population, has led to severe land degradation across the globe (Ahmad and Pandey, 2018; Zhu et al., 2022, Suharyanto et al., 2023). The condition of the watershed area, particularly the Tabunio Watershed, is one with priority treatment due to the condition of the land where it is located, which qualifies for the "very high recovery" category with a critical land area of 19,109.89 hectare (ha). Moreover, the diminishing water absorption also results in flooding during the rainy season and drought in the dry season (Takrina et al., 2023; Enriquez and Tanhueco, 2022). In the last three years, Tanah Laut Regency has frequently become a casualty of flooding. The worst of which occurred in 2021, causing the submergence of approximately 107 residents' houses in floods as deep as two to three meters. The catastrophe also caused damage to the main road, obstructing the in-and-out road access to Tanah Laut Regency. The floods are suspected to be brought about by the environmental degradation due to the hundreds of un-reclaimed mining pits, of which, 50 percent (%) of the 3.7 million hectares of land are controlled by mining and palm oil companies. Environmental damage in the Tabunio Watershed is exacerbated by the existence of traditional gold mining and has become a concern for many parties. With this in mind, the perceived increase in natural disasters, such as floods, landslides, and droughts from year to year requires an evaluation of land degradation in the Tabunio Watershed, which is one of the most important sources of freshwater in the Tanah Laut Regency. Land degradation, often manifested in soil erosion, the loss of quality farmland, and the fall of plant coverage, is affecting the water quality as well. Although Tabunio Watershed is one of the most important supply in Tanah Laut Regency, its water quality continues to be negatively impacted. The degradation of land can have a wide range of negative effects on the surrounding environment, including the amplification of soil loss, a decline in biodiversity, a deterioration in the ecosystem, and a loss in the land's capacity to be used for other

purposes (Dubovyk, 2017; Faisal et al., 2019). Since addressing land degradation effectively is crucial, in 2015 the United Nations applied the "Sustainable Development Goals," one of which consists of combating and restoring degraded land (Dubovyk, 2017; Moonrut et al., 2021). The steps to address land degradation in the affected watersheds (DAS) require a structured approach, involving various stakeholders. One of them is utilizing mapping and field surveys in the identification of areas within the watershed that are experiencing land degradation. This will help prioritize which areas require urgent restoration and conservation actions. This goal aims to achieve land degradation neutrality by the year 2030. The mitigation of climate change and the conservation of biodiversity, as well as the improvement of food security and the upkeep of sustainable livelihoods, all benefit from the management of land degradation (Tolche et al., 2022; Frimawaty et al., 2023). The use of remote-sensing techniques has become increasingly common in the field of land degradation research due to the fact that these techniques have many benefits, including the ability to detect land degradation of varying degrees (Ejegu et al., 2022; Kumsa and Assen, 2022; Shange, 2020); as well as the capability of locating and mapping land degradation. At the moment, there are four major steps in the process of using remote-sensing methods to evaluate land degradation (Gashaw et al., 2014; Hu et al., 2020). Numerous studies use a combination of indices to indicate land degradation—for example, the normalized difference vegetation index (NDVI), soil erosion (SE) (Ghobadi et al., 2012; Kumsa and Assen, 2022), land use/cover change (Gashaw et al., 2014; Moonrut et al., 2021; Van Lynden and Mantel, 2001), and land degradation (Ibrahim et al., 2015). The accuracy of the monitoring cannot be verified in a satisfactory manner. As a result, improving the precision of land-degradation monitoring and creating a comprehensive index of land degradation are both urgent requirements. The ability to simulate and predict the degradation of land can provide important information that can help guide decision-making. The Markov model, System dynamics (SD), modified universal soil loss equation (MUSLE), and multi-agent model are some of the simulation and prediction models that are widely employed in the research on land degradation. MUSLE, as well as an erosion and sedimentation prediction tool called

EROSET (Borrelli *et al.*, 2021; Karydas *et al.*, 2014; Ly *et al.*, 2019; Wiratmoko and Gunawan, 2019). However, it is important to note that none of these models are foolproof, and majority of them concentrate on simulating changes in land use or land cover or on simulating individual indicators of land degradation. In addition, only a few of these models are used to simulate land degradation in its entirety (Borrelli *et al.*, 2021; Febrianti *et al.*, 2018; Karaburun, 2010; Karydas *et al.*, 2014). Quantitatively predicting a dynamic change in landscape characteristic is within the capabilities of Markov models, but these models are incapable of resolving the spatial characteristic of landscape change (García *et al.*, 2019; Liping *et al.*, 2018; MohanRajan and Loganathan, 2021; Oguz and Zengin, 2011). The CA model can predict where the landscape pattern would appear, but it can't tell us when it will change (Liping *et al.*, 2018; MohanRajan and Loganathan, 2021; Oguz and Zengin, 2011). In light of these considerations, it is essential to integrate a variety of modeling approaches to successfully simulate the spatial and temporal characteristics of land degradation. For instance, the CA-Markov model has the ability to simulate the spatio-temporal dynamics of land degradation and has numerous applications in a variety of scientific communities (Mariye *et al.*, 2022; Tadese *et al.*, 2020; Zhu *et al.*, 2022). Despite the satisfactory results that remote sensing and geographic information systems (GIS) have generated in studies of land degradation (Auliana *et al.*, 2018; Kadir and Farma, 2017), commonly used land degradation indices are inadequate because they do not accurately capture the full range of the severity and the temporal and spatial dimensions of land degradation (Zhu *et al.*, 2022). It is necessary to have an integrated remote-sensing index that can track the spatial and temporal features of land degradation to provide coverage for the aforementioned indices. Understanding of the spatial and temporal characteristics of land degradation as well as the factors that cause it, with the goal of improving environmental protection, is a necessity for the case of the Tabunio Watershed. The findings of this study can provide baseline information that can be used in preserving the environmentally sound development of this watershed ecosystem. The purpose of this research is to create an extensive land degradation index (LDI) by combining indices from multiple remote-sensing sources in the evaluation of

the spatial and temporal aspects of land degradation. This study has been carried out in the Tabunio Watershed from 2005 to 2020.

## MATERIALS AND METHODS

### *Study area*

The Tabunio Watershed (3°37'2.72"-3°51' 51.43" SL and 114°36' 12.02"114°57'47.62" EL) is located in Tanah Laut Regency. It has an area of approximately 62,558.56 ha and dominated the area with the lowest elevations. The Tabunio Watershed is shown in Fig. 1. It is not only an essential resource for the economic and social growth of Tanah Laut Regency in a sustainable manner but is also a water resource for the Riam Kanan Dam. The land resources in the Tabunio Watershed are rapidly deteriorating as a result of both natural and human-caused changes in the surrounding environment, drawing an increasing amount of attention to the need for mitigation.

### *Data source*

The multispectral image of the research region, which was taken on January 20 and did not contain any clouds, was retrieved from The Glovis United State of Geological Survey. These data were captured by LANDSAT ETM+ in year 2005 and 2010 and LANDSAT 8 OLI (2015 and 2020). These images have a spatial resolution of 30 meters, six or eight bands at visible and shortwave wavelengths, and one panchromatic band with a resolution of 15 meters (for ETM+ and OLI). ETM+ images have eight spectral bands, while the OLI image only has one. The historic rainfall, relative humidity, and temperature data for January 20 were downloaded from the Center of Hydrometeorology and Remote Sensing (CHRS). The images from the years 2005, 2010, 2015, and 2020 were used for the study. The digital vector data can be found at the following location: Tabunio Watershed administration provided us with a soil-type map, a scale of 1:125.000, and data on land use planning for the Tabunio Watershed.

### *Methods*

The following methodical structure was developed in this research for the purpose of tracking and predicting the degradation of land. It includes the creation of an LDI, the evaluation of the risks associated with land degradation, as well as the observation and simulation accuracy assessments.

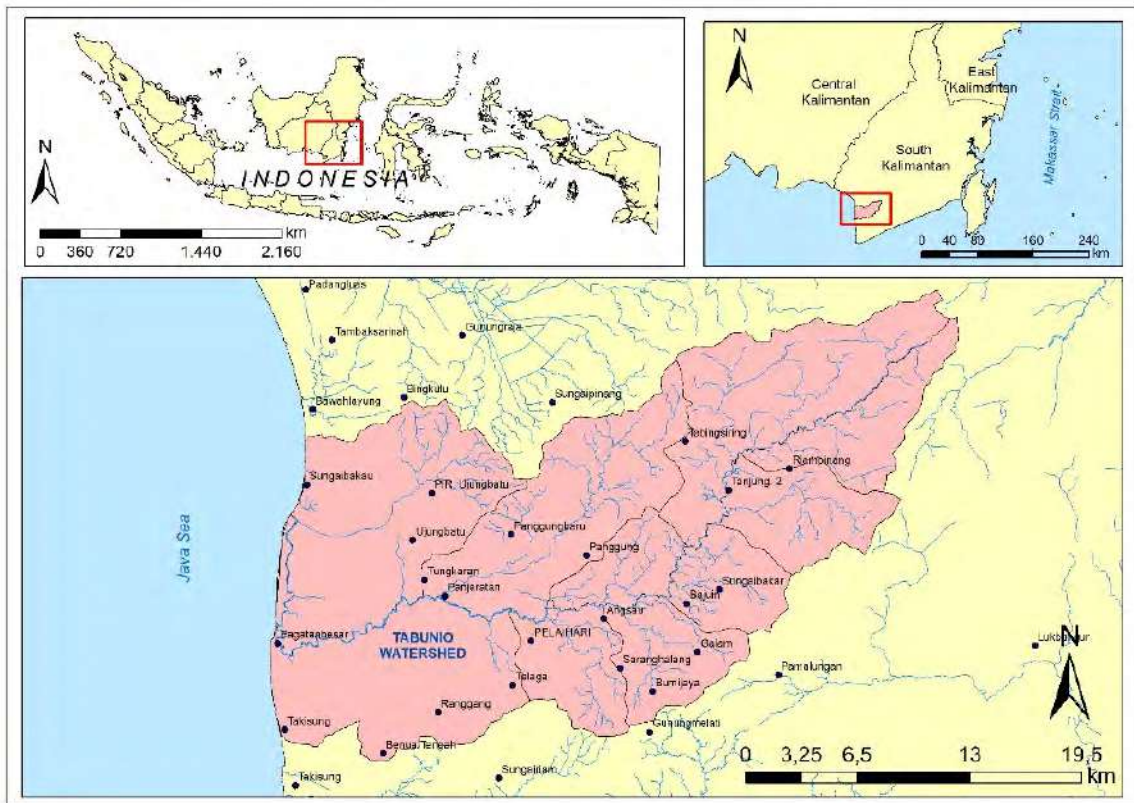


Fig. 1: Geographical location of the study area in the Tabunio Watershed, South Kalimantan, Indonesia.

The most common variety of land degradation are soil erosion, decreased soil fertility, soil pollution, forest degradation, salinization, desertification and urbanization (Loukrakpam and Oinam, 2021). These types of land degradation are primarily responsible for four indicators that describe land degradation, chosen according to actual conditions observed in the field in the Tabunio Watershed. These indicators are land use land cover, vegetation coverage, soil erosion, and soil moisture content.

#### Land use land cover (LULC)

LULC was chosen to be one of the indices used to describe land degradation because changes in LULC are one of the most significant factors that contribute to land degradation in the Tabunio Watershed. For the preprocessing of the LANDSAT TM/ETM+/OLI images that were downloaded, the ENVI 5.3 software was utilized, accomplishing the band combined, FLAASH atmospheric adjustment, combining images, and image selection were all. This technique has

the potential to improve the spatial accuracy of a multispectral bands while maintaining the accuracy of the spectral information included in the source data. The land-use classification process begins with the determination of the land cover/use class based on the dominant land cover in the Tabunio Watershed. This study divides land use into 10 classes, including bodies of water, forests, open land, settlements, plantations, agriculture, swamps, shrubs, ponds, and mines. Then the process of land-cover classification is carried out. Moreover, the classification method used in this study is the support vector machine (SVM) method, which was chosen for its high accuracy (OA > 80%) (Nurlina et al., 2021). Each image was initially categorized into one of ten different LULC types. These LULC types were then arranged in descending order of the likelihood of land degradation, starting from the least likely to the most likely scenario. When looking at the LULC types, a higher score indicates that there is a greater likelihood of land degradation. The order of the score is as follows: water body, forest,

pond, swamp, plantation, agriculture, settlement, shrubs, bare land, and mining.

*Vegetation coverage*

There is a one-to-one correlation between the state of the vegetation cover and the level of land degradation (Aires et al., 2020; Fang et al., 2021; Sun et al., 2020). The composite vegetation index (CVI), a significant metric of vegetation density, was determined in this study using the forest canopy density (FCD) mapping approach. The model is dependent on vegetation indices, and the indices that are generally used to generate the canopy vegetation index (CVI) are the normalized difference vegetation index (NDVI), the shadow index (SI), and the bare soil index (BI), using Eqs. 1-3 (Godinho et al., 2016; Loi et al., 2017; Su Mon et al., 2012)

$$CVI = (NDVI + nBI) * SI \tag{1}$$

$$VC = \frac{(CVI - CVI_{soil})}{(CVI_{veg} - CVI_{soil})}, \tag{2}$$

Where, CVI<sub>veg</sub> and CVI<sub>soil</sub> represent CVI values of vegetation cover and bare soil cover, and using Eqs. 3-5 (Godinho et al., 2016; Loi et al., 2017):

$$NDVI = \frac{\rho_{NIR} - \rho_{RED}}{\rho_{NIR} + \rho_{RED}} \tag{3}$$

$$SI = [(256 - \rho_{BLUE})(256 - \rho_{GREEN})(256 - \rho_{red})]^{1/3} \tag{4}$$

$$BI = \frac{\rho_{swir} + \rho_{RED} - \rho_{NIR} - \rho_{BLUE}}{\rho_{swir} + \rho_{RED} + \rho_{NIR} + \rho_{BLUE}} \tag{5}$$

Where, BLUE, GREEN, RED, NIR, and SWIR each stand for the reflectance of LANDSAT images in the blue band, the green band, the red band, the near-infrared band, and the first shortwave infrared band. According to the FCD model, the percentage of land covered in vegetation has a positive correlation with SI and NDVI but a negative correlation with BI. CVI can reduce the effect of shadow and soil background.

*Soil erosion (SE)*

SE is a complicated physical process that is affected

by a wide range of variables. Some of these variables include precipitation (R), soil erodibility (K), slope (S), vertical continuity (L), plant management (C), land conservation efforts (P) and correction factor 0.6 (f) were used to extract SE values using Eq. 6 (Borrelli and Schütt, 2014; Mariye et al., 2022; Nurlina et al., 2022). Rainfall data, vegetation density, length slope, and land use types were extracted from satellite data and digital elevation model.

$$SE = (R * K * L * S * C * P) * f \tag{6}$$

*Soil moisture content (SMC)*

The SMC is a direct indicator of drought intensity; hence, increasing SMC can help reduce the severity of land degradation (Peng et al., 2020; Perdana et al., 2020; Tajudin et al., 2021). NDVI was integrated with historical temperature data by utilizing an algorithm called a mono-window algorithm, which was done to identify the land surface temperature (LST) of the area that was being researched (El Garouani et al., 2021; Fashae et al., 2020; Guha and Govil, 2021; Nurlina et al., 2023). SMC was calculated using the temperature-vegetation drought index (TVDI) (Eqs. 7–9) in this study. This index is based on the TS-NDVI principle, using Eqs. 7, 8, and 9 (Peng et al., 2020; Wang et al., 2020; Younis and Iqbal, 2015).

$$SMC \approx TVDI = \frac{T_s - T_{s_{min}}}{T_{s_{maks}} - T_{s_{min}}} \tag{7}$$

$$T_{s_{maks}} = a_1 + b_1 * NDVI \tag{8}$$

$$T_{s_{min}} = a_2 + b_2 * NDVI, \tag{9}$$

Where, T<sub>s</sub>, T<sub>smin</sub>, and T<sub>smax</sub> each describe the temperature of the land surface of a single pixel in Kelvin (K), the maximum and minimum surface temperatures that correspond to NDVI (K). The coefficients for the dry edge equation and the wet edge equation are a<sub>1</sub>, b<sub>1</sub>, a<sub>2</sub>, and b<sub>2</sub>.

*Land degradation risk assessment*

The relative importance of each indices that have been previously mentioned was determined by comparison, in accordance with the analytical hierarchy process (AHP) principle. The scoring of all

variable in the LDI valuation matrix were calculated from expert judgment using a questionnaire. (Anh et al., 2014; Ardali, 2016; Kang et al., 2016; Sar et al., 2015; Vaishali and Patil, 2015). The weights of land use, vegetation coverage, soil erosion, and soil moisture content were computed with AHP Software using Eqs. 10 and 11.

$$IDL = w_a LULC + w_b VC + w_c SE + w_d SMC \quad (10)$$

$$W = (w_{TL}, w_{TV}, w_{ET}, w_{KT})^T = (0.34, 0.30, 0.29, 0.10)^T, \quad (11)$$

Where,  $w_a$ ,  $w_b$ ,  $w_c$ , and  $w_d$ , each stand for the respective weights of land use, vegetation coverage, soil erosion, and soil moisture. As a result of the valuation matrix having a consistency of CR = 0.0121 0.1, the requirements for this study were successfully met.

Following are some of the findings that emerged from our investigation of several indices: (a) the level of LDI increase when the values of land use and soil erosion increased (b) the level of LDI decreased when the rates of vegetation coverage and soil moisture increased. Because of this, to simplify the calculations,

the amounts of VC and SMC were standardized using Eq. 12 (Pratt et al., 2004).

$$X = \frac{x_i - x_{min}}{x_{max} - x_{min}}; X = \frac{x_{max} - x_i}{x_{max} - x_{min}}, \quad (12)$$

Where, X is the normalized value of  $x_i$ ,  $x_{min}$ , and  $x_{max}$  are the lowest and highest value of the variable; and X is the value that has been normalized.

Each of the indices that were derived from this process has a value that rises as the amount of degraded land increases. It is intended to reflect the level of land degradation (Eq. 11). Eq. 12 was used to normalize the LDI value so that it falls within the range [0, 1], and a higher LDI value indicates a more severe level of land degradation. Land degradation analysis uses a geographic information system through an overlay process of the four parameters of the LDI with their respective weights and scores (Table 1). LDI values were used to categorize the level of land degradation into five distinct levels, and equal intervals were used for each category. This was done so that it would be easier to compare different years (Table 2 and Fig. 2).

Table 1. Weight value and LDI parameter scoring

Parameter	Weight	Class	Description	Scoring
Land use/land cover	0.3361	Water body		1
		Forest		1
		Bare land		5
		Residential		4
		Plantation		3
		Agriculture		3
		Swamp		2
		Shrubs		4
		Pond		2
		Mining		5
Soil erosion (t/ha/yr)	0.2869	< 15	Very light	1
		15–60	Light	2
		60–180	moderate	3
		180–480	Heavy	4
		> 480	Very heavy	5
Vegetation coverage	0.2802	0–0.2	Not vegetation	5
		0.2–0.4	Vegetation is very sparse	4
		0.4–0.6	Sparse vegetation	3
		0.6–0.8	Dense vegetation	2
Soil moisture content	0.0968	0.8–1	The vegetation is very dense	1
		< 0.2	Very wet	1
		0.2–0.4	Moist	2
		0.4–0.6	Slightly moist	3
		0.6–0.8	Slightly dry	4
		> 0.8	Dry	5

Table 2. LDI Value (Tolche et al., 2022)

LDI Value	Class degradation	Description
0–0.4	No degradation	No degradation, which includes water, areas of complete vegetative cover, building areas, and arable land with high fertility.
0.2–0.4	Mild degradation	The mild degradation is one in which agricultural output has dropped but ecosystem services have not been compromised.
0.4–0.6	Moderate degradation	There has been a moderate decline in land production and some harm to ecosystem function in a region classified as moderately degraded.
0.6–0.8	Severe degradation	The severe degradation category refers to a region that has suffered significant losses in terms of both land production and ecosystem function.
0.8–1	Extreme degradation	Extreme land degradation is characterized by the loss of all land production and ecosystem function.



a. No Degradation



a. Mild Degradation



b. Moderate degradation



c. Severe Degradation



e. Extreme Degradation



Fig. 2: The characteristics of land degradation validation samples

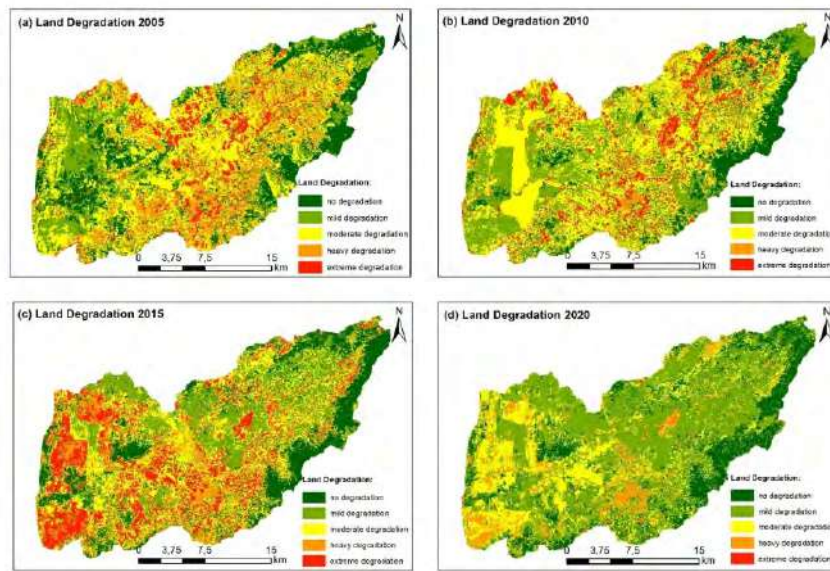


Fig. 3: Spatial and temporal distribution of land degradation index in study area

## RESULTS AND DISCUSSION

The results of the land-cover classification process from 2005 to 2020 show changes in land use as a whole. There are four types of land cover that changed very rapidly with quite significant changes, namely, an increase in the area of plantation land cover followed by a decrease in shrubs and agricultural land and swamp land cover. The positive land use and land cover changes observed in the Tabunio Watershed are a significant increase in the area of plantations, from 502.16 ha in 2005 to 24,313.31 ha in 2020—an increase of 23,811.15 ha (4,841%) and a decrease in the mining area from 2,172.66 ha in 2005 to 350.50 ha in 2020, decreasing by 1,822.17 ha (619.8%) (Nurlina *et al.*, 2021).

### *Monitoring and evaluation of land-degrading conditions*

Fig. 3 shows how the rates of land decline in the Tabunio Watershed changed over the time period of 2005 to 2020. It is split into five levels: areas with no degradation, mild degradation, moderate degradation, serious degradation, and extreme degradation. The degree of land degradation was determined by the area and percentage of LDI in each class.

Spatio-temporal distribution of LDI (Fig. 3), showed

that no degradation areas are found in land cover, bodies of water, and forests, while degradation land are evenly distributed in mining areas, bare land, agricultural land, and plantations with steep and gentle slopes around the Tabunio Watershed. In 2015, most of the areas with severe and extreme LDI were in the south and west areas, and most of them with mild and moderate LDI were in the hilly and plantation zones around the upstream watershed. In terms of the patterns and measurements of land degradation in the Tabunio Watershed, it usually worsened from 2005 to 2020, with the amount of degraded land reduced steadily from 2015 to 2020 except on the years 2005 and 2010. Between the years 2005 and 2015, there was a significant increase in the amount of land that was degraded, which was greater than 50,000 hectares (ha) and 53%. The degree of land degradation underwent drastic changes in 2015–2020; and specifically, the area undegraded increased from 12% in 2010 to 17% in 2015, with an increase in area of 3,271 ha (Table 3); severe degradation decreased from 24,352 ha (38.93%) and 11,810 ha (18.88%) in 2015 to 14,416 ha (23%) and 226.2 (0.36%) in 2020. Total degraded land remains at or beneath 50,000 ha. In terms of the level of land degradation, light to severe land degradation was observed almost throughout the year, while

Table 3: Proportion of land degradation in the Tabunio Watershed from 2005 to 2020

Degradation Class	2005		2010		2015		2020	
	Area (ha)	Proportion (%)						
No degradation	11,266.05	18.01	7,689.62	12.29	10,960.44	17.52	12,282.15	19.63
Mild degradation	15,177.40	24.26	20,638.21	32.99	16,024.79	25.62	30,273.44	48.39
Moderate degradation	21,318.96	34.08	24,352.41	38.93	18,092.33	28.92	14,416.51	23.04
Severe Degradation	8,905.55	14.24	2,908.26	4.65	5,670.68	9.06	5,360.24	8.57
Extreme Degradation	5,890.61	9.42	6,970.05	11.14	11,810.33	18.88	226.22	0.36

the portion of areas with extreme degradation was relatively slight. The rate of land degradation will have dropped by a sizeable amount by the year 2020, and the percentage of land that will be severely and extremely degraded will drop to 9% and 1% (Table 3). Area and proportion of land degradation in the Tabunio Watershed from 2005 to 2020.

The extensive LDI that was proposed in this research proved to be effective in monitoring the spatial and temporal aspects of land degradation (KC > 0.73 and OA > 86%), which is significant when taking into account that a Kappa coefficient that falls within the range of 0.70–0.85 is regarded as having “high accuracy” (Chikhaoui *et al.*, 2005; Ibrahim *et al.*, 2015; Tolche *et al.*, 2022). Even though an accuracy test has been carried out using a confusion matrix, the assessment of the level of land degradation, however, is still subjective, especially for mild and moderate degradation. When compared with individual indices, the LDI is capable of revealing land degradation in a more comprehensive manner. LDI is easily transferable and relevant to various research areas because all of its LDI may be produced quickly from remotely sensed data. As a result, LDI can be used in a wide variety of contexts, making quantitative predictions regarding the possibility of land degradation. In this study, the procedure for deriving the LDI land degradation evaluation matrix was exhaustive, and the assessments matrix was consistent with consistency ratio (CR) is 0.012. This is significant when taking into consideration that a CR of less than 0.1 is considered to be qualified (Atmaja *et al.*, 2019; Solangi *et al.*, 2019). Several studies on land degradation have been estimated quantitatively by analyzing physico-chemical parameters where spatial variability in soil parameters is described through soil maps generated from GIS analysis

(Ahmad and Pandey, 2018). Other studies used the following parameters in this study: rainfall; NDVI LST; topography; and pedological properties (i.e., soil depth, soil pH, soil texture, and soil drainage) (Shange, 2020). Another LDI is based on the concept of a soil line derived from spectroradiometric measurements of soil that compares the LDI and degraded spectral angle (SAM) approaches in assessing and estimating land degradation (Chikhaoui *et al.*, 2005). The results shown from several other studies only used a single index and focused more on soil conditions and did not carry out an accuracy test for the LDI. Our research combines four very complete indices, which are composed of 15 single indices (Eq. 1 to Eq. 9) and with the LDI accuracy test. This study area experienced an acceleration in the loss of biodiversity, destruction of vegetation, and loss of water and soil due to the acceleration of tourism and expansion of oil palm plantation. This resulted LDI with significant region and a percentage of land degraded between 2005 and 2020. It is important to note the dramatic shift that occurred in the land degradation classes between the years 2005 and 2005. The local government began implementing the Grain for Green Programme policy at the beginning of 2015. The goal of this policy was to assist in the conversion of bare land and mining back into forest or plantation. This policy reduced the degree to which land was degraded, which may explain why areas with no degradation increased while areas with severe degradation decreased during the 2005–2020 period. The Tabunio Watershed Management Department engaged in a number of protective efforts, such as delimiting development zones, restricting population expansion and greening scenic regions. These policies and measures resulted in a gradual reduce in the rate of land degradation. It is interesting that the amount

of rain in the Tabunio Watershed affects the level of SE, and that the level of SE goes up in years when there is a lot of rain. The SE is a significant indicator of land degradation; changes in the SE reflect land degradation to a significant degree. During the years 2005–2020, the annual precipitation in the Tabunio Watershed showed a very slight downward trend. Beginning in the year 2015, this precipitation began a significant downward trend (Nurlina et al., 2022). As a result, the disparity between the amount of precipitation and the amount of water lost to evaporation was a driving force behind the reduction of SE in the Tabunio Watershed from 2005 to 2020, which indicated that land degradation was presenting a trend toward improvement, particularly after the year 2010. The proposed comprehensive LDI approach shows that the land degradation classes of the Tabunio Watershed underwent rapid change during the 2005–2022 period, and the vast majority of the effects of these shifts, in terms of slowing down or even reversing land degradation, were beneficial. Some examples of these positive consequences include the expansion of areas with no degradation and the reduction of areas with severe degradation. The control measures for bettering the management of land degradation still need to be worked on. In light of the findings of an investigation into the causes and effects of land degradation, in conjunction with an examination of the characteristics of the Tabunio Watershed, the following proposals for preventative and corrective actions could be made: (a) minimizing the use of pesticides and chemical fertilizers or switching to organic and (b) recommending that biological or engineering building techniques be used in highly degraded areas, such as a more effective slope area management, terraces to store water to minimize water loss and soil erosion, and more plant life make the rehabilitation program work better (Akumu et al., 2018; Khawaldah et al., 2020).

## CONCLUSION

In this study, the proposed comprehensive LDI method is able to describe the spatial and temporal characteristics of land degradation from 2005 to 2020 in *the watershed* area, particularly in *the* Tabunio Watershed. The extensive land degradation index filed in this study combines four major indices that are composed of the presented 15 single indices that were successful in evaluation the spatial and

temporal characteristics of land degradation with Kappa coefficient > 0.73 and overall Accuracy > 86%), being regarded as having “high accuracy.” The degree to which land was degraded from 2005 to 2020 was, on average, lower than it had been during that time period. The increase in areas with no degradation, as well as the decrease in areas with light and severe degradation, were both positive for the mitigation of land degradation. In comparison to the state of the land in 2005, it was anticipated that the degradation of the land would remain relatively increased in 2005 until 2015. Both natural and anthropogenic factors were responsible for the land degradation that took place in this watershed. The control methods for land degradation should be created based on the results of monitoring and forecasting for the Tabunio Watershed. The suggested approach demonstrates that the level of land degradation generally increased from 2005 to 2020, with the extreme year of land degradation being 2010, and most years’ land degradation was moderate, with only a few cases of serious or extreme land degradation. The LDI built from this study shows that the right and very specific combination of variables can produce very good accuracy. Moreover, LD is one of the most serious global threats to people’s livelihoods and the environment. At numerous spatial and temporal scales, remote sensing performs an unprecedented role in LD mapping, assessment, and monitoring. Despite the tremendous promise of remote sensing to aid with LD research, a number of problems have hampered its practical implementation, including limited remote-sensing data with high spatial and temporal resolution. A few strategies for preventing further land degradation ought to be established in advance to ensure the protection of this essential region that is a source for freshwater. The research offers a major new understanding of the impact that the degradation of land has on the sustainable management and development of the environment in the watershed.

## AUTHOR CONTRIBUTIONS

I. Ridwan, the corresponding author, has contributed in GIS data analysis, interpreted the results, prepared maps, Figures and preparing the manuscript. S. Kadir prepared in vegetation cover data analysis and soil erosion, and interpreted the results. N. Nurlina contributed in remote sensing data analysis, all the field data survey, and manuscript preparation.

### ACKNOWLEDGMENTS

The Ministry of Education, Culture, Research, and Technology has funded this study with a National Competitive Applied Research Grant [Number 026/E5/PG.02.00.PL/2023].

### CONFLICT OF INTEREST

The authors declare that there is no conflict of interests regarding the publication of this manuscript. In addition, the ethical issues, including plagiarism, informed consent, misconduct, data fabrication and/or falsification, double publication and/or submission, and redundancy have been completely observed by the authors.

### OPEN ACCESS

©2024 The author(s). This article is licensed under a Creative Commons Attribution 4.0 International License, which permits use, sharing, adaptation, distribution and reproduction in any medium or format, as long as you give appropriate credit to the original author(s) and the source, provide a link to the Creative Commons license, and indicate if changes were made. The images or other third-party material in this article are included in the article's Creative Commons license, unless indicated otherwise in a credit line to the material. If material is not included in the article's Creative Commons license and your intended use is not permitted by statutory regulation or exceeds the permitted use, you will need to obtain permission directly from the copyright holder. To view a copy of this license, visit:

<http://creativecommons.org/licenses/by/4.0/>

### PUBLISHER'S NOTE

GJESM Publisher remains neutral with regard to jurisdictional claims with regard to published maps and institutional affiliations.

### ABBREVIATIONS

%	Percent
°	Degrees
'	minute
''	second
>	more than
<	less than
AHP	Analytical Hierarchy Process

BI	Bare Soil Index
CHRS	Center of Hydrometeorology and Remote Sensing
CR	Consistency Ratio
CVI	Composite Vegetation Index
DEM	Digital elevation model
EL	East Longitude
ENVI	Environment for Visualizing Images
ETM+	Enhanced Thematic Mapper plus
FCD	Forest Canopy Density
FLAASH	Fast Line-of-sight Atmospheric Analysis of Spectral Hypercubes
GIS	Geographic information system
K	Kelvin
KC	Kappa coefficient
Landsat	Land Satellite
LDI	Land degradation index
LULC	Land use land cover
LST	Land Surface Temperature
MUSLE	Modified universal soil loss equation
NDVI	Normalized difference vegetation index
NIR	Near Infra Red
OA	Overall accuracy
OLI	Operational Land Imager
R	Rainfall erosivity factor
SD	System dynamics
SE	Soil Erosion
SI	Shadow Index
SL	South Latitude
SMC	Soil Moisture Content
SWIR	Short Wave Infra Red
TM	Thematic Mapper
TVDI	Temperature Vegetation Drought Index
USGS	United State Geological Survey
USLE	Universal soil loss equation
VC	Vegetation Cover
ha	hectare

<i>MJ</i>	Mili Joule
<i>mm</i>	milimeter
<i>t</i>	Ton
<i>y</i>	year

## REFERENCES

- Ahmad, N.; Pandey, P., (2018). Assessment and monitoring of land degradation using geospatial technology in Bathinda district, Punjab, India. *Solid Earth*. 9(1): 75–90 (16 pages).
- Aires, U.R.V.; da Silva, D.D.; Moreira, M.C.; Ribeiro, C.A.A.S.; Ribeiro, C.B. de M., (2020). The use of the normalized difference vegetation index to analyze the influence of vegetation cover changes on the streamflow in the Manhuaçu River Basin, Brazil. *Water Resour. Manage.*, 34(6): 1933–1949 (17 pages).
- Akumu, C.E.; Henry, J.; Gala, T.; Dennis, S.; Reddy, C.; Teggene, F.; Haile, S.; Archer, R.S., (2018). Inland wetlands mapping and vulnerability assessment using an integrated geographic information system and remote sensing techniques. *Global J. Environ. Sci. Manage.*, 4(4): 387–400 (14 Pages).
- Anh, N.K.; Phonekeo, V.; My, V.C.; Duong, N.D.; Dat, P.T., (2014). Environmental hazard mapping using GIS and AHP – A case study of Dong Trieu District in Quang Ninh Province, Vietnam. *IOP Conference Series: Earth Environ. Sci.*, 18(1): 012045 (7 pages).
- Ardali, M.R., (2016). Application of remote sensing, GIS and AHP potential water sources (Case study: Anticline shyrogoun). *Bulletin of Environment, Pharmacol. Life Sci.*, 5(7): 63–73 (11 pages).
- Atmaja, R.R.S.; Putra, D.P.E.; Setijadji, L.D., (2019). Delineation of groundwater potential zones using remote sensing, GIS, and AHP techniques in southern region of Banjarnegara, Central Java, Indonesia. *Proceeding of SPIE*, 11311 (11 pages).
- Auliana, A.; Ridwan, I.; Nurlina, N., (2018). Analisis tingkat kekritisian lahan di DAS Tabunio Kabupaten Tanah Laut. *Positron*. 7(2): 54–59 (6 pages).
- Borrelli, P.; Alewell, C.; Alvarez, P.; Anache, J.A.A.; Baartman, J.; Ballabio, C.; Bezak, N.; Biddoccu, M.; Cerdà, A.; Chalise, D.; Chen, S.; Chen, W.; De Girolamo, A.M.; Gessesse, G.D.; Deumlich, D.; Diodato, N.; Efthimiou, N.; Erpul, G.; Fiener, P.; Panagos, P., (2021). Soil erosion modelling: A global review and statistical analysis. *Sci. Total Environ.*, 780 146494 (18 pages).
- Borrelli, P.; Schütt, B., (2014). Assessment of soil erosion sensitivity and post-timber-harvesting erosion response in a mountain environment of Central Italy. *Geomorphology*. 204: 412–424 (13 pages).
- Chikhaoui, M.; Bonn, F.; Bokoye, A.I.; Merzouk, A., (2005). A spectral index for land degradation mapping using ASTER data: Application to a semi-arid Mediterranean catchment. *Int. J. Appl. Earth Obs. Geoinf.*, 7(2): 140–153 (14 pages).
- Dubovyk, O., (2017). The role of Remote Sensing in land degradation assessments: opportunities and challenges. *Eur. J. Remote Sens.*, 50(1): 601–613 (13 pages).
- Ejegu, M.A.; Reta, K.G.; Yegizaw, E.S.; Biru, B.Z.; Mekonnen, D.M.; Wassie, G.K.; Tegegne, M.A.; Dirar, T.M.; Dubale, Y.G., (2022). Land management, dynamics and vegetation vulnerability analysis in the Guna-Tana watershed as a predictor of land degradation, using remote sensing data. *J. Degraded Min. Lands Manage.*, 9(4): 3703 – 3714 (12 pages).
- El Garouani, M.; Amyay, M.; Lahrach, A.; Jarar Oulidi, H., (2021). Land Surface Temperature in Response to Land Use/Cover Change Based on Remote Sensing Data and GIS Techniques: Application to Saïss Plain, Morocco. *J. Ecol. Eng.*, 22(7): 100–112 (13 pages).
- Enriquez, M.D.; Tanhueco, R.M., (2022). A basis water quality monitoring plan for rehabilitation and protection. *Global J. Environ. Sci. Manage.*, 8(2): 237–250 (14 pages).
- Faisal, A.; Hossain, M.; Haque, S.; Shaunak, M.; Kafy, A., (2019). Remote Sensing Approach in Wetland and Land Degradation Assessment: a Scenario of Modhumoti Model Town, Savar, Bangladesh. 1st International Conference on Urban and Regional Planning, Bangladesh, 1959: 247–256 (10 pages).
- Fang, H.; Li, S.; Zhang, Y.; Wei, S.; Wang, Y., (2021). New insights of global vegetation structural properties through an analysis of canopy clumping index, fractional vegetation cover, and leaf area index. *Sci. Remote Sens.*, 4: 10–27 (18 pages).
- Fashae, O.A.; Adagbasa, E.G.; Olusola, A.O.; Obateru, R.O., (2020). Land use/land cover change and land surface temperature of Ibadan and environs, Nigeria. *Environ. Monit. Assess.*, 192(2): 109 (18 pages).
- Febrianti, I.; Ridwan, I.; Nurlina, N., (2018). Model SWAT (soil and water assesment tool) untuk analisis erosi dan sedimentasi di catchment area Sungai Besar Kabupaten Banjar. *J. Fisika Flux*. 15(1): 20–25 (6 pages).
- Frimawaty, E.; Ilmika, A.; Sakina, N.A.; Mustabi, J., (2023). Climate change mitigation and adaptation through livestock waste management. *Global J. Environ. Sci. Manage.*, 9(4): 691–706 (16 pages).
- García, M.; Moutahir, H.; Casady, G.; Bautista, S.; Rodríguez, F., (2019). Using Hidden Markov Models for land surface phenology: an evaluation across a range of land cover types in Southeast Spain. *Remote Sens.*, 11(5): 507 (6 pages).
- Gashaw, T.; Bantider, A.; Mahari, A., (2014). Evaluations of land use/land cover changes and land degradation in Dera District, Ethiopia: GIS and remote sensing based analysis. *Int. J. Sci. Res. Environ. Sci.*, 2(6): 199–208 (10 pages).
- Ghobadi, Y.; Pradhan, B.; Kabiri, K.; Pirasteh, S.; Shafri, H.Z.M.; Sayyad, G.A., (2012). Use of multi-temporal remote sensing data and GIS for wetland change monitoring and degradation. 2012 IEEE Colloquium on Humanities, Science and Engineering . 103–108 (6 pages).
- Godinho, S.; Gil, A.; Guiomar, N.; Neves, N.; Pinto-Correia, T., (2016). A remote sensing-based approach to estimating montado canopy density using the FCD model: a contribution to identifying HNV farmlands in southern Portugal. *Agrofor. Syst.*, 90(1): 23–34 (12 pages).
- Guha, S.; Govil, H., (2021). An assessment on the relationship between land surface temperature and normalized difference vegetation index. *Environ. Dev. Sustainability*. 23(2): 1944–1963 (20 pages).
- Hu, T.; Liu, J.; Zheng, G.; Zhang, D.; Huang, K., (2020). Evaluation of historical and future wetland degradation using remote sensing imagery and land use modeling. *Land Degrad. Dev.*, 31(1): 65–80 (16 pages).
- Ibrahim, Y.; Balzter, H.; Kaduk, J.; Tucker, C., (2015). Land degradation assessment using residual trend analysis of GIMMS NDVI3g, soil moisture and rainfall in Sub-Saharan West Africa

- from 1982 to 2012. *Remote Sens.*, 7(5): 5471–5494 **(24 pages)**.
- Kadir, S.; Farma, E., (2017). Power recovery support Tabunio watershed based on analysis of erosion based on geographic information system in the province of South Kalimantan. *Mediterr. J. Soc. Sci.*, 8(4–1): 73–81 **(9 pages)**.
- Kang, H.; Xuxiang, L.; Wang, J.; Zhang, J., (2016). Evaluating ecological vulnerability using the GIS and analytic hierarchy process (AHP) method in Yan'an, China. *Pol. J. Environ. Stud.*, 25(2): 599–605 **(7 pages)**.
- Karaburun, A., (2010). Estimation of C factor for soil erosion modeling using NDVI in Buyukcekmece watershed. *Ozean J. Appl. Sci.*, 3(1): 77–85 **(9 pages)**.
- Karydas, C.G.; Panagos, P.; Gitas, I.Z., (2014). A classification of water erosion models according to their geospatial characteristics. *Int. J. Digital Earth*, 7(3): 229–250 **(22 pages)**.
- Khawaldah, H.A.; Farhan, I.; Alzboun, N.M., (2020). Simulation and prediction of land use and land cover change using GIS, remote sensing and CA-Markov model. *Global J. Environ. Sci. Manage.*, 6(2): 215–232 **(18 pages)**.
- Kumsa, A.; Assen, M., (2022). A Comprehensive framework for itu next generation pons. *J. Electrical Electron Eng.*, 1(1): 1–23 **(23 pages)**.
- Liping, C.; Yujun, S.; Saeed, S., (2018). Monitoring and predicting land use and land cover changes using remote sensing and GIS techniques—A case study of a hilly area, Jiangle, China. *PLOS ONE*, 13(7): e0200493 **(23 pages)**.
- Loi, D.T.; Chou, T.-Y.; Fang, Y.-M., (2017). Integration of GIS and remote sensing for evaluating forest canopy density index in Thai Nguyen Province, Vietnam. *Int. J. Environ. Sci. Dev.*, 8(8): 539–542 **(4 pages)**.
- Loukrakpam, C.; Oinam, B., (2021). Linking the past, present and future scenarios of soil erosion modeling in a river basin. *Global J. Environ. Manage*, 7(3): 457–472 **(16 pages)**.
- Ly, K.; Metternicht, G.; Marshall, L., (2019). Transboundary river catchment areas of developing countries: Potential and limitations of watershed models for the simulation of sediment and nutrient loads. A review. *J. Hydrol. Reg. Stud.*, 24100605 **(14 pages)**.
- Mariye, M.; Mariyo, M.; Changming, Y.; Teffera, Z.L.; Weldegebral, B., (2022). Effects of land use and land cover change on soil erosion potential in Berhe district: a case study of Legedadi watershed, Ethiopia. *Int. J. River Basin Manage.*, 20(1): 79–91 **(13 pages)**.
- MohanRajan, S.N.; Loganathan, A., (2021). Modelling spatial drivers for LU/LC change prediction using hybrid machine learning methods in Javadi Hills, Tamil Nadu, India. *J. Indian Soc. Remote Sens.*, 49(4): 913–934 **(22 pages)**.
- Moonrut, N.; Takrattanasaran, N.; Khamkajorn, T.; Chaikaew, P., (2021). Integrated remote sensing and GIS approaches for land degradation neutrality (LDN) assessment in the agricultural area. *IOP Conference Series: Earth Environ. Sci.*, 626(1): 12-25 **(14 pages)**.
- Nurlina, Kadir, S.; Kurnain, A.; Ilham, W., (2021). Comparison of maximum likelihood and support vector machine classifiers for land use/land cover mapping using multitemporal imagery 12: 126–139 **(14 Pages)**.
- Nurlina, Kadir, S.; Kurnain, A.; Ilham, W.; Ridwan, I., (2022). Analysis of soil erosion and its relationships with land use/cover in Tabunio watershed. *IOP Conference Series: Earth Environ. Sci.*, 976(1): 012027 **(15 pages)**.
- Nurlina, N.; Kadir, S.; Kurnain, A.; Ilham, W.; Ridwan, I., (2023). Impact of land cover changing on wetland surface temperature based on multitemporal remote sensing data. *Pol. J. Environ. Stud.*, 32(3): 2281–2291 **(11 pages)**.
- Oguz, H.; Zengin, M., (2011). Analyzing land use/land cover change using remote sensing data and landscape structure metrics: A case study of Erzurum, Turkey. *Fresenius Environ. Bull.*, 20(12): 3258–3269 **(12 pages)**.
- Peng, W.; Wang, J.; Zhang, J.; Zhang, Y., (2020). Soil moisture estimation in the transition zone from the Chengdu Plain region to the Longmen Mountains by field measurements and LANDSAT 8 OLI/TIRS-derived indices. *Arab. J. Geosci.*, 13(4): 168 **(13 pages)**.
- Perdana, D.; Renaldi, L.; Alinursafa, I., (2020). Performance analysis of soil moisture monitoring based on internet of things with LoRA communications. *J. Southwest Jiaotong Uni.*, 55(5): 55–64 **(10 pages)**.
- Pratt, C.R.; Kaly, U.L.; Mitchell, J., (2004). Manual: How to Use the Environmental Vulnerability Index (EVI) **(98 pages)**.
- Sar, N.; Chatterjee, S.; Das Adhikari, M., (2015). Integrated remote sensing and GIS based spatial modelling through analytical hierarchy process (AHP) for water logging hazard, vulnerability and risk assessment in Keleghai river basin, India. *Model. Earth Syst. Environ.*, 1(4): 31 **(21 pages)**.
- Shange, P., (2020). Mapping land degradation using remote sensing data and an unsupervised clustering algorithm in the eThekweni Metropolitan Area. University of Kwazulu-Natal, January.
- Solangi, Y.A.; Tan, Q.; Mirjat, N.H.; Ali, S., (2019). Evaluating the strategies for sustainable energy planning in Pakistan: An integrated SWOT-AHP and Fuzzy-TOPSIS approach. *J. Cleaner Prod.*, 236117655 **(37 pages)**.
- Su Mon, M.; Mizoue, N.; Htun, N.Z.; Kajisa, T.; Yoshida, S., (2012). Estimating forest canopy density of tropical mixed deciduous vegetation using Landsat data: a comparison of three classification approaches. *Int. J. Remote Sens.*, 33(4): 1042–1057 **(16 pages)**.
- Suharyanto, A.; Maulana, A.; Suprayogo, D.; Devia, Y.P.; Kurniawan, S., (2023). Land surface temperature changes caused by land cover/ land use properties and their impact on rainfall characteristics. *Global J. Environ., Sci. Manage.*, 9(3): 353-372 **(20 pages)**.
- Sun, Y.-L.; Shan, M.; Pei, X.-R.; Zhang, X.-K.; Yang, Y.-L., (2020). Assessment of the impacts of climate change and human activities on vegetation cover change in the Haihe River basin, China. *Phys. Chem. Earth., Parts A/B/C*, 115102834 **(25 pages)**.
- Tadese, M.; Kumar, L.; Koech, R.; Kogo, B.K., (2020). Mapping of land-use/land-cover changes and its dynamics in Awash River Basin using remote sensing and GIS. *Remote Sens. Appl.: Soc. Environ.*, 19100352 **(27 pages)**.
- Tajudin, N.; Ya'acob, N.; Mohd Ali, D.; Adnan, N.A., (2021). Soil moisture index estimation from landsat 8 images for prediction and monitoring landslide occurrences in Ulu Kelang, Selangor, Malaysia. *Int. J. Electr. Comput. Eng.*, 11(3): 2101-2108 **(8 pages)**.
- Takrina, N.D.; Chuan O.M.; Affudin, M.I.; Tristan, L.; Arif, I.; Adiwibowo, A., (2023). Modeling the tropical fish community related to the land uses and environmental determinants. *Global J. Environ. Sci. Manage.*, 9(3): 515-530 **(16 pages)**.
- Tolche, A.D.; Gurara, M.A.; Pham, Q.B.; Anh, D.T., (2022). Modelling

- and accessing land degradation vulnerability using remote sensing techniques and the analytical hierarchy process approach. *Geocarto Int.*, 37(24): 7122–7142 (21 pages).
- Vaishali, G.; Patil, R.R., (2015). Use of remote sensing, GIS and analytical hierarchy process (AHP) in selection of suitable sites for wildlife habitat. *Int. J. Curr. Res.*, 7(3): 14212–14217 (6 pages).
- van Lynden, G.W.J.; Mantel, S., (2001). The role of GIS and remote sensing in land degradation assessment and conservation mapping: some user experiences and expectations. *Int. J. Appl. Earth Obs. Geoinf.*, 3(1): 61–68 (8 pages).
- Wang, J.; Ding, J.; Yu, D.; Teng, D.; He, B.; Chen, X.; Ge, X.; Zhang, Z.; Wang, Y.; Yang, X.; Shi, T.; Su, F., (2020). Machine learning-based detection of soil salinity in an arid desert region, Northwest China: A comparison between Landsat-8 OLI and Sentinel-2 MSI. *Sci. Total Environ.*, 707136092 (11 pages).
- Wiratmoko, B.; Gunawan, T., (2019). Penerapan citra Sentinel 2A dan sistem informasi geografis untuk pemetaan erosi menggunakan pemodelan Musle di DAS Kaligising, Purworejo. *J. Bumi Indonesia* (10 pages).
- Younis, S.M.Z.; Iqbal, J., (2015). Estimation of soil moisture using multispectral and FTIR techniques. *Egypt. J. Remote Sens. Space Sci.*, 18(2): 151–161 (11 pages).
- Zhu, L.; Ke, Y.; Hong, J.; Zhang, Y.; Pan, Y., (2022). Assessing degradation of lake wetlands in Bashang Plateau, China based on long-term time series Landsat images using wetland degradation index. *Ecol. Indic.*, 139: 108903 (12 pages).

#### AUTHOR (S) BIOSKETCHES

**Ridwan, I.**, Ph.D., Associate Professor, Geophysics, Lambung Mangkurat University, Jl. Ahmad Yani km 36, Banjarbaru, South Kalimantan, Indonesia.

- Email: [ichsanridwan@ulm.ac.id](mailto:ichsanridwan@ulm.ac.id)
- ORCID: 0000-0002-8739-5038
- Web of Science ResearcherID: GNP-8509-2022
- Scopus Author ID: 24077087200
- Homepage: <https://physics.ulm.ac.id/profile/19740707-200212-1-003>

**Kadir, S.**, Ph.D., Professor, Forest Faculty, Lambung Mangkurat University, Jl. Ahmad Yani km 36, Banjarbaru, South Kalimantan, Indonesia.

- Email: [syarifuddin.kadir@ulm.ac.id](mailto:syarifuddin.kadir@ulm.ac.id)
- ORCID: 0000-0002-1804-0313
- Web of Science ResearcherID:
- Scopus Author ID: 57130338700
- Homepage: <https://scholar.google.co.id/citations?user=dPspPHwAAAAJ&hl=en>

**Nurlina, N.**, Ph.D., Assistant Professor, Geophysics, Lambung Mangkurat University, Jl. Ahmad Yani km 36, Banjarbaru, South Kalimantan, Indonesia.

- Email: [nurlina\\_abdullah@ulm.ac.id](mailto:nurlina_abdullah@ulm.ac.id)
- ORCID: 0000-0002-9563-1555
- Web of Science ResearcherID: AAU-3158-2021
- Scopus Author ID: 57208673588
- Homepage: <https://physics.ulm.ac.id/profile/19760414-200312-2-001>

#### HOW TO CITE THIS ARTICLE

Ridwan, I.; Kadir, S.; Nurlina, N., (2024). Wetland degradation monitoring using multi-temporal remote sensing data and watershed land degradation index. *Global J. Environ. Sci. Manage.*, 10(1): 83-96.

DOI: [10.22034/gjesm.2024.01.07](https://doi.org/10.22034/gjesm.2024.01.07)

URL: [https://www.gjesm.net/article\\_706487.html](https://www.gjesm.net/article_706487.html)





## ORIGINAL RESEARCH PAPER

## Exploring the upper ocean characteristics of a bay using coastal and regional ocean community model

D. Jaishree\*, P.T. Ravichandran

*Department of Civil Engineering, Faculty of Engineering and Technology, SRM Institute of Science and Technology, Kattankulathur - 603203, Chengalpattu District, Tamil Nadu, India*

## ARTICLE INFO

**Article History:**

Received 25 February 2023

Revised 04 June 2023

Accepted 10 July 2023

**Keywords:**

Bay of Bengal (BoB)

Coastal and Regional Ocean

Community model (CROCO)

Numerical model

Reanalysis data

Salinity and Temperature

## ABSTRACT

**BACKGROUND AND OBJECTIVES:** The innovativeness of this study lies in achieving a comprehensive understanding of the seasonal variations and oceanic characteristics of the Bay of Bengal by addressing the complex interplay of large-scale ocean-atmosphere dynamics. The study aimed to understand the upper ocean characteristics of the Bay of Bengal by analyzing the surface variables such as salinity and temperature using a high-resolution model simulation. To accomplish this, advanced high-resolution numerical simulations were employed, utilizing the coastal and regional ocean community model. This model was crucial for investigating and analyzing the circulation features throughout the entire Bay of Bengal, contributing knowledge and insights about the coastal and regional oceanographic community.

**METHODS:** To investigate the temporal variability of the upper ocean in the Bay of Bengal, climatological simulations were performed over eight years using the coastal and regional ocean community model. Including a three-year spin-up phase facilitated the adjustment of the model to initial conditions and the attainment of equilibrium, ensuring its fidelity to real-world conditions. The follow-up analyses and comparisons were performed five years after the spin-up phase. The primary objective of this study was to examine the temporal evolution of the kinetic energy throughout the eight-year simulation. The volume-averaged kinetic energy was computed, revealing a gradual increase throughout the simulation, with particularly pronounced enhancements observed during the monsoon period. A Taylor diagram was used for predicting the model with the other data sets.

**FINDINGS:** The analysis is performed above the surface and sub-surface oceanic layers with prominent dynamics. The temperature and salinity for the surface and sub-surface layers were validated and analyzed for their seasonal variations. The simulations were validated against the existing satellite, reanalysis, and in situ data.

**CONCLUSION:** The innovativeness of this study lies in its successful demonstration of the seasonal variability of temperature and salinity in the Bay of Bengal. Through extensive validations, it establishes the model to accurately simulate the climatological surface features of the Bay of Bengal. This study highlights the effectiveness of numerical models when combined with observations, and the data were reanalyzed, showcasing their utility as valuable tools for studying oceanic conditions. The utilization of a Taylor diagram further supports the validation and excellent performance of the model compared to other available datasets. During the simulation, there is a high correlation (0.96) between the evolution of the salinity and temperature values obtained from the model and the corresponding data from the World Ocean Atlas. This indicates a strong agreement between the model-based simulations and the assimilated data, as supported by the notable correlation values of 0.96 for salinity and temperature. These findings reinforce the existing knowledge regarding the influential role of monsoon winds in shaping the circulation patterns within the Bay of Bengal. Overall, this study contributes to advancing our understanding of the ocean dynamics of the region and underscores the importance of considering seasonal variations for comprehensive oceanographic research, coastal management, climate modeling, and future studies in the Bay of Bengal.

DOI: [10.22034/gjesm.2024.01.08](https://doi.org/10.22034/gjesm.2024.01.08)This is an open access article under the CC BY license (<http://creativecommons.org/licenses/by/4.0/>).

NUMBER OF REFERENCES

44



NUMBER OF FIGURES

11



NUMBER OF TABLES

2

\*Corresponding Author:

Email: [jaishred@srmist.edu.in](mailto:jaishred@srmist.edu.in)

Phone: +900 3180 202

ORCID: [0000-0003-0401-068X](https://orcid.org/0000-0003-0401-068X)

Note: Discussion period for this manuscript open until April 1, 2024 on GJESM website at the "Show Article".

## INTRODUCTION

The Bay of Bengal (BoB) is a massive body of water situated at the northeastern edge of the Indian Ocean, bordered by the Indian subcontinent and Southeast Asia. (Rao *et al.*, 2011; Masumoto *et al.*, 2005). It spans an approximately 2.2 million km<sup>2</sup> area, with its deepest point reaching around 5,000 m, and is surrounded by some of the most populated regions on Earth. (Schott *et al.*, 2009; Schott and McCreary, 2001). The BoB is an important shipping lane and fishing ground, and it plays a major role in the formation of monsoon rains in the region. (Webster *et al.*, 1998). The BoB experiences a monsoon-dominated climate characterized by clearly distinguishable wet and dry seasons. (Jourdain *et al.*, 2013; Liebmann *et al.*, 1994; Maneesha *et al.*, 2012). During the monsoon season (June – September), the region experiences heavy rainfall and strong winds due to the southwesterly flow of moist air. In the winter months (December – February), the BoB experiences dry and cool weather with winds blowing from the northeast (Roy Chowdhury *et al.*, 2021). Tropical cyclones and storm surges, particularly during the peak pre- and post-monsoon season, are also experienced in the Bay. (Anandh *et al.*, 2018). Oceanographers worldwide have been captivated by the unique dynamics of the BoB, which can be attributed to its geographic location, with a landlocked northern limit causing an alternation in the monsoon winds and seasons. (Akhter *et al.*, 2021; Vinayachandran *et al.*, 1996). The seasonal monsoon precipitation has an impact on the agricultural activity in the neighboring nations as well. Through the advancement of numerical simulation tools, the comprehension of the impact of various physical parameters, such as temperature and salinity as the main parameters, and other parameters like tidal forcing, Rossby and Kelvin waves, along with the wind stress curl have on the ocean circulations has been greatly enhanced. (Sil and Chakraborty, 2012). The BoB is also susceptible to various natural hazards, including tropical cyclones, storm surges, and tsunamis, which cause significant damage and loss of life. As a result, BoB is the focus of extensive research in oceanography, meteorology, geology, disaster risk reduction, and management. In addition, the BoB is strategically important to several regional countries, particularly in maritime trade and security. Additionally, the BoB is a prominent region for energy

exploration and production, harboring substantial oil and gas reserves in its offshore territories. In the BoB, the predominantly warm conditions are one of the foremost reasons for forming seasonal cyclones (Ts *et al.*, 2020). Given the potential scope for the formation of depressions and the intensification of cyclones in the BoB, it becomes crucial to comprehensively understand the intricate interactions among the oceans and atmosphere within the bay. The oceans of the world, mainly the uppermost 700 m, are presently undergoing a warming trend (Levitus *et al.*, 2012) as the oceans are absorbing more amounts of energy that can result in an intensification of the air-sea interactions occurring over the world (Collins *et al.*, 2010). To study the influence of atmosphere-ocean interactions on the variations in temperature and salinity, mixed layer depth (MLD), and circulations in the BoB and the Arabian Sea, a multitude of observational and modeling-based studies have been undertaken. (Gao *et al.*, 2014) These studies aim to better understand these key oceanographic parameters in the area. (Amsalia *et al.*, 2022; Dyn 2010; Akhil *et al.*, 2014; Mahadevan *et al.*, 2016). The part of the Western Bay exhibits various oceanic features, such as the East India Coastal Current (EICC) and the Western Boundary Current (WBC) discontinuities, inconsistency in the boundary current, and a disrupted summer monsoonal boundary current. The BoB contributes markedly to regional climate variability, particularly regarding air-sea exchanges, in a significant manner. (Das *et al.*, 2019; Dey *et al.*, 2017). The BoB has a tropical climate characterized by high sea surface temperatures (SST) ranging from 27 – 30 °C and high sea surface salinity (SSS) levels of around 35 – 37 practical salinity units (psu). The SST and SSS in the BoB vary during the monsoon season and are influenced by the freshwater influx from major rivers like the Ganga and Brahmaputra (Rao and Behera, 2005). In conjunction with the Arabian Sea and the northern Bay, the SSS displays opposite behavior in response to the varying environmental forces. The salinity decreases in the absence of wind and shortwave radiation forces, whereas it increases in the absence of freshwater flux forces. (Srivastava *et al.*, 2018). Comparative studies were adopted for the BoB region (Ts *et al.*, 2020) utilizing two different models, the Regional Ocean Modelling System (ROMS) and the coupled Weather Research and Forecast (WRF). WRF is used to simulate

the oceanic and atmospheric conditions of the Bay. SST, SSS, sea level pressure, net heat flux, currents, and rising sea levels were compared between the simulation data and the original measurements. The findings revealed that the coupled model yielded superior accuracy in simulating the ocean. A study (Dandapat *et al.* 2021) revealed that the air-sea interface experiences a positive net flux which was the primary driver of the shoaling wave of the MLD during the Positive Indian Ocean Dipole (PIOD) year. This net flux had a greater impact on the shortwave radiation than the cooling effect of the latent heat flux. The resolution in the context of the BoB refers to the fineness of details used in computer-generated models or simulations to represent the physical processes and features of the BoB. Higher-resolution models can better capture small-scale features and processes. Forces in the BoB refer to external factors that change the energy levels in the atmospheric circulation and precipitation patterns in the area. Key atmospheric forces in the BoB include monsoon winds, temperature gradients between the land and the sea, and topographical features. Understanding the role of these atmospheric forces is important for improving the accuracy of weather prediction. A study on the BoB that focused on the circulation of the WBC and sea surface height anomaly (SSHA) using the ROMS and COADS was expanded as a Comprehensive Ocean-Atmosphere Data Set model for use in a climatological study (Wu *et al.*, 2019). The study investigated the variations in the seasonal changeabilities of the ocean surface currents in the Eastern Indian Ocean throughout the pre-monsoon, summer monsoon, and post-monsoon periods, taking into account the impact of inconsistencies in the wind patterns between the Advanced Scatterometer (ASCAT) and QuikSCAT (QSCAT) data. (Srivastava *et al.*, 2016; Thankaswamy *et al.*, 2022). The study found that the wind variability was mostly confined to the upper 100 m portion of the water column and had a local effect. Additionally, the study emphasized caution when evaluating the wind-associated variables in ocean models (Sivareddy *et al.*, 2015). This was constructed based on the observed data, and both experiments were compared to evaluate the seasonal variabilities in the temperature, salinity, and currents. (Lee *et al.*, 2000; Sprintall, 2003; Yadav, 2022). They described the mixing of the top layer ranging from 30 – 100 m of the BoB in the seasonal

cycle and was also observed using moored mixing meters. The extent of this salt flux was essential to determine the similarity of the model based on the salt budgets for the upper Bay of the region. (Cherian *et al.*, 2020). Many studies have observed the inflection of Tropical Cyclone activity in the BoB and the influence of atmospheric and oceanic conditions (Ali *et al.*, 2007; Chi, 2013; Goswami *et al.*, 2003; Kikuchi *et al.*, 2009; Lin *et al.*, 2009) which stated that the present condition of the BoB was affected by climatological conditions. Climatological simulations are essential for assessing the circulation features by comprehensively representing the atmospheric processes, reproducing the historical climatic conditions, investigating circulation patterns, conducting sensitivity experiments, and projecting future climate scenarios. These simulations contribute to our understanding of climate dynamics and help in assessing the potential impacts of climate change on circulation patterns and associated weather and climate phenomena. The study aims to understand the upper ocean characteristics of BoB by analyzing the surface variables such as salinity and temperature using a high-resolution model simulation. This study was carried out in 2022 in India's BoB using the numerical model simulation.

## **MATERIALS AND METHODS**

### *Model, data, and methodology*

This study utilized the coastal and regional ocean community model (CROCO), a newly developed oceanic modeling system based on ROMS\_AGRIF and SNH's non-hydrostatic kernel (testing of which is under process). The CROCO model is a free-surface, hydrostatic, primitive equation ocean model that incorporates algorithms from MARS3D (sediments) and HYCOM (vertical coordinates). It is a versatile modeling framework that combines physical, biogeochemical, and ecological processes to simulate and analyze the complex interactions within marine ecosystems. It is important to address the applicability, utility, and advantages of CROCO and its application in various fields, including coastal and ocean dynamics, marine ecology and ecosystems, coastal hazard and risk assessment, climate change, and sea-level rise. Its utility enhances our understanding of the complex interactions within coastal and regional ocean systems by simulating the physical, biogeochemical, and ecological processes.

Additionally, CROCO enables scenario prediction and analysis, data assimilation, and integrated assessments. The advantages of CROCO include high-resolution simulation, a flexible and modular framework, community collaboration, and multi-disciplinary integration. It was configured to cover the Bay of Bengal region (4°N – 24°N; 72°E – 100°E) with a horizontal grid resolution of approximately 10 km (256 × 249 grid points). The model used a stretched terrain-following S-coordinate system. Determination of the boundary conditions involved closed northern, eastern, and major parts of the western boundaries. In contrast, the southern boundary remained open, with temperature and salinity values relaxed to the Levitus monthly climatology. The model consisted of 32 vertical S-coordinate layers, and the bottom topography was derived from the Earth Topography Two-Minute digital terrain model (ETOPO2) data as shown in Fig. 1 and shows the geographic location of the area of study in the BoB, India. Significant attention should be provided to the distinctive bathymetric features of this region, as they potentially play a crucial role in governing deep circulation. This study was carried out in 2022 in the BoB region of India using the numerical model simulation.

*Data sources and evaluation methods*

The reanalysis datasets, along with the *in situ* data sets from Array for Real-time Geostrophic Oceanography (ARGO), World Ocean Atlas (WOA), Comprehensive Ocean-Atmosphere Data Set

(COADS), and Hydro data, were utilized for evaluating the Simulation, Simple Ocean Data Assimilation (SODA) and Estimating the Circulation and Climate of the Ocean (ECCO), and conducting the comparisons between the models. The validation of the model involved the analysis of the correlation coefficient, root mean square difference, and standard deviation (SD) using the Taylor diagram to compare the different datasets and model simulations. The Taylor diagram serves as a comprehensive statistical tool that integrates these measures, aiding in the assessment of the predictability of the model.

*Experimental setup used for the simulation*

To understand the seasonal variability of the upper ocean in the BoB, climatological simulations were conducted for eight years using the CROCO Model. To ensure that the model accurately represented the real-world conditions, a 3-year spin-up period was allowed to adjust to the initial conditions and reach equilibrium. The comparisons made were based on simulations conducted over the next five years. Following the spin-up period, the model analyzed the time required for the evolution of kinetic energy during the 8-year model run, as shown in Fig. 2. The results obtained demonstrated that the volume-averaged kinetic energy gradually increased throughout the simulation, a particularly prominent increase during the monsoon. These were reliably consistent with previous studies highlighting the strong impact of monsoon winds on ocean circulation in the Bay.

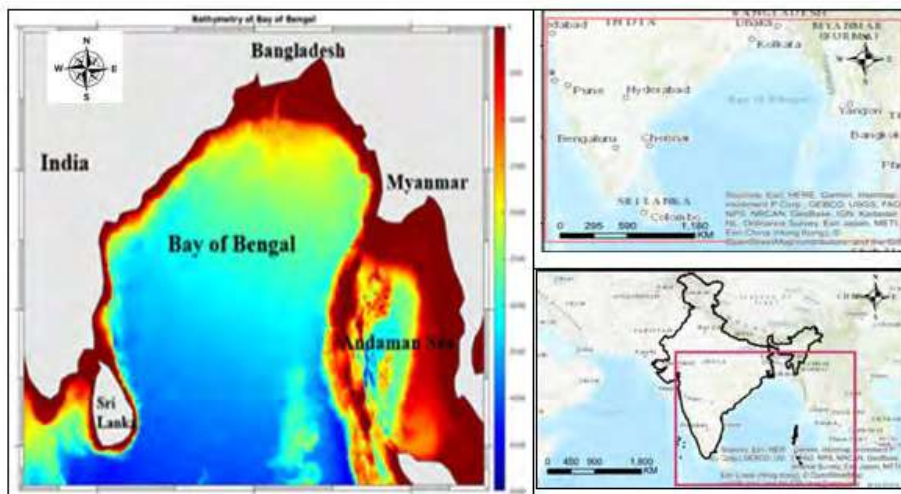


Fig. 1: Geographic location of the study area in the Bay of Bengal, India

These findings provide a valuable understanding of the complex dynamics of ocean drive in the BoB and highlight the importance of careful calibration and optimization of model spin-up periods accurately represent real-world circumstances. SST and SSS datasets from SODA and ECCO were utilized during the different seasons, including pre-monsoon, post-monsoon, monsoon, and winter. The model compared the statistical analysis of the ocean-atmospheric parameters like temperature and salinity. The bias was quantified as the disparity between the model outcomes and observed data. Using the model-based outputs, validating the results obtained with the Taylor diagram was then employed to estimate the correlation coefficient, root mean square deviation (RMSD), and standard deviation across the various datasets and model simulations. These statistical measures are integrated to evaluate the predictability of the model.

## RESULTS AND DISCUSSIONS

In this study, simulation was performed for the comprehensive validation using the CROCO model by comparing the simulation results with the observational data of various oceanic parameters. It evaluated the model's performance in determining the surface and sub-surface temperature and salinity. A validation analysis was conducted on a seasonal basis to ensure the comprehensive evaluation of the model's performance across different timescales. The results of the analysis indicated that the model performed well in capturing the observed changeabilities in the parameters studied.

### *Simulation of seasonal variability in salinity*

Based on Fig. 3, the pre-monsoon simulations of surface salinity for the different datasets were analyzed. The ECCO reanalysis data showed that

the northern bay had the lowest range of salinity distribution, ranging from 26 to 31 psu, while the eastern bay ranged from 31 to 34 psu. The southern and western bay had the highest temperature range of 33 to 35 psu, while the central bay had a one psu bias. The SODA dataset showed that the northern bay ranged from 26 to 31 psu, the eastern bay ranged from 31 to 33 psu, and the eastern bottom part ranged from 32 to 34 psu. The southern and western bay had the highest range of 33 to 35 psu. In the CROCO dataset, the north and eastern bay had the lowest distribution of salinity levels, ranging between 30 to 33 psu, while the southern and partially western bay had a higher distribution between 33 and 35 psu. The central bay had a salinity range of 32 to 33 psu, with a one psu bias. It is important to note that the temperatures in the eastern and western portions of the bay may be similar to those of the northern and southern parts, respectively. However, factors such as airflow and sea currents can cause temperature variations. In their study, [Akhile et al. \(2014\)](#) observed that during the pre-monsoon season, surface waters with salinity values below 31 were confined to the far northeastern region of the BoB. The winter salinity simulation and comparison with reanalysis data are presented in Fig. 4. The ECCO dataset demonstrated the least salinity near the northern, northeastern, and eastern parts of the region. The salinity in the northern bay extends from 28 to 32 psu while the eastern bay varies between 32 and 34 psu. In these regions, the simulation had a bias of one psu. The salinity was higher in the southern bay due to evaporation, ranging from 33 to 35 psu, and the salinity was higher on the southern coast of the western boundary. In the SODA data, the western coast recorded the lowest salinity ranging from 28 to 31 psu. The central bay had a high salinity ranging from 32 to 35 psu, while the open bay of the

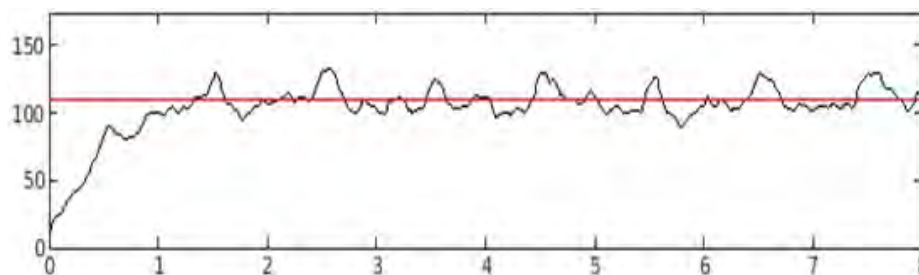


Fig. 2: CROCO 8 years average kinetic energy (cm<sup>2</sup>/s<sup>2</sup>)

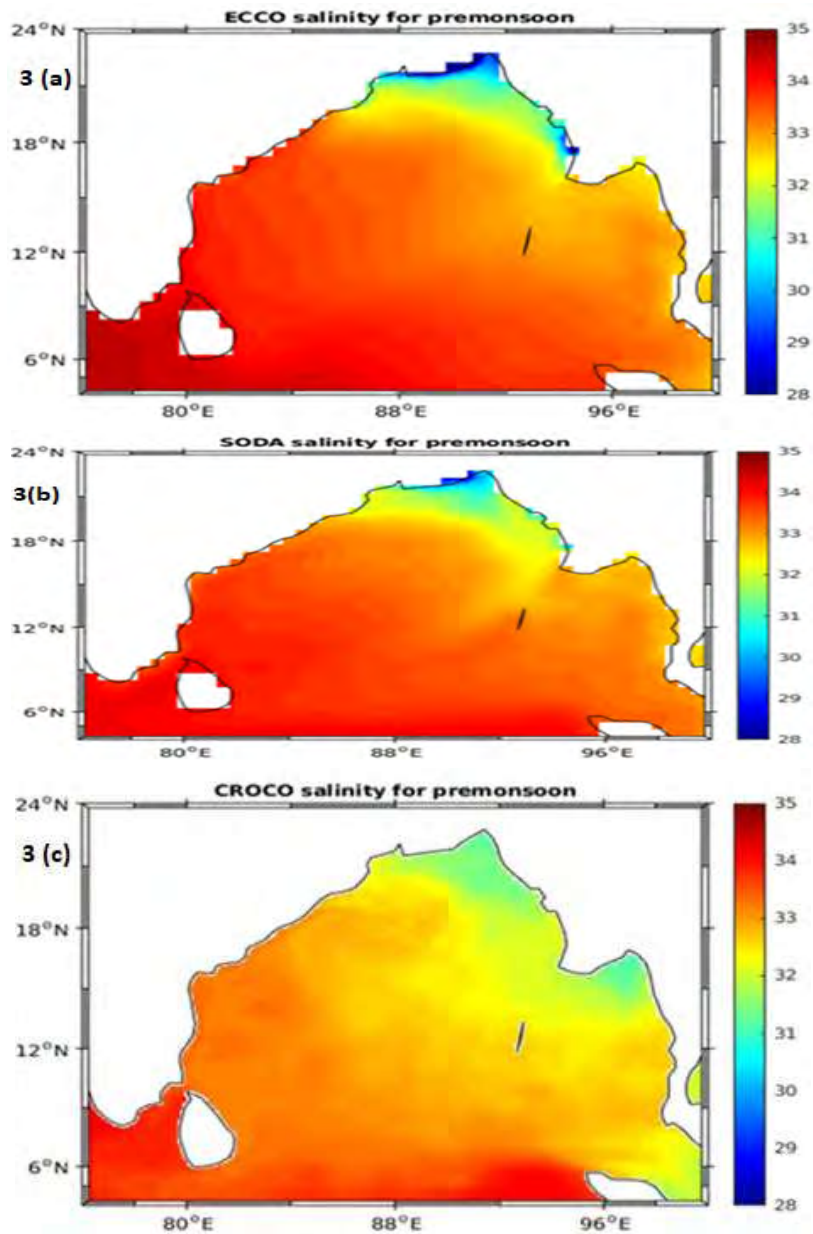


Fig. 3: Simulated salinity climatology plot for pre-monsoon (a) ECCO (b) SODA (c) CROCO

southern area had a high salinity distribution of 34 to 35 psu. The CROCO model simulation could predict better when compared to SODA and ECCO data. Additionally, depending on factors such as airflow and sea currents, the eastern and western parts of the bay had a similar salinity and temperature as in the northern and southern parts, respectively. This

suggests an active role of horizontal advection on the southward migration of the SSS front. Salinity was less than in other seasons and ranged near the bay between 28 to 32 PSU, *Akhil et al. 2014*. In contradiction to expectations, the withdrawal of the fresh tongue takes place in December within the western region of BoB, roughly one month

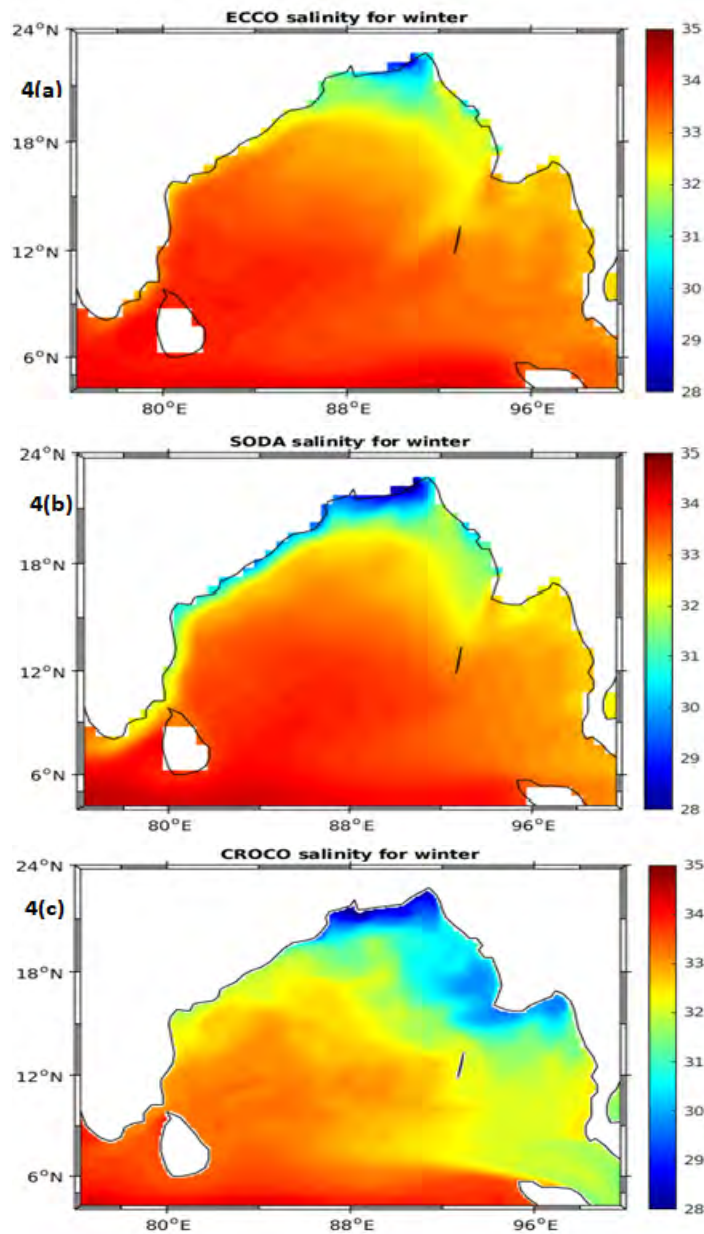


Fig. 4: Simulated salinity climatology plot for Winter (a) ECCO (b) SODA (c) CROCO

preceding the reversal of the prevailing current from equatorward to polewards. This observation implies that the advection process along the shore cannot be attributed to the driving force behind the northward retreat of the SSS front. Fig. 5 illustrates the salinity during the monsoon season. In the ECCO data, the lowest range of salinity distribution (28 – 31 psu)

was located in the north, northeast, and northwest bay due to the influence of the southwest monsoon. The central bay had a salinity distribution of 32 to 34 psu. The south and southwest bays had the highest salinity of 34 to 35 psu, maintained by evaporation and ocean currents entering the bay. The geostrophic current plays a vital role in maintaining the mass

*Numerical simulations in the Bay of Bengal*

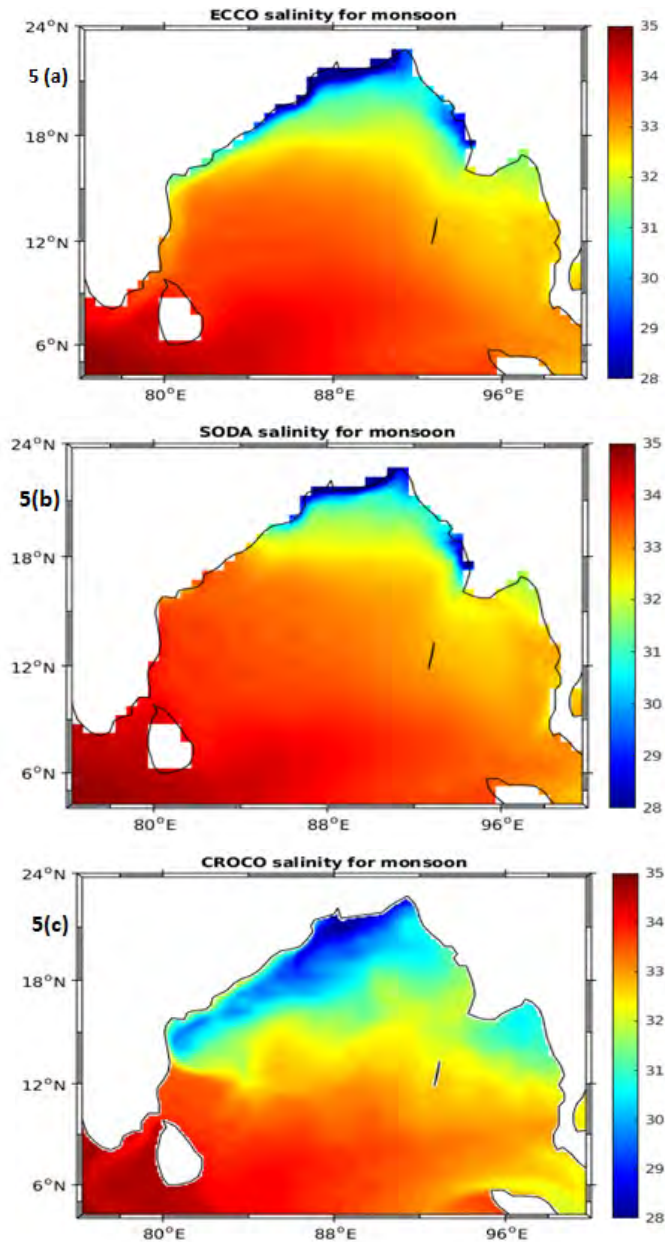


Fig. 5: Simulated salinity climatology plot for monsoon (a)ECCO (b) SODA (c) CROCO

level of low salinity water distribution that covers the bay, as detected from the circulation patterns in the surface salinity. Based on SODA data, it was found that the northern bay had the lowest salinity range of 28 to 31 psu, while the eastern bay had a bias of one psu, and the salinity level ranged between 32 and 33 psu. The south and southeast areas had high salinity

due to ocean currents, and the range of values in all bay areas was the same as that in the ECCO data, with only a one psu bias. The western and partial southern regions (latitude 4° to 12° and longitude 74° to 88°) had a higher salinity range of 34 to 35 psu. Compared with the ECCO and SODA datasets, the model resulted in the same range of lowest salinity (28 to 31 psu) in

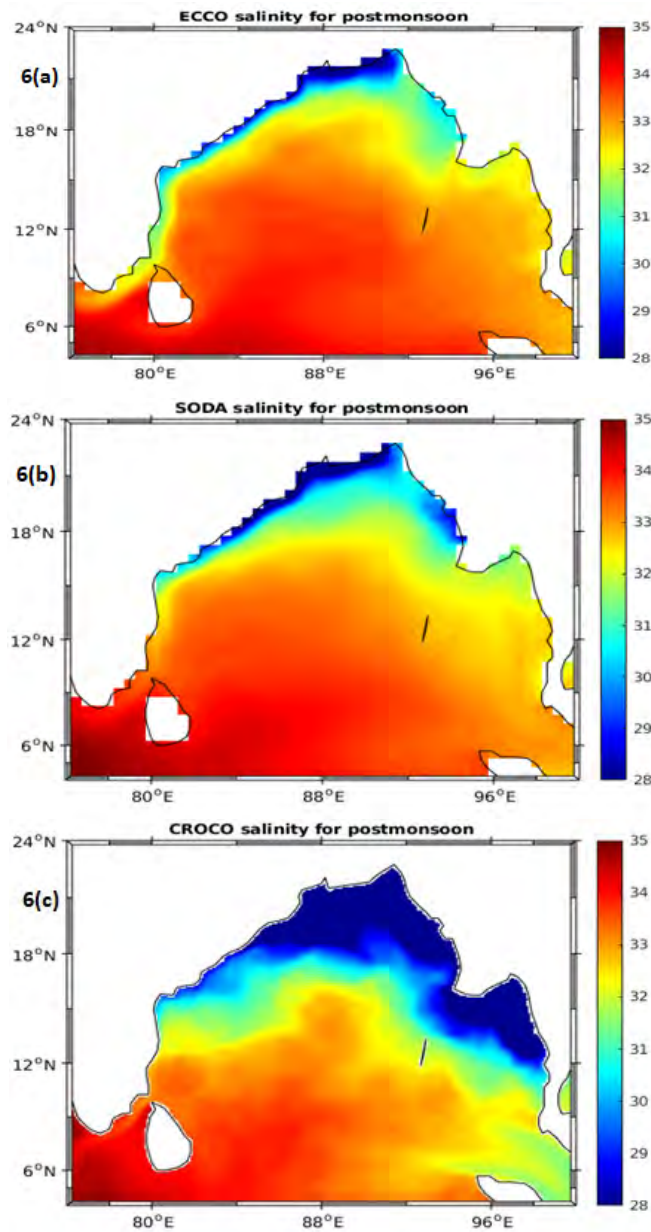


Fig. 6: Simulated salinity climatology plot for post-monsoon (a) ECCO (b) SODA (c) CROCO

the north to northwest regions. The central bay had a bias of one psu, while the east and southeast regions had low salinity due to the geostrophic current. The bottom-most bay opening near the south and west showed a high salinity (34 to 35 psu). The salinity levels in the bay can be affected by factors such as freshwater runoff from monsoon rains, tidal activity,

and ocean currents. During monsoons, the surface salinity was low in the north and the western and eastern boundaries, about 15°N. This information was obtained from a previous study (Chakraborty and Gangopadhyay, 2016).

Fig. 6 presents the simulated salinity distribution in the Bay of Bengal. ECCO analysis showed that the

Table 1: Statistical statement for Salinity

Data	Mean	SD	RMSD	Correlation
WOA	32.4905	0.4604	-	-
CROCO	32.6370	0.3965	0.1338	0.9622
ARGO	33.0993	0.2495	0.3637	0.6179
HYDRO	33.0533	0.3470	0.3212	0.7174

Table 2: Statistical statement for Temperature

Data	Mean	SD	RMSD	Correlation
WOA	28.4886	0.8793	-	-
CROCO	28.9138	0.7001	0.2765	0.9640
ARGO	28.7416	0.8476	0.1307	0.9892
COADS	28.5491	0.8568	0.1750	0.9800

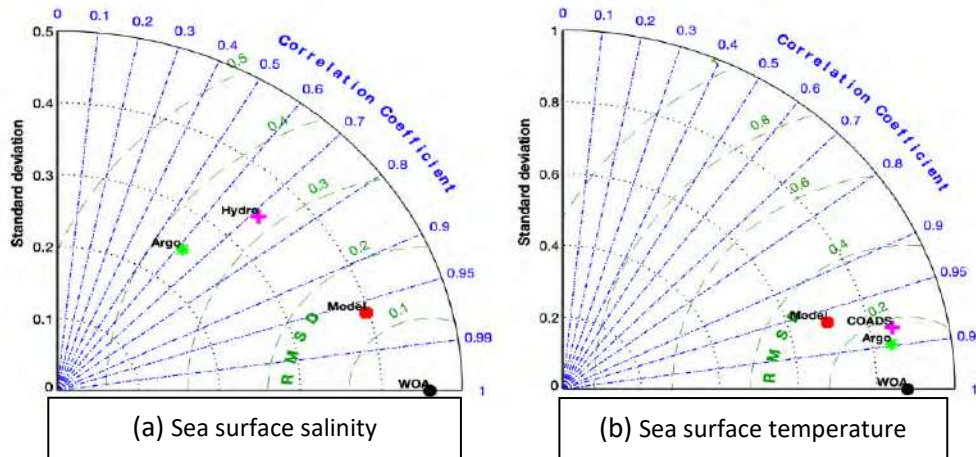


Fig. 7: Taylor Diagrams for CROCO model evaluation: Correlation, RMSD, and standard deviation for (a) Sea surface salinity and (b) Sea surface temperature

lowest salinity ranges from 28 to 31 psu near the north and western parts of the bay, while the central and southern parts had the highest salinity, ranging between 33 to 35 psu. In the western boundary, the salinity varied from 31 to 33 psu. Similarly, SODA data analysis indicated that the lowest salinity, ranging from 28 to 31 psu, was found near the bay's north, east, and western boundary. Also, the southern bay possessed the highest salinity, ranging from 34 to 35 psu. The central bay showed a bias of one psu in the SODA data analysis. Freshwater runoff from the rivers in the post-monsoon season can lead to low salinity levels, while decreased input and increased evaporation during the post-monsoon season can

result in high salinity levels. These changes in salinity levels can affect the local ecosystem and impact the distribution of marine life in the western part of the Bay region. The CROCO model predicted salt levels in the BoB, with the lowest salinity extending from 28 to 30 psu near the north and northeastern part of the bay. The western boundary had a medium range of salinity, ranging from 31 to 33 psu. The salinity ranged from 34 to 35 psu in the southern tip of the bay, which was the highest. The model satisfactorily predicted the salinity in all parts of the Bay, showing values to the ECCO and SODA datasets. In the study conducted by Akhile *et al.* 2014, it was observed that a region of low salinity (< 30 PSU) water formed

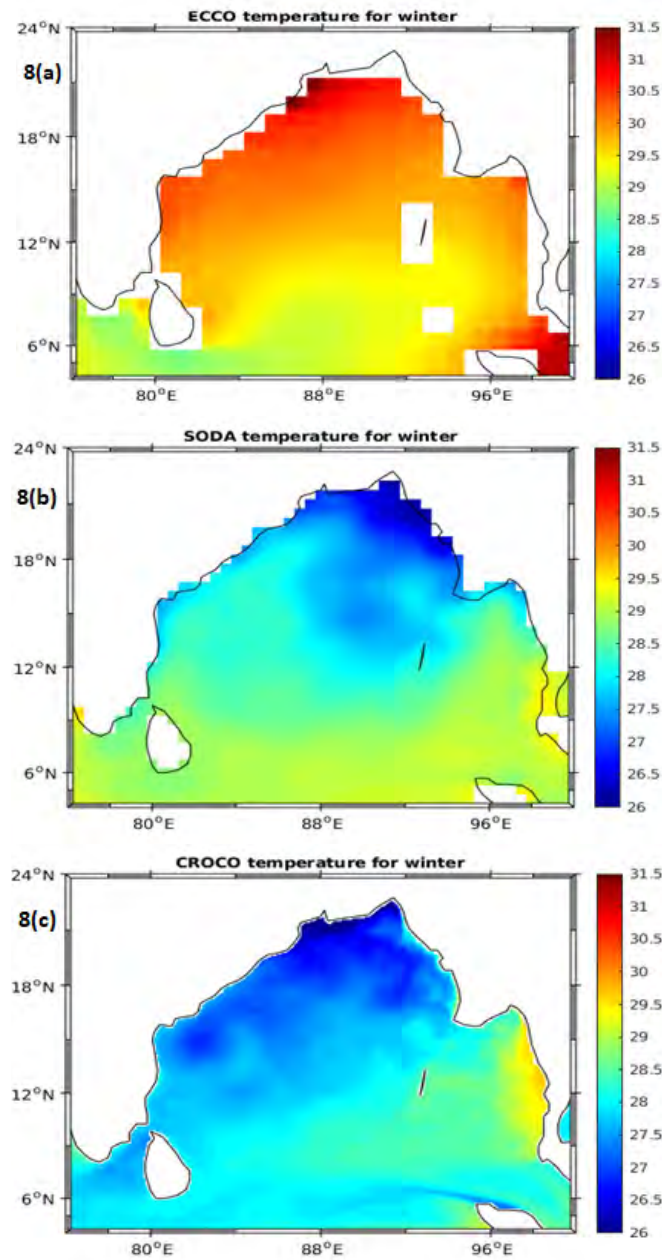


Fig. 8: Simulated temperature climatology plot for winter (a) ECCO (b) SODA (c) CROCO

in the northeastern BoB during August, September, and October. Evaluating the performance of a model often involves considering SSS as one of the main parameters, as shown in Fig 7(a). To validate the model, an analysis was conducted on the correlation coefficients, root mean square differences, and standard deviations using the Taylor diagram.

This diagram enabled the comparison of different datasets and model simulations, functioning as a comprehensive statistical tool for assessing the model's predictability by integrating these measures. The available WOA, Hydro, and AGRO data were used to compare the series of monthly mean SSS values. The correlation coefficient values reveal that the

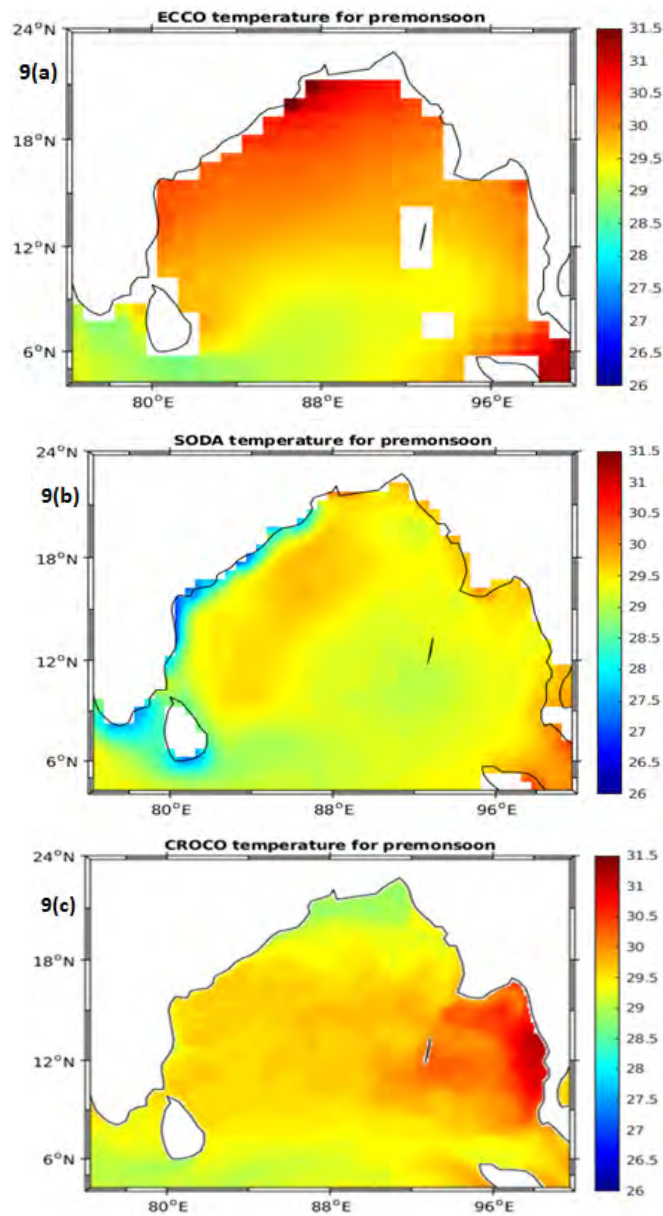


Fig. 9: Simulated Temperature climatology plot for pre-monsoon. (a)ECCO (b) SODA (c) CROCO

CROCO model exhibited a strong positive correlation (0.96) with the WOA dataset, which served as the standard for comparison. The correlation with the Hydro dataset was moderate (0.71), while the correlation with the AGRO dataset was comparatively weaker (0.61). These findings suggested that the CROCO model performed creditably in correlation

with the WOA dataset but may show slightly lower performance with the Hydro and AGRO datasets concerning SSS. Based on the standard deviation values, it was observed that the CROCO model had the highest standard deviation (0.39) when compared to the WOA dataset, which was used as the base for the comparison. The standard deviation was slightly

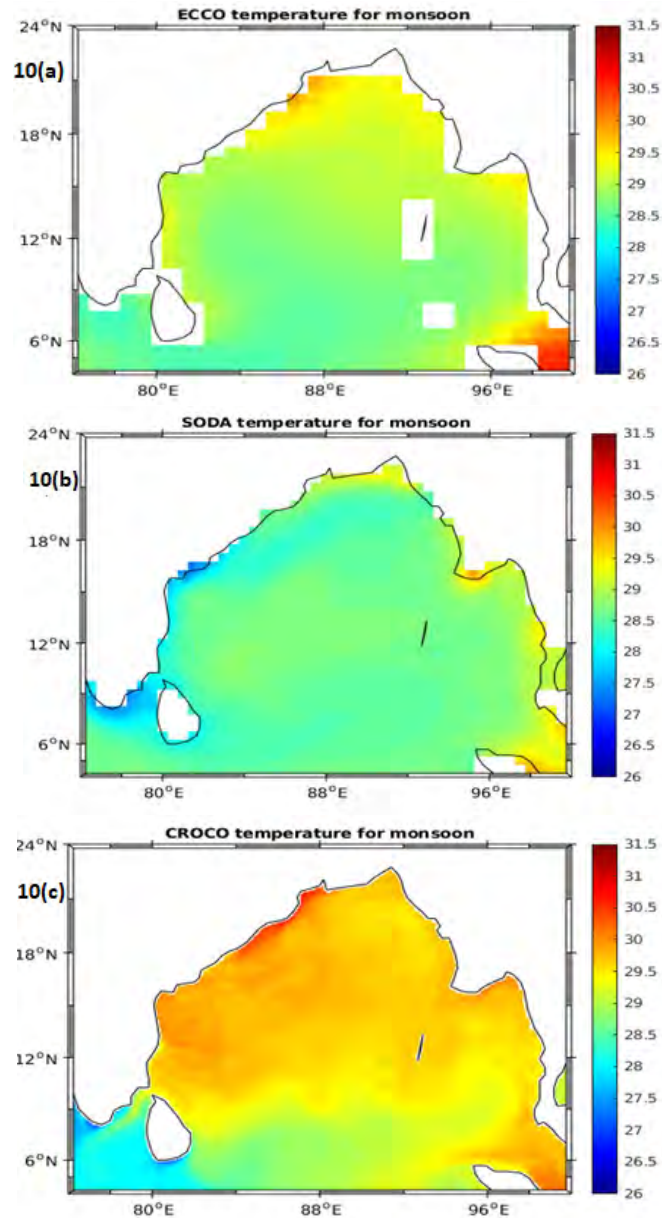


Fig. 10: Simulated Temperature climatology plot for monsoon. (a)ECCO (b) SODA (c) CROCO

lower for the Hydro dataset (0.34), and the lowest for the AGRO dataset (0.24). This suggested that the CROCO model had the highest prediction variability compared to the WOA, Hydro, and AGRO datasets. The CROCO model displayed a high strength when compared to the other datasets. Regarding the RMSD values, it can be observed that the CROCO model

had the lowest RMSD value (0.13) when compared to the WOA dataset, which was used as the base for comparison. The RMSD was higher for the Hydro dataset (0.32) and the highest for the AGRO dataset (0.36). This suggested that the CROCO model had the best agreement with the WOA dataset regarding RMSD, indicating a lower overall deviation between

the model predictions and the WOA dataset values. Although, the Hydro and AGRO datasets showed higher RMSD values, suggesting potentially higher differences between the CROCO model-based predictions and these datasets. The surface salinity, as simulated by the coupled model, exhibited a correlation of 0.78 and a bias of 0.25 psu compared to the SODA values observed by [Anandh et al. \(2020\)](#). In comparison to the aforementioned model results, the current model demonstrated a significantly stronger correlation value of 0.96. The statistical statements for the salinity values are tabulated in [Table 1](#).

#### *Seasonal variability simulation temperature*

[Fig. 8](#) presented the simulation of temperature variations using the reanalysis of the ECCO and SODA datasets and the correlation with the CROCO model, for different seasons, including summer, winter, pre- and post-monsoon seasons. In winter, the ECCO dataset showed a temperature range of 26 °C – 31.5 °C with the north, east, and western regions of the bay having similar ranges and the southern bay having a lower range of 28.5 °C – 29.5 °C. On the other hand, the SODA dataset showed lower temperatures of 26 °C – 27.5 °C in the northern and northeastern regions, with the western boundary having a slightly higher range of 28 °C – 29.5 °C and the south region had a range of 29 °C – 29.5 °C. The analysis of the CROCO model showed that the temperature in the north and the northeastern boundaries ranged from 26 °C – 28 °C, with the western boundary having a higher range of 27 °C – 28 °C. Those of the central and southeastern ranged from 28 °C – 29.5 °C, with a bias of 1 °C, while that of the southern bay ranged from 27.5 °C – 28.5 °C. During the winter, the prevailing winds from the northeast bring cool air from the land to the sea, which causes the temperature in the northern part of the Bay to be slightly lower than in the southern part. The WBC, which flows from the east to the west, influences the temperature in the BoB by bringing warm water from the equatorial region to the bay. This can raise the temperature in the western part of the bay, especially during the winter. Accordingly, the temperature varied conditionally based on the location and season and was influenced by the wind patterns and ocean currents in the BoB. [Akhter et al. \(2021\)](#) stated the winter temperature reached the highest value of 26 °C to 27.3 °C, compared with other results; hence the

model was predicted accurately.

According to [Fig. 9](#), in the pre-monsoon season, the reanalysis of the ECCO dataset showed that the north, east, and western boundaries of the Bay demonstrated temperatures ranging from 30 °C to 31.5 °C, while that of the southern boundary ranged from 28 °C to 29.5 °C. These were typically observed between March and May. The northern part of the bay showed higher temperatures than the southern regions. Although, temperatures in the eastern part and western bay can vary depending on the airflow and sea currents. In the SODA analysis, the temperature near the boundary on the west side of the bay ranged from 26 °C to 28.5 °C. Near the central bay was 28.5 °C to 29.5 °C and near the northeastern bay was 29 °C to 30 °C. In the summer, the Bay experiences a north-northeast wind, which brings cool air from the land to the bay. Coastal upwelling also occurs during this season, causing colder water from the depths to rise to the surface due to winds blowing parallel to the coast and pushing surface water away from the shore. As per the results of the model analysis, the temperature in the north and southern bay ranged from 28.5 °C to 29 °C, whereas, in the eastern bay, it varied from 30 °C to 31.5 °C, [Akhter et al. \(2021\)](#). In spring, it reached 29.6 °C, the highest value, and the western part of the bay ranged from 28.5 °C to 29.5 °C. The bias in the central part was 1, and the temperature in all bay areas depends on the airflow and currents. The BoB is influenced by the equatorial counter-current, a warm ocean current that flows from west to east and can help warm the bay waters during the pre-monsoon season. According to [Fig. 10](#), the ECCO dataset showed that in the northern bay, the temperature range was between 29.5 °C to 31 °C, while the eastern, western, and southern bays ranged from 28 °C to 29 °C. The central bay also recorded similar temperature ranges. These variations were influenced by the southwest monsoon, which brings moist and warm air starting from the Indian Ocean to the BoB region. The SODA dataset indicated that the northern and eastern bays had the highest temperature range, which was between 28 °C to 30.5 °C, while the southern and central bays had a range of 28 °C to 29 °C. The western bay had the lowest temperature range of 26 °C to 28.5 °C. On the other hand, the CROCO model showed that the temperature range varied from 29 °C to 31.5 °C in all three bays, namely the northern,

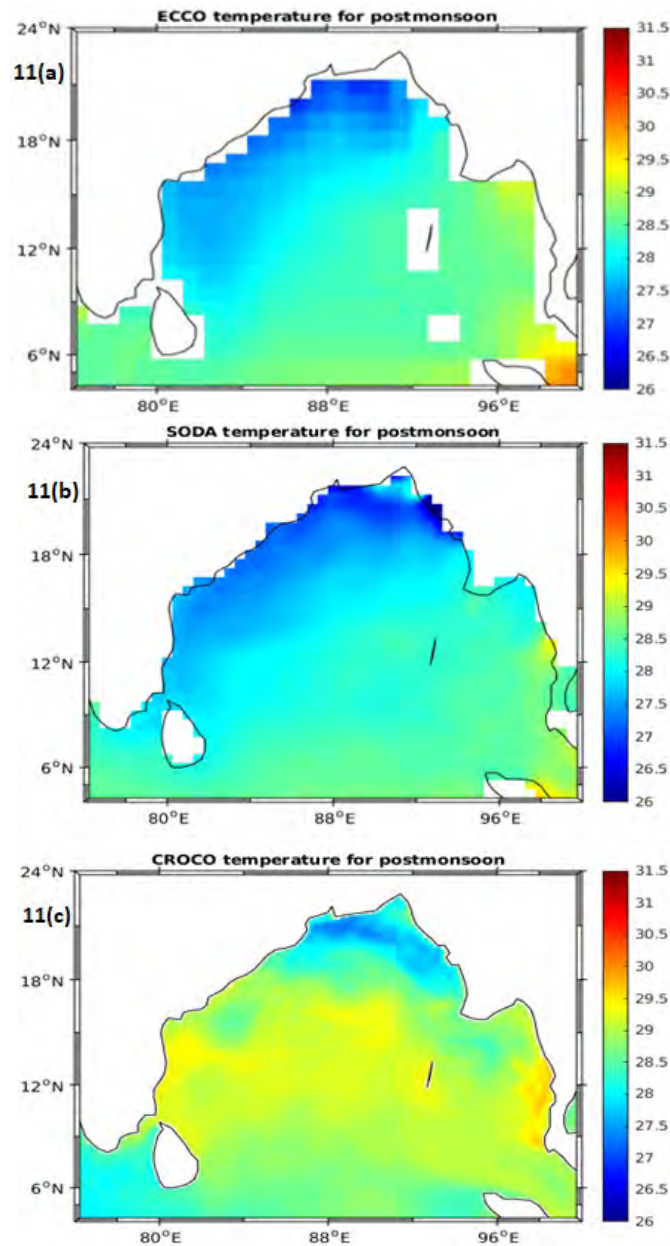


Fig. 11: Simulated Temperature climatology plot for post-monsoon (a) ECCO (b) SODA (c) CROCO

eastern, and southern bays. The central bay also had a maximum temperature range of 29 °C to 30 °C. The tip of the western bay had a minimum temperature range of 27.5 °C to 28.5 °C. It is worth noting that the monsoon winds and ocean currents also influence the wind patterns in the western bay in the BoB. Incidentally, EICC, which flows from east to west, can

bring warm water from the equatorial region to the western side, raising the temperature and affecting the wind patterns. Monsoon seasons also affect the wind patterns in this area, bringing alternating winds from different directions throughout the year. In the eastern bay, wind patterns can vary depending on the location, but the monsoon winds generally influence

them. Throughout the northeast monsoon, winds can be cool and dry, while in the southwest monsoon, they are warm and moist. Overall, the temperature variations and wind patterns in the BoB can have significant implications for marine life, ecosystems, and climate. Additional research is required to comprehensively understand these factors impact on the region and their potential evolution over time. The simulated results from Fig. 11 for the post-monsoon season indicated that the ECCO dataset recorded the highest temperatures, extending from 29 °C to 30 °C, in the eastern portion of the bay of the bottom-most bayline. Meanwhile, the central bay recorded a temperature range of 27 °C to 28.5 °C, and the northern and western bays remained the coldest, with a range of 26 °C to 28 °C. On the other hand, the SODA dataset records varying temperatures depending on the bay, ranging from 26 °C to 27 °C in the western bay, 27.5°C to 28.5°C in the eastern and southern bays, and 28 °C to 30 °C in the southern bay. Although, the central bay had a 1 °C bias. During the post-monsoon season, typically from October to December, the local weather conditions and ocean currents influence the temperature variations in the BoB. As the summer heat dissipates, the water temperature begins to cool, especially more quickly in the part of the northern bayside, leading in the direction of a north-south temperature gradient. The cyclonic activity typically increasing during this season can also impact the water temperature. The surface temperatures exhibited similarity in both simulations, except for a minor cooling effect observed during the summer, monsoon, and post-monsoon periods. The surface temperatures were around 28.9 °C throughout the year, as reported in a study conducted by [Jana et al. \(2015\)](#).

Validating the results obtained from the Taylor Diagram, Fig. 7(b), the CROCO model showed a strong positive linear relationship with the WOA, COADS, and AGRO data sets for the sea surface temperature, with correlation coefficients varying from 0.96 to 0.98. This suggested that the CROCO model was highly correlated with these data sets, particularly AGRO, indicating its potential accuracy in predicting the sea surface temperature. The standard deviation for the CROCO model compared with the WOA data set was 0.7, indicating that a relatively low level of variation occurred between the CROCO model and the WOA data set for sea surface temperature and the level

of variation of the CROCO model when compared with the COADS data set was 0.85. This indicated a slightly higher variation or dispersion between the CROCO model and the COADS data set for sea surface temperature when compared to the WOA data set. The level of variation of the CROCO model compared with the AGRO data set was 0.84, indicating similar variations between the CROCO model and the AGRO data set for sea surface temperature compared to the COADS data set. The CROCO model exhibited an RMSD of 0.27 when compared to the WOA data set, signifying an average difference of 0.3. Similarly, when compared to the COADS data set, the CROCO model yields an RMSD of 0.27, indicating a smaller average difference. The CROCO model demonstrated an RMSD of 0.13 for the AGRO data set, suggesting a similar average difference of 0.1 compared to the COADS data set for the sea surface temperature RMSD was 0.17. Overall, the CROCO model displayed relatively smaller average differences when compared to the WOA, COADS, and AGRO data sets for sea surface temperature, as evident from the RMSD values obtained. Lower RMSD values indicated better agreement between the model and the data, with the COADS and AGRO data sets exhibiting slightly smaller average differences in comparison to the WOA data set. SST is captured well by the coupled model (the correlation coefficient was 0.96 compared to TRMM TMI), ([Anand et.al., 2020](#)). Compared with the above results, the CROCO model correlated well with the temperature as the coefficient was 0.98. The statistical statements for the temperature values are tabulated in [Table 2](#).

## CONCLUSIONS

The findings of this study reveal seasonal variations in temperature and salinity within the BoB region. During the winter and post-monsoon seasons, the southern area of the open bay exhibited a high salinity distribution ranging from 34 to 35 psu. The model used in this study accurately predicted the salinity values throughout the bay, aligning closely with the ECCO and SODA datasets. The salinity and temperature levels in the eastern and western parts of the bay resemble those in the northern and southern parts, respectively, and are influenced by factors such as airflow and sea currents. During the monsoon season, the geostrophic current played a vital role in maintaining the mass level of low

salinity water that covers the bay, as indicated by the observed surface salinity circulation patterns. Factors like freshwater runoff from monsoon rains, tidal activity, and ocean currents can impact salinity levels. The correlation coefficient values demonstrate a strong positive correlation (0.95) between the CROCO model and the WOA dataset, serving as a benchmark for comparison. This suggested that the CROCO model exhibited the closest agreement with the WOA dataset regarding RMSD, indicating minimal deviation between the model-derived predictions and the WOA dataset values. Although, the Hydro and AGRO datasets displayed higher RMSD values, suggesting potential differences between the CROCO model-based predictions and these datasets. Additionally, the analysis of the CROCO model highlighted a temperature range of 27 °C to 28 °C in the western boundary of the bay during winter. The WBC, which flows from the east to the west, influences the temperature in the BoB by transporting warm water from the equatorial region to the bay. This can elevate the temperature in the western part of the bay, particularly during the winter season. The model analysis indicates a temperature range of 30 °C – 31.5 °C in the eastern bay and 28.5 °C – 29.5 °C in the western part. The BoB is influenced by the EICC, a warm ocean current that flows from the west to the east and contributes to the warming of the bay waters during the pre-monsoon season. In the monsoon season, the CROCO model demonstrated a temperature range from 29°C – 31.5°C in all three bays: north, east, and south. The EICC, flowing from the east to the west, can bring warm water from the equatorial region to the western side, raising the temperature, and affecting wind patterns. During the northeast monsoon, winds tend to be cool and dry, while the southwest monsoon brings warm and moist winds. The temperature and wind pattern variations in the BoB significantly affect marine life, ecosystems, and climate. During the post-monsoon period (October to December), the water temperature starts to cool, especially in the North Bay, leading to a north-south temperature gradient. Local weather conditions and ocean currents influenced temperature fluctuations in the northern and eastern regions, as well as the southern and western sides. The presence of a counter-current played a significant role in warming the bay waters, particularly during the pre-monsoon

period. Furthermore, as the summer heat dissipates, the water temperature decreases, with a pronounced cooling effect observed along the northern side of the bay during the post-monsoon phase. Lower RMSD values indicated a higher level of agreement between the model and the data, particularly considering the COADS and AGRO datasets. Existing data were all low resolution (WOA, HYDRO, COADS, ARGO, SODA, and ECCO) and have produced high-resolution data without much deviation from the standard. For validation, the Taylor diagram demonstrated that the model performed satisfactorily compared to the other datasets. The CROCO model exhibited a high correlation between temperature and salinity with a coefficient of 0.98. It is important to note that water salinity may also exhibit seasonal variations, requiring further studies to understand the extent and impact of these variations on the marine ecosystem.

#### **AUTHOR CONTRIBUTIONS**

D. Jaishree reviewed the literature and contributed to the conceptualization, pre-processing, data analysis, preprocessing for simulations, and processing the model outputs and also prepared the manuscript text and edition. P.T. Ravichandran supervised the review work, was involved in the preparation of the manuscript, and reviewed the manuscript for publication.

#### **ACKNOWLEDGEMENT**

Authors express gratitude to Dr. Deeptha Thattai, Dr. Arun Chakraborty (IITK) and Dr. Anandh for their guidance and for conducting scientific discussions which were instrumental in completing the research work.

#### **CONFLICT OF INTEREST**

The author declares that there is no conflict of interests regarding the publication of this manuscript. In addition, the ethical issues, including plagiarism, informed consent, misconduct, data fabrication and/or falsification, double publication and/or submission, and redundancy have been completely observed by the authors.

#### **OPEN ACCESS**

©2024 The author(s). This article is licensed under a Creative Commons Attribution 4.0 International License, which permits use, sharing, adaptation,

distribution and reproduction in any medium or format, as long as you give appropriate credit to the original author(s) and the source, provide a link to the Creative Commons license, and indicate if changes were made. The images or other third-party material in this article are included in the article's Creative Commons license, unless indicated otherwise in a credit line to the material. If material is not included in the article's Creative Commons license and your intended use is not permitted by statutory regulation or exceeds the permitted use, you will need to obtain permission directly from the copyright holder. To view a copy of this license, visit: <http://creativecommons.org/licenses/by/4.0/>

#### PUBLISHER'S NOTE

GJESM Publisher remains neutral with regard to jurisdictional claims in published maps and institutional affiliations.

#### ABBREVIATIONS

%	Percent
°C	Degree Celsius
Cm/s <sup>2</sup>	Centimeter per square second
ASCAT	Advanced scatterometer
ARGO	Array for real-time geostrophic oceanography
BoB	Bay of Bengal
COADS	Comprehensive ocean-atmosphere data set
CROCO	Coastal and regional ocean community model
ECCO	Estimating the circulation and climate of the ocean
EICC	East India Coastal Current
ETOPO2	Earth topography 2–minutes
km	Kilometer
Km <sup>2</sup>	Square kilometer
m	Meter
MLD	Mixed layer depth
PIOD	Positive Indian ocean dipole
Psu	Practical salinity unit
QSCAT	QuikSCAT
RMSD	Root mean square deviation
ROMS	Regional ocean modelling system
SODA	Simulation, simple ocean data assimilation
SSHA	Sea surface height anomaly

SSS	Sea surface salinity
SST	Sea surface temperature
W/m <sup>2</sup>	Watt per square meter
WBC	Western boundary current
WOA	World ocean atlas
WRF	Weather research and forecast

#### REFERENCES

- Akhter, S.; Qiao, F.; Wu, K.; Yin, X.; Chowdhury, K.M.A.; Chowdhury, N.U.M.K., (2021). Seasonal and long-term sea-level variations and their forcing factors in the northern Bay of Bengal: A statistical analysis of temperature, salinity, wind stress curl, and regional climate index data. *Dyn. Atmos. Oceans.*, 95: 1-23 (**23 Pages**).
- Akhil, V.P.; Durand, F.; Lengaigne, M.; Jerome Vialard, J.; Keerthi, M.G.; Gopalakrishna, V.V.; Deltel, C.; Papa, F.; Ement De Boyer, C.; Egut, M., (2014). A modeling study of the processes of surface salinity seasonal cycle in the Bay of Bengal. *J. Geophys. Res. C: Ocean.* 119(6): 3926 – 3947 (**22 Pages**).
- Ali, M.M.; Jagadeesh, P.S.V.; Jain, S., (2007). Effects of eddies on Bay of Bengal cyclone intensity. *Eos, Trans. Am. Geophys. Union.* 88(8): 93-104 (**12 Pages**).
- Amsalia, N.; Haditiar, Y.; Wafdan, R.; Ikhwan, M.; Chaliluddin, M.A.; Sugianto, S.; Rizal, S., (2022). The currents, sea surface temperature, and salinity patterns in the Bay of Bengal. *E3S Web of Conferences.* 339 02001: 1–7 (**7 Pages**).
- Anandh, T.S.; Das, B.K.; Kumar, B.; Kuttippurath, J.; Chakraborty, A., (2018). Analyses of the oceanic heat content during 1980–2014 and satellite-era cyclones over Bay of Bengal. *Int. J. Climatol.*, 38(15): 5619 –5632 (**14 Pages**).
- Anandh, T. S.; Das, B. K.; Kuttippurath, J.; and Chakraborty, A., (2020). A Comparative Analysis of the Bay of Bengal Ocean State Using Standalone and Coupled Numerical Models. *Asia-Pac. J. Atmos. Sci.*, 57(2), 347–359. (**13 Pages**).
- Chakraborty, A.; Gangopadhyay, A., (2016). Development of a high-resolution multiscale modeling and prediction system for Bay of Bengal, Part I: climatology-based simulations. *Open J. Mar. Sci.*, 6: 145–176 (**32 Pages**).
- Chi, N., (2013). The mixed layer salinity budget in the Central Equatorial Indian Ocean. *J. Geophys. Res. C: Oceans.*, 1–18 (**18 Pages**).
- Collins, M.; An, S.II, Cai, W.; Ganachaud, A.; Guilyardi, E.; Jin, F.F.; Jochum, M.; Lengaigne, M.; Power, S.; Timmermann, A.; Vecchi, G.; and Wittenberg, A., (2010). The impact of global warming on the tropical Pacific Ocean and El Niño. *Nat. Geosci.*, 3(6): 391–397 (**17 Pages**).
- Cherian, D.A.; Shroyer, E.L.; Wijesekera, H.W.; Moum, J.N., (2020). The seasonal cycle of upper-ocean mixing at 8°N in the Bay of Bengal. *J. Phys. Oceanogr.*, 50(2): 323–342 (**20 Pages**).
- Dandapat, S.; Chakraborty, A.; Kuttippurath, J.; Bhagawati, C.; Sen, R., (2021). A numerical study on the role of atmospheric forcing on mixed layer depth variability in the Bay of Bengal using a regional ocean model. *Ocean Dyn.*, 71: 963–979 (**17 Pages**).
- Das, B.K.; Anandh, T.S.; Kuttippurath, J.; Chakraborty, A., (2019). Characteristics of the discontinuity of western boundary current

- in the Bay of Bengal. *J. Geophys. Res. C: Oceans*, 124(7): 4464–4479 **(16 Pages)**.
- Dey, D.; Sil, S.; Jana, S.; Pramanik, S.; Pandey, P.C., (2017). An assessment of tropflux and NCEP air-sea fluxes on ROMS simulations over the Bay of Bengal region. *Dyn. Atmos. Oceans.*, 80: 47–61 **(15 Pages)**.
- Dyn, C., (2010). The Indian summer monsoon pre-onset land surface processes and ‘internal’ interannual variabilities of the Indian summer monsoon. *Clim. Dyn.*, 36: 2077–2089 **(13 Pages)**.
- Goswami, B.N.; Ajayamohan, R.S.; Xavier, P.K.; Sengupta, D., (2003). Clustering of synoptic activity by Indian summer monsoon intraseasonal oscillations. *Geophys. Res. Lett.*, 30(8): 1-4 **(4 Pages)**.
- Gao, Z.; Hu, Z.Z.; Zhu, J.; Yang, S.; Zhang, R.H.; Xiao, Z.; Jha, B., (2014). Variability of summer rainfall in Northeast China and its connection with spring rainfall variability in the Huang-Huai region and Indian Ocean SST. *J. Clim.*, 27(18): 7086–7101 **(16 Pages)**.
- Gordon, A.L.; Mahadevan, A.; Hole, W.; Sengupta, D., (2016). Bay of Bengal: 2013 northeast monsoon upper-ocean circulation. *Oceanography*, 29(2): 82-91 **(10 Pages)**.
- Jana, S.; Gangopadhyay, A.; Chakraborty, A., (2015). Impact of seasonal river input on the Bay of Bengal simulation. *Cont Shelf Res* 104:45–62**(18 Pages)**.
- Jourdain, N.C.; Lengaigne, M.; Vialard, J.R.; Madec, G.; Menkes, C.E.; Vincent, E.M.; Jullien, S.; Barnier, B., (2013). Observation-based estimates of surface cooling inhibition by heavy rainfall under tropical cyclones. *J. Phys. Oceanogr.*, 3(1): 1-17 **(17 Pages)**.
- Kikuchi, K.; Wang, B.; Fudeyasu, H., (2009). Genesis of tropical cyclone nargis revealed by multiple satellite observations. *Geophys. Res. Lett.*, 36(6): 1–5 **(5 Pages)**.
- Lee, C.M.; Jones, B.H.; Brink, K.H.; Fischer, A.S., (2000). The upper-ocean response to monsoonal forcing in the Arabian Sea: seasonal and spatial variability. *Deep Sea Res. Part II*, 47(7-8): 1177–1226 **(50 Pages)**.
- Lin, I.I.; Chen, C.H.; Pun, I.F.; Liu, W.T.; Wu, C.C., (2009). Warm ocean anomaly, air sea fluxes, and the rapid intensification of tropical cyclone Nargis (2008). *Geophys. Res. Lett.*, 36(3): 2–6 **(5 Pages)**.
- Levitus, S.; Antonov, J.I.; Boyer, T.P.; Baranova, O.K.; Garcia, H.E.; Locarnini, R.A.; Mishonov, A.V.; Reagan, J.R.; Seidov, D.; Yarosh, E.S.; Zweng, M.M., (2012). World ocean heat content and thermocline sea level change (0-2000m), 1955-2010. *Geophysical Research Letters*, 39(10): 1–5 **(5 Pages)**.
- Liebmann, B.; Hendon, H.; Glick, D., (1994). The relationship and Indian between oceans tropical and the cyclones of the western oscillation pacific by brant liebmann cooperative institute for research in environmental sciences (CIRES), Campus Box 449, University of Colorado, Boulder, Colorado. *J. Meteorolog. Soc. Jpn.*, 72(3): 401–411 **(11 Pages)**.
- Maneesha, K.; Ravichandran, M.; Yu, W., (2012). Upper ocean variability in the Bay of Bengal during the tropical cyclones Nargis and Laila. *Prog. Oceanogr.*, 106: 49-61 **(13 Pages)**.
- Masumoto, Y.; Hase, H.; Kuroda, Y.; Matsuura, H.; Takeuchi, K., (2005). Intraseasonal variability in the upper layer currents observed in the eastern equatorial Indian Ocean. *Geophys. Res. Lett.*, 32(2): 1–4 **(4 Pages)**.
- Mahadevan, A. Hole, W.; Asaro, E.D., (2016). Variability of near-surface circulation and sea surface salinity observed from lagrangian drifters in the northern Bay of Bengal during the waning 2015 southwest monsoon. *Oceanography*, 29(2): 125-133 **(9 Pages)**.
- Rao, S.A.; Saha, S.K.; Pokhrel, S.; Sundar, D.; Dhakate, A.R.; Mahapatra, S.; Ali, S.; Chaudhari, H.S.; Shreeram, P.; Vasimalla, S.; Srikanth, A.S.; Suresh, R.R.V., (2011). Modulation of SST, SSS over northern Bay of Bengal on ISO time scale. *J. Geophys. Res. C: Oceans.*, 116(9): 1-11 **(11 Pages)**.
- Rao, S.A.; Behera, S.K., (2005). Subsurface influence on SST in the tropical Indian Ocean: Structure and interannual variability. *Dyn. Atmos. Oceans.*, 39(1-2): **(11 Pages)**.
- Roy Chowdhury, R.; Prasanna Kumar, S.; Chakraborty, A., (2021). Simultaneous occurrence of tropical cyclones in the northern Indian ocean: differential response and triggering mechanisms. *Front. Mar. Sci.*, 8: 1-25 **(25 Pages)**.
- Schott, F.A.; McCreary, J.P., (2001). The monsoon circulation of the Indian Ocean. *Prog. Oceanogr.*, 1(1): 1-123 **(123 Pages)**.
- Schott, F.A.; Xie, S.P.; McCreary, J.P., (2009). Indian ocean circulation and climate variability. *Rev. Geophys.*, 47(1): 1–46 **(46 Pages)**.
- Sil, S.; Chakraborty, A., (2012). The mechanism of the 20°C isotherm depth oscillations for the Bay of Bengal, *Mar. Geod.*, 35(3): 233–245 **(13 Pages)**.
- Sprattall, J., (2003). Seasonal to interannual upper-ocean variability in the drake passage. *J. Mar. Res.*, 61(1): 27–57 **(31 Pages)**.
- Sivareddy, S.; Ravichandran, M.; Girishkumar, M.S.; Prasad, K.V.S.R., (2015). Assessing the impact of various wind forcing on INCOIS-GODAS simulated ocean currents in the equatorial Indian Ocean. *Ocean Dyn.*, 65(9–10): 1235–1247 **(13 Pages)**.
- Srivastava, A.; Dwivedi, S.; Mishra, A.K., (2016). Intercomparison of high-resolution Bay of Bengal circulation models forced with different winds. *Mar. Geod.*, 39(3–4): 271–289 **(19 Pages)**.
- Srivastava, A.; Dwivedi, S.; Mishra, A.K., (2018). Investigating the role of air-sea forcing on the variability of hydrography, circulation, and mixed layer depth in the Arabian Sea and Bay of Bengal. *Oceanologia*, 60(2): 169–186 **(18 Pages)**.
- Thankaswamy, A.; Xian, T.; Ma, Y.F.; Wang, L.P., (2022). Sensitivity to different reanalysis data on WRF dynamic downscaling for South China sea wind resource estimations. *Atmosphere*, 13(5), 1–23 **(23 Pages)**.
- Ts, A.; Das, B.K.; Kuttippurath, J.; Chakraborty, A., (2020). A coupled model analyses on the interaction between oceanic eddies and tropical cyclones over the Bay of Bengal. *Ocean Dyn.*, 70: 327-337 **(11 Pages)**.
- Vinayachandran, P.N.; Satish Shetye, D.S.; Gadgil, S., (1996). Forcing mechanisms of the Bay of Bengal. *Current Science*, 71(10): 753–763 **(11 Pages)**.
- Vinayachandran, P.N.; Julian, J.P.M.; Hood, R.R.; Kohler, K.E., (2014). Numerical investigation of the phytoplankton bloom in the Bay of Bengal during northeast monsoon. *J. Geophys. Res.*, 110(C12): 1-14 **(14 Pages)**.
- Webster, P.J.; Magaña, V.O.; Palmer, T.N.; Shukla, J.; Tomas, R.A.; Yanai, M.; Yasunari, T., (1998). Monsoons: processes, predictability, and the prospects for prediction. *J. Geophys. Res. C: Oceans*, 103(C7): 14451–14510 **(60 Pages)**.
- Wu, Z.; Jiang, C.; Deng, B.; Chen, J.; Long, Y.; Qu, K.; Liu, X., (2019). Numerical investigation of typhoon Kai-tak (1213) using a mesoscale coupled WRF-ROMS model. *Ocean Eng.*, 175: 1–15 **(15 Pages)**.

#### AUTHOR (S) BIOSKETCHES

**Jaishree, D.**, Ph.D. Candidate, Assistant Professor, Department of Civil Engineering, Faculty of Engineering and Technology, SRM Institute of Science and Technology, Kattankulathur - 603203, Chengalpattu District, Tamil Nadu, India.

- Email: [jaishred@srmist.edu.in](mailto:jaishred@srmist.edu.in)
- ORCID: [0000-0003-0401-068X](https://orcid.org/0000-0003-0401-068X)
- Web of Science ResearcherID: **NA**
- Scopus Author ID: 57193997236
- Homepage: <https://www.srmist.edu.in/faculty/jaishree-d-2/>

**Ravichandran, P.T.**, Ph.D., Professor, Head of the Department of Civil Engineering, Faculty of Engineering and Technology, SRM Institute of Science and Technology, Kattankulathur - 603203, Chengalpattu District, Tamil Nadu, India.

- Email: [ravichap@srmist.edu.in](mailto:ravichap@srmist.edu.in)
- ORCID: [0000-0002-9555-2005](https://orcid.org/0000-0002-9555-2005)
- Web of Science ResearcherID: **NA**
- Scopus Author ID: 23493524100
- Homepage: <https://www.srmist.edu.in/faculty/dr-p-t-ravichandran/>

#### HOW TO CITE THIS ARTICLE

*Jaishree, D.; Ravichandran, P.T., (2024). Exploring the upper ocean characteristics of a bay using coastal and regional ocean community model. Global J. Environ. Sci. Manage., 10(1): 97-116.*

DOI: [10.22034/gjesm.2024.01.08](https://doi.org/10.22034/gjesm.2024.01.08)

URL: [https://www.gjesm.net/article\\_706060.html](https://www.gjesm.net/article_706060.html)





## ORIGINAL RESEARCH ARTICLE

## Application of fuzzy logic in decision-making process for relocation of floating net cages in river fish farming

R. Pramana<sup>1,2</sup>, B.Y. Suprpto<sup>1</sup>, Z. Nawawi<sup>1\*</sup><sup>1</sup> Department of Engineering Science, Faculty of Engineering Universitas Sriwijaya, Palembang 30128, Indonesia<sup>2</sup> Department of Electrical Engineering, Faculty of Engineering Universitas Maritim Raja Ali Haji, Tanjungpinang 29111, Indonesia

## ARTICLE INFO

## Article History:

Received 24 March 2023

Revised 01 June 2023

Accepted 09 August 2023

## Keywords:

Cage relocation

Fuzzy logic

Internet of things

River pollution

Water quality monitoring

## ABSTRACT

**BACKGROUND AND OBJECTIVES:** Land-based aquaculture operations, at present, are intensively conducted to meet the ever-growing demand for food consumption. Floating net cages are one of the traditional methods commonly used by Indonesian fishermen for river fish farming. Increased human activities along the Musi River and coastline have resulted in pollution and waste in the river waters and fluctuating water quality. Yet, floating net cage owners still manually assess the water quality. This study aims to develop an early warning system for water quality and create a decision-making program as a reference for fishermen to relocate floating net cages when the river water quality deteriorates.

**METHODS:** The device was tested at 39 locations within a radius of approximately 3400 meters, and the distance between locations varied between 55 and 334 meters. The river was divided into three sections: the river coast, the middle section, and the other river coast. Water quality sensors were placed at a depth of 0–20 centimeters from the surface of the Musi River, with measurement durations at each location ranging from 1 to 40 minutes. Direct measurements of the Musi River's water quality were obtained by monitoring the water quality using an internet-based computer application. A decision-making Python program utilizing fuzzy logic was then executed to evaluate the suitability of the river water quality for fish cultivation. The program's input variables comprise water temperature, potential of hydrogen, and dissolved oxygen sensor data. Meanwhile, the program output recommends floating net cage owners to either "Stay in position" or "Move." Water quality warnings that exceed the upper and lower threshold limits are displayed using light-emitting diode indicators and a buzzer.

**FINDINGS:** Overall, the water quality values of the Musi River at the test locations generally indicated stable and suitable conditions for river fish cultivation. The average water quality values were 29.20 degrees Celsius for temperature, 3.98 milligrams per liter for dissolved oxygen, and a potential of hydrogen of 6.42. From all the data obtained during the decision-making program, 36 locations suggested that the floating net cages should "Stay in position." Meanwhile, the three remaining locations were recommended to "Move" as they exhibited poor water quality, with potential of hydrogen values below 6. Field observations indicated that these locations were situated near residential areas, factories/industries, and tributaries, which are highly susceptible to waste and pollution. The output of the decision-making program correlated with the issued warnings by the water quality warning indicators when the pH value exceeded the lower threshold limit.

**CONCLUSION:** The fuzzy logic method implemented in the Python program for decision-making regarding the relocation of floating net cages in river fish farming revealed the fluctuating water quality conditions of the Musi River within a specific time duration. These conditions correlated with the proximity of the water bodies to pollution sources such as residential areas, factories, and tributaries. The program's output classified the status of the floating net cages into two conditions: "Stay in position" or "Move." The decision-making application to relocate floating net cages for fish farming in rivers provides a solution for fishermen as the resulting program decisions give the same indication as the reading value of the water quality sensor.

DOI: [10.22034/gjesm.2024.01.09](https://doi.org/10.22034/gjesm.2024.01.09)This is an open access article under the CC BY license (<http://creativecommons.org/licenses/by/4.0/>).

NUMBER OF REFERENCES

38



NUMBER OF FIGURES

9



NUMBER OF TABLES

4

\*Corresponding Author:

Email: [pendidikankimiaumrah@gmail.com](mailto:pendidikankimiaumrah@gmail.com)

Phone: +6282 2845 64481

ORCID: [0000-0002-8472-5126](https://orcid.org/0000-0002-8472-5126)

Note: Discussion period for this manuscript open until April 1, 2024 on GJESM website at the "Show Article".

## INTRODUCTION

As production from capture fisheries continues to decline, intensive fish farming has increased to meet the greater population's ever-growing demand for fisheries products (Sabilillah et al., 2023; Takarina et al., 2023). Aquaculture is a rapidly growing food production sector that involves the cultivation of plants or aquatic animals (Acar et al., 2019). Of the total aquaculture production, 62.5 percent (%) comes from inland aquaculture (FAO, 2020). In Indonesia, rivers are a vital source of life and civilization and serve as focal points for community activities. Rivers are open water bodies that fishermen extensively utilize for cultivation purposes (Torres-Bejarano et al., 2022). Various freshwater fish species are cultivated to meet the increasing demand for fish protein, mainly driven by population growth (Oyinlola, 2019; Maulana et al., 2023). One commonly used method in fish farming is the floating net cage (FNC) method. FNCs are typically placed along the riverbanks, away from crowded areas. With this method, water availability, which is the main component for cultivation, is no longer a concern. However, water quality needs to be managed and given attention (Abinaya et al., 2019), as the increasing human activities in modern times have led to alarming river pollution levels in Indonesia. Water quality in river ecosystems fluctuates and undergoes daily changes that are influenced by various factors. Changes in river water quality can occur due to the surrounding ecosystem, tidal cycles, temperature variations, and weather conditions. External factors such as community waste, industrial waste, agricultural runoff, vessel traffic, excessive utilization of water bodies, and other human activities that utilize the river flow can also contribute to changes in river water quality (Sulistyowati et al., 2023; Ehzari et al., 2022). These external factors pose risks to the survival of living organisms in and around the river. The development and survival of cultured fish depend on optimal water quality (Lekang, 2020). Pollution in one river body can spread to other river waters. Small river streams connected to larger river flows contribute to widespread water contamination. Harmful chemicals and disease-causing agents resulting from pollution can easily spread with the currents, affecting the health of fish in cultivation cages (Cardia and Lovatelli, 2016). Poor water quality also directly affects the growth and well-being of fish. Fish may experience stress, become susceptible

to diseases, and even die. Mass fish mortality is generally caused by factors such as strong winds, lightning, heavy rainfall (Molato, 2022), and high pollution levels in the water bodies. Domestic and industrial wastes can also produce heavy metal pollutants in water, which are hazardous to health (Samimi and Shahriari Moghadam, 2021). Partially treated or untreated waste remains a major threat to the survival of river biodiversity (Maurya et al., 2019). Industrial waste usually contains metal ions such as nickel, copper, cobalt, and timbal, each with a limit on the content levels allowed (Shourije et al., 2023). For traditional fishermen in Indonesia, indicators of polluted river water are changes in the river color and an increased number of dead fish in cultivation ponds within a specific period. If the surface water changes color from its usual state or there is an unusual increase in dead fish in the FNCs, the fishermen will immediately relocate the cages to avoid greater losses. FNCs are relocated by pulling them using motorized boats to another location deemed to have better water quality than the previous one. The longer the delay in relocating the FNCs, the greater the losses incurred by the fishermen. However, there is no established measurement and assessment of water quality for river fish farming. It is advisable to regularly monitor the water quality parameters in the FNCs to ensure optimal growth and development of the fish (Boyd and Lichtkoppler, 1979; Jino Ramson et al., 2019). Water quality parameters need to be evaluated to ensure compliance with existing water quality standards. Thus, this research provides a solution for fishermen using FNCs in making decisions regarding the relocation of their cages when the river water quality deteriorates. This study developed a real-time water quality parameter-based assessment program using fuzzy logic as a reference for fish farmers in making decisions to relocate the FNCs, aiming to avoid greater losses due to river pollution. A Python program using fuzzy logic was employed, and real-time water quality monitoring was conducted using a personal computer with Internet of Things (IoT) technology equipped with an alarm system. The alarm system was incorporated as an early warning for the surrounding water conditions near the FNC to monitor water quality. Cage technology in aquaculture was carried out by (Kim et al., 2011; 2014), who developed and implemented a submersible fish cage system model that works automatically to anticipate

extreme weather. The system comprised an air control system, four batteries, a backup air tank, four air pressure tanks, 12 variable ballast tanks, and a water pump. The fish cage was made of steel with 12 sides and had a diameter of 5.92 meters (m) and a depth of 2.91 m. Meanwhile, (Thangavel *et al.*, 2015) designed a fish cage with an electronic system that can be automatically submerged at the desired depth. The cages were made of high-density polyethylene (HDPE) pipes equipped with control stations, nets, variable ballast frames, submersible pumps, air control systems, buoys, mooring ropes, and anchors. A study on monitoring water quality in cages by (Sung *et al.*, 2014) led to the design of a remote monitoring and control device based on IoT for fish farming. The device utilized Zigbee-based sensors for temperature, dissolved oxygen (DO), potential of hydrogen (pH), and solar panel power sources. (Chen *et al.*, 2016) conducted research on water quality monitoring for aquaculture industries based on a wireless sensor network (WSN) using Zigbee and Wi-Fi. The sensors included temperature, DO, pH, and water level measurements. In addition, (Kyaw and Ng, 2017) developed a control and monitoring device for water quality, which operated automatically through a mobile application or web application, and included light-emitting diode (LED) indicators. (Vishwakarma *et al.*, 2018) constructed an electronic instrument for monitoring pond water with IoT-based technology. Data was wirelessly transmitted to an offshore central server using IoT. (La Madrid *et al.*, 2019) developed a water quality monitoring system for tilapia fish ponds using temperature, pH, DO, and water level sensors. Arduino was used for control, and the system was equipped with a SIM900 global system mobile (GSM) module for data transmission via short message service (SMS). (Shareef and Reddy, 2019) developed a remote water quality monitoring system with an early warning system for aquaculture using temperature, pH, DO, and air humidity sensors. In short, previous researchers have also applied fuzzy logic methods for water quality parameters, such as developing an index model for classifying water quality parameters in lakes (Icaga, 2007), temperature control (Oltean and Ivanciu, 2017), real-time water quality monitoring based on IoT (Bokingkito and Caparida, 2018), and constructing a water quality analysis model for tilapia fish farming (Molato, 2022). Thus, the aim of the current study is to develop an early warning system

for water quality and create a decision-making program to guide fishermen in relocating floating net cages. This study was conducted in the Musi River, South Sumatra Province, Indonesia, in 2022.

## MATERIALS AND METHODS

This research was divided into several stages, including device design, fuzzy logic membership function construction, and the development of a decision-making program for the relocation of FNC. Testing was conducted at 39 locations in the Musi River of South Sumatra. The water quality measurement method divided the river into three sections: riverbank areas (coded U1-U13), the middle section (coded M1-M13), and other riverbank areas (coded D1-D13). The sensor was placed at a depth of 0–20 cm from the river surface. Real-time sensor measurements were performed with the duration at each location ranging from 1 to 40 minutes. Each measured water quality parameter at the test locations was subsequently evaluated using the developed program to assess the water conditions around the FNCs. The results of the water quality assessment serve as a reference for fishermen to determine the status of the FNCs, whether to relocate or keep them in their original positions.

### *Device design*

The device consists of three main components: the sensor unit, the processing unit, and the monitoring and alarm unit. The sensor unit consists of six water quality sensors: temperature, DO, pH, Total Dissolved Solid (TDS), Electric Conductivity (EC), and Turbidity. All sensors used were calibrated according to standard procedures and instructions. The designed device is illustrated in Fig. 1.

This device utilized an Arduino Mega as its processing unit, supported by an ESP8266 for IoT functionality. The alarm and monitoring unit consisted of LED indicators, a buzzer, a liquid crystal display (LCD), and a monitoring application accessed via the Internet. The alarm serves as an early warning for fishermen when the water quality around the fishing area deteriorates. It provides visual and auditory alerts when the water quality reading from the sensor unit exceeds the programmed lower and upper threshold values. The water quality conditions around the fishing area can be remotely monitored through the Blynk version 1.5.4 monitoring application

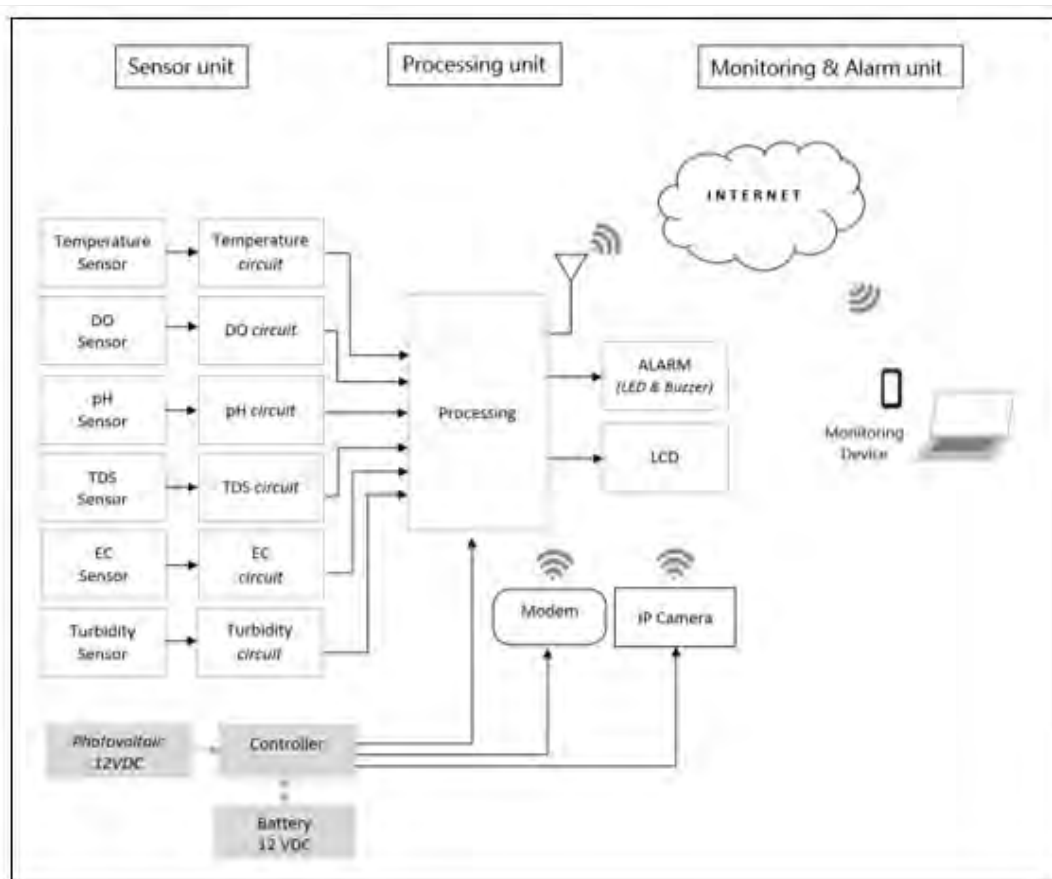


Fig. 1: Design system

using a smartphone or internet-connected personal computer (PC). This application displays real-time data from each sensor reading and can be displayed with average values and selectable time durations. Furthermore, there is an accessible database for administrators to retrieve the data.

#### *The study area and testing location*

The testing was conducted in the Musi River, South Sumatra, Indonesia. The testing location was around Karto Island, with coordinates ranging from -3.041384, 104.662513 to -3.020287, 104.640442, with a radius of approximately  $\pm 3400$  m. The testing location included areas such as forests, settlements, plantations, fish ponds, ports, and community ship crossings.

#### *Water quality alert system*

Every fish has different water quality parameters

according to its habitat and species. Fish living in river habitats have different water quality parameters than those living in marine environments. Suitable water quality for a fish's habitat affects its health, reproduction, and overall survival, which is essential for its growth. In the management of fisheries cultivation, water quality needs to be controlled continuously (Danh *et al.*, 2020). Many factors affect water quality (Wei *et al.*, 2023), such as temperature, pH, and DO, which are the primary parameters that can influence other water quality parameters or serve as indicators for them. These three parameters have also been identified as the causes of mass fish mortality (Molato, 2022). Temperature affects fish metabolism, and the surrounding environmental temperature determines the fish's body temperature (Volkoff and Rønnestad, 2020). Low levels of DO also affect fish growth and survival and may result in fish

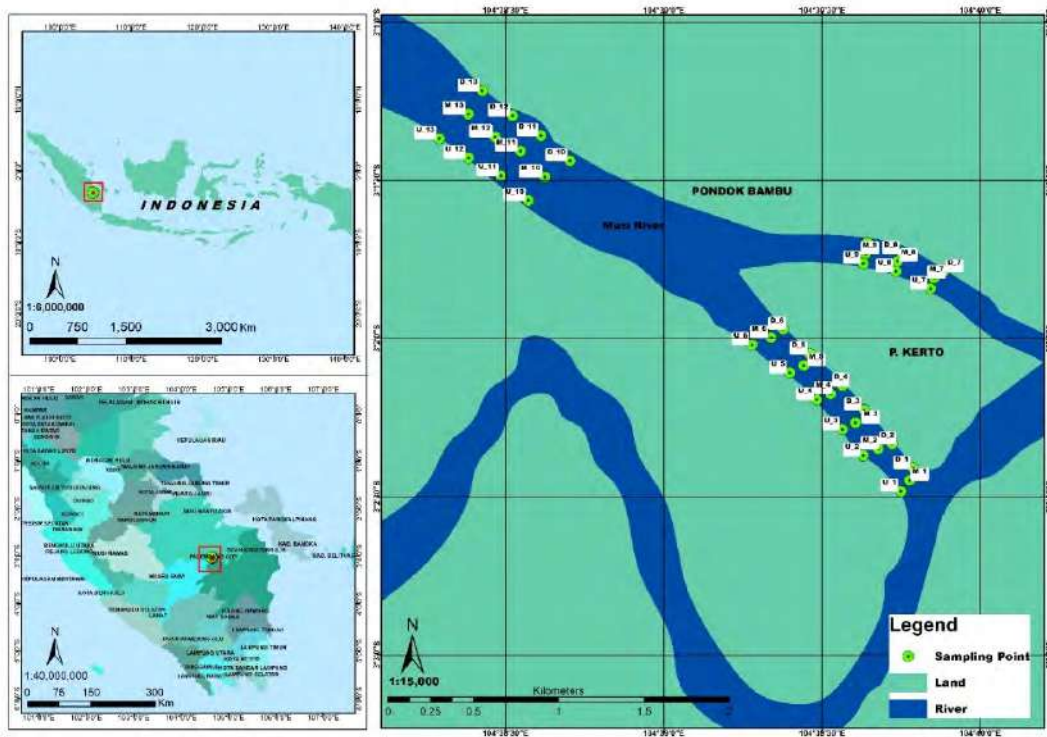


Fig. 2: Geographic location of the study area and the test location in the Musi River, South Sumatra, Indonesia

Table 1: Standard parameters for water quality in river fish cultivation (Pemerintah Republik Indonesia, 2021)

Parameter	Unit	Lower threshold value	Upper threshold value
Temperature	Degrees Celsius (°C)	27°C	32°C
DO	mg/L	3	>3
pH		6	9
TDS	mg/L	1.000	1.000

stress, reduced appetite, susceptibility to diseases, and death. The DO levels vary among different fish species. If the DO levels drop below 3 milligrams per liter (mg/L) within three hours, fish movement becomes sluggish, eventually leading to death if the DO falls below 1.9 mg/L (Prakoso and Chang, 2018). The pH level of water is naturally influenced by the type of rocks, soil, and contaminants discharged into the water, among other variables. Significant changes in the pH value can alter the diversity of freshwater organisms, and only a few species can survive (Abd El-Hack *et al.*, 2022). Standard water quality parameters for fish cultivation in rivers have been formulated in government regulations (Pemerintah

Republik Indonesia, 2021). Based on these regulatory standards, threshold values for the three main water quality parameters were established in this study, as shown in Table 1.

The upper and lower threshold values presented in Table 1 serve as references for the developed program and device. The alarm system provides early warnings for fishermen when the water quality exceeds the predetermined thresholds. The water quality alert system displays this information through a green LED indicator when the water quality surpasses the lower threshold and a red LED indicator when it exceeds the upper threshold. In addition to visual alerts, the system is equipped with a buzzer for



Fig. 3: LED and Buzzer water quality warning indicator

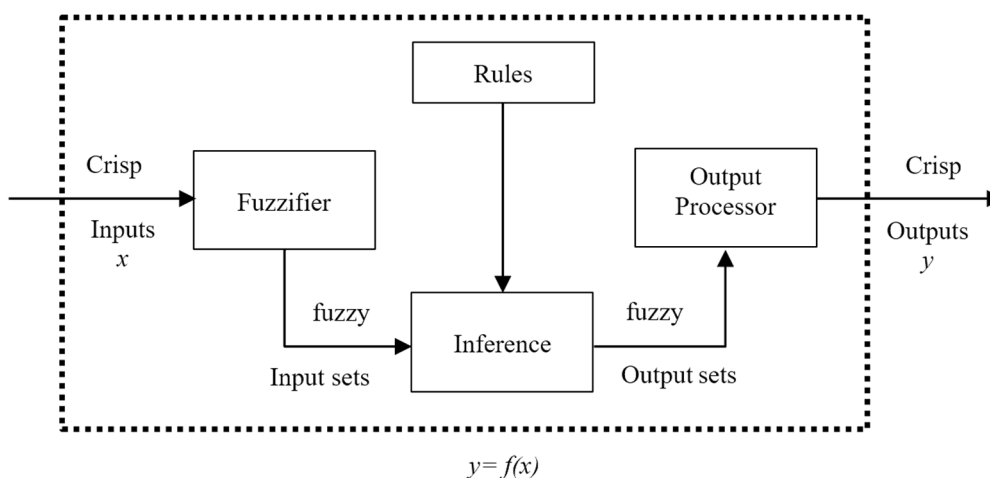


Fig. 4: Fuzzy logic system (Mendel, 2003)

audible warnings. This water quality alert system also aims to facilitate fishermen in accurately monitoring real-time water conditions around the FNC cultivation site.

#### *Decision-making for the relocation of floating net cages based on fuzzy logic*

Fuzzy logic is a type of logic that deals with uncertain or vague values that lie between true and false, ranging from 0 to 1. It resembles human thinking logic, which is different from classical logic, where everything is binary with two possible values: 0 or 1. The values of each input and output variable are determined by their membership functions (Mendel, 1995). Fuzzy logic consists of four interconnected components: fuzzifier, inference, rules, and output processing (Mendel, 2003), as illustrated in Fig. 4.

In this research, the fuzzy method was used as a decision-making tool for relocating the location of

net cages, providing an alternative solution to the traditional method commonly used by fish farmers, who heavily rely on river water color and fish conditions in the ponds. The fuzzy method was implemented using the Python programming language. The fuzzy input variables consist of temperature, DO, and pH data. The standard water quality for fish cultivation in rivers has the following normal ranges: temperature ranges from 27 °C to 32 °C, pH ranges from 6 to 9, and the reference value for DO is greater than 3 mg/L. A DO value above 3 mg/L indicates a higher oxygen content level in the river, which benefits the water environment. Five membership functions were then created for each input variable based on these standard water quality parameters. Table 2 presents the developed parameter values for each input variable's membership function (MF).

Based on the temperature, pH, and DO parameters from the standard water quality for river fish

Table 2: Membership function

Inputs	Range	Name	MF Type	Parameter
Temperature	0-41	cold	gauss2mf	[2.782, 3.434, 17.7, 2.3]
		cool	gaussmf	[24, 1.7]
		normal	gaussmf	[28.5, 1.7]
		warm	gaussmf	[33, 1.7]
		hot	gauss2mf	[38.63, 2.278, 41, 0.034]
Dissolved Oxygen	0-10	very poor	gauss2mf	[0.007, 2.1, 0 0.28]
		poor	gaussmf	[2.8, 0.2]
		normal	gaussmf	[3.5, 0.2]
		good	gaussmf	[4.2, 0.2]
pH	0-14	very good	gauss2mf	[5, 0.28, 10, 0.007]
		very low	gauss2mf	[0, 0.0119, 4, 0.5535]
		low	gaussmf	[5.5, 0.5]
		normal	gaussmf	[7.5, 0.5]
		high	gaussmf	[9.5, 0.5]
		very high	gauss2mf	[11, 0.5535, 14, 0.0119]

cultivation and the constructed membership functions, a decision-making program was designed using the Python language.

```
import skfuzzy as fuzz
import numpy as np
```

```
# Temperature
```

```
temperatur = np.arange(0, 41, 1)
cold = fuzz.gauss2mf(temperatur, 2.782, 3.434, 17.7, 2.3)
cool = fuzz.gaussmf(temperatur, 24, 1.7)
normal = fuzz.gaussmf(temperatur, 28.5, 1.7)
warm = fuzz.gaussmf(temperatur, 33, 1.7)
hot = fuzz.gauss2mf(temperatur, 38.63, 2.278, 41, 0.034)
```

```
# Dissolved Oxygen
```

```
dissolved_oxygen = np.arange(0, 7, 0.1)
very_poor = fuzz.gauss2mf(dissolved_oxygen, 0, 0.007, 2.1, 0.28)
poor = fuzz.gaussmf(dissolved_oxygen, 2.8, 0.2)
normal_DO = fuzz.gaussmf(dissolved_oxygen, 3.5, 0.2)
good = fuzz.gaussmf(dissolved_oxygen, 4.2, 0.2)
very_good = fuzz.gauss2mf(dissolved_oxygen, 5, 0.28, 7, 0.007)
```

```
# pH
```

```
pH = np.arange(0, 14, 0.1)
very_low = fuzz.gauss2mf(pH, 0, 0.0119, 4, 0.5535)
```

```
low = fuzz.gaussmf(pH, 5.5, 0.5)
normal_pH = fuzz.gaussmf(pH, 7.5, 0.5)
high = fuzz.gaussmf(pH, 9.5, 0.5)
very_high = fuzz.gauss2mf(pH, 11, 0.5535, 14, 0.0119)
# Visualize the membership functions
import matplotlib.pyplot as plt
```

```
fig, (ax0, ax1, ax2) = plt.subplots(nrows=3, figsize=(8, 9))
ax0.plot(temperatur, cold, 'b', linewidth=1.5, label='Cold')
ax0.plot(temperatur, cool, 'g', linewidth=1.5, label='Cool')
ax0.plot(temperatur, normal, 'r', linewidth=1.5, label='Normal')
ax0.plot(temperatur, warm, 'm', linewidth=1.5, label='Warm')
ax0.plot(temperatur, hot, 'y', linewidth=1.5, label='Hot')
ax0.set_title('Temperature')
ax0.legend()
ax1.plot(dissolved_oxygen, very_poor, 'b', linewidth=1.5, label='Very Poor')
ax1.plot(dissolved_oxygen, poor, 'g', linewidth=1.5, label='Poor')
ax1.plot(dissolved_oxygen, normal_DO, 'r', linewidth=1.5, label='Normal')
ax1.plot(dissolved_oxygen, good, 'm', linewidth=1.5, label='Good')
ax1.plot(dissolved_oxygen, very_good, 'y', linewidth=1.5, label='Very Good')
```

### Making decisions to relocate floating net cages

```
ax1.set_title('dissolved oxygen')
ax1.legend()
ax2.plot(pH, very_low, 'b', linewidth=1.5, label='Very Poor')
ax2.plot(pH, low, 'g', linewidth=1.5, label='Poor')
ax2.plot(pH, normal_pH, 'r', linewidth=1.5, label='Normal')
ax2.plot(pH, high, 'm', linewidth=1.5, label='Good')
ax2.plot(pH, very_high, 'y', linewidth=1.5, label='Very Good')
ax2.set_title('pH')
ax2.legend()
def decision_making(temperature_value, dissolved_oxygen_value, pH_value):
    if temperature_value >= 27 and temperature_value <= 32 and dissolved_oxygen_value >= 3 and pH_value >= 6 and pH_value <= 9:
        return "Stay_In_Position"
    else:
        return "Move"
# Get user inputs
temperature_value = float(input("Enter the temperature: "))
dissolved_oxygen_value = float(input("Enter the dissolved oxygen value: "))
pH_value = float(input("Enter the pH: "))
# Result
result = decision_making(temperature_value,
```

```
dissolved_oxygen_value, pH_value)
print("The Floating Net Cage should be: ", result)
```

In the running program, enter the values of the three input variables according to the water quality data read from the sensor. The result displays a decision regarding the status of the floating net cage as a fuzzy output variable for the floating net cage, consisting of two possible statuses: "Stay in position" or "Move."

### RESULTS AND DISCUSSION

The field testing results indicate that the sensors are highly responsive to any changes in the river water parameters. The measurements from each sensor are displayed on the Blynk application, which can be accessed through an internet-based personal computer.

The average measurement results from all testing locations are as follows: the average temperature value is 29.50 °C, the average DO value is 3.98 mg/L, and the average pH value is 6.34.

The river water temperature during the testing ranged from 27.44 °C to 31.06 °C, which falls within the acceptable tolerance limits for river fish. The water temperature generally remained stable following the changes in the surrounding air temperature.

The measurements of DO values during testing ranged from 3.00 mg/L to 4.78 mg/L, which is above

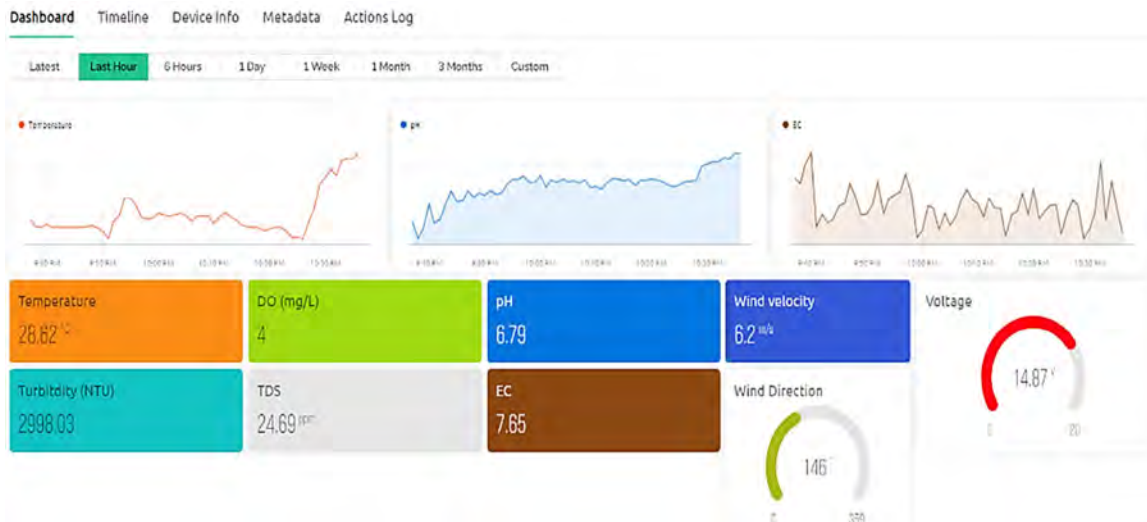


Fig. 5: Display of the water quality monitoring application

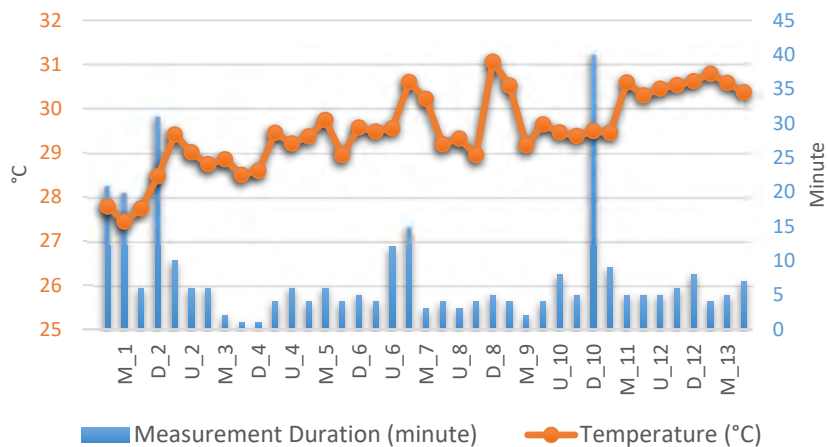


Fig. 6: River water temperature measurement results

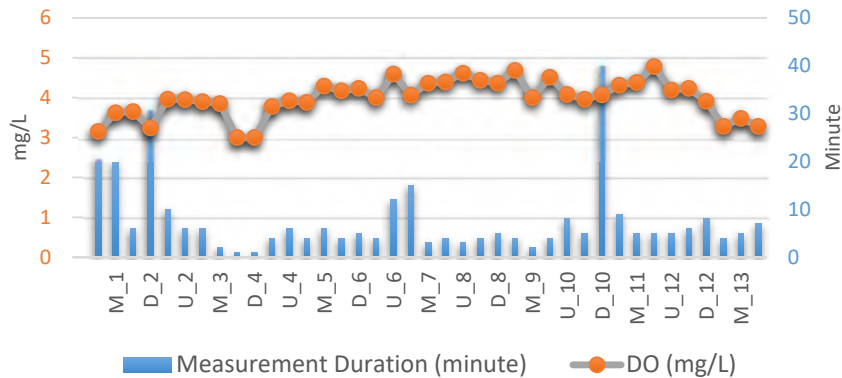


Fig. 7: River water DO measurement results

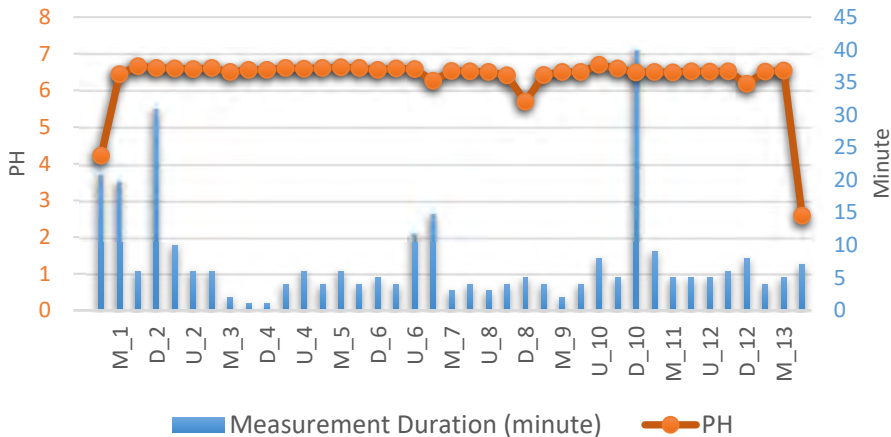


Fig. 8: River water pH measurement results

the standard threshold for river fish. Generally, the measured DO values remained stable with minimal fluctuations.

The pH measurements during testing ranged from 2.58 to 6.70, exceeding the lower threshold value of the standard range (6 to 9). There were fluctuations in the measured pH values, with certain locations experiencing a significant decrease in pH. The Python program generated a decision regarding the status of the floating net cage based on the input water parameter data from the sensor readings. The program considers the water parameter data provided and produces two possible status conditions: "Stay

in position" or "Move." The status "Stay in position" is generated when all the measured input variable values in the net cage meet the predetermined standard water quality thresholds, which are a temperature range of approximately (27°C to 32°C), a pH range of (6 to 9), and a DO value above 3 mg/L. On the other hand, the status "Move" is generated when one or all of the measured output variable values in the net cage exceed the upper and lower threshold values of the predetermined standard water quality. The membership functions for the input variables temperature, pH, and DO are displayed in Fig. 9.

The measurement results of water quality and the

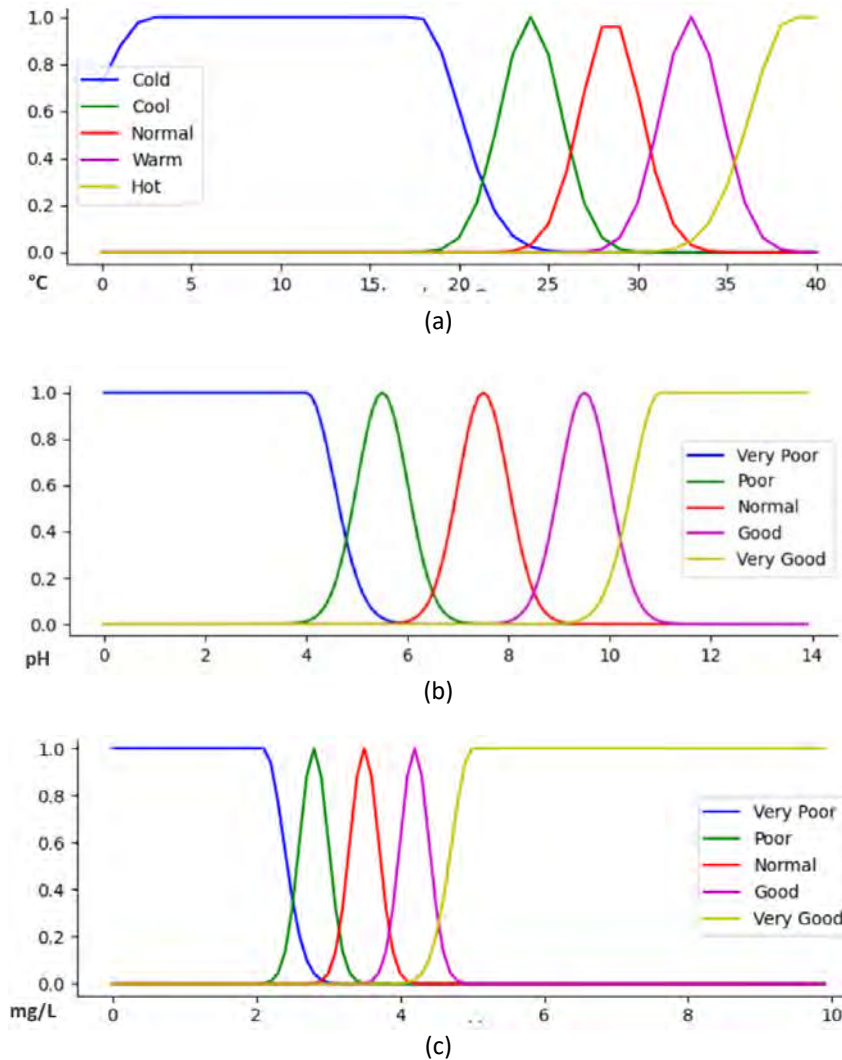


Fig. 9: (a) Temperature membership function. (b) pH membership function (c) DO membership function

Table 3: Measurement results of water quality and recommended status

Location Code	Coordinate	Measurement duration (minute)	Average Value			Recommended FNC Status
			Temp. (°C)	DO (mg/L)	PH	
U_1	-3.041384, 104.662513	21	27.78	3.15	4.22	Move
M_1	-3.040807, 104.662964	20	27.44	3.62	6.44	Stay in position
D_1	-3.040174, 104.663149	6	27.74	3.65	6.66	Stay in position
D_2	-3.038893, 104.662040	31	28.47	3.24	6.61	Stay in position
M_2	-3.039144, 104.661297	10	29.41	3.96	6.60	Stay in position
U_2	-3.039509, 104.660526	6	29.01	3.95	6.58	Stay in position
U_3	-3.038125, 104.659419	6	28.74	3.90	6.61	Stay in position
M_3	-3.037777, 104.660101	2	28.85	3.85	6.50	Stay in position
D_3	-3.037095, 104.660569	1	28.5	3	6.56	Stay in position
D_4	-3.035819, 104.659427	1	28.59	3	6.56	Stay in position
M_4	-3.036249, 104.658797	4	29.45	3.78	6.61	Stay in position
U_4	-3.036555, 104.658063	6	29.21	3.92	6.59	Stay in position
U_5	-3.035142, 104.656636	4	29.37	3.88	6.61	Stay in position
M_5	-3.034752, 104.657388	6	29.74	4.29	6.63	Stay in position
D_5	-3.034148, 104.657702	4	28.95	4.17	6.61	Stay in position
D_6	-3.032848, 104.656301	5	29.57	4.23	6.56	Stay in position
M_6	-3.033291, 104.655666	4	29.48	4	6.60	Stay in position
U_6	-3.033657, 104.654657	12	29.55	4.59	6.58	Stay in position
D_7	-3.029802, 104.664763	15	30.60	4.06	6.26	Stay in position
M_7	-3.030137, 104.664243	3	30.22	4.36	6.53	Stay in position
U_7	-3.030711, 104.664048	4	29.19	4.39	6.52	Stay in position
U_8	-3.029800, 104.662236	3	29.32	4.61	6.50	Stay in position
M_8	-3.029251, 104.662327	4	28.95	4.43	6.41	Stay in position
D_8	-3.028867, 104.662569	5	31.06	4.36	5.69	Move
D_9	-3.028293, 104.660743	4	30.52	4.68	6.42	Stay in position
M_9	-3.028876, 104.660646	2	29.17	4.00	6.50	Stay in position
U_9	-3.029385, 104.660524	4	29.64	4.51	6.50	Stay in position
U_10	-3.026066, 104.642879	8	29.46	4.08	6.70	Stay in position
M_10	-3.024817, 104.643743	5	29.38	3.96	6.60	Stay in position
D_10	-3.023976, 104.645068	40	29.49	4.07	6.49	Stay in position
D_11	-3.022644, 104.643542	9	29.45	4.31	6.50	Stay in position
M_11	-3.023461, 104.642456	5	30.59	4.38	6.49	Stay in position
U_11	-3.024758, 104.641437	5	30.30	4.78	6.52	Stay in position
U_12	-3.023818, 104.639707	5	30.45	4.19	6.51	Stay in position
M_12	-3.022717, 104.641116	6	30.53	4.23	6.52	Stay in position
D_12	-3.021601, 104.642045	8	30.62	3.91	6.18	Stay in position
D_13	-3.020287, 104.640442	4	30.79	3.28	6.51	Stay in position
M_13	-3.021507, 104.639701	5	30.58	3.48	6.54	Stay in position
U_13	-3.022801, 104.638177	7	30.37	3.28	2.58	Move

recommended status from each device's test location are displayed in [Table 3](#).

The test results from all locations indicated that 36 locations possessed suitable water quality for fish cultivation. The sensor data input in the decision-making program suggested that the floating net cages should "Stay in position." However, three locations (U1, D8, U13) showed water quality unsuitable for river fish cultivation and were recommended to "Move" the floating net cages. From the three locations shown in [Table 3](#), it can be observed that the values of temperature and DO parameters are not

significantly different from the 36 locations classified as "Stay in position" and are still within the standard range of river water quality values. However, the pH values of these three locations are below 6 (lower than the standard value for river water quality). The water quality alert system performed well during the testing and aligned with the designed program. The results of the alarm system testing at location U1 are displayed in [Table 4](#).

During the field testing, the sensors responded to every change in the river water parameters, with data updates in the application within 1 to 10

Table 4: Results of LED and buzzer indicator testing for water quality

Time	Water quality measurement			Buzzer (On/Off)	Alert Indicator			Operating LED color
	Temperature (°C)	DO (mg/L)	PH		Temperature (°C)	DO (mg/L)	PH	
11:10:00 AM	28.6	3	1.62	On	-	-	√	Blue
11:11:00 AM	28.63	3	1.65	On	-	-	√	Blue
11:12:00 AM	28.41	3	1.37	On	-	-	√	Blue
11:13:00 AM	27.43	3	0.22	On	-	-	√	Blue
11:14:00 AM	27.32	3	0.02	On	-	-	√	Blue
11:15:00 AM	28.07	3	0.24	On	-	-	√	Blue
11:16:00 AM	28.01	3	0.29	On	-	-	√	Blue
11:17:00 AM	27.83	3	0.21	On	-	-	√	Blue
11:18:00 AM	28.53	3	6.59	Off	-	-	-	None
11:19:00 AM	28.63	3	6.87	Off	-	-	-	None
11:20:00 AM	28.63	3	6.94	Off	-	-	-	None
11:21:00 AM	26.88	4.5	6.5	Off	-	-	-	None

seconds. The measured temperature values of the river water ranged from 27.44 °C to 31.06 °C, the DO values ranged from 3.00 mg/L to 4.78 mg/L, and the pH values ranged from 2.58 to 6.70. The temperature and DO values were within the allowable tolerance limits for river fish, but the measured pH values exceeded the lower threshold of the regulatory standard set at 6-9 (Pemerintah Republik Indonesia, 2021). The testing was conducted at 39 locations, and the decision-making program recommended “Stay in position” for 36 locations, as the measured water quality values were in accordance with the predetermined standards. However, three locations (U1, D8, U13) indicated poor water quality, with pH values below 6, and were recommended to “Move” the FNCs. Observations showed that these three locations were situated near residential areas, factories/industries, and tributaries, which might be contaminated by waste from surrounding activities. These conditions align with previous research by Abd El-Hack et al., (2022), where pH values are influenced by contaminants discharged into the water, resulting in only a few species surviving. The water quality values were within the normal range and were compliant with the existing standards compared to the data from nearby testing locations. Based on the water quality status readings, fish farmers have vital information regarding the water quality conditions around their net cages. Therefore, it is recommended that fish farmers take action and understand the characteristics of the cultivated fish species, and be aware of the duration that the fish can tolerate changes in water quality. If the water

quality conditions continue to deteriorate, fish farmers can make an informed decision on relocating the floating net cages based on factors such as time, water conditions, and the specific species being cultivated. These efforts can minimize the potential losses resulting from river water pollution. Compared with previously published work, the FNCs concept proposed to be carried out horizontally on the river surface is simpler and more effective than the model proposed by (Kim et al., 2011; 2014; Thangavel et al., 2015), which moves vertically. Furthermore, applying the fuzzy logic method in this work uses three primary water quality parameter variables with data taken from direct measurements of river water compared to the previous work by (Oltean and Ivanciu, 2017), which only used one variable. Compared to the work of (Bokingito and Caparida, 2018), fuzzy logic was built for monitoring water quality assessment in real-time using three input variables, namely temperature, pH, and turbidity, with three membership functions each. In contrast, this work implemented fuzzy logic using three input variables: temperature, DO, and pH, with five membership functions each. Furthermore, compared with the work of (Molato, 2022), fuzzy logic was built using three water parameter variables as input with three membership functions each to produce a model to analyze the overall quality of water in tilapia cultivation, monitoring equipment in the form of an LCD and equipped with a database, while in this work fuzzy logic was built to make decisions for FNC transfer with a monitoring application that displays value data and graphics and is equipped with a database.

## **CONCLUSION**

An assessment of the water quality of the Musi River was conducted to classify the status of the floating net cage locations using a Python program. The three main parameters, water temperature, pH, and DO, were measured at 39 testing locations along the Musi River within a radius of 3400 m. All sensors responded to changes in the river water quality. The measured water quality of the Musi River fluctuated over a specific time duration. The program's decision at three testing locations (U1, D8, and U13) recommended moving the floating net cages. The average measured values for the water temperature of the Musi River were 29.20 °C, 3.98 mg/L for DO, and pH 6.42, except for these three locations where the pH values were below 6, which is below the predefined threshold. This condition correlates with the water quality alarm system, which triggers a blue LED indicator and a sounding buzzer at these three locations. Visually, there were no visible changes in the color of the river water at these three locations with poor water quality, which does not correlate with the device testing duration at each location. However, field observations revealed that all three locations were situated along the riverbanks, close to factories/tributaries (U1), and residential areas (D8, U13), which are vulnerable to waste discharge from human activities in the surrounding areas. In this research, the decision-making application for relocating the floating net cages in fish farming is user-friendly, effective in assessing water quality, and efficiently determines cage relocation decisions with accurate results. Applying the fuzzy method in this research provides certainty for fishermen in deciding to relocate the floating net cages. By referring to the program and considering other conditions, fishermen can promptly decide to move the floating net cages and avoid more significant losses. Another benefit is that the monitoring application is accessible through a personal computer or smartphone connected to the Internet. In the future, this work can inspire further research to develop an autonomous system for floating net cages whereby the cages can move automatically when the water quality around the location of the floating net cages deteriorates over a certain period.

## **AUTHOR CONTRIBUTIONS**

Z. Nawawi, the corresponding author, has contributed in supervising the first author in collecting research data, analyzing data and interpreting the results. B.Y. Suprpto prepared test data and images and interpreted the results. R. Pramana participated in the interpretation of the results and manuscript preparation.

## **ACKNOWLEDGEMENT**

The authors are grateful for the support received from the Raja Ali Haji Maritime University LPPM [Grant number: 4/UN53.02/Kontrak-PADD/2022] and the Sriwijaya University Faculty of Engineering team for their contributions to this study in preparing equipment and testing devices in the field.

## **CONFLICT OF INTEREST**

The authors declare that there is no conflict of interests regarding the publication of this manuscript. In addition, the ethical issues, including plagiarism, informed consent, misconduct, data fabrication and/or falsification, double publication and/or submission, and redundancy have been completely observed by the authors.

## **OPEN ACCESS**

©2024 The author(s). This article is licensed under a Creative Commons Attribution 4.0 International License, which permits use, sharing, adaptation, distribution and reproduction in any medium or format, as long as you give appropriate credit to the original author(s) and the source, provide a link to the Creative Commons license, and indicate if changes were made. The images or other third-party material in this article are included in the article's Creative Commons license, unless indicated otherwise in a credit line to the material. If material is not included in the article's Creative Commons license and your intended use is not permitted by statutory regulation or exceeds the permitted use, you will need to obtain permission directly from the copyright holder. To view a copy of this license, visit: <http://creativecommons.org/licenses/by/4.0/>

## **PUBLISHER'S NOTE**

GJESM Publisher remains neutral with regard to jurisdictional claims in published maps and institutional affiliations.

ABBREVIATIONS	DEFINITION
%	Percent
°C	Degree Celsius
Cm	Centimeter
DO	Dissolved oxygen
EC	Electrical conductivity
<i>Et al</i>	And others
<i>Fig</i>	Figure
<i>FNC</i>	Floating net cage
<i>FAO</i>	Food and agriculture organization
<i>Gaussmf</i>	Gaussian membership function
<i>Gauss2mf</i>	Gaussian combination membership function
<i>GSM</i>	Global system mobile
<i>IOT</i>	Internet of things
<i>LCD</i>	Liquid crystal display
<i>LED</i>	Light emitting diode
<i>LoRa</i>	Long range
<i>LPWAN</i>	Low power wide area networks
<i>m</i>	Meter
<i>m/s</i>	Meters per second
<i>MF</i>	Membership function
<i>mg/L</i>	Milligrams per liter
<i>NTU</i>	Nephelometric turbidity unit
<i>PC</i>	Personal computer
<i>pH</i>	Potential hydrogen
<i>ppm</i>	Parts per million
<i>SMS</i>	Short message service
<i>TDS</i>	Total dissolved solid
<i>Temp</i>	Temperature
<i>V</i>	Voltage
<i>VDC</i>	Volt direct current
<i>WSN</i>	Wireless sensor network

## REFERENCES

- Abd El-Hack, M.E.; El-Saadony, M.T.; Nader, M.M.; Salem, H.M.; El-Tahan, A.M.; Soliman, A.S.M.; Khafaga, A.F., (2022). Effect of environmental factors on growth performance of Nile tilapia (*Oreochromis niloticus*). *Int. J. Biometeorol.*, 66(11): 2183–2194 (12 pages).
- Abinaya, T.; Ishwarya, J.; Maheswari, M., (2019). A Novel Methodology for Monitoring and Controlling of Water Quality in Aquaculture using Internet of Things (IoT). 2019 International Conference on Computer Communication and Informatics. 1–4 (4 pages).
- Acar, U.; Frank, K.; Vlacheas, P.; Foteinos, V.; Demestichas, P.; Guven, Y.; Drigkopoulou, L.; Aycan, V., (2019). Designing An IoT cloud solution for aquaculture. *Global IoT Summit, GIoTTS 2019 - Proceedings* (5 pages).
- Bokingkito, P.B.; Caparida, L.T., (2018). Using fuzzy logic for real - Time water quality assessment monitoring system. *ACM International Conference Proceeding Series*. 21–25 (5 pages).
- Boyd, C.E.; Lichtkoppler, F., (1979). Water quality management in pond fish culture. *Int. Center Aquacult.*, 22(22): 1–30 (30 pages).
- Cardia, F.; Lovatelli, A., (2016). Aquaculture operations in floating HDPE cages. *FAO and Ministry of Agriculture of the Kingdom of Saudi Arabia. Rome*. (176 pages).
- Chen, J.H.; Sung, W.T.; and Lin, G.Y., (2016). Automated monitoring system for the fish farm aquaculture environment. *Proceedings - 2015 IEEE International Conference on Systems, Man, and Cybernetics, SMC*. 1161–1166 (6 pages).
- Danh, L.V.Q.; Dung, D.V.M.; Danh, T. H.; Ngon, N.C., (2020). Design and deployment of an IoT-Based water quality monitoring system for aquaculture in mekong delta. *Int. J. Mech. Eng. Rob. Res.*, 1170–1175 (6 pages).
- Ehzari, H.; Safari, M.; Samimi, M.; Shamsipur, M.; Gholivand, M.B., (2022). A highly sensitive electrochemical biosensor for chlorpyrifos pesticide detection using the adsorbent nanomatrix contain the human serum albumin and the Pd: CdTe quantum dots. *Microchem. J.*, 179: 107424 (10 pages).
- FAO, (2020). *The State of World Fisheries and Aquaculture 2020. Rome: Sustainability in action* (224 pages).
- Icaga, Y., (2007). Fuzzy evaluation of water quality classification. *Ecol. Indic.*, 7(3): 710–718 (9 pages).
- Jino Ramson, S.R.; Bhavanam, D.; Draksharam, S.; Kumar, A.; Jackuline Moni, D.; Alfred Kirubaraj, A., (2019). Sensor Networks based Water Quality Monitoring Systems for Intensive Fish Culture -A Review. *Proceedings of the 4th International Conference on Devices, Circuits and Systems, ICDCS 2018*, 54–57 (5 pages).
- Kim, T.; Yang, K.U.; Hwang, K.S.; Jang, D.J.; Hur, J.G., (2011). Automatic submerging and surfacing performance of model submersible fish cage system operated by air control. *Int. J. Aquac. Eng.*, 45(2): 74–86 (13 pages).

- Kim, T.; Hwang, K.S.; Oh, M.H.; Jang, D.J., (2014). Development of an autonomous submersible fish cage system. *IEEE J. Ocean. Eng.*, 39(4): 702–712 **(10 pages)**.
- Kyaw, T.Y.; Ng, A.K., (2017). Smart Aquaponics System for Urban Farming. *Energy Procedia*. 143: 342–347 **(6 pages)**.
- Lekang, O., (2020). *Aquaculture Engineering*. Third Edit, John Wiley and Sons Ltd. Third Edit. West Sussex, UK. **(415 pages)**.
- La Madrid, J.D.; Cruz, J.C.D.; Balisi, V.L.Q., (2019). Real-time water quality monitoring system with predictor for tilapia pond. *IEEE 10th International Conference on Humanoid, Nanotechnology, Information Technology, Communication and Control, Environment and Management, HNICEM*. 1–6 **(6 pages)**.
- Maulana, M.R.; Saiful, S.; Muchlisin, Z.A., (2023). Microplastics contamination in two peripheral fish species harvested from downstream river. *Global J. Environ. Sci Manage.*, 9(2): 299-308 **(10 pages)**.
- Maurya, P.K.; Malik, D.S.; Yadav, K.K.; Kumar, A.; Kumar, S.; Kamyab, H., (2019). Bioaccumulation and potential sources of heavy metal contamination in fish species in River Ganga basin: Possible human health risks evaluation. *Int. J. Toxicol. reports*. 6: 472-481 **(10 pages)**.
- Mendel, J.M., (1995). *Fuzzy-Logic Systems for Engineering: A Tutorial*. Proceedings of the IEEE. 83: 345–377 **(32 pages)**.
- Mendel, J.M., (2003). Uncertainty, type-2 fuzzy sets, and footprints of uncertainty. *Electr. Eng. [Preprint]*, 233-242 **(10 pages)**.
- Molato, M.R.D., (2022). AquaStat: An Arduino-based Water Quality Monitoring Device for Fish Kill Prevention in Tilapia Aquaculture using Fuzzy Logic. *Int. J. Adv. Comput. Sci. Appl.*, 13(2): 557–562 **(6 pages)**.
- Oltean, G.; Ivanciu, L.N., (2017). Implementation of a fuzzy logic-based embedded system for temperature control. *Proceedings of the International Spring Seminar on Electronics Technology*. 1–6 **(6 pages)**.
- Oyinlola, M.A., (2019). *Mariculture: Perception and prospects under climate change, Predicting Future Oceans: Sustainability of Ocean and Human Systems Amidst Global Environ. Change*. Elsevier Inc. **(13 pages)**.
- Pemerintah Republik Indonesia, (2021). *Peraturan Pemerintah Republik Indonesia Nomor 22 Tahun 2021 Tentang Penyelenggaraan Perlindungan dan Pengelolaan Lingkungan Hidup*. Sekretariat Negara Republik Indonesia, 1(078487A) **(483 pages)**.
- Prakoso, V.A.; Chang, Y.J., (2018). Effects of Hypoxia on Oxygen Consumption of Tilapia Fingerlings (*Oreochromis niloticus*). *Oseanologi dan Limnologi di Indonesia*, 3(2): 165-171 **(7 pages)**.
- Sabilillah, A.M.; Palupi, F.R.; Adji, B.K.; Nugroho, A.P., (2023). Health risk assessment and microplastic pollution in streams through accumulation and interaction of heavy metals. *Global J. Environ. Sci. Manage.*, 9(4): 719-740 **(22 pages)**.
- Samimi, M.; Shahriari-Moghadam, M., (2021). Isolation and identification of *Delftia lacustris* Strain-MS3 as a novel and efficient adsorbent for lead biosorption: Kinetics and thermodynamic studies, optimization of operating variables. *Biochem. Eng. J.*, 173: 108091 **(9 pages)**.
- Shareef, Z.; Reddy, S.R.N., (2019). Design and wireless sensor network analysis of water quality monitoring system for aquaculture. *Proceedings of the 3rd International Conference on Computing Methodologies and Communication, ICCMC*. 405–408 **(4 pages)**.
- Shourije, S.M.J.S.; Dehghan, P.; Bahrololoom, M.E.; Cobley, A.J.; Vitry, V.; Azar, G.T.P.; Kamyab, H.; Mesbah, M., (2023). Using fish scales as a new biosorbent for adsorption of nickel and copper ions from wastewater and investigating the effects of electric and magnetic fields on the adsorption process. *Chemosphere*. 317: 137829 **(6 pages)**.
- Sulistyowati, L.; Yolanda, Y.; Andareswari, N., (2023). Harbor water pollution by heavy metal concentrations in sediments. *Global J. Environ. Sci. Manage.*, 9(4): 885-898 **(14 pages)**.
- Sung, W.T.; Chen, J. H.; Huang, D. C.; Ju, Y. H., (2014). Multisensors real-time data fusion optimization for IOT systems. *Conference Proceedings – 2014 IEEE International Conference on Systems, Man and Cybernetics*. 2299–2304 **(6 pages)**.
- Takarina, N.D.; Chuan, O.M.; Pin, T.G.; Femnisy, I.; Fathinah, A.; Ramadhan, A.N.B.; Hermawan, R.; Adiwibowo, A., (2023). Land use variation impacts on trace elements in the tissues and health risks of a commercial fish. *Global J. Environ. Sci. Manage.*, 9(3): 445-462 **(18 pages)**.
- Thangeval, C.; Muthukumaravel, S.; Gowthaman, V.; Sudhakar, T.; Atmanand, M.A., (2015). Mechanical system design of automatic sub-surface floating fish cage. *2015 IEEE Underw. Technol.*, 1-2 **(2 pages)**.
- Torres-Bejarano, F.; Verbel-Escobar, M.; Atencia-Osorio, M.C., (2022). Water quality model-based methodology to assess assimilative capacity of wastewater discharges in rivers. *Global J. Environ. Sci. Manage.*, 8(4): 449-472 **(24 pages)**.
- Vishwakarma, V.; Gurav, A.; Patel, H.; Sahasrabudhe, S., (2018). *Acqua culture monitoring system*. 2018 International Conference on Smart City and Emerging Technology. 1–4 **(4 pages)**.
- Volkoff, H.; Rønnestad, I., (2020). Effects of temperature on feeding and digestive processes in fish. *Temperature*. 7(4): 307–320 **(13 pages)**.
- Wei, T.Y.; Tindik, E. S.; Fui, C. F.; Haviluddin, Hijazi, M. H. A., (2023). Automated water quality monitoring and regression-based forecasting system for aquaculture. *Bull. Electr. Eng. Inf.* 12(1): 570–579 **(10 pages)**.

#### AUTHOR (S) BIOSKETCHES

**Pramana, R.**, ST., MT, Doctoral Student, <sup>1</sup>Department of Engineering Science, Faculty of Engineering Universitas Sriwijaya, Palembang 30128, Indonesia

Assist Professor, Department of Electrical Engineering, Faculty of Engineering Universitas Maritim Raja Ali Haji, Tanjungpinang 29111, Indonesia.

- Email: [rozeff@umrah.ac.id](mailto:rozeff@umrah.ac.id)
- ORCID: [0000-0002-8472-5126](https://orcid.org/0000-0002-8472-5126)
- Web of Science ResearcherID: ABL-0379-2022
- Scopus Author ID: 57226093602
- Homepage: <https://ft.umrah.ac.id/>

**Suprpto, B.Y.**, Dr., Associate Professor, Department of Engineering Science, Faculty of Engineering Universitas Sriwijaya, Palembang 30128, Indonesia.

- Email: [bhakti@ft.unsri.ac.id](mailto:bhakti@ft.unsri.ac.id)
- ORCID: [0000-0002-3995-6347](https://orcid.org/0000-0002-3995-6347)
- Web of Science ResearcherID: AAC-9591-2020
- Scopus Author ID: 57192161634
- Homepage: <https://ft.unsri.ac.id/>

**Nawawi, Z.**, Ph.D., Professor, Department of Engineering Science, Faculty of Engineering Universitas Sriwijaya, Palembang 30128, Indonesia.

- Email: [nawawi\\_z@unsri.ac.id](mailto:nawawi_z@unsri.ac.id)
- ORCID: [0000-0003-4386-9155](https://orcid.org/0000-0003-4386-9155)
- Web of Science ResearcherID: GMW-9162-2022
- Scopus Author ID: 6506923289
- Homepage: <https://ft.unsri.ac.id/>

#### HOW TO CITE THIS ARTICLE

Pramana, R.; Suprpto, B.Y.; Nawawi, Z., (2024). Application of fuzzy logic in decision-making process for relocation of floating net cages in river fish farming. *Global J. Environ. Sci. Manage.*, 10(1): 117-132.

DOI: [10.22034/gjesm.2024.01.09](https://doi.org/10.22034/gjesm.2024.01.09)

URL: [https://www.gjesm.net/article\\_706685.html](https://www.gjesm.net/article_706685.html)





## ORIGINAL RESEARCH PAPER

## Factors affecting cadmium toxicity to rice germinated in soils collected from downstream areas of abandoned zinc mines

P. Chanpiwat<sup>1,2</sup>, A. Numprasanthai<sup>2,3,\*</sup><sup>1</sup> Environmental Research Institute, Chulalongkorn University, Phayathai Road, Pathumwan, Bangkok 10330, Thailand<sup>2</sup> Center of Excellence in Environmental Innovation and Management of Metals, Chulalongkorn University, Phayathai Road, Pathumwan, Bangkok 10330, Thailand<sup>3</sup> Department of Mining and Petroleum Engineering, Faculty of Engineering, Chulalongkorn University, Phayathai Road, Pathumwan, Bangkok 10330, Thailand

## ARTICLE INFO

## Article History:

Received 24 March 2023

Revised 01 July 2023

Accepted 11 August 2023

## Keywords:

Fractionation

Mae Tao

Mobility

Phytotoxicity

Plant availability

Seed germination

Thailand

## ABSTRACT

**BACKGROUND AND OBJECTIVES:** Cadmium contamination in rice grains with a maximum concentration 19 times the national food standard at sites downstream of zinc mines in Thailand has been reported since 2005. These cultivated rice grains are consumed by local residents and have increased the risk of renal dysfunction in residents. Decreasing negative health effects by reducing cadmium accumulation in rice should be considered. Since the soil characteristics affecting the toxicity and accumulation of cadmium in rice cultivated in cadmium-contaminated soils have never been reported, this study was conducted to investigate the soil characteristics affecting the plant availability and mobility of cadmium in paddy soils and the impacts of these soil characteristics on rice seed germination and accumulation in rice.

**METHODS:** The study area is the Mae Tao Subdistrict, Mae Sot District, Tak Province, located downstream of abandoned zinc mines in northwestern Thailand. A total of 36 paddy fields that were reported to produce rice grain with cadmium contents exceeding the national standard for cadmium in rice (0.4 milligrams per kilogram) were randomly selected for composite soil sample collection. The physicochemical characteristics of the soils, including soil texture, redox potential, cation exchange capacity, potential of hydrogen, organic matter, total cadmium concentration, and chemical speciation and concentration of plant-available cadmium, were analyzed. The toxicity of cadmium to rice and the cadmium accumulation ability in rice were assessed through the germination of Khao Dok Mali 105, a popular rice variety for cultivation and consumption in the study area.

**FINDINGS:** Total cadmium concentrations of 0.20 to 89.87 milligrams/kilogram were found in the soils, with 64 percent of all samples containing values greater than the national background value in agricultural soils. Up to 74.2 percent and 99.5 percent of total cadmium was found in the forms of mobile- and plant-available cadmium, respectively. Plant-available cadmium caused significant reductions in the number of seeds germinated and root length. Cadmium toxicity to rice was positively affected by the concentrations of exchangeable, plant-available and total cadmium. The concentrations of plant-available, exchangeable, carbonate-bound, and total cadmium strongly affected the accumulation of cadmium in germinated roots. Cluster analysis showed that plant-available cadmium was the main factor responsible for high cadmium accumulation in rice.

**CONCLUSION:** Based on the overall analyses of soil characteristics affecting the mobility and plant availability of cadmium in soils and its toxicity and accumulation in germinated rice, the immobilization of plant-available cadmium in soils by adding organic matter-rich amendments to soils is recommended. In addition, oxidizing soil conditions should be maintained during rice cultivation to reduce the phytoavailability of Cd in soils.

DOI: [10.22034/gjesm.2024.01.10](https://doi.org/10.22034/gjesm.2024.01.10)This is an open access article under the CC BY license (<http://creativecommons.org/licenses/by/4.0/>).

NUMBER OF REFERENCES

59



NUMBER OF FIGURES

6



NUMBER OF TABLES

6

\*Corresponding Author:

Email: [Apisit.Nu@chula.ac.th](mailto:Apisit.Nu@chula.ac.th)

Phone: +66 2218 8114

ORCID: [0000-0001-6432-0650](https://orcid.org/0000-0001-6432-0650)

Note: Discussion period for this manuscript open until April 1, 2024 on GJESM website at the "Show Article".

## INTRODUCTION

Cadmium (Cd) is principally considered a naturally occurring metal in most environmental samples, including igneous rocks, soils, sediments, freshwater, seawater and crops. Cd is ranked as the 64<sup>th</sup> most abundant element in the Earth's crust, with an average concentration of 0.15 to 0.20 milligrams per kilogram (mg/kg) (Adriano, 2001; Nurhasanah *et al.*, 2023). Although Cd is used in various manufacturing industries, such as the automotive, pigment, coating and plating, plastics (Sabilillah *et al.*, 2023), and battery industries, its usage has drastically decreased since the first discovery of Itai-itai disease in Japan, in which an epidemiological study showed a positive correlation between the disease prevalence rate and the levels of Cd contamination in paddy soils (KMU, 2023; WHO, 2019; Adriano, 2001). In general, the main source of Cd contamination in the environment is anthropogenic activities, including industrial production processes (e.g., mining and smelting of ferrous and nonferrous metals, cement production, application of Cd-containing fertilizer and municipal sewage sludge, disposal and recycling of electronic waste and municipal waste incineration) (WHO, 2019; Nordberg *et al.*, 2018). Of all environmental media, soil is expected to be the major sink of Cd (Adriano, 2001). Once released into the soil, Cd can be absorbed and accumulate in plants at toxic levels, affecting their growth and eventually causing detrimental health effects to humans via the ingestion of contaminated edible plants. In principle, Cd uptake by plants is generally controlled by various soil characteristics as well as plant species. Plant uptake of Cd normally decreases as the soil potential of hydrogen (pH), cation exchange capacity (CEC), oxidation–reduction potential (ORP), and organic matter (OM) increase. On the other hand, a greater amount of Cd uptake by plants is observed in response to higher total and available concentrations of Cd in soil. After uptake, Cd is translocated and accumulates in several plant parts. Since Cd is a nonessential plant nutrient, its accumulation in plants can cause phytotoxic effects, including general growth reduction, leaf curling, chlorosis, necrosis, leaf yellowing, and lowered productivity and yield (Khanna *et al.*, 2022; Haider *et al.*, 2021; Zhao and Wang, 2020). The phytotoxicity of Cd mainly depends on Cd concentration and bioavailability, exposure time, plant species, and plant stage (Khanna *et al.*,

2022; McLaughlin *et al.*, 2021; Samimi, 2024). Rice can accumulate higher amounts of Cd than other staple food crops (Zhao and Wang, 2020). In addition, as Cd is highly soluble in soil, which enhances its transfer to the food chain, its accumulation in grains to levels that can cause potential human health impacts has been reported worldwide (Hussain *et al.*, 2021; Zhao and Wang, 2020). Therefore, reducing Cd bioavailability, uptake, and translocation to grains is expected to be a principal strategy to lower Cd accumulation in grains to a safe level for consumption as well as to protect public health. Since 2005, studies have reported Cd contamination in rice grains in Thailand, especially in the areas downstream of the country's most abundant zinc (Zn) deposit areas in Tak Province, as a result of high Cd background concentrations in the soil and the irrigation of rice using Cd-contaminated water (Srisawat *et al.*, 2021; Chanpiwat *et al.*, 2019; Simmons *et al.*, 2005). The highest Cd concentrations determined in agricultural soils and rice grains were 300.9 mg/kg and 7.7 mg/kg, respectively (Chanpiwat *et al.*, 2019; Simmons *et al.*, 2005). Due to the extremely high levels of Cd contamination in agricultural soils and in rice grains, which are consumed by local residents, extensive research, particularly monitoring studies of Cd contamination in environmental media and human health impact assessments of Cd exposure through rice consumption, has been conducted in the area (Srisawat *et al.*, 2021; Sriprachote *et al.*, 2020, 2012; Suwatvitayakorn *et al.*, 2020; Chanpiwat *et al.*, 2019; Somprasong, 2019; Kosolsaksakul *et al.*, 2018, 2014; Nishijo *et al.*, 2014; Simmons *et al.*, 2005). Briefly, total Cd concentrations in agricultural soils and rice grains exceeding the background concentration in agricultural soil (1.7 mg/kg) and the standard for Cd in polished rice (0.4 mg/kg) have been reported. In addition, more than 40% of local residents were found to have increased risks of renal dysfunction due to Cd-contaminated rice consumption (Nishijo *et al.*, 2014). As a consequence, reduced rice cultivation and a shift toward nonfood crop production, especially sugarcane, have been proposed to local farmers. However, these approaches were not successfully adopted in the long term due to the lower market price of sugarcane than rice. In addition, local residents mainly rely on their home-grown rice for daily consumption (BOD, 2012). Thus, rice production is still the main crop produced in the

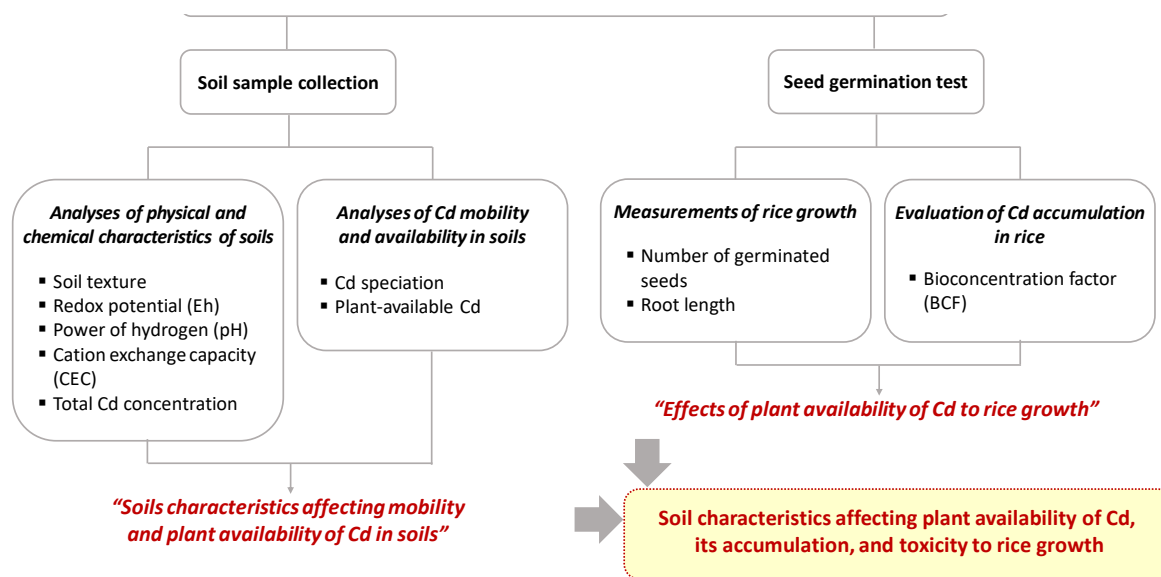


Fig. 1: The research framework of the current study

area. Although several studies, as mentioned earlier, have been conducted in the area, studies on the soil characteristics affecting the plant availability of Cd in paddy soils and the effects of plant-available Cd on rice growth have never been conducted. It was hypothesized that i) soil pH, redox potential (Eh), CEC, and OM would be the soil factors controlling the mobility and availability of Cd in soils, and ii) the higher the total and mobile Cd concentrations in the soil were, the higher the plant-available Cd concentrations and their negative effects on rice growth would be. The results obtained from this study are expected to lead to appropriate mitigation strategies for local farmers and people in other Cd-contaminated areas to reduce the phytotoxicity and accumulation of Cd in rice cultivated in soils with elevated Cd concentrations. Therefore, the aims of the current study are to i) investigate the physical and chemical characteristics of Cd-contaminated paddy soils, ii) determine the soil characteristics affecting the plant availability of Cd in soil, and iii) investigate the effects of plant-available Cd in soil on rice growth. This study was carried out in the Mae Tao Subdistrict, Mae Sot District, Tak Province, and at Chulalongkorn University in 2021. A schematic diagram showing the scope of the study is shown in Fig. 1.

## MATERIALS AND METHODS

### Information on the study area

The study area is the Mae Tao Subdistrict, Mae Sot District, Tak Province, located in northwestern Thailand (Fig. 2). Since this area is rich in primary and secondary Zn deposits, Zn mines yielding 110,000 metric tons/year were operated in the area until 2017 (Chanpiwat *et al.*, 2019; Sriprachote *et al.*, 2012). Following the first report by the International Water Management Institute (IWMI) on Cd contamination in agricultural soils and rice grains in 2005, the Department of Primary Industries and Mines (DPIM) conducted a comprehensive survey on Cd contamination in the area. Particular attention was given to the agricultural areas along Mae Tao Creek, a main source of irrigation water. Since Mae Tao Creek flows through the mine areas, elevated sediment Cd concentrations of up to 7.86 mg/kg have been found (Weeraprapan *et al.*, 2015). In addition, the runoff carrying Cd-laden sediment from the mine areas to the creek during rainfall was reported to increase the contamination level in the creek (Somprasong, 2019). As a result, elevated soil Cd concentrations greater than the background Cd concentration in agricultural soils of 1.7 mg/kg were found. According to a survey conducted by the DPIM, agricultural soils in the area

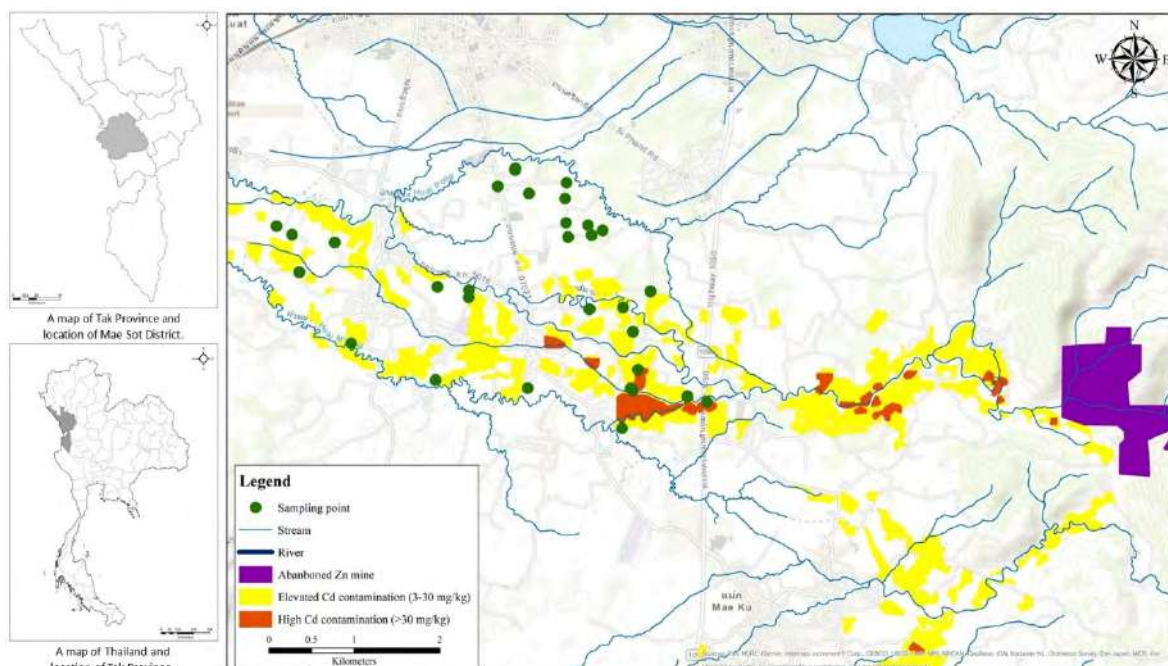


Fig. 2: Geographic location of the study area in the Mae Tao Subdistrict in Thailand, background Cd concentrations in agricultural soils and sampling locations

were categorized into areas with elevated (3 to 30 mg/kg) and high (>30 mg/kg) total Cd contamination (Chanpiwat *et al.*, 2019), as shown in Fig. 2. Rice cultivation is the most popular agricultural practice in the wet season. Cultivation of other crops, such as corn, soybean, and Chinese parsley, is normally adopted in the dry season. The survey also reported a total of 58 paddy fields producing rice grains with total Cd concentrations exceeding the national and Codex standards for total Cd in polished rice of 0.4 mg/kg (Chanpiwat *et al.*, 2019).

#### Sample collection

Considering the number of paddy fields (58 sites) that produced rice grains containing total Cd concentrations higher than the food standard (0.4 mg/kg) (Chanpiwat *et al.*, 2019), a total of 36 paddy fields were randomly selected as the sampling sites (Fig. 2) with a 90% confidence level that these areas could represent all paddy fields that produced Cd-contaminated rice grains. A composite soil sampling technique was applied in this study. At each sampling site, surface soil samples within a 15 centimeter (cm) depth were randomly collected from 5 sampling

points using a shovel. An area of 10'10 square centimeters (cm<sup>2</sup>) was marked as a subsampling point. Thus, approximately 2 kg of composite soil sample was thoroughly mixed and collected in a clean plastic bag before delivery to the laboratory.

#### Soil preparation and analyses

Samples were air-dried and turned over for 3 days in a laboratory. Afterward, the samples were dried in a hot air oven (105 degrees Celsius (°C)) for 16 hours to completely remove soil moisture. Afterward, the samples were ground using an agate mortar and a pestle before sieving to obtain 2-millimeter (mm) soil particles. Finally, the homogenized samples were placed in a clean plastic bag and stored in a desiccator until further analysis.

#### Analyses of physical and chemical characteristics of paddy soils

The physicochemical characteristics of the soil samples, including soil texture, Eh, CEC, pH, OM, total Cd concentration, chemical speciation and plant-available Cd concentration, were analyzed following the methods summarized in Table 1. According to

Table 1: Methods of soil sample analyses

Soil characteristic	Soil sample amount used for analysis (g)	Method of analysis	Reference
Soil texture (sand, silt, and clay)	5	Bouyoucos hydrometer method	DOA, 2010
Eh	10	Mixing with deionized water (1:2 weight per weight (w:w)) and Eh measurement using a glass electrode (ORP meter)	LDD, 2010
CEC	5	Ammonium saturation method	DOA, 2010
pH	10	Mixing with deionized water (1:2.5 w:w) and pH measurement using a glass electrode (pH meter)	LDD, 2010
OM	1	Walkley Black modified acid-dichromate digestion	DOA, 2010
Total Cd	0.5	Aqua regia	Chanpiwat <i>et al.</i> , 2010
Cd speciation	0.5	Tessier sequential extraction	Tessier <i>et al.</i> , 1979; Chanpiwat <i>et al.</i> , 2010
Plant-available Cd	10	Diethylenetriaminepentaacetic acid (DTPA) soil extraction	Lindsay and Norvell, 1978

the different extraction methods, three different categories of Cd, as shown in Table 1, were categorized in this study. Each category of Cd indicates different aspect of Cd contamination in soils. Total Cd was used to indicate gross contamination. The chemical speciation of Cd was used to indicate the mobility of Cd under different environmental conditions. Finally, plant-available Cd was used to indicate the concentration of Cd in soil that is readily taken up through the roots of plants. The concentrations of Cd were quantitatively analyzed by inductively coupled plasma–optical emission spectrometry (ICP–OES, Plasma Quant 9000 Elite, Analytik Jena). The limit of quantitation was 5 micrograms per liter ( $\mu\text{g/L}$ ). The accuracies of soil sample digestion for total Cd determination and ICP–OES analysis were validated with standard reference material (SRM) 1944 (New York/New Jersey waterway sediment) and SRM 1643e (trace elements in water) from the National Institute of Standards and Technology (NIST). The results of digestion method validation (86.3%) and quality assurance and quality control of the ICP–OES analysis (95.0%) were within  $\pm 15\%$  of the certified values. All tests were carried out in triplicate. All glassware and plasticware used for the experiments were previously rinsed with 10% volume per volume (v/v) nitric acid ( $\text{HNO}_3$ ) and deionized water prior to use. Analytical-grade chemicals were used in all experiments.

#### Seed germination test

The seed germination test is a simple toxicity

assessment that is initially used to indicate the potential toxic effects of metals on both plants and humans (Pokorska-Niewiada *et al.*, 2018; Bae *et al.*, 2014). The toxicity of plant-available Cd extracted from the soil samples (Table 1) to the germination of Khao Dok Mali 105 (KDML 105) rice, a popular rice variety for cultivation and consumption in the study area, was assessed in this study. Prior to the test, seed disinfection (Tornuk *et al.*, 2011), comprising soaking in 400 parts per million (ppm) sodium hypochlorite ( $\text{NaOCl}$ ) for 30 minutes and rinsing with deionized water to remove the residual disinfectant, was performed. The germination test was conducted according to Pokorska-Niewiada *et al.* (2018); Bae *et al.* (2014) and Walter *et al.* (2006) with some modifications for 96 hours. In brief, 5 milliliter (mL) of plant-available Cd solution that was extracted from each soil sample was poured into a plastic petri dish (10 cm in diameter and 1.5 cm in depth) containing No. 1 Whatman filter paper. Afterward, 15 disinfected grains were uniformly placed onto the filter paper without touching each other. The dish was then incubated at  $25^\circ\text{C}$  in the dark for 96 hours. In addition, deionized water was used as a control in the germination test. Germination tests of each soil sample were conducted with five replicates. After 96 hours of incubation, the number of seeds with visible breakage of the seed coat was counted as the germinated seeds, and the root length was measured as the key parameter of rice growth. Finally, the percentage of relative seed germination (%RSG),

percentage of relative root growth (%RRG), and germination index (%GI) were calculated using Eqs. 1 to 3 (Walter *et al.*, 2006).

$$\%RSG = \frac{\text{Number of seeds germinated in test group}}{\text{Number of seeds germinated in control group}} \times 100 \quad (1)$$

$$\%RRG = \frac{\text{Mean root length of test group}}{\text{Mean root length of control group}} \times 100 \quad (2)$$

$$\%GI = \frac{RSG \times RRG}{100} \quad (3)$$

#### *Assessment of the bioconcentration of Cd in germinated rice*

After the completion of the seed germination test, all germinated seeds from each test were collected and washed with deionized water three times. Afterward, the germinated seeds were dried in a hot air oven at 80°C for 4 hours before grinding with an agate mortar and pestle. Then, the samples were sieved through a 425 micrometer ( $\mu\text{m}$ ) sieve and dried at 80°C until a constant weight was obtained. A mixture (3:1 v/v) of concentrated, extra-pure nitric acid (67-69%  $\text{HNO}_3$ , Val de Reuil, France) and hydrogen peroxide ( $\text{H}_2\text{O}_2$ ) (35% Chem-supply, Australia) was added to a clean plastic tube containing approximately 0.5 grams (g) dry weight of germinated seeds and predigested overnight before digestion at 80°C in a dry heating block for 2 hours. Finally, the extracted solution was adjusted to 25 mL with deionized water, filtered through a 0.45- $\mu\text{m}$  filtration unit into a new plastic tube and kept at 4°C for total Cd determination by inductively coupled plasma-mass spectrometry (ICP-MS, Agilent 7500c). The limit of quantitation was 1  $\mu\text{g/L}$ . The accuracies of the germinated seed digestion and ICP-MS analyses were validated with NIST SRM 1568a (rice flour) and NIST SRM 1643e (trace elements in water). The results of digestion method validation (92.3%) and quality assurance and quality control of the ICP-MS analysis (88.2%) were within  $\pm 15\%$  of the certified values. Rice sample digestion was carried out in triplicate. Finally, the bioconcentration factor (BCF), as shown in Eq. 4 (Islam *et al.*, 2020; Wang *et al.*, 2020), was calculated to assess the capability of rice plants to adsorb and accumulate Cd. The higher the BCF value is, the greater the capacity of rice to accumulate Cd. According to Wang *et al.* (2020), plants showing BCFs larger than 1 can be considered hyperaccumulator plants for that particular soil pollutant.

$$BCF = \frac{\text{Total Cd concentration in germinated rice root}}{\text{Plant - available Cd concentration in soil}} \quad (4)$$

#### *Data analysis*

All descriptive and inferential statistical analyses in this study were performed using the Statistical Package for Social Science (SPSS) (version 23). The normality of the data distribution was analyzed by the Shapiro-Wilk test ( $n < 50$ ) before conducting further analyses. As the data were not normally distributed, significant differences in all soil characteristics, the concentrations of all Cd species, the concentrations of Cd in germinated roots, and all phytotoxicity indices (%RSG, %RRG, and %GI) among different soil types were analyzed by the Mann-Whitney U test and Kruskal-Wallis H test. Spearman correlations were performed to determine the soil characteristics affecting the plant availability of Cd in soils and the toxic effects of plant-available Cd on the early stage of rice growth. Cluster analysis was used to group soil samples based on their major common characteristics causing different levels of Cd accumulation in the germinated rice roots. A  $p$  value of 0.05 was used to determine significance.

## **RESULTS AND DISCUSSION**

### *Physicochemical characteristics of paddy soils*

The basic physicochemical characteristics of the soils ( $n=36$ ) are summarized in Table 2. According to their different percentages of sand, silt and clay particles, the soil samples can be categorized into 5 types, including sandy loam, loam, clay loam, silty clay and clay. Approximately 42% and 39% of all samples were loam and clay loam, respectively. Regarding the classification of soil pH (LDD, 2010), one sample was very acidic (pH of 5.1). The remaining samples had pH values ranging from 6.1 (slightly acidic) to 7.8 (slightly basic), with 75% of the samples having a neutral pH (6.6 to 7.3). Based on a review of field-scale soil Eh values (Husson, 2013), all samples were moderately reduced soils with Eh values between +100 and +400 millivolt (mV). According to the DOA (2010), various classifications of soil CEC and OM were found in this study. Approximately 19%, 56%, and 25% of all samples had low (3 to 10 centimole per kilogram (cmol/kg)), moderate (10 to 15 cmol/kg), and high CEC values (>15 cmol/kg), respectively. The OM concentrations in the soils ranged from very low (0.5% to 1.0%) to high (3% to 5%). Most of the soils (67% of all samples) had low OM contents (1%

: Physicochemical characteristics of paddy soils

Statistical value	Sand (%)	Silt (%)	Clay (%)	Eh (mV)	pH	CEC (cmol/kg)	OM (%)	Total Cd (mg/kg)
Sandy loam (n=2)								
Minimum	53.4	38.0	8.6	276.2	6.2	3.3	0.7	0.20
Maximum	58.4	25.0	16.6	278.8	6.5	8.4	1.4	3.95
Mean	55.9	31.5	12.6	277.5	6.3	5.9	1.0	2.08
Median	55.9	31.5	12.6	277.5	6.3	5.9	1.0	2.08
SE	2.5	6.5	4.0	1.3	0.1	2.6	0.3	1.88
Loam (n=15)								
Minimum	30.2	28.2	14.6	172.4	6.1	6.3	1.1	0.40
Maximum	51.2	46.0	26.6	262.1	7.3	12.6	1.9	27.53
Mean	40.8	36.0	23.1	224.1	6.8	10.4	1.5	5.82
Median	40.2	34.2	24.6	231.6	6.9	10.5	1.5	2.34
SE	1.4	1.3	0.9	6.9	0.1	0.4	0.1	1.96
Clay loam (n=14)								
Minimum	25.2	28.0	28.6	171.4	5.1	10.1	1.6	0.99
Maximum	41.4	40.2	37.6	278.0	7.8	17.2	2.8	33.56
Mean	33.4	33.7	32.9	222.9	6.8	14.5	2.1	8.92
Median	33.3	32.6	34.1	214.5	6.8	14.9	2.0	6.25
SE	1.3	1.1	0.8	11.5	0.2	0.5	0.1	2.68
Silty clay (n=2)								
Minimum	19.4	40.0	40.6	208.0	6.5	17.6	3.2	2.00
Maximum	19.4	40.0	40.6	258.0	7.2	21.4	3.4	89.87
Mean	19.4	40.0	40.6	233.3	6.9	19.5	3.3	45.93
Median	19.4	40.0	40.6	233.3	6.9	19.5	3.3	45.93
SE	0.0	0.0	0.0	25.0	0.4	1.9	0.1	43.94
Clay (n=3)								
Minimum	18.2	35.0	40.6	223.7	7.0	12.8	1.6	0.40
Maximum	24.4	36.2	45.6	257.1	7.2	21.4	2.3	10.72
Mean	22.0	35.7	42.3	238.6	7.1	16.8	1.9	5.38
Median	23.4	36.0	40.6	235.1	7.1	16.2	1.8	5.01
SE	1.9	0.4	1.7	9.8	0.1	2.5	0.2	2.99
All samples (n=36)								
Minimum	18.2	25.0	8.6	171.4	5.1	3.3	0.7	0.20
Maximum	58.4	46.0	45.6	278.8	7.8	21.4	3.4	89.87
Mean	36.0	35.1	28.9	228.3	6.8	12.8	1.8	9.01
Median	37.2	34.6	28.6	232.4	6.8	12.6	1.8	3.98
SE	1.6	0.8	1.4	5.7	0.1	0.6	0.1	2.68

to 2%). There were significant differences in CEC and OM concentrations in different soil types ( $p < 0.05$ ), in which higher values of both characteristics were found in the silty clay soil than in the remaining soil types. The highest CEC (21.4 cmol/kg) and OM (3.4%) were observed in the silty clay soil (Table 2). On the other hand, compared to the other soil types, significantly lower CEC (3.3 cmol/kg) and OM (0.7%) values were determined in the sandy loam soil. This is because sand particles do not have any electrical charge on their surface; as a result, the higher the percentage of sand particles in the soil is, the lower the CEC value and the lower the capability of the soil to hold and exchange cations on its surface. When comparing the overall physical and chemical characteristics of

all collected soils to the suitable soil characteristics for rice production in Thailand as recommended by the Ministry of Agriculture and Cooperative (LDD, 2019), in which loamy or clayey soils with pH values ranging from slightly acidic to slightly basic as well as OM contents ranging from low to high are considered appropriate for rice production, it was found that two soil samples should not be used as a medium to grow rice, as one soil sample (G24) had a very low OM content (0.7%) and another sample (G34) was very acidic (pH=5.1), which are not appropriate conditions for rice growth. Therefore, soil improvement should be adopted to increase the OM content as well as the pH level of both soils before they can be used as a medium to sustain rice production.

*Total Cd concentrations in paddy soils*

A wide variation in total Cd concentrations (0.20 to 89.87 mg/kg; n=36) in soil samples was observed, as summarized in Table 2. Compared to the national soil quality standard for commercial and agricultural activities to protect against chronic exposure to contaminants (PCD, 2021), in which Cd is limited to not more than 762 mg/kg, all samples had lower total Cd concentrations. However, when comparing the total Cd concentrations in all samples to the national background Cd concentration in agricultural soils (1.7 mg/kg; n=3,186) according to a survey conducted by the LDD (Chanpiwat *et al.*, 2019), approximately 64% of the samples (23 out of 36 samples) contained total Cd concentrations 1.2 to 52.9 times greater than the background value. Although a significant difference in mean total Cd concentration among soil types was not observed ( $p>0.05$ ), the silty clay soils contained approximately 5.1 to 22.1 times the total Cd concentration of the other soil types and exhibited the greatest total Cd concentration in this study (89.87 mg/kg). The highest total Cd concentration was determined in the soils collected from the uppermost stream sampling site, located the closest to the abandoned Zn mines. It is also interesting that 91% of all soils (21 out of 23 samples) containing total Cd concentrations higher than the background Cd concentration were collected from paddy fields that received water for rice cultivation from Mae Tao Creek. When comparing the total Cd concentrations in soils in this study to the total Cd concentrations in agricultural soils collected from areas downstream of the same Zn mines within the past decade (2014 to 2023), as reported by Taepayoon *et al.* (2023); Srisawat *et al.* (2021); Sriprachote *et al.* (2020); Waleeittikul *et al.* (2019); Kosolsaksakul *et al.* (2018, 2014), similar magnitudes were found in previous studies (<0.04 to 106.43 mg/kg) and this study (0.20 to 89.87 mg/kg). In particular, the highest soil total Cd concentrations in this study and in studies by Kosolsaksakul *et al.* (2018, 2014) were found in paddy fields in the upstream section of Mae Tao Creek. However, the sampling site with the highest total soil Cd concentration (106.43 mg/kg) reported by Srisawat *et al.* (2021) was not assessed in the current study.

*Chemical species of Cd in paddy soils*

Since the total concentration can be used to indicate

gross contamination without consideration of the potential effects of different forms of the element bound to soil particles, sequential extraction is normally applied to soils to determine the concentration of the chemical form that may be released into the surroundings once the environmental conditions change (Tessier *et al.*, 1979). Five chemical fractions of Cd, including exchangeable (F1), carbonate-bound (F2), Fe- and Mn-bound (F3), organic-bound (F4) and residual Cd (F5), are the chemical fractions of interest in this study. The percentage distributions of each Cd species in the soils are depicted in Fig. 3. As clearly shown in Fig. 3, significant differences in the distributions of each Cd fraction in different soil types were not observed ( $p>0.05$ ). On average, the order of the percentage distribution was F1 (38.6%) > F5 (20.6%)  $\approx$  F2 (20.0%) > F3 (13.7%) > F4 (7.6%). The paddy soil with the highest concentration of total Cd (89.87 mg/kg) contained the highest concentrations of all Cd fractions except for F5. In contrast, the lowest concentrations of all Cd fractions were determined in the soil sample with the lowest concentration of total Cd. Regarding the environmental conditions that could leach Cd from solid particles, F1 and F2 are generally considered mobile fractions since they can be released from particles when there is a change in the ionic composition and pH of water, respectively (Tessier *et al.*, 1979). The percentage of mobile Cd (F1+F2) in this study ranged from 28.1% to 74.2% (mean $\pm$ SE: 58.6%  $\pm$  1.8%). However, Fe- and Mn-bound Cd (F3), which is normally unstable under anoxic conditions, accounted for 3.1% to 37.1% (mean $\pm$ SE: 13.7%  $\pm$  1.1%). This fraction of Cd is moderately mobile. Moreover, the less mobile fractions had contents of approximately 7.6%  $\pm$  1.1% (F4) and 20.6%  $\pm$  2.4% (F5). The major distribution of mobile Cd in the soils in this study agrees well with the fact that Cd is one of the most mobile elements in the environment. At environmental pH values of 5.1 to 7.8 and Eh values of 171 to 279 mV, which were found in the soils in this study, the majority of Cd is soluble Cd<sup>2+</sup>, according to the pH-Eh diagram of Cd species (Adriano, 2001). Moreover, Kubier *et al.* (2019) found that Cd is the only metal showing an affinity for being easily solubilized and released in the form of the water-soluble, exchangeable, and acid-soluble fractions, which are considered bioavailable Cd. The results obtained in this study were in accordance with the percentages of mobile Cd found in soil collected

Table 3: Concentrations of exchangeable Cd, plant-available Cd and total Cd in paddy soils

Statistical value	Concentration (mg/kg)			Cd plant availability (%)
	Exchangeable Cd	Plant-available Cd	Total Cd	
	Sandy loam (n=2)			
Minimum	0.06	0.07	0.20	33.4
Maximum	2.20	3.49	3.95	88.4
Mean	1.13	1.78	2.08	60.9
Median	1.13	1.78	2.08	60.9
SE	1.07	1.71	1.88	27.5
	Loam (n=15)			
Minimum	0.14	0.55	0.40	9.6
Maximum	6.29	9.35	27.53	99.5
Mean	1.88	2.94	5.82	40.0
Median	1.09	1.25	2.34	37.9
SE	0.53	0.83	1.96	6.1
	Clay loam (n=14)			
Minimum	0.22	0.13	0.99	13.4
Maximum	8.74	8.31	33.56	67.1
Mean	2.91	2.82	8.92	32.7
Median	2.16	1.71	6.25	27.2
SE	0.75	0.78	2.68	4.5
	Silty clay (n=2)			
Minimum	1.06	0.55	2.00	27.4
Maximum	23.36	27.48	89.87	30.6
Mean	12.21	14.01	45.93	29.0
Median	12.21	14.01	45.93	29.0
SE	11.15	13.47	43.94	2.3
	Clay (n=3)			
Minimum	0.13	0.07	0.40	18.5
Maximum	5.57	3.35	10.72	31.3
Mean	2.67	1.58	5.38	25.4
Median	2.30	1.33	5.01	26.5
SE	1.58	0.96	2.99	3.7
	All samples (n=36)			
Minimum	0.06	0.05	0.20	9.6
Maximum	23.36	27.48	89.87	99.5
Mean	2.88	3.33	9.01	36.4
Median	1.68	1.50	3.98	31.3
SE	0.70	0.83	2.68	3.4

from the same study area as reported by Kosolsaksakul *et al.* (2018, 2014). The mean percentages of mobile Cd in the soils containing low (<10 mg/kg), medium (10–50 mg/kg), and high total Cd contents (>50 mg/kg) in this study, according to the contamination categorization scheme in the previous study, were 60.0%, 58.9%, and 59.1%, respectively. These results were lower than the mobile Cd contents of 82.6%, 94.7% and 95.0% found in soils with low, medium, and high Cd contamination, respectively, as reported by Kosolsaksakul *et al.* (2018, 2014). The differences in findings between the two studies can be explained by the highly heterogeneous nature of soil. The high Cd mobility in this study (mean±SE: 58.6% ± 1.8%;

maximum: 74.2%) clearly indicates the potential release of Cd into the environment, which may cause environmental impacts to the surroundings due to its high toxicity.

#### *Plant-available Cd concentrations in paddy soils*

The concentration of plant-available Cd and percentage of plant availability, which is calculated as the ratio of the plant-available Cd concentration to the total Cd concentration, are summarized in Table 3. This fraction of Cd represents Cd species that are readily available for uptake by plants. To obtain results comparable to previous studies conducted in the same study area, the DTPA soil extraction method was

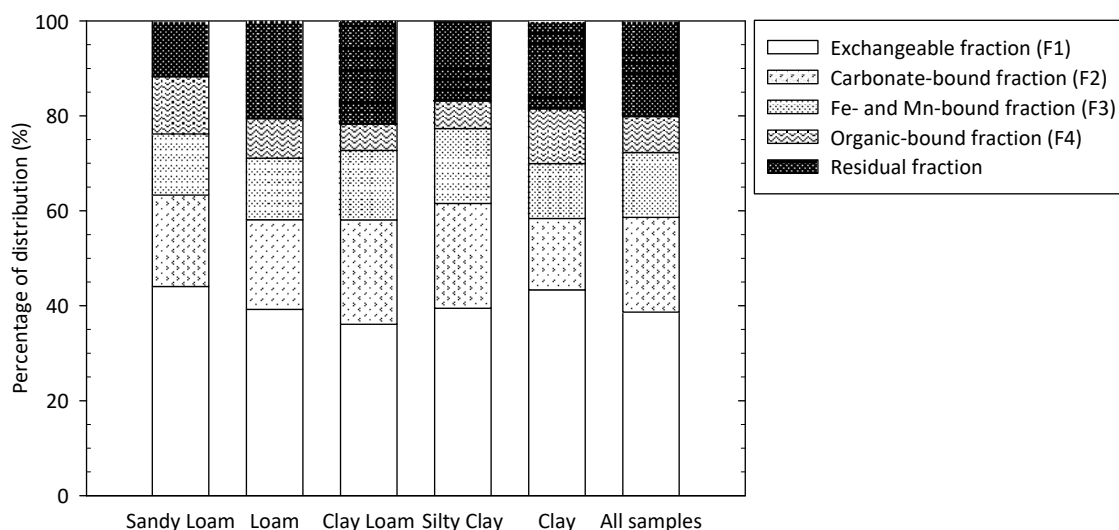


Fig. 3: The distribution of Cd fractions in different soil types

applied in this study. Significant differences in both plant-available concentrations and the percentages of plant availability among different soil types could not be determined ( $p > 0.05$ ). The highest plant-available Cd concentration (27.48 mg/kg) was determined in the soil containing the highest total Cd concentration (89.87 mg/kg) as well as the highest concentration of mobile Cd (F1: 23.36 mg/kg and F2: 29.61 mg/kg). The order of the mean percentage of plant availability was sandy loam (60.9%) > loam (40.0%) > clay loam (32.7%) > silty clay (29.0%) > clay (25.40%). Variations in the concentration of plant-available Cd were found not only in this study (0.05 to 27.48 mg/kg) but also in previous studies (0.38 to 11.8) conducted by [Sriprachote et al. \(2020\)](#) and [Phaenark et al. \(2009\)](#). It is also worth noting that plant availability of Cd among soils can vary by a factor of 10 ([Smolders and Mertens, 2010](#)). A comparison of the concentrations of plant-available Cd found in all soil samples in this study to the soil guideline values set to protect human health and ecosystems, including the predicted no-effect concentration (PNEC) of 0.9 mg/kg regulated by the European Chemical Agency ([ECHA, 2022](#)), the ecological soil guideline value (Eco-SGV) to protect soil quality, particularly for New Zealand productive agricultural land, of 1.5 mg/kg ([Gray and Cavanagh, 2022](#)) and the proposed ecological protective concentration for Korean agricultural soil of 1.58 mg/kg ([Lee et al., 2013](#)), indicated that 36% of all

soil samples in this study were expected to be safe to all receptors and for all purposes of use. However, approximately 47% of all samples may cause negative effects on terrestrial life and lead to the accumulation of Cd to a level that might not be safe for human consumption. Among various organisms, plants and soil microorganisms are more sensitive to Cd toxicity ([Australian Government, 2019, 2017](#); [Adriano, 2001](#)). In addition, root crops, leafy vegetables and cereal grains normally show higher Cd accumulation in their plant parts ([Adriano, 2001](#)). The finding that the average percentages of plant-available Cd in all soil samples ranged between 25.4% and 60.9% ([Table 3](#)) clearly confirms that not all of the Cd present in the soils can be released and is available for plant uptake. Since Cd is a nonessential element for plant growth and cereal grains exhibit high Cd accumulation, the toxicity and accumulation of plant-available Cd in rice in this study were investigated.

#### *Factors affecting the mobility and phytoavailability of Cd in paddy soils*

[Table 4](#) summarizes the soil characteristics that have significant effects on the mobility and phytoavailability of Cd in soils. The levels of association between soil characteristics of concern were interpreted according to [Schober et al. \(2018\)](#). The statistical analyses indicated that the speciation of Cd in the soils was significantly positively and strongly affected by the

Table 4: Correlations between soil characteristics and different Cd species in paddy soils

Characteristic	% Sand	% Silt	% Clay	Eh	pH	CEC	OM	Total Cd	Plant- available Cd	F1 <sup>a</sup>	F2 <sup>b</sup>	F3 <sup>c</sup>	F4 <sup>d</sup>	F5 <sup>e</sup>
% Sand	1.00													
% Silt	-0.46*	1.00												
% Clay	-0.85*	-0.03	1.00											
Eh	0.08	0.05	-0.10	1.00										
pH	-0.10	-0.04	0.16	-0.49*	1.00									
CEC	-0.70*	-0.13	0.90*	-0.12	0.04	1.00								
OM	-0.58*	-0.07	0.71*	-0.26	-0.03	0.80*	1.00							
Total Cd	-0.04	-0.20	0.21	-0.53*	0.45*	0.20	0.38*	1.00						
Plant available Cd	0.16	-0.24	0.01	-0.44*	0.38*	0.04	0.22	0.91*	1.00					
F1 <sup>a</sup>	-0.03	-0.20	0.17	-0.40*	0.32	0.18	0.38*	0.96*	0.90*	1.00				
F2 <sup>b</sup>	-0.05	-0.22	0.22	-0.55*	0.51*	0.24	0.42*	0.94*	0.85*	0.86*	1.00			
F3 <sup>c</sup>	-0.03	-0.19	0.19	-0.57*	0.51*	0.22	0.41*	0.95*	0.85*	0.89*	0.97*	1.00		
F4 <sup>d</sup>	-0.09	-0.19	0.24	-0.58*	0.46*	0.21	0.40*	0.93*	0.79*	0.88*	0.88*	0.91*	1.00	
F5 <sup>e</sup>	-0.08	-0.09	0.16	-0.54*	0.31	0.17	0.30	0.91*	0.82*	0.90*	0.79*	0.82*	0.83*	1.00

\*significant correlation at the 95% confidence level ( $p < 0.05$ );

<sup>a</sup>exchangeable Cd; <sup>b</sup> carbonate-bound Cd; <sup>c</sup> Fe- and Mn-bound Cd; <sup>d</sup> organic-bound Cd; <sup>e</sup> residual Cd7

total Cd concentration in the soil ( $p < 0.05$ ). In addition, significant strong positive correlations were found between Cd fractions ( $p < 0.05$ ). The phytoavailability of Cd was found to be significantly strongly controlled by the concentrations of total Cd and of all Cd species, with correlation coefficients of more than 0.9 ( $p < 0.05$ ). Moreover, significant positive effects of pH and OM on the mobility and availability of Cd in soils were found at moderate levels ( $p < 0.05$ ). Negative moderate correlations were obtained between Eh and all Cd species (F1 to F5) as well as between Eh and plant-available Cd. [Srisawat et al. \(2021\)](#) also reported positive correlations of pH and OM with the concentrations of Cd in agricultural soils collected from the same study area. Previous studies also reported significant effects of total Cd contamination, soil pH, OM, and chemical species on the mobility and availability of Cd ([Li et al., 2021a](#); [McLaughlin et al., 2021](#); [Kubier et al., 2019](#); [Smolders and Mertens, 2010](#)). OM that accumulates at the soil surface has the ability to retain metals, particularly cations, on soil particles ([Adriano, 2001](#)). The different directions of the relationships between pH and Cd mobility and availability in this study and those in previous studies ([Kubier et al., 2019](#); [Smolders and Mertens, 2010](#); [Adriano, 2001](#)) require further investigation.

#### *Toxicity of Cd to rice growth and Cd accumulation in germinated roots*

Since Cd has chemical and charge characteristics similar to those of several macro- and micronutrients for plant growth, including Fe(II), Zn, Mn, and Ca, it competes with these essential nutrients for uptake and translocation by plants ([McLaughlin et al., 2021](#); [Samimi et al., 2023](#)). However, Cd is a nonessential element and is highly toxic to plants ([Khanna et al., 2022](#); [Haider et al., 2021](#); [McLaughlin et al., 2021](#)). The toxicity of plant-available Cd extracted from the soils to rice growth in this study was assessed by using the seed germination test. [Table 5](#) summarizes the toxicity of plant-available Cd in the soil solution to the germination and growth of rice seeds. Significantly lower percentages of RSG, RRG and GI were obtained in all test groups than in the control group ( $p < 0.05$ ). Values of 100% for all indices were obtained for the control group. However, differences in the percentages of RSG, RRG and GI among soil types could not be identified ( $p > 0.05$ ). The number of germinated rice seeds and root length for the control

group were 14 seeds and 1.87 cm, respectively. However, the corresponding values for the test groups varied from 1 to 8 seeds (mean $\pm$ SE: 4.3 $\pm$ 0.3 seeds) and 0.02 to 1.03 cm (mean $\pm$ SE: 0.42 $\pm$ 0.04 cm), respectively. [Fig. 4](#) shows the Cd toxicity to rice germination and root development at the end of the 96-hour incubation. The results shown in [Table 5](#) and [Fig. 4](#) clearly confirmed the toxic effects of Cd on the germination of KDML 105 rice. These results are in line with the findings from previous studies that general visible growth abnormalities induced by Cd include a reduction in plant root elongation after germination ([Khanna et al., 2022](#); [Haider et al., 2021](#)). This is mainly caused by the retardation effects of toxic metals on water penetration into seeds ([Pokorska-Niewiada et al., 2018](#)). Thus, a lower degree of germination was found compared to the control group that used deionized water for germination. The plant-available Cd concentrations in the test groups that caused significant reductions in rice seed germination and root length ranged from 0.05 to 27.48 mg/kg (mean $\pm$ SE: 3.33  $\pm$  0.83 mg/kg). Compared to the concentration of Cd causing reductions in the rice root elongation and germination of seedlings (5.40 mg Cd) ([Haider et al., 2021](#)), the toxicity of Cd in this study showed similar negative effects at a lower Cd concentration (mean $\pm$ SE: 3.33  $\pm$  0.83 mg/kg; minimum: 0.05 mg/kg). The differences in the toxic concentrations of Cd in this study and the previous study might be attributed to the differences in the Cd species, growth media, incubation environment and tested rice variety. As the germination in this study was conducted for only 96 hours, it is expected that a longer germination period in Cd-contaminated soil would cause more negative effects on growth and greater accumulation of Cd in rice roots. In previous studies, cultivation time and soil Cd concentration showed positive relationships with Cd accumulation in the roots, shoots, and grains of rice ([Uraguchi et al., 2009](#)). Cd in soil is transported into grains via xylem–phloem transfer, with a reported range of Cd grain-to-soil ratios of 0.058 to 5.96 ([Zhao and Wang, 2020](#); [Uraguchi et al., 2009](#)). As the mean Cd concentration in germinated roots (1.04 mg/kg) in this study exceeded both the national and Codex standards for Cd in rice (0.4 mg/kg), it is highly likely that the accumulated Cd concentrations in the grains would exceed the standards.

[Table 6](#) summarizes the relationships of the Cd

Table 5: Germination indices and total Cd concentration accumulated in germinated roots after 96 hours of incubation

Statistical value	RSG (%)	RRG (%)	GI (%)	Cd concentration in germinated roots (mg/kg)	BCF
Sandy loam (n=2)					
Minimum	12.4	11.6	1.4	0.04	0.63
Maximum	55.0	44.4	24.4	4.02	1.15
Mean	33.6	28.0	12.9	2.03	0.89
Median	33.6	28.0	12.9	2.03	0.89
SE	21.4	16.4	11.5	1.99	0.26
Loam (n=15)					
Minimum	10.0	1.3	0.1	0.03	0.17
Maximum	54.3	41.0	14.1	2.09	4.06
Mean	30.6	21.5	7.0	0.75	0.59
Median	30.7	21.1	5.5	0.36	0.29
SE	3.5	2.8	1.2	0.20	0.25
Clay loam (n=14)					
Minimum	15.0	7.9	1.2	0.07	0.21
Maximum	57.9	54.0	25.1	5.38	0.69
Mean	29.9	19.3	6.6	1.09	0.38
Median	24.6	15.1	3.5	0.45	0.32
SE	3.6	3.3	1.7	0.40	0.04
Silty clay (n=2)					
Minimum	22.9	8.0	1.8	0.19	0.21
Maximum	45.0	32.8	14.8	5.88	0.35
Mean	33.9	20.4	8.3	3.03	0.28
Median	33.9	20.4	8.3	3.03	0.28
SE	15.7	17.5	9.2	4.02	0.09
Clay (n=3)					
Minimum	20.7	15.5	3.2	0.04	0.02
Maximum	45.7	55.0	25.1	0.48	0.57
Mean	36.2	35.9	14.7	0.19	0.32
Median	42.1	37.2	15.7	0.05	0.28
SE	7.8	11.4	6.4	0.14	0.16
All samples (n=36)					
Minimum	9.5	1.3	0.1	0.03	0.02
Maximum	59.0	55.0	25.1	5.88	4.06
Mean	31.2	22.1	7.9	1.04	0.48
Median	26.9	18.6	5.4	0.42	0.32
SE	2.3	2.2	1.2	0.24	0.11

fractions in the soils with Cd toxicity to rice growth and Cd accumulation in germinated roots. The number of germinated seeds and %RSG were mainly significantly negatively and weakly correlated with the concentration of exchangeable Cd (F1) in the soils ( $p < 0.05$ ). The %RRG, %GI and length of root elongation were significantly negatively affected by the concentrations of total Cd and all Cd species in the soils, with the strengths of the correlations ranging from weak (correlation coefficient of 0.10 to 0.39) to moderate (correlation coefficient of 0.40 to 0.69), except for organic-bound Cd (F4) ( $p < 0.05$ ),

which did not show a significant correlation with either %RRG or %GI ( $p > 0.05$ ). It is interesting that the correlation coefficients of %RRG, %GI and root length with F1 and F2 were higher than those of these three indices with the other Cd fractions (Table 6). These results were in good agreement with a previous study by Cataldo and Wildung (1978), who found that the soluble species of heavy metals strongly controlled the rate and amount of uptake as well as the toxicity in plants, as metals in soils have to be solubilized into the soil solution for root uptake. These conclusions are in accordance

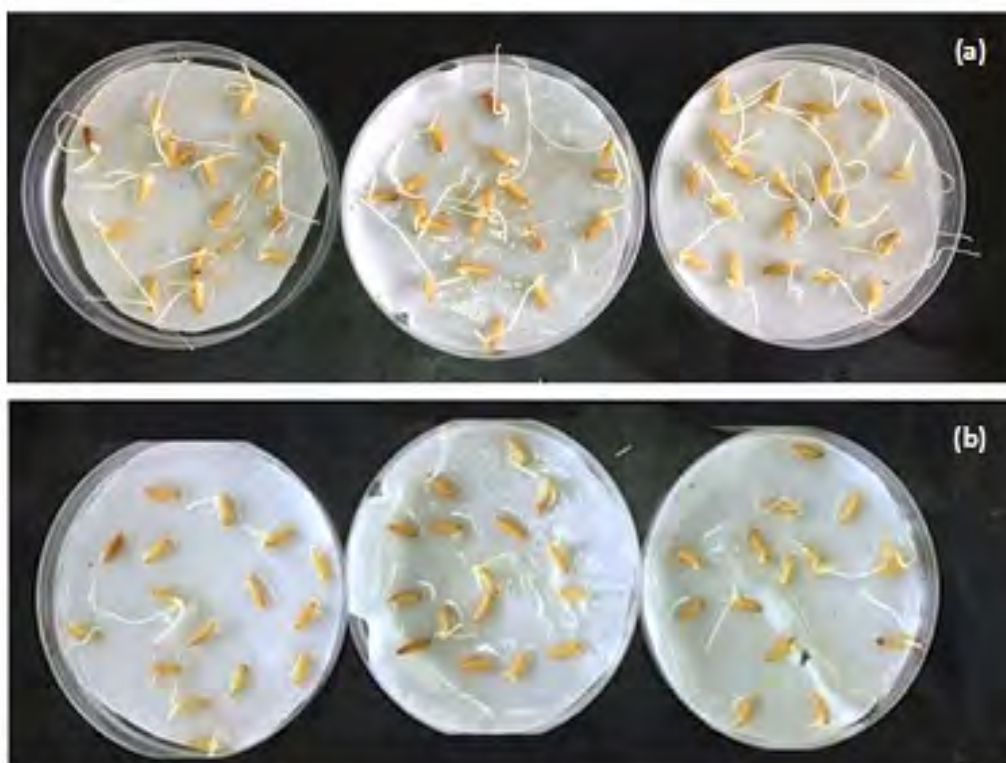


Fig. 4: Germination and length of rice roots germinated with (a) deionized water (control group) and (b) plant-available Cd extracted solution (test group)

with the results of this study (Fig. 5), which revealed significant strong positive correlations ( $p < 0.05$ ) between the total Cd concentration in the germinated roots and the plant-available Cd, exchangeable Cd (F1), carbonate-bound Cd (F2), and total Cd concentrations in soils, with correlation coefficients ranging from 0.77 to 0.89. Furthermore, the less mobile Cd fractions (F3 and F4) and residual Cd fraction (F5) showed positive correlations with the total Cd concentration accumulated in the germinated roots (Table 6). Similar results showing that the accumulation of Cd was principally affected by Cd availability and total Cd concentration were also reported by Li *et al.*, 2022; Nogueira *et al.*, 2022; McLaughlin *et al.*, 2021; Wang *et al.*, 2020).

#### *Common characteristics of paddy soils causing different levels of Cd accumulation in rice*

Cluster analysis was performed on the characteristics of soils, including Eh, pH, CEC, OM, total Cd concentration and percentages of

plant availability and mobility, and the total Cd concentration in germinated roots, to group together the paddy soil samples with similar patterns that caused different levels (low, moderate, and high) of Cd accumulation in germinated rice roots. A total of eight groups of samples with soil characteristics resulting in different levels of Cd accumulation in germinated roots were obtained (Fig. 6). Notably, the levels of Eh, pH, CEC, and OM were similar among the groups. The characteristics that caused different levels of Cd accumulation in germinated roots, which consequently caused Cd accumulation in rice grains, were the concentrations of total Cd, mobile Cd (F1 and F2) and plant-available Cd in soils. Based on the results (Fig. 6), it is possible to infer that high Cd accumulation in rice was mainly affected by a high percentage of plant availability of Cd in the soils regardless of the level of total Cd contamination. Thus, management options to mitigate the plant availability of Cd in soils should be applied to these soils to reduce Cd accumulation in rice.

Table 6: Correlations showing the effects of soil characteristics on the accumulation and toxicity of Cd to rice

Characteristic	Cd in rice	Total Cd	Plant-available Cd	F1 <sup>a</sup>	F2 <sup>b</sup>	F3 <sup>c</sup>	F4 <sup>d</sup>	F5 <sup>e</sup>	BCF	RSG (%)	RRG (%)	GI (%)	No. of seeds germinated	Root length
Cd in rice	1.00													
Total Cd	0.77*	1.00												
Plant-available Cd	0.89*	0.91*	1.00											
F1 <sup>a</sup>	0.79*	0.96*	0.90*	1.00										
F2 <sup>b</sup>	0.78*	0.94*	0.85*	0.86*	1.00									
F3 <sup>c</sup>	0.75*	0.95*	0.85*	0.89*	0.97*	1.00								
F4 <sup>d</sup>	0.67*	0.93*	0.79*	0.88*	0.88*	0.91*	1.00							
F5 <sup>e</sup>	0.66*	0.91*	0.82*	0.90*	0.79*	0.82*	0.83*	1.00						
BCF	-0.27	-0.60*	-0.56*	-0.52*	-0.60*	-0.62*	-0.53*	-0.56*	1.00					
RSG (%)	-0.49*	-0.22	-0.29	-0.34*	-0.23	-0.20	-0.18	-0.19	-0.13	1.00				
RRG (%)	-0.58*	-0.39*	-0.47*	-0.51*	-0.44*	-0.41*	-0.30	-0.35*	0.14	0.60*	1.00			
GI (%)	-0.63*	-0.38*	-0.46*	-0.51*	-0.43*	-0.39*	-0.29	-0.35*	0.04	0.84*	0.92*	1.00		
No. of seeds germinated	-0.49*	-0.22	-0.29	-0.34*	-0.23	-0.20	-0.18	-0.19	-0.13	1.00*	0.60*	0.84*	1.00	
Root length	-0.58*	-0.39*	-0.48*	-0.51*	-0.44*	-0.41*	-0.30	-0.35*	0.14	0.60*	1.00*	0.92*	0.60*	1.00

\*significant correlation at the 95% confidence level (p<0.05);

<sup>a</sup> exchangeable Cd; <sup>b</sup> carbonate-bound Cd; <sup>c</sup> Fe- and Mn-bound Cd; <sup>d</sup> organic-bound Cd; <sup>e</sup> residual Cd .

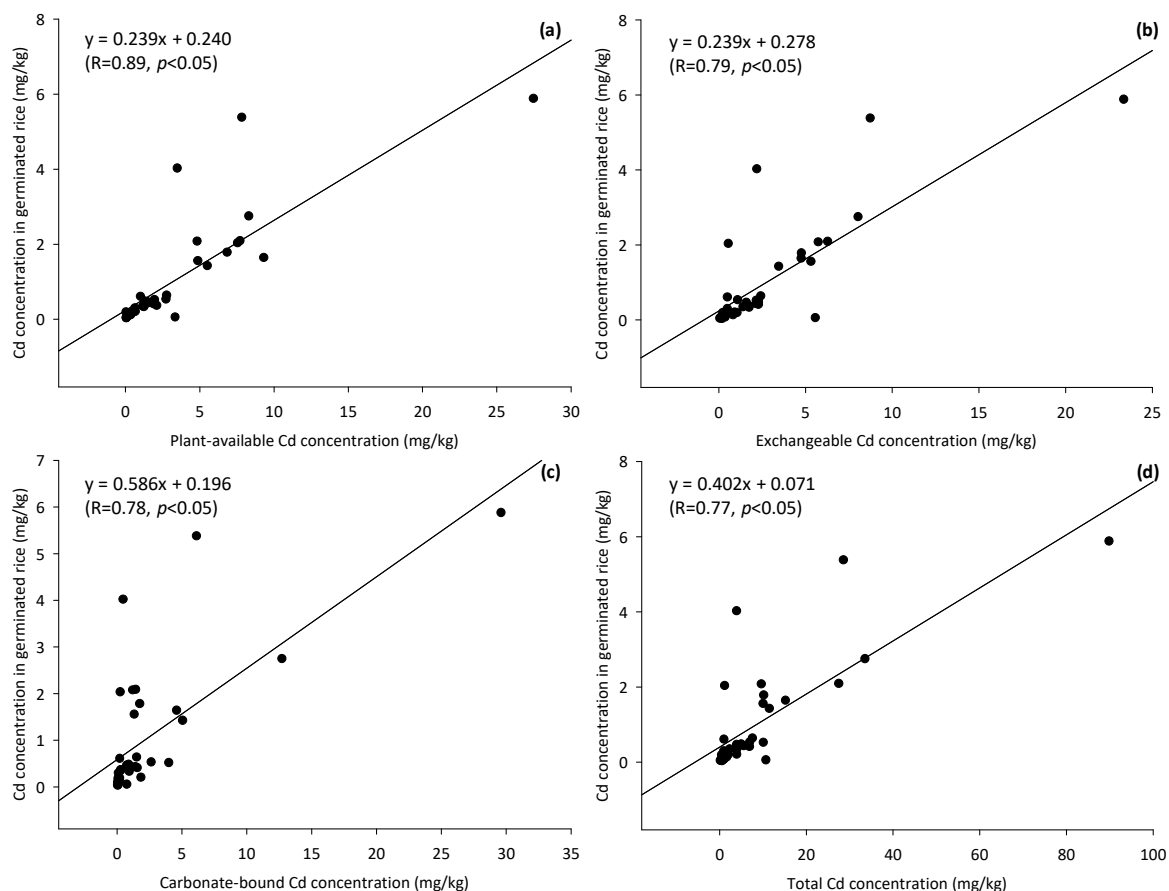


Fig. 5: Significant positive linear relationships between the Cd concentrations accumulated in germinated rice and the concentrations of (a) plant-available Cd, (b) exchangeable Cd, (c) carbonate-bound Cd, and (d) total Cd in the soils

#### Recommended remediation strategy for the study area

According to the authors' previous human health risk assessments of Cd exposure through rice consumption in the study area (Chanpiwat *et al.*, 2019; Suwatvitayakorn *et al.*, 2020), which found that locally grown and consumed rice contained Cd concentrations exceeding the national and Codex standards for Cd in polished rice and that the bioaccessibility of Cd in rice, which is readily absorbed by the human bloodstream, reached 84%, this study was conducted to assess the factors affecting the toxicity and accumulation of Cd in rice. The results showed that the concentrations of total Cd, exchangeable Cd (F1), carbonate-bound Cd (F2), and plant-available Cd were the main soil characteristics affecting the accumulation of

Cd in rice, with plant-available Cd being the most important factor. Therefore, focus should be placed on reducing the plant-available Cd in soils to lower Cd accumulation and protect the public from Cd exposure. As the results further showed that the mobility and phytoavailability of Cd in the soils from the study area were mainly positively controlled by the total Cd and OM concentrations, two potential mitigation measures are i) to change the irrigation water to Cd-free water, as this measure would not add more Cd to the paddy soils, and ii) to add OM-rich amendments to immobilize plant-available Cd in the soils. According to previous studies (Yavari *et al.*, 2023, 2022; Haider *et al.*, 2021; Hussain *et al.*, 2021; Li *et al.*, 2021a, 2021b; McLaughlin *et al.*, 2021; Alam *et al.*, 2020; Zhao and Wang, 2020), organic fertilizer, organic waste compost, organic manure, agrowaste-

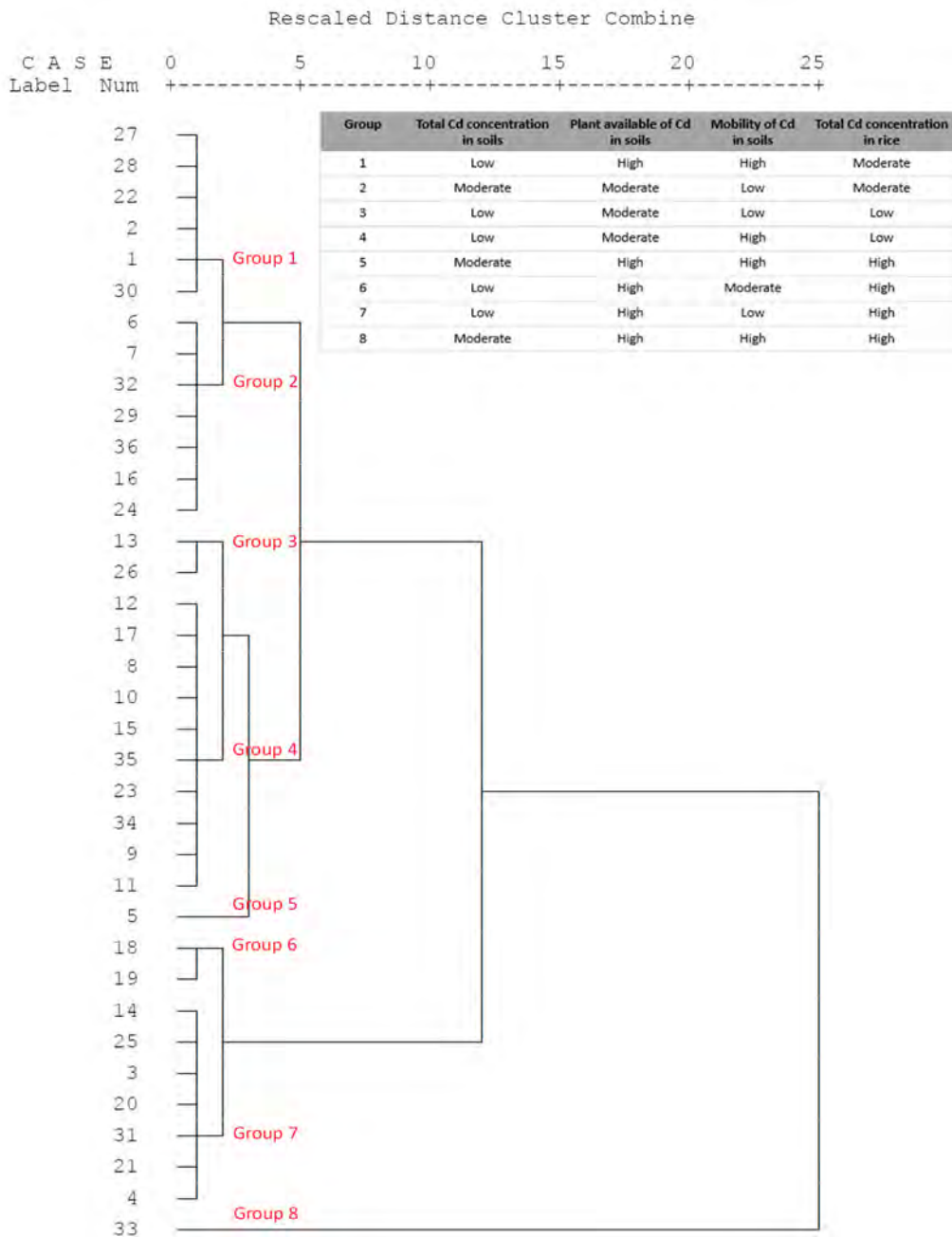


Fig. 6: Dendrogram showing the clustering of sampling sites with similar soil characteristics causing different levels of Cd accumulation in rice

derived biochar, and humic acid have shown a good capability to immobilize various soil pollutants, including metals, and reduce their accumulation in plant parts. However, the application rate of

amendments can differ from those established in previous studies, as the soil characteristics and level of contamination can also differ. Considering the results of this study, which found a negative

relationship between Eh and plant-available Cd, the maintenance of an oxidizing soil environment during cultivation would be another mitigation measure to simultaneously reduce the Cd mobility in soils and Cd accumulation in rice. Moreover, the cultivation of rice cultivars with low grain Cd accumulation, such as those tested in the study area and reported by Sripachote *et al.* (2020), should be promoted.

## CONCLUSION

This study is the first to report the factors affecting the plant availability and mobility of Cd in soils as well as the factors affecting the toxicity and accumulation of Cd in rice grown in paddy soils that were previously reported to produce rice grains with total Cd concentrations exceeding the acceptable level for human consumption of 0.4 mg/kg. Although the total Cd concentrations (0.20 to 89.87 mg/kg) in all soil samples (n=36) were lower than the national soil quality standard for agricultural activities of 762 mg/kg, 64% of the samples contained total Cd concentrations 1.2 to 52.9 times greater than the national background concentration in agricultural soils. The chemical fractions of Cd in the soils were found in the decreasing order  $F_1 > F_5 \approx F_2 > F_3 > F_4$ , with mobile Cd ( $F_1 + F_2$ : 58.60%) composing the majority of species on average, which corresponds well to the mobile characteristics of Cd. A wide variation in plant-available Cd (0.05 to 27.48 mg/kg) was found, with the highest mean percentage of plant availability (60%) found in the sandy loam soils, as sand particles do not have the capacity to absorb cations on their surface. Plant-available Cd exerted significant toxicity to both rice seed germination and root elongation, with approximately 69% and 48% reductions in the two indices, respectively. Cd accumulation in germinated roots (0.03 to 5.88 mg/kg) was observed in 44% of the test samples, with Cd levels exceeding the total Cd standard in rice (0.4 mg/kg). Therefore, the plant-available Cd concentrations in soils should be reduced to lower Cd accumulation in rice. Since the most important soil characteristics affecting the availability of Cd were the total concentration and speciation of Cd, the concentration of plant-available Cd in the soil solution can be decreased by i) reducing the total Cd contamination in the soils by stopping the use of Mae Tao Creek as the irrigation water and ii) increasing the OM concentrations in the soils by adding OM-rich amendments such as compost,

manure, and biochar to immobilize plant-available Cd. By doing so, the concentration of Cd in locally consumed rice as well as the adverse human health impacts will be lessened. As this study did not include an investigation of the toxic effects of Cd throughout the rice cultivation period, it is highly recommended that future work include a study on the effects of local rice cultivation practices on the soil–plant system and the toxic effects throughout the rice growth cycle.

## AUTHOR CONTRIBUTIONS

A. Numprasanthai, the corresponding author, contributed to conceptualization, investigation, methodology, resources, writing - review and editing, supervision, and funding acquisition. P. Chanpiwat, the first author, contributed to the investigation, methodology, data curation, validation, formal analysis, writing - original draft, visualization, and funding acquisition.

## ACKNOWLEDGEMENTS

This research was financially supported by the Thailand Science Research and Innovation Fund (TSRI) [FRB640001\_21\_4] under the project “Georesources Engineering Project: Research and Capacity Building” and the GIST Research Institute (GRI) of the Gwangju Institute of Science and Technology (GIST) in 2023. The authors would like to also express their sincere gratitude to the Environmental Research Institute (ERIC), Chulalongkorn University, for the invaluable support in terms of facilities and scientific equipment.

## CONFLICT OF INTEREST

The authors declare that there are no conflict of interest regarding the publication of this manuscript. In addition, the ethical issues, including plagiarism, informed consent, misconduct, data fabrication and/or falsification, double publication and/or submission, and redundancy, were observed by the authors.

## OPEN ACCESS

©2024 The author(s). This article is licensed under a Creative Commons Attribution 4.0 International License, which permits use, sharing, adaptation, distribution and reproduction in any medium or format, as long as you give appropriate credit to the original author(s) and the source, provide a link to the Creative Commons license, and indicate if changes were made. The images or other third-party material

in this article are included in the article's Creative Commons license, unless indicated otherwise in a credit line to the material. If material is not included in the article's Creative Commons license and your intended use is not permitted by statutory regulation or exceeds the permitted use, you will need to obtain permission directly from the copyright holder. To view a copy of this license, visit: <http://creativecommons.org/licenses/by/4.0/>

#### PUBLISHER'S NOTE

GJESM Publisher remains neutral with regard to jurisdictional claims in published maps and institutional affiliations.

#### ABBREVIATIONS

%	Percent
$\mu\text{g}$	Microgram
$\mu\text{m}$	Micrometer
<i>BCF</i>	Bioconcentration factor
$^{\circ}\text{C}$	Degree Celsius
<i>Ca</i>	Calcium
<i>Cd</i>	Cadmium
<i>CEC</i>	Cation exchange capacity
<i>cm</i>	Centimeter
$\text{cm}^2$	Square centimeter
<i>cmol</i>	Centimole
<i>DOA</i>	Department of Agriculture
<i>DPIM</i>	Department of Primary Industries and Mines
<i>DTPA</i>	Diethylenetriaminepentaacetic acid
<i>Eco-SGV</i>	Ecological soil guideline value
<i>Eh</i>	Redox potential
<i>ERIC</i>	Environmental Research Institute, Chulalongkorn University
<i>F1</i>	Exchangeable fraction
<i>F2</i>	Carbonate-bound fraction
<i>F3</i>	Fe- and Mn-bound fraction
<i>F4</i>	Organic-bound fraction
<i>F5</i>	Residual fraction
<i>Fe</i>	Iron
<i>g</i>	Gram
<i>GI</i>	Germination index

<i>GIST</i>	Gwangju Institute of Science and Technology
<i>GRI</i>	GIST Research Institute
$\text{HNO}_3$	Nitric acid
$\text{H}_2\text{O}_2$	Hydrogen peroxide
<i>ICP-MS</i>	Inductively coupled plasma–mass spectrometry
<i>ICP-OES</i>	Inductively coupled plasma–optical emission spectrometry
<i>IWMI</i>	International Water Management Institute
<i>kg</i>	Kilogram
<i>KDML 105</i>	Khao Dok Mali 105 rice
<i>L</i>	Liter
<i>LDD</i>	Land Development Department
<i>mg</i>	Milligram
<i>mL</i>	Milliliter
<i>mm</i>	Millimeter
<i>Mn</i>	Manganese
<i>mV</i>	Millivolt
<i>n</i>	Sample size
<i>NaOCl</i>	Sodium hypochlorite
<i>NIST</i>	National Institute of Standards and Technology
<i>OM</i>	Organic matter
<i>ORP</i>	Oxidation–reduction potential
<i>p value</i>	Probability value
<i>pH</i>	Potential of hydrogen
<i>PNEC</i>	Predicted no-effect concentration
<i>ppm</i>	Part per million
<i>RRG</i>	Relative root growth
<i>RSG</i>	Relative seed germination
<i>SE</i>	Standard error of the mean
<i>SPSS</i>	Statistical Package for Social Science
<i>SRM</i>	Standard reference material
<i>TSRI</i>	Thailand Science Research and Innovation
<i>v</i>	Volume
<i>w</i>	Weight
<i>Zn</i>	Zinc

## REFERENCES

- Adriano, D.C., (2001). Trace elements in terrestrial environments: Biogeochemistry, bioavailability, and risks of metals. 2nd. Ed. Springer New York.
- Alam, M.; Hussain, Z.; Khan, A.; Khan, M.A.; Rab, A.; Asif, M.; Shah, M.A.; Muhammad, A., (2020). The effects of organic amendments on heavy metals bioavailability in mine impacted soils and associated human health risk. *Sci. Hortic.*, 262: 109067 **(8 pages)**.
- Australian Government, (2017). Water soluble cadmium(2) salts: Environment tier II assessment.
- Australian Government, (2019). Cadmium metal and cadmium oxide: Environment tier II assessment.
- Bae, J.; Mercier, G.; Watson, A.K.; Benoit, D.L., (2014). Seed germination test for heavy metal phytotoxicity assessment. *Can. J. Plant Sci.*, 94: 1519–1521 **(3 pages)**.
- BOD, (2012). A true fear of Mae Tao's local residents (in Thai).
- Cataldo, D.A.; Wildung, R.E., (1978). Soil and plant factors influencing the accumulation of heavy metals by plants. *Environ. Health. Perspect.*, 27: 149–159 **(11 pages)**.
- Chanpiwat, P.; Sthiannopkao, S.; Kim, K.W., (2010). Metal content variation in wastewater and biosludge from Bangkok's central wastewater treatment plants. *Microchem. J.*, 95: 326–332 **(7 pages)**.
- Chanpiwat, P.; Hensawang, S.; Suwatvitayakorn, P.; Ponsin, M., (2019). Risk assessment of bioaccessible arsenic and cadmium exposure through rice consumption in local residents of the Mae Tao Sub-district, Northwestern Thailand. *Environ. Geochem. Health.*, 41: 343–356 **(14 pages)**.
- DOA, (2010). A handbook of soil analysis (in Thai).
- ECHA, (2022). Cadmium chloride.
- Gray, C.W.; Cavanagh, J.A.E., (2022). The state of knowledge of cadmium in New Zealand agricultural systems: 2021. *N.Z.J. Agric. Res.*, 66(4): 285–335 **(51 pages)**.
- Haider, F.U.; Liqun, C.; Coulter, J.A.; Cheema, A.S.; Wu, J.; Zhang, R.; Wenjun, M.; Farooq, M., (2021). Cadmium toxicity in plants: Impacts and remediation strategies. *Ecotoxicol. Environ. Saf.*, 211: 111887 **(22 pages)**.
- Hussain, B.; Umer, M.J.; Li, J.; Ma, Y.; Abbas, Y.; Ashraf, M.N.; Tahir, N.; Ullan, A.; Gogoi, N.; Farooq, M., (2021). Strategies for reducing cadmium accumulation in rice grains. *J. Cleaner Prod.*, 286: 125557 **(20 pages)**.
- Husson, O., (2013). Redox potential (Eh) and pH as drivers of soil/plant/microorganisms systems: A transdisciplinary overview pointing to integrative opportunities for agronomy. *Plant Soil.*, 362: 389–417 **(29 pages)**.
- Islam, Md.D.; Hasan, M.M.; Rahaman, A.; Haque, P.; Islam, Md.S.; Rahman, M.M., (2020). Translocation and bioaccumulation of trace metals from industrial effluent to locally grown vegetables and assessment of human health. *SN Appl. Sci.*, 2: 1315 **(11 pages)**.
- KMU, (2023). Kanazawa Medical University report.
- Khanna, K.; Kohli, S.K.; Ohri, P.; Bhardwaj, R.; Ahmad, P., (2022). Agroecotoxicological aspect of Cd in soil-plant system: Uptake, translocation and amelioration strategies. *Environ. Sci. Pollut. Res.*, 29: 30908–30924 **(17 pages)**.
- Kosolsaksakul, P.; Farmer, J.G.; Oliver, I.W.; Graham, M.C., (2014). Geochemical associations and availability of cadmium (Cd) in a paddy field system, northwestern Thailand. *Environmen. Pollut.*, 187: 153–161 **(9 pages)**.
- Kosolsaksakul, P.; Oliver, I.W.; Graham, M.C., (2018). Evaluating cadmium bioavailability in contaminated rice paddy soils and assessing potential for contaminant immobilization with biochar. *J. Environ. Manage.*, 215: 49–56 **(8 pages)**.
- Kubier, A.; Wilkin, R.T.; Pichler, T., (2019). Cadmium in soils and groundwater: A review. *Appl. Geochem.*, 108: 1–16 **(16 pages)**.
- LDD, (2010). Soil chemical analyses manual (in Thai).
- LDD, (2019). Suitability of Thai soils for agriculture (in Thai).
- Lee, W.M.; Man, S.H.; AN, Y.J., (2013). Deriving ecological protective concentration of cadmium for Korean soil environment. *Environ. Eng. Res.*, 18(4): 241–246 **(6 pages)**.
- Li, X.; Du, J.; Sun, L.; Zhang, Y.; Feng, Y.; Zheng, L.; Wang, G.; Huang, X., (2022). Derivation of soil criteria of cadmium for safe rice production applying soil-plant transfer model and species sensitivity distribution. *Int. J. Environ. Res. Public Health.*, 19: 8854 **(15 pages)**.
- Li, Z.; Liang, Y.; Hu, H.; Shaheen, S.M.; Zhong, H.; Tack, F.M.G.; Wu, M.; Li, Y.F.; Gao, Y.; Rinklebe, J.; Zhao, J., (2021a). Speciation, transportation, and pathways of cadmium in soil-rice systems: A review on the environmental implications and remediation approaches for food safety. *Environ. Int.*, 156: 106749 **(13 pages)**.
- Li, S.; Sun, X.; Li, S.; Liu, Y.; Ma, Q.; Zhou, W., (2021b). Effects of amendments on the bioavailability, transformation and accumulation of heavy metals by packhoi cabbage in a multi-element contaminated soil. *RSC Adv.*, 11: 4395–4405 **(11 pages)**.
- Lindsay, W.L.; Norvell, W.A., (1978). Development of a DTPA soil text for zinc, iron, manganese, and copper. *Soil Sci. Soc. Am. J.*, 42(3): 421–428 **(8 pages)**.
- McLaughlin, M.J.; Smolders, E.; Zhao, F.J.; Grant, C.; Montalvo, D., (2021). Managing cadmium in agricultural systems. *Adv. Agron.*, 166: 1–129 **(129 pages)**.
- Nishijo, M.; Suwazono, Y.; Ruangyuttikarn, W.; Nambunmee, K.; Swaddiwudhipong, W.; Nogawa, K.; Nakagawa, H., (2014). Risk assessment for Thai population: Benchmark dose of urinary and blood cadmium levels for renal effects by hybrid approach of inhabitants living in polluted and non-polluted areas in Thailand. *BMC Public Health.*, 14: 702 **(9 pages)**.
- Nogueira, T.A.R.; Muraoka, T.; Silveira, L.K.; de Silva, J.S.; Abreu-Junior, C.H.; Lavres, J.; Martinelli, A.P.; Filho, M.C.M.T.; He, Z.; Jani, A.D.; Ganga, A.; Capra, G.F., (2022). Comparing soil-to-plant cadmium (Cd) transfer and potential human intake among rice cultivars with different Cd tolerance levels grown in a tropical contaminated soil. *Environ. Monit. Assess.*, 194(1): 20 **(13 pages)**.
- Nordberg, G.F.; Bernard, A.; Diamond, G.L.; Duffus, J.H.; Illing, P.; Nordberg, M.; Bergdahl, I.A.; Jin, T.; Skerfving, S., (2018). Risk assessment of effects of cadmium on human health (IUPAC technical report). *Pure Appl. Chem.*, 90(4): 755–808 **(54 pages)**.
- Nurhasanah; Sulistyowati, L.; Riani, E.; Cordova, M.R., (2023). Cadmium and lead uptake by wild swamp eel in the

- populous river. *Global J. Environ. Sci. Manage.*, 9(3): 497-514 **(18 pages)**.
- Phaenark, C.; Pokethitiyook, P.; Kruatrachue, M.; Ngernsarsaruay, C., (2009). Cd and Zn accumulation in plants from the Padaeng zinc mine area. *Int. J. Phytorem.*, 11: 479–495 **(17 pages)**.
- PCD, (2021). Thailand soil quality standards (in Thai).
- Pokorska-Niewiada, K.; Rajkowska-Mysliwiec, M.; Protasowicki, M., (2018). Acute lethal toxicity of heavy metals to the seeds of plants of high importance to humans. *Bull. Environ. Contam. Toxicol.*, 101: 222–228 **(7 pages)**.
- Sabilillah, A.M.; Palupi, F.R.; Adj, B.K.; Nugroho, A.P., (2023). Health risk assessment and microplastic pollution in streams through accumulation and interaction of heavy metals. *Global J. Environ. Sci. Manage.*, 9(4): 719-740 **(22 pages)**.
- Samimi, M., (2024). Effective biosorption of cadmium by *Eucalyptus globulus* fruit biomass using process parameters optimization. *Global J. Environ. Sci. Manage.*, 10(1) **(11 pages)**.
- Samimi, M.; Mohammadzadeh, E.; Mohammadzadeh, A., (2023). Rate enhancement of plant growth using Ormus solution: optimization of operating factors by response surface methodology. *Int. J. Phytoremediation*, 1-7 **(7 pages)**.
- Schober, P.; Boer, C.; Schwarte, L.A., (2018). Correlation coefficients: Appropriate use and interpretation. *Anesth. Analg.*, 126(5): 1763–1768 **(6 pages)**.
- Simmons, R.W.; Pongsakul, P.; Saiyasitpanich, D.; Klinpholkap, S., (2005). Elevated levels of cadmium and zinc in paddy soils and elevated levels of cadmium in rice grain downstream of a zinc mineralized area in Thailand: Implications for public health. *Environ. Geochem. Health.*, 27: 501–511 **(11 pages)**.
- Smolders, E.; Mertens, J., (2010). Cadmium, in: Allowa, B.J. (Eds.), *Heavy metals in soils: Trace metals and metalloids in soils and their bioavailability*. Springer New York.
- Somprasong, K., (2019). Application of integrated spatial approaches for studying the vegetation alternation's effect on the reclaimed land of contaminated zinc mine. *IOP Conference Series: Earth Environ. Sci.*, 307: 012013 **(11 pages)**.
- Sriprachote, A.; Kanyawongha, P.; Ochiai, K.; Match, T., (2012). Current situation of cadmium-polluted paddy soil, rice and soybean in the Mae Sot District, Tak Province, Thailand. *Soil Sci. Plant Nutr.*, 58: 349–359 **(11 pages)**.
- Sriprachote, A.; Kanyawongha, P.; Boonplang, N.; Phanchindawan, N., (2020). Six years monitoring of the promising low grain-Cd accumulating rice, RD15 cultivar grown on Cd-contaminated paddy soils. *Appl. Environ. Res.*, 42(2): 84–93 **(10 pages)**.
- Srisawat, L.; Satapanajaru, T.; Anurakpongsatorn, P.; Jarusutthirak, C.; Yoo-iam, M., (2021). Agricultural land suitability mapping for rice cultivation in severely heavy metal-contaminated land: Case study of Mae Tao in Thailand. *Water Air Soil Pollut.*, 232: 460 **(18 pages)**.
- Suwatvitayakorn, P.; Ko, M.S.; Kim, K.W.; Chanpiwat, P., (2020). Human health risk assessment of cadmium exposure through rice consumption in cadmium-contaminated areas of the Mae Tao sub-district, Tak, Thailand. *Environ. Geochem. Health.*, 42: 2331–2344 **(14 pages)**.
- Taeprayoon, P.; Printarakul, N.; Somtrakoon, K.; Chunwichit, S.; Yooma, K.; Wiangdao, S.; Avakul, P.; Meeinkuirt, W., (2023). Potentially toxic element accumulation of bryophyte taxa in contaminated soils at Tak Province, Thailand. *Ecol. Indic.*, 147: 109971 **(14 pages)**.
- Tessier, A.; Campbell, P.G.C.; Bisson, M., (1979). Sequential extraction procedure for the speciation of particulate trace metals. *Anal. Chem.*, 51(7): 844–851 **(8 pages)**.
- Tornuk, F.; Ozturk, I.; Sagdic, O.; Yetim, H., (2011). Determination and improvement of microbial safety of wheat sprouts with chemical sanitizers. *Foodborne Pathog. Dis.*, 8(4): 503–508 **(6 pages)**.
- Uraguchi, S.; Mori, S.; Kuramata, M.; Kawasaki, A.; Arao, T.; Ishikawa, S., (2009). Root-to-shoot Cd translocation via xylem is the major process determining shoot and grain cadmium accumulation in rice. *J. Exp. Bot.*, 60(9): 2677–2688 **(12 pages)**.
- Waleeittikul, A.; Chotpantararat, S.; Ong, S.K., (2019). Impacts of salinity level and flood irrigation on Cd mobility through a Cd-contaminated soil, Thailand: Experimental and modeling techniques. *J. Soils Sediments.*, 19: 2357–2373 **(17 pages)**.
- Wang, Y.; Liu, X.; Qin, H., (2020). Bioconcentration and translocation of heavy metals in the soil-plants system in Machangqing copper mine, Yunnan Province, China. *J. Geochem. Explor.*, 200: 159–166 **(8 pages)**.
- Walter, I.; Martinez, F.; Cala, V., (2006). Heavy metal speciation and phytotoxic effects of three representative sewage sludges for agricultural uses. *Environ. Pollut.*, 139: 507–514 **(8 pages)**.
- Weeraprapan, P.; Phalaraksh, C.; Chantara, S.; Kawashima, M., (2015). Water quality monitoring and cadmium contamination in the sediments of Mae Tao Stream, Mae Sot District, Tak Province, Thailand. *Int. J. Environ. Sci. Dev.*, 6(2): 142–146 **(5 pages)**.
- WHO, (2019). Exposure to cadmium: A major public health concern.
- Yavari, S.; Kamyab, H.; Manan, T.S.B.A.; Chelliapan, S.; Asadpour, R.; Yavari, S.; Sapari, N.B.; Baloo, L.; Sidik, A.B.C.; Kirpichnikova, I. (2022). Bio-efficacy of imidazolinones in weed control in a tropical paddy soil amended with optimized agrowaste-derived biochars. *Chemosphere*, 303: 134957 **(8 pages)**.
- Yavari, S.; Kamyab, H.; Asadpour, R.; Yavari, S.; Sapari, N.B.; Baloo, L.; Manan, T.S.B.A.; Ashokkumar, V.; Chelliapan, S. (2023). The fate of imazapyr herbicide in the soil amended with carbon sorbents. *Biomass Covers. Biorefin.*, 13: 7561–7569 **(9 pages)**.
- Zhao, F.J.; Wang, P., (2020). Arsenic and cadmium accumulation in rice and mitigation strategies. *Plant Soil.*, 446: 1–21 **(21 pages)**.

#### AUTHOR (S) BIOSKETCHES

**Chanpiwat, P.**, Ph.D., Assistant Professor, <sup>1</sup>Environmental Research Institute, Chulalongkorn University, Phayathai Road, Pathumwan, Bangkok 10330, Thailand. <sup>2</sup>Center of Excellence in Environmental Innovation and Management of Metals (EnvIMM), Chulalongkorn University, Phayathai Road, Pathumwan, Bangkok 10330, Thailand.

- Email: [Penradee.C@chula.ac.th](mailto:Penradee.C@chula.ac.th)
- ORCID: [0000-0001-7625-0952](https://orcid.org/0000-0001-7625-0952)
- Web of Science ResearcherID: HJY-5028-2023
- Scopus Author ID: 35490058800
- Homepage: <https://eric.chula.ac.th/profile/id/penradee.chanpiwat>

**Numprasanthai, A.**, Ph.D., Assistant Professor, <sup>2</sup>Center of Excellence in Environmental Innovation and Management of Metals (EnvIMM), Chulalongkorn University, Phayathai Road, Pathumwan, Bangkok 10330, Thailand. <sup>3</sup>Department of Mining and Petroleum Engineering, Faculty of Engineering, Chulalongkorn University, Phayathai Road, Pathumwan, Bangkok 10330, Thailand.

- Email: [Apisit.Nu@chula.ac.th](mailto:Apisit.Nu@chula.ac.th)
- ORCID: [0000-0001-6432-0650](https://orcid.org/0000-0001-6432-0650)
- Web of Science ResearcherID: AAA-1335-2020
- Scopus Author ID: 54987315400
- Homepage: <https://www.eng.chula.ac.th/th/staff/asst-prof-apisit-numprasanthai-ph-d>

#### HOW TO CITE THIS ARTICLE

Chanpiwat, P.; Numprasanthai, A., (2024). Factors affecting cadmium toxicity to rice germinated in soils collected from downstream areas of abandoned zinc mines. *Global J. Environ. Sci. Manage.*, 10(1): 133-154.

DOI: [10.22034/gjesm.2024.01.10](https://doi.org/10.22034/gjesm.2024.01.10)

URL: [https://www.gjesm.net/article\\_706724.html](https://www.gjesm.net/article_706724.html)





ORIGINAL RESEARCH PAPER

## Impact of environmental and geographical position on the chemometric classification of ethanol extracts from *Isotoma longiflora* leaves

E. Imelda<sup>1</sup>, K. Khairan<sup>2</sup>, R.R. Lubis<sup>3</sup>, T. Karma<sup>4</sup>, R. Idroes<sup>2\*</sup>

<sup>1</sup> Graduate School of Mathematics and Applied Sciences, Universitas Syiah Kuala, Banda Aceh 23111, Indonesia

<sup>2</sup> Department of Pharmacy, Faculty of Mathematics and Natural Sciences, Universitas Syiah Kuala, Banda Aceh 23111, Indonesia

<sup>3</sup> Department of Ophthalmology, Faculty of Medicine, Universitas Sumatera Utara, Medan 20222, Indonesia

<sup>4</sup> Department of Occupational Health and Safety, Faculty of Health Sciences, Abulyatama University, Banda Aceh 23372, Indonesia

### ARTICLE INFO

#### Article History:

Received 17 February 2023

Revised 23 May 2023

Accepted 28 June 2023

#### Keywords:

Chemometrics

*Isotoma longiflora*

Spectroscopy

Principal component analysis

### ABSTRACT

**BACKGROUND AND OBJECTIVES:** *Isotoma longiflora* L is commonly used as a medicinal plant by the local community in Indonesia, and its geographical position determines its bioactive compounds and hence its efficacy. Ethanol extracts of *Isotoma longiflora* leaves from various locations in Aceh Province were analyzed using a simple infrared spectroscopy technique combined with chemometrics to determine the effect of geographical location and conditions by classification and authentication.

**METHODS:** *Isotoma longiflora* leaf samples were collected from Aceh Besar (a geothermal manifestation of Ie Suum), Banda Aceh, Aceh Jaya, Bireun, and Central Aceh. Principal component analysis was used to categorize the ethanol extract of *Isotoma longiflora* leaves, and a linear discriminant analysis was used for authentication.

**FINDINGS:** The principal component analysis score plot indicated 89 percent of total data variance and that the samples formed three distinct groups: group I consisting of Aceh Tengah and Bener Meriah samples; group II of Aceh Besar and Banda Aceh samples; and group III of Aceh Selatan, Aceh Barat Daya, Aceh Jaya, and Bireun. A linear discriminant analysis was then used to validate these results, and the linear discriminant analysis model derived from the cross-validation predicted the origin of *Isotoma longiflora* samples with 100 percent accuracy rate.

**CONCLUSION:** The *Isotoma longiflora* leaf extracts were successfully classified using Fourier-transform infrared spectroscopy data processed through chemometric calculations (namely, principal component analysis). Based on the cross-validation using linear discriminant analysis showed that the prediction model had a 100 percent accuracy. The present study thus revealed the effect of geographical location on the composition of bioactive compounds in *Isotoma longiflora*, suggesting the potential of chemometric techniques for quality control and assurance in traditional medicine.

DOI: [10.22034/gjesm.2024.01.11](https://doi.org/10.22034/gjesm.2024.01.11)

This is an open access article under the CC BY license (<http://creativecommons.org/licenses/by/4.0/>).



NUMBER OF REFERENCES

45



NUMBER OF FIGURES

6



NUMBER OF TABLES

5

\*Corresponding Author:

Email: [rinaldi.idroes@usk.ac.id](mailto:rinaldi.idroes@usk.ac.id)

Phone: +62 819-7374-4077

ORCID: [0000-0003-2264-6358](https://orcid.org/0000-0003-2264-6358)

Note: Discussion period for this manuscript open until April 1, 2024 on GJESM website at the "Show Article".

## INTRODUCTION

Medicines derived from natural sources are among the most common alternative treatments used in communities in Indonesia. According to the World Health Organization, approximately 80 percent (%) of the world's population uses natural medicines (Gutierrez et al., 2022). Moreover, approximately 80% of the world's plant species can be found in Indonesia, a country with a rich biodiversity of between 25,000 and 30,000 plant species. Natural remedies have been used for thousands of years in Indonesia, before the discovery of modern medicine, and this includes the *Isotoma longiflora* plant. The compounds found in *Isotoma longiflora* leaves contain antioxidants that can neutralize free radicals (Imelda et al., 2022). These antioxidants have multiple applications, including the inhibition of the progression of cataracts or cataractogenesis process (Arrigoni-Blank et al., 2002). Phytochemical studies have revealed that *Isotoma longiflora* leaves contain numerous active compounds, specifically phenolic compounds and flavonoids, which confer antiproliferative, antioxidant, and antibacterial properties (Imelda et al., 2022; Onuigbo et al., 2023). The *Isotoma longiflora* plant can readily grow in multiple locations with sufficient water content, and its leaves can be found in almost every location in Aceh Province, Indonesia. The chemical composition of *Isotoma longiflora* leaves originating from various locations in Aceh Province probably differ in terms of the types and amounts of chemical compounds. As the geographical conditions of Aceh Province are quite diverse, these differences must be analyzed. A previous research on differences in chemical content and geographical origin indicated that secondary metabolites are the result of interactions between plants and their environment, and that the correlation between plants and their environment has a more significant impact on the content of secondary metabolites than on that of primary metabolites (Liu et al., 2008). Both biotic and abiotic environmental factors influence the biosynthesis of secondary metabolites, and abiotic stress factors play a role in decreasing the production of secondary metabolites in medicinal plants (Li et al., 2020). As the secondary metabolites profile is altered due to the influence of environmental factors, a change in bioactivity of the medicinal plant should also be expected. Other reports have stated that plants

interact with their surrounding abiotic environments during growth and development, including water, soil, light, temperature, and chemicals (Verma and Shukla, 2015). Certain abiotic conditions such as drought, flooding, extreme temperatures, and the presence of toxic chemical elements in the soil will cause stress to medicinal plants and variations in the biosynthesis process (Li et al., 2020). Fourier-transform infrared spectroscopy (FTIR) may be useful for identifying plants from different environments as the infrared (IR) spectrum is a fingerprint pattern characteristic of the plant's chemical composition (Sanchez et al., 2018). However, a multivariate statistical approach is necessary for extracting the necessary information from the FTIR spectrum data. Previous studies have reported the results of a combination of FTIR and chemometric methods to identify plants or their geographical origins, including carobs (Christou et al., 2018), *Chomolaena odorata* L (Abubakar et al., 2021), among others (Zulkifli et al., 2023). In addition to analyzing geographical origin, chemometric techniques have also been used for taxonomic discrimination of closely related plants, such as *Panax ginseng* varieties (Liu et al., 2008). Linear discriminant analysis (LDA) has been used for the authentication of red ginger plants (Purwakusumah et al., 2014), horse milk (Arifah et al., 2022), vegetable oils (Jamwal et al., 2021), and beef meatballs (Lestari et al., 2022). Despite the numerous studies conducted to date, there has been no research on the classification and authentication of *Isotoma longiflora* plants originating from various geographical locations. Considering this context, the identification and authentication of *Isotoma longiflora* plants from multiple locations in Aceh Province was performed as a reference for determining the development and quality control of this plant species, which has the potential to be used as a medicinal plant. Therefore, the aim of this study was to construct a chemometric model for the classification of *Isotoma longiflora* collected from different geographical locations. This study was conducted in Banda Aceh, Indonesia, between 2022 and 2023.

## MATERIALS AND METHODS

### Study design

*Isotoma longiflora* plant extract samples from the Aceh Province regencies, including Aceh Besar (AB),

Table 1: Comparison of previously used chemometric methods based on infrared spectra

Sample	Determination	Chemometrics	Sources
Green tea	Geographical origins and processing duration	PCA, PLS-DA, SVM	Liu <i>et al.</i> , 2022
Wine	Geographical origins	PCA, SIMCA, DA	Hu <i>et al.</i> , 2019
Walnut	Geographical origins	PCA, MSC	Arndt <i>et al.</i> , 2020
Tea	Quality control	SIMCA	Zhu <i>et al.</i> , 2019
Sea bass	Geographical origins and quality control	PCA, PLS-DA	Ghidini <i>et al.</i> , 2019
Chestnut	Geographical origins	PLS-DA, SIMCA	Nardecchia <i>et al.</i> , 2020

Note: Discriminant analysis (DA); multiplicative scatter correction (MSC); partial least squares (PLS); soft independent modelling by class analogy (SIMCA); support vector machine (SVM).

Table 2: Sampling locations of *Isotoma longiflora* leaves

No.	Regency	Sample code	Coordinate point	
			Latitude	Longitude
1	Aceh Besar	AB1	5.553216	95.538757
		AB2	5.553216	95.538757
		AB3	5.553216	95.538757
2	Aceh Jaya	AJ1	4.878547	95.400946
		AJ2	4.878547	95.400946
		AJ3	4.878547	95.400946
3	Bireun	B1	5.200639	96.589414
		B2	5.200639	96.589414
		B3	5.200639	96.589414
4	Aceh Tengah	AT1	4.684952	96.738941
		AT2	4.684952	96.738941
		AT3	4.684952	96.738941
5	Banda Aceh	BA1	5.545702	95.351652
		BA2	5.545702	95.351652
		BA3	5.545702	95.351652
6	Bener Meriah	BM1	4.788848	96.736809
		BM2	4.788848	96.736809
		BM3	4.788848	96.736809
7	Aceh Barat Daya	ABD1	3.703605	96.851830
		ABD2	3.703605	96.851830
		ABD3	3.703605	96.851830
8	Aceh Selatan	S1	3.061044	97.325568
		S2	3.061044	97.325568
		S3	3.061044	97.325568

Aceh Jaya (AJ), Biereun (B), Aceh Tengah (AT), Banda Aceh (BA), and Bener Meriah (BM) were obtained. An FTIR instrument was used on each extract to acquire its infrared spectrum at a wavelength of 4000/centimeter (cm) – 400/cm. The spectrum obtained was then analyzed chemometrically using the Unscrambler 10.4 application software (Omar *et al.*, 2019). A comparison of previously employed chemometric methods for analyzing infrared spectra is presented in Table 1.

#### Extract preparation

*Isotoma longiflora* leaf samples were obtained from five locations in Aceh Province, and three

1-kilogram samples were collected from each geographical location. Details on sampling locations are presented in Table 2. The *Isotoma longiflora* leaf samples were washed and air-dried for 14 d. The samples were stored for less than 1 week from collection to treatment. After cleaning, the samples were ground into a fine powder using the maceration method for 48 hours with 70% ethanol. The sample was filtered after 48 hours to obtain the filtrate, was then diluted using a rotary evaporator to obtain a thick extract of *Isotoma longiflora* leaves.

#### FTIR spectrum acquisition

The FTIR spectrometer was calibrated using

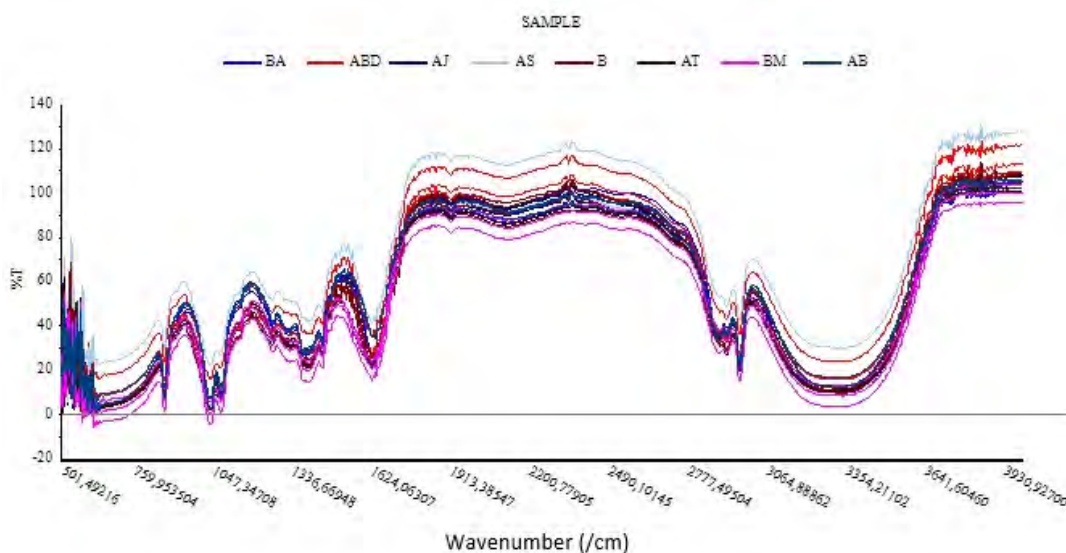


Fig. 1: FTIR spectra of ethanol extracts from *Isotoma longiflora* leaves

a polystyrene film, and the spectral data were compared with those from the National Institute of Standards and Technology. The *Isotoma longiflora* leaf powder sample was analyzed at a 4000–400/cm wavelength, yielding a total of 18 FTIR spectra. The obtained spectral data were saved in Excel (xlsx) for analysis (Cebi *et al.*, 2021; Khanban *et al.*, 2022; Sufriadi *et al.*, 2023; Tan *et al.*, 2021).

#### Chemometric analysis

Each FTIR spectrum underwent data preprocessing using the first derivative method to develop a discriminant model to identify the origin of the sample using wavelengths of 500–4000/cm. Unscrambler Hierarchical cluster analysis (HCA), principal component analysis (PCA), and LDA 10.4 were performed (Adi *et al.*, 2020; Akbar *et al.*, 2021; Arifah *et al.*, 2022; Nadia *et al.*, 2019). Data validation was performed using cross-validation in the LDA model. The equations used in this analysis follow those of a previous study (Chauhan *et al.*, 2021).

## RESULTS AND DISCUSSION

### FTIR spectrum of the *Isotoma longiflora* leaf extract

Identification by infrared spectroscopy is based on the specific vibrational frequencies of certain molecular functional groups (Mellado-Mojica *et*

*al.*, 2016). A previous study acquired the infrared spectrum (wavelength of 4000–500/cm) from ethanol extracts of *Isotoma longiflora* leaves from multiple locations (Christou *et al.*, 2018). Fig. 1 shows the FTIR spectrum of the ethanol extract of *Isotoma longiflora* leaves obtained in the present study.

Fig. 1 shows that the leaves from various locations exhibited the same spectral absorbance pattern, indicating that all samples had identical functional groups. The absorbance at wavelengths of 3000–3700/cm indicates the presence of hydroxyl (O-H) and amine (N-H) functional groups from polysaccharides and proteins (Christou *et al.*, 2018). The bands at 2927/cm and 2935/cm indicate asymmetrical or symmetrical strain to the methylene (CH<sub>2</sub>) functional group. The alkene (C=C) functional group was observed at a wavelength of 1680–1600/cm, whereas the C=C aromatic functional group was observed at wavelength of 1600–1475/cm, the methyl (CH<sub>3</sub>) functional group was observed at wavelength of 1400–1325/cm, and the alkoxy (C-O) functional group was observed at wavelength of 1100–1000/cm (Dogan *et al.*, 2007; Rohman *et al.*, 2011; Rohman and Man, 2010). The global functional categories are listed in Table 3. The absorption peaks from the FTIR spectra of leaves did not vary among locations. Fig. 1 shows that the difference between the samples was

Table 3: Typical peaks in the *Isotoma longiflora* leaf FTIR spectrum

Spectral wavelength (/cm)								Functional Group/ Assignment
AB	BA	AJ	B	AT	BM	ABD	AS	
3361	3342	3331	3330	3338	3342	3331	3330	Bonded O-H Stretching / N-H stretching (Suresh <i>et al.</i> , 2016)
2978	2978	2976	2975	2972	2978	2978	2976	CH <sub>3</sub> symmetric stretching; lipid, protein (Suresh <i>et al.</i> , 2016)
2897	2902	2922	2922	2931	2922	2922	2931	CH <sub>2</sub> asymmetric stretching; mainly lipid and protein (Suresh <i>et al.</i> , 2016)
1658	1643	1639	1638	1643	1639	1638	1643	Stretching carbonyl (C=O) (Smith <i>et al.</i> , 2019)
1633	1627	1633	1634	1622	1633	1634	1622	Assigned to tannins (Smith <i>et al.</i> , 2019) C=C aromatic of condensed tannins (Smith <i>et al.</i> , 2019) C=O stretching in flavones (Hands <i>et al.</i> , 2016) C=O stretching in flavonoids (Smith <i>et al.</i> , 2019) C=C stretching of the aromatic ring (Smith <i>et al.</i> , 2019) N-H bending/C-N stretching (Topalä <i>et al.</i> , 2017)
1456	1456	1456	1456	1448	1456	1456	1448	Amide II of proteins, N-H, alkylamine (C-N) (Thummajitsakul <i>et al.</i> , 2020)
1379	1379	1406	1402	1406	1379	1379	1406	Primary or secondary O-H bending (inplane), and phenol or tertiary alcohol (O-H bend) (Thummajitsakul <i>et al.</i> , 2020)
1332	1332	1334	1336	1340	1332	1334	1336	CH <sub>3</sub> bending (Thummajitsakul <i>et al.</i> , 2020)
1086	1056	1083	1076	1080	1056	1083	1076	C-O stretching vibrations in acid or ester (Thummajitsakul <i>et al.</i> , 2020)

negligible. The absorption intensity of the functional groups differentiated the FTIR spectra of *Isotoma longiflora* leaf samples.

#### Chemometric analysis

Preprocessing was performed on the FTIR spectrum data of the ethanol extract of *Isotoma longiflora* leaves using the Derivative First method. Fig. 3 illustrates the original and preprocessed FTIR spectra using the Savitzky-Golay transform. This first-derivative method can be used to clarify the peaks and valleys of the FTIR/NIR spectra, separate the overlapping peaks, and eliminate the effects of spectral variations. Moreover, the first derivative can be used to remove the background, increase spectral resolution, and eliminate noise caused by differences in particle size in the extract (Akbar *et al.*, 2021; Cen and He, 2007).

#### Principal component analysis

The PCA was used to classify the *Isotoma longiflora* leaf samples from various locations. It is an unsupervised pattern recognition technique that can be used to reduce data and examine information to identify factors that can explain trends in a dataset (Gad *et al.*, 2013). As PCA can be used to construct discriminant models for closely related plants, it was herein used with the Unscrambler 10.4 application to classify and differentiate the leaf extracts from plants grown in locations with different geographical conditions. Fig. 2 shows that the total variance of PC-1 and PC-2 was 89%. The decomposition of spectral data using PCA, where the Y axis displays the number of principal components (PC) and the x-axis displays the proportion of variance explained by the PC, showed that PC-1 explained 79% of the data variance and PC-2 explained 10% of the data

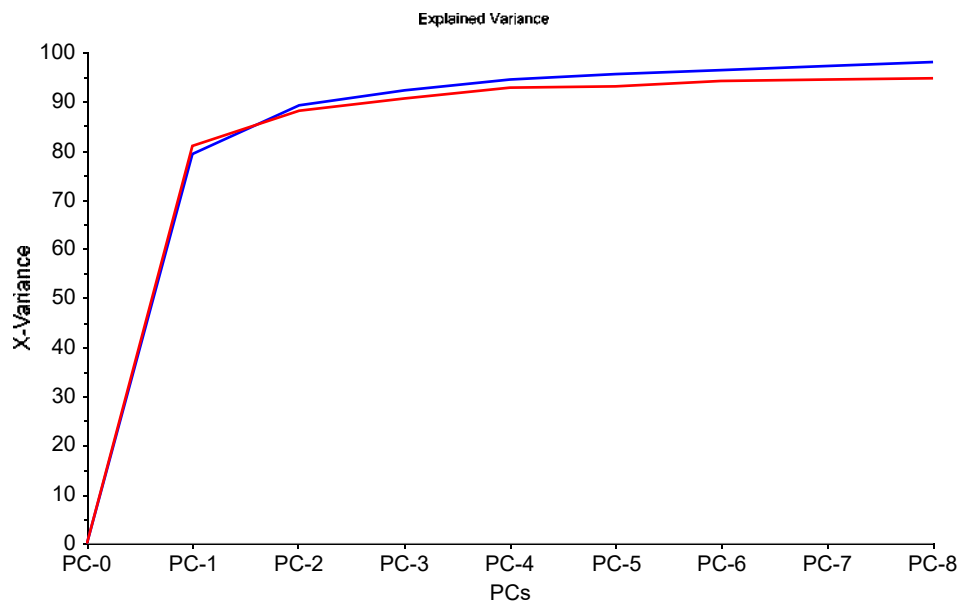


Fig. 2: Results of data variance that PCA can explain

variance. The total percentage of data variance was determined by accumulating the total percentage of variance specified by the previous PC-n and PC (dos Santos Grasel et al., 2016).

Fig. 3 shows the PCA score plot, which revealed the formation of three groups: group I with the AT and BM samples, group II with AB and BA samples, and group III with AS, ABD, AJ, and B samples. These results indicated that the various locations where the *Isotoma longiflora* plants grew corresponded to distinct leaf samples. The samples in group I were from the highlands (mountains), and the pattern of chemical contents in leaves from AT and BM were similar. In contrast, group II (AB and BA) comprised samples from locations far from the coast, whereas group III comprised samples from coastal regions. These results indicate that *Isotoma longiflora* leaf characteristics are influenced by the plants' collection location. This can occur because environmental factors strongly influence the secondary metabolite content of a plant, and the synthesis of secondary plant metabolites is affected by the plant's response to the environment (Gargallo-Garriga et al., 2014; Sampaio et al., 2016). Moreover, abiotic stresses such as the influence of light, temperature, humidity, water availability, nutrients, and salinity in the soil have

been shown to significantly affect the content of secondary metabolites in plants (Bernstein et al., 2010; Khan et al., 2016; Sampaio et al., 2016). The FTIR-chemometric combination has been previously used to identify and authenticate samples. For instance, a study that successfully identified differences in coffee leaves obtained from various locations with different climatic conditions using PCA was based on differences in the FTIR spectra (Sanchez et al., 2018). The results demonstrated that FTIR spectrum analysis with PCA successfully distinguished coffee leaves taken from locations with different climatic conditions. In another study, FTIR spectra were analyzed using the PCA multivariate statistical method, and cluster analysis can be used to distinguish *Fagus sylvatica* L plants from different growth habitats (Rana et al., 2008). Another study stated that FTIR spectroscopy combined with chemometric methods was suitable for distinguishing among different geographical origins (Zhao et al., 2015). Fig. 4 depicts the loading factor, which is essential because it provides information regarding the factors that influence the formation of the PCA score plots (dos Santos Grasel et al., 2016). The loading factor indicated that PC1 had two types of loadings: positive and negative coefficient

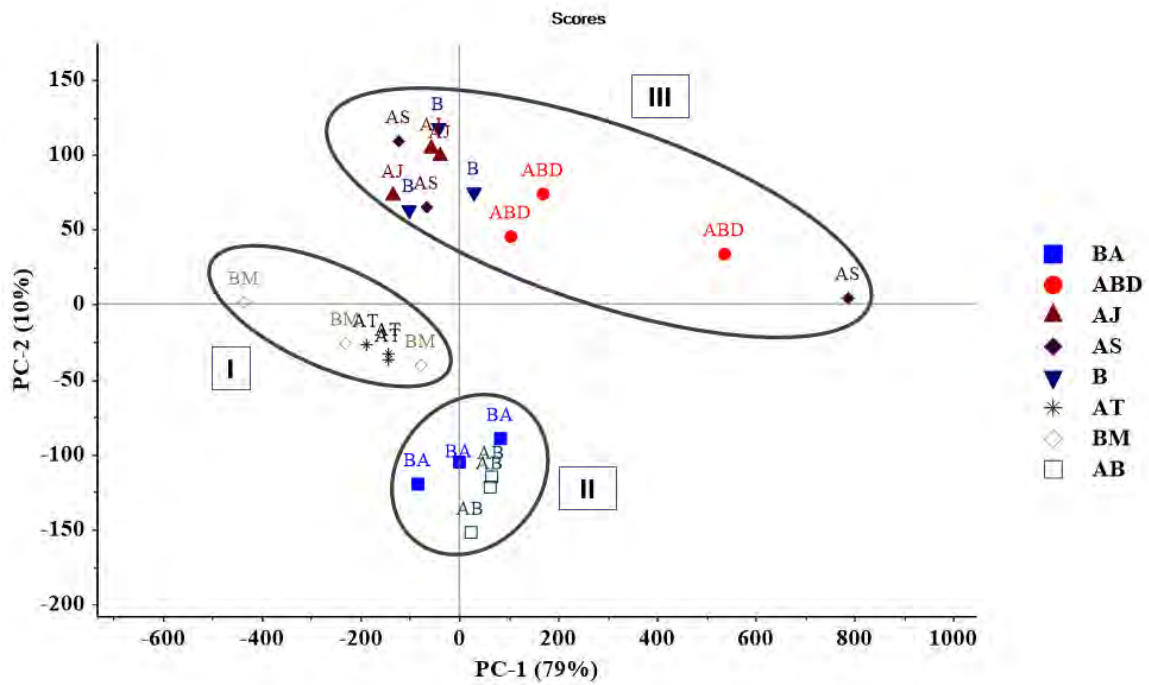


Fig. 3: PCA score plots for the FTIR spectra generated by the ethanolic extract *Isotoma longiflora* leaves

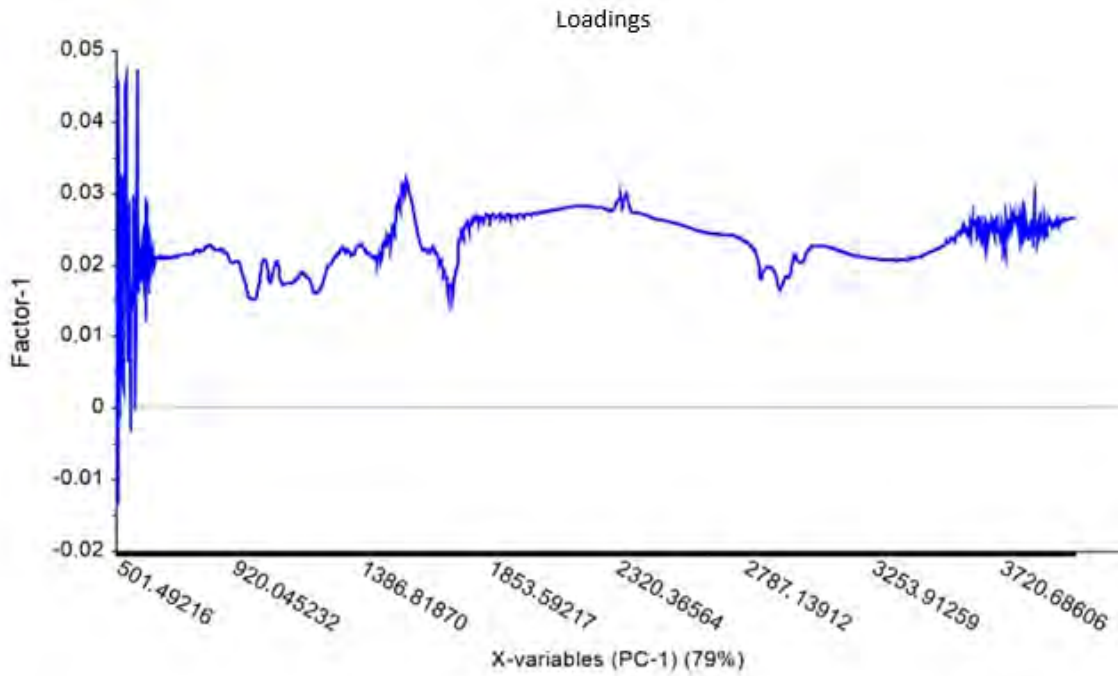


Fig. 4: Loading factor plots PC-1 and PC-2

### Chemometric classification of *Isotoma longiflora* extract

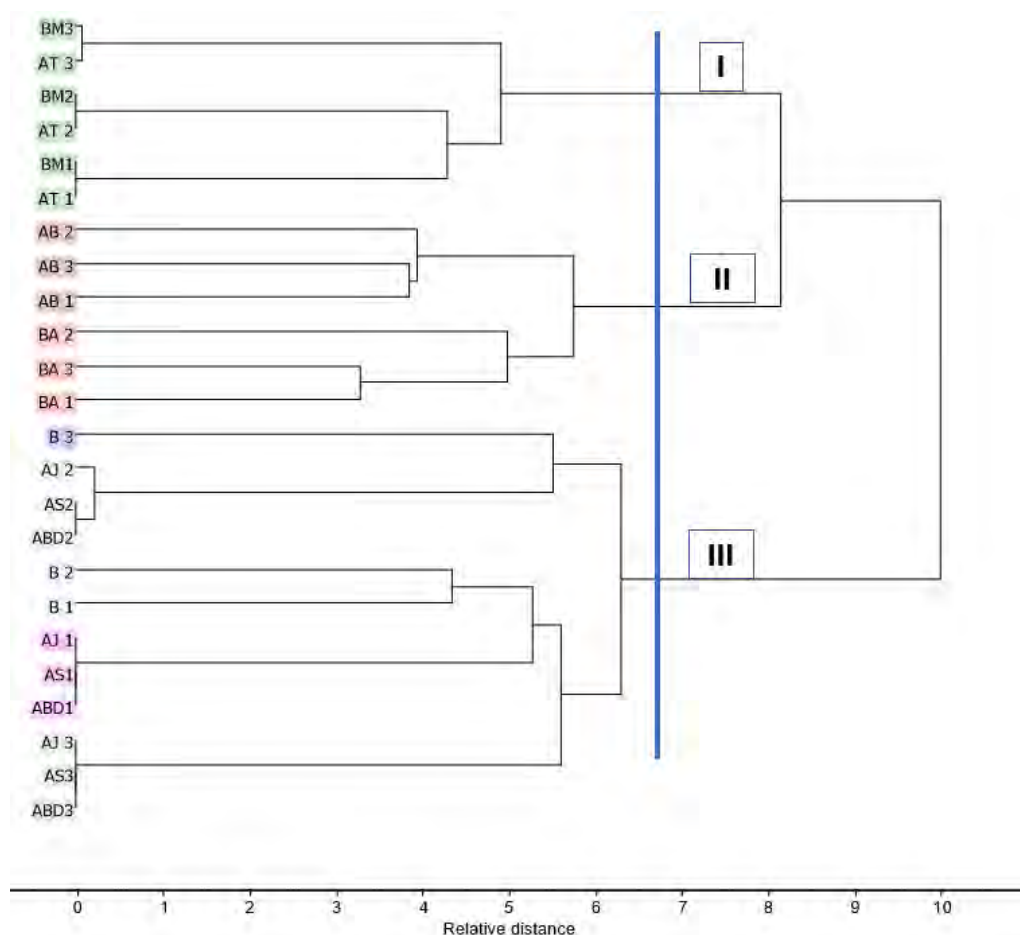


Fig. 5: Dendrogram of FTIR data of the ethanol extract of *Isotoma longiflora* leaves from several locations

values. The spectral band absorptions determined the position of the samples in the PCA score plot. For the PC-1 loading (positive coefficient), several positive absorption bands were dominant, namely at wavelengths 1103/cm, 2997/cm, 2910/cm, 2835/cm, 1573/cm, and 1692/cm. Several functional groups were identified, including C-O, CH<sub>3</sub>, CH<sub>2</sub>, C=O, and C=C. In contrast, loading with a negative coefficient value produced absorption that was dominant at wavelengths below 600/cm, which is in the fingerprint region, thus hindering the identification of functional groups. The loading factor provides information on the wavelengths of the samples. These absorption bands appeared on the loading factor that determined the position of the sample in the PCA plot, indicating that the classification of the ethanol extract of *Isotoma*

*longiflora* leaf samples produced in the PCA plot was influenced by the similarity in some absorptions of the infrared spectra.

#### Hierarchical cluster analysis

HCA was used to confirm the results obtained from the PCA and provide a clearer picture of the similarities and differences among the *Isotoma longiflora* leaf extracts. The HCA results are shown in Fig. 5. Three groups were formed: group I with the AT and BM samples; group II with the AB and BA samples; and group III with the AS, ABD, AJ, and B samples.

#### Linear discriminant analysis

LDA authentication was performed to determine the characteristics of the groups formed in the

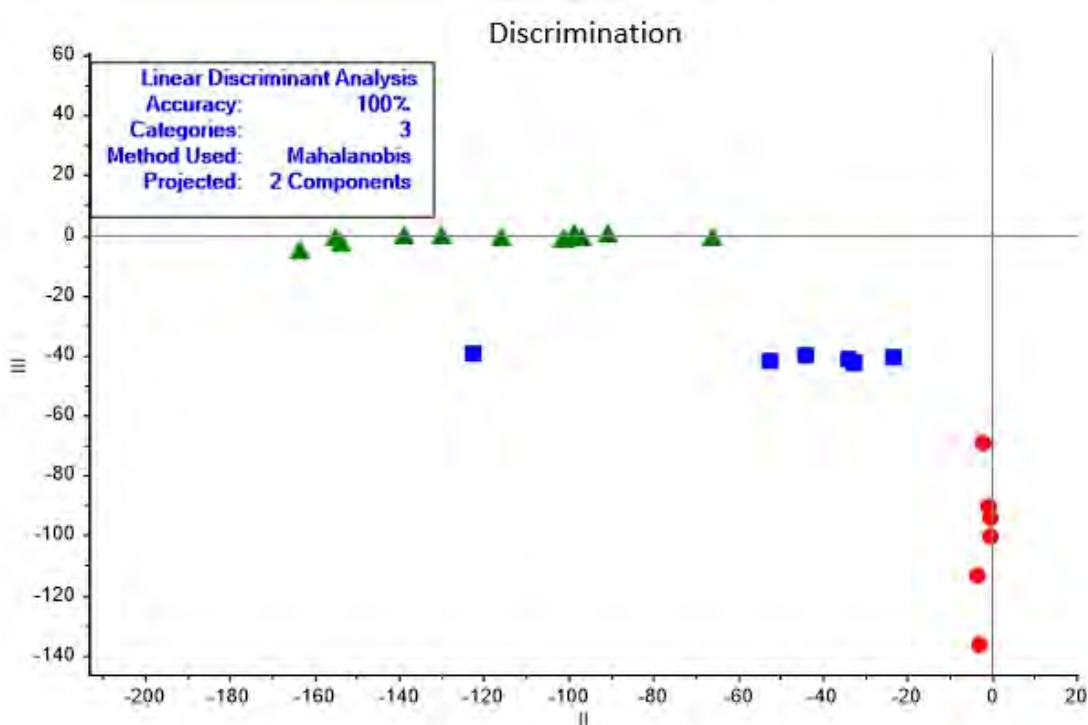


Fig. 6: LDA plot scores

Table 4: Confusion matrix

	Actual	II	III	I
Predicted		1	2	3
II	1	6	0	0
III	2	0	12	0
I	3	0	0	6

PCA (Fig. 6). The LDA prediction model had a 100% accuracy rate, and the LDA model based on the cross-validation results correctly predicted the origin group of *Isotoma longiflora* leaf samples. The confusion matrix for the LDA score plot is in Table 4.

The absence of incorrectly predicted groups indicates that the authentication using LDA was accurate, as supported by the confusion matrix table. The LDA model also demonstrates

a reasonable degree of precision. The LDA calculations that influenced the confusion matrix are presented in Table 5. However, the precise components of the extract were not identified, as retrieving this information would require more complex procedures and many resources. Nevertheless, the chemometric approach might provide an alternative for observing the components of the extract, and hence, its potential use in quality control.

Table 5: Prediction results of the LDA model

Sample	LDA Model			Predicted
	I	II	III	
BA 1	-1183.44	-0.62295	-90.6374	II
BA 2	-2363.75	-3.28124	-113.658	II
BA 3	-379.578	-2.22572	-69.1505	II
ABD1	-3861.08	-66.0575	-1.70126	III
ABD2	-7280.79	-100.863	-2.44604	III
ABD3	-7013.67	-90.5694	-0.31428	III
AJ 1	-3876.14	-115.715	-1.61352	III
AJ 2	-7350.3	-138.922	-1.13064	III
AJ 3	-7031.2	-129.93	-0.75488	III
AS1	-3870.99	-96.9194	-1.47946	III
AS2	-7278.33	-163.261	-5.94169	III
AS3	-7039.81	-154.827	-1.27146	III
B 1	-3523.77	-101.374	-2.11552	III
B 2	-5689.31	-98.4065	-0.04601	III
B 3	-9061.34	-153.558	-3.18524	III
AT 1	-1.02229	-44.0626	-39.7827	I
AT 2	-1.78893	-32.4606	-42.6708	I
AT 3	-0.2388	-33.7401	-41.1731	I
BM1	-1.86294	-23.3225	-40.9473	I
BM2	-1.45359	-52.1477	-41.8311	I
BM3	-3.63345	-122.439	-39.1942	I
AB 1	-1562.17	-0.54158	-100.637	II
AB 2	-1274.18	-0.41189	-94.1179	II
AB 3	-3510.66	-2.91662	-136.738	II

## CONCLUSION

The extracts from *Isotoma longiflora* leaves were successfully classified based on their FTIR spectra using a chemometric approach. The PCA score plot accounted for 89% of the total data variance, and showed the formation of three groups: group I included samples from Central Aceh and Bener Meriah; group II included samples from Aceh Besar and Banda Aceh; and group III included samples from South Aceh, West Aceh Daya, Aceh Jaya, and Bireuen. The differences among the extract samples were confirmed by the HCA results, providing a

clearer picture of the similarities and differences in the observed *Isotoma longiflora* leaf extracts. Authentication was performed using LDA based on the results of the PCA classification with cross-validation of the training and validation sets. The LDA results revealed that the LDA model derived from the cross-validation predicted the origin of the *Isotoma longiflora* samples with 100% accuracy. These findings successfully demonstrate that the geographical conditions of origin affect the composition of the bioactive compounds in *Isotoma longiflora*. The findings of this study suggest the

potential use of FTIR and chemometric spectroscopy to determine the origin of plants, which can be beneficial for the pharmaceutical industry. The chemometric-assisted classification technique could be significant for quality control and assurance, allowing the quality of drug materials (especially from traditional medicine) to be authenticated. This technique is also useful for differentiating among products produced at certain locations, which affects supply chain management, especially when determining the source of the raw material. Further research is required to explore the impact of factors such as climate and soil conditions on the bioactive compounds in *Isotoma longiflora* leaves and other plants. Employing a greater variety of geographical locations can help generate a more comprehensive dataset. These findings can also provide insights into environmental management, to select locations that are suitable for medicinal plant cultivation.

#### AUTHOR CONTRIBUTIONS

E. Imelda contributed in the conceptualization, experiment, and original-draft writing. K. Khairan acted as a supervisor and contributed in reviewing the final version of the manuscript. R.R. Lubis acted as a supervisor and contributed in reviewing the final version of the manuscript. P. Kemala performed the scientific, results validation, and reviewing the final version of the manuscript. U. Zulfiani performed the scientific, results validation, and reviewing the final version of the manuscript. U. Zulfiani assisted the experiment and performed formal analysis. T. Karma assisted the experiment and performed formal analysis. S. Rahayu assisted the experiment and performed formal analysis. G.M. Idroes performed the scientific, results validation, and reviewing the final version of the manuscript. S.M. Adev performed the scientific, results validation, and reviewing the final version of the manuscript. N.B. Maulydia performed the scientific, results validation, and reviewing the final version of the manuscript. R. Idroes acted as a supervisor and contributed in reviewing the final version of the manuscript.

#### ACKNOWLEDGEMENT

Authors appreciate the assistance from Universitas Syiah Kuala for the research facilities.

#### CONFLICT OF INTEREST

The authors declare no conflicts of interest regarding the publication of this manuscript. In addition, ethical issues, including plagiarism, informed consent, misconduct, data fabrication and/or falsification, double publication and/or submission, and redundancy, were observed by the authors.

#### OPEN ACCESS

©2024 The author(s). This article is licensed under a Creative Commons Attribution 4.0 International License, which permits use, sharing, adaptation, distribution and reproduction in any medium or format, as long as you give appropriate credit to the original author(s) and the source, provide a link to the Creative Commons license, and indicate if changes were made. The images or other third-party material in this article are included in the article's Creative Commons license, unless indicated otherwise in a credit line to the material. If material is not included in the article's Creative Commons license and your intended use is not permitted by statutory regulation or exceeds the permitted use, you will need to obtain permission directly from the copyright holder. To view a copy of this license, visit: <http://creativecommons.org/licenses/by/4.0/>

#### PUBLISHER'S NOTE

GJESM Publisher remains neutral with regard to jurisdictional claims in published maps and institutional affiliations.

#### ABBREVIATIONS

%	Percent
AB	Aceh Besar
AJ	Aceh Jaya
AT	Aceh Tengah
B	Biereun
BA	Banda Aceh
BM	Bener Meriah
C=C	Alkene
CH <sub>2</sub>	Methylene
CH <sub>3</sub>	Methyl

cm	Centimeter
C-N	Alkylamine
C-O	Alkoxy
C=O	Carbonyl
DA	Discriminant analysis
IR	Infrared
Fig.	Figure
FTIR	Fourier-transform infrared spectroscopy
HCA	Hierarchical cluster analysis
LDA	Linear discriminant analysis
MSC	<ultiplicative scatter correction
N-H	Amine
O-H	Hydroxyl
PC	Principal component
PCA	Principal component analysis
PLS	Partial least squares
SIMCA	Soft independent modelling by class analogy
SVM	Support vector machine

## REFERENCES

- Abubakar, A.; Yusuf, H.; Syukri, M.; Nasution, R.; Karma, T.; Munawar, A.; Idroes, R., (2021). Chemometric classification of geothermal and non-geothermal ethanol leaf extract of seurapoh (*Chromolaena odorata* Linn) using infrared spectroscopy. IOP Conference Series: Earth Environ. Sci., 667: 012070 (8 pages).
- Adi, D.S.; Hwang, S.-W.; Pramasari, D.A.; Amin, Y.; Cipta, H.; Damayanti, R.; Dwianto, W.; Sugiyama, J., (2020). Anatomical properties and near infrared spectra characteristics of four shorea species from Indonesia. HAYATI J. Biosci., 27: 247-257 (11 pages).
- Akbar, Z.; Idroes, R.; Ginting, B.; Karma, T.; Rahimah, S.; Helwani, Z.; Yusuf, M., (2021). Identification of Gayo arabic coffee beans and powder using the FTIR-PCA combination method. IOP Conference Series: Mater. Sci. Eng., 1087: 012059 (8 pages).
- Arifah, M.F.; Nisa, K.; Windarsih, A.; Rohman, A., (2022). The application of FTIR spectroscopy and chemometrics for the authentication analysis of horse milk. Int. J. Food Sci., 2022: 7643959 (9 pages).
- Arndt, M.; Drees, A.; Ahlers, C.; Fischer, M., (2020). Determination of the geographical origin of walnuts (*Juglans regia* L.) using near-infrared spectroscopy and chemometrics. Foods. 9(12): 1860 (15 pages).
- Arrigoni-Blank, M.D.F.; Oliveira, R.L.B.; Mendes, S.S.; Silva, P.D.A.; Antonioli, Â.R.; Vilar, J.C.; Cavalcanti, S.C.D.H.; Blank, A.F., (2002). Seed germination, phenology, and antiedematogenic activity of *Peperomia pellucida* (L.) HBK. BMC Pharmacol., 2: 1-8 (8 pages).
- Bernstein, N.; Kravchik, M.; Dudai, N., (2010). Salinity-induced changes in essential oil, pigments and salts accumulation in sweet basil (*Ocimum basilicum*) in relation to alterations of morphological development. Ann. App. Biol., 156: 167-177 (12 pages).
- Cebi, N.; Arici, M.; Sagdic, O., (2021). The famous Turkish rose essential oil: Characterization and authenticity monitoring by FTIR, Raman and GC-MS techniques combined with chemometrics. Food Chem., 354: 129495 (10 pages).
- Cen, H.; He, Y., (2007). Theory and application of near-infrared reflectance spectroscopy in determination of food quality. Trends Food Sci. Technol., 18: 72-83 (12 pages).
- Chauhan, R.; Kumar, R.; Kumar, V.; Sharma, K.; Sharma, V., (2021). On the discrimination of soil samples by derivative diffuse reflectance UV-vis-NIR spectroscopy and chemometric methods. Forensic Sci. Int., 319: 110655 (12 pages).
- Christou, C.; Agapiou, A.; Kokkinofa, R., (2018). Use of FTIR spectroscopy and chemometrics for the classification of carobs origin. J. Adv. Res., 10: 1-8 (8 pages).
- Dogan, A.; Siyakus, G.; Severcan, F., (2007). FTIR spectroscopic characterization of irradiated hazelnut (*Corylus avellana* L.). Food Chem., 100: 1106-1114 (9 pages).
- dos Santos Grasel, F.; Ferrão, M.F.; Wolf, C.R., (2016). Development of methodology for identification the nature of the polyphenolic extracts by FTIR associated with multivariate analysis. Spectrochim. Acta A Mol. Biomol. Spectrosc., 153: 94-101: (8 pages).
- Gad, H.A.; El-Ahmady, S.H.; Abou-Shoer, M.I.; Al-Azizi, M.M., (2013). Application of chemometrics in authentication of herbal medicines: a review. Phytochem Anal., 24: 1-24 (24 pages).
- Gargallo-Garriga, A.; Sardans, J.; Pérez-Trujillo, M.; Rivas-Ubach, A.; Oravec, M.; Vecerova, K.; Urban, O.; Jentsch, A.; Kreyling, J.; Beierkuhnlein, C., (2014). Opposite metabolic responses of shoots and roots to drought. Sci. Rep., 4: 6829 (7 pages).
- Ghidini, S.; Varrà, M.O.; Dall'Asta, C.; Badiani A.; Ianieri, A.; Zanardi, E., (2019). Rapid authentication of European sea bass (*Dicentrarchus labrax* L.) according to production method, farming system, and geographical origin by near infrared spectroscopy coupled with chemometrics. Food Chem., 280: 321-327 (6 pages).
- Gutierrez, L.; Lim, J.S.; Foo, L.L.; Ng, W.Y.; Yip, M.; Lim, G.Y.; Wong, M.H.; Fong, A.; Rosman, M.; Mehta, J.S.; Lin, H., (2022) Application of artificial intelligence in cataract management: current and future directions. Eye Vision. 9(1):3 (11 pages).
- Hu, X.-Z.; Liu, S.-Q.; Li, X.-H.; Wang, C.-X.; Ni, X.-L.; Liu, X.; Wang, Y.; Liu, Y., (2019). Geographical origin traceability of Cabernet Sauvignon wines based on Infrared fingerprint technology combined with chemometrics. Sci. Rep., 9: 8256 (9 pages).
- Imelda, E.; Idroes, R.; Khairan, K.; Lubis, R.R.; Abas, A.H.; Nursalim, A.J.; Rafi, M.; Tallei, T.E., (2022). Natural antioxidant activities of plants in preventing cataractogenesis. Antioxidants. 11: 1285 (27 pages).
- Jamwal, R.; Kumari, S.; Sharma, S.; Kelly, S.; Cannavan, A.; Singh, D.K., (2021). Recent trends in the use of FTIR spectroscopy integrated with chemometrics for the detection of edible oil adulteration. Vib. Spectrosc. 113: 103222 (8 pages).

- Khan, M.N.; Mobin, M.; Abbas, Z.K.; ALMutairi, K.A., (2016). Impact of varying elevations on growth and activities of antioxidant enzymes of some medicinal plants of Saudi Arabia. *Acta Ecol. Sinica*, 36: 141-148 **(8 pages)**.
- Khanban, F.; Garmarudi, A.B.; Parastar, H.; Toth, G., (2022). Evaluation of FT-IR spectroscopy combined with SIMCA and PLS-DA for detection of adulterants in pistachio butter. *Infrared Phys. Technol.*, 127: 104369 **(7 pages)**.
- Laouni, A.; El Orche, A.; Elhamaoui, O.; Karrouchi, K.; El Karbane, M.; Bouatia, M., (2023). A preliminary study on the potential of FT-IR spectroscopy and chemometrics for tracing the geographical origin of Moroccan virgin olive oils. *J. AOAC Int.*, 106: 804-812 **(9 pages)**.
- Lestari, D.; Rohman, A.; Syofyan, S.; Yuliana, N.D.; Abu Bakar, N.K.B.; Hamidi, D., (2022). Analysis of beef meatballs with rat meat adulteration using Fourier Transform Infrared (FTIR) spectroscopy in combination with chemometrics. *Int. J. Food Prop.*, 25: 1446-1457 **(12 pages)**.
- Li, Y.; Kong, D.; Fu, Y.; Sussman, M.R.; Wu, H., (2020). The effect of developmental and environmental factors on secondary metabolites in medicinal plants. *Plant Physiol. Biochem.*, 148: 80-89 **(10 pages)**.
- Liu, D.; Li, Y.-G.; Xu, H.; Sun, S.-Q.; Wang, Z.-T., (2008). Differentiation of the root of cultivated ginseng, mountain cultivated ginseng and mountain wild ginseng using FT-IR and two-dimensional correlation IR spectroscopy. *J. Mol. Struct.*, 883: 228-235 **(8 pages)**.
- Liu, Y.; Huang, J.; Li, M.; Chen, Y.; Cui, Q.; Lu, C.; Wang, Y.; Li, L.; Xu, Z. Zhong, Y.; Ning, J., (2020). Rapid identification of the green tea geographical origin and processing month based on near-infrared hyperspectral imaging combined with chemometrics. *Spectrochim. Acta A Mol. Biomol. Spectrosc.*, 267(Pt 1): 120537 **(9 pages)**.
- Mellado-Mojica, E.; Seeram, N.P.; López, M.G., (2016). Comparative analysis of maple syrups and natural sweeteners: Carbohydrates composition and classification (differentiation) by HPAEC-PAD and FTIR spectroscopy-chemometrics. *J. Food Compos. Anal.*, 52: 1-8 **(8 pages)**.
- Nadia, Y.; Ramli, M.; Japnur, A.; Rusyana, A.; Idroes, G.; Suhendra, R.; Sasmita, N.; Tallei, T.; Idroes, R., (2019). Simple combination method of FTIR spectroscopy and chemometrics for qualitative identification of cattle bones, IOP Conference Series: Earth Environ. Sci., 364: 012040 **(7 pages)**.
- Nardecchia, A.; Presutto, R.; Bucci, R.; Marini, F.; Biancolillo, A., (2020). Authentication of the geographical origin of "vallerano" chestnut by near infrared spectroscopy coupled with chemometrics. *Food Anal. Methods*, 13: 1782-1790 **(9 pages)**.
- Omar, J.; Slowikowski, B.; Boix, A., (2019). Chemometric approach for discriminating tobacco trademarks by near infrared spectroscopy. *Foren. Sci. Int.*, 294: 15-20 **(6 pages)**.
- Onuigbo, M.C.; Ukegbu, C.Y.; Uzoigwe, K.C., (2023). Antibacterial activity of *Chrysophyllum albidum* seed oil extract on pathogenic *Staphylococcus aureus*. *Narra X.*, 1(1): e77 **(7 pages)**.
- Purwakusumah, E.D.; Rafi, M.; Safitri, U.D.; Nurcholis, W.; Adzkiya, M.A.Z., (2014). Identifikasi dan autentikasi jahe merah menggunakan kombinasi spektroskopi FTIR dan kemometrik. *Agritech.*, 34: 82-87 **(6 pages)**.
- Rana, R.; Müller, G.; Naumann, A.; Polle, A., (2008). FTIR spectroscopy in combination with principal component analysis or cluster analysis as a tool to distinguish beech (*Fagus sylvatica* L.) trees grown at different sites. *Holzforschung*. 62: 530-538 **(9 pages)**.
- Rohman, A.; Erwanto, Y.; Man, Y.B.C., (2011). Analysis of pork adulteration in beef meatball using Fourier transform infrared (FTIR) spectroscopy. *Meat Sci.*, 88: 91-95 **(5 pages)**.
- Rohman, A.; Man, Y.C., (2010). Fourier transform infrared (FTIR) spectroscopy for analysis of extra virgin olive oil adulterated with palm oil. *Food Res. Int.*, 43: 886-892 **(7 pages)**.
- Sampaio, B.L.; Edrada-Ebel, R.; Da Costa, F.B., (2016). Effect of the environment on the secondary metabolic profile of *Tithonia diversifolia*: a model for environmental metabolomics of plants. *Sci. Rep.*, 6: 29265 **(11 pages)**.
- Sanchez, P.M.; Pauli, E.D.; Scheel, G.L.; Rakocevic, M.; Bruns, R.E.; Scarmenio, I.S., (2018). Irrigation and light access effects on *Coffea arabica* L. leaves by FTIR-chemometric analysis. *J. Braz. Chem. Soc.*, 29: 168-176 **(9 pages)**.
- Sufriadi, E.; Idroes, R.; Meilina, H.; Munawar, A.A.; Lelifajri; Indrayanto, G., (2023). Partial least squares-discriminant analysis classification for patchouli oil adulteration detection by fourier transform infrared spectroscopy in combination with chemometrics. *ACS Omega.*, 8: 12348-12361 **(15 pages)**.
- Tan, C.S.; Leow, S.Y.; Ying, C.; Tan, C.J.; Yoon, T.L.; Jingying, C.; Yam, M.F., (2021). Comparison of FTIR spectrum with chemometric and machine learning classifying analysis for differentiating guan-mutong a nephrotoxic and carcinogenic traditional Chinese medicine with chuan-mutong. *Microchem. J.*, 163: 105835 **(13 pages)**.
- Topală, C.; Tătaru, L.; Ducu, C., (2017). ATR-FTIR spectra fingerprinting of medicinal herbs extracts prepared using microwave extraction. *Arab. J. Med. Aromat. Plants*. 3: 1-9 **(9 pages)**.
- Verma, N. & Shukla, S., (2015). Impact of various factors responsible for fluctuation in plant secondary metabolites. *J. App. Res. Med. Aromat. Plants*. 2: 105-113 **(9 pages)**.
- Zhao, Y.; Zhang, J.; Jin, H.; Zhang, J.; Shen, T.; Wang, Y., (2015). Discrimination of *Gentiana rigescens* from different origins by Fourier transform infrared spectroscopy combined with chemometric methods. *J. AOAC Int.*, 98: 22-26 **(5 pages)**.
- Zhu, M.-Z.; Wen, B.; Wu, H.; Li, J.; Lin, H.; Li, Q.; Li, Y.; Huang, J.; Liu, Z., (2019). The quality control of tea by near-infrared reflectance (NIR) spectroscopy and chemometrics. *J. Spectrosc.*, 2019: 8129648 **(12 pages)**.
- Zulkifli, B.; Fakri, F.; Odigie, J.; Nnabuife, L.; Isitua, C.C.; Chiari, W., (2023). Chemometric-empowered spectroscopic techniques in pharmaceutical fields: A bibliometric analysis and updated review. *Narra X.*, 1(2):e80 **(16 pages)**.

#### AUTHOR (S) BIOSKETCHES

**Imelda, E.**, Ph.D. Candidate, Graduate School of Mathematics and Applied Sciences, Universitas Syiah Kuala, Banda Aceh 23111, Indonesia.

- Email: [evaimeldaspmpo@gmail.com](mailto:evaimeldaspmpo@gmail.com)
- ORCID: 0000-0003-2258-9488
- Web of Science ResearcherID: ITT-1575-2023
- Scopus Author ID: 57765211000
- Homepage: <https://sinta.kemdikbud.go.id/authors/?q=eva%20imelda>

**Khairan, K.**, Ph.D., Associate Professor, Department of Pharmacy, Faculty of Mathematics and Natural Sciences, Universitas Syiah Kuala, Banda Aceh 23111, Indonesia.

- Email: [khairankhairan@usk.ac.id](mailto:khairankhairan@usk.ac.id)
- ORCID: 0000-0003-3028-6022
- Web of Science ResearcherID: GPS-9955-2022
- Scopus Author ID: 37016941000
- Homepage: <https://fsd.usk.ac.id/kkh/>

**Lubis, R.R.**, Ph.D., Professor, Department of Ophthalmology, Faculty of Medicine, Universitas Sumatera Utara, Medan 20222, Indonesia.

- Email: [rodiah@usu.ac.id](mailto:rodiah@usu.ac.id)
- ORCID: 0000-0003-1861-0563
- Web of Science ResearcherID: AAJ-7235-2020
- Scopus Author ID: 566 76056600
- Homepage: <https://www.usu.ac.id/en/directory/rodiah-rahmawaty-lubis>

**Karma, T.**, M.Sc., Assistant Professor, Department of Occupational Health and Safety, Faculty of Health Sciences, Abulyatama University, Banda Aceh 23372, Indonesia.

- Email: [taufiqkarma94@gmail.com](mailto:taufiqkarma94@gmail.com)
- ORCID: 0000-0003-4664-8964
- Web of Science ResearcherID: ABE-3243-2021
- Scopus Author ID: 57222432937
- Homepage: <https://sinta.kemdikbud.go.id/authors/profile/6764829>

**Idroes, R.**, Ph.D., Professor, Department of Pharmacy, Faculty of Mathematics and Natural Sciences, Universitas Syiah Kuala, Banda Aceh 23111, Indonesia.

- Email: [rinaldi.idroes@usk.ac.id](mailto:rinaldi.idroes@usk.ac.id)
- ORCID: 0000-0003-2264-6358
- Web of Science ResearcherID: S-8983-2016
- Scopus Author ID: 57192873366
- Homepage: <https://fsd.usk.ac.id/rinaldi.idroes/>

#### HOW TO CITE THIS ARTICLE

Imelda, E.; Khairan, K.; Lubis, R.R.; Kemala, P.; Zulfiani, U.; Karma, T.; Rahayu, S.; Idroes, G.M.; Adev, S.M.; Mauludya, N.B.; Idroes, R., (2024). Impact of environmental and geographical position on the chemometric classification of ethanolextracts from *Isotoma longiflora* leaves. *Global J. Environ. Sci. Manage.*, 10(1):155-168.

DOI: 10.22034/gjesm.2024.01.11

URL: [https://www.gjesm.net/article\\_705700.html](https://www.gjesm.net/article_705700.html)





## ORIGINAL RESEARCH ARTICLE

**Torrefaction of bamboo pellets using a fixed counterflow multibaffle reactor for renewable energy applications**W. Hidayat<sup>1,\*</sup>, B.A. Wijaya<sup>2,3</sup>, B. Saputra<sup>1</sup>, I.T. Rani<sup>2</sup>, S. Kim<sup>2</sup>, S. Lee<sup>2</sup>, J. Yoo<sup>2</sup>, B.B. Park<sup>3</sup>, L. Suryanegara<sup>4</sup>, M.A.R. Lubis<sup>4</sup><sup>1</sup>Department of Forestry, Faculty of Agriculture, University of Lampung, Jl. Prof. Dr. Ir. Sumantri Brojonegoro No.1, Lampung 35141, Indonesia<sup>2</sup>Climate Change Research Division, Korean Institute of Energy Research, Daejeon, 34129, Republic of Korea<sup>3</sup>Department of Environment and Forest Resources, College of Agriculture and Life Science, Chungnam National University, 99 Daehak-ro, Daejeon, 34134, Republic of Korea<sup>4</sup>Research Center for Biomass and Bioproduct, National Research and Innovation Agency. Jl. Raya Jakarta-Bogor Km. 46, Cibinong, Bogor, 16911, Indonesia

## ARTICLE INFO

**Article History:**

Received 02 May 2023

Revised 08 August 2023

Accepted 14 September 2023

**Keywords:**

Bamboo

biomass

fixed counter-flow multi-baffle

solid fuel

torrefaction

## ABSTRACT

**BACKGROUND AND OBJECTIVES:** The decreasing availability of fossil fuels requires the adoption of renewable energy sources that facilitate the mitigation of greenhouse gas emissions. Meeting Indonesia's goal of achieving a 23 percent mixed energy composition by 2025 through co-firing demands a substantial increase in the availability of renewable energy sources. Bamboo is a valuable biomass resource because of its fast growth rate and potential for energy production. Innovative processes like torrefaction are necessary to improve the quality of biomass due to its challenging low density and hydrophilic properties. The objective of this study is to evaluate the characteristics of torrefied bamboo pellets made from *Gigantochloa pseudoarundinacea* by using a fixed counter-flow multi-baffle reactor. This study aims to investigate the properties and viability of torrefied *G. pseudoarundinacea* pellets for solid fuel applications to fill existing knowledge gaps about this technology's potential.

**METHODS:** A fixed counter-flow multi-baffle reactor was used to torrefy *G. pseudoarundinacea* bamboo pellets. The baffles in the reactor column held the pellets, while hot gas flowed through them. Torrefaction was conducted at 280 degrees Celsius with a 3–5 minutes resident time, and the gas flow rate was 4.25 cubic meters per minute. Torrefied pellets at the column bottom were counted as the first cycle. Three cycles of torrefaction were used, and each cycle was evaluated. The second and third cycles used torrefied pellets from the first and second cycles. The physical, chemical, and bioenergetic properties of the pellets before and after torrefaction were evaluated.

**FINDINGS:** The bamboo pellets' physical, chemical, and thermal properties changed significantly after torrefaction. Torrefaction at 285 degrees Celsius produced 78.5 percent of the production yield, according to thermogravimetric and derivative thermogravimetric analyses. Lightness, red/green, and yellow/blue chromaticity decreased, indicating darker, better solid fuel pellets. Torrefaction in the third cycle reduced moisture content by 99.8 percent. The lower moisture content reduced fungal growth, and improved biomass transport and storage. Torrefaction also raised the bamboo pellets' calorific value and physical and mechanical properties. The highest calorific value of 21.62 megajoules per kilogram was obtained after the third cycle of torrefaction, and it was 16.6 percent higher than that of raw pellets. Torrefaction improved pellet grindability and combustion by decreasing density and compressive strength. Torrefaction increased ash, volatile matter, and fixed carbon. The ultimate analysis showed increased carbon and reduced nitrogen, hydrogen, and oxygen, improving solid fuel quality, energy density, and combustion emissions. According to a Fourier-transform infrared analysis, torrefaction caused extractive and hemicellulose degradation and lignin increase. The chemical analysis showed that temperature and residence time degraded hemicellulose and increased lignin in the torrefied pellets.

**CONCLUSION:** The torrefaction process using a fixed counter-flow multi-baffle reactor demonstrated the enhanced properties of *G. pseudoarundinacea* bamboo pellets for their application as solid fuel. The study's findings contribute to the comprehension of torrefaction and the enhancement of conditions for producing superior biomass products. These findings have implications for exploring the potential applications of torrefaction in diverse industries and energy sectors.

DOI: [10.22034/gjesm.2024.01.12](https://doi.org/10.22034/gjesm.2024.01.12)This is an open access article under the CC BY license (<http://creativecommons.org/licenses/by/4.0/>).

NUMBER OF REFERENCES

75



NUMBER OF FIGURES

9



NUMBER OF TABLES

8

\*Corresponding Author:

Email: [wahyu.hidayat@fp.unila.ac.id](mailto:wahyu.hidayat@fp.unila.ac.id)

Phone: +6282 2115 48516

ORCID: [0000-0002-6015-1623](https://orcid.org/0000-0002-6015-1623)

Note: Discussion period for this manuscript open until April 1, 2024 on GJESM website at the "Show Article".

## INTRODUCTION

Tropical forests contribute essential ecological, climate, and socioeconomic benefits to global and local people in nations like Indonesia. The high biodiversity in Indonesian forests is a source of biomass. Forest-based biomass is an alternative source of renewable energy (Favero et al., 2020). Biomass refers to any organic matter derived from plants through photosynthesis, and it can exist in the form of products or waste (Saputra et al., 2022; Hazbehian et al., 2022; Santoso et al., 2023; Samimi and Monsouri, 2023). The high potential for biomass to become a global energy supply could further reduce fossil fuel use, which has decreased over the years (Dhanasekar and Sathyanathan, 2023). Indonesia's biomass potential is approximately 146.7 million tons/year, equal to 470 gigajoule/year (Rhofita et al., 2022). Biomass is believed to support greenhouse gas reduction in the future (Samimi and Shahriari-Moghadam, 2021). From 2000 to 2013, biomass accounted for approximately 5.8 percent (%) to 8.9% of global electricity production (Bonechi et al., 2017). Global biomass production in 2016 was approximately  $2 \times 10^{11}$  tons (dry carbon bases), making it the most abundant renewable resource on Earth. By 2050, it is predicted that 3,000 terawatt hours (TWh) of electricity could be generated from biomass, avoiding the annual emission of 1.3 billion tons (Bt) of carbon dioxide (CO<sub>2</sub>) equivalent (Gielen et al., 2019). Thus, there is significant potential for utilization. In 2010, woody biomass constituted approximately 9% of global primary energy consumption and 65% of global renewable primary energy consumption (Lauri et al., 2014). The disadvantages of woody biomass include its potential impact on traditional wood users, forestland usage, and management difficulties. The increased utilization of wood for bioenergy could potentially result in underestimation of log volume and associated concerns within the wood market. As a developing nation, Indonesia is susceptible to climate change impacts. The country ratified the Paris Agreement with Law No. 16 in 2016. Indonesia has demonstrated its dedication to mitigating greenhouse gas (GHG) emissions by reinforcing its commitment in the Nationally Determined Contributions (NDC) document (Suroso et al., 2022). Decision 1/Meeting of the Parties to the Paris Agreement (CMA) 3 requires Parties to revise and strengthen their NDC-2030

target to meet the Paris Agreement's temperature goal by 2022. According to this mandate, Indonesia submitted Enhanced NDC to the United Nations Framework Convention on Climate Change (UNFCCC) Secretariat on September 23, 2022, with an emission reduction target of 31.89% on its own efforts and 43.20% with international support. This Enhanced NDC is a transition to Indonesia's Second NDC, which aligns with the Long-Term Strategy for Low Carbon and Climate Resilience (LTS-LCCR) 2050 and aims for net zero emissions by 2060 or sooner (Government of Indonesia, 2022). Biomass-coal co-firing will help Indonesia meet its NDC and net zero emission conditions by replacing coal fuel with biomass waste to reduce organic waste. New technologies such as carbon capture storage (CCS) must be considered to recover/capture the slightly produced carbon from co-firing to generate net zero carbon. This scheme aims to facilitate the realization of the Paris Agreement's objective of attaining net zero emissions by the latter half of this century (Yulianto et al., 2022). Indonesia aims to achieve a 23% share of mixed energy sources by the year 2025. Biomass is significant due to its utilization in co-firing. Nevertheless, the issue of low supply persists in the present day (IESR, 2022). Bamboo, a member of the grass family, is a plant native to Asia, Africa, and South America. The growth rate of bamboo varies among species; however, bamboo generally exhibits rapid maturation. Bamboo is also adaptable to various climates, and its superior properties contribute to its widespread cultivation (Kang et al., 2019). Bamboo has fast growth, as culms mature in 3–6 years depending on species, compared to wood, which takes 15 times longer to be harvested. Bamboo can achieve its full height within 4–6 months, with a daily growth rate of 15–18 centimeters (cm). One clump may have 40–50 stems, producing 10–20 culms annually. Bamboo grows faster than any other plant of its size. The rapid growth of bamboo is a significant factor that motivates its utilization (Liese and Köhl, 2015). Bamboo can grow on degraded and marginal lands with other crops in forestry and agroforestry systems; thus, there is no land competition. Bamboo can be harvested yearly without removing the clump for the next 30–50 years, while other biomass requires replanting after harvesting (Sharma et al., 2018). Bamboo is recognized globally due to its ecological, economic, and social benefits. In 2015, Indonesia had

160 bamboo species from 22 genera that covered approximately 2.1 million hectares of land. As a tropical country, Indonesia grows bamboo that belongs to the sympodial tribe, whereas bamboo grown in temperate climates belongs to the monopodial tribe (Liese and Köhl, 2015). In Indonesia, bamboo biomass has traditionally been utilized as a source of firewood for generating heat in households, primarily for cooking and boiling water (Sharma *et al.*, 2018). Sympodial is a type of bamboo that grows in a clumping or spreading manner, producing multiple culms from a single rhizome and forming clusters of culms. This bamboo has sympodial rhizomes, which are horizontal underground stems that grow parallel to the ground and give rise to new culms (Luo *et al.*, 2019). *Gigantochloa pseudoarundinacea* is one of the endemic bamboos of Indonesia from the genera *Gigantochloa*, which is mostly found in Java and Sumatera Island. *G. pseudoarundinacea* is mostly used in the bamboo industry with other species of bamboo, such as *Dendrocalamus asper*, *Bambusa blumeana*, and *Schizostachyum brachycladum* (Maulana *et al.*, 2021). A previous study reported that bamboo's fuel properties have low ash content, high volatile matter, fixed carbon, and calorific value (Park *et al.*, 2020). Bamboo is considered a sustainable and renewable energy resource due to its efficient fuel properties and rapid growth rate. Using bamboo biomass for co-firing with coal is a promising approach for utilizing biomass in energy production. This method can potentially enhance combustion efficiency and reduce the emissions of pollutants and greenhouse gases compared to coal combustion alone (Xiang *et al.*, 2020). Raw biomass presents challenges due to its low density, high moisture content, nonuniform size, hydrophilic nature, and difficulties in transportation, storage, and combustion due to its nonuniform size and longer residence time (Sher *et al.*, 2020). Therefore, raw biomass is inefficient as a renewable energy source (Iftikhar *et al.*, 2019), requiring additional procedures to improve efficiency. Biomass can serve as a reliable and environmentally friendly energy source by using advanced technologies to convert it into solid, liquid, and gaseous states (Chen *et al.*, 2015). Densification is known to increase the quality of biomass with relatively low energy into a solid form (pellets or briquettes). Pelletization produces pellets through a thermomechanical technique to increase the bulk

density of solid matter such as wood, bamboo, or sawdust containing lignin and cellulose (García *et al.*, 2019; Solihat *et al.*, 2021). Biomass pellets can be utilized for small-scale and industrial heating applications, combined heat and power (CHP), co-firing, and residential heating applications (Manouchehrinejad and Mani, 2018). They can also be used for animal bedding because biomass pellets have hydrophilic properties (Saputra *et al.*, 2022); they can adsorb animal urination well. The pelletization process increases the density of biomass. Liu *et al.* (2013) discovered that the densification process during pelletization resulted in an increase in the density and energy concentration per unit volume of bamboo pellets. This improvement in density and energy concentration turns bamboo pellets into a more efficient source of bioenergy. Bamboo pellets have a higher energy content compared to other biomass materials, such as rice straw and pine (Liu *et al.*, 2013; 2014), providing efficient energy production. However, their bioenergetic properties are relatively lower than those of coal. Bamboo pellets are fibrous, hydrophilic, and prone to attack by fungi during long-term storage. To resolve this issue, thermal treatment with low oxygen can produce high-energy pellets. Torrefaction refers to a gentle thermal treatment conducted at atmospheric pressure with a temperature between 200-300 degrees Celsius (°C) at a particular time in an inert or low oxygen content. Other names for torrefaction include roasting, mild pyrolysis, wood cooking, and high-temperature drying (Hidayat *et al.*, 2021). Torrefaction affects the physical, chemical, mechanical, and bioenergetic properties of biomass, thereby improving its economic value (Chen *et al.*, 2015). The integration of pelletization and torrefaction produces biomass pellets with a darker appearance, generally referred to as black pellets (García *et al.*, 2019), that have better quality than raw pellets (Nunes *et al.*, 2014). Previous research found that torrefaction at high temperatures of 250–350°C increased the calorific value of soybean straw and pinewood sawdust pellets. The hydrophobicity of the pellets was observed to be higher than that of the raw pellets (Zhang *et al.*, 2020). Different types of reactors are currently employed for biomass torrefaction. Fixed-bed reactors are commonly employed for laboratory-scale torrefaction processes. Such reactors are utilized to study the influence of process conditions

on the properties of the sample, and they are easier to use for biomass torrefaction than other reactors (Ribeiro *et al.*, 2018). Because this is a laboratory-scale reactor, only a small number of torrefied pellets can be produced. The rotary kiln reactor is commonly used in pilot plant projects due to its larger capacity. However, its power efficiency is compromised, as the rotation of the kiln requires additional energy consumption. This reactor has limitations in scaling up due to its inability to accommodate a wide range of biomass sizes (Mei *et al.*, 2015). One of the current developments in torrefaction technology is the fixed counter-flow multi-baffle (Fixed COMB) reactor developed by the Korea Institute of Energy Research (KIER) at the University of Lampung, Indonesia. The reactor uses the principle of heating raw material with hot air blowing at a certain flow rate and time (Iryani *et al.*, 2019). The Fixed COMB reactor offers several advantages for torrefaction biomass, specifically pellets. These benefits include a low gas-to-solid ratio (G/S), a short residence time of 3–5 minutes, a constant temperature difference (driving force) along the column, and the reactor's simplicity, flexibility, and mobility. This reactor is designed for pilot plant production, with a processing capacity of 20 kilograms per hour (kg/h) of biomass (Hidayat *et al.*, 2020). The Fixed COMB reactor has the potential to enhance mass production efficiency at an industrial scale, surpassing the capabilities of conventional furnaces. This development is attributed to the direct heating technology in the Fixed COMB reactor, which facilitates uniform heat distribution throughout the material. The concept of vortex flow is applied to achieve uniform heat distribution across the production area. This advantage is significant, as it reduces the risk of product nonuniformity caused by uneven heating, a common occurrence in conventional methods, such as furnaces (Hidayat *et al.*, 2021). The Fixed COMB reactor enhances heat efficiency and distribution and increases product yield. Efficiency is crucial on a commercial scale, as substantial production quantities are necessary to meet demand (Iryani *et al.*, 2019). *G. pseudoarundinacea* is mostly used in the bamboo industry (Maulana *et al.*, 2021) and has a high calorific value compared to other types of biomasses (Park *et al.*, 2020). Thus, *G. pseudoarundinacea* has potential as a bioenergy source. The study of *G. pseudoarundinacea* as torrefied pellets is still limited.

Prior research has focused only on determining the physical characteristics of torrefied *G. pseudoarundinacea* pellets, including moisture content, density, water resistance, and water adsorption (Pah *et al.*, 2021). Presently, no study has been conducted on the characteristics of torrefied *G. pseudoarundinacea* pellets as a form of solid fuel. This study aimed to examine the characteristics of torrefied *G. pseudoarundinacea* pellets using a Fixed COMB reactor, a recent advancement in torrefaction technology. This study was conducted in the forest products workshop in the Integrated Field Laboratory, Faculty of Agriculture, University of Lampung, Indonesia, from 2022–2023.

## MATERIALS AND METHODS

The *G. pseudoarundinacea* bamboo was collected when it was between the ages of three and four years old in Ciawi, located in the Bogor Regency of West Java, Indonesia (latitude 6° 40' 49.3" and longitude 106° 49' 49.6"). Bamboo pellets were produced using a pellet mill with a capacity of one ton of material per hour for processing. Before torrefaction, the bamboo pellets were passed through a strainer and sieved to remove any remaining dust and pellet powder. Afterward, the pellets were categorized into uniform groups based on size, with each measuring 3–4 cm in length. After that, the pellets were dried in an oven for 24 hours at 100°C to evaporate moisture. All pellet samples should have uniform moisture content before torrefaction (Fig. 1). Table 1 displays the characteristics of the unprocessed pellets.

### *Torrefaction process using Fixed COMB reactor*

Torrefaction was performed with a pilot plant Fixed COMB (Fig. 2) reactor developed by KIER. The reactor featured a column with baffles that retained the pellets while hot gas flowed through the column, and it used liquefied petroleum gas (LPG) as the fuel (Fig. 2a). Torrefaction is a thermal process conducted at atmospheric pressure, with temperatures ranging from 200–300°C. According to the preliminary research conducted by Pah *et al.* (2021) and Saputra *et al.* (2022), optimal torrefaction results can be attained at a temperature of 280°C, with a residence time of 40–50 minutes. This study conducted torrefaction at 280°C, with a residence time of 3–5 minutes and three cycles, to imitate the preliminary research and compare the results of each cycle. The gas flow rate



Fig. 1: The process of producing bamboo pellets: (a) Raw materials used; (b) The process of removing the outer and inner skin layers of the bamboo; (c) The production process of transforming the bamboo into its powdered form; (d) Drying the bamboo powder; (e) Producing pellets using the pellet mill; (f) Cooling and conditioning process after pelletization.

Table 1: Proximate and ultimate properties of raw *G. pseudoarundinacea* pellets

Proximate	
Volatile matter weight percent dry basis (wt% db.)	92.40
Ash content wt% db.	1.33
Fixed carbon wt% db.	6.27
Ultimate	
Carbon (C)	47.08
Nitrogen (N)	0.41
Hydrogen (H)	6.33
Oxygen difference (O diff)	46.18
Ratio of O atoms to C atoms in a molecule (O/C)	0.98
Ratio of H atoms to C atoms in a molecule (H/C)	0.13

(column pressure) was 4.25 cubic centimeters per minute ( $\text{cm}^3/\text{min}$ ), and the temperature difference at the column bottom (T1) and the column top (T2) was plus or minus ( $\pm$ )  $50^\circ\text{C}$  (Fig. 2b). The pellet entered the column via the feeder and was torrefied by hot gas from the induced draft fan (ID fan), which blew the air across the combustor and flowed the hot gas from the bottom. Torrefied pellets were collected at the bottom of the column and counted as the first cycle (C1). Torrefaction was conducted in three cycles to determine the characteristics of each cycle. The

second cycle (C2) used torrefied pellets from the first cycle, and the third cycle (C3) used torrefied pellets from the second cycle.

#### Thermogravimetric (TGA) analysis

TGA is a quantitative analytical technique used to inspect the thermal degradation act of *G. pseudoarundinacea* pellets based on the American Society for Testing Materials (ASTM) E1641-16 standard. A thermogravimetric analyzer was used to analyze the raw pellets. A one-gram (g) sample was

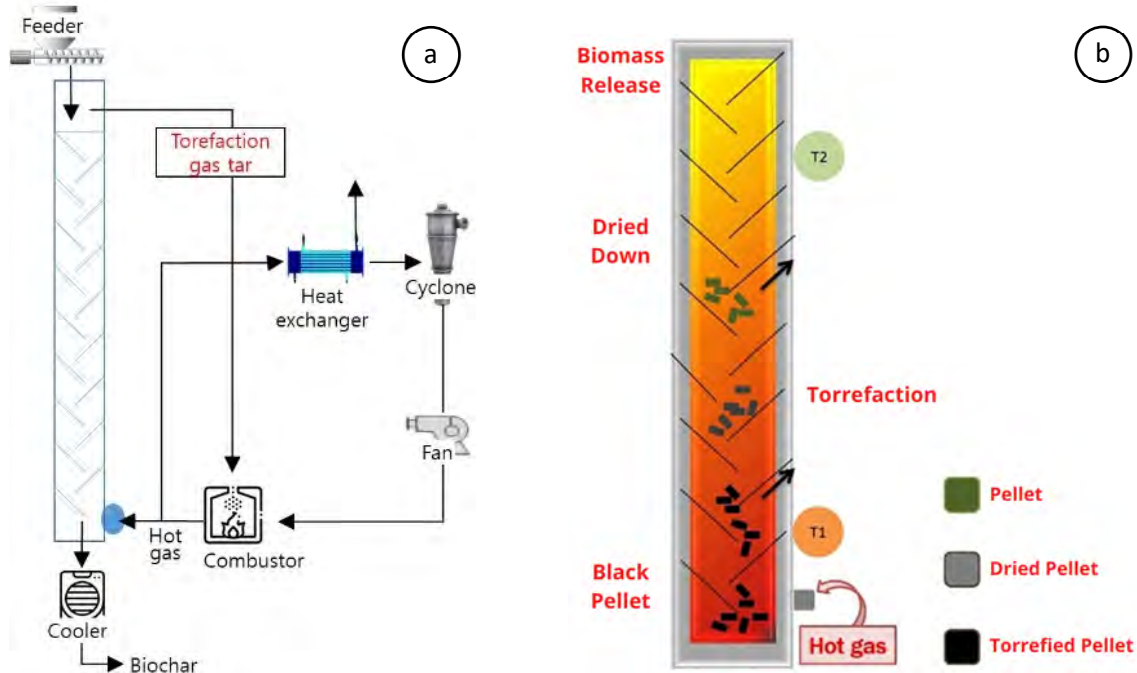


Fig. 2: (a) Fixed COMB reactor schematic; (b) Column condition during the torrefaction process

used and heated in an inert atmosphere from 30–900°C.

#### Physical properties

A colorimeter with a *Commission Internationale de l'Éclairage* (CIE-Lab) system was used to conduct color change tests before and after torrefaction. The overall color change ( $\Delta E^*$ ) was calculated using Eq. 1 (Valverde and Moya, 2014).

$$\Delta E^* = (\Delta L^{*2} + \Delta a^{*2} + \Delta b^{*2})^{1/2} \quad (1)$$

In this context, the variables  $\Delta E^*$ ,  $\Delta L^*$ ,  $\Delta a^*$ , and  $\Delta b^*$  represent the overall color change, change in lightness, change in red/green chromaticity, and change in yellow/blue chromaticity, respectively. The classification of color changes according to Valverde and Moya (2014) is shown in Table 2.

Density is the measure of a sample's weight-to-volume ratio. Obtaining this measurement entailed determining the weight and volume of the samples in both air-dry and oven-dry conditions. In accordance with the Indonesian National Standard (SNI) 8021-2014, density (D) was determined using Eq. 2 (Saputra et al., 2022).

$$D = \frac{W}{V} \quad (2)$$

In this equation, W represents the weight of the pellet (g), and v represents the volume of the pellet in cubic centimeters (cm<sup>3</sup>). Moisture content determination was used primarily to compare the weight loss resulting from heat treatment with the initial weight of the samples. The moisture content of the sample was determined by subjecting it to a 24-hour drying process in an oven at a temperature of 100°C. The sample's weight was measured prior to and following the drying procedure. In accordance with SNI 01-1506, the moisture content (MC) was determined using Eq. 3 (Saputra et al., 2022).

$$MC = \frac{(W_1 - W_0)}{W_0} \times 100\% \quad (3)$$

Where,  $W_1$  is the initial weight (g), and  $W_0$  is the oven-dried weight (g).

#### Mechanical properties

Compressive strength tests were conducted using a universal testing machine. The diameters of the

Table 2: Classification of color changes

No.	Classification value	Description
1	0.0 Is less than (<) $\Delta E^*$ Is less than or equal to ( $\leq$ ) 0.5	Negligible
2	$0.5 < \Delta E^* \leq 1.5$	Slightly Perceivable
3	$1.5 < \Delta E^* \leq 3$	Noticeable
4	$3 < \Delta E^* \leq 6$	Appreciable
5	$6 < \Delta E^* \leq 12$	Very Appreciable
6	$\Delta E^*$ Is greater than (>) 12	Totally Changed

torrefied pellets were measured, and their tips were flattened to ensure stability during machine operation. The pellets were compressed using the machine until they fractured or developed cracks. Subsequently, the machine ceased operation and displayed the graphical representation along with the highest recorded value during the test. The compressive strength (CS) value was determined using Eq. 4 (Saputra *et al.*, 2022).

$$CS = \frac{P}{A} \quad (4)$$

Where, P is the maximum load (N), and A is the surface area (mm<sup>2</sup>).

#### Bioenergetic properties

Calorific value is the heat generated when one unit mass of fuel undergoes complete combustion with water in steam form, and it is quantified in megajoules per kilogram (MJ/kg). A bomb calorimeter was used to conduct the calorific test following the SNI 8675-2018 standard.

#### Proximate analysis

A bomb calorimeter was used to conduct a proximate analysis of volatile matter, fixed carbon, and ash content according to the SNI 8675-2018 standard. Volatile matter denotes the weight percentage lost during the heating of a substance in the absence of external air. The analysis of volatile matter adhered to the SNI 8675-2018 standard and was calculated using Eq. 5 (Hidayat *et al.*, 2017).

$$\text{Volatile matter (\%)} = \frac{\text{Sample Weight Loss (g)}}{\text{Dry Sample Weight (g)}} \times 100\% \quad (5)$$

Fixed carbon is the residual part of a sample that remains after removing moisture content, ash content, and volatile matter fraction. SNI 8675-2018 provided the basis for performing the fixed carbon

analysis, and Eq. 6 (Hidayat *et al.*, 2017) was utilized to compute the fixed carbon.

$$\text{Fixed carbon} = 100\% - (\text{Ash content} - \text{Volatile matter}) \quad (6)$$

Ash content is the residual mineral matter remaining after combustion that does not evaporate. The ash content test analysis followed the guidelines outlined in the SNI 8675-2018 standard, and Eq. 7 (Hidayat *et al.*, 2017) was used to determine the ash content.

$$\% \text{Ash Content} = \frac{\text{Ash Weight (g)}}{\text{Dry Sample Weight (g)}} \times 100\% \quad (7)$$

#### Ultimate analysis

An elemental analyzer was used to conduct the ultimate analysis of the bamboo pellets. The analyzer was calibrated using five tin capsules containing L-cystine sample. A tin capsule contained powdered bamboo pellet sample weighing 0.1 milligram (mg). The experiment involved subjecting the sample to a temperature of 980°C while maintaining a continuous supply of helium gas mixed with oxygen.

#### Fourier-transform infrared (FTIR) analysis

FTIR analysis was conducted using Fourier-transform infrared spectroscopy with the potassium bromide (KBr) technique. FTIR analysis was conducted to evaluate biomass quality and to examine alterations in functional groups (Samimi and Shahriari-Moghadam, 2023). The FTIR spectrum utilizes infrared radiation to pass through the sample gap, where the energy delivered to the sample is regulated by the slit (Ehzari *et al.*, 2022). The sample absorbs specific wavelengths of infrared light and allows others to pass through its surface. The infrared rays are transmitted to the detector, and the resulting signal is then sent to the computer for measurement.

### Chemical properties

The composition of the torrefied products was determined following the method adapted from Datta (1981) with some modifications. Prior to analyzing the composition of the torrefied product, an extraction process was conducted using hot water and an extractor to determine the extractive content. The extractive sample was dried and mixed with 1.5 milliliters (mL) of 72 percent by weight (wt%) sulfuric acid ( $H_2SO_4$ ) at 30°C for 1 hour. The treated sample was hydrolyzed in an autoclave at 121°C for 1 hour after adding 42 mL of water. The hydrolyzed sample underwent cooling, filtration, and multiple washes using hot water. The residue obtained was identified as Klason lignin, which refers to the acid-insoluble solid residue. It was subsequently dried at a temperature of 105°C overnight.

## RESULTS AND DISCUSSION

### Thermogravimetric (TG) and derivative thermogravimetric (DTG) analyses

TG and DTG (Fig. 3) showed that the torrefaction with a temperature of 285°C resulted in a 78.5% production yield. Through thermal degradation, the product decreased by 9.2%, 55.1%, and 38% from 30–900°C, respectively. As shown in the graph's diver-time line, the two peaks were at temperatures of 50.5°C and 350°C. It was suspected that the peak

at 50–100°C was moisture degradation, as reported in a previous study (Rani *et al.*, 2021), and then the degradation peak at 350°C was a biopolymer. Bamboo mainly consists of cellulose, hemicellulose, and lignin, with different responses at specific temperatures (Jagnade *et al.*, 2022). Hemicelluloses undergo decomposition within the temperature range of 200–380°C, whereas cellulose and lignin decompose within the temperature ranges of 250–380°C and 180–900°C, respectively (Chen *et al.*, 2015).

As previously mentioned, weight loss was divided into three phases in agreement with the literature (Burhenne *et al.*, 2013). The initial phase of weight loss was attributed to the removal of moisture and bound water, which is known as the dehydration phase. The next phase, referred to as active pyrolysis, leads to rapid weight loss. The combustion of hemicellulose and cellulose components corresponds to this rapid weight loss (Zakikhani *et al.*, 2015). Lignin decomposition occurred gradually within a broad temperature range of 180–900°C. The reaction exhibited a minor order, leading to a gradual reduction in weight until it reached zero in the final stage. This final stage was identified as passive pyrolysis (Chen *et al.*, 2015).

### Effect of torrefaction using a Fixed COMB reactor on color change

The results showed a distinction between each

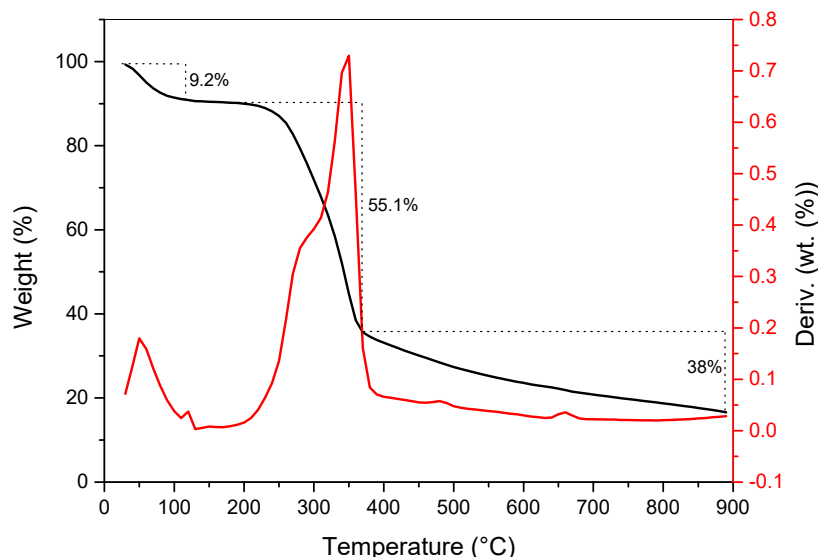


Fig. 3: TG and DTG curves of bamboo pellets.

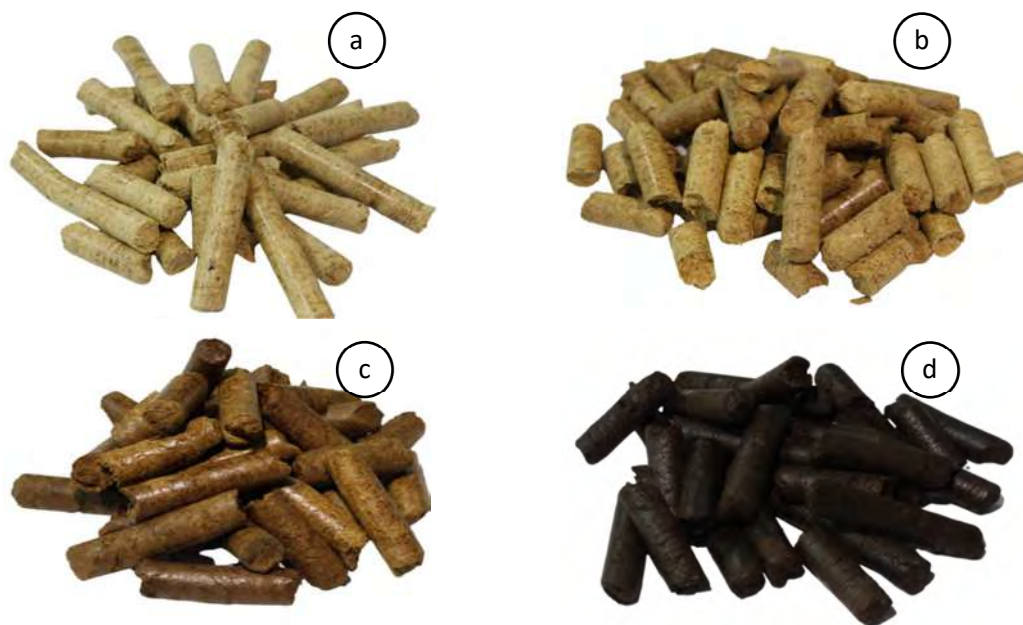


Fig. 4: The visual appearance of the bamboo pellets (a: control, b: C1, c: C2, d: C3)

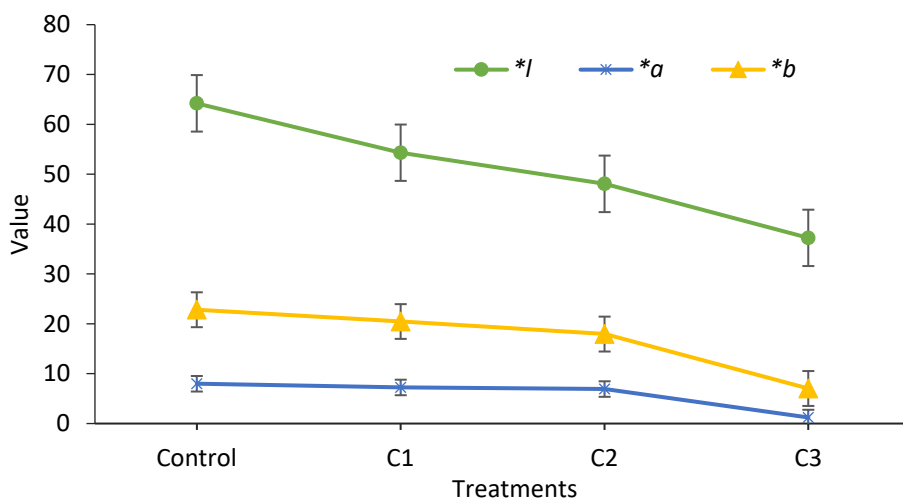


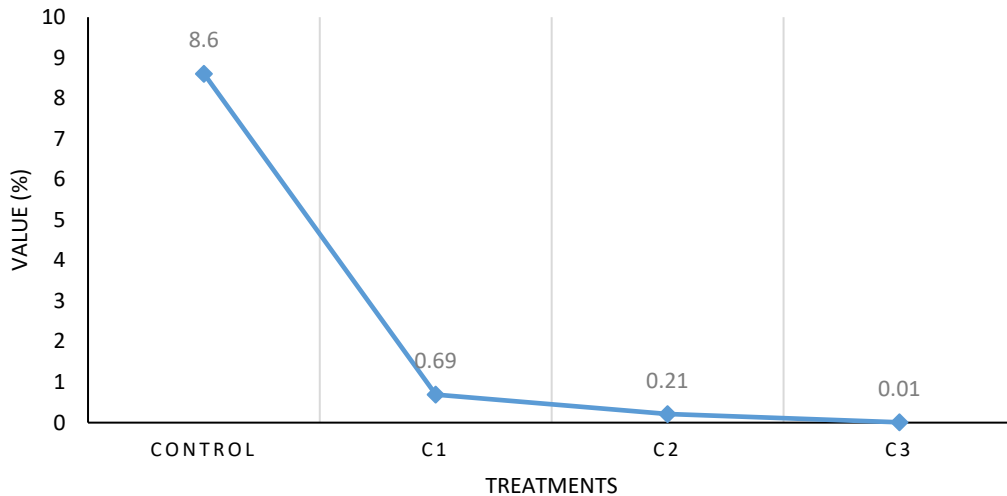
Fig. 5: Effect of the torrefaction cycle process on the change in  $L^*$ ,  $a^*$ , and  $b^*$  in *G. pseudoarundinacea* bamboo pellets

treatment in terms of color change (Fig. 4). The treatment quickly produced a genuine empirical color change in the appearance of each pellet. The raw pellet/control (Fig. 4a), without any heat treatment, had the lightest brown color compared to the treated pellets. Only during C3 did the pellets turn into black pellets (Fig. 4d); in C1 (Fig. 4b) and C2 (Fig. 4c), the torrefaction made the pellets darker but not black.

Based on the *CIE-Lab* system (Fig. 5), all parameters ( $L^*$ ,  $a^*$ , and  $b^*$ ) were decreased to a lower score along with the torrefaction cycle added. The trends in the  $a^*$  and  $b^*$  parameters resulted in a similar pattern in which C1 and C2 underwent plateau conditions and then dropped on the latest treatment. Score-wise (Table. 3), the  $L^*$ ,  $a^*$ , and  $b^*$  parameters show that C3 had the lowest score among treatments by 37.24,

Table 3: Effect of the torrefaction cycle process on the color change of *G. pseudoarundinacea* bamboo pellets

Treatment	Parameters				
	$L^*$	$a^*$	$b^*$	$\Delta E^*$	$\Delta E^*$ Level
Control	64.22	7.26	22.84	-	-
C1	54.32	6.94	20.48	58	Totally Changed
C2	48.08	5.82	17.96	52	Totally Changed
C3	37.24	1.22	7.04	38	Totally Changed

Fig. 6: Effect of the torrefaction cycle process on the change in moisture content in *G. pseudoarundinacea* bamboo pellets.

1.22, and 7.04, respectively, indicating that the C3 pellets had the darkest color compared to the other treatments and the control. The color change levels for C1, C2, and C3, based on the  $\Delta E^*$ , was categorized in total change by 58, 52, and 38, respectively. The results demonstrate a similar pattern to Park et al. (2020), who found that the color of the biomass pellets became darker at higher temperatures and longer residence times. Consistent with the findings of Via et al. (2013), the color of torrefied biomass was observed to transition from a darker brown shade at lower temperatures to nearly black at 300°C. Torrefaction induces a color alteration in biomass through devolatilization and carbonization processes, resulting in a darker or blackened appearance, which varies depending on the level of torrefaction severity. The degradation of hemicellulose and the movement of the extractive component can decrease lightness ( $L^*$ ), and the degradation may accelerate as the treatment temperature rises (Chen et al., 2015). Hidayat et al. (2015) reported that a temperature range of 180–200°C substantially impacted the color change of biomass during heat treatment. According

to Huang et al. (2020), the color change of torrefied biomass can be used as an indicator for predicting the quality of torrefied products. This is because the color parameter of torrefied biomass is strongly correlated with weight loss, volatile matter, and a higher heating value (HHV).

#### Moisture content

Torrefaction conducted with a Fixed COMB reactor during C3 treatment achieved a significant reduction in moisture content, reaching a level of 99.8%. The addition of the torrefaction cycle (Fig. 6) resulted in a decrease in moisture content consistent with the existing literature, which shows a decrease in moisture content with longer residence time. At the maximum temperature and residence time, the macro-TG reactor achieved a moisture content reduction of 76% (Chaves et al., 2021), whereas the atmospheric pressure steam reactor reduced moisture content to 81% (Tu et al., 2022). The results indicate that the Fixed COMB reactor exhibited the lowest moisture content compared to other reactors. The liberation of unbound water from the torrefied

biomass was a result of the elevated temperature and prolonged duration, which coincided with a reduction in moisture content (Peng *et al.*, 2013). Low moisture content is beneficial in degrading the ability of fungi to grow during biomass storage, and it also reduces transportation costs. Reducing moisture content can mitigate storage problems, such as off-gassing and self-heating, and facilitate long-term storage (Pah *et al.*, 2021).

#### *Physical, mechanical, and bioenergetic properties*

The torrefaction process improves the calorific value throughout the added cycle. The HHV of C3 reached 21.13 MJ/kg, which increased by 18.6% from the control pellets' HHV. The density of the control pellets decreased by 40.8% after C3 treatment, dropping from 1.38 grams per cubic centimeter (g/cm<sup>3</sup>) to 0.81 g/cm<sup>3</sup>. This indicates an improvement compared to the torrefaction using the macro-TG reactor at maximum temperature and residence time, which increased the HHV only 2.7% and decreased the density by 8% (Chaves *et al.*, 2021). The decrease in density of torrefied pellets is attributed to the evaporation of moisture, extractives, and partial degradation of hemicellulose during heat exposure via torrefaction (Yang *et al.*, 2007). Furthermore, the compressive strength of the control pellet was 2.46 Newtons per square millimeter (N/mm<sup>2</sup>) and increased to 3.28 N/mm<sup>2</sup> in C1; however, it decreased in C2 and C3. While C1 represents the critical temperature at which the strength remains unaffected, exceeding this cycle can lead to decreased strength (Saputra *et al.*, 2022). The results showed an association between the density and compressive strength of biomass pellets. Denser biomass pellets typically exhibit greater compressive strength and vice versa (Saha *et al.*, 2022). Based on solid fuel utilization, C3 was a preferable pellet compared to the other treatments, producing a higher calorific value and lower density and compressive strength (Table 4). Torrefaction at high temperatures enhances the energy density

and fuel characteristics of torrefied biomass, making it more suited for solid fuels (Pah *et al.*, 2021). Torrefaction temperature and residence time impact the grindability of torrefied biomass. Increasing the temperature and duration of residence will improve grindability. Water evaporation during torrefaction decreases the density of torrefied biomass, making it more brittle but increasing its HHV (Yu *et al.*, 2019). Hemicellulose degradation during heat treatment weakens the hydrogen bonding between particles and reduces cohesiveness inside the biomass, which affects the lowering of compressive strength. As the torrefaction temperature rises, the rate of degradation, primarily in hemicellulose, and the decreased interparticle hydrogen bonding increase. During the torrefaction process, the relative presence of oxygen and hydrogen is reduced compared to carbon, resulting in an increase in the calorific value of biomass that has undergone torrefaction (Peng *et al.*, 2013).

#### *Proximate analysis*

A Fixed COMB reactor could upgrade biomass characteristics, making them more suitable for solid fuel utilization. C3 treatment could increase the fixed carbon by 14.52 wt% db. (Table 5). Increasing fixed carbon content can improve the efficiency of biomass combustion. Nevertheless, the volatile matter and ash content unavoidably accrued when the torrefaction cycle was added. Volatile matter and ash content for C were 89.17 and 1.81, respectively, which means that they increased by 6.18% and 26.5%. Using a macro-TG reactor, Chaves *et al.* (2021) observed the characterization of torrefied *Phyllostachys aurea* bamboo pellets. They stated that the ash content and fixed carbon increased by 1.02% and 17.35%, respectively, while the volatile matter decreased to 81.64%. Saha *et al.* (2022) reported that the torrefaction process of *Gigantochloa scortechinii* bamboo chips in a vertical mass flow reactor resulted in a 39% increase in fixed carbon content and a 58%

Table 4: Effect of the torrefaction cycle process on the physical, mechanical, and bioenergetic properties of *G. pseudoarundinacea* bamboo pellets

Parameters	Treatments			
	Control	C1	C2	C3
Calorific value (MJ/kg)	17.81	18.14	19.23	21.13
Density (g/cm <sup>3</sup> )	1.38	1.24	1.19	0.81
Compressive strength (N/mm <sup>2</sup> )	2.46	3.28	1.84	1.74

Table 5: Effect of the torrefaction cycle process on the proximate of *G. pseudoarundinacea* bamboo pellets

Parameters	Treatments		
	C1	C2	C3
Volatile Matter wt.% db.	89.58	86.25	83.67
Ash Content wt.% db.	1.13	1.41	1.81
Fixed Carbon wt.% db.	9.29	12.34	14.52

Table 6: Effect of the torrefaction cycle process on the ultimate *G. pseudoarundinacea* bamboo pellets

Parameters	Treatments		
	C1	C2	C3
C	47.46	48.99	52.86
N	0.35	0.31	0.29
H	6.23	5.89	5.7
O (diff)	45.96	44.81	41.15
O/C	0.97	0.91	0.78
H/C	0.13	0.12	0.11

decrease in volatile matter content with an increasing torrefaction temperature. These findings align with prior studies on woody biomass (Colin et al., 2017). The ash content in each cycle is relatively low, ranging from 1.13–1.81%, below the maximum limit specified in SNI 8675-2018 of 5%. Increasing the torrefaction temperature of bamboo pellets resulted in higher fixed carbon, increasing their calorific value, which is in line with increased ash content, making the pellets more difficult to burn and resulting in a larger residue. However, a slight increase in ash content did not significantly reduce the calorific value. The high carbon value and low ash content of bamboo pellets directly impact calorific value, improving the quality of solid fuels (Niu et al., 2019).

#### Ultimate analysis

The torrefaction with the Fixed COMB reactor used limited oxygen to prevent combustion, improving the C content in the product (pellet). The C3, with a longer residence time than the other treatments, had the highest C content of 52.86% (Table 6), which is expected for solid fuel. The Fixed COMB reactor increased the C content by 11%. This result shows a higher C content than torrefaction using a slot-spouted rectangular bed reactor at the highest temperature and residence time (Wang et al., 2019). However, under the same conditions, it was still lower than when using a moving bed reactor (Kongto et al., 2021). A high C content is beneficial

for solid fuel because it corresponds to the highest HHV (Niu et al., 2019), as shown in Fig. 6. Formerly, the concentrations of N, H, and O declined by 0.29%, 5.7%, and 41.15%, respectively, after C3 was performed. Less N content in solid fuel will decrease the induced heavy emission of nitrogen oxide ( $\text{NO}_x$ ), which is toxic to the environment, during combustion; simultaneously, reducing the concentrations of H and O can effectively mitigate the production of water vapor and smoke during combustion (Matali et al., 2016) and increase hydrophobic properties (Saputra et al., 2022).

The Van Krevelen diagram indicates that the concentration ratio of C, H, and O determines the quality of solid fuel for combustion. A lower concentration ratio indicates a higher quality of solid fuels. This is supported by the observation that torrefied biomass exhibits properties similar to lignite and coal due to chemical changes caused by heat treatment (Poudel et al., 2018). The diagram in Fig. 6 shows that as a cycle was added, the value lowered. The C3 is the lowest value among the treatments, and the distance is promptly shown, which indicates better solid fuel quality. This follows the same trend in the torrefaction of various biomasses, indicating a preference for coal at temperatures over 250°C. The comparison of the cycle depicted in Fig. 6 reveals that the torrefaction decomposition process involves significant dehydration. This is evident from the observed changes in the O/C and H/C atomic ratios of

the biomass, which align with dehydration pathways. The decrease in hydrogen and oxygen content during the torrefaction process, which leads to increased HHV in torrefied bamboo, is primarily attributed to hydrogen and deoxygenation reactions (Fig. 7; Li et al., 2015). A torrefied biomass with low O/C and H/C ratios is a suitable solid fuel due to its reduced emissions of smoke, water vapor, and energy loss during combustion (Nunes et al., 2014).

**FTIR analysis**

FTIR analysis was performed to determine the

chemical composition of the biomass and to observe changes in the functional groups (Samimi, 2024) (Fig. 8). The peak range at 3,600–3,200/cm, shown in Table 7 and corresponding to the hydroxyl group (OH), decreased as cycles were added. The functional groups of the methyl group (CH) were found in the peak range of 3,000–2,700/cm. The lignin structure or carbon-carbon double bond (C=C) group was found at a peak of 1,800–1,500/cm. The carbon-oxygen single bond (C-O) group was found at a peak range of 1,200–900/cm; it decreased with increasing temperatures. The findings of this study are in

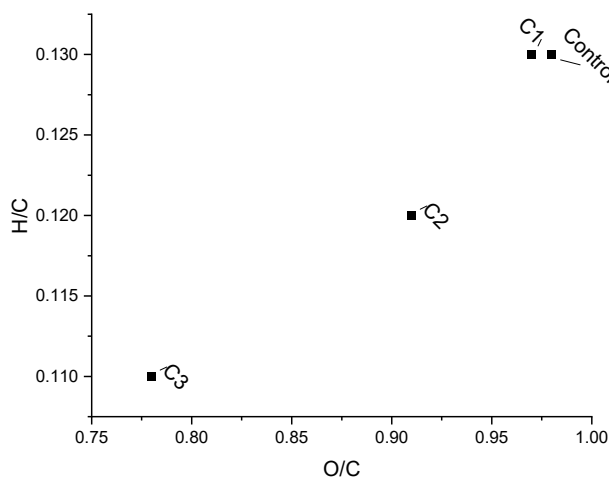


Fig. 7: Van Krevelen diagram of the torrefaction of *G. pseudoarundinacea*.

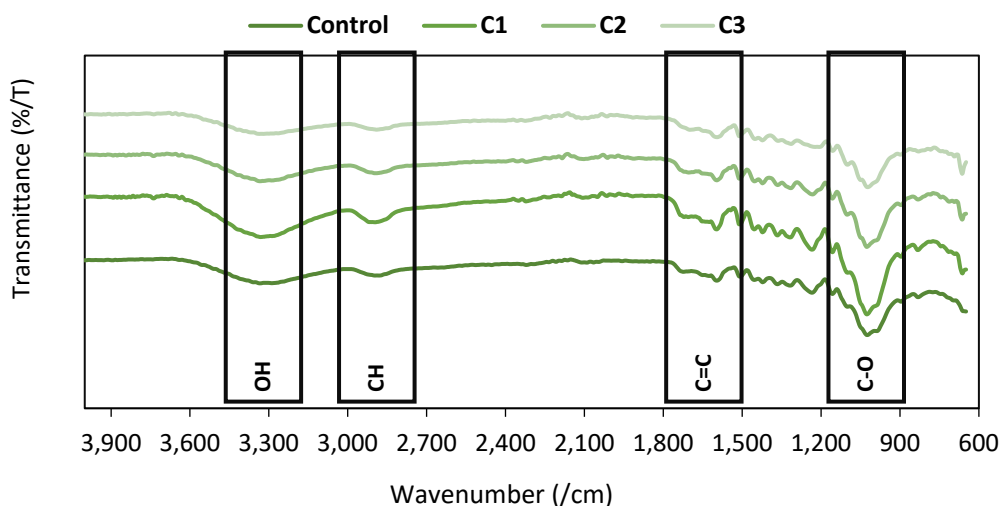


Fig. 8: FTIR analysis of *G. pseudoarundinacea* bamboo pellets before and after torrefaction at various cycles.

Table 7: Compound type for FTIR analysis of *G. pseudoarundinacea* bamboo pellets

Elemental bonds	Peak range (/cm)	Compound type
OH	3,600–3,200	Acid, methanol
CH	3,000–2,700	Alkane
C=C	1,800–1,500	Benzene
C-O	1,200–900	Ethanol

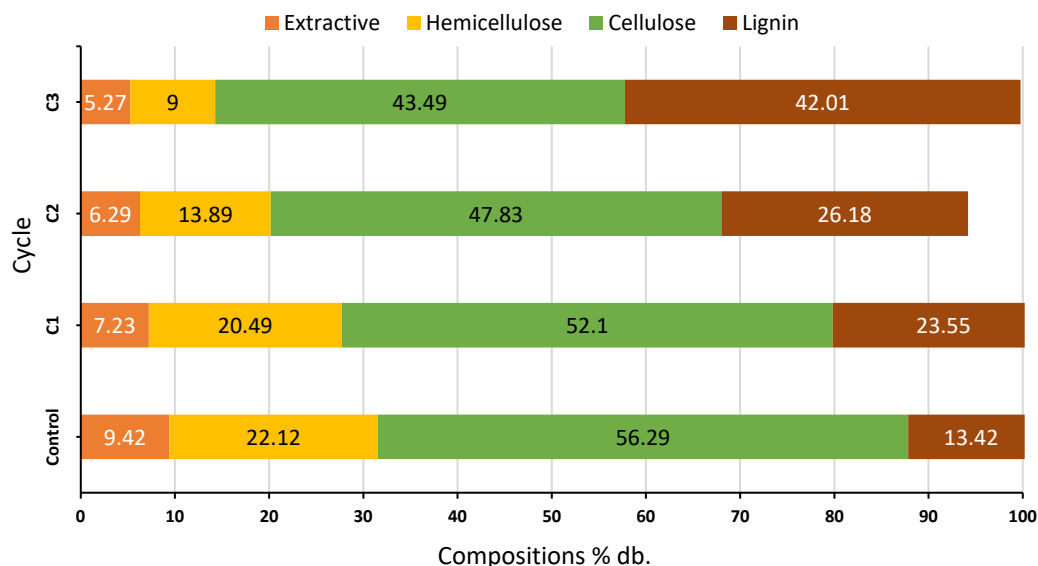


Fig. 9: Chemical compositions change due to the torrefaction cycle.

good agreement with those of [Chen et al. \(2015\)](#) and other studies of soybean straw pellets and pine wood pellets ([Cao et al., 2021](#)) and rice husk, groundnut shell, and corn cob ([Garba et al., 2018](#)). The high temperature during torrefaction triggered a biopolymer breakdown, resulting in a distinct peak between raw and torrefied pellets that declined as the cycle number increased ([Manatura, 2020](#)). [Chen et al. \(2015\)](#) clarified that torrefaction significantly affects the decomposition of carbohydrates, proteins, and lipids. Higher temperatures encourage the degradation of hemicellulose, cellulose, and lignin by adding cycles and changes in functional groups that are becoming larger, as illustrated by the steeper absorption peak ([Fig. 8](#)).

#### Chemical analysis

[Fig. 9](#) shows that the extractive and hemicellulose fractions are more susceptible to degradation through thermal treatment than cellulose and lignin.

Cellulose undergoes partial decomposition in C1. The analytical findings indicate an increase in lignin content following torrefaction. Torrefaction can be achieved rapidly using a Fixed COMB reactor, with a residence time as short as 3 minutes. The impact of temperature on biomass degradation was more significant than residence time. As a result, the C1 process caused only minimal chemical changes due to its short torrefaction duration. The chemical compositions decreased mainly due to hemicellulose degradation and extractive loss after water evaporation in addition to the torrefaction process ([Shoulafar et al., 2014](#)). C3 treatment reduced hemicellulose by 59.31%; however, extractive and cellulose treatments reduced it by only 44.05% and 22.73%, respectively. This is because hemicellulose is substantially more thermally unstable than other compositions ([Shen et al., 2010](#)). At C3, the lignin content increased by 313%, while the other components were reduced. This is attributed to the

wide temperature range of lignin, which spans from 180–900°C (Chen *et al.*, 2015). Lignin is retained in the solid product, while the remaining components undergo decomposition. Because lignin has emerged as the predominant energy source in biomass, a high lignin concentration will enhance HHV (Duranay and Akkuş, 2021).

## CONCLUSION

The bamboo pellets' physical, chemical, and thermal properties changed significantly after the addition of the torrefaction cycle. Torrefaction changed the bamboo pellet color, indicating darker and better pellets for solid fuel use. Torrefaction using a Fixed COMB reactor reduced moisture content by 99.8% at C3, indicating the highest moisture decrease of all reactors. Lower moisture content reduced fungal growth and improved biomass storage and transportation. Torrefaction increased the calorific value and physical and mechanical properties. C3 pellets had the highest HHV of 21.62 MJ/kg, 16.6% higher than the raw pellets. Torrefaction decreases density and compressive strength, improving grindability and combustion to make better pellets. The torrefaction cycle increased fixed carbon, volatile matter, and ash. The final analysis showed increased carbon and decreased nitrogen, hydrogen, and oxygen, improving solid fuel quality, energy density, and combustion emissions. FTIR analysis showed torrefaction-induced changes in functional groups and chemical composition, including extractive and hemicellulose degradation and lignin increase. The chemical analysis showed that temperature and residence time degraded hemicellulose and increased lignin concentration in the torrefied pellets. C3 was a preferable pellet among all treatments, achieving the highest calorific value and a low moisture content that improved biomass storage. In conclusion, the Fixed COMB reactor torrefaction process improved *G. pseudoarundinacea* bamboo pellet properties for solid fuel use. This study's findings help understand torrefaction and how to optimize conditions to produce high-quality biomass products. These findings can be used to investigate torrefaction's potential benefits in various industries and energy sectors.

## AUTHOR CONTRIBUTIONS

W. Hidayat defined the study direction's concept,

decision, and justification. B.A. Wijaya and B.B. Park performed the data analysis and its interpretation. B. Saputra performed the experiments and drafted the manuscript text. I.T. Rani created the figures, tables, and graphics. S. Kim performed the research methodology. S. Lee was responsible for consultation as well as the analysis of the research findings. J. Yoo performed an analysis of the study findings using instrumental methods. L. Suryanegara and M.A.R. Lubis provided consultations and analyzed the characteristics of the bamboo.

## ACKNOWLEDGEMENT

The authors acknowledge the funding received from the project titled "Establishment of Low-Carbon ISWM Center in Indonesia" with the following contact number: [334/UN26.14/TU/2023]. This research was also supported by the FRIEND (Fine Particle Research Initiative in East Asia Considering National Differences) Project through the National Research Foundation of Korea (NRF) funded by the Ministry of Science and ICT (No. 2022M3G1A1020872).

## CONFLICT OF INTEREST

The authors declare that there is no conflict of interest regarding the publication of this manuscript. In addition, the authors protected against ethical issues, including plagiarism, informed consent, misconduct, data fabrication and/or falsification, double publication and/or submission, and redundancy.

## OPEN ACCESS

©2024 the author(s). This article is licensed under a Creative Commons Attribution 4.0 International License, which permits use, sharing, adaptation, distribution, and reproduction in any medium or format, as long as you give appropriate credit to the original author(s) and the source, provide a link to the Creative Commons license, and indicate if changes were made. The images or other third-party materials in this article are included in the article's Creative Commons license unless indicated otherwise in a credit line to the material. If material is not included in the article's Creative Commons license and your intended use is not permitted by statutory regulation or exceeds the permitted use, you will need to obtain permission directly from the copyright holder. To view a copy of this license, visit:

<http://creativecommons.org/licenses/by/4.0/>

**PUBLISHER'S NOTE**

The GJESM publisher remains neutral concerning jurisdictional claims with regard to published maps and institutional affiliations.

**ABBREVIATIONS**

%	Percent	<i>D</i>	Density
<	Is less than	<i>db.</i>	Dry basis
>	Is greater than	<i>DTG</i>	Derivatives thermogravimetric
±	Plus or minus	<i>FTIR</i>	Fourier-transform infrared
$\Delta a^*$	Change in red/green chromaticity	<i>G</i>	Gram
$\Delta b^*$	Change in yellow/blue chromaticity	$g/cm^3$	Gram per cubic centimeter
$\Delta E^*$	Overall color change	<i>G/S</i>	Gas to solid ratio
$\Delta L^*$	Change in lightness	<i>GHG</i>	Greenhouse gas
≤	Is less than or equal to	<i>H</i>	Hydrogen
°C	Degree Celsius	<i>H/C</i>	Ratio of hydrogen (H) atoms to carbon (C) atoms in a molecule
<i>A</i>	Surface area	$H_2SO_4$	Sulfuric acid
$a^*$	Red/green chromaticity	<i>HHV</i>	Higher heating value
<i>ASTM</i>	American Society for Testing Materials	<i>ID Fan</i>	Induced draft fan
$b^*$	Yellow/blue chromaticity	<i>KBr</i>	Potassium bromide
<i>Bt</i>	Billion ton	<i>Kg</i>	Kilogram
<i>C</i>	Carbon	$kg/h$	Kilogram per hour
<i>C=C</i>	Carbon-carbon double bond	<i>KIER</i>	Korea Institute of Energy Research
<i>C1</i>	First cycle	$L^*$	Lightness
<i>C2</i>	Second cycle	<i>LPG</i>	Liquefied petroleum gas
<i>C3</i>	Third cycle	<i>LTS-LCCR</i>	Long-Term Strategy for Low Carbon and Climate Resilience
<i>CCS</i>	Carbon capture storage	<i>MC</i>	Moisture content
<i>CH</i>	Methyl group	<i>Mg</i>	Milligram
<i>CHP</i>	Combined heat and power	<i>MJ</i>	Megajoule
<i>CIE-Lab</i>	Commission Internationale de l'Eclairage	$MJ/kg$	Megajoules per kilogram
<i>Cm</i>	Centimeter	<i>mL</i>	Milliliter
$cm^3$	Cubic centimeter	$mm^2$	Millimeter square
$cm^3/min$	Cubic centimeter per minute	<i>MPa</i>	Megapascal
<i>CMA</i>	Meeting of the Parties to the Paris Agreement	<i>N</i>	Newton
<i>C-O</i>	Carbon-oxygen single bond	<i>N</i>	Nitrogen
$CO_2$	Carbon dioxide	$N/mm^2$	Newton per square millimeter
<i>COMB</i>	Counter-flow multi-baffle	<i>NDC</i>	Nationally determined contributions
<i>CS</i>	Compressive strength	<i>NOx</i>	Nitrogen oxide
		<i>O</i>	Oxygen
		<i>O (diff)</i>	Oxidation (diffusion)
		<i>O/C</i>	Ratio of oxygen (O) atoms to carbon (C) atoms in a molecule
		<i>OH</i>	Hydroxyl group

<i>P</i>	Maximum test load
<i>SNI</i>	Standar Nasional Indonesia (Indonesian National Standard)
<i>T1</i>	Column bottom
<i>T2</i>	Column top
<i>TG</i>	Thermogravimetric
<i>TGA</i>	Thermogravimetric analysis
<i>TWh</i>	Terawatt-hour
<i>UNFCCC</i>	United Nations Framework Convention on Climate Change
<i>W</i>	Weight
<i>wt.%</i>	Percent by weight
<i>wt.% db.</i>	Weight percent dry basis

## REFERENCES

- Bajwa, D.S.; Peterson, T.; Sharma, N.; Shojaeiarani, J.; Bajwa, S.G., (2018). A review of densified solid biomass for energy production. *Renewable Sustainable Energy Rev.*, 96: 296–305 **(10 Pages)**.
- Bonechi, C.; Consumi, M.; Donati, A.; Leone, G.; Magnani, A.; Tamasi, G.; Rossi, C., (2017). Biomass: An overview, in: Dalena, F.; Basile, A.; Rossi, C. (Eds.), *Bioenergy systems for the future: Prospects for biofuels and biohydrogen*. Woodhead Publishing.
- Burhenne, L.; Messmer, J.; Aicher, T.; Laborie, M.P., (2013). The effect of the biomass components lignin, cellulose and hemicellulose on TGA and fixed bed pyrolysis. *J. Anal. Appl. Pyrolysis*, 101: 177–184 **(8 Pages)**.
- Cao, X.; Zhang, J.; Cen, K.; Chen, F.; Chen, D.; Li, Y., (2021). Investigation of the relevance between thermal degradation behavior and physicochemical property of cellulose under different torrefaction severities. *Biomass Bioenergy*. 148: 106061 **(7 pages)**.
- Chaves, B.; Macedo, L.; Galvão, L.; Carlos, A.; Palhano, A.; Vale, A.; Silveira, E.A., (2021). Production and characterization of raw and torrefied *Phyllostachys aurea* pellets and briquettes for energy purposes. 29th European Biomass Conference and Exhibition, 657–661 **(5 pages)**.
- Chen, W.H.; Peng, J.; Bi, X.T., (2015). A state-of-the-art review of biomass torrefaction, densification and applications. *Renewable Sustainable Energy Rev.*, 44: 847–866 **(20 Pages)**.
- Colin, B.; Dirion, J.L.; Arlabosse, P.; Salvador, S., (2017). Quantification of the torrefaction effects on the grindability and the hygroscopicity of wood chips. *Fuel*. 197: 232–239 **(8 Pages)**.
- Datta, R., (1981). Acidogenic fermentation of lignocellulose-acid yield and conversion of components. *Biotechnol. Bioeng.*, 23(9): 2167–2170 **(4 Pages)**.
- Dhanasekar, S.; Sathyanathan, R., (2023). Bioenergy potential of *Chlorella vulgaris* under the influence of different light conditions in a bubble column photobioreactor. *Global J. Environ. Sci. Manage.*, 9(4): 789-804 **(16 pages)**.
- Duranay, N.D.; Akkuş, G., (2021). Solid fuel production with torrefaction from vineyard pruning waste. *Biomass Convers. Biorefin.*, 11(6): 2335–2346 **(12 Pages)**.
- Ehzari, H.; Safari, M.; Samimi, M.; Shamsipur, M.; Gholivand, M.B., (2022). A highly sensitive electrochemical biosensor for chlorpyrifos pesticide detection using the adsorbent nanomatrix contain the human serum albumin and the Pd: CdTe quantum dots. *Microchem. J.*, 179: 107424 **(10 pages)**.
- Favero, A.; Daigneault, A.; Sohngen, B., (2020). Forests: Carbon sequestration, biomass energy, or both? *Sci. Adv.*, 6(13): 1–14 **(14 Pages)**.
- Garba, M.U.; Gambo, S.U.; Musa, U.; Tauheed, K.; Alhassan, M.; Adeniyi, O.D., (2018). Impact of torrefaction on fuel property of tropical biomass feedstocks. *Biofuels*. 9(3): 369–377 **(9 Pages)**.
- García, R.; Gil, M.V.; González, V.M.P.; Rubiera, F.; Pevida, C., (2019). Biomass pelletization: Contribution to renewable power generation scenarios, in: Fang, F.; Smith, R.L.; Tian, X.F. (Eds.), *Production of Materials from Sustainable Biomass Resources*. Springer Singapore.
- Gielen, D.; Boshell, F.; Saygin, D.; Bazilian, M.D.; Wagner, N.; Gorini, R., (2019). The role of renewable energy in the global energy transformation. *Energy Strategy Rev.*, 24: 38–50 **(13 Pages)**.
- Government of Indonesia., (2022). Enhanced Nationally Determined Contribution Republic of Indonesia. Ministry of Environment and Forestry Republic of Indonesia.
- Hazbehean, M.; Mokhtarian, N.; Hallajisani, A., (2022). Converting the cigarette butts into valuable products using the pyrolysis process. *Global J. Environ. Sci. Manage.*, 8(1): 133-150 **(18 pages)**.
- Hidayat, W.; Jang, J.H.; Park, S.H.; Qi, Y.; Febrianto, F.; Lee, S.H.; Kim, N.H., (2015). Effect of temperature and clamping during heat treatment on physical and mechanical properties of okan (*Cylicodiscus gabunensis* [Taub.] Harms) wood. *Open J. Bioresearch*, 10(4): 6961–6974 **(14 Pages)**.
- Hidayat, W.; Qi, Y.; Jang, J.H.; Febrianto, F.; Lee, S.H.; Chae, H.M.; Kondo, T.; Kim, N.H., (2017). Carbonization characteristics of juvenile woods from some tropical trees planted in Indonesia. *J. Fac. Agric., Kyushu University.*, 62(1): 145–152 **(8 Pages)**.
- Hidayat, W.; Rani, I.T.; Yulianto, T.; Febryano, I.G.; Iryani, D.A.; Hasanudin, U.; Lee, S.; Kim, S.; Yoo, J.; Haryanto, A., (2020). Peningkatan kualitas pelet tandan kosong kelapa sawit melalui torefaksi menggunakan reaktor counter flow multi-baffle (COMB). *J. Rekayasa Proses*. 14(2): 169–181 **(13 Pages)**.
- Hidayat, W.; Rubiyanti, T.; Sulistio, Y.; Iryani, D.A.; Haryanto, A.; Amrul.; Yoo, J.; Kim, S.; Lee, S.; Hasanudin, U., (2021). Effects of torrefaction using COMB dryer/pyrolizer on the properties of rubberwood (*Hevea brasiliensis*) and jabon (*Anthocephalus cadamba*) pellets. *Proceedings of the International Conference on Sustainable Biomass (ICSB 2019)*, 202: 209–213 **(5 Pages)**.
- Huang, Z.; Jiang, S.; Guo, J.; Wang, X.; Tan, M.; Xiong, R.; Wang, Z.; Wu, Z.; Li, H., (2020). Oxidative torrefaction of *Phragmites australis*: Gas-pressurized effects and correlation analysis based on color value. *Energy Fuels*. 34(9): 11073–11082 **(10 Pages)**.
- IESR., (2022). Indonesia energy transition outlook 2023: Tracking progress of energy transition in Indonesia: Pursuing energy security in the time of transition. Institute for Essential Services Reform (IESR).
- Iftikhar, M.; Asghar, A.; Ramzan, N.; Sajjadi, B.; Chen, W.Y., (2019). Biomass densification: Effect of cow dung on the physicochemical properties of wheat straw and rice husk based biomass pellets. *Biomass Bioenergy*. 122: 1–16 **(16 Pages)**.
- Iryani, D.A.; Haryanto, A.; Hidayat, W.; Amrul, Talambanua, M.;

- Hasanudin, U.; Lee, S., (2019). Torrefaction upgrading of palm oil empty fruit bunches biomass pellets for gasification feedstock by using COMB (counter flow multi-baffle) reactor. 7th TAE. 212–217 **(6 Pages)**.
- Jagnade, P.; Panwar, N. L.; Agarwal, C., (2022). Experimental investigation of kinetic parameters of bamboo and bamboo biochar using thermogravimetric analysis under non-isothermal conditions. *Bioenergy Res.*, 16: 1143–1155 **(13 Pages)**.
- Kang, D.; Lv, J.; Li, S.; Chen, X.; Wang, X.; Li, J., (2019). Relationship between bamboo growth status and woody plants in a giant panda habitat. *Ecol. Indic.*, 98: 840–843 **(4 Pages)**.
- Kongto, P.; Palamanit, A.; Chaiprapat, S.; Tippayawong, N., (2021). Enhancing the fuel properties of rubberwood biomass by moving bed torrefaction process for further applications. *Renewable Energy*. 170: 703–713 **(11 Pages)**.
- Lauri, P.; Havlík, P.; Kindermann, G.; Forsell, N.; Böttcher, H.; Obersteiner, M., (2014). Woody biomass energy potential in 2050. *Energy Policy*. 66: 19–31 **(13 Pages)**.
- Li, M.F.; Chen, C.Z.; Li, X.; Shen, Y.; Bian, J.; Sun, R.C., (2015). Torrefaction of bamboo under nitrogen atmosphere: Influence of temperature and time on the structure and properties of the solid product. *Fuel*. 161: 193–196 **(4 Pages)**.
- Liese, W.; Köhl, M., (2015). *Bamboo* (vol. 10). Springer International Publishing.
- Liu, X.; Liu, Z.; Fei, B.; Cai, Z.; Jiang, Z.; Liu, X., (2013). Comparative properties of bamboo and rice straw pellets. *Open J. Bioresour.*, 8(1): 638–647 **(10 Pages)**.
- Liu, Z.; Jiang, Z.; Fei, B.; Cai, Z.; Liu, X., (2014). Comparative properties of bamboo and pine pellets. *Wood Fiber Sci.*, 46(4): 510–518 **(9 Pages)**.
- Luo, J.; Lian, C.; Liu, R.; Zhang, S.; Yang, F.; Fei, B., (2019). Comparison of metaxylem vessels and pits in four sympodial bamboo species. *Sci. Rep.*, 9(1): 10876 **(11 Pages)**.
- Mamvura, T.A.; Pahla, G.; Muzenda, E., (2018). Torrefaction of waste biomass for application in energy production in South Africa. *S. Afr. J. Chem. Eng.*, 25: 1–12 **(12 Pages)**.
- Manatura, K., (2020). Inert torrefaction of sugarcane bagasse to improve its fuel properties. *Case Stud. Therm. Eng.*, 19: 100623 **(9 Pages)**.
- Mangurai, S.U.N.M.; Maulana, S.; Murda, R.A.; Muhamad, S.; Hidayat, W.; Bindar, Y., (2022). Physical and mechanical properties of bamboo oriented strand board under various post-thermal treatment duration. *J. Sylva Lestari*. 10(3): 310–320 **(11 Pages)**.
- Manouchehrinejad, M.; Mani, S., (2018). Torrefaction after pelletization (TAP): Analysis of torrefied pellet quality and co-products. *Biomass Bioenergy*, 118: 93–104 **(12 Pages)**.
- Matali, S.; Rahman, N.A.; Idris, S.S.; Yaacob, N.; Alias, A.B., (2016). Lignocellulosic biomass solid fuel properties enhancement via torrefaction. *Procedia Eng.*, 148: 671–678 **(8 Pages)**.
- Maulana, M.I.; Jeon, W.S.; Purusatama, B.D.; Nawawi, D.S.; Nikmatin, S.; Sari, R.K.; Hidayat, W.; Febrianto, F.; Kim, J.H.; Lee, S.H.; Kim, N.H., (2021). Variation of anatomical characteristics within the culm of the three *Gigantochloa* species from Indonesia. *Open J. Bioresour.*, 16(2): 3596–3606 **(11 Pages)**.
- Mei, Y.; Liu, R.; Yang, Q.; Yang, H.; Shao, J.; Draper, C.; Zhang, S.; Chen, H., (2015). Torrefaction of cedarwood in a pilot scale rotary kiln and the influence of industrial flue gas. *Bioresour. Technol.*, 177: 355–360 **(6 Pages)**.
- Niu, Y.; Lv, Y.; Lei, Y.; Liu, S.; Liang, Y.; Wang, D.; Hui, S., (2019). Biomass torrefaction: Properties, applications, challenges, and economy. *Renewable Sustainable Energy Rev.*, 115: 109395 **(18 Pages)**.
- Nunes, L.J.R.; Matias, J.C.O.; Catalão, J.P.S., (2014). A review on torrefied biomass pellets as a sustainable alternative to coal in power generation. *Renewable Sustainable Energy Rev.*, 40: 153–160 **(8 Pages)**.
- Pah, J.M.; Suryanegara, L.; Haryanto, A.; Hasanudin, U.; Iryani, D.A.; Wulandari, C.; Yoo, J.; Kim, S.; Lee, S.; Hidayat, W., (2021). Product characteristics from the torrefaction of bamboo pellets in oxidative atmosphere. *Proceedings of the International Conference on Sustainable Biomass*. 185–189 **(5 Pages)**.
- Park, S.; Kim, S.J.; Oh, K.C.; Cho, L.H.; Kim, M.J.; Jeong, I.S.; Lee, C.G.; Kim, D.H., (2020). Characteristic analysis of torrefied pellets: determining optimal torrefaction conditions for agri-byproduct. *Energies*. 13(2): 423 **(14 Pages)**.
- Peng, J.H.; Bi, H.T.; Lim, C.J.; Sokhansanj, S., (2013). Study on density, hardness, and moisture uptake of torrefied wood pellets. *Energy Fuels*. 27(2): 967–974 **(8 Pages)**.
- Poudel, J.; Karki, S.; Oh, S., (2018). Valorization of waste wood as a solid fuel by torrefaction. *Energies*. 11(7): 1641 **(10 Pages)**.
- Pradhan, P.; Mahajani, S.M.; Arora, A., (2018). Production and utilization of fuel pellets from biomass: A review. *Fuel Process. Technol.*, 181: 215–232 **(18 Pages)**.
- Rani, M.S.A.; Mohammad, M.; Sua'it, M.S.; Ahmad, A.; Mohamed, N.S., (2021). Novel approach for the utilization of ionic liquid-based cellulose derivative biosourced polymer electrolytes in safe sodium-ion batteries. *Polym. Bull.*, 78(9): 5355–5377 **(23 Pages)**.
- Rhofita, E.I.; Rachmat, R.; Meyer, M.; Montastruc, L., (2022). Mapping analysis of biomass residue valorization as the future green energy generation in Indonesia. *J. Cleaner Prod.*, 354: 131667 **(36 Pages)**.
- Ribeiro, J.M.C.; Godina, R.; Matias, J.C.D.; Nunes, L.J.R., (2018). Future perspectives of biomass torrefaction: Review of the current state-of-the-art and research development. *Sustainability*. 10(7): 1–17 **(17 Pages)**.
- Saha, N.; Fillerup, E.; Thomas, B.; Pilgrim, C.; Causer, T.; Herren, D.; Klinger, J., (2022). Improving bamboo's fuel and storage properties with a net energy export through torrefaction paired with catalytic oxidation. *Chem. Eng. J.*, 440: 135750 **(13 Pages)**.
- Samimi, M., (2024). Efficient biosorption of cadmium by *Eucalyptus globulus* fruit biomass using process parameters optimization. *Global J. Environ. Sci. Manage.*, 10(1) 1-11 **(11 pages)**.
- Samimi, M.; Shahriari-Moghadam, M., (2021). Isolation and identification of *Delftia lacustris* Strain-MS3 as a novel and efficient adsorbent for lead biosorption: Kinetics and thermodynamic studies, optimization of operating variables. *Biochem. Eng. J.*, 173: 108091 **(9 pages)**.
- Samimi, M.; Shahriari-Moghadam, M., (2023). The *Lantana camara* L. stem biomass as an inexpensive and efficient biosorbent for the adsorptive removal of malachite green from aquatic environments: kinetics, equilibrium and thermodynamic studies. *Int. J. Phytoremediation*, 25(10): 1-9 **(9 pages)**.
- Samimi, M.; Mansouri, E., (2023). Efficiency evaluation of *Falcaria vulgaris* biomass in Co(II) uptake from aquatic environments: characteristics, kinetics and optimization of operational variables. *Int. J. Phytoremediation*, 1-11 **(11 pages)**.

- Santoso, A.D.; T. Handayani, T.; Nugroho, R.A.; Yanuar, A.I.; Nadirah, N.; Widjaja, E.; Rohaeni, E.S.; Oktaufik, M.A.M.; Ayuningtyas, U.; Erlambang, Y.P.; Herdioso, R.; Rofiq, M.N.; Hutapea, R.; Sihombing, A.L.; Rustianto, B.; Susila, I.M.A.D.; Irawan, D.; Iskandar, D.; Indrijarso, S.; Widiarta, G.D., (2023). Sustainability index analysis of the black soldier fly (*Hermetia illucens*) cultivation from food waste substrate Global J. Environ. Sci. Manage., 9(4): 851-870 (20 pages).
- Saputra, B.; Tambunan, K.G.A.; Suri, I.F.; Febryano, I.G.; Iswandar, D.; Hidayat, W., (2022). Effects of torrefaction temperature on the characteristics of betung (*Dendrocalamus asper*) bamboo pellets. J. Teknik Pertanian Lampung. 11(2): 339-353 (15 Pages).
- Sharma, R.; Wahono, J.; Baral, H., (2018). Bamboo as an alternative bioenergy crop and powerful ally for land restoration in Indonesia. Sustainability. 10(12): 4367 (4 Pages).
- Shen, D.K.; Gu, S.; Bridgwater, A.V., (2010). The thermal performance of the polysaccharides extracted from hardwood: Cellulose and hemicellulose. Carbohydr. Polym., 82(1): 39–45 (7 Pages).
- Sher, F.; Yaqoob, A.; Saeed, F.; Zhang, S.; Jahan, Z.; Klemeš, J.J., (2020). Torrefied biomass fuels as a renewable alternative to coal in co-firing for power generation. Energy. 209: 118444 (13 Pages).
- Shoulaifar, T.K.; DeMartini, N.; Willför, S.; Pranovich, A.; Smeds, A.I.; Virtanen, T.A.P.; Maunu, S.L.; Verhoeff, F.; Kiel, J.H.A.; Hupa, M., (2014). Impact of torrefaction on the chemical structure of birch wood. Energy Fuels. 28(6): 3863–3872 (10 Pages).
- Solihat, N.N.; Sari, F.P.; Falah, F.; Ismayati, M.; Lubis, M.A.R.; Fatrisari, W.; Santoso, E.B.; Syafii, W., (2021). Lignin as an active biomaterial: A review. J. Sylva Lestari. 9(1): 1–22 (22 Pages).
- Suroso, D.S.A.; Setiawan, B.; Pradono, P.; Iskandar, Z.S.; Hastari, M.A., (2022). Revisiting the role of international climate finance (ICF) towards achieving the nationally determined contribution (NDC) target: A case study of the Indonesian energy sector. Environ. Sci. Policy. 131: 188–195 (8 Pages).
- Tu, R.; Sun, Y.; Wu, Y.; Fan, X.; Cheng, S.; Jiang, E.; Xu, X., (2022). The fuel properties and adsorption capacities of torrefied camellia shell obtained via different steam-torrefaction reactors. Energy. 238: 121969 (11 Pages).
- Valverde, J.C.; Moya, R., (2014). Correlation and modeling between color variation and quality of the surface between accelerated and natural tropical weathering in *Acacia mangium*, *Cedrela odorata* and *Tectona grandis* wood with two coatings. Color Res. Appl., 39(5): 519–529 (11 Pages).
- Via, B.K.; Adhikari, S.; Taylor, S., (2013). Modeling for proximate analysis and heating value of torrefied biomass with vibration spectroscopy. Bioresour. Technol., 133: 1–8 (8 Pages).
- Wang, Z.; Lim, C.J.; Grace, J.R., (2019). Biomass torrefaction in a slot-rectangular spouted bed reactor. Particuology. 42: 154–162 (9 Pages).
- Xiang, H.; Feng, Z.; Yang, J.; Hu, W.; Liang, F.; Yang, X.; Zhang, T.; Mi, B.; Liu, Z., (2020). Investigating the co-firing characteristics of bamboo wastes and coal through cone calorimetry and thermogravimetric analysis coupled with Fourier transform infrared spectroscopy. Waste Manage. Res., 38(8): 896–902 (7 Pages).
- Xin, S.; Yang, H.; Chen, Y.; Yang, M.; Chen, L.; Wang, X.; Chen, H., (2015). Chemical structure evolution of char during the pyrolysis of cellulose. J. Anal. Appl. Pyrolysis. 116: 263–271 (9 Pages).
- Yang, H.; Yan, R.; Chen, H.; Lee, D.H.; Zheng, C., (2007). Characteristics of hemicellulose, cellulose and lignin pyrolysis. Fuel. 86: 1781–1788 (8 Pages).
- Yu, S.; Park, J.; Kim, M.; Kim, H.; Ryu, C.; Lee, Y.; Yang, W.; Jeong, Y., (2019). Improving energy density and grindability of wood pellets by dry torrefaction. Energy Fuels. 33(9): 8632–8639 (8 Pages).
- Yulianto, J.; Thamrin, S.; Kuntjoro, Y.D.; Idris, A.M., (2022). Development of biomass co-firing technology by PT. Jawa Bali (PJB) power plant in supporting the energy transition towards net zero emission 2060 during the covid-19 pandemic. Int. J. Innovative Sci. Res. Technol., 7(7): 1555–1564 (10 Pages).
- Zakikhani, P.; Zahari, R.; Hameed S.M.T.; Abang, M.D.L., (2015). Thermal degradation of four bamboo species. Open J. Bioresour., 11(1): 414–425 (12 Pages).
- Zhang, Y.; Chen, F.; Chen, D.; Cen, K.; Zhang, J.; Cao, X., (2020). Upgrading of biomass pellets by torrefaction and its influence on the hydrophobicity, mechanical property, and fuel quality. Biomass Convers. Biorefin., 1–10 (10 Pages).

#### AUTHOR (S) BIOSKETCHES

**Hidayat, W.**, Ph.D., Associate Professor, Department of Forestry, Faculty of Agriculture, University of Lampung, Jl. Prof. Dr. Ir. Sumantri Brojonegoro No.1, Lampung 35141, Indonesia.

- Email: [wahyu.hidayat@fp.unila.ac.id](mailto:wahyu.hidayat@fp.unila.ac.id)
- ORCID: 0000-0002-6015-1623
- Web of Science ResearcherID: F-8410-2017
- Scopus Author ID: 6507549479
- Homepage: <https://www.unila.ac.id/>

**Wijaya, B.A.**, B.A. Research student, Climate Change Research Division, Korean Institute of Energy Research (KIER), Daejeon, 34129, Republic of Korea.

M.Sc. Candidate, Department of Environment and Forest Resources, College of Agriculture and Life Science, Chungnam National University, 99 Daehak-ro, Daejeon, 34134, Republic of Korea.

- Email: [bangun@kier.re.kr](mailto:bangun@kier.re.kr)
- ORCID: 0009-0004-6238-1029
- Web of Science ResearcherID: NA
- Scopus Author ID: 57547377200
- Homepage: <https://www.kier.re.kr/>

#### AUTHOR (S) BIOSKETCHES

**Saputra, B.**, B.A. student, Department of Forestry, Faculty of Agriculture, University of Lampung, Jl. Prof. Dr. Ir. Sumantri Brojonegoro No.1, Lampung 35141, Indonesia.

- Email: [bgs.saputra248@gmail.com](mailto:bgs.saputra248@gmail.com)
- ORCID: 0009-0000-4378-1853
- Web of Science ResearcherID: NA
- Scopus Author ID: NA
- Homepage: <https://www.unila.ac.id/>

**Rani, I.T.**, B.A. Research student, Climate Change Research Division, Korean Institute of Energy Research (KIER), Daejeon, 34129, Republic of Korea. M.Sc. student, Department of Environment and Forest Resources, College of Agriculture and Life Science, Chungnam National University, 99 Daehak-ro, Daejeon, 34134, Republic of Korea.

- Email: [irmathyar@gmail.com](mailto:irmathyar@gmail.com)
- ORCID: 0000-0002-3456-0079
- Web of Science ResearcherID: NA
- Scopus Author ID: NA
- Homepage: <https://www.kier.re.kr/>

**Kim, S.**, Ph.D., Researcher, Climate Change Research Division, Korean Institute of Energy Research (KIER), Daejeon, 34129, Republic of Korea.

- Email: [sdkim@kier.re.kr](mailto:sdkim@kier.re.kr)
- ORCID: 0000-0002-7746-145X
- Web of Science ResearcherID: NA
- Scopus Author ID: 7601601205
- Homepage: <https://www.kier.re.kr/>

**Lee, S.**, Ph.D., Researcher, Climate Change Research Division, Korean Institute of Energy Research (KIER), Daejeon, 34129, Republic of Korea.

- Email: [lsh3452@kier.re.kr](mailto:lsh3452@kier.re.kr)
- ORCID: 0000-0003-2346-3414
- Web of Science ResearcherID: NA
- Scopus Author ID: 56063656500
- Homepage: <https://www.kier.re.kr/>

**Yoo, J.**, Ph.D., Researcher, Climate Change Research Division, Korean Institute of Energy Research (KIER), Daejeon, 34129, Republic of Korea.

- Email: [jyoo@kier.re.kr](mailto:jyoo@kier.re.kr)
- ORCID: 0000-0002-4003-8180
- Web of Science ResearcherID: NA
- Scopus Author ID: 56063656500
- Homepage: <https://www.kier.re.kr/>

**Park, B.B.**, Ph.D., Department of Environment and Forest Resources, College of Agriculture and Life Science, Chungnam National University, 99 Daehak-ro, Daejeon, 34134, Republic of Korea.

- Email: [bbpark@cnu.ac.kr](mailto:bbpark@cnu.ac.kr)
- ORCID: 0000-0002-0620-7374
- Web of Science ResearcherID: NA
- Scopus Author ID: 7402834688
- Homepage: <https://forestry.cnu.ac.kr/forestry/>

**Suryanegara, L.**, Ph.D., Researcher, Research Center for Biomass and Bioproduct, National Research and Innovation Agency (BRIN). Jl. Raya Jakarta-Bogor Km. 46, Cibinong, Bogor, 16911, Indonesia.

- Email: [l\\_suryanegara@yahoo.co.id](mailto:l_suryanegara@yahoo.co.id)
- ORCID: 0000-0003-0060-0981
- Web of Science ResearcherID: AAS-6738-2020
- Scopus Author ID: 26326619700
- Homepage: <https://www.brin.go.id/>

**Lubis, M.A.R.**, Ph.D., Researcher, Research Center for Biomass and Bioproduct, National Research and Innovation Agency (BRIN). Jl. Raya Jakarta-Bogor Km. 46, Cibinong, Bogor, 16911, Indonesia.

- Email: [adlylubis89@gmail.com](mailto:adlylubis89@gmail.com)
- ORCID: 0000-0001-7860-3125
- Web of Science ResearcherID: K-2440-2019
- Scopus Author ID: 57192278476
- Homepage: <https://www.brin.go.id/>

#### HOW TO CITE THIS ARTICLE

Hidayat, W.; Wijaya, B.A.; Saputra, B.; Rani, I.T.; Kim, S.; Lee, S.; Yoo, J.; B.B. Park.; Suryanegara, L.; Lubis, M.A.R., (2024). Torrefaction of bamboo pellets using a fixed counter-flow multi-baffle reactor for renewable energy applications. *Global J. Environ. Sci. Manage.*, 10(1): 169-188.

DOI: [10.22034/gjesm.2024.01.12](https://doi.org/10.22034/gjesm.2024.01.12)

URL: [https://www.gjesm.net/article\\_707632.html](https://www.gjesm.net/article_707632.html)





## ORIGINAL RESEARCH ARTICLE

## Evaluation of mineral and near-infrared forecasting of wheat yield varieties using spectrophotometric techniques

H.A. Pardhe<sup>1</sup>, N. Krishnaveni<sup>1\*</sup>, B.K. Chekraverthy<sup>1</sup>, S. Patel<sup>2</sup>, S. Naveen<sup>3</sup>, V. Rashmi<sup>3</sup>, P.C. Govinden<sup>4</sup><sup>1</sup> Department of Pharmaceutical Analysis, JSS College of Pharmacy, JSS Academy of Higher Education and Research, Ooty, Nilgiris, Tamil Nadu, India<sup>2</sup> Department of Pharmaceutical Analysis, JSS Academy of technical education, Noida, India<sup>3</sup> Food Quality Assurance Division, DRDO-Defence Food Research Laboratory, Mysuru, Karnataka, India<sup>4</sup> Ministry of Agro-Industry and Food Security, Food Science and Technology Division, Mauritius

## ARTICLE INFO

## Article History:

Received 24 May 2023

Revised 18 August 2023

Accepted 12 September 2023

## Keywords:

Biofortified

Fortified

Mineral quantification

Proximate composition

Spectrophotometric techniques

## ABSTRACT

**BACKGROUND AND OBJECTIVES:** Iron, an essential micronutrient, significantly contributes to growth, immune health, and cognitive development in human health. Inadequate dietary iron intake leads to iron deficiency anemia, affecting nearly 1.6 billion people, especially pregnant women and preschool children. Biofortification and fortification of iron in wheat is an acceptable and cost-effective strategy to alleviate iron deficiencies. This study aims to address iron deficiencies through the strategy of fortification and biofortification of wheat varieties. The study places specific emphasis on the proximate composition and iron/mineral content of different wheat varieties. To achieve these objectives, different spectrometric methods were employed to analyze the wheat samples.

**METHODS:** Proximate and mineral quantification were carried out following standard Association of Official Analytical Chemists methods using ultraviolet-visible spectrophotometry, atomic absorption spectrometry, inductive coupled plasma-mass spectroscopy, and prediction was carried out using near-infrared spectra combined with chemometrics.

**FINDINGS:** The samples had moisture content (1.1- 4.5 percent), protein (18.0- 22.6 percent), fat (0.3 - 0.6 percent), gluten (6.3- 10.3 percent), fiber (0.3 - 1.4 percent), alcoholic acidity (0.04- 0.08 percent), ash (0.9- 1.7 percent), and carbohydrate (71.1- 75.2 percent). Iron was determined and compared by spectrophotometric methods. Iron concentration ranged from (0.7 to 6.3 milligrams/100 grams) in ultraviolet-visible analysis, (0.7 to 6.74 milligrams/100 grams) in atomic absorption spectrometry, and (0.81 to 6.8 milligrams/100 grams) in inductive coupled plasma-mass spectroscopy. The obtained results were compared with the standard "Food Composition and Food Safety Standard Authority of India" and predicted using near-infrared spectra combined with chemometrics.

**CONCLUSION:** The work aims to investigate the nutritional content of various wheat varieties, particularly focusing on iron content, which could potentially have implications for improving dietary strategies and addressing nutritional deficiencies. The biofortified varieties (HI-8663 and HI-1605) were found to have high iron content when compared to normal wheat. The acquired results bridge the intricate relationship between plant-based diets, micronutrient deficiencies, providing valuable insights into combating iron deficiencies in public health with the potential achievement of improved nutritional understanding, optimized wheat selection, advanced analytical techniques, education, awareness, and iron deficiency mitigation.

DOI: [10.22034/gjesm.2024.01.13](https://doi.org/10.22034/gjesm.2024.01.13)This is an open access article under the CC BY license (<http://creativecommons.org/licenses/by/4.0/>).

NUMBER OF REFERENCES

45



NUMBER OF FIGURES

5



NUMBER OF TABLES

7

\*Corresponding Author:

Email: [krisath@jssuni.edu.in](mailto:krisath@jssuni.edu.in)

Phone: +944 2083 447

ORCID: [0000-0003-0596-9489](https://orcid.org/0000-0003-0596-9489)

Note: Discussion period for this manuscript open until April 1, 2024 on GJESM website at the "Show Article".

## INTRODUCTION

Iron is an essential micronutrient that significantly contributes to growth, immune health, and cognitive development. As the world's population exceeds billions, malnutrition in public health remains a grave concern, with health issues often going unaddressed. In India, the focus of most health programs remains on children under five, women of reproductive age, and adolescents, while other health issues are often neglected (Vijayshree et al., 2023). Inadequate dietary iron intake, especially during critical periods of growth, development, infancy, and pregnancy, can lead to chronic blood loss, resulting in iron deficiency and increased perinatal risks for mothers and newborns (Chouraqui, 2022; Allen et al., 2018; Chaparro and Suchdev, 2019; Narozhnykh, 2023). Iron deficiency and associated anemia are widespread, affecting nearly 1.2 billion people, especially pregnant women (41.8%) and preschool children (47.4%) (Bruno and Egli, 2008; McLean et al., 2009; White and Broadley, 2009; Chekraverthy et al., 2023). Iron plays a crucial role in various physiological processes within the human body, making the identification of iron deficiency paramount in the biomedical field. Early detection and intervention can prevent the progression of anemia and its associated health complications. Various methods, including blood tests such as serum ferritin, serum iron, transferrin and total iron-binding capacity, hemoglobin, hematocrit levels, and complete blood count, are used to identify iron deficiency. These methods, combined with thorough clinical evaluation, help healthcare professionals diagnose and monitor iron deficiency, enabling timely intervention through dietary changes or addressing underlying causes. Regular monitoring of iron status is crucial, especially in vulnerable populations such as pregnant women, infants, and individuals with chronic diseases (Fernando and Santiago, 2009). Iron deficiency can be related to environmental factors in several ways. Firstly, the availability of iron in the environment can directly affect human intake. In areas where soil and water are low in iron content, there is a higher prevalence of iron deficiency, which can be problematic in agricultural regions where crops may fail to accumulate sufficient iron. This, in turn, can impact soil quality and plant growth. Low iron levels in soil can lead to reduced nutrient availability and poor plant growth, potentially affecting the overall nutritional intake of the

population. Iron deficiency can be addressed through various environmental strategies, including enriching soil with micronutrients/minerals to facilitate nutrient uptake by crops or improving agricultural practices (Rüdiger and Udo, 2003). Despite various supplementation efforts to treat malnutrition in India, the problem persists. In response, cost-effective dietary intervention strategies, such as fortification (physical mixture of ferrous forms) (Uauy et al., 2002) and biofortification (genetic manipulation) (Khush et al., 2012) have been developed to alleviate deficiencies. In recent years, dietary interventions, including the use of iron-fortified and biofortified functional foods, have played a vital role in addressing iron deficits. Among these staple varieties, Wheat (*Triticum aestivum*) is one of the most significant cereal crops grown worldwide, serving as a staple for nearly 2.5 billion people. It is of great interest due to its high consumption as a nutritional food with greater iron bioavailability compared to other staple foods (Arif et al., 2010). Special efforts have been initiated by the Indian Council of Agricultural Research (ICAR) to enrich wheat varieties like HI-8663 and HI-1605 with iron, reaching levels of about 40-43 parts per million (ppm), significantly higher than normal varieties. This biofortified form assumes great significance in achieving the nutritional security of the country (Kumar et al., 2020). When routinely consumed, fortified/biofortified foods can safely and effectively increase iron levels in the body, promoting human health through nutritional advantages. (Bouis and Saltzman, 2017). The Food Safety and Standards Authority of India (FSSAI) recommends daily iron intake of approximately 17 mg for adult men, 21-35 mg for women, 5 mg for infants, and 9 to 32 mg for boys and girls (ICMR, 2010; Chekraverthy et al., 2023). Therefore, there is a need to quantify the iron content in food products such as cereal crops, which are consumed daily. The fortification and biofortification strategies applied to various wheat varieties are expected to significantly improve the mineral content, specifically iron content. It is hypothesized that these strategies will lead to an increase in the iron/mineral content of wheat varieties, potentially contributing to a reduction in iron deficiency anemia and promoting overall human health. In this context, several techniques have been evaluated, including ultraviolet-visible spectrophotometry (UV/Vis), Atomic absorption spectrophotometry (AAS),

Table 1: Overview of the literature for assessment of quality parameters and minerals in wheat and wheat flour

SN	Methodology	Sources
1	Determination of iron in different types of wheat flours	Ihsanullah <i>et al.</i> , 2002
2	Quality assessment of different iron-fortified wheat flours	Arif <i>et al.</i> , 2010
3	Determination of iron species in samples of iron-fortified food	Niedzielski <i>et al.</i> , 2014
4	A comparative assessment of several quality parameters of normal commercial wheat flour in Bangladesh	Saeid <i>et al.</i> , 2015
5	Determination of iron content in wheat flour of organized and unorganized sector	Neerja Usha Kujur <i>et al.</i> , 2019
6	Profiling of nutritional traits in indigenous wheat cultivars	Parvez <i>et al.</i> , 2019
7	Evaluation of iron content in bakery flour samples of Tehran, Iran	Sara Mohamadi <i>et al.</i> , 2023
8	Proximate values and elemental analysis in wheat and soybean using inductively coupled plasma mass spectrometry	Kowmudi <i>et al.</i> , 2023

Inductive coupled plasma- mass spectrophotometry (ICP-MS) for mineral quantification, and near-infrared spectroscopy (NIR) for predicting the mineral content and proximate composition of fortified, biofortified, and normal wheat flours. Although extensive studies have been conducted on the proximate properties of functional wheat varieties globally, limited information is available on Indian biofortified and fortified wheat varieties (Raquel *et al.*, 2013; Poudel and Bhatta, 2017). An overview of the literature for the assessment of quality parameters and minerals in wheat and wheat flour is presented in Table 1.

NIR, a rapid, non-destructive tool, is used as a secondary method for predicting the proximate and mineral composition in wheat samples by developing accurate models. NIR spectrum combined with chemometric regression models, such as the partial least square regression model (PLSR), provides accuracy, with a coefficient of determination ( $r^2$ ), for predicting sample properties (Shun *et al.*, 2022). Limited research has been carried out to compare biofortified and fortified wheat varieties, and there is a gap in the scientific literature concerning NIR calibration development and the prediction of wheat flour composition (Iván *et al.*, 2023). This research work signifies a nutritional strategy to combat iron deficiencies by incorporating different wheat varieties into the diet and focuses on comparing and predicting the composition in terms of proximate and mineral content of various wheat varieties. The current study emphasizes proximate composition along with a comparative analysis of iron content in fourteen different wheat samples (i.e., biofortified, fortified, and normal wheat) using various spectrometric methods. Prediction of mineral and proximate composition is achieved using NIR

spectroscopy combined with chemometrics. The study places specific emphasis on the proximate composition and iron/mineral content of different wheat varieties. To achieve these objectives, various spectrometric methods were employed to analyze the wheat samples. The study was conducted at JSS College of Pharmacy, Ooty, Tamil Nadu, and DRDO-Defence Food Research Laboratory, Mysuru, India, during 2022-2023.

## MATERIALS AND METHOD

### *Samples collection and preparation*

Biofortified (BW) wheat varieties, specifically HI-8663 and HI-1605, as well as normal whole wheat varieties (NW) including HI-803, GW-H57, H-8753, LOK-303, and LOK-807, were sourced from various cultivars across India. Additionally, commercially available fortified (F) and normal wheat flours (NF) were obtained from a local market in Tamil Nadu. The research was conducted collaboratively at JSS College of Pharmacy in Ooty, Tamil Nadu, and the DRDO-Defence Food Research Laboratory in Mysuru, India. The collected samples were meticulously cleaned and allowed to air-dry for 48 hours before being processed using a laboratory pulverizer machine (sieve size - 1). Each flour sample was carefully stored in airtight containers at -4 degrees Celsius ( $^{\circ}\text{C}$ ) until further use. All chemicals utilized in this study were of analytical grade and procured from Sigma-Aldrich, India. Deionized and double-distilled water were employed throughout the entire research process. The proximate composition and mineral quantification were determined using established methods provided by the Association of Official Analytical Chemists (AOAC). For the prediction

of wheat flour composition, near-infrared spectroscopy (NIR) combined with chemometric techniques was employed.

#### *Instruments*

The essential mineral contents were determined using UV/Visible spectrophotometry (Shimadzu UV 1700), Atomic absorption spectrophotometry AAS (Shimadzu Atomic Absorption Spectrophotometer AA 6300), Inductive coupled plasma-Mass spectrophotometry (Nexion 300/350 ICP-MS) and NIR spectrometer (Brimrose luminar 5030) for prediction of wheat flour composition.

#### *Determination of proximate composition*

The analysis of wheat samples encompassed the assessment of moisture, ash, fiber, fat, protein, alcoholic acidity, gluten, and carbohydrate. In brief, the moisture content of the samples was determined through oven drying at 130°C for 2 hours until a constant weight was achieved, expressed as a percentage (Parvez, 2019). Following the determination of moisture content, the oven-dried samples were incinerated in a muffle furnace and maintained at a temperature of 550-600°C until grey ash was obtained. The ash value was then weighed according to the AOAC method (AOAC, 1995). Subsequently, the gluten content was calculated in its dried form, adhering to the AOAC procedure (AOAC, 2002; Kowmudi *et al.*, 2023). Protein extraction was performed using an alkaline extraction method, and quantification was achieved using Bovine serum albumin as a protein standard (Raghuramulu *et al.*, 1983; Plummer, 1988; Mæhre *et al.*, 2018; Samimi and Validov, 2018). The determination of fat content was conducted using the Soxhlet apparatus, employing petroleum ether as an extraction solvent. The extraction process was continued for 6 hours, followed by solvent evaporation and subsequent fat content calculation (AOAC, 2000). Fiber content was determined after fat extraction, utilizing petroleum ether as a solvent, and followed by acid and alkali condensation. Alcoholic acidity was determined following AOAC methods (AOAC, 2005). Lastly, carbohydrate content was calculated using a distinct method, namely: Total Carbohydrate = 100 - (moisture% + ash% + fiber% + fat% + protein%) (Owusua *et al.*, 2022).

#### *Determination of mineral content*

Iron analysis was conducted on 14 samples using Atomic Absorption Spectrophotometry (AAS) with hollow cathode lamps and an air-acetylene mixture. For this analysis, the samples were dry ashed in a muffle furnace at 525°C for 6 hours until white or grey ash was formed. The ash was then dissolved in 0.1N HCl, diluted to 50ml with deionized water, and the analysis was carried out. The fourteen wheat samples underwent mineral estimation, including Iron (Fe), Potassium (K), Magnesium (Mg), Calcium (Ca), Sodium (Na), Zinc (Zn), Manganese (Mn), Copper (Cu), Chromium (Cr), and Selenium (Se), using Inductive Coupled Plasma-Mass Spectrometry (ICP-MS). The following instrumental conditions were maintained: 1L/min Ar gas flow, He nebulizer gas flow of 0.98 L/min, a spray chamber temperature of 2°C; plasma power of 1600W; sample aspiration rate of 300µl/min (Kowmudi *et al.*, 2023). The method was optimized using a National Institute of Standards and Technology (NIST®) 1567b wheat flour as a standard reference material. Given that the selected biofortified and fortified wheat samples are enriched with iron, a comparative assessment of iron content was conducted and reported using different spectrometric techniques in accordance with AOAC official methods (Elemental Analysis Manual, 2015). Microwave digestion was also performed for the sample digestion using 5ml of nitric acid and 2ml of hydrogen peroxide following the digestion program as mentioned in Table 2. The samples underwent 30 minutes of heating followed by 15 minutes of cooling and were then diluted to 50ml using deionized water (Elemental Analysis Manual, 2015). The present work involved a comparative assessment of iron content in different wheat samples using three different spectrometric techniques. Iron quantification was achieved using UV spectrophotometry (Shimadzu UV 1700) in reaction with 2, 2'-bipyridyl in an acetate buffer environment at pH 4.5, employing a photometry wavelength of 520 nanometers (nm). This was followed by Flame Atomic Absorption Spectrophotometry (AAS) (Shimadzu Atomic Absorption Spectrophotometer AA 6300) equipped with standard hollow cathode lamps as a radiation source with air-acetylene flames, Inductive Coupled Mass Spectrometry (NexION 300/350 ICP-MS), and NIR for prediction. The aforementioned

Table 2: Microwave digestion program for iron estimation

Step	Power (W)	Ramp (min.)	Hold (min.)
1	500	01	04
2	1000	05	05
3	1400	05	10
4	00	-	15

spectrometric techniques have significant implications for the agricultural industry, particularly in terms of crop yield forecasting. These techniques enable the analysis of various minerals based on their spectral characteristics. In the context of crop yield forecasting, they provide valuable insights into plant health, growth, and crop quality, allowing for early detection of mineral shortages and quality assessments. These techniques empower farmers to make data-driven decisions that can lead to higher yields and sustainable farming practices

#### *NIR spectroscopy and chemometric methods*

NIR spectra were collected from a total of 15 wheat flour samples, which included NIST 1567b, biofortified, fortified, and normal wheat flours, for calibration development. The samples were analyzed using a Brimrose Lumina 5030 NIR spectrometer. NIR spectroscopy is a rapid and non-destructive technique (Shun *et al.*, 2022) employed for predicting wheat flour composition. The selected spectral range was between 1100-2100nm intervals, and the diffuse reflectance signal of the NIR spectrum is represented as  $\log(1/R)$ , where (R=reflectance) (Uma *et al.*, 2020). Calibration was carried out using the spectra of the samples and their respective proximate and mineral content, which had been analyzed in the laboratory. The obtained spectra were complex due to overtone and combinational vibration bands. To comprehend the intricate nature of the NIR spectra and predict the mineral and proximate composition, Chemometric analysis was employed. The spectral data underwent Chemometric treatment using The Unscrambler X 10.5 (64-bit) software. The Savitzky-Golay Algorithm was applied to minimize noise in the spectrum data, smoothen and enhance signals containing chemical information associated with the samples, and improve the calibration model building (Zhenjiao *et al.*, 2022). From the NIR data, in combination with the reference data, predictive models were developed using Partial Least Squares Regression (PLSR) to

assess the performance of the developed models. The impact of wavelength range and spectral pre-processing methods on the predictive ability of the model is discussed for individual parameters, and the best models were selected.

#### *Statistical analysis*

All measurements were carried out in triplicate for each of the samples and results were expressed as mean  $\pm$  values of standard deviations using Microsoft Excel, 2016, IBM SPSS statistic viewer, and the Unscrambler X 10.5 (64-bit) software.

## RESULTS AND DISCUSSIONS

### *Proximate composition of BW, NW, F, and NF wheat varieties*

The proximate composition of the wheat samples are represented in (Table 3) as Mean $\pm$ SD, and statistical analysis with positive correlation revealed significance at  $p < 0.01$ . The moisture content of the wheat samples ranged from 1.1% to 4.5%, with BW having the highest moisture content at 4.5% and Fortified flours showing the lowest moisture content of 1.1%. These results align with the standard FSSAI value for wheat and flour, which is  $< 14\%$  by weight. Moisture content is critical for maintaining the quality and shelf life of finished products, as lower moisture levels enhance storage stability, prevent mold formation, and inhibit other biochemical processes. The protein content ranged from 18.0% to 22.6%, with FF having the highest protein content at 22.6%, while BW had a protein content of 18.0%. Higher protein content indicates firmer dough, while lower protein content results in softer dough. The protein content found in the wheat flour samples was within acceptable limits, although it exceeded the average amount stated in the Indian Food Composition Table (IFCT, 2017). This discrepancy may be attributed to the higher protein content in the endosperm compared to wheat bran (Uauy *et al.*, 2006). Gluten content in the wheat samples varied from 6.3% to 10.3%, with

Table 3: Proximate composition of different wheat samples (%)

SN (Lab code)	Moisture	Ash	Fibre	Fat	Protein	Alcoholic acidity	Gluten	Carbohydrate
NW1	4.3± 0.05	1.5±0.05	1.36±0.05	0.56±0.05	20.43±0.05	0.08± 0.011	7.56± 0.05	71.6±0.05
NW2	3.66±0.05	1.2±0.01	1.13±0.05	0.60±0.01	21.4±0.05	0.08± 0.005	6.86± 0.05	72.0±0.05
NW3	4.4± 0.05	1.4± 0.05	0.83±0.05	0.26±0.05	20.1±0.05	0.08± 0.005	6.6±0.05	73.0±0.05
NW4	3.5±0.05	1.7±0.05	1.36±0.05	0.36±0.05	18.4±0.05	0.08±0.005	7.2±0.05	74.2±0.05
NW5	4.4±0.05	1.5±0.05	1.1±0.05	0.33±0.05	20.4±0.05	0.08±0.005	7.5±0.05	72.3±0.05
BW1	4.1±0.05	1.4±0.02	1.21±0.01	0.31±0.01	18.0±0.05	0.08±0.005	6.33±0.05	75.2±0.05
BW2	4.5±0.01	1.41±0.01	1.34±0.03	0.31±0.01	21.5±0.01	0.08±0.005	7.0±0.05	71.1±0.05
NF1	4.4±0.05	0.90±0.005	1.40±0.011	0.40±0.011	21.3±0.05	0.08±0.005	8.1±0.05	71.4±0.05
NF2	3.31±0.05	0.90±0.005	1.4±0.011	0.40±0.011	21.3±0.05	0.08±0.005	8.1±0.05	71.4±0.05
NF3	3.03±0.05	1.16±0.05	0.66±0.05	0.36±0.05	21.5±0.05	0.08±0.005	6.3±0.05	73.2±0.05
NF4	3.3±0.05	1.53±0.05	0.36±0.05	0.36±0.05	22.1±0.05	0.05±0.005	10.1±0.05	72.4±0.05
F1	1.13±0.05	1.5±0.05	0.33±0.05	0.33±0.05	22.6±0.05	0.05±0.005	10.3±0.05	74.1±0.05
F2	1.8±0.05	1.3±0.05	0.33±0.05	0.36±0.05	22.3±0.05	0.07±0.005	8.3±0.05	73.8±0.05
F3	1.8±0.05	1.3±0.05	0.36±0.05	0.33±0.05	21.6±0.05	0.04±0.005	6.6±0.05	74.4±0.05

\*NW-Normal wheat, BW- Biofortified wheat, NF-Normal flour, FF- Fortified flour

Values were presented as mean± standard deviation, n = 3. The data show a significant difference ( $p < 0.01$ ) between the different wheat varieties.

BW having the lowest content at 6.3% and NF at 10.3%. Gluten is responsible for the elastic properties and elongation of dough. The research findings comply with regulations stating that the weight of gluten in wheat flour should not be less than 6.0%. Fat content in wheat flour ranged from 0.3% to 0.6%, with NW having the highest fat content at 0.6%, while other samples had a content of 0.3%. These values fall within the acceptable range according to Indian Food Composition Table (IFCT) standards. Fat content is higher in whole wheat bran and germ but lower in flour, and variations can occur due to milling processes and differences in extraction rates (Adams *et al.*, 2002; Nisar *et al.*, 2020). The ash content in wheat varied from 0.9% to 1.7%, with NW having the highest ash content at 1.7% and NF at 0.9%. The total ash content of wheat flour should not exceed 2.0%

by weight, and the present data aligns with FSSAI regulations. Ash content is nutritionally significant as it contains minerals, but excessive ash levels can lead to undesirable darkening of dough and food products. Dietary fiber plays a crucial role in slowing the rate of glucose breakdown and absorption, maintaining glucose levels, and promoting continuous carbohydrate breakdown. The crude fiber content in different wheat flours ranged from 0.3% to 1.4%, with FF having the lowest fiber content of 0.3% and BW at 1.4%. National guidelines dictate that crude fiber in wheat flour should not exceed 2.5%. The alcohol acidity of wheat flour samples ranged from 0.04% to 0.08%, with NF and FF having the highest alcohol acid content at 0.08%. These values are within the permissible limit of 0.18 percent by weight set by FSSAI regulations. Carbohydrates are a significant source of

Table 4: Determination of iron content in wheat samples by UV/Vis, AAS, and ICP MS

Sample lab code	UV/ visible	AAS	ICP MS
	Expressed in mg/100g	Expressed in mg/100g	Expressed in mg/100g
NW1	4.4±0.05	4.2±0.02	4.2±0.05
NW2	1.6±0.05	1.7±0.05	2.0±0.05
NW3	0.7±0.05	0.7±0.005	0.84±0.005
NW4	0.7±0.05	0.74±0.005	0.81±0.005
NW5	2.90±0.005	2.24±0.005	2.86±0.05
BW1	6.33±0.05	6.74±0.011	6.86±0.05
BW2	6.13±0.05	6.24±0.005	6.27±0.01
NF1	2.16±0.05	2.23±0.05	2.36±0.05
NF2	2.23±0.05	2.06±0.05	2.46±0.05
NF3	1.4±0.05	1.24±0.01	1.23±0.005
NF4	1.4±0.05	1.43±0.05	1.53±0.05
F1	1.66±0.05	1.63±0.05	1.72±0.011
F2	4.56±0.05	5.1±0.01	5.33±0.05
F3	2.76±0.05	2.56±0.05	3.16±0.05

\*NW-Normal wheat, BW- Biofortified wheat, NF-Normal flour, FF- Fortified flour

Values were presented as mean± standard deviation, n = 3. The data show a significant difference ( $p < 0.01$ ) between the different wheat varieties.

energy and should be present in high concentrations in breakfast and weaning recipes. Carbohydrate content in various flours ranged from 71.0% to 75.2%, with BW showing the highest carbohydrate content at 75.2% and NF at 71.1%. National standards have not yet established specific criteria for wheat flour's carbohydrate content, although regular wheat flour typically contains around  $64.17 \pm 0.32$  or  $64.72 \pm 1.7$ , as stated in IFCT, 2017.

#### Comparative Iron quantification using three different instrumentation techniques

Mineral analysis using spectrophotometric methods plays a crucial role in predicting wheat composition by measuring the absorbance of light at different wavelengths. When applied to mineral analysis in agriculture, it provides insights into nutrient content in plants, which are crucial for affecting crop yield, nutrient assessment, optimal nutrient management, and early detection of deficiencies. Following the methodology described above, the iron content in fourteen samples of wheat and wheat flour has been presented (Table 4). Considering the samples analyzed by UV, AAS, and ICP-MS, the overall iron concentration ranged from 0.7 mg/100g to 6.8 mg/100g in UV, 0.75 mg/100g to 6.8 mg/100g in AAS, and 0.81 mg/100g to 6.8 mg/100g in ICP-MS. Both BW and FF were found to have high iron content compared to NW and NF. For example, BW1 had iron content of 6.3 mg/100g, 6.74 mg/100g, and 6.86 mg/100g in UV, AAS, and ICP- MS, respectively. BW2 had iron content

of 6.1 mg/100g, 6.24 mg/100g, and 6.27 mg/100g in UV, AAS, and ICP-MS, respectively. FF2 showed iron content of 4.56 mg/100g, 5.1 mg/100g, and 5.3 mg/100g in UV, AAS, and ICP-MS, respectively. As per IFCT standards, wheat and wheat flour should contain  $4.10 \pm 0.67$  mg/100g and  $3.97 \pm 0.78$  mg/100g, respectively. In comparison to these standards, the functional foods BW and FF had higher iron content than NF. Moreover, all the methods/techniques used in this study to quantify iron content were positively correlated, and the correlation was significant at  $p < 0.01$ . The samples were subjected to ICP-MS for mineral estimation because the presence of other minerals may promote or inhibit iron absorption, which also plays a vital role in human health and helps in the prevention of various deficiency disorders. Mineral analysis of NIST®1567b wheat flour was carried out to optimize the quantification method, and the limit of detection (LOD) and limit of quantification (LOQ) were determined and compared with the certified reference values, as shown in (Table 5). A study of the mean elemental composition of wheat samples showed that K, Mg, Ca, and Na were the most abundant elemental species. K values were higher in the flour samples, whereas Cr and Se values were lower in all the samples. All varieties of wheat flour exhibited maximum mineral content, but in the case of NF4, mineral content was found to be in trace amounts, and some minerals were not detected. These variations may be attributed to wide variations in soil and environmental conditions during crop cultivation

Table 5: Mineral analysis of NIST®1567b wheat flour using ICP-MS

	LOD $\mu\text{g/g}$	LOQ $\mu\text{g/g}$		
Na	0.010	0.500	6.71±0.21	6.83±0.07
Ca	0.010	0.500	191±3.3	200.01±3.09
Mg	0.010	0.500	398±12	407±6.34
K	0.010	0.500	1325±20	1334±11.8
Cr	0.001	0.008	NA*	0.04±0.01
Mn	0.001	0.008	9.00±0.78	8.95±0.37
Cu	0.050	0.100	2.03±0.14	1.92±0.06
Zn	0.050	0.100	11.6±0.26	11.8±0.53
Fe	0.050	0.100	14.1±0.33	13.8±0.37

\*NA: Not available

and warrant further investigation. This study revealed that the concentration of minerals followed the order of  $\text{K} > \text{Mg} > \text{Ca} > \text{Na} > \text{Fe} > \text{Zn} > \text{Mn} > \text{Cu} > \text{Cr} > \text{Se}$ . The data on mineral contents in fourteen wheat samples are presented in Table 6. Mineral quantification by ICP-MS was found to be statistically significant at  $p < 0.01$ . As per standard procedures, the present study was conducted to estimate the proximate composition along with iron determination in all fourteen wheat samples. Components like carbohydrates, protein, fat, moisture, etc., were determined and then compared to Indian food standard data (IFCT, 2017). To date, very few analytical techniques have been reported using UV-spectrometry and Atomic Absorption Spectrometry for iron estimation and proximate composition analysis. Limited information is available for a comparative approach to the nutritional and iron composition of fortified and biofortified Indian- based wheat cultivars. For instance, Saeid *et al.*, (2015) investigated different nutritional parameters comparatively in various commercially available wheat flours in Bangladesh, following AOAC protocols. Similarly, Niedzielski *et al.*, (2014) determined iron levels in food samples using UV and AAS techniques. However, there is limited research on the comparative analysis of mineral content in cereal crops. In another study, Akinyele and Shokunbi (2015) conducted a comparative extraction study comparing dry ashing and wet digestion methodologies. Additionally, Arif *et al.*, (2010) emphasized the importance of fortification in the quality assessment of iron in different fortified wheat flours, yielding promising results. Furthermore, Hailu Kassegn (2018) determined the proximate composition and bioactive components of Abyssinian purple wheat. However, no quantification was performed to compare BW

or FF wheat samples in this study. In this study, a comparative assessment of iron estimation was carried out in different functional wheat varieties using higher and more sophisticated instruments. The current study also showed better recovery and less contamination during digestion methods for analysis in wheat samples. Furthermore, it was observed that BW and FF showed significantly higher iron content when compared to the normal samples. The present analytical procedure is very reliable and sensitive in iron analysis, allowing for easy and quick assessment of bioactive components. The results of the analyte were compared with standard regulatory data, and they agreed with the standard reported values. This study highlights the effectiveness of BW and FF wheat by promising an increase in nutritional levels upon human consumption.

#### NIR spectrum and chemometric analysis

NIR spectroscopy is a powerful analytical technique for predicting mineral and wheat composition due to its non-destructive and rapid nature. The samples were scanned to record the reflectance spectra over a range of NIR wavelengths. A calibration model was developed that correlates with the known mineral content of the wheat samples, allowing the prediction of the mineral content of unknown samples by analysing their NIR spectra. When compared with traditional methods of analysis, NIR spectroscopy offers speed, efficiency, non-destructiveness, simultaneous multiple compound analysis, and accuracy. It can provide accurate predictions for various wheat yield components, which are mainly influenced by the quality of the calibration and instrument performance. The accuracy of the prediction was influenced by advanced chemometric

Table 6: Determination of mineral contents in wheat samples by ICP-MS (ppm)

SL. No.	Na	Ca	Mg	K	Cr	Mn	Cu	Zn	Se
NW1	5.1±0.05	1.27±0.005	3.34±0.005	20.63±0.005	0.01±0.005	0.113±0.005	0.03±0.005	0.113±0.005	0.02±0.005
NW2	5.52±0.005	4.95±0.005	26.3±0.011	90.46±0.005	0.021±0.001	0.41±0.005	0.061±0.001	0.40±0.011	0.02±0.005
NW3	5.64±0.005	5.06±0.005	28.9±0.011	110.5±0.005	0.02±0.005	0.40±0.011	0.06±0.001	0.45±0.005	0.02±0.002
NW4	6.52±0.005	10.6±0.01	54.6±0.011	196.9±0.005	0.03±0.001	1.23±0.005	0.14±0.005	1.04±0.005	ND
NW5	6.05±0.01	5.31±0.005	25.8±0.01	100.3±0.005	0.021±0.001	0.41±0.005	0.060±0.001	0.48±0.005	ND
BW1	6.32±0.005	5.32±0.005	25.7±0.005	90.12±0.005	0.02±0.005	0.45±0.005	0.05±0.005	0.40±0.011	ND
BW2	3.01±0.005	3.03±0.005	24.4±0.005	113.3±0.01	0.033±0.005	0.33±0.005	0.07±0.005	0.54±0.005	0.020±0.001
NF1	6.7±0.005	7.15±0.005	29.3±0.005	101.8±0.005	0.030±0.001	0.823±0.005	0.066±0.005	0.443±0.005	0.020±0.001
NF2	5.93±0.005	5.54±0.005	25.5±0.005	95.5±0.005	0.020±0.0011	0.65±0.005	0.07±0.005	0.44±0.005	0.020±0.001
NF3	6.84±0.01	10.7±0.005	19.9±0.005	279.8±0.005	0.04±0.005	0.27±0.005	0.090±0.0011	0.17±0.005	0.020±0.005
NF4	0.07±0.005	0.36±0.005	0.103±0.005	0.25±0.005	ND	0.02±0.005	ND	0.036±0.005	0.033±0.005
F1	0.74±0.005	0.28±0.005	0.56±0.005	5.81±0.005	ND	0.02±0.005	ND	0.010±0.005	ND
F2	0.61±0.01	0.92±0.005	1.98±0.005	46.7±0.005	ND	0.02±0.005	0.010±0.005	0.010±0.005	ND
F3	0.74±0.005	1.17±0.005	1.97±0.005	48.56±0.005	ND	0.030±0.0011	0.010±0.005	0.010±0.005	ND

\*NW-Normal wheat, BW-Bio-fortified wheat, NF-Normal flour, FF-Fortified flour, ND- Not detected

Values were presented as mean± standard deviation, n = 3. The data show a significant difference ( $p < 0.01$ ) between the different wheat varieties.

statistical analysis. The NIR spectrum of the samples was observed in the range of 1100-2100nm. The peak absorbance spectrum of the samples was obtained by the system, and chemometrics were applied for statistical analysis of the spectrum and laboratory-analyzed data. The obtained raw data was plotted in Fig. 1 as a line graph, which was further processed using the Savitzky Golay method for spectrum smoothing (Zhenjiao et al., 2022). Descriptive statistics of the data, as shown in Figs. 2 and 3 and

Table 7, indicated a higher standard deviation in K, Carbohydrate, Protein, and Mg compared to other parameters' data. Furthermore, PLSR analysis was applied along with the Nonlinear Iterative Partial Least Squares (NIPLAS) algorithm. It was observed that the first three factors were sufficient to predict the mineral and proximate composition of the wheat flour, as represented in Figs. 4 and 5. The PLSR analysis was carried out by considering factor 1 and 2 scores. NBW4, BW2, NB5, and NBW2 showed a positive

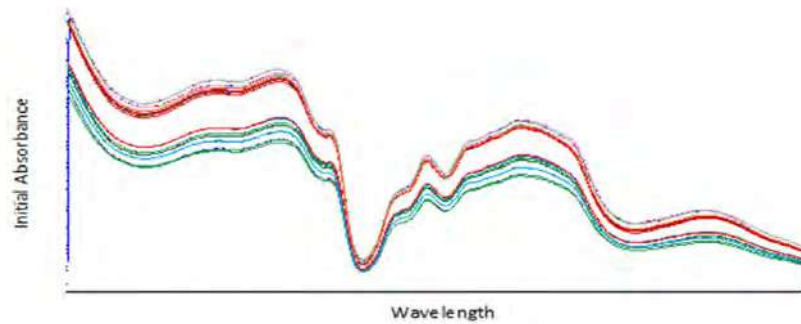


Fig. 1: Line plot of the raw sample spectrum data

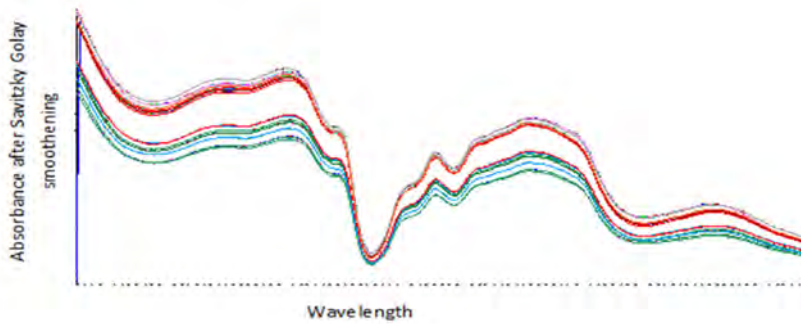


Fig. 2: Line plot after smoothing of the raw data by Savitzky Golay

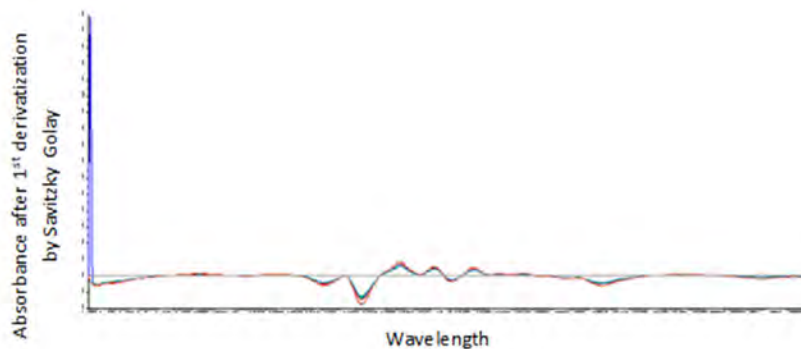


Fig. 3: Line plot after 1<sup>st</sup> derivatization by Savitzky Golay

correlation with each other and had coefficient loadings that predicted higher amounts of Moisture, Ash, Fiber, Carbohydrate, Fat, Alcoholic acidity, Zn, Mg, Fe, Ca, Na than other parameters. On the other hand, NB3, BW1, NBW1 showed a positive correlation with each other and were negatively correlated with other samples. They predicted higher amounts of Mn, Gluten, and Protein than other parameters. NFW1, NF3, NF4, FW3 showed a good correlation with high Moisture, Ash, Fiber, Carbohydrate, Fat, Alcoholic acidity, Zn, Mg, Fe, Ca, Na. NF2, FW1, 1567b, FW2 had a good correlation with high Protein, Gluten, Mn and were negatively correlated with the other independent variable samples.

The correlation coefficients between NIR predictions and reference analysis varied across different parameters. The lowest correlation

coefficient was observed in the prediction of fat content, with an  $r^2$  value of 0.826770, while a notably higher correlation coefficient of  $r^2 = 0.98385$  was found for carbohydrates, as detailed in Table 6. It is generally considered that NIR estimation is robust when the correlation coefficient between NIR readings and the reference method exceeds 0.75. Based on this criterion, it can be concluded that there was an acceptable relationship between observed and predicted values for all calibration parameters. Notably, the NIR data indicated that BW2 and FW3 predicted the highest iron content compared to the other samples, which aligns with the quantification results obtained using UV, AAS, and ICP-OES. These results demonstrate that the developed models are capable of accurately predicting the composition of the wheat samples.

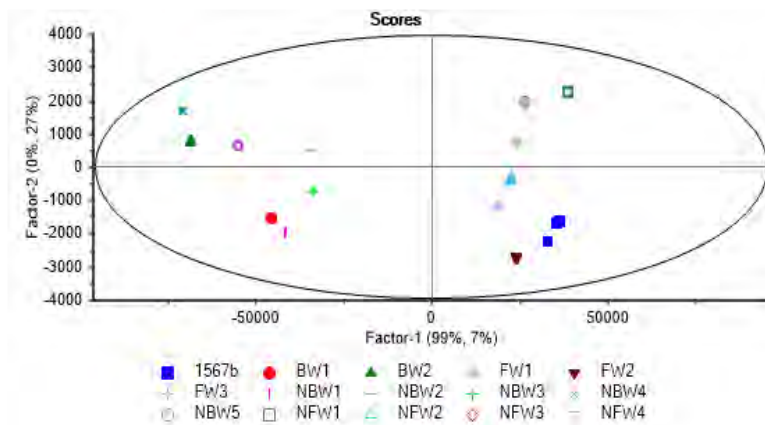


Fig. 4: Scores correlation between the different wheat flour samples

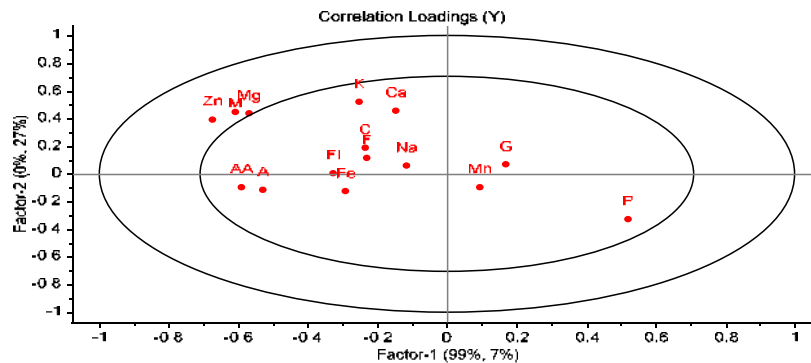


Fig. 5: Correlation loadings of the samples representing different parameters in the sample

Table 7: Standard deviation and correlation coefficient of the sample data by descriptive statistics.

Sl no.	M	A	Fi	F	Pr	AA	G	Cbh	Fe	Na	Ca	Mg	K	Mn	Zn
Mean	3.0	1.3	0.9	0.3	22.2	0.07	7.5	72.1	2.26	4.46	4.26	15.8	81.1	0.50	0.26
Max	4.5	1.8	1.75	0.6	31.7	0.095	10.3	75	5.51	9.05	10.76	54.65	279.84	2	1.04
Min	1.1	0.9	0.3	0.3	18	0.04	5.5	63.89	0.11	0.08	0.29	0.1	0.26	0.02	0.01
Range	3.4	0.9	1.45	0.3	13.7	0.055	4.8	11.11	5.4	8.97	10.47	54.55	279.58	1.98	1.03
SD	1.23	0.23	0.50	0.09	3.34	0.01	1.42	2.93	1.49	2.95	3.32	14.8	76.9	0.58	0.26
r <sup>2</sup>	0.969	0.961	0.961	0.8267	0.895	0.9178	0.8494	0.9838	0.9359	0.9117	0.9505	0.927586	0.94208	0.842214	0.92188

M- moisture; A- ash; Fi- fiber; F- fat; Pr- protein; AA- alcoholic acidity; G- gluten; Cbh- carbohydrate; Fe- iron; Na- sodium; Ca- calcium; Mg- magnesium; K- potassium; Mn- manganese; Zn- zinc; SD- standard deviation.

## **CONCLUSION**

Micronutrient deficiency, often referred to as hidden hunger, remains a widespread concern in populations, particularly among those who rely on undiversified plant-based diets. Adequate nutrition, including essential micronutrients, is pivotal for addressing malnutrition, particularly in vulnerable populations such as children and women who primarily consume plant-based diets. Iron, a crucial nutrient, plays a fundamental role in various biological processes. Nutritional strategies such as fortification and biofortification hold significant potential not only in alleviating micronutrient deficiencies but also in contributing to broader goals of sustainable agriculture and environmental stewardship. This research aims to make a meaningful contribution to the fight against iron deficiencies by thoroughly investigating the nutritional profiles of various wheat varieties, with a particular focus on their iron content. Such investigations have the potential to inform dietary strategies and effectively address nutritional deficiencies. Existing research on fortified and biofortified foods has generally yielded promising outcomes, indicating improvements in the nutritional status of participants. Regular assessment and analysis of mineral content in cereals and food products are essential for gaining a deeper understanding of the effectiveness of biofortification and fortification. To the best of our knowledge, this study represents a pioneering effort, especially in the comparative assessment of iron content in regular, fortified, and biofortified wheat varieties using various spectrophotometric techniques. Additionally, it involves the prediction of proximate and mineral composition through NIR spectroscopy and chemometric analysis. Among the spectrophotometric techniques employed, ICP-MS demonstrated exceptional sensitivity in quantifying iron and other trace elements, followed by AAS and UV-Visible spectrophotometry. The study also comprehensively investigated the proximate components in all wheat varieties, which were found to align with Indian dietary requirements. Notably, the biofortified varieties, namely HI8663 and HI1605, exhibited significantly higher iron content compared to fortified and normal wheat varieties. The calibration evaluation parameters and the development of PLSR models resulted in correlation coefficients between reference values and NIR

measurement values falling within the acceptable range. This demonstrates the efficacy of NIR technology in predicting the composition of samples, and these models can be readily applied to unknown samples, providing results comparable to laboratory determinations. The preliminary comparative analysis and NIR data prediction of biofortified and fortified wheat varieties offer valuable insights for identifying suitable varieties that can contribute to mitigating iron deficiencies and related anemia. The incorporation of spectrophotometric techniques into farming practices has the potential to revolutionize decision-making processes, enabling farmers to gain a deeper understanding of their crops' health, growth, and nutritional needs. This, in turn, can lead to more efficient resource management, reduced environmental impact, and ultimately, higher yields and improved economic returns. It is crucial to maintain vigilance regarding micronutrient intake, as some minerals may have adverse effects and be linked to various health problems. Raising awareness of nutrition and fitness needs is essential. In addition to addressing the single-nutrient deficiency at the heart of this research, biofortification and fortification represent sustainable solutions to tackle a range of micronutrient deficiencies that could affect future generations. Therefore, the findings of this study help bridge the intricate relationship between plant-based diets, micronutrient deficiencies, and sustainable agricultural practices, providing valuable insights for enhancing public health.

## **AUTHOR CONTRIBUTIONS**

H.A. Pardhe conducted the research, performed data analysis, and drafted the manuscript. N. Krishnaveni, the corresponding author, made significant contributions to the conceptualization and design of the study, data analysis and interpretation, and manuscript revision. B.K. Chekraverthy contributed to data analysis and manuscript drafting. S. Patel assisted in the procurement of samples and data analysis. S. Naveen provided technical support for the analysis of samples, and V. Rashmi offered technical assistance for spectrometric analysis. P.C. Govinden provided instrumental support

## **ACKNOWLEDGMENTS**

The authors especially would like to thank ICMR ADHOC [No. F.N.5/9/1323/2020-Nut; Ref No. NUT/

ADHOC/15/2020-21] for the financial support, DFRL Defence Food Research Laboratory, Mysuru for support in analytical work, and Department of Science and Technology- Fund for Improvement of Science and Technology Infrastructure (DST-FIST) and Promotion of University Research and Scientific Excellence (DST-PURSE) for the facilities provided for conducting the research.

#### CONFLICT OF INTEREST

The authors declare that there is no conflict of interest regarding the publication of this manuscript. In addition, the ethical issues, including plagiarism, informed consent, misconduct, data fabrication and/or falsification, double publication and/or submission, and redundancy have been completely observed by the authors.

#### OPEN ACCESS

©2024 The author(s). This article is licensed under a Creative Commons Attribution 4.0 International License, which permits use, sharing, adaptation, distribution and reproduction in any medium or format, as long as you give appropriate credit to the original author(s) and the source, provide a link to the Creative Commons license, and indicate if changes were made. The images or other third-party material in this article are included in the article's Creative Commons license, unless indicated otherwise in a credit line to the material. If material is not included in the article's Creative Commons license and your intended use is not permitted by statutory regulation or exceeds the permitted use, you will need to obtain permission directly from the copyright holder. To view a copy of this license, visit: <http://creativecommons.org/licenses/by/4.0/>.

#### PUBLISHER'S NOTE

GJESM Publisher remains neutral with regard to jurisdictional claims in published maps and institutional affiliations.

#### ABBREVIATIONS

%	Percent
<	Less than
°C	Degree Celsius
µg/g	Microgram/gram
µl/min	Microliter/minute
AAS	Atomic absorption spectrophotometry

AOAC	Association of official analytical chemists
Ar	Argon
BW	Biofortified wheat
Ca	Calcium
Cr	Chromium
Cu	Copper
F	Fortified
FSSAI	Food safety and standards authority of India
H <sub>2</sub> SO <sub>4</sub>	Sulphuric acid
HCl	Hydrochloric acid
He	Helium
ICAR	Indian council of agricultural research
ICP-MS	Inductive coupled plasma-mass spectrophotometry
IFCT	Indian food composition table
K	Potassium
L/min	Litre/minute
LOD	Limit of detection
LOQ	Limit of quantification
Mean±SD	Mean standard deviation
Mg	Magnesium
mg/100g	Milligram/100 gram
mg/day	Milligram/day
Min	Minute
Mn	Manganese
Na	Sodium
nm	Nanometer
NF	Normal flours
NIPLAS	Nonlinear Iterative partial least squares
NIR	Near-infrared spectroscopy
NIST	National institute of standards and technology
NW	Normal wheat
PLSR	Partial least square regression model
PPM	Parts per million
R	Reflectance
r <sup>2</sup>	coefficient of determination
RDA	Recommended daily allowance
Se	Selenium
UV- VIS	UV/Visible spectrophotometry
W	Watts
Zn	Zinc

## REFERENCES

- Adams, M.L.; Lombi, E.; Zhao, F.J.; McGrath, S.P., (2002). Evidence of low selenium concentrations in UK bread-making wheat grain. *J. Sci. Food Agric.*, 82(10): 1160-1165 **(6 pages)**.
- Akinyele, I.; Shokunbi, O.S., (2015). Comparative analysis of dry ashing and wet digestion methods for the determination of trace and heavy metals in food samples. *Food. Chem.*, 173: 682-684 **(3 pages)**.
- Allen, L.; Benoist, D.; Dary, B.; Hurrell O., (2018). Guidelines on Food Fortification with Micronutrients; World Health Organization and Food and Agricultural Organization of the United Nations **(341 pages)**.
- AOAC, (1995). Ash of flour – direct method » in official methods of AOAC International, method 923.03.
- AOAC, (2000). Official Methods of Analysis. 17th Edition. The Association of Official Analytical Chemists, Gaithersburg, MD, USA.
- AOAC, (2002). Association of Official Analytical Chemists 17th Edition. AOAC Official Methods of Analysis.
- AOAC, (2005). Official Journal of the European Communities N° L 344/36 of 26.11.92, Determination of crude fiber, 962.09.
- Arif, M.; Javed, A.; Bangash, F.; Khan, H., (2010). Quality assessment of different iron-fortified wheat flours. *Pak. J. Biochem. Mol. Biol.*, 43(4): 192-194 **(3 pages)**.
- Bouis, H.E.; Saltzman, A., (2017). Improving nutrition through biofortification: A review of evidence from HarvestPlus, 2003 through 2016. *Global Food. Sec.*, 12: 49-58 **(10 pages)**.
- Bruno, De B.I.; Egli, M., (2008). Worldwide prevalence of anemia 1993-2005: WHO global database on anemia. WHO.
- Chaparro, C.M.; Suchdev, P.S., (2019). Anemia epidemiology, pathophysiology, and etiology in low- and middle-income countries. *Ann. N.Y. Acad. Sci.*, 1450(1): 15-31 **(17 pages)**.
- Chekraverthy, B.K.; Pardhe, H.A.; Kiran, A.V.V.R.; Nagappan, K., (2023). Nutritional Strategies for Treating Iron Malnutrition: Implications on Nutrikinetic Approaches. *Curr. Res. Nutr. Food. Sci.*, 11(1).
- Chouraqui, J.P., (2022). Dietary approaches to iron deficiency prevention in childhood-A critical public health issue. *Nutrients*. 14(8): 1604 **(24 pages)**.
- Elemental Analysis Manual., (2015). Inductively Coupled Plasma-Mass Spectrometric Determination of arsenic, cadmium, chromium, lead, mercury, and other elements in food using microwave assisted digestion., 1.
- Fernando, B.; Santiago, G.L., (2009). A guide to diagnosis of iron deficiency and iron deficiency anemia in digestive diseases. *World. J. Gastroenterol.*, 15(37): 4638-4643 **(6 pages)**.
- Hailu Kassegn, H., (2018). Determination of proximate composition and bioactive compounds of the Abyssinian purple wheat. *Cogent. Food. Agric.*, 4(1): 1421415 **(9 pages)**.
- ICMR, (2010). A Report of the Expert Group of the Indian Council of Medical Research.
- Ihsanullah, M.J.; Qureshi, T.N.; khattak, Akhtar, J., (2002). Determination of iron in different types of wheat flours. *Int. J. Agri. Biol.*, 4(2) **(3 pages)**.
- Iván, M.M.; Miriam, H.J.; Isabel, R.; Ana, M.V.Q., (2023). Prediction of mineral composition in wheat flours fortified with lentil flour using NIR technology. *Sensors*. 23: 1491 **(14 pages)**.
- Khush, G.S.; Lee, S.; Cho, J.I.; Jeon, J.S., (2012). Biofortification of crops for reducing malnutrition. *Plant. Biotechnol. Rep.*, 6(3): 195-202 **(8 pages)**.
- Kowmudi, G.; Rashmi, V.; Anoop, K.; Krishnaveni, N.; Naveen, S., (2023). Proximate values and elemental analysis in wheat and soybean using inductively coupled plasma mass spectrometry. *Global J. Environ. Sci. Manage.*, 9(3): 531-544 **(13 pages)**.
- Kumar Yadava, D.; Choudhury, P.R.; Hossain, F.; Kumar, D., (2020). Biofortified Varieties: Sustainable Way to Alleviate Malnutrition 3rd Ed. Indian Council of Agricultural Research.
- Mæhre, H.; Dalheim, L.; Edvinsen, G.; Elvevoll, E.; Jensen, I.J., (2018). Protein determination—method matters. *Foods*. 7(1): 5 **(11 pages)**.
- McLean, E.; Cogswell, M.; Egli, I.; Wojdyla, D.; de Benoist, B., (2009). Worldwide prevalence of anaemia, WHO Vitamin and Mineral Nutrition Information System, 1993-2005. *Public Health Nutr.*, 12(4): 444-454 **(10 pages)**.
- Narozhnykh, K., (2023). Prediction models of iron level in beef muscle tissue toward ecological well-being. *Global J. Environ. Sci. Manage.*, 9(4): 833-850 **(18 pages)**.
- Neerja Kujur, U.; Amol Thakur, R.S.; Arvinadan, A.; Kumar, A.; Saravanan, C., (2019). Determination of iron content in wheat flour of organized and unorganized sector. *Indian J. Nutri. Dietetic.*, 56 (3) **(5 pages)**.
- Niedzielski, P.; Magdalena, Z.D.; Lidia, K.; Pawel, K.; Barbara, S.; Sylwia, Z.; Weronika, W., (2014). Determination of iron species in samples of iron-fortified food. *Food Anal. Methods*. 7(10): 2023-2032 **(9 pages)**.
- Nisar, N.; Faiza, M.; Arifa, T.; Rashad, Q.; Yaodong, Y.; Muhammad, I.K.; Fuyou, W., (2020). Proximate composition, functional properties and quantitative analysis of benzoyl peroxide and benzoic acid in wheat flour samples: effect on wheat flour quality. *Peer J.*, 8(e8788): e8788.
- Owusua Annoh, P.; Sekyere, A.; Kodua, E., (2022). Proximate Composition and Organoleptic Properties of Wheat Rock Cake Fortified With Cassava and Sesame Seeds Flour. *Nat. Volatiles Essent. Oils*. 9: 951-962 **(11 pages)**.
- Parvez, N.; Hardev Choudhary; Swati Parihar; Kelvin Gandhi.; Satveer Singh.; Rajkumar Rathore.; Rudrappa Zulapi.; Bajranglal Kasva.; Ranjit Kumar.; Prakash, S.; Raghuvanshi.; Agyaram Verma., (2019). Profiling of nutritional traits in indigenous wheat cultivars. *J. Exp. Biol. Agric. Sci.*, 7(1): 1-11 **(11 pages)**.
- Plummer, D.T., (1988). An Introduction Practical Biochemistry. Tata Mc Graw-Hill Publishing Company.
- Poudel, R.; Bhatta, M., (2017). Review of Nutraceuticals and functional properties of whole wheat. *J Nutr Food Sci.*, 07(01): 571 **(7 pages)**.
- Raghuramulu, N.; Nair, M.K.; Kalyanasundaram, S., (1983). Manual of laboratory techniques.
- Raquel, L.; Tejera, G.; Luis, D.; Gonzalez-Weller, J.M.; Caballero, A.J.; Gutierrez, C., (2013). Metals in wheat flour; comparative study and safety control. *Nutr. Hosp.*, 8: 506-513 **(8 pages)**.
- Rüdiger, H.; Udo, W.S., (2003). Iron uptake, trafficking and homeostasis in plants. *Planta*. 16(4): 541-51 **(11 pages)**.
- Saeid, A.; Hoque, S.; Kumar, U.; Das, M.; Muhammad, N.; Rahman, M.; Ahmed, M., (2015). Comparative studies on nutritional quality of commercial wheat flour in Bangladesh. *Bangladesh J. Sci. Ind. Res.*, 50(3): 181-188 **(8 pages)**.
- Samimi, M.; Validov, S., (2018). Characteristics of pDNA-loaded chitosan/alginate-dextran sulfate nanoparticles with high transfection efficiency. *Rom. Biotech. Lett.*, 23(5): 13996-14006 **(11 pages)**.
- Mohamadi, S.; Yazdanfar, N.; Ebrahiminejad, B.; Shokri, S.; Pirhadi, M.; Sadighara, P.; Zeinali, T., (2023). Evaluation of iron content in bakery flour samples of Tehran, Iran. *Heliyon*. 9: e12937. **(6 pages)**.
- Shun, Z.; Shuliang, L.; Li, S.; Shujuan, C.; Li, H.; Aiping, L., (2022). Application of near-infrared spectroscopy for the nondestructive analysis of wheat flour: A review. *Cur. Res. Food Sci.*, 5: 1305-1312 **(8 pages)**.
- Uauy, C.; Distelfeld, A.; Fahima, T.; Blechl, A.; Dubcovsky, J., (2006). A NAC Gene regulating senescence improves grain protein, zinc, and iron content in wheat. *Science*. 314(5803): 1298-1301 **(4 pages)**.
- Uauy, R.; Hertrampf, E.; Reddy, M., (2002). Iron fortification of foods: Overcoming technical and practical barriers. *J. Nutr.*, 132(4): S849-S852 **(4 pages)**.
- Uma, K.; Sunita, M.; Paramita, G., (2020). Near infrared spectroscopy

in prediction of the crude protein wheat stored for one year at 4°C. *European J. Mol. Clin. Med.*, 07(07).  
Vijayshree, M.; Shobha, B.; Nitin, M., (2023). Assessment of anemia and malnutrition among adolescent in Kalyan Karnataka region of Karnataka. *Clin. Epidem. Global Health.* 21: 101307 (5 pages).  
White, P.J.; Broadley, M.R., (2009). Biofortification of crops with seven

mineral elements often lacking in human diets-Iron, zinc, copper, calcium, magnesium, selenium, and iodine. *New Phytol.*, 182: 49-84 (36 pages).  
Zhenjiao, D.; Wenfei, T.; Michael, T.; Donghai, W.; Guorong, Z.; Yonghui, L., (2022). Quantitative assessment of wheat quality using near-infrared spectroscopy: A comprehensive review. *Compr. Rev. Food Sci. Food Saf.*, 21: 2956–3009 (55 pages).

#### AUTHOR (S) BIOSKETCHES

**Pardhe, H.A.**, Ph.D. Candidate, Department of Pharmaceutical Analysis, JSS College of Pharmacy, JSS Academy of Higher Education and Research, Ooty, Nilgiris, Tamil Nadu, India.

- Email: [pardhehari97@gmail.com](mailto:pardhehari97@gmail.com)
- ORCID: 0000-0003-3826-9219
- Web of Science Researcher ID: IVH-1511-2023
- Scopus Author ID: NA
- Homepage: <https://jssuni.edu.in/JSSWeb/WebShowFromDB.aspx?MODE=SSMD&PID=10002&CID=6&MID=0&SMID=10402>

**Krishnaveni, N.**, Ph.D., Professor, Head, Department of Pharmaceutical Analysis, JSS College of Pharmacy, JSS Academy of Higher Education & Research, Ooty, Nilgiris, Tamil Nadu, India.

- Email: [krisath@jssuni.edu.in](mailto:krisath@jssuni.edu.in)
- ORCID: 0000-0003-0596-9489
- Web of Science Researcher ID: AAG-2168-2021
- Scopus Author ID: NA
- Homepage: <https://jssuni.edu.in/JSSWeb/WebShowFromDB.aspx?MODE=SSMD&PID=10002&CID=6&MID=0&SMID=10402>

**Chekraverthy, B.K.**, Ph.D. Candidate, Department of Pharmaceutical Analysis, JSS College of Pharmacy, JSS Academy of Higher Education and Research, Ooty, Nilgiris, Tamil Nadu, India.

- Email: [kalyan.b222@gmail.com](mailto:kalyan.b222@gmail.com)
- ORCID: 0000-0002-4139-2341
- Web of Science Researcher ID: Not available
- Scopus Author ID: NA
- Homepage: <https://jssuni.edu.in/JSSWeb/WebShowFromDB.aspx?MODE=SSMD&PID=10002&CID=6&MID=0&SMID=10402>

**Patel, S.**, Ph.D., Assistant professor, Department of Pharmaceutical Analysis, JSS Academy of technical education, Noida, India.

- Email: [sonamp106@gmail.com](mailto:sonamp106@gmail.com)
- ORCID: 0000-0003-4553-0446
- Web of Science Researcher ID: Not available
- Scopus Author ID: NA
- Homepage: <https://jssaten.ac.in/>

**Naveen, S.**, Ph.D., Scientist 'E', Food Quality Assurance Division, DRDO-Defence Food Research Laboratory, Mysuru, Karnataka, India. Food Quality Assurance Division, DRDO-Defence Food Research Laboratory, Mysuru, Karnataka, India

- Email: [naveendfrr@gmail.com](mailto:naveendfrr@gmail.com)
- ORCID: 0000-0003-2981-422X
- Web of Science Researcher ID: AGQ-421-2022
- Scopus Author ID: NA
- Homepage: <https://www.drdo.gov.in/labs-and-establishments/defence-food-research-laboratory-dfrr>

**Rashmi, V.**, M.Sc., Technical Analyst, Food Quality Assurance Division, DRDO-Defence Food Research Laboratory, Mysuru, Karnataka, India

- Email: [rashmidfrr@gmail.com](mailto:rashmidfrr@gmail.com)
- ORCID: 0000-0001-5692-7938
- Web of Science Researcher ID: GYJ-6541-2022
- Scopus Author ID: NA
- Homepage: <https://www.drdo.gov.in/labs-and-establishments/defence-food-research-laboratory-dfrr>

**Govinden, P.C.**, B.Sc., Ministry of Agro-Industry and Food Security, Food Science and Technology Division, Mauritius Ministry of Agro-Industry and Food Security, Food Science and Technology Division, Mauritius.

- Email: [poocat2710@yahoo.com](mailto:poocat2710@yahoo.com)
- ORCID: 0009-0005-7744-4659
- Web of Science Researcher ID: Not Available
- Scopus Author ID: NA
- Homepage: <https://agriculture.govmu.org/Pages/Departments/Departments/Food%20Technology%20Laboratory/Food-Technology-Laboratory-Home.aspx>

#### HOW TO CITE THIS ARTICLE

Pardhe, H.A.; Krishnaveni, N.; Chekraverthy, B.K.; Patel, S.; Naveen, S.; Rashmi, V.; Govinden, P.C., (2024). Evaluation of mineral and near-infrared forecasting of wheat yield varieties using spectrophotometric techniques. *Global J. Environ. Sci. Manage.*, 10(1): 189-204.

DOI: 10.22034/gjesm.2024.01.13

URL: [https://www.gjesm.net/article\\_707573.html](https://www.gjesm.net/article_707573.html)





## ORIGINAL RESEARCH PAPER

## Presence of microplastics contamination in table salt and estimated exposure in humans

D.A. Syamsu<sup>1,2</sup>, D. Deswati<sup>3,\*</sup>, S. Syafrizayanti<sup>3</sup>, A. Putra<sup>4</sup>, Y. Suteja<sup>5</sup><sup>1</sup> Department of Chemistry, Faculty of Mathematics and Natural Sciences, Andalas University, Padang, Indonesia<sup>2</sup> Indonesian Food and Drug Authority, Jambi, Indonesia<sup>3</sup> Department of Chemistry, Faculty of Mathematics and Natural Sciences, Andalas University, Padang, Indonesia<sup>4</sup> Department of Medical Laboratory Technology, Syedza Saintika College of Health Sciences, Padang, Indonesia<sup>5</sup> Department of Marine Science, Faculty of Marine Science and Fisheries, Udayana University, Bali, Indonesia

## ARTICLE INFO

**Article History:**

Received 21 September 2023

Revised 13 August 2023

Accepted 08 June 2023

**Keywords:**

Contaminants

Marine debris

Marine litter

Plastics

Table salt

## ABSTRACT

**BACKGROUND AND OBJECTIVES:** Microplastics are plastic fragments measuring less than 5 millimeters which are formed from degraded plastic materials and have the potential to pollute the environment. Due to their widespread presence in the marine environment, microplastics have become a significant global threat. The presence of microplastics is often considered as causing pollution in various environments, especially aquatic ecosystems such as rivers and oceans. Microplastics contamination can even be found in consumed salt, thus raising concerns about its impact on human health. However, information on the presence of microplastics in salt is still very limited. This study aims to determine the abundance and characteristics of microplastics as contaminants in salt and assess the human exposure to microplastics in Indonesia.

**METHODS:** A total of 21 samples of salt products were taken from various brands available in Padang City and Jambi City, Indonesia for analysis. Microplastics extraction was carried out by removing the organic materials contained in the salt samples using 30 percent hydrogen peroxide and then filtering them with a 0.45 micrometer pore filter. A stereomicroscope was used to detect the abundance, shape, size, and color of microplastics, while the Attenuated Total Reflection-Fourier Transform Infrared Spectroscopy was utilized to identify the polymer type of the microplastics. Furthermore, human exposure to microplastics can be predicted by calculating the estimated dietary intake and taking into account the daily salt intake.

**FINDINGS:** Microplastics were detected in significant amounts ( $p < 0.05$ ) in all salt samples, ranging from 33 to 313 particles/kilogram. The types of microplastics most commonly found in the samples were fragments (67.49 percent), fibers (23.82 percent), films (6.08 percent), and pellets (2.61 percent). The types of polymer identified include polyethylene, polypropylene, polyethylene terephthalate, and polyester. The dominant microplastics were 100-300 micrometers in size (47.3 percent) and black in color (52.88 percent). It is estimated that adults in Indonesia will be exposed to 60.225-571.225 microplastics/year if they consume 5 grams of salt/day or 120.45-1142.45 microplastics/year if they consume 10 grams of salt/day.

**CONCLUSION:** Of the 21 salt samples analyzed, all were detected to contain microplastics. Inadequate and unhygienic salt production and contaminated seawater used as raw material contribute to microplastics contamination of salt, thus posing a risk to human health. By calculating of daily salt intake of the Indonesian population, it is possible to estimate their daily and annual exposure to microplastics. The results of this study contain useful information for the efforts to prevent microplastics contamination by relevant stakeholders and the provision of education and socialization about the proper salt production process in accordance with food safety standards as to reduce or even eliminate microplastics in salt. In addition, this study can provide valuable data on human exposure to microplastics in salt products that can assist policymakers in making standard references for microplastics.

DOI: [10.22034/gjesm.2024.01.14](https://doi.org/10.22034/gjesm.2024.01.14)This is an open access article under the CC BY license (<http://creativecommons.org/licenses/by/4.0/>).

NUMBER OF REFERENCES

79



NUMBER OF FIGURES

7



NUMBER OF TABLES

3

\*Corresponding Author:

Email: [deswati@sci.unand.ac.id](mailto:deswati@sci.unand.ac.id)

Phone: +6285 2639 09573

ORCID: [0000-0002-8655-9838](https://orcid.org/0000-0002-8655-9838)

Note: Discussion period for this manuscript open until April 1, 2024 on GJESM website at the "Show Article".

## INTRODUCTION

Owing to their convenient manufacturing and utilization properties, the demand for plastics has experienced a substantial surge across various sectors, which ultimately leads to a notable escalation in the quantity of plastic waste. Plastic waste is estimated to account for 60-80 percent (%) of all marine debris and even reaches 90-95% in some regions (Moore, 2008; Qiu et al., 2016; Wang et al., 2016). Every year, 9-23 million tons of plastics are dumped into rivers, lakes, and oceans throughout the world (Borrelle et al., 2020). This number is expected to increase to 155-265 million tons by 2060 (Lebreton and Andrady, 2019). Plastic waste entering the oceans has become a global concern because of its negative impact on marine and coastal ecosystems (Sabilillah et al., 2023). Shorelines, seafloors, and surface waterways have all been contaminated by decades of plastic waste dumping into seas and rivers (Selvam et al., 2020). Plastic waste contains microplastics (MPs), plastic particles of less than 5 millimeters (mm) that are considered global environmental pollutants. With their small size, microplastics are persistent in the environment, thus having the potential to produce harmful effects if they enter animal cells (Barboza et al., 2018; Cole et al., 2014). Microplastics enter the environment in two different ways. Primary microplastics are tiny particles produced during industrial processes and then utilized in a wide variety of consumer goods, including face cleansers and cosmetics containing microbeads (Napper et al., 2015). Meanwhile, secondary microplastics are formed when larger pieces of plastics degrade in the environment (by means of biological, photo, or mechanical degradation) (Andrady, 2011). The ability of microplastics to permeate the food chain and accumulate at elevated trophic levels is attributed to their hydrophobic properties, which facilitate the efficient absorption of persistent organic pollutants (POPs) and inorganic substances onto their surfaces (Buwono et al., 2022; Jung et al., 2022; Mamun et al., 2023). According to Jambeck et al. (2015) and Tibbetts (2015), Indonesia is the second largest contributor of plastic waste in the world after China, with annual production of 3.22 million tons. The combination of heightened plastic production and suboptimal recycling rates leads to the substantial disposal of plastics into river systems, subsequently contributing to the influx of plastic

materials into the ocean (Sutherland et al., 2022). This phenomenon exacerbates the accumulation of plastics within the marine ecosystems. Microplastics have been identified as novel food contaminants that may threaten human health and safety (Barboza et al., 2018; Rainieri and Barranco, 2019; Zhang et al., 2020). The presence of microplastics in food products, which then enter the human body, can bring various health problems. Once ingested, microplastics can migrate to organs such as the kidneys and liver and cause adverse effects at the cellular level. Human embryonic kidney cells (HEK 293) and human hepatocellular liver cells (Hep G2) are commonly used to test the potential toxicological effects of 1 micrometer ( $\mu\text{m}$ ) polystyrene microplastics (PS-MPs). Exposure to PS-MPs causes a major reduction in cell proliferation. Kidney and liver cells exposed to polystyrene microplastics result in an increase in reactive oxygen species (ROS) (Goodman et al., 2022). In addition, polystyrene microplastics cause hepatotoxicity and lipotoxicity. These microplastics can also increase production of the hepatocyte nuclear factor-4 alpha (HNF4A) and cytochrome P450 family 2 subfamily e member 1 (CYP2E1) genes in the liver, subsequently increasing the risk of steatosis, fibrosis, and cancer (Cheng et al., 2022). Several studies have evaluated the presence of microplastics in fish, shellfish, bivalves, honey, sugar, lager, and salt (Barboza et al., 2018; Possatto et al., 2011; Rainieri and Barranco, 2019). Microplastics contamination in commercial salt has also been monitored and reported in numerous prior studies conducted in various countries around the world, such as Lebanon (Nakat et al., 2023), Spain (Iñiguez et al., 2017), Turkey (Gündoğdu, 2018), India (Selvam et al., 2020; Seth and Shriwastav, 2018; Vidyasakar et al., 2021), Iran (Makhdoumi et al., 2023), Italy (Renzi and Blašković, 2018), China (Yang et al., 2015), Sri Lanka (Kapukotuwa et al., 2022), South Korea (Lee et al., 2021), Vietnam (Ha, 2021), Australia, France, Japan, Malaysia, New Zealand, Portugal, and South Africa (Karami, et al., 2017). Salt can be contaminated by water taken from the sea to make the salt, which may contain microplastics, organic matters, and sand particles, as well as during its manufacture (Gündoğdu, 2018; Yang et al., 2015). The abundance and characteristics of microplastics in several Indonesian waters have been reported in previous studies (Cordova et al., 2019; Purwiyanto et

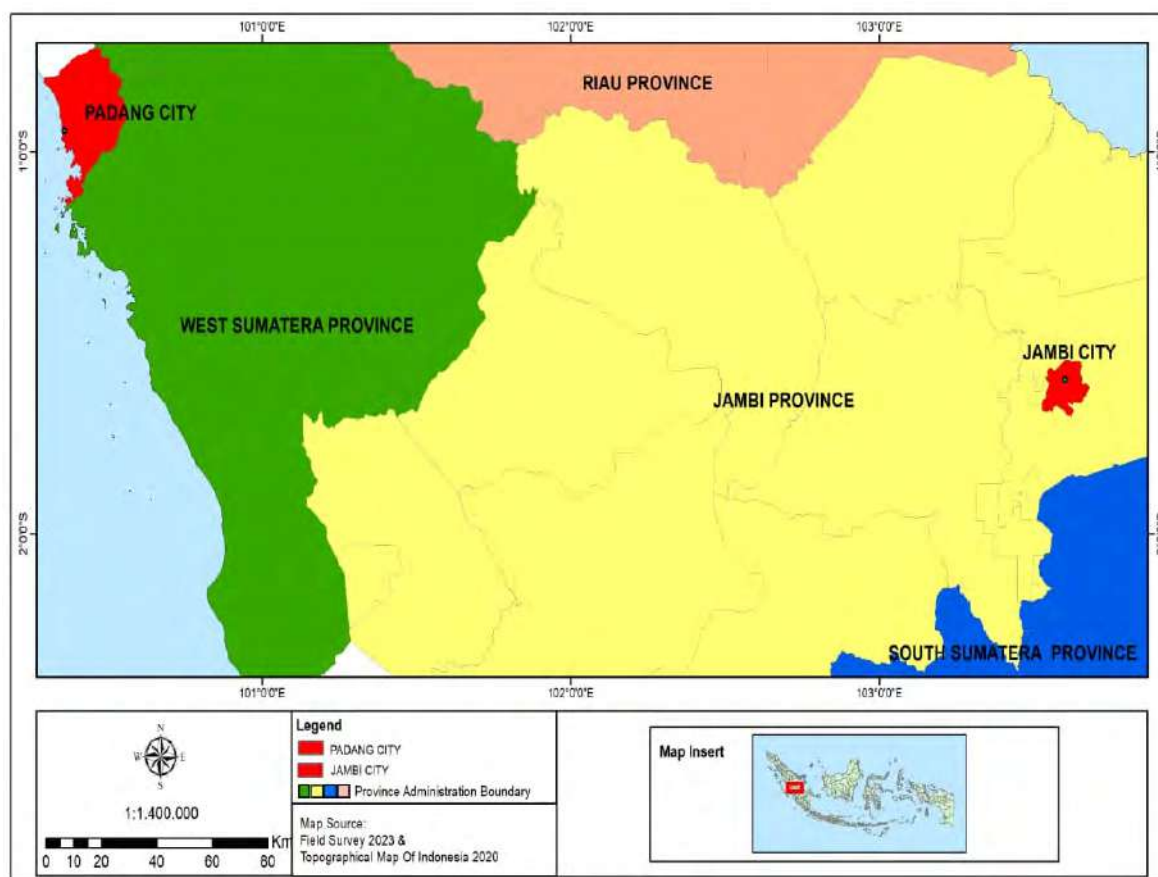


Fig 1: Geographic location of salt sampling areas in Padang and Jambi, Indonesia

*al., 2022; Takarina et al., 2022; Suteja et al., 2021*). Microplastics contamination in marine waters can also be present in the salt taken from these waters using traditional method of extraction and collection in evaporation ponds. The heat of the sun and the wind help the evaporation process, leaving behind concentrated saltwater which then crystallizes into salt; all the solids remain when the water is drained, and the salt is then extracted (*Nilawati et al., 2020; Yang et al., 2015*). Based on the literature review, no research has been conducted on microplastics contamination in table salt available in Padang City and Jambi City, Indonesia. This study identifies and describes microplastic particles found in salt, and compares the level of MPs contamination in Indonesian salt with those produced in other countries worldwide. Furthermore, this study also estimates the exposure of Indonesian adults to

microplastics from their annual salt consumption. This study was carried out in these two cities in 2022 with the aims of determining the abundance and characteristics of microplastics in salt and assessing their exposure in the Indonesian population.

## MATERIALS AND METHODS

### Sample collection

Sampling was carried out in August 2022. Twenty-one salt samples from different brands weighting 250 to 500 grams were collected from various traditional markets and supermarkets in Padang and Jambi, consisting of 10 brands from Padang and 11 brands from Jambi. Of the 21 brands, 19 were fine salt and the remaining two were coarse salt. Five packages were randomly selected to represent each brand. Information about the brands of salt purchased cannot be disclosed to maintain privacy.

#### *Quality assurance and quality control*

Water was used as a control blank. To test for possible water contamination, the (Milli-Q) water used to prepare the sample solution was filtered through a Millipore membrane filter with a diameter of 47 mm and a pore size of 0.45  $\mu\text{m}$ . All laboratory equipment was washed three times with filtered (Milli-Q) water and dried under a fume hood (ESCO) to remove possible contaminants. When not in use, all equipment was immediately covered with aluminum foil (Lusher *et al.*, 2015). During each extraction phase, cotton lab coats and nitrile gloves were consistently worn (Di Fiore *et al.*, 2023). No plastic utensils were used. Before and after each procedure, ethanol (70%) was used to clean all work surfaces and instruments. Before the end of the vacuum pump process, the inside of the vacuum tube was washed with filtered water to prevent loss of plastic particles. Experimental blank tests were also carried out using only 20 milliliters (mL) of filtered 30% hydrogen peroxide ( $\text{H}_2\text{O}_2$ ) in a glass-lidded Erlenmeyer flask, and then all extraction steps were followed. The entire extraction procedure was performed as quickly as possible to avoid contamination during the experiment (Karami, *et al.*, 2017). The results of the blank experiment found no contamination.

#### *Microplastics extraction*

Microplastics extraction was carried out using a modified reference (Seth and Shrivastav, 2018). For each brand, extraction was done in three replicates, each from a different package. Salt samples from each brand were weighed 50 grams and put into a 300 mL glass-lidded Erlenmeyer flask, and then 20 mL of 30%  $\text{H}_2\text{O}_2$  (Merck Millipore) was added to remove organic impurities. The Erlenmeyer flask was placed on a digital hot plate stirrer (Heidolph) with 300 revolutions per minute (rpm) at 65 degrees Celsius ( $^{\circ}\text{C}$ ) for 30 minutes. After being stored at room temperature and allowed to cool, 200 mL of (Milli-Q) water was added to the solution, stirred using a glass stirring rod, and continued with a stirring speed of 300 rpm for another 30 minutes. After the salt was completely dissolved, the Erlenmeyer flask was left at room temperature for 24 hours. After ensuring that the precipitation process was complete, the supernatant was filtered through a Millipore cellulose nitrate membrane filter with a diameter of 47 mm and a pore size of 0.45  $\mu\text{m}$  using a vacuum pump. The

membrane filter was air-dried at room temperature in a sealed petri dish for further analysis of microplastic particles.

#### *Microplastics characterization*

##### *Visual identification*

Olympus SZ61 stereo microscope (Olympus KK, Japan) was utilized to visually identify as well as quantitatively and qualitatively detect the microplastics. Microplastic particles on the membrane filter were counted microscopically, and each particle was photographed. Microplastic particles were analyzed based on their shape, size, and color. In this study, microplastics (MPs) were classified into four categories based on their shape, i.e., fragments, films, fibers, and pellets, and five categories based on their size, namely  $<100 \mu\text{m}$ ,  $\geq 100\text{-}300 \mu\text{m}$ ,  $>300\text{-}500 \mu\text{m}$ ,  $>500\text{-}1000 \mu\text{m}$ , and  $>1000 \mu\text{m}$  (Desforgues *et al.*, 2014; Seth and Shrivastav, 2018). Several representative particles were selected as microplastic particles characterized using Attenuated Total Reflectance-Fourier Transform Infrared (ATR-FTIR) spectroscopy. Nicolet iS10 (Thermo Fisher Scientific) in absorbance mode was utilized to identify the polymeric form of microplastics with a spectral range of 4000–650/cm, spectral resolution of 4/cm, and 16 scans per analysis. Meanwhile, Micro-forceps were used to transfer visible particles onto Attenuated Total Reflectance (ATR) diamonds. Then, the polymer type of the selected particles was identified by comparing their spectra with a polymer database (Agilent Polymer Handheld Library). Identification was based on a match index score greater than or equal to 70% (Song *et al.*, 2014; Yang *et al.*, 2015). Characterization was also carried out to compare the characteristic peaks of each particle assessed with a reference database (Nakat *et al.*, 2023; Deswati *et al.*, 2023). Each wave peak was then analyzed to determine its functional group. Afterwards, the observed functional groups were examined to determine the chemical formula and molecular structure of the plastic monomers being tested (M. R. Jung *et al.*, 2018; Noda *et al.*, 2007).

##### *Assessment of the estimated human exposure to microplastics in salt*

There are no regulations in Indonesia or other countries governing the assessment of human exposure to microplastic particles in food, and it is

not clear whether microplastic particles should be classified as chemical, physical, or microorganism contaminants. The World Health Organization or WHO (WHO, 2012) and the Regulation of the Minister of Health of the Republic of Indonesia Number 30 of 2013 have recommended a daily salt intake limit of 5 grams. However, according to a previous study conducted by Atmarita *et al.* (2017) in Indonesia, 18.9% of Indonesian adults consume more than 10 grams of salt per day. Therefore, to better assess exposure of Indonesian adults to microplastics in salt, the results of this present study were calculated in two categories of daily salt intake, namely 5 grams/day and 10 grams/day. The estimated dietary intake (EDI) of microplastic particles was calculated using Eq. 1 below (Rubio-Armendáriz *et al.*, 2022).

$$EDI = \text{Microplastics in salt} \times \text{daily salt intake per person} \times 365 \quad (1)$$

**Statistical analysis**

Differences in the average abundance of microplastics in particles per kilogram (particles/kg) among salt samples taken from each brand were tested using Analysis of Variance (ANOVA), followed by Tukey’s honest significant difference (HSD) test.

The significance level of difference ( $p < 0.05$ ) (Samimi *et al.*, 2023) was analyzed using SPSS software (SPSS version 27, IBM Inc).

**RESULTS AND DISCUSSION**

*Quantification of microplastics*

All salt samples of 21 different brands were found to contain microplastics (Fig. 2), with the abundance of microplastics in the samples ranging from  $33 \pm 9$  to  $313 \pm 57$  particles/kg. The two samples with the highest abundance were S1 and S6 (both were coarse salt), which had an abundance of  $313 \pm 57$  and  $313 \pm 81$  particles/kg, respectively (Table 1). The ANOVA followed by Tukey’s HSD test on the abundance of microplastics in each salt sample showed significant differences ( $p < 0.05$ ).

This study discovered lower amounts of microplastics than those reported in previous studies on salt conducted in Italy (Renzi and Blašković, 2018), China (Yang *et al.*, 2015), South Korea (Lee *et al.*, 2021), and Vietnam (Ha, 2021). Meanwhile, another prior study by Kim *et al.* (2018) found microplastics of 12,326-14,932 particles/kg in sea salt in Indonesia ( $n = 1$ ). Coarse salt has a high abundance of microplastics compared to fine salt. This is because coarse salt is produced by evaporating seawater under direct sunlight in open fields and is highly dependent

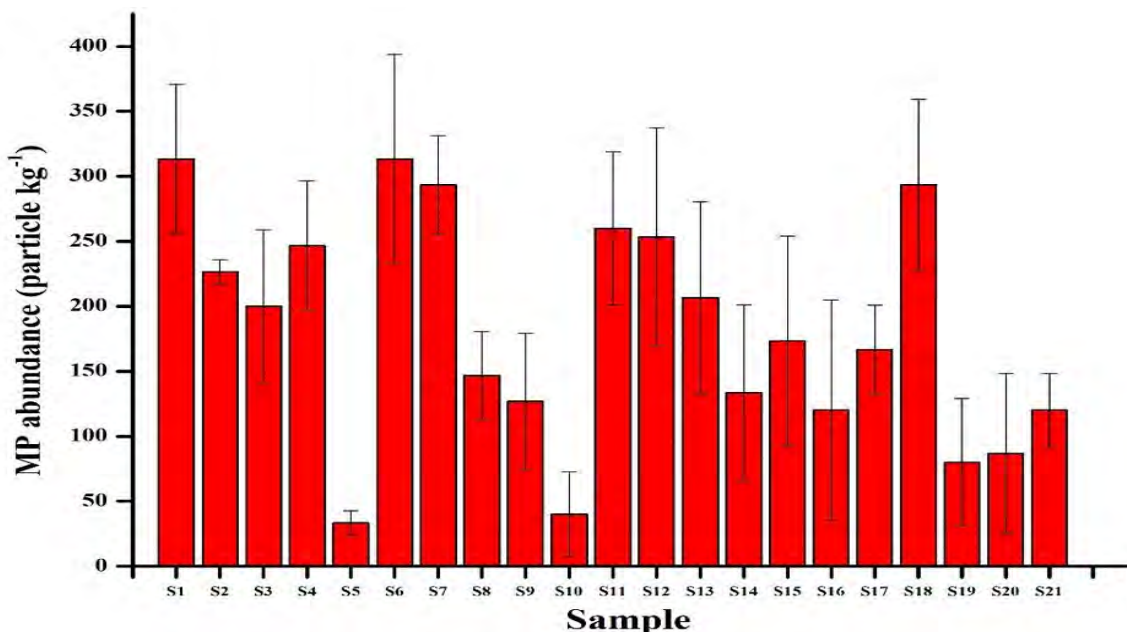


Fig. 2: Histogram of MPs counts in different salt samples

Table 1: The abundance of microplastics in various salt samples in Indonesia

Sample code	Salt type	Average ( $\pm$ SD) of MPs abundance (Particle/kg) <sup>a</sup>
S1	coarse	313 $\pm$ 57
S2	fine	227 $\pm$ 9
S3	fine	200 $\pm$ 59
S4	fine	247 $\pm$ 50
S5	fine	33 $\pm$ 9
S6	coarse	313 $\pm$ 81
S7	fine	293 $\pm$ 38
S8	fine	147 $\pm$ 34
S9	fine	127 $\pm$ 52
S10	fine	40 $\pm$ 33
S11	fine	260 $\pm$ 59
S12	fine	253 $\pm$ 84
S13	fine	207 $\pm$ 74
S14	fine	133 $\pm$ 68
S15	fine	173 $\pm$ 81
S16	fine	120 $\pm$ 85
S17	fine	167 $\pm$ 34
S18	fine	293 $\pm$ 66
S19	fine	80 $\pm$ 49
S20	fine	87 $\pm$ 62
S21	fine	120 $\pm$ 28

<sup>a</sup> Average abundance of microplastics per brand was calculated using the particles detected in each filter of the triplicate samples.

on climate and weather conditions. Airborne microplastics can also contaminate salt production facilities located in open fields. In addition, unlike that of fine salt, there is no further refining stage in the manufacture of coarse salt. The production of fine salt involves three phases of washing: (1) initial washing to remove debris such as grass; (2) washing with brine; and (3) final washing with fresh water. The washed salt solution is then compressed, filtered, and crystallized using the pure-dried vacuum technique. Table 2 lists relevant prior studies on sea salt conducted in several countries.

Despite being contaminated with microplastics, seawater is a major source of salt manufacture, thus having a high potential to produce salt that contains microplastics. Several previous studies have examined the presence of microplastics contamination in Indonesian waters and oceans. The estuary in Benoa Bay, Bali, for example, has a MPs abundance of 1.41-1.88 particles per cubic meter (particles/m<sup>3</sup>) (Suteja et al., 2021). Another study by Syakti et al. (2017) found 16.8-41.6 microplastic particles per square meter (particles/m<sup>2</sup>) in coastal waters in Cilacap, Central Java. The abundance of microplastics in the northern coastal waters of Surabaya, East Java ranges from 0.38

to 0.61 particles/L, with an average of 0.49 particles/L (Cordova et al., 2019). The brands of salt examined in previous studies predominantly come from regions other than Jambi and Padang, such as Jakarta, West Java, Central Java, and East Java. Based on data, the four largest salt-producing regions in Indonesia are East Java, Central Java, East Nusa Tenggara, and West Java (KKP, 2021). Salt production in Padang and Jambi also involves the utilization of raw materials obtained from two salt-producing regions, namely West Java and East Java. The abundance of microplastics in salt samples taken from salt production area in East Java was found to be 303 particles/kg, whereas the abundance of microplastics in seawater used for salt production was 9667 particles/m<sup>3</sup>. The sea itself can be described as the convergence point of various river estuaries. On the other hand, Cordova et al. (2022) conducted a study to monitor marine debris (specifically macro debris) and microplastics in Citarum River located in West Java and revealed that plastics account for 85% of the total waste present in the river, amounting to approximately 5369 $\pm$ 2320 items or 0.92 $\pm$ 0.40 tons per day. Furthermore, the study also estimated that around 6043 $\pm$ 567 items or 1.01 $\pm$ 0.19 tons of macro debris are released into the

Table 2: Abundance, shape, color, size, polymer type, and annual human intake of microplastics

Country	Particles/kg	MPs shape	MPs color	MPs size	Polymer type	EDI (Particles /year)	Sources
Lebanon	0-635,2	Fiber	Transparent, white, yellow, blue, black	NA	PE, Plasticized Rubber, PP, BBP, PES, TPE, Plasticizer	0-2372.5	<a href="#">Nakat et al., 2023</a>
Italy	1653	Fiber, fragment, sphere	Blue, red, black, white	0-500 µm	PP, PA, PE	NA	<a href="#">Di Fiore et al., 2023</a>
Bangladesh	560-1253,33	Fiber, fragment, foam, line, film, pellet	Black, transparent, yellow, red, gray, blue, green	300-5000 µm	PP, PE, PET, PS	1021.74 – 2286.76	<a href="#">Siddique et al., 2023</a>
India	56-103	Fiber, fragment	Black, red, brown, blue, purple	500-2000 µm	PES, PET, PA, PE, PS	NA	<a href="#">Seth and Shrivastav, 2018</a>
India	T/A	Fragment, fiber, sheet	White, blue, green, colorless	<2mm	PE, PP, cellulose, nylon	NA	<a href="#">Selvam et al., 2020</a>
Iran	55,2–151,3	Fragment, fiber	White, black, red, blue, green, colorless	1000-5000 µm	PE, PP	15.540	<a href="#">Makhdoumi et al., 2023</a>
Spanish	50-280	Fiber	Black, red, blue, white, transparent	30-3500 µm	PET, PP, PE	510	<a href="#">Iñiguez et al., 2017</a>
China	550-681	Fragment, fiber	Black, red, white, blue	<200 µm	PET, PE, cellophane	NA	<a href="#">Yang et al., 2015</a>
Türkiye	16-84	Fiber, film, fragment	NA	>1000 µm	PU, PP, PET, PE, PA, PVC	249-302	<a href="#">Gündoğdu, 2018</a>
Italy	1570-8230	Fragment, fiber, film, foam, granule	Black, grey, blue, orange, brown, green, pink, yellow, purple	4-2100 µm	NA	40.6–1085.2	<a href="#">Renzi and Blašković, 2018</a>
Croatia	27,13-31,68	Fiber, film, fragment, granule	Blue, black, white, yellow	15-4628 µm	PP	NA	<a href="#">Renzi and Blašković, 2018</a>
Sri Lanka	11-193	Fiber, fragment	Transparent, red, blue, white, black	65-2500 µm	LDPE, resin dispersion, HDPE	158	<a href="#">Kapukotuwa et al., 2022</a>
Korea	2395	Fragment, fiber	NA	63-100 µm	PP, PE, PS, PET, PVC	12.000	<a href="#">Lee et al., 2021</a>
Vietnam	340-878	Fiber, fragment	Blue, grey, black, yellow, white, red	100-700 µm	PE, PP, PS	637-1270	<a href="#">Ha, 2021</a>
Indonesia	33–313	Fragment, fiber, film, pellet	Black, blue, yellow, red, transparent	≥100-300 µm	PE, PP, PET, PES	60.225–571.225	<a href="#">Current study</a>

Polyethylene (PE), polypropylene (PP), polyester (PES), polyethylene terephthalate (PET), polyamide (PA), polyvinyl chloride (PVC), benzyl butyl phthalate (BBP), thermoplastic elastomers (TPE), low-density polyethylene (LDPE), high-density polyethylene (HDPE). Not Available (NA)

river every day. The concentration of microplastics in Citarum River was found to be reach  $3.35 \pm 0.54$  particles/m<sup>3</sup>, indicating their presence in the river

and their potential transport to the sea. The presence of microplastics was also detected in Brantas River located in East Java, with particle concentrations

ranging from 133 to 5467 particles/m<sup>3</sup>, as reported by [Buwono et al. \(2021\)](#). The water in this river flows into Madura Strait. The Indonesian marine waters located to the north of Java Island and around Madura Island are wide-ranging bodies of water utilized for the production of salt.

*Shape, size, and color of microplastics* This study successfully identified four different forms of microplastics contained in all 21 salt samples, of which fragments are the most common (67.49%), followed by fibers (23.82%), films (6.08%), and pellets (2.61%) as secondary components. The morphologies of microplastics show variations across different brands of salt. However, fragments and fibers have a higher prevalence than films and pellets which only constitute less than 7% of the overall quantity of microplastics detected (Fig. 3a). This is in line with prior studies that have documented that fragments and fibers are the types of microplastics most commonly found in salt samples taken from various countries ([Karami et al., 2017](#); [Makhdoumi et al., 2023](#)). Similar results were also obtained in a study conducted by [Yang et al., \(2015\)](#), where the prevailing forms of microplastics discovered in sea salt in China are fragments and fibers, while other forms such as pellets and films constitute

a smaller proportion (less than 6%). In another previous study carried out by [Seth and Shrivastav \(2018\)](#) in India, the commonly identified types of microplastics are fragments, which accounts for 63% of all microplastics, and fibers, which comprises 37% of all microplastics. The fate and influence of MPs on the health of living organisms are determined by their form. The physicochemical characteristics of microplastics, specifically their shape and size, have the potential to impact the transit of microplastic particles within the digestive organs. [Gray and Weinstein \(2017\)](#) revealed that the morphology of microplastic particles had a statistically significant impact on the quantity of particles consumed by shrimp ( $p < 0.001$ ). The experiment involved exposing shrimp to microplastic particles of different shapes, including pellets, fibers, and fragments. In the study, [Gray and Weinstein \(2017\)](#) found that the mortality rate of crustaceans varied between 5% and 40% when exposed to pellets and fragments larger than 50  $\mu\text{m}$ . [Makhdoumi et al. \(2021\)](#) documented the presence of microplastics in the muscle cells of fish, showing that only 4% of these particles were in the form of fibers, while the other 96% were fragments. As indicated by [Qiao et al. \(2019\)](#), the influence of the shape of microplastics on their impacts and

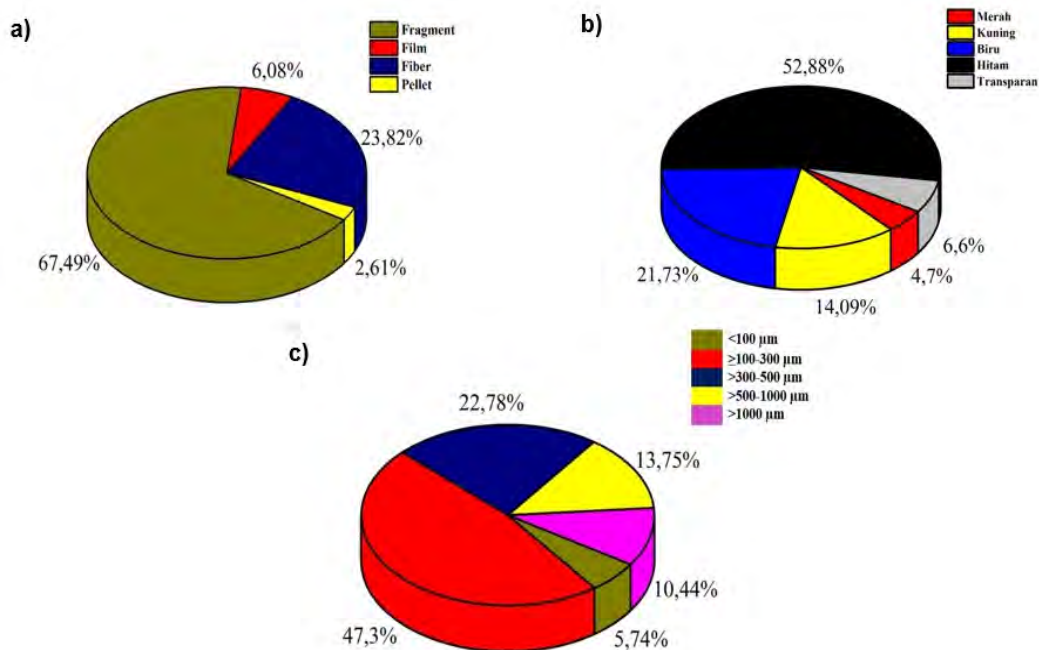


Fig. 3: Composition of microplastics found in salt in Indonesia: (a) shape, (b) color, and (c) size

significance for consideration in the assessment of their health impacts should not be disregarded. In their study, the presence of microplastics in the gastrointestinal tract of zebrafish was also found to be able lead to a range of detrimental consequences, such as damage to the mucosal lining, inflammation, and disruptions of metabolic processes. Notably, the fibrous form of microplastics was observed to have a more pronounced negative impact compared to fragments and pellets.

As presented in Fig. 3c, microplastic particles with sizes ranging from 100-300  $\mu\text{m}$  were the most prevalent, reaching 47.3% of all salt samples. The percentages of microplastics within the size range of >300-500  $\mu\text{m}$ , >500-1000  $\mu\text{m}$ , and >1000  $\mu\text{m}$  were 22.78%, 13.75%, and 10.4%, respectively. Meanwhile, microplastics which are smaller than 100  $\mu\text{m}$  only constituted 5.74% of all samples. The study conducted by Yang *et al.* (2015) revealed that the size of microplastic particles in salt samples varied between 45  $\mu\text{m}$  and 4.3 mm. However, the most prevalent particle size was less than 200  $\mu\text{m}$ , which was 55% of the total amount of microplastics in salt ( $p < 0.05$ ). In a study conducted by Seth and Shrivastav (2018), it was observed that the majority of fibers and fragments had a size range between 500-2000  $\mu\text{m}$  (80%). Iñiguez *et al.* (2017) observed that the size of fibers in 21 table salt samples in Spain varied between 30  $\mu\text{m}$  and 3.5 mm. Researchers around the world have noted the absence of microplastic particles smaller than 30  $\mu\text{m}$ . As seen in Table 2, smaller microplastics are contained in sea salt from China (Yang *et al.*, 2015) and South Korea (Lee *et al.*, 2021), while larger microplastics were present in sea salt from Iran (1000-5000  $\mu\text{m}$ ), India (500- 2000  $\mu\text{m}$ ), Italy (0-500  $\mu\text{m}$ ), Croatia (15-4828  $\mu\text{m}$ ), Spain (30-3500  $\mu\text{m}$ ), Bangladesh (500-1000  $\mu\text{m}$ ), and Vietnam 100-700  $\mu\text{m}$  (Makhdoumi *et al.*, 2023; Seth and Shrivastav, 2018; Renzi and Blašković, 2018; Iñiguez *et al.*, 2017; Siddique *et al.*, 2023; Ha, 2021). According to Rakib *et al.* (2021), variations in the size of microplastics across different countries can be associated with changes in weathering processes induced by factors such as wind, precipitation, temperature, salinity, and sea waves. These weathering patterns may also be influenced by the velocity of wind, as suggested by Kukulka *et al.* (2012).

The areas with the highest concentrations of plastics were observed to be located at a considerable distance

from land, and within the initial kilometers adjacent to the coastline. This pattern may be attributed to the proximity of coastal areas to human populations, with hundreds of thousands of plastic pieces typically found per square kilometer in coastal regions in close proximity to human settlements. This is in line with a study conducted by Pedrotti *et al.* (2016), which found that smaller fragments, measuring less than 2 mm, were more prevalent in areas within 1 kilometer (km) of coastal waters, indicating that high levels of fragmentation occur near the coastline. In this regard, Nilawati *et al.* (2020) stated the establishment of salt ponds by farmers is contingent upon the availability of seawater around the coastal areas. This practice, however, raises concerns regarding the potential for plastic pollutants to enter seawater. According to Yuan *et al.*, (2022), microplastics have the capacity to induce acute toxicity, subchronic toxicity, carcinogenesis, and genotoxicity. As particles ranging in size from 0.2 to 150  $\mu\text{m}$ , microplastics have been observed to exhibit the ability of traversing living cells and infiltrating the human lymphatic and circulatory systems, as documented in several previous studies (Hussain *et al.*, 2001; Rieux *et al.*, 2005; Waring *et al.*, 2018). Stock *et al.* (2019) also reported that intestinal cells have the capability to uptake microplastics with sizes smaller than 4  $\mu\text{m}$ . Meanwhile, microorganisms can absorb particles with a diameter of 150  $\mu\text{m}$  or less. These particles can subsequently traverse the gut walls, lymph nodes, and various organs, releasing detrimental compounds that have the potential to trigger diseases, such as cancer.

The salt samples in this study were found to contain microplastics in different colors, namely red, yellow, blue, black, and transparent, as depicted in Fig. 4. The prevalence of black color was observed to be dominant in all salt samples analyzed, reaching 52.88% of the total samples. The distribution of black microplastics was uniform across all samples, as shown in Fig. 3b. Iñiguez *et al.* (2017) reported in their study that the dominant colors observed in salt samples collected in Spain include black, red, blue, white, and transparent. Microplastics with a size greater than 1000  $\mu\text{m}$  can be seen starting from the extraction stage (Fig. 5). The presence of microplastics in Chinese salt has been documented by Yang *et al.* (2015); these microplastics are generally black, red, blue, or white in color. The color of microplastics is attributed to

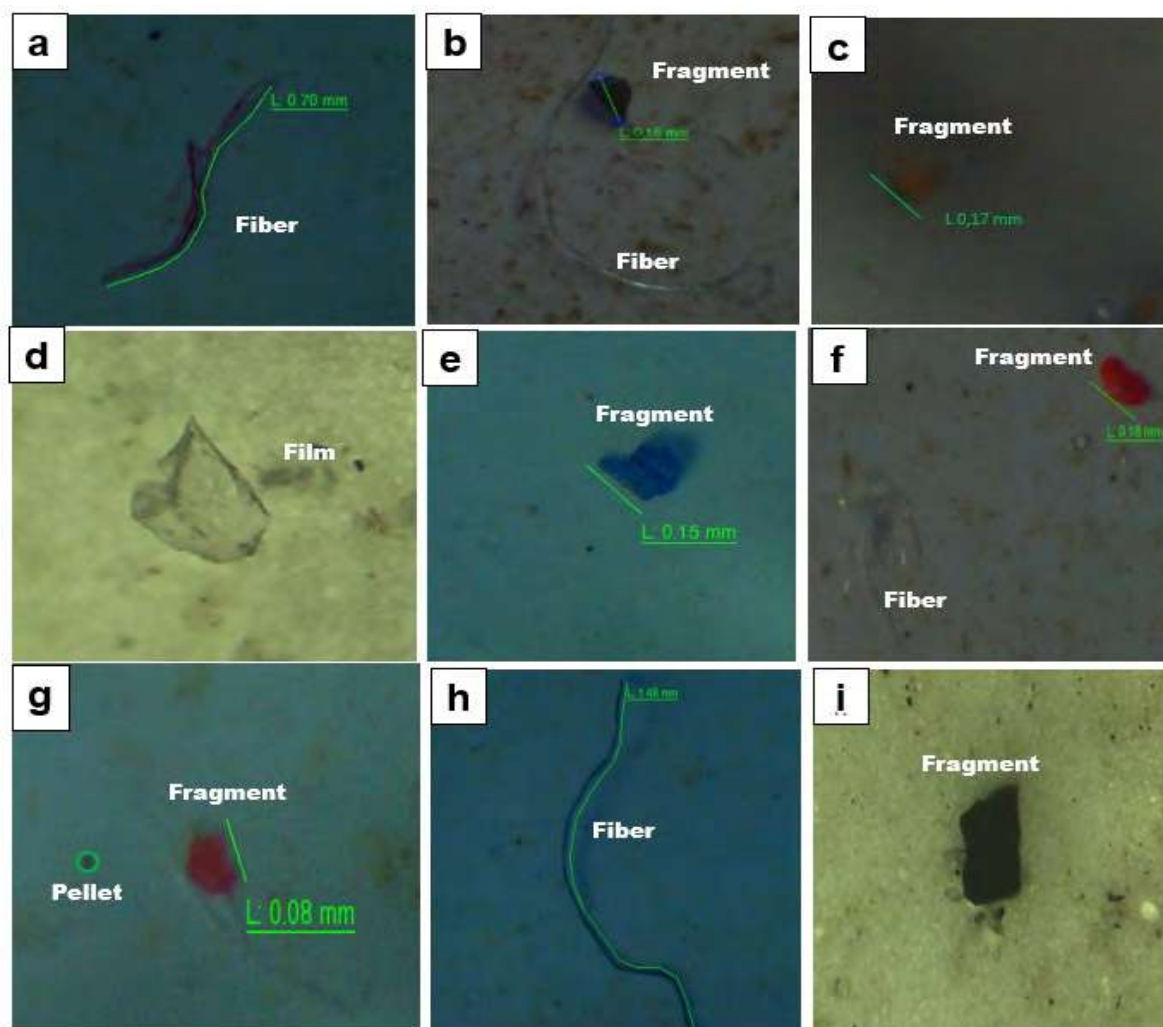


Fig. 4: Microscopic images showing different morphotypes and colors of microplastics obtained from table salt in Indonesia (a) red fiber, (b) black fragment and transparent fiber, (c) yellow fragment, (d) transparent film, (e) blue fragment, (f)-(g) red pellet, (h) blue fiber, (i) black fragment

the degradation of black plastic materials. Black plastic is utilized across a diverse range of industries, encompassing food packaging, cookware, trays, toys, household appliances, and automobile components. The escalating prevalence of black plastic waste in the environment caused by a decline in recycling rates has led to the emergence of black microplastics as its potential consequence (Huang and Xu, 2022). Similarly, transparent microplastics can result from the packaging of various products, including disposable plastic bags, containers, and

bottles. The presence of pigmented microplastics can be associated with the utilization of packaging materials and various plastic consumer products (K. Zhang et al., 2018). Microplastics of various colors, including blue, yellow, and red, can appear as a result of plastic pigmentation and the photoaging process. According to Zhao et al. (2022), the phenomenon of photoaging can induce alterations in the coloration of microplastics, thereby offering a way to determine the duration of plastic particle exposure in the surrounding environment.

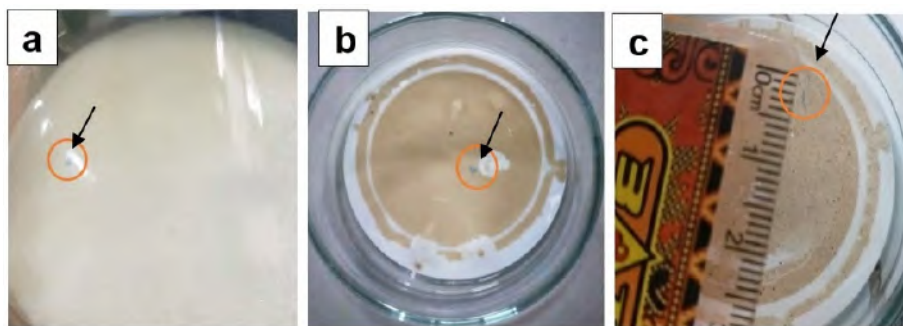


Fig. 5: (a) Microplastics in the form of blue fragments visible at the extraction stage, (b) Microplastics on filter paper, and (c) Microplastics in the form of blue fibers on filter paper.

#### Types of microplastics

Fourier Transform Infrared (FTIR) spectroscopy is a highly effective technique that enables efficient, rapid, and nondestructive identification of samples (Samimi and Shahriari Moghadam, 2023). By analyzing the infrared absorption bands resulting from vibrations of functional groups (Ehzari *et al.*, 2022), FTIR spectroscopy can successfully identify a wide range of plastic polymers. In this study, the ATR-FTIR instrument was utilized to characterize a representative sample of microplastic particles deposited on filter paper, with a total of 26 particles analyzed for their polymer composition. Identification of the polymer type of these particles was achieved through a comparative analysis of their spectra with a polymer database, i.e., the Agilent Polymer Handheld Library. The identification process relied on a match index score that met or exceeded the threshold of 70% (Kim *et al.*, 2018; Yang *et al.*, 2015). Then, identification of the functional groups was performed manually, wherein the characteristic peaks of each evaluated particle were compared with a specific reference database for each polymer, as outlined by Nakat *et al.* (2023). Various microplastic polymers have been identified based on the results of the FTIR spectrum analysis, namely polyethylene (9 particles), polypropylene (8 particles), polyethylene terephthalate (4 particles), polyester (1 particle), and unidentified (4 particles).

Analysis of the type of microplastic polymer in the blue fragment of sample S2 (Fig. 6a) used the Nicolet iS10 ATR-FTIR Spectrometer (Thermo Fisher Scientific) and showed a polyethylene polymer match score of 89%. Furthermore, the FTIR spectrum indicated the presence of C-H stretching at wave numbers 2915/

cm and 2845/cm,  $\text{CH}_3$  bending at 1377/cm,  $\text{CH}_2$  bending at 1467/cm and 1462/cm, and  $\text{CH}_2$  rocking at 730/cm and 717/cm. Likewise, analysis of the type of microplastic polymer in the yellow fragment-shaped particles of sample S1 (Fig. 6b) also used the Nicolet iS10 ATR-FTIR Spectrometer and revealed a polypropylene polymer match score of 80%. In the FTIR spectrum, significant absorbance peaks appeared at wave numbers 2950/cm and 2838/cm, indicating C-H stretching and asymmetric vibrations (Fotopoulou and Karapanagioti, 2012; K appler *et al.*, 2015; L oder *et al.*, 2015), and at wave number 1455/cm signifying  $\text{CH}_2$  bending vibrations (Kappler *et al.*, 2016).  $\text{CH}_3$  bending was detected at wave number 1377/cm. Since the area around 1375-1450/cm refers to  $\text{CH}_3$  bending,  $\text{CH}_3$  rocking was detected at wave numbers 997/cm and 972/cm. meanwhile,  $\text{CH}_2$  rocking was detected at wave numbers 840/cm and 880/cm (Fotopoulou and Karapanagioti, 2012; M. R. Jung *et al.*, 2018; L oder *et al.*, 2015; Syakti *et al.*, 2017). Analysis of the type of microplastic polymer in the black fiber-shaped particles of sample S8 (Fig. 6c) with Nicolet iS10 ATR-FTIR Spectrometer showed a polyethylene terephthalate polymer match score of 88%. PET has a characteristic peak at 720/cm, indicating the presence of the CH Aromatic functional group. C-O stretching was detected at wave numbers 1094 and 1241/cm, C=O stretching at wave number 1713/cm, and OH group vibrations at 3608/cm (M. R. Jung *et al.*, 2018; Noda *et al.*, 2007). The presence of microplastic polyester fibers in the black fiber-shaped particles of sample S5 (Fig. 6c) was analyzed also using Nicolet iS10 ATR-FTIR Spectrometer, indicating a polyester fiber match score of 89%. Polyester is confirmed by the characteristic band of valence

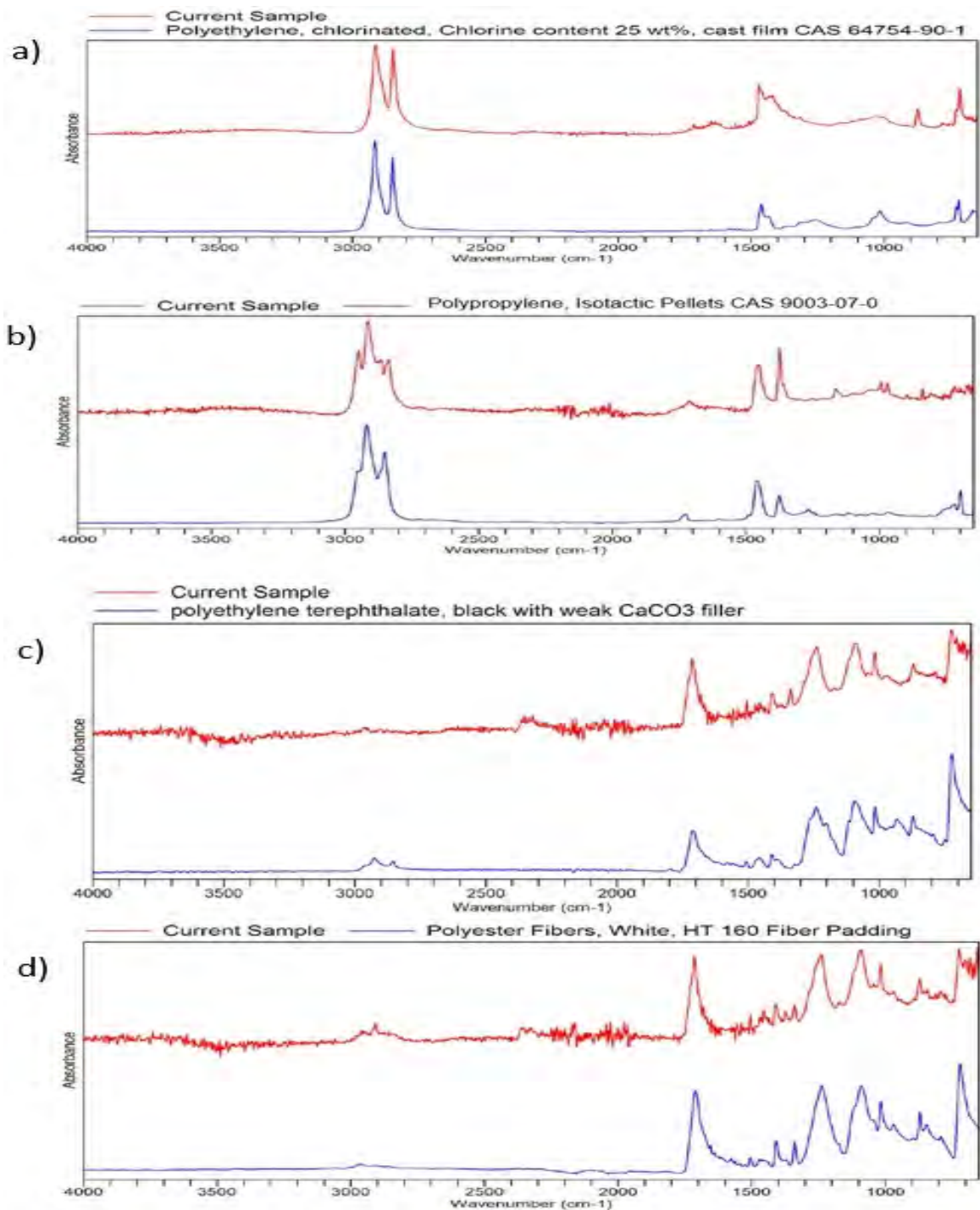


Fig. 6: FTIR spectra of microplastics

vibration of the carbonyl group at 1727/cm. Other special bands were detected at 2819/cm ( $\text{CH}_3$  group), with 725/cm corresponding to carboxylic esters and anhydrides and 971/cm indicating C-C bending (Käppler *et al.*, 2015; Noda *et al.*, 2007).

In this study, four types of microplastics were found (Fig.7), namely PE (34.62%), PP (30.77%), PET (15.38%), and PES (3.85%). Similar results were found in a study by Nakat *et al.* (2023) which identified PE as the dominant polymer type of microplastics in salt available on the market in Lebanon, followed by plasticized rubber and PP. Another study by Selvam *et al.* (2020) also pointed out PE as the most common polymer type, followed by PP, cellulose, and nylon. Meanwhile, a study carried out in India by Seth and Shrivastav (2018) revealed the occurrence of PES, PE, and PA polymer types, with PES being the most prevailing constituent. Sea salts found in African markets mainly contain polyvinyl acetate, PP, and PE (Fadare *et al.*, 2021). PE and PP are major contributors to global plastic production, primarily due to their extensive utilization as packaging materials for various applications, such as containers, bottles, and bags (Andrady, 2011; Geyer *et al.*, 2017). PE and PP are lightweight polymers; PE has a density of 0.85 grams per milliliter (g/mL), while PP has a density of 0.97 g/mL. Both PE and PP are commonly

used in packaging, typically for single-use products with a short shelf life that quickly end up in waste streams and landfills (Pedrotti *et al.*, 2016). PE has been identified as the easiest polymer to identify in both freshwater (Koelmans *et al.*, 2019) and marine ecosystems (Hidalgo-Ruz *et al.*, 2012) due to its lower density compared to water. This property causes PE to float and has the potential to accumulate as residue during the process of sea salt production following water evaporation (UNEP, 2016). The presence of microplastic pollutants in sea salt is initially attributed to the packaging materials used by the community. However, Fadare *et al.* (2021) challenged this hypothesis by demonstrating that packaging materials do not contain any microplastic particles. Instead, Nakat *et al.* (2023) argued that the primary source of microplastics contamination in salt is the seawater itself. PET constitutes a relatively minor fraction of the overall output of non-fiber plastics on a global scale, as indicated by the findings of a study by Lee *et al.* (2021). According to Iñiguez *et al.* (2017), PET is the predominant form of microplastics discovered in salt samples collected in Spain. Previous studies have also reported the presence of PET and polyethylene in salt samples obtained from various countries worldwide (Gündoğdu, 2018; Iñiguez *et al.*, 2017; Karami *et al.*, 2017; Yang *et al.*, 2015).

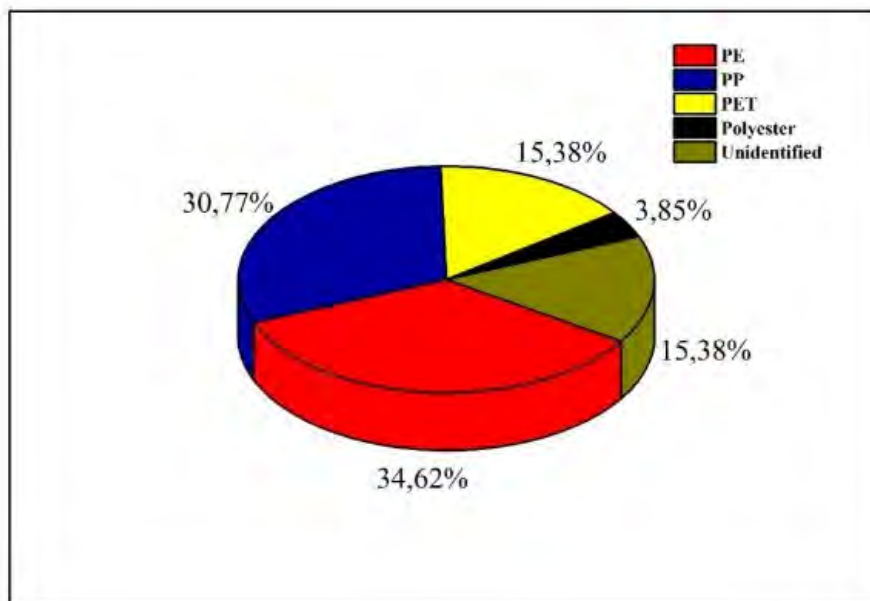


Fig. 7: Polymer types of microplastics in salt samples

Table 3: Estimated dietary intake (EDI)

MPs abundance (Particles/kg)	Level	EDI for adults (microplastics/capita/year)	
		Salt intake of 5 g/day	Salt intake of 10 g/day
33	Lowest	60.225	120.45
183	Median	333.975	667.95
313	Highest	571.225	1142.45

PET, which stands for polyethylene terephthalate, is a type of polyester that is frequently employed as a packaging material in various forms such as flexible films, bottles, and textiles (Iñiguez *et al.*, 2017). According to Acharya *et al.* (2021), various other polyesters and polyamides are mostly sourced from textile materials. Similarly, the utilization of polyethylene and polystyrene polymers in packaging is very extensive (Andrady, 2011). Factors affecting the distribution of microplastics are due to the various human activities around marine and river waters. Polluted rivers become a route for disposal of wastewater, both household and industrial, to the sea (Priya *et al.*, 2023).

#### *Estimated human intake of microplastics in salt*

Salt is one of the food seasonings consumed daily by humans. Therefore, it is extremely important to calculate the estimated contamination with microplastics. The WHO has set a standard for salt intake of 5 grams per day for adults (WHO, 2012). This is in line with the guidelines outlined in the Regulation of the Minister of Health of the Republic of Indonesia Number 30 of 2013 on salt consumption. However, a study conducted by Atmarita *et al.* (2017) revealed that a significant proportion of Indonesian adults, approximately 46.3% of the total population, consumed an average of 5 grams per day, while 18.9% of them consume a higher range of 10-30 grams/day. Based on data on salt consumption in Indonesia, it is absolutely necessary to conduct a careful and precise evaluation of microplastics contamination in salt. This study examines the potential health risks associated with the consumption of microplastics contained in salt available in Padang and Jambi, Indonesia, and calculates the level of contamination based on the estimated daily intake (EDI) of salt by the Indonesian population. For this purpose, the EDI was estimated using microplastic detection techniques and three levels of contamination. The minimum, average,

and maximum levels of microplastics abundance were determined. The minimum, average, and maximum annual exposures of Indonesian adults to microplastics were approximately 60.225 particles/year, 333.975 particles/year, and 571.225 particles/year for the recommended salt intake of 5 grams per day (g/day), or approximately 120.45 particles/year, 667.95 particles/year, and 1142.45 particles/year for salt intake of 10 g/day (Table 3).

Microplastics are considered food contaminants that pose potential risks to human health and food safety. However, studies on the effects of these contaminants on human health are still very limited and little is known about the risks associated with human exposure to microplastics (Barboza *et al.*, 2018; Rainieri and Barranco, 2019; Rubio-Armendáriz *et al.*, 2022). Several studies have evaluated the presence of microplastics in foods, such as fish, shellfish, bivalves, oysters, honey, sugar, and beer (Kasmini *et al.*, 2023; Maulana *et al.*, 2023; Barboza *et al.*, 2018; Rainieri and Barranco, 2019). The exact mechanisms of the damage caused by microplastics to organisms are not yet fully understood. Limited data on this topic suggest that ingestion and accumulation of MPs in animals may cause localized inflammation in the gut and particle toxicity through the induction of immune responses. Besides, MPs enters in various ways into human body, mainly indirectly through the consumption of fish and other seafood (Makhdoumi *et al.*, 2023).

#### *Techniques to reduce microplastics contamination in salt*

Salt can be contaminated with microplastics mainly from polluted seawater and various stages of salt production, handling, and repackaging. Several methods that can reduce microplastics contamination in salt include the sand filtration technology proposed by Seth and Shrivastav (2018) to remove the amount of microplastics from seawater, with an

efficiency of up to 90%. A method with the use of reverse osmosis membranes is also suggested, where the seawater feed is pretreated with microfiltration membranes to remove unwanted particles and then further concentrated by separating the water on reverse osmosis membranes (Yaranal *et al.*, 2020). In addition, coagulation methods using various coagulants such as Aluminum sulfate ( $\text{Al}_2(\text{SO}_4)_3$ ), Aluminum chloride ( $\text{AlCl}_3$ ), and Poly Aluminum Chloride (PAC) can also be employed to remove microplastics, with efficiency exceeding 60% (Ma *et al.*, 2018). Coagulation techniques require simple settings, are cost-effective, and have already been widely used by the community. The magnetic carbon nanotube method is considered to be able to remove microplastic particles in water through adsorption, with results showing 100% efficient removal of PE, PET, and PA. These carbon nanomaterials offer the advantages of being economical and environmentally friendly materials that have a large specific surface area and multiple adsorption sites (Tang *et al.*, 2021). Further studies are highly necessary to prove the usefulness of the new laboratory-tested methods in salt production and to assess the safety of their application in food production. One example of these new innovations is the nano-based technology, which is an important advancement that can affect the food sector by improving the quality of food products (Pushparaj *et al.*, 2022).

## CONCLUSIONS

Based on the results of this study, coarse salt and fine salt circulating in Padang City and Jambi City, Indonesia are found to be contaminated with microplastics. Microplastic particles are found more in coarse salt than in fine salt. The abundance of microplastics in the total samples ranges from  $33 \pm 9$  to  $313 \pm 57$  particles/kg. Most of Indonesian people consume salt every day, thus being at risk of being exposed to microplastics contained in salt. Microplastics contamination in salt can be caused by contaminated seawater as the raw material for salt production, as well as inadequate and unhygienic salt production facilities. The most commonly detected form of microplastics is fragment (67.49%), followed by fiber (23.82%), film (6.08%), and pellet (2.61%). In terms of size, microplastics are classified into size range of  $<100 \mu\text{m}$ ,  $\geq 100\text{-}300 \mu\text{m}$ ,  $>300\text{-}500 \mu\text{m}$ ,  $>500\text{-}1000 \mu\text{m}$ , and  $>1000 \mu\text{m}$ , with the most dominant

size being  $\geq 100\text{-}300 \mu\text{m}$  (47.3%). Microplastics in salt samples are in 5 different colors: black, blue, yellow, red, and transparent, with black being the dominant color of microplastics (52.88%). Lastly, four types of polymers are also identified, namely: polyethylene (34.62%), polypropylene (30.77%), polyethylene terephthalate (15.38%), and polyester (3.85%). It is estimated that each adult in Indonesia is exposed to 60.225-571.225 microplastic particles/year by consuming 5 grams of salt per day, or 120.45-1142.45 particles/year by consuming 10 grams of salt/day. Due to the adverse effects associated with microplastics, further studies are highly necessary to explore strategies for their removal. The process of evaporating seawater into salt can increase the risk of microplastics contained in salt consumed by humans. Some of the available methods that can be employed to reduce the microplastic content in seawater include the implementation of sand filtration technology with an efficiency of up to 90% in removing microplastics from seawater; this simple technique has been widely applied in small-scale salt production in Indonesia. Aside from this technique, the use of reverse osmosis membranes and the application of coagulation methods using coagulants such as  $\text{Al}_2(\text{SO}_4)_3$ ,  $\text{AlCl}_3$ , PAC Aluminum sulfate ( $\text{Al}_2(\text{SO}_4)_3$ ), Aluminum chloride ( $\text{AlCl}_3$ ), and Poly Aluminum Chloride (PAC) with efficiencies exceeding 60% are also strongly recommended. Coagulation techniques require simple settings, are cost-effective, and have already been widely used by the community. The magnetic carbon nanotube method has been proven to efficiently remove microplastic particles (PE, PET, and PA) in water by adsorption. However, further studies should be conducted to prove the usefulness of this new laboratory-tested method in salt production and to assess the safety of its application in food production. Furthermore, to prevent potential airborne microplastics contamination from air pollution and waste incineration, coastal salt production areas are suggested to be located in a significant distance from estuaries, landfills, and other possible polluting industries while monitoring areas on land and off land. In addition, salt producers and handlers must follow good manufacturing practices (GMP) and good hygiene practices (GHP) to improve the safety of salt consumption. Tools, supplies, and ponds should also be properly adapted and maintained in accordance

with the tailor-made food safety training programs by the Ministry of Marine Affairs and Fisheries to reduce physical contamination.

#### AUTHOR CONTRIBUTIONS

D.A. Syamsu conducted literature review, designed and conducted experiments, analyzed and interpreted data, prepared the manuscript, and edited the manuscript. D. Deswati, the corresponding author, supervised co-authors in experiments, analyzed data, interpreted the results, and prepared the manuscript. S. Syafrizayanti conducted data analysis, interpreted the results, prepared the manuscript in the discussion and conclusion sections. A. Putra performed secondary data collection, carried out supporting analysis, linked the findings with existing literature, interpreted data, and arranged the layout of the manuscript. Y. Suteja assisted in drafting, reviewing, and revising the manuscript.

#### ACKNOWLEDGEMENT

The authors would like to express the deepest grateful to the Indonesian FDA for funding this study [PB.02.03.2.9.08.21.223 2021].

#### CONFLICT OF INTEREST

The author declares is no conflict of interest regarding the publication of this manuscript. The ethical issues, including plagiarism, informed consent, misconduct, data fabrication and/or falsification, double publication and/or submission, and redundancy, have been completely observed by the authors.

#### OPEN ACCESS

©2024 The author(s). This article is licensed under a Creative Commons Attribution 4.0 International License, which permits use, sharing, adaptation, distribution, and reproduction in any medium or format, as long as you give appropriate credit to the original author(s) and the source, provide a link to the Creative Commons license, and indicate if changes were made. The images or other third-party material in this article are included in the article's Creative Commons license unless indicated otherwise in a credit line to the material. If material is not included in the article's Creative Commons license and your intended use is not permitted by statutory regulation or exceeds the permitted use, you will need to obtain

permission directly from the copyright holder. To view a copy of this license, visit:

<http://creativecommons.org/licenses/by/4.0/>

#### PUBLISHER'S NOTE

GJESM Publisher remains neutral with regard to jurisdictional claims with regard to published maps and institutional affiliations.

ABBREVIATIONS	DEFINITION
%	Percent
°C	Degrees Celsius
μm	Micrometer
$Al_2(SO_4)_3$	Aluminium sulfate
$AlCl_3$	Aluminium chloride
ANOVA	Analysis of variances
ATR	Attenuated total reflectance
ATR-FTIR	Attenuated total reflectance-fourier transform infra-red
BBP	Benzyl butyl phthalate
CYP2E1	Cytochrome P450 family 2 subfamily E member 1
EDI	Estimated human dietary intake
FDA	Food Drug and Authority
FTIR	Fourier transform infra-red
g/day	Gram per day
g/mL	Gram per milliliter
GHP	Good hygiene practice
GMP	Good manufacturing practice
HDPE	High-density polyethylene
HEK 293	Human embryonic kidney cells
HEP G2	Human hepatocellular liver cells
HNF4A	Hepatocyte Nuclear Factor-4 Alpha
HSD	Honest significant difference
$H_2O_2$	Hydrogen peroxide
km	Kilometer
LDPE	Low-density polyethylene
mL	Milliliter
mm	Millimeter
MPs	Microplastics

NA	Not available
PA	Polyamide
PAC	Poly aluminum chloride
particles/kg	Particles per kilogram
particles/m <sup>2</sup>	Particles per square meter
particles/m <sup>3</sup>	Particles per cubic meter
PE	Polyethylene
PES	Polyester
PET	Polyethylene terephthalate
POPs	Persistent organic pollutants
PP	Polypropylene
PS-MPs	Polystyrene microplastics
PVC	Polyvinyl chloride
ROS	Reactive oxygen species
rpm	Revolutions per minute
TPE	Thermoplastic elastomers
WHO	World Health Organization

## REFERENCES

- Acharya, S.; Rumi, S.S.; Hu, Y.; Abidi, N., (2021). Microfibers from synthetic textiles as a major source of microplastics in the environment: A review. *Text. Res. J.*, 91(17-18): 2136–2156 **(21 pages)**.
- Andrady, A.L., (2011). Microplastics in the marine environment. *Mar. Pollut. Bull.*, 62(8): 1596–1605 **(10 pages)**.
- Atmarita, A.; Jahari, A.B.; Sudikno, S.; Soekatri, M., (2017). Asupan gula, garam, dan lemak di Indonesia: Analisis survei konsumsi makanan individu (SKMI) 2014. *Gizi Indonesia.*, 39(1): 1–14 **(14 pages)**.
- Barboza, L.G.A.; Dick Vethaak, A.; Lavorante, B.R.B.O.; Lundebye, A.K.; Guilhermino, L., (2018). Marine microplastic debris: An emerging issue for food security, food safety, and human health. *Mar. Pollut. Bull.*, 133: 336–348 **(13 pages)**.
- Buwono, N.R.; Risjani, Y.; Soegianto, A., (2021). Distribution of microplastic in relation to water quality parameters in the Brantas River, East Java, Indonesia. *Environ. Technol. Innovation.* 24(2021): 101915 **(10 pages)**.
- Buwono, N.R.; Risjani, Y.; Soegianto, A., (2022). Spatio-temporal patterns of occurrence of microplastics in the freshwater fish *Gambusia affinis* from the Brantas River, Indonesia. *Environ. Pollut.*, 311: 119958 **(9 pages)**.
- Cheng, W.; Li, X.; Zhou, Y.; Yu, H.; Xie, Y.; Guo, H.; Wang, H.; Li, Y.; Feng, Y.; Wang, Y., (2022). Polystyrene microplastics induce hepatotoxicity and disrupt lipid metabolism in the liver organoids. *Sci. Total Environ.*, 806(1): 150328 **(13 pages)**.
- Cordova, M.R.; Nurhati, I.S.; Shiimoto, A.; Hatanaka, K.; Saville, R.; Riani, E., (2022). Spatiotemporal macro debris and microplastic variations linked to domestic waste and textile industry in the supercritical Citarum River, Indonesia. *Mar. Pollut. Bull.*, 175: 113338 **(11 pages)**.
- Cordova, M.R.; Purwiyanto, A.I.S.; Suteja, Y., (2019). Abundance and characteristics of microplastics in the northern coastal waters of Surabaya, Indonesia. *Mar. Pollut. Bull.*, 142: 183–188 **(6 pages)**.
- Desforges, J.-P.W.; Galbraith, M.; Dangerfield, N.; Ross, P.S., (2014). Widespread distribution of microplastics in subsurface seawater in the NE Pacific Ocean. *Mar. Pollut. Bull.*, 79(1-2): 94–99 **(6 pages)**.
- Deswati; Sutopo, J.; Putra, A.; Suparno., (2023). Mikroplastik, sampling dan analisisnya. *Graha Ilmu.*, **(170 pages)**.
- Di Fiore, C.; Sammartino, M.P.; Giannattasio, C.; Avino, P.; Visco, G., (2023). Microplastic contamination in commercial salt: An issue for their sampling and quantification. *Food Chem.*, 404: 134682 **(10 pages)**.
- Ehzari, H.; Safari, M.; Samimi, M.; Shamsipur, M.; Gholivand, M.B., (2022). A highly sensitive electrochemical biosensor for chlorpyrifos pesticide detection using the adsorbent nanomatrix contain the human serum albumin and the Pd: CdTe quantum dots. *Microchem. J.*, 179: 107424 **(10 pages)**.
- Fadare, O.O.; Okoffo, E.D.; Olasehinde, E.F., (2021). Microparticles and microplastics contamination in African table salts. *Mar. Pollut. Bull.*, 164: 112006 **(8 pages)**.
- Fotopoulou, K.N.; Karapanagioti, H.K., (2012). Surface properties of beached plastic pellets. *Mar. Environ. Res.*, 81: 70–77 **(8 pages)**.
- Geyer, R.; Jambeck, J.R.; Law, K.L., (2017). Production, use, and fate of all plastics ever made. *Sci. Adv.*, 3(7): 1700782 **(6 pages)**.
- Goodman, K.E.; Hua, T.; Sang, Q.-X.A., (2022). Effects of polystyrene microplastics on human kidney and liver cell morphology, cellular proliferation, and metabolism. *ACS Omega*, 7(38): 34136–34153 **(18 pages)**.
- Gray, A.D.; Weinstein, J.E., (2017). Size and shape-dependent effects of microplastic particles on adult dagger blade grass shrimp, *Palaemonetes pugio*. *Environ. Toxicol. Chem.*, 36(11): 3074–3080 **(7 pages)**.
- Gündoğdu, S., (2018). Contamination of table salts from Turkey with microplastics. *Food Add. Contam. - Part A Chem.*, 35(5): 1006–1014. **(9 pages)**.
- Ha, D.T., (2021). Microplastic contamination in commercial sea salt of Vietnam. *Vietnam. J. Sci. Technol.*, 59(3): 333–344 **(12 pages)**.
- Hidalgo-Ruz, V.; Gutow, L.; Thompson, R.C.; Thiel, M., (2012). Microplastics in the marine environment: a review of the methods used for identification and quantification. *Environ. Sci. Technol.*, 46(6): 3060–3075 **(16 pages)**.
- Huang, Y.; Xu, E.G., (2022). Black microplastic in plastic pollution: undetected and underestimated? *Water Emerg. Contam. Nanoplastics.*, 1(14): 1-7 **(7 pages)**.
- Hussain, N.; Jaitley, V.; Florence, A.T., (2001). Recent advances in the understanding of uptake of micro particulates across the gastrointestinal lymphatics. *Adv. Drug Deliv. Rev.*, 50(1–2): 107–142 **(36 pages)**.
- Iñiguez, M.E.; Conesa, J.A.; Fullana, A., (2017). Microplastics in Spanish Table Salt. *Sci. Rep.*, 7(8620): 1–7 **(7 pages)**.
- Jambeck, J.R.; Geyer, R.; Wilcox, C.; Siegler, T.R.; Perryman, M.; Andrady, A.; Narayan, R.; Law, K.L., (2015). Plastic waste inputs from land into the ocean. *Science.*, 347(6223): 768–771 **(4 pages)**.

- Jung, M.R.; Horgen, F.D.; Orski, S.V.; Rodriguez C.V.; Beers, K.L.; Balazs, G.H.; Jones, T.T.; Work, T.M.; Brignac, K.C.; Royer, S.-J.; Hyrenbach, K.D.; Jensen, B.A.; Lynch, J.M., (2018). Validation of ATR FT-IR to identify polymers of plastic marine debris, including those ingested by marine organisms. *Mar. Pollut. Bull.*, 127: 704–716 **(13 pages)**.
- Jung, Y.S.; Sampath, V.; Prunicki, M.; Aguilera, J.; Allen, H.; LaBeaud, D.; Veidis, E.; Barry, M.; Erny, B.; Patel, L.; Akdis, C.; Akdis, M.; Nadeau, K., (2022). Characterization and regulation of microplastic pollution for protecting planetary and human health. *Environ. Pollut.*, 315: 120442 **(10 pages)**.
- Käppler, A.; Windrich, F.; Löder, M.G.J.; Malanin, M.; Fischer, D.; Labrenz, M.; Eichhorn, K.-J.; Voit, B., (2015). Identification of microplastics by FTIR and Raman microscopy: A novel silicon filter substrate opens the important spectral range below 1300  $\text{cm}^{-1}$  for FTIR transmission measurements. *Anal. Bioanal. Chem.*, 407: 6791-6801 **(11 pages)**.
- Kapukotuwa, R.W.M.G.K.; Jayasena, N.; Weerakoon, K.C.; Abayasekara, C.L.; Rajakaruna, R.S., (2022). High levels of microplastics in commercial salt and industrial salterns in Sri Lanka. *Mar. Pollut. Bull.*, 174: 113239 **(10 pages)**.
- Karami, A.; Golieskardi, A.; Keong Choo, C.; Larat, V.; Galloway, T.S.; Salamatinia, B., (2017). The presence of microplastics in commercial salts from different countries. *Sci. Rep.*, 7(46173): 1-9 **(9 pages)**.
- Kasmini, L.; Batubara, A.S., (2023). Microplastic contamination and growth pattern of oyster; *Crassostrea gigas* in a coastline. *Global J. Environ. Sci. Manage.*, 9(4): 753-764 **(12 pages)**.
- Kim, J.-S.; Lee, H.-J.; Kim, S.K.; Kim, H.-J., (2018). Global Pattern of Microplastics (MPs) in Commercial Food-Grade Salts: Sea Salt as an Indicator of Seawater MP Pollution. *Environ. Sci. Technol.*, 52(21): 12819–12828 **(9 pages)**.
- KKP., (2021). *Produksi Garam tahun 2020*. Balai Besar Riset Sosial Ekonomi Kelautan dan Perikanan, Badan Riset dan SDM Kelautan dan Perikanan Indonesia.
- Koelmans, A.A.; Mohamed Nor, N.H.; Hermsen, E.; Kooi, M.; Mintenig, S.M.; De France, J., (2019). Microplastics in freshwaters and drinking water: Critical review and assessment of data quality. *Water Res.*, 155: 410–422 **(13 pages)**.
- Lee, H.-J.; Song, N.-S.; Kim, J.-S.; Kim, S.-K., (2021). Variation and Uncertainty of Microplastics in Commercial Table Salts: Critical Review and Validation. *J. Hazard. Mater.*, 402: 123743 **(13 pages)**.
- Löder, M.G.J.; Kuczera, M.; Mintenig, S.; Lorenz, C.; Gerdt, G., (2015). Focal plane array detector-based micro-Fourier-transform infrared imaging for the analysis of microplastics in environmental samples. *Environ. Chem.*, 12(5): 563–581 **(19 pages)**.
- Lusher, A.L.; Tirelli, V.; O'Connor, I.; Officer, R., (2015). Microplastics in Arctic polar waters: The first reported values of particles in surface and sub-surface samples. *Sci. Rep.*, 5(14947): 1-9 **(9 pages)**.
- Ma, B.; Xue, W.; Ding, Y.; Hu, C.; Liu, H.; Qu, J., (2019). Removal characteristics of microplastics by Fe-based coagulants during drinking water treatment. *J. Environ. Sci.*, 78: 267–275 **(9 pages)**.
- Makhdoomi, P.; Hossini, H.; Nazmara, Z.; Mansouri, K.; Pirsaeheb, M., (2021). Occurrence and exposure analysis of microplastic in the gut and muscle tissue of riverine fish in Kermanshah province of Iran. *Mar. Pollut. Bull.*, 173: 112915 **(11 pages)**.
- Makhdoomi, P.; Pirsaeheb, M.; Amin, A.A.; Kianpour, S.; Hossini, H., (2023). Microplastic pollution in table salt and sugar: Occurrence, qualification and quantification and risk assessment. *J. Food Comp. Anal.*, 119(2): 105261 **(11 pages)**.
- Mamun, A.A.; Prasetya, T. A. E.; Dewi, I. R.; Ahmad, M., (2023). Microplastics in human food chains: Food becoming a threat to health safety. *Sci. Total Environ.*, 858: 159834 **(17 pages)**.
- Maulana, M.R.; Saiful, S.; Muchlisin, Z.A., (2023). Microplastics contamination in two peripheral fish species harvested from downstream river. *Global J. Environ. Sci Manage.*, 9(2): 299-308 **(10 pages)**.
- Nakat, Z.; Dgheim, N.; Ballout, J.; Bou-Mitri, C., (2023). Occurrence and exposure to microplastics in salt for human consumption, are present on the Lebanese market. *Food Control*. 145: 109414 **(9 pages)**.
- Nilawati.; Sunarsih.; Sudarno., (2020). Microplastic pollution from sea salt: Its effect on public health and prevention alternatives-a review. *E3S Web Conf.*, 202: 06018 **(10 pages)**.
- Noda, I.; Dowrey, A.E.; Haynes, J.L.; Marcott, C., (2007). Group Frequency Assignments for Major Infrared Bands Observed in Common Synthetic Polymers. *J. E. Mark (Ed.)*. *Phys. Prop. Polym. Handb.* Springer New York, 395–406 **(12 pages)**.
- Pedrotti, M.L.; Petit, S.; Elineau, A.; Bruzard, S.; Crebassa, J.-C.; Dumontet, B.; Martí, E.; Gorsky, G.; Cózar, A., (2016). Changes in the floating plastic pollution of the Mediterranean Sea in relation to the distance to land. *PLoS One*. 11(8): 1-14 **(14 pages)**.
- Possatto, F.E.; Barletta, M.; Costa, M.F.; Ivar do Sul, J.A.; Dantas, D.V., (2011). Plastic debris ingestion by marine catfish: An unexpected fisheries impact. *Mar. Pollut. Bull.*, 62(5): 1098–1102 **(5 pages)**.
- Priya, A.; Anusha, G.; Thanigaivel, S.; Karthick, A.; Mohanavel, V.; Velmurugan, P.; Balasubramanian, B.; Ravichandran, M.; Kamyab, M.; Kirpichnikova, I.M.; Chelliapan, S., (2023). Removing microplastics from wastewater using leading-edge treatment technologies: a solution to microplastic pollution—a review. *Bioprocess Biosyst Eng* 46; 309–321 **(13 pages)**.
- Pushparaj, K.; Liu, W. C.; Meyyazhagan, A.; Orlacchio, A.; Pappusamy, M.; Vadivalagan, C.; Robert, A. A.; Arumugam, V. A.; Kamyab, H.; Klemeš, J. J.; Khademi, T.; Mesbah, M.; Chelliapan, S.; Balasubramanian, B., (2022). Nano- from nature to nurture: A comprehensive review on facets, trends, perspectives, and sustainability of nanotechnology in the food sector. *Energy*, 240; 122732 **(15 pages)**.
- Qiao, R.; Deng, Y.; Zhang, S.; Wolosker, M.B.; Zhu, Q.; Ren, H.; Zhang, Y., (2019). Accumulation of different shapes of microplastics initiates intestinal injury and gut microbiota dysbiosis in the gut of zebrafish. *Chemosphere.*, 236: 124334 **(12 pages)**.
- Rainieri, S.; Barranco, A., (2019). Microplastics, a food safety issue? *Trends Food Sci. Technol.*, 84: 55–57 **(3 pages)**.
- Rakib, M.R.J.; Al Nahian, S.; Alfonso, M.B.; Khandaker, M.U.; Enyoh, C.E.; Hamid, F.S.; Alsubaie, A.; Almalki, A.S.A.; Bradley, D.A.; Mohafez, H.; Islam, M.A., (2021). Microplastic pollution in salt pans from the Maheshkhali Channel, Bangladesh. *Sci.*

- Rep., 11: 23187 **(10 pages)**.
- Renzi, M.; Blašković, A. (2018). Litter & microplastics features in table salts from marine origin: Italian versus Croatian brands. *Mar. Pollut. Bull.*, 135: 62–68 **(7 pages)**.
- Rieux, A.des.; Ragnarsson, E.G.E.; Gullberg, E.; Préat, V.; Schneider, Y.-J.; Artursson, P., (2005). Transport of nanoparticles across an in vitro model of the human intestinal follicle-associated epithelium. *Eur. J. Pharm. Sci.*, 25(4–5): 455–465 **(11 pages)**.
- Rubio-Armendáriz, C.; Alejandro-Vega, S.; Paz-Montelongo, S.; Gutiérrez-Fernández, Á.J.; Carrascosa-Iruzubieta, C.J.; la Torre, A.H., (2022). Microplastics as Emerging Food Contaminants: A Challenge for Food Safety. *Int. J. Environ. Res. Public Health*, 19(3): 1174 **(14 pages)**.
- Sabilillah, A.M.; Palupi, F.R.; Adji, B.K.; Nugroho, A.P., (2023). Health risk assessment and microplastic pollution in streams through accumulation and interaction of heavy metals. *Global J. Environ. Sci. Manage.*, 9(4): 719-740 **(22 pages)**.
- Samimi, M.; Mohammadzadeh, E.; Mohammadzadeh, A., (2023). Rate enhancement of plant growth using Ormus solution: optimization of operating factors by response surface methodology. *Int. J. Phytoremediation*, 1-7 **(7 pages)**.
- Samimi, M.; Shahriari-Moghadam, M., (2023). The Lantana camara L. stem biomass as an inexpensive and efficient biosorbent for the adsorptive removal of malachite green from aquatic environments: kinetics, equilibrium and thermodynamic studies. *Int. J. Phytoremediation*, 25(10): 1-9 **(9 pages)**.
- Selvam, S.; Manisha, A.; Venkatramanan, S.; Chung, S.Y.; Paramasivam, C.R.; Singaraja, C., (2020). Microplastic presence in commercial marine sea salts: A baseline study along Tuticorin Coastal salt pan stations, Gulf of Mannar, South India. *Mar. Pollut. Bull.*, 150: 110675 **(7 pages)**.
- Seth, C.K.; Shriwastav, A., (2018). Contamination of Indian sea salts with microplastics and a potential prevention strategy. *Environ. Sci. Pollut. Res.*, 25: 30122–30131 **(10 pages)**.
- Siddique, M.A.M.; Uddin, A.; Bhuiya, A.; Rahman, S.Md.A.; Kibria, G., (2023). Occurrence, spatial distribution, and characterization of microplastic particles in the salt pans from the Southeastern part of the Bay of Bengal. *Reg. Stud. Mar. Sci.*, 61: 102846 **(10 pages)**.
- Song, Y.K.; Hong, S.H.; Jang, M.; Kang, J.-H.; Kwon, O.Y.; Han, G.M.; Shim, W.J., (2014). Large Accumulation of Micro-sized Synthetic Polymer Particles in the Sea Surface Microlayer. *Environ. Sci. Technol.*, 48(16): 9014–9021 **(8 pages)**.
- Stock, V.; Böhmert, L.; Lisicki, E.; Block, R.; Cara-Carmona, J.; Pack, L.K.; Selb, R.; Lichtenstein, D.; Voss, L.; Henderson, C.J.; Zabinsky, E.; Sieg, H.; Braeuning, A.; Lampen, A., (2019). Uptake and effects of orally ingested polystyrene microplastic particles in vitro and in vivo. *Arch. Toxicol.*, 93: 1817–1833 **(17 pages)**.
- Suteja, Y.; Atmadipoera, A.S.; Riani, E.; Nurjaya, I.W.; Nugroho, D.; Cordova, M.R., (2021). Spatial and temporal distribution of microplastic in surface water of tropical estuary: A case study in Benoa Bay, Bali, Indonesia. *Mar. Pollut. Bull.*, 163: 111979 **(14 pages)**.
- Sutherland, W.J.; Atkinson, P.W.; Butchart, S.H.M.; Capaja, M.; Dicks, L.V.; Fleishman, E.; Gaston, K. J.; Hails, R.S.; Hughes, A.C.; Le Anstey, B.; Le Roux, X.; Lickorish, F. A.; Maggs, L.; Noor, N.; Oldfield, T. E. E.; Palardy, J. E.; Peck, L. S.; Pettorelli, N.; Pretty, J.; Spalding, M. D.; Tonneijck, F. H.; Truelove, G.; Watson, J. E. M.; Wentworth, J.; Wilson, J. D.; Thornton, A., (2022). A horizon scan of global biological conservation issues for 2022. *Trends Ecol. Evol.*, 37(1): 95–104 **(10 pages)**.
- Syakti, A.D.; Bouhroum, R.; Hidayati, N.V.; Koenawan, C.J.; Boulkamh, A.; Sulisty, I.; Lebarillier, S.; Akhlus, S.; Doumenq, P.; Wong-Wah-Chung, P., (2017). Beach macro-litter monitoring and floating microplastic in a coastal area of Indonesia. *Mar. Pollut. Bull.*, 122(1–2): 217–225 **(9 pages)**.
- Tang, Y.; Zhang, S.; Su, Y.; Wu, D.; Zhao, Y.; Xie, B., (2021). Removal of microplastics from aqueous solutions by magnetic carbon nanotubes. *Chem. Eng. J.*, 406: 126804 **(11 pages)**.
- Takarina, N.D.; Purwiyanto, A.I.S.; Rasud, A.A.; Arifin, A.A.; Suteja, Y., (2022). Microplastic abundance and distribution in surface water and sediment collected from the coastal area. *Global J. Environ. Sci. Manag.*, 8(2): 183-196 **(14 pages)**.
- Tibbetts, J., (2015). Managing marine plastic pollution: Policy initiatives to address wayward waste. *Environ. Health Perspect.*, 123(4): A90–A93 **(4 pages)**.
- UNEP, (2016). Marine plastics debris and microplastics Global lessons and research to inspire action and guide policy change.
- Vidyasakar, A.; Krishnakumar, S.; Kumar, K.S.; Neelavannan, K.; Anbalagan, S.; Kasilingam, K.; Srinivasalu, S.; Saravanan, P.; Kamaraj, S.; Magesh, N.S., (2021). Microplastic contamination in edible sea salt from the largest salt-producing states of India. *Mar. Pollut. Bull.*, 171: 112728 **(6 pages)**.
- Waring, R.H.; Harris, R.M.; Mitchell, S.C., (2018). Plastic contamination of the food chain: A threat to human health? *Maturitas.*, 115: 64–68 **(5 pages)**.
- WHO, (2012). Guideline: Sodium intake for adults and children. World Health Organization., **(56 pages)**.
- Yang, D.; Shi, H.; Li, L.; Li, J.; Jabeen, K.; Kolandhasamy, P., (2015). Microplastic Pollution in Table Salts from China. *Environ. Sci Technol.*, 49(22): 13622–13627 **(6 pages)**.
- Yaranal, N. A.; Kumari, S.; Narayanasamy, S.; Subbiah, S., (2020). An analysis of the effects of pressure-assisted osmotic backwashing on the high recovery reverse osmosis system. *J. Water Supply Res. Technol. – Aqua.*, 69(3): 298–318 **(21 pages)**.
- Yuan, Z.; Nag, R.; Cummins, E., (2022). Human health concerns regarding microplastics in the aquatic environment - From marine to food systems. *Sci. Total Environ.*, 823: 153730 **(19 pages)**.
- Zhang, K.; Shi, H.; Peng, J.; Wang, Y.; Xiong, X.; Wu, C.; Lam, P.K.S., (2018). Microplastic pollution in China’s inland water systems: A review of findings, methods, characteristics, effects, and management. *Sci. Total Environ.*, 630: 1641–1653 **(13 pages)**.
- Zhang, Q.; Xu, E.G.; Li, J.; Chen, Q.; Ma, L.; Zeng, E.Y.; Shi, H., (2020). A Review of Microplastics in Table Salt, Drinking Water, and Air: Direct Human Exposure. *Environ. Sci Technol.*, 54(7): 3740–3751 **(12 pages)**.
- Zhao, X.; Wang, J.; Yee Leung, K.M.; Wu, F., (2022). Color: An Important but Overlooked Factor for Plastic Photoaging and Microplastic Formation. *Environ. Sci Technol.*, 56(13): 9161–9163 **(3 pages)**.

#### AUTHOR (S) BIOSKETCHES

**Syamsu, D.A.**, M.Si., <sup>1</sup>Department of Chemistry, Faculty of Mathematics and Natural Science, Andalas University, Padang, Indonesia.

<sup>2</sup>Indonesian Food and Drug Authority (FDA), Jambi, Indonesia.

▪ Email: [desmita.adriani@pom.go.id](mailto:desmita.adriani@pom.go.id)

▪ ORCID: 0009-0006-6437-2905

▪ Web of Science ResearcherID: NA

▪ Scopus Author ID: NA

▪ Homepage: <https://jambi.pom.go.id/>

**Deswati, D.**, Dr., Professor., Department of Chemistry, Faculty of Mathematics and Natural Science, Andalas University, Padang, Indonesia.

▪ Email: [deswati@sci.unand.ac.id](mailto:deswati@sci.unand.ac.id)

▪ ORCID: 0000-0002-8655-9838

▪ Web of Science ResearcherID: AAC-6589-2021

▪ Scopus Author ID: 55682368600

▪ Homepage: <http://kimia.fmipa.unand.ac.id/sivitas/dosen/166-deswati>

**Syafrizayanti, S.**, Dr. Rer.Nat., Associate Professor, Department of Chemistry, Faculty of Mathematics and Natural Science, Andalas University, Padang, Indonesia.

▪ Email: [deswati@sci.unand.ac.id](mailto:deswati@sci.unand.ac.id)

▪ ORCID: 0000-0002-4896-2722

▪ Web of Science ResearcherID: AAE-8090-2021

▪ Scopus Author ID: 56017949100

▪ Homepage: <http://kimia.fmipa.unand.ac.id/sivitas/dosen/189-dr-rer-nat-syafrizayanti>

**Putra, A.**, Ph.D. Candidate, Department of Medical Laboratory Technology, Syedza Sainatika College of Health Sciences, Padang, Indonesia.

▪ Email: [adewirliputra@gmail.com](mailto:adewirliputra@gmail.com)

▪ ORCID: 0000-0001-6500-6241

▪ Web of Science ResearcherID: HLV-6865-2023

▪ Scopus Author ID: 57849105300

▪ Homepage: <https://syedzasaintika.ac.id/web/adewirli/>

**Suteja, Y.**, Dr., Department of Marine Science, Faculty of Marine and Fisheries, Udayana University, Bali, Indonesia.

▪ Email: [yuliantosuteja@unud.ac.id](mailto:yuliantosuteja@unud.ac.id)

▪ ORCID: 0000-0002-7824-5177

▪ Web of Science ResearcherID: AAP-5075-2020

▪ Scopus Author ID: 57201496119

▪ Homepage: <https://fkip.unud.ac.id/pages/view/yulianto-suteja-s-kel-m-si>

#### HOW TO CITE THIS ARTICLE

Syamsu, D.A.; Deswati, D.; Syafrizayanti, S.; Putra, A.; Suteja, Y., (2024). Presence of microplastic contamination in table salt and estimated exposure in humans. *Global J. Environ. Sci. Manage.*, 10(1) 205-224.

DOI: 10.22034/gjesm.2024.01.14

URL: [https://www.gjesm.net/article\\_707785.html](https://www.gjesm.net/article_707785.html)





## ORIGINAL RESEARCH PAPER

## Generalization of artificial neural network for predicting methane production in laboratory-scale anaerobic bioreactor landfills

M.J. Zoqi

Department of Civil Engineering, University of Birjand, Birjand, Iran

## ARTICLE INFO

**Article History:**

Received 06 June 2023

Revised 12 August 2023

Accepted 20 September 2023

**Keywords:**

Anaerobic process

Generalizability

Landfill bioreactor

Leachate treatment

Neural network

## ABSTRACT

**BACKGROUND AND OBJECTIVES:** Leachate recirculation has become a global practice for anaerobic digestion of municipal solid waste. Implementation of artificial neural networks for modeling and prediction of this process still remains challenging. Additionally, there has been a lack of research regarding the generalization capacity of neural networks using the data from other studies. This study aimed to enhance methane production rates and decrease biostabilization time in municipal solid waste treatment. It addressed the research gap in applying and generalizing neural networks to predict biogas production based on laboratory-measured parameters.

**METHODS:** Two distinct systems were utilized for leachate treatment. System 1 involved collecting the leachate delivered by a new municipal solid waste reactor and transferring it to a recirculation tank. System 2 consisted of passing the fresh municipal solid waste leachate through a degraded municipal solid waste and then returning the obtained liquid back to the waste reactor. The experimental data were employed to develop an artificial neural network to predict methane content and cumulative biogas production. The model was trained and optimized using the experimental data. The effectiveness and generalizability of the optimal neural network were evaluated by using it for the unseen data from other studies, ensuring its ability to make accurate predictions beyond the training dataset.

**FINDINGS:** The results demonstrated that in System 1, ammonium and chemical oxygen demand concentrations in the leachate progressively increased to high levels. In System 2, the average removal efficiencies for chemical oxygen demand and ammonium were found to be 85 percent and 34 percent respectively. The methane yield in biogas reached 59 liters per kilogram of dry weight, with a corresponding methane fraction of 63 percent. The neural network model showed an excellent performance, with validation performances of 0.716 and 0.634. The overall performance of the dataset resulted in correlation coefficients of 0.9991 and 0.9975. Finally, high correlation coefficients of 0.88 and 0.82 were achieved by incorporating the test data from other studies.

**CONCLUSION:** Leachate recirculation enhanced the reduction of chemical oxygen demand and the production of methane in bioreactors. Ammonium concentrations initially increased and later decreased due to waste adsorption and bacterial assimilation. The artificial neural network applied for predicting the cumulative methane production from municipal solid waste displayed a robust generalizability when tested on the data from other studies. The neural network was not significantly affected by changes in waste chemical properties, laboratory conditions, and recirculation rate. However, it showed a significant sensitivity to variation of waste mechanical properties.

DOI: [10.22034/gjesm.2024.01.15](https://doi.org/10.22034/gjesm.2024.01.15)This is an open access article under the CC BY license (<http://creativecommons.org/licenses/by/4.0/>).

NUMBER OF REFERENCES

63



NUMBER OF FIGURES

9



NUMBER OF TABLES

5

\*Corresponding Author:

Email: [mj.zoqi@birjand.ac.ir](mailto:mj.zoqi@birjand.ac.ir)

Phone: +98563 102 6423

ORCID: [0000-0002-6999-4221](https://orcid.org/0000-0002-6999-4221)

Note: Discussion period for this manuscript open until April 1, 2024 on GJESM website at the "Show Article".

## INTRODUCTION

Waste landfills are the ultimate repositories for discarded or unusable materials, particularly municipal solid wastes (MSW). For instance, approximately 81 million tons of waste are landfilled annually in the UK. In 2016, 58 percent (%) of the total solid waste generated in the US was disposed (Alabi *et al.*, 2019). Leachate production and management are acknowledged as significant obstacles associated with the environmentally sound operation of municipal landfills. Recirculating leachates through MSW landfill accelerates solid waste stabilization and, consequently, increases gas production (Liu *et al.*, 2023). Over the past two decades, numerous physical, chemical, and biological treatment processes have been evaluated for their ability to treat landfill leachate (Bah *et al.*, 2023; Guo *et al.*, 2022; Luo *et al.*, 2020). These processes are typically employed for *ex-situ* leachate treatments. Nevertheless, treating leachate *ex-situ* can pose significant challenges and incur substantial costs. Moreover, the characteristics and flow of landfill leachates are influenced by some factors such as composition of solid wastes, precipitation and runoff patterns, landfill age, and permeability and type of cover (Luo *et al.*, 2020). Most leachate components are typically present in elevated concentrations during the first year of landfill operation, and these concentrations tend to decrease as the landfill ages (Kulikowska and Klimiuk, 2008). High levels of ammonia and organic matter in landfill leachate lead to significant treatment challenges (Samimi and Shahriari Moghadam, 2018). There are numerous options for landfill leachate treatment, such as complex and expensive *ex-situ* physical-chemical and biological processes, that address high-strength organics and inorganics including different forms of nitrogen. Numerous studies have documented various leachate treatments, including anaerobic sequencing batch reactors and anaerobic hybrid bed filters (Wei *et al.*, 2021), upflow sludge blanket reactors (Govahi *et al.*, 2012), and electro-Fenton method (Guvenc *et al.*, 2019). These treatment procedures can incur substantial costs. Biological processes have proved to be highly effective when applied to relatively young leachates consisting primary volatile fatty acids, but their effectiveness decreases when applied to older leachates (Bove *et al.*, 2015). Numerous scholars have conducted extensive research documenting

the benefits of leachate recirculation in sanitary landfills. According to studies, leachate recirculation generates stabilized leachates with relatively low concentrations of degradable carbon compounds and high concentrations of ammonia (Haydar and Khire, 2005; Hussein and Ibrahim, 2023). In case of biological degradation, the analytical parameters involved exhibit non-linear characteristics (Ćosić *et al.*, 2013). Artificial neural network (ANN) techniques have demonstrated a greater efficiency in accurately modeling these non-linear relationships compared to traditional statistical methods (Desai *et al.*, 2018; Rumaling *et al.*, 2022; Samimi and Mohadesi, 2023). ANNs have become increasingly popular as a useful tool for modeling the environmental systems (Muksin *et al.*, 2023). They have been widely applied in different domains, including air pollution modeling (Cabaneros *et al.*, 2019) and predicting the performance of wastewater treatment plants (El-Rawy *et al.*, 2021). ANNs, however, have not been extensively studied in terms of laboratory settings for anaerobic digestion (Nair *et al.*, 2016; Tufaner and Demirci, 2020). In a study, the utilization of ANN was explored to forecast biogas production and chemical oxygen demand (COD) removal rates in the process of anaerobic digestion (Nair *et al.*, 2016). The results of this experiment demonstrated the effectiveness of the ANN method in accurately predicting biogas production and COD removal rates. Another study indicated a strong correlation between the age of waste and the methane (CH<sub>4</sub>) concentration, which was successfully modeled using an ANN (Ozkaya *et al.*, 2007). Additionally, a separate study proposed an ANN approach to simulate the functionality of a biogas wastewater treatment system, accurately predicting the relationship between the system output and its operational parameters (Karamichailidou *et al.*, 2022). An ANN model developed by Behera *et al.* (2015) was utilized to predict the CH<sub>4</sub> concentration in biogas. The input data from this model consisted of the biogas extraction rate and the ratio of landfill leachate to food waste leachate. The results of this study showed that the backpropagation algorithm effectively predicted the percentage of CH<sub>4</sub> in biogas. Despite the utilization of only two input parameters, the ANN model demonstrated a remarkably high prediction accuracy. This could be attributed to the inclusion of the biogas extraction rate as an input, which had a direct relationship with CH<sub>4</sub> production.

The utilization of ANN was justified by its capability to comprehend intricate non-linear relationships, while the association between biogas extraction rate and CH<sub>4</sub> production was characterized by a simple non-linear pattern. In a recent study, Bao *et al.* (2023) employed a backpropagation ANN to develop a model for optimizing anaerobic digestion. Their findings indicated that the model successfully achieved a high degree of fitting with the actual data, indicating its accuracy in predicting the biogas production. This finding highlighted the practical application value of the model in anaerobic digestion. However, it is important to note that the study included an excessive number of factors in predicting biogas production, involving ten parameters. One of the primary objectives of ANN design is accurate output prediction with minimal data requirements. The selection of input data plays a critical role in determining the applicability, economy, and accuracy of ANNs. The present study emphasized the importance of selecting the best input data for ANNs based on experimental results and previous studies. The current study explored two distinct anaerobic systems as *in-situ* organic and nitrogen removal methods (System 1 and System 2). In System 1, which consisted of a reactor for fresh waste, the leachate produced by the reactor was recirculated directly into the fresh waste. In contrast, System 2 was established where the fresh waste reactor and a degraded waste reactor were connected, and the process involved recirculating leachate between the two reactors. The primary objective of this study was to investigate the methods for enhancing the rate of CH<sub>4</sub> production and reducing the biostabilization time for MSW treatment. The experiment aimed to examine the impact of operational parameters on the biodegradation of MSW within a simulated anaerobic bioreactor landfill. There was limited exploration of the application and generalization of ANN in predicting cumulative biogas production and CH<sub>4</sub> content, based on the laboratory-measured parameters that influenced the process. This study aimed to address this gap by investigating the potential of ANN in predicting the degradation rate of MSW in the bioreactors. Generalizability of the ANN was assessed by evaluating its performance on completely unseen data from other studies, representing the pioneer application of such test. This study has been conducted in the Environmental Engineering Laboratory, Department of Civil

Engineering, University of Birjand, Birjand, Iran in 2023.

## MATERIALS AND METHODS

The MSW was sourced from the Saravan Landfill, a municipal landfill located in the northern region of Tehran, Iran. This landfill has been operational since 1984. The waste sorting process involved the removal of plastic bags and inorganic waste. The remaining waste was then pretreated and tattered by blade shredder to ensure optimal flow of leachate in the laboratory-scale landfills.

### Experimental apparatus

The simulated landfill reactors consisted of square-based columns with internal dimensions of 400 square centimeters (cm<sup>2</sup>) and vertical height of 130 centimeters (cm), yielding a volume of 40 liters (L). These columns were made up of steel and Plexiglas. To maintain the internal temperature, 10 cm-thick polystyrene panels were used in order to insulate the columns, which were then placed in a temperature-controlled room at 30±2 °C. To prevent leachate outlet clogging, a 15-cm gravel drainage layer was incorporated into the lower portion of the reactors. Approximately 24 kilograms (kg) of fresh waste was used to load Reactor A and Reactor B, while Reactor C was loaded with approximately 44 kg of degraded waste. Afterward, the 15-cm layer of fine gravel was applied to cover the waste, and a water distributor was installed on top of each reactor. Subsequently, approximately 2 L of deionized water was used to generate the desired amount of leachate.

### Sampling and analytical methods

Two distinct experimental methods were employed. In System 1, the leachate from Reactor A was collected and recirculated into a tank every 24 hours (Fig. 1). In System 2, Reactor C was supplied with the leachate from Reactor B. The leachate produced in Reactor C was recirculated back to Reactor B on a 24-hour cycle. The process of leachate recirculation in both systems was facilitated using peristaltic pumps. The schematic diagram of both systems is presented in Fig. 1.

The composition of the MSW was analyzed in terms of its elemental composition including carbon (C), hydrogen (H), nitrogen (N), oxygen (O), and sulfur (S) using the PerkinElmer 2400 Series II CHNS/O Elemental Analyzer. Table 1 presents the physical

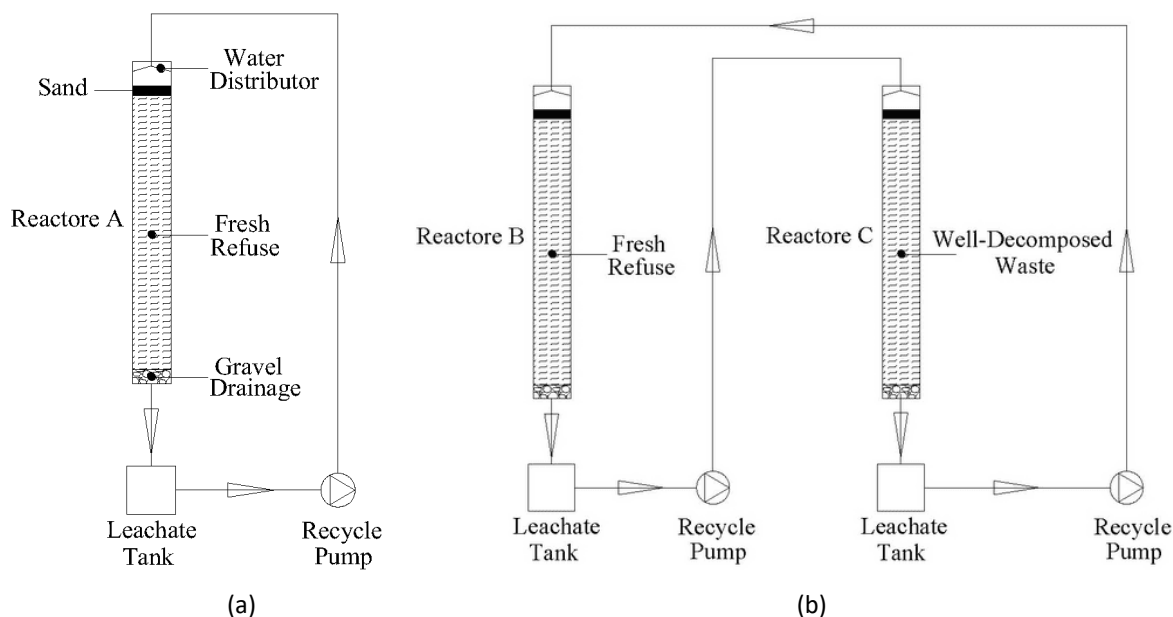


Fig. 1: Schematic diagram of (a) System 1, and (b) System 2

Table 1: Characteristics of fresh and degraded MSW (% of total weight)

Physical composition	Fresh	Degraded	Chemical characteristics	Fresh	Degraded
Food waste	65	0	Moisture content	28.32	46.23
Plastic	12	10.2	C	41.26	24.86
Paper	9	7.5	H	6.28	6.31
Textiles	2	1.2	O	39.72	42.54
Metal	0.5	0.2	N	2.57	2.15
Wood	2	1.5	S	0.51	0.26
Glass and others	9.5	9.7	Volatile solid	39.41	12.46
Soil	0	69.7			

and chemical characteristics of the MSW. Leachate samples were collected from the reactors every 6 days to measure the concentrations of biological oxygen demand ( $BOD_5$ ), COD, ammonium-nitrogen ( $NH_4^+-N$ ), and potential of hydrogen (pH) values. The pH value was measured using a HACH pH meter, while  $BOD_5$ , COD, and  $NH_4^+-N$  concentrations were determined according to the standard methods for the examination of water and wastewater (Rice *et al.*, 2012). A modified water displacement set-up was employed to measure the biogas from various runs. To quantify the total  $CH_4$  produced, biogas was passed through water containing 2% volume per volume (v/v) sulfuric acid ( $H_2SO_4$ ). The set-up involved connecting the biogas outlet of the reactor to a gas collection vessel filled with a  $H_2SO_4$

solution. As the biogas released from the reactor, it bubbled through the solution. The  $H_2SO_4$  solution was intended to absorb and react with specific components of the biogas, such as  $CO_2$ . The volume of  $CH_4$ , which did not react with the solution, was determined by measuring the displacement of water in the gas collection vessel (Sponza and Ağdağ, 2004). To determine the  $CH_4$  content, biogas samples were collected at 6-day intervals during the study. These samples were analyzed using a Young Lin gas chromatograph (model YL6100). The measurement setup was equipped with a PORO PACK Q column and a thermal conductivity detector (TCD).

#### ANN modelling

The  $CH_4$  content and cumulative biogas production

were modeled using ANN methodology. The pH, COD, hydraulic retention time (HRT), and  $\text{NH}_4^+\text{-N}$  were selected as input parameters for the ANN. These parameters were selected based on their profound influence on the microbial processes integral to methane production (Al-Dailami *et al.*, 2022). These parameters served as pivotal indicators, enabling the neural network to unravel both the qualitative and quantitative nuances of biological activity within the reactor. The ANN model was developed using a matrix laboratory (MATLAB) R2018b, a multi-paradigm numerical computing environment, with the support of the Neural Network Toolbox provided by MathWorks, Inc. The ANN architecture utilized included different layers such as input, hidden, and output layers. The neurons in the input layer indicated the independent variables and were connected to the neurons in the hidden layers by weighted connections. These weights determined the importance of the input data for each node, and a bias term was integrated to govern the size of the input data. The obtained values were multiplied by the Tan-Sigmoid activation function. The output layer determined the values of the output variables through the Pure-linear activation function. Tan-Sigmoid activation function is frequently utilized in ANNs to introduce non-linearity, enabling complex mappings within the hidden layer. In contrast, the output layer employs the Linear activation function to create a mapping that is linear in nature without any further non-linear transformation. This pairing of activation functions allowed for efficient modeling and prediction within the ANN architecture (Lee *et al.*, 2020). The values obtained from the ANN model were compared to the experimentally measured values. The error between the predicted and observed values was calculated and used to update the weights and bias of each neuron in the network. This approach enabled precise modeling and prediction of the intended outcomes. The proposed ANN model comprised two distinct ANNs. The first ANN (ANN1) was designed to predict the  $\text{CH}_4$  content (%), while the second ANN (ANN2) was developed to estimate the cumulative  $\text{CH}_4$  production liter per kilogram (L/kg) dry weight. The inputs to the model included analytical parameters such as pH, COD,  $\text{NH}_4^+\text{-N}$ , and HRT. To ensure objective evaluation, the experimental data were divided into three sets which had been randomly selected from different stages of the experimental study to prevent

bias towards any particular stage. The first set comprised 70% of the data and was used for training the model and optimizing its parameters. The second set accounted for 15% of the data and was used for independent testing while serving as a benchmark for evaluating the model performance. The validation set constituted the remaining 15% of the data and was utilized to refine the hyperparameters of the model. In the ANNs training, the Levenberg Marquardt feed-forward back propagation perceptron (LMFFBP) algorithm was utilized, and the performance assessment was done using the mean squared error (MSE) metric. LMFFBP enables faster prediction and correction of limitations by manipulating the flow of input data within the ANN layers. This technique demonstrates excellent capability and robustness in addressing fitting problems (Mougari *et al.*, 2021). Control of the randomly-selected datasets, as well as determining the number of hidden layers, neurons, and activation functions are crucial in identifying the optimal architecture of ANN in terms of accuracy and simplicity. It is also essential to balance model complexity and data learning capacity. An ANN with overabundance of hidden layers and neurons may only store data without effectively learning from it. Hence, the most optimal structure for an ANN is the one that leads to accurate predictions with the least hidden layers and neurons in the hidden layer (Kerdan and Gálvez, 2020). In this study, the adopted ANN architecture included one hidden layer. The optimal number of neurons in the hidden layer was determined through an iterative process of trial and error. The performance of the ANN model was evaluated based on the statistical criteria including MSE and correlation coefficient. Once the optimal ANN was obtained, its effectiveness and generalizability was evaluated by testing it on previously unseen data from other studies. Such an evaluation was done for the first time to ensure the ability of the ANN to generalize beyond the specific dataset used for training, testing, and validation.

## RESULTS AND DISCUSSION

Fig. 2 depicts the concentrations of COD in the leachate from Reactors A, B, and C. The experiment showed significant variations in the COD concentrations. At the beginning of the experiment, COD of the leachate from the fresh MSW in System 1 increased rapidly, reaching a maximum of 91,400

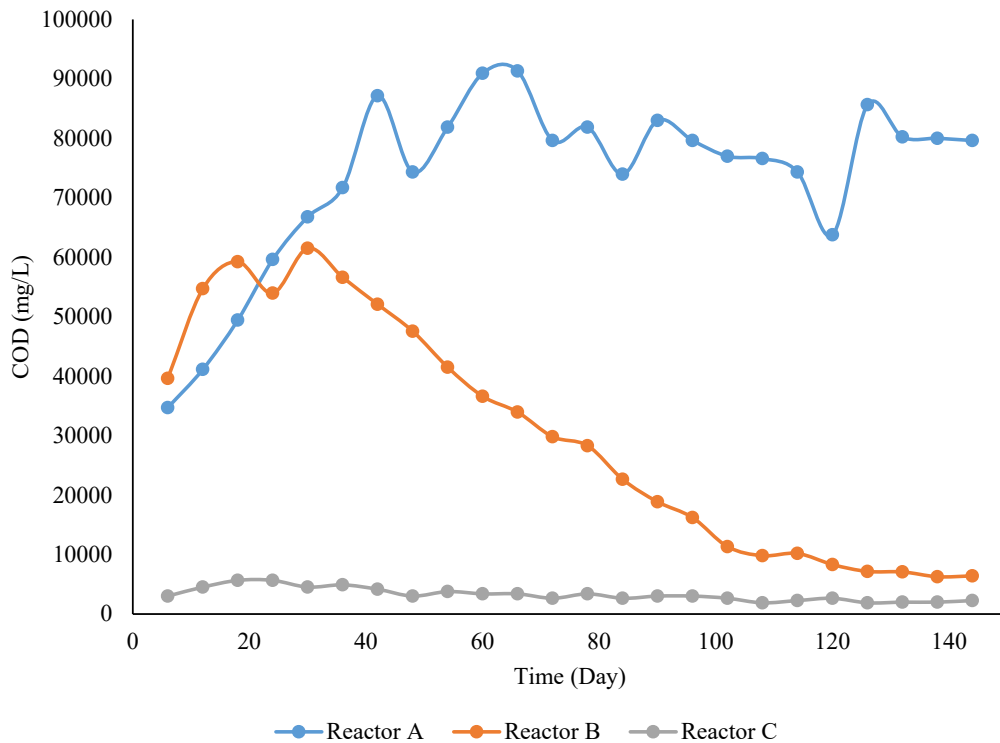
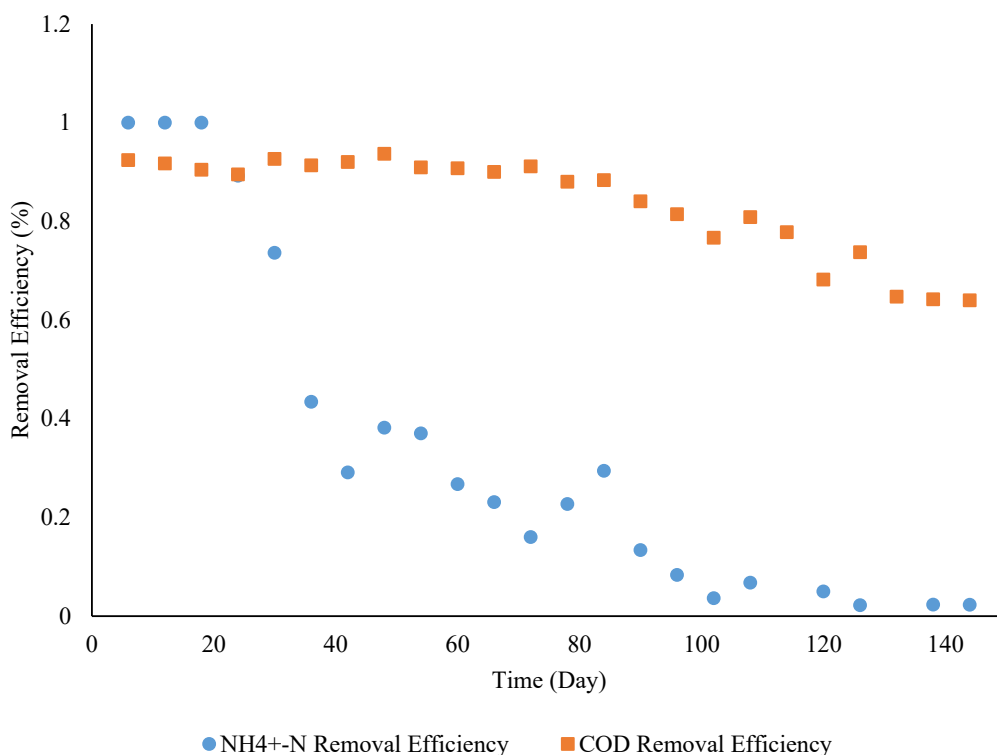


Fig. 2: Changes in the COD concentration of leachate over time in the bioreactors

mg/L on day 66. Notably, no significant decrease in COD concentrations was observed in the leachate produced by System 1. The rapid increase in COD concentrations in Reactor A could be explained by the presence of easily biodegradable organic matter in leachate from young landfills. This result was consistent with the findings of the study conducted by [Ahn et al. \(2002\)](#) and [Marttinen et al. \(2013\)](#). They observed higher COD concentrations in leachate from young landfill sites due to the higher proportion of biodegradable organic material. In reactor A, the absence of acetogenic bacteria in the fresh waste led to the occurrence of only two stages: hydrolysis and acidogenesis. Acidogenic bacteria (clostridium, bacteroides, and enterococcus), convert complex organic compounds into simpler compounds such as volatile fatty acids (VFAs) ([Marttinen et al., 2013](#)). This breakdown of organic matter typically results in the release of COD, leading to an increase in COD concentration in the leachate. In System 2, the leachate COD concentrations in Reactor B increased initially for 30 days after recirculation. This was

followed by a gradual decrease from 61,600 mg/L on day 30 to 6,270 mg/L on day 144. ([Fig. 2](#)), which could be attributed to the accumulation of carboxylic acid ([Saadoun et al., 2021](#)). In contrast, Reactor C consistently maintained low effluent COD, indicating the successful removal of organic contaminants from the leachate by System 2.

[Fig. 3](#) depicts the time-dependent degradation efficiency of COD and  $\text{NH}_4^+\text{-N}$  in System 2. During the entire operation, the degradation efficiency of COD fluctuated between 65% and 90%. In degraded MSW, the presence of acetogenic bacteria (acetobacterium, clostridium, and syntrophomonas) facilitated further metabolism of VFAs generated during acidogenesis. These acetogenic bacteria convert VFAs into acetic acid, hydrogen ( $\text{H}_2$ ), and carbon dioxide ( $\text{CO}_2$ ) through their metabolic activities ([Saadoun et al., 2021](#)). Consequently, this conversion process contributed to a notable reduction in COD concentration. COD removal efficiency in System 2 decreased with the decrease of COD concentration in the leachate. The highest COD removal efficiency in Reactor B was

Fig. 3: COD and NH<sub>4</sub><sup>+</sup>-N removal efficiencies in System 2

obtained as 90% (Fig. 3). The different biodegradability of organic matter was widely recognized in leachate. The BOD<sub>5</sub>/COD ratio is frequently used to evaluate biodegradability; a higher value indicates a greater proportion of biodegradable organic material. On day 144, the BOD<sub>5</sub>/COD ratio of the leachate from System 1 was 0.38, while the BOD<sub>5</sub>/COD ratio of leachate from System 2 was 0.09. Due to the presence of large molecule compounds, such as humic acids, which are challenging to biodegrade, the residual organic matter in the leachate was nonbiodegradable (Keyikoglu *et al.*, 2021). Consequently, the maximum COD removal efficiency was capped at 90%.

#### NH<sub>4</sub><sup>+</sup>-N

According to Fig. 4, the concentrations of ammonium in leachate in reactor A increased due to the accumulation of ammonium from the recirculated leachate (Feng *et al.*, 2019). Similarly, the concentrations of ammonium in the leachate in Reactors B and C experienced an initial increase within the first 42 days, which could be attributed

to the breakdown of nitrogenous compounds specifically in Reactor B. As the two reactors (System 1 and System 2) operated under anaerobic conditions, the absence of nitrification microorganisms, which are effective in aerobic conditions (Peng *et al.*, 2022), caused ammonia-nitrogen to accumulate in them. The concentrations of NH<sub>4</sub><sup>+</sup>-N in the leachate in Reactor A showed a significant increase, with the highest amount recorded on day 96 when the NH<sub>4</sub><sup>+</sup>-N concentrations reached 3060 mg/L (Fig. 4). During hydrolysis, complex organic compounds are broken down into simpler forms, such as sugars, amino acids, fatty acids, and other organic nitrogen-containing compounds releasing ammonium as a byproduct (Price *et al.*, 2013).

However, under anaerobic conditions in System 2, the NH<sub>4</sub><sup>+</sup>-N concentrations in Reactors B and C began to decrease on day 42 due to the degraded MSW adsorption capacity and the assimilation of NH<sub>4</sub><sup>+</sup>-N by anaerobic microorganisms to support their growth (Feng *et al.*, 2019). On day 42, the maximum concentrations of ammonium in Reactors B and C were

### Predicting methane production.

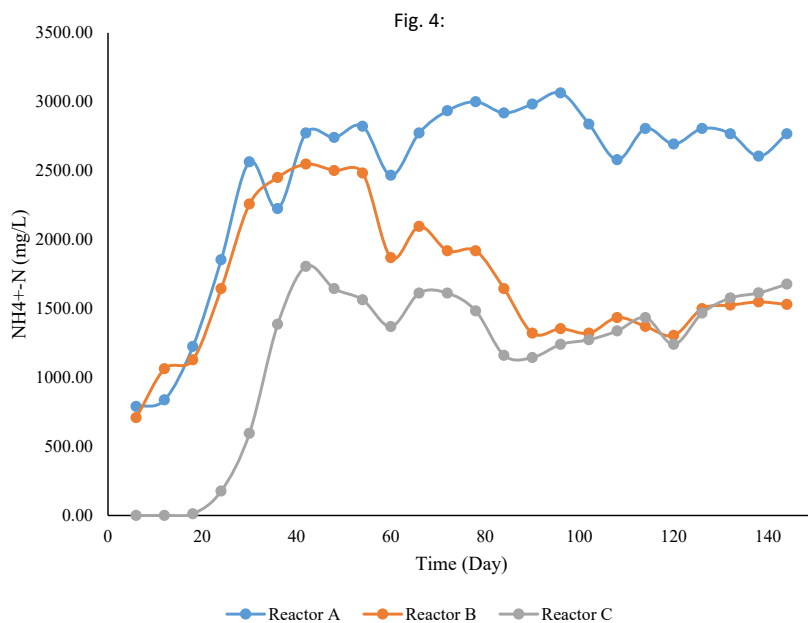


Fig. 4: Changes in the  $\text{NH}_4^+\text{-N}$  concentration of leachate over time in the bioreactors

obtained as 2650 mg/L and 1800 mg/L, respectively. After 42 days, the  $\text{NH}_4^+\text{-N}$  concentrations in leachates in Reactors B and C decreased, with Reactor B exhibiting a greater rate of  $\text{NH}_4^+\text{-N}$  decrease. On day 144, both reactors gave an identical  $\text{NH}_4^+\text{-N}$  concentration of 1600 mg/L. In System 2,  $\text{NH}_4^+\text{-N}$  was removed from the leachate by adsorption in Reactor C. In this system, the initial efficiency of ammonium removal was high and subsequently decreased gradually. Once the absorption capacity of  $\text{NH}_4^+\text{-N}$  in degraded waste reached saturation, the removal efficiency of System 2 decreased to approximately 0.5% on day 96 and remained around 0% in later stages. Obviously, the removal efficiencies of both COD and  $\text{NH}_4^+\text{-N}$  decreased over a certain period, with the  $\text{NH}_4^+\text{-N}$  removal efficiency declining more rapidly compared to the COD removal efficiency (Fig. 3). In biological treatment systems, microorganisms compete for available COD and  $\text{NH}_4^+\text{-N}$  as energy sources. If there is an excess of COD or other easily degradable organic matter, microorganisms may prioritize the utilization of COD over  $\text{NH}_4^+\text{-N}$  (Wang *et al.*, 2020).

#### pH

Variation in pH levels of anaerobic leachate in all reactors is illustrated in Fig. 5. In Reactor A, the pH of the leachate increased marginally throughout

recirculation. Following recirculation, the pH in Reactor A rose from 5.9 on day 6 to 7.2 on day 144. These results indicated a tendency for pH to increase after leachate recirculation, which could be attributed to the stimulation of hydrolytic and fermentative bacteria. Hydrolytic and fermentative bacteria breakdown complex organic compounds into simpler forms through hydrolysis and fermentation as a part of recirculation process. The breakdown of organic compounds results in the release of different byproducts, such as VFAs and organic acids (Ratti *et al.*, 2013). The accumulation of VFAs and organic acids may decrease the pH of the leachate. The accumulation of VFAs and similar compounds in high-temperature reactors has been attributed to their anaerobic degradation in syntrophic reactions. Syntrophic bacteria play a vital role in anaerobic digestion by promoting the conversion of VFAs into  $\text{CH}_4$ . The bacteria and methanogens form a symbiotic relationship in the final step of  $\text{CH}_4$  production (Li *et al.*, 2012). Syntrophic bacteria consume the VFAs produced by fermentative bacteria, thereby producing hydrogen and carbon dioxide as byproducts. Methanogens use these byproducts to produce  $\text{CH}_4$ . Additionally, sulfate-reducing and homoacetogenic bacteria consume VFAs and organic acids, resulting in the production of hydrogen sulfide

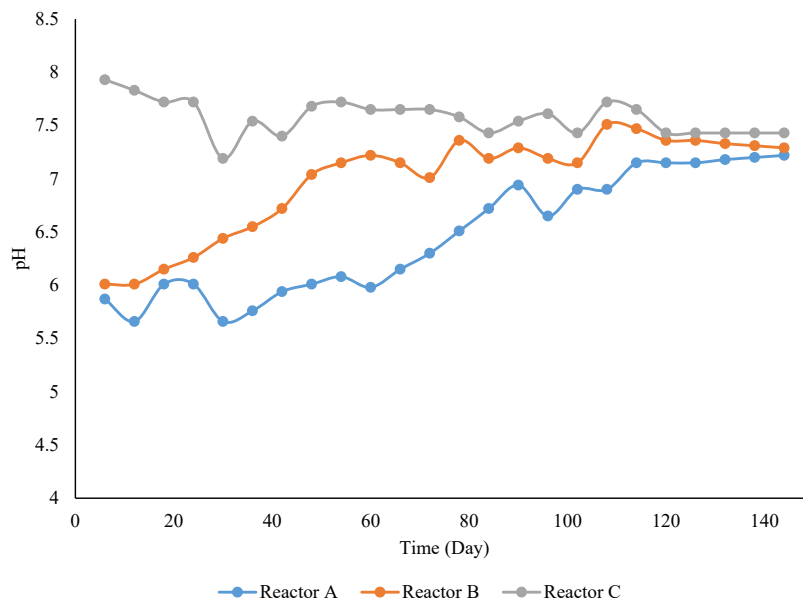


Fig. 5: Changes in the leachate pH over time in the bioreactors

and acetate, respectively (Singh *et al.*, 2021). Acetate, as a compound to other organisms, can be valuable, or it may be converted into  $\text{CH}_4$  by methanogens in later steps of anaerobic digestion. This process leads to a decrease in the concentration of VFAs and organic acids and an increase in pH in the leachate. In Reactor B, the pH of the leachate increased from 6 to 7 during the first 48 days of recirculation and then continued to rise to over 7 from day 48 to day 144 (Fig. 5). The highest pH value in this reactor was recorded on day 108 reaching 7.5. Throughout the operation, the pH of leachate in Reactor C remained above 7 as a result of the presence of degraded waste in this reactor. The maximum and minimum pH values for leachate in Reactor C were 8 and 7.2, respectively. In Reactor B, fermentation and bacterial processes acting on biodegradable compounds produced and accumulated acids (Ratti *et al.*, 2013). Methanogenic bacteria in Reactor C converted the acids accumulated in Reactor B into  $\text{CH}_4$  and carbon dioxide. As a result, the leachate pH in the Reactor B was found to be lower compared to the pH of the effluent leachate from Reactor C. Therefore, the pH value of the effluent leachate from Reactor C decreased over time as leachate was recirculated from Reactor B to Reactor C. However, the pH variation, occurring after 114 days, was minimal during the stable phase. The stable

phase of leachate recirculation is characterized by pH stabilization, which results from the development of a balanced microbial community and stable metabolic processes (Talalaj, 2015). In Reactor B, pH balance resulted from the steady-state consumption of acids by the methanogenic bacteria in Reactor C. The decomposition of solid waste undergoes three distinct phases within the lab-scale landfills (Reactors A and B). Initially, complex organic matter undergoes hydrolysis, resulting in the formation of soluble molecules. During the next stage, these molecules are further transformed into carbon dioxide, hydrogen, simple organic compounds, and VFAs. The third stage involves the production of  $\text{CH}_4$  through the decomposition of acids into  $\text{CH}_4$  and  $\text{CO}_2$ , or the reduction of  $\text{CO}_2$  with  $\text{H}_2$ . In this study, Reactor C balanced the growth of the acid-production and  $\text{CH}_4$ -production phases, accelerating the decomposition of organic matter in System 2. Based on Fig. 5, the recirculation of leachate from degraded MSW to fresh MSW resulted in a notable increase in pH values in Reactor B compared to Reactor A. Consequently, a faster degradation of MSW in System 2 was expected. These findings were consistent with the results of other studies (Luo and Wong, 2019). The characteristics of the leachate effluent from Reactors A and B before and after completion of treatment are

Table 2: Characteristics of the leachate from Reactors A and B

Parameter	Initial leachate		Treated leachate	
	Reactor A and B		Reactor A	Reactor B
COD (mg/L)	31525		79620	6410
NH <sub>4</sub> <sup>+</sup> -N (mg/L)	772		2768	1530
pH	6		7.22	7.29
BOD (mg/L)	16850		30255	580

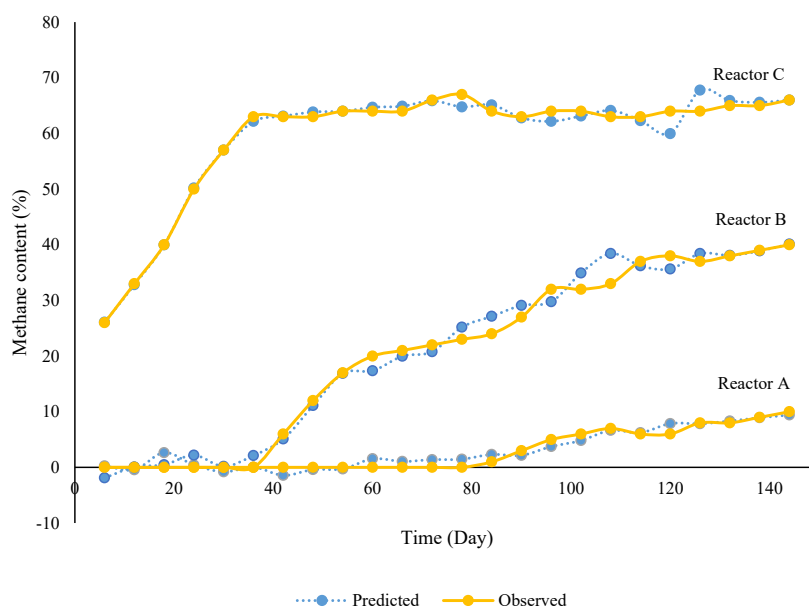


Fig. 6: Methane content observed and predicted over time in the bioreactors

presented in Table 2.

#### *CH<sub>4</sub> content and cumulative CH<sub>4</sub> production*

Figs. 6 and 7 illustrate the results for CH<sub>4</sub> content in the biogas and cumulative CH<sub>4</sub> production from Reactors A, B, and C. Fig. 6 shows that the type of recirculation method and the age of waste are involved in the CH<sub>4</sub> gas concentration variations. The CH<sub>4</sub> content in Reactor A was below 10% during the whole experiment. The CH<sub>4</sub> content in biogas from System 2 indicated the stability and performance of anaerobic digestion. The CH<sub>4</sub> content in reactor B showed a rapid increase after 36 days of digestion and reached 48% on day 144. The CH<sub>4</sub> concentration in the biogas from reactor C showed a significant increase from 26% to 63% between day 6 and day 36 and then remained stable (Fig. 6). Cumulative CH<sub>4</sub> production in fresh waste in reactor B reached 26.8 L/kg dry weight, which was 4.31 times higher

than those in Reactor A (6.21 L/kg dry weight) (Fig. 7). These findings were consistent with the results reported in previous studies (Behera *et al.*, 2015; Gao *et al.*, 2023). According to Figs. 2, 5, and 6, on day 36, reactor B entered the methanogenesis phase, indicated by the increase of CH<sub>4</sub> content and leachate pH and decrease of leachate COD concentrations. Reactor B reached this stage 48 days earlier as compared to Reactor A. The performances of reactors A and B indicated that the addition of leachate from degraded waste decreased the startup time and enhanced the biogas production from fresh waste. Recirculation of the leachate in fresh waste triggers accelerated hydrolysis and acidification, leading to the accumulation and inhibition of intermediates (Gao *et al.*, 2023). When the leachate is recirculated back into fresh waste, it introduces additional moisture and soluble compounds, providing optimal conditions for microbial activity. It also enhances the

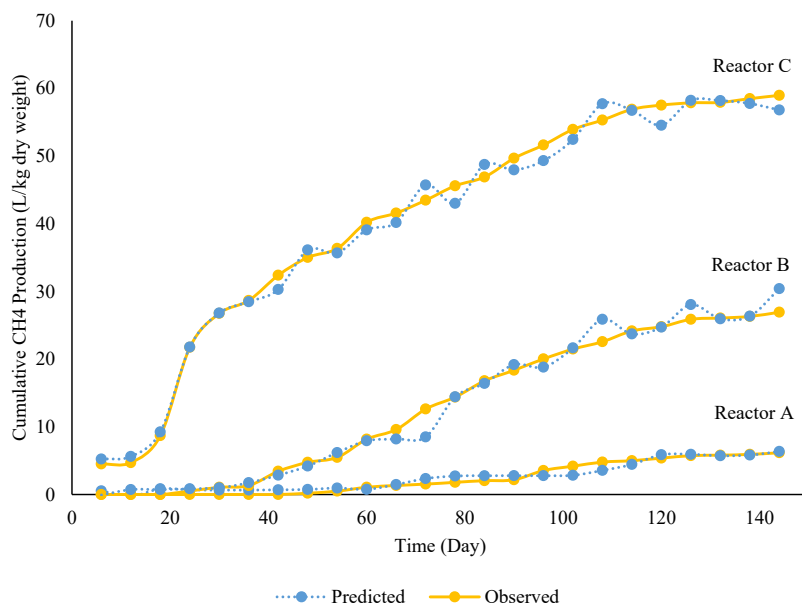


Fig. 7: Cumulative methane production observed and predicted over time in the bioreactors

availability of water and nutrients, promoting the growth and activity of hydrolytic microorganisms.

The stabilization phase in reactor C, as indicated by stable concentration of COD (Fig. 2), was attained prior to the commencement of leachate recirculation. Subsequently, a considerable increase in  $\text{CH}_4$  production following the initiation of recirculation indicated the ability of methanogens to effectively utilize organic acids from the fresh waste leachate, even when the waste decomposition had already reached the stabilization phase. Confirmation of this ability of methanogens has been established in previous studies (Yang *et al.*, 2021). Methanogens utilized these organic acids as a carbon source for their metabolism, converting them into  $\text{CH}_4$  gas. Consequently, the consumption of organic acids by methanogens reduced the concentration of organic acids in reactor B and increased the carbon source in reactor C, enhancing  $\text{CH}_4$  production in both reactors. As a result of this process, reactor C showed a notable increase in cumulative  $\text{CH}_4$  production, with the volume significantly rising from day 24 onwards. By day 144, the cumulative  $\text{CH}_4$  production reached 59 L/kg dry weight, indicating a substantial enhancement in  $\text{CH}_4$  production within the system. The maximum daily  $\text{CH}_4$  production in Reactor C occurred from day 18 to day 24 of the experiment, reaching 2.09 L/day/

kg dry weight (Fig. 7). These findings were consistent with the results reported in previous studies. In a study conducted by Sandip *et al.* (2012), the cumulative  $\text{CH}_4$  production on day 270 of the experiment was 67 L/kg dry weight, with a maximum daily  $\text{CH}_4$  production of 1.68 L/day/kg dry weight. Another study reported a cumulative  $\text{CH}_4$  production of 50 L/kg dry weight on day 250 for degraded MSW (Sanphoti *et al.*, 2006). In a study by Ahmadifar *et al.* (2016), the cumulative  $\text{CH}_4$  production for degraded MSW was recorded as 54.87 L/kg dry weight on day 180, with a maximum daily  $\text{CH}_4$  production of 1.35 L/day/kg dry on day 112. Methanogenic bacteria in a bioreactor containing degraded waste need time to adjust to a new organic load when fresh waste is introduced. Consequently, the initiation of methane production in such reactors can be protracted (Ahmadifar *et al.*, 2016). Starting from day 36 (Fig. 2), COD concentration in reactor B exhibited a simultaneous decrease with the increase of  $\text{CH}_4$  production in reactors B and C. This decline could be attributed to the carbon consumption by the methanogenic bacteria existing in reactor C. It has been established that an  $\text{NH}_4^+\text{-N}$  concentration of over 2500 mg/L is toxic to methanogenesis, regardless of temperature and pH levels (Feng *et al.*, 2019; Liu and Sung, 2002). In this study, a comparison was made between  $\text{NH}_4^+\text{-N}$  concentration (Fig. 4) and

CH<sub>4</sub> yields, revealing that NH<sub>4</sub><sup>+</sup>-N played a crucial role in determining the initiation time of CH<sub>4</sub> production. Based on the analysis on day 36 (Figs. 4 and 6), a significant increase in the CH<sub>4</sub> content was observed in reactor B. This increase occurred simultaneously with a decrease in NH<sub>4</sub><sup>+</sup>-N concentration.

#### ANN modelling

To perform comprehensive analysis, the modeling samples were randomly selected from different stages of the experiment and included in training, validation, and testing sets. The data used for testing the ANN are presented in Table 3.

The optimal network architecture was determined based on statistical criteria, MSE, and correlation coefficient (R). According to Table 4 in ANN1 and ANN2, as the number of neurons exceeded 4 and 6 respectively, MSE of the training data decreased, but MSE of the test data increased. Increase of the number of neurons in ANN improved the fitting of the training data, potentially decreasing the MSE of the training data. However, it was likely that very high number of neurons could cause the ANN to overfit the training data, leading to an elevated MSE for the test data (McElroy *et al.*, 2021). This increase in MSE for the test data indicated that the ANN was not generalizing effectively and could not preserve the patterns and relationships in the data.

For accurate prediction of CH<sub>4</sub> content, the optimal configuration for ANN1 included one hidden layer with 4 neurons. The best setup for ANN2 to precisely forecast the cumulative CH<sub>4</sub> production entailed one hidden layer containing 6 neurons. Both ANNs utilized the Tan-Sigmoid activation function for the hidden layer and the Pure-linear activation function for the output layer. Utilization of the datasets obtained from MATLAB neural network learning for this analysis, and

the results of ANN1 and ANN2 training performances are shown in Fig. 8a and 8b, respectively. By representing the experimental data (target value) and the predicted results (output) in plot form, the regression results demonstrated the relationship between them. Fig. 9a and 9b show the regression results of the significant correlation coefficient for CH<sub>4</sub> content and cumulative CH<sub>4</sub> production in the training, validation, and testing data.

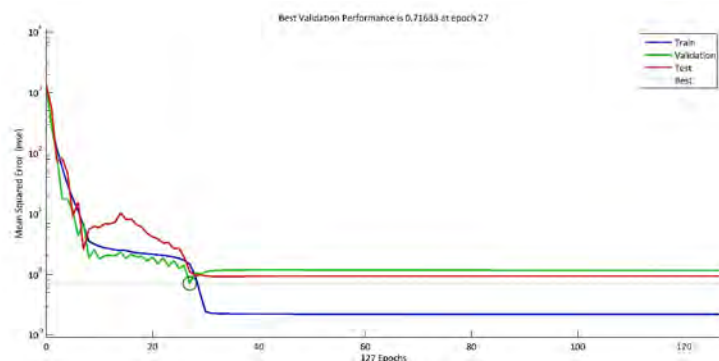
The ANN1 and ANN2 models exhibited exceptional performances during the validation, leading to the best validation performances of 0.716 and 0.634, respectively (Fig. 8). This indicated the models' ability to accurately predict the CH<sub>4</sub> content and cumulative CH<sub>4</sub> production based on the input parameters. The training determination coefficients of 0.9990 for ANN1 and 0.9995 for ANN2 further confirmed the successful learning of the relationship between input and output variables by the ANNs. In addition, the validation R-values of 0.9997 for ANN1 and 0.9981 for ANN2 indicated the strong generalization ability of the models. The overall performance of the dataset showed high R-values of 0.9991 and 0.9975 for ANN1 and ANN2 respectively, suggesting a thorough comprehension of the complex biological process in the system (Fig. 9). The strong correlation in among the test data indicated the model's capacity to understand the complex modeling process. Modeling biological systems is inherently more challenging than physical or chemical processes due to the involvement of living microorganisms and their complex characteristics and responses to changing conditions (Nair *et al.*, 2016). The high R-value obtained for the test data indicated an optimized selection of effective parameters in the input data. ANNs are mathematical models that learn patterns and relationships from data. However, they do not possess an inherent

Table 3: Input data for testing the ANN model

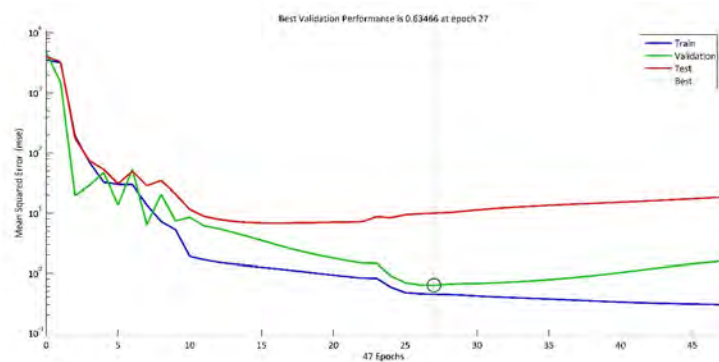
Reactor	HRT (Day)	COD(mg/L)	NH <sub>4</sub> <sup>+</sup> -N (mg/L)	pH
A	6	34710	790	5.87
	60	91320	2467	5.98
	132	79620	2580	7.22
B	12	54710	1064	6.01
	84	22640	1645	7.19
	114	10180	1371	7.47
	126	7160	1500	7.36
C	6	3010	0	7.93
	72	2640	1612	7.65
	126	1880	1467	7.43

Table 4: MSE values for ANNs with different numbers of neurons in the hidden layer

Number of neurons	CH <sub>4</sub> content		Cumulative CH <sub>4</sub> production	
	Train	Test	Train	Test
3	2.13	9.86	76.24	95.62
4	0.74	0.72	15.75	38.67
5	0.71	3.59	2.61	11.65
6	0.68	9.17	0.52	0.63
7	0.53	23.63	0.48	6.85
8	0.31	22.25	0.41	19.42



(a)

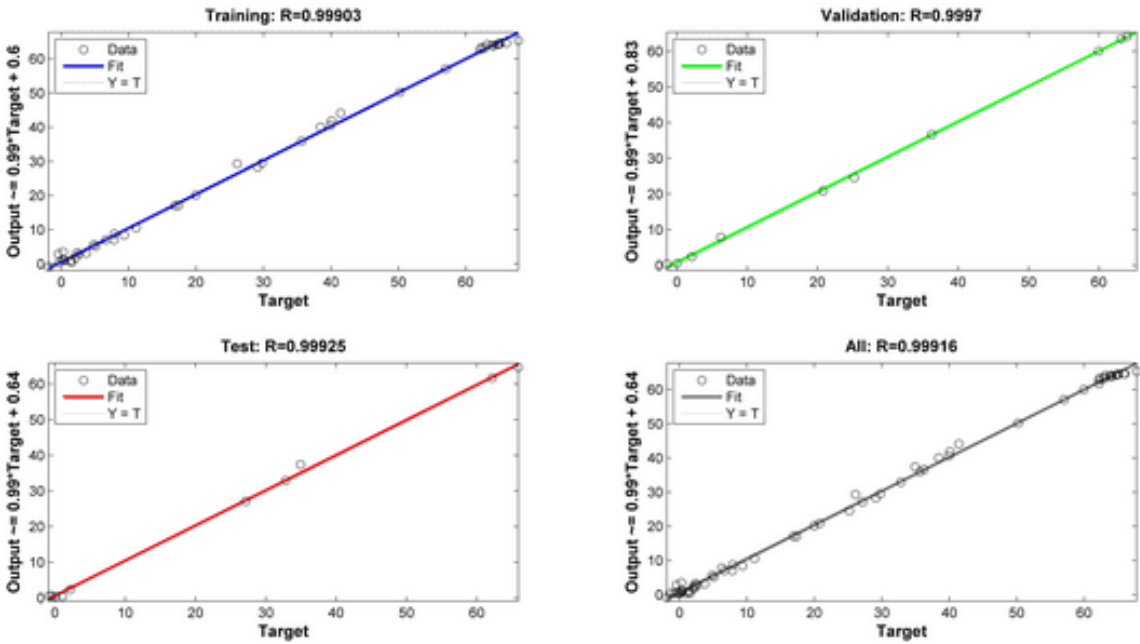


(b)

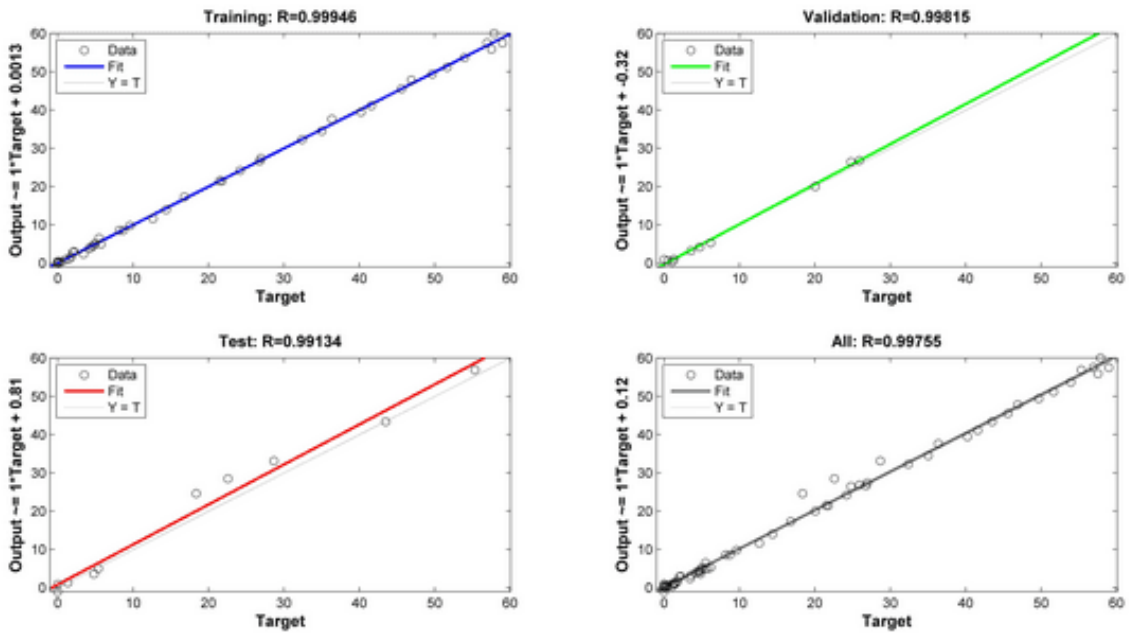
Fig. 8: MSE variation with Epochs during the training process of (a) ANN1, and (b) ANN2

understanding of the modeled process. For effective learning and predicting, ANNs depend on accurately selected and represented inputs (Hatata *et al.*, 2021). In a study, pH, moisture content, total volatile solids, VFAs, and HRT values were included as the input data for ANN (Nair *et al.*, 2016). In the current study, the analysis of test data revealed a notably higher R-value surpassing the R-value reported by Nair *et al.* (2016). This finding provided a compelling evidence for the advanced proficiency of the developed ANN in understanding the complexities of the biological

processes. As discussed earlier, biological factors that affect biogas production could significantly impact the concentration of COD and NH<sub>4</sub><sup>+</sup>-N. In the present study, these parameters along with pH and HRT were included in the input data. This approach effectively improved the comprehension of the biological process by the ANN. The performance of ANN in predicting CH<sub>4</sub> production was compared with other methods (Table 5). The ANN demonstrated a better performance compared to other methods for predicting CH<sub>4</sub> production (Table 5). However, it is



(a)



(b)

Fig. 9: Comparison of the observed and predicted (a) CH<sub>4</sub> content, and (b) cumulative CH<sub>4</sub> production for training, validation, and testing sets

Table 5: Comparison of the CH<sub>4</sub> production prediction models

Feedstock	Reactor type	Input parameters	Method	R-value	MSE	References
MSW	Landfill	Total waste landfilled, organic content, temperature, precipitation, landfill age, depth, and landfill cover	Fuzzy	0.951	71.31	Mohsen and Abbassi, 2020
			LandGEM	0.804	96.75	
MSW	Anaerobic bioreactor landfill	Amount of leachate, temperature, methane content, pH, COD	Neuro-fuzzy	0.71	3.62	Mehrdad et al., 2021
			Support vector machine	0.90	3.37	
Sewage sludge	Anaerobic digester reactor	Sludge inflow, temperature, pH, total solid, volatile solid, organic acid, alkalinity, HRT, and organic loading rate (OLR)	ANN	0.98	3.21	Bao et al., 2023
			Multiple linear regression	0.722	11.03	
Molasses wastewater	Pilot-scale upflow anaerobic sludge blanket	OLR, COD removal rate, influent and effluent alkalinity, and pH	Fuzzy-logic	0.8721	8.15	Turkdogan-Aydinol and Yetilmezsoy, 2010
			ANN	0.9847	4.86	
Palm oil mill effluent	Anaerobic digester reactor	Recirculation ratio, pH and temperature	Response surface methodology	0.9512	0.51	Chong et al., 2023
			ANN	0.977	0.23	
			ANFIS	0.976	0.23	
High polluted wastewater	Anaerobic reactor	Reactor fill ratio, OLR, influent and effluent pH, alkalinity, COD, suspended solids	Nonlinear regression	0.9852	18.22	Tufaner and Demirci, 2020
			ANN	0.9878	14.74	
MSW	Anaerobic bioreactor landfill	COD, HRT, NH <sub>4</sub> <sup>+</sup> -N, pH	ANN	0.998	0.634	The current study

worth noting that there was no significant difference between the ANN and the adaptive neuro-fuzzy inference system (ANFIS) in terms of performance. The results presented in Table 5 also demonstrated that the achieved prediction quality was superior to the prediction quality reported in recent studies focusing on biogas production modeling.

The impact of removing specific input variables on the performance of ANN was investigated for their combined effect on cumulative CH<sub>4</sub> production. Eliminating the pH parameter resulted in a lower R-value (0.8801) and a higher MSE (21.79) compared to ANN2 in the test and validation data, respectively. Exclusion of the COD concentration led to a lower R-value (0.751) and higher MSE (44.52). Similarly, removing the HRT parameter resulted in a R-value of 0.7731 and a MSE of 29.73. Moreover, exclusion of the NH<sub>4</sub><sup>+</sup>-N concentration yielded a R-value of 0.835 and a MSE of 23.39. The results suggested that the combined influence of the selected parameters could affect cumulative CH<sub>4</sub> production. According to the results obtained from MSE and R-values in

the test and validation data, it could be inferred that the COD concentration had the highest influence on cumulative CH<sub>4</sub> production. Conversely, the pH level was found to have the lowest impact on cumulative CH<sub>4</sub> production among the studied parameters. The weights of the ANN were employed to estimate the relative importance of the operational parameters on cumulative CH<sub>4</sub> production. The results showed that COD and HRT had a stronger influence, with relative importance values of 39.03 and 28.34, respectively. NH<sub>4</sub><sup>+</sup>-N and pH had relative importance values of 18.54 and 14.09, respectively. After successful development of a reliable and high-performing ANN model, the trained ANN was employed to optimize the process conditions with the aim of maximizing cumulative CH<sub>4</sub> production. Utilizing the trained ANN as a fitness function, a genetic algorithm (GA) was implemented for this purpose. For each GA iteration, the ANN model assessed methane production, yielding a fitness value. The GA was executed for 200 iterations with a population size of 25 individuals. During each generation, the individuals producing

the highest methane estimates, as determined by the ANN, underwent reproduction, mutation, and crossover to form the subsequent generation. The optimized values for HRT, COD,  $\text{NH}_4^+\text{-N}$ , and pH were determined as 81 days, 12680 mg/L, 1712 mg/L, and 7.28, respectively. The maximum cumulative  $\text{CH}_4$  production under these optimum parameters was found to be 61.94 L/kg dry weight.

#### *Assessing the generalizability of the ANN*

If all the influential parameters were selected and the ANN was properly trained, the ANN would have a potential to accurately predict outputs under different conditions. In this study, the input data for the ANN consisted of COD and  $\text{NH}_4^+\text{-N}$  concentration, pH value, and HRT. These parameters were selected based on their known influence on the biogas production process. By incorporating these input data, the ANN was able to effectively capture and accommodate the influence of variations in biological processes on the output. The hypothesis was that any variation in the biological characteristics of the waste, the waste quality parameters (such as carbon, nitrogen, moisture, sulfur, etc.), laboratory conditions (temperature, volume, number of reactors, etc.), and recirculation rate might not have a substantial impact on accuracy of the ANN in forecasting the output. Since these variations affected the input data, the ANN accounted for their effects on the output. In this section, the data from four additional studies were utilized as inputs to the ANN. These studies were selected to provide a diverse range of conditions and inputs in order to ensure the robustness of the ANN model. In the first study, three types of bioreactors containing MSW had been employed. One of these bioreactors operated without leachate recirculation, while the others (remaining two bioreactors) had leachate recirculation systems. The leachate recirculation rate in one of the reactors was 9 liters per day (L/day), while the other reactor had a recirculation rate of 21 L/day (Sponza and Ağdağ, 2004). The simulation results obtained using ANN1 demonstrated significant effectiveness in predicting the performance of the bioreactors. By incorporating the data from the study conducted by Sponza and Ağdağ (2004) into the input data of ANN1, the R-value and MSE for the experimental data and the predicted data were determined to be 0.88 and 5.35, respectively. In the second study, the biological

degradation of MSW had been investigated in both anaerobic and hybrid bioreactors (Xu *et al.*, 2015). To assess the generalization ability of ANN1, only the anaerobic bioreactor data were employed. By incorporating the data from the study conducted by Xu *et al.* (2015) into the ANN1, the values of MSE and R-value for the observed and predicted data were determined as 9.06 and 0.83, respectively. Despite the reduction of the R-value in these two studies, it should be considered that any R-value exceeding 0.8 was widely accepted as suitable for modeling the biological processes (Bao *et al.*, 2023; Turkdogan-Aydinol and Yetilmezsoy, 2010). By comparing these results with those presented in Table 5 and taking into account that the data utilized at this stage were completely unseen by the ANN, the performance of the ANN could be deemed appropriate. Additionally, it was important to consider other statistical indices, such as MSE, in conjunction with the R-value (Rahman *et al.*, 2022). Considering the predicted data range, with the highest value of 70 and the lowest value of 0, a MSE of 9.06 represented an acceptable level of accuracy. In the third and fourth studies, the MSW had undergone mechanical treatment followed by biological treatment (Di Addario and Ruggeri, 2018; Sormunen *et al.*, 2008). The primary objective of the mechanical treatment of MSW was to separate different components such as organic materials for recycling and metals for reuse, and prepare the remaining waste for subsequent treatment. This process involved sieving and sorting methods, resulting in smaller particle sizes in the residual waste. It should be noted that when the smaller particles are landfilled, the initial degradation phase may be impacted and the leaching of organic materials and nitrogen from waste may be increased (Di Addario and Ruggeri, 2018). The mechanical properties of waste, including porosity, hydraulic conductivity, particle sizes, and surface areas, play a crucial role in anaerobic decomposition. The hydraulic conductivity of waste can directly affect the availability of water for microbial activity, which is essential for the growth and metabolism of methanogenic bacteria. Additionally, smaller particle sizes and larger surface areas provide more contact sites for microbial colonization and enhance the breakdown of organic compounds, leading to an increased methane production (Johnravindar *et al.*, 2021). Reducing the porosity of MSW can improve mass transfer and

increase the rate of CH<sub>4</sub> production (Ko *et al.*, 2015). It is important to note that the ANN trained in this study did not consider the input parameters related to the mechanical characteristics of the waste, such as porosity, particle size, and hydraulic conductivity. Consequently, ANN1 did not consider the potential impact of these variables on the prediction of cumulative CH<sub>4</sub> production from the waste. Therefore, the performance of ANN1 in accurately predicting the CH<sub>4</sub> content was significantly reduced for the data from the latter two studies. In the study conducted by Di Addario and Ruggeri (2018), the R-value and MSE of ANN1 were determined as 0.28 and 186, respectively. Similarly, in the study done by Sormunen *et al.* (2008) the R-value and MSE of ANN1 were found to be 0.39 and 137, respectively.

## CONCLUSION

This study demonstrated that the recirculation of leachate between fresh and degraded waste led to a substantial improvement in COD reduction in System 2. Acetogenic bacteria in Reactor C contributed to a notable reduction in COD concentration. The COD removal efficiency in System 2 fluctuated between 65% and 90%. NH<sub>4</sub><sup>+</sup>-N concentrations in Reactors B and C initially increased to maximum levels of 2650 mg/L and 1800 mg/L, respectively. However, after day 42, the concentrations started to decrease. By day 144, both reactors reached the same NH<sub>4</sub><sup>+</sup>-N concentration of 1600 mg/L. The decrease in NH<sub>4</sub><sup>+</sup>-N was mainly due to the adsorption of degraded waste and assimilation by anaerobic bacteria. Throughout the experiment, reactor A had a CH<sub>4</sub> content of below 10%, while reactors B and C showed significant increases. Reactor B reached 48% CH<sub>4</sub> content on day 144, with its cumulative CH<sub>4</sub> production being 4.31 times higher compared to reactor A. Leachate recirculation in Reactor B accelerated the startup time, enhancing biogas production. Reactor C exhibited a notable CH<sub>4</sub> production reaching 59 L/kg dry weight by day 144. The performance of the ANN models during the validation was exceptional, with validation performances of 0.716 and 0.634 achieved for ANN1 and ANN2, respectively. The high R value obtained for the test data demonstrated the model's capacity to understand the complex modeling process, despite the inherent challenges in biological systems modeling. The accuracy of ANN1 prediction was evaluated under different experimental conditions. The data

from two previous studies supported its effectiveness and significant accuracy in predicting the bioreactor performance. However, ANN1 did not account for variations in mechanical characteristics of waste, impacting its ability to accurately predict cumulative CH<sub>4</sub> production. Specifically, the ANN performance in predicting the CH<sub>4</sub> content for the two studies, which involved mechanical treatment and smaller particle sizes in the waste, showed a significant decline.

## ACKNOWLEDGEMENT

This study was conducted with the support of the University of Birjand, Birjand, Iran. The authors would like to acknowledge the authorities of the University of Birjand for their valuable support and contribution to this study.

## CONFLICT OF INTEREST

The author declares that there is no conflict of interests regarding the publication of this manuscript. In addition, the ethical issues, including plagiarism, informed consent, misconduct, data fabrication and/or falsification, double publication and/or submission, and redundancy have been completely observed by the authors.

## OPEN ACCESS

©2024 The author(s). This article is licensed under a Creative Commons Attribution 4.0 International License, which permits use, sharing, adaptation, distribution and reproduction in any medium or format, as long as you give appropriate credit to the original author(s) and the source, provide a link to the Creative Commons license, and indicate if changes were made. The images or other third-party material in this article are included in the article's Creative Commons license, unless indicated otherwise in a credit line to the material. If material is not included in the article's Creative Commons license and your intended use is not permitted by statutory regulation or exceeds the permitted use, you will need to obtain permission directly from the copyright holder. To view a copy of this license, visit: <http://creativecommons.org/licenses/by/4.0/>

## PUBLISHER'S NOTE

GJESM Publisher remains neutral with regard to jurisdictional claims in published maps and institutional affiliations.

## ABBREVIATIONS

%	Percent
ANFIS	Adaptive Neuro-Fuzzy Inference System
ANN	Artificial Neural Network
ANN1	First type of artificial neural network
ANN2	Second type of artificial neural network
BOD <sub>5</sub>	Biochemical Oxygen Demand
C	Carbon
CH <sub>4</sub>	Methane
cm	Centimeter
cm <sup>2</sup>	Square centimeter
CO <sub>2</sub>	Carbon Dioxide
COD	Chemical Oxygen Demand
GA	Genetic Algorithm
H	Hydrogen
H <sub>2</sub> SO <sub>4</sub>	Sulfuric Acid
HRT	Hydraulic Retention Time
kg	Kilogram
L	Liter
L/day	Liter per Day
L/kg	Liter per Kilogram
LMFFBP	Levenberg Marquardt Feed-Forward Back Propagation Perceptron
m	Meter
m <sup>2</sup>	Meter square
MATLAB	Matrix Laboratory
mg/L	Milligram per Liter
MSE	Mean Squared Error
MSW	Municipal Solid Waste
N	Nitrogen
NH <sub>4</sub> <sup>+</sup> -N	Ammonium-Nitrogen
O	Oxygen
OLR	Organic Loading Rate
S	Sulfur
TCD	Thermal Conductivity Detector
v/v	Volume per Volume
VFA	Volatile Fatty Acid

## REFERENCES

- Ahn, W.Y.; Kang, M.S.; Yim, S.K.; Choi, K.H., (2002). Advanced landfill leachate treatment using an integrated membrane process. *Desalination*, 149(1-3): 109-114 (6 pages).
- Ahmadifar, M.; Sartaj, M.; Abdallah, M., (2016). Investigating the performance of aerobic, semi-aerobic, and anaerobic bioreactor landfills for MSW management in developing countries. *J. Mater. Cycles Waste Manage.*, 18: 703-714 (12 pages).
- Al-Dailami, A.; Ahmad, I.; Kamyab, H.; Abdullah, N.; Koji, I.; Ashokkumar, V.; Zabara, B., (2022). Sustainable solid waste management in Yemen: environmental, social aspects, and challenges. *Biomass Convers. Biorefin.*, 10: 1-27 (27 pages).
- Alabi, O.A.; Ologbonjaye, K.I.; Awosolu, O.; Alalade, O.E., (2019). Public and environmental health effects of plastic wastes disposal: a review. *J. Toxicol. Risk Assess.*, 5(021): 1-13 (13 pages).
- Bah, A.; Chen, Z.; Bah, A.; Qian, Q.; Tuan, P.D.; Feng, D., (2023). Systematic literature review of solar-powered landfill leachate sanitation: Challenges and research directions over the past decade. *J. Environ. Manage.*, 326(Pt B): 116751 (11 pages).
- Bao, Y.; Koutavarapu, R.; Lee, T.G., (2023). Derivation of optimal operation factors of anaerobic digesters through artificial neural network technology. *Systems*, 11(7): 375-384 (10 pages).
- Behera, S.K.; Meher, S.K.; Park, H.-S., (2015). Artificial neural network model for predicting methane percentage in biogas recovered from a landfill upon injection of liquid organic waste. *Clean Technol. Environ. Policy*, 17: 443-453 (11 pages).
- Bove, D.; Merello, S.; Frumento, D.; Arni, S.A.; Aliakbarian, B.; Converti, A., (2015). A critical review of biological processes and technologies for landfill leachate treatment. *Chem. Eng. Technol.*, 38(12): 2115-2126 (12 pages).
- Cabaneros, S.M.; Calautit, J.K.; Hughes, B.R., (2019). A review of artificial neural network models for ambient air pollution prediction. *Environ. Model. Software*, 119: 285-304 (20 pages).
- Chong, D.J.S.; Chan, Y.J.; Arumugasamy, S.K.; Yazdi, S.K.; Lim, J.W., (2023). Optimisation and performance evaluation of response surface methodology (RSM), artificial neural network (ANN) and adaptive neuro-fuzzy inference system (ANFIS) in the prediction of biogas production from palm oil mill effluent (POME). *Energy*, 266: 126449 (12 pages).
- Čosić, I.; Vuković, M.; Gomzi, Z.; Briški, F., (2013). Modelling of kinetics of microbial degradation of simulated leachate from tobacco dust waste. *Chem. Pap.*, 67(9): 1138-1145 (8 pages).
- Desai, K.M.; Survase, S.A.; Saudagar, P.S.; Lele, S.; Singhal, R.S., (2018). Comparison of artificial neural network (ANN) and response surface methodology (RSM) in fermentation media optimization: case study of fermentative production of scleroglucan. *Biochem. Eng. J.*, 41(3): 266-273 (8 pages).
- Di Addario, M.; Ruggeri, B., (2018). Experimental simulation and fuzzy modelling of landfill biogas production from low-biodegradable MBT waste under leachate recirculation. *Environ. Technol.*, 39(20): 2568-2582 (15 pages).
- El-Rawy, M.; Abd-Ellah, M.K.; Fathi, H.; Ahmed, A.K.A., (2021). Forecasting effluent and performance of wastewater treatment plant using different machine learning techniques. *J. Water Process Eng.*, 44: 102380 (10 pages).

- Feng, S.; Hong, X.; Wang, T.; Huang, X.; Tong, Y.; Yang, H., (2019). Reutilization of high COD leachate via recirculation strategy for methane production in anaerobic digestion of municipal solid waste: Performance and dynamic of methanogen community. *Bioresour. Technol.*, 288: 121509 **(9 pages)**.
- Gao, X.; Li, Z.; Zhang, K.; Kong, D.; Gao, W.; Liang, J.; Liu, F.; Du, L., (2023). Layer inoculation as a new technology to resist volatile fatty acid inhibition during solid-state anaerobic digestion: Methane Yield Performance and Microbial Responses. *Ferment.*, 9(6): 535 **(14 pages)**.
- Govahi, S.; Karimi-Jashni, A.; Derakhshan, M., (2012). Treatability of landfill leachate by combined upflow anaerobic sludge blanket reactor and aerated lagoon. *Int. J. Environ. Sci. Technol.*, 9: 145-151 **(7 pages)**.
- Guo, Z.; Zhang, Y.; Jia, H.; Guo, J.; Meng, X.; Wang, J., (2022). Electrochemical methods for landfill leachate treatment: A review on electrocoagulation and electrooxidation. *Sci. Total Environ.*, 806(Pt 2): 1505-1529 **(25 pages)**.
- Guvenc, S.Y.; Dincer, K.; Varank, G., (2019). Performance of electrocoagulation and electro-Fenton processes for treatment of nanofiltration concentrate of biologically stabilized landfill leachate. *J. Water Process Eng.*, 31: 100863 **(15 pages)**.
- Hatata, A.; Galal, O.H.; Said, N.; Ahmed, D., (2021). Prediction of biogas production from anaerobic co-digestion of waste activated sludge and wheat straw using two-dimensional mathematical models and an artificial neural network. *Renewable Energy*, 178: 226-240 **(15 pages)**.
- Haydar, M.M.; Khire, M.V., (2005). Leachate recirculation using horizontal trenches in bioreactor landfills. *J. Geotech. Geoenviron. Eng.*, 131(7): 837-847 **(11 pages)**.
- Hussein, O.A.; Ibrahim, J.A. A., (2023). Leachates Recirculation Impact on the Stabilization of the Solid Wastes-A Review. *J. Eco. Eng.*, 24(4): 103816 **(11 pages)**.
- Johnravindar, D.; Patria, R.D.; Lee, J.T.; Zhang, L.; Tong, Y.W.; Wang, C.-H.; Ok, Y.S.; Kaur, G., (2021). Syntrophic interactions in anaerobic digestion: how biochar properties affect them? *Sustainable Environ.*, 7(1): 1945282 **(14 pages)**.
- Karamichailidou, D.; Alexandridis, A.; Anagnostopoulos, G.; Syriopoulos, G.; Sekkas, O., (2022). Modeling biogas production from anaerobic wastewater treatment plants using radial basis function networks and differential evolution. *Comput. Chem. Eng.*, 157: 107629 **(11 pages)**.
- Kerdan, I.G.; Gálvez, D.M., (2020). Artificial neural network structure optimisation for accurately prediction of exergy, comfort and life cycle cost performance of a low energy building. *Appl. Energy*, 280: 115862 **(10 pages)**.
- Keyikoglu, R.; Karatas, O.; Rezanian, H.; Kobya, M.; Vatanpour, V.; Khataee, A., (2021). A review on treatment of membrane concentrates generated from landfill leachate treatment processes. *Sep. Purif. Technol.*, 259: 118182 **(16 pages)**.
- Ko, J.H.; Li, M.; Yang, F.; Xu, Q., (2015). Impact of MSW compression on methane generation in decelerated methanogenic phase. *Bioresour. Technol.*, 192: 540-546 **(7 pages)**.
- Kulikowska, D.; Klimiuk, E., (2008). The effect of landfill age on municipal leachate composition. *Bioresour. Technol.*, 99(13): 5981-5985 **(5 pages)**.
- Lee, D.-H.; Kim, Y.-T.; Lee, S.-R., (2020). Shallow landslide susceptibility models based on artificial neural networks considering the factor selection method and various non-linear activation functions. *Remote Sens.*, 12(7): 1194 **(11 pages)**.
- Li, J.; Ban, Q.; Zhang, L.; Jha, A.K., (2012). Syntrophic propionate degradation in anaerobic digestion: a review. *Int. J. Agric. Biol.*, 14(5): 843-850 **(8 pages)**.
- Liu, K.; Lv, L.; Li, W.; Wang, X.; Han, M.; Ren, Z.; Gao, W.; Wang, P.; Liu, X.; Sun, L.; Zhang, G., (2023). Micro-aeration and leachate recirculation for the acceleration of landfill stabilization: Enhanced hydrolytic acidification by facultative bacteria. *Bioresour. Technol.*, 387: 129615 **(9 pages)**.
- Liu, T.; Sung, S., (2002). Ammonia inhibition on thermophilic aceticlastic methanogens. *Water Sci Technol*, 45(10): 113-20 **(8 pages)**.
- Luo, H.; Zeng, Y.; Cheng, Y.; He, D.; Pan, X., (2020). Recent advances in municipal landfill leachate: A review focusing on its characteristics, treatment, and toxicity assessment. *Sci. Total Environ.*, 703: 135468 **(11 pages)**.
- Luo, L.; Wong, J.W.C., (2019). Enhanced food waste degradation in integrated two-phase anaerobic digestion: Effect of leachate recirculation ratio. *Bioresour. Technol.*, 291: 1213-18 **(6 pages)**.
- Marttinen, S.K.; Kettunen, R.H.; Rintala, J.A., (2013). Occurrence and removal of organic pollutants in sewages and landfill leachates. *Sci. Total Environ.*, 301(1-3): 1-12 **(12 pages)**.
- McElroy, P.D.; Bibang, H.; Emadi, H.; Kocoglu, Y.; Hussain, A.; Watson, M.C., (2021). Artificial neural network (ANN) approach to predict unconfined compressive strength (UCS) of oil and gas well cement reinforced with nanoparticles. *J. Nat. Gas Sci. Eng.*, 88: 103816 **(10 pages)**.
- Mehrdad, S.M.; Abbasi, M.; Yeganeh, B.; Kamalan, H., (2021). Prediction of methane emission from landfills using machine learning models. *Environ. Prog. Sustainable Energy*, 40(4): e13629 **(12 pages)**.
- Mohsen, R.A.; Abbasi, B., (2020). Prediction of greenhouse gas emissions from Ontario's solid waste landfills using fuzzy logic based model. *Waste Manage.*, 102: 743-750 **(8 pages)**.
- Mougari, N.; Largeau, J.; Himrane, N.; Hachemi, M.; Tazerout, M., (2021). Application of artificial neural network and kinetic modeling for the prediction of biogas and methane production in anaerobic digestion of several organic wastes. *Int. J. Green Energy*, 18(15): 1584-1596 **(13 pages)**.
- Muksin, U.; Riana, E.; Rudyanto, A.; Bauer, K.; Simanjuntak, A.V.H.; Weber, M., (2023). Neural network-based classification of rock properties and seismic vulnerability. *Global J. Environ. Sci. Manage.*, 9(1): 15-30 **(16 pages)**.
- Nair, V.V.; Dhar, H.; Kumar, S.; Thalla, A.K.; Mukherjee, S.; Wong, J.W., (2016). Artificial neural network based modeling to evaluate methane yield from biogas in a laboratory-scale anaerobic bioreactor. *Bioresour. Technol.*, 217: 90-99 **(10 pages)**.
- Ozkaya, B.; Demir, A.; Bilgili, M.S., (2007). Neural network prediction model for the methane fraction in biogas from field-scale landfill bioreactors. *Environ. Model. Software*, 22(6): 815-822 **(8 pages)**.
- Peng, Y.; Li, L.; Yuan, W.; Wu, D.; Yang, P.; Peng, X., (2022). Long-term evaluation of the anaerobic co-digestion of food waste and landfill leachate to alleviate ammonia inhibition. *Energy Convers. Manage.*, 270: 116195 **(11 pages)**.
- Price, G.A.; Barlaz, M.A.; Hater, G.R., (2013). Nitrogen management in bioreactor landfills. *Waste Manage.*, 23(7): 675-688 **(14 pages)**.
- Rahman, S.; Ramli, M.; Arnia, F.; Muharrar, R.; Ikhwan, M.; Munzir, S., (2022). Enhancement of convolutional neural network

- for urban environment parking space classification. *Global J. Environ. Sci. Manage.*, 8(3): 315-326 **(12 pages)**.
- Ratti, R.P.; Botta, L.S.; Sakamoto, I.K.; Varesche, M.B.A., (2013). Microbial diversity of hydrogen-producing bacteria in batch reactors fed with cellulose using leachate as inoculum. *Int. J. Hydrogen Energy*, 38(23): 9707-9717 **(11 pages)**.
- Rice, E.W.; Bridgewater, L.; Association, A.P.H., (2012). Standard methods for the examination of water and wastewater. American public health association Washington, DC. **(724 pages)**.
- Rumaling M.I.; Chee, F.P.; Chang, H.W.J.; Payus, C.M.; Kong, S.K.; Dayou, J.; Sentian, J., (2022). Forecasting particulate matter concentration using nonlinear autoregression with exogenous input model. *Global J. Environ. Sci. Manage.*, 8(1): 27-44 **(18 pages)**.
- Saadoun, L.; Campitelli, A.; Kannengiesser, J.; Stanojkovski, D.; El Alaoui El Fels, A.; Mandi, L.; Ouazzani, N., (2021). Potential of medium chain fatty acids production from municipal solid waste leachate: Effect of age and external electron donors. *Waste Manage.*, 120: 503-512 **(10 pages)**.
- Samimi, M.; Shahriari Moghadam, M., (2018). Optimal conditions for the biological removal of ammonia from wastewater of a petrochemical plant using the response surface methodology. *Global J. Environ. Sci. Manage.*, 4(3): 315-324 **(10 pages)**.
- Samimi, M.; Mohadesi, M., (2023). Size estimation of biopolymeric beads produced by electrospray method using artificial neural network. *Particulate Science and Technology*, 41(3): 371-377 **(7 pages)**.
- Sandip, T.M.; Kanchan, C.K.; Ashok, H.B., (2012). Enhancement of methane production and bio-stabilisation of municipal solid waste in anaerobic bioreactor landfill. *Bioresour. Technol.*, 110: 10-17 **(8 pages)**.
- Sanphoti, N.; Towprayoon, S.; Chaiprasert, P.; Nopharatana, A., (2006). The effects of leachate recirculation with supplemental water addition on methane production and waste decomposition in a simulated tropical landfill. *J. Environ. Manage.*, 81(1): 27-35 **(9 pages)**.
- Singh, N.K.; Kumari, P.; Singh, R., (2021). Intensified hydrogen yield using hydrogenase rich sulfate-reducing bacteria in bio-electrochemical system. *Energy*, 219: 119583 **(10 pages)**.
- Sormunen, K.; Einola, J.; Ettala, M.; Rintala, J., (2008). Leachate and gaseous emissions from initial phases of landfilling mechanically and mechanically-biologically treated municipal solid waste residuals. *Bioresour. Technol.*, 99(7): 2399-2409 **(11 pages)**.
- Sponza, D.T.; Ağdağ, O.N., (2004). Impact of leachate recirculation and recirculation volume on stabilization of municipal solid wastes in simulated anaerobic bioreactors. *Process Biochem.*, 39(12): 2157-2165 **(9 pages)**.
- Talalaj, I.A., (2015). Mineral and organic compounds in leachate from landfill with concentrate recirculation. *Environ Sci Pollut Res Int.*, 22(4): 2622-2633 **(12 pages)**.
- Tufaner, F.; Demirci, Y., (2020). Prediction of biogas production rate from anaerobic hybrid reactor by artificial neural network and nonlinear regressions models. *Clean Technol. Environ. Policy*, 22: 713-724 **(12 pages)**.
- Turkdogan-Aydinol, F.I.; Yetilmezsoy, K., (2010). A fuzzy-logic-based model to predict biogas and methane production rates in a pilot-scale mesophilic UASB reactor treating molasses wastewater. *J. Hazard. Mater.*, 182(1-3): 460-471 **(12 pages)**.
- Wang, Y.; Singh, R.P.; Geng, C.; Fu, D., (2020). Carbon-to-nitrogen ratio influence on the performance of bioretention for wastewater treatment. *Environ. Sci. Pollut. Res. Int.*, 27(15): 17652-17660 **(9 pages)**.
- Wei, Y.; Ye, Y.; Ji, M.; Peng, S.; Qin, F.; Guo, W.; Ngo, H.H., (2021). Microbial analysis for the ammonium removal from landfill leachate in an aerobic granular sludge sequencing batch reactor. *Bioresour. Technol.*, 324: 124639 **(11 pages)**.
- Xu, Q.; Tian, Y.; Wang, S.; Ko, J.H., (2015). A comparative study of leachate quality and biogas generation in simulated anaerobic and hybrid bioreactors. *Waste Manage.*, 41: 94-100 **(7 pages)**.
- Yang, S.; Li, L.; Peng, X.; Zhang, R.; Song, L., (2021). Methanogen Community Dynamics and Methanogenic Function Response to Solid Waste Decomposition. *Front Microbiol.*, 12: 743827 **(11 pages)**.

**AUTHOR (S) BIOSKETCHES**

**Zoqi, M.J.**, Ph.D., Assistant Professor, Department of Civil Engineering, University of Birjand, Birjand, Iran.

- Email: [mj.zoqi@birjand.ac.ir](mailto:mj.zoqi@birjand.ac.ir)
- ORCID: 0000-0002-6999-4221
- Web of Science ResearcherID: NA
- Scopus Author ID: 36626901400
- Homepage: <https://cv.birjand.ac.ir/zoghi>

**HOW TO CITE THIS ARTICLE**

Zoqi, M.J., (2024). *Application and generalization of artificial neural network for predicting methane production in laboratory-scale anaerobic bioreactor landfills.* *Global J. Environ. Sci. Manage.*, 10(1): 225-244.

DOI: [10.22034/gjesm.2024.01.15](https://doi.org/10.22034/gjesm.2024.01.15)

URL: [https://www.gjesm.net/article\\_707793.html](https://www.gjesm.net/article_707793.html)





## CASE STUDY

## Modeling regional aboveground carbon stock dynamics affected by land use and land cover changes

A.D. Malik<sup>1,\*</sup>, M.C.W. Arief<sup>2</sup>, S. Withaningsih<sup>3</sup>, P. Parikesit<sup>4</sup><sup>1</sup>Center for Environment and Sustainability Science, Universitas Padjadjaran, Bandung, West Java, Indonesia<sup>2</sup>Department of Fisheries, Faculty of Fisheries and Marine Science, Universitas Padjadjaran, Sumedang, West Java, Indonesia<sup>3</sup>Sustainability Science Masters Study Program, Graduate School, Universitas Padjadjaran, West Java, Indonesia<sup>4</sup>Department of Biology, Faculty of Mathematics and Natural Sciences, Universitas Padjadjaran, Sumedang, West Java, Indonesia

## ARTICLE INFO

## Article History:

Received 06 February 2023

Revised 11 March 2023

Accepted 23 May 2023

## Keywords:

Ecosystem services  
Integrated Valuation of  
Ecosystem Services and  
Tradeoffs (InVEST)  
Landscape; Sequestration  
Spatial model  
Vegetation

## ABSTRACT

**BACKGROUND AND OBJECTIVES:** Land use and land cover changes are affected by massive construction, urban expansion, and exploitative agricultural management. These pressures threaten the potential of aboveground carbon storage in Rancakalong District, West Java, Indonesia. In that massive construction and agricultural expansion are ongoing, it is critical to detect the potential changes in carbon stocks in the region. This study evaluated the impact of land use and land cover changes on aboveground carbon stock potential in Rancakalong District, West Java, Indonesia, by incorporating several ground-based carbon inventories into geographic information systems and remote sensing approaches. The spatiotemporal dynamics of the aboveground carbon stocks were assessed using Integrated Valuation of Ecosystem Services and Tradeoffs models.**METHODS:** Aboveground carbon stocks were estimated using the integrated approach of field inventory and geographic information systems. Land use and land cover changes were assessed from remotely sensed imagery data recorded in 2009 and 2021 using the maximum likelihood classification method in the geographic information system as a collection of layers and other elements in a map 10.6 package. Tree height and diameter were collected within the purposively distributed plots with a size of 30 × 30 square meters. Vegetation biomass was assessed using an allometric equation, and aboveground carbon stock data were extrapolated to the landscape scale using a linear regression model of measured carbon stocks and the Normalized Difference Vegetation Index derived from recent satellite imagery.**FINDINGS:** Vegetated areas were predominant in 2009 and 2021. Vegetation covered 51 percent of the total area in 2009, increasing to 57 percent in 2021. Regarding agricultural area, mixed gardens and drylands decreased between 2009 and 2021. Meanwhile, paddy fields were the only agricultural land use to increase between 2009 and 2021. The bare land and built-up expansion related to the observed land clearing for the Cisumdawu Highway mainly came from the conversion of mixed gardens, paddy fields, and drylands. The results show that the land use and land cover changes in Rancakalong District have caused a reduction in aboveground carbon stocks by 11,096 tons between 2009 and 2021. The highest reduction in aboveground carbon stocks occurred in mixed gardens, while a slight increase in aboveground carbon stocks occurred in forests, shrubs, and paddy fields. The results highlight the contribution of mixed gardens to carbon storage as they are visually similar to forests in the structure and composition of vegetation.**CONCLUSION:** Land use and land cover changes directly affected the aboveground carbon stock potential in Rancakalong District, indicated by an 11,096-ton reduction in the stocks. This shortage of carbon stock potential was mainly attributed to the massive reduction in mixed garden areas between 2009 and 2021 by 12 percent, which caused a significant decrease in aboveground carbon stocks. The application of the Integrated Valuation of Ecosystem Services and Tradeoffs model is efficient in analyzing the effect of land use and land cover change on aboveground carbon stock dynamics and can be widely used in environmental engineering studies involving remote sensing approaches.DOI: [10.22034/gjesm.2024.01.16](https://doi.org/10.22034/gjesm.2024.01.16)This is an open access article under the CC BY license (<http://creativecommons.org/licenses/by/4.0/>).

NUMBER OF REFERENCES

88



NUMBER OF FIGURES

6



NUMBER OF TABLES

3

\*Corresponding Author:

Email: [annas12001@mail.unpad.ac.id](mailto:annas12001@mail.unpad.ac.id)

Phone: +6283 8265 60209

ORCID: [0000-0003-0588-387X](https://orcid.org/0000-0003-0588-387X)

Note: Discussion period for this manuscript open until April 1, 2024 on GJESM website at the "Show Article".

## INTRODUCTION

Climate change and global warming have become major threats to global ecosystems (Hassan and Nile, 2021; Frimawaty et al., 2023; Arredondo Trapero et al., 2023). The recent increase in greenhouse gas emissions that has resulted from massive human social development and industrialization is one of the main causes of climate change (Javaherian et al., 2021). Temperatures in places inhabited by more than one-fifth of humanity have already risen by 1.5 degrees Celsius (C) over preindustrial levels in at least one season (Javaherian et al., 2021). Without mitigation efforts to reduce greenhouse gases, the global temperature is expected to continue to rise in the 21st century, ranging from a median increase of 3.7°C to 4.8°C (IPCC, 2014).

The primary factors causing climate change are thought to be carbon emissions and greenhouse gases, and their levels continue to meet the upper limit of the model scenario developed by the IPCC (Jagdish et al., 2013). As a consequence of landscape modification, land use and land cover (LULC) change impacts the ability of a landscape to reduce carbon emissions. LULC changes further impact the distribution of soil organic matter as an area shrinks over time (Zhao et al., 2018; KARBASSI et al., 2015). Moreover, modifications in LULC exert increasing pressure on regulatory ecosystem services such as carbon sequestration (Solomon et al., 2018). The benefits humans gain from ecosystems are referred to as "ecosystem services" (Millennium Ecosystem Assessment, 2005). All ecosystem services are needed for human survival and livelihoods (Solomon et al., 2017). The regulation of gas concentrations that circulate between the ecosystem and atmosphere of the earth and have an impact on the world's climate is carbon sequestration (Lee et al., 2022). The dynamics of the carbon cycle are affected by LULC changes, which affect emission rates and carbon sequestration (Coutinho et al., 2015). The ability of terrestrial carbon pools may also be disturbed by these impacts, which can affect the accumulation of many sources of carbon (Zhao et al., 2018). Terrestrial ecosystems play an essential role in carbon sequestration. According to the FAO (2016), carbon sequestered in above- and belowground biomass is estimated at approximately 296 gigatons (Gt) and 44% is stored in plant biomass. Conversely, the emission of carbon dioxide (CO<sub>2</sub>)

resulting from vegetation biomass deterioration was estimated at 12.5% of the total CO<sub>2</sub> emissions (Masripatin et al., 2010). Aboveground biomass consists of all living things and vegetation that exists in terrestrial ecosystems, such as trees, shrubs, and herbaceous plants (Piyathilake et al., 2022). According to a report from the Forest Resource Assessment, the world's carbon stored in forest biomass was 289 Gt (Ostadhashemi et al., 2014). The carbon stocks in natural forests are believed to be one of the most vital ecosystems for combating anthropogenic climate change (Thom et al., 2017). Forest areas have ten times greater potential for carbon stocks than other types of vegetation; however, many forests are currently being deforested (Masripatin et al., 2010). Changes in forest cover and other land use with carbon sequestration potential influence carbon dynamics (Dida et al., 2021). Between 2005 and 2010, the carbon contained in the world's forest biomass was expected to decrease by 0.5 Gt each year. This reduction was primarily due to a decrease in worldwide forest area (Forestry Economics and Policy Division, 2010). Likewise, between 2015 and 2016, it was estimated that forests in Indonesia experienced 0.63 million hectares (ha) of deforestation (KLHK, 2018). Most carbon emissions come from the coal energy sector, and this rate is predicted to increase further until reaching 434.96 parts per million (ppm) in 2050, where carbon increases that exceed 400 ppm can be categorized as a global phenomenon (Cahyono et al., 2022). In this context, investigating the potential loss of valuable ecosystem components as a result of LULC change is essential (Lahiji et al., 2020). Numerous studies in Indonesia have analyzed the potential of various ecosystems to sequester carbon, for example, in state forests (Darmawan et al., 2022), production forests (Situmorang et al., 2016), urban green spaces (Dewanto and Jatmiko, 2021), mangroves (Kusumaningtyas et al., 2022), and agroforestry systems (Latifah et al., 2018). However, limited studies have discussed how LULC changes impact ecosystem services, and a spatiotemporal model of carbon stock dynamics has not been produced. The recent rapid development of geographic information systems (GIS) provides an opportunity to identify LULC changes over time and comprehensively detect disturbances in a particular ecosystem service (Zhao et al., 2019). Furthermore,

a spatial model provides a clearer explanation of how disturbance impacts ecosystem services (Jiang *et al.*, 2021). The study of LULC changes and measurement of the aboveground carbon stock may vary using remote sensing and GIS. Several previous studies have focused on revealing the significant effects of LULC changes on carbon stocks using GIS and remote sensing approaches. A typical simulation model for carbon stock dynamics incorporating annual maps was performed to analyze the effect of LULC changes on vegetation biomass and carbon stocks (Liu *et al.*, 2016). The assessment of LULC changes and vegetated aboveground carbon stocks using multispectral data in remote-sensing-based methodology revealed a relevant decrease in vegetated areas (Masseti and Gil, 2020). Another study conducted by Piyathilake *et al.* (2021) used the GIS approach and InVEST model to predict the LULC type containing the largest carbon stocks on a regional scale. Later, the use carbon budget model, which focuses on the prediction of carbon dynamics affected by several disturbances and LULC variations, was performed by (Tang *et al.* 2022). The empirical model also incorporates some ecological processes regarding the plant species' traits and characteristics and climate data. However, these studies used secondary data, such as available vegetation maps, geodatabase of vegetation stand attributes, and national statistics data of biomass growth to obtain carbon stocks. Detailed information regarding the combination of remote sensing and integrated field surveys at the regional scale remains limited. In this study, rather than relying only on carbon data sources from published studies and reports, the integration of a few field carbon inventory data points with GIS and remote sensing methods is expected to obtain more accurate and precise carbon estimation results. The normalized difference vegetation index (NDVI) is a metric derived from remotely sensed images that is commonly used in predicting biophysical factors, such as aboveground biomass and carbon (Wani *et al.*, 2021). Typically, some parametric models have been applied to discover the direct relationship between aboveground biomass and metrics/spectral values derived from satellite imagery (Vafaei *et al.*, 2018; Zhu and Liu, 2015). Several spatially based decision models for ecosystem services assessment have

been widely applied (Bagstad *et al.*, 2013), one of which is Integrated Valuation of Ecosystem Services and Tradeoffs (InVEST) (Sharp *et al.*, 2020). InVEST is a distinguished model that has been widely applied to assess global ecosystem services (Piyathilake *et al.*, 2022). The advantages of this model include its low data requirements and ease of use (Cong *et al.*, 2020). Models for regulatory ecosystem services have been commonly applied in InVEST, and the model has been used to assess carbon sequestration under multiple scenarios (Posner *et al.*, 2016). The InVEST model uses LULC projection maps and quantitative data on ecosystem services (Nelson *et al.*, 2009). The model needs an estimation of the carbon stocks in at least one of the four carbon pools for each LULC map. These data can be used to create a projection model of the amount of carbon stored in a class of land cover over time and predict carbon sequestration (Sharp *et al.*, 2018). This study employs the aboveground biomass of vegetation as it is the most active carbon pool in the carbon cycle (Harper *et al.*, 2018). Land deterioration has occurred in Sumedang Regency, West Java, Indonesia. According to Khaerani *et al.* (2018), a protected forest and production forest conversion of 7,817 ha between 2015 and 2017 violated the regional planning for the Sumedang Regency. In recent years, forest cover degradation has been affected by the megaproject in Sumedang Regency. They are the Cisumdawu Highway project, which connects Bandung, the capital city of West Java, with Kertajati International Airport, and the Jatigede Hydropower Plant, which is expected to generate  $2 \times 25$  megawatts (MW) of electricity. As a result of this forest cover degradation, carbon sequestration has likely been significantly diminished. Rancakalong is a district in Sumedang Regency. Segments of the Cisumdawu Highway also pass through this District, resulting in LULC change. Since these massive constructions are ongoing, determining the link between LULC change and carbon stocks in this area is critical, as various LULC classes have varying effects on carbon stocks (Toru and Kibret, 2019). The aim of this study is to analyze spatial and temporal dynamics of aboveground carbon stocks associated with LULC change in Rancakalong using the InVEST model. This study was conducted in Rancakalong District, which is situated in Sumedang Regency, West Java Province, Indonesia in 2009 and 2021.

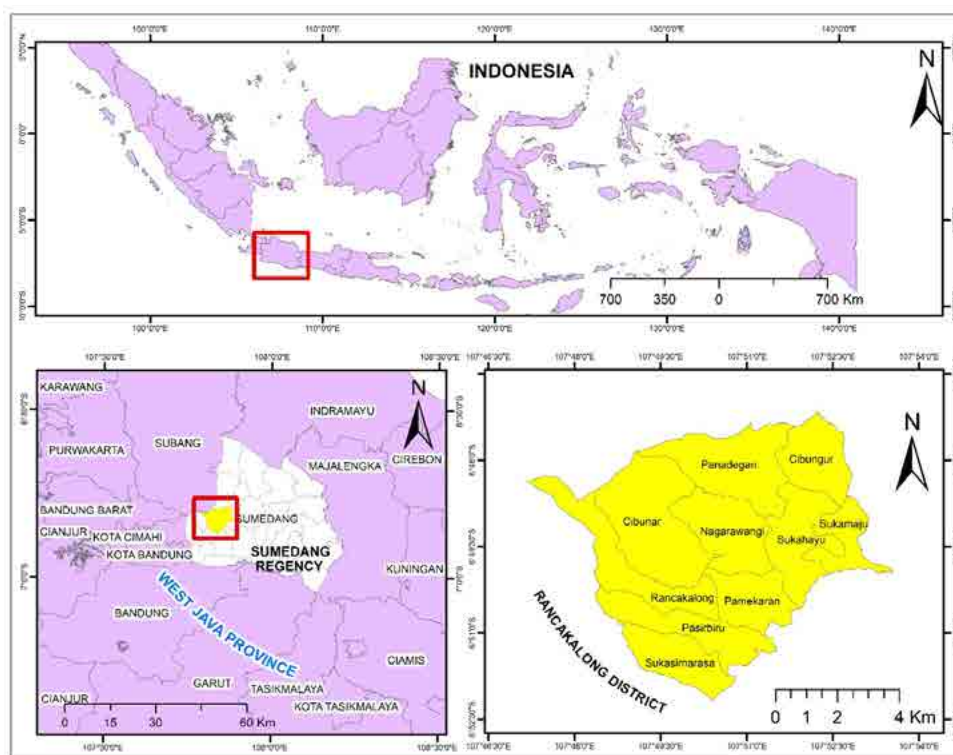


Fig. 1: Geographic location of the study area in Rancakalong District, Indonesia

## MATERIALS AND METHODS

### Research site

Rancakalong District is located in the western part of Sumedang Regency 16 kilometers (km) from the capital of Sumedang Regency, West Java Province, Indonesia (Fig. 1). The mean temperature in the study area is 24.7°C, and the mean precipitation is 2570 millimeters per year (mm/y) (Sampurno and Thoriq, 2016). The total area of Rancakalong District is 5574.12 ha, dominated by hills and mountainous landscapes, and the elevation ranges from 500 to 1500 meters (m) above sea level (Sumedang Regency, 2019). The geographic conditions indicated that large parts of the area are barely accessible. Most of Rancakalong's people are working in the agricultural sector, reflected by the agriculture area as the major land use in Rancakalong, with the characteristics of upland agricultural systems and paddy fields reaching 3383.77 ha or 60.71 percent (%) of the Rancakalong District (Sumedang Regency, 2019). The forests lie on the very steep slope hillside of Cibunar Mountain and cover 146.29 ha of the area. In recent days, the

Rancakalong area has been exposed to environmental pressure from the development of the Cisumdawu Highway as segments of the toll road pass through the area and have affected massive LULC changes.

### Data collection and sampling design

The magnitude of the data collected was at the Rancakalong District scale as part of the Sumedang Regency. The integrated approach combining the direct measurement of carbon stocks and spatial analysis was conducted to assemble the required primary and secondary data. The primary data of the carbon stocks collected by direct measurement of aboveground biomass of the vegetation stands measures the diameter at breast height (DBH) and height. Most of the area was difficult to access due to very steep slopes around the hills and mountains and the high rainfall that occurred during the research. The vegetation stands were sampled in the study area and quantified using a purposive sampling technique considering safety, climate, and topographic factors. The sample plot size of 30 × 30 square meters (m<sup>2</sup>)

refers to the pixel size of medium-resolution remotely sensed satellite imagery (~30 m). The secondary data contain the global spatial distribution of crop yield data in tons/hectare (tons/ha) for all commodities in Rancakalong (rice, sweet potato, maize, groundnut, banana, and cassava), which can be considered biomass in tons/ha and tree density of all measured trees. The crop yield information was collected from the Global Agroecological Zones+ (GAEZ+) (Frolking *et al.*, 2020) data on global gridded crop harvest areas, crop production, and crop yields. Tree density was obtained from the global wood density database (Zanne *et al.*, 2009). Furthermore, the secondary data of the multispectral image of Landsat 5 Thematic Mapper (TM) recorded on 3 May 2009 and Landsat 8 Operational Land Imager (OLI) recorded on 16 September 2021 were used as spatial data for InVEST modeling.

#### Preprocessing

Satellite imagery pre-analysis was required to correct the atmospheric disturbance of the multispectral image data. This process corrected the pixel value of the image data and allowed the pixel value to depict the true condition of the terrestrial ecosystem. Without this correction, the image sensor may have failed to absorb the object's reflection of the earth due to atmospheric disturbance. The preprocessing step consisted of radiometric calibration and atmospheric correction. Before calibration, the satellite images were cropped to the area of interest. Next, the vector administrative boundary of Rancakalong District was selected as the masking area. In radiometric calibration, the multispectral image data, or so-called digital numbers (DN), were converted into the top of atmosphere (TOA) radiance and reflectance by rescaling the DN values in the metadata text file extension (MTL). This process is a prerequisite for DN value conversion into a surface reflectance value when correcting for atmospheric disturbance (Chavez, 1989). This reflectance measurement produces a vegetation index of the imagery data (Jaya *et al.*, 2022). To generate the TOA radiance value, the radiance rescaling factors of the MTL were used and included in Eq. 1 (Hua and Ping, 2018).

$$L_{\lambda} = M_L Q_{cal} + A_L \quad (1)$$

where:

$L_{\lambda}$  = TOA spectral radiance

$M_L$  = The MTL-derived multiplicative rescaling factor

$A_L$  = MTL's additive rescaling factor

$Q_{cal}$  = Standard product pixel values or DN value of a specific pixel

The following stage involved converting TOA spectral radiance to TOA reflectance. The images in spectral radiance were converted to reduce the in-between-scene variability through normalization for solar irradiance (Chander and Markham, 2003). This step is imperative to cross-calibrate all Landsat sensors (Li *et al.*, 2018). For the Landsat 5 TM, the spectral radiance ( $L_{\lambda}$ ) was converted to the surface and atmospheric reflectance using Eq. 2 (Chander and Markham, 2003).

$$\rho_p = (\pi L_{\lambda} d^2) / (ESUN_{\lambda} \cos \theta_s) \quad (2)$$

where:

$\rho_p$  = Planetary reflectance

$\pi$  = phi

$L_{\lambda}$  = TOA spectral radiance

$d$  = The astronomic distance between Earth and Sun

$ESUN_{\lambda}$  = The mean value of solar exoatmospheric irradiances

$\theta_s$  = Angle of the sun's zenith in degrees (90° – solar elevation)

Meanwhile, all rescaling factors for Landsat 8 OLI imagery were found in the MTL, meaning that the conversion to TOA radiance was unnecessary. The conversion was conducted using Eq. 3 (Nijhawan and Jain, 2018).

$$\rho_{\lambda}' = M_{\rho} Q_{cal} + A_{\rho} \quad (3)$$

where:

$\rho_{\lambda}'$  = TOA reflectance, in which the sun's angle correction is not necessary for OLI

$M_{\rho}$  = MTL-derived band-specific multiplicative rescaling factor

$A_{\rho}$  = Additive rescaling factor from the MTL for each band

$Q_{cal}$  = Standard product pixel values or DN value of a specific pixel

The effects of atmospheric scattering should be considered when measuring reflectance at the

ground, also known as surface reflectance (Chavez, 1989). The surface reflectance is applied using Eq. 4 (Moran et al., 1992).

$$\rho = \left[ \pi * (L_{\lambda} - L_p) * d^2 \right] / [T_v * ((ESUN_{\lambda} * \cos \theta_s * T_z) + E_{down})] \quad (4)$$

where:

$\rho_{\lambda}$  = Surface reflectance

$\pi$  = phi

$L_{\lambda}$  = TOA spectral radiance

$L_p$  = Path radiance

$d$  = The astronomic distance between Earth and Sun

$T_v$  = Atmospheric transmittance in the viewing direction

$\theta_s$  = Solar zenith angle in degrees ( $90^\circ$  – solar elevation)

$T_z$  = Atmospheric transmittance in the illumination direction

$ESUN_{\lambda}$  = The mean value of solar exoatmospheric irradiances (ESUN is not required for Landsat 8 OLI bands)

$E_{down}$  = The downwelling diffuse irradiance

All preprocessing steps were run in the Semiautomatic Classification Plugin (SCP) integrated into the QGIS 3.16 software. The SCP is a free plugin for QGIS that facilitates satellite image conversion to reflectance to generate the best condition of the Earth's surface by reducing the atmospheric condition. As the final step of preprocessing (atmospheric correction/surface reflectance), dark object subtraction 1 (DOS1) atmospheric correction was applied in the plugin.

#### LULC classification

LULC classification was applied to both Landsat 5 TM and Landsat 8 OLI images. This process produces raster data of LULC classes and later will serve as the data for InVEST modeling. All raster images were stacked or composited to produce a single raster and multispectral image. Since a pansharpened raster band is available in the multispectral image of Landsat 8 OLI, an image enhancement tool was used to sharpen the image resolution and clarify the image during the remote sensing process. The image classification process using maximum likelihood classification (MLC) was run in the geographic information as a collection of layers and other elements in a map.

(ArcMap) 10.6. Numbers of training samples were drawn on each satellite image representing the LULC classes (forests, mixed gardens, paddy fields, shrubs, built-up land, drylands, and bare land). This nomenclature variation of LULC classes was selected following guidance from the Ministry of Forestry and Environment of Indonesia and the Regional Planning Agency of Sumedang regarding the remote sensing method for medium-resolution satellite imagery data. The supervised technique identifies and classifies the pixel values drawn in the training sample with other identical pixel values. Visual interpretation of the satellite imagery was assisted by high-resolution Google Earth imagery and ground-truthing at the study site. The determination of selected variations of LULC classes was also helped by the Google Earth imagery and ground-truthing approach. The best band combination for built-up area classification is the natural color band combination, that is, band 4-3-2 for Landsat 8 OLI and band 3-2-1 for Landsat 5 TM (Liu et al., 2018). Conversely, the false color band combination is the most suitable for vegetation mapping, namely, band 5-4-3 for Landsat 8 OLI and band 4-3-2 for Landsat 5 TM (Liu et al., 2018). The false color band is superior because tree leaves have a large amount of chlorophyll, which can better absorb red light from the infrared spectrum (Zhang et al., 2012). Later, an accuracy assessment was conducted to minimize LULC classification errors due to the sampling technique and the potential for misinterpretation of pixel values in the imagery data. The assessment employed a matrix of the error to identify pixel misclassification (Yesserie, 2009). The Kappa coefficient is an appropriate analysis for nominal data image classification models that partially rely on ground-truth data (Senseman et al., 1995).

#### Vegetation index identification

A vegetation index distribution map was produced to extrapolate the direct biomass and carbon stock measurements of vegetation stands from the plot scale to the landscape scale. This index was also useful to identify the index value of the vegetation present in the study site. The most commonly used spectral vegetation index is NDVI. To identify the current state of vegetation in the study area, the multispectral image data were converted into a raster map containing the values of the vegetation

index. In this study, NDVI provided information about the canopy and vegetation coverage and depicted this information in a vegetation distribution map (Calderón-Contreras and Quiroz-Rosas, 2017). According to Marchetti *et al.* (2016), NDVI patterns can map the physiognomy and elevation of various vegetation types. This process permits mapping of different areas covered by vegetation (e.g., forests, mixed gardens, shrubs, and paddy fields). In this study, the Landsat 8 OLI recorded on 16 September 2021 was used to obtain the NDVI. The NDVI of the multispectral image is a division between the near-infrared and red bands, which in Landsat 8 OLI is related to Bands 5 and 4. The NDVI used to identify the difference in vegetation quality was obtained using Eq. 5 (Rouse *et al.*, 1974).

$$NDVI = \frac{NIR-Red}{NIR+Red} \quad (5)$$

where:

NDVI = Normalized Difference Vegetation Index

NIR = Near-infrared band (Band 5)

Red Band = Red band (Band 4)

The NDVI produces a value between -1.0 and 1.0, where negative values represent water bodies or bare lands and higher positive values indicate dense vegetation (Calderón-Contreras and Quiroz-Rosas, 2017). Such higher values are due to dense vegetation's capacity to absorb much of the red spectrum while reflecting much of the near-infrared (Davies *et al.*, 2016). The higher the value of the NDVI, the higher the photosynthetic activity of a particular identified area of vegetation (Jamali *et al.*, 2011).

#### Biomass and Carbon Stock Measurement

The sampling technique considered the spatial distribution of each NDVI class. The sample was ensured to represent each class of NDVI. Deforestation was heavily affected by LULC changes; therefore, only the aboveground biomass of vegetation was measured. In the sample plots, the name of the species, DBH, and the height of the trees were measured. The estimation of biomass was conducted using Eq. 6. This allometric equation and coefficient are suitable for aboveground biomass estimation in most tropical moist regional locations, considering DBH, wood density ( $\rho$ ), and tree height (T) as the most important predictive variables (Chave *et al.*, 2005).

$$AGB = 0.0509 * \rho * DBH^2 * T \quad (6)$$

where:

AGB = Total aboveground biomass (kg)

DBH = Diameter at breast height (~1.3 m)

$\rho$  = Wood density (gr/cm<sup>3</sup>)

T = tree height (m)

The biomass carbon content was calculated by multiplying the biomass estimation result with a default value of 46% (Hairiah *et al.*, 2011). Carbon stocks obtained from field measurements were extrapolated to the landscape scale using correlation analysis. A single explanatory variable regression was selected to identify the correlation between NDVI values and the field measurement of carbon stocks (Batsaikhan *et al.*, 2020). In the regression model, the dependent variable (Y) was the plot-level carbon stock measurement result, and the independent variable (X) was the NDVI value distribution map. A scatterplot of NDVI values was produced, and the carbon stock was measured in all permanent plots to ensure that the distribution of plot carbon data matched the trend of the NDVI (Basalumi *et al.*, 2018). The correlation analysis was performed in IBM SPSS Statistics 26 software. To confirm that the study area's real carbon stocks could be modeled by the simple linear regression equation, a standard error of estimate (SEE) accuracy test was conducted on the result of the obtained carbon model and compared with the actual field carbon data in all permanent plots. The SEE analysis was calculated using Eq. 7 (Smith, 2015).

$$SEE = \sqrt{\frac{\sum_{i=1}^n (y_i - \hat{y}_i)^2}{n - 2}} \quad (7)$$

where:

SEE = Standard Errors of Estimate (tons/pixel)

$\sum_{i=1}^n (y_i - \hat{y}_i)^2$  = Difference value between the carbon model and actual field carbon stocks

n = number of plots

The carbon stocks model was extrapolated from the plots to the landscape scale by the Raster Calculation feature in QGIS 3.6 software. This process produced the final carbon model distribution map in a raster image format.

*InVEST carbon storage model*

A product of the Natural Capital Project, the InVEST Carbon Storage and Sequestration Model is software for ecosystem services mapping and calculation. In this study, InVEST was used to model the carbon stock dynamics in the study site. Specifically, the results of the older carbon stocks spatial model were compared with the more recent model. InVEST carbon modeling requires maps of LULC classification and carbon stock data in tons/ha. This study uses aboveground biomass as the only carbon pool. The model produces both numeric and spatial data in a raster output for further GIS analysis and decision-making processes (Shrestha *et al.*, 2021). The LULC raster data, which are necessary for the carbon storage model, were obtained from the LULC image classifications from 2009 and 2021. The LULC classifications contained attribute tables with information on LULC classes (forests, mixed gardens, paddy fields, shrubs, built-up land, dryland, and bare land). The result of the carbon stock estimation spatial data from the previous extrapolation process was converted into numeric values of carbon density for each LULC class. Carbon density values were then aggregated in a comma-separated value (csv) file format. All LULC raster images and the .csv file were integrated into the InVEST software to begin modeling the current aboveground carbon storage. The final result

contained carbon storage distribution maps in a temporary instruction file format (tiff).

**RESULTS AND DISCUSSION**

*Land use and land cover changes*

As shown in Fig. 2, the classification identified LULC changes in the Rancakalong District. As seen in Table 1, the largest LULC class area in both 2009 and 2021 was mixed gardens. In 2009, mixed gardens (31%) were followed by drylands (21% as the second most common class). Meanwhile, mixed gardens (25%) and paddy fields (13%) were the most common LULC classes in 2021. According to LULC change detection, the area of mixed gardens and drylands decreased between 2009 and 2021 by 6% and 8%, respectively. The areas of shrubs, forests, paddy fields, and bare land increased by 9%, 2%, 2%, and 2%, respectively. The supervised classification detected that vegetated land was predominant in 2009 and 2021. In this study, forests, mixed gardens, and shrubs were considered to be vegetated areas, as vegetation cover was predominant in each area. Vegetation covered 51% of the total area in 2009. In 2021, the vegetated area covered 57% of the total area, indicating a 6% increase in vegetated areas. This increase was driven by shrubs, as this type of vegetation expanded 10% between 2009 and 2021.

At the LULC level, the conversions occurred at

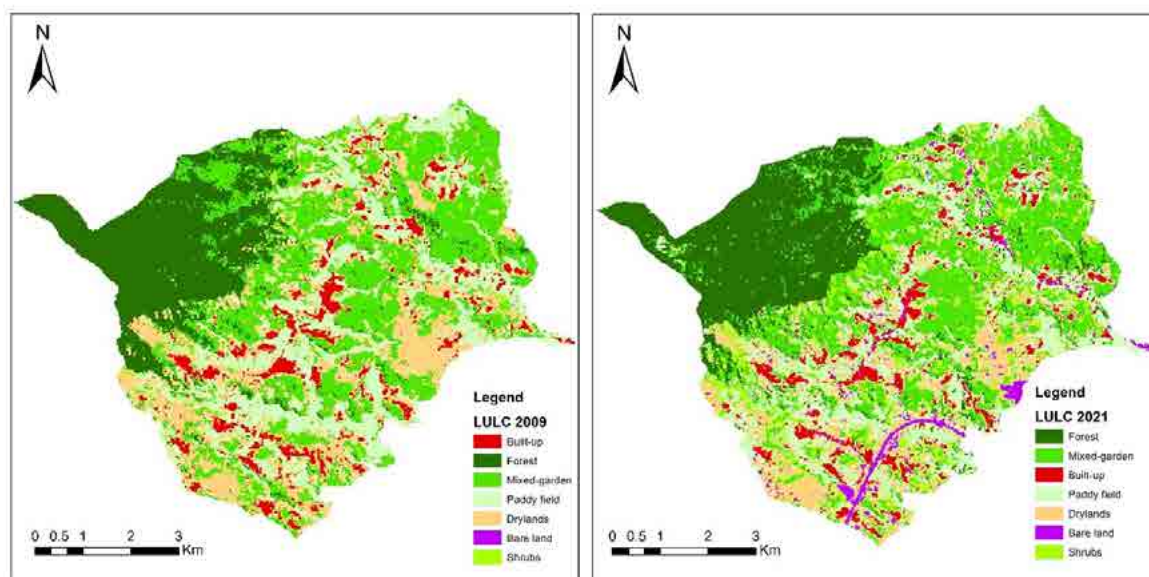


Fig. 2: Map of LULC classification in Rancakalong District in 2009 and 2021

different rates depending on the type of LULC class (Table 2). For example, forests were mostly converted to mixed gardens (12%), followed by these areas' conversion to paddy fields (3%) and shrubs (2%). Mixed gardens—the most common LULC class in the study site—experienced a 12% conversion to forests, followed by conversion to shrubs (13%) and paddy fields (11%). The estimated conversions between forests and mixed gardens may have been biased by the visual characteristics of these LULC classes potentially leading to misclassification. According to the remote sensing method, forests and mixed gardens are visually similar since the mixed garden in the study area can be considered an agroforestry system managed by local communities that take part as forest buffer areas. As agriculture is the main occupation of Rancakalong District's people, the conversion of forests and mixed gardens to paddy fields was mainly attributed to these areas expanding to fulfill the needs of Rancakalong's people for this type of agricultural system.

The increase in forest cover can be largely attributed to the rise in mixed gardens because mature mixed gardens are visually similar to forest cover and are both dominated by perennial plants. In contrast, the mixed garden area decreased between 2009 and 2021. The mixed gardens were mostly converted into shrubs, indicating some abandonment of mixed gardens following plant-clearance activities by farmers. Paddy fields were the only agricultural land use to become more prevalent, increasing from 20% to 22% between 2009 and 2021 (Table 1). Meanwhile, the other agricultural areas, mixed gardens, and drylands, decreased between 2009 and 2021. As in the nonvegetated and non-agricultural areas, the newly built-up areas largely resulted from the conversion of drylands (6%) and paddy fields (2%) (Table 2). The largest bare land conversion came from paddy fields (4%), followed by drylands (3%) (Table 2). The bare land conversion was related to the observed land-clearing activities for the Cisumdawu Highway project, which started

Table 1: Estimated area for each LULC class in 2009 and 2021

LULC classes	2009 (ha)	2021 (ha)	2009 (%)	2021 (%)	Area change (%)
Drylands	1150.17	712.90	21%	13%	-8%
Forests	1134.54	1218.73	20%	22%	2%
Mixed gardens	1736.90	1413.36	31%	25%	-6%
Bare land	0.18	138.70	0%	2%	2%
Built-up	342.10	286.61	6%	5%	-1%
Paddy fields	1130.93	1245.90	20%	22%	2%
Shrubs	57.59	536.22	1%	10%	9%
Total	5552.41	5552.41	100%	100%	

Table 2: Conversion area matrix of LULC classes between 2009 and 2021

LULC	2021 ha (%)							
	Drylands	Forests	Mixed gardens	Bare land	Built-up	Paddy fields	Shrubs	
2009 ha (%)	Drylands	372.39 (32%)	30.13 (3%)	149.87 (13%)	35.78 (3%)	65.29 (6%)	315.09 (-27%)	181.61 (16%)
	Forests	8.7 (-1%)	928.50 (82%)	134.10 (12%)	2.76 (0.24%)	0.40 (0.03%)	38.38 (-3%)	21.70 (2%)
	Mixed gardens	98.88 (-6%)	205.20 (12%)	977.72 (56%)	31.18 (1.8%)	6.67 (0.38%)	198.81 (-11%)	218.45 (13%)
	Bare land	0.05 (-29%)	0	0	0.03 (17%)	0	0.09 (-52%)	0
	Built-up	64.95 (-19%)	0.89 (0.26%)	4.12 (-1%)	25.21 (7%)	196.09 (57%)	46.86 (-14%)	3.98 (-1%)
	Paddy fields	162.38 (14%)	51.90 (5%)	122.26 (11%)	42.58 (4%)	17.88 (2%)	641.11 (-57%)	92.82 (8%)
	Shrubs	5.54 (-10%)	2.11 (-4%)	25.30 (44%)	1.15 (2%)	0.29 (-1%)	5.55 (-10%)	17.65 (31%)

in 2013. According to [Thonfeld et al. \(2020\)](#), the change in forest cover may have minor impacts on biodiversity and ecosystem services compared to the stronger effects from the conversion of natural or non-agricultural landscapes such as forests, shrubs, and mixed gardens to agricultural and nonvegetated land uses (e.g., drylands, paddy fields, built-up areas, and bare lands).

#### Vegetation index in the study area

The NDVI map in this study ranged from 0.0796807 to 0.880033 ([Fig. 3](#)). Higher NDVI values were distributed in the northwest compared to other parts of the Rancakalong District because there was an undisturbed forest in this area. The high NDVI value was indicative that the green biomass was mainly distributed in the northwest area ([Bosino et al., 2019](#)). Conversely, the lowest NDVI was distributed in the south, which contained the majority of built-up areas and bare lands. This situation was mainly attributed

to the land-clearing process for the construction of the Cisumdawu Highway, which passes through Rancakalong District. According to [Suharyanto et al. \(2021\)](#), man-made materials can strongly reflect solar radiation, resulting in a massive reduction in NDVI. High NDVI values, which indicate the presence of dense vegetation, were evident in forest areas and some mixed garden areas. Although some areas were considered bare lands, the absence of a negative value indicates there were still vegetated parts of these areas. This evidence of vegetation might be related to replanting activities and succession progress in abandoned areas following land clearing. In turn, NDVI can provide insight and predict vegetation recovery after some disturbance events ([Saito et al., 2022](#)). Moderate vegetation cover (indicated in yellow) was largely located in some nonperennial plant-based agricultural lands, such as paddy fields and drylands. The NDVI value distribution in the study site can superficially predict the amount of

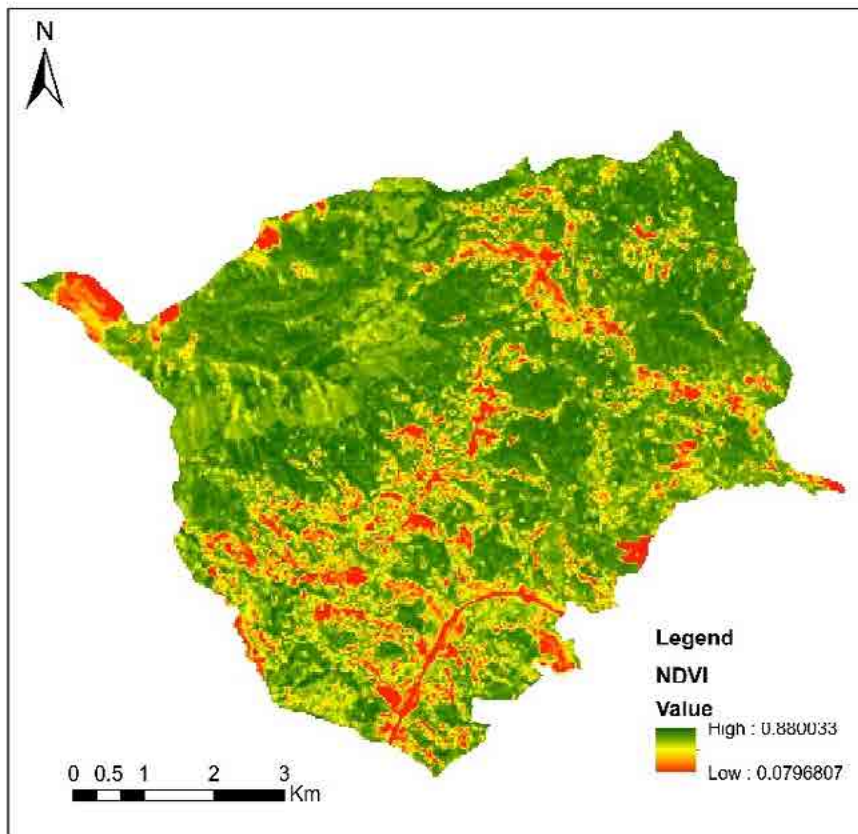


Fig. 3: Map of NDVI distribution in Rancakalong District

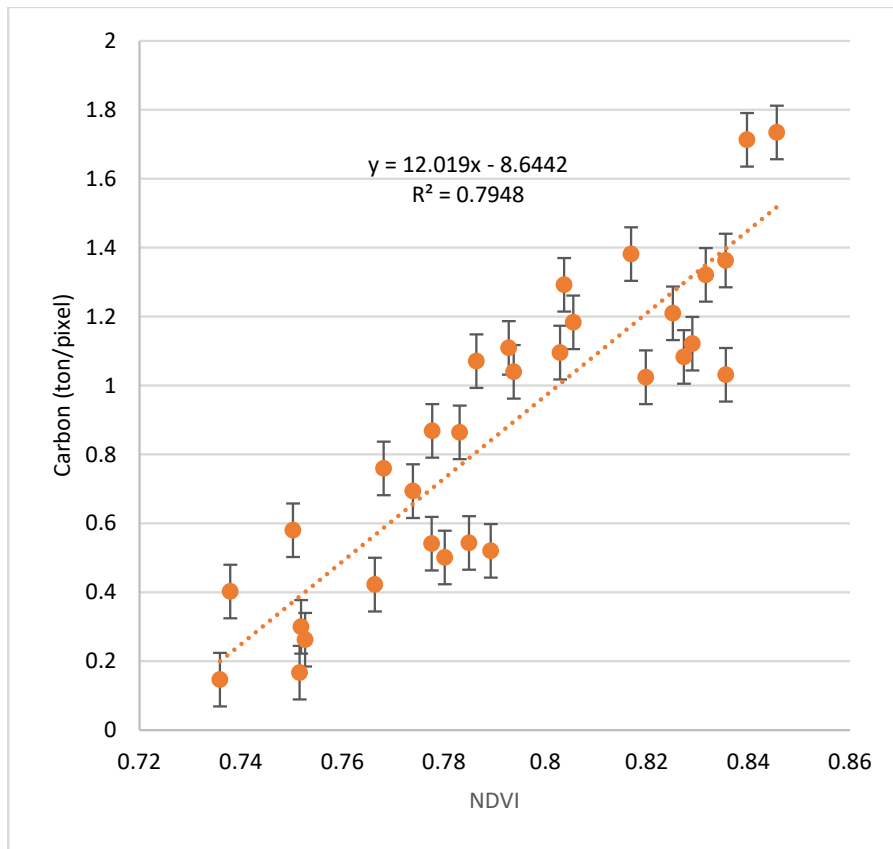


Fig. 4: Scatterplot of NDVI and aboveground carbon stocks in a linear regression model

vegetation biomass (Astsatryan *et al.*, 2015), which was useful in extrapolating the aboveground biomass and carbon content to a landscape scale.

#### *Extrapolation of field carbon inventory data to the landscape scale*

The aboveground carbon stock estimation model was built using correlation analysis. A simple linear regression analysis was carried out to identify the degree of correlation between NDVI values and the plot-level result of carbon stocks. As shown in Fig. 4, the regression model revealed a positive relationship between aboveground carbon stocks in the field and NDVI values. The scatterplot shows a positive trend: the higher the NDVI value, the higher the aboveground carbon stocks in the study site. A determination value ( $R^2$ ) of 0.7948 shows a significant correlation between field measurements of aboveground carbon stocks and NDVI values.

The result shows that approximately 79% of aboveground carbon stocks in the study area can be determined by NDVI values in this regression model, while 21% of aboveground carbon stocks were determined by other factors. This relatively strong determination value suggests that the regression model can effectively extrapolate aboveground carbon stocks to the landscape scale. To demonstrate this, an accuracy test was conducted comparing the aboveground carbon stocks from the model and data from the field measurements in all permanent plots. The SEE test resulted in an estimated error of 0.445195549 tons/pixel. The relatively low estimated error suggests that the simple linear regression is the optimal model for aboveground carbon stock estimation using NDVI as the vegetation index in the study area.

The results of the aboveground carbon stock extrapolation and crop yield data obtained from

Table 3: Carbon pool values (tons/ha/y) for each LULC class in the study site

Code	LULC class name	C-above
1	Drylands	30.90717857
2	Forests	56.93176429
3	Mixed gardens	123.9699638
4	Bare land	0
5	Built-up	0
6	Paddy fields	3.5290878
7	Shrubs	80.03822364

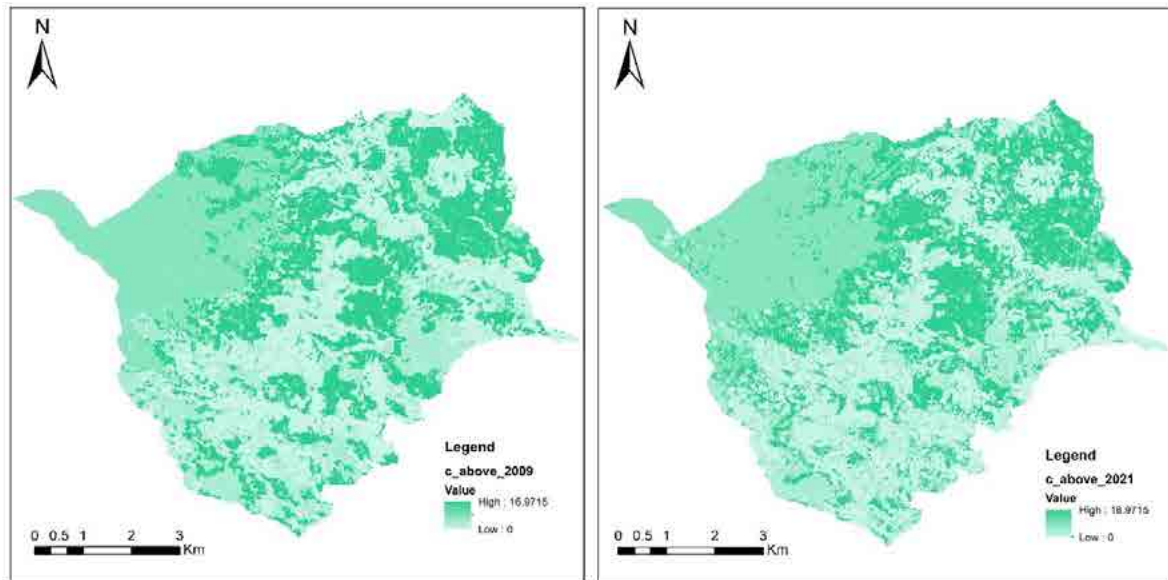


Fig. 5: Distribution of estimated aboveground carbon stocks in 2009 and 2021

GAEZ+ were aggregated and assigned to each LULC class. The aboveground biomass value for built-up and bare land areas was set at zero because an extremely low vegetation cover can be neglected when generating an optimal carbon stock model. This decision followed the assumption that those LULC classes did not have any potential aboveground carbon content. An aboveground carbon pool tabulation for each LULC class is presented in Table 3.

*Spatial distribution of carbon stocks*

The InVEST carbon storage and sequestration model generated a raster representing the spatial distribution of carbon stocks in the research area (Fig. 5). Between 2009 and 2021, the spatial distribution of aboveground carbon stocks in Rancakalong District became less varied. The highest aboveground carbon stock value in Rancakalong

District was 16.97 tons, which was located in the dense vegetation area. Carbon stock values were generally highest in the western and northeastern regions, where the climate and topographic conditions were favorable for the growth of the forest. These areas were considered part of a mountain range in the study area. Meanwhile, the lowest aboveground carbon stock was 0, as it was assumed that bare land and built-up land did not contain aboveground carbon stock potential in the long term. The lower carbon stock values were mainly distributed in the southern region where drylands and other land uses that had scant carbon stock potential predominated. In particular, the drylands were mainly dominated by upland commodity cultivation with no vegetation stands. As a result, there was less vegetation coverage and relatively low carbon stocks. The spatial distribution of carbon stocks in the study area was related to

the LULC class distribution. The area dominated by dense forest and tree-based agricultural landscapes contained more carbon stocks than the region dominated by undergrowth vegetation-based agriculture and other unused lands, such as the bare lands resulting from land-clearing activities. Between 2009 and 2021, there was a significant decrease in aboveground carbon stocks in the southern areas of Rancakalong District. This reduction is due to widespread conversion of mixed garden locations to built-up and bare land areas. In northeastern areas, the increase in upland agricultural LULC classes resulted in a reduction of vegetation coverage in tree-based agricultural LULC classes. This reduction led to a slight decrease in aboveground carbon stocks in this area. The major causes of vegetation cover reduction were mainly attributed to the conversion of forests and mixed gardens (as the most vegetated LULC classes) to paddy fields. The expansion of paddy fields at the expense of forests and mixed gardens might be driven by population growth coupled with an increase in the requirement for paddy field cultivation as subsistence. Another cause for this vegetation cover reduction might be related to the abandonment of mixed garden areas after harvesting perennials, resulting in the areas being converted to shrublands.

*The effect of land use and land cover changes on carbon stocks*

The spatial model of aboveground carbon stocks generated by InVEST shows that in 2009, the total stock of aboveground carbon in Rancakalong District was 324,821 tons. In comparison, the total stock of aboveground carbon in 2021 was 313,725 tons. The aboveground carbon stock potential varied among all LULC classes. In 2009, the highest aboveground carbon stocks were from mixed gardens, which had a total carbon stock of 64%. This carbon stock level was followed by forest (20%) and other agricultural LULC classes, namely, drylands (12%) and paddy fields (2%) (Fig. 6). In 2021, the highest aboveground carbon stocks were also in mixed gardens, which contributed 52%. This level was followed by forests (22%), shrubs (15%), and drylands (7%) (Fig. 6). According to the numeric statistics model generated by InVEST, there was a decrease in aboveground carbon density in the study area by 11,096 tons between 2009 and 2021. A significant decrease occurred in the mixed-garden LULC class. The number of aboveground carbon stocks in mixed gardens decreased from 64% to 52%. A decrease in aboveground carbon density also occurred in drylands, with a reduction from 12% to 7%. Conversely, there was an increase in

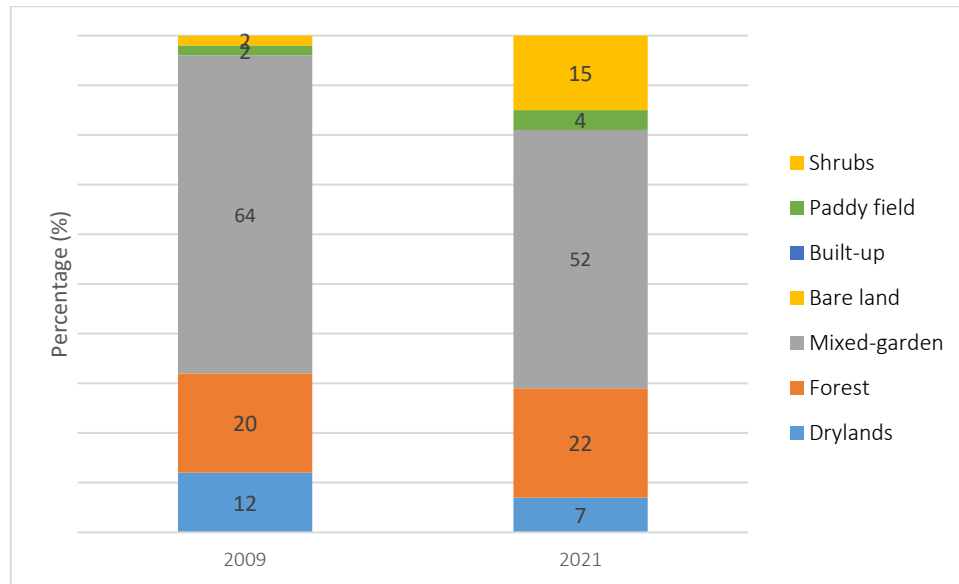


Fig. 6: Percentage of aboveground carbon stock distribution for each LULC class

aboveground carbon stocks in forests (20%–22%), shrubs (2%–15%), and paddy fields (2%–4%) (Fig. 6).

The aboveground carbon stocks of vegetated areas were greater than the potential carbon stocks of other LULC classes. Forests and mixed gardens were considered to be vegetated areas because vegetation stand coverage was dominant in both classes. As shown in Fig. 6, the combined aboveground carbon stocks in forests and mixed gardens were significantly higher than those in other LULC classes (84% in 2009 and 74% in 2021). Forest aboveground carbon density was relatively higher than that in agricultural areas. As presented in Fig. 6, in both 2009 and 2021, forests contributed more carbon storage (20% and 22%, respectively) than agricultural areas, such as drylands (14%) and paddy fields (11%), respectively. However, mixed gardens were the only exception. As agricultural areas, mixed gardens have significantly higher aboveground carbon stock densities than forests. For both 2009 and 2021, mixed gardens contributed more to aboveground carbon stocks than forests, with a comparison of 64% to 20% in 2009 and 52% to 22% in 2021. This advantage is because the total area of the mixed garden was larger than the forest area, as shown in Table 1. In 2009, mixed gardens were the largest LULC class, with an area of 1736.90 ha, compared to forests, which had a total area of 1134.54 ha. Although the forest area increased to 1218.73 ha in 2021, the total area of the mixed gardens was still the largest in the study site, with 1413.36 ha.

Hairiah et al. (2011) stated that the aboveground carbon stock potential of forests is relatively higher than that of any other vegetated land cover. However, in this study area, the aboveground carbon stocks in mixed gardens were higher than stocks in forests. This preponderance is associated with the structure and composition of the tree-based farming system. The case study in Rancakalong District, Sumedang, Indonesia shows that different LULC activities lead to variability in aboveground carbon storage potential within all LULC classes in a landscape with a mix of agriculture and forest.

In the study area, more vegetated LULC classes had increased aboveground carbon stock potential compared to less vegetated LULC classes, although less vegetated LULC classes covered a larger area. In comparison to open agricultural areas, shrubs, built-

up areas, and bare land, dense forests have higher aboveground carbon stocks. A study conducted by Piyathilake et al. (2022) revealed that carbon storage in natural forests was significantly higher than that in agricultural LULC classes, although the area of forest cover was much lower than that in the other LULC classes combined. Additionally, a sparse forest was shown to have more potential for carbon storage than agricultural land (Bera et al., 2022). Carbon storage and sequestration were also positively correlated with the degree of green density of vegetation growth, and a dense forest had the greenest density (Chacko et al., 2018). Confirming these findings, the highest number of aboveground carbon stocks in Rancakalong District was located in the LULC classes with the highest density of vegetation cover. However, in the study site, mixed gardens were the largest contributor to carbon stocks, not forests. Mixed-gardens, which are a tree-based agricultural system, contained the highest number of carbon stocks, even though these stocks were greatly depleted between 2009 and 2021. The percentage of carbon stored in mixed gardens decreased from 64% to 52%, mainly due to a reduction in this LULC class area from 1736.90 ha to 1413.36 ha between 2009 and 2021. However, the carbon density data for mixed gardens may fluctuate concerning the influence of carbon deposition during the harvesting time of vegetation stands. This may result in uncertainty about the change in aboveground carbon stocks over time (Wang et al., 2022). Furthermore, the carbon sequestration and carbon storage potentials of agricultural areas were probably underestimated, as the carbon sinks were potentially offset during harvesting time (Paquit and Mindana, 2017). The fact that mixed gardens had a higher carbon storage potential than forests was related to the structure and composition of the vegetation in this tree-based agricultural system. Mixed gardens, which are generally located on hillslopes of Rancakalong District, are agroforestry systems. They are a common agroforestry system in West Java, Indonesia, and are known locally as *talun* or *kebon tatangkalan* (Parikesit et al., 2005). In the study area, this type of agroforestry comprises bamboo species (*Gigantochloa atter*, *Schizostachyum brachycladum*, *Dendrocalamus asper*), fruit trees (*Durio zibethinus*, *Artocarpus heterophyllus*, *Persea americana*), and timber trees

(*Swietenia macrophylla*, *Maesopsis eminii*, and *Tectona grandis*). These trees are cultivated with a mixture of aromatics and rhizomes, such as clover, coffee, ginger, and cardamom. The *talun* gradually evolved from a mixture of annual crops and tree seedlings. The field was frequently abandoned after the annuals were harvested, after which perennials dominated the agricultural area (Christanty *et al.*, 1986). During the abandonment phase, the perennials continually grew and became mature. As the perennials dominated, the agricultural area resembled secondary forest fallow and was essentially a man-made forest (Soemarwoto, 1984). The *talun* consisted of a mixture of perennial trees with a multilayered canopy as a key characteristic of this traditional agroforestry system (Soemarwoto, 1984). The findings on the carbon stock potential of this tree-based *talun* agricultural system corroborated a previous study on aboveground carbon stocks in Rancakalong revealing that the coffee-based agroforestry system had higher carbon storage potential than secondary forests. This greater potential was due to the dominance of sparse vegetation with a smaller diameter in some of the secondary forests (Luth and Setiyono, 2019). The result is in line with findings by Natalia *et al.* (2016), who stated that the basal area of trees is strongly correlated with total carbon stocks in natural forests and agroforestry. This study found that the change in aboveground carbon stocks was mainly attributed to LULC change. There was a decrease in total aboveground carbon stocks by 11,096 tons between 2009 and 2021. This carbon storage reduction was mainly related to urban expansion in Rancakalong District. The construction of the Cisumdawu Highway, which started in 2013, was at the expense of vegetated LULC classes. This construction might have contributed to the reduction in aboveground carbon stocks in the study area. Data from 2021 show that the construction of the highway resulted in a significant increase in bare land cover as a result of LULC conversion from tree-based agroforestry and other agricultural land use classes. A 138.70-ha increase in bare land in 2021 was due to the change in LULC classes with larger carbon inventories, such as mixed gardens, paddy fields, and drylands. This change reduced the total number of aboveground carbon stocks in the Rancakalong District. A study conducted in the

Silang-Santa Rosa Watershed in the Philippines also showed that the continuous expansion of urban areas resulted in a decrease in the total number of carbon stocks (Dida *et al.*, 2021). Similarly, the rapid increase in built-up land because of farmland conversion was linked to a decline in carbon storage capability in northwestern China (Liang *et al.*, 2017). The reduction in aboveground carbon stocks was also related to the conversion of forest cover and other vegetated LULC classes into croplands. The findings of Pellikka *et al.* (2018) in Afromontane in Kenya showed that the deterioration of forest cover and shrublands directly caused a reduction in carbon sequestration. In this study, the reduction in aboveground carbon stocks in the vegetated area generally resulted from the abandonment of some mixed gardens after the mature trees were harvested. This process led to the massive conversion of mixed gardens to shrublands between 2009 and 2021, which contain lower aboveground carbon stock potential. As a result, during the fallow period, there were only shrubs and undergrowth vegetation cover. Developing a spatial distribution of aboveground carbon storage within different LULC classes provides information about the potential of different LULC classes in carbon storage and sequestration. The spatial dynamics of aboveground carbon stocks reveal how aboveground carbon stocks fluctuate over time within different LULC classes as a result of anthropogenic interventions such as urban expansion and agricultural management. Carbon stocks in other carbon pools (belowground biomass, soil, litter, and necromass) must be further studied, including the use of higher resolution remote sensing data and enhancing the sample size at the plot level to comprehensively map the dynamics of carbon storage and carbon stock potential in the research area across a variety of land uses. As this study only relies on business-as-usual LULC trends, it is essential to develop various LULC change scenarios. The results of carbon stock estimation and modeling using INVEST should be considered in decision-making processes related to environmental management and regional development plans (spatial plans). These data could be used as a basis for a carbon credit scheme to protect vegetated areas and combat climate change.

Tree-based agricultural systems (mixed gardens) have shown significant potential in carbon storage.

Therefore, this LULC class needs appropriate management strategies to enhance carbon storage potential while simultaneously reducing carbon emissions. Conservative farming practices in the form of mixed gardens should be enhanced to boost subsistence farming without undermining the potential of this agricultural landscape to contribute to carbon sequestration and climate change mitigation.

## CONCLUSION

This study emphasizes the correlation between LULC changes and aboveground carbon stocks. Furthermore, this work examines how LULC conversions such as urban expansion and agricultural management put direct pressure on carbon storage potential in different LULC classes. Massive construction and agricultural expansion are still occurring in the study area; therefore, it is critical to detect the carbon stock levels affected by LULC changes. The present study attempts to incorporate a few ground-based inventories of carbon stocks into GIS and remote sensing approaches and integrates the inventory data with the InVEST spatial carbon dynamics model. The results of supervised classification on remotely sensed satellite images showed that vegetated land was predominant in 2009 and 2021. Vegetation covered 51% of the total area in 2009 and increased by 6% in 2021, resulting in 57% of vegetation area coverage. Regarding agricultural area, mixed gardens and drylands decreased between 2009 and 2021 by 6% and 8%, respectively. Meanwhile, paddy fields were the only agricultural land use to increase by 2% between 2009 and 2021. The bare land and built-up expansion related to the observed land clearing for the Cisumdawu Highway mainly came from the conversion of mixed gardens, paddy fields, and drylands. This study has demonstrated that LULC changes in the Rancakalong District have caused a reduction in aboveground carbon stocks by 11,096 tons between 2009 and 2021. Based on the results of the InVEST spatial and statistical models, a reduction in aboveground carbon stocks occurred in the mixed gardens and drylands, with the highest reduction occurring in mixed gardens. Indeed, the number of aboveground carbon stocks in mixed gardens declined from 64% to 52%. In those mixed gardens were the most common LULC

class in the study area in both 2009 and 2021, the massive reduction in this agricultural area caused a significant decrease in aboveground carbon stocks, although a slight increase in aboveground carbon stocks occurred in forests, shrubs, and paddy fields. This shortage of carbon stock potential was mainly attributed to the abandonment of this tree-based agricultural system after harvesting and led to the massive conversion of mixed gardens to shrublands, which contain lower aboveground carbon stock potential. The construction of the Cisumdawu Highway, which started in 2013, was at the expense of vegetated LULC classes. This development might have contributed to the reduction in aboveground carbon stocks in the study area. The results of remotely sensed data from 2021 show that the construction of the highway resulted in a significant increase in bare land cover as a result of LULC conversion from tree-based agroforestry and other agricultural land use classes. A 138.70-ha increase in bare land in 2021 was due to the conversion of LULC classes to those with larger carbon stocks, particularly mixed gardens. In the future, it is crucial to conserve this bioproduction system with long-term protection mechanisms as this tree-based agricultural system (mixed gardens) showed great potential in aboveground carbon storage. The model should be considered in decision-making processes related to environmental management and regional development plans (spatial plans). Further studies may consider alternative scenarios in LULC changes.

## AUTHOR CONTRIBUTIONS

A.D. Malik performed the study conceptualization, literature review, data collection, analysis and interpretation of results, spatial data preparation, and draft manuscript preparation. M.C.W. Arief performed the interpretation of results, spatial data preparation, and draft manuscript preparation. S. Withaningsih performed the draft manuscript preparation and manuscript editing. Parikesit helped in manuscript text preparation and manuscript text evaluation.

## ACKNOWLEDGEMENT

The research was funded by the Ministry of Research and Higher Education (DIKTI) of Indonesia in the research Grant of 'Penelitian Dasar Unggulan Perguruan Tinggi (PDUPT)' [Grant number 2393/UN6.3.1/PT.00/2022] and Universitas Padjadjaran

in the internal research Grant of ‘Hibah Riset Universitas Padjadjaran 2023’ [Grant number 1549/UN6.3.1/PT.00/2023]. The authors also thank the E-Asia Joint Research Program (JRP) ITMoB for supporting this study.

### CONFLICT OF INTEREST

The author declares that there is no conflict of interest regarding the publication of this manuscript. In addition, ethical issues, including plagiarism, informed consent, misconduct, data fabrication and/or falsification, double publication and/or submission, and redundancy, have been completely observed by the authors.

### OPEN ACCESS

©2024 The author(s). This article is licensed under a Creative Commons Attribution 4.0 International License, which permits use, sharing, adaptation, distribution, and reproduction in any medium or format, as long as you give appropriate credit to the original author(s) and the source, provide a link to the Creative Commons license, and indicate if changes were made. The images or other third-party material in this article are included in the article’s Creative Commons license, unless indicated otherwise in a credit line to the material. If material is not included in the article’s Creative Commons license and your intended use is not permitted by statutory regulation or exceeds the permitted use, you will need to obtain permission directly from the copyright holder. To view a copy of this license, visit: <http://creativecommons.org/licenses/by/4.0/>

### PUBLISHER’S NOTE

GJESM Publisher remains neutral with regard to jurisdictional claims in published maps and institutional affiliations.

### ABBREVIATIONS

%	Percent
$\theta_s$	Angle of the sun’s zenith in degrees
$\rho$	Wood density
$\rho\lambda'$	Top of atmosphere reflectance
$\rho_p$	Planetary reflectance

$\rho_\lambda$	Surface reflectance
$\pi$	Phi
%	Percent
$A_L$	The metadata’s additive rescaling factor
-	Additive rescaling factor from the metadata for each band
$A_p$	
AGB	Total aboveground biomass
<i>ArcMap</i>	Geographic information as a collection of layers and other elements in a map
C	Celsius
$CO_2$	Carbondioxide
csv	Comma separated value
d	The astronomic distance between earth and sun
DBH	Diameter at breast height
DN	Digital numbers
DOS1	Dark object subtraction 1
$E_{down}$	The downwelling diffuse irradiance
$ESUN_\lambda$	The mean value of solar exo-atmospheric irradiances
GIS	Geographic information systems
$gr/cm^3$	Gram per cubic centimeter
GAEZ+	Global agro-ecological zones’ +
Gt	Gigatons
ha	Hectares
<i>InVEST</i>	Integrated valuation of ecosystem services and tradeoffs
IPCC	Intergovernmental Panel on Climate Change
km	Kilometers
$L_\lambda$	Top of atmosphere spectral radiance
$L_p$	Path radiance
LULC	Land use and land cover
$M_p$	Metadata-derived band-specific multiplicative rescaling factor

$M_L$	Metadata-derived multiplicative rescaling factor
$m$	Meters
$m^2$	Square meters
$mm/y$	Milimeters per year
$MLC$	Maximum likelihood classification
$MTL$	Metadata text file extension
$MW$	Megawatts
$n$	Number of plots
$NDVI$	Normalized difference vegetation index
$NIR$	Near-infrared band
$OLI$	Operational land imager
$ppm$	Parts per million
$Q_{cal}$	Standard product pixel values or digital number value of a specific pixel
$SCP$	Semiautomatic classification plugin
$SEE$	Standard errors of estimate
$T$	Tree height
$T_v$	Atmospheric transmittance in the viewing direction
$T_z$	Atmospheric transmittance in the illumination direction
$tiff$	Temporary instruction file format
$TM$	Thematic mapper
$TOA$	Top of atmosphere
$tons/ha$	Tons per hectare
$Y_i$	Carbon value in plot number- $i$

## REFERENCES

- Arredondo-Trapero, F.G.; Guerra-Leal, E.M.; Kim, J., (2023). Effectiveness of the voluntary disclosure of corporate information and its commitment to climate change. *Global J. Environ. Sci. Manage.*, 9(4): 1033-1048 **(16 pages)**.
- Atsatryan, H.; Hayrapetyan, A.; Narsisian, W.; Asmaryan, S.; Saghatlyan, A.; Muradyan, V.; Giuliani, G.; Guigoz, Y.; Ray, N., (2015). An interoperable cloud-based scientific GATEWAY for NDVI time series analysis. *Comput. Stand. Interfaces.* 4: 79-84 **(6 pages)**.
- Bagstad, K.J.; Semmens, D.J.; Waage, S.; Winthrop, R., (2013). A comparative assessment of decision-support tools for ecosystem services quantification and valuation. *Ecosyst. Serv.*, 5: 27-39 **(13 pages)**.
- Basalumi, L.; Kilawe, C.J.; Mauya, E.W., (2018). Linking ground forest inventory and NDVI in mapping above ground carbon stock in Kasane Forest Reserve, Botswana. *Open J. For.*, 8(3): 429-438 **(10 pages)**.
- Batsaikhan, B.; Lkhamjav, O.; Batsaikhan, G.; Batsaikhan, N.; Norovsuren, B., (2020). Carbon stock estimation using remote sensing data and field measurement in haloxylon ammodendron dominant winter cold desert region of Mongolia. In XXIV ISPRS Congress, Commission III (Volume V-3-2020)- 2020 edition.
- Bera, B.; Bhattacharjee, S.; Sengupta, N.; Shit, P.K.; Adhikary, P.P.; Sengupta, D.; Saha, S., (2022). Significant reduction of carbon stocks and changes of ecosystem service valuation of Indian Sundarban. *Sci. Rep.*, 12: 7809 **(17 pages)**.
- Bosino, A.; Omran, A.; Maerker, M., (2019). Identification, characterisation and analysis of the Oltrepo Pavese calanchi in the Northern Apennines (Italy). *Geomorphology*, 340: 53-66 **(14 pages)**.
- Cahyono, W.; Parikesit; Joy, B.; Setyawati, W.; Mahdi, R., (2022). Projection of CO<sub>2</sub> emissions in Indonesia. In 2nd International Conference on Chemical Engineering and Applied Sciences. Semarang, Indonesia 3 - 4 November. UNDIP: Indonesia.
- Calderón-Contreras, R.; Quiroz-Rosas, L.E., (2017). Analysing scale, quality and diversity of green infrastructure and the provision of urban ecosystem services: A case from Mexico City. *Ecosyst. Serv.*, 23: 127-137 **(11 pages)**.
- Chacko, S.; Ravichandran, C.; Vairavel, S.M.; Mathew, J., (2018). Employing measurers of spatial distribution of carbon storage in Periyar Tiger Reserve, Southern Western Ghats, India. *J. Geovisualization Spatial Anal.*, 3(1): 1-7 **(7 pages)**.
- Chander, G.; Markham, B., (2003). Revised Landsat-5 TM radiometric calibration procedures and postcalibration dynamic ranges. *IEEE Trans. Geosci. Remote Sens.*, 41(11): 2674-2677 **(4 pages)**.
- Chave, J.; Andalo, C.; Brown, S.; Cairns, M. A.; Chambers, J.Q.; Eamus, D.; Fölster, H.; Fromard, F.; Higuchi, N.; Kira, T.; Lescure, J.-P.; Nelson, B.W.; Ogawa, H.; Puig, H.; Riéra, B.; Yamakura, T., (2005). Tree allometry and improved estimation of carbon stocks and balance in tropical forests. *Oecologia*. 145(1): 87-99 **(13 pages)**.
- Chavez Jr., P.S., (1989). Radiometric calibration of Landsat Thematic Mapper multispectral images. *Photogramm. Eng. Remote Sens.*, 55(9): 1285-1294 **(10 pages)**.
- Christanty, L.; Abdoellah, O.S.; Marten, G.; Iskandar, J., (1986). Traditional agriculture in southeast Asia: A human ecology perspective. Westview Press.
- Cong, W.; Sun, X.; Guo, H.; Shan, R., (2020). Comparison of the SWAT and InVEST models to determine hydrological ecosystem service spatial patterns, priorities and trade-offs in a complex basin. *Ecol. Indic.*, 112: 1-13 **(13 pages)**.
- Coutinho, H.L.C.; Noellemeyer, E.; Balieiro, F.de C.; Piñeiro,

- G.; Fidalgo, E.C.C.; Martius, C.; Silva, C. F.da., (2015). Impacts of land-use change on carbon stocks and dynamics in central-southern South American biomes: Cerrado, Atlantic Forest and Southern Grasslands, in : Banwart S.A., Noellemeyer E., Milne, E. (Eds.), Soil carbon: science, management and policy for multiple benefits. CABI Digital Library.
- Darmawan, A.A.; Ariyanto, D.P.; Basuki, T.M.; Syamsiyah, J.; Dewi, W.S., (2022). Biomass accumulation and carbon sequestration potential in varying tree species, ages and densities in Gunung Bromo Education Forest, Central Java, Indonesia. *Biodiversitas*. 23(10): 5093-5100 **(8 pages)**.
- Davies, T.; Everard, M.; Horswell, M., (2016). Community-based groundwater and ecosystem restoration in semi-arid north Rajasthan (3): evidence from remote sensing. *Ecosyst. Serv.*, 21(2016): 20-30 **(11 pages)**.
- Dewanto, B.E.B.; Jatmiko, R.H., (2021). Estimation of aboveground carbon stock using SAR Sentinel-1 imagery in samarinda city. *IJReSES*. 18(1): 103-116 **(14 pages)**.
- Dida, J.J.; Tiburan Jr.,C.; Tsutsumida, N.; Saizen, I., (2021). Carbon stock estimation of selected watersheds in Laguna, Philippines Using InVEST. *Philipp J. Sci.*, 150(2): 501-513 **(13 pages)**.
- FAO, (2016). Global forest resources assessment 2015: How are the world's forests changing? (second edition). Food and Agriculture Organization of the United Nations, Rome.
- Forestry Economics and Policy Division, (2010). Global forest resources assessment 2010—main report. Food and Agriculture Organization of the United Nations, Rome.
- Frolking, S.; Wisser, D.; Grogan, D.; Prousevitch, A.; Glidden, S., (2020). GAEZ+<sub>2015</sub> crop yield. Harvard Dataverse.
- Frimawaty, E.; Ilmika, A.; Sakina, N.A; Mustabi. J., (2023). Climate change mitigation and adaptation through livestock waste management. *Global J. Environ. Sci. Manage.*, 9(4): 691-706 (16 pages).
- Hairiah, K.; Dewi, S.; Agus, F.; Velarde, S.; Ekadinata, A.; Rahayu, S.; van Noordwijk, M., (2011). Measuring carbon stocks across land use systems: a manual. World Agroforestry Centre (ICRAF) SEA Region Office, Bogor.
- Harper, A.B.; Wiltshire, A.J.; Cox, P.M.; Friedlingstein, P.; Jones, C.D.; Mercado, L.M.; Sitch, S.; Williams, K.; Duran-Rojas, C., (2018). Vegetation distribution and terrestrial carbon cycle in a carbon cycle configuration of JULES4.6 with new plant functional types. *Geosci. Model Dev.*, 11(7): 2857-2873 **(17 pages)**.
- Hassan, W.H.; Nile, B.K., (2021). Climate change and predicting future temperature in Iraq using CanESM2 and HadCM3 modeling. *Model. Earth Syst. Environ.*, 7(2): 737-748 **(12 pages)**.
- Hua, A.K.; Ping, O.W., (2018). The influence of land-use/land-cover changes on land surface temperature: A case study of Kuala Lumpur metropolitan city. *Eur. J. Remote Sens.*, 51(1): 1049-1069 **(21 pages)**.
- IPCC, (2022). Global Warming of 1.5°C: IPCC special report on impacts of global warming of 1.5°C above pre-industrial levels in context of strengthening response to climate change, sustainable development, and efforts to eradicate poverty (1st ed.). Cambridge University Press, Cambridge.
- IPCC, (2014). AR5 synthesis report: climate change 2014: Intergovernmental Panel for Climate Change.
- Jagdish, J.; Erayya; Makanur, B.; Sajeesh, P.K.; Managanvi, K., (2013). Prospects for mitigation of greenhouse gas emission: in context to agriculture and climate change. *Environ. Ecol.*, 31(2): 551-557 **(7 pages)**.
- Jamali, S.; Seaquist, J.W.; Ardö, J.; Eklundh, L., (2011). Investigating temporal relationships between rainfall, soil moisture and Modis-Derived NDVI and EVI for six sites in Africa. in 34th International Symposium on Remote Sensing of Environment. Sydney, Australia 10-15 April. International Center for Remote Sensing of Environment: Tucson.
- Javaherian, M.; Ebrahimi, H.; Aminnejad, B., (2021). Prediction of changes in climatic parameters using CanESM2 model based on RCP scenarios (case study): Lar dam basin. *Ain. Shams. Eng. J.*, 12(1): 445-454 **(10 pages)**.
- Jaya, L.M.G.; Saputra, R.A.; Idrus, S.H., (2022). Using support vector machine to identify land cover change during covid-19 pandemic in Komodo National Park, Indonesia. *Geogr. Environ. Sustainability*. 15(3): 70-79 **(10 pages)**.
- Jiang, H.; Wu, W.; Wang, J.; Yang, W.; Gao, Y.; Duan, Y.; Ma, G.; Wu, C.; Shao, J., (2021). Mapping global value of terrestrial ecosystem services by countries. *Ecosyst. Serv.*, 52(2021): 101361 **(10 pages)**.
- Karbassi, A.R.; Tajziehchi, S.; Afshar, S., (2015). An investigation on heavy metals in soils around oil field area. *Global J. Environ. Sci. Manage.*, 1(4): 275-282 **(8 pages)**.
- Khaerani, R.; Sitorus, S.R.P.; Rusdiana, O., (2018). Analysis of land use deviation based on spatial plan in Sumedang Regency. *TATALOKA*. 20(4): 399-409 **(11 pages)**.
- KLHK, (2018). The state of Indonesia's forests 2018. Ministry of Environment and Forestry Republic of Indonesia (KLHK), Jakarta.
- Kusumaningtyas, M.A.; Kepel, T.L.; Solihuddin, T.; Lubis, A.A.; Putra, A.D.P.; Sugiharto, U.; Ati, R.N.A.; Salim, H.L.; Mustikasari, E.; Heriati, A.; Daulat, A.; Sudirman, N.; Suryono, D.D.; Rustam, A., (2022). Carbon sequestration potential in the rehabilitated mangroves in Indonesia. *Ecol. Res.*, 37(1): 80-91 **(12 pages)**.
- Lahiji, R. N.; Dinan, N.M.; Liaghati, H.; Ghaffarzadeh, H.; Vafaeinejad, A., (2020). Scenario-based estimation of catchment carbon storage: Linking multi-objective land allocation with InVEST model in a mixed agriculture-forest landscape. *Front. Earth Sci.*, 14(3): 637-646 **(10 pages)**.
- Latifah, S.; Muhdi, M.; Purwoko, A.; Tanjung, E., (2018). Estimation of aboveground tree biomass *Toona sureni* and *Coffea arabica* in agroforestry system of Simalungun, North Sumatra, Indonesia. *Biodiversitas*. 19(2): 670-675 **(6 pages)**.

- Lee, H.; Seo, B.; Cord, A.F.; Volk, M.; Lautenbach, S., (2022). Using crowdsourced images to study selected cultural ecosystem services and their relationships with species richness and carbon sequestration. *Ecosyst. Serv.*, 54(2022): 101411 **(12 pages)**.
- Li, S.; Wang, W.; Ganguly, S.; Nemani, R.R., (2018). Radiometric characteristics of the Landsat collection 1 dataset. *Int. J. Adv. Remote Sens.*, 7(3): 203-217 **(14 pages)**.
- Liang, Y.; Liu, L.; Huang, J., (2017). Integrating the SD-CLUE-S and InVEST models into assessment of oasis carbon storage in northwestern China. *PLoS One.* 12(2): e0172494 **(15 pages)**.
- Liu, J.; Sleeter, B.M.; Zhu, Z.; Heath, L.S.; Tan, Z.; Wilson, T.S.; Sherba, J.; Zhou, D., (2016). Estimating carbon sequestration in the piedmont ecoregion of the United States from 1971 to 2010. *Carbon Balance Manage.*, 11(10): 10-22 **(13 pages)**.
- Liu, J.; Mason, P.J.; Bryant, E.C., (2018). Regional assessment of geohazard recovery eight years after the Mw7.9 Wenchuan earthquake: A remote-sensing investigation of the Beichuan region. *Int. J. Remote Sens.*, 39(6): 1671-1695 **(25 pages)**.
- Luth, F.; Setiyono, H., (2019). Capacity of coffee-based agroforestry in carbon storage. *Paspalum*, 7(1): 34-41 **(8 pages)**.
- Marchetti, Z.Y.; Minotti, P.G.; Ramonell, C.G.; Schivo, F.; Kandus, P., (2016). NDVI patterns as indicator of morphodynamic activity in the middle Paraná River floodplain. *Geomorphology*, 253: 146-158 **(13 pages)**.
- Masseti, A.; Gil, A., (2020). Mapping and assessing land cover/land use and aboveground carbon stocks rapid changes in small oceanic islands' terrestrial ecosystems: a case study of Madeira Island, Portugal (2009–2011). *Remote Sens. Environ.*, 239(2020): 111625 **(11 pages)**.
- Masripatin, N.; Gustan, P.; Wayan, S.; Chairil, A.; Ari, W.; Dyah, S.; Arief, Niken, S.; Mega, L.; In-dartik; Wening, W.; Saptadi, D.; Ika, H.; Heriyanto, N.; Haris, S.; Rath, D.; Dian, A.; Haruni, K.; Bayu, S., (2010). Carbon stocks in many types of forests and plants in Indonesia. Pusat Penelitian dan Pengembangan Perubahan Iklim dan Kebijakan, Bogor.
- Millennium Ecosystem Assessment, (2005). *Ecosystems and human well-being: wetlands and water synthesis: a report of the Millennium Ecosystem Assessment.* World Resources Institute, Washington DC.
- Moran, M.S.; Jackson, R.D.; Slater, P.N.; Teillet, P.M., (1992). Evaluation of simplified procedures for retrieval of land surface reflectance factors from satellite sensor output. *Remote Sens. Environ.*, 41(2): 169-184 **(16 pages)**.
- Natalia, D.; Arisoelaningsih, E.; Hairiah, K., (2016). Are high carbon stocks in agroforests and forest associated with high plant species diversity? *AGRIVITA.* 39(1): 74-82 **(9 pages)**.
- Nelson, E.; Mendoza, G.; Regetz, J.; Polasky, S.; Tallis, H.; Cameron, Dr.; Chan, K.M.; Daily, G.C.; Goldstein, J.; Kareiva, P.M.; Lonsdorf, E.; Naidoo, R.; Ricketts, T.H.; Shaw, Mr., (2009). Modeling multiple ecosystem services, biodiversity conservation, commodity production, and tradeoffs at landscape scales. *Front. Ecol. Environ.*, 7(1): 4-11 **(8 pages)**.
- Nijhawan, R.; Jain, K., (2018). Glacier terminus position monitoring and modeling using remote sensing data, in: M. Singh, P.K., Gupta, V., Tyagi, J., Flusser, Ören, T. (Eds.), *Advances in computing and data sciences.* Springer Singapore. Singapore.
- Ostadhashemi, R.; Rostami, S.T.; Roehle, H.; Mohammadi, L.S., (2014). Estimation of biomass and carbon storage of tree plantations in northern Iran. *J. For. Sci.*, 60(9): 363-371 **(9 pages)**.
- Paquit, J.; Mindana, F., (2017). Modeling the spatial pattern of carbon stock in Central Mindanao University using InVEST tool. *J. Bio. Environ. Sci.*, 10(4): 103-113 **(11 pages)**.
- Parikesit; Takeuchi, K.; Tsunekawa, A.; Abdoellah, O.S., (2005). Kebon tatangkalan: a disappearing agroforest in the Upper Citarum Watershed, West Java, Indonesia. *Agrofor. Syst.*, 63(2): 171-182 **(12 pages)**.
- Pellikka, P.K.E.; Heikinheimo, V.; Hietanen, J.; Schäfer, E.; Siljander, M.; Heiskanen, J., (2018). Impact of land cover change on aboveground carbon stocks in Afriomontane landscape in Kenya. *Appl. Geogr.*, 94: 178-189 **(12 pages)**.
- Piyathilake, I.D.U.H.; Udayakumara, E.P.N.; Ranaweera, L.V.; Gunatilake, S.K., (2022). Modeling predictive assessment of carbon storage using InVEST model in Uva province, Sri Lanka. *Model. Earth Syst. Environ.*, 8(2): 2213-2223 **(11 pages)**.
- Posner, S.; Verutes, G.; Koh, I.; Denu, D.; Ricketts, T., (2016). Global use of ecosystem service models. *Ecosyst. Serv.* 17(2016): 131-141 **(11 pages)**.
- Rouse, J.W.Jr.; Haas, R.H.; Schell, J.A.; Deering, D.W., (1974). *Monitoring vegetation systems in the great plains with erts.* NASA Special Publication, Washington DC.
- Saito, H.; Uchiyama, S.; Teshirogi, K., (2022). Rapid vegetation recovery at landslide scars detected by multitemporal high-resolution satellite imagery at ASO volcano, Japan. *Geomorphology.* 398(2022): 107989 **(9 pages)**.
- Sampurno, R.M.; Thoriq, A., (2016). Land cover classification using Landsat 8 Operational Land Imager (OLI) data in Sumedang Regency. *Teknotan.* 10(2): 61-70 **(10 pages)**.
- Senseman, G.M.; Bagley, C.F.; Tweddale, S.A., (1995). Accuracy assessment of the discrete classification of remotely-sensed digital data for landcover mapping. *US Army Corps of Engineers, Virginia.*
- Sharp, R.; Douglass, C.; Wolny, S.; Arkema, K.; Bernhardt, J.; Bierbower, N.; Chaumont, N.; Denu, D.; Fisher, D.; Glowinski, K.; Griffin, R.; Guannel, G.; Guerry, A.; Johnson, J.; Hamel, P.; Kennedy, C.; Kim, C.K.; Lacayo, M.; Lonsdorf, E.; Mandle, L.; Rogers, L.; Silver, J.; Toft, J.; Verutes, G.; Vogl, A.L.; Wood, S.; Wyatt, K., (2018). *InVEST 3.7.0 user's guide.* The Natural Capital Project, Stanford University,

- University of Minnesota, The Nature Conservancy, and World Wildlife Fund, California.
- Sharp, R.; Douglass, C.; Wolny, S.; Arkema, K.; Bernhardt, J.; Bierbower, N.; Chaumont, N.; Denu, D.; Fisher, D.; Glowinski, K.; Griffin, R.; Guannel, G.; Guerry, A.; Johnson, J.; Hamel, P.; Kennedy, C.; Kim, C.K.; Lacayo, M.; Lonsdorf, E.; Mandle, L.; Rogers, L.; Silver, J.; Toft, J.; Verutes, G.; Vogl, A.L.; Wood, S.; Wyatt, K., (2020). InVEST 3.10.2 user's guide. The Natural Capital Project, Stanford University, University of Minnesota, The Nature Conservancy, and World Wildlife Fund, California.
- Shrestha, M.; Piman, T.; Grünbühel, C., (2021). Prioritizing key biodiversity areas for conservation based on threats and ecosystem services using participatory and GIS-based modeling in Chindwin River Basin, Myanmar. *Ecosyst. Serv.*, 48: 101244 **(11 pages)**.
- Situmorang, J.P.; Sugianto, S.; Darusman., (2016). Estimation of carbon stock stands using EVI and NDVI vegetation index in production forest of Lembah Seulawah Sub-district, Aceh Indonesia. *Aceh Int. J. Sci. Technol.*, 5(3): 126-139 **(14 pages)**.
- Smith, G., (2015). *Essential statistics, regression, and econometrics*. Academic Press, California.
- Soemarwoto, O., (1984). The talun-kebun system, a modified shifting cultivation, in West Java. *The Environmentalist*. 4(1984): 96-98 **(3 pages)**.
- Solomon, N.; Birhane, E.; Tadesse, T.; Treydte, A.C.; Meles, K., (2017). Carbon stocks and sequestration potential of dry forests under community management in Tigray, Ethiopia. *Ecol. Processes*. 6(1): 20-30 **(11 pages)**.
- Solomon, N.; Pabi, O.; Annang, T.; Asante, I.K.; Birhane, E., (2018). The effects of land cover change on carbon stock dynamics in a dry Afromontane forest in northern Ethiopia. *Carbon Balance Manage.*, 13(1): 14-26 **(13 pages)**.
- Suharyanto, A.; Maulana, A.; Suprayogo, D.; Devia, Y.P.; Kurniawan, S., (2023). Land surface temperature changes caused by land cover/ land use properties and their impact on rainfall characteristics. *Global J. Environ., Sci. Manage.*, 9(3): 353-372 **(20 pages)**.
- Sumedang Regency, (2019). Decree of Sumedang Regent No. 51 Year 2019 : strategic plan for Rancakalong District, 2018—2023.
- Tang, Y.; Quaqin, S.; Tiezhu, S.; Zhensheng, L.; Guofeng, W., (2022). Spatiotemporal dynamics of forest ecosystem carbon budget in Guizhou: customisation and application of the CBM-CFS3 model for China. *Carbon Balance Manage.*, 17(1): 10-33 **(23 pages)**.
- Thom, D.; Rammer, W.; Seidl, R., (2017). The impact of future forest dynamics on climate: Interactive effects of changing vegetation and disturbance regimes. *Ecol. Monogr.*, 87(4): 665-684 **(19 pages)**.
- Thonfeld, F.; Steinbach, S.; Muro, J.; Hentze, K.; Games, I.; Näschen, K.; Kauzeni, P.F., (2020). The impact of anthropogenic land use change on the protected areas of the Kilombero catchment, Tanzania. *IISPRS J. Photogramm. Remote Sens.*, 168: 41-55 **(15 pages)**.
- Toru, T.; Kibret, K., (2019). Carbon stock under major land use/land cover types of Hades sub-watershed, astern Ethiopia. *Carbon Balance Manage.*, 14(1): 7-20 **(14 pages)**.
- Vafaei, S.; Soosani, J.; Adeli, K.; Fadaei, H.; Naghavi, H.; Pham, T.D.; Tien B.D., (2018). Improving accuracy estimation of forest aboveground biomass based on incorporation of ALOS-2 PALSAR-2 and Sentinel-2a imagery and machine learning: a case study of the hyrcanian forest area (Iran). *Remote Sens.*, 10(2): 172-192 **(21 pages)**.
- Wang, L.; Zhu, R.; Yin, Z.; Chen, Z.; Fang, C.; Lu, R.; Zhou, J.; Feng, Y., (2022). Impacts of land-use change on the spatio-temporal patterns of terrestrial ecosystem carbon storage in the Gansu Province, Northwest China. *Remote Sens.*, 14(13): 3164-3190 **(27 pages)**.
- Wani, A.A.; Bhat, A.F.; Gattoo, A.A.; Zahoor, S.; Mehraj, B.; Najam, N.; Wani, Q.S.; Islam, M.A.; Murtaza, S.; Dervash, M.A.; Joshi, P.K., (2021). Assessing relationship of forest biophysical factors with NDVI for carbon management in key coniferous strata of temperate Himalayas. *Mitigation Adapt. Strategies Global Change*. 26(1): 1-22 **(23 pages)**.
- Yesserie, A., (2009). Spatio-temporal land use/land cover changes analysis and monitoring in the Valencia Municipality, Spain. Ph.D. Dissertation, Universitat Jaume I Castellón, Spain.
- Zanne, A.E.; Lopez-Gonzalez, G.; Coomes, D.A.; Ilic, J.; Jansen, S.; Lewis, S.L.; Miller, R.B.; Swenson, N.G.; Wiemann, M.C.; Chave, J., (2009). Towards a worldwide wood economics spectrum (Version 5, p. 2047488 bytes). Dryad.
- Zhang, C.; Chen, K.; Liu, Y.; Kovacs, J.M.; Flores-Verdugo, F.; Santiago, F.J.F.de., (2012). Spectral response to varying levels of leaf pigments collected from a degraded mangrove forest. *J. Appl. Remote Sens.*, 6(1): 063501 **(14 pages)**.
- Zhao, K.; Wulder, M.A.; Hu, T.; Bright, R.; Wu, Q.; Qin, H.; Li, Y.; Toman, E.; Mallick, B.; Zhang, X.; Brown, M., (2019). Detecting change-point, trend, and seasonality in satellite time series data to track abrupt changes and nonlinear dynamics: a bayesian ensemble algorithm. *Remote Sens. Environ.*, 232(2019): 111181 **(20 pages)**.
- Zhao, Z.; Liu, G.; Mou, N.; Xie, Y.; Xu, Z.; Li, Y., (2018). Assessment of carbon storage and its influencing factors in Qinghai-Tibet Plateau. *Sustainability*. 10(6): 1864-1880 **(17 pages)**.
- Zhu, X.; Liu, D., (2015). Improving forest aboveground biomass estimation using seasonal Landsat NDVI time-series. *IISPRS J. Photogramm. Remote Sens.*, 102: 222-231 **(10 pages)**.

#### AUTHOR (S) BIOSKETCHES

**Malik, A.D.**, M.Sc., Assistant Professor, Center for Environment and Sustainability Science, Universitas Padjadjaran, Bandung, West Java, Indonesia.

- Email: [annas12001@mail.unpad.ac.id](mailto:annas12001@mail.unpad.ac.id)
- ORCID: 0000-0003-0588-387X
- Web of Science ResearcherID: HZL-2698-2023
- Scopus Author ID: 57683705500
- Homepage: [https://cess.unpad.ac.id/easia\\_annas/](https://cess.unpad.ac.id/easia_annas/)

**Arief, M.C.W.**, Ph.D., Associate Professor, Department of Fisheries, Faculty of Fisheries and Marine Science, Universitas Padjadjaran, Sumedang, West Java, Indonesia.

- Email: [mochamad.candra@unpad.ac.id](mailto:mochamad.candra@unpad.ac.id)
- ORCID: 0000-0003-3077-5934
- Web of Science ResearcherID: HZL-4715-2023
- Scopus Author ID: 56469720200
- Homepage: <https://fpik.unpad.ac.id/en/program-studi-perikanan/>

**Withaningsih, S.**, Ph.D., Associate Professor, Sustainability Science Masters Study Program, Graduate School, Universitas Padjadjaran, West Java, Indonesia.

- Email: [susanti.withaningsih@unpad.ac.id](mailto:susanti.withaningsih@unpad.ac.id)
- ORCID: 0000-0002-5893-0222
- Web of Science ResearcherID: AAB-6734-2021
- Scopus Author ID: 57195276031
- Homepage: <https://pasca.unpad.ac.id/en/about-graduate-school/organizational-structure/>

**Parikesit, P.**, Ph.D., Professor, Department of Biology, Faculty of Mathematics and Natural Sciences, Universitas Padjadjaran, Sumedang, West Java, Indonesia.

- Email: [parikesit@unpad.ac.id](mailto:parikesit@unpad.ac.id)
- ORCID: 0000-0001-8214-7126
- Web of Science ResearcherID: AAC-9331-2021
- Scopus Author ID: 55934491300
- Homepage: <https://www.biologi-unpad.ac.id/dosen/>

#### HOW TO CITE THIS ARTICLE

Malik, A.D.; Arief, M.C.W.; Withaningsih, S.; Parikesit, P., (2024). Modeling regional aboveground carbon stock dynamics affected by land use and land cover changes. *Global J. Environ. Sci. Manage.*, 10(1): 245-266.

DOI: [10.22034/gjesm.2024.01.16](https://doi.org/10.22034/gjesm.2024.01.16)

URL: [https://www.gjesm.net/article\\_704982.html](https://www.gjesm.net/article_704982.html)





## ORIGINAL RESEARCH PAPER

## Root growth and arbuscular mycorrhizal fungi on woody plants for vegetative stabilization of tropical slopes

I.G. Tejakusuma<sup>1</sup>, E.H .Sittadewi<sup>1\*</sup>, T. Handayani<sup>2</sup>, T. Hernaningsih<sup>3</sup>, W. Wisyanto<sup>1</sup>, A. Rifai<sup>2</sup><sup>1</sup> Center for Geological Disaster, National Research and Innovation Agency, Indonesia<sup>2</sup> Research Centre for Sustainable Production System and Life Cycle Assessment, National Research and Innovation Agency, Indonesia<sup>3</sup> Research Centre for Environmental and Clean Technology, National Research and Innovation Agency, Indonesia

## ARTICLE INFO

## Article History:

Received 08 January 2023

Revised 13 March 2023

Accepted 18 May 2023

## Keywords:

Arbuscular Mycorrhizal Fungi

Bamboo

Nutrient uptake

Root direction

Tree-root growth

Woody plants

## ABSTRACT

**BACKGROUND AND OBJECTIVES:** Arbuscular mycorrhizal fungi improve plant growth but have not been studied for slope stabilization. Inoculation of these fungi and bamboo intervention can enhance root growth toward the slip plane. The study tests tree roots' responses to seeding in bamboo tubes and the fungi consortium.**METHODS:** The growth of three fast-growing native Indonesian woody plants: *Paraserianthes falcataria*, *Acacia mangium*, and *Gmelina arborea*, was monitored in a screen house. These plants were seeded in bamboo tubes containing soil from Jati Radio and Citatah. The tubes were placed on an inclined plane resembling a 20o slope. Arbuscular mycorrhizal fungi were added in three doses and controlled by the plots without mycorrhiza and bamboo.**FINDINGS:** The results showed that bamboo could direct root growth toward the slip plane. The best arbuscular mycorrhizal fungi inoculation results were obtained in *Gmelina arborea* with a treatment dose of M3 or 30 grams on Jati Radio and Citatah soils. Both treatments did not show significant differences in both locations.**CONCLUSION:** *Gmelina arborea* has the highest phosphorus absorption at 80 percent and the highest biomass weight at 660 grams with M3 dose in Citatah, and 71 percent with 330 g at the same dose in Jati Radio, which is related to the optimal level of arbuscular mycorrhizal fungi inoculation. Therefore, this species provides the best option for implementing biotechnological strategies to stabilize slopes in areas prone to landslides. Combining bamboo with arbuscular mycorrhizal fungi can direct and accelerate root growth, with the goal of crossing landslide slip planes.DOI: [10.22034/gjesm.2024.01.17](https://doi.org/10.22034/gjesm.2024.01.17)This is an open access article under the CC BY license (<http://creativecommons.org/licenses/by/4.0/>).

NUMBER OF REFERENCES

57



NUMBER OF FIGURES

9



NUMBER OF TABLES

5

\*Corresponding Author:

Email: [euth001@brin.go.id](mailto:euth001@brin.go.id)

Phone: +6281 2903 8409

ORCID: [0000-0001-5240-3926](https://orcid.org/0000-0001-5240-3926)

Note: Discussion period for this manuscript open until April 1, 2024 on GJESM website at the "Show Article".

## INTRODUCTION

Climate-related disasters are expected to become more common in the coming years due to climate change. Climate change is expected to increase the frequency and intensity of extreme precipitation, resulting in landslide occurrence (Lin et al., 2020). Shifts in precipitation patterns caused by climate change contribute to an increase in the frequency of shallow landslides (Guo et al., 2023). Soil conditions, morphology, vegetation cover, and land use, all contribute to the site conditions that cause shallow landslides (Masi et al., 2023). In Indonesia, from 1815 to 2019, disaster events were dominated by climate-related disasters, comprising floods with 10.438 events, landslides with 6.050 events, droughts with 2.124 events, and forest fires with 1.914 events (Yulianto et al., 2021). Mitigation of landslide hazards depends on understanding the causes and triggering processes, which depend directly on soil properties, land use, and changes over time (Folletau et al., 2023). Slopes are the main topographic drivers for landslides, soil erosion, and nutrient loss (Abdalla et al., 2020). Vegetation stabilizes steep slopes, especially by increasing soil cohesion (Phillips et al., 2021). However, vegetation cover changes over time due to natural processes and land management practices or disturbances such as forest fires (Rengers et al., 2020). Vegetation restoration can reduce runoff and soil loss and increase solid organic carbon content (Yang et al., 2023). Deep-rooted vegetative cover is a potential solution to stabilize newly constructed slopes or repair shallow landslides (Asima et al., 2022). Plants, soil physical properties, thickness, and lithology stratigraphy are critical components. The aboveground parts of plants may limit erosion by intercepting raindrops and retarding surface runoff. Roots may help stabilize soil while reducing its water content through absorption and transpiration. However, it is not easy to improve slope stability through the growth of plants without detailed and in-depth knowledge of slope movements, soil properties, and the plants themselves. This study describes the experimental manipulation of the tree-root growth of three woody plant species native and economically beneficial to Indonesia, *Paraserianthes falcataria*, *Acacia mangium*, and *Gmelina arborea*, as a strategy for reducing shallow landslide hazards. Using arbuscular mycorrhizal fungi (AMF) and bamboo, we encouraged roots to grow downward across

imaginary slip planes, and were induced roots to increase the overall shear strength of the soil. A study on plant manipulation using these methods for landslide mitigation has not been performed elsewhere. In this study, AMF was intended to trigger and accelerate the growth of roots and plants. AMF is the most common fungus in the terrestrial ecosystem and forms a symbiotic relationship with the plant roots belonging to Glomeromycota (Thiergart et al., 2019). AMF infects the host plant's root system to produce external hyphae tissue that grows expansively and penetrates the subsoil layer, thereby increasing root capacity in nutrient and water absorption (Fattahi et al., 2021). The role of AMF in increasing the availability and absorption of P and other nutrients through the following process mechanisms: 1) chemical modification by mycorrhiza in the process of soil P solubility so that plants exude organic acids and acid phosphatase enzymes which accelerate the process of P mineralization. Root exudation occurs as a response of plants to P-deficient soil conditions, which affects the chemistry of the rhizosphere; 2) the diffusion distance of the phosphate ions can be shortened by the external hyphae of AMF, which can also function as phosphate absorbing and translocation tools; 3) P absorption still occurs in mycorrhizal plants even though it is below the minimum concentration where the roots are no longer able to absorb P and other nutrients. This process occurs due to higher external hyphae affinity or increased attraction of phosphate ions which causes faster P movement into the AMF hyphae (Bahadur et al., 2019). The role of AMF affects soil health and nutrient cycling in tropical slope environments. AMF plays an essential role in the conservation of nutrient cycles, helps to improve the soil structure (Fall et al., 2022), transports carbon in the root system (Busso and Busso, 2022), overcomes the degradation of soil fertility (Sekar et al., 2019), and protects plants from disease (Hou et al., 2022). AMF is a group of fungi belonging to the phylum Glomeromycota, which live in symbiosis with plant roots (Husna et al., 2022). Root infection obtained the best results in infecting roots when the plants began to adapt to the growing media because the roots in the soil have started to grow a lot or evenly in the roots so that AMF can infect more effectively. The optimal dose of AMF for woody plants is 20 g/plant containing approximately 200–250 spores (Rini et al.,

2021). The optimal time of inoculation and dose of AMF accelerated plant growth. Research by Khan *et al.* (2021) explained that AMF inoculation in the form of root pieces could increase the dry weight of shoots of signal grass by 0.15 gram (g) and the root dry weight by 0.06 g compared to plants without AMF. *Gmelina arborea*, *Acacia mangium*, and *Paraserianthes falcataria* are fast-growing, adaptable, and versatile plants that have invaded beyond their native areas (Koutika and Richardson, 2019). Taproots in woody plants grow downward parallel to plant growth. New lateral roots can be produced by the parent root at any stage of development, at any location along the parent root axis, and whenever necessary to modify the architecture of the root system in response to environmental stimuli (Montagnoli, 2019). The state of the art of root growth direction modification was performed using bamboo pots placed on a simulated inclined plane resembling a 20° slope. The bamboo pot method is combined with AMF to stimulate root growth. The bamboo is installed not in the form of a tube but in bamboo sticks which are placed around the tree in a certain diameter. For example, the estimated diameter is 0.5–1 m and the depth is adjusted to the depth of the slip plane at the site. Around the plants bordered by bamboo, soil is added with compost and AMF, which acts as a biological fertilizer. Thus, to a depth of more than 30–45 centimete (cm), nutrients are still used for growth until the time limit for root growth to come out of the bamboo circle and penetrate into the slip plane. Planting trees will have a good reinforcement effect on 20° and 35° slopes (Lan *et al.*, 2020). The proposed combined methods are breakthroughs in slope reinforcement and can be applied to prevent landslides. The growth of the root system is usually very plastic and acclimatized in response to specific stresses, for example, physical, soil chemical, or mechanical. Roots can respond to mechanics of varying strength. On steep slopes, the source of root strength is primarily located in the lower slope quadrant and is followed by the wind direction quadrant. The cross-sectional area of the roots at the point of attachment of the lateral roots to the taproot is more comprehensive in the lower slope quadrant. The critical role of roots is anchoring trees to the soil where they grow (Montagnoli, 2019). Roots can change the direction of growth in response to mechanical forces and other environmental

influences (Bujoczek *et al.*, 2021). The direction of root growth was modified using a bamboo tube placed on an inclined plane. Landslides on unstable slopes greater than 30° require appropriate bio and eco engineering techniques (Lan *et al.*, 2020). AMF has been widely used to enhance plant growth but is not intended for slope stabilization. Research on AMF inoculation for the improvement of lemongrass plants has been carried out by De Souza *et al.*, (2022). Combining bamboo tubes with AMF to stimulate root growth and direction provides a new technique for further landslide disaster mitigation that can be used on slopes to prevent landslides. Planting on sloping land has been conducted using various techniques, for example, palisades, brush layering, bamboo fences, and grass planting (Suresh and Dwivedi, 2022). However, this technique has a weakness: the direction of root growth does not reach deep; thus, the lower soil is easily eroded by water, and the plants fall easily. The technology of using bamboo to direct root growth and stimulate root growth with AMF is a breakthrough and a novelty of this study. There is currently no literature on these methods in other publications. Furthermore, because the plants have spread globally, the findings of this study have the potential to be widely used. Some fungi are infectious diseases if they penetrate cells (Jangjou, *et al.*, 2019), but AMF benefits plant growth. Concerning fungi, AMF has also been widely used in improving nutrient crisis land (Asmelash *et al.*, 2016). One of the causes of landslide-prone soil is in terms of the physical and chemical conditions of the soil so that plants do not thrive. Conditions like this can be corrected in advance with biochar. Biochar is a black carbon sorbent that can stabilize organic substances in soil (Yavari *et al.*, 2022a). Biochar, a carbon-rich bio-sorbent, has shown its ability to stabilize organic substances in soils and, therefore, potentially can reduce their leaching (Yavari *et al.*, 2022b). The experimental set-up in this study emulated conditions in slide-prone areas in Indonesia, where landslides and debris flows compose large proportions of the yearly disasters. The experiment replicated the slide-prone areas of Jati Radio (JR) and Citatah (CT) in West Java, where both regions have experienced landslides. This study aimed to test the effectiveness of several AMF doses, determine the appropriate dose to increase root growth and use bamboo tubes to modify the root growth direction. The most significant

results are the correct dose of AMF and the environmentally friendly technique to modify the direction of root growth for further plantings on a slope to mitigate landslide disasters. This study was conducted in JR and CT, West Java, Indonesia in 2021.

## MATERIALS AND METHODS

### Field landslide observations

Field observations for this study were performed in two Indonesian areas where shallow landslides had occurred: Citatah Town, Cipatat District, and Jati RadioTown, Cililin District. Both are located in the West Bandung Regency of West Java Province, Indonesia. The observations in the field were focused on the geology of landslides. A simple geological model of the landslides was developed based on the observations. The model guided experiments in a screened house.

### Artificial plant-root growth and growing media

The experiment was conducted in a screen house of plastic-screened bamboo with a 65 percent (%) paranet shade. The screen house was first designed and constructed to resemble the conditions of the two landslide models, CT and JR. A split plot design was used in a randomized block design, with three replications for each treatment. One plot was designed for the slope movement model for CT, and the other for JR. The CT plot was filled with bentonite clay, corresponding to the slip plane lithology in CT. The JR plot, by contrast, was filled with igneous rock clasts in the form of gravel with a small amount of sand as the slip plane in Jati Radio. The identification of mycorrhiza spores was performed in the laboratory. In this study, soil for growing media was collected from the two landslide areas, CT, and JR. The growing medium used was a 3:1 mixture of soil and compost. This medium was placed inside bamboo tubes. The bamboo's bottom was slanted, mimicking the slope in the field with a slope angle of 20°. The tube was 25 cm long on the short side and 30 cm long on the long side, with diameters ranging from 8 to 9 cm, allowing root growth to be directed vertically during the early stages of development. The plants were growing vertically as normal. In the experiments, the base of the bamboo was inclined to replicate the slope in the field. This is due to the slope which is a factor that influences the asymmetrical belowground development of the root (Wang *et al.*,

2023). For 4 months, all seedlings were enclosed in a screen house. The control plots refer to plots without AMF and not using bamboo tubes but polybags.

### Plant species

Three species of woody plants were used in this study: *Paraserianthes falcataria*, *Gmelina arborea*, and *Acacia mangium*. The plant seeds used were seedlings measuring 20 cm in height. These plants can be found in CT and JR. These fast-growing plants are essential for protecting against landslides as they can mitigate the risk faster. In addition, these trees offer economic benefits to the local community.

### Inoculum

Endogenous mycorrhiza, also known as AMF, was used in this study. The number of spores per 100 g of mycorrhiza consortium contained in the packaging was *Glomus* sp., 766 spores; *Glomus moseae*, 168 spores; *Scutellospora* sp., 29 spores; *Acaulospora* sp., 23 spores; *Gigaspora* sp., 11 spores; and *Gigaspora margarita*, 9 spores. The following four dosages were prepared: M0 = without mycorrhiza, M1 = 10 g containing  $\pm$  100 spores, M2 = 20 g containing  $\pm$  200 spores, and M3 = 30 g having  $\pm$  300 spores. M0 refers to the control plot without mycorrhiza. The dose determination for this experiment was based on the results of a previous study in which the best dose was micro aggregates (200–250 spores), equivalent to 20 g/plant (Rini *et al.*, 2021). The dose is given once at the beginning of planting woody plant seeds.

### Plant height and biomass weight observations

Plant height was measured on all plots to monitor plant growth. Measurements began at the start and continued every 2 weeks until the experiment concluded at week 16. The length was measured from the stem's base to the growing shoots' tip. Root growth was not observed every 2 weeks because removing the plants from the medium and replanting them caused them to wither and even die. Root length measurements were taken at the beginning and end of the experiment. At the end of the observation, plant biomass, including roots, shoots, and leaves, was measured by cutting plant samples.

### Root observation

Fresh roots were cut into 1 cm fragments, washed, and cleaned in 10% KOH at 90°C for 2 h. The segments

were acidified with 5% lactic acid for 20 min, stained with 0.05% weight per volume (w/v) Trypan blue for 30 min at 90°C, and then microscopically observed for root mycorrhiza colonization. The frequency of fungal structures in the root fragments (F%) and the intensity of the mycorrhiza colonization (M%) were evaluated in 20 randomly chosen root fragments (1 cm length) per glass slide, repeated five times for each sample. Mycorrhiza parameters (F% and M%) were calculated according to [Alhadidi et al. \(2021\)](#). The root growth direction was observed at the end of the experiment, on the 16<sup>th</sup> week after planting. The comparison was observed between plots using bamboo and those without bamboo.

#### *Percentage of nutrient uptake (%)*

The percentage of nutrient uptake was calculated based on the analysis of the initial and final soil samples. The nutrient parameters analyzed were mainly nitrogen (N), phosphorus (P), and kalium (K). The difference in the nutrient content in the initial soil samples and at the end of the experiment was the value of nutrients absorbed by plants.

#### *Experimental design and data analysis*

Subplots were designed for the two main plots of JR and CT, and each main plot received four doses of mycorrhiza (M0, M1, M2, and M3). In the two main plots, 12 treatment combinations were used, consisting of 4 doses of AMF and 3 species of woody plants. Each treatment was repeated three times for 36 plants observed. The SAS 9.4 variance program was used to analyze the results. The analysis results were then used Duncan Multiple Range Test at 5% to perform if the treatment was significantly affected. Numbers followed by the same letter on the row show no significant difference at the level of F 5%. The F test is a test that measures the magnitude of the difference in variance between the two groups, namely the CT and JR soils, which received the addition of AMF treatment.

## **RESULTS AND DISCUSSION**

### *Citatah landslide*

The landslide in CT, according to [Johnson et al. \(2023\)](#) classification, corresponds to a complex type, changing from a debris slide to earth flow. The slope is quite steep, measuring around 35° on the uphill side, 23° in the middle, and 10° on the

foothill side. The lithology is layered sedimentary rock consisting of sandstone, siltstone, claystone, and sedimentary breccia. The thickness of the soil ranges from approximately 3–5 m. The soil was formed by the weathering of these underlying rocks and by amendments from landslides. The degree of weathering can be seen in the field, with the weathering level being completely weathered near the ground surface and slightly weathered in the depth. The landslides event was triggered by rainfall and the conversion of vegetation cover from forest to mixed plantation, shrub, and bushes. The CT landslide can be described as a debris slide to earthflow or a sand/silt/debris flowslide. Sedimentary rock, primarily siltstone and claystone, exists at the bottom of the landslide, and moderately to completely weathered rock or soil with a 3–5 m thickness lies above it. The slip plane is claystone, and siltstone lies at the boundary between weathered and slightly weathered rock. The CT landslide can be seen in [Fig. 1a](#).

### *Jati Radio landslide*

The landslide in JR was triggered by rainfall and was likely promoted by the human removal of vegetation. The landslide was additionally controlled by hydrogeological conditions, in which the bottom topography of the land that slide is a channel like structure. The slope exceeds a 40° height on the slope and diminishes downward to approximately 20° at the foot of the slope. The hill is composed of andesitic rock that is both jointed and weathered. The upper reaches have in situ soil, whereas the lower reaches have much soil transported by slopewash and slope failure. The soil thickness in the upper and middle hills ranges from a few tens of centimeter to 2 m, while, at the bottom of the hill, the thickness of the soil reaches more than 5 m. The slip plane is underlain by fresh or unweathered to slightly weathered andesite, and is overlain by slightly to completely weathered rock or soil above it. The vegetation covering the area is a mixed forest interspersed with seasonal crops planted by people. The simple model of the JR landslide can be described as earthflow or sand/silt/debris flowslide. Andesitic rock forms the foundation, and moderately to completely weathered rock or soil lies above it, with a thickness of up to around 2 m. The slip plane is the boundary between slightly weathered rock and soil. The JR landslide can be seen in [Fig. 1b](#).



(a)

(b)

Fig. 1: Landslides in Citatah (a) and Jati Radio (b) with the crowns on top

Table 1: Results of analysis of CT and JR soils

Parameter	CT		JR	
	Results of analyses	Criteria	Results of analyses	Criteria
pH H <sub>2</sub> O (1:5)	5.9	acid	5.3–6.8	Acid-neutral
C organic (%)	2.98	low	1.17–1.72	Low
N total (%)	0.28	low	0.11–0.19	Low
C/N ratio	11	low	9	Low
P <sub>2</sub> O <sub>5</sub> (ppm)	7–7.2	low	6.6–11	Low
K <sub>2</sub> O (ppm)	430	high	348	High
<i>Grain size: (%)</i>				
Gravel	0–0.59	Clayey silt	0.41–0.50	Sandy silt
Sand	7.46–14.91		9.86–11.95	
Silt	67.59–72.95		76.14–80.63	
Clay	17.5–19		9–11.5	

#### Growing media

According to the soil analysis results (Table 1), the CT and JT fertility level and C/N (carbon per nitrogen) ratio are low to moderate. Soils' C/N ratios should be increased so plants can absorb nutrients directly. This was accomplished by adding compost at a 3:1 soil-to-compost ratio. Compost can also help to improve the structure of soil media. Grain size analyses revealed that the JR soil was coarser than the CT soil. Soil

observations in the field also demonstrated by the grain size macroscopically.

The results of CT and JR soil analysis showed that both soils were acid-neutral with a pH between 5.3 and 6.8. While organic C, total N, C/N ratio and P<sub>2</sub>O<sub>5</sub> showed low values. Conversely, K<sub>2</sub>O shows a high value. Grain size based on gravel, sand, silt, and clay criteria indicated clayey silt on CT and sandy silt on JR.



Fig. 2: Physical growth of *Paraserianthes falcataria*, *Acacia mangium*, and *Gmelina arborea* at the end of the experiment, namely in the 16<sup>th</sup> week after planting

#### Plant growth and height observations

The physical characteristics of *Paraserianthes falcataria*, *Acacia mangium*, and *Gmelina arborea* were observed regularly every 2 weeks. The physical growth of the plants exhibited a positive response, appeared to grow well and showed no plant nutrient deficiency (Fig. 2). An increase in plant height is markedly correlated with an increased number of leaves that grow on each stem. Root growth is also strongly correlated with the development of plant height. The growth of stunted plants is also correlated with the slow growth of roots; vice versa, the growth of fertile plants also shows the development of abundant roots. Cao *et al.* (2020) also discovered that the root growth rate is strongly related to the number and area of leaves, demonstrating that these plant organs are interconnected in photosynthesis. Trees continuously adapt the spatial distribution of the roots in response to environmental conditions through new lateral roots, changes in the growth direction, and wood production reactions (Montagnoli, 2019). In this study, the mycorrhiza showed a positive effect on plant growth. Plants have grown significantly as a result of the optimal mycorrhiza doses. Fig. 3 depicts the plant height growth trends up to 16 weeks. Pearson's correlation revealed a similar trendline in all CT and JR plots.

The variance analysis showed that treatments mycorrhiza doses of *Paraserianthes falcataria* were not significantly different in both main plots of JR and CT, and the best dose was M3. Similarly, *Gmelina arborea* treatments were not significantly different

in the two locations, and the best dosage was also M3. However, for *Acacia mangium*, neither area was significantly different, and all doses had a positive effect.

#### Biomass weight analysis

Wet biomass weight was measured to determine the effect of the mycorrhiza intervention on root growth 16 weeks after planting. The results of the analysis are presented in Table 3. The table shows the wet weight of the biomass of *Paraserianthes falcataria* and *Gmelina arborea* showed extreme growth with the best mycorrhiza dose, M3, except for *Acacia mangium*, which showed the best mycorrhiza dose, M1. The wet weight of the root biomass from these three woody plants was compared to that of the control. The table shows that plants infected by mycorrhiza had a higher wet biomass than controls.

The plots in a polybag (C) and bamboo (M0), both without AMF, at the two sample locations (JR and CT), showed no significant difference in biomass weight. Only *Acacia mangium* planted in CT soil was better in bamboo than polybag plots.

#### The abundance of mycorrhiza species

The positive effect of the mycorrhiza intervention on root and plant growth was also shown by the infection of the three woody plant species. At the end of the experiment, 16 weeks after planting, samples were taken from the two main plots, the CT and JR plots, by choosing the best-growing plants. The results obtained from laboratory observations

Root growth and arbuscular mycorrhizal fungi

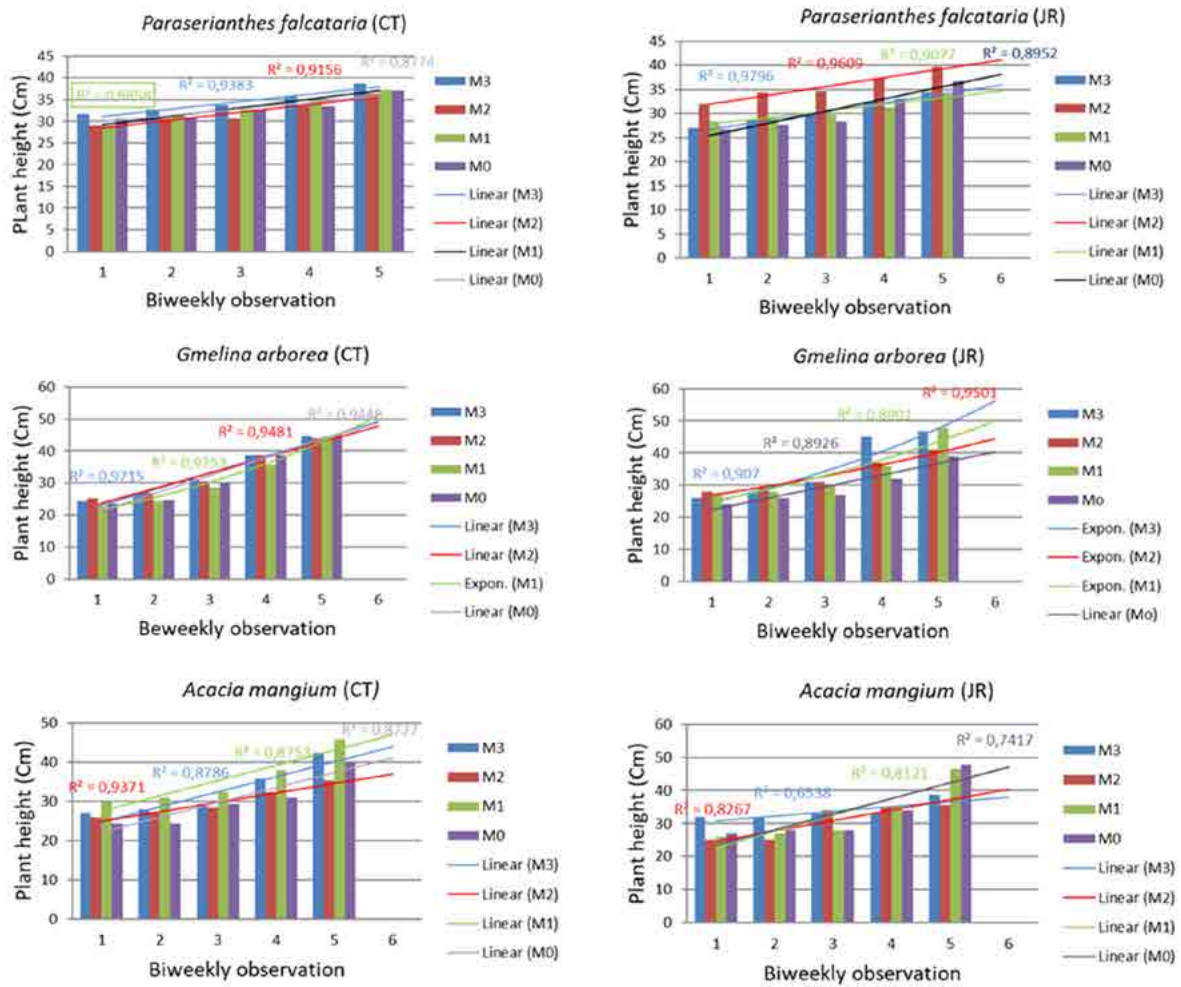


Fig. 3: Effect of mycorrhiza doses on plant growth with height characteristics of *Paraserianthes falcataria*, *Acacia mangium*, and *Gmelina arborea* in CT and JR plots.

Table 2: Effect of mycorrhiza doses on the average plant height of the woody plants.

Locality	Plant species	Mycorrhiza doses			
		M0	M1	M2	M3
CT	<i>Paraserianthes falcataria</i>	70.33 c	63.33 c	87.66 b	95.66 a
	<i>Gmelina arborea</i>	95.66 a	97.33 a	71.66 b	100.33 a
	<i>Acacia mangium</i>	8.66 a	88.33 a	73 b	84.66 a
JR	<i>Paraserianthes falcataria</i>	68 b	71.33 a	65 b	76.66 a
	<i>Gmelina arborea</i>	55.66 c	97.66 a	85.66 b	94.33 a
	<i>Acacia mangium</i>	81.66 a	79.66 a	56.66 b	63 b

Note: Numbers followed by the same letter on the same row show no significant difference at the level of F 5%.

are shown in Table 3. The highest level of mycorrhiza infection occurred in the roots of *Gmelina arborea* with the treatment level of M3 mycorrhiza in CT two plots, which reached 67.4%, with the highest wet biomass weight of 660 g. However, it was not significantly different from the M3 treatment in JR plots. The predominant mycorrhiza in both locations' soil samples were *Glomus* sp. and *Gigaspora* sp. The diversity of mycorrhiza species affects nutrient uptake, increasing the growth rate. Table 4 shows that the number of mycorrhiza species *Glomus* sp. and *Gigaspora* sp. in the soil of both locations (CT and JR) planted with *Acacia mangium* was significantly lower

than that of *Gmelina arborea* and *Paraserianthes falcataria*. The low number of *Glomus* sp. and *Gigaspora* sp. spores led to the slow growth of *Acacia mangium* (Table 4), which was also indicated by the weight of the biomass at the end of the experiment (Table 3). The macroscopic observations and laboratory tests showed that JR soil is coarser than CT soil (Table 1). The coarser grain is why *Glomus* sp. and *Gigaspora* sp. develop healthily, because their hyphae can spread more widely. AMF's ability to absorb water from soil pores is due to the smaller and more delicately branching mycorrhiza hyphae outside the roots, with a diameter of approximately 2 μm.

Table 3: Biomass weights of the three plants species

No.	Locality	Plant species	Control (Plot without AMF)		AMF dose (Plot with bamboo)			
			Media code	Wet weight (g)	Media code	Wet weight (g)	Media code	Wet weight (g)
1	Citatah	<i>Paraserianthes falcataria</i>	C	105b	M0	153b	M3	205a
		<i>Gmelina arborea</i>	C	205b	M0	396b	M3	660a
		<i>Acacia mangium</i>	C	80b	M0	82a	M3	80b
2	Jati Radio	<i>Paraserianthes falcataria</i>	C	65b	M0	76b	M3	105a
		<i>Gmelina arborea</i>	C	310b	M0	316b	M3	330a
		<i>Acacia mangium</i>	C	105b	M0	164a	M1	165a

Table 4: Number of mycorrhiza spores in the roots of the three plant species in CT and JR soils

CT			JR		
Sample code	Species	Number of spores	Sample code	Species	Number of spores
Pf-M3	<i>Glomus</i> sp.	598a	Pf-M3	<i>Glomus</i> sp.	698a
	<i>Gigaspora</i> sp.	102a		<i>Gigaspora</i> sp.	72a
	<i>Scutellospora</i> sp.	15b		<i>Scutellospora</i> sp.	11a
	<i>Acaulospora</i> sp.	21a		<i>Acaulospora</i> sp.	13a
Am-M1	<i>Glomus</i> sp.	458b	Am-M3	<i>Glomus</i> sp.	646b
	<i>Gigaspora</i> sp.	98b		<i>Gigaspora</i> sp.	66b
	<i>Scutellospora</i> sp.	26a		<i>Scutellospora</i> sp.	10b
	<i>Acaulospora</i> sp.	22a		<i>Acaulospora</i> sp.	9b
Ga-M3	<i>Glomus</i> sp.	589a	Ga-M3	<i>Glomus</i> sp.	708a
	<i>Gigaspora</i> sp.	112a		<i>Gigaspora</i> sp.	74a
	<i>Scutellospora</i> sp.	18b		<i>Scutellospora</i> sp.	12a
	<i>Acaulospora</i> sp.	20b		<i>Acaulospora</i> sp.	14a

Note: Numbers followed by the same letter on the same column show no significant difference at the level of F 5%.

### Root growth direction

At the end of the experiment, 16 weeks after planting, observations were made in the direction of root growth for all plants. The bamboo tube intervention on the root growth direction was intended to direct roots downward across the imaginary slip plane and anchor the plants in the underlying rock. The experimental results showed that the roots of *Paraserianthes falcataria*, *Acacia mangium*, and *Gmelina arborea* followed the bamboo shape to grow in a vertical direction downwards (Figs. 4, 5, and 6). The directed growth occurred in all plots with bamboo tubes but did not occur in the

control plot without the bamboo intervention. Roots change growth direction due to mechanical forces (Montagnoli, 2019).

### Nutrient uptake

The calculation results for the nutrient uptake percentage were obtained from the best-growing plants. The symbiotic responses of AMF and suspected plants showed differences in nutrient uptake. Results of Duncan's analysis showed a significant difference between *Gmelina arborea* and the two other plants, *Paraserianthes falcataria* and *Acacia mangium*. *Gmelina arborea* showed the best response in CT and

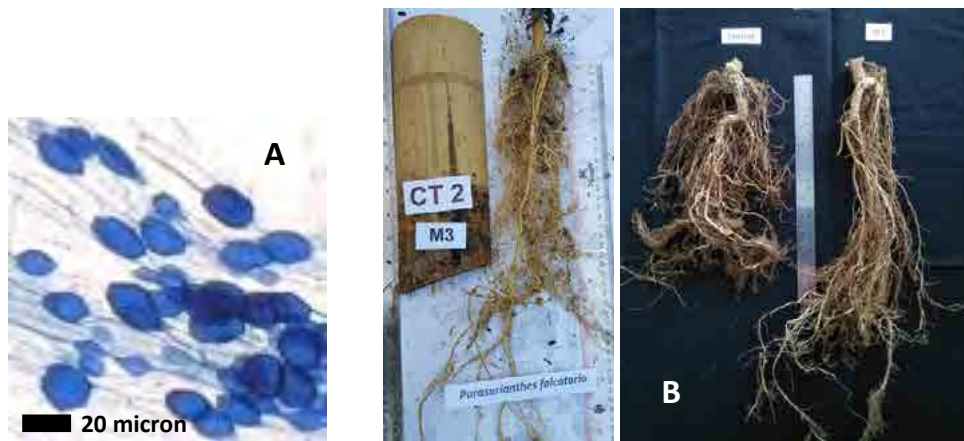


Fig. 4: (A) Mycorrhizal infections in *Paraserianthes falcataria* roots (M3). (B) AMF (M3) and *Paraserianthes falcataria* symbiosis planted in CT soil with a bamboo tube at 16 weeks old. The bamboo modified the root growth and grew longer than the control



Fig. 5: (A) Mycorrhizal infections in *Acacia mangium* roots (M3). (B) AMF (M3) and *Acacia mangium* symbiosis planted in CT soil with a bamboo tube at 16 weeks old. Bamboo strongly affected root growth. Roots grown without bamboo tubes grew heavier than those grown with bamboo tubes.



Fig. 6: (A) Mycorrhizal infections (M3) in the roots of *Gmelina arborea* plant. (B) The symbiosis of AMF (M3) and *Gmelina arborea* planted in JR soil with a bamboo tube at 16 weeks old. The bamboo-modified roots grew longer and more extensively than those without bamboo

Table 5: Percentage of nutrient uptake in an AMF-woody plant symbiosis.

Nutrient	Woody plant species	Soil before experiment		Soil after experiment		Nutrient uptake (%)	
		CT	JR	CT	JR	CT	JR
Phosphate	<i>Paraserianthes falcataria</i>	611.3	519	509.9	267	17 a	48 a
	<i>Acacia mangium</i>	611.3	519	416.6	221	31 a	57 a
	<i>Gmelina arborea</i>	611.3	519	120.4	146	80 b	71 b
Nitrogen	<i>Paraserianthes falcataria</i>	0.51	0.59	0.33	0.4	35 a	32 a
	<i>Acacia mangium</i>	0.51	0.59	0.39	0.24	23 a	59 b
	<i>Gmelina arborea</i>	0.51	0.59	0.25	0.19	50 b	67 b
Kalium	<i>Paraserianthes falcataria</i>	907	1582	890	609	21 a	61 a
	<i>Acacia mangium</i>	907	1582	704	644	22 b	59 a
	<i>Gmelina arborea</i>	907	1582	736	559	18 b	64 b

Note : Numbers followed by the same letter on the row show no significant difference at the level of F 5%.

JR soils (Table 5). The highest nutrient absorption in P was good for *Gmelina arborea*, at approximately 80% in CT soil and 71% in JR soil. In contrast, the two other plants yielded values of 17% and 31% in CT soil and 48% and 57% in JR soil.

#### Effect of mycorrhiza on plant growth

In this experiment, the effect of mycorrhiza on plant growth could be observed from the plant height (Table 2) and biomass weight (Table 3). All

plants could grow from CT and JR on both soil media. It could be observed that there were differences in the plant responses to AMF doses. In CT plots, the chosen amounts of M0 and M1 were beneficial for the growth of *Gmelina arborea* and *Acacia mangium*, whereas M3 was suitable for all plants. For JR plots, the M1 dose was suitable for the growth of the three types of plants. The M3 dose was only beneficial for *Paraserianthes falcataria* and *Gmelina arborea*. An interesting result is that *Acacia mangium* had the best

growth on M0, both in CT and JR. Therefore, *Acacia mangium* grows well without mycorrhiza application. The result also indicates that the AMF consortium is incompatible with *Acacia mangium*. Doses of M1 and M3 showed growth effects at both locations for *Paraserianthes falcataria* and *Gmelina arborea*. Therefore, the M1 dose is the best dose considering economical mycorrhiza application. The dose of M3 showed the best plant height growth in line with a high biomass weight at both test sites (CT and JR) for *Gmelina arborea*, followed by *Paraserianthes falcataria* and *Acacia mangium*, respectively (Table 3). The dose of M3 (30 g/plot) was the best dose for *Paraserianthes falcataria*, which was also shown by the fact that doses of 15, 20, and 25 g appeared to cause the best growth and results were not significantly different between the three doses (Listiani and Yuniati, 2021). Mycorrhiza inoculation at 20 g/plot in *Gmelina arborea* increased growth to 2.4 times the biomass weight compared to the case without mycorrhizae (Akhavue et al., 2020). The application of rhizobium and mycorrhizae on *Acacia crassicarpa* caused variations in growth parameters. The highest growth rate and increase in dry weight indicated symbiotic compatibility between rhizobium strains and mycorrhizal species (Liu et al., 2020). This study used AMF containing various types of spora and found promising results for both soil types (CT and JR) and all woody plants tested, even at the lowest dose (M1).

indicated by the increase in nutrient uptake, which impacted the increase in root length. Modification of the root growth direction was achieved using bamboo. This was seen in *Paraserianthes falcataria* and *Gmelina arborea* (Figs. 4 and 6). *Acacia mangium* in the control (C) was denser. Still, root growth in bamboo was longer (Fig. 5). AMF inoculation increases the growth of woody plants such as teak, cocoa, and coffee (Bezza Beyene et al., 2022). Through symbiosis with the AMF, the host plant obtains nutrients from the fungus, while the AMF receives carbohydrates from the host plant (Wira Yuwati et al., 2020). For host plants, AMF is very beneficial in the absorption of nutrients and water, tolerance to drought, the inhibition of infection by disease organisms (Tao et al., 2022), increasing seedling growth, tree height, and crop yield (Umer et al., 2021), improving soil aggregation (Fall et al., 2022) addressing non-biological and biological stresses in plants, and increasing ecosystem productivity (Xiao et al., 2023). Mycorrhiza can generally increase plant tolerance to abiotic conditions (Begum et al., 2019). Plant growth indicates effective P absorption. At the end of the experiment, wet biomass data for the three woody plant species revealed that *Gmelina arborea* had the most significant biomass weight, as shown in Table 3. AMF mainly leads to plants' increased uptake of nutrients, particularly phosphate (Zai et al., 2021). Much progress has been made in research on P-deficiency-induced root architecture remodeling, and several reports suggest that the root tip is a useful site for locally sensing the status of P deficiency (Bi et al., 2023). Functional analyses of the different

Effects of mycorrhiza on nutrient uptake

In the results, the effectiveness of AMF was

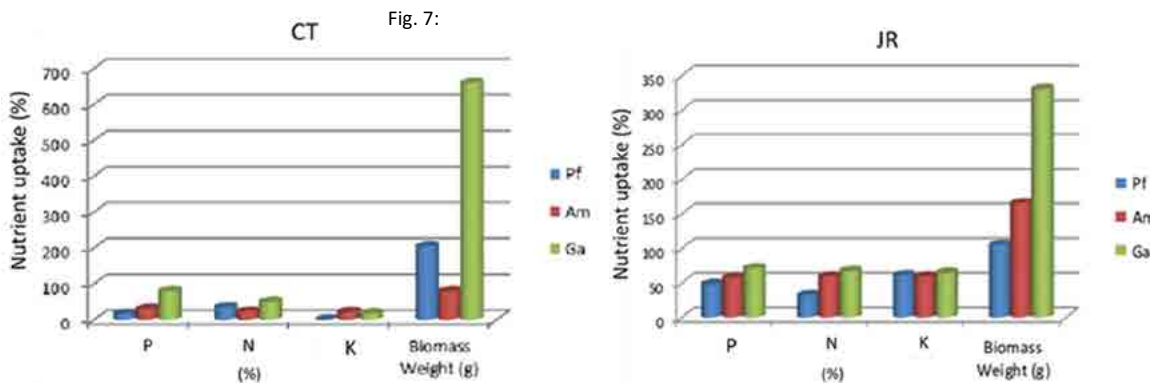


Fig. 7: Percentage of nutrient uptake (N, P, and K) in symbiosis between AMF and woody plants is compared with biomass weight (g) in Citatah and Jati Radio soil.

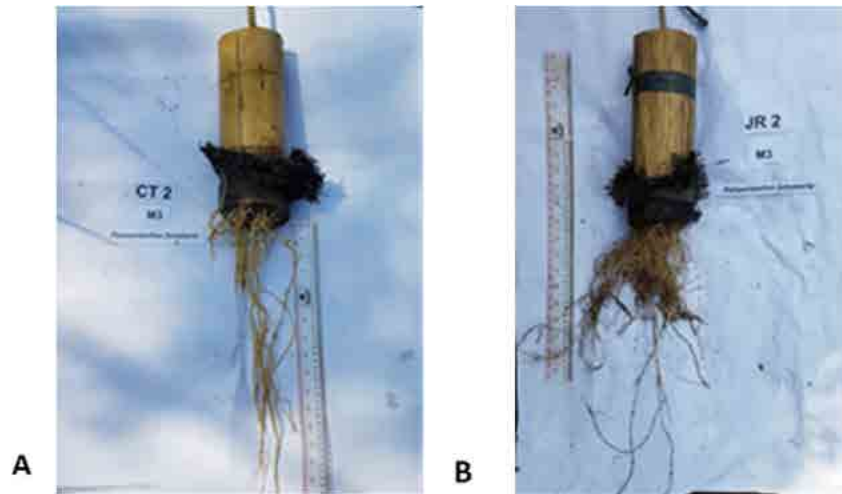


Fig. 8: Root growth of *Paraserianthes falcataria* in JR soil media (A) and CT soil media (B)

root tissues of the root tip are required to identify the early steps of P starvation responses. Several phytohormones, particularly auxins, are involved in the modulation of root architecture adaptation (Dixit *et al.*, 2022). The nutrients N, P, and K absorbed by the three tested woody plants showing AMF activity are presented in Fig. 7. The best nutrient uptake measured by the wet biomass weight parameter was shown by *Gmelina arborea* grown on both test soils, namely CT and JR.

#### Effect of bamboo on root growth direction

Three types of plants were planted in bamboo tubes filled with planting medium on a 20° slope, and inhibited growth was observed at the roots, which normally grow laterally. Taproots appear to be longer than lateral roots. Because of its role as an anchor, the longer taproot can theoretically strengthen plant growth by penetrating deeper into the ground. Taproots that are longer than lateral roots will also protect the plant from the wind so that it is more stable and can grow on slopes (Dumroese *et al.*, 2019). The downslope quadrant gets the greatest quantity of root resources on steep slopes, followed by the wind direction quadrant. The larger cross-sectional area at the point of attachment of the lateral root to the taproot in the downslope quadrant indicates the shallow roots play an essential role in tree anchorage. Roots change growth direction due to mechanical forces (Montagnoli, 2019). The root

growth direction can be modified using bamboo tubes and AMF, which has been proven in this study (Figs. 4, 5 and 6). The results of this study showed that, in general, in CT and JR soil media, bamboo intervention can force root growth in the vertical direction, different from the growth in the control plant (Figs. 3b, 4b, and 5b). The roots can penetrate the bamboo base and grow into the slip plane medium. Roots are expected to penetrate the actual slip planes for future applications, and rock crevices and roots can strengthen the grip on the soil. This follows Zhang *et al.* (2020) statement that deepening roots into soil layers provide good shear strength and bending effects. This will undoubtedly provide support for the above soil layer and be effective in controlling shallow landslides. The extent to which plant roots penetrate the bamboo appears to be dependent on the grain size of the soil medium. For example, the difference in root growth of *Paraserianthes falcataria* in JR and CT soil media, demonstrates this. In JR, roots can penetrate the bamboo base more quickly than in CT (Fig. 8). JR soil media (sandy silt) is porous in comparison to CT soil media (clayey silt). This is consistent with the results of research by Biehl *et al.* (2023) on the growth and root morphology of *Picea abies* seedlings, and soil strength due to the hydrogels effect. Their results showed that the compaction of clay soil caused the total length of primary and lateral roots to decrease, but root growth was stronger. Furthermore, Xiong *et al.*, (2022) described that, in

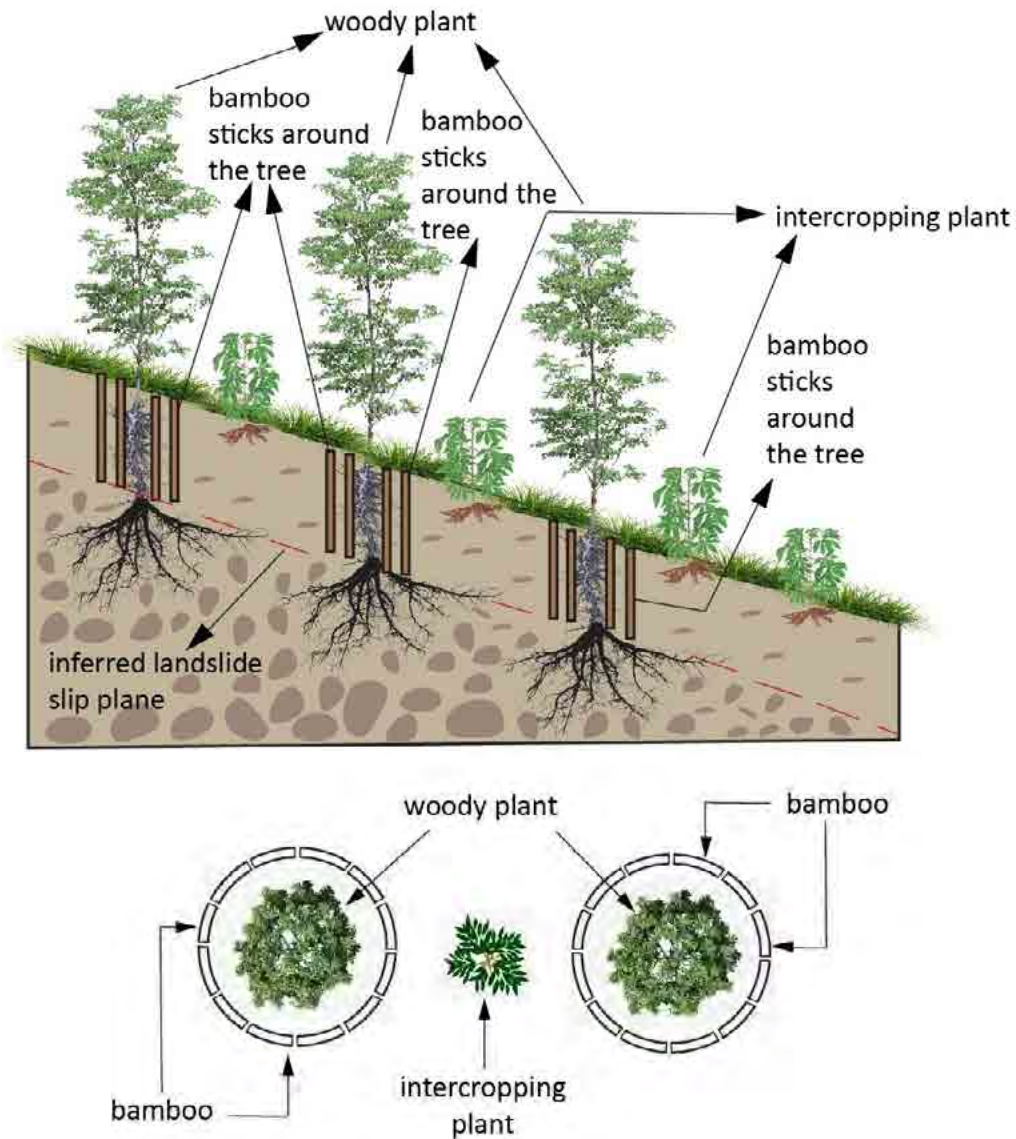


Fig. 9: Illustration of the use of bamboo sticks in conjunction with AMF interventions in tree planting on a slope to stabilize the slope. The figure depicts a cross-section on top and a plane section on the bottom.

uncompacted soil, the number of biopores crossed by roots was much greater than in compacted soil.

#### *Effects of arbuscular mycorrhizal fungi on soil shape*

Mycorrhiza significantly increased root growth in the woody plants tested in the experiment. The study also revealed that the roots spread into the soil beneath the bamboo tubes, resulting in more stable soil. The growth and decomposition of roots and

mycorrhizal hyphae control the soil macroaggregates' stability. AMF appears to be the most important mediator of soil aggregation (Carrara et al., 2023). As a helpful resource in AMF associations, the external hyphae provide a direct physical link between the host plant and soil. External hyphae of AMF can bind the small soil debris into micro aggregates by generating a glycoprotein (glomalin), accounting for 30%–60% of C in undisturbed soils (Villa-Rivera et al.,

2021). The entanglement of macroaggregates results in a stepped-forward shape and soil aggregation balance. The results suggest that inoculating seedlings with AMF and supplementing with P should be a management strategy, especially for the best species, *Gmelina arborea*. These results are similar for pioneer woody plant species when revegetating riparian areas or for late secondary species when planting secondary forests for enrichment (Ishad et al., 2021; Araiza-Aguilar et al., 2020). In ecosystems, mycorrhizae play a role in cycling and conserving nutrients through soil mycelia, is a food source for numerous soil fauna, improve soil structure, play a role in carbon transport from plant roots in other soil organisms, and act as a bioindicator environmental quality in terms of fungal diversity (Muhammad et al., 2021). In nature, temperature and humidity regimes are intimately connected, and temperature may be a more significant driver for the success of mycorrhiza types than previously assumed. The poorer performance of AMF in low-temperature and drought conditions may reflect stress avoidance rather than stress tolerance by AMF (Kilpeleinen et al., 2020). Applying mycorrhizae, cow dung, and biochar improved the sandy soil characteristics (Herawati et al., 2021).

## CONCLUSION

The soil thickness of the landslide areas in CT and JR is approximately 2–5 m, with the slip plane at the boundary between the weathered and slightly weathered rock. This setting is suitable for applying the proper vegetation to stabilize the slopes. AMF and bamboo interventions can accelerate plant growth and change the direction of root growth. Plants on the slopes can grow faster with these interventions. The plant's root system acts as an anchor, increasing the slope's stability. The grain size of JR soil is coarser than CT soil, and JR soil is more porous than CT soil, causing the taproot to grow and penetrate the bamboo base faster in JR soil than in CT soil. As a result, the potential slip plane in JR soil can be reached and grip more quickly for landslide mitigation than in CT soil. The AMF treatment of *Gmelina arborea* produced the best results in this experiment. The optimal level of AMF is related to *Gmelina arborea*'s highest phosphorus absorption at 80% and the highest biomass weight of 660 g with the M3 dose in CT, and 71% with 330 g at the same dose in JR. The

high absorption of phosphorus nutrients then affects the increase in root growth and length. The results are not significantly different to those of AMF treated with M1. Consequently, from an economic point of view, M1 doses are recommended and can be used to stimulate tree-root growth in *Gmelina arborea* trees. Based on *Gmelina arborea* distribution and soil characteristics, similar to JR and CT, M1 AMF doses can be applied in other locations. According to the findings of this study, bamboo tubes combined with AMF can stimulate root growth and direction. These provide a new technique for environmentally friendly landslide disaster mitigation and can be used to prevent landslides. Based on the root growth rate and biomass weight, *Gmelina arborea* can be recommended as the best woody plant for stabilizing slopes at the CT and JR test sites. These findings can also be applied in other area which the similar soil characteristics as CT and JR. The symbiotic relationship between AMF and plant roots can enhance nutrient and water absorption, leading to faster and better plant growth. Therefore, excellent and fast plant growth can contribute to faster slope stabilization, essential for landslide protection.

## RECOMMENDATION

This study recommends that bamboo and AMF can be used to direct and accelerate the growth of woody tree roots so that they grow lengthwise to reach and grip the slip plane. The area of land between woody trees can be used for intercropping plants, thereby increasing the economic value for the community. This type of ecosystem will eventually give rise to agroforestry, a way of land conservation and a method of landslide protection (Fig. 9).

1. *Gmelina arborea* is a recommended plant for use in slope stabilization. Adding 10 g or  $\pm 100$  spores of AMF is sufficient to be given once at the beginning of tree planting growth.

2. The role of bamboo is to direct the growth of vertical roots so that they grow further into the slip plane, allowing the tree to prevent slope movements.

3. In practical application, bamboo can be installed as sticks around the tree instead of bamboo tubes. The recommended diameter for bamboo sticks is 0.5 m with a depth according to the estimated slip plane depth and up to at least 2 m.

4. Intercropping plants such as *Manihot* sp. can be used between the woody trees, adding economic

value to the local people.

Despite the favorable elements of this technology, several restrictions can create hurdles to the beneficial implications of this application, such as the fact that this procedure is partially dependent on the plant's dormant seasons, which is an availability limitation of the site. The application of this technique is prospective in Indonesia, because lots of land is prone to landslides; bamboo is easy to get in any area because it is easy to grow; AMF and woody plant symbiosis is very beneficial because it can restore problematic soil conditions especially the lack of nutrients for plants; the combination of bamboo and AMF is an environmentally friendly and economical technology. The challenge faced in the restoration program using new techniques, namely planting woody plants combined with bamboo and AMF on sloping land, is an approach to empowering the community in terms of participating in caring for plants for rehabilitation so they can grow well. It requires an expert with experience working on restorations with challenging soils, and another with a different perspective and understanding of this kind of complication. The attention and support of the local government significantly contributed to the success of the restoration. The implementation of planting on sloping land before planting is identifying those site factors that inhibit vegetation growth. Identify primary vegetation limiting features: steep slopes, poor nutritional status, unpleasant chemical characteristics, and soil temperature extremes. Forest erosions are closely related to steep slopes, poor texture/compaction, and low nutrient status. Restorative technology that employs AMF is also known as soil bioengineering or biotechnique. This technique is advantageous since it only necessitates a little maintenance after implementation. Because it is relatively inexpensive, this technique can be an excellent tool for mitigating landslides and unstable slopes. Bioengineering systems, like living systems, require little or no maintenance and continue to improve over time. Bioengineering can act as a link between traditional engineering treatments and standard seeding work. Bioengineering can help with the reclamation of forest lands.

#### **AUTHOR CONTRIBUTIONS**

I.G. Tejakusuma contributed to the conceptualization, methodology, preparation of

photos and figures, and manuscript writing. E.H. Sittadewi, the corresponding author, conducted observations, formal analyses, funding acquisition, project administration, and manuscript writing. T. Handayani performed the methodology, formal analyses, data curation, writing, reviewing, and editing. T. Hernaningsih supported the conception and design of the manuscript, conducted a literature review, and drafted and prepared the manuscript. W. Wisyanto performed data acquisition, analysis, and interpretation and sharpened the background. A. Rifai assisted with experimental and administrative work and provided technical and material assistance. All authors read and approved the final manuscript.

#### **ACKNOWLEDGEMENT**

The authors are grateful to the Head of Research Center for Geological Disaster, the Head of Research Center for Sustainable Production System and Life Cycle Assessment, and the Head of Research Center for Environmental and Clean Technology of the National Research and Innovation Agency, Indonesia. The authors thank the editors and anonymous reviewers for their constructive comments.

#### **CONFLICT OF INTEREST**

The author declares that there is no conflict of interests regarding the publication of this manuscript. In addition, the ethical issues, including plagiarism, informed consent, misconduct, data fabrication and/or falsification, double publication and/or submission, and redundancy have been completely observed by the authors.

#### **OPEN ACCESS**

©2024 The author(s). This article is licensed under a Creative Commons Attribution 4.0 International License, which permits use, sharing, adaptation, distribution, and reproduction in any medium or format, as long as you give appropriate credit to the original authors and the source, provide a link to the Creative Commons license, and indicate if changes were made. The images or other third-party material in this article are included in the article's Creative Commons license, unless indicated otherwise in a credit line to the material. If material is not included in the article's Creative Commons license and your intended use is not permitted by statutory regulation or exceeds the permitted use, you will need to obtain

permission directly from the copyright holder. To view a copy of this license, visit <http://creativecommons.org/licenses/by/4.0/>

#### PUBLISHER'S NOTE

GJESM Publisher remains neutral with regard to jurisdictional claims in published maps and institutional affiliations.

#### ABBREVIATIONS

AMF	Arbuscular mycorrhizal fungi
Ac	Acacia mangium
C	Carbon
cm	centimetre
C/N Ratio	Carbon/nitrogen ratio
CT	Citatah
F%	Root fragments
Ga	Gmelina arborea
K	Kalium
K <sub>2</sub> O	Kalium oxide
KOH	Kalium hydroxide
JR	Jati Radio
M%	Mycorrhiza colonization
Mo	Without AMF
M1	AMF 10 mg
M2	AMF 20 mg
M3	AMF 30 mg
P	Phosphorus
P <sub>2</sub> O <sub>5</sub>	Phosphore pentoxide
Pf	<i>Paraserianthes falcataria</i>

#### REFERENCES

Abdalla, K.; Mutema, M.; Hill, T., (2020). Soil and organic carbon losses from varying land uses: a global meta-analysis. *Geogr. Res.*, 58: 167–185 (29 pages).

Akhabue, E.F.; Chima, U.D.; Eguakun, F.S., (2020). Comparative evaluation of growth performance and soil quality of two age sequences of *Gmelina arborea* plantation in University of Port Harcourt, Nigeria. *J. Appl. Sci. Environ. Manage.*, 24(10): 1767-1773 (7 pages).

Alhadidi, N.; Pap, Z.; Ladányi, M.; Szentpéteri, V.; Kappel, N., (2021). Mycorrhizal inoculation effect on sweet potato (*Ipomoea batatas* (L.) lam) seedlings. *Agronomy*. 11(10): 1-10 (10 pages).

Araiza-Aguilar, J.A.; Rojas-Valencia, M.N.; Aguilar-Vera, R.A., (2020). Forecast generation model of municipal solid waste using multiple linear regression. *Global J. Environ. Sci. Manage.*, 6(1): 1-14 (14 pages).

Asima, H.; Niedzinski, V.; O'Donnell, F.C.; Montgomery, J., (2022). Comparison of vegetation types for prevention of erosion and shallow slope failure on steep slopes in the Southeastern USA. *Land*. 11(10): 1-20 (20 pages).

Asmelash, F.; Bekele, T.; Birhane, E., (2016). The potential role of arbuscular mycorrhizal fungi in the restoration of degraded lands. *Front. Microbiol.*, 7: 1-15 (15 pages).

Bahadur, A.; Batool, A.; Nasir, F.; Jiang, S.; Mingsen, Q.; Zhang, Q.; Pan, J.; Liu, Y.; Huyuan Feng, H., (2019). Mechanistic insights into arbuscular mycorrhizal fungi-mediated drought stress tolerance in plants. *Int. J. Mol. Sci.*, 20(17): 1-18 (18 pages).

Begum, N.; Qin, C.; Ahanger, M.A.; Raza, S.; Khan, M.I.; Ashraf, M.; Ahmed, N.; Zhang, L., (2019). Role of arbuscular mycorrhizal fungi in plant growth regulation: implications in abiotic stress tolerance. *Front. Plant Sci.*, 10: 1-15 (15 pages).

Berza Beyene, B.; Pagano, M.C.; Vaiyapuri, R.P.; Assefa Tuji, F., (2022). Microbial consortia inoculation of woody legume *Erythrina brucei* increases nodulation and shoot nitrogen and phosphorus under greenhouse conditions. *Biotechnol. Rep.*, 33:1-10 (10 pages).

Biehl, J.; Sanden, H.; Rewald, (2023). Contrasting effects of two hydrogels on biomass allocation, needle loss, and root growth of *Picea abies* seedlings under drought. *For. Ecol. Manage.*, 538: 1-9 (9 pages).

Bi, B.; Yin, Q.; Hao, Z., (2023). Root phosphatase activity is a competitive trait affiliated with the conservation gradient in root economic space. *For. Ecosyst.*, 10: 1-8 (8 pages).

Bujoczek, L.; Bujoczek, M.; Zięba, S., (2021). How much, why and where? Deadwood in forest ecosystems: The case of Poland. *Ecol. Indic.*, 121: 1-14 (14 pages).

Busso, M.A.; Busso, M.B.; (2022). Arbuscular mycorrhizal fungi and common mycorrhizal networks benefit plants through morphological, physiological and productive traits and soil quality. *Lilloa*. 59(2) (17 pages).

Cao, Z.; Li, Y.; Ye, C.; Shu, S.; Sun, B.; Huang, J.; Wu, L., (2020). Model for monitoring tiller number of double cropping rice based on hyperspectral reflectance. *Nongye Gongcheng Xuebao/Trans. Chin. Soc. Agric. Engine.*, 36(4): 185-192 (8 pages).

Carrara, J.E.; Lehotay, S.J.; Lightfield, A.R.; Sun, D.; Richie, J.P.; Smith, A.H.; Heller, W.P., (2023). Linking soil health to human health: Arbuscular mycorrhizae play a key role in plant uptake of the antioxidant ergothioneine from soils. *Plants People Planet*. 10: 1-10 (10 pages).

Dixit, R.; Agrawal, L.; Srivastava, S.; Chauhan, P.S., (2022). *Paenibacillus lentimorbus* enhanced abiotic stress tolerance through lateral root formation and phytohormone regulation. *J. Plant Growth Regul.*, 41(6): 1-12 (12 pages).

De Souza, B.C., Da Cruz, R.M.S., Lourenco, E.L.B., Pinc, M.M., Dalmagro, M., Da Silva, C., Faria Nunes, M.G., De Souza, S.G.H., Alberton, O., (2022). Inoculation of lemongrass with

- arbuscular mycorrhizal fungi and rhizobacteria alters plant growth and essential oil production. *Rizhosphere*. 22 (4 pages).
- Dumroese, R.K.; Terzaghi, M.; Chiatante, D.; Scippa, G.S.; Lasserre, B.; Montagnoli, A., (2019). Functional traits of *Pinus ponderosa* coarse roots in response to slope conditions. *Front. Plant Sci.*, 10: 1-12 (12 pages).
- Fall, A.F.; Nakabonge, G.; Ssekandi, J.; Founoune-Mboup, H.; Apori, S.O.; Ndiaye, A.; Badji, A.; Ngom, K., (2022). Roles of arbuscular mycorrhizal fungi on soil fertility: contribution in the improvement of physical, chemical, and biological properties of the soil. *Front. Fungal Biol.*, 3: 1-11 (11 pages).
- Fattahi, M.; Mohammadkhani, A.; Shiran, B.; Baninasab, B.; Ravash, R.; Gogorcena, Y., (2021). Beneficial effect of mycorrhiza on nutritional uptake and oxidative balance in pistachio (*Pistacia* spp.) rootstocks submitted to drought and salinity stress. *Sci. Hortic.*, 281 (12 pages).
- Folleau, S.; Uhlemann, S.; Falco, N.; Dafflon, B., (2023) Assessing probability of failure of urban landslides through rapid characterization of soil properties and vegetation distribution. *Geomorphol.*, 423: 1-11 (11 pages).
- Guo, Z.; Ferrer, J.V.; Hurlimann, M.; Medina, V.; Polo, C.P.; Yin, K.; Huang, D., (2023). Shallow landslide susceptibility assessment under future climate and land cover changes: A case study from southwest China. *Geosci. Front.*, 14 : 1 - 21 (21 pages).
- Herawati, A.; Syamsiyah, J.; Mujiyo, M.; Rochmadtulloh, M.; Susila, A.A.; Romadhon, M.R., (2021). Mycorrhizae and a soil ameliorant on improving the characteristics of sandy soil. *J. Soil Sci.*, 18(1): 1-8 (8 pages).
- Hou, T.; Yang, M.; Yan, K.; Fan, X.; Ci, X.; Peng, L., (2022). Amentoflavone ameliorates carrageenan-induced pleurisy and lung injury by inhibiting the NF- $\kappa$ B/STAT3 pathways via Nrf2 activation. *Front. Pharmacol.*, 13: 1-15 (15 pages).
- Husna, Tuheteru, F.D.; Albasri, Arif, A.; Basrudin, Nurdin, W.R.; Arman, E.; Agustin, D.I.; Saribadu, J.; Rahmat, Dermawansyah, A.; Daliana, Lody, L.P.; Deri, A.S.; Safitri, I., (2022). Diversity of arbuscular mycorrhizal fungi of *Kalappia celebica*: An endemic and endangered plant species in Sulawesi, Indonesia. *Biodiversitas*. 23(10): 3844-3853 (10 pages).
- Jangjou, A.; Zarehsharabadi, Z.; Abbasi, M.; Talaiekhosani, A.; Kamyab, H.; Chelliapan, S.; Vaez, A.; Golchin, A.; Tayebi, L.; Vafa, E.; Amani, A.M.; Faramarzi, H., (2019). Time to conquer fungal infectious diseases: employing nanoparticles as powerful and versatile antifungal nanosystems against a wide variety of fungal species. *Sustainability*. 14(19): 1-33 (33 pages).
- Johnson, C.; Affolter, M.D.; Inkenbrandt, P.; Mosher, C., (2023). An Introduction To Geology, LibreTexts. 1-121 (121 pages).
- Ishaq, L.; Adu Tae, A.S.J.; Airthur, M.A.; Bako, P.O., (2021). Effect of single and mixed inoculation of arbuscular mycorrhizal fungi and phosphorus fertilizer application on corn growth in calcareous soil. *Biodiversitas*. 22(4): 1920-1926 (7 pages).
- Khan, Y.; Sohail, A.; Yaseen, T.; Rehman, K.U.; Noor, M.; Akbar, K., (2021). Arbuscular mycorrhizal fungi improved the growth and yield productivity of lens esculenta under the influence of poultry litter. *Pakistan J. Phytopath.*, 33(1): 145-151 (7 pages).
- Kilpeleainen, J.; Aphalo, P.J.; Lehto, T., (2020). Temperature affected the formation of arbuscular mycorrhizas and ectomycorrhizas in *Populus angustifolia* seedlings more than a mild drought. *Soil Biol. Biochem.*, 146: 1- 12 (12 pages).
- Koutika, L.S.; Richardson, D.M., (2019). *Acacia mangium* willd: Benefits and threats associated with its increasing use around the world. *For. Ecosyst.*, 6(2): 1-13 (13 pages).
- Lan, H.; Wang, D.; He, S.; Fang, Y.; Chen, W.; Zhao, P.; Qi, Y., (2020). Experimental study on the effects of tree planting on slope stability. *Landslides*. 17: 1021–1035 (15 pages).
- Lin, Q.; Wang, Y.; Glade, T.; Zhang, J.; Zhang, Y., (2020). Assessing the spatiotemporal impact of climate change on event rainfall characteristics influencing landslide occurrences based on multiple on multiple GCM projections in China. *Climatic Change*, 162: 761 - 779 (18 pages).
- Listiani, S.; Yuniati, R., (2021). The effect of mycorrhizae on the growth of *Paraserianthes falcataria* L. (Nielsen) in an artificial growth medium containing copper and cadmium. *J. Phys. Conference Series*. 1725: 1-9 (9 pages).
- Liu, A.; Ku, Y.S.; Contador, C.A.; Lam, H.M., (2020). The impacts of domestication and agricultural practices on legume nutrient acquisition through symbiosis with rhizobia and arbuscular mycorrhizal fungi. *Front. Genet.*, 11: 1-11 (11 pages).
- Masi, E.B.; Tofani, V.; Rossi, G.; Cuomo, S.; Wu, W.; Salciarini, D.; Caporali, E.; Filippo Catani, F., (2023). Effects of roots cohesion on regional distributed slope stability modelling. *Catena*. 222: 1 - 10 (10 pages).
- Montagnoli, A.; Terzaghia, M.; Chiatantea, D.; Scippab, G.S.; Lasserreb, B.; Dumroesec, R.K., (2019). Ongoing modifications to root system architecture of *Pinus ponderosa* growing on a sloped site revealed by tree-ring analysis. *Dendrochronologia*. 58: 1-11 (11 pages).
- Muhammad, M.; Umi Isnatin, U.; Peeyush Soni, P.; Adinurani, P.G., (2021). Effectiveness of Mycorrhiza, plant growth promoting rhizobacteria and inorganic fertilizer on chlorophyll content in *Glycine max* (L.) cv. Detam-4 Prida. *E3S Web Conference*. 226: 1-8 (8 pages).
- Phillips, C.; Hales, T.; Smith, H.; Basher, L., (2021). Shallow landslides and vegetation at the catchment scale: a perspective. *Ecol. Eng.*, 173: 1-14 (14 pages).
- Rengers, F.K.; McGuire, L.A.; Oakley, N.S.; Kean, J.W.; Staley, D.M.; Tang, H., (2020). Landslides after wildfire: initiation, magnitude and mobility. *Landslides*. 17: 2631–2641 (10 pages).
- Rini, M.V.; Yansyah, M.P.; Arif, M.A.S., (2021). The application of arbuscular mycorrhizal fungi reduced the required dose of compound fertilizer for oil palm (*Elaeis Guineensis* Jacq.) Nursery. *IOP Conf. Ser.: Earth Environ.*, 1012(1): 1-7 (7 pages).
- Sekar, J.; Saharan, K.; Raju, K.; Singh, U.; Vaiyapuri, P.R., (2019). Consequences of bioinoculants and intercropping approach to alleviate plant drought and salinity stress for sustainable

- agriculture. Salt Stress, Microbes, and Plant Interactions: Mechanisms and Molecular Approaches. 2: 161-182 (22 pages).
- Suresh, B., Dwivedi, V., (2022). Soil bioengineering to deal with soil erosion and landslides in developing nations. Technoarete Transactions on Recent Research. Appl. Microbiol. Biotec., 1(2): 1-7 (7 pages).
- Tao, J.; Dong, F.; Wang, Y.; Chen, H.; Tang, M., (2022). Arbuscular mycorrhizal fungi enhance photosynthesis and drought tolerance by regulating MAPK genes expressions of *Populus simonii* × *P. nigra*. *Physiol. Plant.* 174(6): 1-22 (22 pages).
- Thiergart, T.; Zgadzaj, R.; Bozsóki, Z.; Garrido-Oter, R.; Radutoiu, S.; Schulze-Leferta, P., (2019). *Lotus japonicus* symbiosis genes impact microbial interactions between symbionts and multikingdom commensal communities. *American Society for Microbiology: MBio*, 10(5): 5-19 (15 pages).
- Umer, M.; Mubeen, M.; Iftikhar, Y.; Ali Shad, M.; Usman, H. M.; Sohail, M.A.; Atiq, M. N., Abbas, A., Ateeq, M., (2021). Role of rhizobacteria on plants growth and biological control of plant diseases: A review. *Plant Protect.*, 5(1): 59-71 (15 pages).
- Villa-Rivera, M.G.; Cano-Camacho, H.; López-Romero, E.; Zavala-Páramo, M.G., (2021). The role of arabinogalactan type ii degradation in plant-microbe interactions. *Front. Microbiol.*, 12: 1-14 (14 pages).
- Wang, H.; Qin, J.; Hu, Y.; Guo, C., (2023). Asymmetric growth of belowground and aboveground tree organs and their architectural relationships: a review. *Can. J. For. Res.*, 53(5): 315-327 (13 pages).
- Wira Yuwati, T.; Septiana Putri, W.; Badruzsaufari, (2020). Comparison of arbuscular mycorrhizal spores abundance under sengon (*Falcataria moluccana* (Miq.) Barneby & Grimes) planted on deep peat and mineral soils. *J. Trop. Peatl.*, 10(2): 1-8 (8 pages).
- Xiao, X.; Liao, X.; Yan, Q.; Xie, Y.; Chen, J.; Liang, G.; Chen, M.; Xiao, S.; Chen, Y.; Liu, J., (2023). Arbuscular mycorrhizal fungi improve the growth, water status, and nutrient uptake of *cinnamomum migao* and the soil nutrient stoichiometry under drought stress and recovery. *J. Fungi.* 9(3): 1-23 (23 pages).
- Xiong, P.; Zhang, Z.; Wang, Y.; Peng, X., (2022). Variable responses of maize roots at the seedling stage to artificial biopores in noncompacted and compacted soil. *J. Soils Sed.*, 22: 1155–1164 (10 pages).
- Yang, R.; Yang, S.; Chen, L.; Yang, Z.; Xu, L.; Zhang, X.; Liu, G.; Zhang, X.; Jiao, C.; Bai, R.; Zhang, X.; Zhai, B.; Wang, Z.; Zheng, W.; Li, Z.; Zamanian, K., (2023). Effect of vegetation restoration on soil erosion control and soil carbon and nitrogen dynamics: A meta-analysis. *Soil and Tillage Res.*, 230: 1-11 (11 pages).
- Yavari, S.; Kamyab, H.; Manan, T.S.A.; Chelliapan, S.; Asadpour, R.; Yavari, S.; Sapari, N.; Baloo, L.; Sidik, A.B.C., (2022a). Bio-efficacy of imidazolinones in weed control in a tropical paddy soil amended with optimized agrowaste-derived biochars. *Chemosphere.* 303: 1-8 (8 pages).
- Yavari, S.; Asadpour, R.; Kamyab, H.; Yavari, S.; Kutty, S.R.M.; Baloo, L.; Manan, T.S.A.; Chelliapan, S.; Sidik, A.B.C., (2022b). Efficiency of carbon sorbents in mitigating polar herbicides leaching from tropical soil. *Clean Technol. Environ.*, 24: 251–260 (10 pages).
- Yulianto, S.; Apriyadi, R.K.; Aprilyanto, A.; Winugroho, T.; Ponangsera, I.S.; Wilopo, W., (2021). Histori bencana dan penanggulangannya di indonesia ditinjau dari perspektif keamanan nasional. *PENDIPA J. Sci. Educ.*, 5(2): 180-187 (8 pages).
- Zai, X.M.; Fan, J. J.; Hao, Z.P.; Liu, X.M.; Zhang, W.X., (2021). Effect of co-inoculation with arbuscular mycorrhizal fungi and phosphate solubilizing fungi on nutrient uptake and photosynthesis of beach palm under salt stress environment. *Sci. Rep.*, 11(1): 1-11 (11 pages).
- Zhang, X.; Knappett, J.A.; Leung, A.K.; Ciantia, M.O.; Liang, T.; Danjon, F., (2020). Small-scale modelling of root-soil interaction of trees under lateral loads. *Plant Soil.* 456: 289–305 (7 pages).

#### AUTHOR (S) BIOSKETCHES

**Tejakusuma, I.G.**, Ph.D, Professor, Center for Geological Disaster, National Research and Innovation Agency, Indonesia.

- Email: [iwan004@brin.go.id](mailto:iwan004@brin.go.id)
- ORCID: 0000-0002-2660-4828
- Web of Science ResearcherID: 2655-2023
- Scopus Author ID: 6504148333
- Homepage: <https://brin.go.id/>

**Sittadewi, E.H.**, M.Sc., Senior Researcher, Center for Geological Disaster, National Research and Innovation Agency, Indonesia.

- Email: [euth001@brin.go.id](mailto:euth001@brin.go.id)
- ORCID: 0000-0001-5240-3926
- Web of Science ResearcherID: 2865-2023
- Scopus Author ID: 57200330811
- Homepage: <https://brin.go.id/>

**Handayani, T.**, Ph.D., Professor, Research Centre for Sustainable Production System and Life Cycle Assessment, National Research and Innovation Agency, Indonesia.

- Email: [titi001@brin.go.id](mailto:titi001@brin.go.id)
- ORCID: 0000-0002-4403-5948
- Web of Science ResearcherID: 8677-2022
- Scopus Author ID: 57195628023
- Homepage: <https://brin.go.id/>

**AUTHOR (S) BIOSKETCHES**

**Hernaningsih, T.**, M.Sc., Senior Researcher, Research Centre for Environmental and Clean Technology, National Research and Innovation Agency, Indonesia.

- Email: [taty001@brin.go.id](mailto:taty001@brin.go.id)
- ORCID: 0000-0003-3465-2157
- Web of Science ResearcherID: 8260-2023
- Scopus Author ID: NA
- Homepage: <https://brin.go.id/>

**Wisyanto, W.**, M.Sc., Senior Researcher, Center for Geological Disaster, National Research and Innovation Agency, Indonesia.

- Email: [wisy001@brin.go.id](mailto:wisy001@brin.go.id)
- ORCID: 0009-0007-3583-6536
- Web of Science ResearcherID: 8474-2023
- Scopus Author ID: 57488973700
- Homepage: <https://brin.go.id/>

**Rifai, A.**, B.Sc., Researcher, Research Center for Sustainable Production System and Life Cycle Assessment, National Research and Innovation Agency, Indonesia.

- Email: [akhm001@brin.go.id](mailto:akhm001@brin.go.id)
- ORCID: 0000-0002-4403-5948
- Web of Science ResearcherID: 5138-2023
- Scopus Author ID: NA
- Homepage: <https://brin.go.id/>

**HOW TO CITE THIS ARTICLE**

Tejakusuma, I.G.; Sittadewi, E.H.; Handayani, T.; Hernaningsih, T.; Wisyanto, W.; Rifai, A., (2024). Root growth and arbuscular mycorrhizal fungi on woody plants for vegetative stabilization of tropical slopes. *Global J. Environ. Sci. Manage.*, 10(1): 267-286.

DOI: 10.22034/gjesm.2024.01.17

URL: [https://www.gjesm.net/article\\_704899.html](https://www.gjesm.net/article_704899.html)





## ORIGINAL RESEARCH ARTICLE

Role of *Cylindrospermopsis* sp. in vertical nitrogen changes observed in tropical oxidation wastewater treatment pondsM. Srichomphu<sup>1</sup>, O. Phewnil<sup>1\*</sup>, T. Pattamapitoon<sup>1</sup>, R. Chaichana<sup>2</sup>, K. Chunkao<sup>3</sup>, W. Wararam<sup>1</sup>, N. Dampin<sup>1</sup>, P. Maskulrath<sup>3</sup><sup>1</sup> Department of Environmental Science, Faculty of Environment, Kasetsart University, Bangkok, Thailand<sup>2</sup> Department of Environmental Technology and Management, Faculty of Environment, Kasetsart University, Bangkok, Thailand.<sup>3</sup> The King's Royally Initiated Laem Phak Bia Environmental Research and Development Project, Chaipattana Foundation, Ban Laem District, Phetchaburi Province, Thailand

## ARTICLE INFO

## Article History:

Received 14 January 2023

Revised 19 May 2023

Accepted 28 June 2023

## Keywords:

Community wastewater

*Cylindrospermopsis* sp.

Nitrogen Change

Oxidation pond

Phytoplankton

Tropical climate zone

Vertical distribution

## ABSTRACT

**BACKGROUND AND OBJECTIVES:** As a producer within the ecological food chain, phytoplankton provides the base energy and oxygen to the environment through photosynthesis and higher trophic levels. These benefits can be applied in five consecutive nature-by-nature oxidation ponds for the treatment of community wastewater coming through a high density polyethylene pipeline from the Phetchaburi Municipality located at the King's Royally Initiated Laem Phak Bia Environmental Research and Development Project, Ban Laem District, Phetchaburi Province (Universal Transverse Mercator 47P 1442725 North 617774 East). This study focuses on the vertical distribution of the phytoplankton *Cylindrospermopsis* sp. and its relationship with nitrogen compounds in oxidation ponds.**METHODS:** Samples were collected from a community wastewater treatment system at various depths (30, 60, 90, 120, and 150 centimeters) below the water surface in April 2019 between 11:00 and 13:00 hours and analyzed for their chemical and physical properties. The analysis revealed a vertical relationship between *Cylindrospermopsis* sp. and wastewater. In the density of phytoplankton which were collected by measuring 20 liters of water and filtered using a 36-micron plankton net, calculated and counted under a high magnification microscope, as the species are classified according to the taxonomy.**FINDINGS:** The results of the wastewater quality were as follows: the content of suspended solids was 65–81 milligram per liter, water temperature was 31.8–33.2°C, potential of hydrogen was 8.7–9.2, total nitrogen content was 4.0–5.3 milligram per liter, ammonium content was 0.03–0.06 milligram per liter, nitrate content was 0.09–0.12 milligram per liter, total phosphorus content was 0.9–1.3 milligram per liter, and phosphate content was 0.4–0.5 milligram per liter. In the density of phytoplankton, a significant correlation was observed between the population of *Cylindrospermopsis* sp. and water depth ( $R^2 = 0.9324$ ). The number of populations at the depths of 30, 60, 90, 120, and 150 centimeters were  $3.2 \times 10^7$ ,  $1.6 \times 10^7$ ,  $1.1 \times 10^7$ ,  $5.5 \times 10^7$ , and  $1.1 \times 10^8$  cells per cubic meter, respectively.**CONCLUSION:** The different densities of *Cylindrospermopsis* sp. found at different depths throughout the treatment pond are related to the nitrogen dynamics of the water body. The results of this study revealed that organic nitrogen, including ammonium, was assimilated and converted to inorganic nutrients, which promoted the growth of other phytoplankton species. The correlation between *Cylindrospermopsis* sp. and total nitrogen and ammonium showed significance at  $R^2 = 0.7268$  and  $0.797$ , respectively, with a confidence level of 0.05. Therefore, to ensure treatment effectiveness, the depth of wastewater treatment ponds should be considered during their construction because phytoplankton regulation plays an important role to maintain the overall treatment efficiency.DOI: [10.22034/gjesm.2024.01.18](https://doi.org/10.22034/gjesm.2024.01.18)This is an open access article under the CC BY license (<http://creativecommons.org/licenses/by/4.0/>).

NUMBER OF REFERENCES

41



NUMBER OF FIGURES

4



NUMBER OF TABLES

4

\*Corresponding Author:

Email: [onanong.p@ku.th](mailto:onanong.p@ku.th)

Phone: +668 1824 8649

Note: Discussion period for this manuscript open until April 1, 2024 on GJESM website at the "Show Article".

## INTRODUCTION

Phytoplankton are an important ecosystem species and primary producers of food for marine fauna larvae and dissolved oxygen (DO) in water (Cahyonugroho et al., 2023). As a bioindicator for water fertility and quality, different types of plankton require different environmental factors for growth and blooming (Yossan et al., 2015; Enawgaw et al., 2023). For water contaminated with high levels of organic substances, such as community oxidation pond systems, phytoplankton can produce oxygen for the aerobic digestion of bacteria, which reduces contaminated organic substances and is effective in wastewater treatment (Chunkao et al., 2014; Gautam and Saini, 2020). Environmental factors affecting phytoplankton growth include sunlight, temperature, and chemical compounds, such as nitrogen and phosphorus (Chaichana et al., 2016), which are necessary for protein synthesis and cell formation (Klotz et al., 2016). In addition, some phytoplankton, such as cyanobacteria and blue-green algae, including *Microcystis* sp., *Oscillatoria* sp., *Annabena* sp., and *Cylindrospermopsis* sp., are capable of fixing nitrogen from the air (Paerl, 2017; Ammar et al., 2022). However, some cyanobacteria produce biotoxins, such as microcystin, nodularin, cylindrospermopsin, anatoxin, and saxitoxins, which often affect the nervous system, liver, kidney, skin, and cell membranes of aquatic species, such as fish (Sivonen, 2009; Pelaez et al., 2010; Boopathi et al., 2014; Mowe et al., 2015; Sotton et al., 2015; Mohamed et al., 2018). The importance of nitrogen on phytoplankton can be observed based on the nutrients that affect the growth of plankton by stimulating the production of pigments in the cells used in photosynthesis. In particular, pigments affect energy absorption at different wavelengths, facilitating photosynthesis and producing energy for cell division and growth (Cira et al., 2016). In open water bodies, nitrogen fixation occurs through the transformation of organic nitrogen by ammonification into ammonia nitrogen ( $\text{NH}_4^+$ ), generating nitrite ( $\text{NO}_2^-$ ) and nitrate ( $\text{NO}_3^-$ ), which promote the growth of phytoplankton (Wang et al., 2022). In municipal wastewater treatment systems, nitrogen is transformed through nitrification without significant affects caused by both the depth and seasons. Studies on community wastewater oxidation ponds in Thailand have shown that environmental factors, such as high nutrient levels and organic contaminants, promote high growth rates

of cyanobacteria. Such nutrients were measured with total nitrogen (TN) ranging between 5.0 and 7.1 milligram per liter (mg/L), total phosphorus (TP) at 0.5 and 1.0 mg/L. In terms of energy, solar radiation wavelengths ranging from 381 to 450 nm, 501 to 570 nanometer (nm), and 621 to 750 nm support the growth of cyanobacteria, and each wavelength is specifically important for individual pigments, such as chlorophyll-a, chlorophyll-b, and phycoerythrin, within cyanobacteria cells (Chunkao et al., 2014; Chaichana et al., 2016; Li et al., 2017; Sukchinda et al., 2019). However, since the wastewater treatment systems are highly turbid, solar radiation reaches only up to a water depth of around 30 centimeters (cm) below the surface. Studies have also shown that cyanobacteria, such as *Cylindrospermopsis* sp., grow well under low-light-intensity conditions and are distributed vertically. *Cylindrospermopsis* sp. is a phytoplankton species that fixes nitrogen from the atmosphere for its growth and causes eutrophication. In addition, *Cylindrospermopsis* sp. produces cylindrospermopsin (CYN), a hepatotoxin or cytotoxin that targets the liver, kidney, intestine and muscles (Fernandez et al., 2014; Sotton et al., 2014; Mohamad et al., 2018). Furthermore, *Cylindrospermopsis* sp. cyanobacteria are members of the *Nostocaceae* family and have a filamentous structure, with their cell structures containing pigments, such as chlorophyll-a, carotenoids, phycocyanin, and phycoerythrin. They can produce saxitoxin and cylindrospermopsin (Krienitz et al., 2013; Boopathi et al., 2014; Pierangelini et al., 2014; Vico et al., 2020; Huo et al., 2021; Swe, 2021), which affect fish livers and accumulate in fish muscles (Mohamed et al., 2018; Sotton et al., 2015). Thus, the knowledge gained from this study can be applied for the management of wastewater treatment systems considering the pond depth, especially in stabilization ponds, which allow light to reach the bottom of the pond for an appropriate retention period, thereby realizing an efficient and sustainable water treatment. Cyanobacteria contain phycocyanin, a type of pigment in photosystem II, as they also have the ability to fix nitrogen in low nitrogen environments (Pierangelini et al., 2014; Noreña-Caro et al., 2018). *Cylindrospermopsis* sp. grows well at temperatures ranging from 27.5 to 32.5 degrees Celsius ( $^{\circ}\text{C}$ ) (Antunes et al., 2015; Pierangelini et al., 2015). The TN were 1.81–3.53 mg/L, the TP were 0.046–0.119

mg/L, with all together making the TN to the TP ratio of 23:1 (Chapman *et al.*, 1997). *Cylindrospermopsis* sp. does not grow well on the water surface, mainly because of the effects of hydrogen peroxide (H<sub>2</sub>O<sub>2</sub>) and hydroxyl radicals formed as a result of solar radiation penetrating the water surface and DO molecules. Free radicals created by photolysis damage and destroy *Cylindrospermopsis* sp. cell membranes via lipid peroxidation, resulting in ripped cell membranes that leave cells unable to exchange substances and energy, thereby leading to cell death (Pattamapitoon *et al.*, 2013; Smith *et al.*, 2015; Zarantonellot *et al.*, 2018). Most studies on *Cylindrospermopsis* sp. were conducted in freshwater reservoir, lakes, and rivers (Antunes *et al.*, 2015; Yamamoto and Shiah, 2016). This study aimed to investigate the distribution of *Cylindrospermopsis* sp. and its correlation with nitrogen compounds to demonstrate its ability to remove and fix atmospheric nitrogen into bodies of water, especially in domestic treatment ponds (Yang *et al.*, 2018), where the addition of nitrogen compounds can lead to toxicity and blooming. The study site is the community wastewater treatment

system of the King's Royally Initiated Laem Phak Bia Environmental Research and Development Project: Phetchaburi Province, Thailand, in 2019, which was investigated at different depths.

## MATERIALS AND METHODS

### Study area

The study site of the community wastewater treatment system is located at the King's Royally Initiated Laem Phak Bia Environmental Research and Development Project, Ban Laem District, Phetchaburi Province (Universal Transverse Mercator 47 P 1442725 N 617774 E). The project site consists of five oxidation ponds used for the treatment of domestic wastewater from the Phetchaburi Municipality located near the coastal region of Thailand. The wastewater is gathered through 18.5 kilometers (km) of 40-cm-diameter high density polyethylene pipeline (HDPE) pipes that transfer 6,167 cubic meter per day (m<sup>3</sup>/day) of wastewater to the treatment system (Figs. 1 and 2 and Table 1). The wastewater used for treatment in the system is the municipal wastewater of the Phetchaburi Municipality, which

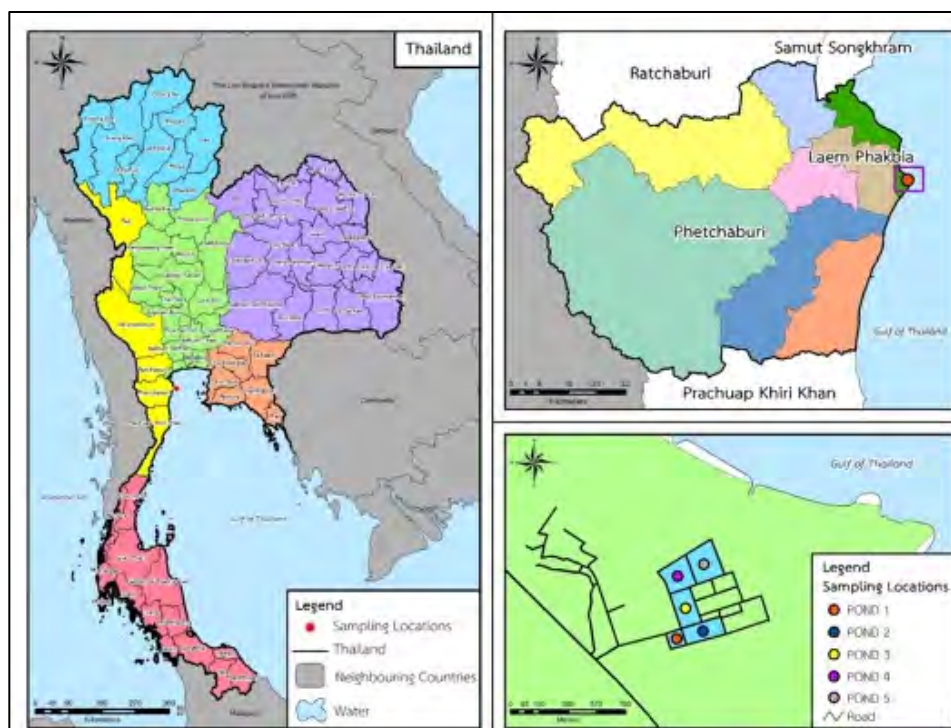


Fig. 1: Geographical location of the study area at the King's Royally Initiated Laem Phak Bia Environmental Research and Development Project, Ban Laem District, Phetchaburi Province, Thailand

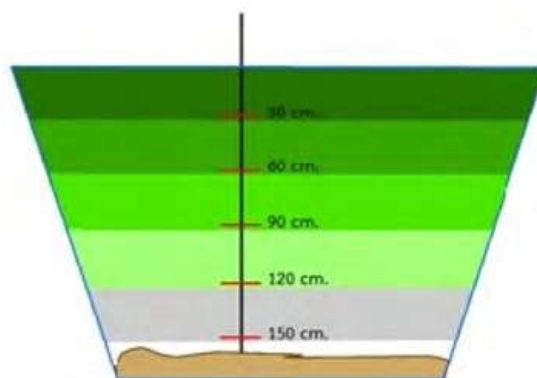


Fig. 2: Wastewater sampling collection depth in pond no. 3 at the King's Royally Initiated Laem Phak Bia Environmental Research and Development Project

Table 1: Pond capacity and dimension

Pond	Pond No. 1	Pond No. 2	Pond No. 3	Pond No. 4	Pond No. 5
Capacity (m <sup>3</sup> )	21,970	60,906	59,007	54,011	59,155
Depth (m)	2.43	2.23	1.93	1.64	1.42
HRT (day)	5	12	15	15	16

is mainly derived from household activities, including that from fresh markets, cooking, and washing. The combined sewer system transfers the wastewater from the source into the wastewater collection pond and retains it for 26 hour (h) before pumping through HDPE pipes in a closed (anaerobic) system at a distance of 18 km and rate of 5000–6000 m<sup>3</sup>/day (Jinjaruk *et al.*, 2018). Regarding the changes in the nitrogen compounds, when community wastewater enters the system, it undergoes nature-by-nature treatment to decrease the biological oxygen demand (BOD), phosphorus, and nitrogen contents while increasing the suspended solid (SS) content owing to the growth of phytoplankton in the system (Chunkao *et al.*, 2018). These processes may affect the nitrogen content as most of the growing plankton are cyanobacteria (Sukchinda *et al.*, 2019), which can fix nitrogen. Moreover, when the phytoplankton die, their cells increase the amount of organic matter in the system.

#### Water sampling and analysis

Wastewater samples were collected from the community wastewater treatment ponds during the dry period in April 2019. This work only focused on pond no. 3, which has the highest density of *Cylindrospermopsis sp.* Before sampling, the

collection depths of the pond were defined and indicated to ensure that the water was sampled from the desired depth. The samples were collected from the center of the pond at five different depths (30, 60, 90, 120, and 150 cm from the surface) (Noikondee *et al.*, 2019) using water samplers in a vacuum water pump attached to a tube placed at the desired depths of 30, 60, 90, 120, and 150 cm between 11:00 a.m. and 14:00 p.m. Once the pump was operated for 60 s before obtaining the actual sample water, 1 liter (L) water sample was collected in polyethylene bottles, which were wrapped in aluminum foil and stored at 4°C to prevent exposure to light and slow down microorganism activities. The samples were then analyzed in laboratories following standard procedures (APHA, 2012) for the physical parameters temperature and total dissolved solids and the chemical parameters dissolved oxygen, pH, nitrogen compounds (Organic nitrogen, total Keldahl nitrogen, ammonium, and nitrate), phosphorus, and phosphate. The temperature and pH were measured on site; the results are shown in Table 2.

#### Phytoplankton analysis

Phytoplankton were collected by filtering 20 L from each depth through a 36-micrometer (µm) plankton net. Once filtered, 4% formalin solution was added

Table 2: Parameters analyzed and the methods used

Parameters	Units	Method
Temperature (Degree Celsius)	°C	Thermometer
DO (Dissolve oxygen)	mg/L	DO meter
pH (Potential of hydrogen)	-	pH meter
TN (Total nitrogen)	mg/L	Kjeldahl
TKN (Total Kjeldahl nitrogen)	mg/L	Kjeldahl
NH <sub>4</sub> <sup>+</sup> (Ammonium nitrogen)	mg/L	Colorimetric
NO <sub>3</sub> <sup>-</sup> (Nitrate nitrogen)	mg/L	Brucine
TP (Total phosphorus)	mg/L	Ascorbic acid
PO <sub>4</sub> <sup>3-</sup> (Orthophosphate)	mg/L	Colorimetric
SS (Suspended solids)	mg/L	Filter with glass microfiber filter (GF/C), dried at 103-105°C
Transparency	cm	Secchi disk

to maintain the sample (Figs. 1 and 2) (Wongrat *et al.*, 2017). The samples were then analyzed under a high magnification microscope to classify the phytoplankton species according to their taxon using molecular and morphological methods (Bellinger and Sigeo, 2010; Li *et al.*, 2017; Wongrat, 2017). The size and particles in 1 L samples were determined under a Sedgewick–Rafter chamber thrice and averaged in terms of cells per cubic meter (cells/m<sup>3</sup>), using Eq. 1 (USEPA, 2021).

$$C = \frac{NV_2}{V_1} \quad (1)$$

Where,

C = plankton density in cells/L (a conversion (×1000) was conducted to obtain the value in cells/m<sup>3</sup>)

N = average density of per 1 milliliter of plankton

V<sub>2</sub> = volume of water filtered through the plankton filter bag (liters)

V<sub>1</sub> = volume of sample water contained in the sample bottle (milliliters)

In the data analysis, the average value was used to create graphs in terms of the depth and its correlation with the water quality and *Cylindrospermopsis* sp. For the community wastewater treatment, pond no. 3 was used as the best representation of the treatment system of the water quality, which demonstrated the water treatment to meet standards. However, when the system processes progressed and the plankton bloomed, *Cyanobacteria* sp. grew.

#### Statistical analysis

All data of this study were analyzed using one-way

analysis of variance, and correlation graphs were prepared for comparing the relationship between *Cylindrospermopsis* sp. and different nitrogen compounds.

## RESULTS AND DISCUSSION

### Type and amount of Cyanobacteria

According to the sample analysis, cyanobacteria were detected in all five oxidation ponds at the following population levels: 5.19 × 10<sup>6</sup>, 9.00 × 10<sup>6</sup>, 3.10 × 10<sup>7</sup>, 1.36 × 10<sup>5</sup>, and 1.27 × 10<sup>4</sup> cells/m<sup>3</sup>. The cyanobacteria were classified into two orders, three families, five genera, and six species: *Oscillatoria* sp., *Spirulina patensis*, *S. subsalsa*, *Anabenopsis* sp., *Cylindrospermopsis* sp., and *Microcystis aroginosa*. The highest cyanobacteria population was found in pond no. 3 and was distributed across all depths with the population 2.9 × 10<sup>7</sup>, 4.4 × 10<sup>7</sup>, 1.6 × 10<sup>7</sup>, 2.1 × 10<sup>7</sup>, and 4.2 × 10<sup>7</sup> cells/m<sup>3</sup> at 30, 60, 90, 120, and 150 cm from the surface, respectively (Table 3 and Fig. 3).

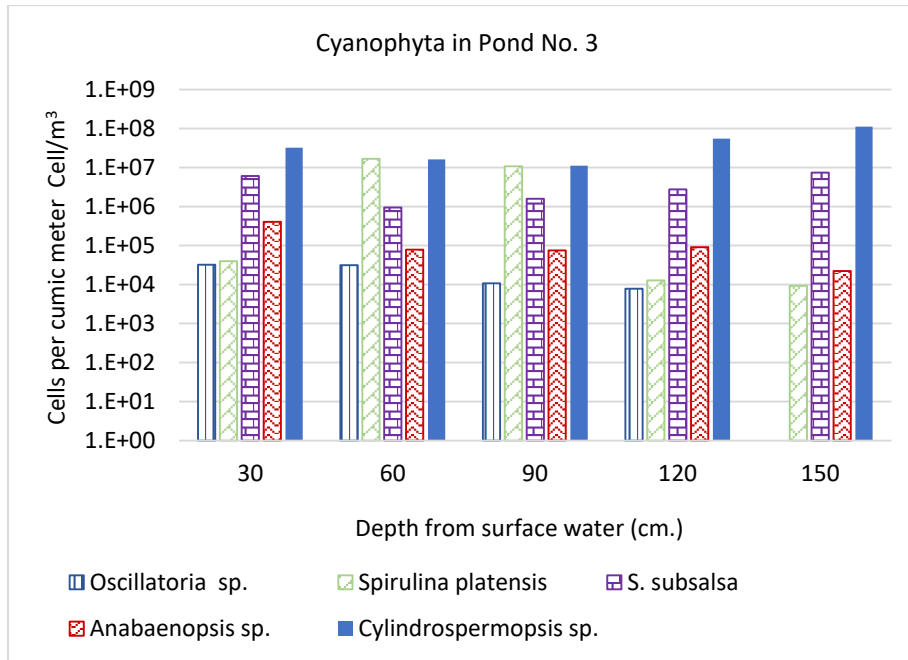
Five species of cyanobacteria were found in pond no. 3: *Oscillatoria* sp., *Spirulina patensis*, *S. subsalsa*, *Anabenopsis* sp., and *Cylindrospermopsis* sp. In particular, *Cylindrospermopsis* sp. was distributed at all depths and tended to increase with the depth (R<sup>2</sup> = 0.9324). At 30, 60, 90, 120, and 150 cm, the populations of *Cylindrospermopsis* sp. were 3.2 × 10<sup>7</sup>, 1.6 × 10<sup>7</sup>, 1.1 × 10<sup>7</sup>, 5.5 × 10<sup>7</sup>, and 1.1 × 10<sup>8</sup> cells/m<sup>3</sup>, respectively. The density of the phytoplankton is related to the nitrogen content, as *Cylindrospermopsis* sp. was that the assimilate the nitrogen compound in which they support the removal of ammonium in the oxidation pond, however under their optimal habitat of low light and temperature (Yamamoto, and Shiah, 2016) leading to differences in density resulting in the vertical distribution of the species as well as the

Table 3: Average populations of cyanobacteria in the community wastewater treatment system oxidation ponds in April 2019

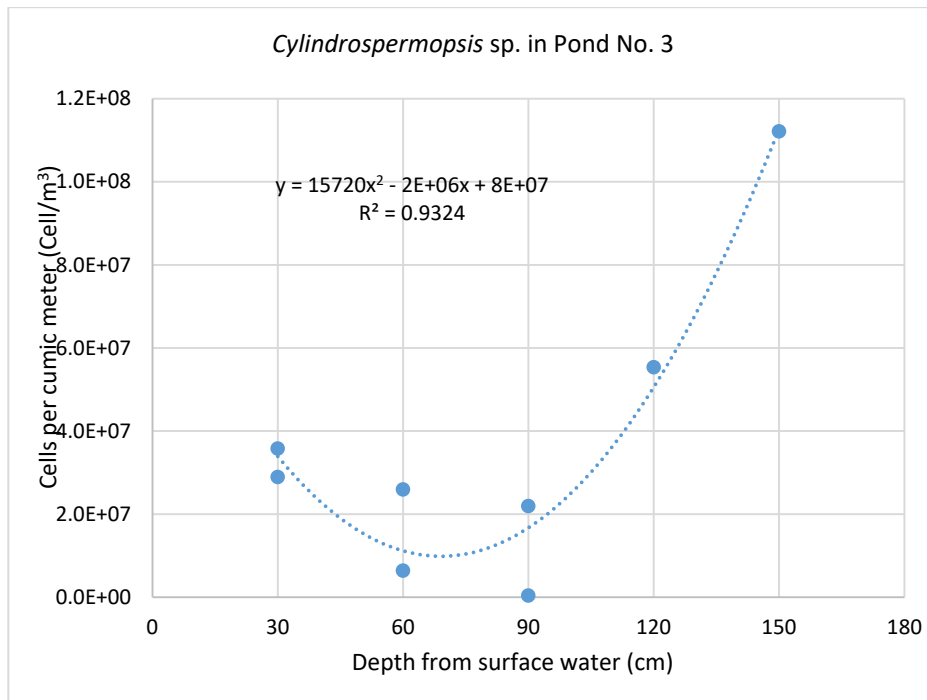
Depth (cm)	Temp (°C)	DO (mg/l)	pH	TN (mg/L)	TKN (mg/L)	NH <sub>4</sub> <sup>+</sup> (mg/L)	NO <sub>3</sub> <sup>-</sup> (mg/L)	TP (mg/L)	[PO <sub>4</sub> ] <sup>3-</sup> (mg/L)	SS (mg/L)
30	33.23 ± 0.11 <sup>a</sup>	10.85 ± 1.45 <sup>a</sup>	9.17 ± 0.11 <sup>a</sup>	5.17 ± 0.56 <sup>a</sup>	5.04 ± 0.56 <sup>a</sup>	0.04 ± 0.01 <sup>ab</sup>	0.10 ± 0.03 <sup>a</sup>	1.37 ± 0.25 <sup>a</sup>	0.50 ± 0.04 <sup>a</sup>	65.33 ± 7.63 <sup>b</sup>
60	32.80 ± 0.20 <sup>b</sup>	8.74 ± 0.35 <sup>b</sup>	9.12 ± 0.04 <sup>a</sup>	4.63 ± 0.98 <sup>a</sup>	4.48 ± 0.96 <sup>a</sup>	0.05 ± 0.02 <sup>ab</sup>	0.10 ± 0.01 <sup>a</sup>	0.94 ± 0.13 <sup>ab</sup>	0.48 ± 0.04 <sup>a</sup>	63.33 ± 3.51 <sup>b</sup>
90	32.40 ± 0.30 <sup>bc</sup>	5.80 ± 0.93 <sup>c</sup>	9.05 ± 0.04 <sup>a</sup>	4.04 ± 1.46 <sup>a</sup>	3.92 ± 1.48 <sup>a</sup>	0.03 ± 0.005 <sup>b</sup>	0.10 ± 0.01 <sup>a</sup>	0.97 ± 0.39 <sup>b</sup>	0.47 ± 0.02 <sup>a</sup>	68.67 ± 2.88 <sup>b</sup>
120	32.07 ± 0.30 <sup>cd</sup>	3.80 ± 0.58 <sup>d</sup>	8.88 ± 0.07 <sup>b</sup>	4.48 ± 2.58 <sup>a</sup>	4.29 ± 2.58 <sup>a</sup>	0.06 ± 0.02 <sup>a</sup>	0.12 ± 0.005 <sup>a</sup>	1.16 ± 0.19 <sup>ab</sup>	0.52 ± 0.07 <sup>a</sup>	70.00 ± 1.73 <sup>b</sup>
150	31.80 ± 0.10 <sup>d</sup>	2.21 ± 0.75 <sup>d</sup>	8.74 ± 0.06 <sup>c</sup>	5.38 ± 1.98 <sup>a</sup>	5.23 ± 1.96 <sup>a</sup>	0.03 ± 0.02 <sup>ab</sup>	0.12 ± 0.01 <sup>a</sup>	1.11 ± 0.24 <sup>ab</sup>	0.51 ± 0.04 <sup>a</sup>	81.33 ± 6.11 <sup>a</sup>
STD**	-	-	5.5–9.0*	<20*	-	-	-	<2*	-	<50*

\*Pollution Control Department of Thailand (2010)

\*\*STD = Standard



(a)



(b)

Fig. 3: Species of cyanobacteria in pond no. 3 relationship between *Cylandrospermopsis* sp. and depth in pond no. 3. (a) Cyanophyta density in pond no. 3. (b) *Cylandrospermopsis* sp. in pond no. 3

Table 4: Water quality in pond no.3

Depth (cm)	Temp (°C)	pH	TN (mg/L)	TKN (mg/L)	NH <sub>4</sub> <sup>+</sup> (mg/L)	NO <sub>3</sub> <sup>-</sup> (mg/L)	TP (mg/L)	PO <sub>4</sub> <sup>3-</sup> (mg/L)	TN:TP (mg/L)	SS (mg/L)
30	33.23	9.17	5.17	5.04	0.04	0.10	1.37	0.50	3.80	65.33
60	32.80	9.12	4.63	4.48	0.05	0.10	0.94	0.48	5.06	63.33
90	32.40	9.05	4.04	3.92	0.03	0.10	0.97	0.47	4.40	68.67
120	32.07	8.88	4.48	4.29	0.06	0.12	1.16	0.52	4.22	70.00
150	31.80	8.74	5.38	5.23	0.03	0.12	1.11	0.51	4.73	81.33

nitrogen content. Furthermore, it was suggested that the phytoplankton prefer different nitrogen sources, mainly NH<sub>4</sub><sup>+</sup> over NO<sub>3</sub><sup>-</sup>, followed by N-free; therefore, dissolved inorganic nitrogen was considered the main source of nitrogen for *Cylindrospermopsis* sp., which is related to the nitrogen removal efficiency (Antunes *et al.*, 2015).

#### Water quality

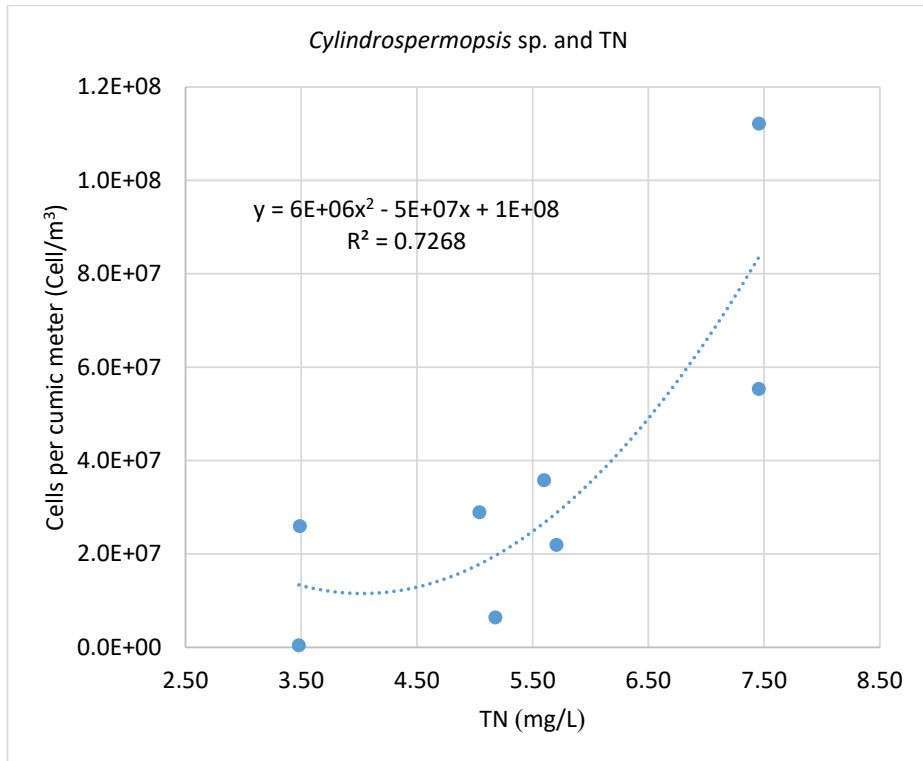
The community wastewater at the study site contains high levels of organic substances contamination is rested within the sedimentation pond (pond no. 1) for 7 days to settle out the heavy sediment. The water then flows into pond no. 2, 3, and 4. Microorganisms in oxidation ponds use oxygen produced by plankton through photosynthesis and the thermosiphon process (Pattamapitooon *et al.*, 2013; Chunkao *et al.*, 2014; Noikondee *et al.*, 2019; Kumar *et al.*, 2019) to digest organic substances and produce inorganic substances, which are used by phytoplankton for growth. The wastewater is retained in oxidation pond nos. 2, 3, and 4 for 12, 15, and 15 days, respectively. After the community wastewater is treated, it flows into pond no. 5, the stabilization pond. This is the shallowest pond as the pond function were to allow for sunlight to penetrate into the bottom of the pond killing bacteria, while also adds oxygen produced by the phytoplankton to the water before it is released into natural environment. The wastewater treatment process takes 49 days, and the results of water quality sampling indicated that the water quality reached standards for community wastewater treatment system set by the Ministry of Natural Resource and Environment, Thailand. Depicting into pond no. 3, the transparency was 27 cm, and the dissolved oxygen content was 2.2–10.8 mg/L. However, the

dissolved oxygen tended to decrease with depth because of decreasing levels of sunlight. Sunlight supports phytoplankton photosynthesis at the water surface, thereby increasing the oxygen levels in water. Dissolved oxygen at deeper levels is used by microorganisms for organic digestion, resulting in higher levels of dissolved oxygen at the water surface than at the deeper levels. The suspended solid content was 65–81 mg/L, and it tended to increase with depth due to the increasing density of *Cylindrospermopsis* sp. at deeper levels (Table 4).

#### Relationship between nitrogen and *Cylindrospermopsis* sp.

The TN tended to increase with an increase in the density of *Cylindrospermopsis* sp. because of their nitrogen-fixing ability. Moreover, NH<sub>4</sub><sup>+</sup> increased with an increase in water depth due to ammonification; NH<sub>4</sub><sup>+</sup> was used by *Cylindrospermopsis* sp. for their growth (Yang *et al.*, 2018). This showed a reverse relationship between the amount of NH<sub>4</sub><sup>+</sup> and the density of *Cylindrospermopsis* sp., considering the relationship between *Cylindrospermopsis* sp. to TN and NH<sub>4</sub><sup>+</sup> according to water depth. The results revealed that TN and NH<sub>4</sub><sup>+</sup> were significantly correlated (R<sup>2</sup> = 0.7268 and 0.797, respectively) (Fig. 4).

The water temperature ranged from 31.8°C to 33.2°C and tended to decrease with depth because of the heating by solar radiation at the surface (Noikondee *et al.*, 2019). Solar radiation and wind promote evaporation and cool the surface of the pond, creating a denser water column. These changes in density promote vertical circulation of the water within the pond as there is a thermal gradient. Such phenomena makes the water temperature at the bottom of the pond suitable for the growth of



(a)

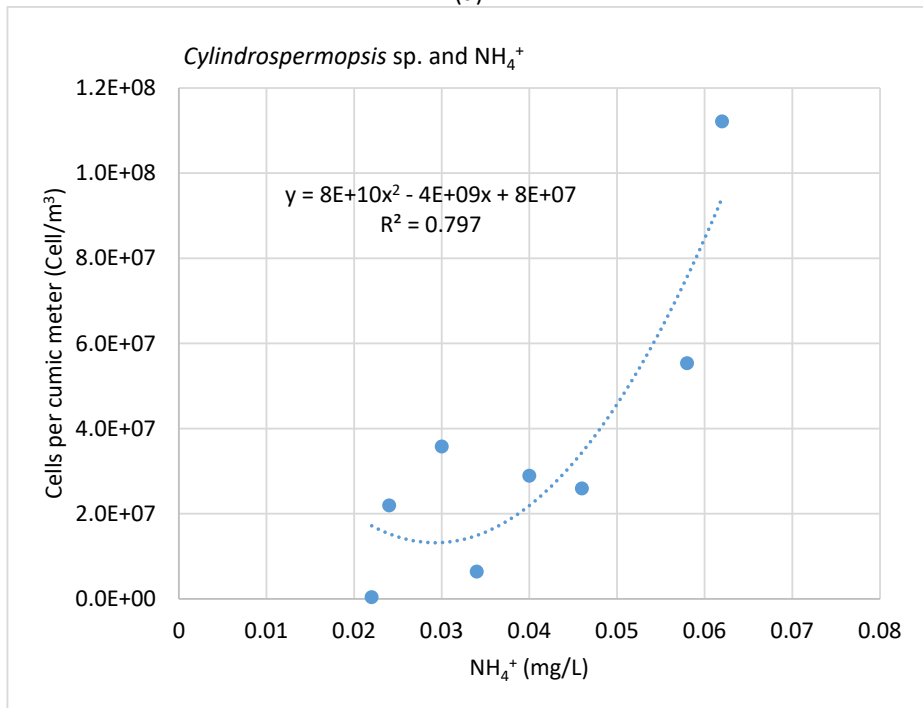


Fig. 4: Relationship between *Cylindrospermopsis* sp. and (a) total nitrogen (TN), (b) ammonium (NH<sub>4</sub><sup>+</sup>)

*Cylindrospermopsis* sp. The results showed that the pH at the surface of water (30 cm) was 9.2; however, it decreased to 8.7 at deeper levels (150 cm) due to the release of carbon dioxide from microbial digestion. The carbon dioxide reacts with water and is dissociated into bicarbonate, which releases hydrogen ions. At the same time, nitrification turns  $\text{NH}_4^+$  into hydrogen ions, increasing the alkalinity of water. The nutrient levels in pond no. 3 were indicated by the TN (4.04-5.38 mg/L) and TP (0.94-1.37 mg/L) levels, which decreased with water depth. However, it increased slightly at 90 cm below the water surface due to the greater distribution of *Cylindrospermopsis* sp. at deeper levels, which fix nitrogen from the air, resulting in increased organic substances in the water.  $\text{NH}_4^+$  levels decreased from 0.03–0.06 mg/L according to the depth of the water because of the ammonification process, which decomposes nitrogen from organic substances into inorganic substances in the form of  $\text{NH}_4^+$ . At deeper levels, the nitrification process converts  $\text{NH}_4^+$  into  $\text{NO}_3^-$ . At the bottom of the pond, where oxygen is low, *Cylindrospermopsis* sp. is capable of photosystem II that produced oxygen for the microorganisms through nitrification. This resulted in an increase in  $\text{NO}_3^-$  to 0.09–0.12 mg/L. Moreover, the TP level was 0.9–1.3 mg/L and the orthophosphate ( $\text{PO}_4^{3-}$ ) level was 0.4–0.5 mg/L, which decreased at the surface and middle depths of the pond but increased at deeper levels (Table 3). From (Fig. 4), the correlation between *Cylindrospermopsis* sp., TN and  $\text{NH}_4^+$  presented a high significant relation, where this is explained through the process of nitrogen fixation by *Cylindrospermopsis* sp. from the atmosphere together with the ammonification process within the pond. *Cylindrospermopsis* sp. cyanobacteria in pond no. 3 had the highest growth rate and density. *Cylindrospermopsis* sp. was distributed at every depth without significant difference because it is capable of growing under low-light intensities, with preferable temperature ranging between 27.5°C and 32.5°C (Antunes et al., 2015; Pierangelini et al., 2015; Xiao et al., 2017). Under high-light-intensity conditions, high levels of UVA and UVB breakdown water molecules and transform DO into a new compound, such as  $\text{H}_2\text{O}_2$  (Pattamapitoon et al., 2013), which can destroy the cell membrane of *Cylindrospermopsis* sp. It also results in vesicle leakage, leading to malformation and rendering cells incapable of cell division and growth, thereby

reducing cell density and division (Pattamapitoon et al., 2015; Smith et al., 2015; Zantonellot et al., 2018). However, at low-light intensities, *Cylindrospermopsis* sp. uses more phycocyanins for photosystem II (Pierangelini et al., 2014; Noreña-Caro et al., 2018). Overall, it can be concluded that the distribution of *Cylindrospermopsis* sp. was greater in low-light-intensity areas than in high-light-intensity areas at the study site. Nitrogen compounds in the municipal wastewater treatment system are transformed from organic nitrogen compounds to  $\text{NH}_4^+$ ,  $\text{NO}_2^-$ , and  $\text{NO}_3^-$  through nitrification. Considering the depth, the TN and organic nitrogen contents were higher than  $\text{NH}_4^+$  and  $\text{NO}_3^-$  at the bottom of the pond. As more than 15 types of microorganisms were found in the community wastewater treatment system, each group contributed to the transformation of nitrogen compounds together. Moreover, the growth of *Cylindrospermopsis* sp. in the pond increased the high organic nitrogen concentration due to the increased nitrogen fixation owing to the use of  $\text{NH}_4^+$  and  $\text{NO}_3^-$  to produce more cells (Rose et al., 2021; Saneha et al., 2023). The process is described by the conversion of organic nitrogen into inorganic nitrogen ( $\text{NH}_4^+$  and  $\text{NO}_3^-$ ), which are the N sources for *Cylindrospermopsis* sp. growth, by nitrification. The inorganic nitrogen is then converted back into its organic form in the plankton's cells through cellular assimilation (Spröber et al., 2003). When the cells die, the amount of organic nitrogen at the bottom of the pond increases. Overall, nitrogen fixation refers to the conversion of nitrogen into  $\text{NH}_4^+$ , and cyanobacteria can photosynthesize and supply oxygen to the environment. However, *Cylindrospermopsis* sp. can adapt to nitrogen fixation under low-light conditions, such as that at the bottom of the pond (Paerl, 2017; Rose et al., 2021).

## CONCLUSION

In the identification of the total phytoplankton species found in the nature-by-nature (an oxidation process which is not assisted or enhanced by any artificial aeration or mixing) oxidation treatment pond for domestic wastewater at The King's Royally Initiated Laem Phak Bia Environmental Research and Development Project, Phetchaburi Province, Thailand. This work investigated the distribution in domestic wastewater treatment system. The findings suggested that the most abundant species was *Cylindrospermopsis* sp., which has the ability

to move freely throughout the treatment pond and fix free atmospheric nitrogen into the water body. Furthermore, through the oxidation process in the treatment system, the conversion of organic nitrogen, including  $\text{NH}_4^+$ , into inorganic nutrients promotes the growth of other phytoplankton species and the photosynthesis process. The distribution of *Cylindrospermopsis* sp. was the highest in pond no. 3 at 150 cm below the surface ( $1.1 \times 10^8$  cells/ $\text{m}^3$ ). This population affected the overall water quality by increasing the nitrogen and phosphorus-containing SS, TN, and  $\text{NH}_4^+$  concentrations that were significantly correlated with the *Cylindrospermopsis* sp. population. Therefore, the depth of wastewater treatment ponds should be considered for the treatment effectiveness when constructing wastewater treatment systems, as regulation by phytoplankton plays an important role in maintaining the overall treatment efficiency with the implication of the potential impact would be through their ability to remove nitrogen from the oxidation pond as this would increase plankton bloom leading to a potential *cylindrospermopsin* build up. This study determined the appropriate pond depth to be less than 1.5 m to eliminate low-light areas, which could decrease the density of *Cylindrospermopsis* sp.; however, further studies are recommended to determine the correlation among ponds deeper than 1.5 m, *cylindrospermopsin*, light, and seasonal variations.

#### AUTHOR CONTRIBUTIONS

M. Srichomphu performed literature review, experimental design, material preparation, data collection, analysis, and interpretation, and manuscript preparation. O. Phewnil performed study conception, experimental design, material preparation, data collection and analysis, and manuscript preparation and editing. T. Pattamapitooon performed experimental design and data collection and interpretation. R. Chaichana performed experiments and commented on a previous version of the manuscript. K. Chunkao performed experimental design and manuscript editing. W. Wararam performed data collection, analysis, and interpretation. N. Dampin performed some experiments and data collection. P. Maskulrath performed material preparation, data collection, and manuscript preparation.

#### ACKNOWLEDGEMENT

The authors appreciate the King's Royally Initiated Laem Phak Bia Environmental Research and Development Project, the Chapiattan Foundation for its research funding (LERD RDS2-2/2562) and facilitation during the research process. We also thank professors from the Faculty of Environment, Kasetsart University, for their invaluable consultation.

#### CONFLICT OF INTEREST

The authors declare that there is no conflict of interests regarding the publication of this manuscript. In addition, the ethical issues, including plagiarism, informed consent, misconduct, data fabrication and/or falsification, double publication and/or submission, and redundancy, have been completely observed by the authors.

#### OPEN ACCESS

©2024 The author(s). This article is licensed under a Creative Commons Attribution 4.0 International License, which permits use, sharing, adaptation, distribution and reproduction in any medium or format, as long as you give appropriate credit to the original author(s) and the source, provide a link to the Creative Commons license, and indicate if changes were made. The images or other third-party material in this article are included in the article's Creative Commons license, unless indicated otherwise in a credit line to the material. If material is not included in the article's Creative Commons license and your intended use is not permitted by statutory regulation or exceeds the permitted use, you will need to obtain permission directly from the copyright holder. To view a copy of this license, visit: <http://creativecommons.org/licenses/by/4.0/>

#### PUBLISHER'S NOTE

GJESM Publisher remains neutral with regard to jurisdictional claims in published maps and institutional affiliations.

#### ABBREVIATIONS

%	Percent
°C	Degree celsius

$\mu m$	Micrometer
BOD	Biological oxygen demand
cm	Centimeter
Cells/m <sup>3</sup>	Cell per cubic meter
CYN	Cylindrospermopsis
DO	Dissolved oxygen
GF/C	Glass microfiber filter
h	Hour
HDPE	High density polyethylene
H <sub>2</sub> O <sub>2</sub>	Hydrogen peroxide
km	Kilometer
L	Liter
m	Meter
m <sup>3</sup>	Cubic meter
m <sup>3</sup> /Day	Cubic meter per day
mg/L	Milligram per liter
mL	Milliliter
NH <sub>4</sub> <sup>+</sup>	Ammonium nitrogen
nm	Nanometer
No.	Number
NO <sub>2</sub> <sup>-</sup>	Nitrite
NO <sub>3</sub> <sup>-</sup>	Nitrate
pH	Potential of hydrogen
PO <sub>4</sub> <sup>3-</sup>	Orthophosphate
R <sup>2</sup>	Coefficient of determination
SS	Suspended solid
TN	Total nitrogen
TP	Total phosphorus
TKN	Total Kjeldahl nitrogen
STD	Standards

## REFERENCES

- APHA, (2012). Standard methods for examination of water and wastewater, 22nd ed. Washington (541 pages).
- Ammar, E.E.; Aioub, A.A.A.; Elesawy, A.E.; Karkour, A.M.; Mouhamed, M.S.; Amer, A.A.; EL-Shershaby, N.A., (2022). Algae as bio-fertilizers: between current situation and future prospective. Saudi Journal of Biol. Sci., 29(5): 3083-3096 (14 pages).
- Antunes, J.T.; Leão, P.N.; Vasconcelos, V.M., (2015). Cylindrospermopsis raciborskii: review of the distribution, phylogeography, and ecophysiology of a global invasive species. Front Microbiol., 6: 1-13 (13 pages).
- Bellinger, E.G., Sigeo, D.C., (2010). Freshwater algae: identification and use as bioindicators. John Wiley & Sons, Ltd.: 157-254 (11 pages).
- Boopathi, T.; Ki, J-S., (2014). Impact of environmental factors on the regulation of cyanotoxin production. Toxins. 6(7): 1951-1978 (28 pages).
- Cahyonugroho, O.H.; Hariyanto, S.; Supriyanto, G., (2022). Dissolved organic matter and its correlation with phytoplankton abundance for monitoring surface water quality. Global J. Environ. Sci. Manage., 8(1): 59-74 (16 pages).
- Chaichana, R.; Dampin, N., (2016). Unialgal blooms of Cyanobacteria in oxidation ponds the King's Royally Initiated Laem Phak Bia Environmental Research and Development Project, Thailand. Environment Asia. 12(3): 54-61 (8 pages).
- Chunkao, K.; Tarnchalanukit, W.; Prabuddham, P., (2014). The King's Royally Initiated LERD project on community wastewater treatment through small wetlands and oxidation pond in Phetchaburi, Thailand. Mod Appl Sci., 8(5): 233-246 (14 pages).
- Cira, E.K.; Paerl, H.W.; Wetz, M.S., (2016). Effects of nitrogen availability and form on phytoplankton growth in a eutrophied estuary (Neuse River Estuary, NC, USA). PLoS One. 11(8): 1-15 (15 pages).
- Fernandez, D.A.; Louzao, M.C.; Vilarino, N.; Fraga, M.; Espina, B.; Vieytes, M.R.; Botana, L.M., (2014). Evaluation of the intestinal permeability and cytotoxic effects of cylindrospermopsis. Toxicon. 91: 23-34 (12 pages).
- Gautam, S.; Saini, G., (2020). Use of natural coagulants for industrial wastewater treatment. Global J. Environ. Sci. Manage., 6(4): 553-578 (26 pages).
- Huo, D.; Gan, N.; Geng, R.; Cao, Q.; Song, L.; Yu, G.; Li, R.; (2021). Cyanobacterial blooms in China: diversity, distribution, and cyanotoxins. Harmful Algae. 109: 102106 (14 pages).
- Klotz, A.; Georg, J.; Bučinská, L., (2016). Awakening of a dormant cyanobacterium from nitrogen chlorosis reveals a genetically determined program. Curr. Biol., 26: 2862-2872 (11 pages).
- Krienitz, L.; Dadheech, P.K.; Fastner, J.; Kotut, K., (2013). The rise of potentially toxin producing cyanobacteria in Lake Naivasha, Great African Rift Valley, Kenya. Harmful Algae 27: 42-51 (10 pages).
- Kumar, N.; Rajshree, A.; Yadav, A.; Malhotra, N.H.; Gupta, N.; Pushp, P., (2019). Validation of eco-enzyme for improved water quality effect during large public gathering at river bank. Int. J. Hum. Capital Urban Manage., 4(3): 181- 188 (8 pages).
- Li, X.; Huo, S.; Cai, F., (2017). The taxonomy and phylogeny of the genus Cylindrospermopsis (Cyanobacterium) evaluated by adding five new records from China. Phytotaxa. 316: 224-238 (15 pages).
- Mohamed, ZA.; Bakr, A., (2018). Concentrations of cylindrospermopsis toxin in water and tilapia fish of tropical fishponds in Egypt, and assessing their potential risk to human health. Environ. Sci. Pollut. Res. Int., 25: 36287-36297 (11 pages).
- Mowe, MAD.; Mitrovic, SM.; Lim, RP., (2015). Tropical cyanobacterial blooms: a review of prevalence, problem taxa, toxins and influencing environmental factors. J. Limnol., 73: 205-224 (19 pages).
- Noikondee, R.; Chunkao, K.; Bualert, S., (2019). Evaluation of dissolved oxygen stratification in an oxidation pond for community wastewater treatment through King's Royally Initiated "nature by nature. process. Environ. Asia. 12: 169-177 (9 pages).
- Noreña-Caro, D.; Benton, MG., (2018). Cyanobacteria as

- photoautotrophic biofactories of high-value chemicals. *J. CO<sub>2</sub> Util.*, 28: 335-366 (32 pages). Paerl H., (2017). The cyanobacterial nitrogen fixation paradox in natural water. *F1000 Research*. 6(244): 1-6 (6 pages).
- Pattamapitooon, T.; Sirirote, P.; Pakkong, P., (2013). Nature of solar radiation as encouraged to produce an increment of dissolved oxygen and hydrogen peroxide in oxidation ponds for community wastewater treatment at H.M.The King's LERD project site in Phetchaburi Province, Thailand. *Mod. Appl. Sci.*, 7(6): 26-41 (16 pages).
- PCDT, (2010). Announcement of the Ministry of Natural Resources and Environment: Standards controlling the discharge of wastewater from all wastewater treatment systems. Pollution Control Department of Thailand. 27-28 (2 page).
- Pierangelini, M.; Stojkovic, S.; Orr, P.T., (2014). Elevated CO<sub>2</sub> causes changes in the photosynthetic Apparatus of a toxic cyanobacterium, *Cylindrospermopsis raciborskii*. *J. Plant Physiol.*, 171: 1091-1098 (8 pages).
- Pierangelini, M.; Stojkovic, S.; Orr, P.T., (2015). Photo-acclimation to low light—changes from growth to antenna size in the cyanobacterium *Cylindrospermopsis raciborskii*. *Harmful Algae*. 46: 11-17 (7 pages).
- Rose, A.; Padavan, A.; Christian, K.; Van de Kamp, J.; Kaeatli, M; Tsoukalis, S; Bodrossy, L.; Gibb, K., (2021). The Diversity of nitrogen-cycling microbial genes in a waste stabilization pond reveals changes over space and time that is uncoupled to changing nitrogen chemistry. *Microb. Ecol.*, 81: 1029-1041 (13 pages).
- Saneha, S., Pattamapitooon, T.; Bualert, S.; Phewnil, O.; Wararam, w.; Semvimol, N.; Chunkao, K.; Tudsanaton, C.; Srichonphu, M.; Nachaiboon, U.; Wongsrikaew, O.; Wichittrakarn, P.; Chanthasoon, C., (2023). Relationship between bacteria and nitrogen dynamics in wastewater treatment oxidation ponds. *Global J. Environ. Sci. Manage.*, 9(4): 707-718 (11 pages).
- Smith, BR.; Edds, DR.; Goeckler, JM., (2015). Lowhead dams and the downstream dispersal of zebra mussels. *Hydrobiologia*. 755: 1-12 (12 pages).
- Sotton, B.; Domaizon, I.; Anneville, O., (2015). Nodularin and cylindrospermopsin: a review of their effects fish. *Rev. Fish. Biol. Fish.*, 15: 1-19 (19 pages).
- Spröber, P., Shafik, H.M., Présing, M., Kovács, A.W., Herodek, S., (2003). Nitrogen uptake and fixation in the cyanobacterium *Cylindrospermopsis raciborskii* under different nitrogen conditions. *Hydrobiologia* 506: 169-174 (6 pages).
- Sukchinda, S.; Bualert, S.; Phewnil, O.; Pattamapitooon, T.; Srichomphu, M., (2019). Effect of solar radiation on cyanobacteria bloom in oxidation ponds community wastewater treatment at the King's Royally Initiated Laem Phak Bia Environmental Research and Development Project, Phetchaburi, Thailand. *Environ. Asia*. 12: 54-61 (8 pages).
- Swe, T.; Miles C.O.; Cerasino L.; Mjelde, M.; Kleiven, S.; Ballot, A., (2021). *Microcystis*, *Raphidiopsis raciborskii* and *Dolichospermum smithii*, toxin producing and non-toxigenic cyanobacteria in Yezin Dam, Myanmar. *Limnology*. 90: 125901 (9 pages).
- USEPA, (2021). Standard operating procedure for phytoplankton analysis LG401. 1-35 (35 pages).
- Vico, P.; Bonilla, S.; Cremella, B.; Aubriot, L.; Iriarte, A.; Piccini, C., (2020). Biogeography of the cyanobacterium *Raphidiopsis (Cylindrospermopsis) raciborskii*: integrating genomics, phylogenetic and toxicity data. *Mol. Phylogenet. Evol.*, 148: 106824 (10 pages).
- Wang, M.; Fan, Z.; Wang, R.; Liu, Z.; Gao, F.; Zhang, Z.; Yi, M.; Lu., M., (2022). Nitrogen removal performance, and microbial community structure of water and its association with nitrogen metabolism of an ecological engineering pond aquaculture system. *Aquacult. Rep.*, 25: 101258 (9 pages).
- Wongrat, L., Wongrat, P., Ruangsomboon, S., (2017). Freshwater phytoplankton in Thailand I: Euglenophyceae. *J. Fish. Environ.*, 27: 1-34 (34 pages).
- Xiao, M.; Willis, A.; Burford, MA., (2017). Differences in cyanobacterial strain responses to light and temperature reflect species plasticity. *Harmful Algae*. 62: 84-93 (13 pages).
- Yamamoto, Y., Shiah, F., (2016). Appearance of *Cylindrospermopsis raciborskii* in winter in an artificial pond in northern Taiwan. *Ann. Limnol.- Int. J. Lim.*, 52: 335-341 (7 pages).
- Yang, Y.; Chen, Y.; Cai, F.; Liu, X.; Wang, Y.; Li., R., (2018). Toxicity-associated changes in the invasive cyanobacterium *Cylindrospermopsis raciborskii* in response to nitrogen fluctuations. *Environ. Pollut.*, 237: 1041-1049 (9 pages).
- Yossan, S.; Moonsin, P., (2015). Using dominant phytoplankton as a bioindicator of water quality in Huay Samran, Sisaket Province. *Res. Dev. J.*, 38: 295-309 (15 pages).
- Zarantonello, V.; Silvat, TP.; Noyma, NP., (2018). The cyanobacterium *Cylindrospermopsis raciborskii* (CYRF-01) responds to environmental stresses with increased vesiculation detected at single-cell resolution. *Front Microbiol.*, 9: 272 (12 pages).

#### AUTHOR (S) BIOSKETCHES

**Srichomphu, M.**, Ph.D. Candidate. Department of Environmental Science, Faculty of Environment, Kasetsart University, Bangkok, Thailand.

- Email: [manlikasri@gmail.com](mailto:manlikasri@gmail.com)
- ORCID: [0009-0004-4965-5769](https://orcid.org/0009-0004-4965-5769)
- Web of Science ResearcherID: NA
- Scopus Author ID: 57202059256
- Homepage: <https://www.lerd.org/>

**Phewnil, O.**, Ph.D., Assistant Professor, Department of Environmental Science, Faculty of Environment, Kasetsart University, Bangkok, Thailand.

- Email: [onanong.p@ku.th](mailto:onanong.p@ku.th)
- ORCID: [0000-0001-9616551X](https://orcid.org/0000-0001-9616551X)
- Web of Science ResearcherID: NA
- Scopus Author ID: 56252364600
- Homepage: <https://envi.ku.ac.th>

**AUTHOR (S) BIOSKETCHES (continued)**

**Pattamapitoon, T.**, Ph.D., Assistant Professor, Department of Environmental Science, Faculty of Environment, Kasetsart University, Bangkok, Thailand.

- Email: [thanit.pa@ku.th](mailto:thanit.pa@ku.th)
- ORCID: 0009-00051664450X
- Web of Science ResearcherID: NA
- Scopus Author ID: 55822416300
- Homepage: <https://envi.ku.ac.th>

**Chaichana, R.**, Ph.D., Associate Professor, Department of Environmental Technology and Management, Faculty of Environment, Kasetsart University, Bangkok, Thailand.

- Email: [fscircc@ku.ac.th](mailto:fscircc@ku.ac.th)
- ORCID: 0000-0003-0244-9736
- Web of Science ResearcherID: NA
- Scopus Author ID: 35766295700
- Homepage: <https://envi.ku.ac.th>

**Chunkao, K.**, Ph.D., Professor, The King's Royally Initiated Laem Phak Bia Environmental Research and Development Project, Chaipattana Foundation, Ban Laem District, Phetchaburi Province, Thailand.

- Email: [prof.kasemc@gmail.com](mailto:prof.kasemc@gmail.com)
- ORCID: 0009-0002-80354732
- Web of Science ResearcherID: NA
- Scopus Author ID: 54683551800
- Homepage: <https://www.lerd.org>

**Wararam, W.**, Ph.D., Assistant Professor, Department of Environmental Science, Faculty of Environment, Kasetsart University, Bangkok, Thailand.

- Email: [watcharapong.warar@ku.th](mailto:watcharapong.warar@ku.th)
- ORCID: 0009-0000-1487-4284
- Web of Science ResearcherID: NA
- Scopus Author ID: 57096032600
- Homepage: <https://envi.ku.ac.th>

**Dampin, N.**, Ph.D., Lecturer, Department of Environmental Science, Faculty of Environment, Kasetsart University, Bangkok, Thailand.

- Email: [ecncd@ku.ac.th](mailto:ecncd@ku.ac.th)
- ORCID: 0009-0000-5540-5281
- Web of Science ResearcherID: NA
- Scopus Author ID: 57194972798
- Homepage: <https://envi.ku.ac.th>

**Maskulrath, P.**, The King's Royally Initiated Laem Phak Bia Environmental Research and Development Project, Ban Laem District, Phetchaburi Province, Thailand.

- Email: [parkin.ma@ku.th](mailto:parkin.ma@ku.th)
- ORCID: 0000-0002-1352-4247
- Web of Science ResearcherID: NA
- Scopus Author ID: 57202060728
- Homepage: <https://www.lerd.org/>

**HOW TO CITE THIS ARTICLE**

Srichomphu, M.; Phewnil, O.; Patamapitoon, T.; Chaichana, R.; Chunkao, K.; Wararam, W.; Dampin, N.; Maskulrath, P., (2024). Role of *Cylindrospermopsis* sp. in vertical nitrogen changes observed in tropical oxidation wastewater treatment ponds. *Global J. Environ. Sci. Manage.*, 10(1): 287-300.

DOI: [10.22034/gjesm.2024.01.18](https://doi.org/10.22034/gjesm.2024.01.18)

URL: [https://www.gjesm.net/article\\_705701.html](https://www.gjesm.net/article_705701.html)





## ORIGINAL RESEARCH PAPER

## Flood susceptibility mapping based on watershed geomorphometric characteristics and land use/land cover on a small island

B.H. Narendra<sup>1,\*</sup>, O. Setiawan<sup>1</sup>, R.A. Hasan<sup>2</sup>, C.A. Siregar<sup>1</sup>, Pratiwi<sup>1</sup>, N. Sari<sup>1</sup>, A. Sukmana<sup>1</sup>, I.W.S. Dharmawan<sup>1</sup>, R. Nandini<sup>1</sup><sup>1</sup> Research Center for Ecology and Ethnobiology, National Research and Innovation Agency, Jl. Raya Jakarta-Bogor Km. 46, Cibinong 16911, Jawa Barat, Indonesia<sup>2</sup> Research Center for Society and Culture, National Research and Innovation Agency, Jl. Gatot Subroto No.10, Jakarta 12710, Indonesia

## ARTICLE INFO

**Article History:**

Received 06 February 2023

Revised 15 June 2023

Accepted 21 July 2023

**Keywords:**Flood susceptibility  
Hydrological response  
Geomorphometrics  
Land use/land cover

## ABSTRACT

**BACKGROUND AND OBJECTIVES:** Flooding is the most frequent hydrological disaster which greatly impacts humans and the environment. Lombok, a small tropical island, experiences severe flooding almost yearly. Flood susceptibility mapping is important to determine the priority watershed in implementing flood mitigation action, including improving the spatial planning in watershed management. Several methods of determining flood susceptibility require the support of long data series and a variety of monitoring equipment in the field where not every region has the resource capacity. Compared to other methods that require the support of long data series and a large number of evenly distributed monitoring equipment, the geomorphometric parameters and land use/cover in a watershed are closely related to the hydrological responses and are potentially applicable in flood susceptibility mapping. This research aimed to classify the watershed flood susceptibility on a small island based on the geomorphometric characteristics and land use/land cover of the watershed.**METHODS:** This study was carried out on Lombok Island, located in southern Indonesia, representing a small island in the tropical region. Watershed classification was carried out using 24 geomorphometric variables and land use/land cover, representing aspects of the river network, geometry, texture, and watershed relief. The principal component analysis approach was carried out to determine the most significant variable, and the weight of each variable was determined using the weighted sum approach method. Then, compound values were calculated based on the weighted values and preliminary ranking to indicate the flood susceptibility levels, which were divided into five classes.**FINDINGS:** The analysis found that the variables most related to flood events are the total number of rivers, relief ratio, elongation ratio, river density, stream frequency, and dry agricultural land use. These most related geomorphometrics indicate that the watersheds with higher flood susceptibility have low rock permeability, relatively low infiltration capacity, and relatively high surface runoff, thus triggering flooding. The flood susceptibility mapping classified 16 watersheds as having very high flood susceptibility. This research shows that analysis of the geomorphometric characteristics and land use/land cover can be relied upon to determine the flood susceptibility level, which is useful in spatial planning and flood disaster mitigation.**CONCLUSION:** Geomorphometric characteristics and land use/land cover can be used to determine a watershed's hydrological characteristics or behaviour. Based on the geomorphometric characteristics of the watersheds on Lombok Island, some identifying variables that are highly related to flood processes were obtained. Based on these characteristics, watersheds with high and very high flood susceptibility levels have low rock permeability, relatively low potential infiltration capacity, and relatively high surface runoff potential. Flooding still occurs despite good forest cover because the geomorphometric characteristics of the watershed also play a major role in flood events.DOI: [10.22034/gjesm.2024.01.19](https://doi.org/10.22034/gjesm.2024.01.19)This is an open access article under the CC BY license (<http://creativecommons.org/licenses/by/4.0/>).

NUMBER OF REFERENCES

57



NUMBER OF FIGURES

6



NUMBER OF TABLES

3

\*Corresponding Author:

Email: [budi065@brin.go.id](mailto:budi065@brin.go.id)

Phone: +6281 2420 3265

ORCID: [0000-0001-8856-5687](https://orcid.org/0000-0001-8856-5687)

Note: Discussion period for this manuscript open until April 1, 2024 on GJESM website at the "Show Article".

## INTRODUCTION

Vulnerability to hydrometeorological catastrophes is one of the repercussions of Indonesia's astronomical position (Djalante et al., 2017). Natural disasters caused by hydrometeorology, such as floods, droughts, landslides, forest fires, and extreme climates, are the most frequent disasters in Indonesia (Rosyida et al., 2018). Among the hydrometeorological disasters, floods are the most frequent and have wide-reaching impacts (Das, 2019). Indonesia is a country that has a high frequency of flood events and the intensity is increasing every year (Nurulita and Ningrum, 2018). Floods are caused by various natural factors, e.g., meteorological factors, physical characteristics, and land cover (Pariartha et al., 2023) and anthropogenic factors, e.g., community behaviour, land use/land cover (LULC) changes, deforestation (Ramadhan et al., 2023), and environmental management (Handayani et al., 2020). Various studies have stated that the rise in hydrometeorological disasters is related to the global climate change phenomenon in the world in the last few decades (Thomas and López, 2015; Frimawaty et al., 2023). The flood risk level is increasing due to extreme weather phenomena caused by climate change (Brunner et al., 2018; Puno et al., 2022). Coastal areas will be more vulnerable to climate change disasters (Mycoo et al., 2022), such as flooding, due to water level rises (Gaborit, 2022). Lombok, a small island in Indonesia, has specific characteristics in terms of the landscape, geology, hydrology, and climate patterns that influence resource management (Bengen et al., 2012). With a diverse topography ranging from mountainous to coastal areas, the island also has different climatic conditions. A climate analysis conducted by Nandini and Narendra (2011) stated that Lombok Island has been experiencing climate change, characterized by the tendencies of decreased rainfall, increased air temperature, and shifts in climate types from 1961 to 2008. In addition, Yasa et al. (2022) predicted climate changes marked by rain patterns in 2018–2035, during which the pattern will tend to be wetter, thereby increasing the chances of flooding. Several factors, such as rainfall, watershed characteristics, LULC changes, and an increase in degraded land, have influenced the occurrence of floods on Lombok Island. In the last few years, floods have inundated rice fields, settlements, and infrastructures in Mataram, the biggest city on

the island, which has caused large material losses (Rahadiati et al., 2021). In 2022, there were 30 flood incidents on Lombok Island. The high number of flood events on Lombok Island cannot be separated from the level of susceptibility of this island regarding the potential for flooding. The Regional Disaster Management Agency also stated that in 2017–2022, 57,301 people spread across 758 villages with a moderate level of flood susceptibility were affected by the flood disaster that occurred on Lombok Island (Yunus et al., 2019). Flood events, such as those occurring in Senggigi Beach and the Mandalika area, have disrupted tourism and economic activities by cutting off road access and several bridges (Suarantb, 2023). Mitigation measures, including spatial planning based on the level of disaster susceptibility of an area, must be taken to minimize disaster risk (Umar and Dewata, 2018). Lombok, as a small island, necessitates rigorous spatial planning, including flood susceptibility mapping (Setiawan and Nandini, 2021). Information on flood susceptibility for watershed level in Indonesia has not been mapped in detail. Several methods, such as statistical and hydrological modelling, can be used to map the flood susceptibility level. However, these methods require the support of long data series from many widely distributed monitoring equipment (Ahmed et al., 2021). Good DEM and LULC data availability and easy acquisition are other reasons the use of geomorphological and LULC parameters has good potential for flood susceptibility mapping in Indonesia. Research on flood events related to the geomorphological aspects of a watershed on a small island is rarely performed in Indonesia. Flood events with extreme magnitudes are largely influenced by geomorphological characteristics, which are uncontrollable natural factors. Flood disasters can be minimized by taking into account other aspects, including LULC, which is influenced by human activities and constitutes the main factor determining flood vulnerability (Ahn and Merwade 2015). This study aims to map flood susceptibility based on geomorphological conditions and watershed LULC on a small island. The results of the mapping of flood-prone areas will be useful for spatial planning and flood disaster mitigation strategies, and they methods can also be applied to other small islands. This study was carried out on Lombok Island in 2021.

## MATERIALS AND METHODS

Descriptions of the study area, data sources for analysis, the geomorphometric characterization, LULC classification, and integrated approach (PCA and WSA) are explained in detail as follows.

### Description of the study area

The study was carried out on Lombok Island, which is positioned in the southern region of Indonesia (Fig. 1). The island is categorized as a small island and covers an area of approximately 4,700 square kilometers (km<sup>2</sup>). Geographically, Lombok Island lies between 115°49'28" and 116°43'22" east (E) and between 8°12'41" and 8°57'20" south (S). The island has experienced flood events, including flash

floods, in at least the past five years. Another reason was that the island represents small islands in the tropical region, which are relatively vulnerable to climate change by the trigger factor of floods. These are essential reasons in the context of an evaluation of the applicability of the methods used for flood susceptibility mapping. Based on the watershed map of Indonesia (scale 1:50,000), the island has 194 watersheds. Watersheds on small islands are characterized by relatively small areas, flows directly heading to the sea relatively steep terrain in the upstream area, and flat terrain in the downstream area. The elevation of each watershed varies; generally, the elevation ranges from 0 to 3,726 meters above sea level (masl), with the highest elevation

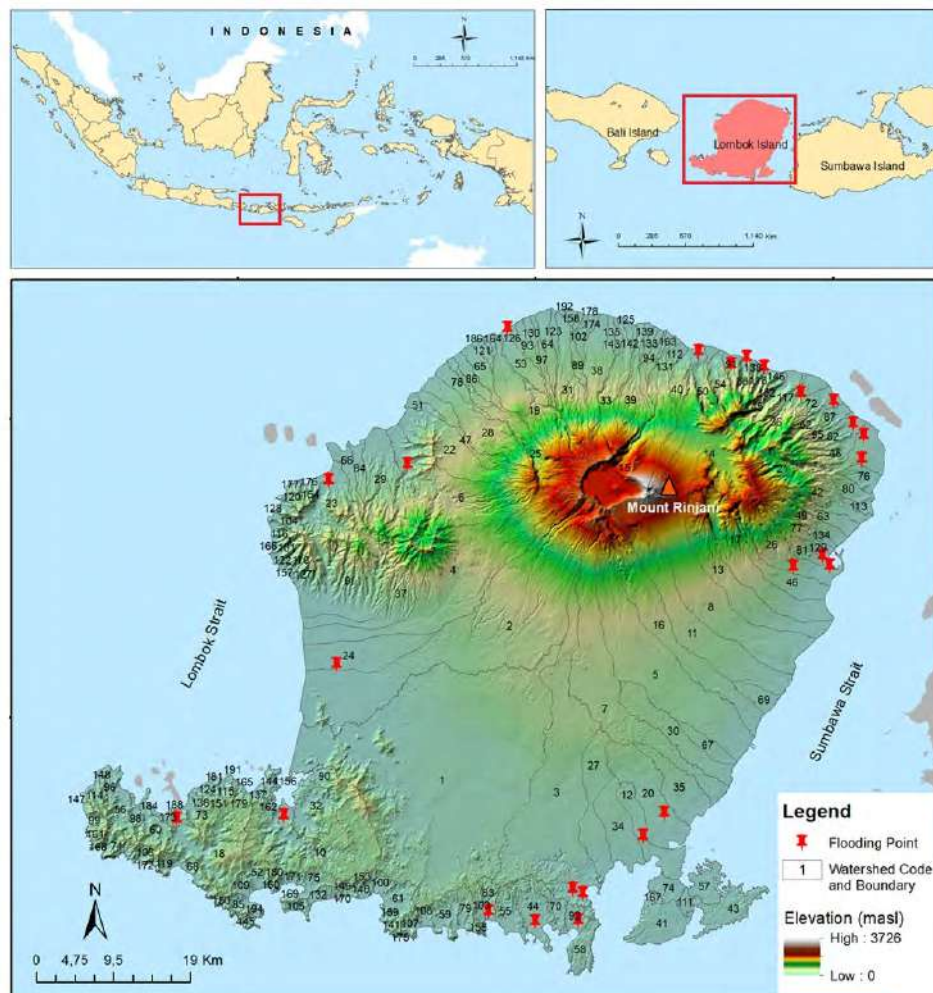


Fig. 1: Geographic location of the study area in Lombok Island, positioned in the southern region of Indonesia

being the peak of Mount Rinjani. Low areas mostly lie in the study area's southern part, while mountainous regions are in the northern part. Relatively flat slope gradients dominate the low areas, while steep slope gradients dominate the high-lying areas.

The research area's climate differs geographically. Based on the Schmidt-Fergusson classification, Lombok Island is dominated by a moderate climate (type D) distributed on the western and eastern parts of the island. Meanwhile, a slightly wet climate (type C) is found in the island's middle part, especially around Mount Rinjani. The northern and southern parts of Lombok Island have a slightly dry climate (type E) (Yasa *et al.*, 2022). The average rainfall reaches 1,568 millimeters (mm)/year, with a unimodal rainfall pattern. The unimodal pattern indicates that rainfall has only one peak from December to March. Spatially, the areas at the high elevation of Mount Rinjani experience high rainfalls (> 1,000 mm), while the western and southern parts experience low rainfalls (< 1,000) (Widiatmaka *et al.*, 2015). The highest and the lowest temperatures on Lombok Island occur in August and December, ranging from 24.7 degrees Celsius (°C) to 27.2 °C. Lombok Island's lithology is formed of sediment material that is Tertiary to Quaternary in age. The geology of Lombok Island is characterized by volcanic rocks, such as volcanic breccias, lavas, and sandstones. Some areas are also dominated by a fresh and unconsolidated sediment quarter. Tertiary rock formation dominates the eastern part of Lombok Island, including breccias, lavas, and tuffs. The rock arrangement in the west, generally an alluvial region, is formed of alluvial or loose rocks. Quaternary volcanic rocks from Mount Rinjani cover the northern part and almost two-thirds of Lombok Island (Agustawijaya and Syamsuddin, 2009). Lombok Island consists of four primary soil types: Litosols, Cambisols, Alluvials, and Vertisols. In a few areas, Mediterranean soil exists as a slightly developed soil type. According to the FAO soil system, these primary soil types are equal to Leptosols, Fluvisols, Cambisols, Vertisols, and Luvisols. Shallow solum, sandy texture, low soil nutrients, a low cation-exchange capacity (CEC), and low organic carbon content characterize Litosols/Leptosols. The soils with a quite a deep solum are Cambisols or Undepts. These are also slightly fertile with a loamy texture and medium organic carbon content and CEC. Alluvial or Fluvent soils are primarily used for paddy cultivation

with various clay and organic carbon contents and depths and relatively fertile soil. Vertisols, also known as Uderts, are distinguished by a dominant clay texture, great difficulty in cultivation, high CEC, and moderately productive soil. Mediterranean soils or Udalfs are more developed soils with moderate CEC and moderately fertile soil (Priyono *et al.*, 2019).

#### *Data and data sources*

Variables collected as the source data consisted of geomorphometric and LULC variables. Data from the digital elevation model were used for geomorphometric characterization. The DEM data, released by the Geospatial Information Agency of Indonesia, had 8.3 meters (m) spatial resolution (Sihombing *et al.*, 2021) and consisted of 12 tiles in total for the study area. The boundaries of the watersheds on Lombok Island were obtained from the watershed map of Indonesia at a scale of 1:50,000. LULC data were interpreted from Landsat 8 multi-band optical images. The images, available on the United States Geological Survey website, have a medium spatial resolution and can be optimized up to 15 m resolution by using panchromatic band (Roy *et al.*, 2014). An inventory of flood events in Lombok Island was carried out by mapping the last two years of flood occurrences from several sources, including report documents of the National Disaster Management Agency, online and offline news, previous research, and ground check. The complete workflow of this study is shown in Fig. 2.

#### *Geomorphometric characterization*

Geomorphometric characterization aimed to extract the geometric features of all the watersheds in the study area. Many studies have shown that geomorphometric analysis can be used to prioritize watersheds regarding hydrological issues, such as erosion (Obeidat *et al.*, 2021) and flooding (Mahmood and Rahman, 2019). The relationship between geomorphological features and hydrological processes can provide comprehension of the hydrological behavior within the watershed. There were several steps involved in the analysis of the geomorphological parameters: mosaicking 12 DEM data tiles, overlaying the DEM data and the provided watershed map, and computation of the geomorphological parameters for each watershed. The environment of a geographic information system

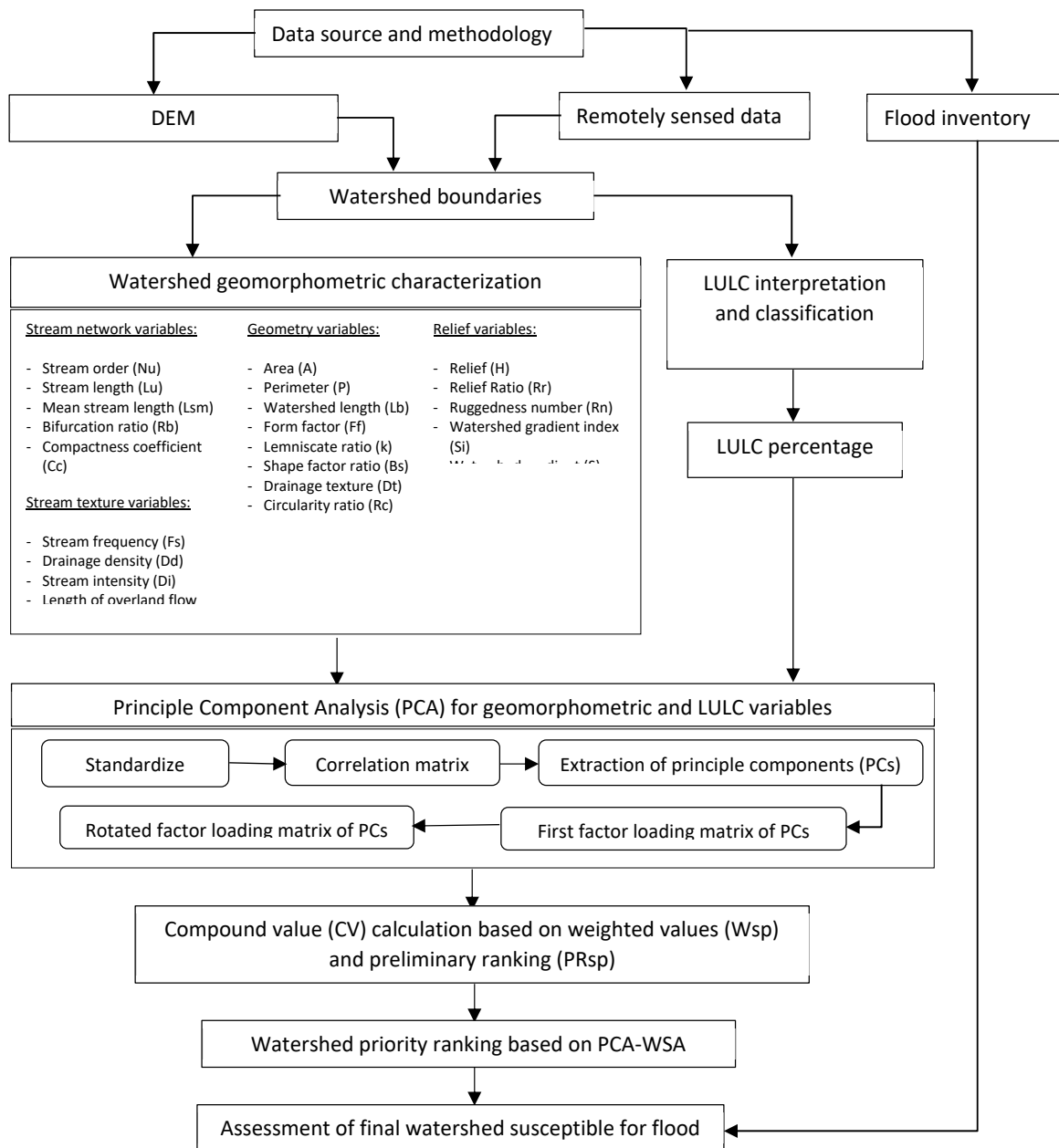


Fig. 2: The workflow of the study

was employed to derive the main parameters from the DEM data, drainage network, and watershed maps. The main parameters included the area, perimeter, watershed length, stream order, number of streams, stream length, and relief. Computation

of the main parameters was conducted to obtain the stream network variables, stream texture variables, geometry variables, and relief variables. All the variables (Table 1) were calculated using standard and well-known formulas proposed by previous

Table 1: Geomorphological variables used in the study

Geomorphometric variables	Formula
<b>Geometry variables</b>	
Area (km <sup>2</sup> )	Estimated by GIS
Perimeter kilometer (km)	Estimated by GIS
Watershed length (km)	Estimated by GIS
Form factor	$Ff = A/Lb^2$
Lemniscate ratio	$K = Lb^2/4 \times A$
Shape factor ratio	$Bs = Lb^2/A$
Drainage texture	$Dt = Nu/P$
Circularity ratio	$Rc = 4 \times \pi \times A/P^2$
Elongation ratio	$Re = 1.129 \times \sqrt{A/Lb}$
<b>Stream network variables</b>	
Stream length	$Lu = L1 + L2 + \dots + Ln$
Stream order	$Nu = N1 + N2 + N3 + \dots + Nn$
Mean stream length (km)	$Lsm = Lu/Nu$
Compactness coefficient	$Cc = 0.282 \times P/\sqrt{A}$
Channel maintenance (km)	$Cm = 1/Dd$
Bifurcation ratio	$Rb = Nu/Nu + 1$
<b>Stream texture variables</b>	
Stream frequency (no./km <sup>2</sup> )	$Fs = Nu/A$
Drainage density (km/km <sup>2</sup> )	$Dd = Lu/A$
Stream intensity	$Di = Fs/Dd$
Length of overland flow (km)	$Lg = 1/2 Dd$
<b>Relief variables</b>	
Relief	$R = Hmax - Hmin$
Relief ratio	$Rr = R/Lb,$
Ruggedness number	$Rn = Dd*(H/1000)$
Gradient index	$Si = H/Lb$
Average gradient	$S = Lb/H$

studies (Ghasemlounia and Utlu, 2021; Obeidat et al., 2021; Kant et al., 2022; Tiwari and Kushwaha, 2021).

*LULC classification*

The LULC map was obtained by image interpretation of Landsat 8 remote sensing data of 2020. Mosaicking, radiometric and geometric correction conducted prior to the interpretation process. The method used for interpretation was the maximum likelihood method (Chandniha and Kansal, 2017). The LULC categorization employed the national standard of LULC classes (Badan Standardisasi Nasional, 2010), including forest, dryland farming, paddy field, fishpond, shrub, bare land, pasture, water body, airport, mangrove, and resettlement. The obtained LULC map was then overlaid with the watershed boundaries to acquire an LULC map of each watershed, which was calculated as a percentage of the total area of watersheds.

*Integrated approach: PCA and WSA*

This study combined principal component analysis

with the weight sum approach (WSA) in defining flood susceptibility at a watershed scale. The PCA aimed to reduce the geomorphometric and LULC variables based on variance within inter-correlated variables into principal components. As the roles of the influenced variables in flooding are in equal naturally, the WSA was used to define the weight value of each variable. Several studies have found that integrating PCA and the WSA provides more sophisticated results in watershed prioritization. (Singh and Pandey, 2021). The PCA technique in this study was carried out in several steps. First, the dataset was standardized as each variable had a different unit and aimed to gain PCA performance. Second, correlation matrix computation was carried out to define all possibilities of variable relationships. Third, the eigenvalues were determined for the PC number selection. In this case, the PC with eigenvalues of more than one were chosen. The fourth and fifth steps were the computation of the first-factor loading matrix and the rotated factor loading matrix of the PCs, respectively. Based on the rotated factor loading

matrix, the variable of each PC with the highest value was considered the most influenced variable used for the WSA and CV calculation for susceptibility class determination. The WSA was applied to the most influenced variables resulting from the PCA. Compound values were determined for the final flood susceptibility ranking based on the ranking and weights of the influenced variables. CV calculation was employed using Eq. 1 (Siddiqui *et al.*, 2020).

$$CV = Riv \times Wiv \quad (1)$$

Where; CV = compound value, Riv = ranking of influenced variable, and Wiv = weight of influenced variable. The weight values of the influenced variables were obtained using a cross-validation technique using Eq. 2 (Malik *et al.*, 2019).

$$W_{iv} = \frac{\text{Sum of correlation coefficients}}{\text{Total of coefficients}} \quad (2)$$

The ranking for each influenced variable was determined based on the relationship between the variable and the flooding process, whether ranking was directly proportional (ordered from the smallest) or inversely (sorted from the largest) for each watershed. The class of susceptibility to flooding was determined based on the CV. Susceptibility was divided into five classes: very low, low, medium, high, and very high, with the interval between classes obtained using the Jenks natural breaks approach. A high or very high flood susceptibility class illustrates a higher level of potential for flooding and a higher priority watershed to minimize flood risk. The final flood susceptibility map was also crosschecked with historical flood events based on flood inventory data.

## RESULTS AND DISCUSSION

### *Geomorphometric characteristics*

Geomorphometrics analysis is the assessment and mathematical examination of the shape and pattern of the Earth's surface in a given landscape (Hajam *et al.*, 2013). The results of the geomorphometric analysis are presented in Fig. 3. The evaluation of the morphometric and stream network plays a very significant role in identifying the geo-hydrological merit of the catchment area. The relation indicates the predominant function of geology, geomorphology, and climate in the formation of the catchment area in the landscape. Moreover, catchment area analysis

is essential in any hydrological review to evaluate the groundwater hydrology, groundwater management, the soil as a natural landscape body, and the environment. The important geomorphometric elements are the stream network, drainage texture, geometry, and watershed relief.

### *a. Stream network*

The first step in the catchment area analysis was to describe the river or stream order. Stream is defined as a positive whole number employed in morphometry to indicate the number or level of branching in a river system. The total number of streams has the highest range of all variables, with the value starting from 3 (Batu Payung Watershed) up to 2,876 (Dodokan Watershed). A high stream number in a watershed often reflects large discharge and rapid peak flow during rainstorm events, in comparison to a low number of streams (Ahmed *et al.*, 2021). The stream length is a dimensional feature that reveals the distinctive size of the drainage network components and their contributing watershed surface. The value is calculated by dividing the overall length of an order's stream by the total number of segments in the order. A higher stream order, in most cases, indicates a smaller total stream length. In the field, however, a higher number of stream orders also reveals a greater total stream length. This study's highest stream length was 1,709.9 for the Dodokan Watershed, indicating lower infiltration and higher runoff. The mean stream length is a dimensional attribute reflecting the typical size of drainage network components and their contributing catchment surface. The value is produced by dividing the total stream length by the total stream cover for each stream order. A greater mean stream length is associated with a higher stream order, in which case the value of stream order 1 is less than that of stream order 2, and the value of stream order 2 is less than that of stream order 3, and so on. The characteristics of this catchment area are significantly influenced by some important variables, namely, the lithology, slope, and topography (Vinutha and Janardhana, 2014). The bifurcation ratio is the ratio of several stream segments of a specified order to several streams in the next higher order. The bifurcation ratio is directly connected to the river network structure. In this study, the highest bifurcation ratio value (21) was found in the Hangat Watershed. The high bifurcation ratio value represents significant structural control.

Flood susceptibility mapping

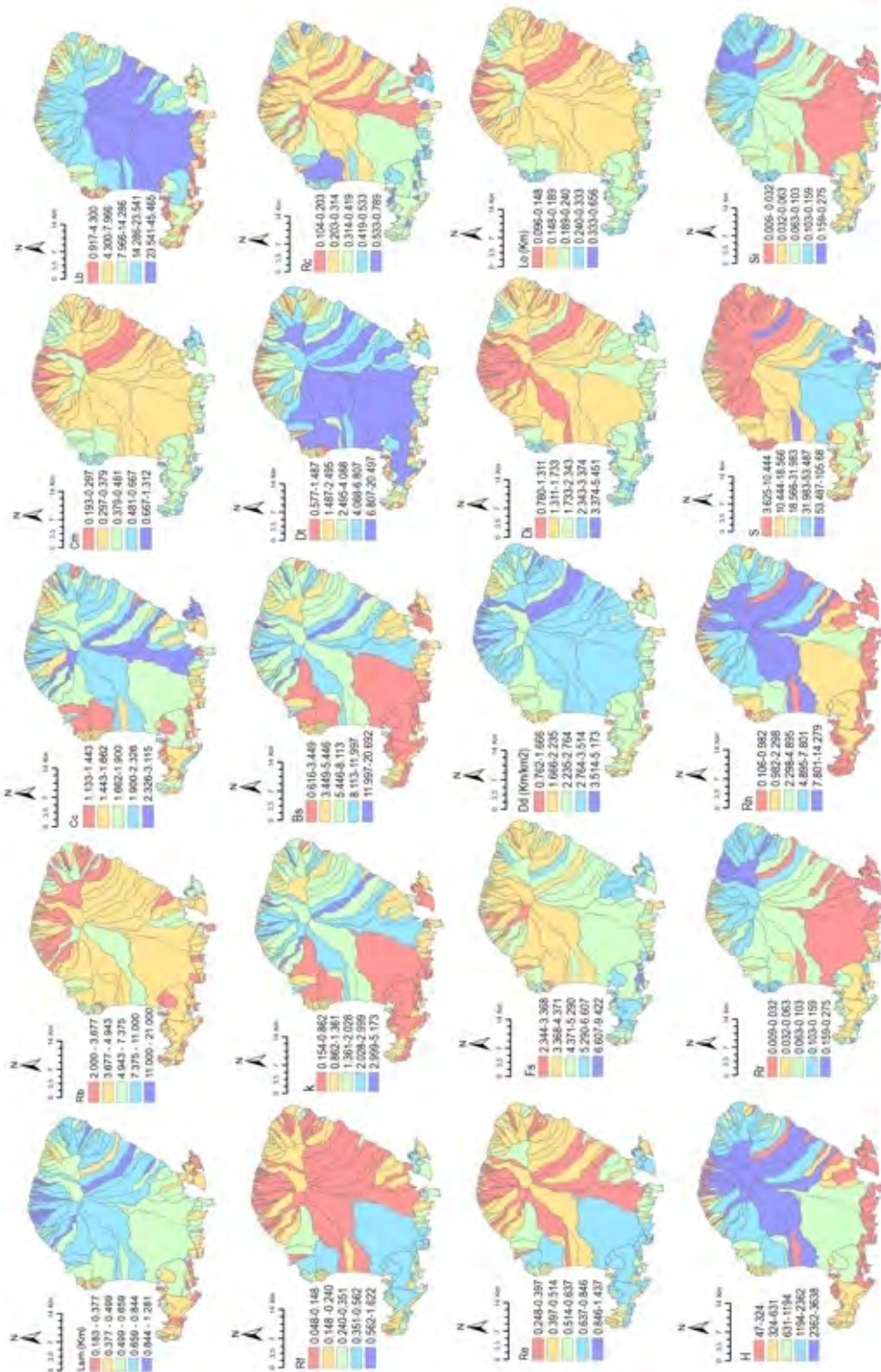


Fig. 3: Variable maps of stream network, stream texture, geometry, and relief

#### *b. Drainage texture*

There are four drainage texture variables, namely, stream frequency, drainage density, drainage intensity, and length of overland flow. In general, stream frequency values range from 3.00 to 9.99. The value of  $F_s$  depends on the lithological conditions of the catchment area and reflects the drainage texture (Albaroot *et al.*, 2018). The stream frequency values observed in the flooded watersheds on Lombok Island ranged from 3.06 to 6.61. Based on the  $F_s$  values, these watersheds have steep slopes, with low permeability rocks, relatively low water infiltration, and greater surface runoff, resulting in a greater potential for flooding (Markose *et al.*, 2014). Such conditions are also indicated by the characteristics of the soil found in the study site. The soil in the study area is formed out of volcanic rock, in which the weathering process produces a fairly high clay content (> 40%), as found in the Cambisol and Vertisol soil types in the study area (Iqbal *et al.*, 2020). The higher the clay content, the soil tends to have a lower infiltration capacity (Tejedor *et al.*, 2013). Water that is not able to infiltrate will become surface runoff, which under certain conditions will cause environmental problem (Sartohadi *et al.*, 2018). A high drainage density in a watershed implies high runoff and erosion potential (Malik and Shukla, 2018), resulting in low infiltration rates. Based on the classification of Altaf *et al.* (2013), the flooded watersheds on Lombok Island are described as follows: included in the low class (<2 km/km<sup>2</sup>) is the Melempo Watershed; included in the medium class (2–2.5 km/km<sup>2</sup>) are the Mentareng, Nangka, Pesiran, Pelangan, Asin, Bentek, and Belik Watersheds; the rest (15 watersheds) are classified as high (>2.5 km/km<sup>2</sup>). Flooded watersheds have surface material with low permeability and a relatively low infiltration capacity, so the chances of surface runoff will be greater. A low stream intensity value reveals that the stream frequency and the drainage density have minimal influence on the degree of watershed subsidence by denudational processes (Gautam *et al.*, 2020). The intensity of the drainage for flooded watersheds on Lombok Island is quite high, namely, between 0.97 and 2.46, with an average of 1.72. This indicates that these watersheds are more vulnerable to flooding, valley erosion, and soil movement. The average length of overland flow is generally about half of the

distance between river channels, or in other words, about half of the drainage density. The lengths of the overland flow values of flooded watersheds on Lombok Island are relatively low (0.12–0.27 km). This indicates that these watersheds have steep slopes and shorter flow paths.

#### *c. Geometry*

The geometry of the river network a critical function in determining river flow direction and the frequency and magnitude of flood incidents. The form factor is a part of the geometry parameter obtained from the proportion of the watershed area to the watershed length squared. The analysis results show that the form factor values ranged from 0.05 (Mumbul Watershed) to 0.62 (Tanjung Munah Watershed). Based on various studies, a high form factor value indicates a higher discharge of short-duration events (Bashir, 2023). The lemniscate ratio shows a watershed's elongated or circular shape. In this study, lemniscate ratio values ranged from 0.15 to 5.17, with an average of 1.38. A low K value confirms the watershed's circular shape and shorter lag time, making the watershed prone to flooding (Bhat *et al.*, 2019). The circularity ratio indicates the ratio of the watershed area to a circle area with the same circumference. This variable is essential in determining flood susceptibility in a watershed. The circularity ratio values of the study area varied from 0.1 to 0.79. A high circularity ratio value indicates a circular-shaped watershed with a high flash flood risk due to the peak flow being reachable in a relatively shorter time (Ahmed *et al.*, 2021). The elongation ratio compares the watershed area to the length of the watershed. The watersheds on Lombok Island have an average elongation ratio value of 0.53, with the highest value being 0.86 (Kelapa Watershed) and the lowest being 0.25 (Mumbul Watershed). A watershed that has a low elongation ratio value tends to be elongated with low flood risk.

#### *d. Watershed relief*

There are five variables of watershed relief, namely the relief value, relief ratio, ruggedness number, watershed slope, and watershed slope index. The flooded watersheds on Lombok Island generally have relatively high watershed relief. A high relief value indicates the potential for high erosion energy from the watershed system, especially during flood events

(Pathere and Pathere, 2021). The relief ratio allows for a comparison of the relative relief of any watershed regardless of differences in the topographical scale. The relief ratio values of the flooded watersheds on Lombok Island ranged from 0.01 to 0.24. If this parameter alone is used to determine erosion intensity, then the watersheds with larger relief ratio values are more susceptible to erosion. The ruggedness number implies a watershed's susceptibility degree to soil erosion (Puno and Puno, 2019). The flooded watersheds on Lombok Island had relatively large ruggedness number values, except for the Tebelo Asin, Pemokong, and Balak Watersheds. These watersheds are generally more susceptible to erosion. The average watershed slope of the flooded watersheds on Lombok Island was the lowest at 4.16 for the Mentareng Watershed and the highest at 95.42 for the Pemokong Watershed. In general, the S values of all watersheds were relatively high. The values show the magnitudes of the watershed relief. A great watershed slope plays an important role in flood events. A steep slope can cause severe flash floods, but the velocity of water will increase as the slope of the watershed increases. As the time required for water to reach the outlet decreases, the danger of flooding will ultimately increase. The slope index indicates the rate at which the erosion process occurs on the slopes of the watershed. Steep slopes will certainly contribute large amounts of eroded material into the river channel. The river's steep gradient allows the river flow to carry debris as a base load. The flooded watersheds on Lombok Island have relatively small slope index values, which indicates that the concentration time is relatively longer.

Based on the analysis of the geomorphometric characteristics of the flooded watersheds on Lombok Island, the uniformity of several variables was obtained. These variables consist of the total number of drainage, drainage density, stream frequency, watershed relief, and bifurcation ratio. According to these identifying variables, watersheds that experience flooding are generally characterized by many drainage segments, a high drainage density, a relatively high stream frequency, large watershed relief, and a relatively high bifurcation ratio value. This indicates that these watersheds have low rock permeability, a relatively low potential infiltration capacity, and relatively high surface runoff potential (Malik and Shukla, 2018).

#### *Land use and land cover*

LULC is another important factor that influences the incidence of flooding in a watershed. LULC changes are one of the triggers for an environmental change, which can increase the erosion process. LULC are generally influenced by anthropogenic factors (Malik and Bhat, 2014). The type of land use and vegetation cover also affect the runoff (volume and speed) that flows to lower areas (Alaghmand et al., 2014). Areas with a higher density of vegetation cover tend to have higher infiltration and abstraction. Areas with sparse vegetation cover have increased shares of runoff. The LULC of the watersheds on Lombok Island is presented in Fig. 4.

The map shows that most of the watersheds on the island of Lombok are dominated by cultivated areas (66%). This agricultural land is mainly in the form of dryland agriculture (34%) and paddy fields (32%). Field observations show that dryland agriculture is mostly carried out on hillsides. Planting is only carried out during the rainy season, and land that is no longer productive is abandoned as shrubland. Forest cover also has a large proportion (21%). However, some watersheds have little forest cover, and others do not have forest cover at all. The Dodokan Watershed, the largest on Lombok Island, only has 2% forest cover. There are three watersheds with forest cover, namely, the Peretan, Balangpaku, and Batubuton Watersheds.

#### *Flood susceptibility mapping using the PCA and WSA*

The PCA was used to determine the most significant of both the geomorphometric and LULC variables. The results of the PCA show that six principal components can explain 89.16% of the variance of the data used and have more than one eigenvalue. The PCA also produces factor weights (loading factors) for each variable and each principal component. The variables in each principal component have correlation values ( $r$ ) of various strengths: strong ( $r > 0.90$ ), good ( $0.90 \geq r > 0.75$ ), and moderate ( $0.75 \geq r > 0.60$ ). The first principal component is directly proportional to the stream number, stream length, watershed area, circumference of the watershed, and drainage density, and is inversely proportional to the lemniscate index, shape factor ratio, and relief ratio. The second principal component correlates with the mean stream length, compactness coefficient, watershed length, circularity ratio, drainage density, relief, and ruggedness number. The constants of

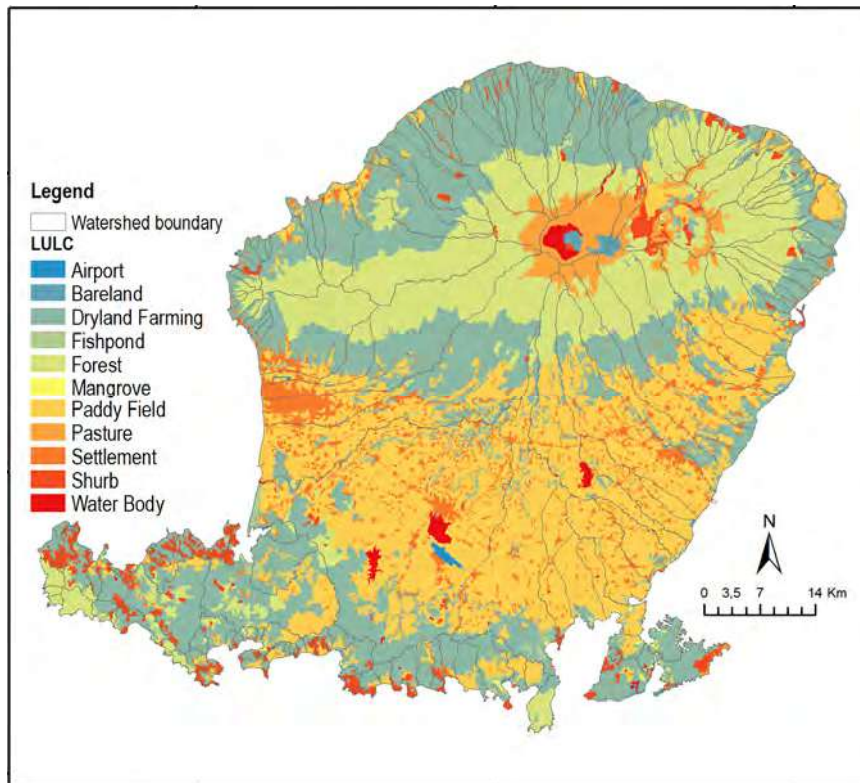


Fig. 4: LULC on Lombok Island

channel maintenance, drainage density, length of overland flow, and relief are either directly or inversely proportional to the third principal component. The fourth principal component only correlates with the compactness coefficient. The fifth principal component correlates only with stream frequency variables. The LULC variables, namely; dry land agriculture and settlements, correlate with the sixth principal component. The first factor weights do not show the most significant variable for each principal component. Therefore, the factor weights were rotated using the varimax method. Based on the factor weight rotation results, the most significant variables were obtained for each principal component, namely the total stream number, relief ratio, elongation ratio, drainage density, stream frequency, and dry land agriculture cover. Each variable represents aspects of the stream network, watershed geometry, river texture, and relief as geomorphometric variables, as well as LULC aspects. Based on these characteristics, the geomorphometric

variables with low rock permeability, a relatively low potential infiltration capacity, and relatively high surface runoff potential can increase flooding. This study's findings align with several studies on sub-watershed prioritization using geomorphometric and land use variables and the PCA approach. For example, these previous studies have found various influenced variables, such as the stream frequency and relief ratio (Pathere and Pathere, 2021), drainage density and stream frequency (Kumar *et al.*, 2023), elongation ratio and stream number (Rahman *et al.*, 2022), and agricultural land use (Setiawan and Nandini, 2021). Each significant variable naturally has a different contribution to the flood event. The calculation of each variable weight is necessary for determining the final compound value. The variable weights were determined using the WSA approach. Table 2 presents the weight calculation using the WSA.

Based on the WSA value and the variable rating value for each watershed, the compound value was

Table 2: Cross-correlation of influenced variables of the PCA

Variables	Nu	Rr	Re	Dd	Fs	PL_P
Nu	1	-0.363	0.079	0.086	0.179	-0.183
Rr	-0.363	1	-0.302	-0.266	-0.316	-0.288
Re	0.079	-0.302	1	-0.266	0.115	0.176
Dd	0.086	-0.266	-0.266	1	0.341	0.373
Fs	0.179	-0.316	0.115	0.341	1	0.067
PL_P	-0.183	-0.288	0.176	0.373	0.067	1
Sum	0.799	-0.533	0.801	1.268	1.387	1.144
Grand Total	4.866	4.866	4.866	4.866	4.866	4.866
WSA	0.164	-0.110	0.165	0.261	0.285	0.235

Table 3: Flood hazard classes of the watersheds on Lombok Island

No	Compound value	Susceptibility class	Watershed
1	<44.217	Very low	Bengkang, Blongas 1, Blongas 2, Brangbantun, Jelateng, Kumbu, Labuanpoh, Lancing, Lendang Lombok, Leong, Luk Lombok, Medang, Midang, Palung, Rambanperia, Temeran, Tiupupus
2	44.218–82.673	Low	Airberi, Ankopang, Bagekrarit, Bat, Bentek, Braringan, Bumbang, Jerengkang, Kemangi, Kengkang, Ketapang Lombok, Koloh Belik, Kukusan, Labu Lombok, Lokok Peria, Luncing, Malimbu, Menanggan, Mumbul, Nangka, Nawan, Ngolang, Padek 1, Padek 2, Peak, Pemokong 1, Pemokong 2, Persani, Pewaringan, Rangso, Sacut, Sauh, Segara, Segoar, Selindungan, Selodong, Sependok, Supak, Tawun, Temodo, Ujunggol Aikampat, Amoramor, Aruina, Balak, Bangkobangko, Batu Payung, Batubuton, Batulayar, Batuleong, Cereme, Dodokan, Duduk, Dundang, Eat Brang, Erat Pandanan, Jerenjeng, Jorong, Kali Geres, Kandang, Kelep, Kenyaru, Koangan, Kokok Menanga Paok, Krandangan, Kuang, Kuang Bulu, Labuankuwe, Lebahpebali, Lendangluar, Lendangre, Lengkulun, Mawun, Meang, Moyot, Orongudang, Pancor, Paok, Penggolong, Peretan, Pesugulan, Putih, Rajak, Rambat, Rere Penembem, Rowok, Selinggahan, Selongblanak, Sepang 2, Serangan, Sesager, Siung, Sokong, Tampah, Tanjung Puramalikan, Tanjungkates, Tantang, Tebelo, Tebi, Teluk Kowal, Tibu, Tibuborok, Tomangomang, Torokaikbelik
3	82.674–108.363	Medium	Airsintu, Akar, Asin, Babak, Bange, Bangketlamin, Batubolong, Bebanan, Belangpaku 1, Belik, Berenyok / Ancar, Buangpaok, Desa, Eat Panggang, Embarembur, Gereneng, Gol, Hangat, Jangkok, Kedome, Kelapa, Koloh Pandanan, Koloh Tujorong, Kombang, Kurbian, Lebuanbetung, Lempenge, Lendang Bahagia, Mansit, Melemo, Menangabaris, Meninting, Mentareng, Mentigi, Pangsing, Pekendangan, Pelangan, Pemalikanagung, Pengantap, Pengembulan, Puramalikan, Reak, Renggung Perempung, Sambelia, Senggigi, Sengkurik, Teba, Teluk Mekaki 1, Teluknara, Tembawang, Tenung, Terake, Tg. Munah, Tibulele, Tongker, Trawas, Uluan
4	108.364–137.286	High	Batu Jonggat, Beburung, Blimbing, Kelui, Leper, Marmadi, Nipah, Pemalikanalit, Pengawisan, Pesiran, Runggang, Selain, Sepi 2, Sidutan, Tibubunut, Tojang
5	>137.287	Very high	

determined using Eq. 3 (Siddiqui et al., 2020).

$$CV = (0.164 \times R\_Nu) + (-0.110 \times R\_Rr) + (0.165 \times R\_Re) + (0.261 \times R\_Dd) + (0.285 \times R\_Fs) + (0.235 \times R\_PL\_P) \quad (3)$$

The values of variables for each watershed were determined by ranking according to the variable's relationship with flood events. Variables with a directly proportional relationship determine the ranking from the smallest value to the largest. If the variables are

inversely proportional, the ranking starts from the largest value. Based on some of the literature, only the significant elongation ratio variable is inversely related to flooding events. The compound value calculation was held for all watersheds. The flood susceptibility class was determined using the Jenks natural breaks approach based on the compound value. Table 3 presents the distribution of the flood susceptibility classes of the watersheds on Lombok Island, while the spatial distribution is presented in Fig. 5.

High or very high flood susceptibility categories

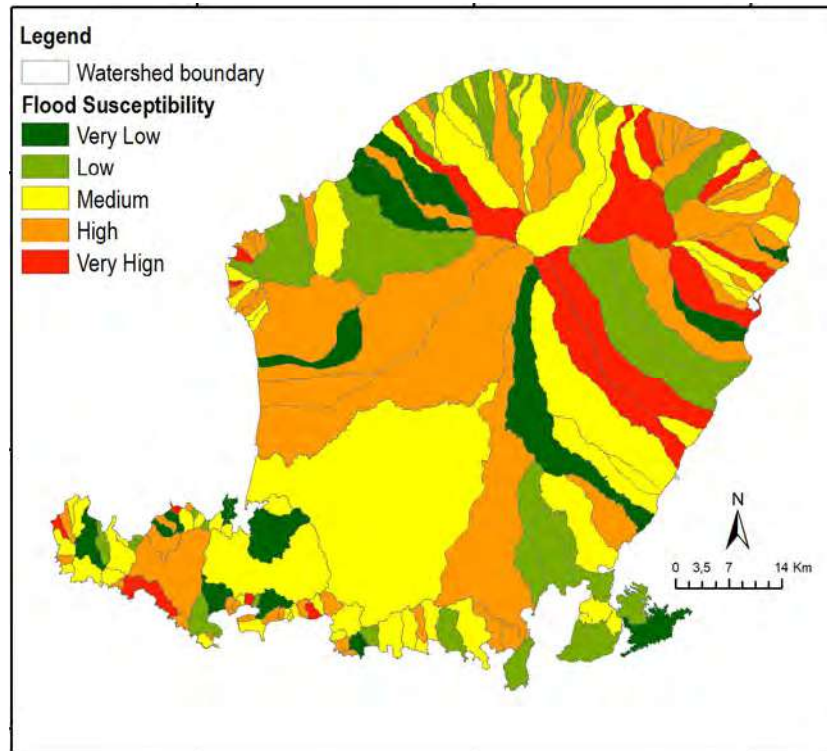


Fig. 5: Spatial distribution of watershed susceptibility to flooding on Lombok Island

illustrate a higher potential for flooding and a higher potential to be designated as priority watersheds to minimize flood susceptibility. The low category has good geomorphometric characteristics and existing LULC in response to rainfall.

Flood susceptibility mapping results can have several critical applications and uses for disaster preparedness and land management on a small island. The potential applications include developing early warning systems, assisting emergency management agencies in developing effective response plans, utilizing land use planning, guiding the planning and design of critical infrastructure, contributing to effective environmental management and conservation efforts, raising public awareness about flood risks and educating communities on preparedness and mitigation measures. When comparing flood susceptibility on small islands to larger landmasses or mainland areas, some unique challenges and considerations are specific to the island environment. A few key points to consider include 1) limited land area, which amplifies the potential

impacts of flooding coastal vulnerability due to their exposure to storm surges, sea-level rise, and tidal influences; 2) diverse topographical features, which influence the flow of water during flooding events and can lead to localized areas of higher susceptibility; 3) challenges related to limited data availability, including historical flood records, topographic data, and hydrological information; 4) limited connectivity and access to remote or less developed areas that impact data collection efforts, field surveys, and the implementation of flood mitigation measures; and 5) vulnerability to the impacts of climate change, including sea-level rise, changing rainfall patterns, and increased frequency and intensity of storms. The strategy for flood mitigation based on disaster mitigation in flood-prone areas in Lombok Island is divided into two, namely 1) Structural mitigation in the form of construction of flood control buildings, such as making embankments, making drainage network structures, and making drop structures; 2) non-structural mitigation in the form of training and simulation of disaster mitigation, as well as evaluating

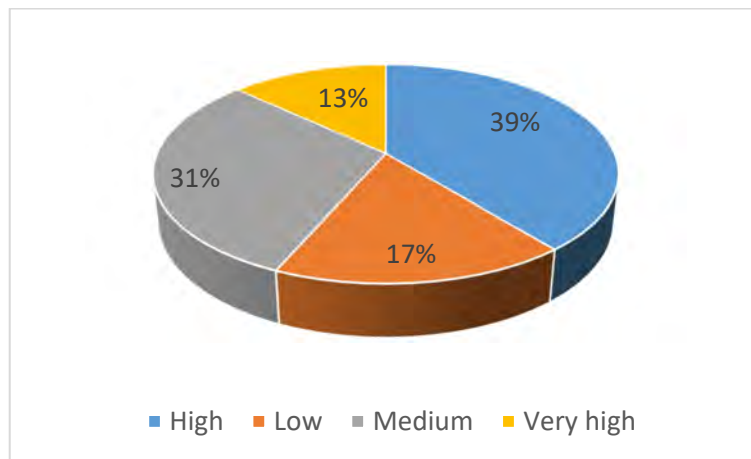


Fig. 6: Percentage of 23 flood event watersheds related to obtaining the flood susceptibility map

policies on reducing the risk of flood disasters in flood-prone areas in Lombok Island. Regarding spatial planning, local governments are required to rearrange their territorial space and create a water-friendly environment in a sustainable manner. Five steps can be taken: 1) check the applicable regulations through space or land use audits that can be carried out in accordance with applicable regulations such as master plans, regional spatial planning, and detailed spatial planning; 2) check the legality of the land/house for violations against the use of space in water resources conservation areas with applicable laws or regulations; 3) the government, academia, the community, and experts are expected to sit together to formulate directions and strategies that can be implemented to find a win-win solution for all parties regarding flood mitigation efforts; 4) regional governments can normalize rivers, canals, lakes, and reservoirs and save beaches and mangrove forests whose land has been converted; 5) the regional government needs to carry out social engineering on residents who live close to water conservation areas such as riverbanks, beaches and so on to help the residents change habits such as littering and throwing wastewater into rivers so that these bad habits can be gradually reduced and even eliminated.

#### *Comparison of flood susceptibility map and flood inventory*

The results of the flood susceptibility mapping have been validated by comparison with records of flood

events on the island of Lombok, as shown in Fig. 6.

The validation results show that the resulting flood susceptibility map is good enough to describe the watershed conditions on Lombok Island. Of the 23 flood events whose damage was recorded, only four flood events (17%) occurred in the low-susceptibility areas, precisely at the Nangka, Segara, Bentek, and Pemokong Watersheds. This indicates that the accuracy of this flood susceptibility map is approximately 83%, where the flood-experienced watersheds were included in the medium- to very high-susceptibility classes. The map accuracy is good enough to represent the flood susceptibility in the study area. The accuracy is also supported by the result of Samanta et al. (2018), who found the accuracy of their study to be about 81%. The limitation of this study lies in the flood event data used, which provide only information on the total inundated areas and damage levels and no information on flooding depths. The results of the flood susceptibility map may help guide local policy- and decision-making to better cope with future floods. Some of the flooded watersheds on Lombok Island have forest land cover of more than 30%, namely the Mentareng, Melempo, Tibubunut, Nangka, Pesiran, Sambelia, Rajak, Segara, and Belik Watersheds. Other watersheds have agricultural land use as the dominant land use. More than 30% of forest cover still allows flooding to occur. The natural factors of a watershed, in this case, the geomorphometric characteristics of the watershed, have a major role in flood events.

## **CONCLUSION**

Lombok, a small tropical island, now frequently experiences floods, threatening the economic potential and welfare of the people. Flood mitigation measures, including better spatial planning, need to be supported by the availability of a flood susceptibility map. Geomorphometric characteristics and land use/land cover supported by a geographic information system, remote sensing techniques, and a detailed digital elevation model able to determine the hydrological characteristics and behavior of the watersheds were used as the basis for flood susceptibility mapping. Based on the analysis of the geomorphometric characteristics of the watersheds on Lombok Island, the identifier variables strongly related to flood events were obtained, namely the total number of drainage, relief ratio, elongation ratio, drainage density, and stream frequency. Dry land agricultural cover, which is predominantly carried out on hillsides, has the most influence on flood susceptibility from the LULC aspect. Based on these characteristics, the watersheds with high or very high flood susceptibility have low rock permeability, a relatively low potential infiltration capacity, and relatively high surface runoff, thus triggering flooding. High or very high flood susceptibility categories indicate a greater risk of flooding and a greater likelihood of being identified as priority watersheds to reduce flood susceptibility. Several watersheds that experience flooding on Lombok Island have more than 30% forest land cover. Other watersheds have agricultural land use as the dominant land use. In other words, more than 30% of forest cover still allows flooding to occur. Thus, the natural factors of a watershed, in this case, the geomorphometric characteristics of the watershed, have a major role in flood events. The flood susceptibility map, a result of utilizing the geomorphometric characteristics and land use/land cover parameters, has adequate validation in describing the level of flood susceptibility for each watershed on Lombok Island. The use of geomorphometric characteristics and land use/land cover parameters in this study was able to produce a flood susceptibility map in an accurate and efficient manner. Documenting more detailed flood disaster events will help improve the accuracy of the resulting susceptibility map, because this map is important for consideration in prioritizing flood disaster mitigation including improving the spatial planning in each watershed.

## **AUTHOR CONTRIBUTIONS**

All Authors have equal roles as main contributors in this study. B.H. Narendra performed the research conception, and literature review. O. Setiawan performed the study methodologies, and managed data collection. R.A. Hasan drafting of the manuscript, and managed data collection. C.A. Siregar performed the research conception, and edited the manuscript. Pratiwi analysed the data, and preparation the manuscript text. N. Sari drafting of the manuscript, and literature review. A. Sukmana compiled the data and performed data processing. I.W.S. Dharmawan analysed the data, and edited manuscript. R. Nandini compiled the data and performed data processing.

## **ACKNOWLEDGEMENT**

This study was supported and funded by the Ministry of Environment and Forestry through decree number [SP DIPA-029.07.1.465015/2021] on November 23<sup>th</sup>, 2020.

## **CONFLICT OF INTEREST**

The author declares that there is no conflict of interest regarding the publication of this manuscript. In addition, the ethical issues, including plagiarism, informed consent, misconduct, data fabrication and/or falsification, double publication and/or submission, and redundancy, have been completely observed by the authors.

## **OPEN ACCESS**

©2024 The author(s). This article is licensed under a Creative Commons Attribution 4.0 International License, which permits use, sharing, adaptation, distribution and reproduction in any medium or format, as long as you give appropriate credit to the original author(s) and the source, provide a link to the Creative Commons license, and indicate if changes were made. The images or other third-party material in this article are included in the article's Creative Commons license, unless indicated otherwise in a credit line to the material. If material is not included in the article's Creative Commons license and your intended use is not permitted by statutory regulation or exceeds the permitted use, you will need to obtain permission directly from the copyright holder. To view a copy of this license, visit:

<http://creativecommons.org/licenses/by/4.0/>

### PUBLISHER'S NOTE

GJESM Publisher remains neutral with regard to jurisdictional claims in published maps and institutional affiliations.

### ABBREVIATIONS

%	Percent
°C	Degree Celsius
A	Area
Bs	Shape factor ratio
CEC	Cation-exchange capacity
Cm	Channel maintenance
Co	Compactness coefficient
CV	Compound value
Dd	Drainage density
DEM	Digital elevation model
Di	Stream intensity
Dt	Drainage Texture
E	East
FAO	Food and Agriculture
Ff	Form factor
Fs	Stream frequency
GIS	Geographic information system
H	Relief
ha	Hectare
K	Lemniscate ratio
km	Kilometer
km <sup>2</sup>	Square kilometer
Lb	Watershed Length
Lo	Length of overland flow
Lsm	Mean stream length
Lu	Stream length
LULC	Land use and land cover
LULC	Stream length
m	Meter
masl	Meter above sea level
mm	Milimeter
Nu	Stream order

P	Perimeter
PCA	Principle component analysis
PCs	Principal components
PRsp	Preliminary ranking
r	Correlation value
Rb	Bifurcation ratio
Rc	Circularity ratio
Re	Elongation ratio
Riv	Ranking of influence variable
Rn	Ruggedness number
Rr	Relief ratio
S	South
S	Average gradient
SD	Standard deviation
Si	Gradient index
Wiv	Weight of influence variable
WSA	Weight sum approach
Wsp	Weighted value

### REFERENCES

- Agustawijaya, D.S.; Syamsuddin, (2009). The development of hazard risk analysis method: a case study in Lombok Island. *Dinamika Teknik Sipil*, 12(2): 146–150 (5 pages).
- Ahmed, A.; Hewa, G.; Alrajhi, A., (2021). Flood susceptibility mapping using a geomorphometric approach in South Australian basins. *Nat. Hazard*. 106: 629–653 (25 pages).
- Ahn, K.; Merwade, V., (2015). Role of watershed geomorphic characteristics on flooding in Indiana, United States. *J. Hydrol. Eng.*, 21(2): 501-521 (21 pages).
- Alaghmand, S.; Beecham, S.; Hassanli, A., (2014). Impacts of vegetation cover on surface-groundwater flows and solute interactions in a semi-arid saline floodplain: A case study of the Lower Murray River. Australia. *Environ. Process*. 1(1): 59–71 (13 pages).
- Albaroot, M.; Al-Areeq, N.M.; Aldharab, H.S.; Alshayef, M.; Ghareb, S.A., (2018). Quantification of morphometric analysis using remote sensing and GIS techniques in the Qa' Jahran Basin. Tamar Province, Yemen. *International Journal of New Technology and Research (IJNTR)*, 4(8): 12-22 (11 pages).
- Altaf, F.; Meraj, G.; Romshoo, S.A., (2013). Morphometric analysis to infer hydrological behaviour of Lidder Watershed, Western Himalaya, India. *Geogr. J.*, 2013, 178021 (14 pages).
- Badan Standardisasi Nasional, (2010). *Klasifikasi penutup lahan*. SNI 7654: 1–28 (28 pages).

- Bashir, B., (2023). Morphometric parameters and geospatial analysis for flash flood susceptibility assessment: a case study of Jeddah City along the Red Sea Coast, Saudi Arabia. *Water*. 15(5): 870-889 **(20 pages)**.
- Bengen, D.G.; Retraubun, A.S.W.; Saad, S., (2012). Menguak realitas dan urgensi pengelolaan berbasis eko-sosio sistem pulau kecil. Pusat Pembelajaran dan Pengembangan Pesisir dan Laut (P4L).
- Bhat, M.S.; Alam, A.; Ahmad, S.; Farooq, H.; Ahmad B., (2019). Flood hazard assessment of upper Jhelum basin using morphometric parameters. *Environ. Earth. Sci.*, 78(54):1-17 **(17 pages)**.
- Brunner, M.I.; Sikorska, A.E.; Seibert, J., (2018). Bivariate analysis of floods in climate impact assessments. *Sci. Total Environ.*, 616: 1392-1403 **(12 pages)**.
- Chandniha, S.K.; Kansal, M.L., (2017). Prioritisation of sub-watersheds based on morphometric analysis using geospatial technique in Piperiya watershed, India. *Appl. Water Sci.*, 7(1): 329-338 **(10 pages)**.
- Das, S., (2019). Geospatial mapping of flood susceptibility and hydro-geomorphic response to the floods in Ulhas basin, India. *Remote Sens. Appl.: Soc. Environ.*, 14: 60-74 **(15 pages)**.
- Djalante, R.; Garschagen, M.; Thomalla, F.; Shaw, R., (2017). Disaster risk reduction in Indonesia: progress, challenges, and issues. In R. Djalante, M. Garschagen, F. Thomalla, R. Shaw (Eds.), *Disaster Risk Reduction in Indonesia*. Disaster Risk Reduct, 1-17 **(17 pages)**.
- Frimawaty, E.; Ilmika, A.; Sakina, N.A; Mustabi. J., (2023). Climate change mitigation and adaptation through livestock waste management. *Global J. Environ. Sci. Manage.*, 9(4): 691-706 **(16 pages)**.
- Gaborit, P., (2022). Climate adaptation to Multi-Hazard climate related risks in ten Indonesian Cities: Ambitions and challenges. *Clim. Risk Manage.*, 37: 100453 **(14 pages)**.
- Gautam, P.K.; Singh, D.S.; Kumar, D.; Singh, A.K., (2020). A GIS-based approach in drainage morphometric analysis of Sai River Basin, Uttar Pradesh, India. *J. Geol. Soc.*, 95: 366-376 **(11 pages)**.
- Ghasemlounia, R.; Utlu, M., (2021). Flood prioritization of basins based on geomorphometric properties using principal component analysis, morphometric analysis and Redvan's priority methods: A case study of Harşit River basin. *J. Hydrol.*, 603: 127061 **(16 pages)**.
- Hajam, R.A.; Hamid, A.; Bhat, S., (2013). Application of morphometric analysis for geo-hydrological studies using geospatial technology - A case study of Vishav Drainage Basin. *Hydrol. Current Res.*, 4(3): 1-12 **(12 pages)**.
- Handayani, W.; Chigbu, U.E.; Rudiarto, P.I.H.S., (2020). Urbanization and increasing flood risk in the Northern Coast of Central Java-Indonesia: an assessment towards better land use policy and flood management. *Land*. 9(10) 343 **(22 pages)**.
- Iqbal, P., Muslim, D., Zakaria, Z., Permana, H., Satriyo, N. A., Syahbana, A. J., Yunarto, Khoirullah, N., Asykarullah, A. W. (2020). Swelling potential of volcanic residual soils in Sumatra (Indonesia) in relation to environmental issues. *Environmental and Socio-Economic Studies*, 8(4), 1-10 **(10 pages)**.
- Kant, C.; Kumar, G.; Meena, R.S., (2022). Modeling morphometric and geomorphological parameters of mountainous river basin for water resource management using remote sensing and GIS approach. *Model. Earth Syst. Environ.*, 9: 2151-2163 **(13 pages)**.
- Kumar, M., Tiwari, R. K., Kumar, K., Rautela, K. S. (2023). Prioritization of Sub-watersheds for the Categorization of Surface Runoff and Sediment Production Rate Based on Geo-spatial Modeling and PCA Approach: A Case from Upper Beas River, Himachal Pradesh, India. *Journal of the Geological Society of India*, 99(4), 545-553 **(8 pages)**.
- Mahmood, S.; Rahman, A.ur., (2019). Flash flood susceptibility modeling using geo-morphometric and hydrological approaches in Panjkora Basin, Eastern Hindu Kush, Pakistan. *Environ. Earth Sci.*, 78(43): 1-16 **(16 pages)**.
- Malik, A.; Kumar, A.; Kushwaha, D.P.; Kisi, O.; Salih, S.Q.; Al-Ansari, N.; Yaseen, Z.M., (2019). The implementation of a hybrid model for hilly sub-watershed prioritisation using morphometric variables: Case study in India. *Water*. 11(6): 1138 **(19 pages)**.
- Malik, M.I.; Bhat, M.S., (2014). Integrated approach for prioritizing watersheds for management: A study of lidder catchment of Kashmir Himalayas. *Environ. Manage.*, 54(6): 1267-1287 **(21 pages)**.
- Malik, M.S.; Shukla, J.P., (2018). A GIS-based morphometric analyses of Kandaihimmat Watershed. Hoshangabad District. M.P. India. *Indian J. Geo Mar. Sci.*, 47 (10):1980-1985 **(6 pages)**.
- Markose, V.; Dinesh, A.; Jayappa, K., (2014). Quantitative analysis of morphometric parameters of Kali River Basin. Southern India, using bearing azimuth and drainage (bAd) calculator and GIS. *Environ. Earth Sci.*, 72: 2887-2903 **(17 pages)**.
- Mycoo, M.; Wairiu, M.; Campbell, D.; Duvat, V.; Golbuu, Y.; Maharaj, S.; Nalau, J.; Nunn, P.; Pinnegar, J.; Warrick, O., (2022). Small Island. In *Climate Change 2022: impacts, adaptation and vulnerability*. Intergovernmental Panel on Climate Change. 2043-2123 **(80 pages)**.
- Nandini, R.; Narendra, B.H., (2011). Study of rainfall, temperature and type of climate change in Lombok Island ecosystem zone. *J. Anal. Kebijakan Kehutanan*, 8(3): 228-244 **(17 pages)**.
- Nurulita, I.; Ningrum, W., (2018). Extreme flood event analysis in Indonesia based on rainfall intensity and recharge capacity. *IOP Conference series. Earth Environ. Sci.*, 118, 012045, **(5 pages)**.
- Obeidat, M.; Awawdeh, M.; Al-Hantouli, F., (2021).

- Morphometric analysis and prioritisation of watersheds for flood risk management in Wadi Easal Basin (WEB), Jordan, using geospatial technologies. *J. Flood Risk Manage.*, 14(2): 1–19 (19 pages).
- Pariartha, I.P.G.S.; Aggarwal, S.; Rallapalli, S.; Egodawatta, P.; McGree, J.; Goonetilleke, A., (2023). Compounding effects of urbanization, climate change and sea-level rise on monetary projections of flood damage. *J. Hydrol.*, 620(PB), 129535 (12 pages).
- Pathare, J. A., Pathare, A.R., (2021). Watershed prioritization for soil and water conservation in Darna River basin: a PCA approach. *Sustainable Water Resources Management*, 7(4) (15 pages).
- Priyono, J.; Yasin, I.; Dahlan, M.; Bustan, B., (2019). Identifikasi sifat, ciri, dan jenis tanah utama di Pulau Lombok. *Jurnal Sains Teknologi & Lingkungan*, 5(1): 19–24 (6 pages).
- Puno, G.R., Puno, R.C.C., (2019). Watershed conservation prioritization using geomorphometric and land use-land cover parameters. *Global J. Environ. Sci. Manage.*, 5(3), 279–294 (16 pages).
- Puno, G.R., Puno R.C.C., Maghuyop I.V. (2022). Flood hazard simulation and mapping using digital elevation models with different resolutions. *Global J. Environ. Sci. Manage.*, 8(3): 339-352 (14 pages).
- Rahadiati, A.; Munawaroh, Suryanegara, E., (2021). The impact of flooding on settlement along the Jangkok River Mataram, Indonesia. *IOP Conference series. Earth Environ. Sci.*, 750(1) (9 pages).
- Rahman, M.M.; Zaman, M.N.; Biswas, P.K., (2022). Optimisation of significant morphometric parameters and sub-watershed prioritisation using PCA and PCA-WSM for soil conservation: a case study in Dharla River watershed, Bangladesh. *Model. Earth Syst. Environ.*, 8(2): 2661–2674 (14 pages).
- Ramadhan, C.; Dina, R.; Nurjani, E., (2023). Spatial and temporal based deforestation proclivity analysis on flood events with applying watershed scale (case study: Lasolo watershed in Southeast Sulawesi, Central Sulawesi, and South Sulawesi, Indonesia). *Int. J. Disaster Risk Reduct.*, 93, 103745 (10 pages).
- Rosyida, A.; Nurmasari, R.; Suprpto, (2018). Data bencana Indonesia 2017. Pusat Data, Informasi dan Humas Badan Nasional Penanggulangan Bencana.
- Roy, D.P.; Wulder, M.A.; Loveland, T.R.; Woodcock, C.E.; Allen, R.G.; Anderson, M.C.; Helder, D.; Irons, J.R.; Johnson, D.M.; Kennedy, R.; Scambos, T.A.; Schaaf, C.B.; Schott, J.R.; Sheng, Y.; Vermote, E.F.; Belward, A.S.; Bindschadler, R.; Cohen, W.B.; Gao, F.; Hipple, J.D.; Hostert, P.; Huntington, J.; Justice, C.O.; Kilic, A.; Kovalsky, V.; Lee, Z.P.; Lymburner, L.; Masek, J.G.; McCorkel, J.; Shuai, Y.; Trezza, R.; Vogelmann, J.; Wynne, R.H.; Zhu, Z., (2014) Landsat-8: science and product vision for terrestrial global change research. *Remote Sens. Environ.*, 145: 154-172 (19 pages).
- Samanta, R. K., Bhunia, G. S., Shit, P. K., Pourghasemi, H. R. (2018). Flood susceptibility mapping using geospatial frequency ratio technique: a case study of Subarnarekha River Basin, India. *Modeling Earth Systems and Environment*, 4(1), 395–408 (13 pages).
- Sartohadi, J., Pulungan, N. A. H. J., Nurudin, M., Wahyudi, W. (2018). The ecological perspective of landslides at soils with high clay content in the Middle Bogowonto Watershed, Central Java, Indonesia. *Applied and Environmental Soil Science*, 2018(Article ID 2648185) (9 pages).
- Setiawan, O.; Nandini, R., (2021). Sub-watershed prioritization inferred from geomorphometric and landuse/landcover datasets in Sari Watershed, Sumbawa Island, Indonesia. *IOP Conference Series: Earth Environ. Sci.*, 747(1) (16 pages).
- Siddiqui, R.; Said, S.; Shakeel, M., (2020). Nagmati River sub-watershed prioritisation using PCA, integrated PCWS, and AHP: a case study. *Nat. Resour. Res.*, 29: 2411-2430 (20 pages).
- Sihombing, F.M.H.; Sahdarani, D.N.; Supriyanto, (2021). DEMNAS: a recently released nation-wide digital elevation model from the Indonesian Government and its implication for geothermal exploration – study case of Gunung Endut Geothermal Prospect, Banten Province, Indonesia. In *Proceedings World Geothermal Congress*. Reykjavik, Iceland April – October. International Geothermal Association: The Hague.
- Singh, G.; Pandey, A., (2021). Flash flood vulnerability assessment and zonation through an integrated approach in the Upper Ganga Basin of the Northwest Himalayan region in Uttarakhand. *Int. J. Disaster Risk Reduct.*, 66: 102573 (18 pages).
- Suarantb, (2023). Bencana banjirancam citra pariwisata Senggigi.
- Tejedor, M., Neris, J., Jiménez, C. (2013). Soil Properties Controlling Infiltration in Volcanic Soils (Tenerife, Spain). *Soil Science Society of America Journal*, 77(1), 202–212 (11 pages).
- Thomas, V.; López, R., (2015). Global increase in climate-related disasters. No. WPS157775-2. The ADB Economics Working Paper Series, Issue 466.
- Tiwari, R.N.; Kushwaha, V.K., (2021). Watershed prioritization based on morphometric parameters and PCA technique: a case study of Deonar River Sub Basin, Sidhi Area, Madhya Pradesh, India. *J. Geol. Soc. India*, 97(4): 396–404 (9 pages).
- Umar, I.; Dewata, I., (2018). Arah kebijakan mitigasi pada zona rawan banjir Kabupaten Limapuluh Kota, Provinsi Sumatera Barat. *Environ. Nat. Resour. J.*, 8(2): 251–257 (7 pages).
- Vinutha, D.N.; Janardhana, M.R., (2014). Morphometry of the Payaswini watershed, Coorg District, Karnataka, India using remote sensing and GIS techniques. *Int. J. Innov. Res. Technol. Sci. eng.*, 3(5): 516-524 (9 pages).
- Widiatmaka, W.; Ambarwulan, W.; Sutandi, A.; Murtiلاسو, K.; Munibah, K.; Daras, U., (2015). Suitable and available land for

cashew (*Anacardium occidentale* L.) in the island of Lombok, Indonesia. *J. Appl. Hortic.*, 17(2): 129–139 (11 pages).  
Yasa, I.W.; Sulistiyono, H.; Saadi, Y.; Hartana, (2022). Spatial climate forecasting for climatology disaster mitigation.

*Environ. Ecol. Res.*, 10(6): 786–796 (11 pages).  
Yunus, R.; Amri, M.R.; Wartono; Kristanto, Y.; Nugraheni, A.D., (2019). Katalog desa/kelurahan rawan bencana banjir. Badan Nasional Penanggulangan Bencana NTB.

#### AUTHOR (S) BIOSKETCHES

**Narendra, B.H.**, Ph.D., Researcher, Principal Researcher, Research Center for Ecology and Ethnobiology, National Research and Innovation Agency (BRIN), Jalan Raya Jakarta-Bogor Km 46, Cibinong 16911, Indonesia.

- Email: [budi065@brin.go.id](mailto:budi065@brin.go.id)
- ORCID: 0000-0001-8856-5687
- Web of Science ResearcherID: ABD-5972-2020
- Scopus Author ID: 55935042500
- Homepage: <https://brin.go.id/page/civitas>

**Setiawan, O.**, Ph.D., Senior Researcher, Research Center for Ecology and Ethnobiology, National Research and Innovation Agency (BRIN), Jalan Raya Jakarta-Bogor Km 46, Cibinong 16911, Indonesia.

- Email: [ogi.setiawan@brin.go.id](mailto:ogi.setiawan@brin.go.id)
- ORCID: 0000-000 2-8682-4849
- Web of Science ResearcherID: ABG-9899-2021
- Scopus Author ID: 57205433334
- Homepage: <https://brin.go.id/page/civitas>

**Hasan, R.A.**, M.PA., Junior Researcher, Research Center for Society and Culture, National Research and Innovation Agency (BRIN), Jl. Gatot Subroto No.10, Jakarta 12710, Indonesia.

- Email: [ruba001@brin.go.id](mailto:ruba001@brin.go.id)
- ORCID: 0000-0002-9090-178X
- Web of Science ResearcherID: NA
- Scopus Author ID: 57361998700
- Homepage: <https://brin.go.id/page/civitas>

**Siregar, C.A.** Ph.D., Professor, Research Center for Ecology and Ethnobiology, National Research and Innovation Agency (BRIN), Jalan Raya Jakarta-Bogor Km 46, Cibinong 16911, Indonesia.

- Email: [chai008@brin.go.id](mailto:chai008@brin.go.id)
- ORCID: 0000-000 3-0172-7554
- Web of Science ResearcherID: NA
- Scopus Author ID: 43661890800
- Homepage: <https://brin.go.id/page/civitas>

**Pratiwi, Ph.D.**, Professor, Research Center for Ecology and Ethnobiology, National Research and Innovation Agency (BRIN), Jalan Raya Jakarta-Bogor Km 46, Cibinong 16911, Indonesia.

- Email: [prat007@brin.go.id](mailto:prat007@brin.go.id)
- ORCID: 0000-0001-6423-2351
- Web of Science ResearcherID: IQU-1436-2023
- Scopus Author ID: 5721423229
- Homepage: <https://brin.go.id/page/civitas>

**Sari, N.**, M.Sc., Senior Researcher, Research Center for Ecology and Ethnobiology, National Research and Innovation Agency (BRIN), Jalan Raya Jakarta-Bogor Km 46, Cibinong 16911, Indonesia.

- Email: [nila006@brin.go.id](mailto:nila006@brin.go.id)
- ORCID: 0000-0002-1135-4520
- Web of Science ResearcherID: NA
- Scopus Author ID: 57208221830
- Homepage: <https://brin.go.id/page/civitas>

**Sukmana, A.**, M.Sc., Senior Researcher, Research Center for Ecology and Ethnobiology, National Research and Innovation Agency (BRIN), Jalan Raya Jakarta-Bogor Km 46, Cibinong 16911, Indonesia.

- Email: [asep057@brin.go.id](mailto:asep057@brin.go.id)
- ORCID: 0009-0009-1953-2297
- Web of Science ResearcherID: NA
- Scopus Author ID: 57297916100
- Homepage: <https://brin.go.id/page/civitas>

**CONTINUED AUTHOR (S) BIOSKETCHES**

**Dharmawan, I.W.S.**, Ph.D., Senior Researcher, Research Center for Ecology and Ethnobiology, National Research and Innovation Agency (BRIN), Jalan Raya Jakarta-Bogor Km 46, Cibinong 16911, Indonesia.

- Email: [iway028@brin.go.id](mailto:iway028@brin.go.id)
- ORCID: [0000-0002-3587-693X](https://orcid.org/0000-0002-3587-693X)
- Web of Science ResearcherID: NA
- Scopus Author ID: 58097512800
- Homepage: <https://brin.go.id/page/civitas>

**Nandini, R.**, Ph.D., Senior Researcher, Research Center for Ecology and Ethnobiology, National Research and Innovation Agency (BRIN), Jalan Raya Jakarta-Bogor Km 46, Cibinong 16911, Indonesia.

- Email: [ryke001@brin.go.id](mailto:ryke001@brin.go.id)
- ORCID: [0000-0002-5003-2735](https://orcid.org/0000-0002-5003-2735)
- Web of Science ResearcherID: F-2933-2019
- Scopus Author ID: 57205494099
- Homepage: <https://brin.go.id/page/civitas>

**HOW TO CITE THIS ARTICLE**

Narendra, B.H.; Setiawan, O.; Hasan, R.A.; Siregar, C.A.; Pratiwi; Sari, N.; Sukmana, A.; Dharmawan, I.W.S.; Nandini, R., (2024). Flood susceptibility mapping based on watershed geomorphometric characteristics and land use/land cover on a small island. *Global J. Environ. Sci. Manage.*, 10(1): 301-320.

DOI: [10.22034/gjesm.2024.01.19](https://doi.org/10.22034/gjesm.2024.01.19)

URL: [https://www.gjesm.net/article\\_706336.html](https://www.gjesm.net/article_706336.html)





## ORIGINAL RESEARCH PAPER

**Machine learning using random forest to model heavy metals removal efficiency using a zeolite-embedded sheet in water**N.D. Takarina<sup>1\*</sup>, N. Matsue<sup>2</sup>, E. Johan<sup>2</sup>, A. Adiwibowo<sup>3</sup>, M.F.N.K. Rahmawati<sup>1</sup>, S.A. Pramudyawardhani<sup>1</sup>, T. Wukirsari<sup>4</sup><sup>1</sup> Department of Biology, Faculty of Mathematics and Natural Sciences, Universitas Indonesia, Gedung E, Kampus UI Depok, Depok 16424, Indonesia<sup>2</sup> The United Graduate School of Agricultural Sciences, Ehime University, 3-5-7 Tarumi, Matsuyama 790-8566, Japan<sup>3</sup> Occupational Health and Safety Department, Faculty of Public Health Universitas Indonesia, Depok 16424, Indonesia<sup>4</sup> Occupational Department of Chemistry, Faculty of Mathematics and Natural Sciences, Universitas Indonesia, Gedung E, Kampus UI Depok, Depok 16424, Indonesia

## ARTICLE INFO

**Article History:**

Received 06 March 2023

Revised 17 June 2023

Accepted 23 July 2023

**Keywords:**

Adsorbent

Heavy metals

Random forest

Removal efficiency

Zeolite

## ABSTRACT

**BACKGROUND AND OBJECTIVES:** Zeolite has been recognized as a potential adsorbent for heavy metals in water. The form of zeolite that is generally available in powder has challenged the use of zeolite in the environment. Embedding powder zeolite in a nonwoven sheet, known as a zeolite-embedded sheet can be an alternative to solve that. Another challenge is that information and models of zeolite-embedded sheet removal efficiency are still limited. The novelty of this study is, first, the development of a zeolite-embedded sheet to remove heavy metals from water, and second, the use of the random forest method to model the heavy metal removal efficiency of a zeolite-embedded sheet in water.**METHODS:** The heavy metals studied were copper, lead and zinc, considering that those are common heavy metals found in water. For developing the zeolite-embedded sheet, the methods include fabrication of the zeolite-embedded sheet using a heating procedure and heavy metals adsorption treatment using the zeolite-embedded sheet. The machine learning analysis to model the heavy metal removal efficiency using zeolite-embedded sheet was performed using the random forest method. The random forest models were then validated using the root mean square error, mean square of residuals, percentage variable explained and graphs depicting out-of-bag error of a random forest.**FINDINGS:** The results show the heavy metal removal efficiency was 5.51-95.6 percent, 42.71-98.92 percent and 13.39-95.97 percent for copper, lead and zinc, respectively. Heavy metals were reduced to 50 percent at metal concentrations of 10.355 milligram per liter for copper, 171.615 milligram per liter for lead and 4.755 milligram per liter for zinc. Based on the random forest models, the important variables affecting copper removal efficiency using zeolite-embedded sheet were its contents in water, followed by water temperature and potential of hydrogen. Conversely, lead and zinc removal efficiency was influenced mostly by potential of hydrogen. The random forest model also confirms that the high efficiency of heavy metals removal (>60 percent) will be achieved at water potential of hydrogen ranges of 4.94–5.61 and temperatures equal to 29.1 degrees Celsius.**CONCLUSION:** In general, a zeolite-embedded sheet can adsorb diluted heavy metals from water because there are percentages of adsorbed heavy metals. The random forest model is very useful to provide information and determine the threshold of heavy metal contents, water potential of hydrogen and temperature to optimize the heavy metal removal efficiency using a zeolite-embedded sheet and reducing pollutants in the environment.DOI: [10.22034/gjesm.2024.01.20](https://doi.org/10.22034/gjesm.2024.01.20)This is an open access article under the CC BY license (<http://creativecommons.org/licenses/by/4.0/>).

NUMBER OF REFERENCES

62



NUMBER OF FIGURES

10



NUMBER OF TABLES

5

\*Corresponding Author:

Email: [noverita.dian@sci.ui.ac.id](mailto:noverita.dian@sci.ui.ac.id)

Phone: +62217 721 7019

ORCID: [0000-0003-1766-7445](https://orcid.org/0000-0003-1766-7445)

Note: Discussion period for this manuscript open until April 1, 2024 on GJESM website at the "Show Article".

## INTRODUCTION

Water is a basic necessity for humans (Corbella, 2010; Daneshvar Rad et al., 2023; Sarmurzina et al., 2023). Water sources for human consumption include well (Schneider et al., 2016), rainwater collection (Evantri et al., 2021), and surface water that service providers treat (Dinh et al., 2020). Water that meets health requirements must be safe in terms of physical, chemical, microbiological, and radioactive aspects (WHO, 2022). Heavy metals are naturally occurring environmental components and are considered pollutants in high concentrations (Sabiha-Javied et al., 2009; Astuti et al., 2021; Ehzari et al., 2022; Sulistyowati et al., 2023a). The higher the pollution of heavy metals in a body of water, the higher the bioaccumulation of heavy metals in the tissues of aquatic organisms (Junianto et al., 2017; Safari et al., 2019; Nurhasanah et al., 2023; Sulistyowati et al., 2023b). The increasing human population and its anthropogenic activities affect the supply of groundwater and surface water contaminated with heavy metals, causing disruptions to the balance of organisms and aquatic biota (Waqar et al., 2013; Fahimah et al., 2023; Sabillillah et al., 2023). These may disturb the ecological balance of the environment and the diversity of aquatic organisms (Budijono and Hasbi, 2021). Several methods for removing heavy metals from water have been developed, including chemical precipitation (Djedidi et al., 2009), ion exchange (Al-Othman et al., 2011), reverse osmosis (Aljendeel, 2011) and membrane separation (O'Connel et al., 2008). These methods produced encouraging results. The metal removal efficiency and dewatering ability of the resulting sludge were assessed using studies of simple and combined precipitation treatment modes (Djedidi et al., 2009), physicochemical properties and higher ion exchange capacity of composite cation exchangers, which improves the efficiency of toxic metal separation, adsorption and removal (Al-Othman et al., 2011). Metals are efficiently separated by reverse osmosis (Aljendeel, 2011) and the membrane separation approach uses cellulose as the foundation for building new adsorbents that are reasonably straightforward to chemically change (O'Connel et al., 2008). However, these technologies are too expensive for treating and disposing secondary toxic metal sludge, take too long to treat, consume too much energy or are ineffective when heavy metals are present in the

wastewater at low concentrations (Kabwadza-Corner et al., 2015). Researchers are investigating low-cost adsorbents for heavy metal removal, such as chitosan beads (Nghah et al., 2006), alginate beads (Samimi and Moeini, 2020), sago waste (Quek et al., 1998), rice husks (Wong et al., 2003), bacterial biomass (Samimi and Shahriari Moghadam, 2021), sawdust (Larous et al., 2005) and zeolites (Peric, 2004). One of the potential adsorbents is zeolite, which contains silicon (Si), aluminum (Al) and oxygen (O) atoms. The primary roles of zeolite are ion exchange or as an adsorbent, molecular sieve, catalyst and soil amendment. Because zeolite and clays contain negative charges, zeolite can absorb heavy metals or positively charge dyes, including textile waste. Zeolites are efficient adsorbent materials with numerous uses in the removal of heavy metals from wastewater. Zeolite was synthesized from by-products such as fly ash and rice husk. The sorption process of zeolites was generally spontaneous and endothermic, and heavy metal ions were removed by adsorption and ion exchange processes. Sadia et al. (2021) found that zeolites have good cation exchange capabilities and sorption performance. One difficulty in using zeolites for metal removal is that, despite their strong adsorptive capacity for heavy metals, recovering zeolites after adsorption is challenging because zeolites are in powder form. Then, a solution is required to use other zeolite form in water, one of them is creating a zeolite-embedded sheet (ZES). This method is proposed as an effective adsorbent for heavy metals, primarily in water. The advantage of embedding powder zeolite in a nonwoven sheet is the convenience with which an adsorbent can be collected after adsorption, and they require instruments to separate the adsorbent and adsorbate. Botoman et al. (2018) demonstrated the efficacy of a Linde type A (LTA)-embedded sheet in eliminating lead (Pb) from water. Random forest (RF) methods have been widely used, including in heavy metal studies. Tan et al. (2018) have explored heavy metal estimation of soil using RF due to its built-in modeling expressiveness and feature selection ability. RF has also been used to estimate, validate and model the heavy metal removal efficiency from environments. Currently, advanced data analysis approaches, including machine learning (ML), have become versatile tools for modeling and developing estimation and prediction of the future of unknown data based on hidden information

related to massive input data. In heavy metal removal studies, RF has been used to accurately predict heavy metal adsorption efficiency using biochar (Zhu *et al.*, 2019). According to Chun *et al.* (2022), the heavy metal removal efficiency based on flocculant properties, flocculation conditions and heavy metal properties can be predicted using RF with high accuracy with a coefficient of determinant ( $R^2$ ) equal to 0.9354. In Indonesia, estimating the efficiency of heavy metal removal from water using both ZES and RF analyses is still lacking and accurate information on the heavy metal removal efficiency of ZES is needed because of the rising heavy metal contents in water. Considering this situation, this study attempts to address the following questions: Can ZES remove heavy metals like copper (Cu), lead (Pb) and zinc (Zn) from water? And if ZES can remove heavy metals, can RF model the removal efficiency of ZES? The objectives of this study are to assess the Cu, Pb and Zn removal efficiency of ZES and model the removal efficiency using RF. The result of this study can contribute to heavy metal removal practices, in particular by providing information on the heavy metal concentration at which ZES can be used and providing the optimum removals. This study has been conducted at the Department of Biology and Chemistry, Faculty of Mathematics and Natural Sciences, Universitas Indonesia in 2023.

## MATERIALS AND METHODS

### Materials

Chemical reagents for adsorption testing, namely copper (II) sulfate pentahydrate ( $\text{Cu}(\text{SO}_4)_2 \cdot 5\text{H}_2\text{O}$ ), zinc sulfate heptahydrate ( $\text{ZnSO}_4 \cdot 7\text{H}_2\text{O}$ ), lead (II) nitrate ( $\text{Pb}(\text{NO}_3)_2$ ), sodium nitrate ( $\text{NaNO}_3$ ) and sodium sulfate ( $\text{Na}_2\text{SO}_4$ ), were ordered from MERCK. Aquades was bought directly from Brataco, limited (Ltd), Indonesia. Raw materials were purchased from different marketplace. Nonwoven sheets made of polypropylene (PP) and polyethylene (PE) were bought from Platec, Ltd, Japan. The zeolite A-4 powder was acquired from Wako Pure Chemical Industries, Ltd, Japan.

### Fabrication of ZES

In this study, ZES was fabricated, referring to Sadiya *et al.* (2021). The nonwoven sheets were cut into 81 centimeter squared ( $\text{cm}^2$ ) and divided into nine pieces. Each of them was then numbered and

weighed. The amount of zeolite powder was poured into a stainless tray. The sheets were placed into the tray, and then pressed slowly and inverted by hand. The sheets were then heated at  $160^\circ\text{C}$  for 8 minutes. After chilling, ten embedded sheets were put into a 1 liter (L) Duran bottle, added with 500 milliliter (mL) of water and shaken by hand for 2 minutes. After the water is removed, this shuffling is repeated one more time. Then, the sheet in the bottle is shaken with 500 mL water for 1 hour to remove zeolite powder that does not attach to the filter. Shaking was repeated once, and the filter was dried at room temperature ( $25^\circ\text{C}$ ). The dry weight of the sheet was weighed to determine the mass of zeolite contained in each embedded sheet.

### Characterization of ZES

ZES was recorded for their structure, chemical composition, and vibrational properties. A scanning electron microscope–energy-dispersive X-ray (SEM-EDX) (Jeol JSM-IT200) was used to observe the surface morphology and chemical properties of ZES. Fourier transform infrared (FTIR) (Thermo Scientific Nicolet iS50 FTIR) was applied for vibrational properties. SEM-EDX analysis was conducted in the National Research and Innovation Agency (BRIN) and the FTIR was conducted in the Integrated Laboratory and Research Center (ILRC), University of Indonesia.

### Cu, Pb, and Zn adsorption using ZES

Adsorption solutions were prepared with different concentrations. First, 1 molar (M)  $\text{NaNO}_3$  and  $\text{Na}_2\text{SO}_4$  solution as a background solution were composed. Second, stock solutions of 0.1 M  $\text{Cu}(\text{SO}_4)_2 \cdot 5\text{H}_2\text{O}$  (1000 mL), 0.1 M  $\text{Pb}(\text{NO}_3)_2$  (1000 mL) and 0.1 M  $\text{ZnSO}_4 \cdot 7\text{H}_2\text{O}$  (1000 mL) were prepared. Third, stock solutions of 5 millimolar (mM) Cu, 5 mM Pb and 5 mM Zn were then prepared. The Cu, Pb and Zn solutions were diluted from various concentrations to experiment with the adsorption of Cu, Pb and Zn solutions with ZES. For  $\text{Cu}(\text{SO}_4)_2 \cdot 5\text{H}_2\text{O}$ ,  $\text{Pb}(\text{NO}_3)_2$  and  $\text{ZnSO}_4 \cdot 7\text{H}_2\text{O}$  50 mL solution at each concentration: 0.025, 0.05, 0.10, 0.20, 0.40 and 0.60 mM were taken for initial concentration analysis using the Inductively Coupled Plasma (ICP) method and the potential of hydrogen (pH) was measured. In adsorption experiments,  $\text{Cu}(\text{SO}_4)_2 \cdot 5\text{H}_2\text{O}$ ,  $\text{Pb}(\text{NO}_3)_2$  and  $\text{ZnSO}_4 \cdot 7\text{H}_2\text{O}$  solutions were put into a PP bottle according to the weight of ZES, with ZES-solution ratio of 0.1 gram (g): 500 g.

Table 1: Summary of initial heavy metal contents in water

Prepared solution (mM)	Contents in water (mg/L)		
	Cu	Pb	Zn
0.025	1.365	6.765	1.575
0.05	2.7	9.38	3.31
0.1	5.685	28.035	6.44
0.15	8.3	30.92	4.755
0.2	10.355	38.895	6.11
0.3	14.84	74.62	4.67
0.4	19.395	100.515	26.95
0.5	21.015	139.01	34.24
0.6	28.26	171.615	41.125

One sheet of ZES was put in each bottle and shaken vertically 10 times. The bottle was chilled for 3 hours and shaken every 1 hour. Then, the ZES in the bottle is taken with tweezers. Finally, the pH of the solution was measured again and the final concentration of Cu in the solution was measured using ICP. The same treatment was also conducted on Zn and Pb adsorption. The heavy metal content analyses were performed at Saraswanti Indo Genetech Ltd, Indonesia. A summary initial heavy metal contents in water is shown in [Table 1](#).

#### Environmental variables

In this experiment, two water environmental variables were measured. Those variables were water pH and temperature. The equipment used to measure the these variables was a Lutron pH meter 5510.

#### Cu, Pb, and Zn adsorption experiment

Heavy metal removal of ZES was measured on the basis of the remaining heavy metal contents after treatment with ZES. The percent removal of heavy metals was calculated using Eq. 1 ([Chibuzo et al., 2016](#); [Azimi et al., 2019](#)).

$$\% \text{adsorption} = \frac{C_i - C_e}{C_i} \times 100 (\%) \quad (1)$$

Where,  $C_i$  and  $C_e$  are the initial and final concentration of heavy metals, respectively.

#### RF model statistical analysis

The statistical analysis used in this study is RF. The RF model was developed following [Fathi et al. \(2014\)](#). An RF is a collection of hundreds of decision trees

with identical distribution. Classification algorithms, such as classification and regression trees, are used to create these trees. RF, proposed by Leo Breiman, constructs many decision trees and blends them to obtain a more accurate and consistent prediction. This model, in terms of the strength of the individual predictors and their relationships, provides insight into the RF's capacity to forecast. The predictors in this study were water pH, temperature and heavy metal content in mM and milligram per liter (mg/L). Within RF, a classification tree is iteratively defined by a division criterion (node) obtained from one of the variables,  $x_j$ , which results in the construction of two subsets in the training sample consisting of a subset that contains the observations (i) that satisfy the condition  $x_j^i < a$  real number, which is defined by the algorithm (T), whereas the other subset contains the observations i that satisfy the condition  $x_j^i > T$  ([Ruiz-Gazen and Villa, 2008](#)). For both classification and regression models, we utilized the RF package in R platform version 3.6.3 for statistical computing and making visuals. The reference contains a full description of the RF method.

#### Model validation for error analysis

The removal efficiency model developed using RF was validated and measured for its error. The validation was based on several statistical tests. Those tests include the root mean square error (RMSE), mean square of residuals (MSR), percentage variable explained and graphs depicting the out-of-bag (OOB) error of an RF model for Cu, Pb, and Zn. The lowest RMSE closed to zero ([Sang et al., 2022](#)) and the more trees within the OOB mean the model is providing the best accuracy.

## RESULTS AND DISCUSSION

### Characterization of ZES

Fig. 1 shows the appearance of ZES morphology using SEM and the presence of zeolite - a cubical structure attached to sheet fibers. The sticking of zeolite occurs because of heating. The chemical composition of ZES analyzed using EDX is shown in Table 2. ZES in the study contained elements carbon (C) (66.86%), O (26.87%), natrium (Na) (2.56%), Al (1.75%), Si (1.96%) and chloride (Cl) (0.28%). The presence of O, Na, Al and Si indicated that zeolite is successfully attached to the sheet. Related to adsorption ability, silicon per aluminum (Si/Al) ratio is considered important. In this study, the Si/Al ratio present in the ZES is 0.96. According to Hudcová *et al.* (2021), the smaller the value of the ratio, the better the adsorption ability of a material. Because the lower in Si/Al ratio of the zeolite indicates the higher

in its CEC (cation exchange capacity).

The vibrational properties of ZES using FTIR are shown in Fig. 2. The peak band at 3381.33 reciprocal centimeter (/cm) and 3643.07/cm indicate oxygen hydrogen (OH) stretch as reported by Corona *et al.* (2009) and Jacas-Rodríguez *et al.* (2020) stated that OH stretch usually detected in the range 3400–3700/cm that has interaction between the water hydroxyl and cations. Spectral regions between 3000/cm and 2800/cm enable an analysis of the peak on 2848.33/cm and 2915.36/cm related to the asymmetric and symmetric stretching vibrations of carbon hydrogen (C–H) bonds in the methoxy (O–CH<sub>3</sub>) group (Portaccio *et al.*, 2011). C–H bending was observed at the peak of 1479.63/cm (Merck, 2023). The vibration at 969.69/cm is attributed to the asymmetric stretching vibrations characteristic of asymmetrical stretching vibrations ( $V_{as}$ ) siloxane (Si–O–Si) and  $V_{as}$  silicon–

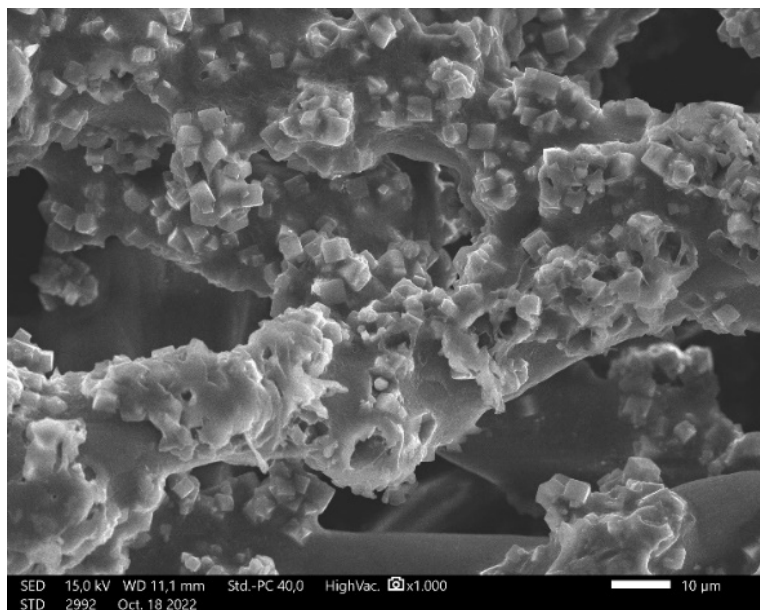


Fig. 1: Morphological structure of ZES

Table 2: Chemical composition of ZES

Element	Atomic concentration (%)
C	66.86
O	26.87
Na	2.56
Al	1.75
Si	1.69
Cl	0.28

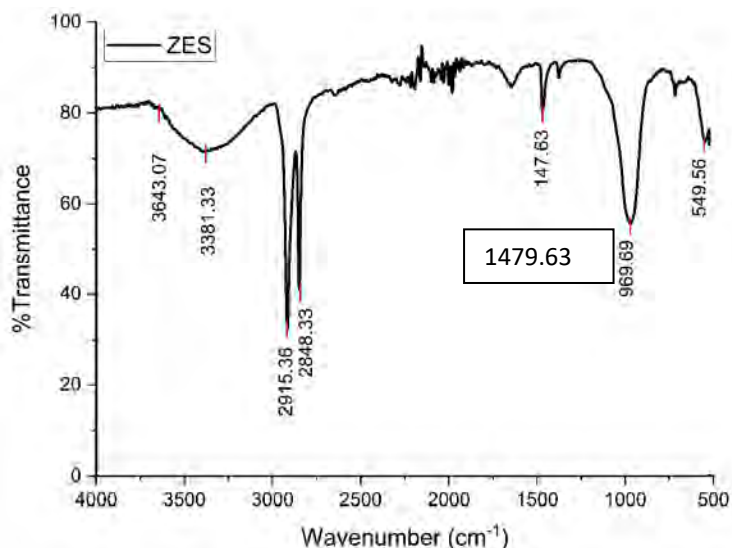


Fig. 2: FTIR spectrum of ZES

Table 3: Summary of model validation for Cu, Pb and Zn

Variables	Cu	Pb	Zn
RMSE	1.805	1.080	2.229
MSR	0.383	2.202	0.674
% var explained	99.09	99.33	99.92

oxygen–aluminum (Si–O–Al) (Mozgawa et al., 2011). The peak of 549.56/cm has a complex band as the superposition of different vibrations, composed of the symmetrical stretching vibrations ( $\nu_s$ ) of Si–O–Si and the bending vibrations ( $\delta$ ) corresponding to siloxane (O–Si–O) (Jacas-Rodríguez et al., 2020). The peaks related to the carbon hydrogen (C–H) bonds (2848.33 and 2915.36/cm) and the C–H bending (1479.63/cm) were due to PE (Madhu et al., 2014) and PP (Ummartyotin and Pechyen, 2016) respectively, derived from the sheet. The other peaks were belong to zeolite.

#### Adsorption trends of Cu, Pb, and Zn

The adsorption trends and removal efficiency of Cu, Pb and Zn are shown in Figs. 3–5 after 60 minute contact times. In general, ZES can adsorb diluted heavy metals from water because percentages of adsorbed heavy metals are present. The adsorptive effects of this experiment were influenced by the initial heavy metal contents in water. It is clear that an

increase in heavy metal contents in water will reduce heavy metal adsorption of ZES. The heavy metal removal efficiency of ZES was reduced to 50 percent (%) at metal concentrations of 10.355 mg/L for Cu, 171.615 mg/L for Pb and 4.755 mg/L for Zn. It can be concluded that ZES was more efficient at adsorbing Pb because the Pb removal efficiency has a threshold as high as 171.615 mg/L. The adsorption trends of Cu, Pb, and Zn were related to cation exchange capacity and porous structure. Solid materials with a porous structure can be used as adsorbents (Irani et al., 2011). Zeolite has high adsorption efficiency due to its low cation exchange capacity in the form of high Si/Al ratios. These properties explain the adsorption result of zeolite and its potency as an adsorbent for those heavy metals in water. On the basis of Pratama et al. (2021), zeolite particles contributed Cu and Zn adsorption sites. Copper ion ( $\text{Cu}^{2+}$ ) form complex with silicon–oxygen bonds (Si–O) and aluminum–oxygen bonds (Al–O). According to Chang and Shih (2000), zeolite’s features and

the characteristics of those metal ions impact the variation in adsorption capacity. Metal ions may pass through pores that have a particular size. The adsorption capacity would be reduced if a metal ion was larger than the pore size. Compared with Cu, Zn has a larger atomic diameter (Barak and Helmke, 1993). These characteristics explain the higher levels of Cu adsorption in the zeolite than Zn adsorption.

More central metal ions have low capacities for solidity and electrostatic adsorptive power, these will restrict the ability of metals of particular dimensions to interact with one another (Minceva et al., 2007). On the other hand, ions having a greater ion valence and a small ion radius will be firmly and densely adsorbed. According to Minceva et al. (2007), metals with higher electronegativity values will be simpler

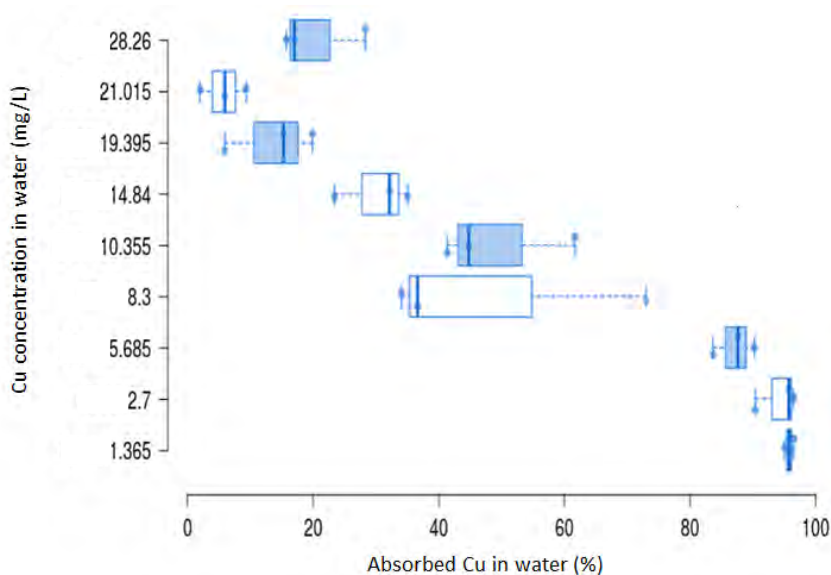


Fig. 3: Percentages of adsorbed Cu (x-axis) in water related to Cu concentration (y-axis; 1.365, 2.7, 5.685, 8.3, 10.355, 14.84, 19.395, 21.015, 28.26 mg/L) (means between population / distribution (F) = 87.999, probability (P) = 0.000)

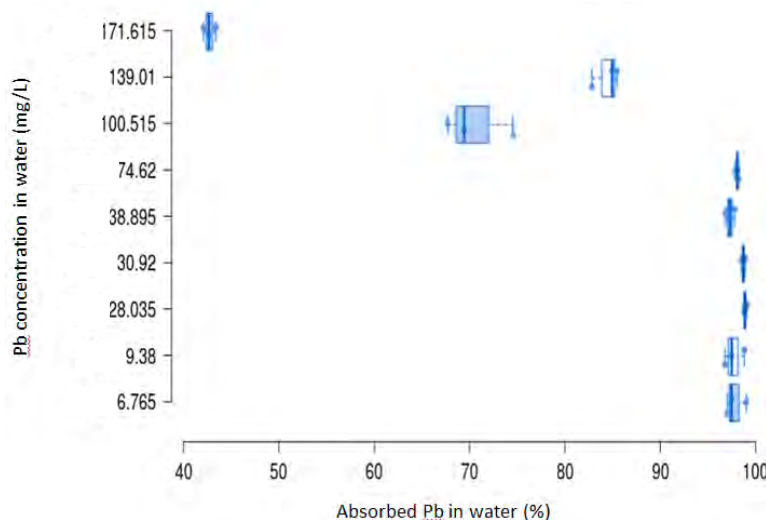


Fig. 4: Percentages of adsorbed Pb (x-axis) in water related to Pb concentrations (y-axis; 6.765, 9.38, 28.035, 30.92, 38.895, 74.62, 100.515, 139.01, 171.615 mg/L) (F = 570.797, P = 0.000)

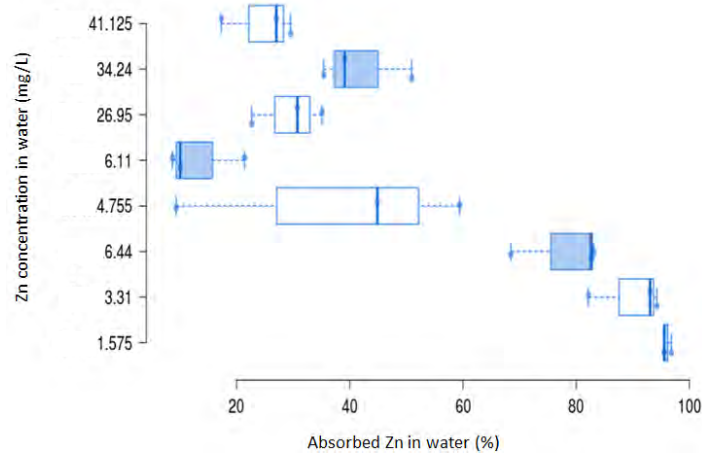


Fig. 5: Percentages of adsorbed Zn (x-axis) in water related to Cu concentrations (y-axis; 1.575, 3.31, 6.44, 4.755, 6.11, 26.95, 34.24, 41.125 mg/L) ( $F = 24.954$ ,  $P = 0.000$ )

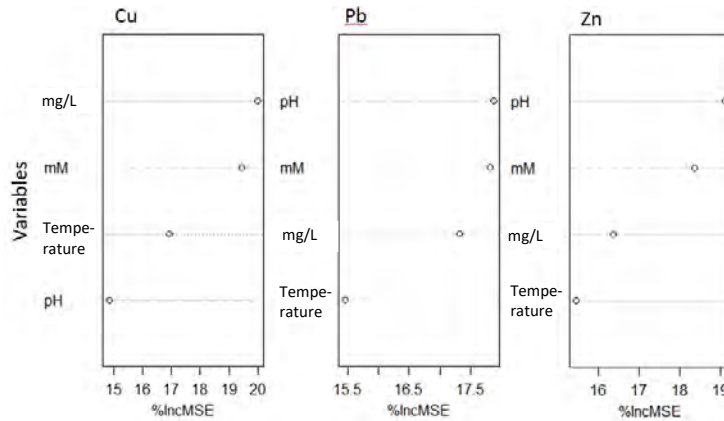


Fig. 6: Important variables for Cu, Pb and Zn adsorption by ZES

to absorb than those with lower electronegativity values. Additionally, zeolite displayed a typical silicon dioxide ( $\text{SiO}_2$ ) and aluminum oxide ( $\text{AlO}_3$ ) bond structure. Zeolite contains an extra negative ion capacity due to this connection, which is exploited in a cation exchange process to bind the metal ions. Our findings show that at metal concentrations such as 10.355 mg/L for Cu and 4.755 mg/L for Zn, heavy metals decreased to 50%. This makes ZES more efficient at adsorbing Cu ions because it can adsorb a higher concentration of 10.355 mg/L than Zn. If Zn concentrations were close to 10.355 mg/L, the removal efficiency of ZES was only <50%. Cu is more highly adsorbed in zeolite than Zn. Cu can be highly adsorbed in zeolite because Cu has a smaller atomic

size than Zn. Zn has a larger electron number than Cu, so the size of the Zn ion is larger than that of the Cu ion.

#### Important variables affecting the efficiency of removing Cu, Pb and Zn

Fig. 6 presents the important variables for Cu, Pb and Zn adsorption by ZES. The important variables affecting Cu removal efficiency by ZES were its contents in water, followed by water temperature and pH. In the other hand, for Pb and Zn, removal efficiency was influenced mostly by pH. According to [Kulkarni et al. \(2013\)](#), pH has an influence on metal adsorption using zeolite because pH affects the  $\text{H}^+$  between adsorbents and metals ([Mubarak et al., 2022](#)).

Besides pH, temperature also contributes to metal sorption by zeolite (Chibuzo *et al.*, 2016).

#### Model validation for Cu, Pb, and Zn

Model validation for Cu, Pb, and Zn are shown in Table 3. Zn has the highest RMSE, whereas Pb has the lowest RMSE. Lower RMSE means better accuracy. Then the prediction accuracy of the model is good in this case of Pb and Zn.

#### OOB error

The OOB error for Cu, Pb, and Zn is shown in Fig. 7. All OOB shows a large number of trees when the OOB error is decreasing, which indicates the model has good accuracy. Between heavy metals, the best model was observed for Zn and Cu, followed by Pb. The number of trees in Zn and Cu had already stabilized at 300 and 400, respectively. Conversely the number of trees in Pb was still fluctuating after 400.

#### RF model

The RF model (Fig. 8) confirms that the high removal efficiency of Cu from water with a probability of 100% (>66%, average efficiency = 92.2%; confidence intervals (CI): 87%–97.4%) was significantly determined by the Cu(II) solution in water ( $P < 0.001$ ), equal to  $\leq 5.685$  mg/L. While with a Cu(II) solution of  $> 5.685$  mg/L in water, ZES can only remove <66% (average efficiency = 25.5%; CI: 12.7%–38.3%) of Cu from water. On the basis of the RF model, Pb and Zn removal efficiency was affected by pH. A high removal efficiency of Pb from water with a probability of 100% (Fig. 9) was significantly determined by water pH equal to  $\leq 4.94$

and water temperature equal to  $\leq 29.1$  degrees Celsius ( $^{\circ}\text{C}$ ) ( $P < 0.001$ ). When water pH equals to  $> 4.94$  and water temperature equals to  $> 29.1$   $^{\circ}\text{C}$ , ZES can only adsorb 30–60% of Pb from water. The Zn adsorption pattern was also similar to that of Pb adsorption. Based on the RF model for Zn (Fig. 10), the high removal efficiency of Zn from water with a probability of 100% was significantly determined by water pH equal to  $\leq 5.61$  ( $P < 0.001$ ). With a high water pH equal to  $> 5.61$  and water temperature equal to  $> 29.6$   $^{\circ}\text{C}$ , ZES can only adsorb 30–60% of Zn from water. In this study, several heavy metal removal efficiency has been modeled using RF. According to Shi *et al.* (2022), ML methods have been used in heavy metal content assessment studies that include artificial neural networks (ANN) (Sakizadeh *et al.*, 2017), least absolute shrinkage and selection operators (LASSO), genetic algorithms (GA), and error back-propagation neural networks (BPNN), namely the LASSO-GA-BPNN model, support vector regression (SVR) (Huang *et al.*, 2021) and RF (Taghizadeh-Mehrjardi *et al.*, 2021). The RF model used in this study has obvious high accuracy and recognition capability for predicting the removal efficiency of heavy metals from water. The results also show that the RF model is effective at predicting adsorbed Cu, Pb and Zn, confirming the science and the advancement of the RF prediction model in heavy metal removal studies (Cao *et al.*, 2023). According to the model, removal efficiency was also affected by water pH and temperature, as can be seen for Pb and Zn. In this study, high removal efficiency was observed when the pH was  $< 4.94$  for Pb and 5.61 for Zn. This finding contradicts the general pattern. Shaker (2007) confirms that an increase in pH will increase adsorption

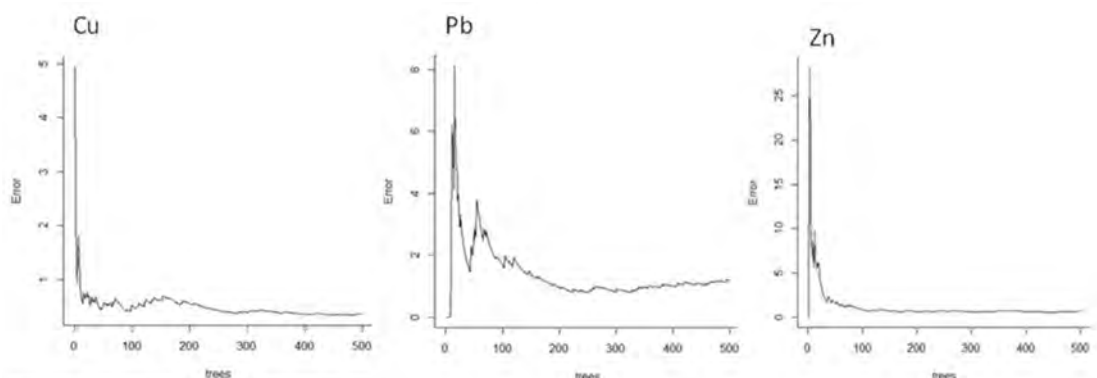


Fig. 7: Graphs depicting the OOB error of an RF model for Cu, Pb and Zn

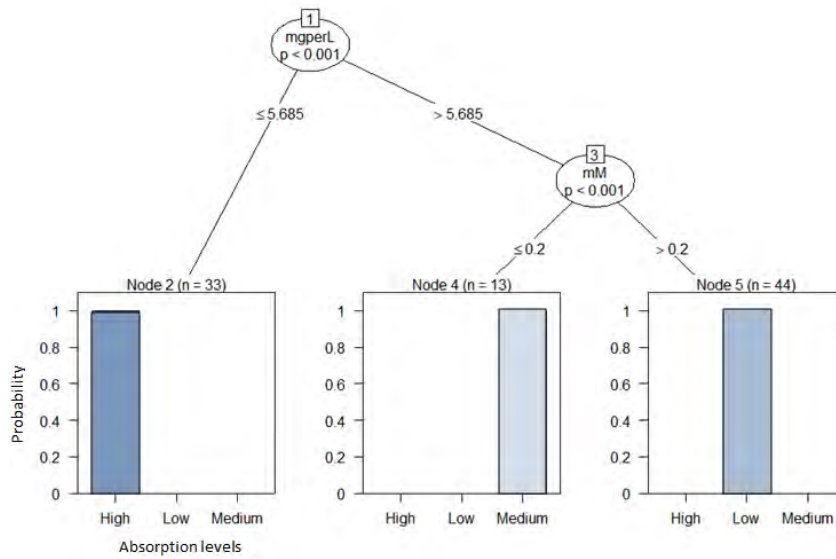


Fig. 8: RF model of adsorbed Cu (x-axis, absorption levels: low, 0–30%; medium, 31–60% and high, 61–100%) in water related to water pH, temperature and Cu concentration in mM and mg/L.

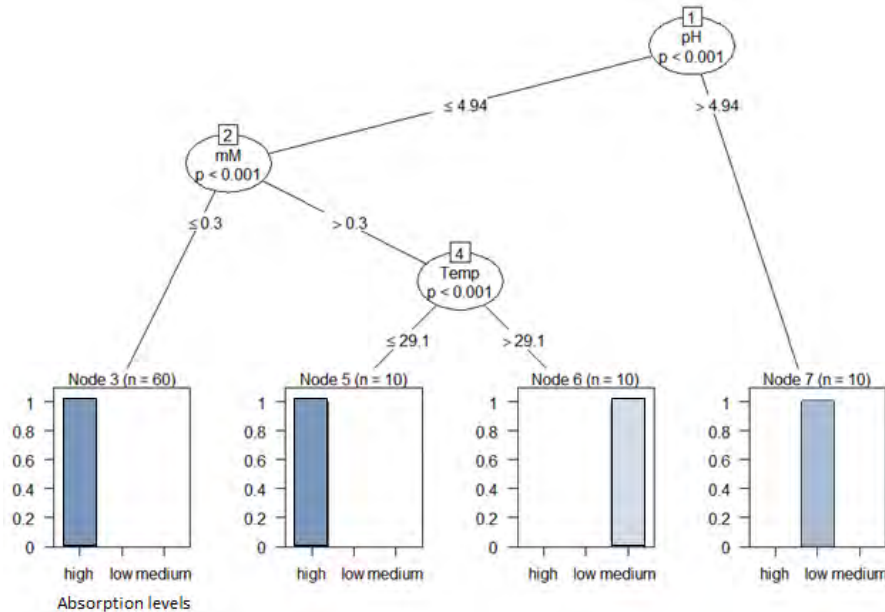


Fig. 9: RF model of adsorbed Pb (x-axis, absorption levels: low, 0–30%; medium, 31–60% and high, 61–100%) in water related to water pH, temperature and Pb concentration in mM and mg/L.

since, at low pH, there is a high concentration of  $H^+$  with high mobility due to metal ions, and this increases the competition between  $H^+$  and metal ions, causing reductions in its adsorption. The removal efficiency

using ZES in this study was comparable to the previous study (Table 4). For zeolite adsorption, an increase in pH will reduce the adsorption. Kulkarni *et al.* (2013) observed that when pH increased from 6 to 8, the

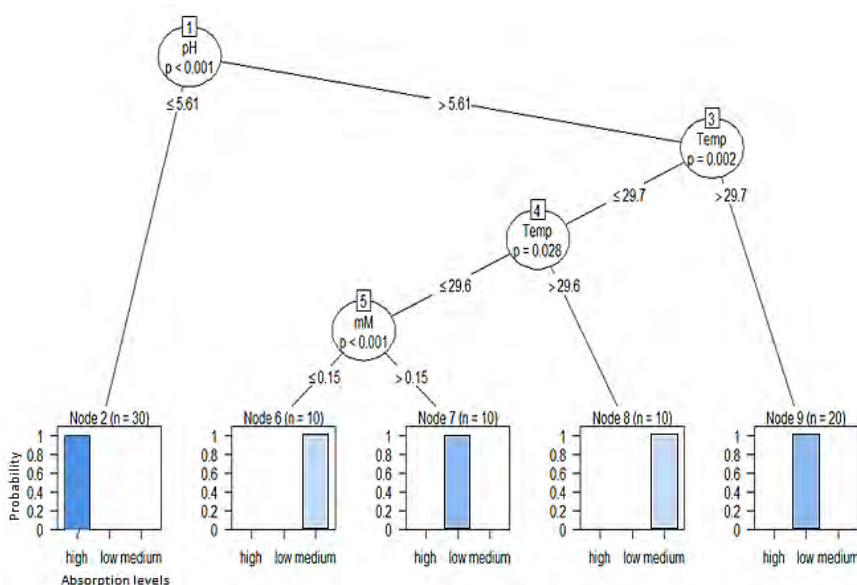


Fig. 10: RF model of adsorbed Zn (x axis, absorption levels: low, 0–30%; medium, 31–60% and high, 61–100%) in water related to water pH, temperature and Zn concentration in mM and mg/L.

Table 4: Comparisons with previous studies and other zeolite adsorbents

Heavy metals	Adsorbents	Removal efficiency (%)	pH ranges	Temperature (°C)	Sources
Calcium (Ca)	Zeolite 4A	70–90	3–8	NA	Kulkarni <i>et al.</i> (2013)
iron (Fe) and manganese (Mn)	Titanium dioxide (TiO <sub>2</sub> )@Zeolites-4A nanocomposite	70–100	2–9	NA	Mubarak <i>et al.</i> (2022)
Pb	Zeolite solution	80–100	2–10	29.8–39.8	Chibuzo <i>et al.</i> (2016)
Cu, Pb and Zn	ZES	5.51–98.92	4–7	29.1–29.9	This study

removal efficiency decreased from 90% to 70%. Even at a low pH of 2 to 3, the removal efficiency of zeolite can reach 70-80%. Temperature was also considered an important variable for removing heavy metals from water. In this study, adsorptions was observed at temperatures of 29.1–29.9 °C. This temperature range is in agreement with that in previous studies. Chibuzo *et al.* (2016) reported that 29 °C is the optimum temperature for zeolite. Instead, although this study was successful in predicting metal adsorption, the RF approach still has significant shortcomings that must be addressed (Fernández-Delgado *et al.*, 2014). The RF model makes a prediction based on a set of hundreds of decision trees with identical distribution. The development of the trees may slow down the algorithm’s prediction. Hyperparameters and tuning

methods can be used to optimize RF. Tuning is the process of determining the best hyperparameters for a learning algorithm for a particular dataset. Aside from tuning, numerous ways for optimizing the RF model were suggested. These methods include grid search, F-race, the OOB approach and generic simulated annealing (Seibold *et al.*, 2017).

#### Heavy metal removal optimization

Heavy metal removal optimization by ZES varied depending on the zeolite dose, metal contents, water pH and temperature (Table 5). For Cu, optimized removal was achieved at 86.98% when the concentration of Cu in water was 5.685 mg/L. Optimization for Pb and Zn was different and was influenced more by pH and temperature than metal

Table 5: Heavy metal removal optimization parameters

Heavy metals	Removal efficiency (%)	Zeolite dose (g)	Metal contents (mg/L)	Water	
				pH	Temperature (°C)
Cu	86.98	0.08	5.685	4.69	29.5
Pb	98.92	0.08	28.035	4.67	29.0
Zn	95.97	0.074	1.575	5.2	29.9

contents in water. For Pb, the optimum pH and temperature were found to be <4.94 and 29.1 °C, respectively with 98.92% Pb reduction. In contrast, for 95.97% of Zn reduction, the optimum pH and temperature were found to be <5.61 and 29.7 °C.

### CONCLUSION

This study has shown that zeolite can be embedded in sheets by heating because the zeolite powder sticks to the sheet during the heating process. Additionally, the sandwich method used allows the zeolite powder embedded in the sheet to become denser. This study succeeded in showing the removal of heavy metals from water using ZES and modeling the contribution of variables that affect heavy metal removal using an RF model. The heavy metal removal efficiency by ZES was reduced to 50% at metal concentrations of 10.355 mg/L for Cu, 171.615 mg/L for Pb and 4.755 mg/L for Zn. According to the model, the important variables affecting the heavy metal removal efficiency of ZES were metal contents in water, followed by water temperature and pH. This modeling is supported by validation based on the RMSE, MSR, percentage variable explained and graphs depicting the OOB error. The RMSE values obtained in this study were in the order of Zn > Cu > Pb, whereas the MSR values obtained were in the order of Pb > Zn > Cu. On the basis of OOB error, all models show a large number of trees when the OOB error is decreasing, which indicates the model has good accuracy. Between heavy metals, the best model was observed for Zn and Cu, followed by that for Pb. An RF model can determine the threshold of heavy metal contents, water pH and temperature to optimize the heavy metal removal efficiency of ZES. Although this study was successful in predicting metal adsorption, the RF approach still has significant limitations that must be addressed. The RF model makes a prediction based on a set of hundreds of decision trees with identical distribution and the development of those trees may slow down the algorithm's prediction. In conclusion, high removal

of Cu from water by ZES is observed if the Cu content is ≤5.685 mg/L. Conversely, the high removal of Pb and Zn from water by ZES is observed if the water pH ranges from 4.94 to 5.61 and the temperature is ≤29.1 °C. The application of this model can assist in the development of adsorbents in reducing pollutant levels in water. This study can also be a reference for environmentalists as an alternative material in handling waste that enters the water system.

### AUTHOR CONTRIBUTIONS

N.D. Takarina as corresponding author has contributed in funding. N. Matsue provided references for the manuscript. E. Johan verified the data and results. A. Adiwibowo drafted the manuscript, analyzed and interpreted data using RF. M.F.N.K. Rahmawati conducted material preparation and fabrication of ZES. S.A. Pramudyawardhani helped in the Cu, Pb and Zn adsorption experiments using ZES. T. Wukirsari assisted in the preparation of stock solutions of Cu, Pb and Zn.

### ACKNOWLEDGEMENT

The authors thank the Directorate of Research and Development, University of Indonesia (Risbang UI) for its funding through PUTI Q2 Research Grant with contract number [NKB-658/UN2.RST/HKP.05.00/2022].

### CONFLICT OF INTEREST

The authors declare that there is no conflict of interests regarding the publication of this manuscript. In addition, the ethical issues, including plagiarism, informed consent, misconduct, data fabrication and/or falsification, double publication and/or submission, and redundancy have been completely observed by the authors.

### OPEN ACCESS

©2024 The author(s). This article is licensed under a Creative Commons Attribution 4.0 International

License, which permits use, sharing, adaptation, distribution and reproduction in any medium or format, as long as you give appropriate credit to the original author(s) and the source, provide a link to the Creative Commons license, and indicate if changes were made. The images or other third-party material in this article are included in the article's Creative Commons license, unless indicated otherwise in a credit line to the material. If material is not included in the article's Creative Commons license and your intended use is not permitted by statutory regulation or exceeds the permitted use, you will need to obtain permission directly from the copyright holder. To view a copy of this license, visit: <http://creativecommons.org/licenses/by/4.0/>

#### PUBLISHER'S NOTE

GJESM Publisher remains neutral with regard to jurisdictional claims in published maps and institutional affiliations.

#### ABBREVIATIONS

%	Percent
°C	Degree Celsius
$\delta$	Symmetrical bending vibrations
/cm	Reciprocal centimeter
Al	Aluminum
Al–O	Aluminum–oxygen bonds
AlO <sub>3</sub>	Aluminum oxide
ANN	Artificial neural networks
BPNN	Back propagation neural networks
BRIN	The National Research and Innovation Agency
C	Carbon
Ca	Calcium
C–H	Carbon–hydrogen
Cl	Chloride
CI	Confidence intervals
Cl	Chloride
cm <sup>2</sup>	Centimeter squared
Cu	Copper
Cu <sup>2+</sup>	Copper ion
CuSO <sub>4</sub> ·5H <sub>2</sub> O	Copper (II) sulfate pentahydrate
Fe	Iron
F	Means between population / distribution

FTIR	Fourier transform infrared
g	Gram
GA	Genetic algorithms
H <sub>i</sub>	Heavy metal concentration before treatment using ZES
H <sub>t</sub>	Heavy metal concentration after treatment using ZES
i	A subset that contains the observations
ICP	Inductive couple plasma
ILRC	The Integrated Laboratory and Research Center University of Indonesia
L	Liter
LASSO	Least absolute shrinkage and selection operators
LASSO-GA-BPNN	Least absolute shrinkage and selection operators–genetic algorithms– back-propagation neural networks
LTA	Linde type A
Ltd	Limited
M	Molar
mg/L	Milligram per liter
mL	Milliliter
ML	Machine learning
mM	Millimolar
Mn	Manganese
NaNO <sub>3</sub>	Sodium nitrate
Na <sub>2</sub> SO <sub>4</sub>	Sodium sulfate
MSR	Mean square of residuals
Na	Natrium
O	Oxygen
O–CH <sub>3</sub>	Methoxy
O–Si–O	Siloxane – bending form
OOB	Out of bag error
OH	Oxygen hydrogen
P	Probability
pH	Potential of hydrogen
Pb	Lead
Pb(NO <sub>3</sub> ) <sub>2</sub>	Lead (II) nitrate
PE	Polyethylene
PP	Polypropylene

$R^2$	Coefficient of determinant
RF	Random forest
RMSE	Root mean square error
SEM-EDX	Scanning electron microscope–energy-dispersive X-ray
Si	Silicon
Si/Al	Silicon per aluminum
Si–O–Al	Silicon–oxygen–aluminum
Si–O–Si	Siloxane – stretching form
Si–O	Silicon–oxygen bonds
SiO <sub>2</sub>	Silicon dioxide
SVR	Support vector regression
T	A real number which is defined by the algorithm
TiO <sub>2</sub>	Titanium dioxide
V <sub>os</sub>	Asymmetrical stretching vibrations
V <sub>s</sub>	Symmetrical stretching vibrations
x <sub>j</sub>	Variables
ZES	Zeolite-embedded sheet
Zn	Zinc
ZnSO <sub>4</sub> ·7H <sub>2</sub> O	Zinc sulfate heptahydrate

## REFERENCES

- Aljendeel, H.A., (2011). Removal of heavy metals using reverse osmosis. *J. Eng.*, 17(3): 647–658 (12 pages).
- Al-Othman, Z.A.; Naushad, Mu.; Inamuddin, (2011). Organic–inorganic type composite cation exchanger poly-o-toluidine Zr(IV) tungstate: Preparation, physicochemical characterization and its analytical application in separation of heavy metals. *Chem. Eng. J.*, 172(1): 369-375 (7 pages).
- Astuti, R.D.P.; Mallongi, A.; Rauf, A.U., (2021). Natural enrichment of chromium and nickel in the soil surrounds the karst watershed. *Global J. Environ. Sci. Manage.*, 7(3): 383-400 (18 pages).
- Azimi, N.; Azimi, P.; Samimi, M.; Mansouri Jalilian, T., (2019). Ultrasonic-assisted adsorption of Ni (II) ions from aqueous solution onto Fe<sub>3</sub>O<sub>4</sub> nanoparticles. *Adv. Nanochem.*, 1(2): 66-72 (7 pages).
- Barak, P.; Helmke, P.A., (1993). The Chemistry of zinc. In: Robson, A.D. (eds) *Zinc in Soils and Plants*. Dev. Plant Soil Sci., 55. Springer (13 pages).
- Botoman, L.; Shukla, E.; Johan, E.; Mitsunobu, S.; Matsue, N., (2018). Sorbent-embedded sheets for safe drinking water in developing countries: a case study of lead(II) removal by a zeolite-embedded sheet. *J. Water Health*. 16(1): 159-163 (5 pages).
- Cao, J.; Guo, Z.; Lv, Y.; Xu, M.; Huang, C.; Liang, H., (2023). Pollution risk prediction for cadmium in soil from an abandoned mine based on Random Forest Model. *Int. J. Environ. Res. Public Health*. 20(6): 5097 (11 pages).
- Chang, H.L.; Shih, W.H., (2000). Synthesis of zeolites A and X from fly ashes and their ion-exchange behavior with cobalt ions. *Ind. Eng. Chem. Res.*, 39(11): 4185-4191 (7 pages).
- Chibuzo, A.A., Asadu, C.O., Ikechukwu, O., Arinze, A., (2016). Kinetics and isotherm studies on divalent lead ions adsorption by zeolite solution. *Int. J. Nov. Res. Eng. Sci* 3(1): 49-61 (13 pages).
- Corbella, H.M., (2010). *Urban Water Management and Market: Environmentalism: A Historical Perspective for Barcelona and Madrid*. Universitat Autònoma de Barcelona.
- Corona, O. L.; Hernández, M.A.; Hernández, F.; Rojas, F.; Portillo, R.; Lara, V. H.; Carlos, F. M., (2009). Propiedades de adsorción en zeolitas con anillos de 8 miembros I. Microporosidad y superficie externa. *Rev. Mater.*, 14(3): 918–931 (14 pages).
- Daneshvar rad, R.; Heidari Sharifabad, H.; Torabi, M.; Azizinejad, R.; Salemi, H.; Heidarisoltanabadi, M., (2023). Drought stress tolerance based on selection índices of resistant crops variety. *Global J. Environ. Sci Manage.*, 9(2): 287-298 (12 pages).
- Dinh, D.A.T., Nguyen, T.L., Nguyen, T.N.P., Nguyen, H.T., (2020). Assessing existing surface water supply sources in the Vietnamese Mekong delta: case study of Can Tho, Soc Trang, and Hau Giang provinces. *VJSTE*, 62(4): 65-70 (6 pages).
- Djedidi, Z.; Bouda, M.; Souissi, M.A.; Cheikh, R.B.; Mercier, G.; Tyagi, R.D.; Blais, J.F., (2009). Metals removal from soil, fly ash and sewage sludge leachates by precipitation and dewatering properties of the generated sludge. *J. Hazard. Mater.*, 172(2-3): 1372-1382 (11 pages).
- Evantri, D.; Purwanto, M.Y.D.; Waspodo, R.S.B.; Pandjaitan, R.H., (2021). Panen air hujan sebagai sumber air bersih alternatif di wilayah DAS Bekasi hulu. *Jurnal Keteknik Pertanian*. 9(2): 73-78 (5 pages).
- Ehzari, H.; Amiri, M.; Safari, M.; Samimi, M., (2022). Zn-based metal-organic frameworks and p-aminobenzoic acid for electrochemical sensing of copper ions in milk and milk powder samples. *Int. J. Environ. Anal. Chem.*, 102(16): 4364-4377 (14 pages).
- Fathi, F.; Majari-Kasmaee, L.; Mani-Varnosfaderani, A.; Kyani, A.; Rostami-Nejad, M.; Sohrabzadeh, K.; Naderi, N.; Zali, M.R.; Rezaei-Tavirani, M.; Tafazzolia, M.; Arefi-Oskouie, A., (2014). H-1 NMR based metabolic profiling in Crohn’s disease by random forest methodology. *Magn. Res. Chem.*, 52(7): 370-376 (7 pages).
- Fahimah, N.; Salami, I.R.S.; Oginawati, K.; Yapfirin, S.J.; Supriatin, A.; Thaher, Y.N., (2023). Mapping and determining chemical of potential concerns from heavy metals in water usage in the uppers watershed. *Global J. Environ. Sci. Manage.*, 9(4): 765-788 (24 pages).
- Fernández-Delgado, M., Cernadas, E., Barro, S., Amorim, D., (2014). Do we need hundreds of classifiers to solve real world classification problems? *J. Mach. Learn. Res.*, 15:3133–3181 (49 pages).
- Huang, Y.T.; Lin, J.; Lin, X.; Zheng, W., (2021). Quantitative analysis of Cr in soil based on variable selection coupled with multivariate regression using laser-induced breakdown spectroscopy. *J. Anal. At. Spectrom.*, 36: 2553-2559 (7 pages).
- Hudcová, B.; Osacký, M.; Vítková, M.; Mitzia, A.; Komárek, M., (2021). Investigation of zinc binding properties onto natural and synthetic zeolites: Implications for soil remediation. *Microporous Mesoporous Mater.*, 317(2021): 111022 (10 pages).
- Irani, M.; Amjadi, M.; Mousavian, M.A., (2011). Comparative study of lead sorption onto Natural Perlite, Dolomite and Diatomite. *Chem. Eng. J.*, 178(2011): 317-323 (7 pages).
- Jacas-Rodríguez, A.; Rodríguez-Pascual, P.; Franco-Manzano, D.; Contreras, L.; Polop, C.; Rodríguezacaz, M.A., (2020). Mixed matrix membranes prepared from polysulfone and linde type a zeolite. *Sci. Eng. Compos. Mater.*, 27: 236–244 (9 pages).
- Junianto; Zahidah; Apriliani, I.M., (2017). Evaluation of heavy metal contamination in various fish meat from Cirata Dam, West Java, Indonesia. *AAFL Bioflux.*, 10(2): 241-246 (6 pages).
- Kabwadza-Corner, P.; Johan, E.; Matsue, N., (2015). pH dependence of lead adsorption on zeolites. *J. Environ. Prot.*, 6: 45-53 (9 pages).
- Kulkarni, R.M.; Srinikethan, G.; Shetty, K.V., (2012). Equilibrium and

- kinetic studies for the adsorption of cadmium ion on Zeolite 4A. *J. Biochem. Technol.*, 3(5): S158-S160 (3 pages).
- Larous, S.; Meniai, A.H.; Lehocine, M.B., (2005). Experimental study of the removal of copper from aqueous solutions by adsorption using sawdust. *Desalination*. 185(1-3): 483-490 (8 pages).
- Lu, C.; Xu, Z.; Dong, B.; Zhang, Y.; Wang, M.; Zeng, Y.; Zhang, C., (2022). Machine learning for the prediction of heavy metal removal by chitosan-based flocculants. *Carbohydr. Polym.*, 285(4): 119240 (8 pages).
- Madhu, G.; Bhunia, H.; Bajpai, P.K.; Chaudhary, V., (2014). Mechanical and morphological properties of high density polyethylene and polylactide blends. *J. Polym. Eng.*, 34(9): 813-821 (9 pages).
- MERCK, (2023). IR spectrum and chart, Germany.
- Minceva, M.; Markovska, L.; Meshko, V., (2007). Removal of Zn<sup>2+</sup>, Cd<sup>2+</sup> and Pb<sup>2+</sup> from binary aqueous solution by natural zeolite and granulated activated carbon. *Maced. J. Chem. Chem. Eng.*, 26(2): 125-134 (9 pages).
- Mubarak M.F., Mohamed, A.M.G., Keshawy, M., Moghny, T.A., Shehata, N., (2022). Adsorption of heavy metals and hardness ions from groundwater onto modified zeolite: Batch and column studies. *Alex. Eng. J.*, 61(6): 4189-4207 (9 pages).
- Mozgawa, W.; Król, M.; Barczyk, K., (2011). FT-IR studies of zeolites from different structural groups. *CHEMIK* 65(7): 667-674 (8 pages).
- Ngah, W.S.W.; Kamari, A.; Fatinathan, S.; Ng, P.W., (2006). Adsorption of chromium from aqueous solution using chitosan beads. *Adsorption*, 12: 249-257 (9 pages).
- Nurhasanah; Sulistyowati, L.; Riani, E.; Cordova, M.R., (2023). Cadmium and lead uptake by wild swamp eel in the populous river. *Global J. Environ. Sci. Manage.*, 9(3): 497-514 (18 pages).
- O'Conneall, D.W.B.; Colin, B.; O'Dwyer, T.F., (2008.) Heavy metal adsorbents prepared from the modification of cellulose: A review. *Bioresour. Technol.*, 99(15): 6709-6724 (16 pages).
- Perić, J.; Trgo, M.; Medvidovic, N., (2004). Removal of Zinc, Copper and Lead by natural zeolite—a comparison of adsorption isotherms. *Water Res.*, 38(7): 1893-1899 (7 pages).
- Portaccio, M., Della Ventura, B.; Mita, D.G.; Manolova, N.; Stoilova, O.; Rashkov, I.; Lepore, M., (2011). FT-IR microscopy characterization of sol-gel layers prior and after glucose oxidase immobilization for biosensing applications. *J. Sol-Gel Sci. Technol.*, 57: 204-211 (8 pages).
- Pratama, B.S.E.; Hambali, M.; Matsue, N., (2004). Kinetic and isotherm studies of Cu(II) adsorption by beads and film of alginate/zeolite 4A composites. *IOP Conference Series: Earth Environ. Sci.*, 749: 012013 (12 pages).
- Quek, S.Y.; Wase, D.A.J.; Forster, C.F., (1998). The use of sago waste for the sorption of lead and copper. *Water SA*, 24(3): 251-256 (6 pages).
- Ruiz-Gazen, A.; Villa, N., (2008). Storms prediction : Logistic regression vs random forest for unbalanced data. *Arxiv*, 1(2): 91-101 (11 pages).
- Sabiha-Javied; Mehmood, T.; Chaudhry, M.M.; Tufail, M.; Irfan, N., (2009). Heavy metal pollution from phosphate rock used for the production of fertilizer in Pakistan. *Microchem. J.*, 91(1): 94-99 (6 pages).
- Sadia, S.; Johan, E.; Mitsunobu, S.; Shukla, E.A.; Matsue, N., (2021). Effective washing removal of radioactive cesium from soils using adsorbents: a proposed adsorbent-coexistence method. *J. Radioanal. Nucl. Chem.*, 329: 1439-1445 (7 pages).
- Sakizadeh, M.; Mirzaei, R.; Ghorbani, H., (2017). Support vector machine and artificial neural network to model soil pollution: A case study in Semnan Province, Iran. *Neural Comput. Appl.*, 28: 3229-3238 (10 pages).
- Sang, L.; Wang, Y.; Zong, C.; Wang, P.; Zhang, H.; Guo, D.; Yuan, B.; Pan, Y., (2022). Machine learning for evaluating the cytotoxicity of mixtures of Nano-TiO<sub>2</sub> and heavy metals: QSAR model apply random forest algorithm after clustering analysis. *Molecules*. 27(18): 6125 (14 pages).
- Schaider, L.A.; Ackerman, J.M.; Rudel, R.A., (2016). Septic systems as sources of organic wastewater compounds in domestic drinking water wells in a shallow sand and gravel aquifer. *Sci. Total Environ.*, 547: 470-481 (12 pages).
- Sabilillah, A.M.; Palupi, F.R.; Adji, B.K.; Nugroho, A.P., (2023). Health risk assessment and microplastic pollution in streams through accumulation and interaction of heavy metals. *Global J. Environ. Sci. Manage.*, 9(4): 719-740 (22 pages).
- Safari, M.; Moghadam, M.S.; Samimi, M.; Azizi, Z., (2019). Study of the Optimal Conditions for Zn<sup>2+</sup> Removal Using the Biomass of Isolated Bacteria from Ravang Mine. *Iran. J. Soil Water Res.*, 50(1): 149-160 (12 pages).
- Samimi, M.; Moeini, S., (2020). Optimization of the Ba<sup>2+</sup> uptake in the formation process of hydrogels using central composite design: Kinetics and thermodynamic studies of malachite green removal by Ba-alginate particles. *J Part. Sci. Technol.*, 6(2): 95-102 (8 pages).
- Samimi, M.; Shahriari-Moghadam, M., (2021). Isolation and identification of *Deftia lacustris* Strain-MS3 as a novel and efficient adsorbent for lead biosorption: Kinetics and thermodynamic studies, optimization of operating variables. *Biochem. Eng. J.*, 173: 108091 (9 pages).
- Sarmurzina, R.G.; Boiko, G.I.; Kenzhaliyev, B.K.; Karabalin, U.S.; Lyubchenko, N.P.; Kenyaikin, P.V.; Ilmaliyev, Zh.B., (2023). Coagulants for water based on activated aluminum alloys. *Global J. Environ. Sci. Manage.*, 9(4): 673-690 (18 pages).
- Seibold, H.; Bernau, C.; Boulesteix, A.-L.; De Bin, R., (2017). On the choice and influence of the number of boosting steps for high-dimensional linear Cox-models. *Comput. Stat.*, 1-21 (21 pages).
- Shaker, M.A., (2007). Thermodynamic profile of some heavy metal ions adsorption on to biomaterial surfaces. *Am. J. Appl. Sci.*, 4(8): 605-612 (8 pages).
- Shi, S.; Hou, M.; Gu, Z.; Jiang, C.; Zhang, W.; Hou, M.; Li, C.; Xi, Z., (2022). Estimation of heavy metal content in soil based on machine learning models. *Land*. 11(7): 1037 (19 pages).
- Sulistyowati, L.; Nurhasanah; Riani, E.; Cordova, M.R., (2023b). Heavy metals concentration in the sediment of the aquatic environment caused by the leachate discharge from a landfill. *Global J. Environ. Sci. Manage.*, 9(2): 323-336 (14 pages).
- Sulistyowati, L.; Yolanda, Y.; Andareswari, N., (2023a). Harbor water pollution by heavy metal concentrations in sediments. *Global J. Environ. Sci. Manage.*, 9(4): 885-898 (14 pages).
- Taghizadeh-Mehrjardi, R.; Fathizad, H.; Ardakani, M.A.H.; Soudiazadeh, H.; Kerry, R.; Heung, B.; Scholten, T., (2021). Spatio-temporal analysis of heavy metals in arid soils at the catchment scale using digital soil assessment and a random forest model. *Remote Sens.*, 13(9): 1698 (23 pages).
- Tan, K.; Ma, W.; Wu, F.; Du, Q., (2019). Random forest-based estimation of heavy metal concentration in agricultural soils with hyper spectral sensor data. *Environ. Monit. Assess.*, 191: 446 (14 pages).
- Ummartyotin, S.; Pechyen, C., (2016). Microcrystalline-cellulose and polypropylene based composite: A simple, selective and effective material for microwavable packaging. *Carbohydr. Polym.*, 142: 133-140 (8 pages).
- Waqar, K.; Ahmad, I.; Kausar, R.; Tabassum, T.; Muhammad, A.,

- (2013). Use of bioremediated sewage effluent for fish survival. *Int J Agric Biol.*, 15(5): 988-992 (5 pages).
- WHO, (2022). Guidelines for drinking-water quality. World Health Organization.
- Wong, K.K.; Lee, C.K.; Low, K.S.; Haron, M.J., (2003). Removal of Cu and Pb by tartaric acid modified rice husk from aqueous solutions. *Chemosphere.* 50(1): 23–28 (6 pages).
- Zhu, X.; Wang, X.; Okm Y.S., (2019). The application of machine learning methods for prediction of metal sorption onto biochars. *J. Hazard. Mater.*, 378(2019): 120727 (9 pages).

#### AUTHOR (S) BIOSKETCHES

**Takarina, N.D.**, Ph.D., Professor, Department of Biology, Faculty of Mathematics and Natural Sciences, Universitas Indonesia, Gedung E, Kampus UI Depok, Depok 16424, Indonesia.

- Email: [noverita.dian@sci.ui.ac.id](mailto:noverita.dian@sci.ui.ac.id)
- ORCID: 0000-0003-1766-7445
- Web of Science ResearcherID: GPX-2701-2022
- Scopus Author ID: 6505460222
- Homepage: <https://scholar.ui.ac.id/en/persons/noverita-dian-takarina>

**Matsue, N.**, Ph.D, Professor, The United Graduate School of Agricultural Sciences, Ehime University, 3-5-7 Tarumi, Matsuyama 790-8566, Japan.

- Email: [matsue.naoto.mj@ehime-u.ac.jp](mailto:matsue.naoto.mj@ehime-u.ac.jp)
- ORCID: 0000-0002-0029-4788
- Web of Science ResearcherID: NA
- Scopus Author ID: 6507852978
- Homepage: <https://www.researchgate.net/profile/Naoto-Matsue>

Dr. **Johan, E.**, M.Agr., The United Graduate School of Agricultural Sciences, Ehime University, 3-5-7 Tarumi, Matsuyama 790-8566, Japan.

- Email: [johan@agr.ehime-u.ac.jp](mailto:johan@agr.ehime-u.ac.jp)
- ORCID: 0000-0002-1745-6085
- Web of Science ResearcherID: NA
- Scopus Author ID: 55759036000
- Homepage: <https://www.researchgate.net/profile/Erni-Johan>

**Adiwibowo, A.**, M.Sc., Occupational Health and Safety Department, Faculty of Public Health Universitas Indonesia, Depok 16424, Indonesia.

- Email: [awbio2021@gmail.com](mailto:awbio2021@gmail.com)
- ORCID: 0000-0001-7787-5735
- Web of Science ResearcherID: NA
- Scopus Author ID: 57226558692
- Homepage: <https://staff.ui.ac.id/andrio.adiwibowo>

**Rahmawati, M.F.N.K.**, B.Sc. Student, Department of Biology, Faculty of Mathematics and Natural Sciences, Universitas Indonesia, Gedung E, Kampus UI Depok, Depok 16424, Indonesia.

- Email: [mariafatimanikena99@gmail.com](mailto:mariafatimanikena99@gmail.com)
- ORCID: 0000-0001-8451-7418
- Web of Science ResearcherID: NA
- Scopus Author ID: NA
- Homepage: <https://biologi.ui.ac.id/en/home/>

**Pramudyawardhani, S.A.**, B.Sc. Student, Department of Biology, Faculty of Mathematics and Natural Sciences, Universitas Indonesia, Gedung E, Kampus UI Depok, Depok 16424, Indonesia.

- Email: [sekararpramudya@gmail.com](mailto:sekararpramudya@gmail.com)
- ORCID: 0000-0003-4823-4191
- Web of Science ResearcherID: NA
- Scopus Author ID: NA
- Homepage: <https://biologi.ui.ac.id/en/home/>

**Wukirsari, T.**, S.Si, M.Agr, Ph.D, Occupational Department of Chemistry, Faculty of Mathematics and Natural Sciences, Universitas Indonesia, Gedung E, Kampus UI Depok, Depok 16424, Indonesia.

- Email: [tutiwukirsari@sci.ui.ac.id](mailto:tutiwukirsari@sci.ui.ac.id)
- ORCID: 0000-0002-8457-5578
- Web of Science ResearcherID: NA
- Scopus Author ID: 55681676600
- Homepage: <https://kimia.ui.ac.id/en/home/>

#### HOW TO CITE THIS ARTICLE

Takarina, N.D.; Matsue, N.; Johan, E.; Adiwibowo, A.; Rahmawati, M.F.N.K.; Pramudyawardhani, S.A.; Wukirsari, T., (2024). Machine learning using random forest to model heavy metal removal efficiency by zeolite-embedded sheet in wáter. *Global J. Environ. Sci. Manage.*, 10(1): 321-336.

DOI: 10.22034/gjesm.2024.01.20

URL: [https://www.gjesm.net/article\\_706365.html](https://www.gjesm.net/article_706365.html)





## CASE STUDY

**Cocoa farmers' characteristics on climate variability and its effects on climate change adaptation strategy**I. Idawati<sup>1,\*</sup>, N.A. Sasongko<sup>2,4</sup>, A.D. Santoso<sup>2</sup>, M. Septiani<sup>2</sup>, T. Handayani<sup>3</sup>, A.Y.N. Sakti<sup>2</sup>, B.D. Purnamasari<sup>2</sup><sup>1</sup> Department of Agribusiness, Faculty of Agriculture, Andi Djemma University, Indonesia<sup>2</sup> Research Centre for Sustainable Production System and Life Cycle Assessment, National Research and Innovation Agency, Indonesia<sup>3</sup> Research Policy and Innovation, National Research and Innovation Agency, Indonesia<sup>4</sup> Republic of Indonesia Defense University, Indonesia Peace and Security Centre, Bogor, Indonesia

## ARTICLE INFO

**Article History:**

Received 07 February 2023

Revised 14 May 2023

Accepted 22 June 2023

**Keywords:**

Climate

Cocoa

Environment

Knowledge

Relationship

## ABSTRACT

**BACKGROUND AND OBJECTIVES:** Climate change has a greater influence on agriculture through local climate variability than global climate patterns. The impact of climate change on agricultural productivity and shifts in crop patterns varies significantly across regions. Its impact is closely tied to the technical abilities of farmers in managing their cocoa farming businesses. Technical skills encompass the proficiency of farmers in adopting adaptive cocoa cultivation techniques for planting, maintaining cocoa plants, as well as handling harvest and postharvest processes. The technical capability is interconnected with factors such as crop dependency on rainfall patterns, availability of infrastructure for quality inputs, soil degradation and fertility, nutrient levels, limited farmers' resources, and technology penetration. Given the significant impact of climate change on cocoa farmers, it becomes crucial to enhance their adaptive capacity to address these challenges. Therefore, this study aimed to analyze the relationship between the characteristics of farmers and their adaptive capacity in responding to the impact of climate change.

**METHODS:** Data were collected from 960 populations from two regencies, 4 districts, and 8 villages using the stratified sampling technique through interviews with 282 respondents. The sample size was determined using the Slovin formula through in-depth interviews with five key informants. The data collected were descriptively and statistically analyzed using the Excel program, which involved generating frequency distribution tables. Furthermore, the Mann-Whitney test, utilizing Statistical Product and Service Solution version 24, was employed to conduct a comparative analysis.

**FINDINGS:** This result showed that the characteristics of farmers in the two areas were relatively the same in terms of age, non-formal education, number of family dependents, and perceptions of the climate. In terms of age, most farmers fell within the mature group of 36-48 years, with an average age of 44.63, considering in low category. The low productive age of farmers (44.63), along with their non-formal education, including training in climate field schools and integrated pest management field schools, as well as the number of dependents and their perceptions of climate change, emerged as significant parameters impacting farmers' decision-making processes. These factors also influenced their ability to cope, adapt, and seek new approaches to manage and mitigate the effects of climate change on their farming operations.

**CONCLUSION:** The relationship between farmers' characteristics and adaptive capacity showed that the larger the land owned by farmers, the higher the managerial adaptability of farmers with lower technical ability.

DOI: [10.22034/gjesm.2024.01.21](https://doi.org/10.22034/gjesm.2024.01.21)This is an open access article under the CC BY license (<http://creativecommons.org/licenses/by/4.0/>).

NUMBER OF REFERENCES

43



NUMBER OF FIGURES

3



NUMBER OF TABLES

4

\*Corresponding Author:

Email: [badrulaida1@gmail.com](mailto:badrulaida1@gmail.com)

Phone: +62 853 9744 0270

ORCID: [0009-0007-5276-8176](https://orcid.org/0009-0007-5276-8176)

Note: Discussion period for this manuscript open until April 1, 2024 on GJESM website at the "Show Article".

## INTRODUCTION

Indonesia has consistently ranked as one of the world's top three cocoa producers for the past twenty years, producing 656,817 tons in 2016 (FAO, 2017). More than half of cocoa are smallholders in Sulawesi, who account for about 60 to 71% of the national production. However, climate change poses significant challenges for cocoa cultivation, impacting the biophysical environment of the plant as well as the socioeconomic conditions of farmers (Feola et al., 2015; Schroth et al., 2016; Frimawaty et al., 2023). Luwu and North Luwu Regencies, which serve as major cocoa production centres and cover 61.4% of the national cocoa area, are particularly affected by climate change. It is characterized by changes in rainfall patterns leading to high humidity and increased attacks by pests and diseases during the rainy season. Conversely, prolonged dry seasons result in flower loss, wilting, plant mortality, and reduced cocoa production. On average, climate change has caused a decline in cocoa production from 800-1000 kilograms per hectare per year (kg/ha/y) to 600 kg/ha/y. For instance, cocoa production in North Luwu Regency was 30,854.56 tons in 2020, from a land area of 40,814.56 ha, but decreased to 28,573.37 tons in 2021 (Oyekale, 2018; Idawati et al., 2019). This means that water availability plays a critical role in the physiological processes of cocoa plants, either directly or indirectly. Therefore, adaptation efforts in minimizing vulnerability to exposure, sensitivity, and adaptive capacity are needed to overcome these impacts. Farmers' ability to adopt information and technology is a key factor in determining their adaptive capacity. It is closely linked to individual farmers' characteristics, such as their education, age, farming experience, number of dependents, income level, land area, perception of climate, risk assessment, and evaluation of information. The adaptive capacity of cocoa farmers is influenced by a) their characteristics in non-formal education which consists of training, Climate Field Schools, Integrated Pest Management Field Schools, and length of farming that influences decision making, b) Counseling support from the government, private and self-help groups in increasing the ability and mastery of climate-adaptive material for extension workers, and c) government support in climate information services and availability of farming capital for cocoa farmers to realize sustainable cocoa

farming. The challenge of sustainable livelihoods of rural farmers in the context of climate change is in accordance with the response to government policy on mitigation strategies (Asante et al., 2017). Non-formal education plays a significant role in fostering farmers' acceptance of extension activities in the two regencies. According to Suh and Molua (2022), non-formal education provides practical learning opportunities outside traditional classrooms or field schools. It employs adult learning methods that effectively address specific problems and align with the goals and targets of the learners. In addition, non-formal education also influences farmers' attitudes, actions, and mindsets, enabling them to make innovative decisions, increase productivity, improve the quality of their work, and expedite task completion. Private extension workers, who have firsthand experience and success in cocoa farming, play a crucial role in delivering non-formal education to doctors who are skilled farmers. They serve as direct examples and provide practical guidance to the surrounding farmers. These extension workers undergo training programs conducted by cocoa plantation agribusiness management partners, including governmental and corporate entities. These partners are assigned to assist and support farmers in their respective target areas. The presence of government, private, and non-governmental extension agents varies in terms of their duties and functions in the field. They collaborate to address implementation challenges related to climate change mitigation strategies (Ameyaw et al., 2018), comprehensive evaluation of integrated energy plantation models for cocoa production (Wessel and Quist-Wessel, 2015), and climate change adaptation and mitigation strategies for cocoa farmers. These strategies include ensuring sufficient water availability, managing pest attacks and diseases, and addressing the threats of floods and droughts. It is also essential to understand cocoa farmers' perceptions of climate change, the availability of capital, extension support, and the involvement of the private sector in enhancing adaptability to the impacts of climate change (Kosoe and Ahmed, 2022). These factors contribute to the sustainability of cocoa farmers' lives and their families (Peprah, 2015). Moreover, it is important to recognize non-climate stressors in semi-arid areas (Ahmed et al., 2016) and consider cocoa farmers'

perceptions of climate variability (Ehiakpor *et al.*, 2016). Given the background mentioned above, this study aims to analyze the relationship between cocoa farmers' characteristics and adaptive capacity in managing farming business in the face of climate change in 2022.

## MATERIALS AND METHODS

### Study area

This study was conducted from October to December 2022 in Luwu and North Luwu Regencies, South Sulawesi Province, Indonesia. The map of the study site locations is shown in Fig. 1.

### Data collection

The target population for this study consisted of cocoa farmers who met specific criteria, including being actively involved in managing cocoa plantations and authorized to make decisions. The sample size of 282 farmers was determined from a total of 960 eligible agribusiness actors using the Slovin equation. The distribution of the sample was conducted across several villages in different districts, including Batu Lappa and La'loa Villages in South Larompong District, Lamasi Pantai and Pompengan Villages in East Walenrang District, Marobo and Bakka Villages in Sabbang District, as well as Teteuri and Terpedo Jaya

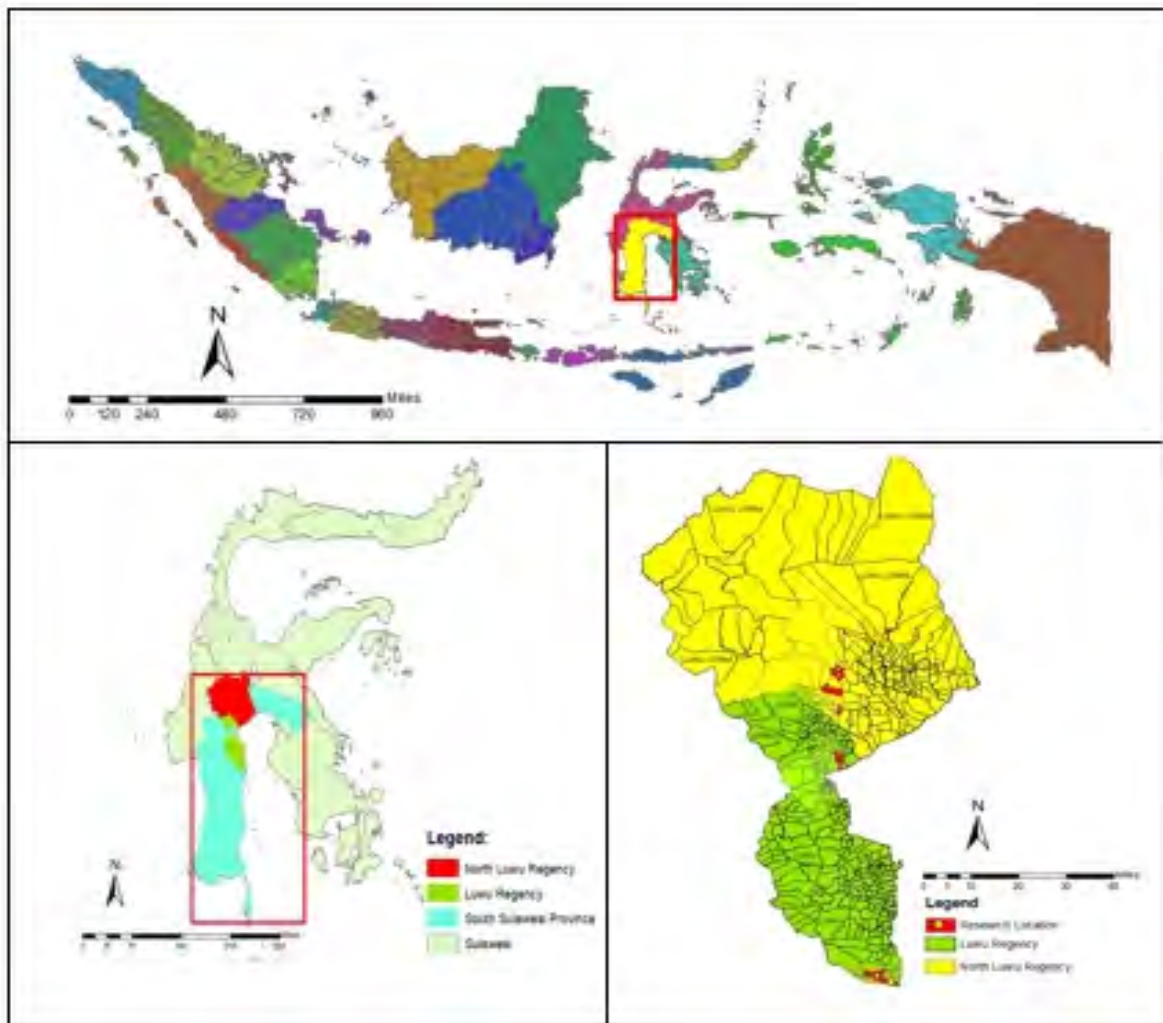


Fig. 1: Geographic location of the study area in Luwu and North Luwu Regencies, Indonesia

Table 1: The distribution of locations, population, and study samples

Regency	District	Village	Total population (person)	Farmers' group/sample (person)
Luwu	South Larompong	Batu Lappa	150	44
		La'loa	100	29
	East Walenrang	Lamasi Pantai	125	37
		Pompengan	60	18
		Marobo	110	32
North Luwu	Sabbang	Bakka	125	37
		Teteuri	170	50
	South Sabbang	Terpedo Jaya	120	35
Total			960	282

Villages in South Sabbang District. Data collection from respondents in each village was carried out using stratified sampling, targeting specific farmers' groups within each village. From the eight selected villages, one farmers' group was randomly selected, ensuring the inclusion of both members and administrators, using a simple random sampling method in accordance with the group's specific provisions, as shown in Table 1.

The questionnaire used was tested for validity using the Pearson Product Moment correlation with a calculated value of 0.603-0.966 ( $r$  is greater (>) than the table  $r$  value). Reliability testing was performed using the Cronbach Alpha method, which measured the correlation coefficient between 0 and 1. The questionnaire exhibited a reliability range of 0.743 across its items. These validation and reliability tests were conducted outside the study population using similar characteristics and conditions to the respondents. Specifically, the tests were performed among 30 farmers in the Siwata Farmer Group in Noling Village, Luwu Regency.

#### Statistical analysis

Structured interviews were conducted with 282 respondents using questionnaires. Additionally, in-depth interviews were carried out with five key informants, consisting of extension workers, coordinators of private partners (PT Mars Sustainability Indonesia), community leaders, and officials from the Department of Agriculture and other relevant institutions. The questionnaires used a Likert scale to measure respondents' opinions or feelings, with categories ranging from strongly disagree (1.00-1.99), undecided (2.00-2.99), agree

(3.00-3.99), to strongly agree (4). The collected interview data and results were tabulated and analyzed descriptively and qualitatively using frequency tables in the Excel program. This analysis aimed to provide an overview of the characteristics and adaptability of farmers. The Mann-Whitney test was employed for statistical analysis using the social science software (SPSS) version 24. This study also sought to explore the relationship between the characteristics of cocoa farmers and their adaptive capacity through inferential statistical analysis using Spearman's Rank correlation. Qualitative data were used to complement and describe the quantitative data findings.

## RESULTS AND DISCUSSION

### Rainfall conditions in Luwu and North Luwu Regencies

The rainfall patterns and the number of rainy days in Luwu Regency from 2020 to 2022 are illustrated in Fig. 2. The data showed that rainfall was significantly low or even absent from July to November. This indicates that the climatic conditions over the past four years have impacted the physiological processes of cocoa plants during those years and may continue to affect them in the future. Cocoa plants generally thrive when rainfall is evenly distributed in the year. Fluctuations in rainfall can have adverse effects on cocoa plants' physiological processes. During the dry season, cocoa plant growth is inhibited, and the fruit may fall prematurely at approximately two months of age. Conversely, excessive humidity during the rainy season can lead to fruit rot and increased susceptibility to pests, necessitating regular pruning. The distribution of cocoa cultivation

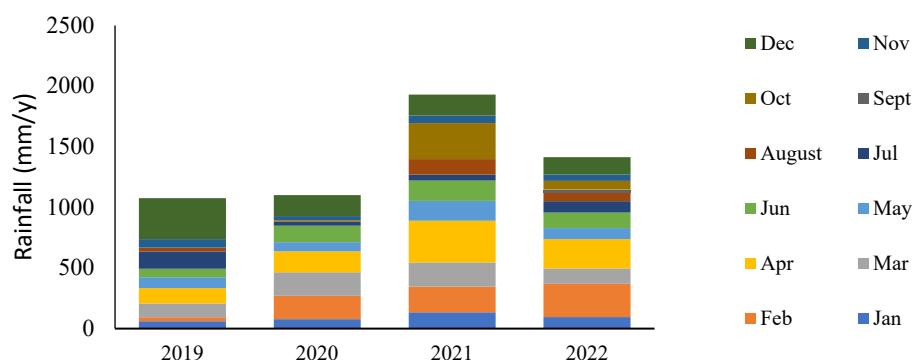


Fig. 2: Annual rainfall in the study sites Luwu and North Luwu Regencies

is typically observed between 7 degrees North Latitude (NL) and 18 degrees South Latitude (SL), corresponding to the rainfall and sunshine patterns throughout the year. However, cocoa can still be grown in regions of 20 NL to 20 SL, making Indonesia, located between 5 NL and 10 SL, suitable for cocoa cultivation. The ideal altitude for cocoa cultivation in Indonesia is below 800 meters above sea level (asl).

According to [Riyanto et al. \(2022\)](#), the upper slopes at an elevation of 900 meters above sea level (asl) have a significantly higher potential phosphate (P) content compared to the lower slopes. This indicates variations in nutrient availability in the soil, highlighting the importance of using fertilizers containing P elements, specifically on lower slopes. For optimal cocoa growth, the ideal rainfall distribution is consistent in the year, with an average annual rainfall ranging from 1,100 to 3,000 mm. Rainfall exceeding 4,500 mm/year is unfavorable as it is closely associated with the occurrence of fruit rot disease. In areas with rainfall below 1,200 mm/year, cocoa cultivation is still feasible but will require irrigation. This is because the amount of water lost through transpiration by the plants would exceed the water received from rainfall alone.

#### Characteristics of farmers

The analysis of farmers' characteristics in the two regencies revealed several similarities and differences. The characteristics that showed relatively similar values between the regencies were

age, non-formal education, number of dependents, and farmers' perceptions of the climate. On the other hand, the characteristics that differed between the regencies were formal education, agribusiness experience, land area, cosmopolitanism, and information exposure, as shown in [Table 2](#). In terms of age, the majority of farmers in both regencies fell within the mature category, ranging from 36 to 48 years old, with an average age of 44.63. This age group is considered productive and allows farmers to focus on the development of their cocoa farming business. This finding is consistent with the study by [Anning et al., 2022](#) that those between 44-64 years are of productive age because the farmers are still young, with the potential and physical ability to ensure adequate management. Farmers still showed enthusiasm and motivation to care for their farming business, accept innovation, and change lives by earning a better income. [Arifah et al. \(2022\)](#) stated that the productive age of cocoa farmers significantly influenced their farming abilities. Those in this age group can implement good cultivation practices and make decisions, including adopting new knowledge and technologies for cocoa cultivation. Farmers at this age can quickly make decisions through the support of ideas and information while still actively participating in agricultural extension activities. The number of family dependents also plays a crucial role in determining the effectiveness of extension agents in influencing farmers' behavior. The number of family dependents can have positive and negative implications for farmers. A small number of dependents or having non-productive family

Table 2: Frequency distribution of cocoa farmers according to individual characteristics in Luwu and North Luwu Regencies

Individual characteristic	Category	Regency		Mann Whitney difference test
		Luwu (%)	North Luwu (%)	
Average age = 44.63	Young (24-26.25 years)	18.75	21.43	0.242
	Adults (36.26-48.50 years)	50.78	55.84	
	Old (48.51-60.75 years)	26.56	20.13	
	Very Old (60.76-73 years)	3.91	2.60	
Average formal education = 8.77	Very Low (Elementary School)	34.38	29.87	0.011**
	Junior High School	41.41	27.92	
	Senior High School	24.22	42.21	
	Higher Education (University)	0.00	0.00	
Average non-formal education = 3.72	Very Low (1-2.5)	10.94	27.92	0.208
	Low (2.51-4)	61.72	16.23	
	High (4.1-5.5)	27.34	44.16	
	Very High (5.51-7)	0.00	11.69	
Average agribusiness experience = 17.87	Very Low (3-9.75 Tahun)	5.47	9.74	0.038*
	Low (9.76-16.50 Tahun)	33.59	39.61	
	High (16.51-23.25 Tahun)	35.94	29.87	
	Very High (23.26-30 Tahun)	25.00	20.78	
Average land area = 1.25	Narrow (0.5-1 ha)	73.44	28.57	0.000**
	Medium (1.1-2 ha)	25.00	70.78	
	Large (3.1-4 ha)	0.78	0.00	
	Vast (4.1-5 ha)	0.78	0.65	
The average number of dependents = 4.96	Very Low (3-4 people)	58.00	46.10	0.742
	Low (4.1-5 people)	17.00	17.53	
	High (5.1-6 people)	44.00	28.57	
	Very High (6.1-7 people)	9.00	7.79	
Average cosmopolitanism = 3.84	Very Low (2-3)	23.44	22.73	0.001**
	Low (3.1-4)	46.88	20.13	
	High (4.1-5)	27.34	54.55	
	Very High (5.1-6)	2.34	2.60	
Average information exposure = 5.71	Very Low (3-4.75)	21.09	29.22	0.000**
	Low (4.76-6.50)	56.25	31.82	
	High (6.51-8.25)	15.63	35.06	
	Very High (8.26-10)	7.03	3.90	
Average Farmer's Perception of Climate = 20.83	Very Low (10-14.25)	17.97	7.79	0.495
	Low (14.26-18.52)	0.00	0.00	
	High (18.52-22.76)	54.69	64.29	
	Very High (22.77-27)	27.34	27.92	

\*significantly different at the level of 0.05 \*\* significantly different at the level of 0.01

members can contribute to household poverty. However, the presence of family dependents, particularly those in the productive age range, can motivate farmers to expand their businesses and increase their income. In cocoa farming, having family members who can contribute to labour can be beneficial. [Coopmans et al., \(2021\)](#) stated that family dependents in the productive age range could provide additional labour for cocoa farming activities. This can help farmers manage their farms more effectively and increase productivity. The number of dependents can also serve as a source of motivation for them to work harder and achieve

greater success. Farmers may be driven to increase their efforts and income generation to support the needs and welfare of their family members. Additionally, their perceptions in the two regencies regarding climate change were relatively similar, indicating a shared understanding of the challenges they face and the need for adaptation, as shown in [Table 1](#). According to [\(May et al., 2019\)](#), some of the internal characteristics, such as education, age, and area of arable land, influence farmers' decision-making process to implement adaptive choices related to climate change. They acknowledged the impact of climate change on cocoa plants and

Table 3: Distribution of cocoa farmers based on their adaptive capacity in the two study locations in Luwu and North Luwu Regencies

Farmers' adaptive capacity	Category	Regency		Mann Whitney difference test
		Luwu (%)	North Luwu (%)	
Average technical ability = 17.20	Very Low (8-13)	14.84	30.52	0.002**
	Low (13.1-18)	43.75	23.38	
	High (18.1-23)	25.78	46.10	
	Very High (23.1-28)	15.63	0.00	
Average managerial Ability = 12.40	Very Low (5-8.25)	7.81	5.19	0.000**
	Low (8.26-11.50)	55.47	21.43	
	High (11.51-14.75)	21.88	55.84	
	Very High (14.76-18)	14.84	17.53	
Average socio-cultural ability = 18.73	Very Low (10-13.5)	12.50	2.60	0.000**
	Low (13.51-17)	21.09	8.44	
	High (17.1-20.5)	49.22	54.55	
	Very High (20.51-24)	17.19	34.42	

\*significantly different at the level of 0.05 \*\* significantly different at the level of 0.01

recognized the importance of implementing Good Agriculture Practices (GAP) and other techniques such as pruning, pest control, fertilizing, and sanitation (P3SP) to ensure optimal farming care. This is in accordance with the findings of (Asante *et al.*, 2022) regarding the influence of rainfall and temperature changes on cocoa cultivation. The analysis in Table 2 showed significant differences between the two regencies regarding formal education, agribusiness experience, land area, cosmopolitanism, and exposure to information, with higher values observed in North Luwu Regency. This showed that cocoa farmers in North Luwu Regency had better access to information and were more engaged in managing their businesses, potentially due to policy support and attention from the local government. The involvement of the private sector, as exemplified by the Sustainable Farming in Tropical Asian Landscape (SFITAL) Program and collaborations between various stakeholders, including the private sector, government, universities, and farmers, contributed to the optimization of cocoa farming practices in North Luwu Regency. These collaborative efforts aimed to establish a sustainable cocoa roadmap and achieve common goals in cocoa production (Tothmihaly *et al.*, 2019). The presence of the private sector served as a motivating factor and played a role in influencing farmers' behavior and success in managing their agribusinesses, particularly in North Luwu Regency.

#### *Farmers' Adaptive Capacity in Overcoming the Climate Change Impacts*

The analysis results of cocoa farmers' adaptive capacity in the two regencies in Table 3 showed that their technical, managerial, and socio-cultural adaptive capacities differed. The percentage of farmers with technical and managerial skills was low in Luwu but high in North Luwu. On the other hand, both regencies showed high levels of socio-cultural adaptive capacity.

#### *Technical ability*

The statistical test results indicate significant differences in the technical adaptation abilities between the two regencies, as well as variations in farmers' distribution. The technical ability scores for both Luwu and North Luwu Regencies were 17.20 (Table 3) and in the low category. In general, the unique tropical climate of both regencies, characterized by distinct rainy and dry seasons, directly influences cocoa farming practices from a technical standpoint. When the technical abilities of farmers in the two regencies were compared, Luwu exhibited lower scores than North Luwu. The key technical skills assessed were regular monitoring of soil pH, utilization of organic fertilizers, biannual soil liming, manual weed removal (without herbicides), appropriate disposal of cocoa shells, and sanitation practices. Others include a) cocoa GAP techniques, b) water-saving technology, management and use,

c) implementation of Climate Field Schools and Integrated Pest Management Field Schools, d) demonstration plots/gardens, e) plant rejuvenation by carrying out crop diversification (agroforestry concept), and f) application of a climate adaptation cacao cultivation calendar. The findings of this research are in accordance with the study conducted by (Daniele *et al.*, 2022), which stated the varying degrees of adaptation abilities among Danish farmers. Some of them expressed indifference toward the impact of climate change and encountered obstacles to adaptation, while others recognized ongoing efforts as proactive actions to capitalize on potential opportunities arising from climate change impacts. The technical ability assessed in this study focused on implementing GAP for cultivating cocoa plants, with specific emphasis on adaptive strategies to address climate change, including the P3SP approach. However, the findings revealed that the technical capacity of farmers was still very low due to their failure to apply the climate-adaptive GAP technique during the initial stages of cocoa tree planting. The adaptive technical ability of farmers is demonstrated when they effectively carry out maintenance activities in accordance with GAP techniques, particularly those that are climate-adaptive. These climate-adaptive practices are in accordance with the cocoa cultivation calendar, which serves as a guideline for growing cocoa plants and allows farmers to adapt their practices to local weather conditions. The technical ability of farmers in North Luwu Regency excelled in areas such as plant pest organism (PPO) control and weed management, according to the specific timing outlined in the cocoa cultivation calendar. They also showed adaptive behavior by following the cocoa cultivation calendar, which aimed at increasing cocoa productivity and supported by external assistance provided by partners. This is in accordance with the findings of Dessart *et al.* (2019), stating that the adaptive capacity of farmers was influenced by internal factors such as land area, family size, and understanding of climate change. These factors enable farmers to manage their cultivation activities following prevailing weather conditions effectively. Additionally, external support from decision-making bodies and relevant stakeholders plays a crucial role in enhancing farmers' access to market information, loans, services, counselling,

and involvement in study, thereby offering solutions to agricultural challenges associated with climate change adaptation. Buitenhuis *et al.* (2020) recommended increasing the involvement of group leaders, providing training opportunities, and strengthening cooperation among stakeholders to overcome disharmonious relations between relevant stakeholders, government and private institutions. Furthermore, the presence of assistants or facilitators who can foster better relationships between cocoa farmers and stakeholders is essential. Taking these measures makes it possible to overcome deadlocks and minimize communication barriers, ultimately achieving better communication convergence among all stakeholders involved in the cocoa farming sector.

#### *Managerial ability*

The average managerial ability in the two regencies was significantly different, with an average score of 12.40 in the high category. Managerial ability encompasses various indicators, including financial record-keeping, allocation of capital for the next season, fertilizer usage calculation, cocoa seedling requirements during rejuvenation, and efficient use of labour. In Luwu Regency, these indicators were found to be in a low category, indicating a lower level of managerial ability than in North Luwu Regency, as shown in Table 3. Farmers in Luwu Regency focused on setting aside farming capital for the following season and maintaining financial records. However, they faced challenges in allocating sufficient funds for their farming business due to the difficulties in generating income, which led to a decline in production. The income earned primarily met basic family needs, leaving little capital available for farming. Consequently, farmers estimated their capital requirements based on financial resources without a comprehensive and detailed farming business plan. To address these challenges, it is crucial to enhance farmers' understanding of the circular economy concept, which emphasizes optimizing the utilization of resources and promoting sustainable farming practices. This includes improving the farmers' managerial cycle processes, such as effectively managing inputs and reusing resources as farming capital, updating farming business plans, and understanding the production process and the recycling of raw materials needed

for cocoa products. The circular economy is a closed economic, managerial cycle system that aims to maintain the value of products, by-products, and materials within the supply chain process (Sasongko & Pertiwi, 2021). This system can be integrated as a component within different areas, with varying impacts at the local and wider levels. The value chain of circular economic products and services presents opportunities for various areas with unique characteristics and effects. Coopmans *et al.* (2021) identified four internal factors that influenced the adaptability of farmers. The first factor is the personal characteristics of the farmers, including their ability to recognize talents and skills, self-motivation, problem-solving capabilities, adherence to norms, values, customs, culture, ideas, and emotional control. These factors play a significant role in agricultural management decision-making and are closely related to farmers' motivation, such as their desire for self-actualization versus economic considerations, as well as the survival of farmers and their families. The second factor is the initial involvement in farming and family habits that affect complex social life, including gender. The third factor is career paths, where higher formal education and work experience in non-agricultural sectors may deter the younger generation from pursuing careers in agriculture, resulting in a lack of interest and ability among the youth in the agricultural sector. The fourth factor is the individual's perception of agriculture. Farmers' perceptions influence their ability to manage time between work and family life, which in turn affects socio-cultural aspects (e.g., primogeniture, gender roles) and sociological factors (e.g., modernization, individualization) in their managerial adaptation within cocoa farming (Sianipar, 2022).

#### *Socio-cultural ability*

Socio-cultural ability exhibited significant differences between the two regencies, with an average score of 18.73, indicating a high ability level. This disparity was evident in farmers' participation in activities organized by partner companies, who not only provided counselling on cocoa farming but also purchased the products, as shown in Table 3. The local culture of farmers further contributed to this discrepancy, as indigenous people tended

to settle down, retire early, and transfer their land to migrants from Bugis, Makassar, Enrekang, Java, and Toraja. The advanced age of the farmers also influenced their physical fitness and work ethic, exacerbating the lack of regeneration in the agricultural business. According to Meuwissen *et al.* (2019), supporting factors of agricultural production are closely related to the family in the context of social dynamics. The first factor is human capital, one of the agricultural succession supports. Successful farmers possess the necessary skills to navigate personal, household, and entrepreneurial challenges. Therefore, learning capacity is needed to face various dangerous challenges in the development and sustainability of agriculture. The second is interpersonal dynamics which are defined as participation and reciprocal interaction between fellow farmers and the involvement of supporting factors as socio-economic networks in the agricultural sector. Prain *et al.* (2020) further investigated the influence of roles and interpersonal dynamics on technology transfer in the livestock sector, and examined how these factors impacted farmers and the local community. The ability to communicate and collaborate effectively relies heavily on the local cultural context of the two regencies, as well as the government's involvement in decision-making processes that engage all relevant stakeholders. The third factor is the characteristics of agriculture which refer to the production inputs involved in capital, land, labour and management as factors of production owned by farmers. Balanced activity between production factors and demographics of agricultural areas, including infrastructure in agricultural organizational institutions, is a determinant of the sustainability of agricultural businesses. This balance also serves as an attractive incentive for the regeneration of millennial farmers, as it aligns with their inclination towards technology adoption and problem-solving approaches, contributing to achieving sustainable development goals (SDGs). The fourth factor is the farmer-family dynamics which include all processes related to agricultural life as a whole with the family. Given that agricultural businesses often involve families, it is inevitable that there will be overlapping aspects between work and residence, as well as matters related to finance and resources.

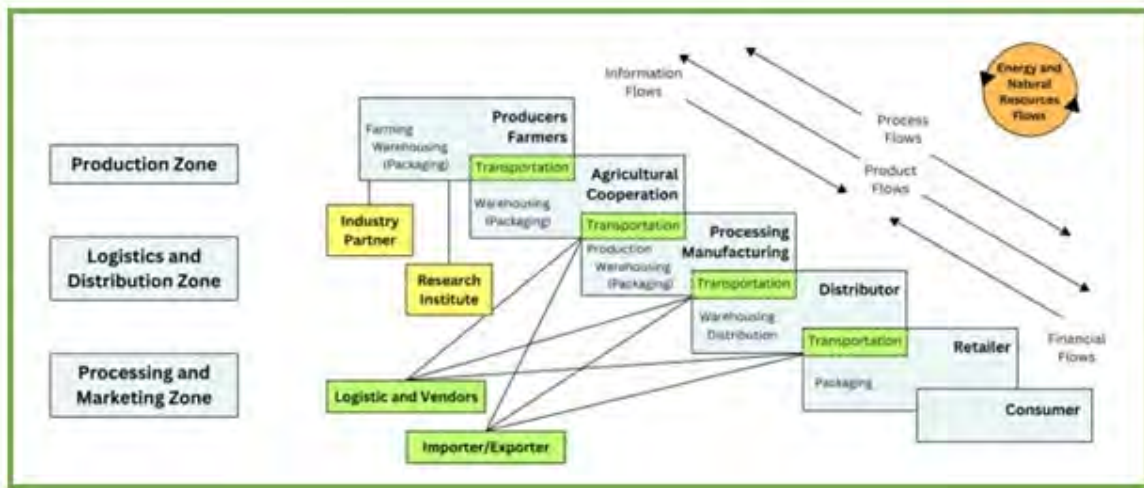


Fig. 3: Supply chain of cocoa Agribusiness in North Luwu Regency

*Relationship between farmers' characteristics and adaptive capacity*

The correlation coefficient analysis shown in Table 4 provides insights into the relationship between the adaptability of farmers and their characteristics. The characteristics of farmers, specifically the length of agribusiness experience and land area, are related to managerial ability. Land area is positively associated with the technical skills and farmers perceptions of climate change, as well as socio-cultural abilities. Meanwhile, other characteristic variables such as age, education, number of family members, cosmopolitanism, and level of information exposure do not show any significant relationship with the technical, managerial, or socio-cultural adaptability.

According to Shereen et al. (2020), the entrepreneurial context in agriculture is shaped by three factors related to agricultural resources and the current circular economy developments. Firstly, the competitive external environment challenges agricultural regeneration, as individuals are enticed by non-agricultural job opportunities that offer higher financial rewards, improved lifestyles, and increased leisure time. Factors such as wage differentials, economic status, and the desire for vacations contribute to this competition. Furthermore, Dhir et al. (2021) highlighted the significance of non-agricultural labour market options, access to credit facilities, availability of agricultural inputs, land conditions, prices, and the

ability to process raw materials into final products. These factors influence farmers' aspirations to become managers of their agricultural businesses. Secondly, limited knowledge and skills in product processing pose obstacles to the formation of entrepreneurial farmers. Insufficient expertise in processing agricultural products may hinder the development of value-added products and limit opportunities for entrepreneurship among farmers. Thirdly, policy support is crucial to safeguard the potential of human resources as a skilled workforce and reduce dependence on government assistance. It is important to provide accessible behavior change training programs for farmers, fostering an entrepreneurial mindset in agriculture and minimizing off-farm migration. The changes in the biophysical environment of cocoa plants indirectly affect the socio-economic environment of farmers, who are the main stakeholders in cocoa production. These impacts also influence the cocoa trading system in the two regencies. The cocoa trading system begins with farmers and farmers' groups (such as Koptan Masagena) who produce and ferment cocoa beans. These farmers and cooperatives then sell the dry beans to buyers, including the Chalodo Chocolate cocoa bean processing factory, Olam Food Ingredients (OFI) company, and Mars Sustainability company. The companies further process the beans into cocoa flour or final products ready for consumers. Based on Fig. 3 and in accordance with

Table 4: Correlation coefficient between farmers' characteristics and adaptive capacity

Farmers' characteristic	Farmers' adaptive capacity		
	Technical ability	Managerial ability	Socio-cultural ability
1. Age	-0.049	-0.110	-0.072
2. Formal education	-0.026	0.036	0.015
3. Non-formal education	0.012	-0.069	0.040
4. Agribusiness experience	0.057	-0.137*	-0.072
5. Land area	-0.127*	0.133**	0.040
6. Number of family members	-0.031	0.029	-0.059
7. Cosmopolitanism	-0.061	-0.072	0.039
8. Information level of exposure	-0.042	-0.112	0.025
9. Farmers perception of climate change	-0.053	-0.039	0.136*

\* Has a significant correlation at the level of 0.05

\*\* Has a significant correlation at the level of 0.019

the study by [Dhir et al. \(2021\)](#), the cocoa agribusiness supply chain system should be supported by a policy framework that covers both upstream and downstream processes. The supply chain system can be divided into 3 zones, including 1) Production zone encompasses agricultural production, including cultivation, product processing, warehousing, and packaging. The key actors involved in this zone are farmers, partners/companies/vendors providing facilities and infrastructure, industrial processing companies, and research institutions. 2) Logistics and distribution zones bridge the production zone, facilities and infrastructure providers, processing industries, and consumers. Logistics companies play a crucial role in effectively planning, implementing, and supervising the transportation process of goods or services, energy, and other resources from the point of origin to the point of use. They work closely with suppliers or logistics vendor companies. 3) Processing and marketing zone encompasses production, warehousing, and packaging activities. The main actors in this zone are processing companies, suppliers of raw materials and supporting materials, logistics companies and vendors, as well as importers/exporters.

Farmers in North Luwu Regency showed superior managerial abilities in handling their farming business finances and keeping detailed records of income and expenditures compared to those in Luwu Regency. This finding is supported by studies highlighting the significance of managerial skills for cocoa farmers in understanding and adapting to changes in the farming environment ([Sianipar, 2022](#); [Asante et al., 2022](#)). Farmers need to possess inherent capacities and a strategic management

mindset, similar to business managers, enabling them to predict and address challenges arising from the farming environment. This was in accordance with the study by ([Mbow et al., 2014](#); [Prain et al., 2020](#)), which emphasized the role of Non-Governmental Organizations (NGOs) in developing the managerial capabilities of farmers through personality and farming management training, participatory decision-making, empowerment, and community capacity building. These efforts aim to strengthen the relationship between farmers and markets while fostering rural development. [Buitenhuis et al. \(2020\)](#) stated that the prevalence of high socio-cultural abilities within a society or specific segments instilled hope for improved capabilities and trust in innovation. In both regencies, the socio-cultural abilities remained high, thereby facilitating the development of enhanced adaptive capacities among farmers through collaborative efforts within institutions. Farmers also exhibit substantial social capital, which promotes the coordination and development of institutions. Some important factors in enhancing the capacity of rice farmers include their active involvement, partnerships, the adoption of innovative practices and technology transfer, social capital, and access to business capital ([Idawati et al., 2018](#)). The age range observed in this study shows that cocoa agribusiness activities can be optimally carried out with the available physical labour, and farmers still possess significant enthusiasm for agricultural activities. ([Giovanopoulou et al., 2011](#)) showed a statistically significant positive correlation between age and adopting good agricultural practices, highlighting the greater effectiveness of young and productive

farmers in implementing such practices. Despite cocoa experts in the area, motivating farming communities to replant cocoa trees has proven challenging. Therefore, efforts should be made to enhance the capacity of individual farmers through knowledge acquisition, attitudinal development, critical awareness, and skill building (Jallow et al., 2017). The perceptions of farmers show limited information regarding the impacts of climate change and the support provided by government policies for the sustainability of cocoa agribusiness (Hirons et al., 2018). Non-formal education plays a crucial role in influencing the ability of farmers to develop their agribusiness and stay abreast of advancements in agricultural technology influenced by local practices. It has been proven that educational factors, specifically non-formal education, heavily influence adoption of new technologies and the dissemination of extension information.

#### *Adaptive capacity of farmers in overcoming climate change impacts*

##### *Technical ability*

Technical adaptation is essential for successful cocoa cultivation, particularly when facing challenges such as climate change. To overcome the impact of the rainy season, farmers must focus on frequent harvesting, regular pruning, the use of shade trees, and following the cacao growing season calendar. During the rainy season, farmers must diligently prune cocoa plants and shade trees to reduce moisture. Similarly, they should ensure a water source for their cocoa fields during the dry season to prevent issues such as flower dropping, wilting, and plant death. Some farmers lack discipline in implementing these practices, but those who devote their time and effort to cocoa agribusiness and diligently care for their farms enjoy a prosperous period with high income. Technical skills are acquired through intentional, systematic, and continuous effort, enabling farmers to perform well in managing cocoa cultivation. As a significant environmental factor, climate greatly influences various stages of cocoa cultivation, such as land preparation, seed selection, flushing, flowering, fertilizing, pruning, harvesting, and post-harvesting. Cocoa plants thrive in conditions with a moderately distributed and consistent combination of temperature, humidity and rainfall throughout the year. Therefore, it is crucial to employ cocoa

cultivation techniques that are adaptive to climate change. The strategic positioning of cocoa plantations in open areas allows maximum sunlight penetration, facilitating renewable energy generation through optimal photovoltaic panels (Naderipour et al., 2020). This renewable energy can be used to improve the irrigation system of cocoa plants efficiently. Water pumps powered by photovoltaic energy, equipped with a meta-heuristic Intelligent Water Drops Algorithm (IWDA), can effectively supply water in remote areas (Naderipour et al., 2021). Widespread implementation of this innovation has the potential to increase cocoa plantation productivity. The decreasing cocoa yield in Luwu Regency is attributed to the shrinking cocoa plantation area caused by farmers rejuvenating cocoa plants or converting land for seasonal or other plantation crops. The conversion of cocoa fields into rainfed rice fields through government programs is prevalent due to decreased cocoa productivity primarily caused by increased pest attacks, which are associated with the low adaptive level of farmers in plant care. Adaptive level refers to the technical ability of farmers to adjust their farming practices based on the cacao cultivation calendar when faced with climate change. For instance, during the rainy season, characterized by high rainfall, adaptive farmers prune cocoa plants and shade trees to prevent moisture accumulation, which can lead to pest and disease development (Karpouzoglou et al., 2016).

##### *Managerial ability*

Farmers in North Luwu Regency exhibit superior managerial skills compared to their counterparts in Luwu Regency. They show competence in financial management and allocate sufficient working capital for their agribusiness operations. To enhance the managerial capabilities of farmers, assistance from NGOs is essential. This support can be provided through personality development and agribusiness management training, emancipatory participation, empowerment, and community capacity building. These initiatives aim to strengthen the relationship between farmers and markets and promote rural development (Kosoe & Ahmed, 2022). It has been observed that the income of farmers from cocoa farming positively impacts their managerial abilities, as higher income generates better business planning outcomes, particularly in terms of input support and

resulting production output. This finding aligned with the study conducted by [Ayanlade et al. \(2018\)](#), which highlighted the significant influence of capital and production facilities on the planning of fish farming businesses. Access to capital also influences business development, as greater capital resources contribute to improved managerial decision-making in using funds for business management. To enhance financial management efficiency and reliability among farmers, it is advisable for farmers' organizations, in collaboration with partners, to introduce modules that assist farmers in managing their finances effectively. Local companion organizations can collaborate with banks or institutions experienced in financial management at the district or village level to facilitate this process. According to [Meuwissen et al. \(2019\)](#), adaptive cycle processes, encompassing agricultural practices, regional demography, risk management, and governance, are integral components of a managerial system that shapes the adaptive frameworks of farmers within agricultural resilience systems.

#### *Socio-cultural ability*

Socio-cultural abilities facilitate collaboration and connection among individuals, groups, communities, organizations, and society. Farmers possess the ability to collaborate in developing their farming businesses and search for information from various sources such as the government, partnerships, and the general public. In a constantly changing society, it is important to recognize that society should not be viewed as a fixed state but as an ongoing process or a continuous flow of events without interruption. Society, including groups, communities, organizations, nations, and countries, is contingent upon actions, changes, and perpetual processes within it ([Tschora and Cherubini, 2020](#)). The socio-cultural capabilities of cocoa farmers, specifically their ingrained habits and persistent behaviors, significantly influence the development of farming practices ([Schroth et al., 2016](#)). Farmers continuously strive to enhance their farming businesses through intensified efforts. A notable indicator of this intensification is the deliberate selection of plant species with high economic value based on agroecological conditions and land suitability ([Karpouzoglou et al., 2016](#)). Cocoon farmers maintain high expectations in both Luwu

and North Luwu Regencies, and their socio-cultural abilities fall within the high category. These regions exhibit social capital capabilities characterized by trust in extension workers, which enables active participation in development meetings. Adaptation, effective farming management, and institutional structures play significant roles, guided by socio-cultural values and community outreach abilities ([Lobley & Potter, 2004](#)). According to [Meuwissen et al. \(2019\)](#), ensuring the economic, social, and ecological sustainability of agricultural systems in Europe necessitates proactive engagement from agricultural actors, supply chain stakeholders in the circular economy, farmers' institutions and organizations, and the availability of relevant products and services. These efforts aim to address agricultural and environmental challenges within a regional context while upholding the resilience of agricultural systems. This entails harnessing the functions and systems that facilitate economic problem-solving, climate-related concerns, and environmental factors. Moreover, the evolving landscape of farmers' institutions calls for increased adaptability and the adoption of transformative technologies.

#### *Relationship between farmers' characteristics and adaptive capacity*

The cocoa agribusiness industry requires advanced technical skills due to its complex nature. Small land holdings and intricate challenges make it crucial for farmers to possess the expertise to maximize their income. The heightened awareness regarding climate change impacts public willingness to interact and collaborate with farmers' groups and the broader community. The ability of a group or community to withstand and overcome challenges in the farming environment, known as individual resilience, is influenced by cultural characteristics. This resilience empowers farmers to prioritize information exchange within their community, enabling them to develop their knowledge and skills. It also involves using regional local wisdom for technology transfer, fostering institutional development and partnerships, as well as leveraging the social capital and role of society ([Idawati et al., 2018](#); [Adger, 2000](#); [Idawati et al., 2019](#)). Developing human resources through technical knowledge alone is insufficient to address the problems of farmers.

It requires the involvement of stakeholders from multiple sectors in a sustainable manner. Problem-solving involves identifying the sources of problems, offering technical solutions, and integrating farm management skills, planning, control, evaluation, and socio-cultural approaches. This step aims to modify the behavior of rural communities, which hold deep attachments to their local customs and culture. It is an adaptive action that considers the cultural, social, and economic conditions of the target innovation area. Agriculture is a way of life, profession, and lifestyle for farmers within local communities and the broader agricultural context. The public perception regarding the future of farmers due to negative information portrayed by the media, emphasizing their dependence on nature and climate, need to change. Additionally, the increasing emphasis on big data in the global landscape has shifted the expectations of people and reduced the attractiveness of agricultural professions. This perception is exacerbated by the minimal profits receive from operations compared to large processing factories that source their raw materials. The lifestyle connotations associated with rural farming, such as lack of leisure time and unbalanced work hours, further discourage individuals from pursuing careers in agriculture. The attractiveness of agriculture in rural areas is crucial for the next generation of farmers. It heavily relies on the appeal of agricultural locations and their natural resources, which are determined by the accessibility and quality of essential infrastructure and services, including education. Enhancing the promotion of rural villages and creating a sense of comfort and peace in natural surroundings are essential for both residents and visitors to rural areas.

## **CONCLUSION**

In conclusion, the characteristics of farmers in the two regencies showed similarities in age, non-formal education, number of dependents, and their perception of climate. Differences were observed in terms of formal education, years of experience in agribusiness, land area, cosmopolitanism, and level of information exposure. Farmers with larger land holdings required higher levels of managerial adaptability, but their technical abilities tended to be lower. The length of agribusiness experience did not necessarily lead to improved managerial

adaptability. Conversely, farmers with stronger socio-cultural abilities had a more positive perception of the impact of climate change. The adaptive capacity of cocoa farmers is directly influenced by internal factors, including non-formal education and years of farming experience, affecting their technical, managerial, and socio-cultural abilities. The technical adaptive ability of farmers involves practices such as regular measurement of soil pH, use of organic fertilizers, biannual soil liming, manual weed clearance (without herbicides), and proper disposal of cocoa shells. Farmers should adopt a) cocoa Good Agricultural Practices (GAP), b) water-saving technologies, c) participate in Climate Field Schools and Integrated Pest Management Field Schools, d) establish demonstration plots/gardens, e) implement crop diversification through agroforestry, and f) develop a climate adaptation cacao cultivation calendar. The adaptive managerial ability of farmers, particularly in determining the quantity and pricing of inputs, as well as keeping records of production costs, was found to be very low. Planning, farming knowledge, and cost recording were lacking among most farmers, leading to increasing production costs and insufficient income to meet their family and business capital needs. Farmers mostly relied on estimations and information from fellow farmers who employed similar practices. The strength of social capital within the farming community played a crucial role in fostering trust among farmers, extension workers, and stakeholders. It also promoted tolerance among residents and the adherence to customary rules for adaptive environmental management, thereby supporting sustainable cocoa farming. Sustainable cocoa farming entails increased income and independence for farmers and their groups, environmental sustainability, and farmers' regeneration. This can be achieved through a) increased income and independence of farmers, environmental sustainability and regeneration through efforts to ensure the implementation of the counselling, b) the institutional activity of cocoa farmers' groups as a vehicle for learning and c) government support in terms of infrastructure and facilities. Collaboration with the Meteorology, Climatology, and Geophysics Agency (BMKG) and extension agents can be beneficial, along with providing adequate water sources, drainage systems

and enhancing the skills of extension agents to cater to the specific needs of the superior commodities of the target areas. It is important to provide guidance, monitoring, and ongoing evaluation, beyond mere subsidies to enable farmers to focus professionally on their commodities. Implementing counselling based on needs, fostering active organizations in rural areas, and fulfilling cocoa infrastructure are key strategies to achieve these objectives.

#### **AUTHOR CONTRIBUTIONS**

Idawati conducted a thorough literature review, designed the study, supervised the experimental work, and drafted the manuscript. N.A. Sasongko played a key role in conceptualizing the study, designing the study, interpreting the data, supervising all experiments, and contributing to manuscript preparation. A.D. Santoso contributed to the literature review, supported data collection, validated data, conducted statistical analysis, and edited the manuscript. M. Septiani supported data collection, validation, and graphing maps and figures. T. Handayani contributed to data collection, validation, analysis, interpretation, manuscript preparation, and graphing maps and figures. A.Y.N. Sakti conducted the literature review, supported experimental and administrative work, and offered technical and material assistance. B.D. Purnamasari performed the literature review, supported experimental and administrative work and provided technical and material assistance. A. Albahry performed the literature review, supported experimental and administrative work and provided technical and material assistance.

#### **ACKNOWLEDGEMENT**

The authors are grateful to the National Research and Innovation Agency for providing this Post Doctoral Program.

#### **CONFLICT OF INTEREST**

The author declares no conflict of interest regarding the publication of this manuscript. In addition, the ethical issues, including plagiarism, informed consent, misconduct, data fabrication/falsification, double publication/submission, and redundancy, have been completely observed by the authors.

#### **OPEN ACCESS**

©2024 The author(s). This article is licensed under a Creative Commons Attribution 4.0 International License, which permits use, sharing, adaptation, distribution and reproduction in any medium or format, as long as you give appropriate credit to the original author(s) and the source, provide a link to the Creative Commons license, and indicate if changes were made. The images or other third-party material in this article are included in the article's Creative Commons license unless indicated otherwise in a credit line to the material. If material is not included in the article's Creative Commons license and your intended use is not permitted by statutory regulation or exceeds the permitted use, you will need to obtain permission directly from the copyright holder. To view a copy of this license, visit: <http://creativecommons.org/licenses/by/4.0/>

#### **PUBLISHER'S NOTE**

GJESM Publisher remains neutral with regard to jurisdictional claims in published maps and institutional affiliations.

#### **ABBREVIATIONS**

%	Percent
AGS	Aerobic granular sludge
BMKG	Badan meteorology klimatologi, dan geofisika (meteorological, climatological, and geophysical agency of Indonesia)
FAO	Food and agricultural organization
GAP	Good agriculture practices
IWDA	Intelligent water drops algorithm
kg/ha/y	Kilogram per hectare per year
m	Meter
mm	Mili meter
NL	North latitude
NGOs	Non-governmental organization
OFI	Olam Food Ingredients
P	Phosphate

P3SP	Harvesting, pruning, plant-disturbing organism control, fertilizing, and sanitation
PPO	Plant pest organisme
SDGs	Sustainable development goals
SFITAL	Sustainable farming in tropical Asian landscape
SL	South latitude
SLI	Climate fiels schools
SLPHT	Integrated pest management field schools
SPSS	Statistical analysis in social science
y	Year

## REFERENCES

- Adger, W.N., (2000). Social and ecological resilience: Are they related? *Prog. Hum. Geog.*, 24: 347–364 **(17 pages)**.
- Ahmed, A.; Lawson, E. T.; Mensah, A.; Gordon, C.; Padgham, J., (2016). Adaptation to climate change or non-climatic stressors in semi-arid regions? Evidence of gender differentiation in three agrarian districts of Ghana. *Environ. Dev.*, 20: 45–58 **(14 pages)**.
- Ameyaw, L.K.; Ettl, G.J.; Leissle, K.; Anim-Kwapong, G.J., (2018). Cocoa and climate change: Insights from smallholder cocoa producers in Ghana regarding challenges in implementing climate change mitigation strategies. *Forests.*, 9: 1–20 **(20 pages)**.
- Anning, A.K.; Ofori-Yeboah, A.; Baffour-Ata, F.; Owusu, G., (2022). Climate change manifestations and adaptations in cocoa farms: perspectives of smallholder farmers at Adansi South District, Ghana. *Curr Res. Environ. Sustainability.* 4: 100196 **(9 pages)**.
- Arifah; Salman, D.; Yassi, A.; Demmallino, E., (2022). Climate change impacts and the rice farmers' responses at irrigated upstream and downstream in Indonesia. *Heliyon.* 8: e11923 **(12 pages)**.
- Asante, P.A.; Rahn, E.; Zuidema, P.A.; Rozendaal, D.M.A.; van der Baan, M.E.G.; Läderach, P.; Asare, R.; Cryer, N.C.; Anten, N.P.R., (2022). The cocoa yield gap in Ghana: A quantification and an analysis of factors that could narrow the gap. *Agric. Sys.*, 201: 103473 **(13 pages)**.
- Asante, W.A.; Acheampong, E.; Kyereh, E.; Kyereh, B., (2017). Farmers' perspectives on climate change manifestations in smallholder cocoa farms and shifts in cropping systems in the forest-savannah transitional zone of Ghana. *Land Use Policy.* 66: 374–381 **(8 pages)**.
- Ayanlade, A.; Radeny, M.; Morton, J.F.; Muchaba, T., (2018). Rainfall variability and drought characteristics in two agro-climatic zones: An assessment of climate change challenges in Africa. *Sci. Total Environ.*, 630: 728–737 **(10 pages)**.
- Buitenhuis, Y.; Candel, J.J.L.; Termeer, K.J.A.M.; Feindt, P.H., (2020). Does the common agricultural policy enhance farming systems' resilience? Applying the resilience assessment tool (ResAT) to a farming system case study in the Netherlands. *J. Rural Stud.*, 80: 314–327 **(14 pages)**.
- Coopmans, I.; Dessein, J.; Accatino, F.; Antonioli, F.; Bertolozzi-Caredio, D.; Gavrilescu, C.; Gradziuk, P.; Manevska-Tasevska, G.; Meuwissen, M.; Peneva, M.; Pettit, A.; Urquhart, J.; Wauters, E., (2021). Understanding farm generational renewal and its influencing factors in Europe. *J. Rural Stud.*, 86: 398–409 **(12 pages)**.
- Daniele, B.C.; Barbara, S.; Isabel, B.; Alberto, G., (2022). Analysis of perceived robustness, adaptability and transformability of Spanish extensive livestock farms under alternative challenging scenarios. *Agric. Syst.*, 202: 103487 **(15 pages)**.
- Dessart, F.J.; Barreiro-Hurlé, J.; Van Bavel, R., (2019). Behavioural factors affecting the adoption of sustainable farming practices: A policy-oriented review. *Eur. Rev. Agric. Econ.*, 46: 417–471 **(55 pages)**.
- Dhir, A.; Sadiq, M.; Talwar, S.; Sakashita, M.; Kaur, P., (2021). Why do retail consumers buy green apparel? A knowledge-attitude-behaviour-context perspective. *J. Retail. Consum. Serv.*, 59: 102398 **(11 pages)**.
- Ehiakpor, D.S.; Danso-Abbeam, G.; Baah, J.E., (2016). Cocoa farmer's perception of climate variability and its effects on adaptation strategies in the Suaman district of the western region, Ghana. *Cogent Food Agric.*, 2:1210557 **(12 pages)**.
- FAO., (2017). The future of food and agriculture – trends and challenges. Food and Agriculture Organization of the United Nations. Rome **(180 pages)**.
- Foela, G.; Lerner, A.M.; Jain, M.; Montefrio, M.J.F.; Nicholas, K.A., (2015). Researching farmer behaviour in climate change adaptation and sustainable agriculture: Lessons learned from five case studies. *J. Rural Stud.*, 39: 74–84 **(11 pages)**.
- Frimawaty, E.; Ilmika, A.; Sakina, N.A; Mustabi, J., (2023). Climate change mitigation and adaptation through livestock waste management. *Global J. Environ. Sci. Manage.*, 9(4): 691-706 **(16 pages)**.
- Giovanopoulou, E.; Nastis, S.A.; Papanagiotou, E., (2011). Modelling farmer participation in agri-environmental nitrate pollution reducing schemes. *Ecol. Econ.*, 70: 2175–2180 **(6 pages)**.
- Hirons, M.; Boyd, E.; McDermott, C.; Asare, R.; Morel, A.; Mason, J.; Malhi, Y., Norris, K. (2018). Understanding climate resilience in Ghanaian cocoa communities – Advancing a biocultural perspective. *J. Rural. Stud.*, 63: 120–129 **(10 pages)**.
- Idawati; Fatchiya, A.; Ariyanto, D. (2019). Sustainable cocoa farming strategies in overcoming the impact of climate change through SEM PLS 2. *Int. J. Innov. Techn. Expl. Eng.*, 9: 291–297 **(7 pages)**.
- Idawati; Hubeis; Fatchiya; Asngari, T., (2018). The implication of climate adaptation and mitigation research: Capacity adaptation of rice paddy farmers to climate change. *IOP*

- Conf Ser: Earth Environ. Sci., 200: 1–6 **(6 pages)**.
- Jallow, M.F.A.; Awadh, D.G.; Albaho, M.S.; Devi, V.Y.; Thomas, B.M., (2017). Pesticide knowledge and safety practices among farm workers in Kuwait: Results of a survey. *Int. J. Environ. Res. Public Health*, 14: 1–15 **(15 pages)**.
- Karpouzoglou, T.; Dewulf, A.; Clark, J., (2016). Advancing adaptive governance of social-ecological systems through theoretical multiplicity. *Environ. Sci. Policy*, 57: 1–9 **(9 pages)**.
- Kosoe, E.A.; Ahmed, A., (2022). Climate change adaptation strategies of cocoa farmers in the Wassa East District: Implications for climate services in Ghana. *Clim. Serv.*, 26: 100289 **(9 pages)**.
- Lobley, M., Potter, C., (2004). Agricultural change and restructuring: Recent evidence from a survey of agricultural households in England. *J. Rural Stud.*, 20: 499–510 **(12 pages)**.
- May, D.; Arancibia, S.; Behrendt, K.; Adams, J., (2019). Preventing young farmers from leaving the farm: Investigating the effectiveness of the young farmer payment using a behavioural approach. *Land Use Policy*, 82: 317–327 **(11 pages)**.
- Mbow, C.; Van Noordwijk, M.; Luedeling, E.; Neufeldt, H.; Minang, P.A.; Kowero, G., (2014). Agroforestry solutions to address food security and climate change challenges in Africa. *Curr. Opin. Environ. Sustainabl.*, 6: 61–67 **(7 pages)**.
- Meuwissen, M.P.M.; Feindt, P.H.; Spiegel, A.; Termeer, C.J.A.M.; Mathijs, E.; de Mey, Y.; Finger, R.; Balman, A.; Wauters, E.; Urquhart, J.; Vigan, M.; Zawalińska, K.; Herrera, H.; Nicholas-Davies, P.; Hansson, H.; Paas, W.; Slijper, T.; Coopmans, I.; Vroege, W.; Reidsma, P., (2019). A framework to assess the resilience of farming systems. *Agric. Syst.*, 176: 102656 **(10 pages)**.
- Naderipour A.; Abdul-Malek, Z.; , Noor Azlinda Ahmad, N.A.; Kamyab, H.; Ashokkumar, V.; Ngamcharussrivichai, C.; Chelliapan, S., (2020). Effect of COVID-19 virus on reducing GHG emission and increasing energy generated by renewable energy sources: A brief study in Malaysian context. *Environ. Technol. Inn.*, 20: 101151 **(8 pages)**.
- Naderipour, A.; Nowdeh, S.A.; Babanezhad, M.; Najmi, E.S.; Kamyab, H.; Abdul-Malek, Z., (2021). Technical-economic framework for designing of water pumping system based on photovoltaic clean energy with water storage for drinking applications. *Environ. Sci. Pollut. Res.*, 30: 71754–71765 **(12 pages)**.
- Oyekale, A.S., (2018). Impact of climate change on cocoa agriculture and technical efficiency of cocoa farmers in South-West Nigeria. *J. Hum. Ecol.*, 40: 143–148 **(6 pages)**.
- Peprah, K., (2015). Sustainability of cocoa farmers' livelihoods: A case study of Asunafo District, Ghana. *Sustain. Prod. Consum.*, 4: 2–15 **(14 pages)**.
- Prain, G.; Wheatley, C.; Odsey, C.; Verzola, L.; Bertuso, A.; Roa, J.; Naziri, D., (2020). Research-development partnerships for scaling complex innovation: Lessons from the Farmer Business School in IFAD-supported loan-grant collaborations in Asia. *Agric. Syst.*, 182: 102834 **(15 pages)**.
- Riyanto, D.; Dianawati, M.; Sutardi; Susanto, H.; Sasongko, N.A.; Sri Ratmini, N.P.; Rejekiingrum, P.; Yustisia; Susilawati, H.L.; Hanafi, H.; Jauhari, S.; Anda, M.; Arianti, F.D.; Praptana, R.H.; Pertiwi, M.D.; Martini, T. (2022). The Effect of P2O5 Fertilizer, Zeolite, and Volcanic Soil Media from Different Altitudes on the Soil Mineral, Growth, Yield, and Asiaticoside Content of *Centella asiatica* L. *Sustainability*, 14: 15394 **(16 pages)**.
- Schroth, G.; Läderach, P.; Martinez-Valle, A.I.; Bunn, C.; Jassogne, L., (2016). Vulnerability to climate change of cocoa in West Africa: Patterns, opportunities and limits to adaptation. *Sci. Total Environ.*, 556: 231–241 **(11 pages)**.
- Shereen, M.A.; Khan, S.; Kazmi, A.; Bashir, N.; Siddique, R. (2020). COVID-19 infection : Emergence, transmission, and characteristics of human coronaviruses. *J. Adv. Res.*, 24: 91–98 **(8 pages)**.
- Sianipar, C.P.M., (2022). Environmentally-appropriate technology under lack of resources and knowledge: Solar-powered cocoa dryer in rural Nias, Indonesia. *Clean. Eng. Technol.*, 8: 100494 **(16 pages)**.
- Simão, S.A.V.; Rohden, S.F.; Pinto, D.C., (2022). Natural claims and sustainability: The role of perceived efficacy and sensorial expectations. *Sustainable Prod. Consum.*, 34: 505–517 **(13 pages)**.
- Suh, N.N.; Molua, E.L., (2022). Cocoa production under climate variability and farm management challenges: Some farmers' perspective. *J. Agric. Food Res.*, 8: 100282 **(9 pages)**.
- Sasongko, N.A.; and Pertiwi, G.A. (2021). Life cycle cost (LCC) and the economic impact of the national biofuels development through biorefinery concept and circular economy. *IOP Conference Series: Earth Environ. Sci.*, 924: 012074 **(8 pages)**.
- Tschora, H.; Cherubini, F., (2020). Co-benefits and trade-offs of agroforestry for climate change mitigation and other sustainability goals in West Africa. *Global Ecol. Conserv.*, 22: e00919 **(13 pages)**.
- Tothmihaly, A.; Ingram, V.; von Cramon-Taubadel, S., (2019). How can the environmental efficiency of Indonesian cocoa farms be increased? *Ecol. Econ.*, 158: 134-145 **(12 pages)**.
- Wessel, M.; Quist-Wessel, P.M.F., (2015). Cocoa production in West Africa, a review and analysis of recent developments. *NJAS - Wageningen J. Life Sci.*, 74–75: 1–7 **(7 pages)**.

#### AUTHOR (S) BIOSKETCHES

**Idawati, I.**, Ph.D., Lecturer, Department of Agribusiness, Faculty of Agriculture, Andi Djemma University, Indonesia.

- Email: [badrulaida1@gmail.com](mailto:badrulaida1@gmail.com)
- ORCID: 0009-0007-5276-8176
- Web of Science Researcher ID: -
- Scopus Author ID: 57204941378
- Homepage: <https://unanda.ac.id/>

**Sasongko, N.A.**, Ph.D., Director, Research Center for Sustainable Production System and Life Cycle Assessment, National Research and Innovation Agency (BRIN), Tangerang Selatan, Indonesia. Associate Professor, Republic of Indonesia Defense University (UNHAN), Indonesia Peace and Security Centre, Bogor, Indonesia.

- Email: [nugroho.adi.sasongko@brin.go.id](mailto:nugroho.adi.sasongko@brin.go.id)
- ORCID: 0000-0002-6546-1348
- Web of Science ResearcherID: NA
- Scopus Author ID: 56709544200
- Homepage: <https://www.linkedin.com/in/nugroho-adi-sasongko-94558ab9/>

**Santoso, A.D.**, Ph.D., Senior Researcher, Research Centre for Sustainable Production System and Life Cycle Assessment, National Research and Innovation Agency, Indonesia.

- Email: [arif.dwi.santoso@brin.go.id](mailto:arif.dwi.santoso@brin.go.id)
- ORCID: 0000-0003-3595-9265
- Web of Science Researcher ID: HJY-1972-2023
- Scopus Author ID: 56516534000
- Homepage: <https://brin.go.id/>

**Septiani, M.**, S.Ds., Assistant Researcher, Research Centre for Sustainable Production System and Life Cycle Assessment, National Research and Innovation Agency, Indonesia.

- Email: [mari032@brin.go.id](mailto:mari032@brin.go.id)
- ORCID: 0000-0002-7058-1192
- Web of Science Researcher ID: NA
- Scopus Author ID: 57990906700
- Homepage: <https://brin.go.id/>

**Handayani, T.**, S.Kom., M.S.M., Assistant Researcher, Deputy of Research Policy and Innovation, National Research and Innovation Agency, Indonesia.

- Email: [trih014@brin.go.id](mailto:trih014@brin.go.id)
- ORCID: 0000-0002-6734-4102
- Web of Science Researcher ID: NA
- Scopus Author ID: NA
- Homepage: <https://brin.go.id/>

**Sakti, A.Y.N.**, S.T., Assistant Researcher, Research Centre for Sustainable Production System and Life Cycle Assessment, National Research and Innovation Agency, Indonesia.

- Email: [ardh007@brin.go.id](mailto:ardh007@brin.go.id)
- ORCID: 0000-0001-9586-6541
- Web of Science Researcher ID: NA
- Scopus Author ID: NA
- Homepage: <https://brin.go.id/>

**Purnamasari, B.D.**, S.T., M.A.B., Assistant Researcher, Research Centre for Sustainable Production System and Life Cycle Assessment, National Research and Innovation Agency, Indonesia.

- Email: [beni004@brin.go.id](mailto:beni004@brin.go.id)
- ORCID: 0000-0003-1106-8601
- Web of Science Researcher ID: NA
- Scopus Author ID: 57991096800
- Homepage: <https://brin.go.id/>

#### HOW TO CITE THIS ARTICLE

Idawati, I.; Sasongko, N.A.; Santoso, A.D.; Septiani, M.; Handayani, T.; Sakti, A.Y.N.; Purnamasari, B.D., (2024). Cocoa farmers characteristics on climate variability and its effects on climate change adaptation strategy. *Global J. Environ. Sci. Manage.*, 10(1): 337-354.

DOI: [10.22034/gjesm.2024.01.21](https://doi.org/10.22034/gjesm.2024.01.21)

URL: [https://www.gjesm.net/article\\_705576.html](https://www.gjesm.net/article_705576.html)





## CASE STUDY

## An analysis on the economic development and deforestation

E.S. Siregar\*, S.U. Sentosa, A. Satrianto

Department of Environmental and Development Studies, Faculty of Economy, Universitas Negeri Padang, Padang, Indonesia

## ARTICLE INFO

## Article History:

Received 22 January 2023

Revised 29 April 2023

Accepted 06 June 2023

## Keywords:

Deforestation

Economic development

Environmental consequences

Human resource

Natural resource

## ABSTRACT

**BACKGROUND AND OBJECTIVES:** This study aimed to investigate endogenous variables namely, economic development and deforestation, in North Sumatra, and examine their determinants. Both variables are substantial in a country community welfare with harmonized environmental sustainability as a legacy for future generations.

**METHODS:** In this quantitative study, secondary data in the form of time series data from 1991 to 2020 with a total of 30 years were analyzed. The novelty of this study is its aim to combine deforestation variables and their determinants in a research model related to economic development. In this study, the determinants of economic development used were education, health, mineral resources and forest resource, whereas those of deforestation, were forest resource, institutional factors, population density, and economic development.

**FINDINGS:** The data analysis revealed that the economic development in North Sumatra was significantly influenced by education, health, and mineral resources, excluding forest resources. Simultaneously, the determinants influenced economic development by 74.15 percent. Education contributed 27 percent, health 71 percent, mineral resources 12 percent and forest resources 29 percent to economic development. Forest resources and institutions had a significant influence on deforestation in North Sumatra, whereas population density and economic development did not have a significant effect. Simultaneously, the determinants influenced deforestation by 77.24 percent. Partial, forest resources and institutions were identified and significant effect but population density does not significantly affect it. Forest resources contributed 14 percent to deforestation, institutional factors 72 percent, population density 3 percent and economic development 57 percent.

**CONCLUSION:** The findings of this study, indicated that education and health have a major effect on economic development whereas forest resources do not however, forest resources significantly affect deforestation. This means that an increasing environmental damage removes forest cover. Thus, it is recommended that the government increase human resource in terms of education and health, which are essential in prioritizing human resource development as a fundamental factor. It is also important to set the limit to long-term natural resource exploitation, consider environmental damages, and improve institutional quality. The government needs to explore alternative sources that are more sustainable and environmentally friendly, such as ecotourism, and renewable energy. Renewable energy can be a reliable source of energy that will help reduce reliance on fossil fuels while also minimizing environmental impacts.

DOI: [10.22034/gjesm.2024.01.22](https://doi.org/10.22034/gjesm.2024.01.22)This is an open access article under the CC BY license (<http://creativecommons.org/licenses/by/4.0/>).

NUMBER OF REFERENCES

37



NUMBER OF FIGURES

4



NUMBER OF TABLES

5

\*Corresponding Author:

Email: [ennisari056@gmail.com](mailto:ennisari056@gmail.com)

Phone: 0853 7036 7600

ORCID: [0000-0002-0225-3533](https://orcid.org/0000-0002-0225-3533)

Note: Discussion period for this manuscript open until April 1, 2024 on GJESM website at the "Show Article".

**INTRODUCTION**

Economic development is a substantial aspect of a nation, as it deals with the attempts to improve community welfare and eradicate poverty. Gross domestic product (GDP) is the popular parameter of a nation’s economic development (Sun and Tang, 2011). The success of economic development is reflected on economic growth, in which these two variables are intercorrelated. Economic development can encourage economic growth, and increased economic growth, in turn, will assist in the process of economic development. Community welfare can be improved by increasing national and per capita income, providing employment opportunities, and reducing poverty rate. Natural resources also significantly influence economic development, particularly in Indonesia. Abundant natural resources encourage the production of various products and services. The government, in cooperation with private sectors, create, and encourage employment opportunities to enhance economic development. Redmond and Nasir (2020) highlighted the significant contribution of natural resources to economic development, hence natural resource exploitation needs to be regulated. Exploration of natural resources needs to consider the possible environmental damages. Natural resource exploration is linked to deforestation, in which the trees cover area decreases due to the direct exploration of natural resources and land conversion. North Sumatra has the largest population on Sumatra island and ranked fourth in Indonesia following West Java, Central Java and East Java, with a total of 15,136,522 people. With a fairly

dense population, its economic development is similar to that of Indonesia in general. The enactment of regional autonomy encourages the local governments to strive to improve the welfare of their community and eradicate poverty by accelerating economic development. Economic development is affected by a variety of factors. Kamaroellah and Kutsiyah (2018) perceived environment as a factor affecting economic development. Deforestation is a major environmental issue that emerges after economic development. Cuaresma and Heger (2018) stated that countries with high economic development also have high deforestation rates. Fig. 1 presents economic development as reflected by the gross regional domestic product (GRDP), in North Sumatra between 2016 and 2020.

Fig. 1 presents the data on the GRDP and deforestation which continue to fluctuate. GDP is the total goods and services produced within one period, usually within 1 year (y). It is defined as economic performance in social welfare. GRDP increased by 5.12 percent (%) and 5.17% in 2017 and 2018, respectively. Furthermore, in 2018, the deforestation rate has drastically decreased by 67.54% or 7,319.10 hectares (ha), which is not an ideal situation. Various factors can affect economic development, including social, economic and environmental factors (Klapper et al., 2016). Then Kamaroellah and Kutsiyah (2018) also mentioned some economic factors that influence economic development, including natural resources, human resources, capital formation, and expertise, or entrepreneurship. No economic factors include sociocultural environment, political conditions and

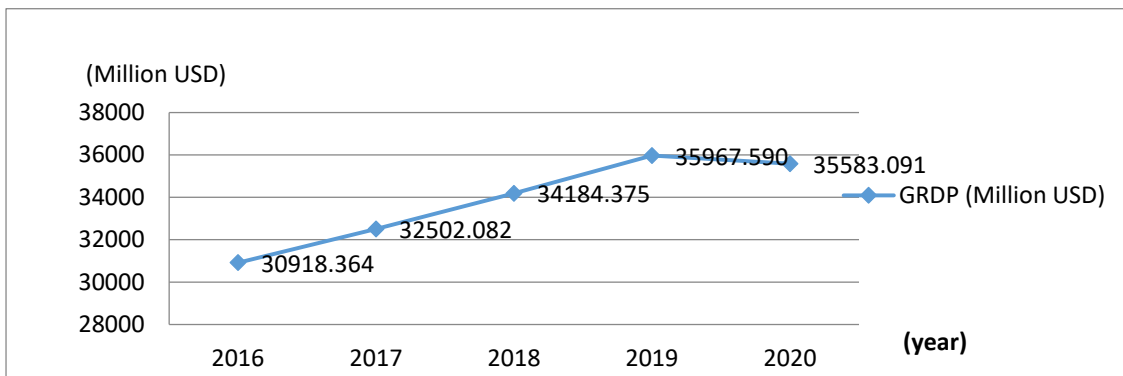


Fig. 1: Economic development shown in GRDP in North Sumatra in 2016 to 2020 (Badan Pusat Statistik, 2021)

Table 1: Determinants of economic development in North Sumatra in 2016–2020 (Badan Pusat Statistik, 2021)

Tahun	Education (year)	Health (year)	Mineral resource ( Million USD)	Forest resources ( Million M3)
2016	9,12	68,33	564,96	2,24
2017	9,25	68,37	593,55	0,95
2018	9,34	68,61	636,8	0,15
2019	9,45	68,95	677,37	1,08
2020	9,54	69,1	691,56	1,65

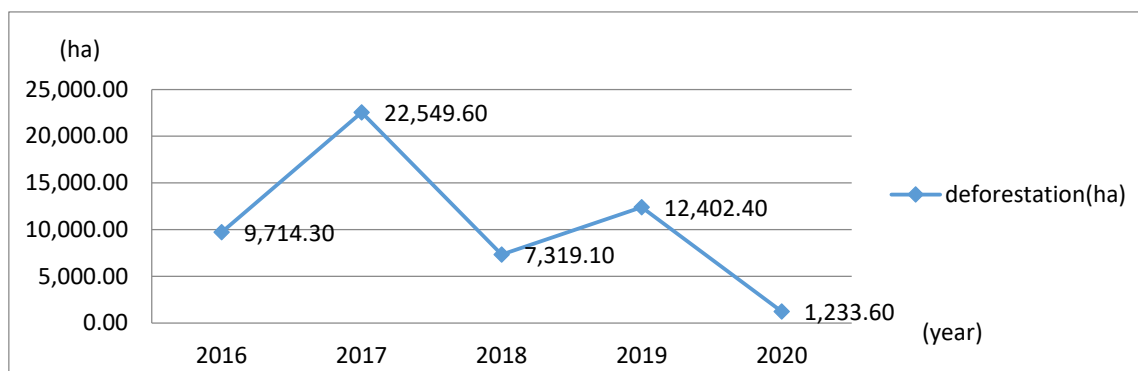


Fig. 2: Deforestation in North Sumatra in 2016-2020 (Badan Pusat Statistik, 2021)

institutions. Atalay (2015) explained that human capital relates to the knowledge, skills, experience, behavior and talents possessed by individuals which can be improved through education. Furthermore, health is the factor that constructs human capital. On the other hand, natural resources such as forests, mineral resources, and mining products also contribute to the production process that drives the national economy. In this study, economic development is defined as government performance for welfare as measured by GDP. Based on several studies, the determinants of economic development in this study are human resources, natural resources and the linkage of economic development to deforestation as environmental factor. Human resources are more broadly described as education and health, whereas natural resources are described as mineral and forest resources. Adequate natural and human resources are the capital of a nation in carrying out the development and providing government support to encourage investment while handling environmental issues (Azam, 2015). Oryani et al. (2022) evaluated the environmental impact of economic activities. Table 1 presents the determinants of economic development in North

Sumatra.

Environmental factors also play considerable role. Deforestation can lead to other environmental problems. Human activities on land, increase, land conversion also increase causing environmental damages such as decreased tree cover that will result in climate change problems, loss of plant diversity, and even landslides, floods and erosion (Waluyo and Terawaki, 2016). On the other hand, exploration of natural resources creates opportunities for economic development, but also affect deforestation strong interaction between forest cover and economic development in relation to the deforestation (Ewers, 2006). Similar view was also shared who found a significant relationship between economic development and the level of deforestation. Table 2 presents the determinants of deforestation in North Sumatra. In 2016, the deforestation in North Sumatra reached 9,714.30 Ha which then significantly increased by 132.13% in 2017. In the same year, the economic development as seen from the GRDP also increased by 5.12%. Contrarily, in 2018, the deforested area decreased by 67.54%, but the economic development somehow increased by 5.17%. Unlike the general expectation

Table 2: Determinants of deforestation in North Sumatra in 2016 – 2020 (Badan Pusat Statistik, 2021)

Tahun	Forest resources (Milion M3)	Institutional (Total of role)	Population density (People)	GRDP (Million USD)
2016	2,24	32	193	30918,36
2017	0,95	50	196	32502,08
2018	0,15	55	198	34184,38
2019	1,08	41	200	35967,59
2020	1,65	49	203	35583,09

where increases in deforestation would lead to higher economic development, the aforementioned findings were opposite. Angelsen and Kaimowitz (1999) mentioned the factors that influence deforestation namely, economic development, demographics, institutions and macroeconomic factors. Deforestation increases following the increases in investment in land and property, which eventually enhance land productivity (Liscow, 2013)

Increasing population also leads to higher deforestation rates, particularly people living in rural areas who tend to explore the forest for living. Institutional factors also contribute to this matter, where regulations should be elucidated to provide no loophole for anyone to conduct deforestation. This matter also relates to capital formation and economic development, which are macroeconomic factors that can affect the extent of deforestation. Economic development is a key variable, where GDP is generally used as the main indicator in the development of a nation or country which, in turn, encourages improvement in community welfare (Sun and Tang, 2011; Kenzheguzin and Yessekina, 2004). Economic development is carried out by reorienting and improving human factors on all sides, for example, education, and community culture so that they can stimulate creativity. Investment in human resources and capital is the most important and effective means to improve community welfare. To date, economic development remains the main parameter for community welfare, where improvement should be made in all aspects, including human and capital resources and various other variables deemed to have influences. The model of sustainable economic development balances the management of capital, human, and natural resources by adding features of the social environment, institutions and economic politics (Ravago et al., 2015). Furthermore the factors that

affect a nation’s economic development include human labor and capital inputs (Sun and Tang, 2011). The main goal of economic development is poverty eradication. In this study, we used the Solow growth model, a neoclassical aggregate production function, and focused on the factors that directly affect the growth using Eq. 1 (Onyinye et al., 2017).

$$Y_t = f(K_t, A_t L_t) \tag{1}$$

where

Y : real output or GDP

K : capital ability (human capital and tangible capital)

L : workforce input

A : technology

Health and education are the main parameters of economic development. Several studies conducted by Satrianto explained that human resources are the main key to increasing economic productivity. The concept of human development also indicates that the role of education is important for enhancing the ability of developing countries to absorb modern technology and develop capacities to achieve sustainable growth and development (Satrianto and Juniardi, 2023; Aravind et al., 2016). Health is central to human well-being, and education is essential for a quality life. Education affects the ability to adopt and utilize the technology, whereas health supports productivity. Hence, human capital is seen as a vital component in development as input for aggregate production function (Todaro and Smith, 2012). Effective and efficient management of natural resources as well as quality human resources will accelerate a nation’s economic development. Deforestation is an equally crucial issue. Intensified human activity reduces the tree cover. Deforestation is the consequence of continuous human activity

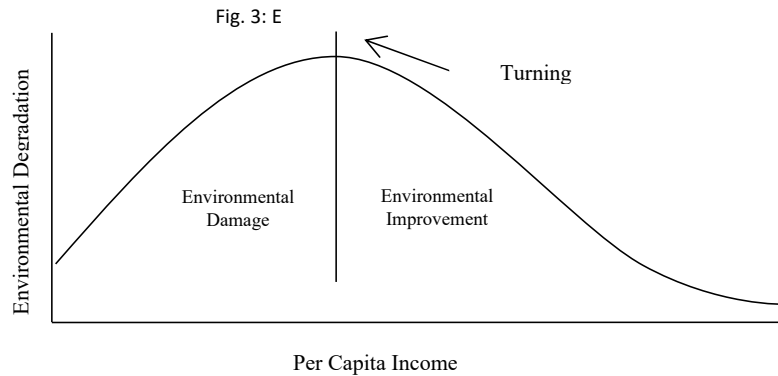


Fig. 3: Environmental Kuznets curve (Singh and Yadav, 2021)

in a long period of time, resulting in a significant decline in forest area, particularly in the tropics (Lee and Lemieux, 2010). Lewis also stated similar view, where they found that human activities can degrade and decrease environmental quality (Cuaresma and Heger, 2018). Countries with abundant natural resources have greater opportunities to accelerate their economic development. Utilization of natural resources such as forests for timber production and land conversion reduce forest area but increase economic activities, which later increase the GDP of a country. Therefore, deforestation affects economic development. In 1955, Kuznets analyzed the relationship between per capita income and environmental quality as described in the environmental Kuznets curve (Fig. 3).

During the initial phase of economic development, damage to the environment will continue to increase, but after economic growth reaches a certain threshold, a reverse movement will occur, where income will continue to increase along with environmental quality (Singh and Yadav, 2021). Angelsen stated that the factors underlying deforestation indirectly affect deforestation through various models, such as institutional factors, economic development, demography, and other macroeconomic factors (Damette and Delacote, 2012). Previous empirical studies viewed institutional quality as a critical factor in deforestation. (Afawubo and Noglo (2019) found that weak governance, high corruption rate, and low institutional quality are often associated with higher rates of deforestation. Bhattarai and Hammig demonstrated that improving the quality of politics and governance institutions

can effectively reduce the deforestation rates (Bhattarai and Hammig, 2001). They specifically analyzed the political rights and civil liberties as key institutional variables that influence deforestation. Improvement in institutional quality promotes democracy, strengthens individual and civil liberties, and establishes the rule of law, leading to better forest area conservation that ultimately reduces environmental degradation. Aquilas et al. (Aquilas et al., 2022) also suggested that institutions, population growth, and GDP are important factors that influence deforestation. As stated by those experts, sustainable development requires balance between economic development and environmental sustainability. While economic growth is necessary to address social and economic issues, it should not bring environmental damages. A healthy environment should be preserved to prevent the occurrence of natural disasters such as floods and landslides that occur during the rainy season as tree roots fail to hold water when the rainfall is high, loss of biodiversity, and other environmental problems that can severely impact the society. Environmental sustainability should be a top priority. Despite the challenges that follow, balance between economic development, and environmental sustainability should be realized for a better future. Based on the initial data presented, it can be concluded that economic development and deforestation in North Sumatra have not shown ideal conditions. Imagine if this is allowed to continue, welfare will not be achieved, people's trust in the government will decrease, the poverty, rate will increase, and unemployment, and economic growth will decline.

In terms of deforestation, climate change, increased emissions, and the threat of natural disasters. This study, investigated the determinants of economic development namely, education, health, mineral resources and forest resources. Education and health are used to explain the role of human resources in more detail, whereas mineral, and forest resources are used to determine the types of natural resources that affect economic development. Deforestation determined in forest resources, institutional, population density, and economic development. This study addresses the following question: How do these determinants affect economic development and deforestation in North Sumatra? At present, the government of North Sumatra has integrated sustainable development into regional development plans to minimize deforestation by ensuring the preservation of ecosystems based on international agreements. Implementing global afforestation, and deforestation, restoring degraded land, inhibiting the hunting and trading of protected flora and fauna, and integrating ecosystem values into poverty reduction budgeting plans (Dinas kehutanan, 2022). This issue is a problem faced by countries worldwide, particularly the developing ones; thus, it is a shared responsibility. Lambin et al. (2018) highlighted multinational companies also take initiatives to reduce deforestation such as collective aspirations of stakeholders to determine common goals in reduced deforestation and establishment of company commitments, code ethics and sectoral standards in produced goods with a moratorium of sanctions for companies that ignore reduced deforestation. This study aimed to prove the effect of the identified endogenous variables on economic development and deforestation in a model. The

study is expected to compensate for the lack of previous research. It has been conducted in North Sumatra, Indonesia, during 2021 to 2022.

**MATERIALS AND METHODS**

*Method of the study*

This quantitative study was conducted using descriptive and associative methods. Secondary data collected from the North Sumatra Central Bureau of Statistics were used. The observation year ranged from 1991 to 2020, a period of 30 years. The determinants of economic development used in this study were education, health, mineral resources and forest resources. Deforestation was affected by forest resource, institutions, population density, and economic development.

*Operational definition of the variables*

Measurement of the data of each variable is presented in Table 3. The data was collected from the documentation, annual reports or records issued by the North Sumatra Central Bureau of Statistics

As can be seen from the conceptual framework in Fig. 4, the mathematical measurements are expressed using Eqs. 2 and 3 (Kamaroellah and Kutsiyah, 2018; Angelsen and Kaimowitz, 1999).

First, the economic development:

$$Y_{1t} = \alpha_0 + \alpha_1 X_{1t} + \alpha_2 X_{2t} + \alpha_3 X_{3t} + \alpha_4 X_{4t} + \epsilon_{1t} \tag{2}$$

Second, the deforestation equation model:

$$Y_{2t} = \alpha_5 + \alpha_6 Y_{1t} + \alpha_7 X_{4t} - \alpha_8 X_{5t} + \alpha_9 X_{6t} + \epsilon_{2t} \tag{3}$$

*Identification test*

The order condition in identification from in model of *M* simultaneous equations. To identify an

Table 3 : Operational definition of the research variables

Variable	Measurement	Unit	Sources
Economic development (Y1)	GRDP	billion/y	Badan Pusat Statistik, 1991_2020
Deforestation (Y2)	Area of deforestation	ha/y	Badan Pusat Statistik, 1991_2020
Education (X1)	Average school period	y	Badan Pusat Statistik, 1991_2020
Health (X2)	Life expectancy rate	y	Badan Pusat Statistik, 1991_2020
Mineral resources (X3)	Mining output value in	Billion/y	Badan Pusat Statistik, 1991_2020
Forest resources (X4)	Number of timber production	M <sup>3</sup> /y	Badan Pusat Statistik, 1991_2020
Institutional factors (X5)	The number of regulations and law	No./y	Badan Pusat Statistik, 1991_2020
Population density (X6)	The population every kilometers	km <sup>2</sup> /y	Badan Pusat Statistik, 1991_2020

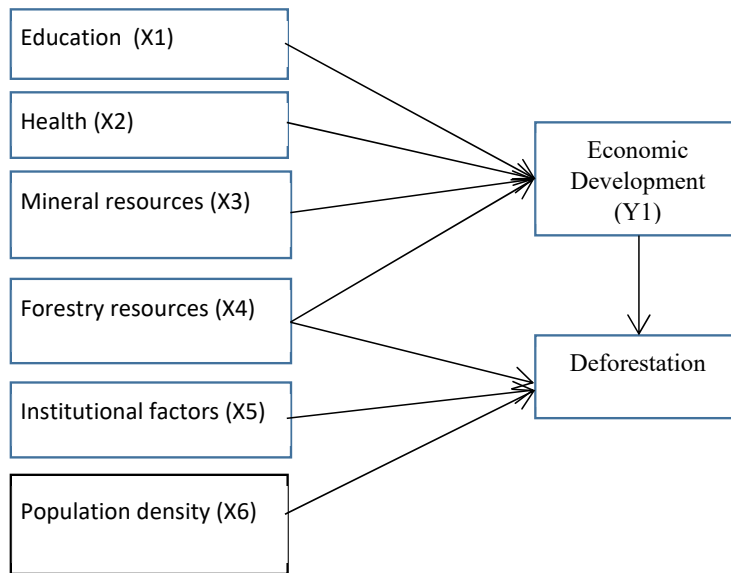


Fig. 4: Conceptual framework

equation, the number of predetermined variables excluded from the equation must not be less than the number of endogenous variables included in that equation less 1, that is,  $K - k \geq m - 1$ .

If  $K - k = m - 1$ , the equation is just identified, but if  $K - k > m - 1$ , it is overidentified

The identification test using order condition in this study is explained using Eqs. 4 and 5 (Gujarati and Porter, 2009).

$$K - k = 6 - 4 = m - 1 = 1 - 1 : \text{therefore, } 2 > 0 \text{ (overidentified) (4)}$$

$$K - k = 6 - 3 = m - 1 = 1 - 1 : \text{therefore, } 3 > 0 \text{ (overidentified) (5)}$$

The comparative test using order conditions for the two agreements showed that some equations were overidentified, thereby, they can be measured using the *two-stage least squares* (TSLS).

*Research hypothesis*

1. Education, health, mineral resources, and forest resources toward economic development in North Sumatra, using Eqs. 6 and 7 (Redmond and Nasir, 2020 ; Todaro and Smith, 2012).

$$H_0 : \alpha_1 = \alpha_2 = \alpha_3 = \alpha_4 = 0 \tag{6}$$

$$H_a : \alpha_1 \neq \alpha_2 \neq \alpha_3 \neq \alpha_4 \neq 0 \tag{7}$$

2. Forest resources, institutions, population density, and economic development toward deforestation in North Sumatra, using Eqs. 8 and 9 (Damette and Delacote, 2012).

$$H_0 : \beta_1 = \beta_2 = \beta_3 = \beta_4 = 0 \tag{8}$$

$$H_a : \beta_1 \neq \beta_2 \neq \beta_3 \neq \beta_4 \neq 0 \tag{9}$$

**RESULTS AND DISCUSSIONS**

The results of the data analysis are presented in Eq. 10 and Table 4. The estimation results of the economic development equation in Table 4 indicate that education and health have a significant positive impact, whereas mineral resources a significant negative impact on economic development. On the other hand, forest resources did not significantly affect economic development. Simultaneously, education, health, mineral resources, and forest resources have a significant impact on economic development, as shown by the F-statistic probability

Table 4: Results of the analysis of economic development variables (Y1)

Variable	Coefficient	SE	t-Statistic	Prob.
C	37.24584	12.67842	2.937736	0.0070
X1	0.270944	0.502717	5.389609	0.0000
X2	0.712908	0.240783	2.960796	0.0066
X3	-0.12E-05	4.04E-06	-2.992549	0.0061
X4	-0.29E-07	2.65E-07	-1.116627	0.2748
R-Squared	0.741531	Mean dependent var		11.51169
Adjusted R-squared	0.741531	S.D. dependent var		1.384772
S.E. of regression	0.700176	Akaike info criterion		2.435401
Sum squared resid	0.758249	Schwarz criterion		2.668934
Log likelihood	14.37352	Hannan_Quinn criter		2.510110
F-statistic	17.93085	Durbin_Watson stat		2.125756
Prob (F-statistic)	0.000000			

Table 5: Result of analysis of deforestation variables (Y2)

Variable	Coefficient	SE	t-Statistic	Prob.
C	17.23470	5.769993	2.986952	0.0062
Y1	0.570E-07	1.30E-06	0.438412	0.6649
X4	0.149E-06	4.03E-07	3.712818	0.0010
X5	-0.728867	0.321696	-2.265701	0.0324
X6	-0.031700	0.040052	-0.791467	0.4361
R-Squared	0.772362	Mean dependent var		10.25441
Adjusted R-squared	0.735939	SD dependent var		2.411007
S.E. of regression	1.238940	Akaike info criterion		3.417401
Sum squared resid	38.37429	Schwarz criterion		3.650934
Log likelihood	-46.26101	Hannan_Quinn criter		3.492110
F-statistic	21.20582	Durbin_Watson stat		1.587684
Prob (F-statistic)	0.000000			

value of 0.0000 (lower than 0.05). The partial of each variable is summarized in Eq. 10, education (X1) has a regression coefficient value of 0.27. This means that an increase in education of 1% will lead to an increase in economic development by 27% assumed ceteris paribus. Similar to health (X2) with a coefficient of 0.71, mineral resources (X3) with a coefficient of 0.12 and forest resources (X4) with a coefficient of 0.29 it means the contribution of each variable to economic development with the assumption of ceteris paribus, this is the answer to previous hypothesis, using Eq. 10 (Redmond and Nasir, 2020 ; Todaro and Smith, 2012).

$$Y1 = 37,25 + 0,27X1+ 0,71X2-0,12X3-0,29X4 \quad (10)$$

$$R^2 = 0,7415$$

$$\text{Probability } F = 0,0000$$

In North Sumatra, education has a significant, and positive impact on economic development. This highlights the importance of education in

increasing human capital, productivity, and overall development. This finding is consistent with the opinion of Raheem *et al.* (2018), who argued that human resource development is crucial for promoting economic development. According to the theory of human capital, better human capacity generates greater economic value, leading to higher labor productivity and overall economic development (Rahim *et al.*, 2021). Thus, to achieve sustainable development, it is important to prioritize human resource development as a fundamental factor. In addition to education, health significantly affects economic development in North Sumatra. Health also contributes to the improvement of human capital and positively affects economic performance. According to Inwood, health and economic development have a positive relationship (Inwood, 2017). Health is an essential input factor in the production process, and healthy working conditions can lead to higher productivity, resulting in increased production. Albarrán also viewed

life expectancy as an important component of human capital in addition to education (Albarran, 2018). Health is a source of variation in income. Meanwhile, discrepancies in life expectancy can cause income inequality. Furthermore, populations with better health are more likely to invest in new technologies, adapt to changes, and invest more leading to faster economic growth. Therefore, health is an essential component of human capital that contributes to economic development by supporting productivity and increasing production capacity. In North Sumatra, mineral resources also have a significant effect on economic development. Natural resources are products obtained from nature that can be utilized by humans to meet their needs; they are beneficial for economic development as the abundance of natural resources provides the energy required for such a development (Wang et al., 2021; Qiang and Jian, 2020). Natural resources are the foundation of economic development as regions with abundant energy and mineral resources effectively leverage their resource advantages into economic development advantages. Mineral resources, in particular, contribute to the GDP. However, continuous exploitation of mineral resources can have negative impacts on the economy. Overexploitation and improper management of mineral resources can lead to resource depletion, environmental degradation, and conflicts, which can hamper economic development. Therefore, proper management and sustainable use of natural resources, including mineral resources, are important to ensure long-term economic development. Furthermore, the utilization of forest resources does not have a significant impact on the economic development in North Sumatra, indicating that changes in forest resource yields do not lead to significant changes in economic growth. However, this finding contradicts previous research by Hao et al. (2018) which suggested that natural resource utilization, particularly forest resources, contributes to the improvement of the economy and living standards (Qiang and Jian, 2020; Hao et al., 2018). The forestry sector is closely intertwined with the economy, as sustained economic growth is often accompanied by a substantial decline in forest resources. The author of this study attributed these inconsistent findings to the long-term environmental damage and natural disasters resulting from the continued

utilization of forest resources, ultimately negatively affecting economic development. These findings are consistent with those of empirical studies, such as that by Hao et al., which demonstrated an inverted U-shaped relationship between forest resources and economic development, as seen in the GDP, which in the initial use of forest resources use leads to output growth until a tipping point is reached, after which forest depletion results in deforestation and greater losses. The results of the deforestation (Y2) are shown using Eq. 11 (Damette and Delacote, 2012).

$$Y2 = 17,23 + 0,57Y1 + 0,14X4 - 0,72X5 - 0,03X6 \quad (11)$$

$$R^2 = 0,7724$$

Probability F value = 0,0000

According to the given equation, forest resources exhibit a partial significant positive impact whereas institutions have a significant negative impact on deforestation in North Sumatra. However, population density has no significant effect on deforestation. When considered together, forest resources, institutions, and population density exert a significant effect on deforestation, as evidenced by the probability value of the f-statistic, which is less than 0.05 (i.e., 0.0000). The partial of each variable is summarized in Eq. 11, forest resources (X4) have a regression coefficient value of 0.14. This means that an increase in forest resources of 1% will lead to an increase in deforestation by 14% assumed *ceteris paribus*. Similar to institutional factor (X5) with a coefficient of 0.72, population density (X6) with a coefficient of 0.03 and economic development (Y1) with a coefficient of 0.57 it means the contribution of each variable to deforestation with the assumption of *ceteris paribus*.

According to the given information, forest resources have a partial significant positive effect on deforestation in North Sumatra, indicating that continuous utilization of forest products can lead to environmental degradation and become a factor in deforestation. Expert opinions suggest that the triggers for deforestation include the quantity of harvested forest products and development issues. Ewers suggested that high-income countries often have low forest cover and focus on afforestation by establishing of new plantations, whereas low-income countries with smaller forest tend to consume their remaining share at a proportionally

faster rate than low-income countries with larger forest. In addition, countries with large forests have a higher rate of deforestation (Ewers, 2006). Similarly Cuaresma and Heger, (2018) suggest that low-income countries tend to have high economic development with high deforestation rates. North Sumatra is one of the areas with extensive forests in Indonesia, which is developing country. Forests are a source of income for the region and will expand deforestation. In North Sumatra, Institutions have a significant negative effect on deforestation, indicating that a decrease in institutional quality, as measured by the number of existing legal regulations, can lead to an increase in deforestation, whereas an improvement in institutional quality can lead to a decrease in deforestation. This finding is consistent with Angelsen's statement that institutional factors indirectly affect deforestation through various models, including institutions (Damette and Delacote, 2012). Institutional quality associated with deforestation, where the risk of ownership provides incentives for increasing deforestation. Better institutions lead to better environmental management, forward-looking behavior, higher efficiency, and better enforcement of public policies related to the environment. In addition, empirical studies, such as those of Afawubo and Noglo, highlighted the critical role of institutional quality in the deforestation process (Afawubo and Noglo, 2019). Weak governance, high corruption, and low institutional quality often result in higher deforestation rates. In North Sumatra, population density does not have a significant effect on deforestation. This indicates that changes in population density, whether an increase, or decrease, will not directly impact deforestation in North Sumatra. However, these findings differ from those of the studies conducted by Culas and Bhattarai and Hammig, who explained that population growth and density increase demand for forest products and land use, leading to deforestation (Culas, 2007). Population growth can increase labor force and affect the labor market, ultimately leading to high unemployment rates. With a large number of unemployed workers, forests can become an alternative, leading to an increase in deforestation rates. These findings are consistent with the idea that excessive population growth and pressure in developing countries are key

factors that drive tropical deforestation (Bhattarai and Hammig, 2001). Once the population reaches a certain level, the production process changes to increase efficiency and preserve natural resources. The inconsistencies in the results of previous studies were likely indirectly influenced by the effect of population density on employment rather than on deforestation. As population density increases, people may migrate from rural to urban areas in search of higher-paying jobs, leading to a reduction in traditional activities such as farming and a decrease in interactions between individuals and forests. Therefore, population density may affect employment first before affecting the deforestation. Some highly populated areas have low deforestation rates, which could be attributed to public awareness of environmental preservation (Tritsch and Tourneau, 2016). Widespread deforestation will barrier various policies included the development of education and health. Deforestation also contributes to environmental problems such as loss of flora and fauna to natural disasters. This is an economic cost that must be paid. Ewer (2006) demonstrated that the occurrence of environmental problems, such as climate change, loss of biodiversity, and increased rates of soil erosion, caused by deforestation increases the frequency and severity of floods.

## CONCLUSION

Based on the results of this study, it can be concluded that education, health, mineral resources and forest resources exert a significant effect on economic development in North Sumatra. Simultaneously the determinants of economic development have an effect of 74.15% (R square 0.7415). Education, health and mineral resources exert partial significant effects, whereas forest resources have no significant effect on economic development. Variable coefficient is the contribution of each variable to economic development. Education contributed 27% to economic development, health 71%, mineral resources 12%, and forest resources 0.29%. To realize economic development in North Sumatra, the government is recommended to increase human resources in terms of education and health, and prioritize human resource development as a fundamental factor. Differences in life expectancy can lead to income inequality. Populations with better health

are more likely to invent new technologies, adapt to changes, and invest more which will lead to faster economic growth. Health factor is an essential component of human capital that contributes to economic development by supporting productivity and increasing production capacity. The government must reduce the utilization of natural resources as an effort to save the environment for future generations. As an efforts to increase economic development, the government is currently focusing on household consumption, investment, and exports. The second hypothesis in this study to accepted, forest resources, institutions, population density and economic development have a significant effect on deforestation in North Sumatra. Simultaneously the determinants of deforestation have an effect of 77.24% (R square 0.7724). Partial of forest resources and institutions were identified and significant influences but population density does not significantly affect it. In North Sumatra, forest resources contributed 14% to deforestation, institutional factors 72%, population density 3%, and economic development 57%. The government continues to perform afforestation and reforestation to restore some forest cover. It is recommended that stakeholders explore alternative sources that are more sustainable and environmentally friendly, such as ecotourism, and renewable energy. Ecotourism can generate revenue for local communities while promoting conservation of natural resources and biodiversity. Renewable energy can be a reliable source of energy which will help reduce reliance on fossil fuels while also minimizing environmental impacts. The government can also implement policies and programs that promote sustainable practices in agriculture, fisheries, and forestry, such as sustainable land use planning, conservation of biodiversity, and community-based forest management. By adopting a sustainable and holistic approach to economic development, the government can ensure that economic growth is inclusive, equitable, and environmentally sustainable.

#### **AUTHOR CONTRIBUTIONS**

E.S. Siregar helped in the design and development of models in the research, collection and analysis of data, and creation of research reports. S.U. Sentosa directed and mentored the literature review. A.

Satrianto accompanied and guided the writing of the manuscript.

#### **ACKNOWLEDGMENT**

The authors would like to thank Padang State University as a facilitator for supporting this study.

#### **CONFLICT OF INTEREST**

The authors declare that there is no conflict of interests regarding the publication of this manuscript. In addition, the ethical issues including plagiarism, informed consent, misconduct, data fabrication, and/or falsification, double publication and/or submission, and redundancy, have been completely observed by the authors.

#### **OPEN ACCESS**

©2024 The author(s). This article is licensed under a Creative Commons Attribution 4.0 International License, which permits use, sharing, adaptation, distribution, and reproduction in any medium or format, as long as you give appropriate credit to the original author(s) and the source, provide a link to the Creative Commons license, and indicate if changes were made. The images or other third-party material in this article are included in the article's Creative Commons license, unless indicated otherwise in a credit line to the material. If material is not included in the article's Creative Commons license and your intended use is not permitted by statutory regulation or exceeds the permitted use, you will need to obtain permission directly from the copyright holder. To view a copy of this license, visit <http://creativecommons.org/licenses/by/4.0/>

#### **PUBLISHER'S NOTE**

GJESM Publisher remains neutral with regard to jurisdictional claims in published maps and institutional affiliations.

#### **ABBREVIATIONS**

%	Percent
+	Plus sign
=	Equal sign
≠	Non equal sign
>	Strict inequality (greater than)

$\geq$	Greater equals	X5	Institutional factors
/	Per	X6	Population density
A	Alpha	Y	Real output or gross domestic product
E	Error term	Y	Year
A	Technology	Y1	Economic development
C	Constant	Y2	Deforestation

Eq	Equation
F	Simultaneous
Fig.	Figure
GDP	Gross domestic product
GRDP	Gross regional domestic product
ha	Hectare
i.e	Id est
K	Capital ability (human capital and tangible capital)
K	Number of predetermined variable in model including intercept
k	Number of predetermined variable in a given equation
KM	Kilometers
L	Workforce input
Log	Logarithm
M	Number of endogenous variable in the model
M <sup>3</sup>	Cubic meter
M	Number of endogenous variable in a given equation
Prob	Probability
R2	Correlation coefficient
SD	Standard deviation
S.E	Standard error
T	Time
TSLS	Two stage least squares
Var	Variable
X1	Education
X2	Health
X3	Mineral resources
X4	Forest resources

## REFERENCES

- Afawubo, K.; Noglo, Y.A., (2019). Remittances and deforestation in developing countries: is institutional quality paramount? *Res. Econ.*, 73(4): 304-320 **(17 pages)**.
- Albarrán, D.G., (2018). Health and economic development. *Econ. Hum. Biol.*, 31(C): 228-237 **(10 pages)**.
- Angelsen, A.; Kaimowitz, D., (1999). Rethinking the causes of deforestation: lessons from economic models. *World Bank Res. Obs.*, 14(1): 73–98 **(26 pages)**.
- Aquillas, N.A.; Mukong, A.K.; Kimengsi, J.N.; Ngangnchi, F.H., (2022). Economic activities and deforestation in the congo basin: an environmental kuznets curve framework analysis. *Environ. Challenges*, 8: 100553 **(12 pages)**.
- Aravind, J.; Kanmani, P.; Sudha, G.; Balan, R., (2016). Optimization of chromium(VI) biosorption using gooseberry seeds by response surface methodology. *Global J. Environ. Sci. Manage.*, 2(1): 61-68 **(8 pages)**.
- Atalay, R., (2015). The education and the human capital to get rid of the middle-income trap and to provide the economic development. *Procedia Soc. Behav. Sci.*, 174: 969–976 **(8 pages)**.
- Azam, M., (2019). Relationship between energy, investment, human capital, environment, and economic growth in four brics countries. *Environ. Sci. Pollut. Res.*, 26: 34388-34400 **(13 pages)**.
- Badan Pusat Statistik, (2021). *Sumatra Utara Dalam Angka*. Badan Pusat Statistik.
- Bhattarai, M.; Hammig, M., (2001). Institutions and the environmental kuznets curve for deforestation: a crosscountry analysis for latin america, africa and asia. *World Develop.*, 29(6): 995–1010 **(16 pages)**.
- Cuaresma, J.C; Heger, M., (2018). Deforestation and economic development: evidence from national borders. *Land Use Policy*. 84: e347 –e353 **(7 pages)**.
- Culas, R.J., (2007). Deforestation and the environmental kuznets curve: an institutional perspective. *Ecol. Econ.*, 61(2-3): 429–437 **(9 pages)**.
- Damette, O.; Delacote, P., (2012). On the economic factors of deforestation: what can we learn from quantile analysis?. *Econ. Model.*, 29 (6) : 2427–2434 **(8 pages)**.

- Dinas Kehutanan, (2022). Perubahan rencana strategis provinsi Sumatra utara tahun 2019-2023. Dinas Kehutanan. **(99 pages)**.
- Ewers, R.M., (2006). Interaction effects between economic development and forest cover determine deforestation rates. *Global Environ. Change*. 16(2): 161–169 **(9 pages)**.
- Gujarati, D.N.; Porter, D.C., (2009). Basic econometrics fifth edition. Mc Graw Hill Series. **(922 pages)**.
- Hao, Y.; Xu, Y.; Zhang, J.; Hu, X.; Huang, J.; Chang, C.; Guo, Y., (2018). Relationship between forest resources and economic growth : empirical evidence from china. *J. Clean Product.*, 214: 848-859 **(12 pages)**.
- Inwood, S., (2017). Agriculture, health insurance, human capital and economic development at the rural-urban-interface. *J. Rural Stud.*, 54: 1–14 **(14 pages)**.
- Kamaroellah, A.; Kutsiyah, F., (2018). Isu-isu strategi makro ekonomi. CV. Zifatama Jawara. **(286 pages)**.
- Kenzheguzin, M.B.; Yessekina, B.K., (2004). Methodological basis of forecasting of sustainable development of economic system. *Math. Comput. Simul.*, 67(4-5): 343–349 **(7 pages)**.
- Klapper, L.; El-Zoghbi, M.; Hess, J., (2016). Achieving the sustainable development goals : the role of financial inclusion. *UNSGSA*, 1–15 **(15 pages)**.
- Lambin, E.F.; Gibbs, H.K.; Heilmayr, R.; Carlson, K.M.; Fleck, L.C.; Garrett, R.D.; Waroux, Y.P.; McDermott, C.L.; McLaughlin, D.; Newton, P.; Nolte, C.; Pacheco, P.; Rausch, L.L.; Streck, C.; Thorlakson, T.; Walker, N.F., (2018). The role of supply chain initiatives in reducing deforestation. *Nature Climate Change*. 8: 109-116 **(8 pages)**.
- Lee, D.S.; Lemieux, T., (2010). Regression discontinuity designs in economics. *Econ. Lit.*, 48(2): 281–355 **(75 pages)**.
- Liscow, Z.D., (2013). Do property rights promote investment but cause deforestation? Quasi-experimental evidence from nicaragua. *J. Environ. Econ. Manage.*, 65(2) : 241–261 **(21 pages)**.
- Onyinye, N.G.; Idenyi, O.S.; Ifeyinwa, A.C., (2017). Effect of capital formation on economic growth in nigeria. *Asian J. Econ. Bus. Accounting*. 5(1) : 1–16 **(16 pages)**.
- Oryani, B.; Kamyab, H.; Moridian, A.; Azizi, Z.; Rezania, S.; Chelliapan, S., (2022). Does structural change boost the energy demand in a fossil fuel-driven economy? new evidence from iran. *Energy*. 254(C) **(12 pages)**.
- Qiang, Q.; Jian, C., (2020). Natural resource endowment, institutional quality and china’s regional economic growth. *Resour. Policy*. 66 (101644) : 1-9 **(9 pages)**.
- Raheem, I.D.; Isah, K.O.; Adedeji, A.A., (2018). Inclusive growth, human capital development and natural resource rent in ssa. *Econ. Change Restructuring*. 51 : 29–48 **(20 pages)**.
- Rahim, S.; Murshed, M.; Umarbeyli, S.; Kirikkaleli, D.; Ahmad, M.; Tufail, M.; Wahab, S., (2021). Do natural resources abundance and human capital development promote economic growth? A study on the resource curse hypothesis in next eleven countries. *Resour. Environ. Sustainability*. 4 (100018): 1–8 **(8 pages)**.
- Ravago, M.L.V.; Balisacan, A.M.; Chakravorty, U., (2015). The principles and practice of sustainable economic development: overview and synthesis. *Sustainable Econ. Develop: Resour. Environ. Institutions*. 3 -10 **(8 pages)**.
- Redmond, T.; Nasir, M.A., (2020). Role of natural resource abundance, international trade and financial development in the economic development of selected countries. *Resour. Policy*. 66(1015910): 1–15 **(15 pages)**.
- Satrianto, A.; Juniardi, E., (2023). Inclusive human development and inclusive green growth: a simultaneous approach. *J. Sustainable Develop. Planning*, 18(2), 523–530 **(8 pages)**.
- Singh, S.; Yadav, A., (2021). Interconnecting the environment with economic development of a nation. *Environ. Sustainability Econ.*, 35-60 **(26 pages)**.
- Sun, Q.; Tang, Y., (2011). The grey relational degree measurement of city’s s&t input and sustainable economic development based on the data from hunan province. *Procedia Eng.*, 21: 457–463 **(7 pages)**.
- Todaro, M.P.; Smith, S.C., (2012). Economic development. PEARSON **(829 pages)**.
- Tritsch, I.; Tourneau, F.M.Le., (2016). Population densities and deforestation in the brazilian amazon: new insights on the current human settlement patterns. *Appl. Geogr.*, 76 : 163–172 **(10 pages)**.
- Waluyo, E.A.; Terawaki, T., (2016). Environmental kuznets curve for deforestation in indonesia: an ardl bounds testing approach. *J. Econ. Cooperation Develop.*, 37(3): 87–108 **(22 pages)**.
- Wang, R.; Tan, J.; Yao, S., (2021). Are natural resources a blessing or a curse for economic development? The importance of energy innovations. *Resour. Policy*. 72: 102042 **(8 pages)**.

**AUTHOR (S) BIOSKETCHES**

**Siregar, E.S.**, Ph.D. Candidate, Faculty of Economy, Universitas Negeri Padang, Padang, Indonesia.

- Email: [ennisari056@gmail.com](mailto:ennisari056@gmail.com)
- ORCID: 0000-0002-0225-3533
- Web of Science ResearcherID: NA
- Scopus Author ID: NA
- Homepage: <http://fe.unp.ac.id/faculty/>

**Sentosa, S.U.**, Ph.D., Professor, Faculty of Economy, Universitas Negeri Padang, Padang, Indonesia.

- Email: [sriulfasentosa1961@gmail.com](mailto:sriulfasentosa1961@gmail.com)
- ORCID: 0000-0002-7630-4751
- Web of Science ResearcherID: NA
- Scopus Author ID: 57200199998
- Homepage: <http://fe.unp.ac.id/faculty/sri-ulfa-sentosa>

**Satrianto, A.**, Ph.D., Professor, Faculty of Economy, Universitas Negeri Padang, Padang, Indonesia.

- Email: [alponsatrianto@fe.unp.ac.id](mailto:alponsatrianto@fe.unp.ac.id)
- ORCID: 0000-0002-8412-8524
- Web of Science ResearcherID: NA
- Scopus Author ID: 57200204759
- Homepage: <http://fe.unp.ac.id/faculty/alpon-satrianto>

**HOW TO CITE THIS ARTICLE**

*Siregar, E.S.; Sentosa S.U.; Satrianto A., (2024). An analysis on the economic development and deforestation, 10(1): 355-368.*

DOI: [10.22034/gjesm.2024.01.22](https://doi.org/10.22034/gjesm.2024.01.22)

URL: [https://www.gjesm.net/article\\_705271.html](https://www.gjesm.net/article_705271.html)





## ORIGINAL RESEARCH ARTICLE

Ecotoxicological insight of phytochemicals, toxicological informatics, and heavy metal concentration in *Tridax procumbens* L. in geothermal areasN.B. Maulydia<sup>1</sup>, R. Idroes<sup>2\*</sup>, K. Khairan<sup>2</sup>, T.E. Tallei<sup>3</sup>, F. Mohd Fauzi<sup>4</sup><sup>1</sup> Graduate School of Mathematics and Applied Sciences, Universitas Syiah Kuala, Banda Aceh, 23111, Indonesia<sup>2</sup> Department of Pharmacy, Faculty of Mathematics and Natural Sciences, Universitas Syiah Kuala, Banda Aceh 23111, Indonesia<sup>3</sup> Department of Biology, Faculty of Mathematics and Natural Sciences, Universitas Sam Ratulangi, Manado, Indonesia<sup>4</sup> Faculty of Pharmacy, Universiti Teknologi MARA Selangor, Puncak Alam Campus, 42 300 Bandar Puncak Alam, Selangor, Malaysia

## ARTICLE INFO

## Article History:

Received 09 June 2023

Revised 13 August 2023

Accepted 22 September 2023

## Keywords:

Geothermal area

Heavy metals

Ie-Seu'um

Mount Seulawah Agam

Phytol

Tridax procumbens

## ABSTRACT

**BACKGROUND AND OBJECTIVES:** *Tridax procumbens* L. is a plant that grows abundantly in the Ie-Seu'um geothermal area in Aceh Province, Indonesia. The objective of this study is to determine metabolite compounds from *Tridax procumbens* plants in a geothermal area using qualitative and quantitative analyses. In addition, the contents of six heavy metals in plants and their toxicology were assessed using an in silico approach.**METHODS:** The ethanolic extract of *Tridax procumbens* was analyzed qualitatively using reagents to determine the contents of secondary metabolites such as flavonoids, alkaloids, tannins, steroids, triterpenoids, and saponins. In addition, quantitative analysis was conducted using gas chromatography–mass spectroscopy to obtain the chromatograms and mass spectra of the metabolite compounds of the ethanolic extract of *Tridax procumbens*, which were used in computational toxicology analysis using a simplified molecular input system in a predictor server. Atomic absorption spectrometry was conducted to confirm the contents of six heavy metals harmful to medicinal plants.**FINDINGS:** The results showed that *Tridax procumbens* from the Ie-Seu'um geothermal area, Aceh, has secondary metabolites such as flavonoids, saponins, steroids, and tannins, with phytol from diterpenoid group having the highest content (32.72 percent). Toxicological analysis showed that the compounds in the ethanolic extract of *Tridax procumbens* were nontoxic or inactive in five toxicity parameters. The other results of the heavy metal analysis showed the dominance of chromium among the other six metals tested (copper, not detected; cadmium,  $0.91 \pm 0.03$  milligram per kilogram; zinc,  $3.50 \pm 0.03$  milligram per kilogram; iron,  $4.65 \pm 0.02$  milligram per kilogram; lead,  $6.42 \pm 0.05$  milligram per kilogram; and chromium,  $13.81 \pm 0.07$  milligram per kilogram).**CONCLUSION:** This study highlights the unique secondary metabolite composition of *Tridax procumbens* under such extreme conditions and underscores the potential implications of heavy metal accumulation in plants in geothermal areas.DOI: [10.22034/gjesm.2024.01.23](https://doi.org/10.22034/gjesm.2024.01.23)This is an open access article under the CC BY license (<http://creativecommons.org/licenses/by/4.0/>).

NUMBER OF REFERENCES

47



NUMBER OF FIGURES

3



NUMBER OF TABLES

7

\*Corresponding Author:

Email: [rinaldi.idroes@usk.ac.id](mailto:rinaldi.idroes@usk.ac.id)

Phone: +6281 9737 44077

ORCID: [0000-0003-2264-6358](https://orcid.org/0000-0003-2264-6358)

Note: Discussion period for this manuscript open until April 1, 2024 on GJESM website at the "Show Article".

## INTRODUCTION

Heavy metal contamination is a potential problem in geothermal regions. Effluents containing heavy metals from geothermal energy sources are rare and difficult to interpret because of interference from geysers and other naturally existing thermal phenomena (Sabadell and Aaxtmann, 1975; Sabilillah et al., 2023). Geothermal fluids are prone to having elevated chemical concentrations, which can have a negative effect on nearby water sources. One of the hydrothermal areas in Aceh Province, Indonesia, is *le-Seu'um* (local name: hot air), which is reported to have the highest arsenic-containing hot springs with levels of  $166.73 \pm 0.0081$  microgram per liter ( $\mu\text{g/L}$ ), (Irnawati et al., 2021). *le-Seu'um* is a hot spring which is one of the manifestations of Mount Seulawah Agam with temperatures up to 86.09 degrees Celsius ( $^{\circ}\text{C}$ ), (Idroes et al., 2019). The examination of the chloride–bicarbonate–sulfate ( $\text{Cl-HCO}_3\text{-SO}_4$ ) triangle diagram and Piper diagram indicates that the hydrological characteristics and prevailing chemical composition of the fluids in *le-Seu'um* are primarily chloride based, with significant amounts of sodium, potassium, and chloride ions (Idroes et al., 2019). The potential for pollution caused by trace heavy metals originating from geothermal sources is considerable, but available field measurements are limited. The Seulawah Agam mountain is known as one of the most active volcanoes in Aceh Province, Indonesia. Aceh Province is well known for its many geothermal sites, including *le-Seu'um*, *le-Jue*, and *le-Brouk* in the Aceh Besar District. Surface manifestations of geothermal locations include thermal springs, gases or solfatara, streaming earth, altered rock, and phreatic eruptions. Geological phenomena have the ability to change ambient environmental conditions, such as temperature, moisture levels, and humidity (Idroes et al., 2019). The flora found in these geothermal regions possesses distinct characteristics and synthesizes metabolic chemicals that are associated with various health advantages (Nurasikin et al., 2020). Limited study has been conducted on plants in geothermal areas in Aceh Province. However, the findings of existing studies indicate the promising potential of these plants as candidates for pharmaceutical applications. The investigation of the possibility of utilizing weeds from geothermal zones as complementary-based therapy

warrants further exploration. Currently, published research on the exploration of geothermal medicinal plants, particularly plants from the Asteraceae family, is limited. The Asteraceae family, also known as Compositae, is considered to be among the most extensive families of flowering plants, encompassing a remarkable assemblage of over 1600 genera and approximately 25,000 species distributed across various regions of the world (Rolnik and Olas, 2021). Asteraceae has a high biodiversity that spreads across all regions in all conditions and continents, except Antarctica (Funk et al., 2005). Many species of the Asteraceae family have therapeutic properties and have been used in traditional medicine for a long time. Certain members of this family have been cultivated for over three millennia, largely for its nutritional and medicinal utilities (Rolnik and Olas, 2021). One member of this family is the plant *Tridax procumbens* L., described by Linnaeus in 1753, with various pharmaceutical and traditional uses (Ingole et al., 2022). *T. procumbens* is native to Mexico and is found southward throughout Central America and the majority of South America, demonstrating its robust capacity for proliferation and dissemination due to its extensive natural occurrence over tropical and subtropical regions worldwide (PPQ, 2018). *T. procumbens* is a perennial plant with light green color, 15–40 centimeter (cm) height, roots that emerge from nodes, stems that emerge from the base of the wood, and ovate to lanceolate hairy leaves that are 4–30 millimeter (mm) long (Powell, 1965). In the *le-Seu'um* geothermal area, *T. procumbens* can be seen around hot springs and surrounding areas (Fig. 1). The soil conditions in the geothermal area surrounding the spring of *le-Seu'um* exhibit temperatures ranging from approximately 27.16 $^{\circ}\text{C}$  to 36.13 $^{\circ}\text{C}$  (Irnawati et al., 2021). The findings of the study by Chauhan and Johnson (2008) indicated that *T. procumbens* exhibits optimal seed germination ability in temperature conditions of 35 $^{\circ}\text{C}$ /25 $^{\circ}\text{C}$  and 30 $^{\circ}\text{C}$ /20 $^{\circ}\text{C}$ . In addition, the research suggests that the seed germination of *T. procumbens* is significantly enhanced under light conditions compared to dark conditions, with a range of 58 percent (%) to 70% germination observed. This observation implies that *T. procumbens* plants thrive in geothermal environments because of their adaptive traits that enable them to tolerate soil conditions characterized by elevated temperatures.



Fig. 1: *T. procumbens* plants

Medicinal plants are often used over a long period to improve health, but this can lead to the accumulation of harmful heavy metals in the body, which can cause various health problems if not managed properly (Kandić *et al.*, 2023; Samimi and Mansouri, 2023). *T. procumbens* plants are used in traditional medicine, but research on its chemical content is limited. Currently, research using computational or *in silico* techniques is growing rapidly. Various research using *in silico* approaches such as quantitative relationship structure analysis (Noviandy *et al.*, 2023) and molecular docking to molecular dynamics (Tallei *et al.*, 2020). This currently study we conducted research that included i) qualitative (using reagents) and quantitative (using gas chromatography–mass spectroscopy (GC–MS)) phytochemical analyses of plant constituents, ii) the assessment of the heavy metal (i.e., lead (Pb), copper (Cu), chromium (Cr), cadmium (Cd), iron (Fe), and Zinc (Zn)) concentrations in the ethanolic extract of *T. procumbens*, and (iii) toxicological informatics studies using an *in silico* approach. The objective of the study is to investigate and analyze the chemical composition of *T. procumbens*, a plant species found in the *le-Seu'um* geothermal area, Aceh.

Specifically, the study aims to achieve the following objectives: confirmation of secondary metabolites, identification of dominant bioactive compounds and their toxicology using an *in silico* approach, and analysis of the heavy metal concentration of the ethanolic extract *T. procumbens*. This study was conducted in Aceh Province, Indonesia, in 2023.

## MATERIALS AND METHODS

### *Plant preparation and extraction*

*T. procumbens* was obtained from the manifestation geothermal of Seulawah Agam *le-Seu'um*, which is located at 05°32'50" north (N), 95°32'45" east (E) (Fig. 2). The plant parts that were collected include branches, leaves, and flowers. The voucher for the species was given the number B-2238 in National Research and Innovation Agency, Indonesia. To prepare the extracts, various plant parts were mixed, cleaned, air-dried at room temperature, and then ground into powder. Maceration at a ratio of 1:10 weight: volume (w:v) for three days resulted in the production of an ethanolic extract. Immediately after that, extract was dried using a rotary evaporator (Butchi Rotavapor®, Switzerland), followed by a vacuum filtering process to obtain a dry extract.

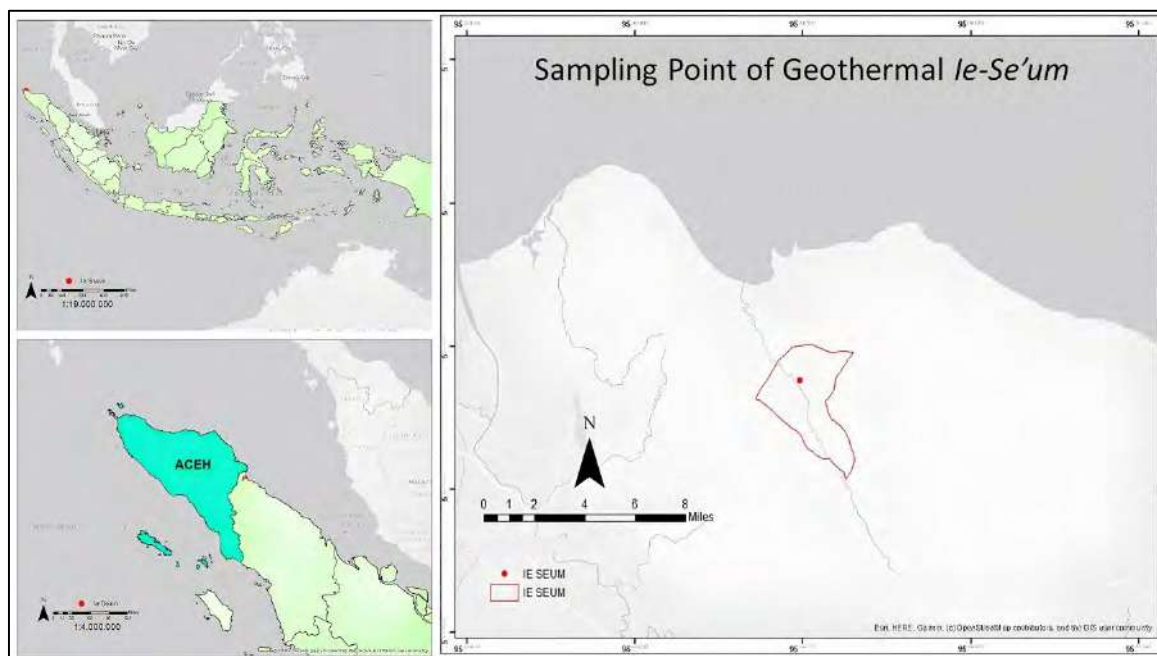


Fig. 2: Geographical location of the study area in *Ie-Seu'um*, Indonesia

#### Phytochemical analysis

Phytochemical analysis was conducted on six classes of secondary metabolites, namely, flavonoids, tannins, saponins, terpenoids, steroids, and alkaloids. The method used in this study was based on the method used by Harbone (1987), with slight modifications.

#### Gas chromatography–mass spectroscopy (GC–MS) analysis

GC–MS was conducted using a TRACE 1310 GC and single quadrupole (ISQ) 7000 equipped with a TraceGOLD TG-35MS column- 30 meter (m) × 0.25 millimeter (mm) × 0.25 micrometer (μm); Thermo Fisher Scientific, Inc., United States of America) to examine the ethanolic extracts of *T. procumbens*. The temperature of the injector was kept constant at 250°C, and the ion source temperature was adjusted to 250°C. The programmed temperature of the column was set to gradually increase from 60°C to 280°C at a rate of 10°C/minutes. Helium was used as the carrier gas at a flow rate of 1 μL/min. Mass spectra were acquired using an energy level of 75 electron volt (eV) while scanning a range of 400 to 500 atomic mass units (Amu).

#### Heavy metal analysis

The samples for heavy metal analysis were prepared by placing plant samples that weighed up to 1.00 ± 0.05 gram (g) in a tube vessel, adding 10 ± 0.1 milliliter (mL) of pure nitric acid (HNO<sub>3</sub>) (Merck, Darmstadt, Germany), and then placing the tube vessel in a microwave to destruct the sample. The destruction was carried out at 180°C for 10 minutes and then the analyte was cooled to room temperature. After the destruction step was completed, the analyte was transferred to a 25 mL volumetric flask and diluted with demineralized water. The test sample solution was analyzed using an atomic absorption spectrophotometer (AAS) (PinAAcle 900H PerkinElmer, Waltham, MA, USA). The calibration curves for the metals Pb, Cd, Cu, Cr, Fe, and Zn were established using specific wavelengths of 217.0, 220.8, 324.8, 357.9, 248.1, and 213.9 nanometer (nm), respectively. These wavelengths were employed in accordance with the guidelines from Association of Official Analytical Collaboration (AOAC) International (AOAC official method, 2022).

#### Method validation

Method validation was conducted to determine

Table 1: Method validation

No.	Parameters	Heavy metals					
		Pb	Cd	Cu	Cr	Fe	Zn
1	Slope	0.0402	0.2422	0.0991	0.0519	0.0526	0.0419
2	Intercept	0.0001	0.0050	-0.0005	$1.77 \times 10^{-5}$	0.0007	0.0101
3	R <sup>2</sup>	0.9999	0.9999	0.9999	0.9999	0.9999	0.9999
4	LoD	0.018	0.016	0.022	0.019	0.021	0.019
5	LoQ	0.049	0.056	0.067	0.042	0.065	0.066
6	Precision (%RSD)	1.07	1.09	1.09	1.03	0.98	1.12
7	Recovery (%R)	100.99	100.35	100.29	100.49	100.33	100.82

Table 2: SMILES structure of metabolite compounds

SMILES structure	Compound CID
<chem>CC1=CC(N=N1)(C2=CC=CC=C2)C3=CC=CC=C3</chem>	605783
<chem>C[C@@H](CCC[C@@H](C)CCC/C(=C/CO)/C)CCCC(C)C</chem>	5280435
<chem>CC(C)CCCC(C)CCCC(C)CCCC(=C)C=C</chem>	10446
<chem>CCCCC/C=C\C(C)CCCCCOC(=O)C</chem>	5363222
<chem>CCCCCCCCCCCCC(=O)OC</chem>	8181
<chem>CC(C)(C)C1=CC(=CC(=C1O)C(C)(C)CCC(=O)OC</chem>	62603
<chem>CCCCCCCCCCCCC(=O)O</chem>	985
<chem>CCCCC/C=C\C#CC#C[C@H](C=C)O</chem>	5469789
<chem>CCCCC/C=C\C#CCCCC(=O)O</chem>	5282800
<chem>CC/C=C\C/C=C\C/C=C\C#CCCCC(=O)O</chem>	5280934

the reliability of the research results (Winarsih *et al.*, 2023). To achieve linearity, six different concentration levels of each metal were determined and expressed using the coefficient of determination (R<sup>2</sup>). Method precision was determined by performing measurements six times on one concentration of standard solution to percent of relative standard deviation (%RSD), and the value of recovery was determined by performing a spike on the sample percent of recovery (%R). The values for the limits of detection (LoD) and quantification (LoQ) for each metal were determined based on the standard curve, and the measurement uncertainty for each metal was computed using the LINEST function in Microsoft Excel based on the standard deviation of concentration (Sc). As shown in Table 1, method validation exhibited a significant level of linearity and sensitivity, demonstrating acceptable levels of recovery and precision. In addition, every experiment displayed a strong R<sup>2</sup> of 0.9999. This finding suggests that the calibration curve exhibited a strong association between the standard concentration and the instrument response.

#### Toxicology computational analysis

The chemical compounds that were successfully identified using GC-MS then underwent verification for their presence in the PubChem database (Rachmawati *et al.*, 2022). Data regarding the PubChem identifier using the compound identifier (CID), chemical formula, simplified molecular input line-entry system (SMILES), and two-dimensional structure were collected (Kim *et al.*, 2023). Then, toxicology computational analysis was conducted using a ProTox-II system (Banerjee *et al.*, 2018). Toxicology assessments were conducted using the SMILES structure presented in Table 2. Four toxicity endpoints (carcinogenicity, immunotoxicity, mutagenicity, and cytotoxicity) and one organ toxicity (hepatotoxicity) were subjected to probability calculations with values ranging from 0 to 1, and the final results were either active or inactive.

## RESULTS AND DISCUSSION

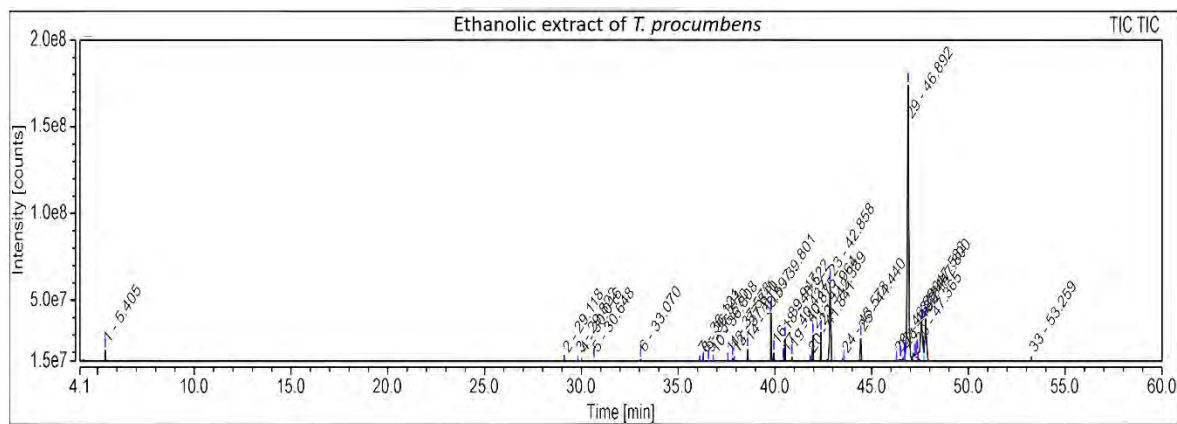
#### Qualitative phytochemical analysis

Qualitative analysis commonly entails the identification of specific compounds or chemical qualities using diverse reagents, which are

Table 3: Phytochemical analysis using qualitative methods

No	Secondary metabolites	Results
1	Alkaloids	-
2	Flavonoids	+
3	Saponins	+
4	Steroids	+
5	Triterpenoids	-
6	Tannins	+

(-) absent; (+) present

Fig. 3: Total ion chromatogram of *T. procumbens* extract

specialized chemicals employed for testing purposes (Rachmawati et al., 2022). Phytochemical analysis showed that *T. procumbens* plants from the *le-Seu'um* geothermal area in Aceh Province have secondary metabolites such as flavonoids, saponins, steroids, and tannins (Table 3). These results corroborate that there is diversity in the content of secondary metabolite compounds in these plants. In the study conducted by Ingole et al. (2022), it was found that the metabolite compounds derived from *T. procumbens* include alkaloids, flavonoids, saponins, tannins, steroids, terpenoids, essential oils, carbohydrates, carotenoids, and various other chemicals. The study by Christudas et al. (2012) showed that the phytochemical screening of *T. procumbens* using different solvents such as petroleum ether, chloroform, and ethanol extract showed the presence of alkaloids, tannins, steroids, purines, carbohydrates, and proteins. The diversity of the active compounds found in *T. procumbens* may hold promise as a complementary medicine. Recent studies have shown that *T. procumbens* extracts have several pharmacological activities, including

antihyperuricemic, antioxidant, antibacterial, and antifungal activities (Andriana et al., 2019).

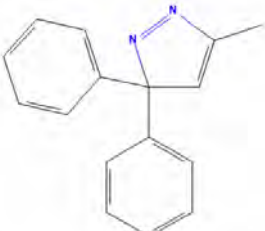
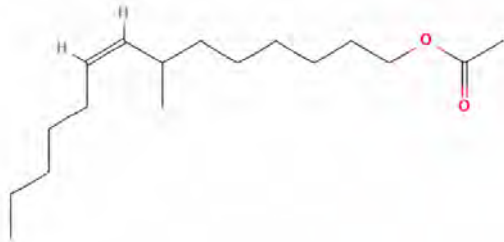
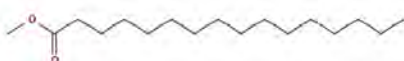
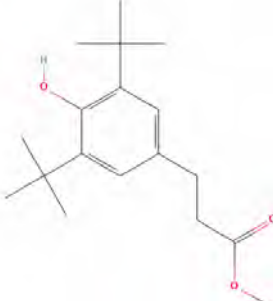
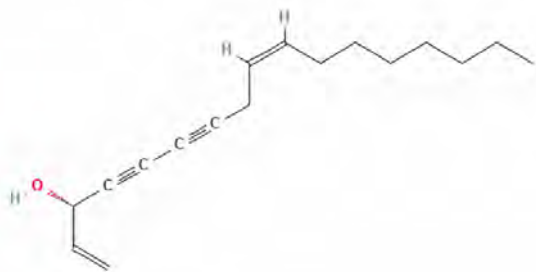
#### Quantitative phytochemical analysis

Gas chromatography–mass spectroscopy analysis was performed using a nonpolar column. The results showed 32 peaks in the total ion chromatogram analysis with a running time of 60 min (Fig. 3). The results showed one highest peak with a retention time of 46.98 min known as phytol. Another study also found phytol in *T. procumbens* mainly in the leaf essential oil with a percentage of 0% to 7.2% (Coulibaly et al., 2020).

In addition, metabolite compounds with a percentage area >2% are classified in Table 4. Terpenoids (neophytadiene and phytol) and fatty acids (hexadecanoic acid methyl ester, n-hexadecanoic acid, 10(E),12(Z)-conjugated linoleic acid, and 9,12,15-octadecatrienoic acid, (Z,Z,Z)) dominated these results.

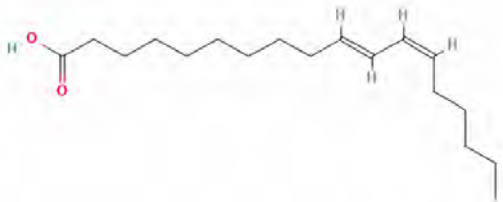
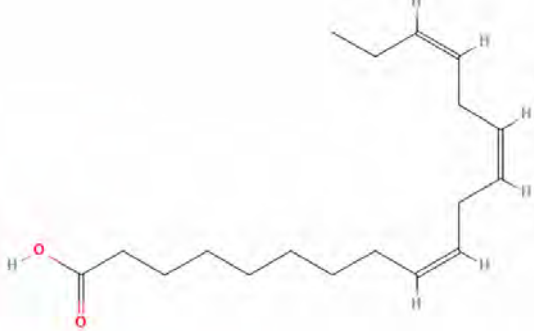
As shown in Table 4, the compound with the highest relative percentage was phytol. Phytol is an isoprenoid alcohol with 20 carbon atoms and

Table 4: Chemical profiling of the *T. procumbens* extract using GC-MS

Compound name	Retention time (min)	Relative area (%)	Molecular formula	Chemical structure
3,3-Diphenyl-5-methyl-3H-pyrazole	30.648	3.12	C <sub>16</sub> H <sub>14</sub> N <sub>2</sub>	
Neophytadiene	39.801	4.14	C <sub>20</sub> H <sub>38</sub>	
7-Methyl-Z-tetradecen-1-ol acetate	40.522	2.78	C <sub>17</sub> H <sub>32</sub> O <sub>2</sub>	
Hexadecanoic acid, methyl ester	41.964	3.32	C <sub>17</sub> H <sub>34</sub> O <sub>2</sub>	
Benzenepropanoic acid, 3,5-bis(1,1-dimethylethyl)-4-hydroxy-, methyl ester	42.389	3.73	C <sub>18</sub> H <sub>28</sub> O <sub>3</sub>	
n-Hexadecanoic acid	42.858	9.23	C <sub>16</sub> H <sub>32</sub> O <sub>2</sub>	
(S,Z)-Heptadeca-1,9-dien-4,6-diyn-3-ol	44.44	3.72	C <sub>17</sub> H <sub>24</sub> O	

Chemical Characterization of *Tridax procumbens* L

Continued Table 4: Chemical profiling of the *T. procumbens* extract using GC–MS

Compound name	Retention time (min)	Relative area (%)	Molecular formula	Chemical structure
Phytol	46.892	32.72	C <sub>20</sub> H <sub>40</sub> O	
10(E),12(Z)-Conjugated linoleic acid	47.582	7.94	C <sub>18</sub> H <sub>32</sub> O <sub>2</sub>	
9,12,15-Octadecatrienoic acid, (Z,Z,Z)-	47.8	6.81	C <sub>18</sub> H <sub>30</sub> O <sub>2</sub>	

1 double bond (C<sub>20</sub>H<sub>40</sub>O) that is known to have the highest peak area with a value of 32.72%. Phytol is a compound of the terpenoid group, that is, acyclic diterpenoids, which also metabolize chlorophyll in plants; therefore, it is widely available in nature. Chlorophyll is the most abundant photosynthetic pigment in higher plants (Gutbrod *et al.*, 2019). During the aging process, chlorophyll is hydrolyzed to release phytol and free chlorophyllide in a ratio of 1:1 (Ischebeck *et al.*, 2006). As shown in the results of the GC–MS analysis, the most abundant compound was phytol. It can be connected that *T. procumbens* weed plants in the *Je-Seu'um* geothermal area have a high chlorophyll content and will be useful for the surrounding environment because it increases oxygen levels in the air. Phytol is also known as the precursor of synthetic vitamin E and vitamin K (Santos *et al.*, 2013), which are known to be toxic to breast cancer cells, that is, Michigan Cancer Foundation-7 (MCF7), and have the potential to provide antioxidant and antinociceptive effects (Pejin

*et al.*, 2014). Pharmacokinetic analysis of phytol was found to have good characteristics as a drug candidate and can be used against enzyme targeted *Staphylococcus aureus* (Maulydia *et al.*, 2023). Other substances in Table 2 support the uniqueness of *T. procumbens* growing in severe environments, such as in geothermal areas, because geographical origin influences the makeup of bioactive compounds (Imelda *et al.*, 2024).

#### Heavy metal concentrations

Metals can be categorized into two groups based on their relevance to human metabolism: essential and nonessential. Metals such as Fe, Cu, and Zn play crucial roles in human metabolism, but excessive amounts of these metals can lead to hazardous effects (Samimi and Nouri, 2023). Metals such as Pb, Cd, and mercury (Hg) lack nutritional and helpful properties for metabolism and can exert hazardous effects on living organisms even when present in extremely low amounts (Varol and

Table 5: Heavy metal contents of the ethanolic extract of *T. procumbens*

Sample	Heavy metal concentrations $\pm$ Sc milligram per kilogram (mg/kg)					
	Pb	Cu	Cr	Cd	Fe	Zn
Ethanolic extract of <i>T. procumbens</i>	6.42 $\pm$ 0.05	N.D.	13.81 $\pm$ 0.07	0.91 $\pm$ 0.03	4.65 $\pm$ 0.02	3.50 $\pm$ 0.03

N.D.= not detected

Table 6: Heavy metal limits and adverse effects

Metals	WHO recommended limits for toxic metals in herbal medicines and products	Possible adverse effects on the human body	Sources
Cu	-	Nausea, vomiting, and diarrhea	Balali-Mood <i>et al.</i> , 2021
Cd	0.3 mg/kg	Kidney dysfunction, prostate, breast cancer, osteomalacia, and reproductive deficiencies	Naseri <i>et al.</i> , 2021
Cr	-	Respiratory irritation, lung damage, and cancer	Naseri <i>et al.</i> , 2021
Fe	-	Nausea, vomiting, and diarrhea	Balali-Mood <i>et al.</i> , 2021
Zn	-	Nausea, vomiting, and diarrhea	Balali-Mood <i>et al.</i> , 2021
Pb	10 mg/kg	Developmental delays in children, anemia, and damage to the nervous system	Naseri <i>et al.</i> , 2021

Sunbul, 2020; Sulistyowati *et al.*, 2022; Samimi *et al.*, 2023; Nurhasanah *et al.*, 2023; Samimi, 2024). Heavy metals can be present in small amounts in soil and plants because living organisms need certain metals to perform metabolic processes. According to the validated assay method, this study presents the quantities of the heavy metals found in the ethanolic extract of *T. procumbens* leaves taken from *le-Seu'um*, as shown in Table 5.

The validated methodology was utilized to assess the amounts of Pb, Cu, Cr, Fe, Zn, and Cd in the geothermal area known as *le-Seu'um* by employing AAS. As shown in Table 5, the heavy metal concentrations in the ethanolic extract of *T. procumbens* in *le-Seu'um* were Cu, not detected; Cd, 0.91 mg/kg; Zn, 3.50 mg/kg; Fe, 4.65 mg/kg; Pb, 6.42 mg/kg; and Cr, 13.81 mg/kg. Of the six metals found in the ethanolic extract of *T. procumbens*, chromium (Cr: electron configuration: [Ar] 3d<sup>5</sup>4s<sup>1</sup>) had the highest concentration of 13.81 mg/kg. Cr is a trace element that is essential for the metabolism of glucose. Research conducted on both humans and animals has shown evidence for the crucial significance of small quantities of Cr(III) 50  $\mu$ g/day to 200  $\mu$ g/day in regulating proper glucose metabolism. The administration of substances through the oral route does not pose a significant risk of toxicity (Dayan and Paine, 2001). Although Cr(III) interacts

with biomolecules such as deoxyribonucleic acid, its limited capacity to traverse cell membranes has been linked to its diminished biological and toxicological effects. Currently, conclusive research that establishes the indispensability of chromium in biomolecular or physiological mechanisms is lacking (Pavesi and Moreira, 2020). Shamsul and Mangaonkar (2010) reported that *T. procumbens* plants from India have the highest amounts of Cu at 29.96 ppm; Pb, 6.48 ppm, and Cd, 0.46 ppm. Existing literature does not provide any specific information regarding the impact of heavy metals present in *T. procumbens* L. on human health. Additional investigation is required to ascertain the potential health implications associated with the consumption of *T. procumbens* L. that is contaminated with heavy metals. According to the guidelines provided by the World Health Organization (WHO), there are specific restrictions imposed on the presence of hazardous metals such as Cu and Pb in medicines and herbal products. The suggested limits set by WHO state that the permissible levels of Cu should not exceed 0.3 mg per/kg and the maximum allowable concentration of Pb should not exceed 10 mg/kg (WHO, 2007). On the basis of the available evidence, the concentrations of the metals present in the ethanol extract of *T. procumbens* did not exceed the set limits of Cu (not detected) and Pb (6.42  $\pm$

Table 7: Toxicology prediction of metabolite compounds in *T. procumbens*

Compound name	Hepatotoxicity		Carcinogenicity		Immunotoxicity		Mutagenicity		Cytotoxicity		LD <sub>50</sub> (mg/kg)	Toxicity class
	Pred.	Prob.	Pred.	Prob.	Pred.	Prob.	Pred.	Prob.	Pred.	Prob.		
3,3-Diphenyl-5-methyl-3H-pyrazole	Inactive	0.51	Active	0.59	Inactive	0.99	Inactive	0.54	Inactive	0.76	1000	4
Phytol	Inactive	0.79	Inactive	0.76	Inactive	0.99	Inactive	0.97	Inactive	0.85	5000	5
Neophytadiene	Inactive	0.79	Inactive	0.73	Inactive	0.99	Inactive	0.98	Inactive	0.81	5050	6
7-Methyl-Z-tetradecen-1-ol acetate	Inactive	0.76	Active	0.50	Inactive	0.88	Inactive	0.98	Inactive	0.74	3460	5
Hexadecanoic acid, methyl ester	Inactive	0.58	Inactive	0.55	Inactive	0.99	Inactive	0.98	Inactive	0.73	5000	5
Benzenepropanoic acid, 3,5-bis(1,1-dimethylethyl)-4-hydroxy-, methyl ester	Active	0.55	Inactive	0.60	Inactive	0.96	Inactive	0.90	Inactive	0.77	5000	5
n-Hexadecanoic acid	Inactive	0.52	Inactive	0.63	Inactive	0.99	Inactive	1	Inactive	0.74	900	4
(S,Z)-Heptadeca-1,9-dien-4,6-dien-3-ol	Inactive	0.69	Inactive	0.61	Inactive	0.69	Inactive	0.95	Inactive	0.80	8000	6
10(E),12(Z)-Conjugated linoleic acid	Inactive	0.55	Inactive	0.64	Inactive	0.98	Inactive	1	Inactive	0.71	3200	5
9,12,15-Octadecatrienoic acid, (Z,Z,Z)-	Inactive	0.54	Inactive	0.63	Inactive	0.99	Inactive	0.95	Inactive	0.71	10000	6

Pred = Prediction  
 Prob = Probability  
 LD<sub>50</sub> = Lethal dose 50%

0.05 mg/kg). These metal contents as chemical compounds may also have harmful effects on the human body if taken in large quantities (Samimi and Shahriari Moghadam, 2021). Some of these illnesses are chronic, with gastrointestinal issues being the most frequent (Table 6).

Similar findings regarding the presence of heavy metals in *Chromolaena odorata* (local name: *seurapoh*) leaves were reported by Abubakar et al., (2023), who found Cd ( $0.0219 \pm 0.005$ ) and Pb of 0.0181 to 0.0356 mg/kg, but no As or Hg. The ability of plants to absorb and utilize heavy metals in their metabolism may explain the discrepancy in the results of the two analyses. *T. procumbens* has been shown to possess significant bioremediation capabilities, particularly in the removal of heavy metals such as Cr, Cu, Pb, and Cd from soil that has been contaminated by industrial effluents (Govarthanan et al., 2016). *T. procumbens* is also reported to have the ability to absorb heavy metals in large quantities. The desiccated leaves of *T. procumbens* can remove 91% of copper from a synthetic metal solution at pH 5.0 and 250 rpm with constant stirring. This adsorbent is an excellent choice for the adsorption of heavy metal ions in wastewater stream, including copper ions (Karthika et al., 2010). Due to its favorable characteristics, *T. procumbens* has potential as a viable option for the implementation of phytoremediation initiatives in regions characterized by significant levels of heavy metal contamination. It is essential to note that the risks associated with heavy metal contamination in geothermal regions can vary depending on the location and quantity of contamination. Consequently, it is essential to conduct field measurements and research to better comprehend the environmental issue and its potential health dangers. This research is needed to explore the potential and safety of plants in geothermal areas if they are to be used as traditional medicines.

#### Ecotoxicological analysis

The GC-MS analysis revealed the abundance of compounds in the ethanol extract of *T. procumbens*. Some of these compounds are hazardous to other organisms, such as humans, animals, microbes, and plants. Ecotoxicology of secondary metabolite compounds in plants investigates the potential impact of these compounds on ecosystems and the

creatures that inhabit them. Ecotoxicology is one of the fields of science that studies the impact of chemicals or other pollutants on the environment and living organisms. One approach in measuring the toxicity impact of these substances is using an *in silico* approach (CDESCS, 2014). The *in silico* approach in ecotoxicology refers to the use of software and computers to predict the potential impact of a substance on organisms and ecosystems without the need to conduct direct trials on living organisms (Benfenati, 2013). *T. procumbens* is frequently used as a traditional medicine, and the toxicological discussion in this paper refers to the human body. In this particular study, the ecotoxicology of the secondary metabolites from the ethanolic extracts of *T. procumbens* was analyzed using a ProTox-II system. The ProTox-II model utilizes a combination of molecular similarity, fragment propensities, most frequent features, and machine learning techniques, specifically employing a cross-validation method known as fragment similarity-based cluster. This approach involves the use of 33 different models to predict a range of toxicity endpoints, including acute toxicity, hepatotoxicity, cytotoxicity, carcinogenicity, mutagenicity, immunotoxicity, adverse outcomes in Tox21 pathways, and toxicity targets (Banerjee et al., 2018). Table 7 shows the results of the toxicity prediction against five toxicity targets, showing the dominance of nontoxic. The results of the hepatotoxic analysis showed that the compound 3,5-bis(1,1 dimethylethyl)-4-hydroxy-,methyl ester has an active potential with a probability of 0.55. Next, 3,3-diphenyl-5-methyl-3H-pyrazole with potential toxicity because it is carcinogenic with a probability of 0.59. The results of other tests show that all compounds have nontoxic potential in immunotoxicity, mutagenicity, and cytotoxicity. Toxicity examination also supported by the results of the lethal dose 50% ( $LD_{50}$ ), which is the dose that causes 50% of subjects to die from a chemical after exposure in milligrams per kilogram of body weight. Toxicity classes are defined according to the globally harmonized chemical labeling classification system (GHS) ranging from class I (fatal) to class VI (nontoxic). Secondary metabolites from *T. procumbens* showed class 4 (harmful if swallowed  $300 < LD_{50} \leq 2000$ ), class 5 (may be harmful if swallowed  $2000 < LD_{50} \leq 5000$ ), and class 6 (nontoxic  $LD_{50} > 5000$ ). Research on acute oral toxicity studies in albino mice has been

conducted on extracts of *T. procumbens*, and the results showed that they did not cause acute toxicity or severe liver damage (Burgos-Pino et al., 2023). This supports the evidence that *T. procumbens* extracts are safe to consume at controlled doses. According to the findings of this investigation, toxicological informatics has been demonstrated to have the capability to determine the toxicity of the chemicals present in the ethanol extracts of *T. procumbens*. Understanding the aforementioned subject matter is of utmost significance because of its potential to offer comprehensive understanding of the adverse effects of metabolite compounds from plants on human health resulting from the consumption of traditional medicine and exposure to the environment.

### CONCLUSION

*T. procumbens* is a plant species that can be found in the *Ie-Seu'um* geothermal area in Aceh Province, Indonesia. The primary purpose of this research is to determine whether this plant possesses secondary metabolites and to evaluate the plant's potential for usage in medical and therapeutic applications. Secondary metabolites are chemical substances produced by plants, and they frequently participate in a wide variety of biological processes. The research demonstrated that *T. procumbens*, which was collected from the geothermal region specified, contains secondary metabolites. These secondary metabolites include tannins, steroids, and saponins. It is important to note the presence of these chemicals because, in many cases, diverse pharmacological and therapeutic qualities are linked to them. The discovery of these secondary metabolites indicates that *T. procumbens* may have the potential for a variety of uses in the fields of medicine and therapy. Traditional medicine, medicines, and various other healthcare-related applications could all fall under this category of potential uses. The research highlights the presence of the diterpenoid phytol as one of the secondary metabolites that were found. The highest concentration of phytol was 32.72%. It is known that phytol possesses bioactive qualities, and the fact that there is a large amount of it in *T. procumbens* suggests that it may play a significant role in the pharmacological actions of the plant. This lends credence to the hypothesis that phytol-rich extracts of *T. procumbens* may provide a number of advantageous health effects.

In addition, an investigation of the presence of heavy metals in *T. procumbens* was conducted using samples taken from the geothermal region, and a number of heavy metals were found. This aspect of the research is very important because it helps in determining whether *T. procumbens* is safe to use and whether it is suitable for a variety of applications. Understanding the presence of heavy metals is vital, particularly if the plant will be used for medical or nutritional purposes, because excessive amounts of heavy metals can be harmful to one's health. It is imperative to emphasize the significance of conducting studies of this nature to establish a cohesive connection between the state of a plant and the possible toxicity associated with its metabolite composition. The subsequent procedure involves performing tests on the biological activity of *T. procumbens* plants to verify their therapeutic potential and enhance their efficacy for medicinal purposes.

### ACKNOWLEDGMENT

This research was funded by Kementerian Pendidikan, Kebudayaan, Riset dan Teknologi Nasional through "Program Magister Menuju Doktor Sarjana Unggul" scheme, grant number: [95/UN11.2.1/PT.01.03/DRPM/2022].

### CONFLICT OF INTEREST

The authors declare that there is no conflict of interests regarding the publication of this manuscript. In addition, ethical issues such as plagiarism, informed consent, misconduct, data fabrication and/or falsification, double publication and/or submission, and redundancy have been completely observed by the authors.

### OPEN ACCESS

©2024 The author(s). This article is licensed under a Creative Commons Attribution 4.0 International License, which permits use, sharing, adaptation, distribution and reproduction in any medium or format, as long as you give appropriate credit to the original author(s) and the source, provide a link to the Creative Commons license, and indicate if changes were made. The images or other third-party material in this article is included in the article's Creative Commons license, unless indicated otherwise in a credit line to the material. If material

is not included in the article's Creative Commons license and your intended use is not permitted by statutory regulation or exceeds the permitted use, you will need to obtain permission directly from the copyright holder. To view a copy of this license, visit: <http://creativecommons.org/licenses/by/4.0/>

#### PUBLISHER'S NOTE

GJESM Publisher remains neutral with regard to jurisdictional claims in published maps and institutional affiliations.

#### ABBREVIATIONS

%	Percent	$HNO_3$	Nitric acid
°C	degrees Celsius	<i>iSQ</i>	Single quadropole
AAS	Atomic absorption spectrometry	$LD_{50}$	Lethal dose 50%
AOAC	Association of Official Analytical Collaboration	<i>LoD</i>	Limits of detection
<i>Amu</i>	Atomic mass units	<i>LoQ</i>	Limits of quantification
<i>Cd</i>	Cadmium	<i>m</i>	Meter
<i>CDESCS</i>	Committee on the Design and Evaluation of Safer Chemical Substitutions	<i>MCF7</i>	Michigan cancer foundation-7
<i>CID</i>	Compound identifier	<i>mg/kg</i>	Milligram per kilogram
$Cl-HCO_3-SO_4$	Chloride-bicarbonate-sulfate	<i>Min</i>	Minute
<i>cm</i>	Centimeter	<i>mL</i>	Milliliter
<i>Cr</i>	Chromium	<i>mm</i>	Millimeter
<i>Cu</i>	Copper	<i>N</i>	North
<i>E</i>	East	<i>N.D.</i>	Not detected
<i>eV</i>	Electron volt	<i>nm</i>	Nanometer
<i>Fe</i>	Iron	<i>Pb</i>	Lead
<i>g</i>	Gram	<i>pH</i>	Power of hydrogen
<i>GC-MS</i>	Gas chromatography-mass spectroscopy	<i>Ppm</i>	Part per million
<i>GHS</i>	Globally harmonized chemical labeling classification system	<i>Pred</i>	Prediction
<i>Hg</i>	Mercury	<i>Prob</i>	Probability
		<i>R</i>	Recovery
		$R^2$	Coefficient of determination
		<i>rpm</i>	Rotation per minutes
		<i>RSD</i>	Relative standard deviation
		<i>Sc</i>	Standard deviation of concentration
		<i>SMILES</i>	Simplified molecular input line-entry system
		w:v	Weight:volume
		<i>WHO</i>	World Health Organization
		<i>Zn</i>	Zinc
		$\mu g/L$	Microgram per liter
		$\mu m$	Micrometer

## REFERENCES

- Abubakar, A.; Yusuf, H.; Syukri, M.; Nasution, R.; Yusuf, M., Idroes, R., (2023). Heavy metals contamination in geothermal medicinal plant extract; *Chromolaena odorata* Linn. *Global J. Environ. Sci. Manage.* 9: 995–1004 (10 Pages).
- Andriana, Y.; Xuan, T.D.; Quy, T.N.; Minh, T.N.; Van, T.M.; Viet, T.D., (2019). Antihyperuricemia, antioxidant, and antibacterial activities of *Tridax procumbens* L. *Foods* 8: 1–12 (12 Pages).
- AOAC, (2002). AOAC official method 999.10, in: Evaluation. AOC International. 18–20 (3 pages).
- Balali-Mood, M.; Naseri, K.; Tahergorabi, Z.; Khazdair, M.R.; Sadeghi, M., (2021). Toxic mechanisms of five heavy metals: mercury, lead, chromium, cadmium, and arsenic. *Front. Pharmacol.*, 12, 1–19 (19 Pages).
- Banerjee, P.; Eckert, A.O.; Schrey, A.K.; Preissner, R., (2018). ProTox-II: A webserver for the prediction of toxicity of chemicals. *Nucleic Acids Res.*, 46: W257–W263.
- Benfenati, E., (2013). In silico methods for predicting drug toxicity, methods in molecular biology. Springer. 1425: 237-304 (68 pages).
- Burgos-Pino, J.; Gual-Orozco, B.; Vera-Ku, M.; Loría-Cervera, E.N.; Guillermo-Cordero, L.; Martínez-Vega, P.P.; Torres-Tapia, L.W.; Castro-Valencia, K.; Peraza-Sánchez, S.R.; Gamboa-León, R., (2023). Acute oral toxicity in BALB/C mice of *Tridax procumbens* and *Allium sativum* extracts and (3s)-16,17-didehydrofalcarinol. *J. Ethnopharmacol.*, 301: 115840.
- Chauhan, B.S.; Johnson, D.E., (2008). Germination Ecology of two troublesome asteraceae species of rainfed rice: siam weed (*Chromolaena odorata*) and coat buttons (*Tridax procumbens*). *Weed Sci.* 56, 567–573 (7 Pages).
- Christudas, S.; Kulathivel, T.M.; Agastian, P., (2012). Phytochemical and antibacterial studies of leaves of *Tridax procumbens* L. *Asian Pac. J. Trop. Biomed.*, 2: S159–S161 (3 pages).
- CDESCS, (2014). A framework to guide selection of chemical alternatives. Committee on the Design and Evaluation of Safer Chemical Substitutions. The National Academic Press (281 pages).
- Coulibaly, A.; Soro, Y.; Siaka, S.; Nea, F.; Tonzibo, Z.F., (2020). Chemical variability of essential oils from the leaves of *Tridax procumbens* linn (Asteraceae) from five cities of Côte d'Ivoire. *Int. J. Biol. Chem. Sci.*, 14: 1843–1852 (10 pages).
- Dayan, A.; Paine, A.J., (2001). Mechanisms of chromium toxicity, carcinogenicity and allergenicity: Review of the literature from 1985 to 2000. *Hum. Exp. Toxicol.*, 20: 439–451 (13 Pages).
- Funk, V.A.; Bayer, R.J.; Keeley, S.; Chan, R.W.L.; Gemeinholzer, B.; Schilling, E.; Panero, J.L.; Baldwin, B.G.; Garcia-Jacas, N.; Susanna, A.; Jansen, R.K. (2005). Everywhere but antarctica: using a supertree to understand the diversity and distribution of the compositae. *Biol.Skr.*, 55: 343-373 (32 pages).
- Govarthanan, M.; Mythili, R.; Selvankumar, T.; Kamala-Kannan, S.; Rajasekar, A.; Chang, Y.C., (2016). Bioremediation of heavy metals using an endophytic bacterium *Paenibacillus* sp. RM isolated from the roots of *Tridax procumbens*. *3 Biotech.* 6: 1–7 (7 Pages).
- Gutbrod, K.; Romer, J.; Dörmann, P., (2019). Phytol metabolism in plants. *Prog. Lipid Res.*, 74: 1–17 (17 pages).
- Harborne, J.B., (1987). *Phytochemical methods: A guide to modern techniques of plant analysis*. Springer Dordrecht (300 pages).
- Idroes, R.; Yusuf, M.; Saiful, S.; Alatas, M.; Subhan, S.; Lala, A.; Muslem, M.; Suhendra, R.; Idroes, G.M.; Marwan, M.; Mahlia, T.M.I., (2019). Geochemistry exploration and geothermometry application in the north zone of seulawah agam, Aceh Besar District, Indonesia. *Energies.* 12: 4442 (17 pages).
- Imelda, E.; Khairan, K.; Lubis, R.R.; Taufik, K.; Rinaldi, I., (2024). Impact of environmental and geographical position on the chemometric classification of ethanol extracts from *Isotoma longiflora* leaves. *Global J. Environ. Sci. Manage.* 10: 1–14 (14 pages).
- Ingole, V. V.; Mhaske, P.C.; Katade, S.R., (2022). Phytochemistry and pharmacological aspects of *Tridax procumbens* (L.): A systematic and comprehensive review. *Phytomed. Plus.* 2: 100199 (26 pages).
- Irnawati, I.; Idroes, R.; Zulfiani, U.; Akmal, M.; Suhartono, E.; Safitri, E.; Jalil, Z., (2021). Assessment of arsenic levels in water, sediment and human. *Water*, 13(17): 23 (12 pages).
- Ischebeck, T.; Zbierzak, A.M.; Kanwischer, M.; Dörmann, P., (2006). A salvage pathway for phytol metabolism in *Arabidopsis*. *J. Biol. Chem.*, 281: 2470–2477 (8 pages).
- Kandić, I.; Kragović, M.; Petrović, J.; Janačković, P.; Gavrilović, M.; Momčilović, M.; Stojmenović, M., (2023). Heavy metals content in selected medicinal plants produced and consumed in Serbia and their daily intake in herbal infusions. *Toxics.* 11: 1–19 (19 Pages).
- Karthika, T.; Thirunavukkarasu, A.; Ramesh, S., (2010). Biosorption of copper from aqueous solutions using *Tridax procumbens*. *Recent Res. Sci. Technol.*, 2: 86–91 (6 pages).
- Kim, S.; Chen, J.; Cheng, T.; Gindulyte, A.; He, J.; He, S.; Li, Q.; Shoemaker, B.A.; Thiessen, P.A.; Yu, B.; Zaslavsky, L.; Zhang, J.; Bolton, E.E., (2023). PubChem 2023 update. *Nucleic Acids Res.* 51: D1373–D1380 (7 Pages).
- Mauludya, N.B.; Khairan, K.; Noviandy, T.R., (2023). Prediction of pharmacokinetic parameters from ethanolic extract mane leaves (*Vitex pinnata* L.) in geothermal manifestation of seulawah agam le-Seu'um, Aceh. *Malacca Pharm.*, 1: 16–21 (6 pages).

- Naseri, K.; Salmani, F.; Zeinali, M.; Zeinali, T., (2021). Health risk assessment of Cd, Cr, Cu, Ni and Pb in the muscle, liver and gizzard of hen's marketed in East of Iran. *Toxicol. Reports*, 8: 53–59 (7 Pages).
- Ningsih, D.S.; Celik, I.; Abas, A.H.; Bachtiar, B.M.; Kemala, P., (2023). A review of the ethno-dentistry activities of *Calotropis gigantea*. *Malacca Pharm.*, 1: 8–15 (8 pages).
- Noviandy, T.R.; Maulana, A.; Idroes, G.M.; Mauludya, N.B., (2023). Integrating genetic algorithm and lightgbm for qsar modeling of acetylcholinesterase inhibitors in alzheimer's disease drug discovery. *Malacca Pharm.*, 1: 48–54 (7 pages).
- Nurhasanah; Sulistyowati, L.; Riani, E.; Cordova, M.R., (2023). Cadmium and lead uptake by wild swamp eel in the populous river. *Global J. Environ. Sci. Manage.*, 9(3): 497-514 (18 pages).
- Pavesi, T.; Moreira, J.C., (2020). Mechanisms and individuality in chromium toxicity in humans. *J. Appl. Toxicol.*, 40: 1183–1197 (15 Pages).
- Pejin, B.; Savic, A.; Sokovic, M.; Glamoclija, J.; Ciric, A., (2014). Further in vitro evaluation of antiradical and antimicrobial activities of phytol. *Nat. Prod. Res.*, 37–41 (5 pages).
- Powell, A.M., (1965). Taxonomy of tridax (Compositae). *Brittonia*, 17: 47–96 (50 pages).
- PPQ, (2018). Weed Risk Assessment for *Tridax procumbens* L. (Asteraceae) – Coat buttons. United States Department of Agriculture, Animal and Plant Health Inspection Service, Plant Protection and Quarantine (PPQ), New York (26 pages).
- Rachmawati, R.; Idroes, R.; Suhartono, E.; Mauludya, N.B.; Darusman, D., (2022). In silico and in vitro analysis of *tacca tubers* (*Tacca leontopetaloides*) from Banyak Island, Aceh Singkil Regency, Indonesia, as antihypercholesterolemia agents. *Molecules* 27 (14 Pages).
- Rolnik, A.; Olas, B., (2021). The plants of the asteraceae family as agents in the protection of human health. *Int. J. Mol. Sci.*, 22: 1–10 (10 pages).
- Sabilillah, A.M.; Palupi, F.R.; Adji, B.K.; Nugroho, A.P., (2023). Health risk assessment and microplastic pollution in streams through accumulation and interaction of heavy metals. *Global J. Environ. Sci. Manage.*, 9(4): 719-740 (22 pages).
- Santos, C.C.M.P.; D.M.; Salvadori, M.S.; Mota, V.G.; Costa, L.M.; Almeida, A.A.C.; Oliveira, G.A.L.; Costa, J.P.; Sousa, D.P.; Freitas, R.M.; Almeida, R.N., (2013). Antinociceptive and antioxidant activities of phytol in vivo and in vitro models. *Neurosci. J.*, 2013 (9 pages).
- Sabadell, J.E.; Axtmann, R.C., (1975). Heavy metal contamination from geothermal sources. *Environ. Health Perspect.* 12: 1–7 (7 pages).
- Samimi, M., (2024). Efficient biosorption of cadmium by *Eucalyptus globulus* fruit biomass using process parameters optimization. *Global J. Environ. Sci. Manage.*, 10(1): 1-11 (11 pages).
- Samimi, M.; Shahriari-Moghadam, M., (2021). Isolation and identification of *Delftia lacustris* Strain-MS3 as a novel and efficient adsorbent for lead biosorption: Kinetics and thermodynamic studies, optimization of operating variables. *Biochem. Eng. J.*, 173: 108091 (9 pages).
- Samimi, M.; Zakeri, M.; Alobaid, F.; Aghel, B., (2023). A Brief Review of Recent Results in Arsenic Adsorption Process from Aquatic Environments by Metal-Organic Frameworks: Classification Based on Kinetics, Isotherms and Thermodynamics Behaviors. *Nanomater.*, 13(1): 60 (12 pages).
- Samimi, M.; Mansouri, E., (2023). Efficiency evaluation of *Falcaria vulgaris* biomass in Co(II) uptake from aquatic environments: characteristics, kinetics and optimization of operational variables. *Int. J. Phytoremediation*, 1-11 (11 pages).
- Samimi, M.; Nouri, J., (2023). Optimized Zinc Uptake from the Aquatic Environment Using Biomass Derived from *Lantana Camara* L. Stem, *Pollution*, 9(4).
- Sulistyowati, L.; Nurhasanah; Riani, E.; Cordova, M.R., (2022). Heavy metals concentration in the sediment of the aquatic environment caused by the leachate discharge from a landfill. *Global J. Environ. Sci. Manage.*, 9(2): 323-336 (14 pages).
- Shamshul, S., Mangaonkar, K. V., 2010. Heavy metal analysis from *Tridax procumbens* plant powder and effect of regional variation on its copper content using ICP-AES technique Shaikh. *Anal. Chem. An Indian J.*, 9: 256–259 (4 pages).
- Tallei, T.E.; Tumilaar, S.G.; Niode, N.J.; Fatimawali, F.; Kepel, B.J.; Idroes, R.; Effendi, Y., (2020). Potential of plant bioactive compounds as SARS-CoV-2 main protease (mpro) and spike (s) glycoprotein inhibitors: A molecular docking study. *Scientifica (Cairo)*. 2020: 2020040102 (18 pages).
- Varol, M., Sünbül, M.R., 2020. Macroelements and toxic trace elements in muscle and liver of fish species from the largest three reservoirs in Turkey and human risk assessment based on the worst-case scenarios. *Environ. Res.*, 184: 109298 (8 pages).
- Winarsih, A.; Idroes, R.; Zulfiani, U.; Yusuf, M.; Mahmudi, M.; Saiful, S.; Rahman, S.A., (2023). Method validation for pesticide residues on rice grain in Aceh Besar District Indonesia using gas chromatography-electron capture detector (GC-ECD). *Leuser J. Environ. Stud.*, 1: 18–24 (7 pages).

#### AUTHOR (S) BIOSKETCHES

**Maulydia, N.B.**, M.Si., Ph.D. Candidate, Graduate School of Mathematics and Applied Sciences, Universitas Syiah Kuala, Banda Aceh, 23111, Indonesia.

- Email: [maulydiabalqis@gmail.com](mailto:maulydiabalqis@gmail.com)
- ORCID: 0009-0000-6497-5825
- Web of Science ResearcherID: NA
- Scopus Author ID: 57424387500
- Homepage: <https://usk.ac.id/>

**Idroes, R.**, Ph.D., Professor, Department of Pharmacy, Faculty of Mathematics and Natural Sciences, Universitas Syiah Kuala, Banda Aceh 23111, Indonesia.

- Email: [rinaldi.idroes@usk.ac.id](mailto:rinaldi.idroes@usk.ac.id)
- ORCID: 0000-0003-2264-6358
- Web of Science ResearcherID: S-8983-2016
- Scopus Author ID: 57192873366
- Homepage: <https://fsd.usk.ac.id/rinaldi.idroes/>

**Khairan, K.**, Ph.D., Associate Professor, Department of Pharmacy, Faculty of Mathematics and Natural Sciences, Universitas Syiah Kuala, Banda Aceh 23111, Indonesia.

- Email: [khairankhairan@usk.ac.id](mailto:khairankhairan@usk.ac.id)
- ORCID: 0000-0003-3028-6022
- Web of Science ResearcherID: GPS-9955-2022
- Scopus Author ID: 37016941000
- Homepage: <https://fsd.usk.ac.id/kkh/>

**Tallei, T.E.**, Ph.D., Professor, Department of Biology, Faculty of Mathematics and Natural Sciences, Universitas Sam Ratulangi, Manado, Indonesia.

- Email: [trina\\_tallei@unsrat.ac.id](mailto:trina_tallei@unsrat.ac.id)
- ORCID: 0000-0002-7963-7527
- Web of Science ResearcherID: U-1322-2019
- Scopus Author ID: 57193317686
- Homepage: <http://fmipa-unsrat.com/biologi.php>

**Mohd Fauzi, F.**, Ph.D., Associate Professor, Faculty of Pharmacy, Universiti Teknologi MARA Selangor, Puncak Alam Campus, 42 300 Bandar Puncak Alam, Selangor, Malaysia.

- Email: [fazlin5465@uitm.edu.my](mailto:fazlin5465@uitm.edu.my)
- ORCID: 0000-0002-1572-9449
- Web of Science ResearcherID: J-5819-2015
- Scopus Author ID: 57219347587
- Homepage: <https://pharmacy.uitm.edu.my/index.php/discover-us/directory/27-corporate/staff-directory/53-dr-fazlin-mohd-fauzi>

#### HOW TO CITE THIS ARTICLE

Maulydia, N.B.; Idroes, R.; Khairan, K.; Tallei, T.E.; Mohd Fauzi, F., (2024). Ecotoxicological insight of phytochemicals, toxicological informatics and heavy metal concentration in *tridax procumbens* L. in geothermal areas. *Global J. Environ. Sci. Manage.*,10(1): 369-384.

DOI: 10.22034/gjesm.2024.01.23

URL: [https://www.gjesm.net/article\\_707943.html](https://www.gjesm.net/article_707943.html)





## REVIEW PAPER

## A state-of-the-art review on geotechnical reinforcement with end-life tires

M. Shariati<sup>1</sup>, M. Afrazi<sup>2</sup>, H. Kamyab<sup>3\*</sup>, S. Rouhanifar<sup>4</sup>, E. Toghrol<sup>5</sup>, M. Safa<sup>6</sup>, Sh. Chelliapan<sup>3</sup>, H. Afrazi<sup>7</sup><sup>1</sup> Faculty of Architecture and Urbanism, UTE University, Calle Rumipamba S/N and Bourgeois, Quito, Ecuador, Ecuador<sup>2</sup> Mechanical Engineering department, New Mexico Institute of Mining and Technology, Socorro, NM 87801 USA<sup>3</sup> Engineering Department, Razak faculty of Technology and Informatics, Universiti Teknologi Malaysia Jalan sultan Yahya Petra 56100 Kuala Lumpur, Malaysia<sup>4</sup> Department of Civil Engineering, Tarbiat Modares University, Tehran, Iran<sup>5</sup> Department of Civil Engineering, Calut Company Holding, Melbourne, 800, Australia<sup>6</sup> School of Engineering and Technology, Duy Tan University, Da Nang, Vietnam<sup>7</sup> Department of Civil Engineering, Shahid Bahonar University of Kerman, Kerman, Iran

## ARTICLE INFO

**Article History:**

Received 01 June 2023

Revised 12 August 2023

Accepted 19 September 2023

**Keywords:**

Geotechnical engineering

Rubber

Scrap tires

Sustainable management

## ABSTRACT

This study provides a comprehensive exploration of the utilization of scrap tires in geotechnical engineering, focusing on their applications, mechanical behavior, environmental impact, and potential challenges. The utilization of waste tires in engineering applications is of paramount importance, offering a sustainable solution to the escalating challenge of waste tire management. The accumulation of discarded tires poses significant environmental and economic concerns globally, with traditional disposal methods often leading to environmental degradation, fire hazards, and increased land use. By harnessing the inherent properties of scrap tires, such as their durability and energy-absorbing characteristics, geotechnical engineering presents a promising path for repurposing these materials. This review examines how integrating scrap tires into geotechnical projects, such as retaining walls, slopes, and drainage systems, can offer sustainable alternatives while addressing environmental concerns. The paper extensively analyzes the mechanical behavior of sand-rubber mixtures through laboratory investigations. Factors including rubber proportions, aspect ratios, and interaction mechanisms are dissected to understand their influence on shear strength, deformation behavior, and modulus properties. These insights pave the way for optimizing the performance of sand-rubber mixtures in engineering applications. Additionally, the article delves into modeling approaches that simulate the intricate behavior of these mixtures, facilitating better design and analysis. The economic feasibility of incorporating scrap tires is investigated, emphasizing the cost-effectiveness achieved through reduced material costs and enhanced infrastructure durability. The environmental benefits of diverting rubber waste from landfills are discussed, highlighting the alignment with sustainability goals and regulations. Despite the advantages, engineering challenges associated with rubber particles' behavior are acknowledged, and potential solutions are explored. Through a comprehensive synthesis of research findings and practical implications, this review aims to provide a deep understanding of the potential of scrap tires in geotechnical engineering. It concludes by advocating for further research and innovation to harness the full potential of scrap tires, ultimately contributing to a more sustainable and resilient built environment.

DOI: [10.22034/gjesm.2024.01.24](https://doi.org/10.22034/gjesm.2024.01.24)This is an open access article under the CC BY license (<http://creativecommons.org/licenses/by/4.0/>).

NUMBER OF REFERENCES

129



NUMBER OF FIGURES

10



NUMBER OF TABLES

1

\*Corresponding Author:

Email: [hesam\\_kamyab@yahoo.com](mailto:hesam_kamyab@yahoo.com)

Phone: +6017 782 0054

ORCID: [0000-0002-5272-2297](https://orcid.org/0000-0002-5272-2297)

Note: Discussion period for this manuscript open until April 1, 2024 on GJESM website at the "Show Article".

## INTRODUCTION

The accumulation of discarded tires is an escalating concern, due to the environmental hazards like long-term degradation, observed in both developing and developed nations because of the widespread use of vehicles (Daghistani et al., 2023; Ru et al., 2023; Wu et al., 2023a). The conventional methods of disposing of these waste products, such as landfilling or stockpiling, have been proved to be environmentally harmful and economically burdensome (Ahmed, 1993; Safa et al., 2020; Zehtab Yazdi et al., 2022). Tire waste poses a significant challenge as they are non-biodegradable and can take centuries to decompose naturally. The utilization of scrap tires can substantially decrease landfill waste volume and prevent these tires from contaminating ecosystems (Mansouri et al., 2016). To provide a sense of the scale of this issue, statistics from the RMA (2013) indicate that an estimated 3.8 million metric tons of discarded tires have been accumulated in the United States alone. The continuous growth of the stockpile of scrap tires is primarily attributed to the usage of tires in automobiles and trucks (Fareghian et al., 2023; Zeybek; Eyin, 2023). Typically, the composition of these discarded tires includes elements such as carbon black, synthetic rubber, fillers, natural rubber, steel, fabric, and accelerators (Fareghian et al., 2023) (Fig. 1). However, a discernible global trend in the field of civil engineering has emerged, wherein scrap tires are being increasingly utilized, either in their entirety or after undergoing processing, across various applications (Cui et al., 2022; Nikitas and Bhattacharya, 2023; Arefnia et al., 2013; Veena and James, 2023; Trung et al., 2019). This paradigm shift towards the incorporation of discarded tires in civil engineering practices not only provides a viable solution for their sustainable management but also presents an opportunity to address environmental and economic concerns (Abbas-Abadi et al., 2022; Tian and Senetakis, 2022; Valente et al., 2023; Armaghani et al., 2020). The objective of this review paper is to comprehensively examine the integration of scrap tires in geotechnical engineering. By conducting a thorough analysis of existing research studies and industry practices, the study aims to explore the wide range of applications where scrap tires have been used, identify the associated benefits, and address the challenges that may arise. Furthermore, this study will assess the environmental implications of

implementing scrap tire applications in geotechnical projects. This study has been conducted in Iran in 2023.

### *Applications and practical implementations*

The utilization of scrap tires, both in their intact form and subsequent processing, has found extensive applications in the realms of civil engineering (Fakhimi and Afrazi, 2023; Gabry, 2023; Zrar and Younis, 2022). In the industrial sector, scrap tires undergo pyrolysis, a thermal treatment process, to extract valuable resources such as carbon black, oil, and scrap steel from the organic constituents of tires (Roy et al., 1990; Shariati et al., 2019; Hosseini and Toghrol, 2021). Within civil engineering, a multitude of applications have emerged (Vratsikidis and Pitolakis, 2023; Wu et al., 2023b; Khari et al., 2019). Scrap tires have been employed as additives to enhance asphalt in road construction, act as effective sound barriers, serve as insulating layers beneath gravel-surfaced roads, function as lightweight aggregates in concrete, and exhibit exceptional performance in the creation of low-noise pavements (Edil and Bosscher, 1992; Eldin and Senouci, 1993; Meiarashi, 2004). In the scope of geotechnical engineering, both intact scrap tires and processed forms have garnered significant attention due to their practical implementation (Erfanianpour et al., 2022; Tasalloti et al., 2021; Zrar and Younis, 2022). These applications encompass a wide range of uses, including the reinforcement of retaining walls and slopes, stabilization of slopes with economic and technical benefits, rehabilitation of tropical soil slopes, improved drainage performance, and the mitigation of settlement and backfill pressure on retaining structures (Ahmed, 1993; Garga and O'Shaughnessy, 2000; Hazarika et al., 2010; Huat et al., 2008; Majedi et al., 2020; Ghanizadeh et al., 2022; O'Shaughnessy and Garga, 2000; Poh and Broms, 1995; Tweedie et al., 1998). Processed scrap tires have exhibited effectiveness in various geotechnical applications. They have been successfully incorporated as subgrade materials to impede water capillary rise and enhance drainage systems. Furthermore, their utilization as lightweight backfills has proven advantageous in terms of settlement reduction, stability improvement, and enhanced drainage characteristics for retaining structures (Bernal et al., 1996; Hazarika et al., 2010; Zornberg et al., 2004a; Riaz et al., 2023). Additionally, the utilization of rubber particles derived from scrap



Fig. 1: Stockpiling scrap tires in the environment

tires as a drainage layer in embankment structures has demonstrated high permeability and non-clogging attributes (Hazarika *et al.*, 2010; Mohajerani *et al.*, 2020; Momeni *et al.*, 2023; Rezamand *et al.*, 2021). The reinforcement of embankments with processed scrap tires has been extensively investigated, revealing enhanced strength and reduced settlement compared to non-reinforced structures (Li *et al.*, 2016; Shah *et al.*, 2016b). Noteworthy studies have examined real-scale highway embankments utilizing sand-rubber mixtures, assessing settlement behavior, environmental impacts, and temperature variations (Abdolrahim, 2012). These investigations have showed the advantages of sand-rubber mixtures, including their lightweight nature, cost-effectiveness, ease of compaction, and efficient drainage (Majedi *et al.*, 2021; Yadav and Tiwari, 2019; Faizi *et al.*, 2017). Nevertheless, challenges arise when employing rubber particles alone in geotechnical structures, encompassing issues related to high deformation, compaction, and self-heating mechanisms. Addressing these concerns necessitates the removal of exposed steel components from intact scrap tires and the incorporation of soil particles to mitigate self-heating and reduce the deformation response (Youwai and Bergado, 2003). Importantly, extensive studies have indicated that rubber particles have negligible effects on groundwater quality within the specified ranges of civil engineering applications.

#### *Size classification of processed scrap tires*

The size classification of processed scrap tires

holds significant importance within the realm of geotechnical engineering, particularly concerning its applications in construction projects (Shah *et al.*, 2016a). Geotechnical engineers frequently employ processed scrap tires as a sustainable and economically viable substitute for traditional materials. Accurate size classification of these tires is essential to ascertain their suitability for specific applications (Akbarimehr *et al.*, 2020; Tiwari *et al.*, 2012; Yang *et al.*, 2020; Shariat *et al.*, 2018). By systematically categorizing processed scrap tires into distinct size groups, engineers can effectively evaluate their physical characteristics, including particle size distribution, void ratio, and compaction behavior (Dabic-Miletic *et al.*, 2021; Li *et al.*, 2010; Tran *et al.*, 2022). This knowledge proves to be helpful in the design and optimization of geotechnical constructions, for instance embankments, retaining walls, and road pavements. Moreover, the size classification of processed scrap tires enables the appropriate selection of engineering techniques and the formulation of efficient waste management strategies, thereby advancing environmentally conscious practices within the field of geotechnical engineering. Well-established standards, such as ASTM D6270-08 (2012) and the ETRA (2013), provide guidelines for effectively classifying these rubber particles. These standards outline specific size ranges for the resulting rubber particles obtained through cutting methods, with magnetic separation being employed to remove any metallic strips or

Table 1: Size classification of processed scrap tires

ASTM D6270–08 (2012)		ETRA (2013)	
Name	Size	Name	Size
Powdered Rubber	< 425µm	Fine Powders	< 500µm
Ground Rubber	425µm-2mm	Powders	< 1 mm
Granulated Rubber	425µm-12mm	Granulate Rubber	1mm-10mm
Rough Shred	50*50*50-762*50*50	Rubber Chips	10mm-50mm
Tyre Chips	12mm-50mm	Rubber Shreds	50mm-300mm
Tyre Shreds	50mm-305mm	-	-



Fig. 2: Visual representation of types of rubber particles (Mistry *et al.*, 2021)

components. Table 1 presents the size classifications of processed tires as defined by the ETRA (2013) and ASTM D6270–08 (2012). Moreover, Fig. 2 visually depicts four distinct types of rubber particles, observed in prior studies (Edinçliler *et al.*, 2013; Foose *et al.*, 1996).

*laboratory analysis of discarded tires in geotechnical engineering*

Thorough laboratory investigations are imperative for obtaining comprehensive insights into the behavior of soil-rubber mixtures to ensure the optimal utilization of scrap tires in geotechnical applications. Considerable investigations have been undertaken to examine the behavior of soils when

mixed with rubber fragments. Most of the research conducted has concentrated on granular materials that have been strengthened using rubber particles, also significant investigations have been carried out regarding the behavior of rubber-reinforced clay soils (Al-Tabbaa and Aravinthan, 1997; Cabalar, 2011; Özkul and Baykal, 2007). Achieving homogeneity and preventing segregation between constituents are critical aspects for successful laboratory and field applications of soil-rubber mixtures (Jahandari *et al.*, 2021). Segregation may arise due to disparities in size, density, stiffness, and shape between rubber and soil particles, particularly when mixtures contain higher rubber proportions (Fareghian *et al.*, 2023; Pincus *et al.*, 1994). Visual inspections have traditionally been

employed to assess segregation, although quantitative evaluation of segregation has been proposed using sieve analysis on samples obtained from various locations within an embankment (Badarayani *et al.*, 2021; Toghroli *et al.*, 2020). However, a systematic approach to evaluating the uniformity of laboratory experiments involving sand-rubber mixtures and field applications is currently lacking. Various fabrication techniques have been implemented to mix sand and rubber materials and investigate segregation phenomena. Several variables, including rubber type, size, rubber content, and the ratio of rubber particle size to sand particle size ( $\frac{D_{Rubber}}{D_{Sand}}$ ), impact the mechanical characteristics of sand-rubber mixtures. Previous studies have predominantly focused on the strength and compression characteristics of sand-rubber mixtures. Traditional triaxial tests have been extensively employed to analyze the behavior of these mixtures (Ahmed, 1993; Akbarimehr and Hosseini, 2022; Bergado *et al.*, 2005; Chaney *et al.*, 1996; Hazarika *et al.*, 2012; Jastrzębska, 2019; Kawata *et al.*, 2007; Mashiri *et al.*, 2015; Noorzad and Raveshi, 2017; Promputthangkoon, 2009; Takano *et al.*, 2014; Youwai and Bergado, 2003; Zornberg *et al.*, 2004a). Additionally, direct shear tests (Edil and Bosscher, 1992; Foose *et al.*, 1996; Ghazavi, 2004; Ghazavi and Sakhi, 2005) have been employed to investigate the strength behavior of sand-rubber mixtures. Furthermore, the influence of rubber content on the compressive response of sand-rubber mixtures has been extensively explored through oedometer apparatus (Jamshidi Chenari *et al.*, 2019; Kim and Santamarina, 2008; Neaz Sheikh *et al.*, 2012; Zhou *et al.*, 2022; Fakharian *et al.*, 2023; Ngo and Valdes 2007; Valdes and Evans, 2008).

#### *Influence of rubber proportion*

The mechanical performance of sand-rubber mixtures is notably affected by the proportion of rubber integrated into the mixtures (Fu *et al.*, 2023). Accurate evaluation and selection of the rubber proportion are essential for achieving the desired performance and functional properties of these mixtures. Several methodologies have been proposed to quantitatively assess the rubber proportion, including the sand fraction ( $S_f$ ), rubber fraction (FR), and gravimetric or rubber content ( $\chi$ ). The sand and rubber fractions represent volume-based proportions, while the gravimetric or rubber content

is expressed in terms of mass-based proportions. To calculate the volume of rubber in the content, these measures are defined using Eqs. 1 to 6 (Terzaghi and Peck, 1948). Equations 1 and 2 define the sand and rubber fractions and equation 3 shows how to calculate rubber content.

$$S_f = \frac{V_S}{V_S + V_R} \quad (1)$$

$$F_R = \frac{V_R}{V_S + V_R} \quad (2)$$

$$\chi = \frac{M_R}{M_S + M_R} \quad (3)$$

Where,  $V_S$  and  $V_R$  correspond to the volumes of sand and rubber particles, respectively, and  $M_S$  and  $M_R$  represent the masses of sand and rubber particles, respectively. These parameters can be interrelated using Eqs. 4 to 6 (Terzaghi and Peck, 1948).

$$S_f = 1 - F_R \quad (4)$$

$$\chi = \frac{G_R}{G_R + G_S \left( \frac{1}{F_R} - 1 \right)} \quad (5)$$

$$\chi = \frac{S_f}{G_R + G_S \left( \frac{S_f}{1 - S_f} \right)} \quad (6)$$

Where,  $G_S$  and  $G_R$  signify the specific gravities of soil and rubber particles, respectively.

Several researches have been conducted to analyze how varying the rubber content affects the mechanical properties, including strength and deformation behavior of mixtures, consisting of sand and rubber (Bandyopadhyay *et al.*, 2023; Dai *et al.*, 2023; Farooq and Nimbalkar, 2023; Afrazi *et al.*, 2022). These studies aim to identify the optimal rubber content that enhances the mechanical properties while ensuring stability and performance. The findings from these investigations contribute to an improved understanding and design of sand-

rubber mixtures for geotechnical applications.

#### *Strength response of sand-rubber mixtures*

A substantial volume of research has been conducted to explore the strength characteristics exhibited by sand-rubber mixtures at different rubber content levels (Zhang et al., 2023). Lee et al. (2007) performed drained conventional Triaxial tests on sand-rubber mixtures with a rubber-to-sand diameter ratio ( $D_{\text{Rubber}}/D_{\text{Sand}}$ ) of approximately 0.25 and different sand fractions ( $s_f$ ). The results revealed a decrease in peak strength and an increase in axial strain at peak strength for mixtures with lower sand fractions. To study the strength and deformation behavior of sand-rubber mixtures, Youwai and Bergado (2003) conducted Triaxial drained compression tests under different confining pressures. The mixtures consisted of various rubber fractions (FR) ranging from 0 Percent (%) to 100%, using cubical rubber particles. The findings indicated a reduction in maximum strength with increasing rubber volume fraction, accompanied by an increase in shear strain at peak strength. Notably, mixtures with higher rubber fractions exhibited no apparent peak strength. Bergado et al. (2005) investigated the behavior of sand-rubber mixtures under various confining pressures, with a rubber-to-sand diameter ratio ( $D_{\text{Rubber}}/D_{\text{Sand}}$ ) of approximately 20 and different rubber fractions (FR) ranging from 0% to 100%. The experimental results showed a decrease in peak strength and an increase in distortional strain as the rubber fraction increased. Additionally, the stiffness of the mixtures decreased with the incorporation of rubber particles, while the volumetric behavior demonstrated an increased tendency to compress with higher rubber fractions. Noorzad and Raveshi (2017) conducted Triaxial testing on sand-rubber mixtures under different confining pressures, varying the rubber fractions (FR) from 0% to 50% and maintaining a rubber-to-sand diameter ratio ( $D_{\text{Rubber}}/D_{\text{Sand}}$ ) of approximately 25. The results indicated a reduction in peak strength and an increase in residual strength with increasing rubber content, corroborating the findings reported by Bergado et al. (2005). Several investigations have examined the shear strength behavior of sand-rubber mixtures under varying conditions. Chaney et al. (1996) performed Triaxial compression tests on sand-rubber mixtures with a rubber-to-sand diameter ratio ( $D_{\text{Rubber}}/D_{\text{Sand}}$ ) of approximately 20, subjecting

the mixtures to different confining pressures. The addition of rubber particles resulted in reduced shear strength and an increase in axial strain at peak shear strength. Hazarika et al. (2012) conducted drained Triaxial compression tests on sand-rubber mixtures with a rubber-to-sand diameter ratio ( $D_{\text{Rubber}}/D_{\text{Sand}}$ ) of approximately 2, revealing a decrease in peak shear strength, accompanied by increased axial strain for mixtures with higher rubber fractions. Additionally, researchers have investigated the impact of different rubber fractions on the decrease in shear strength observed in sand-rubber mixtures when exposed to varying levels of confining pressures. Kawata et al. (2007) performed Triaxial drained compression tests on sand-rubber mixtures with a rubber-to-sand diameter ratio ( $D_{\text{Rubber}}/D_{\text{Sand}}$ ) of approximately 0.4, demonstrating a decrease in shear strength with increasing rubber fractions in both loose and dense mixtures. Fu et al. (2014), Lee et al. (2014) and Takano et al. (2014) conducted shear tests on sand-rubber mixtures, observing reductions in shear strength as the rubber fraction increased. Moreover, researchers have examined the effect of rubber particle size, shape, and aspect ratio on the strength response of sand-rubber mixtures. Mashiri et al. (2015) investigated the behavior of sand-rubber mixtures containing tire chips with a specific aspect ratio. The experimental results indicated a dependence of the optimum rubber percentage on the aspect ratio, shape, and rubber particles' size. Zornberg et al. (2004a) conducted Triaxial compression tests on sand-rubber mixtures containing tire shreds with a specific aspect ratio, revealing an initial increase followed by a decrease in shear strength as the rubber fraction increased.

#### *Deformation behavior of sand-rubber mixtures*

The deformation behavior of sand-rubber mixtures is greatly affected by the rubber content present in the mixtures. To investigate this behavior, Neaz Sheikh et al. (2012) conducted one-dimensional compression tests on sand-rubber mixtures with varying rubber fractions (FR) of 0%, 10%, 20%, 30%, and 40%. The mixtures were subjected to incremental pressures up to 745 Kilopascal (kPa), followed by unloading to 38 kPa. The results revealed that higher rubber fractions contributed to increased compressibility and swelling responses, indicating the significant role of rubber content in controlling the compressible and swelling

behaviors. The swelling and compression indexes exhibited a consistent increase corresponding to the rubber fractions (Fig. 3).

To further comprehend the deformation behavior of sand-rubber mixtures, Lee et al. (2007) performed oedometer tests on mixtures with a rubber-to-sand diameter ratio ( $\frac{D_{Rubber}}{D_{Sand}}$ ) of approximately 0.25. The sand fraction (Sf) varied from 0 to 1, and the mixtures were subjected to various effective stresses up to 556 kPa. The findings indicated that the vertical strain decreased with increasing Sf. Additionally, the

investigation of constrained modulus ( $M = \frac{\Delta\sigma_v}{\Delta\epsilon_v}$ ) and maximum shear modulus demonstrated that both modulus values increased with higher sand fractions (or reduced rubber fractions) under all confinement conditions. Notably, mixtures with a sand fraction of 0.6 exhibited an intermediate behavior, transitioning from sand-like behavior at higher confinement to rubber-like behavior at lower confinement (Figs. 4 and 5).

Similarly, Kim and Santamarina (2008) conducted oedometer tests on sand-rubber mixtures with

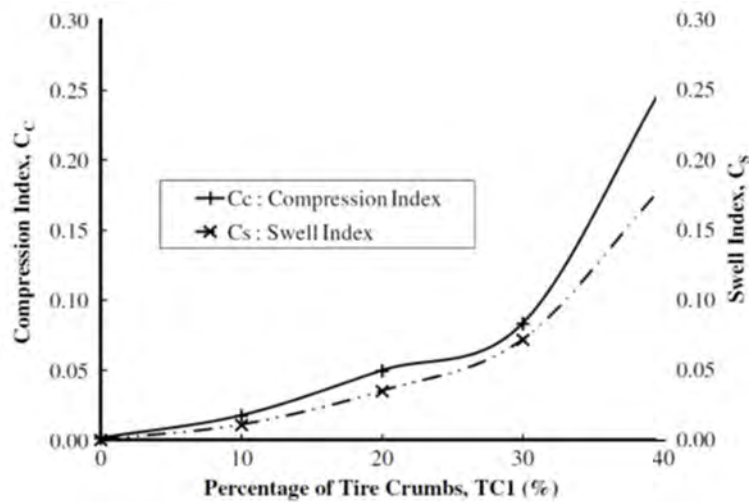


Fig. 3: Compression and swelling indexes of sand-rubber mixtures (Neaz Sheikh et al., 2012)

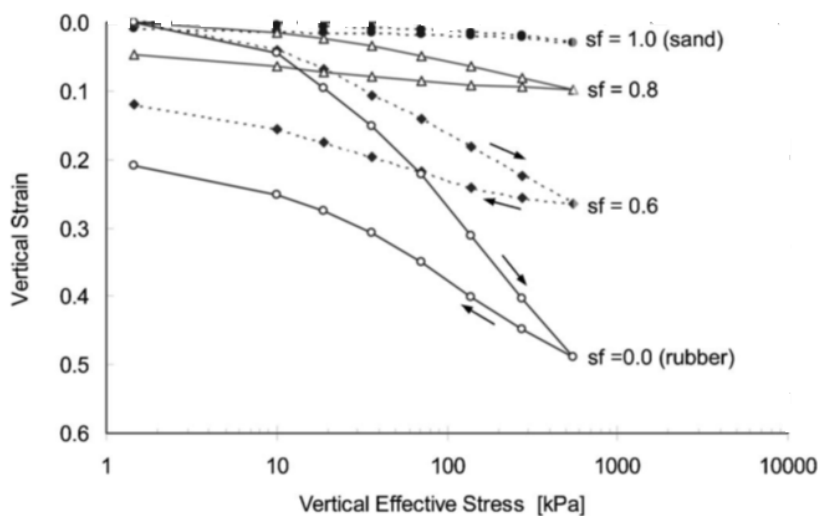


Fig. 4: Vertical strain vs. vertical stress in oedometer tests (Lee et al., 2007)

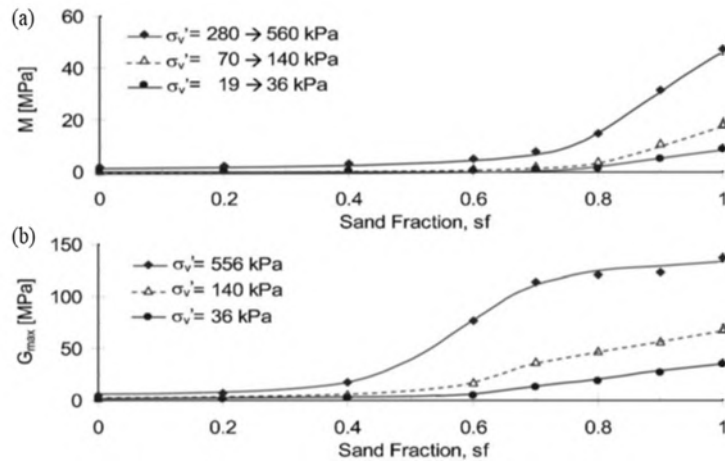


Fig. 5: (a) Constrained modulus at middle strain; (b) Small strain shear modulus (Lee et al., 2007)

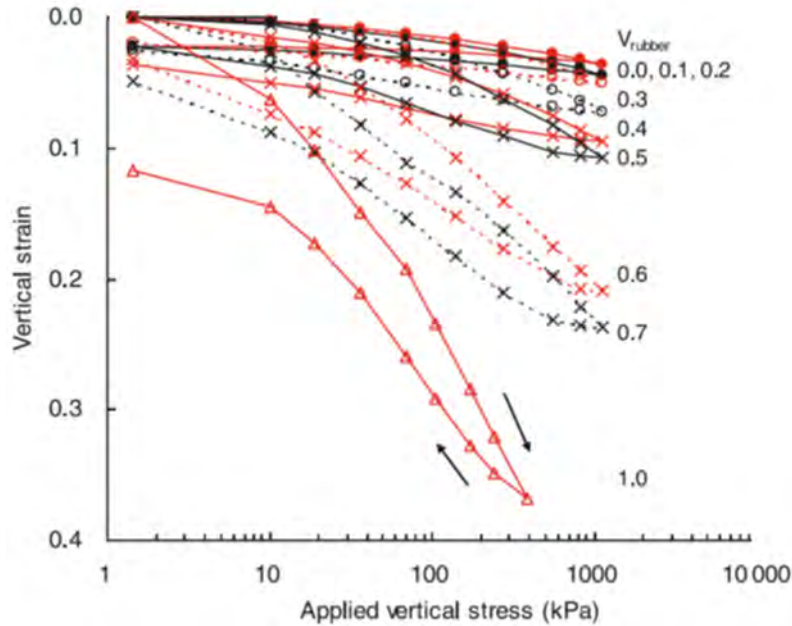


Fig. 6: Vertical strain vs. vertical stress in oedometer tests (Kim and Santamarina, 2008)

a rubber-to-sand diameter ratio ( $\frac{D_{rubber}}{D_{sand}}$ ) of approximately 10, encompassing varied rubber fractions (FR) from 0 to 1. The investigation revealed that increased rubber fractions led to higher compression and swelling behavior. Mixtures with sand fractions of 0.4-0.5 exhibited an intermediate behavior, transitioning from sand-like to rubber-like behavior. Additionally, the constrained modulus

decreased with increasing rubber fractions, aligned with the findings of Lee et al. (2007) (Figs. 6 and 7) and Kim and Santamarina (2008).

#### Influence of rubber particle aspect ratio

The aspect ratio ( $\eta$ ) of the rubber particles, indicating the relationship between their length and width, play a substantial role in affecting the

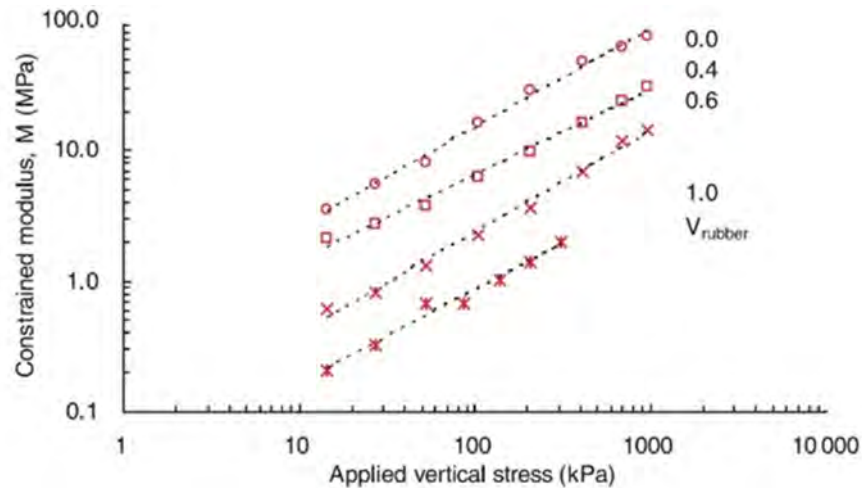


Fig. 7: Constrained modulus of sand-rubber mixtures (Kim and Santamarina, 2008)

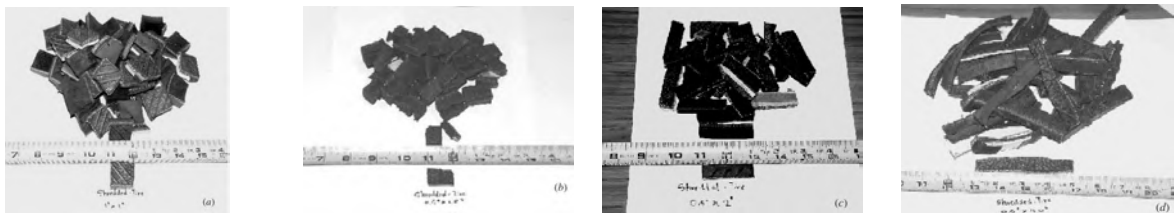


Fig. 8: The visual depiction of tire shreds exhibiting various aspect ratios: (a)  $\eta = 1$  (25.4 mm \* 25.4 mm); (b)  $\eta = 2$  (12.7 mm \* 25.4 mm); (c)  $\eta = 4$  (12.7 mm \* 50.8 mm); (d)  $\eta = 8$  (12.7 mm \* 101.6 mm) (Zornberg et al., 2004a)

mechanical characteristics of sand-rubber blends. Visual examination reveals four distinct types of tire shreds having aspect ratios of 1, 2, 4, and 8 (Zornberg et al., 2004a). The incorporation of tire shreds into sand mixtures introduces characteristics reminiscent of fiber-reinforced sand, resulting in improved peak shear strength (Foose et al., 1996; Zornberg et al., 2004a).

To investigate the impact of rubber particle aspect ratio on the behavior of sand-rubber mixtures, a study conducted by Zornberg et al. (2004a) utilized Triaxial compression tests. The tests involved samples that included tire shreds with the aspect ratios mentioned earlier (Fig. 8). These tests were conducted under three different confining pressures: 48.3 kPa, 103.5 kPa, and 207 kPa. The experimental results, as illustrated in Fig. 9, indicated that increasing the aspect ratio of the rubber particles leads to higher deviatoric stresses regardless of the applied confining

pressures. This observation can be attributed to the enhanced pull-out resistance experienced by the tire shreds, thereby promoting increased tensile forces within the rubber particles.

#### *Influence of rubber-sand size ratio*

The size ratio between rubber and sand in soil mechanics holds considerable importance as it directly impacts diverse engineering properties and soil behaviors. The adding of rubber particles to sand can modify the mechanical characteristics of the soil mixture (Hsiao and Lin, 2023; Mei et al., 2023; Wu et al., 2023a).

#### *Strength response of sand-rubber mixtures*

The mechanical characteristics of sand-rubber mixtures are notably impacted by the size ratio ( $S_r$ ) between rubber and sand, which describes the relationship between the average grain sizes

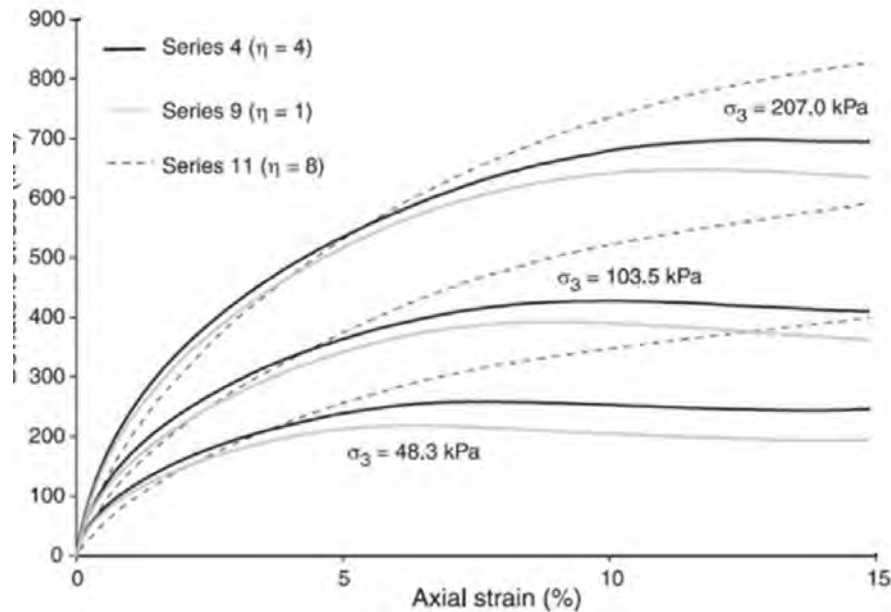


Fig. 9: The deviatoric stress-axial strain response for sand-rubber mixtures with various aspect ratios (Zornberg et al., 2004a)

of rubber and sand particles (Cheng et al., 2023; Yimsiri and Soga, 2010; Zornberg et al., 2004b; Wu et al., 2023b). Triaxial compression tests were carried out on sand-rubber mixtures by Neaz Sheikh et al. (2012), employing size ratios of 4 and 7, while subjecting the samples to a confining pressure of 207 kPa. The findings indicated that mixtures characterized by a higher size ratio demonstrated increased shear strength in comparison to mixtures with a lower size ratio (Neaz Sheikh et al., 2012). Similarly, Noorzad and Raveshi (2017) investigated the impact of size ratio on sand-rubber mixtures under various confining pressures and observed that mixtures with higher size ratios displayed higher deviatoric stresses compared to mixtures with lower size ratios. The reason behind this phenomenon lies in the greater interfacial area between smaller rubber particles and sand particles found in mixtures characterized by lower size ratios. As a result, the interactions between sand particles are diminished, thus causing a reduction in sand-sand interactions. In another study by Promputthangkoon (2009), undrained Triaxial monotonic tests were conducted on sand-rubber mixtures with different rubber-

sand size ratios of approximately 1.7, 3.3, 5.7, and 11.4. The results clearly showed that the shear strength of the mixtures was significantly influenced by the size of the rubber particles. Specifically, an increase in rubber particle size resulted in higher shear strength. Moreover, the utilization of larger rubber particles led to the development of more pronounced negative pore pressure within the sand-rubber mixtures. In their research, the authors examined loose sand-rubber mixtures with a void ratio of 0.86. Three rubber particle types with D-rubber/D-sand ratios of 0.25, 1, and 4 were used, along with varying rubber-sand ratios (5%-50%) in over 300 shear tests. Shear strength and deformation responses depended on rubber proportions and size ratios. Initially, friction angle increased and cohesion intercept reduced up to 20% rubber, then reversed. Shear strength's sensitivity to rubber fraction was limited, as indicated by dimensional analysis.

#### *Deformation behavior of sand-rubber mixtures*

The size ratio (Sr) and rubber proportions have an impact on the deformation response and interaction mechanisms of sand-rubber mixtures

(Akbarimehr *et al.*, 2023; Al-Fatlawi *et al.*, 2023; Dehghanbanadaki *et al.*, 2021; Badarayani *et al.*, 2023). Kim and Santamarina (2008) conducted studies that highlighted the impact of these factors. Mixtures with a lower ratio of rubber particle diameter to sand particle diameter ( $D_{\text{Rubber}}/D_{\text{Sand}}$ ) exhibit pore filling at the particle level and distortion of rubber chains. On the other hand, mixtures with a higher  $D_{\text{Rubber}}/D_{\text{Sand}}$  ratio display stiffness and arching effects. The behavior of these mixtures is governed by fabric, particle-level mechanisms, and macroscale characteristics. Particle segregation and spatial percolation phenomena are observed in samples with varying size ratios (Lee *et al.*, 2014). Further investigations by Lee *et al.* (2009) explored the effect of  $D_{\text{Rubber}}/D_{\text{Sand}}$  using different size ratios (Sr) ranging from 4.7 to 0.35. The constrained modulus of the mixtures was analyzed. It was found that for mixtures with  $Sr < 1$ , the constrained modulus remained relatively constant, while for mixtures with  $Sr > 1$ , the constrained modulus increased. The behavior was attributed to the formation of load carrying chains before rubber particle deformation in mixtures with smaller sand and larger rubber particles. Conversely, in mixtures with smaller rubber particles and larger sand particles, rubber particle deformation occurred before the establishment of load carrying chains between sand particles. The small strain shear modulus was also examined to assess the influence of size ratio. Lee *et al.* (2009) found that the contact area between particles played a crucial role in determining the small shear modulus. Mixtures with  $Sr < 1$  and  $Sr > 1$  exhibited increased shear modulus due to the contact area effect. The lowest small strain shear modulus was observed in mixtures with  $Sr \sim 1$ , indicating a lower stiffness at the particle contacts. Interparticle contacts were identified as significant contributors to the shear strength stiffness.

#### *Effect of confining pressure*

The behavior of sand-rubber mixtures under confining pressure follows a similar pattern to that observed in traditional sand specimens. The shear strength characteristics of the mixtures are notably influenced by the applied confining pressures, regardless of the rubber proportions. Noteworthy investigations by Ahmed (1993), Bergado *et al.* (2005), Chaney *et al.* (1996), Neaz Sheikh *et al.*

(2012), and Zornberg *et al.* (2004a) have highlighted the pronounced effect of confining pressure on the shear strength behavior of sand-rubber mixtures. Specifically, Zornberg *et al.* (2004a) underscored the intensified reinforcement mechanism of rubber particles at lower confining pressures. Experimental results, exemplified by the deviatoric stress response of sand-rubber mixtures illustrated in Fig. 10 provide compelling evidence of the confinement-induced influence on the behavior of these mixtures.

#### *Modeling of soil-rubber mixtures*

The modeling of soil-rubber mixtures is a complex and multidisciplinary task in the field of geotechnical engineering. It involves the development of mathematical models and computational techniques to simulate the behavior of soil mixed with rubber particles (Fu *et al.*, 2023; Zhang *et al.*, 2023). Various aspects need to be considered in the modeling process, including the mechanical properties of both the soil and rubber, the distribution and arrangement of rubber particles within the soil matrix, and the interaction between the two materials. The modeling approaches can range from simplified analytical models to more sophisticated numerical simulations, such as finite element or discrete element methods. These models aim to capture the unique behavior exhibited by soil-rubber mixtures, including their enhanced energy dissipation, improved damping characteristics, and altered mechanical response under different loading conditions. Accurate and reliable modeling of soil-rubber mixtures is crucial for understanding their performance in geotechnical applications and facilitating the design and optimization of structures built on or with these materials (Lv *et al.*, 2023; Wang *et al.*, 2023; Zhang *et al.*, 2023). In the study conducted by Lee *et al.* (1999), a constitutive model was proposed to simulate the behavior of sand-rubber mixtures with a rubber fraction of 40% by weight. However, the model had limitations in accurately representing post-peak strength, plastic strain, and dilative response, which were identified as significant drawbacks. Although the model provided accurate predictions under at-rest conditions, it tended to overestimate the behavior under active conditions. Youwai and Bergado (2003) proposed another constitutive model to simulate the stress and deformation behavior of sand-rubber mixtures. While the model showed

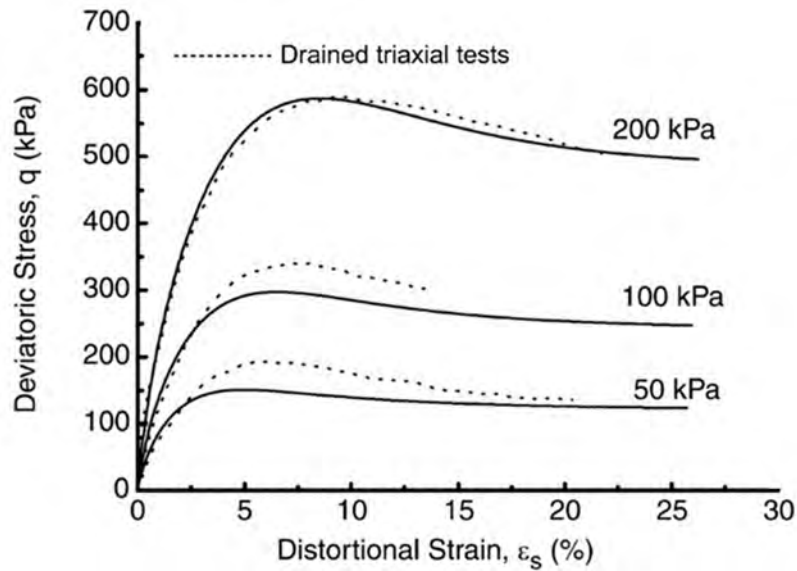


Fig. 10: Deviatoric stress-distortional strain under three different confining pressures

promise in capturing the overall behavior, challenges were encountered in accurately predicting the critical state at large strains due to the observed dilation of the mixtures. To address these limitations, Mashiri et al. (2015) developed a semi-empirical constitutive model based on the critical state framework. This model successfully predicted the stress-strain and volumetric behaviors observed in monotonic Triaxial drained tests conducted by Zornberg et al. (2004a) and Mashiri et al. (2015). In a different approach, Takano et al. (2014) employed a 3D discrete element method based on molecular dynamics to simulate sand-rubber mixtures. Unlike conventional models using spherical particles, this approach utilized non-spherical particles (clumps) to represent the mixtures. To account for computational limitations, the width of the simulated shear box was reduced to 20 mm. While the model effectively predicted the shear strength behavior of the mixtures under a confining pressure of 100 kPa, limitations were observed in accurately predicting the vertical displacement of mixtures with rubber fractions of 0% and 20%.

#### Cost effectiveness of using sand-rubber mixtures

The utilization of alternative materials in civil engineering applications has gained considerable attention in recent years due to the need for sustainable and cost-effective construction practices.

One such innovative approach is the incorporation of rubber particles into traditional construction materials like sand, leading to the formation of sand-rubber mixtures. These mixtures not only offer potential engineering benefits but also present an avenue for cost savings in various construction projects (Tsiavos et al., 2019).

#### Material cost

The cost effectiveness of using sand-rubber mixtures primarily stems from the utilization of waste rubber, which can be sourced from discarded tires, conveyor belts, and other rubber products (Lopera Perez et al., 2017). Compared to the traditional production of construction materials, such as concrete or asphalt, which often require costly extraction and processing of raw materials, incorporating waste rubber particles can significantly reduce the material cost component of construction projects (Assaggaf et al., 2022). The availability of waste rubber at lower or even zero cost, along with potential savings in transportation and disposal fees for rubber waste, contributes to the economic viability of sand-rubber mixtures.

#### Reduced maintenance and longevity

While initial construction costs are a significant consideration, the long-term cost effectiveness of construction materials cannot be overlooked (Alwi

Assaggaf *et al.*, 2022; Bisht and Ramana, 2017). Sand-rubber mixtures have demonstrated improved resilience and durability due to the unique properties of rubber particles, such as their ability to absorb impact and distribute loads (Al-Tayeb *et al.*, 2013; Al-Tayeb *et al.*, 2013; Ngo *et al.*, 2019). This enhanced durability can translate to reduced maintenance and repair needs over the lifespan of the constructed infrastructure, leading to potential long-term cost savings. The decreased frequency of repairs and replacements, particularly in high-traffic areas like roads and pavements, adds to the overall cost effectiveness of employing sand-rubber mixtures.

#### *Environmental and regulatory benefits*

In addition to economic advantages, the use of sand-rubber mixtures aligns with sustainability goals and environmental regulations (Gigli *et al.*, 2019). Incorporating waste rubber into construction materials diverts rubber waste from landfills, contributing to waste reduction and a more circular economy. This alignment with environmental objectives might lead to potential incentives or support from regulatory bodies, further enhancing the cost effectiveness of this innovative approach.

#### *Engineering considerations*

While the economic benefits are promising, it is essential to acknowledge the potential engineering considerations associated with sand-rubber mixtures. These mixtures might require modifications in construction techniques, equipment, and quality control procedures. Therefore, a thorough assessment of the construction process, including any additional labor or equipment requirements, must be conducted to accurately evaluate the overall cost effectiveness of using sand-rubber mixtures.

#### *Application of scrap tires in geotechnical engineering Retaining walls and embankments*

Scrap tires can be used as lightweight fill materials in the construction and building of retaining walls and embankments. Their low density and their essential characteristics reduce the lateral earth pressure exerted on retaining walls, reducing the requirements for additional structural reinforcements. Many researchers around the world studied this application of waste tires (Ma *et al.*, 2023; Hazarika *et al.*, 2023; Garga *et al.*, 2000; Li *et al.*, 2020). For instance, Li *et al.* (2020) studied the dynamic behavior of using waste

tires in retaining walls and showed that using waste tires enhance the dynamic performance of retaining walls. However, it should be mentioned that adding and mixing rubber particles is not an easy task and it's one of the obstacles which need attention and some real project studies.

#### *Drainage properties*

The void spaces within the scrap tires particles provide effective drainage pathways, allowing for the efficient removal of excess pore water. This characteristic makes them suitable for use in drainage systems, such as leachate collection layers in landfills and beneath roadways to combat waterlogging (Edil *et al.*, 2005; Czarna *et al.*, 2023). To determine the effects of drainage properties of waste tires in landfills, Edil *et al.* (2005) showed that using waste tires can efficiently increase the quality of the leachate.

#### *Ground improvement*

The use of scrap tires as a geotechnical fill material can improve the load-bearing capacity of weak or compressible soils. As mentioned earlier, tire-derived aggregate (TDA) could be used to reinforce soils and increase their shear strength, making them suitable for supporting heavy structures like buildings and bridges. Various studies have assessed the efficacy of scrap tires in ground improvement and showed that using scrap tire can significantly increase the shear behavior of soils (Wang *et al.*, 2023; Nikitas and Bhattacharya, 2023).

## **CONCLUSION**

This review study has provided a comprehensive examination of the application of scrap tires in geotechnical engineering, aiming to explore diverse applications, identify associated benefits, and address challenges. By analyzing existing research studies and industry practices, this paper has shed light on the integration of scrap tires in geotechnical engineering projects such as retaining wall reinforcement, slope stabilization, and improved drainage systems. The evaluation of environmental implications and economic feasibility has underscored the importance of sustainable practices in geotechnical engineering. Through literature investigations, the behavior of sand-rubber mixtures has been thoroughly analyzed, considering various factors such as rubber proportions, aspect ratios, and interaction

mechanisms. The findings have revealed the effects of rubber content on the shear strength, strain behavior, compressibility, and constrained modulus of the mixtures. These insights contribute to the advancement and understanding of sustainable geotechnical engineering practices, facilitating the effective utilization of scrap tires while minimizing plagiarism concerns. The accumulation of scrap tires poses significant environmental and economic challenges worldwide. Conventional methods of disposal have proven to be environmentally harmful and economically burdensome. By integrating scrap tires into geotechnical engineering methods, the aim is to tackle these issues and concurrently advance sustainability goals. The utilization of scrap tires in various applications, such as retaining wall reinforcement, slope stabilization, and improved drainage systems, has shown promising results. Extensive research has been conducted on the mechanical behavior of sand-rubber mixtures, yielding valuable insights into their strength and deformation characteristics. It is important to note that challenges exist when employing rubber particles alone in geotechnical structures, including issues related to high deformation, compaction, and self-heating mechanisms. However, through proper removal of exposed steel components from scrap tires and the incorporation of soil particles, these challenges can be mitigated. Furthermore, extensive studies have indicated that rubber particles have negligible effects on groundwater quality within specified ranges of civil engineering applications. To maximize the benefits of scrap tire integration, the size classification of processed tires is crucial. Established standards provide guidelines for effectively categorizing rubber particles based on size, allowing for their optimal utilization in various applications. Additionally, modeling approaches have been developed to simulate the behavior of sand-rubber mixtures, although further research is needed to accurately capture the post-peak strength, plastic strain, and dilative response of these mixtures. In conclusion, the utilization of scrap tires in geotechnical engineering presents an opportunity to address the environmental and economic challenges associated with their accumulation. By exploring the diverse range of applications, evaluating environmental implications, and understanding the behavior of sand-rubber mixtures, this review paper

contributes to the advancement and understanding of sustainable geotechnical engineering practices.

#### **AUTHOR CONTRIBUTIONS**

M. Shariati performed the literature review, analyzed and interpreted the data, prepared the manuscript text, and manuscript edition. M. Afrazi performed the literature review, analyzed and interpreted the data, prepared the manuscript text, and manuscript edition. H. Kamyab performed the literature review, analyzed and interpreted the data, prepared the manuscript text, and manuscript edition. S. Rouhanifar performed the literature review, analyzed and interpreted the data, prepared the manuscript text, and manuscript edition. E. Toghrolhi helped in the literature review and manuscript preparation. M. Safa helped in the literature review and manuscript preparation. C. Shreeshivadasan helped in the literature review and manuscript preparation. H. Afrazi helped in the literature review and manuscript preparation.

#### **ACKNOWLEDGEMENT**

The authors are deeply grateful to all those who played a role in the success of this study. Authors would also like to thank the anonymous reviewers for their invaluable input and support throughout this study.

#### **CONFLICT OF INTEREST**

The authors declare that there is no conflict of interests regarding the publication of this manuscript. In addition, the ethical issues, including plagiarism, informed consent, misconduct, data fabrication and/or falsification, double publication and/or submission, and redundancy have been completely observed by the authors.

#### **OPEN ACCESS**

©2024 The author(s). This article is licensed under a Creative Commons Attribution 4.0 International License, which permits use, sharing, adaptation, distribution and reproduction in any medium or format, as long as you give appropriate credit to the original author(s) and the source, provide a link to the Creative Commons license, and indicate if changes were made. The images or other third-party material in this article are included in the article's Creative Commons license, unless indicated otherwise in a

credit line to the material. If material is not included in the article's Creative Commons license and your intended use is not permitted by statutory regulation or exceeds the permitted use, you will need to obtain permission directly from the copyright holder. To view a copy of this license, visit:

<http://creativecommons.org/licenses/by/4.0/>

**PUBLISHER'S NOTE**

GJESM Publisher remains neutral with regard to jurisdictional claims with regard to published maps and institutional affiliations.

ABBREVIATIONS	DEFINITION
%	Percent
$\frac{D_{Rubber}}{D_{Sand}}$	Rubber-to-sand diameter ratio
$\Delta\sigma_V$	Volumetric stress change
$\Delta\epsilon_V$	Volumetric strain change
$G_R$	Specific gravities of rubber particles
$G_S$	Specific gravities of soil particles
$M_R$	Masses of rubber particles
$M_S$	Masses of sand particles
$V_R$	Volumes of rubber particles
$V_S$	Volumes of sand particles
ASTM	American Society for Testing and Materials
FR	Rubber fraction
kPa	Kilopascal
mm	Millimeter
Sf	Sand fraction
Sr	Size ratio
$\eta$	Aspect ratio
$\mu m$	Micrometer
$\chi$	Gravimetric or rubber content

$$M = \frac{\Delta\sigma_V}{\Delta\epsilon_V} \quad \text{Constrained modulus}$$

**REFERENCE**

Abbas-Abadi, M.S.; Kusenber, M.; Shirazi, H.M.; Goshayeshi, B.; Van Geem, K.M., (2022). Towards full recyclability of end-of-life tires: Challenges and opportunities. *J. Cleaner Product.*, 374: 134036.

Abdolrahim, J. (2012). "Seismic performance of structures with pre-bent strips as a damper. *Int. J. Phys. Sci.*, 7(26): 4061-4072 (12 pages).

Afrazi, M.; Lin, Q.; Fakhimi, A., (2022) Physical and Numerical Evaluation of Mode II Fracture of Quasi-Brittle Materials. *Int. J. Civ. Eng.* 20: 993–1007 (15 pages).

Ahmed, I., (1993). Laboratory study on properties of rubber-soils. Joint highway research project. Purdue University.

Akbarimehr, D.; Hosseini, S.M., (2022). Elasto-plastic characteristics of the clay soil mixed with rubber waste using cyclic triaxial test results. *Arab. J. Geosci.*, 15(14): 1280.

Akbarimehr, D.; Eslami, A.; Aflaki, E., (2020). Geotechnical behaviour of clay soil mixed with rubber waste. *J. Cleaner Product.*, 271: 122632.

Akbarimehr, D.; Rahai, A.; Eslami, A.; Karakouzian, M., (2023). Deformation Characteristics of Rubber Waste Powder–Clay Mixtures. *Sustainability.* 15(16): 12384.

Al-Fatlawi, S. A.; Al-Jumaili, M.A.; Eltwati, A.; Enieb, M., (2023). Experimental-numerical model of permanent deformation in asphalt paving mixtures modified with waste plastic and rubber. In *AIP Conference Proceedings* 2775 (1). AIP Publishing.

Al-Tabbaa, A.; Aravinthan, T., (1997). Engineered clay-shredded tyre mixtures as barrier materials. University of Birmingham,UK. International Containment Technology Conference: Proceedings.

Al-Tayeb, M.M.; Abu Bakar, B.H.; Akil, H.M.; Ismail, H., (2013). Performance of Rubberized and Hybrid Rubberized Concrete Structures under Static and Impact Load Conditions. *Exp. Mech.*, 53(3): 377–384 (8 pages).

Al-Tayeb; Maher, M.; Abu Bakar, B.H.; Ismail, H.; Md Akil, H., (2013). Effect of partial replacement of sand by fine crumb rubber on impact load behavior of concrete beam: experiment and nonlinear dynamic analysis. *Mater. Struct.*, 46(8): 1299–1307 (8 pages).

Alwi Assaggaf, R.; Uthman Al-Dulajjan, S.; Maslehuddin, M.; Baghabra Al-Amoudi, O.S.; Ahmad, S.; Ibrahim, M., (2022). Effect of different treatments of crumb rubber on the durability characteristics of rubberized concrete. *Constr. Build. Mater.*, 318: 126030.

Arefnia, A.; Armaghani, D.J.; Momeni, E., (2013). Comparative Study on the Effect of Tire-Derived Aggregate on Specific Gravity of Kaolin. *Electron. J. Geotech. Eng.*, 18: 335-344 (10 pages).

Arefnia, A.; Momeni, E.; Armaghani, D.J.; Kassim, K.A.;

- Ahmad, K., (2013). Effect of tire derived aggregate on maximum dry density of Kaolin. *Jurnal Teknologi*, 66(1): 19-23 **(5 pages)**.
- Armaghani, D.J.; Mirzaei, F.; Togholi, A.; Shariati, A., (2020). Indirect measure of shear strength parameters of fiber-reinforced sandy soil using laboratory tests and intelligent systems. *Geomech. Eng.*, 22(5): 397.
- Assaggaf, R.A.; Maslehuddin, M.; Al-Dulaijan, S.U.; Al-Osta, M.A.; Ali, M.R.; Shameem, M., (2022). Cost-effective treatment of crumb rubber to improve the properties of crumb-rubber concrete. *Case Stud. Constr. Mater.*, 16: e00881.
- ASTM D6270-08, (2012). Standard Practice for Use of Scrap Tires in Civil Engineering Applications, ASTM International.
- Badarayani, P.; Cazacliu, B.; Ibraim, E.; Artoni, R.; Richard, P., (2023). Sand Rubber Mixtures under Oedometric Loading: Sand-like vs. Rubber-like Behavior. *Appl. Sci.*, 13(6): 3867.
- Badarayani, P.R.; Artoni, R.; Cazacliu, B.; Ibraim, E.; Richard, P., (2021). Segregation of sand-rubber chips mixtures subject to vertical tapping under confinement. *Powder Technol.*, 393: 764–772 **(9 pages)**.
- Bandyopadhyay, T.S.; Chakraborty, P.; Hegde, A., (2023). Interaction between geogrid and sand-crumb rubber mixtures in laboratory pullout conditions. *Innovative Infrastruct. Solutions*, 8(5): 141.
- Bergado, D.T.; Youwai, S.; Rittirong, A., (2005). Strength and deformation characteristics of flat and cubical rubber tyre chip-sand mixtures. *Géotechnique*, 55(8): 603–606 **(4 pages)**.
- Bernal, A.; Lovell, C.; Salgado, R., (1996). Laboratory study on the use of tire shreds and rubber-sand in backfilled and reinforced soil applications. *Joint Transportation Research Program*, 136.
- Bisht, K.; Ramana, P.V., (2017). Evaluation of mechanical and durability properties of crumb rubber concrete. *Constr. Build. Mater.*, 155: 811–817 **(7 pages)**.
- Cabalar, A.F., (2011). Direct Shear Tests on Waste Tires–Sand Mixtures. *Geotech. Geol. Eng.*, 29(4), 411–418.
- Chaney, R.; Demars, K.; Masad, E.; Taha, R.; Ho, C.; Papagiannakis, T., (1996). Engineering Properties of Tire/Soil Mixtures as a Lightweight Fill Material. *Geotech. Test. J.*, 19(3): 297.
- Cheng, Z.; Wang, J.; Zhou, B.; Xiong, W., (2023). The micro-mechanical behaviour of sand–rubber mixtures under shear: A numerical study based on X-ray micro-tomography. *Comput. Geotech.*, 163: 105714.
- Cui, S.; Zhou, C.; Zhang, J., (2022). Experimental Investigations on the State-Dependent Thermal Conductivity of Sand-Rubber Mixtures. *J. Mater. Civil Eng.*, 34(3).
- Dabic-Miletic, S.; Simic, V.; Karagoz, S., (2021). End-of-life tire management: a critical review. *Environ. Sci. Pollut. Res.*, 28(48): 68053–68070 **(18 pages)**.
- Daghistani, F.; Baghbani, A.; Abuel Naga, H.; Faradonbeh, R.S., (2023). Internal friction angle of cohesionless binary mixture sand–granular rubber using experimental study and machine learning. *Geosciences*. 13(7): 197.
- Dai, B.B.; Liu, Q.; Mao, X.; Li, P.Y.; Liang, Z.Z., (2023). A reinterpretation of the mechanical behavior of rubber-sand mixtures in direct shear testing. *Constr. Build. Mater.*, 363: 129771.
- Dehghanbanadaki, A.; Khari, M.; Amiri, S.T.; Armaghani, D.J., (2021). Estimation of ultimate bearing capacity of driven piles in c- $\phi$  soil using MLP-GWO and ANFIS-GWO models: a comparative study. *Soft Comput.*, 25: 4103-4119 **(17 pages)**.
- Edil, T.B.; Bosscher, P.J., (1992). Development of engineering criteria for shredded waste tires in highway applications, final report.
- Edinciller, A.; Cabalar, A.F.; Cevik, A., (2013). Modelling dynamic behaviour of sand–waste tires mixtures using Neural Networks and Neuro-Fuzzy. *Eur. J. Environ. Civ. Eng.*, 17(8): 720–741 **(22 pages)**.
- Eldin, N.N.; Senouci, A.B., (1993). Rubber-tire particles as concrete aggregate. *J. Mater. Civ. Eng.*, 5(4), 478–496 **(9 pages)**.
- Erfanianpour, A.E.; Afrazi, M.; Golshani, A., (2022). Experimental Study of the Effect of Length and Angle of Cross-Cracks on Tensile Strength of Rock-Like Material. *Iran. J. Sci. Technol. Trans. Civ. Eng.*, 46: 4543–4556 **(8 pages)**.
- ETRA, (2013). Introduction to tyre recycling. *European Tyre Recycling Association*.
- Faizi, K.; Rashid, A.S.A.; Armaghani, D.J.; Nazir, R.; Momeni, E., (2017). The influence of bituminous coating on uplift resistance of short pile foundations in sand. *Soil Mech. Found. Eng.*, 54, 177-182.
- Fakharian, P.; Eidgahee, D.R.; Akbari, M.; Jahangir, H.; Taeb, A.A., (2023). Compressive strength prediction of hollow concrete masonry blocks using artificial intelligence algorithms. *Structures*. 47: 1790-1802 **(13 pages)**.
- Fakhimi, A.; Afrazi, M., (2023). *Elastic Theory of Materials*. Tarbiat Modares University Publisher.
- Fareghian, M.; Afrazi, M.; Fakhimi, A., (2023). Soil Reinforcement by Waste Tire Textile Fibers: Small-Scale Experimental Tests. *J. Mater. Civ. Eng.*, 35(2).
- Farooq, M.A.; Nimbalkar, S., (2023). Static and cyclic performance of polyurethane foam adhesive bound soil–rubber mixtures under drained conditions. *Acta Geotech.*, 1-29 **(29 pages)**.
- Foose, G.J.; Benson, C.H.; Bosscher, P.J., (1996). Sand Reinforced with Shredded Waste Tires. *J. Geotech. Eng.*, 122(9): 760–767 **(8 pages)**.
- Fu, R.; Coop, M.R.; Li, X.Q., (2014). The mechanics of a compressive sand mixed with tyre rubber. *Géotechnique Lett.*, 4(3): 238–243 **(6 pages)**.
- Fu, R.; Yang, B.; Hu, X.; Zhou, B.; Coop, M.R., (2023). A micromechanical investigation of sand–rubber mixtures using the discrete element method. *Eng. Geol.*, 318: 107106.
- Gabryś, K., (2023). Experimental research on compressibility characteristics of recycled concrete aggregate: recycled tire waste mixtures. *J. Mater. Cycles Waste Manage.*

- 25(4): 1966–1977 **(12 pages)**.
- Garga, V.K.; O’Shaughnessy, V., (2000). Tire-reinforced earthfill. Part 1: Construction of a test fill, performance, and retaining wall design. *Can. Geotech. J.*, 37(1): 75–96 **(22 pages)**.
- Ghanizadeh, A.R.; Delaram, A.; Fakharian, P.; Armaghani, D.J., (2022). Developing predictive models of collapse settlement and coefficient of stress release of sandy-gravel soil via evolutionary polynomial regression. *Appl. Sci.*, 12(19): 9986.
- Ghanizadeh, A.R.; Ziaee, A.; Khatami, S.M.H.; Fakharian, P., (2022). Predicting resilient modulus of clayey subgrade soils by means of cone penetration test results and back-propagation artificial neural network. *J. Rehabil. Civ. Eng.*, 10(4): 146-162 **(17 pages)**.
- Ghazavi, M., (2004). Shear strength characteristics of sand-mixed with granular rubber. *Geotech. Geolo. Eng.*, (22): 401–416 **(16 pages)**.
- Ghazavi, M.; Sakhi, M.A., (2005). Influence of Optimized Tire Shreds on Shear Strength Parameters of Sand. *Int. J. Geomech.*, 5(1): 58–65 **(8 pages)**.
- Gigli, S.; Landi, D.; Germani, M., (2019). Cost-benefit analysis of a circular economy project: a study on a recycling system for end-of-life tyres. *J. Cleaner Prod.*, 229: 680–694 **(15 pages)**.
- Hazarika, H.; Otani, J.; Kikuchi, Y., (2012). Evaluation of tyre products as ground improving geomaterials. *Proceedings of the Institution of Civil Engineers: Ground Improvement*. 165(4): 267–282 **(16 pages)**.
- Hazarika, H.; Yasuhara, K.; Kikuchi, Y.; Karmokar, A.K. and Mitarai, Y., (2010). Multifaceted potentials of tire-derived three dimensional geosynthetics in geotechnical applications and their evaluation. *Geotext. Geomembr.*, 28(3): 303–315 **(13 pages)**.
- Hosseini, S.A.; Togholi, A., (2021). Effect of mixing Nano-silica and Perlite with pervious concrete for nitrate removal from the contaminated water. *Adv. Concr. Construct.*, 11(6): 531-544 **(14 pages)**.
- Hsiao, D.H.; Lin, C.C., (2023). Effects of the Properties of Fines on the Pore Water Pressure Generation Characteristics of Sand–Silt–Clay Mixtures during Cyclic Loading. *Appl. Sci.*, 13(14): 8126.
- Jahandari, S.; Tao, Z.; Saberian, M.; Shariati, M.; Li, J.; Abolhasani, M.; Kazemi, M.; Rahmani, A.; Rashidi, M., (2021). Geotechnical properties of lime-geogrid improved clayey subgrade under various moisture conditions. *Road Mater. Pavement Des.*, 1-19 **(19 pages)**.
- Jamshidi Chenari, R.; Alaie, R.; Fatahi, B., (2019). Constrained compression models for tire-derived aggregate-sand mixtures using enhanced large scale oedometer testing apparatus. *Geotech. Geol. Eng.*, 37(4): 2591–2610 **(10 pages)**.
- Jastrzębska, (2019). Strength characteristics of clay-rubber waste mixtures in UU triaxial tests. *Geosciences*. 9(8): 352.
- Kawata, S.; Hyodo, M.; Orense, P.; Yamada, S.; Hazarika, H.; Orense, R.P., (2007). Undrained and drained shear behavior of sand and tire chips composite material. In *Proceedings of the international workshop on scrap tire derived geomaterials—opportunities and challenges*. Yokosuka, Japan. 277–283 **(7 pages)**.
- Khari, M.; Dehghanbanadaki, A.; Motamedi, S.; Armaghani, D.J., (2019). Computational estimation of lateral pile displacement in layered sand using experimental data. *Meas.*, 146: 110-118 **(19 pages)**.
- Kim, H.B.; Abdul Aziz, A.; Loh, W.C.; Huat, B.B.; Aziz, A.A.; Chuan, L.W., (2008). Application of scrap tires as earth reinforcement for repair of tropical residual soil slope. *Electron. J. Geotech. Eng.*, 13: 1–9 **(9 pages)**.
- Kim, H.K.; Santamarina, J.C., (2008). Sand–rubber mixtures (large rubber chips). *Can. Geotech. J.*, 45(10): 1457–1466 **(10 pages)**.
- Lee, C.; Shin, H.; Lee, J.S., (2014). Behavior of sand-rubber particle mixtures: experimental observations and numerical simulations. *Int. J. Numer. Anal. Methods Geomech.*, 38(16): 1651–1663 **(13 pages)**.
- Lee, C.; Truong, Q.H.; Lee, W.; Lee, J.S., (2009). Characteristics of rubber-sand particle mixtures according to size ratio. *J. Mater. Civ. Eng.*, 22(4): 323–331 **(9 pages)**.
- Lee, J.H.; Salgado, R.; Bernal, A.; Lovell, C.W.; Lee, J.; Salgado, R.; Bernal, A.; Lovell, C., (1999). Shredded tires and rubber-sand as lightweight backfill. *J. Geotech. Geoenviron. Eng.*, 125(2): 132–141 **(10 pages)**.
- Lee, J.S.; Dodds, J.; Santamarina, J.C., (2007). Behavior of Rigid-Soft Particle Mixtures. *J. Mater. Civ. Eng.*, 19(2): 179–184 **(6 pages)**.
- Li, L.; Xiao, H.; Ferreira, P.; Cui, X., (2016). Study of a small scale tyre-reinforced embankment. *Geotext. Geomembr.*, 44(2): 201–208 **(8 pages)**.
- Li, X.; Xu, H.; Gao, Y.; Tao, Y., (2010). Comparison of end-of-life tire treatment technologies: A Chinese case study. *Waste Manage.*, 30(11): 2235–2246 **(12 pages)**.
- Lopera Perez, J.C.; Kwok, C.Y.; Senetakis, K., (2017). Micromechanical analyses of the effect of rubber size and content on sand-rubber mixtures at the critical state. *Geotext. Geomembr.*, 45(2): 81–97 **(17 pages)**.
- Lv, Y.; Yang, S.; He, Y.; Ma, X.; Pang, M.; Xiong, L., (2023). Discrete element analysis of sand-tyre chips mixtures with different tyre chip orientations under triaxial compression tests. *Constr. Build. Mater.*, 365: 130081.
- Majedi, M.R.; Afrazi, M.; Fakhimi, A., (2020). FEM-BPM simulation of SHPB testing for measurement of rock tensile strength. In *54th US rock mechanics / geomechanics symposium*, at: Colorado School of Mines. Golden, Colorado.
- Majedi, M.R.; Afrazi, M.; Fakhimi, A., (2021). A micromechanical model for simulation of rock failure under high strain rate loading. *Int. J. Civ. Eng.*, 19(5): 501–515 **(15 pages)**.
- Mansouri, I.; Safa, M.; Ibrahim, Z.; Kisi, O.; Tahir, M.M.; Baharom, S.; Azimi, M., (2016). Strength prediction of rotary brace damper using MLR and MARS. *Struct. Eng.*

- Mech., 60(3): 471-488 **(18 pages)**.
- Mashiri, M.S.; Vinod, J.S.; Sheikh, M.N.; Tsang, H.H., (2015). Shear strength and dilatancy behaviour of sand–tyre chip mixtures. *Soils Found.*, 55(3): 517–528 **(12 pages)**.
- Mei, X.; Li, C.; Sheng, Q.; Cui, Z.; Zhou, J.; Dias, D., (2023). Development of a hybrid artificial intelligence model to predict the uniaxial compressive strength of a new aseismic layer made of rubber-sand concrete. *Mech. Adv. Mater. Struct.*, 30(11): 2185–2202 **(18 pages)**.
- Meiarashi, S., (2004). Porous elastic road surface as urban highway noise measure. *Transp. Res. Rec.*, 1880(1): 151–157 **(7 pages)**.
- Mistry, M.K.; Shukla, S.J.; Solanki, C.H., (2021). Reuse of waste tyre products as a soil reinforcing material: a critical review. *Environ. Sci. Pollut. Res.*, 28(20): 24940–24971 **(32 pages)**.
- Mohajerani, A.; Burnett, L.; Smith, J.; Markovski, S.; Rodwell, G.; Rahman, M.T.; Kurmus, H.; Mirzababaei, M.; Horpibulsuk, S.; Maghool, F., (2020). Recycling waste rubber tyres in construction materials and associated environmental considerations: A review. *Resources, Resour. Conserv. Recycl.*, 155: 104679.
- Momeni, E.; He, B.; Abdi, Y.; Armaghani, D.J., (2023). Novel Hybrid XGBoost Model to Forecast Soil Shear Strength Based on Some Soil Index Tests. *CMES-Comput. Model. Eng. Sci.*, 136(3).
- Neaz Sheikh, M.; Mashiri, M.S.; Vinod, J.S.; Tsang, H.H., (2012). Shear and compressibility behavior of sand–tyre crumb mixtures. *J. Mater. Civ. Eng.*, 25(10): 1366–1374 **(9 pages)**.
- Ngo, A.T.; Valdes, J.R., (2007). Creep of sand–rubber mixtures. *J. Mater. Civ. Eng.*, 19(12): 1101–1105 **(5 pages)**.
- Ngo, T.N.; Indraratna, B.; Rujikiatkamjorn, C., (2019). Improved performance of ballasted tracks under impact loading by recycled rubber mats. *Transp. Geotech.*, 20: 100239.
- Nikitias, G.; Bhattacharya, S., (2023). Experimental study on sand–tyre chip mixture foundations acting as a soil liquefaction countermeasure. *Bull. Earthquake Eng.*, 21(8): 4037–4063 **(17 pages)**.
- Noorzad, R.; Raveshi, M., (2017). Mechanical Behavior of Waste Tyre Crumbs–Sand Mixtures Determined by Triaxial Tests. *Geotech. Geol. Eng.*, 35(4): 1793–1802 **(10 pages)**.
- O’Shaughnessy, V.; Garga, V.K., (2000). Tyre-reinforced earthfill. Part 2: Pull-out behaviour and reinforced slope design. *Can. Geotech. J.*, 37(1): 97–116 **(20 pages)**.
- Özkul, Z.H.; Baykal, G., (2007). Shear Behavior of Compacted Rubber Fiber-Clay Composite in Drained and Undrained Loading. *J. Geotech. Geoenviron. Eng.*, 133(7): 767–781 **(15 pages)**.
- Pincus, H.; Edil, T.; Bosscher, P., (1994). Engineering properties of tyre chips and soil mixtures. *Geotech. Test. J.*, 17(4): 453–464 **(12 pages)**.
- Poh, P.S.H.; Broms, B.B., (1995). Slope stabilization using old rubber tires and geotextiles. *J. Perform. Constr. Facil.*, 9(1): 76–79 **(4 pages)**.
- Promptthangkoon, P., (2009). Liquefaction of sand-tyre chip mixtures. Ph.D thesis, The University of Sheffield, UK.
- Rezamand, A.; Afrazi, M.; Shahidikhah, M., (2021). Study of convex corners’ effect on the displacements induced by soil-nailed excavations. *J. Adv. Eng. Comp.*, 5(4): 277-290 **(14 pages)**.
- Riazi, E.; Yazdani, M.; Afrazi, M., (2023). Numerical Study of Slip Distribution at Pre-existing Crack in Rock Mass using Extended Finite Element Method (XFEM). *Iran. J. Sci. Technol. Trans. Civ. Eng.*, 47: 2349–2363 **(15 pages)**.
- Roy, C.; Labrecque, B.; de Caumia, B., (1990). Recycling of scrap tires to oil and carbon black by vacuum pyrolysis. *Resour. Conserv. Recycl.*, 4(3): 203–213 **(11 pages)**.
- RMA, (2013). Scrap tire markets. Rubber manufacturers association.
- Safa, M.; Sari, P.A.; Shariati, M.; Suhatriil, M.; Trung, N.T.; Wakil, K.; Khorami, M., (2020). Development of neuro-fuzzy and neuro-bee predictive models for prediction of the safety factor of eco-protection slopes. *Phys. Stat. Mech. Appl.*, 550: 124046.
- Shah, S.N.R.; Sulong, N.H.R.; Shariati, M.; Khan, R.; Jumaat, M.Z., (2016b). Behavior of steel pallet rack beam-to-column connections at elevated temperatures. *Thin-Walled Struct.*, 106: 471-483 **(13 pages)**.
- Shah, S.N.R.; Sulong, N.H.R.; Khan, R.; Jumaat, M.Z.; Shariati, M., (2016a). Behavior of Industrial Steel Rack Connections. *Mech. Syst. Signal Process.*, 70: 725-740 **(26 pages)**.
- Shariati, M.; Heyrati, A.; Zandi, Y.; Laka, H.; Toghroli, A.; Kianmehr, P.; Safa, M.; Salih, M.N.A.; Poi-Ngian, S., (2019). Application of waste tyre rubber aggregate in porous concrete.” *Smart Struct. Syst.*, 24(4): 553-566 **(14 pages)**.
- Suhatriil, M.; Osman, N.; Azura Sari, P.; Shariati, M.; Marto, A., (2019). Significance of Surface Eco-Protection Techniques for Cohesive Soils Slope in Selangor, Malaysia. *Geotech. Geol. Eng.*, 37(3): 2007–2014 **(8 pages)**.
- Takano, D.; Chevalier, B.; Otani, J., (2014). Experimental and numerical simulation of shear behavior on sand and tyre chips. In 14th International Conference of the International Association for Computer Methods and Advances in Geomechanics. Kyoto, Japan: CRC Press. 1545–1550 **(6 pages)**.
- Tasaloti, A.; Chiaro, G.; Murali, A.; Banasiak, L., (2021). Physical and Mechanical Properties of Granulated Rubber Mixed with Granular Soils—A Literature Review. *Sustainability*. 13(8): 4309.
- Terzaghi, K.; Peck, R.B., (1948). Soil mechanics. Engineering Practice. John Wiley and Sons, Inc., New York.
- Tian, Y.; Senetakis, K., (2022). Influence of creep on the small-strain stiffness of sand–rubber mixtures. *Géotechnique*, 72(10): 899–910 **(12 pages)**.
- Tiwari, B.; Ajmera, B.; Moubayed, S.; Lemmon, A.; Styler, K., (2012). Soil Modification with Shredded Rubber Tires. In *GeoCongress*. Reston, VA: Am. Soc. Civ. Eng., 3701–3708 **(8 pages)**.
- Toghroli, A.; Nasirianfar, M.S.; Shariati, A.; Khorami, M.;

- Paknahad, M.; Ahmadi, M.; Gharehaghaj, B.; Zandi, Y., (2020). Analysis of extended end plate connection equipped with SMA bolts using component method. *Steel Compos. Struct.*, 36(2): 213-228 **(6 pages)**.
- Tran, T.Q.; Skariah Thomas, B.; Zhang, W.; Ji, B.; Li, S.; Brand, A.S., (2022). A comprehensive review on treatment methods for end-of-life tire rubber used for rubberized cementitious materials. *Constr. Build. Mater.*, 359: 129365.
- Trung, N. T., Alemi, N.; Haido, J.H.; Shariati, M.; Baradaran, S.; Yousif, S.T., (2019). Reduction of cement consumption by producing smart green concretes with natural zeolites. *Smart Struct. Syst.*, 24(3): 415-425 **(11 pages)**.
- Tsiavos, A.; Alexander, N.A.; Diambra, A.; Ibraim, E.; Vardanega, P.J.; Gonzalez-Buelga, A.; Sextos, A., (2019). A sand-rubber deformable granular layer as a low-cost seismic isolation strategy in developing countries: Experimental investigation. *Soil Dyn. Earthquake Eng.*, 125: 105731.
- Tweedie, J.; Humphrey, D.; Sandford, T., (1998). Tire shreds as lightweight retaining wall backfill: active conditions. *J. Geotech. Geoenviron. Eng.*, 124(11): 1061–1070 **(10 pages)**.
- Valdes, J.R.; Evans, T.M., (2008). Sand–rubber mixtures: Experiments and numerical simulations. *Can. Geotech. J.*, 45(4): 588–595 **(8 pages)**.
- Valente, M.; Sambucci, M.; Chougan, M.; Ghaffar, S.H., (2023). Composite alkali-activated materials with waste tire rubber designed for additive manufacturing: an eco-sustainable and energy saving approach. *J. Mater. Res. Technol.*, 24: 3098–3117 **(20 pages)**.
- Veena, U.; James, N., (2023). Natural rubber latex treatment of sand: A novel remediation technique for soil liquefaction. *Soil Dyn. Earthquake Eng.*, 165: 107661.
- Vratsikidis, A.; Pitilakis, D., (2023). Field testing of gravel-rubber mixtures as geotechnical seismic isolation. *Bull. Earthquake Eng.*, 21(8): 3905–3922 **(18 pages)**.
- Wang, T.; Wautier, A.; Zhu, J.; Nicot, F., (2023). Stabilizing role of coarse grains in cohesionless overfilled binary mixtures: A DEM investigation. *Comput. Geotech.*, 162: 105625.
- Wu, M.; Liu, F.; Li, Z.; Bu, G., (2023). Micromechanics of granulated rubber–soil mixtures as a cost-effective substitute for geotechnical fillings. *Mech. Adv. Mater. Struct.*, 30(13): 2701–2717 **(17 pages)**.
- Wu, M.; Liu, F.; Yang, J., (2023). Stress–strain–strength behavior of geosynthetic reinforced rubber–sand mixtures. *Acta Geotech.*, 1-12 **(12 pages)**.
- Wu, M.; Tian, W.; He, J.; Liu, F.; Yang, J., (2023). Seismic isolation effect of rubber-sand mixture cushion under different site classes based on a simplified analysis model. *Soil Dyn. Earthquake Eng.*, 166: 107738.
- Wu, M.; Tian, W.; Liu, F.; Yang, J., (2023). Dynamic behavior of geocell-reinforced rubber sand mixtures under cyclic simple shear loading. *Soil Dyn. Earthquake Eng.*, 164: 107595.
- Yadav, J.S.; Tiwari, S.K., (2019). The impact of end-of-life tires on the mechanical properties of fine-grained soil: A Review. *Environ. Dev. Sustainability*. 21(2): 485–568 **(14 pages)**.
- Yang, Z.; Zhang, Q.; Shi, W.; Lv, J.; Lu, Z.; Ling, X., (2020). Advances in properties of rubber reinforced soil. *Adv. Civ. Eng.*, 2020, 1–16 **(16 pages)**.
- Yazdani, M.; Kabirifar, K.; Frimpong, B.E.; Shariati, M.; Mirmozaffari, M.; Boskabadi, A., (2021). Improving construction and demolition waste collection service in an urban area using a simheuristic approach: A case study in Sydney, Australia. *J. Cleaner Prod.*, 280: 124138.
- Yimsiri, S.; Soga, K., (2010). DEM analysis of soil fabric effects on behaviour of sand. *Géotechnique*, 60(6): 483–495 **(13 pages)**.
- Youwai, S.; Bergado, D.T., (2003). Strength and deformation characteristics of shredded rubber tire and sand mixtures. *Can. Geotech. J.*, 40(2): 254–264 **(11 pages)**.
- Zehtab Yazdi, Y.; Mansouri, N.; Atabi, F.; Aghamohammadi, H., (2022). Dispersion modelling of particulate matter concentrations of sand product plants in a mineral complex. *Global J. Environ. Sci. Manage.*, 8(2): 265-280 **(16 pages)**.
- Zeybek, A.; Eyin, M., (2023). Experimental Study on Liquefaction Characteristics of Saturated Sands Mixed with Fly Ash and Tire Crumb Rubber. *Sustainability*. 15(4): 2960.
- Zhang, J.Q.; Wang, X.; Yin, Z.Y., (2023). DEM-based study on the mechanical behaviors of sand-rubber mixture in critical state. *Constr. Build. Mater.*, 370: 130603.
- Zhou, J.; Huang, S.; Zhou, T.; Armaghani, D.J.; Qiu, Y., (2022). Employing a genetic algorithm and grey wolf optimizer for optimizing RF models to evaluate soil liquefaction potential. *Artif. Intell. Rev.*, 55(7): 5673-5705 **(23 pages)**.
- Zornberg, J.G.; Cabral, A.R.; Viratjandr, C., (2004b). Behaviour of tire shred tire ans sand mixtures. *Can. Geotech. J.*, 41(2): 227–241 **(15 pages)**.
- Zornberg, J.G.; Cabral, A.R.; Viratjandr, C., (2004a). Behaviour of tire shred sand mixtures. *Can. Geotech. J.*, 41(2): 227–241 **(15 pages)**.
- Zrar, Y.J.; Younis, K.H., (2022). Mechanical and Durability Properties of Self-Compacted Concrete Incorporating Waste Crumb Rubber as Sand Replacement: A Review. *Sustainability*. 14(18): 11301.

#### AUTHOR (S) BIOSKETCHES

**Shariati, M.**, Ph.D., Professor, Faculty of Architecture and Urbanism, UTE University, Calle Rumipamba S/N and Bourgeois, Quito, Ecuador, Ecuador.

- Email: [mahdi.shariati@ute.edu.ec](mailto:mahdi.shariati@ute.edu.ec)
- ORCID: 0000-0002-0440-7612
- Web of Science ResearcherID: C-9626-2019
- Scopus Author ID: 36769148300
- Homepage: [https://scholar.google.com/citations?hl=en&user=w\\_Inx3gAAAAJ](https://scholar.google.com/citations?hl=en&user=w_Inx3gAAAAJ)

**Afrazi, M.**, M.Sc., Mechanical Engineering department, New Mexico Institute of Mining and Technology, Socorro, NM 87801 USA.

- Email: [Mohammad.afrazi@student.nmt.edu](mailto:Mohammad.afrazi@student.nmt.edu)
- ORCID: 0000-0002-0024-1432
- Web of Science ResearcherID: ABD-8432-2020
- Scopus Author ID: 57218269319
- Homepage: <https://scholar.google.com/citations?user=YxXMYTQAAAAJ&hl=en>

**Kamyab, H.**, Ph.D., Assistant Professor, Engineering Department, Razak faculty of Technology and Informatics, Universiti Teknologi Malaysia Jalan sultan Yahya Petra 56100 Kuala Lumpur, Malaysia

- Email: [hesam\\_kamyab@yahoo.com](mailto:hesam_kamyab@yahoo.com)
- ORCID: 0000-0002-5272-2297
- Web of Science ResearcherID: H-4583-2016
- Scopus Author ID: 55355146400
- Homepage: <https://www.scopus.com/authid/detail.uri?authorId=55355146400>

**Rouhanifar, S.**, Ph.D., Assistant Professor, Department of Civil and environmental Engineering, Tarbiat Modares University, Tehran, Iran.

- Email: [Salman.rouhanifar@modares.ac.ir](mailto:Salman.rouhanifar@modares.ac.ir)
- ORCID: 000-0001-8777-5551
- Web of Science ResearcherID: FVA-2146-2022
- Scopus Author ID: 57188982175
- Homepage: <https://scholar.google.com/citations?hl=en&user=2jeTmCwAAAAJ>

**Toghrolji, E.**, Ph.D. Candidate, Department of Civil Engineering, Calut Company Holding, Melbourne, 800, Australia.

- Email: [toghrolji@calut.au](mailto:toghrolji@calut.au)
- ORCID: 0009-0001-6279-3806
- Web of Science ResearcherID: JDQ-0868-2023
- Scopus Author ID: N/A
- Homepage: [https://scholar.google.com/citations?view\\_op=list\\_works&hl=en&authuser=2&user=\\_8dwQPIAAAAJ](https://scholar.google.com/citations?view_op=list_works&hl=en&authuser=2&user=_8dwQPIAAAAJ)

**Safa, M.**, Ph.D., Assistant Professor, School of Engineering and Technology, Duy Tan University, Da Nang, Vietnam.

- Email: [maryamsafa@duytan.edu.vn](mailto:maryamsafa@duytan.edu.vn)
- ORCID: 0000-0003-0158-4450
- Web of Science ResearcherID: ABA-8983-2021
- Scopus Author ID: 57038525200
- Homepage: [https://scholar.google.com/citations?hl=en&user=VsCi\\_64AAAAJ&view\\_op=list\\_works&sortBy=pubdate](https://scholar.google.com/citations?hl=en&user=VsCi_64AAAAJ&view_op=list_works&sortBy=pubdate)

**Chelliapan, S.**, Ph.D., Professor, Engineering department, Razak faculty of technology and Informatics, Universiti Teknologi Malaysia Jalan sultan Yahya Petra 56100 Kuala Lumpur, Malaysia.

- Email: [shreesshivadasan.kl@utm.my](mailto:shreesshivadasan.kl@utm.my)
- ORCID: 0000-0002-3580-3351
- Web of Science ResearcherID: J-6997-2019
- Scopus Author ID: 12140068900
- Homepage: [https://scholar.google.com/citations?hl=en&user=oo\\_okhUAAAAJ](https://scholar.google.com/citations?hl=en&user=oo_okhUAAAAJ)

**Afrazi, H.**, M.Sc., Department of Civil Engineering, Shahid Bahonar University of Kerman, Kerman, Iran.

- Email: [hosseinafrazi@aol.com](mailto:hosseinafrazi@aol.com)
- ORCID: 0009-0007-5543-7399
- Web of Science ResearcherID: ABH-2037-2021
- Scopus Author ID: 57216860861
- Homepage: [https://scholar.google.com/citations?view\\_op=list\\_works&hl=en&user=JcJhP6kAAAAJ](https://scholar.google.com/citations?view_op=list_works&hl=en&user=JcJhP6kAAAAJ)

#### HOW TO CITE THIS ARTICLE

Shariati, M.; Afrazi, M.; Kamyab, H.; Rouhanifar, S.; Toghrolji, E.; Safa, M.; Chelliapan, Sh., Afrazi, H., (2024). *Global J. (2024). A state-of-the-art review on geotechnical reinforcement with end life tires. Global J. Environ. Sci. Manage., 10(1): 385-404.*

DOI: [10.22034/gjesm.2024.01.24](https://doi.org/10.22034/gjesm.2024.01.24)

URL: [https://www.gjesm.net/article\\_707739.html](https://www.gjesm.net/article_707739.html)





## CASE STUDY

## Abnormality in optimal forest management by indigenous people in deforestation

A. Mutolib<sup>1,2,\*</sup>, Y. Yonariza<sup>3</sup>, A. Rahmat<sup>2</sup><sup>1</sup> *Agribusiness and Natural Resources Management, University of Siliwangi, Jl. Siliwangi No. 24, Kahuripan, Tawang, Kota Tasikmalaya, Jawa Barat 46115, Indonesia*<sup>2</sup> *Research Center for Limnology and Water Resources, National Research and Innovation Agency, Jl. Raya Jakarta-Bogor km. 46, Cibinong 16911, Bogor Jawa Barat, Indonesia*<sup>3</sup> *Department of Integrated Natural Resources Management, School of Graduate, Andalas University. Limau Manis, Kecamatan Pauh, Kota Padang, Sumatra Barat 25175 Indonesia*

## ARTICLE INFO

## Article History:

Received 15 June 2023

Revised 25 August 2023

Accepted 03 October 2023

## Keywords:

Deforestation

Indigenous people

Social network

Ulayat forest

## ABSTRACT

**BACKGROUND AND OBJECTIVES:** Deforestation threatens 120.5 million hectares of forest, and it occurs at a rate of 115 thousand hectares per year. Economic needs and livelihoods encourage people to cut and farm forest areas. Deforestation is considered to be a random and unstructured process that does not involve indigenous people. This research found that indigenous people and various other parties are continuously involved in forest land encroachment. Social networks have facilitated indigenous people and encroachers (buyers of forest land). This research aims to identify the actors involved in forest encroachment and the social network structure in the deforestation process in the production forest of Dharmasraya, Indonesia.**METHODS:** This study employs an ethnographic case study approach to understanding the drivers of deforestation in the Production Forest Management Unit of Dharmasraya. The Production Forest Management Unit of Dharmasraya covers an area of 33,550 hectares. In customary law, the production forest is owned by four indigenous communities from the *Nagari* (villages): Bonjol, Abai Siat Nagari Sikabau, and Sungai Dareh. In this research, the data were collected through interviews that asked the respondent to report on those with whom she/he shared particular relations. Primary data were collected using in-depth interviews employing the snowball sampling method. The data collection used interview guides relating to the actors involved in forest sales and the deforestation process. Key informant interviews involving 34 key informants were conducted with traditional leaders, representatives of a lineage unit (*Ninik Mamak*) and adat functionaries (*Datuak customary authorities*), *Wali Nagari* (village chiefs), local institutional leaders, the government, companies, and those holding concessions. The secondary data were collected from relevant agencies in the research area. The data were analyzed using descriptive-qualitative tools.**FINDINGS:** Three parties are interested in forest production, namely, the local indigenous people, the companies, and the government and each parties claims the production forest because each party sees itself as being the most eligible for forest ownership; this causes an overlap of forest management and ownership among the actors. The indigenous people have become the most powerful party in the ownership of the production forest. The claims of ownership of forests as customary forests have caused the traditional authorities to sell forests massively. The land sale price varies according to the position of the forest and its distance from villages, the topography, and the access. *Ulayat* (forest) land is considered cheap, ranging between USD 300 and USD 1,300 per hectare, including the *Alas hak*. The *Alas hak* is a signed letter showing that the forest land or communal land has been sold to someone else. There are three models of *ulayat* forest land selling: selling by the customary authorities, selling through a broker, and selling by local people. The research has identified 40 actors involved in production forest management in Dharmasraya. Eight actors were not involved in deforestation or *ulayat* forest selling. Ten actors were involved in deforestation and *ulayat* forest selling indirectly, and 22 actors were directly involved in deforestation through forest selling.**CONCLUSION:** Deforestation occurred because the indigenous people sold forest land massively. The sale of the land claimed as *ulayat* forest is not restricted; anyone interested in opening a plantation in a forest area can buy the land from the customary authorities. Hence, deforestation has occurred as part of a systematic process involving critical figures in the community. *Ulayat* forest land sales involved government officers, such as high-ranking police officers and army personnel, and entrepreneurs, officials, civil servants, and other parties who supposedly understand forestry law. The study also confirmed that the economic factors driving deforestation are facilitated by the social networks between indigenous people and the people holding power. The findings of this study contradict the general fact that indigenous people can manage forests sustainably.DOI: [10.22034/gjesm.2024.01.25](https://doi.org/10.22034/gjesm.2024.01.25)This is an open access article under the CC BY license (<http://creativecommons.org/licenses/by/4.0/>).

NUMBER OF REFERENCES

49



NUMBER OF FIGURES

0



NUMBER OF TABLES

6

\*Corresponding Author:

Email: [amutolib24@yahoo.com](mailto:amutolib24@yahoo.com)

Phone: +6282 3867 17542

ORCID: [0000-0002-0788-4991](https://orcid.org/0000-0002-0788-4991)

Note: Discussion period for this manuscript open until April 1, 2024 on GJESM website at the "Show Article".

## INTRODUCTION

Indonesia has a forest area of 120.5 million hectares (ha), including production, protection, and conservation forests (MOEF, 2021). It has the most significant tropical peatland in the world, with approximately 15 million hectares of peatland (both forested and non-forested), spread across Sumatra, Kalimantan, Sulawesi, and Papua (CBS, 2018). Unfortunately, from 2000 to 2012, 6 million hectares of primary forest were lost in Indonesia (Margono et al., 2014). From 2018 to 2019, the rate of deforestation in Indonesia was 462.5 thousand hectares, and from 2019 to 2020, the rate of deforestation was 115.5 thousand hectares (MOEF, 2023). As a result, the forest cover decreased to 91 million hectares (49.8 percent (%) of the total land area) in 2015 (FAO, 2015). Deforestation is driven by economic pressure and population growth (Vanclay, 2005), agriculture, and plantation expansion (Ting et al., 2011; Dalla-Nora et al., 2014), illegal logging (Ji et al., 2017), resettlement, road construction, and forest fires (Sunderlin and Resosudarmo, 1996; Geist and Lambin, 2002; Herdiansyah). Forests and indigenous people cannot be separated. In many cases around the world, indigenous people can manage forests sustainably. Several similar studies have shown that indigenous people are particularly effective at reducing deforestation and protecting the forest (Barsimantov and Kendall, 2012). For example, the indigenous land experienced lower deforestation rates in the Brazilian Amazon (Nolte et al., 2013) and lower fire incidence across Latin America (Nelson and Chomitz, 2011); and sustainable forest management by indigenous people in Tanzania (Fragallah et al., 2021) and in the Brazilian Amazon (Walker et al., 2020; Garcia et al., 2021). The research showed the application of local wisdom in independent forest management to maintain the harmony of ecological, economic, and social culture. This fact proves that the local community can preserve the forest if involved. In Indonesia, 50-60 million people live in forest areas and depend on forest resources for survival (Nunes et al., 2019; Kraus et al., 2021). Forests are the only source of livelihood for the community; consequently, however, this causes conflicts regarding forest ownership between local communities and the government (Feurer et al., 2018; Rochmayanto et al., 2023). The literature on the Indonesian forest noted that there has been some land ownership conflict

between indigenous people and the state/forest companies (Muur, 2018; Maring, 2022). Generally, the indigenous people are against the state and the companies that grab the forest for plantation. In retaliation, the indigenous people removed the forest from the companies and changed the forest into plantation areas (Suryadi et al., 2020; Rangga et al., 2021). In other cases, deforestation occurred as the forest was changed into a plantation (Harun and Dwiprabowo, 2014). In West Rinjani, Indonesia, the indigenous people who claimed the forest as an adat forest changed it into a plantation (Mukarom et al., 2015). These cases show that the indigenous people who live around the forest can become actors in deforestation. Several studies explain that indigenous people have the potential to be the main actors in deforestation; however, many believe that deforestation is purely due to economic factors (Wicke et al., 2011; Brun et al., 2015; Siregar et al., 2023). This research explains new facts about structured and systematic deforestation by indigenous people. This study describes the localized deforestation of 33,000 ha of production forest claimed by indigenous people as customary land (*ulayat*) in Dharmasraya District, West Sumatra Province. Furthermore, it describes the systematic and structured process through which this has happened; the process has involved local people and outsiders in a social network. Forest conversion into agricultural land has reached 85% of the total forest production in the last ten years (Mutolib et al., 2017). From 2000 to 2019, the forest area of the Production Forest Management Unit (PFMU) of Dharmasraya reduced from 86 to 12%, and plantations increased from 10 to 81% of the total area (Rudy et al., 2021). The indigenous people are leaders in a social network with many actors that are cutting and opening the forest for agriculture and plantation land through land transactions. At the same time the Ministry of Environment and Forestry has declared the forest land as the working area of the PFMU of Dharmasraya to strengthen its status as a state forest (Rudy et al., 2021). By setting up a PFMU, the central government expects the state body to conduct management activity on the ground. Unfortunately, indigenous people and various other parties are continuously involved in forest land encroachment. Social networks have facilitated indigenous people and encroachers (buyers of forest land). However, a case like this has yet to be reported. Consequently,

a measure taken to combat deforestation has yet to be effective. As this paper argues, there is no random process of deforestation. Instead, it is a result of the social networks among the parties involved. This study aims to identify the actors involved in forest encroachment and the social network structure in the deforestation process in the production forest of Dharmasraya, Indonesia. It is hoped that this research can explain how deforestation occurs in a structured manner through the contribution of local communities. This study was carried out in the PFMU of Dharmasraya, West Sumatra, Indonesia, from 2016 to 2018; it then continued in 2021 to identify the level of deforestation in the PFMU of Dharmasraya.

## MATERIALS AND METHODS

### *Methods and Research site*

This study employs an ethnographic case study approach to understanding the deforestation process. The ethnographic method was chosen deliberately so that the problem of deforestation at the research location could be explained well and in detail. Obtaining research data on the actors who have been involved in deforestation tends to be difficult if using non-participatory interview methods. An ethnographic approach is considered to be the most appropriate method to describe the problem of deforestation and to provide input to policy makers to prevent continuous deforestation; this is in line with research that uses ethnographic methods to identify cases of forest decline in the Goderich community, Canada (Jackson, 2015). This study was conducted in Dharmasraya District, West Sumatra Province, Indonesia. Dharmasraya is 220 kilometers (km) to the east of Padang City, the provincial capital of West Sumatra. In this district, the PFMU of Dharmasraya covers an area of 33,550 ha (Mutolib et al., 2016). In accordance with customary law, four indigenous communities own the production forest: Nagari Bonjol, Abai Siat Nagari Sikabau, and Sungai Dareh

### *Data Collection and informants*

In this research, the data were collected by interviews in order to gather social network data (Marsden, 2011); the respondent was asked to report on those with whom she/he shared particular relations. Collecting network data can be conducted by presenting the respondent with a list of network

members and the people who have a relationship with the respondent (Marin and Wellman, 2010). The secondary data were collected from relevant agencies, such as representatives of the PFMU of Dharmasraya, the Dharmasraya Bureau of Statistics, and the Dharmasraya Forestry Service. In contrast, additional primary data were collected using an in-depth interview employing the snowball sampling method. The data collection used interview guides relating to the actors involved in the forest sales and the deforestation process. Key informant interviews involving 34 key informants were conducted with the traditional leaders (Nagari Custom Density or KAN leader), representatives of the lineage unit (*Ninik Mamak*) and adat functionaries (*Datuak customary authorities*), *Wali Nagari* (village chief), local institutional leaders, the government, companies, and those holding concessions. The research also included anthropological observations, in which the researcher stayed within the community for five months, giving more reliable, valid, and accurate information. The distribution of the informants is displayed in Table 1.

### *Data analysis*

The data were analyzed using descriptive–qualitative tools. Data analysis followed the approach described, using data reduction, data display, and conclusions (drawing or verifying) to provide a descriptive answer to the research questions (Miles and Huberman, 1994). To identify the actors and social structure involved in production forest encroachment, we used a qualitative research approach with the stakeholders and social network analysis (SNA), employing UCINET and NetDraw software (Borgatti et al., 2002; Prell, 2011). This research used the centrality approach to measure the actors who were more “central” to the social structures and more likely to be influential or powerful according to three indicators: 1) degree of centrality, 2) closeness centrality, and 3) betweenness (Hanneman and Riddle, 2011). UCINET is a comprehensive package used for the analysis of social network data as well as other 1-mode and 2-mode data. This technology uses the following SNA methods to identify the centrality of the actors in deforestation. In addition, UCINET is integrated with the NetDraw program to draw social network diagrams (Borgatti et al., 2002).

Table 1. Key Informants

Stakeholder	Number of informants	Information
<i>Nagari</i> Bonjol	7	Customary authorities (3), Wali <i>Nagari</i> , Head of KAN, and <i>Ninik mamak/adat</i> leader
<i>Nagari</i> Abai Siat	7	Customary authority (1), Wali <i>Nagari</i> , Head of KAN, and <i>Ninik mamak/adat</i> leader
<i>Nagari</i> Sungai Dareh	4	Wali <i>Nagari</i> , Head of KAN, and <i>Ninik mamak/adat</i> leader
<i>Nagari</i> Sikabau	7	Customary authority (1), Wali <i>Nagari</i> , Head of KAN, and <i>Ninik mamak/adat</i> leader
Dharmasraya Forestry service	3	Head of Dharmasraya forestry service, Secretary, and Head of protection of forest division
PFMU Dharmasraya	1	Head of PFMU of Dharmasraya
BPN (National Land Agency) of Dharmasraya	1	Head of infrastructure division
Koto Besar Chiefdom	2	Father of king, council of elders chief, KAN of Koto Besar
Private companies	2	PT. AWB and PT. SMP
Total	34	

PT (Private Limited Company), AWB (Andalas Wahana Berjaya), SMP (Silago Makmur Plantation)

Table 2. Stakeholders claim in PFMU of Dharmasraya management

Stakeholders	Claim to the forest
Government/PFMU of Dharmasraya	Production forest of Dharmasraya as state forest and forest managed by PFMU of Dharmasraya. Ministry of Forestry Republic of Indonesia Decree Number SK.695/Menhut-II/2013 Date 21 October 2013.
HTI Company	IUPHHK (forest timber product exploitation permits) with Minister of Forestry of Republic Indonesia decree No.621/Kpts-II/2009, October 5th, 2009, for PT. Dhara Silva Lestari with area of 15,357 ha and PT. Inhutani with 13,721.68 Ha.
Local/Indigenous People	Forest in PFMU as <i>ulaya land</i> /communal land and owned by local people. This is in accordance with the <i>Adat</i> of Minangkabau, West Sumatra.

## RESULTS AND DISCUSSION

### *Multiple claims on forest land*

Forest management in the PFMU of Dharmasraya is complicated. Three parties are interested in forest production, i.e., local indigenous people, the companies, and the government (PFMU of Dharmasraya) (Table 2). Three parties are claimed the production forest because each party sees itself as being the most eligible for forest ownership; this causes an overlap of forest management and ownership among the actors. In reality, the indigenous people have become the most powerful party with regard to the ownership of the production forest. All the communities in Dharmasraya and West Sumatra claim that the forest is customary/*ulayat* forest, not state forest, which strengthens the indigenous people's claim over the forest land. This condition was exploited by customary authorities and a few local elites to sell the *ulayat* forest. The overview of the stakeholders interested in the PFMU of Dharmasraya is displayed in Table 2.

The central government only recently tried to regain

control over forest land by creating the Production Forest Management Unit (PFMU). As a result, the Ministry of Environment and Forestry issued decree No. SK.695/Menhut-II/2013, dated 21 October 2013, on the PFMU of Dharmasraya. The decree was issued after almost 15 years of the forest management of a previously forested concession area with an area of about 66,000 ha; the concession lasted from 1972 to 2002. The history of forest management in the FMU of Dharmasraya is shown in Table 3.

At present, the entire forest of the PFMU of Dharmasraya is claimed as *ulayat* forest by the indigenous people in Dharmasraya. According to customary law, the *ulayat* forest is an asset to be used for the welfare of the entire community and therefore its members. The indigenous people only recognize forests as communal land and do not recognize the state law and state forests. The study area, which is the working area of the PFMU of Dharmasraya, is considered by indigenous people to be Tanah *ulayat*. In general, *ulayat* land is owned by two parties, namely the Kingdom of Koto Besar

Table 3. History of forest management in PFMU of Dharmasraya

Year	Owner	Function of Forest	Area (ha)
1972	PT. Ragusa Ltd.	Forest Concession Rights (HPH)	66,000
2002	PT. Inhutani	HTI 15, 000 ha for Meranti trees ( <i>Shorea leprosula</i> )	32,749
2002	PT. Incasi Raya, PT. AWB, and PT. SMP	Land use rights (HGU) of oil palm plantation	33,251
2007	PT. BRM	HTI (part of HTI Inhutani)	764
2007	PT. Dhara Silva	HTI (part of HTI Inhutani)	17,114
2013	PFMU Dharmasraya	HTI (including PT. Dhara Silva Lestari, Inhutani and BRM)	32,749

HTI (industrial plantation forest), BRM (Bukit raya mudisa)

(*Nagari* Bonjol and Abai Siat) and the other kingdoms (*Nagari* Sikabau and Sungai Dareh). Under the current administrative system, the area falls into four *Nagaris*, but Bonjol, the dominant area, covers more or less 70% of the total PFMU of Dharmasraya working area. While *ulayat* Abai Siat is predicted to be only around 1,000 ha, the rest is *ulayat Nagari* Sikabau and Sungai Dareh (as estimated by the head of the PFMU of Dharmasraya). The *ulayat* of Sikabau and Sungai Dareh is under the authority of *Datuak Gadang*, who lives in Sikabau. Therefore, this independent *ulayat* is unrelated to Koto Besar or the other kingdoms. Meanwhile, the *ulayats* of Bonjol and Abai Siat were part of the Koto Besar kingdom. The *ulayat* of the Koto Besar kingdom was initially one *ulayat*, but with the population growth, the *Nagari* land was divided into clan land in each *Nagari*. However, oral history keeps spreading from generation to generation. As a traditional hierarchy, the *ulayat* of *Nagari* Abai Siat is under the authority of *Datuak Tanaro Mudo*. At the same time, *Nagari* Bonjol shares the largest *ulayat* with Kerajaan Koto Besar, which has an area as large as 50,000 ha. According to the oral history, Bonjol has its privilege as a former agricultural area of the *Puti Langguak Princess*, the founder of the Koto Besar kingdom. Hence, the name Bonjol means agricultural field. The Koto Besar kingdom delegated authority to "*Datuak Mandaro Kuniang*" as treasurer to manage the *ulayat* land, which belonged to the Melayu clan and exists in the present *Nagari* Bonjol. The present *Datuak Mandaro Kuniang* is held by S (disguised name) after he received it from his predecessor *Sulaiman Datuak Mandaro Kuniang*. Aside from *Datuak Mandaro Kuniang*, two other figures also have authority over part of the *Nagari* Bonjol *ulayat* land. These are A (disguised name) and D (disguised name), both of whom have limited authority.

However, *Datuak Mandaro Kuniang* has more extensive authority, which is recognized by many, even though the government claims this *ulayat* land as a state forest. With a permit obtained from these traditional rulers, people feel secure about buying and clearing the forest. The same thing was found at the other two *Nagaris*. These traditional leaders play a crucial role in managing communal land; people only obtain access to the land with their permission, and they also play a central role in deforestation.

#### *Deforestation, forest land selling, and the role of indigenous people*

Under Minangkabau customs, *ulayat* forest land is communally owned (Alandra et al., 2018; Medaline et al., 2022). Therefore, it is forbidden to sell it. However, much of this land in the study area has recently been sold by the elites of a clan. It is difficult to pinpoint a specific reason for this, but in earlier times, the land was sold at a low price to high-ranking military personnel and government officials. It is also clear that the *ulayat* rights holders had close links with these influential figures, facilitating the land sales. Social network analysis achieved its purpose in analyzing this case. Table 4 shows the parties that hold power and have the authority to manage the *ulayat* forest.

The land sale price varies according to the position of the forest and its distance from villages, the topography, and the access. The price of *ulayat* (forest) land is considered to be cheap, ranging between USD 300 and USD 1,300, including the *Alas hak*. The *Alas hak* is a signed paper showing that the forest land or communal land has been sold to someone else. The *Alas hak* is issued by the *Nagari* and signed by the customary authorities, *Mamak Kepala Waris* (MKW), *Mamak Kepala Kaum* (MKK),

Table 4. Parties involved in the sale of *ulayat* forest land

Position	Authority
<i>Ulayat</i> land rightsholder	To sell the <i>ulayat</i> forest
Ruler of customary land (MKW)	To sell the <i>ulayat</i> forest
Chief of council of elders	Proof of sale for <i>ulayat</i> forest
Wali Nagari ( <i>village chief</i> )	Purchase <i>ulayat</i> forest

the head of KAN (*Kerapatan Adat Nagari*), Wali Nagari, and the witnesses. The size of the land sold varies between 25 and 1,000 ha (Mutolib et al., 2016). This forest land has become an attractive proposition for outsiders at such a low price. The buyers come from various professions and backgrounds from outside of Dharmasraya District. Why do they dare to cut down and sell in a state forest area? In Indonesia, in the eyes of the state, the forest is legally owned by the government, but the local community does not recognize the legitimacy of this claim (Hapsari, 2018; Anugrah et al., 2022). The recognition of customary law in the PFMU of Dharmasraya is robust, and the local community is not concerned about the repercussions if the forest is used in illegal ways in the eyes of the state. However, cutting down trees and selling *ulayat* forest land must be approved by the customary authorities or MKW. Indigenous people only dare to open and sell the forest with this approval. The existence of the customary authorities is highly influential in forest land selling. Hence, the forest encroachment/cutting activities started with slashing and felling trees in the forest, followed by burning to clear the land. After the forest was burned and cleared, the farmers planted oil palm and/or rubber, but strangely, many left the cleared plot without planting a single seedling. There is speculation regarding the selling of the land by using the forest clearing to mark the *ulayat* land ownership. Companies or other parties who want to take land that local people have opened must compensate those who have cleared the forest. As a result, forest land sales increase, and the forest is increasingly threatened. However, this finding is not an isolated case. Although legally the forest is owned by the state, indigenous locals assume that their customary rights have greater legitimacy than the state claims because the indigenous people were there before the state (Larson, 2012; Shrinkhal, 2021). In addition, recognizing customary law, which is very strong in the community, has caused them to have no fear or

worry when clearing forest land, which is prohibited by state law.

#### *Mechanism of ulayat forest land selling*

In *Ulayat* forest selling in the PFMU of Dharmasraya, the customary authorities and buyers only use the *Alas hak* as a basis for ownership, and they do not necessarily use a statutory legal certificate from the government. The *Alas hak* is issued by the Nagari government under the approval of the customary authorities. Furthermore, the *Alas hak* is signed by Wali Nagari, head of KAN. What is the *Alas hak*? Based on Basic Agrarian Law (BAL), Law Number 5, of the year 1960, the Government of Indonesia has determined that the land in the whole of the Republic of Indonesia should be registered, as is envisaged in Article 19 of the BAL for the legal certainty of land. Land registration for the first time, according to the Government Regulation of Indonesia no 24, of the year 1997, Article 1 clause 9, is the process of land registration activities against the land object that has not been registered based on Government Regulation No. 10, of the year 1961, on land registration. The *Alas hak* is defined as evidence of land tenure and can be an evidence tool to show the juridical relationship between the land and owner; it can also show the formal and official history of land ownership published by the village government. Juridically, the *Alas hak* is usually in the form of written evidence, such as a letter of decision, an affidavit or a letter of recognition of customary land ownership. The implementation of *ulayat* land registration in Minangkabau preceded the creation of an *Alas hak*. Therefore, the requirement for the national land title is the existence of an *Alas hak*. Consequently, an interesting question related to the sales of the *ulayat* forest in Dharmasraya concerns whether the *ulayat* forest can be the basis for the land title. Based on state law, the answer is no because the *ulayat* forest falls within the state claim as a forest area. Therefore, the National Land Agency of Indonesia (BPN) will refuse and not issue

a formal land title for the land inside the forest area. So, what caused the people to dare to buy land when it is legally prohibited by the state? The buyers of the *ulayat* forest do not consider the state land law and only recognize the customary law regarding forest ownership in Dharmasraya. Therefore, the buyers argue that cutting down and changing the forest into rubber and oil palm plantations is not against the law because the forest is customary and not a state forest. Hence, the Constitutional Court's Decision no. 35/PUU-X/2012 on customary forests provides the opportunity for forest land sales (especially *ulayat* forest) that incur deforestation. The process of *ulayat* forest selling in the production forest of Dharmasraya is conducted by three actors with different processes. The customary authorities are the leading actor in *ulayat* forest selling. In addition, there is the broker, who serves as the accomplice of the customary authorities, and the local people who have bought the *ulayat* forest from customary authorities and resold it. So, there are three models of *ulayat* forest land selling in the PFMU of Dharmasraya.

#### *Model 1*

*Selling by customary authorities:* In this process, the customary authorities become the sole actor in the *ulayat* forest selling. The customary authorities conduct the transactions and communicate directly with prospective buyers of the *ulayat* forest land. The prospective buyers and customary authorities negotiate over the *ulayat* forest land to determine the price, location, and land area. After the agreement, the customary authorities will take care of the *Alas hak* in the *Nagari* office as proof that the *ulayat* forest has been owned by the buyers. An *Alas hak* means that *ulayat* forest land has been transferred and no longer bears communal land property rights.

#### *Model 2*

*Selling through a broker:* In this process, the customary authorities do not sell the *ulayat* forest directly but authorize someone to sell the *ulayat* forest. The broker will offer prospective buyers and negotiate the price, location, and area. After the agreement, the brokers assist the buyers in making the *Alas hak* in the *Nagari* office. This case is evidence of a social network in forest selling between the customary authorities and the buyers through the broker.

#### *Model 3*

*Selling by local people:* The meaning of local people in this research is not only the members of the clan in the *ulayat* forest but the people from the four *Nagaris* who sell the land inside the forest area. In some cases, local people purchase the *ulayat* forest from customary authorities, but not for farming; they purchase the *ulayat* forest for resale. The locals who purchase the *ulayat* forest get lower prices than prospective buyers from outside Dharmasraya because they are members of a clan or a kinship. Local people sell land ranging from two ha to hundreds of hectares. When they resell the land, it is facilitated by social networks. Customary authorities have a central role in granting permits to sell *ulayat* land. Related parties, in this case the government, can reduce the rate of deforestation of *ulayat* forests by collaborating with the customary authorities. The government can provide sustainable forest management options that benefit the customary authorities and indigenous communities. Decisions taken by the customary authorities in managing *ulayat* forest land become absolute decisions that are followed by the community. The model for selling *ulayat* forest land in Dharmasraya is different from that in North Sumatra, where the role of the customary authorities is less dominant. Local communities who sell do not need permission from the customary authorities but are required to hand over money to obtain permission to sell *ulayat* land (Hidayat and Lukitaningsih, 2022).

#### *Social network of the actors in deforestation*

The research has identified 40 actors involved in production forest management in Dharmasraya. Eight actors were not involved in deforestation or *ulayat* forest selling. Ten actors were involved in deforestation and *ulayat* forest selling indirectly, and twenty-two actors were directly involved in deforestation through forest selling, as shown in Table 5.

This study investigated whether forest encroachment and deforestation were the results of systematic processes; these processes are different from what is commonly understood. More interestingly, the economy is not the only driving factor of deforestation; deforestation is also due to misconduct by local elites. They can also do it through the facilitation of social networks among traditional rulers with other influential figures in government

*Systematic deforestation by indigenous people*

Table 5. The actors involved in deforestation and forest selling in production forest in Dharmasraya

No.	Actors	Explanation	Role in deforestation
1	King of Koto Besar	<i>Ulayat</i> land in some sub-districts is part of the <i>ulayat</i> owned by the kingdom of Koto Besar. However, control of the <i>ulayat</i> has been given to every customary authority in each <i>Nagari</i> .	Indirect
2	<i>Adat</i> leaders of Koto Besar Kingdom	Koto Besar kingdom has an <i>adat</i> structure; they have the authority to manage all aspects of the <i>adat</i> , including <i>ulayat</i> property. They can rebuke the customary authorities from each <i>Nagari</i> if they deviate from the <i>adat</i> .	Indirect
3	Customary authorities/CAs (S)	Someone from the <i>Nagari</i> /clan/subclan who has the power to control and manage the <i>ulayat</i> land. In Bonjor, there are three Cas and one in Abai Siat and Sikabau. The <i>ulayat</i> of <i>Nagari</i> Sungai Dareh is affiliated with Sikabau.	Direct
4	Head of KAN Wali <i>Nagari</i>	The highest leader of the <i>adat</i> in a <i>Nagari</i> in Minangkabau society.	Direct
5	(Village/ <i>Nagari</i> chief)	Leader of <i>Nagari</i>	Direct
6	Notary	Working under the control of the customary authorities, they work to issue a buy and sell agreement. Some of the buyers request it.	Indirect
7	Broker (S)	Someone who has a relationship with the customary authorities. The broker helps the customary authorities to sell the <i>ulayat</i> forest	Direct
8	<i>Adat</i> leader (S)	Seller of <i>ulayat</i> forest.	Direct
9	Dharmasraya Forestry service	After the PFMU is established, the management of the forest is given to the PFMU. The Dharmasraya forestry service has the task of coordinating with the PFMU in forest management.	No
10	PFMU	Forest management authority of production forest of Dharmasraya.	No
11	Local Community (S)	Indigenous people who take the forest for resale.	Direct
12	Local community (Encroachers who take forest)	Indigenous people who take the forest for farming.	Direct
13	Police (B)	Buyers of forest <i>ulayat</i>	Direct
14	Soldiers (B)	Buyers of forest <i>ulayat</i>	Direct
15	Investors/Businessmen (B)	Buyers of forest <i>ulayat</i>	Direct
16	Officials (B)	Buyers of forest <i>ulayat</i>	Direct
17	Civil servants (B)	Buyers of forest <i>ulayat</i>	Direct
18	Dharmasraya community (B)	Buyers of forest <i>ulayat</i>	Direct
19	West Sumatera community (B)	Buyers of forest <i>ulayat</i>	Direct
20	West Sumatera outsiders (B)	Buyers of forest <i>ulayat</i>	Direct
21	Pensionary of police (B)	Buyers of forest <i>ulayat</i>	Direct
22	Pensionary of soldiers (B)	Buyers of forest <i>ulayat</i>	Direct
23	Pensionary of civil servants (B)	Buyers of forest <i>ulayat</i>	Direct
24	House of Representatives (B)	Buyers of forest <i>ulayat</i>	Direct
25	PT. SMP	NESHP is owned by PT SMP. SMP collaborates with Koskopabo to sell the oil palm FFB (fresh fruit bunches).	Indirect
26	PT. AWB	None. Conflict of forest claim between AWB and local people from Sikabau still continues.	No
27	PT. Dhara Silva	Almost all forest area owned by PT Inhutani grabbed by local people.	No
28	PT. Inhutani	Almost all forest area owned by PT Inhutani grabbed by local people.	No
29	Buyer of FFB	Consists of Koperasi, companies, and traders. They purchase FFB from the people who have plantations in forest areas.	Indirect
30	Co-operative of KOSKOPABO	Koskopabo purchases the oil palm FFB (fresh fruit bunches) from NESHP, which is an area in the forest.	Indirect
31	Workers of forest cutting	Forest buyers hire the workers to cut and clean the forest.	Direct

Continued Table 5. The actors involved in deforestation and forest selling in production forest in Dharmasraya

No.	Actors	Explanation	Role in deforestation
32	Workers of plantation	Plantation owners are dominated by those outside Dharmasraya. Some people are hired to manage the plantation. The workers stay on the plantation, and plantation owners pay for all the needs of the workers, including living costs and plantation costs.	Indirect
33	Gold miners	They take the gold in the rivers and must obtain permission from the customary authorities.	No
34	Encroachers who take logs	Encroachers obtain the permission from the customary authorities to take the logs. They must open the access and share the benefits with the customary authorities.	Direct
35	Wood factory	The wood factory purchases the logs from the encroachers.	Indirect
36	Bulldozer owners	Encroachers hire the bulldozers to open the access and flatten the land in the forest area.	Direct
37	Agriculture and Plantation Service	Does not have the authority in production forest management. But sometimes indigenous people take oil palm and rubber seedlings to be planted in forest areas.	No
38	BPN Dharmasraya	National Land Agency of Dharmasraya	No
39	Ex-Bupati (Ex-regent)	Ex-regent of Dharmasraya purchased the land for plantation in production forest area from customary authorities.	Direct
40	NESHP	NESHP (nucleus estate smallholder oil palm <i>plantation</i> ). Some of the NESHP is located in the production forest. Palm oil companies, local people, and Koperasi have a role in establishing the NESHP.	Indirect

S (seller of *ulayat* land), B (buyer of *ulayat* land)

bodies, such as the military, members of the legislative bodies, police officers, and other civilian officials. Forest encroachment and deforestation are a result of this network. The findings of this study are at odds with other studies that explain deforestation as an unstructured and accidental process resulting from economic demands (Bhattarai *et al.*, 2021; Billah *et al.*, 2021). Unfortunately, this fact has been less documented (Table 5). PT. SMP is involved in deforestation because it has opened an oil palm plasma plantation in a forest area. The company and the local communities through the co-operative of Koskopabo claim that the plasma plantation (palm oil) is included in a non-forest area, but the results of satellite image identification show that the plasma plantation (palm oil) is included in the production forest area. Social networks facilitate land acquisition in the PFMU of Dharmasraya; it all began with the land acquisition by the local high-ranking police officer who purchased forest land with an area of 140 ha from a local elite in the years 2004-2005. This acquisition created at least two impetuses; first, land sale was perceived as legal; second, it paved the way for a social network of land sales. This social network developed rapidly as more police officers purchased *ulayat* land from local elites. Later, like a snowball, the networks got bigger and bigger, attracting

other sectors of government officials, military men, pensioners, legislative members, and the middle class. It also triggered locals to obtain land clearing permits to sell the plots. These networks caused systematic deforestation. Social networks of forest land sales are becoming more prominent as many have found them profitable. The buyers meet the right holder network to buy cheap land for investment with robust proper recognition since the right holders transfer the right. The right holders also feel secure against state laws on forest land encroachment, especially in dealing with forest use permit holders and the PFMU since the buyers are of the state apparatus. The buyers would help to strengthen the recognition of *ulayat* land ownership to maintain their plantation inside the state forest area. Consequently, the forest land sale is unstoppable and leads to massive deforestation. In the future, the Dharmasraya production forest will be under threat and clear danger, especially with its status as a production forest. Regarding the utilization of *ulayat* land among the Minangkabau, land sale and the deforestation that it has caused can also be viewed as inconsistent with ideal communal land usage. Among the Minangkabau people, *ulayat* land is a reserve land for the future expansion of agriculture; so, it is forbidden to transfer the land rights. Minangkabau people consider *ulayat* land as

belonging to future generations, and its usage must be considered for the future generations. What has happened in the Dharmasraya districts is against tradition. It is not a collective action in managing the local forest but a collaboration to grab benefits from the selling of *ulayat* land. The interviews reveal that the current practices of *ulayat* sales are against local custom, but they admitted that time had changed many things. It is not considered as wrongdoing, and the *ulayat* land institution is no longer relevant due to the current economic pressures. However, it is probably changing the mindset of local people; their perception accelerates *ulayat* land sales and causes severe deforestation. SNA identifies the actor roles through approaches to the degree of centrality, the betweenness centrality, and the closeness centrality. The degree of centrality is thus seen as a measure of an actor's level of involvement or activity in the network. Indegree centrality is the number of ties received by an actor from others, and outdegree centrality is the number of ties given by an actor to others. In this case, the customary authorities have most of the ties in the network (indegree centrality and outdegree centrality have 27 paths/links); this means that the customary authorities became the actors most involved in deforestation and forest land selling in the PFMU of Dharmasraya. Betweenness centrality calculates how often an actor sits on the geodesic path (the shortest path), linking two other actors together (Prell, 2011). In the communication network, betweenness centrality measures how many potentially controlling actors are in the network. For example, in the deforestation and selling of *ulayat* forest land, the customary authorities become an actor with the most links with other actors (187 links/path). The logic of closeness centrality can be summarized as follows: if an actor is not central, he generally needs to rely on others to relay messages through the network (Freeman, 1978). Closeness centrality is determined by the short path lengths linking actors together: it measures centrality as the distance between actors, whereas actors with the shortest distance to other actors are seen as having the most closeness centrality (Prell, 2011). For example, in the deforestation in Dharmasraya, the customary authorities became the actor who had the shortest distance from the other actors (score: 35). The results of the centrality analysis prove that the customary authorities are the parties who play

the greatest role in the deforestation process in the PFMU of Dharmasraya.

## CONCLUSION

Three parties are interested in forest production: local indigenous people, the companies, and the government (the PFMU of Dharmasraya) and each party claims the production forest because each party sees itself as being the most eligible for forest ownership; this causes an overlap of forest management and ownership among the actors. The indigenous people have become the most powerful party in the ownership of the production forest. The claims of ownership of the forests as customary forests have caused the traditional authorities to sell forests massively. All the communities in Dharmasraya and West Sumatra claimed that the forest was the customary/*ulayat* forest, not state forest; this strengthens the indigenous people's claim over forest land. The customary authorities and a few local elites have exploited this condition to sell the *ulayat* forest. The land sale price varies according to the position of the forest and its distance from villages, the topography, and the access. The price of *ulayat* (forest) land is considered cheap, ranging between USD 300 and USD 1,300, including the *Alas hak*. The *Alas hak* is a signed paper showing that the forest or communal land has been sold to someone else. The traditional leaders who play a role in the sale of customary land are 1) the *ulayat* land rights holder (customary authorities), 2) the ruler of the customary land (MKW), and 3) the chief of the council of elders. The *Nagari* (village chief) plays a role by issuing *alas hak* of the *ulayat* forest. There are three models of *ulayat* forest land selling in the PFMU of Dharmasraya, namely selling by customary authorities, selling through the broker, and selling by local people. The research identified 40 actors involved in production forest management in Dharmasraya. Eight actors were not involved in deforestation or *ulayat* forest selling. Ten actors were involved in deforestation and *ulayat* forest selling indirectly, and twenty-two actors were directly involved in deforestation through forest selling. The social network facilitates deforestation through land sales. Land encroachment is not a random process; it makes use of the social structure in the community where the *ulayat* land rights holders play a crucial role. Land buyers come from various sectors of society that understand the statutory and

customary laws. Legal pluralism paves the way for land transactions using customary law. The buyers are from various backgrounds; they are civil servants, police officers, members of the legislative bodies, and local figures at the district and provincial levels. They are tied by a mutual relationship and protect each other from state law. Strong recognition of customary land rights provides secure land transactions. The land was sold at a low price, which triggered huge transactions involving forest land. The social network has become large and more significant and involves many actors. The fact that indigenous people and local elites are the main actors in the forest land transactions that led to deforestation has severe implications for forest management in Indonesia. Moreover, these findings provide feedback on the recent Constitutional Court ruling stating that the *ulayat* forest was excluded from the state forests through the Constitutional Court's Decision no. 35/PUU-X/2012. Therefore, the criteria and indicators of customary land management by indigenous people must be integrated into forest management to ensure forest conservation in the future. Integrated forest management to prevent the abuse of customary authority through the management of forests in an irresponsible and unsustainable manner.

#### AUTHOR CONTRIBUTIONS

A. Mutolib performed the literature review, designing research, collecting research data, analyzed and interpreted the data. Y. Yonariza performed has contributed in arranging study permits, managing and providing the study locations, compiled the data and manuscript preparation. A. Rahmat performed the spatial analysis to identify the deforestation, interpretation of the data results and manuscript preparation.

#### ACKNOWLEDGEMENT

The authors thank to PFMU Dharmasraya, Dharmasraya District Forestry Service, and Local Communities at the research location who gave permission and participated in the research. This study was funded by Ministry of Research, Technology and Higher Education through Program Menuju Doktor Sarjana Unggul (PMDSU) Grant 2014-2017 and supported by National Research and Innovation Agency, Indonesia through Researcher Mobility Program [Contract No. 151/II/HK/2022].

#### CONFLICT OF INTEREST

The author declares that there is no conflict of interests regarding the publication of this manuscript. In addition, the ethical issues, including plagiarism, informed consent, misconduct, data fabrication and/or falsification, double publication and/or submission, and redundancy have been completely observed by the authors.

#### OPEN ACCESS

©2024 The author(s). This article is licensed under a Creative Commons Attribution 4.0 International License, which permits use, sharing, adaptation, distribution and reproduction in any medium or format, as long as you give appropriate credit to the original author(s) and the source, provide a link to the Creative Commons license, and indicate if changes were made. The images or other third-party material in this article are included in the article's Creative Commons license, unless indicated otherwise in a credit line to the material. If material is not included in the article's Creative Commons license and your intended use is not permitted by statutory regulation or exceeds the permitted use, you will need to obtain permission directly from the copyright holder. To view a copy of this license, visit: <http://creativecommons.org/licenses/by/4.0/>

#### PUBLISHER'S NOTE

GJESM Publisher remains neutral with regard to jurisdictional claims in published maps and institutional affiliations.

#### ABBREVIATIONS DEFINITION

%	Percent
BAL	Basic agrarian law
BPN	Badan pertanahan nasional (National land agency)
CBS	Central Bureau of Statistics
FAO	Food and agriculture organization
FFB	Fresh fruit bunches
ha	Hectare
HGU	Hak guna usaha (Land use rights)

<i>HPH</i>	Hak penguasaan hutan (Forest concession rights)
<i>HTI</i>	Hutan tanaman industri (Industrial plantation forest)
<i>IUPHHK</i>	Izin usaha pengelolaan hasil hutan kayu hutan tanaman industri (Forest timber product exploitation permits)
<i>KAN</i>	Kerapatan adat nagari (Council of the elder chief)
<i>KOSKOPABO</i>	Koperasi Sawit Koto Besar Padang Bungur dan Bonjol (Cooperative Organization)
<i>Km</i>	Kilometer
<i>MKK</i>	Mamak kepala kaum (Leader of a tribe or clan)
<i>MKW</i>	Mamak kepala waris (Ruler of customary land)
<i>MOEF</i>	Ministry of environment and forestry
<i>NESHP</i>	Nucleus estate smallholder oil palm plantation
<i>PFMU</i>	Production forest management unit
<i>PT</i>	Perseroan terbatas (Private limited company)
<i>PT AWB</i>	PT Andalas wahana berjaya
<i>PT BRM</i>	PT Bukit raya mudisa
<i>PT DSL</i>	PT Dhara silva lestari
<i>PT SMP</i>	PT Silago Makmur Plantation
<i>SNA</i>	Social network analysis
<i>USD</i>	United states dollars

## REFERENCES

- Alandra, Y.; Amelia, F.U.D.; Iskandar, J., (2018). The traditional Rimbo Larangan system of forest management: An ethnoecological case study in Nagari Paru, Sijunjung District, West Sumatra, Indonesia. *Asian J. Ethnobiol.*, 1(2): 61-68 **(8 pages)**.
- Anugrah, D.; Muin, A.V.F.; Irlan, I.; Tomasina, M.A.; Azila, N.; Sirimorok, N.; Dungga, N.E.; Alam, S., (2022). Injustice against Women in a Social Forestry Program: Case Studies from Two Indonesian Villages. *For. Soc.*, 6(2): 723-741 **(19 pages)**.
- Barsimantov, J.; Kendall, J., (2012) Community forestry, common property and deforestation in eight Mexican states. *J. Environ. Develop.*, 21 (4): 414-437 **(24 pages)**.
- Bhattarai, S.; Pant, B.; Laudari, H.K.; Rai, R.K.; Mukul, S.A., (2021). Strategic Pathways to Scale Up Forest and Landscape Restoration: Insights from Nepal's Tarai. *Sustainability.*, 13(9): 1-16 **(16 pages)**.
- Billah, M.M.; Rahman, M.M.; Abedin, J.; Akter, H., (2021). Land cover change and its impact on human–elephant conflict: a case from Fashiakhali forest reserve in Bangladesh. *SN Appl. Sci.*, 3(649): 1-17 **(17 pages)**.
- Borgatti, S.P.; Everett, M.G.; Freeman, L.C., (2002). UCINET 6 for Windows: Software for social network analysis (Version 6.102). Harvard, Ma: Analytic Technologies.
- Brun, C.; Cook, A.R.; Lee, J.S.H.; Wich, S.A.; Koh, L.P.; Carrasco, L.R., (2015). Analysis of deforestation and protected area effectiveness in Indonesia: A comparison of Bayesian spatial models. *Global Environ. Change.* 319: 285–295 **(11 pages)**.
- CBS, (2018). Statistik Produksi Kehutanan. Forestry Production Statistics 2018. Central Bureau of Statistics, Jakarta.
- Dalla-Nora, E.L.; de Aguiar, A.P.D.; Lapola, D.M.; Woltjer, G., (2014). Why have land use change models for the Amazon Failed to Capture the Amount of Deforestation Over the Last Decade? *Land Use Policy.*, 39(2014): 403–411 **(9 pages)**.
- FAO., (2015). Global Forest Resources Assessment 2015. Global For. Resour. Assess., FAO, Rome.
- Feurer, M.; Gritten, D.; Than, M.M., (2018). Community Forestry for Livelihoods: Benefiting from Myanmar's Mangroves. *Forests.* 9(2018): 1-15 **(15 pages)**.
- Fragallah, S.A.D.A.; Lulandala, L.L.L.; Eltahir, M.E.S.; Khalifa, A.E.S.O.; Ahmed, S.E.E.; Suliman, K.H.; Ahmed, E.H.; Musa, F.I.; Ligate, E.J., (2021). Participation of Local Community in Tree Conservation Practices for Sustainable Forest Management in Mzinga River Catchment, Uluguru Mountains – Tanzania. *Asian J. Res. Rev. Agric.*, 3(1): 148–168 **(21 pages)**.
- Freeman, L.C., (1978). Centrality in Social Networks Conceptual Clarification. *Social Networks.*, 1(3): 215-239 **(24 pages)**.
- Garcia, B.; Rimmer, L.; Vieira, L.C.; Mackey, B., (2021). REDD+ and forest protection on indigenous lands in the Amazon. *Rev. Europ. Comp. Int. Environ. Law.*, 30(2): 207-219 **(13 pages)**.
- Geist, H.J.; Lambin, E.F., (2002). Proximate Causes and Underlying Driving Forces of Tropical Deforestation. *BioScience.* 52 (2): 143–150 **(8 pages)**.
- Hapsari, M., (2018). Contesting deforestation: civil society movements and knowledge co-production in Indonesia. *Power Conflict Democracy J.*, 6(1): 117-145 **(28 pages)**.
- Harun, M.K.; Dwiprabowo, H., (2014). Model resolusi konflik lahan di Kesatuan Pemangkuan Hutan Produksi Model Banjar (Resolution model of land conflicts in Production Forest Management Unit of Banjar). *J. Penelitian Sosial dan Ekonomi Kehutanan.*, 11: 265–280 **(16 pages)**.
- Hidayat.; Lukitaningsih., (2022). Changes in Ownership and Ulayat Land Use in Lumban Rau Timur Village, Toba Samosir. *Indones. Hist. Stud.*, 5(2): 161-186 **(26 pages)**.
- Jackson, E.A., (2015). Ethnographic Narrative of Forest Decline in the Goderich Community: The People's Perspectives. *Forest Res.*, 4(4): 157-163 **(7 pages)**.
- Ji, Y.; Ranjan, R; Truong, C., (2017). Determinants of illegal logging in Indonesia: An empirical analysis for the period 1996–2010. *J. Sustainable For.*, 36: 197-220 **(24 pages)**.

- Kraus, S.; Liu, J.; Kocha, N.; Fuss, S., (2021). No aggregate deforestation reductions from rollout of community land titles in Indonesia yet. *PNAS.*, 118 (43): e2100741118 **(3 pages)**.
- Larson, A.M., (2012). Tenure rights and access to forests. A training manual for research. Jakarta: Center for International Forestry Research. 1-71 **(71 pages)**.
- Margono, B.A.; Potapov, P.V.; Turubanova, S.; Stolle, F.; Hansen, M.C., (2014). Primary forest cover loss in Indonesia over 2000–2012. *Nat. Clim. Change.* 4: 1–6 **(6 pages)**.
- Marin, A.; Wellman, B., (2010). Social Network Analysis: An Introduction. In J. Scott and P. J. Carrington (Eds.), *Handbook of Social Network Analysis*. New York: Sage Publications. 11–25 **(15 pages)**.
- Maring, P., (2022). Conflict transformation and collaboration in developing social forestry in Flores, Indonesia. *For. Soc.*, 6(1): 40-66 **(17 pages)**.
- Marsden, P.V., (2011). Survey Methods for Network Data. In J. Scott and P. J. Carrington (Eds.), *The Sage Handbook of Social Network Analysis*. New York: Sage Publications. 370–388 **(19 pages)**.
- Medaline, O.; Fatmawati, I.; Nurhayati, S., (2022). The “Social Advocacy” Model Of Wakf Land Settlements of Minangkabau Province West Sumatra. *J. Positive School Psychol.*, 6 (9): 542-549 **(7 pages)**.
- Miles, M.B.; Huberman, A.M., (1994). *Qualitative Data Analysis: A Sourcebook of New Methods*. Sage Publication: Inc Beverly Hills USA **(354 pages)**.
- MOEF, (2021). Status status of forests and forestry. Ministry of Environment and Forestry, Ministry of Environment and Forestry. Jakarta.
- MOEF., (2023). Status Lingkungan Hidup Indonesia 2022. Ministry of Environment and Forestry, Jakarta.
- Mukarom, M.; Yuwono, T.G.; Sirajuddin, S.; Suryadinata, S.; Maududi, A.; Anshar, C.; Tuarita, A.; Perdana, A.A.; Jatiningsih, I.; Herman, H.; Sakinah, A.; Jusmawarni, J.; Yumantoko, Y.; Maidianto, M., (2015). *Memberdayakan Masyarakat melalui Kemitraan Kehutanan* Kompilasi Tulisan Pengalaman dari KPH Rinjani Barat. Kemitraan Partnership & Kedutaan Besar Norwegia dan Ford Foundation, Jakarta **(66 pages)**.
- Muur, W.V.D., (2018). Forest conflicts and the informal nature of realizing indigenous land rights in Indonesia. *Citizenship Stud.*, 22(2): 160-174 **(15 pages)**.
- Mutolib, A.; Yonariza, Y.; Mahdi, M.; Ismono, H., (2016). Gender inequality and the oppression of women within Minangkabau matrilineal society: A Case study of the management of *Ulayat* forest land in Nagari Bonjol, Dharmasraya District, West Sumatra Province, Indonesia. *Asian Women.* 32(3): 23–49 **(27 pages)**.
- Mutolib, A.; Yonariza, Y.; Mahdi, M.; Ismono, H., (2017). Forest ownership conflict between a local community and the state: A case study in Dharmasraya, Indonesia. *J. Trop. For. Sci.*, 29(2): 163–171 **(9 pages)**.
- Nelson, A.; Chomitz, K.M., (2011). Effectiveness of strict vs Multiple use protected areas in reducing tropical forest fires: a global analysis using matching methods. *PLoS One.* 6 (2011): 1-14 **(14 pages)**.
- Nolte, C.; Agrawal, A.; Silvius, K.M.; Soares-Filho, B.S., (2013). Governance regime and location influence avoided deforestation success of protected areas in the Brazilian Amazon. *PNAS.*, 110 (13): 4956–4961 **(96 pages)**.
- Nunes, L.J.R.; Meireles, C.I.R.; Gomes, C.J.P.; Ribeiro, N.M.C.A., (2019). Forest Management and Climate Change Mitigation: A Review on Carbon Cycle Flow Models for the Sustainability of Resources. *Sustainability.* 11(9): 5276 **(10 pages)**.
- Prell, C., (2011). *Social Network Analysis: History, Theory and Methodology*. Sage Publication, Thousand Oaks, USA **(272 pages)**.
- Rangga, K.K.; Yonariza.; Yanfika, H.; Mutolib, A., (2020). Perception, attitude, and motive of local community towards forest conversion to plantation in Dharmasraya District, West Sumatra, Indonesia. *Biodiversitas.*, 21(10): 4903-4910 **(8 pages)**.
- Rochmayanto, Y.; Nurrochmat, D.R.; Nugroho, B.; Darusman, D.; Satria, A.; Casse, T.; Erbaugh, J.T.; Wicaksono, D., (2023). Devolution of forest management to local communities and its impacts on livelihoods and deforestation in Berau, Indonesia. *Heliyon.* 9(5): e16115 **(16 pages)**.
- Rudy, R.; Yonariza, Y.; Yanfika, H.; Rahmat, A.; Ramadhani, W.; and Mutolib, A. (2021). Forest Cover Change and Legal Pluralism in Forest Management: A Review and Evidence from West Sumatra, Indonesia. *Indonesian J. Sci. Technol.*, 6(2): 299-314 **(16 pages)**.
- Shrinkhal, R., (2021). Indigenous sovereignty” and right to self-determination in international law: a critical appraisal. *AlterNative. An Int. J. Indigenous People.* 17(1): 71–82 **(12 pages)**.
- Siregar, E.; Sentosa, S.; Satrianto, A., (2023). An analysis on the economic development and deforestation. *Global J. Environ. Sci. Manage.*, 10(1): 1-14 **(14 pages)**.
- Sunderlin, W.D.; Resosudarmo, I.A.P., (1996). Rates and Causes of Deforestation in Indonesia: Towards a Resolution of Ambiguities. *Occasional Papers Number 9: 1-19 (19 pages)*.
- Suryadi, S.; Dharmawan, A.H.; Barus, B., (2020). Ekspansi Perkebunan Kelapa Sawit: Persoalan Sosial, Ekonomi dan Lingkungan Hidup (Studi Kasus Kab. Pelalawan, Riau) [Palm Oil Plantation Expansion: Social, Economic and Environmental Issues (Case Study of Pelalawan District, Riau)]. *J. Ilmu Lingkungan.* 18 (2): 367-374 **(8 pages)**.
- Ting, Z.; Haiyun, C.; Shivakoti, G.P.; Cochard, R.; Homchaim, K., (2011). Revisit to community forest in northeast of Thailand: Changes in status and utilization. *Enviro. Dev. Sustainability.* 13(2): 385–402 **(17 pages)**.
- Vanclay, J.K., (2005). Deforestation: correlations, possible causes and some implications. *Int. For. Rev.* 7(4): 278–293 **(16 pages)**.
- Walker, W.S.; Gorelik, S.R.; Baccini, A.; Aragon-Osejo, J.L.; Josse, C., (2020). The role of forest conversion, degradation, and disturbance in the carbon dynamics of Amazon indigenous territories and protected areas. *PNAS.* 117(6): 3015–3025 **(11 pages)**.
- Wicke, B.; Sikkema, R.; Dornburg, V.; Faaij, A., (2011). Exploring land use changes and the role of palm oil production in Indonesia and Malaysia. *Land Use Policy.* 28(1): 193–206 **(14 pages)**.

#### AUTHOR (S) BIOSKETCHES

**Mutolib, A.**, Ph.D., Assistant Professor, Department of Agribusiness, Graduate Program, University of Siliwangi, Jl. Siliwangi No. 24, Kahuripan, Tawang, Kota Tasikmalaya, Jawa Barat 46115, Indonesia.

- Email: [amutolib24@yahoo.com](mailto:amutolib24@yahoo.com)
- ORCID: [0000-0002-0788-4991](https://orcid.org/0000-0002-0788-4991)
- Web of Science ResearcherID: H-5168-2017
- Scopus Author ID: 57191584252
- Homepage: <https://sinta.kemdikbud.go.id/authors/profile/6675434>

**Yonariza, Y.**, Ph.D., Professor, Department of Integrated Natural Resources Management, School of Graduate, Andalas University. Limau Manis, Kecamatan Pauh, Kota Padang, Sumatra Barat 25175 Indonesia

- Email: [yonariza@yahoo.com](mailto:yonariza@yahoo.com)
- ORCID: [0000-0003-4667-744X](https://orcid.org/0000-0003-4667-744X)
- Web of Science ResearcherID: AAC-8557-2021
- Scopus Author ID: 34968859700
- Homepage: <https://yonariza.com/>

**Rahmat, A.**, Ph.D., Associate Professor, Research Center for Limnology and Water Resources, The National Research and Innovation Agency (BRIN), Jl. Raya Jakarta-Bogor km. 46, Cibinong 16911, Bogor Jawa Barat, Indonesia

- Email: [alirahmat@gmail.com](mailto:alirahmat@gmail.com)
- ORCID: [0000-0003-3475-775X](https://orcid.org/0000-0003-3475-775X)
- Web of Science ResearcherID: AAM-5139-2020
- Scopus Author ID: 57189066685
- Homepage: <https://sinta.kemdikbud.go.id/authors/profile/6761124>

#### HOW TO CITE THIS ARTICLE

Mutolib, A.; Yonariza, Y.; Rahmat, A.; (2024). *Abnormality in optimal forest management by indigenous people in deforestation. Global J. Environ. Sci. Manage.*, 10(1): 405-418.

DOI: [10.22034/gjesm.2024.01.25](https://doi.org/10.22034/gjesm.2024.01.25)

URL: [https://www.gjesm.net/article\\_708192.html](https://www.gjesm.net/article_708192.html)



## PUBLICATION ETHICS

The ethical policy of GJESM is based on the Committee on Publication Ethics (COPE) guidelines and complies with International Committee of GJESM Editorial Board codes of conduct. Readers, authors, reviewers and editors should follow these ethical policies once working with GJESM. The ethical policy of GJESM is liable to determine which of the typical research papers or articles submitted to the journal should be published in the concerned issue. For information on this matter in publishing and ethical guidelines please visit <http://publicationethics.org>

### Duties and Responsibilities of Publishers

1. GJESM is committing to ensure that editorial decisions on manuscript submissions are the final.
2. GJESM is promising to ensure that the decision on manuscript submissions is only made based on professional judgment and will not be affected by any commercial interests.
3. GJESM is committing to maintain the integrity of academic and research records.
4. GJESM is monitoring the ethics by Editor-in-Chief, Associate Editors, Editorial Board Members, Reviewers, Authors, and Readers.
5. GJESM is always checking the plagiarism and fraudulent data issues involving in the submitted manuscript.
6. GJESM is always willing to publish corrections, clarifications and retractions involving its publications as and when needed.

### Duties and Responsibilities of Editors

1. The Editors of the journal should have the full authority to reject/accept a manuscript.
2. The Editors of the journal should maintain the confidentiality of submitted manuscripts under review or until they are published.
3. The Editor-in-Chief should take a decision on submitted manuscripts, whether to be published or not with other editors and reviewers
4. The Editors of the journal should preserve the anonymity of reviewers.
5. The Editors of the journal should disclose and try to avoid any conflict of interest.
6. The Editors of the journal should maintain academic integrity and strive to meet the needs of readers and authors.
7. The Editors of the journal should be willing to investigate plagiarism and fraudulent data issues and willing to publish corrections, clarifications, retractions, and apologies when needed.
8. The Editors of the journal should have the limit themselves only to the intellectual content.
9. The Editors of the journal must not disclose any information about submitted manuscripts to anyone other than the corresponding author, reviewers, potential reviewers, other editorial advisers, and the publisher, as appropriate.
10. Unpublished materials disclosed in a submitted paper will not be used by the editor or the members of the editorial board for their own research purposes without the author's explicit written consent.

### Duties and Responsibilities of Reviewers

1. The Reviewers of the journal should assist the Editors in taking the decision for publishing the submitted manuscripts.
2. The Reviewers should maintain the confidentiality of manuscripts, which they are invited to review.
3. The Reviewers should provide comments in time that will help editors to make decision on the submitted manuscript to be published or not.
4. The Reviewers are bound to treat the manuscript received for peer reviewing as confidential, and must not use the information obtained through peer review for personal advantage.
5. The Reviewers comments against each invited manuscript should be technical, professional and objective.
6. The Reviewers should not review the manuscripts in which they have found conflicts of interest with any of the authors, companies, or institutions.
7. The Reviewers should disclose and try to avoid any conflict of interest.

### Duties and Responsibilities of Authors

1. Manuscripts must be submitted only in English and should be written according to sound grammar and proper terminology.
2. Manuscripts must be submitted with the understanding that they have not been published elsewhere (except in the form of an abstract or as part of a published lecture, review, or thesis) and are not currently under consideration by another journal published by or any other publisher.
3. The submitting (corresponding) author is responsible for ensuring that the manuscript article's publication has been approved by all the other coauthors.
4. In order to sustain the peer review system, authors have an obligation to participate in peer review process to evaluate manuscripts from others.
5. It is also the authors' responsibility to ensure that the manuscripts emanating from a particular institution are submitted with the approval of the necessary institution.
6. It is a condition for submission of a manuscript that the authors permit editing of the paper for readability.
7. Authors are requested to clearly identify who provided financial support for the conduct of research and/or preparation of the manuscript and briefly describe the role of the funder/sponsor in any part of the work.
8. A copy right release and conflict of interest disclosure form must be signed by the corresponding author in case of multiple authorships, prior to the acceptance of the

manuscript, by all authors, for publication to be legally responsible towards the Journal ethics and privacy policy.

9. Under open access license, authors retain ownership of the copyright for their content, but allow anyone to download, reuse, reprint, modify, distribute, and/ or copy the content as long as the original authors and source are cited properly.
10. All authors have agreed to allow the corresponding author to serve as the primary correspondent with the editorial office, to review the edited manuscript and proof.
11. When author(s) discovers a significant error or inaccuracy in his/her own published work, it is the author's obligation to promptly notify the journal editor or publisher to retract or correct the manuscript.
12. All authors must know that that the submitted manuscripts under review or published with GJESM are subject to screening using Plagiarism Prevention Software. Plagiarism is a serious violation of publication ethics.

#### Violation of Publication Ethics

1. **Plagiarism:** Plagiarism is intentionally using someone else's ideas or other original material as if they are one's own. Copying even one sentence from someone else's manuscript, or even one of your own that has previously been published, without proper citation is considered by GJESM Journals as plagiarism. All manuscripts under review or published with GJESM are subject to screening using plagiarism prevention software. Thus, plagiarism is a serious violation of publication ethics. The development of CrossCheck is a service that helps editors to verify the originality of papers. CrossCheck is powered by the iThenticate software from iParadigms, known in the academic community as providers of Turnitin. For a searchable list of all journals in the CrossCheck database, please visit: [www.ithenticate.com/search](http://www.ithenticate.com/search)
2. **Data Fabrication and Falsification:** Data fabrication and falsification means the researcher did not really carry out the study, but made up data or results and had recorded or reported the fabricated information. Data falsification means the researcher did the experiment, but manipulated, changed, or omitted data or results from the research findings.
3. **Simultaneous Submission:** Simultaneous submission occurs when a manuscript (or substantial sections from a manuscript) is submitted to a journal when it is already under consideration by another journal.
4. **Duplicate Publication:** Duplicate publication occurs when two or more papers, without full cross referencing, share essentially the same hypotheses, data, discussion points, and conclusions.
5. **Redundant Publications:** Redundant publications involve the inappropriate division of study outcomes into several articles, most often consequent to the desire to plump academic vitae.

6. **Improper Author Contribution or Attribution:** All listed authors must have made a significant scientific contribution to the research in the manuscript and approved all its claims. Don't forget to list everyone who made a significant scientific contribution, including students and laboratory technicians.
7. **Citation Manipulation:** Citation Manipulation is including excessive citations, in the submitted manuscript, that do not contribute to the scholarly content of the article and have been included solely for the purpose of increasing citations to a given author's work, or to articles published in a particular journal. This leads to misrepresenting the importance of the specific work and journal in which it appears and is thus a form of scientific misconduct.

#### Handling Cases of Misconduct

Once GJESM confirms a violation against GJESM's publication ethics, GJESM addresses ethical concerns diligently following an issue-specific standard practice as summarized below.

1. The first action of the journal Editor is to inform the Editorial Office of GJESM by supplying copies of the relevant material and a draft letter to the corresponding author asking for an explanation in a nonjudgmental manner.
2. If the author's explanation is unacceptable and it seems that serious unethical conduct has taken place, the matter is referred to the Publication Committee via Editorial Office. After deliberation, the Committee will decide whether the case is sufficiently serious to warrant a ban on future submissions.
3. If the infraction is less severe, the Editor, upon the advice of the Publication Committee, sends the author a letter of reprimand and reminds the author of GJESM publication policies; if the manuscript has been published, the Editor may request the author to publish an apology in the journal to correct the record.
4. Notification will be sent to corresponding author and any work by the author responsible for the violation or any work these persons coauthored that is under review by GJESM journal will be rejected immediately.
5. The authors are prohibited from serving on GJESM editorial board and serving as a reviewer for GJESM Journal. GJESM reserves the right to take more actions.
6. In extreme cases, notifications will be sent to the affiliations of the authors and the authors are prohibited from submitting their work to GJESM for 5 years.
7. In serious cases of fraud that result in retraction of the article, a retraction notice will be published in the journal and will be linked to the article in the online version. The online version will also be marked "retracted" with the retraction date.

## GUIDE FOR AUTHORS

"Global Journal of Environmental Science and Management" (GJESM) is a double blind peer reviewed electronic and print quarterly publication concerned with all aspects of environmental science and management. GJESM publishes original research papers, review papers, case reports and short communications, letters to editor and authors' response about letters to editor across the broad field of environment. These include but are not limited to environmental science, environmental management, environmental engineering, environmental planning and design, urban and regional landscape design and industrial ecology. Environmentalist disciplines are invited to contribute their knowledge and experience. The publication appears at regular intervals time quarterly. The Journal database is fully open access and full text of published articles are available for everyone who can get access to the Journal website free of cost. The authors never pay any charges for submission, article processing and publication.

**Guide for Authors:** More details on guide for authors refer: <http://gjesm.net/journal/authors.note>

### GENERAL

1. Authors should submit their contributions electronically through the GJESM website submission system to the Editorial Office.
2. Manuscripts must be submitted only in English and should be written according to sound grammar and proper terminology. Manuscripts should be typed in Times New Roman of 11 pt. font and in MS-Word format in one column with 2.5 cm margin at each side. Manuscript submission must be applied once in order to obtain only one submission ID number. More than one submission for a single manuscript can lose the chance of the manuscript consideration. Manuscript must be accompanied by a covering letter including title and author(s) name.
3. There are no strict formatting requirements but all manuscripts must contain the essential elements needed to convey your manuscript, for example Abstract, Keywords, Introduction, Materials and Methods, Results, Conclusions, Artwork and Tables with Captions. Please ensure the figures and the tables included in the single file are placed next to the relevant text in the manuscript, rather than at the bottom or the top of the file. There are no strict requirements on reference formatting at submission. References can be in any style or format as long as the style is consistent.

### BEFORE YOU BEGIN

**1. Peer-Review Process:** In order to sustain the peer review system, authors have an obligation to participate in peer review process to evaluate manuscripts from others. When appropriate, authors are obliged to provide retractions and/or corrections of errors to the editors and the Publisher. All papers submitted to GJESM journal will be peer reviewed for at least one round. GJESM journal adopts a double-blinded review policy: authors are blind to reviewers, but reviewers are not blind to authors. After receiving reviewers' comments, the editorial team member makes a decision. Because reviewers sometimes do not agree with each other, the final decision sent to the author may not exactly reflect recommendations by any of the reviewers. The decision after each round of peer review may include (a) Accept without any further changes, (b) Accept with minor revision, (c) Major changes are necessary for resubmission and (d) Decline without encouraging resubmission.

**2. Post-Publication Evaluation:** In addition to rapid Peer Review Process, the GJESM Journal has Post-Publication Evaluation by the scientific community. Post-Publication Evaluation is concentrated to ensure that the quality of published research, review and case report meets certain standards and the conclusions that are presented are justified. The post-publication evaluation includes online comments and citations on published papers. Authors may respond to the comments of the scientific community and may revise their manuscript. The Post-Publication Evaluation is described in such a way; it is allowing authors to publish quickly about Environmental science, management, engineering and technology concepts.

**3. Publication Ethics:** The ethical policy of GJESM is based on the Committee on Publication Ethics (COPE) guidelines and complies with International Committee of GJESM Editorial Board codes of conduct. Readers, authors, reviewers and editors should follow these ethical policies once working with GJESM. The ethical policy of GJESM is liable to determine which of the typical research papers or articles submitted to the journal should be published in the concerned issue. The ethical policy insisted the Editor-in-Chief, may confer with other editors or reviewers in making the decision. Visit at: <http://publicationethics.org>

**4. Conflict of Interest:** Authors are requested to evident whether impending conflicts do or do not exist. A copyright transfer agreement is signed by the corresponding author, upon the acceptance of the manuscript, on behalf of all authors, for publication to be legally

responsible towards the journal ethics and privacy policy. Authors will be notified as soon as possible of decisions concerning the suitability of their manuscripts for publication in the journal. The submitted materials may be considered for inclusion but cannot be returned and Editors of the journal reserve the right to accept or reject any article in any stage, if necessary. Conflict of Interest Disclosure form can be found at: [www.gjesm.org/conflict\\_of\\_interest\\_disclosure\\_form.docx](http://www.gjesm.org/conflict_of_interest_disclosure_form.docx)

**5. Submission Declaration and Verification:** While submitting a manuscript to GJESM, all contributing author(s) must verify that the manuscript represents authentic and valid work and that neither this manuscript nor one with significantly similar content under their authorship has been published or is being considered for publication elsewhere including electronically in the same form, in English or in other language, without the written consent the copy right holder.

**6. Authorship:** All contributing authors should qualify for authorship and corresponding author should sign the authorship form while submitting the manuscript. It can be found at: [http://www.gjesm.net/data/gjesm/news/authorship\\_form.docx](http://www.gjesm.net/data/gjesm/news/authorship_form.docx).

**7. Changes to Authorship:** After the manuscript is submitted or accepted for publication, the corresponding author is required to send a request to add or remove an author or to rearrange the author names of the submitted/accepted manuscript by sending the change of authorship form to editorial office. No authorship change is allowed after publication of manuscript. More details may be found at: [http://www.gjesm.net/data/gjesm/news/change\\_of\\_authorship\\_form.docx](http://www.gjesm.net/data/gjesm/news/change_of_authorship_form.docx)

**8. Retained Author Rights:** As an author, author or authors' employer or institution retains certain rights. For more information on author rights, found at: [www.gjesm.org/retained\\_authors\\_right.docx](http://www.gjesm.org/retained_authors_right.docx).

**9. Copy Right:** Journals should make clear the type of copyright under which authors' work will be published. For open access articles the publisher uses an exclusive licensing agreement in which authors retain copyright in their manuscript. More details may be found at: [www.gjesm.org/copyright\\_form.docx](http://www.gjesm.org/copyright_form.docx)

**10. User license Agreement:** GJESM provides access to archived material through GJESM archives. Manuscripts are the parts of an open archive are made freely available from GJESM website after certain period, which begins from the final publication date of the manuscript. All articles published open access will be immediately and permanently free for everyone to read and download. Permitted reuse is defined by Creative Commons user license called **Creative Commons Attribution**. Visit at: [Creative Commons Attribution 4.0 International \(CC BY 4.0\)](http://creativecommons.org/licenses/by/4.0/)

**11. Plagiarism Prevention and Violation of Publication Ethics:** All manuscripts under review or published with GJESM are subject to screening using Plagiarism Prevention Software. Plagiarism is a serious violation of publication ethics. Other violations include duplicate publication, data fabrication and falsification, and improper credit of author contribution. Thus, the Plagiarism or Fraudulent or knowingly inaccurate statements constitute unethical behavior are unacceptable and submitting the same manuscript to more than one journal concurrently constitutes unethical publishing behavior and is unacceptable. The development of CrossCheck is a service that helps editors to verify the originality of papers. CrossCheck is powered by the Ithenticate software from iParadigms, known in the academic community as providers of Turnitin. For more details visit at: [www.ithenticate.com/search](http://www.ithenticate.com/search)

**12. Handling Cases of Misconduct:** Once GJESM confirms a violation against GJESM's publication ethics, the following actions will be taken.

- a. The work is rejected / retracted immediately. Notification will be sent to corresponding authors. In extreme cases, notifications will be sent to the affiliations of the authors.
- b. The authors are prohibited from submitting their work to GJESM for 5 years.
- c. Any work by the authors responsible for the violation or any work these persons coauthored that is under review by any GJESM journal will be rejected immediately.
- d. The authors are prohibited from serving on GJESM editorial board. GJESM reserves the right to take more actions.

## MANUSCRIPT PREPARATION

**1. Title Page:** The title page should include: the name(s) of the author(s), a concise and informative title, the affiliation(s) and address (es) of the author(s), and e-mail address, telephone and fax numbers of the corresponding author.

**2. Manuscript Title:** Title of up to 17 words should not contain the name of locations, countries or cities of the research as well as abbreviations. The title should be oriented to Environmental issues while not being obscure or meaningless.

**3. Abstract:** An abstract of 150 to 250 words that sketches the purpose of the study; basic procedures; main findings its novelty; discussions and the principal conclusions, should not contain any undefined abbreviations or references.

**4. Keywords:** Provide 5 to 7 keywords which can be used for indexing purposes. Keywords should not repeat the words of the manuscript title or contain abbreviations and shall be written in alphabetical order as separated by semicolon.

**5. Introduction:** The Introduction should state the purpose of the investigation and identify clearly the gap of knowledge that will be filled in the Literature review study. Date and location of the research carried out throughout the study must be mentioned at the end of this section.

**6. Materials and methods:** The Materials and Methods section should provide enough information to permit repetition of the experimental work. It should include clear descriptions and explanations of sampling procedures, experimental design, and essential sample characteristics and descriptive statistics, hypothesis tested, exact references to literature describing the tests used in the manuscript, number of data involved in statistical tests, etc.

**7. Results and Discussion:** The Results section should describe the outcome of the study. Data should be presented as concisely as possible - if appropriate in the form of tables or figures, although very large tables should be avoided. The Discussion should be an interpretation of the results and their significance with reference to work by other authors. Please note that the policy of the Journal with respect to units and symbols is that of SI symbols.

**8. Tables:** Do not submit tables and graphs as photograph. Place explanatory matters in footnotes, not in the heading. Do not use internal horizontal and vertical rules. Tables should be called out in the text and should have a clear and rational structure and consecutive numerical order. All tables should be numbered 1, 2, 3, etc. Give enough information in subtitles so that each table is understandable without reference to the text. Footnotes to tables should be indicated by superscript lower-case letters (or asterisks for significance values and other statistical data) and included beneath the table body.

**9. Figures:** Figures/ illustrations should be in high quality art work, within 200-300 dpi and separately provided in Excel format. Ensure that figures are clear, labeled, and of a size that can be reproduced legibly in the journal. Each figure should have a concise caption describing accurately what the figure depicts. Figure captions begin with the term Fig. Figures should be with the captions placed below in limited numbers. No punctuation is to be placed at the end of the caption.

**10. Conclusion:** This section should highlight the major, firm discoveries, and state what the added value of the main finding is, without literature references.

**11. Acknowledgements:** Acknowledgments of people, grants, funds, etc. should be placed in a separate section before the reference list. The names of funding organizations should be written in full. Financial support

affiliation of the study, if exists, must be mentioned in this section. Thereby, the Grant number of financial support must be included.

**12. References:** All the references should be cited throughout the manuscript text as well as in the Reference section organized in accordance with Harvard system. Groups of references should be listed first alphabetically, then chronologically. The number of references extracted from each journal should not exceed 3 to 5 citations, which is the average acceptable amount. The number of references should not be less than 30 for original paper, less than 100 for review paper. It is substantially recommended to the authors to refer to more recent references rather than old and out of date ones. Volume, issue and pages of the whole references must be specified according to the GJESM format.

**Citing and listing of Web references:** As a minimum, the full URL should be given. Any further information, if known (Author names, dates, reference to a source publication, etc.), should also be given.

**Text:** All citations in the text should refer to: 1. Single author: the author's name (without initials, unless there is ambiguity) and the year of publication; 2. Two authors: both authors' names and the year of publication; and 3. Three or more authors: first author's name followed by "et al." and the year of publication. Citations may be made directly (or parenthetically). Groups of references should be listed first alphabetically, then chronologically. Examples: "as demonstrated (Allan, 1996a, 1996b, 1999; Allan and Jones, 1995). Kramer *et al.*, (2000) have recently shown ...".

**List:** References should be arranged first alphabetically and then further sorted chronologically if necessary. More than one reference from the same Author(s) in the same year must be identified by the letters "a", "b", "c", etc., placed after the year of publication.

**Journal article:** Nouri J.; Lorestani B.; Yousefi N.; Khorasani N.; Hassani A. H.; Seif, F.; Cheraghi M., (2011). Phytoremediation potential of native plants grown in the vicinity of Ahangan lead-zinc mine. *Environ. Earth Sci.*, 62(3): 639-644.

**Book:** Davis, M. L., (2005). *Introduction to Environmental Engineering*, 3rd. Ed. McGraw Hill Inc.

**Book chapter:** Mettam, G. R.; Adams, L. B., (1999). How to prepare an electronic version of your article, in: Jones, B. S., Smith, R. Z. (Eds.), *Introduction to the electronic age*. E-Publishing Inc., New York.

**Conference paper:** Brown, J., (2005). Evaluating surveys of transparent governance. In UNDESA, 6th. *Global forum on reinventing government: towards participatory and transparent governance*. Seoul, Republic of Korea 24-27 May. United Nations: New York.

**Dissertation:** Trent, J. W., (1975). *Experimental acute renal failure*. Ph.D. Dissertation, University of California. USA.

**Online document:** Cartwright, J., (2007). Big stars have weather too. IOP Publishing Physics Web. <http://physicsworld.com/cws/article/news/2007/jun/26/big-stars-have-weather-too>

## AFTER ACCEPTANCE

**1. Online Proof Correction:** Corresponding authors will receive an e-mail with a link to our online proofing system, allowing annotation and correction of proofs online. Use this proof only for checking the typesetting, editing, completeness and correctness of the text, tables and figures. Significant changes to the article as accepted for publication will only be considered at this stage with permission from the Editor-in-Chief. It is important to ensure that all corrections are sent back to us in one communication. Please check carefully before replying, as inclusion of any subsequent corrections cannot be guaranteed. Proofreading is solely the corresponding author responsibility.

**2. Offprints:** The offprints can be downloading from the GJESM website once the final corrected manuscripts are disseminated.

## AUTHORS INQUIRIES

Authors can track their submitted article through GJESM website on author's login section at: [http://gjesm.net/contacts?\\_action=login](http://gjesm.net/contacts?_action=login)

# Global Journal of Environmental Science and Management (GJESM)

## Copyright Transfer Agreement

### 1. Parties of the agreement

#### Author (s):

Manuscript Title:

Manuscript ID:

(Herewith referred to as the "materials"),

**Journal Title:** Global Journal of Environmental Science and Management (GJESM)

### 2. Subject of the agreement

#### A) Copyright

1- The Author and each co-authors shall transfer and sell to the Publisher for the length of the copyright starting from the moment the present agreement comes into force the exclusive rights to the materials, including the rights to translate, reproduce, transfer, distribute or otherwise use the materials or parts (fragments) contained therein, for publication in scientific, academic, technical or professional journals or other periodicals and in derivative works thereof, worldwide, in English, in print or in electronic editions of such journals, periodicals and derivative works in all media or formats now existing or that may exist in future, as well as the right to license (or give permission to) third parties to use the materials for publication in such journals, periodicals and derivative works worldwide. The transfer under this agreement includes the right to adapt the presentation of the materials for use in conjunction with computer systems and programs, reproduction or publication in machine-readable format and incorporation into retrieval systems.

2- Reproduction, placement, transfer or any other distribution or use of the materials, or any parts of the materials contained therein, in any way permitted under this Agreement, shall be accompanied by reference to the Journal and mentioning of the Publisher, namely: the title of the article, the name of the Author (Co-authors), the name of the Journal, volume/number, copyright of the publisher.

#### B) Reserved Rights

The Author (Co-authors) or the employer of the Author (Co-authors) of the materials shall retain all proprietary rights (with the exception of the rights transferred to the Publisher under the present Agreement).

#### C) Author Guarantee

The Author (Co-authors) guarantees that the materials are an original work, submitted only to GJESM, and have not been published previously.

In case the materials were written jointly with co-authors, the Author guarantees that he/she has informed them of the terms of this Agreement and obtained their signatures or written permission to singe on their behalf.

The Author guarantees as well that:

The materials do not contain libelous statements.

The materials do not infringe on other persons' rights (including without limitation copyrights, patent rights and the trademark right).

The materials do not contain facts or instructions that can cause damage or injury to third parties and their publication does not cause the disclosure of any secret or confidential information

#### Author (Corresponding Author):

Correspondence Address:

Phone:

Fax:

Email:

Corresponding Author Name:

Signature

Date

#### On Behalf of the Publisher:

Iran Solid Waste Association,  
Faculty of Environment, University of Tehran,  
Postal Code: 1417854511, Tehran,  
**Iran**

Telefax: (+9821) 2610 5110

Email: [editor@gjesm.net](mailto:editor@gjesm.net)

[Gjesm.publication@gmail.com](mailto:Gjesm.publication@gmail.com)

Website: [www.gjesm.net](http://www.gjesm.net)

Accepted for publication

Signature

Date

**PLEASE NOTE:** The accepted manuscript cannot be processed for publication until the publisher has received this signed form. The form MUST be signed by the Corresponding Author and then scanned and sent through the system or email. If the manuscript is not published in the Journal, this release will not take effect.

The sole responsibility for the whole content (s) of the article remains only with the corresponding author. However, Editor would reserve the right to adjust the style to certain standards of uniformity before publication.

## CONFLICT OF INTEREST DISCLOSURE FORM

Conflict of Interest is defined as a set of conditions in which professional judgment concerning a primary interest, such as the validity of research, may be influenced by a secondary interest, such as financial gain. A Conflict of Interest Disclosure is an agreement or notification from the authors that they have not been paid for the work, or if they have, stating the source of their payment. The purpose of Conflict of Interest Disclosure form is to provide readers of authors' manuscript with information about authors' interests that could influence how the authors receive the work. The corresponding author (on behalf of all co-authors) should submit a conflict of interest disclosure form and is responsible for the accuracy and completeness of the submitted manuscript. Conflict of Interest Disclosure form can be signed by the corresponding author on behalf of all co-authors and stating that the submitted manuscript is the authors' original work, has not received prior publication and is not under consideration for publication elsewhere, permission has been received to use any material in the manuscript such as tables, figures etc. or no permissions have necessary to publish the authors' work.

1. Name of the corresponding author
2. Affiliation including e-mail and phone number
3. Manuscript Title
4. Do the authors or authors' institution at any time receive payment or services from a third party (government, commercial, private foundation, etc.) for any aspect of the submitted manuscript (including but not limited to grants, data monitoring board, study design, manuscript preparation, statistical analysis, etc.)?

Are there any relevant conflicts of interest? Yes / No

5. Do the authors have any patents, whether planned, pending or issued, broadly relevant to the work?

Are there any relevant conflicts of interest? Yes / No

6. Are there other relationships or activities that readers could perceive to have influenced, or that give the appearance of potentially influencing, what the authors' information in the submitted manuscript?

Are there any relevant conflicts of interest? Yes / No

7. Are there any aspect of the work covered in this manuscript that has involved either experimental animals or human patients has been conducted with the ethical approval of all relevant bodies or not.

Are there any relevant conflicts of interest? Yes / No

Corresponding Author  
Signature

Print Name

Date

## AUTHORSHIP FORM

By completing and signing the following statements, the corresponding author acknowledges and accepts the responsibility on behalf of all contributing authors, if any, concerning Authorship Responsibility.

Manuscript title:

Corresponding author:

Affiliation:

Email:

Phone No:

By signing and filling this form, the corresponding author certifies that each author has met all criteria below (A, B, C, and D) and indicates each author general and specific contributions by listing his or her name next to the relevant section.

A. I certify that

- The manuscript is authentic and valid and that neither this manuscript nor one with considerably similar content under my authorship has been published or is being considered for publication elsewhere, except as described in an attachment, nor copies of closely related manuscripts are provided.
- I will provide the data or will contribute fully in providing and obtaining the data on which the manuscript is based for examination by the editors or their assignees, if requested.
- Every author has agreed to allow the corresponding author to serve as the primary correspondent with the editorial office, to review the edited manuscript and proof.

B. Each author has given final approval of the submitted manuscript.

C. Each author has participated sufficiently in the work to take public responsibility for the whole content.

D. Each author qualifies for authorship by listing his or her name on the appropriate line of the categories of contributions listed below. List appropriate author next to each section – each author must be listed in at least 1 field. More than 1 author can be listed in each field.

- conception and design
- acquisition of data
- analysis and interpretation of data
- drafting of the manuscript
- critical revision of the manuscript for important intellectual content
- statistical analysis
- obtaining funding
- administrative, technical, or material support
- supervision
- no additional contributions
- other (specify)

**Corresponding Author Signature**

**Print Name**

**Date**

## CHANGE OF AUTHORSHIP FORM

Manuscript Title:

Corresponding Author:

**Please check all that apply.**

- New author(s) have been added.
- There is a change in the order of authorship.
- An author wishes to remove his/her name. An author's name may only be removed at his/her own request in writing.

### ORIGINAL AUTHORSHIP

List ALL AUTHORS in the same order as the original (first) submission.

Print Name	Print Name
Name (1)	Name (6)
Name (2)	Name (7)
Name (3)	Name (8)
Name (4)	Name (9)
Name (5)	Name (10)

### NEW AUTHORSHIP

List the ALL AUTHORS in same order as the new version.

Print Name	Print Name
Name (1)	Name (6)
Name (2)	Name (7)
Name (3)	Name (8)
Name (4)	Name (9)
Name (5)	Name (10)

### I attest that:

1. The manuscript is not currently under consideration, in press, or published elsewhere, and the research reported will not be submitted for publication elsewhere until a final decision has been made as to its acceptability by the journal (posting of submitted material on a web site may be considered prior publication-note this in your cover letter).
2. The manuscript is truthfully original work without fabrication, fraud, or plagiarism.
3. I have made an important scientific contribution to the study and am thoroughly familiar with the primary data.
4. I have read the complete manuscript and take responsibility for the content and completeness of the manuscript and understand that I share responsibility if the paper, or part of the paper, is found to be faulty or fraudulent.

Corresponding Author Signature

Name

Date

# SUBSCRIPTION FORM

# Subscription form

## Global Journal of Environmental Science and Management

Please enter my annual subscription to the Global Journal of Environmental Science and Management (GJESM), including 4 quarterly issues for the Year ..... Vol. .... Nos.....

	Domestic (Rials)	International (USD)
▪ Institutional	3,000,000	150
▪ Individual	2,000,000	100
▪ Student	1,000,000	80
▪ Single Copy	500,000	50

Name:

Tel.:

Email:

Mailing Address:

**Payment method:** Check or money order must be made in order of:  
Account #. 0101834143005, Account name: J. Nouri  
Bank Melli Iran, IAU Branch, Code 1017, Tehran, Iran

Bank receipt enclosed

\* Please allow 3 to 5 weeks for delivery

Please send this filled in order form along with the Bank receipt payment to:

Global Journal of Environmental Science  
and Management  
No. 2, Kouhestan Deadend, Janpour Street,  
Darabad, Tehran 1956934461 Iran

# Global Journal of Environmental Science and Management

## CONTENTS

Volume 10, Number 1, Winter 2024

Economics and cost effectiveness of a rain garden for flood-resistant urban design D. Rinchumphu; N. Suriyanon; N. Phichetkunbodee; S. Munlikawong; C. Wanitchayapaisit; S. Sittikankun ( <a href="#">ORCID</a> , <a href="#">Scopus</a> )	1 - 12
Green synthesis of titanium dioxide photocatalyst using <i>Lactobacillus bulgaricus</i> for processing palm oil mill effluent L. Agustina; M. Romli; P. Suryadarma; S. Suprihatin ( <a href="#">ORCID</a> )	13 - 26
Efficient biosorption of cadmium by <i>Eucalyptus globulus</i> fruit biomass using process parameters optimization M. Samimi ( <a href="#">ORCID</a> )	27 - 38
Silver-based plasmonic nanoparticles for biosensor organophosphate pesticides using a single film containing acetylcholinesterase/choline oxidase D. Hermanto; N. Ismillayli; H. Muliastari; R. Wirawan; S.R. Kamali ( <a href="#">ORCID</a> , <a href="#">Scopus</a> ) ( <a href="#">ORCID</a> )	39 - 50
Analyzing cellulolytic bacteria diversity in mangrove ecosystem soil using 16 svedberg ribosomal ribonucleic acid gene I. Dewiyanti; D. Darmawi; Z.A. Muchlisin; T.Z. Helmi ( <a href="#">ORCID</a> )	51 - 68
Evaluation of municipal waste collection performance using operational data G.M. Hoang; H.T.T. Ung; N.T.L. Le; T.D. Nguyen ( <a href="#">ORCID</a> )	69 - 82
Wetland degradation monitoring using multi-temporal remote sensing data and watershed land degradation index I. Ridwan; S. Kadir; N. Nurlina ( <a href="#">ORCID</a> , <a href="#">Scopus</a> )	83 - 96
Exploring the upper ocean characteristics of a bay using coastal and regional ocean community model D. Jaishree; P.T. Ravichandran ( <a href="#">ORCID</a> )	97 - 116
Application of fuzzy logic in decision-making process for relocation of floating net cages in river fish farming R. Pramana; B.Y. Suprpto; Z. Nawawi ( <a href="#">ORCID</a> )	117 - 132
Factors affecting cadmium toxicity to rice germinated in soils collected from downstream areas of abandoned zinc mines P. Chanpiwat; A. Numprasanthai ( <a href="#">ORCID</a> )	133 - 154
Impact of environmental and geographical position on the chemometric classification of ethanol extracts from <i>Isotoma longiflora</i> leaves E. Imelda; K. Khairan; R.R. Lubis; T. Karma; R. Idroes ( <a href="#">ORCID</a> )	155 - 168
Torrefaction of bamboo pellets using a fixed counterflow multibaffle reactor for renewable energy applications W. Hidayat; B.A. Wijaya; B. Saputra; I.T. Rani; S. Kim; S. Lee; J. Yoo; B.B. Park; L. Suryanegara; M.A.R. Lubis ( <a href="#">ORCID</a> , <a href="#">Scopus</a> )	169 - 188
Evaluation of mineral and near-infrared forecasting of wheat yield varieties using spectrophotometric techniques H.A. Pardhe; N. Krishnaveni; B.K. Chekraverthy; S. Patel; S. Naveen; V. Rashmi; P.C. Govinden ( <a href="#">ORCID</a> , <a href="#">Scopus</a> )	189 - 204
Presence of microplastics contamination in table salt and estimated exposure in humans D.A. Syamsu; D. Deswati; S. Syafrizayanti; A. Putra; Y. Suteja ( <a href="#">ORCID</a> )	205 - 224
Generalization of artificial neural network for predicting methane production in laboratory-scale anaerobic bioreactor landfills M.J. Zoqi ( <a href="#">ORCID</a> )	225 - 244
Modeling regional aboveground carbon stock dynamics affected by land use and land cover changes A.D. Malik; M.C.W. Arief; S. Withaningsih; P. Parikesit ( <a href="#">ORCID</a> )	245 - 266
Root growth and arbuscular mycorrhizal fungi on woody plants for vegetative stabilization of tropical slopes I.G. Tejakusuma; E.H. Sittadewi; T. Handayani; T. Hernaningsih; W. Wisyanto; A. Rifai ( <a href="#">ORCID</a> )	267 - 286
Role of <i>Cylindrospermopsis</i> sp. in vertical nitrogen changes observed in tropical oxidation wastewater treatment ponds M. Srichomphu; O. Phewnil; T. Pattamapitoon; Ratcha Chaichana; K. Chunkao; W. Wararam; N. Dampin; P. Maskulrath ( <a href="#">ORCID</a> )	287 - 300
Flood susceptibility mapping based on watershed geomorphometric characteristics and land use/land cover on a small island B.H. Narendra; O. Setiawan; R.A. Hasan; C.A. Siregar; , Pratiwi; N. Sari; A. Sukmana; I.W.S. Dharmawan; R. Nandini ( <a href="#">ORCID</a> )	301 - 320
Machine learning using random forest to model heavy metals removal efficiency using a zeolite-embedded sheet in water N.D. Takarina; N. Matsue; E. Johan; A. Adiwibowo; M.F.N.K. Rahmawati; S.A. Pramudyawardhani; T. Wukirsari ( <a href="#">ORCID</a> , <a href="#">Scopus</a> )	321 - 336
Cocoa farmers' characteristics on climate variability and its effects on climate change adaptation strategy I. Idawati; N.A. Sasongko; A.D. Santoso; M. Septiani; T. Handayani; A.Y.N. Sakti; B.D. Purnamasari ( <a href="#">ORCID</a> )	337 - 354
An analysis on the economic development and deforestation E.S. Siregar; S.U. Sentosa; A. Satrianto ( <a href="#">ORCID</a> )	355 - 368
Ecotoxicological insight of phytochemicals, toxicological informatics, and heavy metal concentration in <i>Tridax procumbens</i> L. in geothermal areas N.B. Mauliyda; R. Idroes; K. Khairan; T.E. Tallei; F. Mohd Fauzi ( <a href="#">ORCID</a> , <a href="#">Scopus</a> ) ( <a href="#">ORCID</a> )	369 - 384
Economics and cost effectiveness of a rain garden for flood-resistant urban design M. Shariati; M. Afrazi; H. Kamyab; S. Rouhanifar; E. Toghrol; M. Safa; Sh. Chelliapan; H. Afrazi ( <a href="#">ORCID</a> , <a href="#">Scopus</a> )	385 - 404
Abnormality in optimal forest management by indigenous people in deforestation A. Mutolib; Y. Yonariza; A. Rahmat ( <a href="#">ORCID</a> )	405 - 418